IN-LINE AND TRANSVERSE FORCES ON A CYLINDER NEAR A BOUNDARY IN OSCILLATORY FLOW

GREGORY JAMES TUCKER

CIVIL ENGINEERING DEPARTMENT

UNIVERSITY OF CAPE TOWN

FEBRUARY 1991

A dissertation submitted in partial fulfillment of the requirements of the degree of Master of Science in Civil Engineering

DECLARATION OF CANDIDATE

I, Gregory James Tucker, hereby declare that this is my own work unless otherwise stated and that this document has not been submitted for a degree at another university.

Signed by candidate

G.J.Tucker

February 1991

ACKNOWLEDGMENTS

I would like to take this opportunity to express my thanks to those people who assisted me during the course of this work.

In particular I am most grateful to:

- Assoc. Prof. Tony Kilner, who supervised this work, for his guidance, advice and encouragement.

- Dr Gerald Rosenthal for his expertise with the programming and electronic equipment.

- Dave Dean for his help with the electronic equipment.

- Dirk Pienaar for his help with the hydraulic apparatus.

I would also like to thank :

- Eike von Guerard, Denis Botha, Giovanni Bertuzzi and Robin Edge, each of whom was of great assistance with the experimental apparatus.

SYNOPSIS

It was endeavoured to measure the in-line and transverse forces that act on a cylinder placed near a plane boundary in oscillatory flow. The value of performing such work is that it provides information on the forces that may be exerted by surface waves on a pipeline or cable mounted near the sea bed.

Investigations were carried out in a laboratory, using a water filled flume. The test cylinder was attached to a plywood surface which was fastened to an hydraulic ram which could oscillate horizontally in a sinusoidal mode. Furthermore, this plywood surface, which acted as the boundary, was in contact with the upper free surface of the water in the flume, with the test cylinder submerged in the water under the plywood surface. The situation as it occurs in the field has therefore been inverted for this work, and the test cylinder is oscillated while the water remains stationary. Instead of measuring the lift and drag forces directly, pressure transducers were used to obtain the pressure distribution around the circumference of the test cylinder. An integration of these pressures then yielded the lift and drag forces.

The primary variables to be considered were test cylinder diameter, amplitude of oscillation, period of oscillation and the gap distance between the cylinder and the boundary. At different values of these primary variables, the dimensionless constants Reynolds number, Keulegan-Carpenter number and βd were obtained. Tests were performed in the ranges Re=4200-56600, Kc=0.8-56 and G/d=0.01-1.0. (See page xiii for definitions of constants)

The results of these tests were presented in the form of a plot of instantaneous force vs the phase angle in a cycle. This showed the measured force over a complete cycle and it was found that for certain flow conditions, regular waveform patterns would develop. Of equal importance were the maxima of these curves or rather, the maximum lift forces towards and away from the boundary and the inertia and drag coefficients. These were plotted against the Reynolds number, gap ratio and Keulegan-Carpenter number but the latter was found to be the most useful parameter.

These plots produced even more regular and repeatable curves than the force vs phase plots. The information gained from these plots was of particular importance since both axes of the plots are dimensionless. This meant that regardless of the primary variables, the maxima can be reasonably well predicted by considering the values of the dimensionless constants.

It was concluded that the proximity of the boundary does not significantly affect the fluid flow when the gap ratio is larger than 0.5. For gap ratios less than 0.5, the boundary actually increases the force coefficients. It was further concluded that the method of obtaining the forces via pressure measurement is quite efficient and accurate.

It has been recommended that a larger test cylinder be used to obtain results at prototype conditions and at a higher range of Reynolds number. It was also recommended that an extensive series of testing be performed in the range Kc=2-10, since it was found that force coefficients are most critical in this range.

TABLE OF CONTENTS

NOMENCLATURE

Symbol	Description
A	amplitude
A_P	projected area of cylinder
Cd	average drag coefficient (Fourier)
C_D	instantaneous drag coefficient
C_{DMAX}	maximum C_D measured over a cycle
CL_{amp}	amplitude of lift coefficient
CL+	maximum lift coefficient away from boundary
CL-	maximum lift coefficient towards boundary
Cm	average inertia coefficient (Fourier)
d	cylinder diameter
F_D	drag force
F_L	lift force (positive away from boundary)
g	gravitational constant = 9.81 m/s^2
K	Karman constant
L	wave length
P	pressure
P.I.D	proportional, integral and differential controller
SHM	simple harmonic motion
t	time
T	period
u	horizontal component of velocity
$\bar{u}$	time mean value of u
u_*	shear velocity at the boundary = $(\tau_o/\rho)^{1/2}$
$\bar{u}_*$	time mean value of u_*
$\hat{u}_*$	maximum shear velocity
U_m	maximum free stream velocity = ω A = $\frac{2\pi A}{T}$

$\bar{U}_1$	velocity at the outer edge of boundary layer
v	velocity
w	specific weight of water = 9.81 kN/m^3
V	voltage (or volts)
x	distance measured in horizontal direction
y	distance away from the boundary
y_o	constant depending on ratio of bed roughness to boundary layer thickness
y_1	boundary layer thickness
z	elevation

β	$\sqrt{\frac{\omega}{2\nu}}$
δ	thickness of viscous sub layer
Δ	thickness of wall layer
ε	vertical eddy viscosity
μ	dynamic viscosity of fluid
ν	kinematic viscosity of fluid
ρ	density of fluid = 1000 kg/m^3 for pure water
τ	shear stress
$\bar{\tau}$	time mean value of τ
τ_o	shear stress at boundary
ω	angular frequency = $(2\pi / T)$

Dimensionless parameters

βd $$\sqrt{\frac{\omega}{2\nu}} \times d = \sqrt{\frac{\pi}{\nu T}} \times d$$
$$= \sqrt{\frac{Re}{KC}} \times \pi^2$$

Cd $$\frac{-3}{4} \int_0^{2\pi} \frac{F \cos\theta}{\rho\, U_m^2\, A_p}\, d\theta$$ (Fourier average)

C_D inst. drag coeff. $= \dfrac{F_D}{1/2\ \rho\, U_m^2\, A_p}$

C_L lift coefficient $= \dfrac{F_L}{1/2\ \rho\, U_m^2\, A_p}$

Cm $$\frac{2\, U_m\, T}{\pi^3\, d} \int_0^{2\pi} \frac{F \sin\theta}{\rho\, U_m^2\, A_p}\, d\theta$$ (Fourier average)

G/d gap ratio

K-C Keulegan Carpenter number

$$= \frac{U_m\, T}{d} = \frac{Re.\pi}{(\beta_d)^2} = \frac{2.\pi.A}{d}$$

Re Reynolds number $= \dfrac{U_m\, d}{\nu}$

$$= \frac{\beta_d^2\, KC}{\pi}$$

Explanation of phase origin and coefficients

Lift coefficients

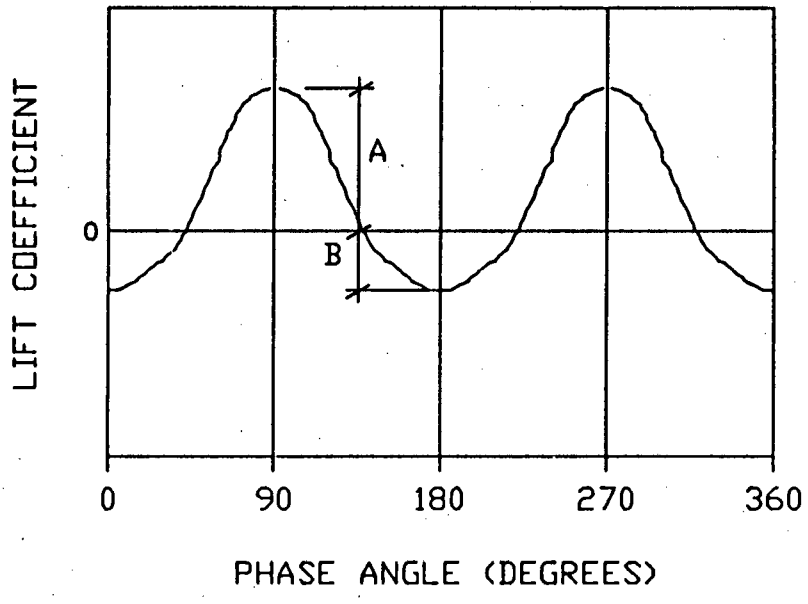

$Cl_+ = A$

$Cl_- = B$

$Cl_{amp} = A + B$

Velocity reversal occurs at 0 degrees

Drag coefficients

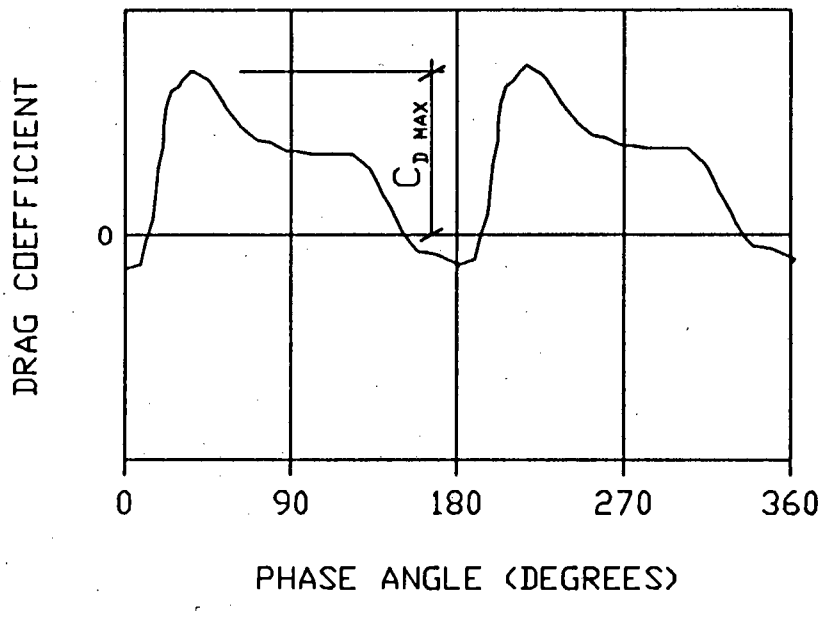

1. INTRODUCTION

The subject of the dynamics of fluid flow around cylinders is of particular importance since quantitative knowledge on the subject is necessary for the design of pipes and cables submerged near the sea bed in different flow conditions.

One of the most important aspects in the design of offshore pipelines is the calculation of the forces exerted on them. Movement of these pipelines can lead to serious economic and environmental consequences, an example of which is the Green Point sewer outfall which recently failed, leading to widespread pollution of the vicinity.

Although offshore pipelines are subjected to both uni-directional flow (currents) and oscillatory flow (waves), it is convenient to investigate these two effects separately. The concept of uni-directional flow is well researched and understood, but quantitative knowledge of oscillatory flow is not as abundant. The subject has been difficult to understand thoroughly because of the complicated flow regimes which depend on velocity distribution, near boundary conditions and the random phenomenon of vortex shedding.

The purpose of conducting this work was to measure the in-line and transverse forces exerted on a circular cylinder near a plane boundary when it is subjected to oscillatory flow which is perpendicular to the cylinder's central axis. It was acceptable to use oscillatory flow to simulate wave effects at the sea bed , since the elliptical orbits of a particle's displacement become

flatter when the bed is approached. Figure 1.1 shows that at the bed, the flow is purely oscillatory for shallow water conditions. The flow conditions which are of most concern are gap ratio, amplitude of oscillation and period of oscillation, all of which have been varied. The pressure distribution around the cylinder was measured over a complete cycle and then integrated to give the resultant in-line and transverse forces.

Since experimental work in an environment as hostile as the sea is difficult and costly, this work, as most others, was conducted in a laboratory. The apparatus used consisted of a flume containing stationary water, in which the test cylinder could be oscillated. The test cylinder was mounted below a plywood tray which was in contact with the upper water surface. A hydraulic drive system then oscillated this arrangement in a sinusoidal fashion.

This document outlines the background hydrodynamic theory associated with lift and drag forces. It goes on to describe the apparatus and explains how it is operated. Results of both lift and drag force under oscillatory flow conditions are analyzed, and finally conclusions are drawn and recommendations for further work given.

u = LOCAL HORIZONTAL VELOCITY

A = AMPLITUDE (MAJOR AXIS)

B = AMPLITUDE (MINOR AXIS)

L = WAVELENGTH

d = DEPTH

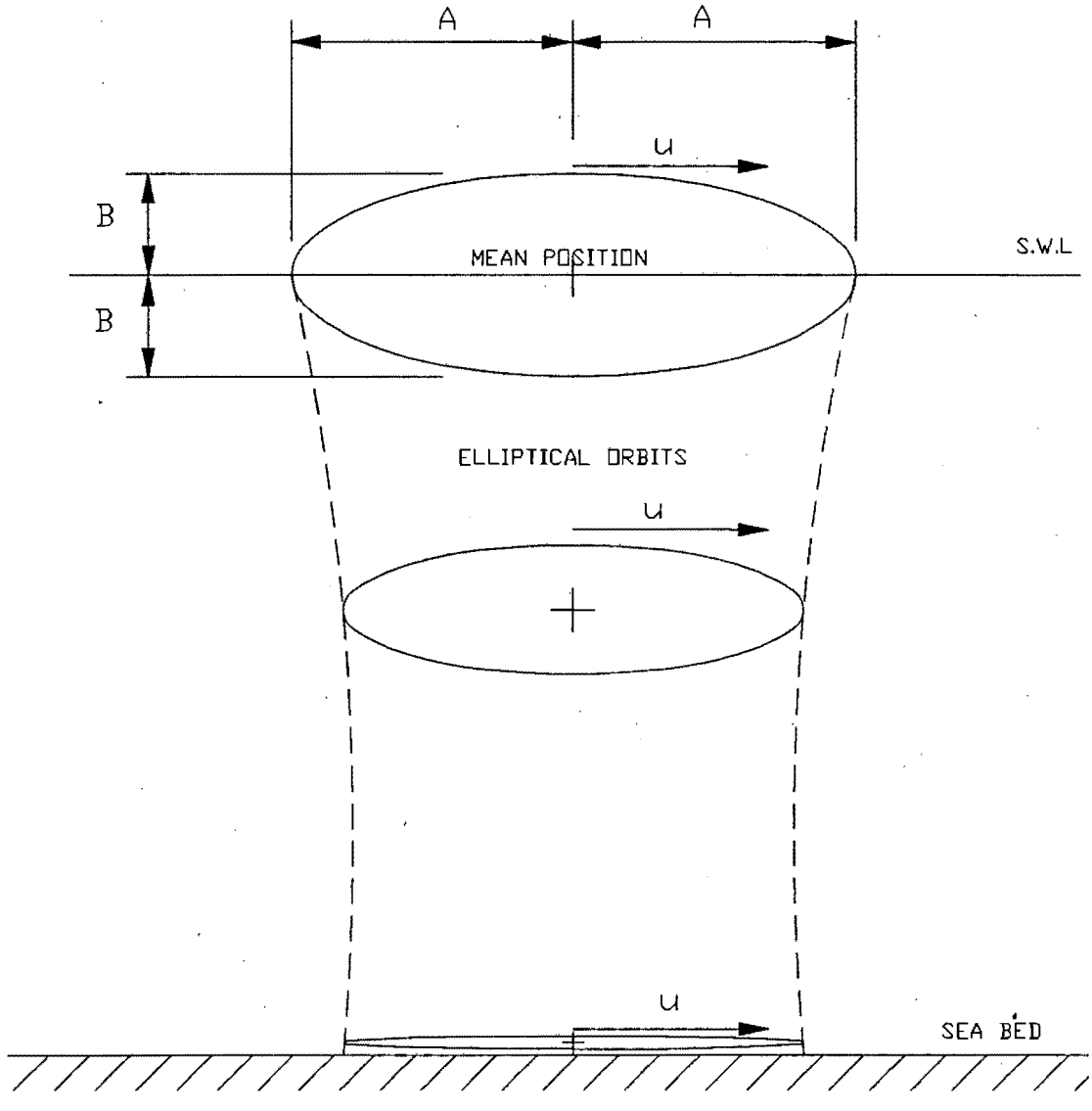

SHALLOW WATER WAVE OR TRANSITIONAL WATER WAVE

WHERE d/L < 1/2

Figure 1.1 : Water particle displacements from the mean position for shallow water (CERC manual 1977)

2. LITERATURE REVIEW

It should be acknowledged that some of the following text is a paraphrase of the work by Sarpkaya(1975,1976,1977,1986), Bellamy(1989), Rosenthal(1986) and some other authors that have been referenced. The theory in this chapter is therefore not original and should not be considered a result of work undertaken for this thesis.

The purpose of this chapter is to introduce the relevant fluid mechanics involved in both steady and oscillatory flow, so that the role of lift and drag forces may be better understood.

2.1 VELOCITY DISTRIBUTION

Consider a flat plate located in a stream of uniform flow and extending to infinity in the direction of flow. The resulting flow includes a relatively thin shear layer which is attached to the plate.

The stream is stationary at the point of contact with the plate and there is a velocity gradient between the plate and a point where the plate no longer affects the fluid flow. The region where this velocity gradient exists is known as the boundary layer, which can be defined as a zone where viscous forces acting on fluid elements cannot be neglected, when compared with the inertial forces. Therefore, at the surface of the plate, the velocity of the stream is zero and outside the boundary layer the velocity is equal to the free stream velocity U_m.

Flow in the boundary layer may be either laminar or turbulent. Flow is said to be laminar when fluid particles follow each other along streamlines which are parallel. As the velocity of the flow increases or if there are substantial disturbances, the path of the streamlines may become disturbed and only the time averaged flow is along the streamline. Flow is now said to be turbulent.

Initially, and in the absence of surface protrusions, the boundary layer is laminar. Due to the action of viscosity, the fluid elements inside the boundary layer decelerate, and as they move downstream they entrain more and more fluid elements from outside the boundary layer. A momentum exchange takes place between the particles and in this way the boundary layer becomes thicker with increasing downstream distance.

If this process continues, a stage is reached where there is a transition from laminar to turbulent flow, resulting in a turbulent boundary layer. In this turbulent boundary layer, the velocities substantially fluctuate with time and as a result there is a greater rate of momentum exchange. This leads to a significant increase in the thickness of the boundary layer.

2.1.1 Velocity distribution in uni-directional flow

(i) Laminar boundary layer in uni-directional flow

In laminar flow the velocity distribution adjacent to a flat plate has the form of the Blasius profile, see figure 2.1. In the Blasius profile, $u / \bar{U}_1$ represents the ratio of local velocity to the free stream velocity, and y / Y_1 represents the ratio of the

distance from the boundary to the boundary layer thickness.

(ii) Turbulent boundary layer in uni-directional flow

Turbulent boundary layers are of particular importance since the boundary layers encountered in practice are turbulent for most of their length. Turbulent boundary layers are usually thicker than laminar boundary layers and the velocity gradient is usually steeper.

For convenience, the turbulent boundary layer may be divided into three regions - the inner layer, the overlap layer and the outer layer (Sleath 1984). See figure 2.2.

a) The inner layer or viscous sub layer is a very thin laminar sub layer, where Newtonian viscosity applies and where the velocity gradient is steep. From the equations,

$$\bar{\tau} = \mu \frac{d\bar{u}}{dy} \qquad \text{and} \qquad \bar{u}_* = \sqrt{\frac{\tau_o}{\rho}}$$

where :
- $\bar{\tau}$ = average shear stress
- μ = dynamic viscosity
- $\bar{u}$ = ave. horizontal component of velocity
- y = distance away from boundary
- $\bar{u}_*$ = average shear velocity
- τ_o = shear stress at boundary
- ν = kinematic viscosity

and assuming that the shear stress is constant, due to the layer being so thin, the velocity distribution is given by,

$$\bar{u} = \frac{y\,\bar{u}_*^2}{\nu}$$

The thickness of the viscous sub layer is given by,

$$\delta = 11.6 \times \frac{\nu}{\bar{u}_*}$$

b) The overlap layer is the region of overlap between the wall layer and the defect layer. For the wall layer the velocity is a function of the shear stress at the bed, however, the defect layer is unaffected by viscosity.

The velocity distribution in the overlap layer can be described by the Prandtl-von Karman formula,

$$\frac{\bar{u}}{\bar{u}_*} = \frac{1}{K} \ln\left(\frac{y}{y_o}\right)$$

where y_o is a constant dependent on the ratio of bed roughness to boundary layer thickness. The Karman constant, K is usually taken as 0.4.

c) The outer layer is that part of the defect layer that does not overlap the wall layer. Coleman (1981), suggests the following expression for the velocity distribution in this region.

$$\frac{U_m - \bar{u}}{\bar{u}^*} = -\frac{1}{K} \times \ln\left(\frac{y}{y_1}\right) + \frac{2 \cdot P}{K}\left(1 - \sin^2 \frac{\pi y}{2y_1}\right)$$

where: U_m = maximum free stream velocity

y_1 = thickness of the boundary layer

P = 0.19 for pure water

$\bar{u}$ = mean horizontal velocity

Clauser (1956), showed that a reasonable approximation of the velocity profile for the entire turbulent boundary layer is,

$$\frac{\bar{u}}{\bar{U}_1} = \left(\frac{y}{y_1} \right)^{(1/7)}$$

where : $\bar{U}_1$ = free stream velocity

y_1 = thickness of boundary layer

This equation does not hold for 10% of the boundary layer nearest the boundary.

2.1.2 Velocity distribution in oscillatory flow

As in uni-directional flow, the oscillatory boundary layer may be either laminar or turbulent. However, in oscillatory flow, the velocity distribution near the bed is far more complex. In particular jets of fluid are thrown up from the boundary at velocity reversal. These jets appear to be associated with the ejection of vortices that form around elements of bed roughness which occurs as the direction of flow changes. These jets can cause considerable mixing of the different layers in the boundary layer mentioned above, even when the flow in the layer is essentially laminar.

An important feature in describing the velocity distribution in

oscillatory flow is the transition from laminar to turbulent flow. Sleath (1984) concluded that a Reynolds number = 1.6×10^5 should be used to describe the transition. This is somewhat confirmed by Jonsson (1980) who proposed a Reynolds number = 1×10^5.

(i) Laminar boundary layer in oscillatory flow

Consider an infinite, smooth bed oscillating in its own plane with a velocity,

$$u = U_m \cos \omega t$$

The Navier-Stokes equation may be reduced to,

$$\frac{\partial u}{\partial t} = \nu \times \frac{\partial^2 u}{\partial y^2}$$

By neglecting non-linear terms, Stokes (1851) derived the following equation.

$$u = U_m \, e^{-\beta y} \cos(\omega t - \beta y)$$

where: $U_m = \omega \cdot A$

$$\beta = \sqrt{\frac{\omega}{2\nu}}$$

β^{-1}, which is a measure of the extent to which viscosity effects penetrate the fluid, may be used as a measure of the oscillatory boundary layer thickness.

β^{-1} is used as a measure of length in oscillatory laminar flow and therefore the product $\beta \times d$ (d/β^{-1}) gives the ratio of cylinder diameter to oscillatory boundary layer thickness. Therefore, a

large value of βd implies that the diameter is large in comparison with the boundary layer thickness and a small value ($\beta d=1$) means that they are of a comparable size.

(ii) Turbulent boundary layer in oscillatory flow

Owing to the complexity of the flow, there are no purely analytical solutions for oscillatory turbulent boundary layers. As for uni-directional flow, the onset of turbulence is associated with significant momentum or vorticity exchange from one fluid layer to another.

Kajiura (1968), whose results compared reasonably well with those of Horikawa and Watanabe (1968), proposed that as for uni-directional flow, the turbulent layer could be divided into three regions - the inner layer, the overlap layer and the outer layer. He also defined the vertical eddy viscosity separately for smooth and rough beds for each of the three layers. The basis of this model is beyond the scope of this review but is discussed in some detail by Horikawa and Watanabe (1968).

Kajiura's model has been described in further detail by Sleath (1984) as follows.

$$\tau = \rho \cdot \varepsilon \cdot \frac{du}{dy}$$

$$\frac{\partial u}{\partial t} = - \hat{U}_s . \omega . \sin \omega t + \rho . \varepsilon \frac{\partial^2 u}{\partial y^2} + \frac{\partial u}{\partial y} \frac{\partial \varepsilon}{\partial y} \rho$$

where : ε = vertical eddy viscosity

$$\varepsilon_{\left\{\begin{smallmatrix}\text{smooth}\\ \text{bed}\end{smallmatrix}\right\}} = \begin{cases} \nu & \text{for} \quad 0 < y < 12\nu / \hat{u}_* \quad \text{(inner layer)} \\ K.\hat{u}_* y & \text{for} \quad 12\nu/\hat{u}_* < y < \Delta \quad \text{(overlap layer)} \\ K.\hat{u}_* \Delta & \text{for} \quad y > \Delta \quad \text{(outer layer)} \end{cases}$$

where : $\hat{U}_s$ = maximum velocity at the centre of the cylinder, relative to the fluid velocity at that point in the absence of the cylinder.

$\hat{u}_*$ = maximum shear velocity = $\sqrt{\tau_o / \rho}$

Δ = thickness of the wall layer = $0.05\ \hat{u}_* / \omega$

K = 0.02

ρ = density of the fluid

2.2 SEPARATION EFFECTS

2.2.1 Uni-directional flow

In a non-viscous flow, a deceleration is accompanied by a rise in pressure along the streamline and conversely, in an acceleration there must be fall in pressure along the streamline. A convex surface in irrotational flow would cause the streamlines to converge upstream of the crest of the surface and then to diverge downstream, thus creating a zone of acceleration and decreasing pressure followed by a zone of deceleration and increasing pressure.

Consider therefore, the flow over a curved surface as shown in figure 2.3. As the fluid is deflected around the surface, it is accelerated over the left hand section until at point C, the velocity just outside the boundary layer is a maximum. Here the pressure is a minimum, therefore the pressure gradient from A to C

is negative due to the acceleration of flow. Therefore, the net force on an element in the boundary layer is in the direction of flow.

Beyond C, the fluid decelerates resulting in a pressure increase and so the net force on an element opposes the direction of flow. Within a real fluid and allowing for boundary layer effects, the accelerating fluid upstream of point C tends to offset the retarding influence of viscous stress and consequently the boundary layer remains thin instead of expanding in the direction of flow as would be in the case of a flat plate. Downstream of point C these viscous stresses are enhanced by the increasing pressure gradient. This reduces the momentum and energy of the fluid particles, causing a rapid growth of the boundary layer. A point is eventually reached where the velocity at the surface is zero (point D). Beyond D, the flow close to the surface is actually reversed. The fluid, no longer able to follow the contour of the surface breaks away from it. This breakaway is termed separation and it first occurs at what's known as the separation point, where the velocity at the surface is zero. For continuity, there must be an increase in forward flow to compensate the reverse flow and hence the formation of eddies and vortices.

The location of the separation point depends largely on Reynolds number. In the case of the cylinder, the separation point is located on the lee side, moving towards the shoulder with increasing Reynolds number.

2.2.2 Oscillatory flow

There are many fundamental differences between the fluid effects occurring in uni-directional and oscillatory flow. With oscillatory flow, the fluid not only accelerates from and decelerates to zero, but also reverses direction within each half cycle.

Furthermore, the boundary layer may change from fully laminar to partially turbulent or fully turbulent conditions. When the flow reverses, there will be a change in the location of the separation point, and also a reversal of the wake from the downstream side to the "upstream side". Thus, formation of vortices within one half cycle will also be reversed during the wake reversal and this sudden reversal of vortices results in vortex shedding which significantly modifies the forces acting on the cylinder.

Therefore, it may be expected that sudden changes in the transverse and in-line forces will occur at velocity reversal.

2.3 LIFT FORCES ON CYLINDERS NEAR A BOUNDARY

When cylinders are exposed to fluid flow, there is a rapid rise in the rate of change of pressure from the shoulder to the tail of the cylinder. See figure 2.4.

The boundary layer over this region becomes stalled near the shoulder which greatly affects the pressure distribution around the cylinder. Separation often occurs at this point and this separation leads to the formation of vortices and a wake.

The cylinder will experience an in-line force in the direction of flow. This is commonly known as the drag force. The fluid will also exert a force in a direction transverse to the direction of flow. This transverse force is referred to as lift, irrespective of whether it acts towards or away from the boundary.

Lift forces may be developed in flow situations where a bluff body (cylinder, sphere, or any object that is an obtrusion to the flow) is,

a) spinning
b) near a boundary
c) in a shear flow
d) in a distorted fluid flow

This dissertation includes the study of in-line and transverse forces acting on a cylinder near a plane boundary in oscillatory flow. The lift forces are associated with the shear flow created within the boundary layers generated by the cylinder and bed and with the interaction of these boundary layers. They are also associated with the distortion of the fluid flow between the cylinder and the bed.

2.3.1 Lift forces in uni-directional flow

When a cylinder is placed near a plane boundary in an infinite, inviscid, steady and parallel flow of free stream velocity $\overline{U}_1$, there is a distortion of the streamlines as shown in figure 2.4.

A smaller gap distance will result in a higher fluid velocity between the boundary and the cylinder, and in accordance with the Bernoulli equation,

$$\frac{P}{w} + \frac{v^2}{2g} + z = \text{constant}$$

OR $$P + \frac{1}{2}\rho v^2 + \rho g z = \text{constant}$$

this higher velocity results in a lower pressure at the 'boundary shoulder' than the pressure at the 'free stream shoulder'. This pressure differential results in a net lift force that acts towards the boundary, the magnitude of which is primarily dependent on the gap distance G. Therefore, the further the cylinder is from the bed, the smaller this lift force will be. Under different conditions of 'gap', the flow may become restricted and the net lift force may act away from the bed.

2.3.2 Lift forces in oscillatory flow

The oscillatory flow situation is substantially different from that of uni-directional flow. Whereas in uni-directional flow, momentum exchange leads to a substantial increase in the viscous boundary layer thickness with increasing downstream distance, the periodic flow reversal of oscillatory flow prevents this growth of the boundary layer and consequently it is relatively thin. Furthermore, the wake that forms in the first half cycle interacts with that of the second and, since vortex shedding occurs in conditions of changing velocity, a whole range of complex vortex shedding frequencies arises.

Investigations into lift forces on cylinders oscillating near a boundary have necessarily been undertaken experimentally due to the extremely complicated flow patterns. Investigations of

relevance include Sarpkaya (1975,1976,1977), Wright et al (1979), Ikeda and Yamamoto (1989), Verley et al (1989) and Yamamoto et al (1974).

The lift coefficient, which is expressed in terms of the lift force, is given by the following expression,

$$C_L = \frac{F_L}{\frac{1}{2} \rho U_m^2 A_p}$$

where : F_L = measured lift force (N)

ρ = fluid density = 1000 kg/m^3 for pure water

U_m = maximum free stream velocity (m/s)

A_p = projected cylinder area (m^2)

The phase was assumed to be equal to zero at the velocity reversal and therefore, maximum velocity occurred at phases $\frac{\pi}{2}$ and $\frac{3\pi}{2}$.

2.4 DRAG FORCES ON CYLINDERS NEAR A BOUNDARY

When a fluid flows past a flat surface parallel to the flow, the fluid exerts a drag force on the surface as a direct result of viscous action. This drag force is termed skin friction.

When a bluff body such as a cylinder is placed in this fluid flow, there is an additional force resulting from the pressure distribution over the surface. This force is known as pressure drag or form drag since this drag force is dependent on the form or shape of the object.

2.4.1 Drag forces in uni-directional flow

In almost all cases, the separation point occurs on the lee side of the body. As a result of the wake downstream of the body, the pressure at the tail is reduced and therefore the pressure drag is increased. For a cylinder, the flow is separated over much of the surface, causing a wide wake which in turn results in the pressure drag being much greater than skin friction.

In uni-directional flow, the drag coefficient is a function of the Reynolds number. A remarkable phenomenon connected with the transition from laminar to turbulent flow occurs with bluff bodies such as cylinders. The drag coefficient undergoes a sudden and dramatic decrease near Reynolds number, $Re=5x10^5$. It is a consequence of transition which causes the separation point to move downstream, because, in the case of a turbulent boundary layer, the accelerating influence of the external flow extends further due to turbulent mixing. Hence the downstream migration of the separation point. This phenomenon is also associated with a drastic reduction in wake size.

2.4.2 Drag forces in oscillatory flow

As with lift forces, the oscillatory flow situation is substantially more complex than the uni-directional flow situation and the oscillatory boundary layer is relatively thin. Again, this is due to the velocity reversal giving rise to vortex shedding and sudden changes in the drag force at velocity reversal.

As the velocity of the stream is increased, the boundary layer

near the nose of the cylinder remains thin but increases in thickness towards the rear. Within this boundary layer there is reversal of the fluid motion and the boundary layer thus separates from the cylinder near the shoulder.

As the velocity of the stream is still further increased, the point of separation of the boundary layer moves further forward and the layer widens out behind into an eddying wake in which energy is constantly washed away downstream with vortex shedding.

Data reduction for the in-line forces is based on Morison's equation and a Fourier analysis. The in-line force, which consists of the inertia force F_I and the drag force F_d, is assumed by Morison to be expressible by :

$$F = \frac{1}{2} \rho A_p U|U| C_d + \frac{1}{4} \pi \rho d A_p C_m \frac{dU}{dt}$$

where : $U = -U_m \sin \theta$

$$\theta = \frac{2 \pi t}{T}$$

C_d and C_m represent the drag and inertia coefficients respectively. The coefficients of inertia have in most cases been experimentally determined, however, the inertia coefficient may be analytically determined from potential flow theory.

The average drag and inertia coefficients over a full cycle were developed by Fourier and are given by :

$$C_d = \frac{-3}{4} \int_0^{2\pi} \frac{F \cos\theta}{\rho U_m^2 A_p} d\theta$$

$$C_m = \frac{2\ U_m\ T}{\pi^3\ d} \int_0^{2\pi} \frac{F\ \sin\theta}{\rho\ U_m^2\ A_p}\ d\theta$$

The in-line force coefficient for the instantaneously measured force was given by :

$$C_D = \frac{F_D}{\frac{1}{2}\ \rho\ U_m^2\ A_p}$$

where : F_D= measured in-line force

This term was developed merely to present the instantaneous in-line force in non-dimensional terms.

2.5 DIMENSIONLESS PARAMETERS

The problem of defining lift and drag forces on a cylinder near a boundary in oscillatory flow may be controlled by the following dimensionless parameters.

i) Reynolds number = Re = $\frac{U_m\ d}{\nu}$

ii) Gap ratio = Gap distance between cylinder and boundary divided by the cylinder diameter.

iii) βd = ratio of cylinder diameter to oscillatory boundary layer thickness.

$$= \sqrt{\frac{\omega}{2\nu}} \times d$$

$$= \sqrt{\frac{Re}{KC}} \times \pi^2$$

iv) Keulegan Carpenter no. = KC = Period parameter

$$= \frac{2\ \pi\ A}{d} = \frac{U_m\ T}{d}$$

With respect to measured lift forces, the lift coefficient may be defined as:

$$C_L = \frac{F_L}{\frac{1}{2}\ \rho\ U_m^2\ A_p}$$

The term CL+ is associated with the maximum measured lift force away from the bed in a cycle in terms of the equation above. Also, the term CL- is associated with the maximum measured lift force towards the bed in a cycle in terms of the equation above. C_{Lamp} is the amplitude of lift coefficient given by (CL+) - (CL-).

The <u>instantaneous</u> drag coefficient C_D given by,

$$C_D = \frac{F_D}{\frac{1}{2}\ \rho\ U_m^2\ A_p}$$

should not be confused with the relation,

$$C_d = \frac{-3}{4} \int_0^{2\pi} \frac{F\ \cos\theta}{\rho\ U_m^2\ A_p}\ d\theta$$

C_d is an <u>average</u> drag coefficient for one complete cycle, derived by Fourier, whereas C_D is an instantaneously measured coefficient that was implemented merely to express the measured in-line force in non-dimensional terms. C_{Dmax} is the maximum value of the coefficient C_D in a cycle.

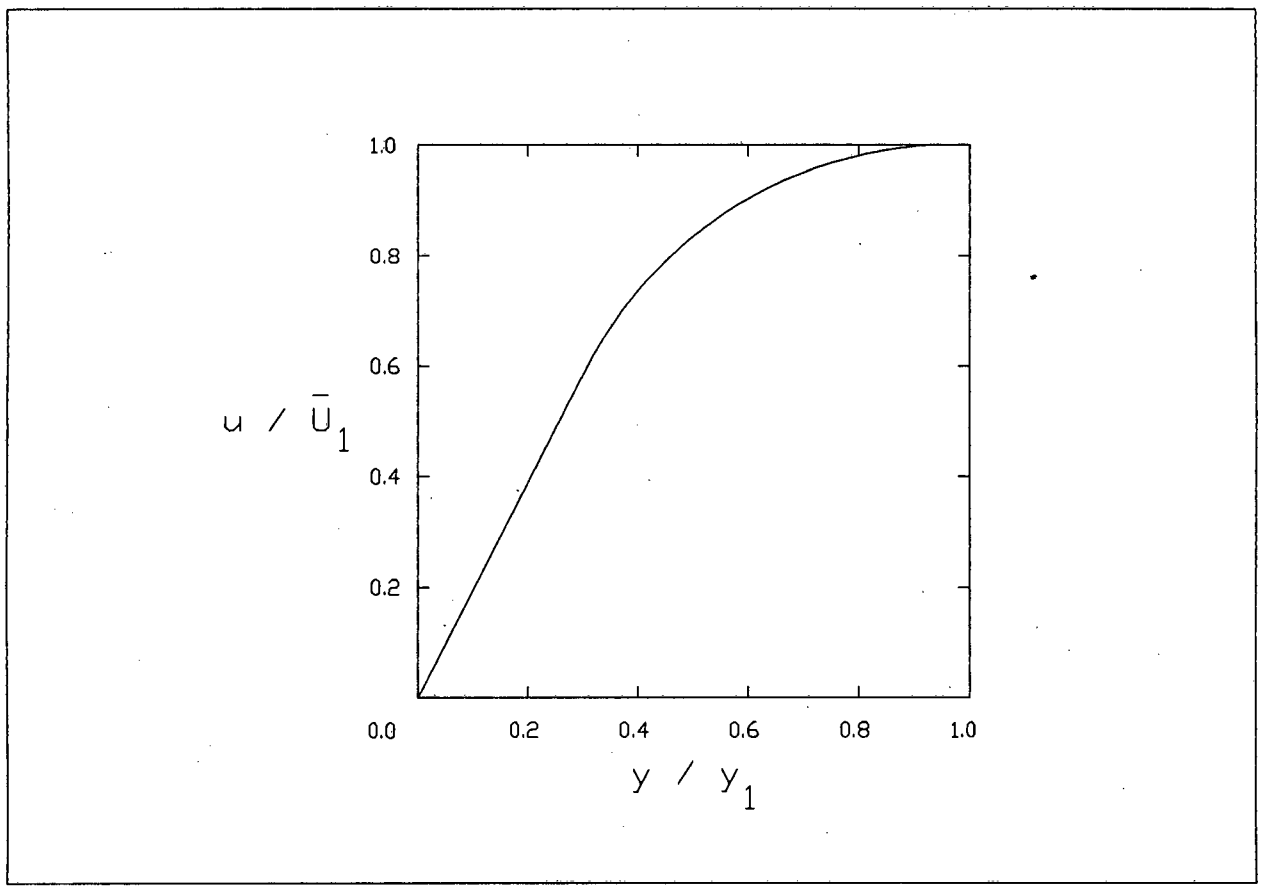

Figure 2.1 : The Blasius profile for laminar boundary layers (Clauser, 1956)

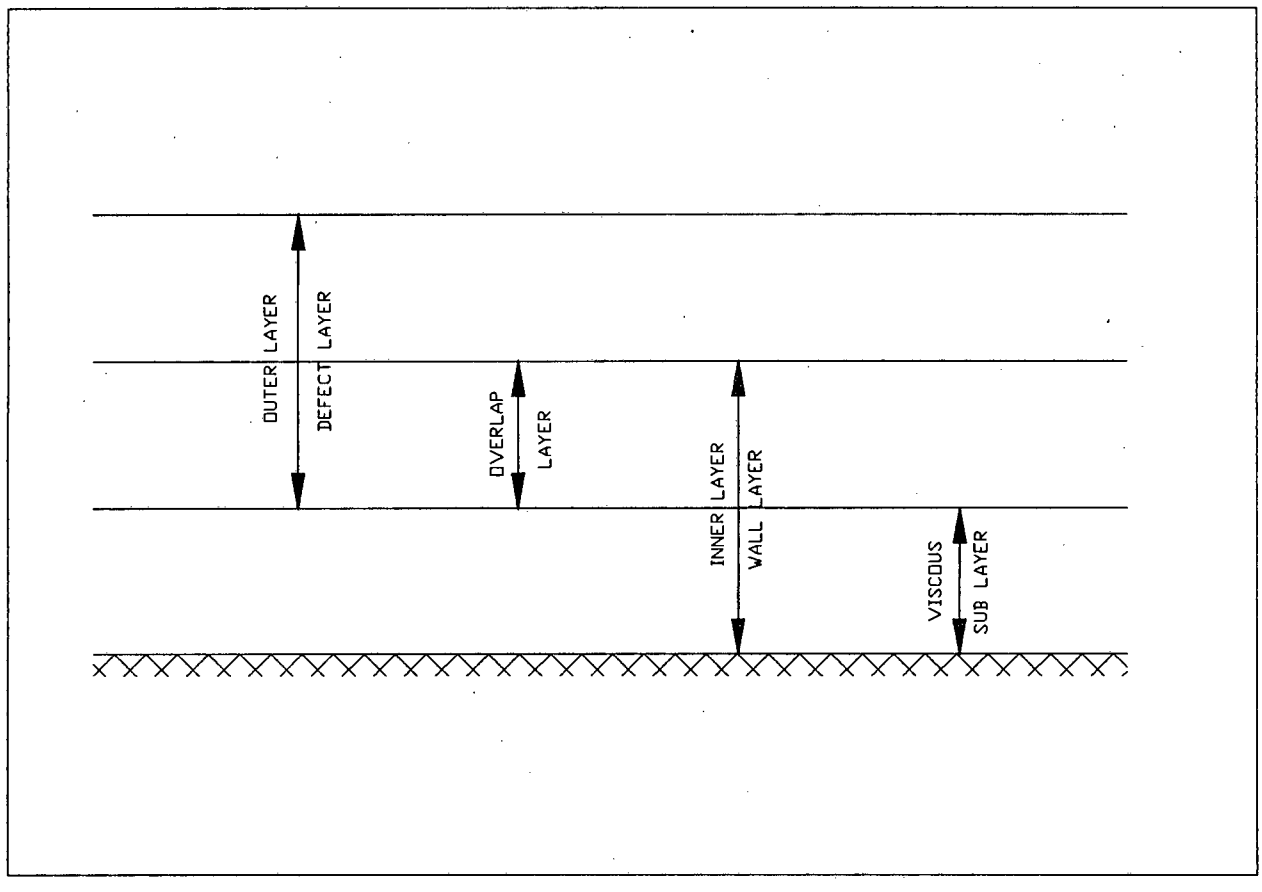

Figure 2.2 : The division of turbulent boundary layers into various different regions (Kajiura, 1968)

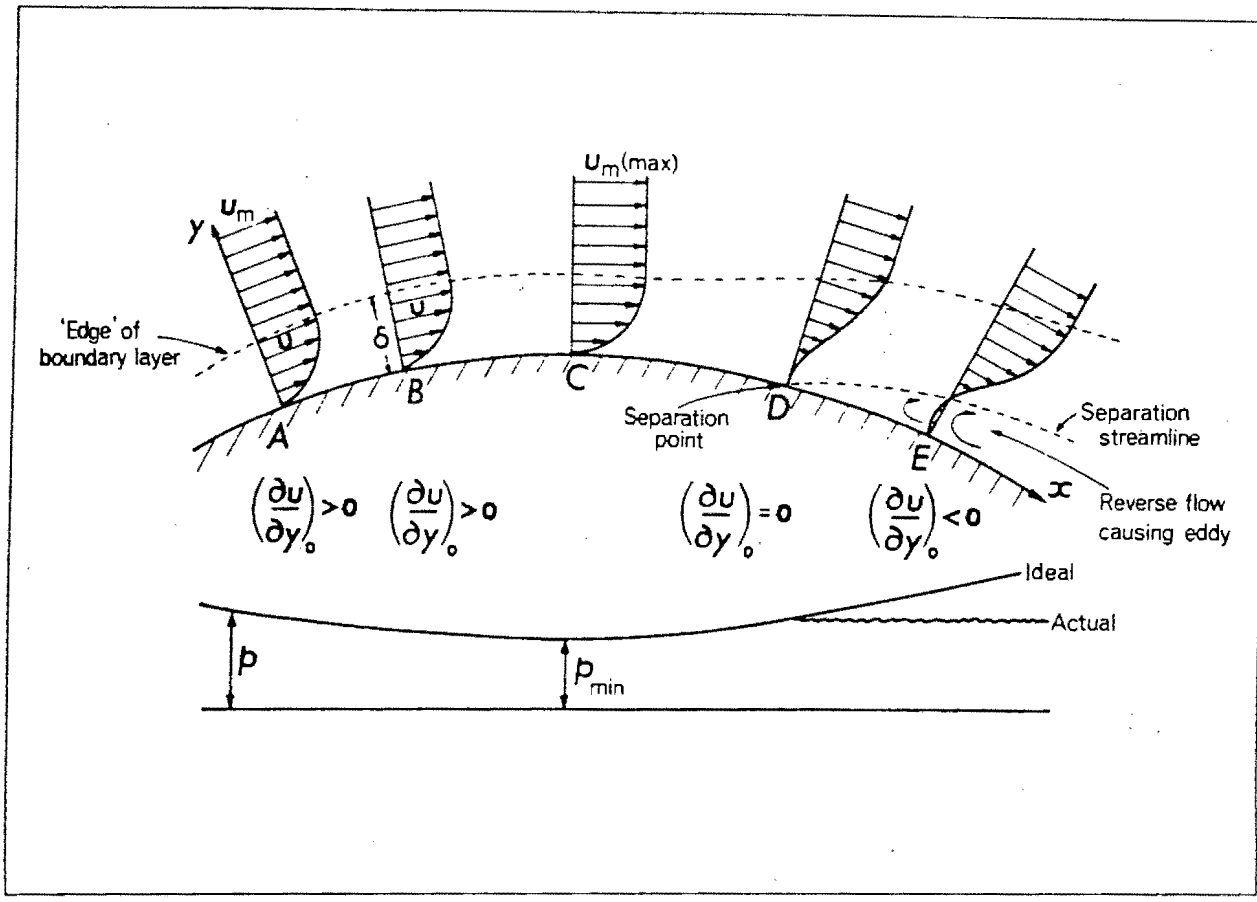

Figure 2.3 : Flow patterns around a convex surface showing separation point and velocity distribution (Massey 1979)

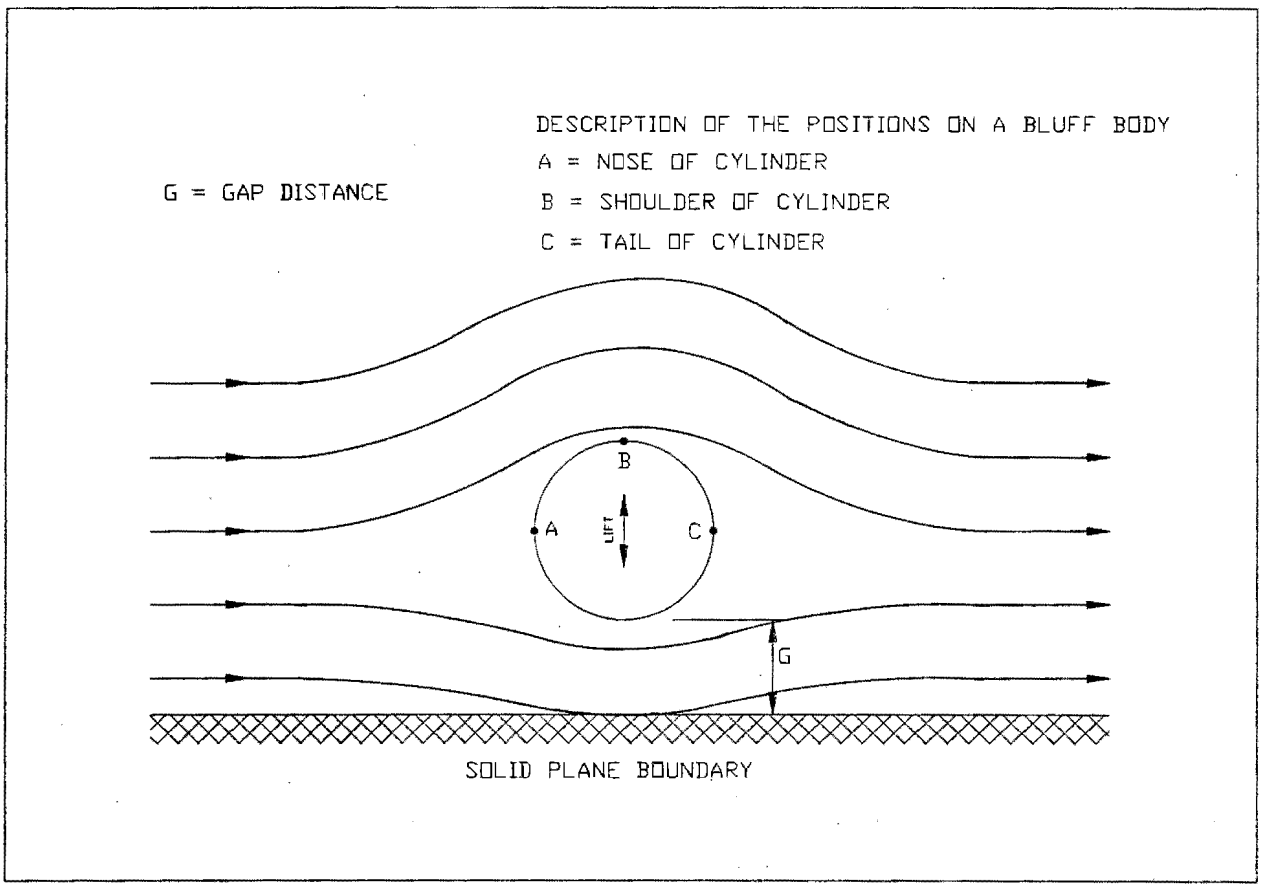

Figure 2.4 : Cylinder near a plane boundary in steady, inviscid flow

3. EXPERIMENTAL APPARATUS

This chapter describes the apparatus that was developed to simulate the effects incurred by a cylinder near a plane boundary in oscillatory flow. Since this work is an extension of an experimental programme that began some time ago, much of the experimental apparatus used was developed by previous researchers. It is for this reason that a distinction between previous developments and developments undertaken for this thesis is given. It should be noted that the majority of the experimental apparatus was developed by Martin Bellamy (1989) who carried out similar work using spherical test objects, and reference should be made to his dissertation for further apparatus details. The developments have been separated into three classes.

	Developed by:
i) Mechanization	
- Oscillatory tray, air support system and hydraulic drive.	Bellamy(1989)
- Position control system	Stevens (1989) / Bellamy(1989)
- Extension to position control system	Tucker(1991)
- Test cylinders and mounting arrangements	Tucker(1991)
ii) Instrumentation	
- Hydraulic drive monitoring and control	Bellamy(1989)
- Computer logging system and sine wave generator	Bellamy(1989)
- Multiple pressure transducers ,pressure signal control and multiple switching	Tucker(1991)

iii) Computer Software

- Data logging (force measurement,lift only) Bellamy(1989)
- Data logging (pressure measurement,lift only) Armitage(1989)
- Data logging (pressure measurement,lift and drag) Tucker(1991)
- Hydraulic drive monitoring Bellamy(1989) / Tucker(1991)

3.1 MAJOR MECHANICAL COMPONENTS

The rig included a flume which was filled with water until it reached the underside of a plywood tray. This tray was connected to a hydraulic piston which could oscillate back and forth in a sinusoidal fashion.

Suspended below this tray was a cylinder in which seven pressure transducers were mounted. As the fluid flowed around the cylinder, these pressure transducers would record the pressures acting on the cylinder at that stage of the cycle. These pressures, recorded over a number of oscillations or cycles, could then be integrated to provide the in-line and transverse forces acting on the cylinder. Figure 3.1 shows an overall view of the apparatus.

3.1.1 Wave flume and inverted tray

There are essentially two methods in which the flow conditions may be simulated, both of which have been used in previous research and provided comparable results.

The first method is to accelerate the chosen fluid past the test object, as occurs in the field. The second method was to have a stationary fluid and oscillate the test object. Both methods

simulate the hydrodynamic forces acting on the test object effectively. The second method is acceptable since the flow conditions past a body in an incompressible fluid of constant density are kinematically the same whether one oscillates the fluid or the test object.

Practically, to simulate fluid oscillating about a stationary object requires the construction of a U-tube. This would have provided physical construction difficulties with regard to available laboratory space and equipment. Furthermore, providing a means to vary the amplitude was considered to involve many difficulties and, because the water column would oscillate at it's own natural frequency, the range of testing would be limited.

It was therefore decided that it would be more feasible to oscillate the test object in stationary water. A 480mm deep by 600mm wide flume was filled with water and it was necessary now to oscillate the test object through this water. The problem of providing adequate sealing to protect the electrical measurement instrumentation and the associated drive systems was overcome by inverting a plywood tray and placing it in contact with the top surface of the water, with the test cylinder suspended below the tray. The edges of the tray were then mounted on to tracks to enable movement back and forth. The test cylinder could now be fixed beneath the tray and oscillated if the tray was oscillated. The tray was built 5m long to eliminate end effects.

In short, the situation as it occurs in the field has been inverted and the test object is oscillated through stationary water instead of the water oscillated past a stationary test

object. See figure 3.2.

3.1.2 Air bearing and support

To support the tray mentioned above, two 7.2m long aluminium channel sections were mounted to the top edges of the wave flume in an inverted position. Two sealed aluminium box section air chambers were then placed on top of these base tracks and rigidly supported apart from each other by eight aluminium box sections. The plywood surface representing the bed was reinforced by a series of compartments, which were then fastened to these air chambers. See figure 3.1.

To ensure directional stability when moving back and forth, an inverted aluminium angle section was mounted on top of one base track and an identical angle section mounted under the corresponding air chamber in a complimentary fashion.

Now the tray could slide over the base channels, but because the friction between the two aluminium surfaces would result in mechanical noise and vibrations that would disturb the signal from the pressure transducers, it was decided to implement an air bearing system to separate the two surfaces.

To lift the tray above the base channels, pressurized air was injected into the air chambers from two fan blowers. The air would then escape the air chamber via 600 holes on the underside of the air chamber. The diameter of these holes was chosen to be 3.5mm to maximize the lift force and they were equally spaced along the length of the air chamber to provide a uniform lift. See figure

3.3. The efficiency of this system was improved when a skirt of industrial felt, 3mm thick and 10mm wide was glued to the underside perimeter of the air chamber.

The air supply was provided by two Continental Fan Works Model 500/100/100 blowers, each driven by a Femco Model 1502316, 1.1 KW motor turning at 2780 r.p.m. They delivered approximately 250 l/s of air at a pressure of 3 kPa. The air flow from each blower was separated into two flexible air ducts, each 2m long and connected to the air chamber at it's quarter points. With this system, a 1mm gap between the two surfaces was formed. See figure 3.4.

Since aluminium is difficult to weld, an epoxy adhesive (Epidermix 350) was used to ensure that all bonds in the air chamber were air tight. This compound had a tensile strength of 8 MPa and a compressive bond strength of 55 MPa.

Apart from reducing the frictional vibrations between the two surfaces, this bearing method had the added advantage of isolating the tray from any mechanical noise that did not originate from the tray itself.

3.1.3 Hydraulic drive mechanism

The hydraulic drive mechanism had to meet the following requirements :

- An ability to drive an 82 kg tray in a sinusoidal fashion.
- Stroke to be variable up to a maximum of 2m with a repeatability of 1mm.

- Period to be variable up to 15s with a repeatability within two milliseconds.
- A natural frequency (vibration resonance) above 90 Hz.
- A maximum speed of 1 m/s.

Numerous methods and equipment to achieve the above requirements were investigated, and for both economic and suitability reasons, a Mannesmann-Rexroth servo valve system was adopted.

This was a hydraulic system, consisting of a hydraulic cylinder and a ram (to be connected to the tray). See figure 3.5. A servo valve, controlled by a variable analogue input, controlled the rate of fluid flow to the hydraulic cylinder.

The available laboratory hydraulic power was provided by a HYREC type A10VS2S power pack. Unfortunately, this power pack only has a hydraulic fluid flow rate of 35 l/min which allowed a maximum velocity of only 0.58 m/s. By incorporating a hydraulic accumulator, a maximum velocity of 0.71 m/s was attainable. This meant that the maximum stroke of 2 m could be completed in a minimum period of 8.8 s. See figure 3.6.

The term "servo" describes the function where a small input results in a large output. A nominal signal is supplied to the servo valve from the sine wave generator. The position of the "spool" in the servo valve is measured and then any difference between the measured signal and the nominal signal is corrected for.

The disadvantage of this system is that it is open loop, or there

is no compensation for any error that may occur in the hydraulic system beyond the servo valve. Because of the high repeatability required for this work, the system was incorporated in a closed loop circuit. This means that instead of measuring the value within the servo valve, the physical position of the ram was measured by a position transducer attached to the end of the ram. This signal would be continuously compared with the nominal signal, and compensation would be applied for any difference. This comparison was achieved by the proportional module of a P.I.D circuit.

Due to the high sensitivity of the servo valve, it was necessary to install a high pressure filter with a 5 micron rating to prevent the ingress of dirt particles into the servo valve. Also, because the servo valve could only operate at pressures above 40 MPa, a pressure switch was installed to ensure that this pressure was always available. This activated a bypass valve if the pressure dropped below 40 MPa.

3.1.4 Test cylinders

A 455mm × 455mm portion of the plywood tray was removed and replaced with a perspex surface. This perspex tray could then be removed to attach or adjust the test object. See figure 3.7.

Two pipe diameters, 120mm and 90mm were investigated, both of which were PVC cylinders with a wall thickness of approximately 3mm. They were sealed at both ends by solid PVC plugs, one of which was glued and the other left unglued for accessibility purposes. The total length of the cylinder, including plugs was

420mm.

Two aluminium support arms were bolted to the centre of these plugs. These support arms fitted through two slots in the perspex inspection hatch and were bolted to supports mounted on the hatch. By moving these arms up or down, the required "gap" could be obtained. The magnitude of this gap was measured by feeding a Vernier caliper through two holes in the hatch directly above the centre line of the cylinder.

Seven holes, 4mm in diameter were drilled radially at 30° intervals over a range of 180°. The cylinder was mounted in such a way that an imaginary line between the 0° and 180° holes would be perpendicular to the plane of the bed. It was not necessary to measure the pressure distribution around the full 360° of the cylinder because the pressure acting on a tapping in one half cycle is identical to the pressure, acting at the same orientation on the opposite semi circle, in the next half cycle. Intervals of 30° were chosen because this allows the best measurement of both lift and drag forces. It should be noted that when measuring both lift and drag force, it is most desirable to have pressure tappings in line and transverse to the direction of flow. (i.e. 0° 90°and 180°) Armitage (1989) recommends that tappings be located at 30° intervals, yet any fraction of 30° would be acceptable, provided tappings are located at 0°, 90° and 180°.

The pressure transducers were mounted to a fixture that could be removed from the test cylinder. This fixture comprised a series of PVC discs that were tapered in such a way that when the pressure transducers were fixed to them, their pressure ports would lie in

the 30° interval orientations. There were two support discs on either side of the tapered discs to provide stability and prevent vibration at velocity reversal. O-rings around these support discs ensured that the fixture had a snug fit when inside the test cylinder. See figure 3.8.

3.2 CONTROL INSTRUMENTATION (See figure 3.9 and 3.9a)

3.2.1 Pressure transducers

The pressure transducers used were Sensym model SCX01DNC. These sensors are fully calibrated for offset and span and will provide a stable output over a 0° C to 70° C temperature range.

The devices feature an integrated circuit sensor element and laser trimmed thick film ceramic all housed in a compact nylon case. This package provides excellent corrosion resistance and provides isolation from external stresses.

This sensor is available for differential or gauge applications, however for this work, only the gauge mode was used. This meant that port A was left open to the atmosphere and the fluid pressure was applied to port B. See figure 3.10. With this arrangement, all pressures are measured relative to atmospheric pressure. For differential applications, a reference pressure is applied to port A and this pressure is then kept constant. The pressure applied to port B is then considered to be the change in pressure relative to the applied reference pressure. Differential mode was not chosen because it would be difficult to ensure that a constant pressure was maintained on the A ports.

The sensor is intended for use with non-corrosive and non-ionic fluids and because water does not exhibit these properties, a few drops of Dow Corning 200 water clear silicon fluid were used as a buffer between the pressure sensing chip and the water in the flume.

Since these devices have a very low noise output and a 100 micro second response time, they were considered an excellent choice for this work. The performance characteristics for these pressure transducers are given in Appendix A.

3.2.2 Strain gauge amplifiers

Since the output from the strain gauge bridge of a pressure transducer was in the order of micro volts, it was necessary to amplify this signal to a range of 0-10V, suitable for the A/D converter. This was done by incorporating a small op-amp circuit which amplified the signal to this range. The zero offset and degree of amplification (gain), could be adjusted by variable resistors.

Because both positive and negative pressures would be encountered, the offset (static head signal) was set to give an output in the middle of the range ie. ± 5 V. Since the offset for each tapping orientation would differ due to different static heads, it was necessary to have a strain gauge amplifier for each pressure transducer.

In actual fact, the A/D converter was able to record the signal in millivolts from the pressure transducers. This, however, would

mean that the signal to noise ratio could have been small enough to seriously effect the results. By incorporating the strain gauge amplifiers as close to the source as possible, this signal to noise ratio is increased substantially.

The circuit diagram for the strain gauge amplifiers is given in figure 3.11. By shorting connections J2 and J5 and opening the connections J1,J3,J4,J6 and J7, the upper and lower limits of the voltage output were 10V and ±0V respectively.

3.2.3 Low pass filter

A Krohn-Hite filter model 3340 was used to reduce electrical noise from the signal produced by the pressure transducers. This filter had digitally tuned cut off frequencies over the range 0.001 Hz to 99 Hz and can function in either high or low pass mode. It was used in MFLP (maximum flat low pass) mode giving 7th order Butterworth low pass filtering. The device was set to reduce electrical noise above 5 Hz.

3.2.4 Sine wave generator (Servo control)

The sine wave generator, developed by Bellamy(1989), fulfilled three objectives:

1. To provide an electrical sine wave with a variable amplitude between +10V and -10V. The frequency of the sine wave was to be variable between 0.05 Hz and 1 Hz. This electrical signal provided the input signal to the servo amplifier (P.I.D) and subsequently to the servo valve. This input signal therefore

controlled the velocity of the cylinder.

2. To create a high frequency pulse train that was variable between 50 and 400 pulses/cycle. 200 pulses/cycle were used in this work. These 5V pulses triggered the recording mechanism of the A/D converter, so that whenever the pulse went high, the A/D converter would record the signal from the pressure transducer in use at that particular time. These 200 pulses are generated in sequence with the sine wave signal as shown in figure 3.12.

3. To produce a low frequency pulse signal of one pulse/cycle. This 5V pulse was used to :

   a. Measure the period of the sine wave. The computer could record the period of time between each pulse and hence provide the period of one cycle.

   b. Initiate the sampling procedure. This was necessary to ensure that the sampling started at the same phase position for each test.

The low frequency pulse is shown in relation to the sine wave in figure 3.13.

3.2.5 Inverter

An inverter was connected to the lead carrying the 200 samples/cycle. This inverter ensured that the pulse signal was in a range of 0-5V. It also grounded the +5V charge on the input

connection of the A/D converter. This meant that the signal would be zero unless the sine wave generator pulsed high to +5V.

3.2.6 P.I.D Controller (Servo amplifier)

The P.I.D would take the actual position of the ram and compare it to the required position as specified by the sine wave generator. If the two signals differed, the P.I.D would automatically implement a change in the servo valve until the two signal were identical.

The input analogue signal was received by the P.I.D. in the form of a sine wave from the sine wave generator and the feedback signal was, theoretically, exactly the same sine wave received from the position transducer.

P.I.D (proportional, integral, differential) describes the manner in which the P.I.D responds to the difference in signals. For this work, the proportional mode was used. This meant that the input voltage and the feedback voltage are proportional to each other. Also, if there was a difference in input and feedback signals, there would be a proportional adjustment to the servo valve.

Both of these signals were connected to the isolated earth module of the P.I.D, with a negative input signal and a positive feedback signal.

3.2.7 Position transducers

Two position transducers using exactly the same principal of

operation were incorporated into the system. One was used to provide the feedback signal to the P.I.D controller as discussed above, and the other was used purely to measure the amplitude of oscillation. Theoretically, only one position transducer was necessary to perform both duties but it was found that electrical noise from the amplitude measurement line could cause slight variations in the signal for the P.I.D circuit, which affected the motion of the tray. For this reason it was decided to isolate the P.I.D circuit entirely and develop a separate position transducer system purely for amplitude measurement. Bellamy(1989) appeared also to have encountered this problem since he used two isolated position transducers as well.

Both of these position transducers consisted of a multi-turn potentiometer (10 turns) connected to a rotating drum. Tensioned lengths of wire were fastened to the end of the ram and then looped around these drums. Therefore, when the ram moved, it would cause the drums to rotate and this would yield an electrical signal from the potentiometers, ranging from -10V to +10V from the P.I.D feedback potentiometer and ranging from 0V to 6V for the amplitude measurement potentiometer. See figure 3.14.

3.2.8 Analogue to digital converter (A/D)

The A/D converter used was a Microlink interface manufactured by Biodata Ltd., Manchester, England.

The A/D converter was used to convert an input signal of electrical volts to digital numbers. These numbers could be calibrated and then used in the computer program. The A/D

converter can only read voltages in the range of 0V to 10.25V which subsequently results in a digital output range of 0 - 4095 arbitrary units.

Three modules were used in this work. One was used to trigger the sampling sequence when the low frequency pulse went high. The second module was used to record the signal supplied by the position transducer and hence provide the amplitude of oscillation. The third module recorded the signal from that particular pressure transducer that was being monitored.

The high frequency pulse train was connected to the high speed clock (HSC) module which was set to the externally clocked mode. This triggered the pressure measurement module to record the pressure transducer signal whenever the pulse went high.

All seven pressure transducers supplied a voltage signal simultaneously and since the A/D converter could only record one signal at a time, it was necessary to record them individually. The RR8 module of the A/D converter was therefore used to switch the signals. It consisted of seven switches, one for each pressure transducer circuit. These switches were always in the opened position and the switch would only be closed when a certain pressure transducer signal was to be recorded. Once 10 cycles for a particular pressure transducer had elapsed, the RR8 module would automatically open that particular transducer's switch and simultaneously close the next pressure transducer's switch.

3.2.9 Power supplies

A Farnell power supply which had two variable modules, 4-6V and 8-16V, was used as a power source to various items of equipment. The lower range module was used at 6.0VDC for the amplitude measurement position transducer and the upper range module was used at 15.0VAC for the sine wave generator and the feedback position transducer.

A separate power supply model SOLV15 was used to supply the pressure transducers and strain gauge amplifiers. It was preferable to isolate the supplies for the following reasons :

a) The pressure transducers and strain gauge amplifiers required 15VDC which was not available from the Farnell without hampering the sine wave generator requirements.

b) A stable supply, free of fluctuations and drift was required by the pressure transducers since their output voltages were ratiometric to the supply voltage.

3.2.10 Safety limit switches

The working pressure of the ram was 10 MPa. This represents a maximum ram force of approximately 12 KN. It was therefore necessary to have safety switches at either end of the ram's stroke so that, if for any reason the ram was out of control, these switches would be activated and they would immediately halt the motion by cutting off the hydraulic fluid supply.

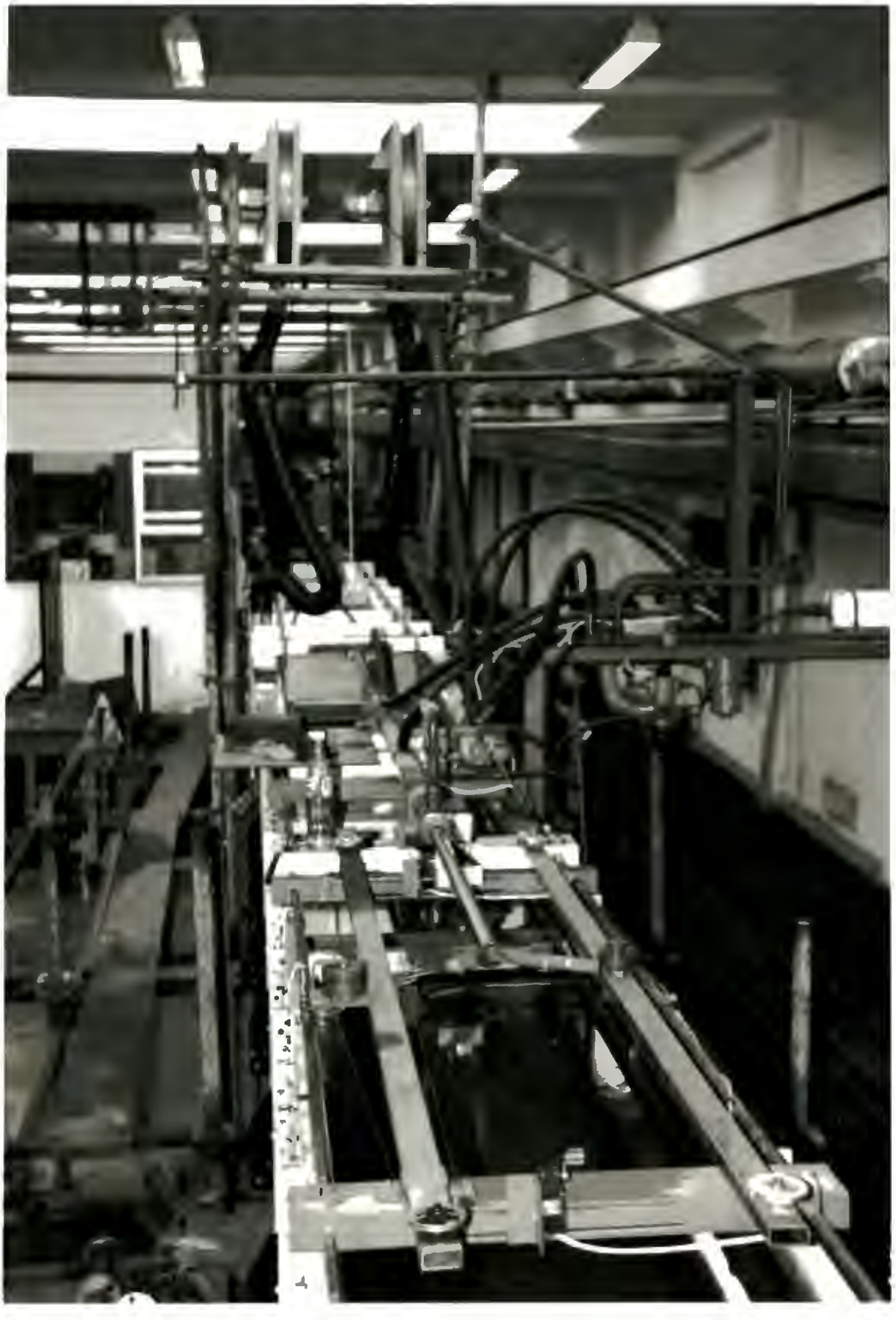

Figure 3.1 : Overall view of the test apparatus

Figure 3.2 : Side view of the apparatus showing the test cylinder suspended below the plywood tray

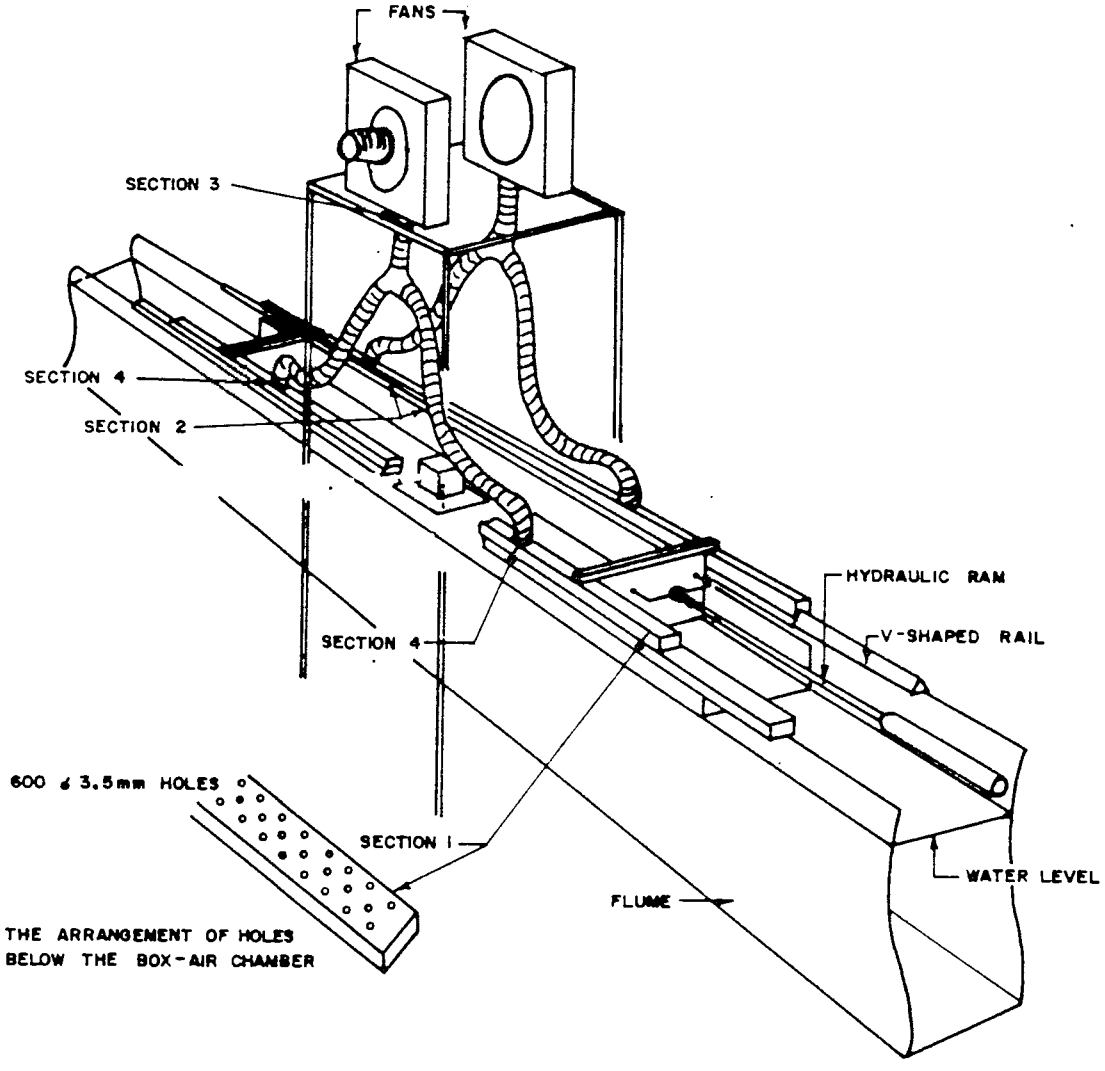

AREAS OF PRESSURE LOSS

SECTION 1 - 600 HOLES

SECTION 2 - AIR DUCTING

SECTION 3 - BLOWER OUTLETS

SECTION 4 - INLET TO AIR CHAMBER

Figure 3.3 : Simplified view of the apparatus showing the air bearing and blowers (Bellamy 1989)

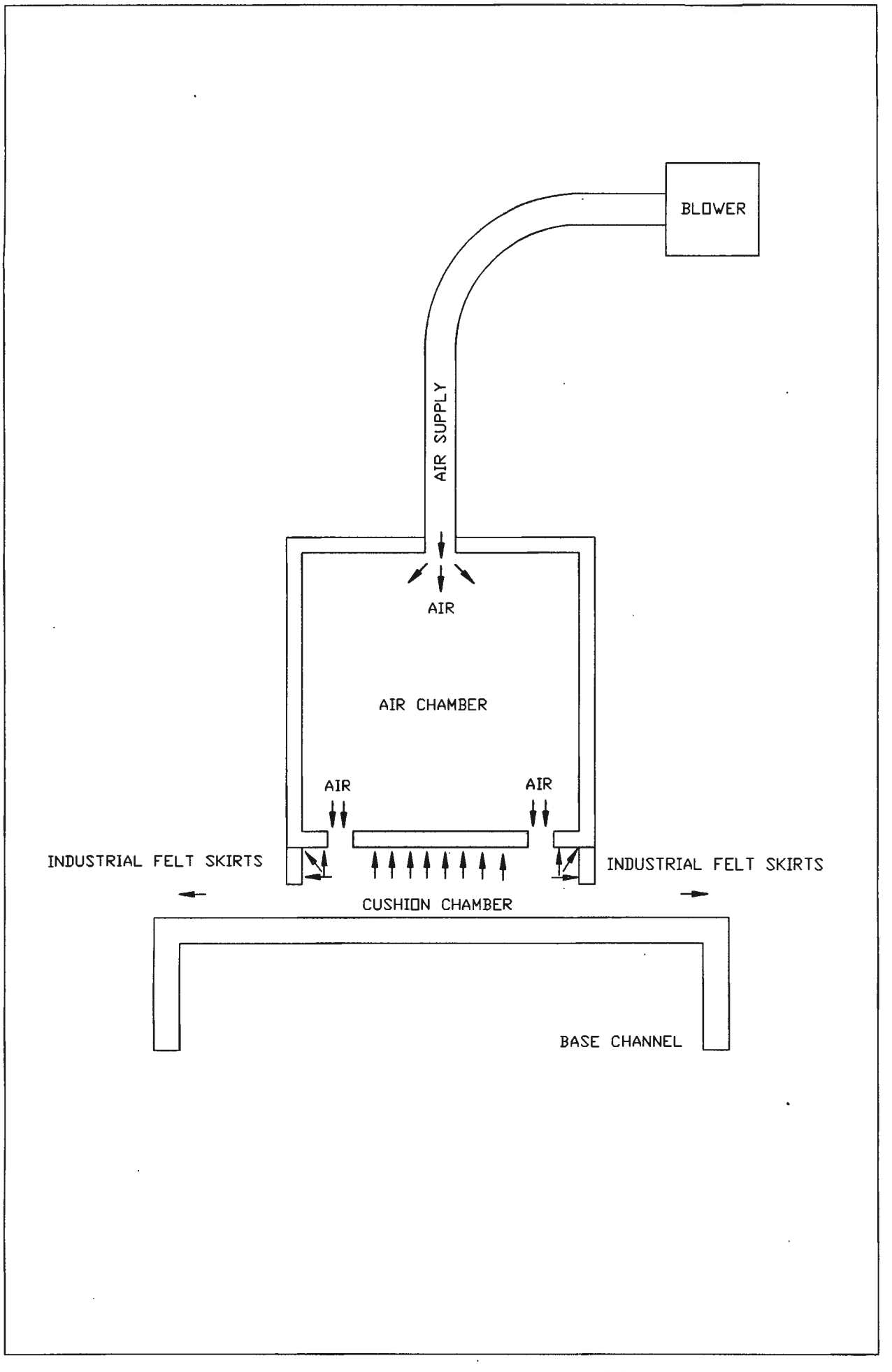

Figure 3.4 : Cross section of air bearing using hovercraft principle (Bellamy 1989)

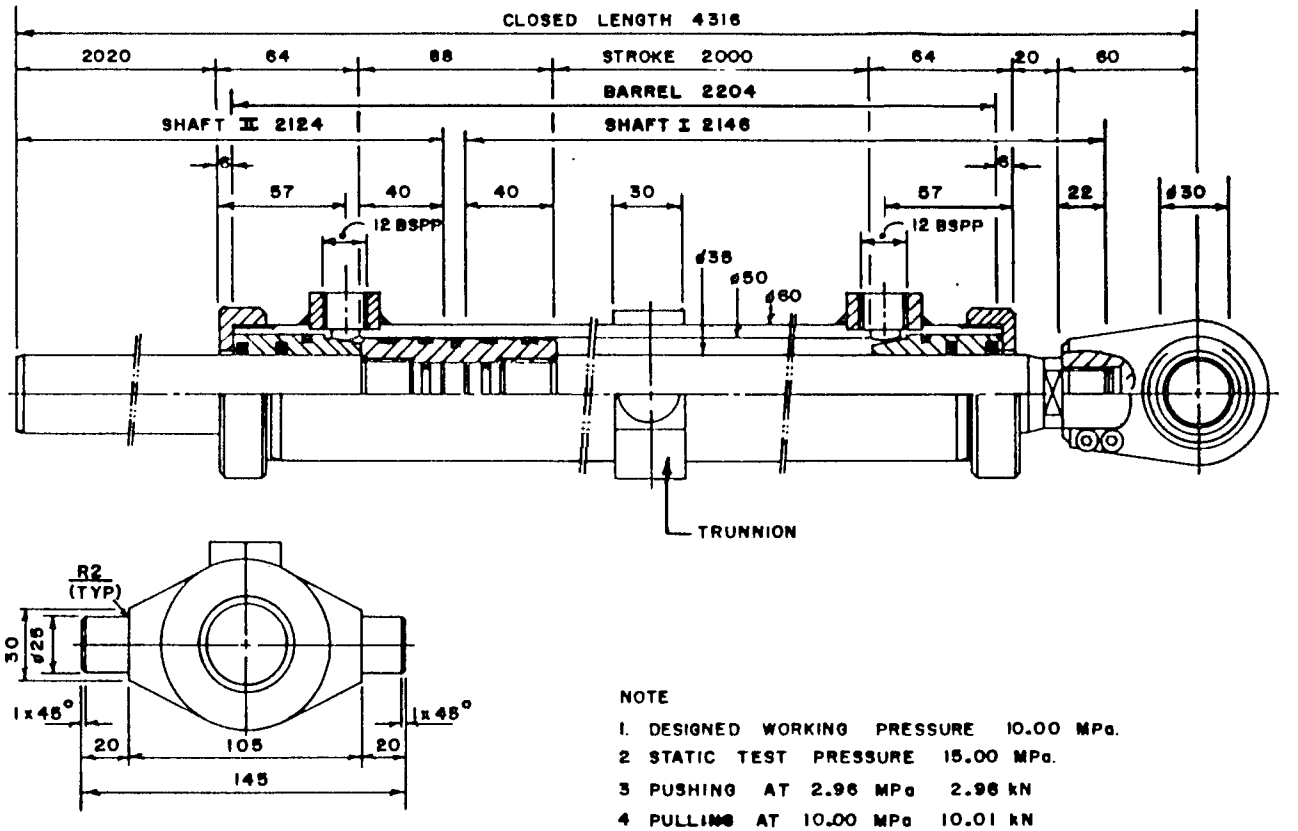

Figure 3.5 : Hydraulic cylinder with maximum stroke of 2m (Bellamy 1989 - designed by Hytec(Ltd.))

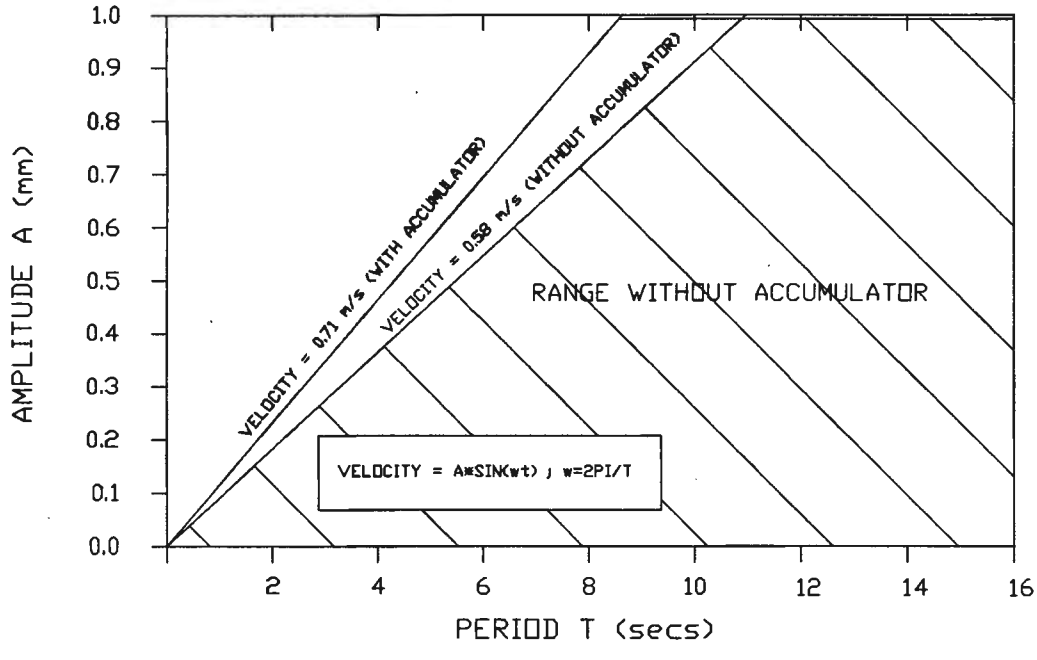

Figure 3.6 : Range of the period and amplitude with and without the hydraulic accumulator (Bellamy 1989)

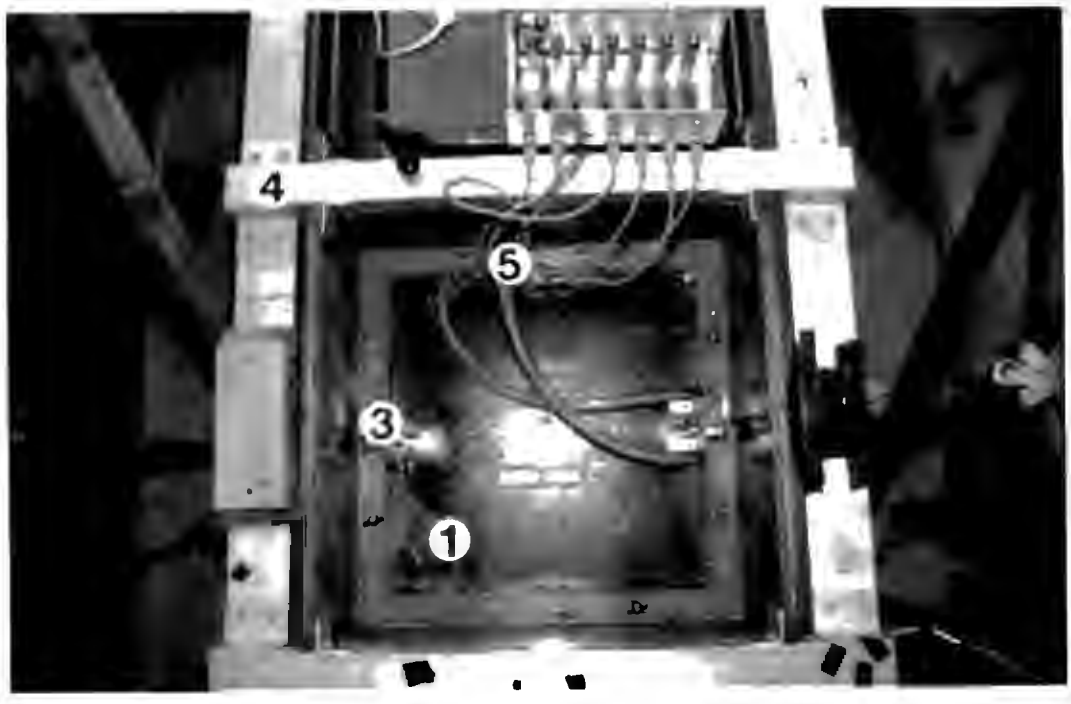

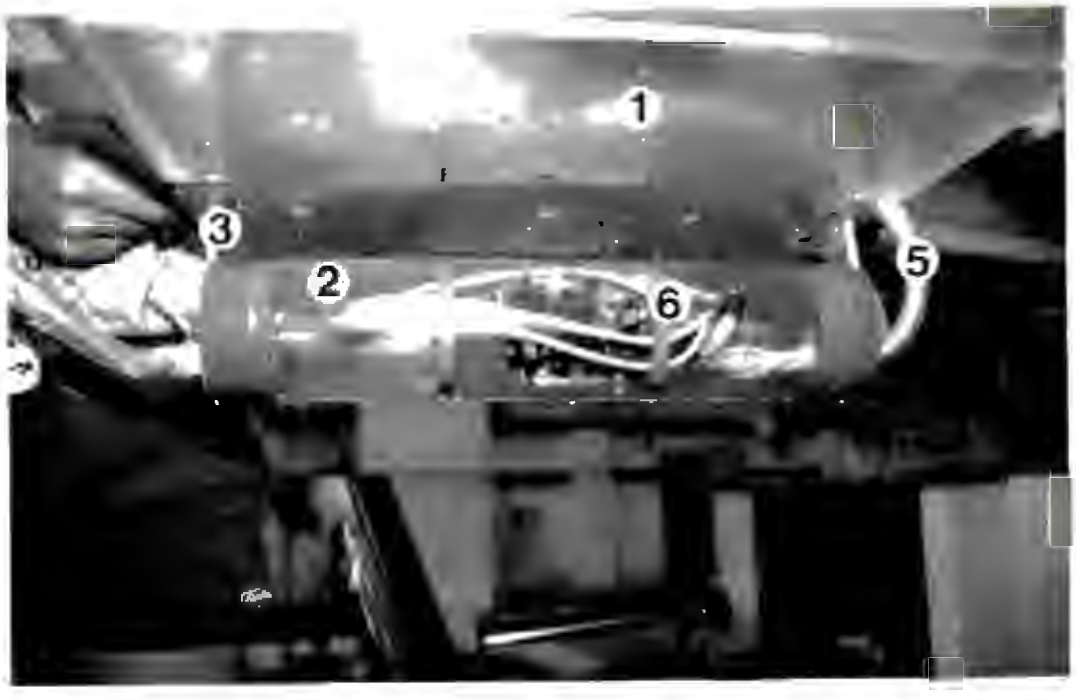

1. Test tray
2. Test cylinder
3. Cylinder mounting arm
4. Oscillatory tray
5. Pressure signal leads
6. Pressure transducers and mounting inside test cylinder

Figure 3.7 : Plan view of the perspex tray in the flume with the test cylinder attached and front view of the tray and test cylinder

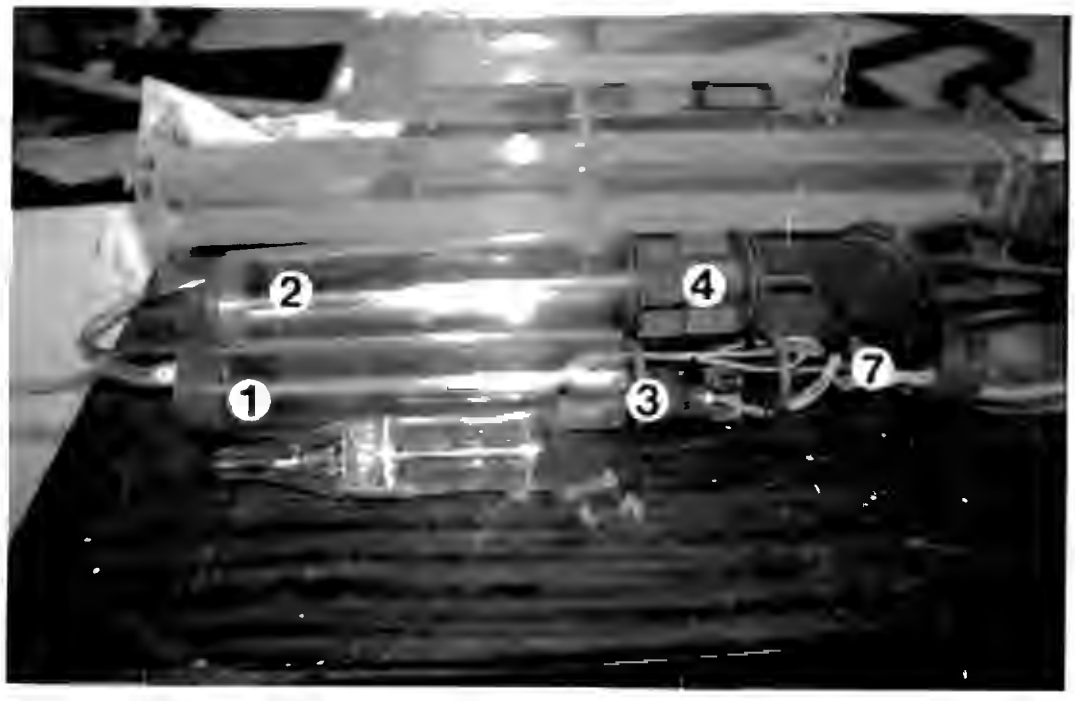

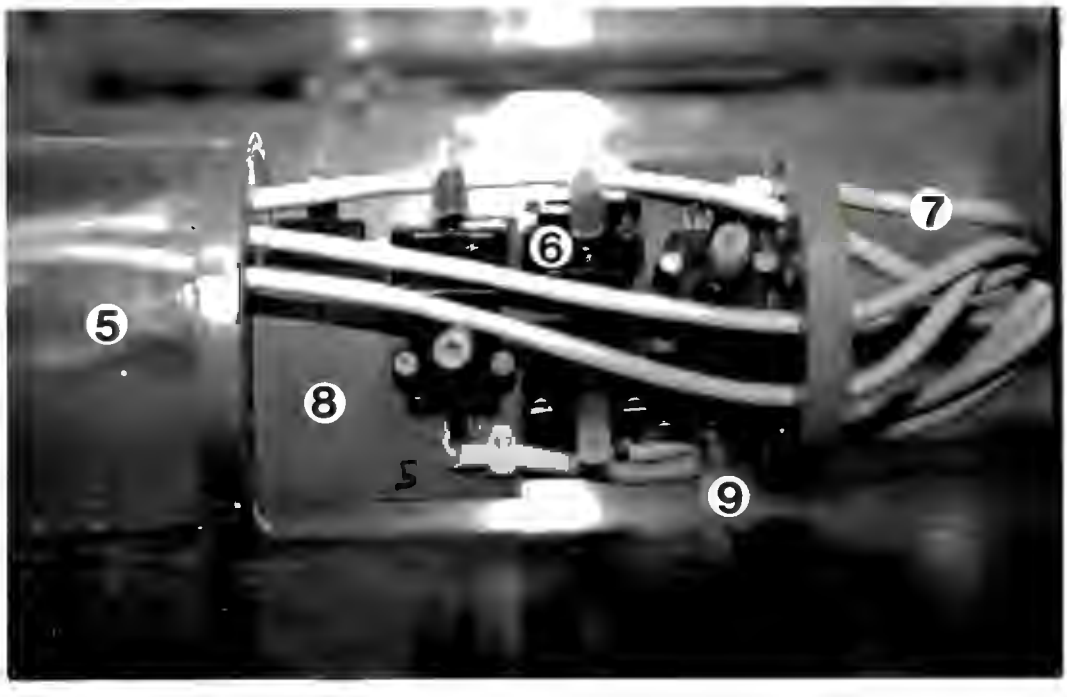

1. 90mm diameter test cylinder
2. 120mm diameter test cylinder
3. 90mm diameter transducer mounting
4. 120mm diameter transducer mounting
5. Test cylinder
6. Pressure transducer
7. Pressure signal lead
8. Pressure transducer mounting
9. Surgical tubing connector

Figure 3.8 : Pressure transducer mountings for both test cylinders and a close up view of the transducers on the 90mm cylinder mounting

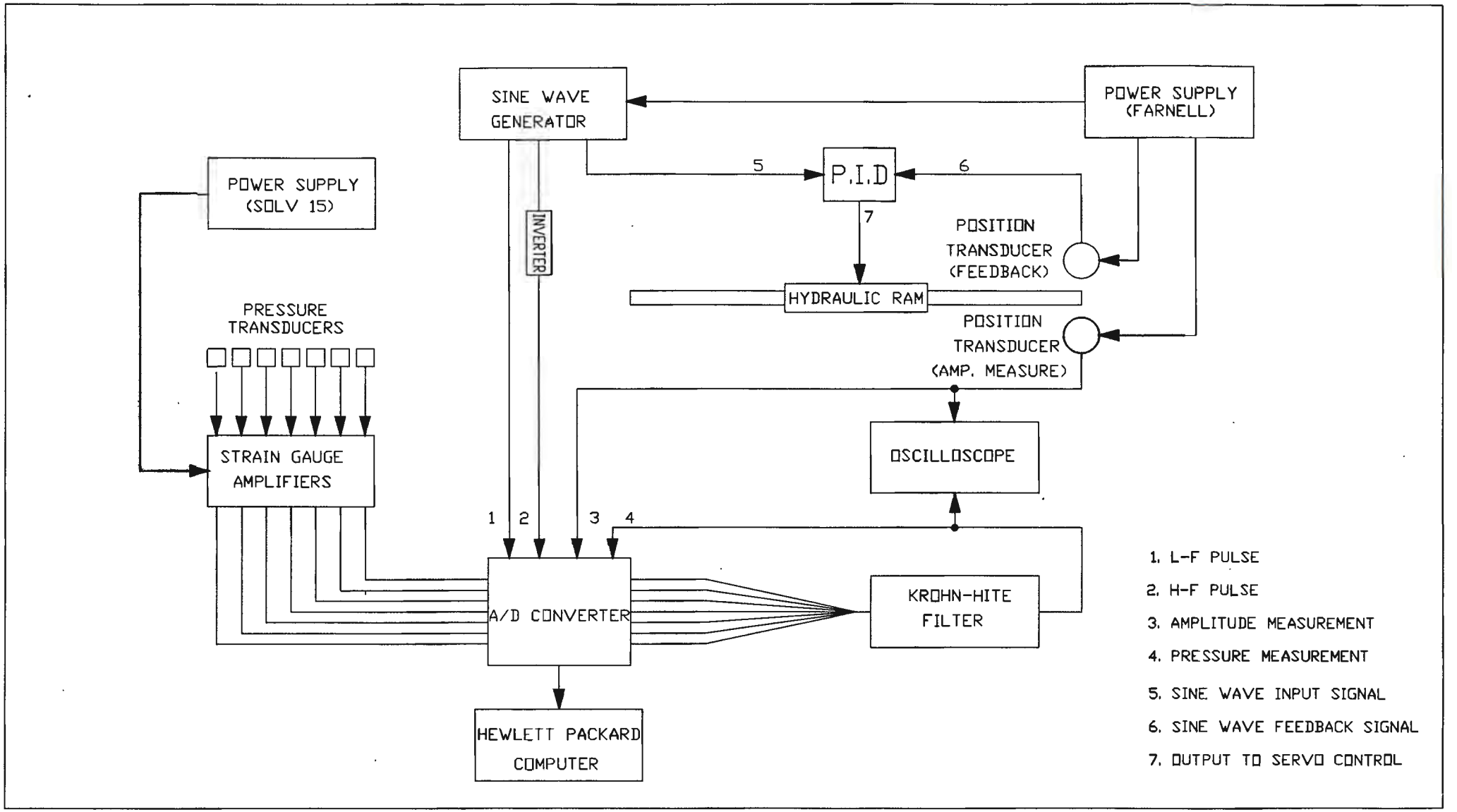

Figure 3.9 : Schematic layout of the instrumentation

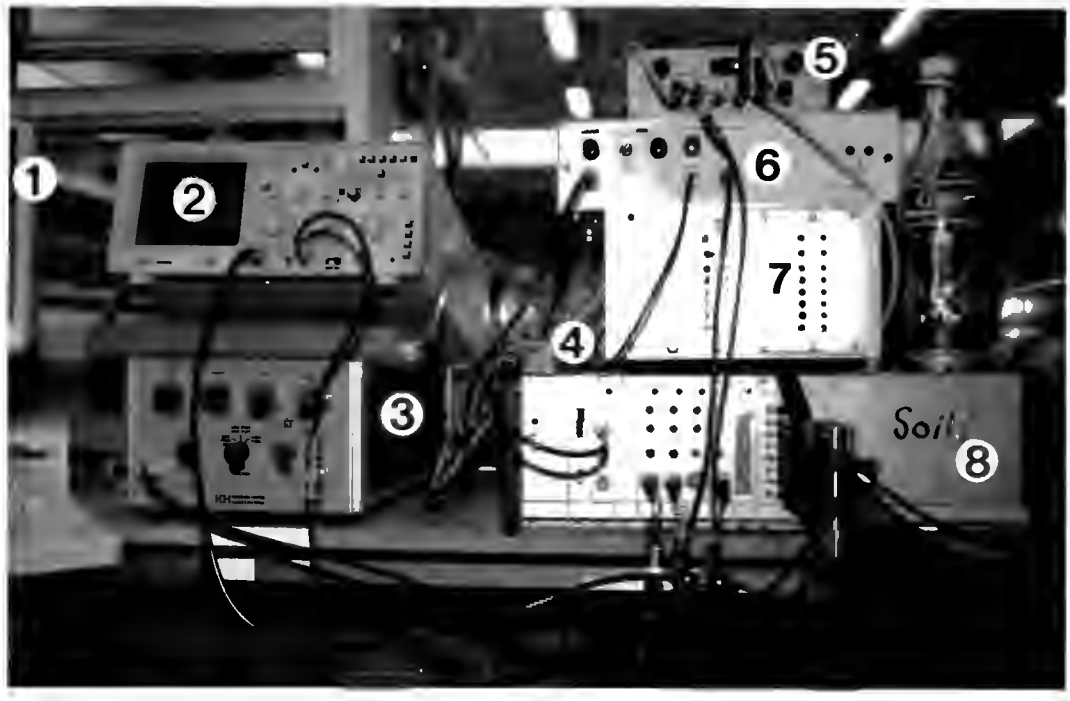

1. HP Computer
2. Oscilloscope
3. Krohn - Hite filter
4. Inverter
5. Power Supply
6. Sine Wave Generator
7. P.I.D.
8. A/D Converter
9. Strain Gauge Amplifiers

Figure 3.9a : Control instrumentation and the strain gauge amplifier box

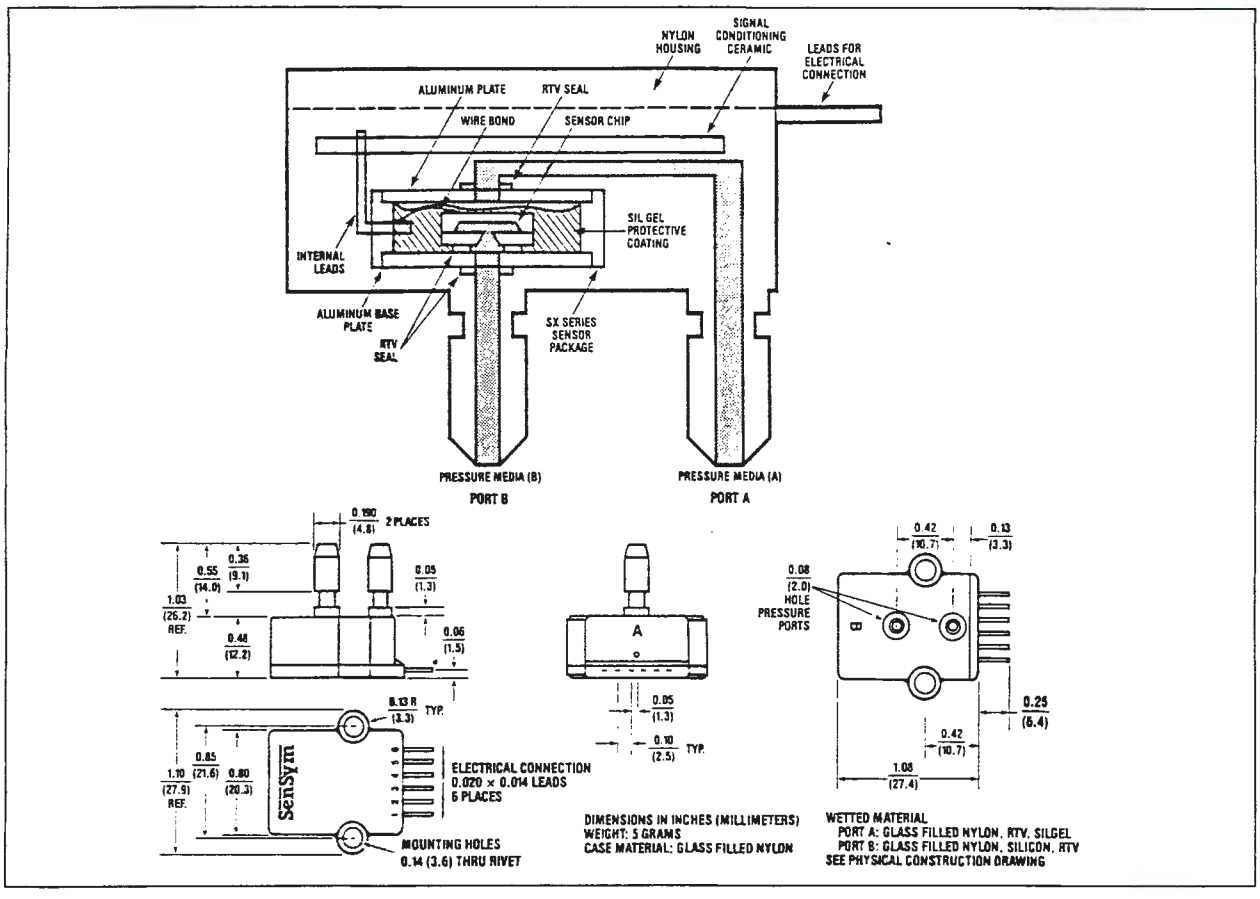

Figure 3.10 : Physical construction and dimensions of a pressure transducer (From Sensym catalague)

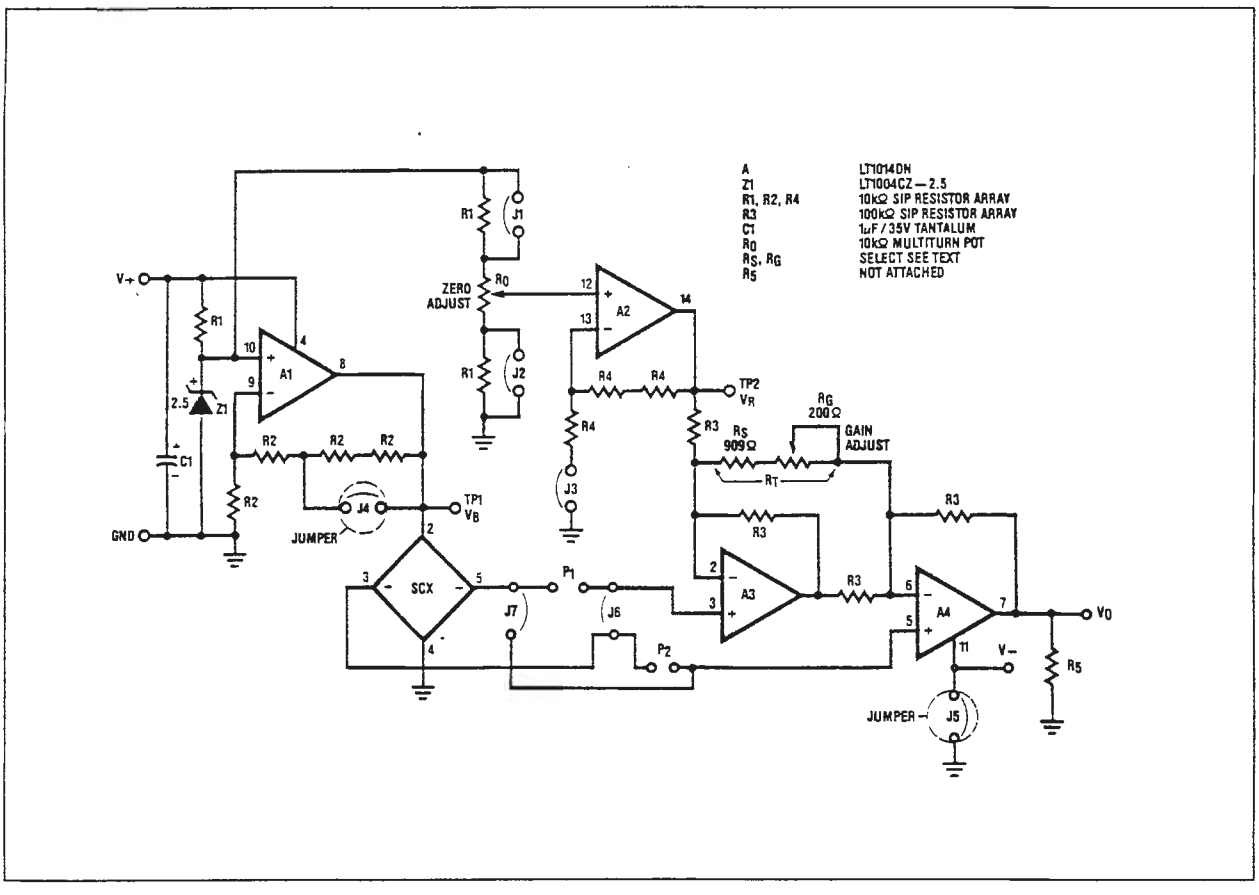

Figure 3.11 : Strain gauge amplifier circuit diagram (From Sensym catalogue)

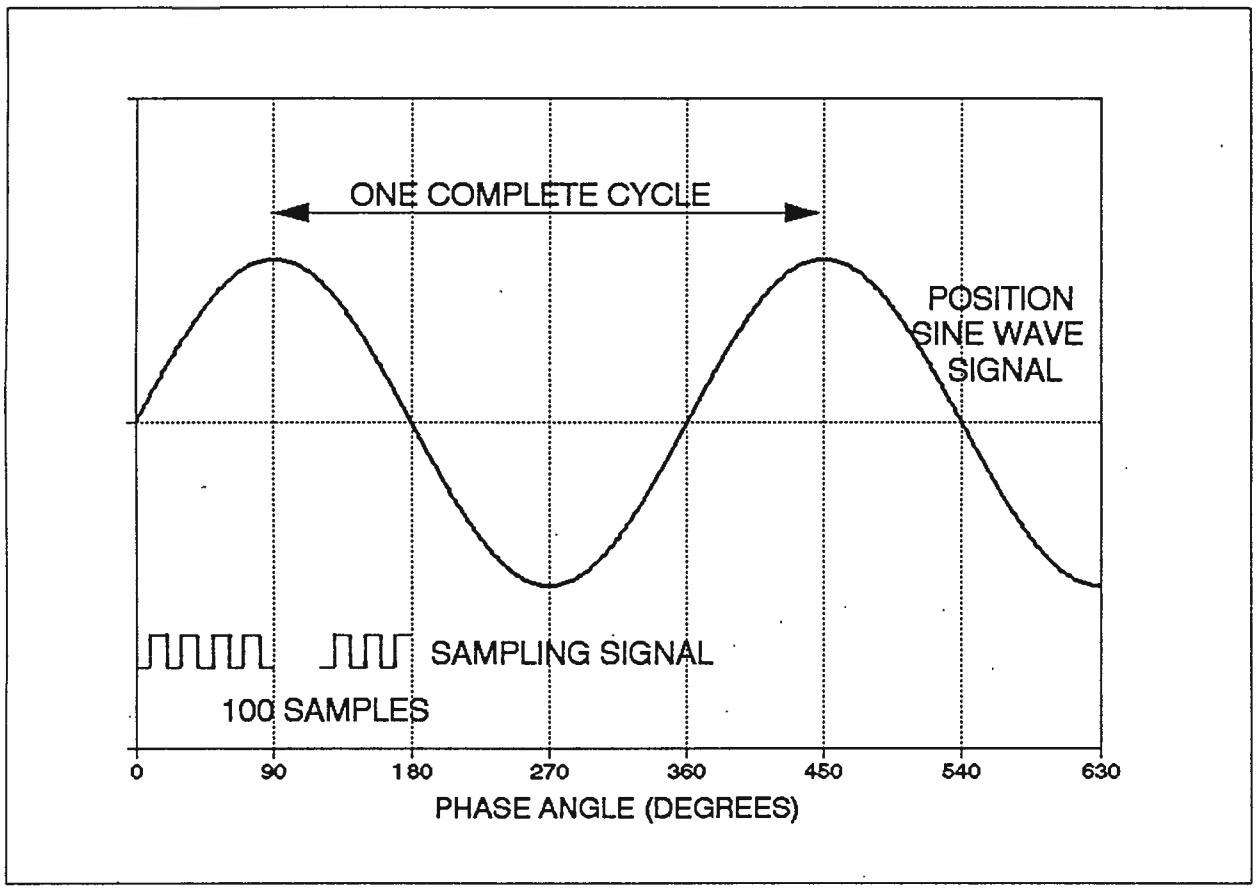

Figure 3.12 : High frequency pulse (sampling pulse) shown as a function of period (From Bellamy 1989)

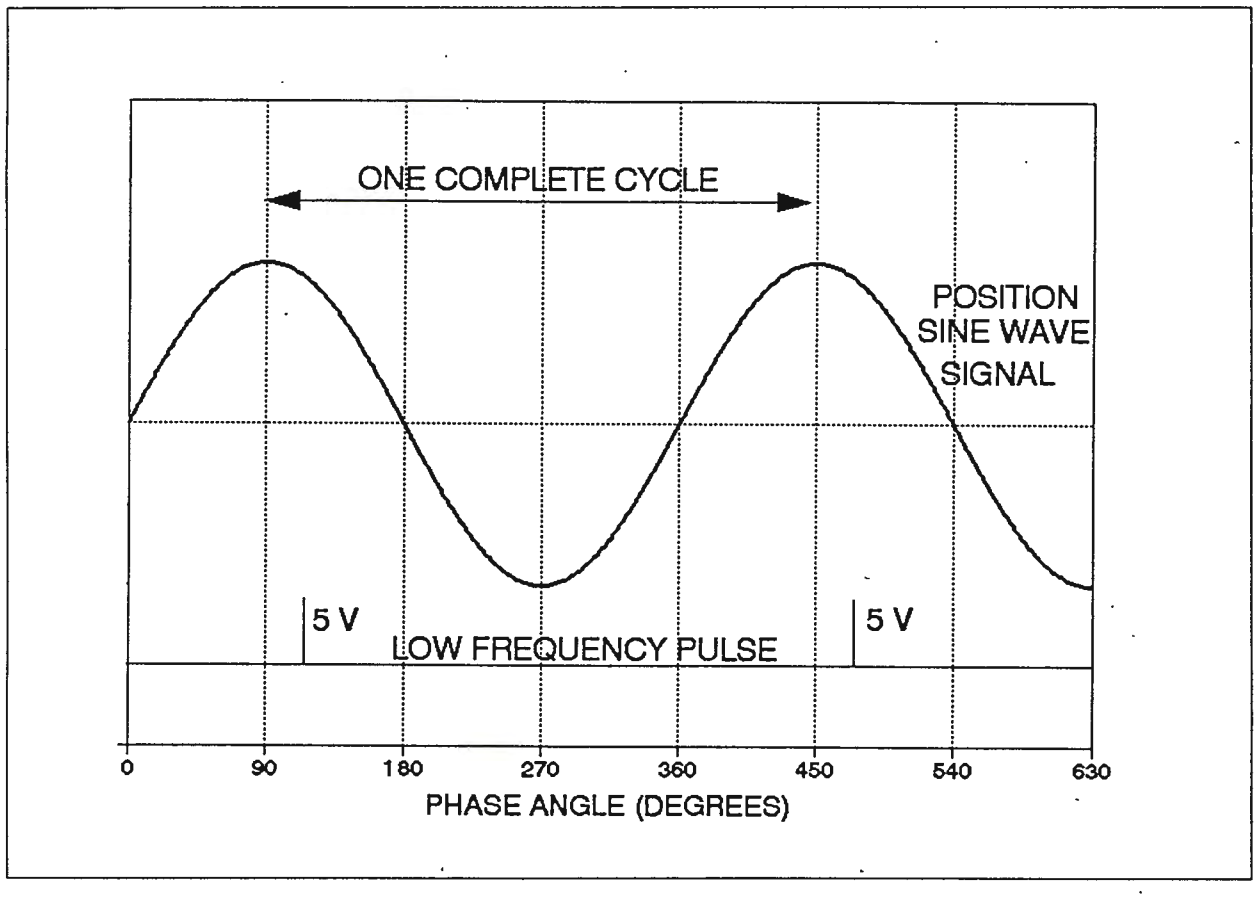

Figure 3.13 : Low frequency pulse always occurs at the same phase in a cycle (From Bellamy 1989)

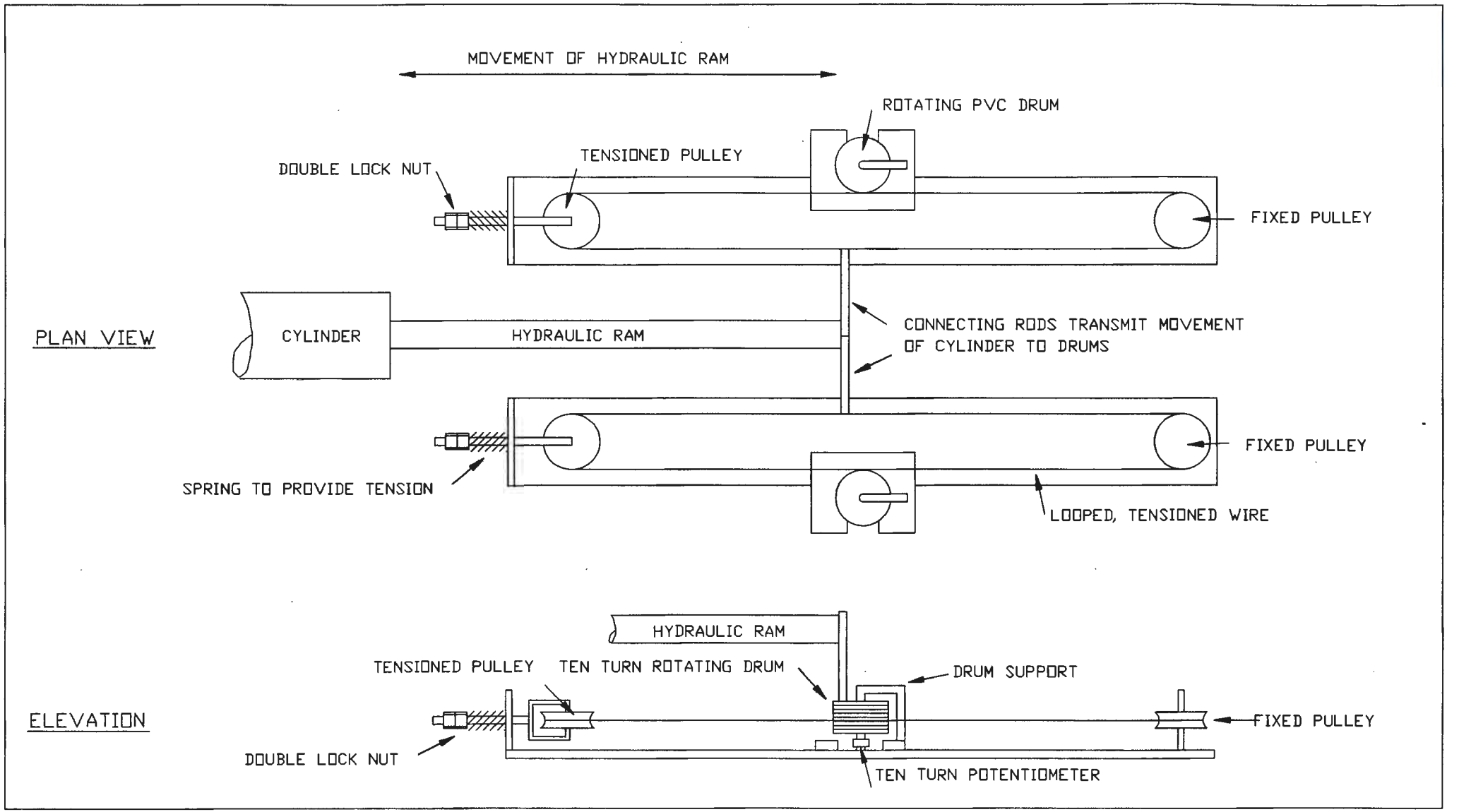

Figure 3.14 : Position transducers for closed loop system

4. EXPERIMENTAL PROCEDURE

4.1 INITIAL PREPARATION

4.1.1 Calibration of the amplitude measurement

A 6VDC power supply was connected to the position transducer discussed in 3.2.7. The signal that the potentiometer supplied was connected to a module of the A/D converter, and the gain of this module was set such that at maximum amplitude, (±850mm and ±6V) it would record 4095 units. The offset was adjusted to make the module record ± 2000 when the tray was stationary. (zero amplitude and 3V signal)

Therefore, as the tray moved back and forth, the position transducer would yield an electrical signal oscillating about 3V and not exceeding the limits of 0V and 6V. The arbitrary figures from the A/D converter corresponding to these limits were 0-4095.

Because these arbitrary units are meaningless without a conversion factor, the tray was set in motion and the actual amplitude of oscillation was measured with a tape measure. This procedure was repeated for a host of different amplitudes which finally allowed a least squares regression analysis to yield a straight line through all the measured points with A/D units on one axis and amplitude in mm on the other. See figure 4.1

The slope of this line was used as a calibration factor to convert A/D units into mm which could then be instantaneously displayed on the computer screen while the tray was in motion.

4.1.2 Phase lag measurement

It was required that the pressure sampling began at a phase angle of zero degrees and since the low frequency pulse initiated the sampling process, this was not the case because the low frequency pulse occurred out of phase. Therefore it was necessary to measure the phase angle at which the low frequency pulse did occur and then compensate for the difference between this phase and zero. See figure 4.2. Since the phase lag was dependant on the frequency of the sine wave, phase lags had to be measured for each period of oscillation at which testing was performed.

To do this, The A/D converter first recorded the amplitude signal when the tray was in the zero amplitude position. (± 2000) The tray could then be set in motion and the A/D converter would wait until a low frequency pulse occurred. As soon as it pulsed, the A/D converter would switch to the amplitude measurement module and record this signal until the tray reached zero amplitude. A counter installed in the program would count how many samples (200 samples/cycle) had been recorded in this period, and this number of samples was converted and adjusted to yield the phase lag in degrees.

The results of this method were confirmed by connecting the low frequency pulse signal and the amplitude signal to the oscilloscope. Here one could visually see where the pulses went high in relation to the sine wave. The phase lag could be obtained by 'freezing' the screen and measuring the phase lag using the graded units on the screen.

4.1.3 Adjusting the range of the pressure transducers

By supplying 15VDC to the strain gauge amplifiers, an output range of 0-10V could be generated by the pressure transducers.

The maximum static head on a transducer was to be 240mm (diameter=120mm ; G/d=1 ; transducer furthest from bed) and allowing for dynamic pressure, the gain on the A/D converter was set such that the transducers would yield a signal of 10V at a pressure equivalent to ±300mm of water. This was done while the gains on the strain gauge amplifiers were set to maximum amplification, ensuring that the full A/D range(0-4095) would be read over the 0-300mm range. With the offsets of each transducer set to a minimum on the strain gauge amplifiers, the offset on the A/D converter was set to ±1800. The offset for each transducer was then adjusted to 2000 on the strain gauge amplifiers.

The offset and gain on the A/D module would now remain unchanged as would the gains on the strain gauge amplifiers. Only the offsets on the strain gauge amplifiers would be varied to accommodate the different pressure ranges associated with each gap.

4.2 PREPARATION FOR DATA LOGGING

4.2.1 Setting the voltage offset of the pressure transducers

At each gap ratio, a certain static head would act on each transducer when the test cylinder was placed in the flume.

These heads could be calculated and applied to the

pressure transducers using the U-tube manometer. The offset on the respective strain gauge amplifiers could then be set such that the pressure transducers yielded ±2000 A/D units at these static heads. This value was termed the "offset" for a particular transducer.

Once the test cylinder was placed in the flume, the offsets could be further corrected if necessary. The magnitude of the offset was not critical because it is cancelled in the data manipulation procedure.

4.2.2 Calibration of the pressure transducers

Due to the high sensitivity of the pressure transducers, accurate equipment was needed to calibrate them. Initially an inclined U-tube manometer at a slope of 1:10 was used but due to the friction between the column of water and the tube walls at this slope, the menisci fluctuated substantially.

It was then decided to use the U-tube manometer in the vertical plane. See figure 4.3. This limited the range of pressures available since now 1mm=10Pa whereas in the inclined case, 1mm=1Pa. However the range proved to be within the required limits and extremely high repeatability was achieved.

Firstly, the pressure transducers, strain gauge amplifiers and power supply were all brought into the office in order to be within reach of the U-tube manometer. The transducer mounting was then supported in such a way that the transducers lay in the same orientation as they would in the flume. With the offsets and gains

preset, each transducer would be calibrated individually.

The ports of a transducer would be left to atmosphere and the A/D converter would record the reading. Then the maximum positive pressure would be applied by the U-tube manometer to the pressure port (the reference port is still left open to atmosphere) and the reading taken. The pressure in the limb of the U-tube manometer would then be reduced and again applied to the pressure port. This procedure would be repeated ±6 times for each pressure transducer.

A least squares regression analysis was then performed on these readings. The slope of the curve was taken as the calibration factor, and the Y-intercept was of little consequence since it cancelled in the data manipulation process. However, it did act as a check to ensure that :

a) There was no open circuit in the line.
b) The transducer was in the correct range.

This procedure was performed for each pressure transducer and the calibration factors of each were found to be within 5% of each other. The transducers were calibrated before each set of tests at a certain gap ratio and the results of the calibrations were found to be repeatable to within 1%.

4.2.3 Preparation of the test cylinder

Once the calibration had been completed, the test cylinder had to be prepared for data logging.

Firstly, the pressure transducer mounting was inserted in such a way that the pressure ports were aligned directly behind the holes in the wall of the cylinder. Short lengths of surgical latex tubing were inserted through these holes and over the pressure ports. The silicon oil, discussed in 3.2.1 was then inserted into these lengths of tubing using a syringe.

PVC cylinders are drawn in such a way that they are not 100% cylindrical and therefore, despite the O-ring on the end plug, water still managed to seep into the cylinder. To prevent this, a Dow Corning vacuum grease was smeared over the shoulder of the end plug and this proved successful in keeping the inside of the test cylinder dry.

During the construction of the test cylinder, a marker was accurately scribed onto one of the supporting arms and the corresponding end plug to indicate the test cylinder orientation that exactly matched the required transducer orientations. Whenever a test was to be run, the cylinder would be rotated until these markers matched.

The required gap distance was obtained by setting a Vernier caliper to this distance and feeding it through holes that were drilled through the perspex tray directly above the cylinder. The cylinder was then brought up to meet the Vernier caliper and then locked in this position. This method provided an accuracy of 0.05mm.

The perspex tray and test cylinder could now be lowered into the inspection hatch and bolted down firmly. The air vent, which

supplied atmospheric pressure to the reference ports while the test cylinder was submerged, and transducer leads were fed through slots in the perspex tray and plugged with pres-stik to prevent air entrainment.

The next step was to turn on the air supply for the air bearing and the power to the hydraulic pump for the servo valve and hydraulic cylinder. At this stage the rig was ready for testing to begin.

4.3 DATA LOGGING PROCEDURE

4.3.1 Setting the period of oscillation

The period of oscillation was set by adjusting the frequency of the sine wave signal from the sine wave generator. The computer would then measure the difference in time between low frequency pulses. This had to be done before each range of tests at a certain period.

4.3.2 Entering the test parameters

Before a test could be run, the operator would have to enter certain variables into the computer. They include date, number of cycles per run, number of samples per cycle, test cylinder diameter, gap distance, water temperature, phase lag, period and amplitude.

4.3.3 Measuring the pressure transducers' offsets

Before a series of tests, the computer would measure the offset of each transducer. This means that just prior to testing, with the water absolutely stationary, the static heads on the transducers would be measured and recorded for the data manipulation process.

During a data logging run, the A/D converter will record instantaneous readings from the transducers and after the run, the offsets were subtracted from these readings to yield only the instantaneous dynamic pressures. See Appendix B.

Typically, the offsets were measured before each series of tests at a certain period, i.e. every eight tests.

4.3.4 Setting the amplitude of oscillation

The amplitude of oscillation could be set by adjusting the amplitude of the sine wave signal from the sine wave generator. The required amplitude could be obtained by adjusting the sine wave signal, noting the actual response of the tray from the position transducer and making the necessary compensation until the amplitude was correct.

4.3.5 Recording of data

Now that all the test constraints had been set, the data logging could be initiated from the keyboard. The sampling would begin immediately after a low frequency pulse occurred and 200 samples/cycle would be recorded over 10 cycles for each pressure

transducer.

The A/D converter would switch the signals of the pressure transducers using the RR8 module discussed in 3.2.8. Once all seven pressure transducers had been recorded, the program would convert the raw data into in-line and transverse force coefficients. Once the conversion was complete, the data was stored to disc and the parameters of the next test could now be entered and testing initiated.

4.3.6 Data manipulation

At the end of one run, a total of 14000 samples have been recorded. (7 transducers × 10 cycles × 200 samples/cycle) The program takes the average of the 10 cycles for each transducer's readings and then it makes an adjustment for the phase lag. It then takes these samples and converts each of them with the corresponding calibration factor and offset into pressure units of pascals. At this stage there are 1400 samples.

These pressures are then converted into in-line and transverse forces and an integration of all seven transducer readings at a particular phase is performed. The end result was 200 samples each for in-line and transverse force coefficients which were then stored to disc along with the test parameters. See Appendix E.

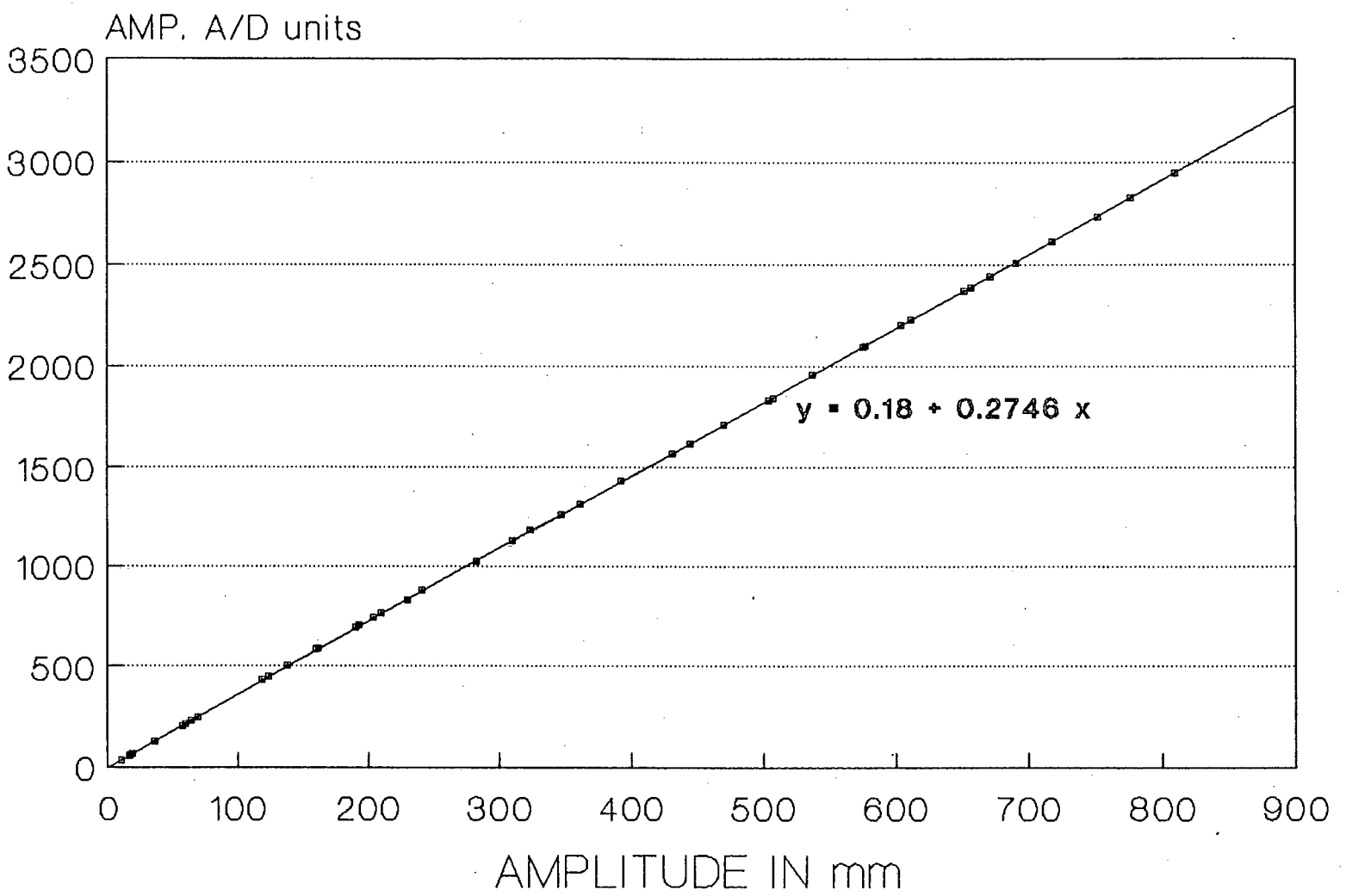

Figure 4.1 : Calibration curve for the amplitude measurement

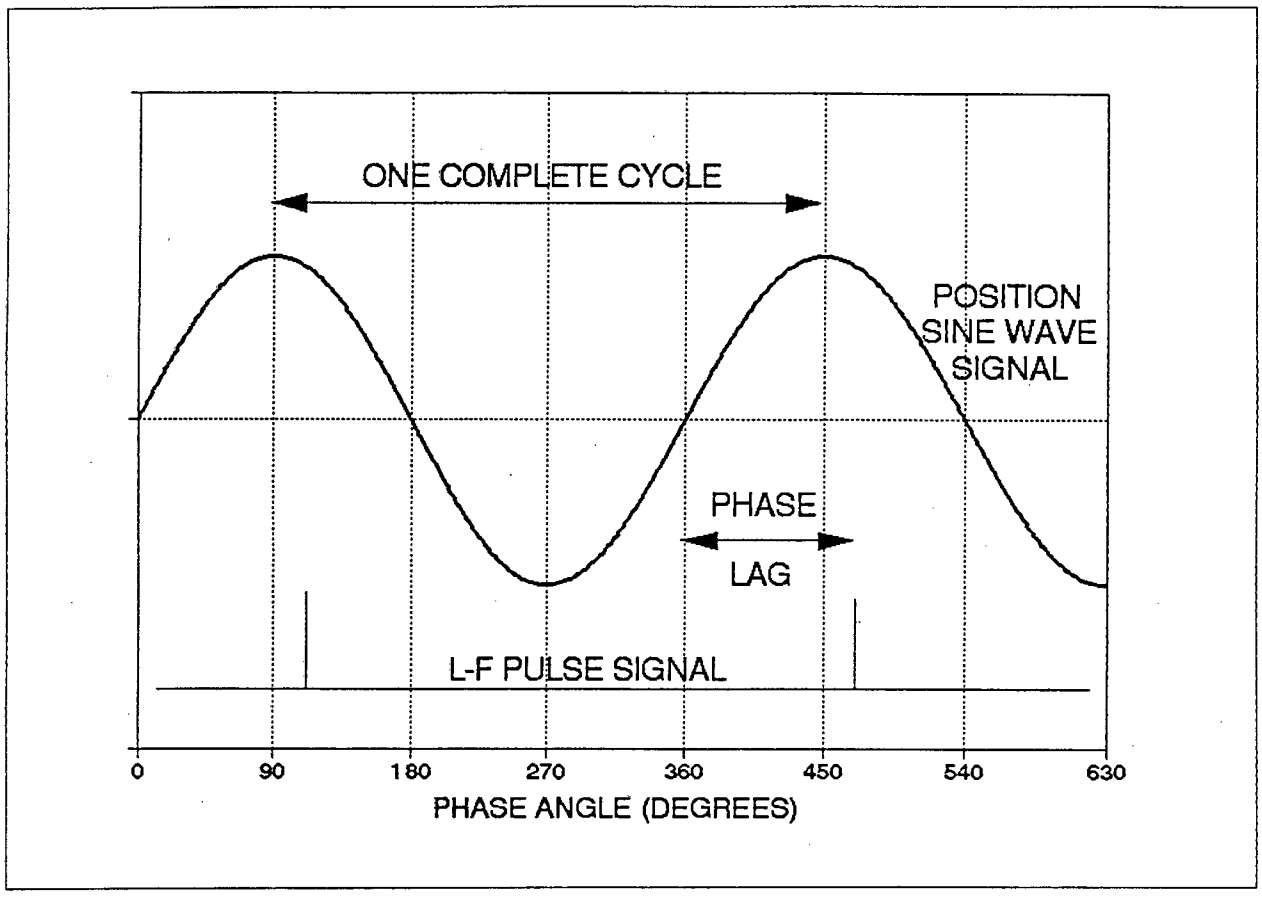

Figure 4.2 : Phase lag between low frequency pulse and sine wave signal

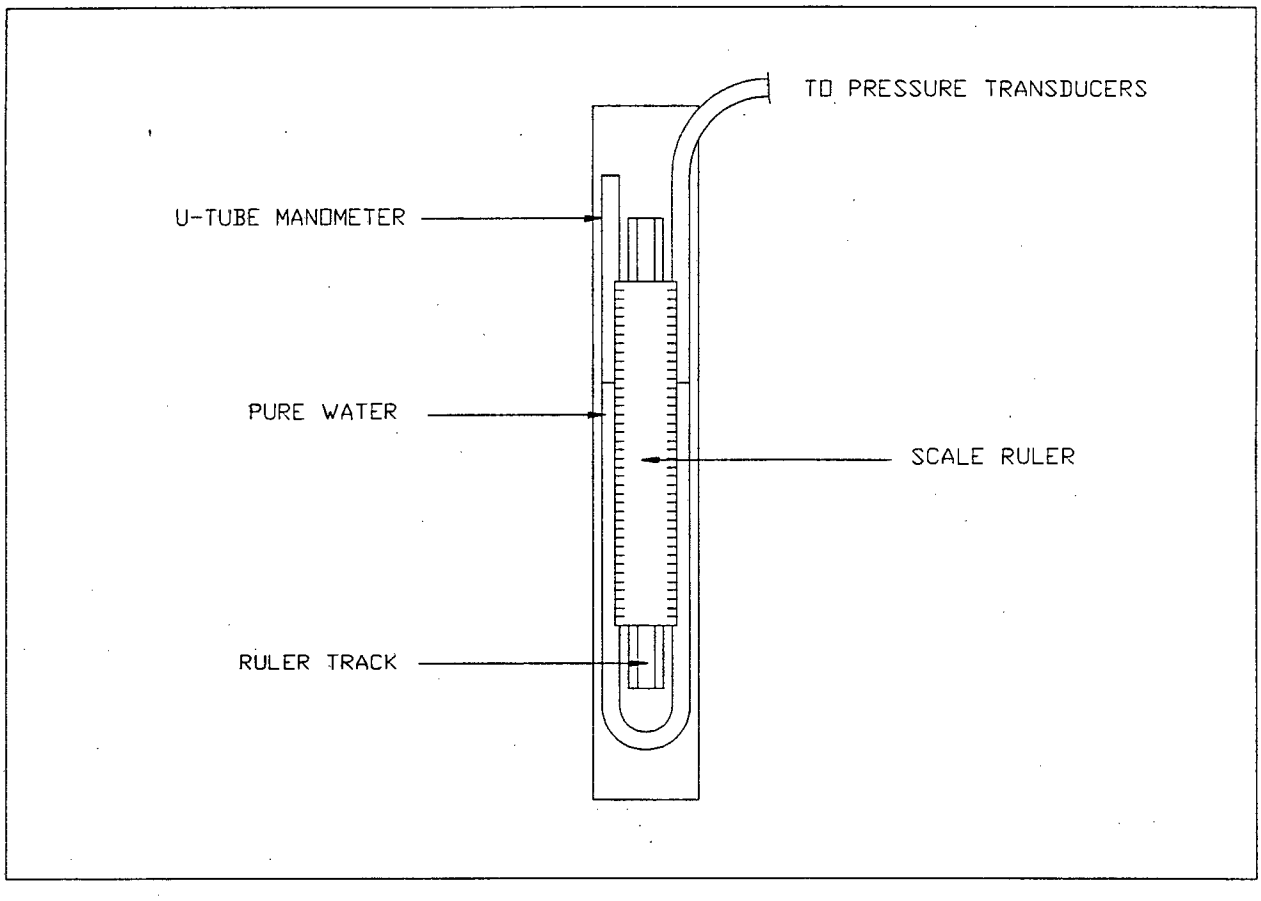

Figure 4.3 : U-tube manometer used to calibrate the pressure transducers

5. LIMITATIONS AND ERRORS

The results of this work were affected by errors due to both random effects and systematic effects.

5.1 RANDOM ERRORS

These errors were related to mechanical and electrical noise and instrument precision. In most cases it was impossible to compensate them. They include the following:

5.1.1 Environmental conditions

The density of water, ρ was assumed to be 1000 kg/m^3 although this value does vary slightly with temperature.

Massey (1979) proposed that the kinematic viscosity is a function of the water temperature, and is given by:

$$\nu = \log^{-1} \left(19.182 - 7.776 \times \log(273 + T) \right) \quad (mm^2/s)$$

Where T is the temperature in degrees Celsius. The specific weight of water was taken to be 9.81 kN/m^3.

5.1.2 Calibration of pressure transducers

A possible source of error in the signal from the pressure transducers was voltage supply drift since the signal is ratiometric to the supply voltage. This was prevented by :

a) Providing a power supply to be used only by the pressure transducers and strain gauge amplifiers.

b) Op-amps in the strain gauge amplifiers that provide a regulated voltage to the pressure transducers. In this manner the circuit becomes independent of supply variations, power supply noise and ripple.

The pressure transducers were calibrated at regular intervals to avoid any possible variations similar to those described above. For each calibration, ±6 pressure measurements were taken for each pressure transducer using the U-tube manometer. The results of these calibrations were repeatable to within 1%.

5.1.3 Gap distance

Using a Vernier caliper to measure the gap distance meant that a resolution of 0.05 mm was possible. For the most critical case (d = 90 mm), this amounts to a maximum possible error of 0.055%.

5.1.4 Amplitude and period

The amplitude measurement system had the advantage that it measured the actual response of the tray itself in comparison to a system where the expected movement of the tray is measured. (e.g. measuring the amplitude of the input sine wave) The measurement of the amplitude of oscillation was accurate to within 1mm. For the most critical case this amounts to an error of 6%, but for the majority of the amplitudes at which testing took place, the error was less than 0.2%.

By measuring the period of oscillation with the oscilloscope and the low frequency pulse, the period measurement was found to be accurate to within 0.01 s. Although this is a high resolution, it is expected to be higher since human error would play a large role when milliseconds are being measured.

5.1.5 Effects of waves on measured pressure

When one considers a wave of 1mm height travelling down the flume, this results in a pressure of 10 Pa, which is of the order of magnitude of the pressures to be measured. Therefore any disturbance of this sort would upset the results.

However, because the plywood bed is 580mm wide and the flume is 600mm wide, there is a gap of only 10 mm on either side where ripples may travel up and down the flume. Directly underneath the plywood tray however, no wave motion is allowed to exist. The pressure distribution below the water surface due to these ripples is not thought to affect the measured pressures since the pressure tappings are distributed well within the middle third of the flume.

5.1.6 Repeatability of test results

When one considers all the possible sources of error, the repeatability of the test results is found to be extremely high.

Some tests have been run more than once. They were performed under exactly the same conditions only the following tests were run at later dates which means that in the interim, these conditions had

been varied. This therefore provides a check on the accuracy of gap measurement, amplitude measurement, period measurement, test cylinder orientation and calibration factor collectively.

The results of these tests have been plotted using the same axes. Figure 5.1 shows repeat tests at the three primary variables, namely gap ratio, amplitude and period.

Furthermore, a single test was performed under exactly the same conditions using 20,15 and 10 cycles per run. The data storage facility of the computer would not allow more than 20 cycles to be tested since the maximum number of real numbers that can be stored is 30000. It will be seen from figure 5.2 that there is little difference in the force versus phase plots when the number of cycles per run is varied. This indicates that the results of one cycle are of such a high repeatability that the average of only 10 cycles is sufficient.

5.2 SYSTEMATIC ERRORS

These are errors that occur repeatedly and therefore adjustments could be made. They include the following :

5.2.1 Pressure tapping orientation

Because the holes for the pressure tappings were drilled in the workshop, the control of the accuracy may be assumed to be high. However, if the test cylinder itself was rotated out of line, all the pressure tappings would be out of orientation by the same angle. The markers used to align the test cylinder are described

in 4.2.3. This method is expected to give errors no larger than 1° or 0.3%.

5.2.2 Phase lag measurement

The phase lag between the start of the sampling process and the 0° phase of the sine wave was corrected as described in chapter 4.1.2. After numerous measurements this method was calculated to be accurate to within 0.4%.

Further, the Krohn-Hite low pass filter, which was set at 5 Hz resulted in a maximum phase shift of 5° for small periods which meant a maximum error of 1.4%. For the majority of tests, the phase shift was less than 1° (0.3% error), because the amplitudes were higher. Figure 5.3 shows plots of lift versus phase for identical tests at four different periods, one with phase lag compensation and the other without.

5.2.3 Side wall effects

Milliner (1978) concluded from tests with an oscillating cylinder and a pair of false vertical walls that test piece area to wave flume area ratios larger than 20% were necessary to substantially affect measurements. Blockage is said to occur when the effects of the side walls begin to affect the results.

According to this information, the largest possible test cylinder diameter that could be used with the available apparatus was 130mm.

5.2.4 Asymmetry of pressure tappings

By measuring the forces in each half-cycle separately it was found that it was quite acceptable to assume that forces acting on the cylinder in one half cycle were the same as those acting in the other half cycle.

5.2.5 Pressure distribution

It has been assumed, for programming simplicity, that the pressure measured by a pressure transducer at a certain orientation is constant over the circumference of the cylinder up to 15° on either side of that orientation. See figure 5.5.

This was thought to be a reasonably poor estimation of the pressure distribution around the circumference of the cylinder. However, two tests were performed using thirteen pressure transducer orientations. This was done by testing conventionally and then rotating the test cylinder through 15% and measuring the pressures at these orientations. Effectively there are thirteen tapping orientations at 7.5° intervals.

It was found that both methods yielded almost identical force versus phase plots as shown in figure 5.4. It is expected that this high accuracy is obtained due to the fact that the results obtained for the 7 tapping test were used along with the further 6 series of results for the 13 tapping tests. This meant that seven tapping orientations were sufficient to measure the pressure distribution around the cylinder.

5.2.6 Test cylinder diameter

Merely to confirm existing non-dimensional theory, tests using the 90mm and 120mm diameter test cylinders were performed under certain conditions that yielded identical non-dimensional parameters such as Re, KC, βd and G/d. The results of these tests are plotted on the same axes in figure 5.6 which shows that the comparison is rather good. The comparison appears to improve with decreasing βd and increasing Re and KC.

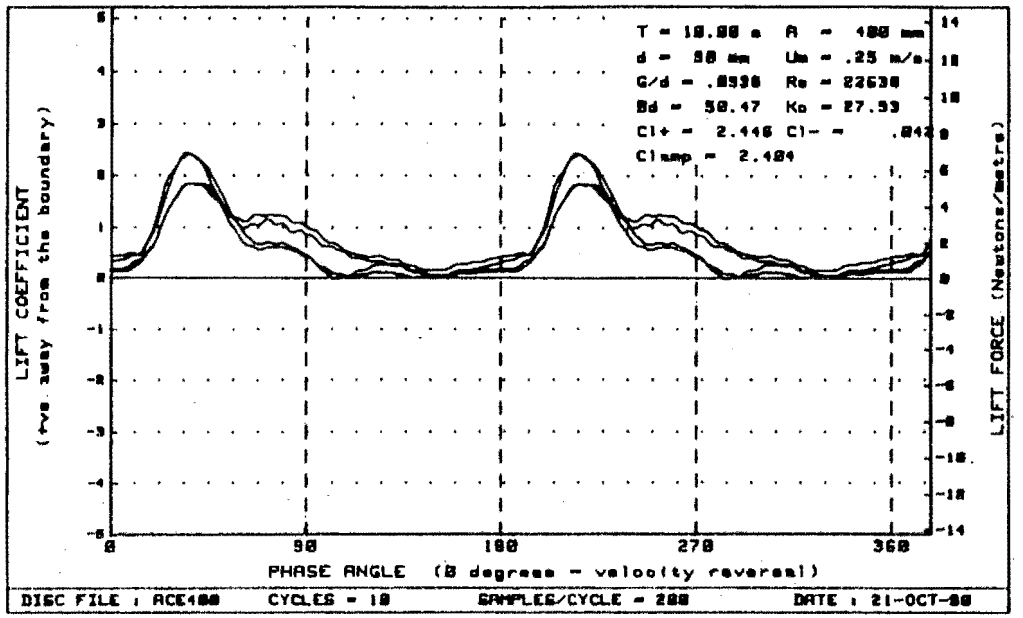

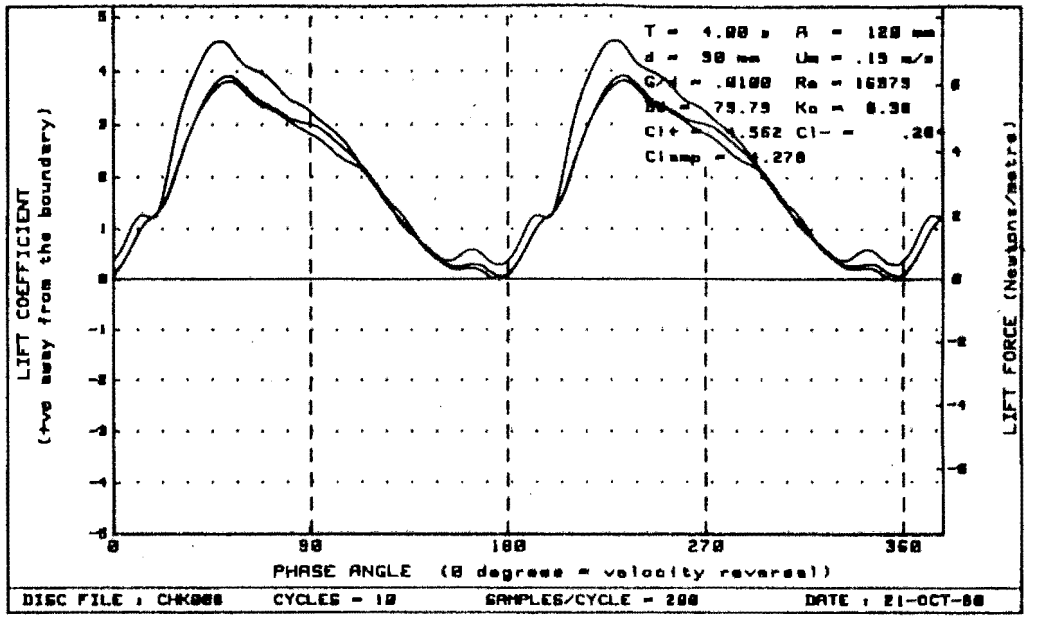

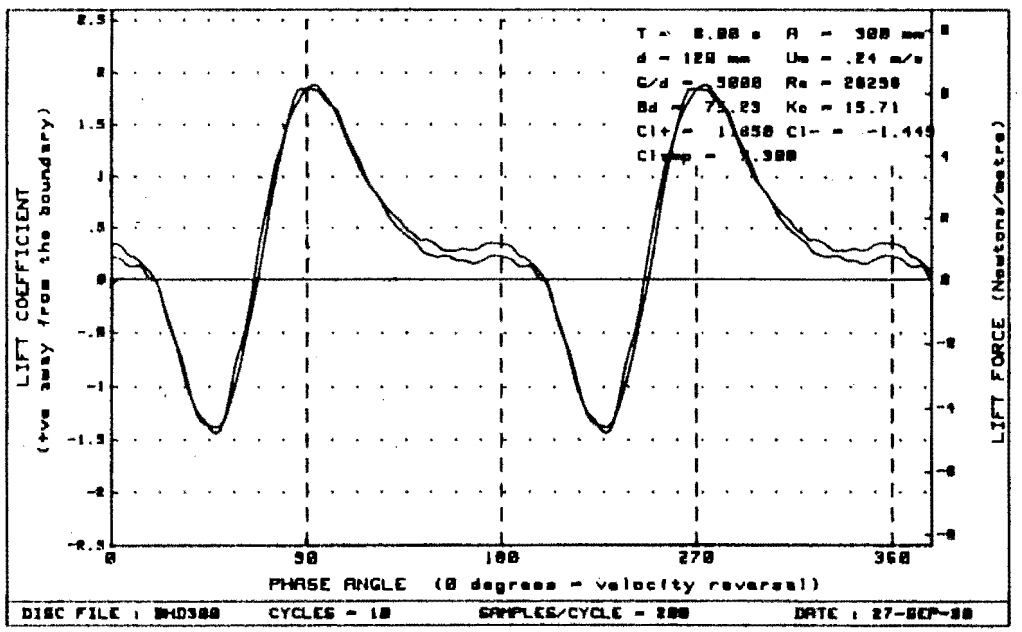

Figure 5.1 : Repeatability tests at different gap ratios, periods and amplitudes.

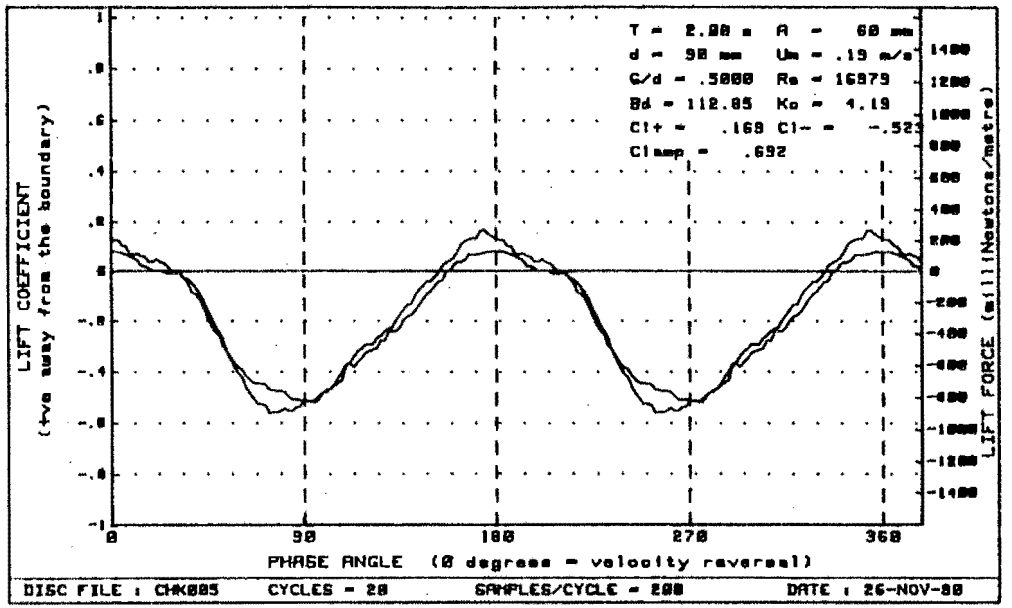

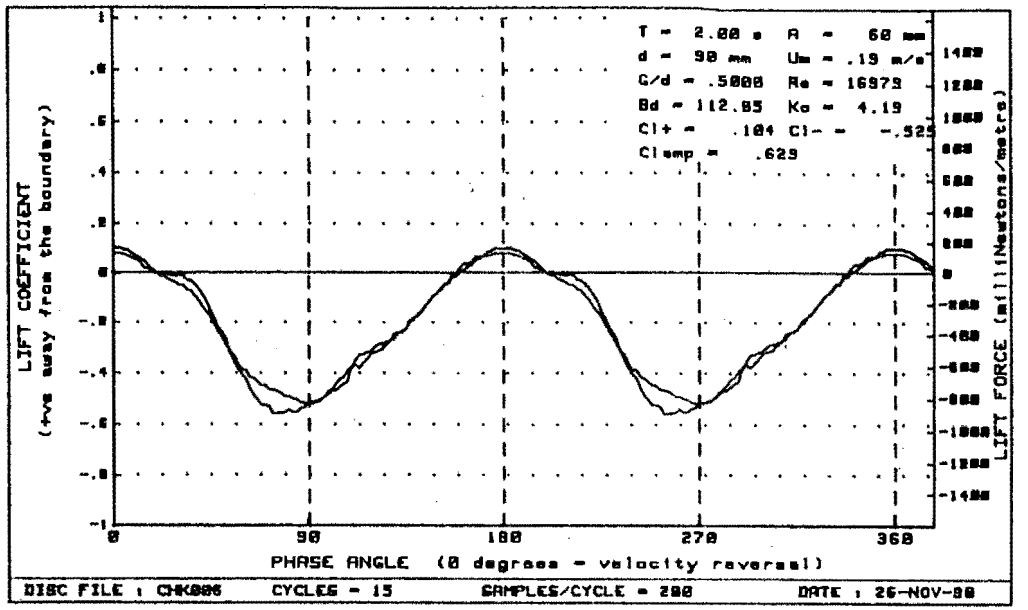

Figure 5.2 : Tests performed at different cycles/run under identical conditions.

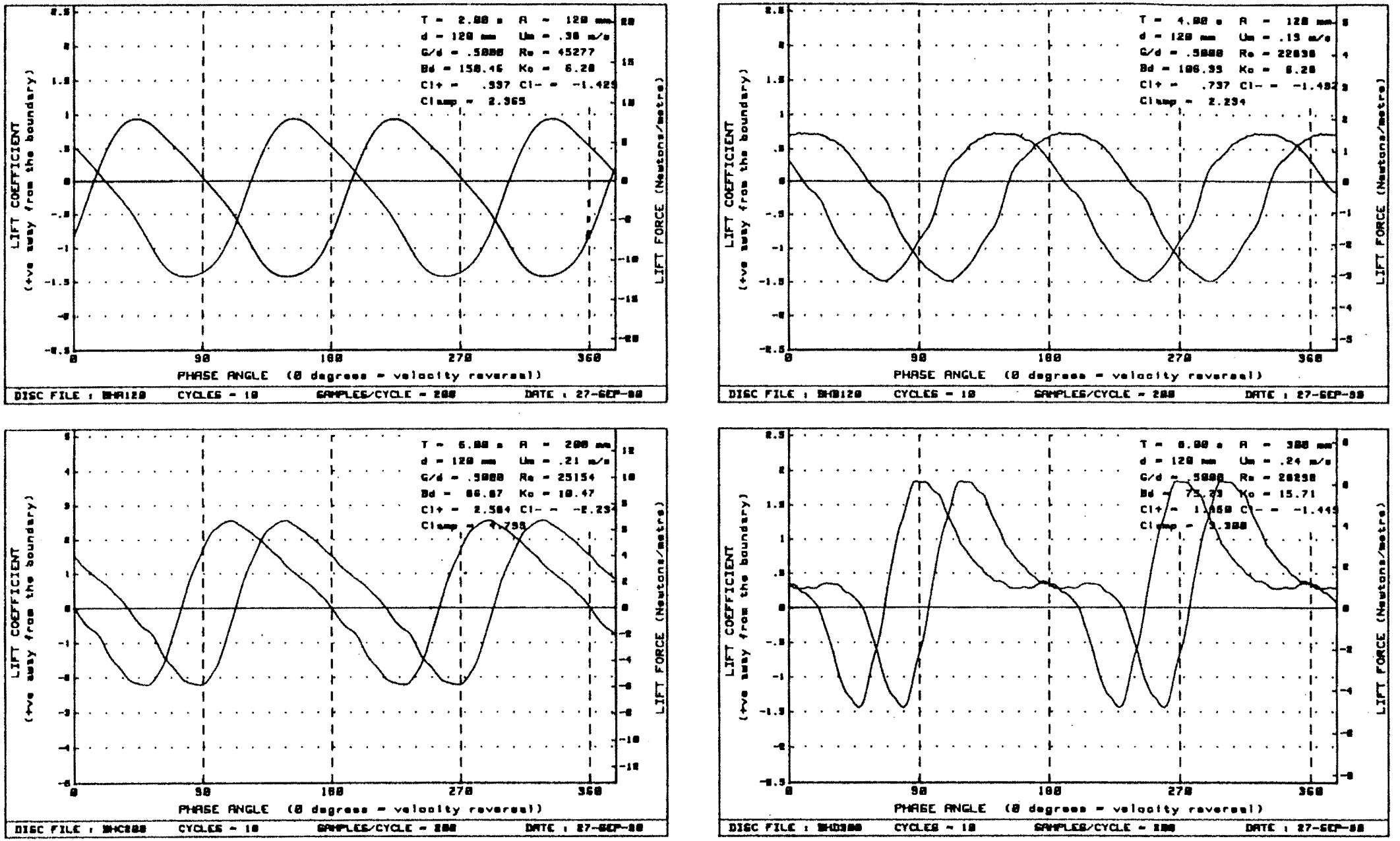

Figure 5.3 : Phase lag compensation shown as a function of period.

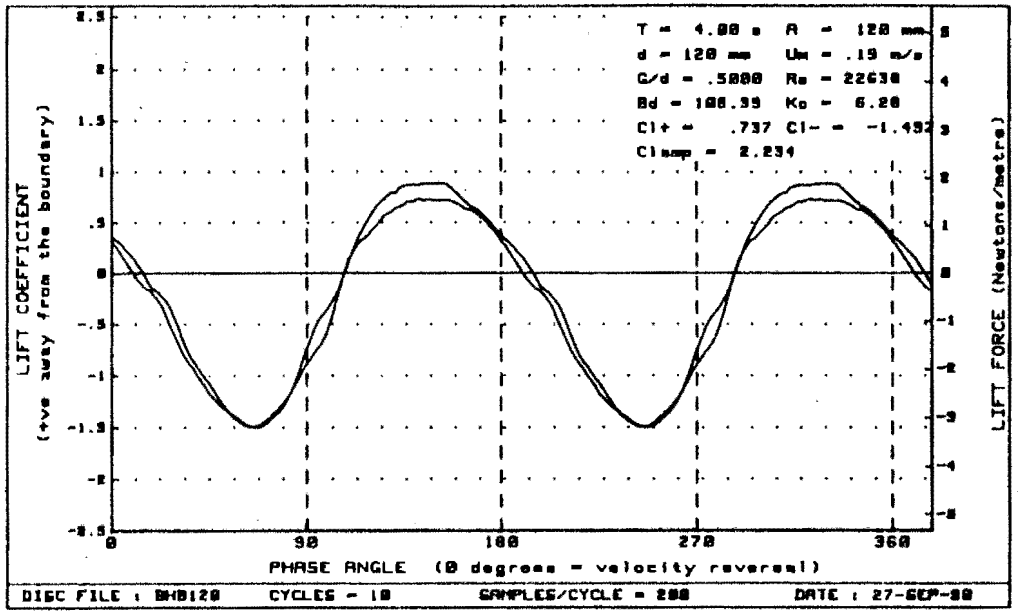

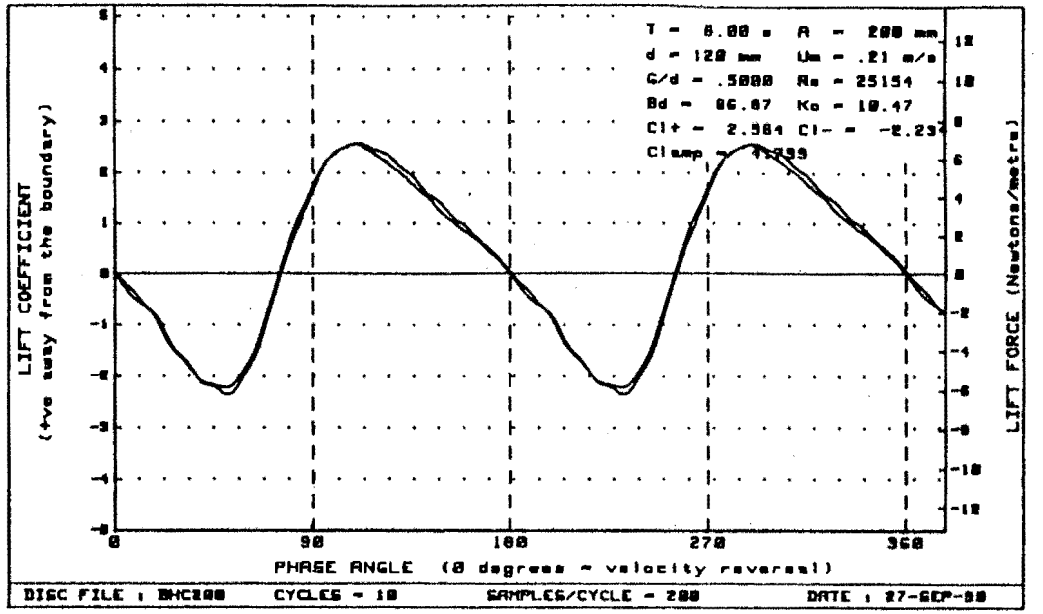

Figure 5.4 : Tests performed at identical conditions with 7 and 13 tapping orientations.

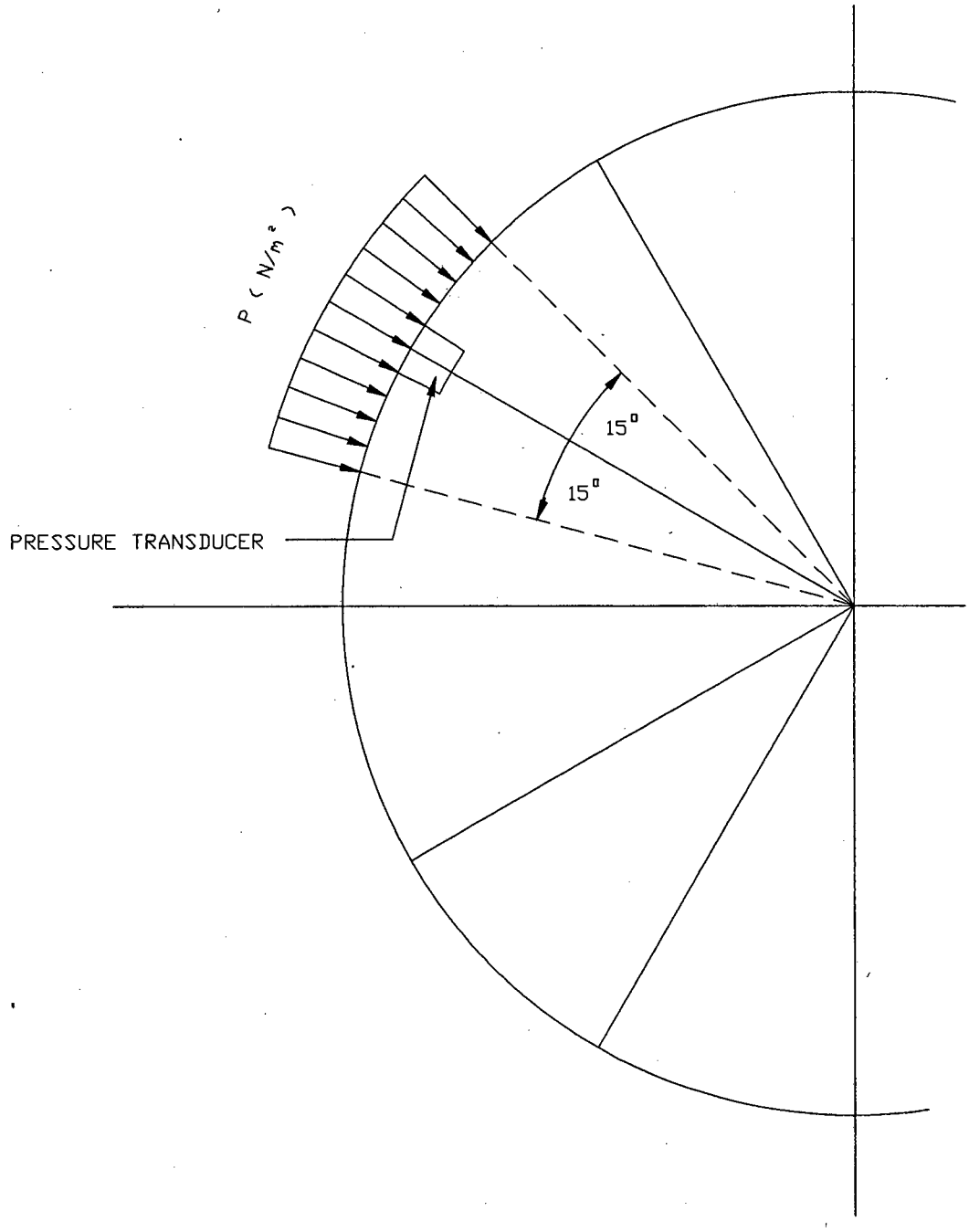

Figure 5.5 : Assumed pressure distribution in the vicinity of a pressure tapping

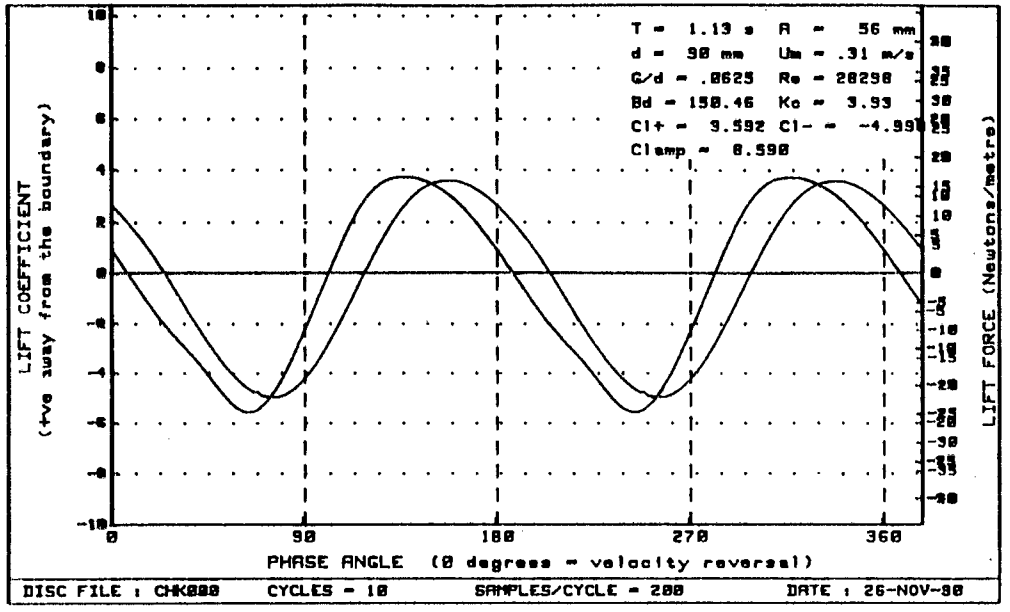

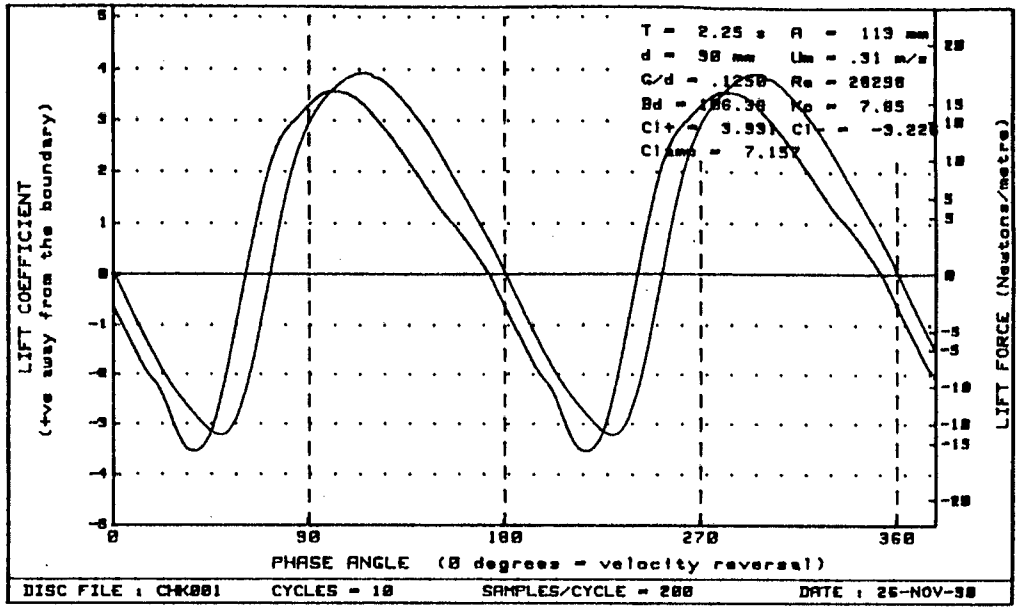

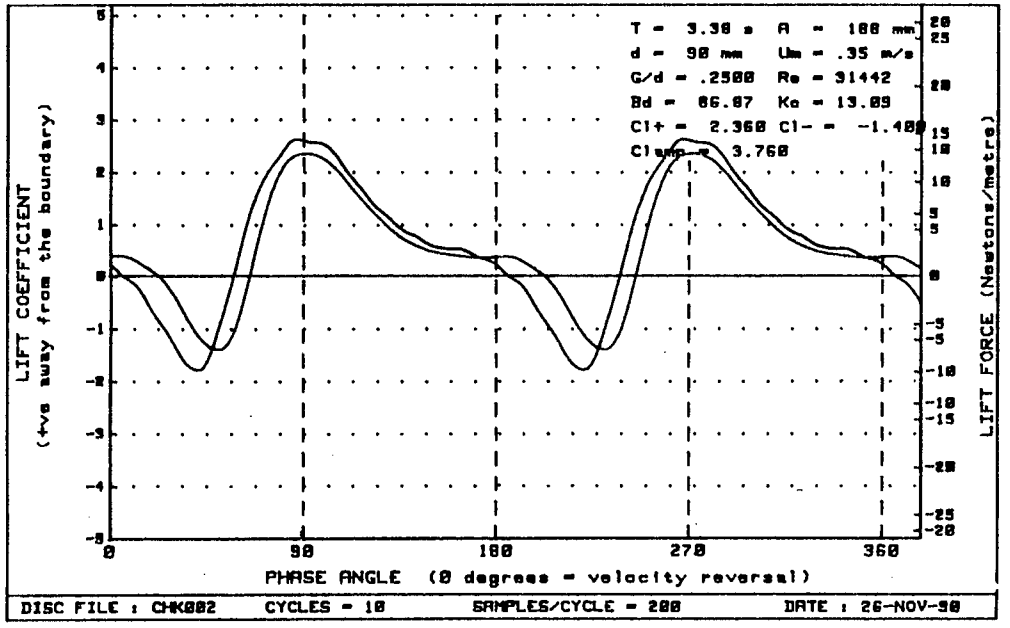

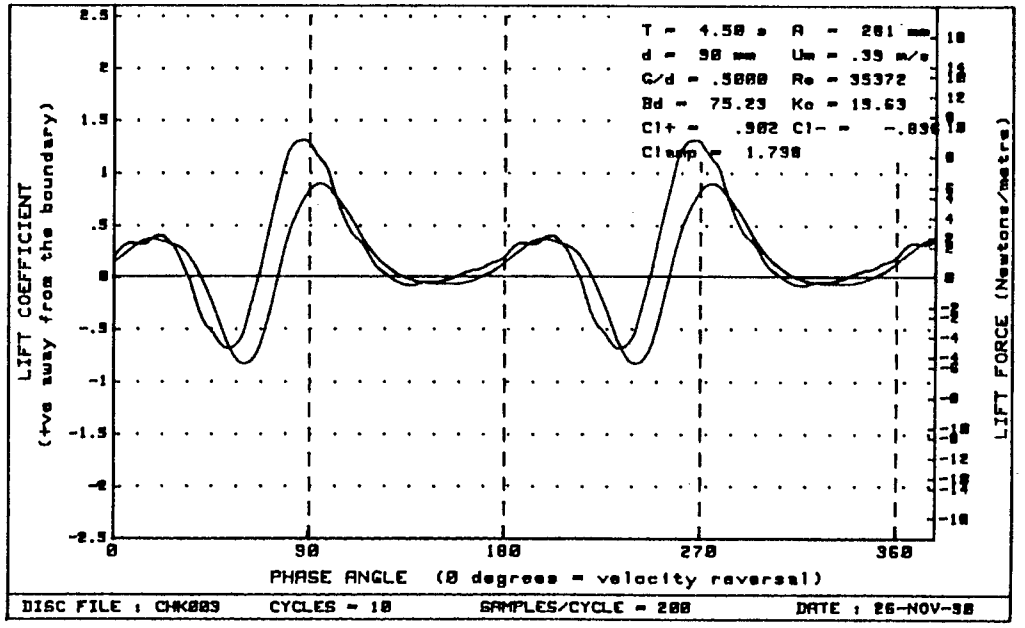

Figure 5.6 : Tests performed at identical Re, KC and Bd with different cylinder diams.

6. RESULTS OF LIFT FORCE MEASUREMENT

This chapter involves a discussion of each individual test with respect to lift force versus phase angle. The range of tests undertaken are given in Table 8.1 and the results of these tests are given in Appendix F. This chapter is to be read in conjunction with the lift versus phase plots given in Appendix G.

The results are discussed in groups of gap ratio, starting with the smallest gap ratio and moving up. Within each group, the tests have been further subdivided from high to low values of βd.

6.1 Lift measurements for G/d = 0.01 (fig G.1 - G.8)

This group of tests was performed with the 90mm diameter test cylinder at periods of T=4,6,8 and 10s. The amplitudes of oscillation were varied from 30mm to 800mm. This amounted to the ranges Re=4245-45277 and Kc=2.09-55.85.

For βd=79.79 or T=2s, the curve has the shape of a rectified sine wave for Kc=2.09-6.28, with the maximum lift force away from the bed occurring at maximum velocity. The maximum lift force towards the bed occurs at velocity reversal. In this range, the lift forces act predominantly towards the bed as confirmed by theory, becoming more positive with increasing Kc. In the range of Kc=8.38-16.76, the shape of the curve deviates from the rectified sine wave somewhat, with a more rapid rise in lift away from the bed and a slower fall to Cl-. Furthermore, the peak of Cl+ migrates to a point midway between velocity reversal and maximum

velocity. The lift forces in this range of Kc tend to become more and more away from the bed with increasing Kc and at the same time the phase transition from Cl+ to Cl- becomes greater with increasing Kc.

For βd=65.15 or T=4s, a striking factor is that the lift forces are almost all away from the bed throughout the range. This range shows a definite trend of a sudden rise to Cl+ and a gradual decline to Cl- which are located at phases of $\pm 30^{\circ}$ and $\pm 160^{\circ}$ respectively. At the higher range of Kc (17.45-27.93) the curve tends to adopt a plateau shortly after the Cl+ peak, becoming more predominant with increasing Kc.

For βd=56.42 or T=8s, the lift forces are again predominantly away from the bed as for βd=65.15. Here the curve takes on the plateau shape for the lower range of Kc (10.47-20.94) and this feature falls away more and more until Kc=41.89 where the plateau is very short. Once again, Cl+ is located at a phase of $\pm 30^{\circ}$ with Cl- at $\pm 160^{\circ}$. According to the above observations, the change from Cl+ to Cl- is rather gradual at low Kc, becoming slightly more rapid with increasing Kc due to the shortening of the plateau.

For βd=50.47 or T=10s, the lift forces in the range Kc=6.98 -13.96 are completely away from the bed and at the same time the Cl+ values for this range are relatively high. In the range Kc= 20.94-55.05 the lift becomes more negative, reducing in value with increasing Kc. The curve has a slight plateau after Cl+ at low Kc, becoming less pronounced with increasing Kc. The positive peak occurs at $\pm 40^{\circ}$ and the negative peak just before velocity

reversal.

Considering the gap ratio of 0.01 as a whole, it may be deduced that the lift forces act towards the bed at low Kc, acting more away from the bed with decreasing βd. Curve shapes take on the rectified sine shape for all βd at low Kc, with the positive peak at maximum velocity and the negative peak at velocity reversal. For the higher Kc at each βd range, the curves adopt the plateau formation after the positive peak, the plateau usually becoming shorter with increasing Kc. This gap ratio may generally be characterized by a rather gradual change from positive to negative peak with these peaks generally occurring at approximately 30°-45° and 160°-180° respectively in the higher Kc range for each βd.

6.2 Lift measurements for G/d = 0.03125 (Figs G.9-G.16)

This group of tests was performed with the 120mm diameter test cylinder at periods of T=2,4,6,8s. The amplitudes of oscillation were varied from 15mm to 600mm. This amounted to the ranges Re=5660-56596 and Kc=0.79-31.42.

For βd=150.46 or T=2s, the curve is a prominent rectified sine wave. Unlike the case for G/d=0.01, the positive peaks occur near velocity reversal and the negative peaks near maximum velocity. The curve maintains this shape throughout, but both the positive and negative peaks migrate to lower phase angles with increasing Kc or rather, for Kc=0.79, Cl+ and Cl- occur at $\pm$ 185° and $\pm 100^{\circ}$ respectively and steadily move back to $\pm 130^{\circ}$ and $\pm 25^{\circ}$ for Kc=6.28. At the lower range, the lift forces are slightly more negative,

gradually becoming more positive with increasing Kc. The curves are of a definite shape with little fluctuation from the rectified sine wave except that a high Kc, there appears to be a mild upward kink in the curve at the negative peak. There is a rather uniform rate of change over from maximum positive to maximum negative lift force and vice versa.

For βd=106.39 or T=4s, the curve shape is similar to the βd=150.46 case in that it is a rectified sine wave throughout. Again, the kink at Cl- appears but it does so only at small Kc whereas for βd=150.46 it occurred at high Kc. The peaks migrate backwards with increasing Kc, however in the upper range of Kc (6.28- 12.57) the positive peak remains at maximum velocity while the negative peak remains at velocity reversal. Again there is a relatively uniform change between peaks. As with the previous case, the lift forces are predominantly negative at low Kc, becoming more positive with increasing Kc.

For βd=86.87 or T=6s, the shape varies with Kc. At low Kc (2.62-7.85) the rectified sine wave occurs and in the upper Kc range (10.47-20.94) the curve tries to take on a secondary peak soon after the first but the plateau is very short so the curves may therefore be considered to be distorted rectified sine waves. There is a rather pronounced backward migration of the peaks with increasing Kc. At Kc=2.62 the positive and negative peaks occur at phases $\pm 130^{o}$ and $\pm 210^{o}$ respectively, moving back to $\pm 90^{o}$ and $\pm 180^{o}$ for Kc=10.47. For Kc=13.09-20.94, the negative peak remains at velocity reversal while the positive peak continues to migrate backwards. At this value of βd the lift forces are completely

positive, regardless of Kc.

For βd=75.23 or T=8s, the most outstanding feature is the location of the negative peak which occurs at velocity reversal throughout. There is a backward migration of the positive peak from $\pm 90^{\circ}$ for Kc=3.93 to $\pm 30^{\circ}$ for Kc=31.42. The lift forces act mostly away from the bed at low Kc but for the majority of the range they act away from the bed completely. At low Kc the curve takes on the shape of a slightly distorted rectified sine wave with Cl+ at maximum velocity and Cl- at velocity reversal. From Kc=11.78-31.42 a short plateau appears after Cl+. This results in a distinctively longer phase angle between positive and negative peaks.

To summarize this gap ratio as a whole, the most outstanding feature is the change from the rectified sine wave of βd=150.46 and 106.39 to the plateau or distorted rectified sine wave of βd=86.87 and 75.23. For βd=150.46, there appears to be no dominant direction of lift force but they become distinctly away from the bed at Kc=4.71 remaining more positive thereafter. Another trend that appears is the location of the negative peak. For all βd other than 150.46, the negative peak remains at velocity reversal while the positive peaks continue to migrate accordingly.

6.3 Lift measurements for G/d = 0.046875 (figs G.17 - G.24)

This group of tests was performed with the 120mm diameter test cylinder at periods of T=2,4,6 and 8s. The amplitudes of oscillation were varied from 15mm to 600mm. This amounted to the ranges Re=5366-53660 and Kc=0.79-31.42.

For βd=146.51 or T=2s, the lift versus phase plots have a definite rectified sine wave shape throughout the range of Kc. Both the positive and negative peaks migrate backward from phases of $\pm 210^{\circ}$ and $\pm 120^{\circ}$ for Cl+ and Cl- respectively at Kc=0.79 to phases of $\pm 120^{\circ}$ and $\pm 30^{\circ}$ for Kc=6.28. Lift forces are predominantly toward the bed up to Kc=4.71 and from Kc=5.5-6.28 they tend to be somewhat equally distributed towards and away from the bed.

For βd=103.6 or T=4s, the curves are slightly distorted rectified sine waves becoming more distorted with increasing Kc. The positive peak appears to be more rounded or smooth than the negative peak which occurs rather rapidly. This is complemented by an upward kink just prior to the negative peak. Once again there is a backward migration of the peaks with increasing Kc. Cl+ migrates from a phase of $\pm 150^{\circ}$ for Kc=1.57 to $\pm 90^{\circ}$ for Kc= 12.57. Cl- appears to migrate from $\pm 70^{\circ}$ for Kc=1.57 to $\pm 10^{\circ}$ for Kc=12.57 ie. a steady backward migration of 60°. As before the lift forces are predominantly towards the bed for low Kc up to Kc =4.71. From Kc=6.28-12.57 the lift forces become increasingly away from the bed with increasing Kc.

For βd=84.59 or T=6s, a rectified sine wave is the predominant shape for low Kc up to Kc=7.85. From Kc=10.47 upwards, the rectified sine wave becomes distorted, taking on a short plateau after a rather flat positive peak. This creates a sudden transition from Cl- to Cl+ especially at the high range of Kc. In practical terms this means that a sudden upward force will be exerted on the cylinder which could lead to the cylinder's failure. The transition from Cl+ to Cl- takes longer and longer

with increasing Kc due to the fact that in the range Kc=13.09 -20.94 the negative peak remains at velocity reversal while the positive peak migrates backwards from ±90° for Kc=13.09 to ±40° for Kc=20.94. In the lower range, Kc=2.62-10.47, both Cl+ and Cl- migrate steadily from ±130° and ±40° for Kc=2.62 to ±90° and ±10° for Kc=10.47 respectively. Once again, lift forces act predominantly towards the bed at low Kc acting more away from the bed with increasing Kc.

For βd=73.25 or T=8s, the rectified sine wave exists only in the range Kc=3.93-7.85. From Kc=11.78 upwards, this form is distorted, changing to the general shape of a plateau, with a positive peak followed by a rather short plateau, followed by a sudden decrease to the zero lift position where another plateau occurs just prior to the negative peak. On the whole it appears that the negative peak does not migrate, remaining at velocity reversal. The positive peak migrates from ±100° for Kc=3.93 to ±30° for Kc=31.42. Yet again lift forces are predominant towards the bed but now the lift becomes more positive at lower Kc, (Kc= 7.85) so that the lift forces are away from the bed for most of the range.

Considering the 0.046875 gap ratio as a whole, the most outstanding feature is the trend for the lift forces to act towards the bed for low Kc and away from the bed for high Kc. The transition from predominantly negative to predominantly positive lift situations occur at lower and lower Kc when βd is reduced. Another striking observation is the rectified sine wave which occurs for most of the range except at low values of βd and high Kc. For the range βd=103.6-73.25, the negative peak occurs at

velocity reversal almost all the time. The positive peak however continues its backward migration causing a slower rate of change between Cl+ and Cl- and an increased rate of change from Cl- to Cl+.

6.4 Lift measurement for G/d = 0.0625 (figs G.25 - G.32)

This group of tests was performed with the 120mm diameter test cylinder at periods of T=2,4,6 and 8s. The amplitudes of oscillation were varied from 15mm to 600mm. This amounted to the ranges Re= 5511-55111 and Kc=0.79-31.42.

For βd=148.47 and T=2s, the curves are clearly rectified sine waves over the entire range, with no distortions whatsoever. As usual, the lift forces are predominantly towards the bed at low Kc, gradually becoming predominantly away from the bed with increasing Kc until only at Kc=6.28, the lift forces away from the bed slightly outweigh those towards the bed. There is a curve migration of $\pm 60^{\circ}$, with Cl+ and Cl- at Kc=1.57 $\pm 190^{\circ}$ and $\pm 110^{\circ}$ respectively and $\pm 130^{\circ}$ and $\pm 50^{\circ}$ at Kc=6.28.

For βd=104.99 or T=4s, the curves are the perfect rectified sine wave up to Kc=9.42 where the curves start become slightly distorted. Once again, at low Kc the lift forces act predominantly towards the bed, acting more away from the bed with increasing Kc. The transition from predominantly negative to predominantly positive takes place at Kc=6.28. There is a migration of the curve from Kc=3.14, where the zero lift condition occurs at velocity reversal and maximum velocity, to the case where Cl+

occurs at maximum velocity with zero lift at velocity reversal for Kc=12.57.

For βd=85.72 or T=6s, the plateau takes form at Kc=10.47 with a slightly distorted rectified sine wave at lower Kc. The lift forces are dominant towards the bed up to Kc=5.24 where the lift becomes dominant away from the bed, this effect increasing with increasing Kc. The negative peak migrates from $\pm 225^{\circ}$ for Kc=2.62 to $\pm 190^{\circ}$ at Kc=7.85 where it remains for the remainder of the Kc range. Positive peaks move steadily from $\pm 145^{\circ}$ for Kc=2.62 to $\pm 45^{\circ}$ for Kc=20.94.

For βd=74.24 or T=8s, the curve is a rectified sine wave up to Kc=7.85. The secondary peak then begins to develop for higher Kc. Again, lift forces towards the bed dominate for low Kc but for Kc=7.85 and up, forces away from the bed dominate. Again the migration occurs but the negative peak remains at $\pm 185^{\circ}$ from Kc=11.78 upwards. The positive peaks migrate in a similar fashion to previous cases causing a slow transition from Cl+ to Cl- and a very rapid rise from Cl- to Cl+ which is undesirable.

On the whole it appears that lift forces act towards the bed up to Kc=±6 where they then act away from the bed, becoming more positive with increasing Kc. The curve takes the shape of the rectified sine wave up to Kc=±9.5 and then secondary peak or plateau type curves begin to develop.

6.5 Lift measurements for G/d = 0.09375 (figs G.33 - G.40)

This group of tests was performed with the 90mm diameter test cylinder at periods of T = 4,6,8 and 10s. The amplitudes of oscillation were varied from 30mm to 800mm. This amounted to the ranges Re= 4025-45277 and Kc=2.09-55.85.

For βd=77.7 or T=4s, lift forces act towards the bed up to Kc=6.28 whereafter the lift acts predominantly away from the bed, becoming more positive with increasing Kc. The rectified sine wave occurs until Kc=8.38 with a slight upward kink at the negative peak and thereafter becomes distorted, taking on a slight plateau type trend. Yet again the migration takes place with increasing Kc, however the negative peak remains at $\pm 190^{o}$ from Kc=10.47-16.76 causing the gradual decline from Cl+ to Cl- followed by a rapid lift away from the bed.

For βd=63.44 or T=6s, the curve in the range Kc=3.49-6.98 may be described as a rectified sine wave with a particularly sharp or quick negative peak in comparison with the smooth positive peak.From Kc=10.47-27.93, the curve becomes more plateau like with increasing Kc. Transition from predominantly negative lift to predominantly positive lift takes place at Kc=6.98. From Kc=13.96 onwards Cl- remains at a phase of $\pm 190^{o}$ while the positive peak Cl+ migrates backwards. A gradual decline from Cl+ to Cl- occurs but a very rapid jump from Cl- to Cl+ takes place.

For βd=54.94 or T=8s, the plateau shape begins to develop at Kc=10.47. Lift forces are predominantly away from the bed at

Kc=10.47. Strangely enough, in the range Kc=15.71-41.89, there is little migration of the curve with Cl+ and Cl- at ±40° and ±190° respectively. There is a sudden fall from Cl+ followed by a short plateau. A gradual drop to a plateau of the zero lift is then followed by an extremely quick rise to Cl+.

For βd=50.47 or T=10s, the curve is generally that of the plateau, becoming distorted at Kc=48.87 and 55.85. Lift forces act away from the bed throughout the range i.e. from Kc=6.98. The location of Cl- is difficult to locate since there is usually a very gradual drop to Cl- but it would seem that it occurs just before velocity reversal. The form of the curve is a sharp positive peak followed by a rather gradual decline to the plateau at zero lift. This is followed by a very rapid rise back to Cl+. It appears that little migration occurs.

For this gap ratio as a whole the most striking factor is the gradual decline from Cl+ to Cl- followed by an extremely rapid jump back to Cl+. Also there is a transition from the case where the majority of lift acts towards the bed to the case where the majority of lift acts away from the bed; this generally occurs at Kc=±7.

6.6 Lift measurement for G/d = 0.125 (figs G.41 - G.48)

This group of tests was performed with the 120mm diameter test cylinder at periods of T = 2,4,6 and 8s. The amplitudes of oscillation were varied from 15mm to 600mm. This amounted to the ranges Re= 5660-56596 and Kc=0.79-31.42.

For βd=150.46 or T=2s, the curves are of the rectified sine wave type throughout the range. Lift forces act predominantly toward the bed right through to Kc=6.28. Generally, Cl+ occurs at velocity reversal and Cl- at maximum velocity, however there is a backward migration from $\pm 210^{\circ}$and $\pm 120^{\circ}$ for Kc=1.57 to $\pm 145^{\circ}$ and $\pm 70^{\circ}$ for Kc=6.28 of Cl+ and Cl- respectively.

For βd=106.39 or T=4s, the curves are rectified sine waves throughout except at Kc=11.0 and 12.57 they become slightly distorted, attempting to create a plateau after the positive peak. The transition from predominantly negative to predominantly positive lift forces takes place at Kc=7.85. The negative peak remains at $\pm 210^{\circ}$ for the range Kc=7.85 - 12.57 while the positive peaks migrate only slightly. In the lower range Kc=1.57-6.28, there is a backward migration of $\pm 30^{\circ}$.

For βd= 86.87 or T=6s, the curves take on the rectified sine wave shape in the range Kc=2.62-10.47. and changes to a plateau shape in the range Kc=13.09-20.94. Transition from predominantly negative to predominantly positive lift forces occurs at Kc=7.85. The negative peak remains at $\pm 200^{\circ}$ for most of the range, Kc=7.85 -20.94 with the positive peak migrating from $\pm 95^{\circ}$ to $\pm 50^{\circ}$in this range.

For βd=75.23 or T=8s, the curves are rectified sine waves in the lower range, Kc=3.93-7.85 becoming plateaux for the rest of the range up to Kc=31.42. Transition from predominantly negative to predominantly positive lift forces takes place at Kc=7.85. Again the negative peak remains at $\pm 200^{\circ}$ while the positive peak moves

±45° over the range Kc=7.85-31.42.

In conclusion, this gap ratio clearly shows that the transition from predominantly negative to predominantly positive lift forces takes place at Kc=7.85. Also, clearly rectified sine waves occur up to Kc=±8.5 where the shape changes to that of the plateau. With the plateau type curve the change from Cl- to Cl+ is rather rapid.

6.7 Lift measurements for G/d = 0.25 (figs G.49 - G.56)

This group of tests was performed with the 120mm diameter test cylinder at periods of T = 2,4,6 and 8s. The amplitudes of oscillation were varied from 15mm to 600mm. This amounted to the ranges Re=5660-56596 and Kc=0.79-31.42.

For βd=150.46 or T=2s, the curves have the rectified sine wave shape throughout, with Cl+ occurring near velocity reversal and Cl- near maximum velocity in most cases. There is however a backward migration of the curve by ±45. As Kc is increased, the slopes of the curve becomes steeper or rather transition from peak to peak becomes quicker. Lift forces are predominantly toward the bed in a cycle throughout (up to Kc=6.28).

For βd=106.39 or T=4s, the curves once again had the rectified sine wave shape, becoming slightly distorted on the transition from Cl+ to Cl- at Kc=11.0. Lift forces act predominantly toward the bed up to Kc=9.42. Here there is a migration of nearly 90°, with Cl+ at ±180° and Cl- at ±80° for Kc=3.14 and Cl+ at ±90° and Cl- at ±45° for Kc=12.57. The gradients of the curves appear to

increase up to Kc=7.85 whereafter they remain constant.

For βd=86.87 or T=6s, rectified sine waves occur up to Kc=10.47. They then form the plateau shape for the higher Kc range. Lift forces act predominantly toward the bed up to Kc=10.47 and for Kc=18.33 and 20.94 forces are almost all away from the bed except for the negative peak. The slope of transition from Cl- to Cl+ remains constant throughout and of course the transition from Cl+ to Cl- becomes flatter with the changing curve shape. The backward migration is relatively slight, with the negative peak remaining at $\pm 45^{\circ}$.

For βd=75.23 or T=8s, the curves are of the rectified sine wave type for Kc=3.93 and 7.85, becoming distorted at Kc=11.78 and forming the twin peaks shape for Kc=15.71 and 19.63. A secondary peak begins to develop and then subsides to form a plateau for Kc=23.56-31.42. Lift forces predominantly act toward the bed up to Kc=11.78. The negative peak remains at ±40 throughout, with the positive peak moving from $\pm 160^{\circ}$ for Kc=3.93 to $\pm 60^{\circ}$ for Kc=31.42.

In summary, rectified sine waves occur up to Kc=±10 forming the plateau shape in the higher Kc range. Lift forces act predominantly toward the bed up to Kc=±10.5. Again there is a backward migration of the curves for all βd.

6.8 Lift measurements for G/d = 0.5 (figs G.57 - G.64)

This group of tests was performed with the 120mm diameter test cylinder at periods of T = 2,4,6 and 8s. The amplitudes of

oscillation were varied from 15mm to 600mm. This amounted to the ranges Re= 5660-56596 and Kc=0.79-31.42.

For βd=150.46 or T=2s, it may be assumed that the curve shape is that of the rectified sine wave throughout, although at the lower Kc range (0.79-3.14) this is difficult to determine since the lift forces are of such small magnitudes (milliNewtons/metre). In contrast to previous trends, the lift forces act predominantly away from the bed up to Kc=3.14 and then for Kc=3.93 the lift forces act almost completely towards the bed, and then become more positive with increasing Kc. Migration of the curves is difficult to determine at low Kc but it appears that there is a $\pm 20^{\circ}$ migration in the upper range of Kc=4.71-6.28.

For βd=106.39 or T=4s, the rectified sine wave curve shape occurs throughout. Cl- clearly remains at $\pm 60^{\circ}$ throughout while Cl+ migrates from $\pm 150^{\circ}$ to $\pm 100^{\circ}$ for Kc=6.28 and 12.57 respectively, causing an increase in slope from Cl- to Cl+ with increasing Kc. Lift forces act predominantly towards the bed up to Kc=11.0.

For βd=86.87 or T=6s, the rectified sine wave occurs up to Kc=10.47; at Kc=13.09 the downward slope becomes distorted and for Kc=15.71-20.94 the curve develops a secondary peak. Lift forces are predominantly towards the bed up to Kc=7.85. The negative peak remains at $\pm 60^{\circ}$ throughout while the positive peak moves from $\pm 160^{\circ}$ to $\pm 90^{\circ}$ for Kc=5.24 and 20.94 respectively. This causes the transition from Cl- to Cl+ to become more rapid.

For βd=75.23 or T=8s, the rectified sine wave curve occurs up to

Kc=11.78 and thereafter the secondary peak develops. Lift forces are predominantly negative up to Kc=7.85. As before, the negative peak remains at ±60° and the positive peak migrates steadily from ±120° for Kc=7.85 to ±80° for Kc=31.42, causing a steepening of the curve from Cl- to Cl+.

In summary, lift forces for this gap ratio are predominantly negative up to Kc=±8.9. The curve type is a rectified sine wave up to Kc=±11.0 whereafter the secondary peak type curve occurs. In general, the negative peak remains at ±60° while the positive peak migrates backwards by ±60°. This change in waveform and the extremely small magnitudes of lift force at high βd tend to indicate that the boundary does not have a large effect on the flow around the cylinder at this gap ratio. Further data analysis in Chapter 8 confirms that this is the case.

6.9 Lift measurements for G/d = 0.6, 0.75 and 1.0

This group of tests was performed with the 90mm diameter test cylinder at periods of T=2 and 8s. The amplitudes of oscillation were varied from 15mm to 600mm. This amounted to the ranges Re= 4245-42447 and Kc=1.05-41.89.

These gap ratios have been grouped together because it has been found that they each yield similar trends, meaning that the boundary has little effect on their results. It has therefore been concluded that the boundary affects the flow patterns around cylinders for gap ratios up to G/d=0.5 and the results for tests performed at gap ratios greater than 0.5 approach their freestream

values. This conclusion is in direct agreement with previous research. Force versus phase plots for these gap ratios have therefore been omitted due to their irrelevance with regard to the boundary and to conserve space. However, a brief description of the plots is given.

For βd=112.85 or T=2s, the curve type is the rectified sine wave throughout. The lift forces act predominantly toward the bed up to Kc=8.38. There is very little backward migration of the curve.

For βd=56.42 or T=8s, the curve is a rectified sine wave only up to Kc=10.47 whereafter a rather pronounced secondary peak develops, similar to the case for G/d=0.5. The lift forces are predominantly negative up to Kc=15.71 and again there is little or no migration of the curve.

7. RESULTS OF DRAG FORCE MEASUREMENT

This chapter involves a discussion of each test with respect to the drag force vs phase angle. The range of tests undertaken are given in Table 8.1 and the results of each test are given in Appendix F. This chapter is to be read in conjunction with the drag vs phase plots in Appendix H.

Tests have been discussed in groups of gap ratio in ascending order. They have been further subdivided into descending order of βd.

7.1 Drag measurements for G/d=0.01 (figs H.1 - H.8)

This group of tests was performed with the 90mm diameter test cylinder at periods T=4,6,8 and 10s. The amplitudes of oscillation were varied from 30-800mm. These amounted to the following ranges Re=4245-45277 and Kc=2.09-55.85.

For βd=79.79 or T=4s, the point of zero drag moves from $\pm 110^{\circ}$ for Kc=2.09 to $\pm 140^{\circ}$ for Kc=16.76. This means that with increasing Kc, wake effects become more pronounced. The peak occurs just after velocity reversal where there is a rapid increase in drag force. This "spike" is a result of the cylinder interacting with the wake in the previous half-cycle.

For βd=65.15 or T=6s, the spike is rather conspicuous for low Kc but with increasing Kc, the drop from the peak of the spike becomes smaller. The point of zero drag steadily moves from $\pm 120^{\circ}$ for Kc=3.49 to $\pm 165^{\circ}$ for Kc=27.93.

For βd=56.42 or T=8s, exactly the same trend as before occurs in that the drop from the peak of the spike becomes less with increasing Kc. Zero drag points move from $\pm 110^{\circ}$ for Kc=5.24 to $\pm 150^{\circ}$ for Kc=41.89.

For βd=50.47 or T=10s, the drag curve is quite erratic however the spike after velocity reversal is still evident.

In summary, the drag curves are extremely repeatable. There is always a sudden rise in the drag force just after velocity reversal, preceded by an equally sudden but less pronounced fall in drag force. The position of zero drag migrate forwards from ± 110 to $\pm 150^{\circ}$.

7.2 Drag measurement for a G/d=0.03125 (figs H.9 - H.16)

This group of tests was performed with the 120mm diameter test cylinder at periods T=2,4,6 and 8s. The amplitudes of oscillation were varied from 15-600mm. These amounted to the following ranges Re=5660-56596 and Kc=0.79-31.42.

For each series of tests at a particular value of βd, the shape of the drag curves are highly repeatable. The shape of the curves at different βd differ only slightly. All curves exhibit the spike after velocity reversal, regardless of βd or Kc.

For βd=150.46 the spike occurs relatively late at low Kc, followed by a gradual decrease in drag force. With increasing Kc, the magnitude of the drag force remains at the magnitude of the spike and is followed by a more sudden decrease in drag. The position of

zero drag appears to remain at approximately 130° throughout. For βd=106.39, 86.87 and 75.23 the spikes occur immediately after velocity reversal but otherwise follow exactly the same trends as those for βd=150.46.

7.3 Drag measurements for G/d=0.046875 (figs H.17 - H.24)

This group of tests was performed with the 120mm diameter test cylinder at periods T=2,4,6 and 8s. The amplitudes of oscillation were varied from 15-600mm. These amounted to the following ranges Re=5366-53660 and Kc=0.79-31.42.

As for the previous gap ratio, the drag curves are highly repeatable at a particular βd and varying only slightly at different βd.

For βd=146.51 the spike occurs relatively late followed by a gradual decrease in drag force. With increasing Kc, a plateau forms after the spike at the spike's magnitude which is followed by a sudden decrease in drag force. The zero drag position remains at ±125° throughout.

For βd=103.6, 84.59 and 73.25 the spike occurs immediately after velocity reversal and again, the plateau develops after the spike with increasing Kc. The zero drag positions for the different values of βd are given by:

βd=103.6 : ±125° for Kc=1.57 and ±150° for Kc=12.57.
βd=84.59 : ±125° for Kc=2.62 and ±160° for Kc=20.94.
βd=73.25 : ±110° for Kc=3.93 and ±160° for Kc=31.42.

7.4 Drag measurements for G/d=0.0625 (figs H.25 - H.32)

This group of tests was performed with the 120mm diameter test cylinder at periods T=2,4,6 and 8s. The amplitudes of oscillation were varied from 15-600mm. These amounted to the following ranges Re=5511-55111 and Kc=0.79-31.42.

Once again, drag curves are highly repeatable with the spike occurring relatively late at high βd and forming a slight plateau with increasing Kc. The zero drag position remains at approximately 125°.

For the remaining values of βd the spikes occur immediately after velocity reversal and exhibit identical curve trends except for the zero drag positions, given by:

βd=104.99: ±125° for Kc=1.57 and ±150° for Kc=12.57.
βd=85.72 : ±125° for Kc=2.62 and ±165° for Kc=20.94.
βd=74.24 : ±115° for Kc=3.93 and ±155° for Kc=31.42.

7.5 Drag measurements for G/d=0.09375 (figs H.33 - H.40)

This group of tests was performed with the 90mm diameter test cylinder at periods T=4,6,8 and 10s. The amplitudes of oscillation were varied from 30-800mm. These amounted to the following ranges Re=4025-45277 and Kc=2.09-55.85.

The general waveform of the drag force occurs yet again with the late spike at high βd and low Kc, and the plateau becoming more pronounced with increasing Kc.

The zero drag position migrates forwards with increasing Kc, the magnitude of migration becoming slightly larger with increasing βd.

7.6 Drag measurements for G/d=0.125 (figs H.41 - H.48)

This group of tests was performed with the 120mm diameter test cylinder at periods T=2,4,6 and 8s. The amplitudes of oscillation were varied from 15-600mm. These amounted to the following ranges Re=5660-56596 and Kc=0.79-31.42.

For βd=150.46 the spike occurs relatively late and at high Kc appears to be rather small in magnitude. The zero drag position remains in approximately the same position.

At the lower values of βd, the waveform is characterized by a severe spike followed by a gradual decrease at low Kc with the plateau developing at higher values of Kc. At higher Kc the peak is sometimes slightly larger than the spike and is followed by a rather sudden drop in drag force. Zero drag positions move forwards by $\pm 50^{\circ}$.

7.7 Drag measurements for G/d=0.25 (figs H.49 - H.56)

This group of tests was performed with the 120mm diameter test cylinder at periods T=2,4,6 and 8s. The amplitudes of oscillation were varied from 15-600mm. These amounted to the following ranges Re=5660-56596 and Kc=0.79-31.42.

Waveforms for this gap ratio are of a virtually identical nature

to those for the gap ratio of 0.125. See paragraph 7.6.

7.8 Drag measurements for G/d=0.5 (figs H.57 - H.64)

This group of tests was performed with the 120mm diameter test cylinder at periods T=2,4,6 and 8s. The amplitudes of oscillation were varied from 15-600mm. These amounted to the following ranges Re=5660-56596 and Kc=0.79-31.42.

For βd=150.46, at low Kc the spike occurs even later than is usually the case, and it is preceded by an equally severe negative spike. This phenomenon reduces in magnitude with increasing Kc.

As before, with the remaining βd, the spike is followed by a slight rise in drag force up to the peak at high Kc and the zero drag position migrates by $\pm 50^{\circ}$.

7.9 Drag measurements for G/d=0.6, 0.75 and 1.0

As discussed in chapter 6 the boundary does not influence the flow patterns at a gap ratio larger than 0.5. A detailed discussion is therefore not considered to be necessary and the drag force vs phase plots have been omitted. However, the results of the tests are given in Appendices F and I.

8. EXAMINATION OF TRENDS

The variations of the waveforms of both lift and drag forces with differing flow conditions have been discussed in the previous two chapters. This chapter involves a discussion of the force coefficients associated with particular flow conditions namely, Cl+, Cl-, Clamp, Cd, Cm and Cdmax. These coefficients have been plotted against Kc, Re and G/d but it was found that plots of coefficients vs Kc were most useful and hence the majority of the data has been plotted against Kc. Also, since the available literature uses Kc as parameter, this is more advantageous from a comparison point of view. Plots of coefficient vs Kc are given in two ways.

1) For a constant βd with all corresponding gap ratios plotted on the same axes.
2) For a constant gap ratio with the results of all the corresponding βd plotted on the same axes.

Direct results may be obtained from Appendix F and the plots mentioned above are given in Appendix I. This chapter has been divided into lift coefficient vs parameter and drag coefficient vs parameter. They have been further subdivided according to the type of plots mentioned above.

The range of testing undertaken in this work is shown in Table 8.1 overleaf.

Bd / G/d	50-51	55-56	63-65	73-80	84-87	103-106	113	146-151
0.01	5660-45277 6.98-55.85	5306-42447 5.24-41.89	4716-37731 3.49-27.93	4245-33958 2.09-16.76				
0.03125				7074-56596 3.93-31.42	6288-50307 2.62-20.94	5660-45277 1.57-12.57		5660-45277 0.79-6.28
0.046875				6708-53660 3.93-31.42	5962-47698 2.62-20.94	5366-42928 1.57-12.57		5366-42928 0.79-6.28
0.0625				6889-55111 3.93-31.42	6123-48988 2.62-20.94	5511-44089 1.57-12.57		5511-44089 0.79-6.28
0.09375	5660-45277 6.98-55.85	5031-43587 5.24-41.89	4472-38744 3.49-27.93	4025-32196 2.09-16.76				
0.125				7074-56596 3.93-31.42	6288-50307 2.62-20.94	5660-45277 1.57-12.57		5660-45277 0.79-6.28
0.25				7074-56596 3.93-31.42	6288-50307 2.62-20.94	5660-45277 1.57-12.57		5660-45277 0.79-6.28
0.5				7074-56596 3.93-31.42	6288-50307 2.62-20.94	5660-45277 1.57-12.57		5660-45277 0.79-6.28
0.6	5306-42447 5.24-41.89						4245-33958 1.05-8.38	
0.75	5306-42447 5.24-41.89						4245-33958 1.05-8.38	
1	5306-42447 5.24-41.89						4245-33958 1.05-8.38	

LEGEND
Reynolds no.
K-C no.

Table 8.1 : Dimensionless parameter ranges

8.1 Lift coefficients vs parameter

8.1.1 Lift coefficients vs Kc for constant gap ratio and differing βd.

1) Positive peak (Cl+) ; Figs I.61-I.68 ; One figure constitutes the results of tests undertaken at different βd for one gap ratio. The most outstanding feature when considering this series of figures is the repeatability of the curves or in other words, the curves tend to follow a similar pattern regardless of βd. This is most likely due to the fact that the values of βd are rather high ie. the cylinder diameter is large in comparison to the oscillatory boundary layer.

   Regardless of gap ratio, the curves all rise sharply to a peak at low Kc and then fall gradually with increasing Kc, until Cl+ is very small at large Kc. For G/d=0.01 the peak occurs at Kc=±5 and increases slightly with increasing gap ratio up to G/d=0.5 where the peak occurs at Kc=±10.

   Also, it appears that the general trend is for higher values of Cl+ to be found at higher βd, although there is only a slight variance. The ranges of the curves for each βd are different seeing as the period controls the maximum amplitude due to the available maximum velocity.

   The magnitude of Cl+ peaks decrease with increasing gap ratio as would be expected. It decreases steadily from approximately Cl+=6 for G/d=0.01 to approximately Cl+=2.5 for G/d=0.5.

2) Negative peak (Cl-) ; Figs I.69-I.76 ; As with Cl+ the curves follow similar paths regardless of βd. The form of the curves may be described as an opposite hand version of the Cl+ curves with a sudden downward fall to the negative peak at low Kc followed by a gradual increase with increasing Kc. These peaks move steadily from approximately Kc=2 for G/d=0.01 to approximately Kc=9 for G/d=0.5. Again the magnitude of Cl- peaks increase with increasing gap ratio, increasing steadily from Cl-=±-8 for G/d=0.01 to Cl-=±-2.5 for G/d=0.5. There does not appear to be any definite trend with regard to magnitudes of Cl- at different βd.

3) Amplitude of lift coefficient (Clamp) ; Figs I.77-I.84 ; Yet again the curves follow similar paths regardless of βd, however the curve shape does vary from Cl+ and Cl- curves slightly. At low gap ratios the curve starts from a peak at low Kc and then Clamp reduces steadily with increasing Kc. For gap ratios G/d=0.0625-0.5 the curve is similar to that for Cl+, with a sudden rise to a peak at low Kc followed by a gradual fall with increasing Kc. There is a general decrease in magnitude of the peak with increasing gap ratio, falling from Clamp=±10 for G/d=0.03125 to Clamp=±4.5 for G/d=0.5. There appears to be no trend with regard to magnitudes of Clamp at different βd since the curves follow very similar paths. As with Cl+ and Cl-, these peaks of Clamp occur in the range Kc=0-10, with Kc=±2.5 for G/d=0.01 and increasing steadily up to Kc=±10 for G/d=0.5.

8.1.2 Lift coefficients vs Kc for constant βd and differing gap ratio.

For this series of figures, one figure represents a series of results at different gap ratios performed at the same value of βd.

1) Positive peak (Cl+) ; Figs I.1-I.4 and I.13-I.16 ; As found in the previous paragraph, the magnitudes of Cl+ do not vary substantially with βd. As expected, the magnitudes of Cl+ are highest at the smallest gap ratio and decrease with increasing gap ratio. As stated before the peaks generally occur in the range Kc=0-10, depending on the gap ratio, but usually at Kc=±6.

2) Negative peak (Cl-) ; Figs I.5-I.8 and I.17-I.20 ; Curves are of the usual shape with a fall to the peak at low Kc followed by a gradual increase with increasing Kc. The position of the peak varies with gap ratio but remains in the region Kc=0-10. Curves are usually most negative for the small gap ratios and become less negative with increasing gap ratio.

3) Amplitude of lift coefficient (Clamp) ; Figs I.9-I.12 and I.21-I.24 ; The curves have a rather flatter rise to the peak which is followed by the gradual decline with increasing Kc. These peaks, in the range Kc=0-10 differ in location according to gap ratio. As before the largest amplitudes of lift coefficient are to be found with the smallest gap ratios, becoming smaller with increasing gap ratio. Magnitudes of Clamp do not differ substantially with βd.

8.1.3 Lift coefficients vs Kc for constant βd and G/d=0.6, 0.75 and 1.0

1) Positive peak (Cl+) ; Figs I.25-I.26 ; Curves for these three gap ratios follow almost identical paths and since it was found in chapters 6 and 7 that the waveforms for these gap ratios differed from that for a gap ratio of 0.5 and less, it has been concluded that the boundary does not play a role for gap ratios larger than 0.5. At low Kc there is a slight fall to a short plateau which is followed by a sudden increase in Cl+. The peak occurs at approximately Kc=13 and then gradually falls to zero with increasing Kc. The maximum magnitude of Cl+ appears to be ±2.

2) Negative peak (Cl-) ; Figs I.27-I.28 ; Again similar curves are followed by all three gap ratios indicating that they are unaffected by the boundary. A slight increase to a plateau at low Kc is followed by a sudden decrease in Cl- to the peak which is followed by a gradual increase to zero with increasing Kc. The peak would appear to exist in the region Kc=5-8 and Cl- has a magnitude =±-3

3) Amplitude of lift coefficient (Clamp) ; Figs I.29-I.30 ; Very similar curves exist for each gap ratio with the peak at Kc=±13 of magnitude approximately Clamp=3.5. For both Cl+ and Clamp there appears to be a crossover at Kc=±3. Below Kc=3, the magnitudes of the coefficients for G/d=0.6 are smallest and above Kc=3 they are largest.

8.1.4 Clamp vs other parameters

1) Clamp vs gap ratio for constant βd and different Re ; Figs I.109-I.112 ; It is clear from this series of curves that the amplitude of lift coefficient increases with decreasing values of Re or Kc. Also, for a particular value of Re, the Clamp vs G/d curve rises slowly in the region G/d=0.03-0.06 and then undergoes a steeper rise which soon flattens out and continues at the same value. This curve type holds true for the higher Re range, depending also on the value of βd.

2) Clamp vs Re for constant gap ratio and different βd ; Figs I.117-I.118 ; These curves are provided merely to illustrate the similarity between curves of parameter Kc or Re. Kc was found to be more useful in the discussion of waveforms in chapters 6 and 7 and therefore it was used in this chapter primarily to maintain continuity and to provide a comparison with other research. Considering figures I.78 and I.84, it will be noted that the curves show identical trends except that the X-axis range is different.

8.2 Drag coefficients vs parameter

8.2.1 Drag coefficients vs Kc for constant gap ratio and differing βd.

1) Drag coefficient (Cd) ; Figs I.85-I.92 ; As for the lift coefficients the curves follow similar paths at different βd. However, the curves for βd=±85 generally appears to be elevated above the other βd curves, the degree of this

elevation decreasing with increasing Kc. The curves generally all begin with a rapid fall in Cd, and with increasing Kc the fall becomes more gradual. The curves usually begin to flatten in the region Kc=5-10. Magnitudes of Cd become smaller with increasing gap ratio with the exception of G/d=0.01 where magnitudes are comparatively small.

2) Inertia coefficient (Cm) ; Figs I.93-I.100 ; There are no apparent trends with regard to curve shape for the inertia coefficient although there is a remarkable repeatability of the curve shapes at the different values of G/d. For a given gap ratio, the largest magnitude of Cm is achieved with βd=±85 up to Kc=±10 where βd=±75 becomes the curve of largest magnitude of Cm. The highest βd always yields the lowest curve of Cm. Magnitudes of Cm drop steadily with increasing gap ratio from an average Cm of ±3 for G/d=0.01 down to an average Cm of ±1 for G/d=0.5.

3) Maximum drag coefficient (Cdmax) ; Figs I.101-I.108 ; This curve type is very similar to that of Cd with a sudden fall followed by a gradual fall. The transition from rapid to gradual fall occurs in the region Kc=5-10 for all gap ratios. As for Cd, the magnitudes of Cdmax appear to be largest for the largest value of βd, decreasing in magnitude with decreasing βd. Magnitudes of Cdmax do tend to decrease slightly with increasing G/d although this trend is not very noticeable.

8.2.2 Drag coefficients vs Kc for constant βd and differing gap ratio.

1) Drag coefficient (Cd) ; Figs I.31-I.34 and Figs I.43-I.46 ; Remarkably similar curves are followed at each gap ratio indicating that, as determined in the previous paragraphs, the boundary does not have as large an influence on the drag coefficient as it does on the lift coefficient. It is quite clear that the drag coefficients decrease with increasing gap ratio. Curve shapes are quite uniform with a steep fall followed followed by a gradual fall, the transition taking place at roughly Kc=2-10. It appears that the value of Kc at which transition takes place increases with decreasing βd. The magnitude of the drag coefficients decrease with decreasing βd.

2) Inertia coefficient (Cm) ; Figs I.35-I.38 and I.47-I.50 ; As discovered in 8.2.1, there are no apparent trends with the curve shape for Cm other than a slight tendency for the curve to rise up to Kc=±6 and then drop gradually with increasing Kc, although there are exceptions. As previously noted, the magnitudes of Cm increase slightly with decreasing βd although this trend is more apparent in 8.2.1.(2). There is a definite trend for inertia coefficients to decrease with increasing gap ratio.

3) Maximum drag coefficient (Cdmax) ; Figs I.39-I.42 and I.51-I.54 ; Highly repeatable curves occur with a steep fall followed by a gradual fall with the transition in the region Kc=2-10, the value of Kc increasing with decreasing βd. It is

quite clear that magnitudes of Cdmax decrease with increasing gap ratio and just as clear is the decrease in magnitude with decreasing βd.

8.2.3 Drag coefficients vs Kc for constant βd and G/d=0.6, 0.75 and 1.0

1) Drag coefficient (Cd) ; Figs I.55-I.56 ; Curve trends are remarkably similar and differ from the curve shape for G/d=0.5 and less, therefore again confirming the conclusion that the boundary does not effect fluid flow when the gap ratio is larger than 0.5. These curves rise up to Kc=±10 and then fall with increasing Kc. The values of Cd are actually mostly negative at βd=112.9.

2) Inertia coefficient (Cm) ; Figs I.57-I.58 ; As noted before, few trends are evident with the curve shape for Cm except that at βd=56.4 the magnitude of Cm remains relatively constant. Repeatability is extremely high, indicating once more that the boundary has little effect at these gap ratios.

3) Maximum drag coefficient (Cdmax) ; Figs I.59-I.60 ; The usual Cdmax curve is exhibited here with high repeatability. Transitions from steep to gradual falls takes place at approximately Kc=3 for βd=112.9 and Kc=15 for βd=56.4.

8.2.4 Cd vs other parameters

1) Cd vs gap ratio for constant βd and different Re ; Figs I.113-I.116 ; The most outstanding feature with this series of

curves is the trend for magnitudes of Cd to decrease with increasing Re or Kc. There is also the expected trend for the magnitude of Cd to decrease with increasing gap ratio for a constant value of Re, although this decrease is less than one would expect. Also, the magnitudes clearly decrease with decreasing βd.

2) Cd vs Re for constant gap ratio and differing βd ; Figs I.119-I.120 ; Once again these curves are given merely to illustrate that the information gained from a curve with Kc as parameter is also obtained when Re is made parameter. Reference to figures I.86 and I.92 will show that the only difference between curves of different parameter is the X-axis range. For reasons discussed earlier, Kc was chosen as parameter.

9. COMPARISON WITH OTHER WORK

The purpose of this chapter is to compare the results and techniques of previous research to that of the present work. There is an abundance of literature covering similar topics, including oscillatory and steady flow for spheres, cylinders, plates, rectangles etc. The forces on these objects have been investigated near a boundary or in a free stream and quite often with a series of test objects. The categories of research that are relevant to this work are:

i) A cylinder in steady flow near a boundary.
ii) A cylinder in oscillatory flow in a freestream.
iii) A cylinder in oscillatory flow near a boundary.

with the latter of course being of most significance. Each category will be dealt with individually.

9.1 A CYLINDER NEAR A BOUNDARY IN STEADY FLOW

Because the oscillatory and steady flow conditions differ substantially, one research paper of this category is provided merely as a reference. The most repeatedly referenced paper of this category was presented by Bearman and Zdravkovich (1978).

9.1.1 Bearman and Zdravkovich (1978)

Bearman and Zdravkovich used air as the fluid medium by placing a 19mm test cylinder in a 3m long wind tunnel with its axis normal to the freestream. The cylinder was pressure tapped at midspan and

by rotating it, pressure measurements could be made at any angular position. They performed tests at gap ratios up to G/d=3.5 and also used a smoke tunnel for flow visualization purposes.

The tests were carried out at two Reynolds numbers, $Re=2.5 \times 10^4$ and $Re=4.8 \times 10^4$. They found, in agreement with theory that the pressure distribution in the gap region decreases rapidly, causing a lift force away from the bed. They did however find that the bed influenced flow patterns for gap ratios less than G/d=0.3, whereas in this work it was found that the boundary affected the forces on the cylinder up to a gap ratio of G/d=0.5. The most likely reason for this disagreement is that the irregular vortex shedding influences the forces in conjunction with the influence of bed proximity. It is therefore expected that the transition gap ratio would be larger in the oscillatory case. Further, the velocity distributions differ substantially for the two flow conditions since oscillatory flow is associated with a boundary layer growth whereas for steady flow the distribution remains much the same.

Apart from this no further agreements or disagreements of any consequence were noted.

9.2 A CYLINDER IN OSCILLATORY FLOW IN A FREE STREAM

The results of this work show that flow forces approach their free stream values for gap ratios larger than G/d=0.5. Therefore, present work conducted at gap ratios larger than 0.5 may be compared with previous research in this category. It is usually the case that previous work is compared to the present case G/d= 1.0, $\beta_d = 56.42$.

9.2.1 Sarpkaya (1975, 1977, 1986)

Sarpkaya used a U-shaped vertical water tunnel of cross sectional area 456mm × 508mm. The test body was placed in one of the vertical shafts and he then oscillated the fluid medium with a slider crank mechanism. This mechanism was operated at a frequency that matched the natural frequency of the water column in the shaft. This consequently limited the range of frequencies at which testing could be undertaken. He measured force directly with a series of cantilever beams at the outer surfaces of the test section. He used Morison's equation together with the Fourier analysis, least squares method and modified least squares method to determine the drag and inertia coefficients and found that all three methods yielded "nearly identical results".

In his 1975 publication, Sarpkaya found no correlation between lift and drag coefficients with Reynolds number yet he concluded a good relation with the Keulegan Carpenter number. He does not produce much comment on the influence of KC on the drag and inertia coefficients. However, for lift he finds C_L reaching a maximum as high as three and even exhibiting more than one maxima. See figure 9.1. He found high scatter in the region KC=20-25 and very high lift forces in the region KC=4-10. The results of the present work performed at gap ratio G/d=1.0 and β_d=56.42 have been compared with those of Sarpkaya in figure 9.1. They exhibit quite similar shapes although present values appear to be slightly larger. His lift curves show two maxima which is unusual and are generally larger in magnitude than the present results. The present magnitudes of drag and inertia coefficients are slightly larger than those shown by Sarpkaya, yet they follow similar

paths. He comments that in the range KC=4-10, the in-line force is essentially of an inertial nature and he suggests that in this range the drag and transverse forces may be ignored. The present results indicate that this would be an unacceptable decision since this would seriously underestimate the total force acting on the cylinder.

In his 1977 publication, Sarpkaya went about the research using a different approach. He decided that Reynolds number was not the most suitable parameter "since the effects of viscosity are small." He replaced Reynolds number with the parameter β=Re/KC and performed tests over a wide range of KC (KC=0-150), but he also tested at a wide range of β. Since β is constant at any particular period, this means that he performed tests at numerous periods whereas in this research only two periods were investigated at the gap ratio G/d=1. A graphical comparison is therefore not suitable because his graphs are drawn with β as parameter and only two points of the present work could be superimposed. He did, however, comment that Cd decreases with increasing Reynolds number to a value of Cd=±0.5 (depending on KC) and then gradually rises to a constant value of Cd=±0.65 for Reynolds number larger than 40,000. Present results indicate that no subsequent rise in drag force would occur in this region. He concludes that the inertia coefficient increases with increasing Re, reaches a maximum and then gradually approaches a value of Cm=±1.75. Further, the lift coefficient depends on Reynolds number for Re>20,000 and rapidly decreases to about 0.2 for larger Re.

Sarpkaya's 1986 publication has been devoted to a very low range of Keulegan Carpenter number (KC=0.2-10) and typically only two

present data points fall in this range. It has therefore been decided that this publication is not suitable for comparison.

9.2.2 Sawamoto et al (1980)

Sawamoto and his colleagues used the standing wave approach. The test cylinder was placed horizontally at a nodal point of a standing wave in a wave tank 20m long, 0.4m wide and 0.6m deep. The length of the tank was adjusted by a movable vertical wall, so that the standing wave would resonate under the given period. They measured lift and drag force using strain gauges that were attached to springs supporting the cylinder at both ends.

They examined the applicability of the Morison equation in which Cm and Cd were determined by the Fourier analysis. They found that for KC<5, Cd=±2 and the Morison equation expresses the instantaneous forces rather well. They also found that for KC>30, the equation can be used with good agreement to experimental work. They found, however, that for the range KC=10-30, the equation cannot express the force with sufficient accuracy, especially in the range KC=10-15. Sarpkaya (1975), however found rather good expression by the equation in this region and only found some scatter in the lift force at approximately KC=20-25. Sawamoto et al suggest a modification to the Morison equation that builds in a phase angle factor, to be determined by experiment.

Unfortunately, although present tests were conducted in a similar range of KC, Sawamoto et al tested in the range Re=200-13000, a range in which only two of the present test results fall. This means that the parameter β=Re/KC are quite different and for this

reason a graphical comparison is not suitable.

9.2.3 Maull and Milliner (1978)

Maull and Milliner used a U-tube with cross section 450mm x 450mm to oscillate water past a cylindrical test object. The column of water is driven by oscillating a piston in one of the limbs at the natural frequency of the column. They used two test cylinders of polished aluminium alloy with diameters 25.4mm and 38.1mm. The forces were measured using strain gauges and the signals recorded on magnetic tape for subsequent analysis by computer.

They carried out testing at two values of the viscous parameter β=Re/KC, β=200 and 443. KC was varied between 0 and 30. The lowest magnitude of β for the present work at G/d=1 is β=1013 but despite this difference, figure 9.2 shows a very good comparison between the respective results. Figure 9.2 is a relationship between KC and the root mean square of the drag force, the latter given by:

$$C_{F(RMS)}^2 = \frac{KC^2}{2} \left(3/4 \; Cd^2 \; KC^2 + \pi^4 \; Cm^2 \right)$$

The above equation is used in figure 9.2 with the inertia coefficient replaced by its potential flow value of 2. They choose a value of 1.45 for Cd but don't mention how they arrived at this figure, although most likely by trial and error to produce the best fit. Present results are rather well matched to this curve, despite the difference in β. Maull and Milliner point out that for this range of KC and that particular β, the constant values of Cd and Cm are adequate to predict the root mean square of the drag force.

Their lift data, also at β=200, shows considerable scatter and therefore a comparison has not been made. They conclude, that for β=200, the the root mean square drag coefficient may be used by assuming Cm=2, and the drag coefficient during a cycle may be considered as the addition of the inertia term and a further term which is a function of the vortex movement. The lift force and that part of the drag force due to vortex movement are thus strongly related.

9.3 A CYLINDER IN OSCILLATORY FLOW NEAR A BOUNDARY

9.3.1 Sarpkaya (1975, 1976, 1977)

Sarpkaya used the same experimental apparatus discussed in paragraph 9.2.1, except he placed the test cylinder closer to the side wall to investigate the effects of the wall proximity on the flow forces.

In his 1975 publication, he investigated the regions KC=2-40, Re=4,000-35,000 and G/d=0.01-1.0. He states that his results show in-line and transverse force could acquire large magnitudes and give rise to serious oscillations. For KC<3 the flow around the cylinder does not separate, the drag force is very small or negligible and the in-line and transverse forces are essentially from wave acceleration. The results of this work generally contradict this statement since it is usual that the highest Cd is found at this low range of KC. It is apparent in some cases however that the drag coefficient curve appears to increase in this low range of KC. He also finds that the drag coefficient peaks to a value of Cd=±3.75 at KC=7. See figure 9.4. He does not

however mention the magnitude of β=Re/KC or βd therefore it is difficult to isolate a family of present tests to compare directly. The present results for G/d=0.01, 0.09375 and 0.25 have been chosen for a comparison with Sarpkaya's G/d=0.014, 0.1 and 0.22 respectively. Figure 9.3 shows that the lift coefficients are rather well matched considering the difference in gap ratios. For G/d=0.09375, the present values for Cl+ are lower than Sarpkaya's values in the range KC=20-30. Figure 9.4 shows the drag coefficients to be well matched but for the inertia coefficient present values are significantly smaller than Sarpkaya's values, although they do possess similar curve shapes.

He concludes that for G/d larger than unity Cd and Cm values approach their freestream values. The present results show this transition to be G/d=0.5. He concludes further that it is not possible to explain the complex variations of Cd with KC since it is largely determined by separation effects. He is of the opinion that the predictions of the potential flow theory are in error, explaining that for intermediate values of KC, potential theory underestimates the transverse forces whereas for large KC it grossly overestimates them.

His 1976 publication is virtually a reprint of the 1975 edition and no new information is introduced.

In his 1977 publication, he cleverly arranged his testing in such a way that for a constant KC, he could vary the Reynolds number by changing the period. The testing in this work was not performed in this manner, and therefore only one point could be superimposed on his force plots which is inadequate for comparison.

With flow visualization he found that for very small gap ratios a jet like flow exists between the cylinder and the boundary. The flow separating from the top of the cylinder contained high frequency oscillations but did not curl up into vortices immediately behind the cylinder. He concluded that the gap blocks the flow and gives rise to earlier separation of the flow above the cylinder. This in turn increases the in-line and transverse forces.

He divided the transverse force into a component towards the wall (C_{LT}) and away from the wall (C_{LA}). He states that the former occurs at low velocity since the separation effects are minor, and that it is relatively small and fairly independent of gap ratio. This is supported by the results of this work since Cl+ is predominantly larger in magnitude than Cl-. The independence of gap ratio is however questionable since there is a noticeable trend for the force to reduce with increasing gap ratio. It has also been noted that the lift force towards the bed tends to decrease to approximately zero in the range KC=0-20.

He concluded that the dependence of Cl+ and Cl- on Kc is stronger than that on Re for values of Re less than 25000 and at that time he expected the dependence on Re to become stronger with larger Re. He concluded further that the effect of boundary proximity is to increase the force coefficients for gap ratios less than 0.5 which is confirmed by the results of this work. He explains that in this range $0<G/d<0.5$, the non-linear interaction between the shear layers emanating from the top and bottom of the cylinder is reduced and the frequency of oscillations in the shear layer is asynchronised. For gap ratios larger than 0.5, the regular vortex

shedding resumes, more or less unimpeded by the presence of the boundary and the lift, drag and inertia coefficients nearly assume their free cylinder values. This is supported by the results of this work yet he concluded a gap ratio G/d=1 for the inertia coefficients in the 1975 publication.

9.3.2 Ikeda and Yamamoto (1989)

Ikeda and Yamamoto used a plexiglass, U-shaped water tunnel 14m long with cross section 300mm × 300mm. They oscillated the fluid (water) with a piston driven by a DC motor. The test cylinders were placed horizontally in the middle of the working section. Force was measured by a strain gauged cantilever beam mounted rigidly to one side wall and connected to the cylinder on the free end. They used a hotfilm anemometer to measure the flow, conducting tests in the range KC=0-70. Unfortunately they only performed tests with the cylinder in contact with the boundary (i.e. G/d=0), yet there are some interesting similarities. A graphical comparison has not been presented since present testing at a gap ratio G/d=0 was not conducted. Their results have, however, been presented in figure 9.5.

They found that the force coefficients are significantly correlated to Kc and their flow visualization revealed the separation point to be closely correlated with the flow acceleration. They established that the inertia coefficients have a minimum value of approximately 1.75 at Kc=±12 and increase gradually to reach 3.5 for Kc>100. Figure 9.5 shows that the drag coefficient decreases gradually with increasing Kc for Kc>7 and finally reaches a value of approximately 1.2 at sufficiently high

Kc. They concluded from the steep slope in Cd at low Kc, that the coefficients depend not only on Kc but also on the period of oscillation.

The lift coefficients shown in figure 9.5 show considerable scatter but they do have the apparent trend to decrease with increasing Kc, to reach a constant value of approximately Cl=2.5. They are also about three times larger than the drag coefficients for a wide range of Kc. Their results indicate that the lift force generation for cylinders placed on the boundary is mainly due to the mean flow field such as undisturbed flow velocity and acceleration, and the vortices play a relatively minor role in the lift force generation when the cylinder is in contact with the boundary.

9.3.3 Wright et al (1979)

Wright et al generated gravity waves in a wave basin. This apparatus was capable of 1.5m wave heights and the wave energy was dissipated in a beach section. They used a 1m long extruded aluminium tube as their test cylinder and measured forces directly by using strain gauges which recorded the deflection of the test object. They performed testing in the ranges Re=2,000-200,000, KC=0.06-19 and G/d=0-2.

Because they passed gravity waves over the test cylinder and varied the still water level depth, their results have been presented in terms such as H/L, H/T^2, h/T^2 etc. which are not applicable to the results of this work. Where possible however, their results have been reworked to enable comparison.

For a gap ratio of G/d=0.042 they investigated the conditions KC=0.3 to 10.8. They established that for KC<1.3 both the horizontal and vertical forces vary nearly sinusoidally and result from an inertia dominated potential flow. The present work shows that lift varies sinusoidally up to KC=±2. For the range KC=1.3-5 the horizontal velocity begins to contribute to negative vertical forces, magnifying them threefold, while the transverse force away from the bed remains much the same. The in-line force appears to have doubled and keeps the sine wave pattern. For KC>0.8 the forces toward the bed approach a constant value while the forces away from the bed become dominant. They found that the point at which a wake forms and drag effects must be considered is KC=5. This is supported by Sarpkaya (1976) who predicts a 90% chance that flow asymmetrics will occur at this point.

They also found that the curve underwent a phase migration with varied KC. It is expected that if they had performed more tests, a very good comparison of this migration could have been made. They concluded that Cm increased as the gap ratio decreased. This was not found to be the case in the present work, where no relation with gap ratio could be established. They do not draw any conclusion as to the effect of gap ratio on the drag and inertia coefficients.

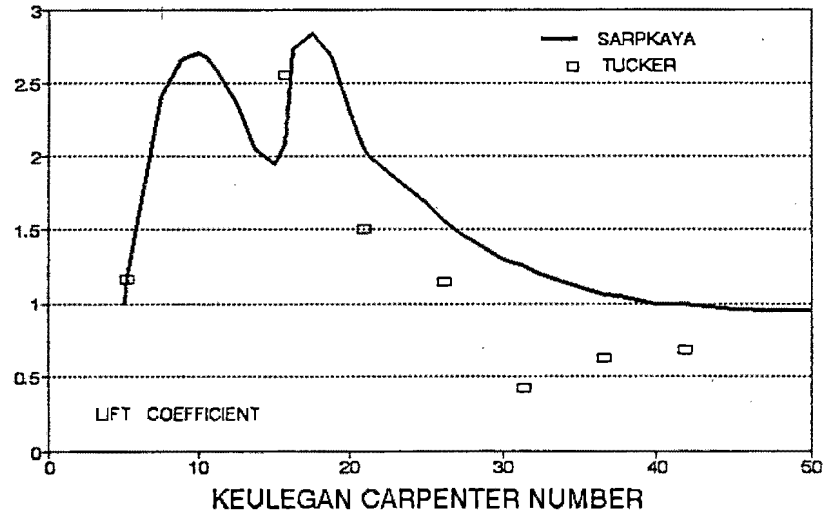

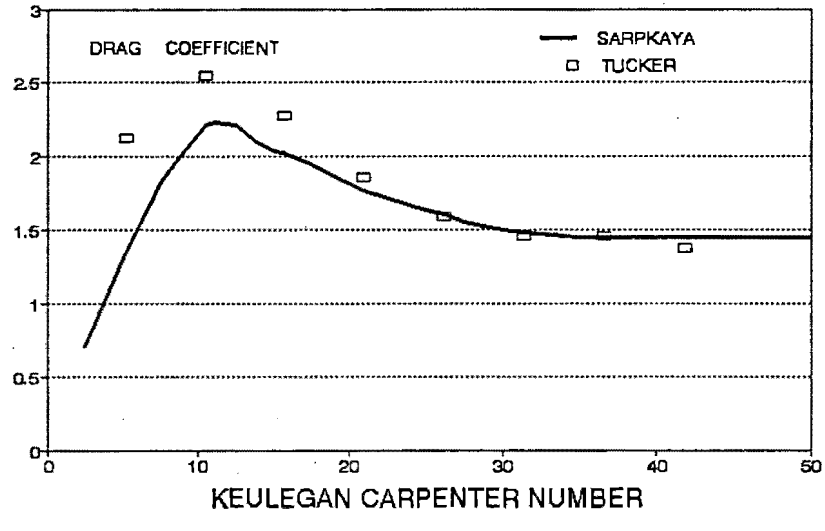

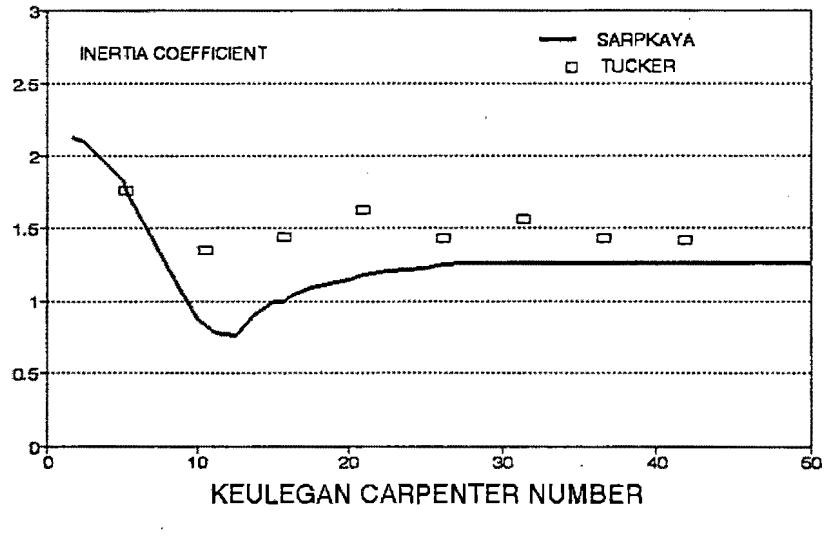

Figure 9.1 : Sarpkaya(1975) results for oscillatory flow in a freestream

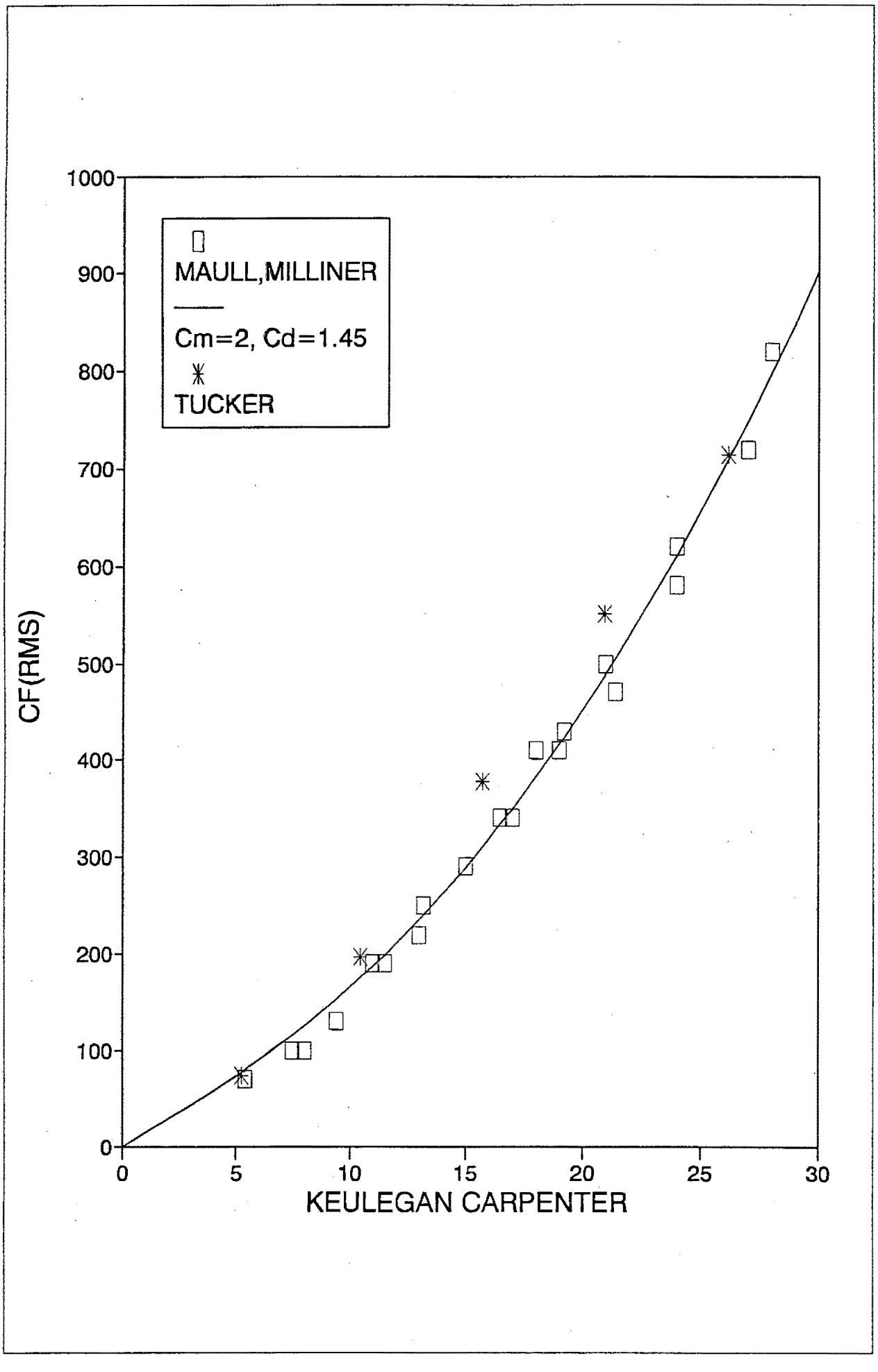

Figure 9.2 : Maull and Milliner (1978) results for oscillatory flow in a free stream

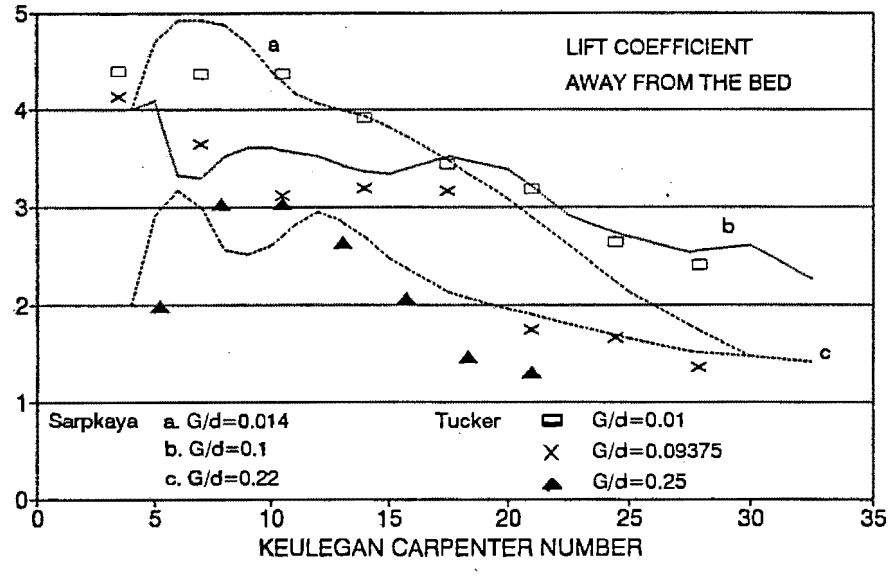

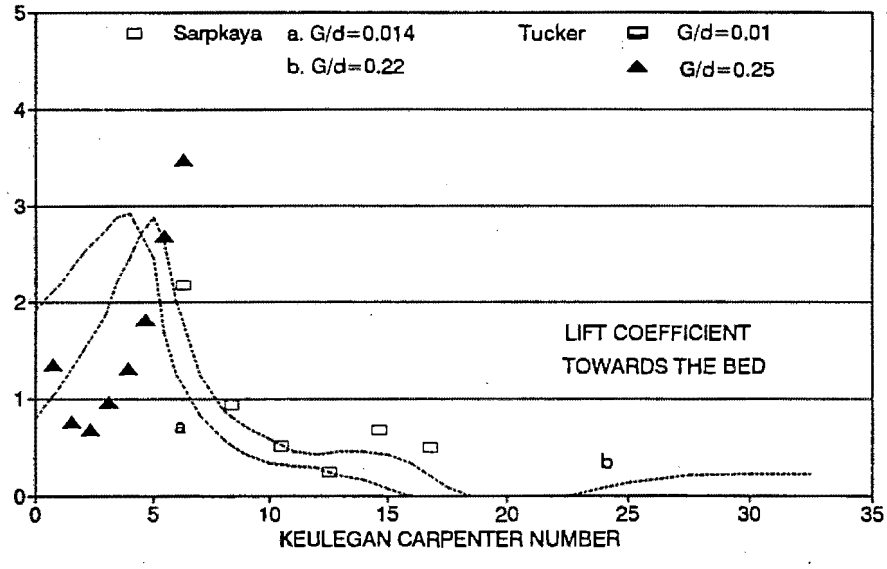

Figure 9.3 : Sarpkaya (1975,1976) lift coefficients for oscillatory flow near a boundary

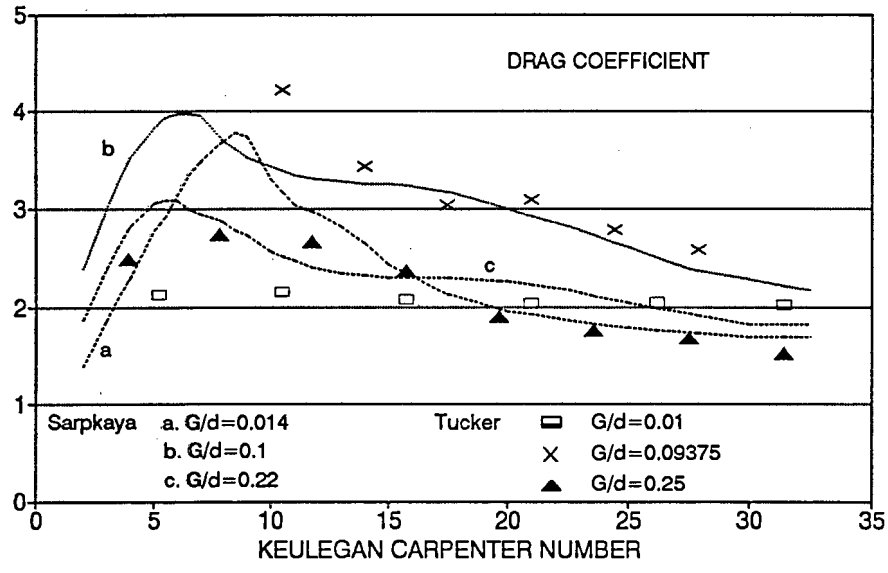

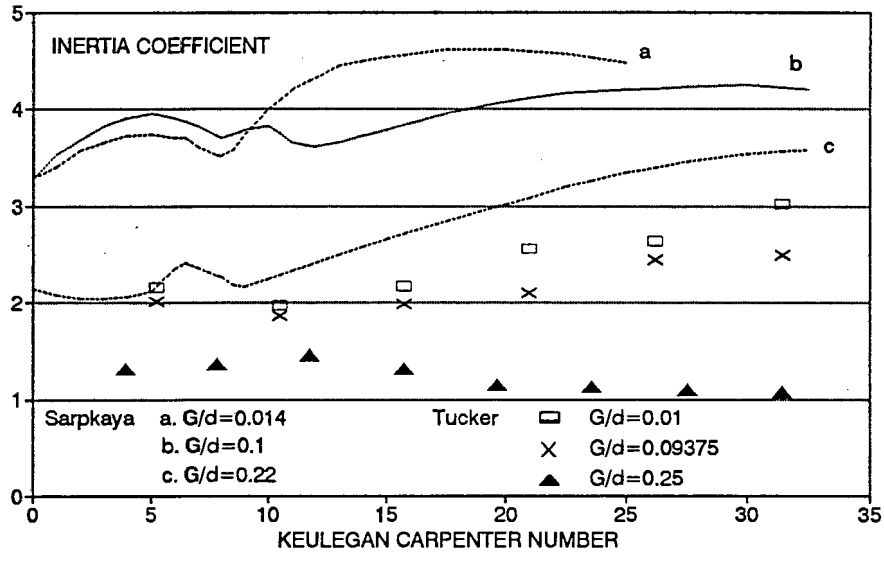

Figure 9.4 : Sarpkaya (1975,1976) drag and inertia coefficients for oscillatory flow near a boundary

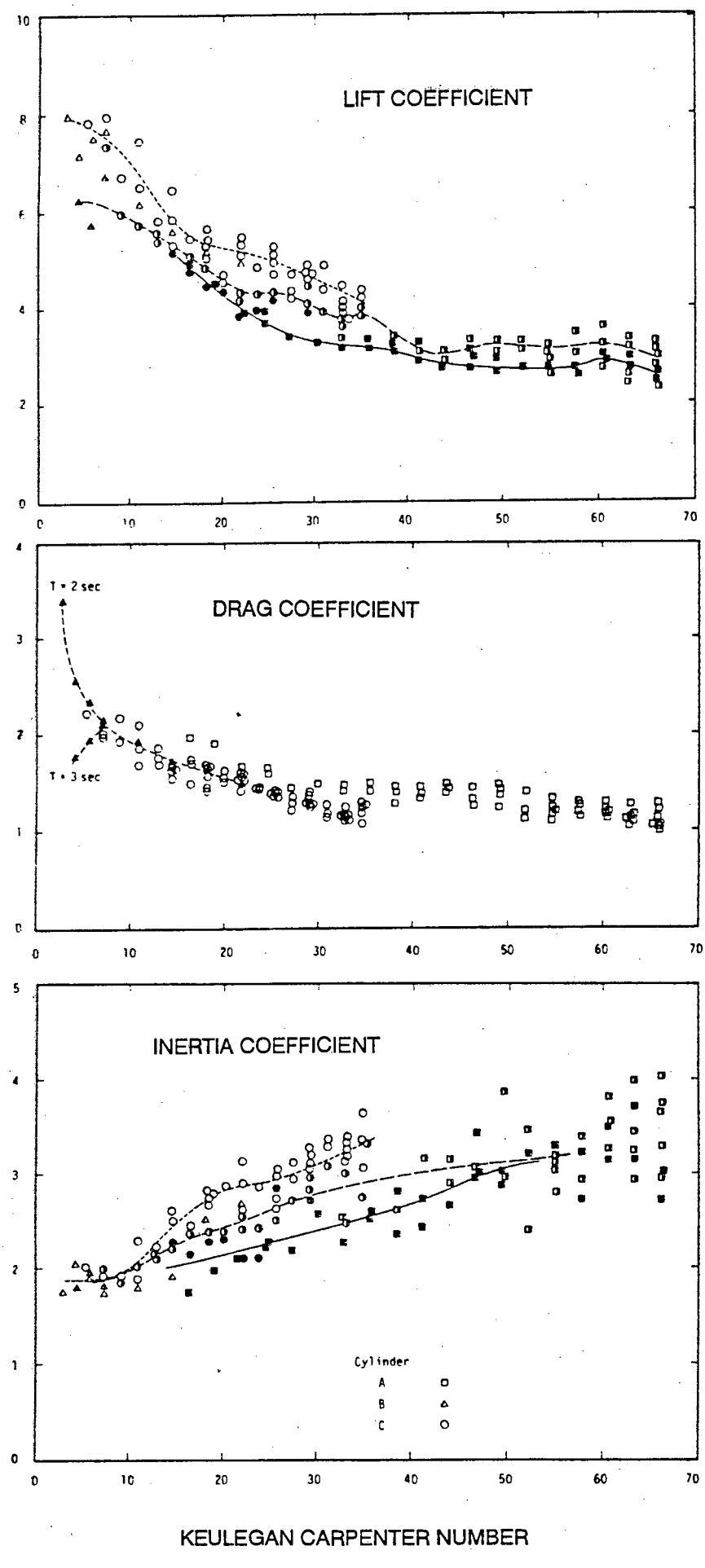

Figure 9.5 : Ikeda and Yamamoto (1989) lift, drag and inertia coefficients for oscillatory flow near a boundary

10. CONCLUSIONS

From the results and findings of this work, the following conclusions have been drawn.

1) The maximum value of Reynolds number at which tests were performed in this work was Re=56600 or 0.57×10^5. This means that only laminar boundary layers have been investigated since at this value of Reynolds number, the turbulent boundary layer has not yet developed.

2) Since the curves follow an extremely repeatable pattern at short periods, it may be assumed that lift force measurements at short periods, or high βd, yield more accurate results than those at long periods, or low βd.

3) For a certain set of flow conditions, the lift force vs phase curve migrates backwards with increasing Keulegan Carpenter number or Reynolds number. In some instances the negative peak will remain at a particular phase while the positive peak continues to migrate, causing an increased slope from negative to positive peak.

4) Lift forces usually act away from the boundary at small values of the Keulegan Carpenter number with the direction tending to act more towards the boundary as the Keulegan Carpenter number is increased.

5) Lift and drag force vs phase plots develop regular curve shapes at certain conditions but unfortunately it is difficult

to characterize a certain curve shape with a range of Keulegan Carpenter or Reynolds number.

6) It appears that if the lift force vs phase curve has a shape other than that of the rectified sine wave, then the increasing slope (from Cl- to Cl+) invariably tends to be steeper than the falling slope (from Cl+ to Cl-). In some cases this transition is very sudden, causing a rapid change from lift towards the bed to lift away from the bed.

7) If the cylinder is mounted at a gap ratio larger than G/d=0.5, then lift and drag forces approach their freestream values. This has been confirmed by both the waveforms and the coefficient curves. It was also found that for gap ratios less than 0.5, the force coefficients were increased.

8) The drag force vs phase plot always has a sudden increase preceded by equally sudden but less pronounced decrease in drag force immediately after velocity reversal. This occurs due to the interaction of the wakes of the two half-cycles.

9) Both lift and drag coefficient peaks tend to be largest in the range Kc=2-10. For values of Keulegan Carpenter number larger than approximately 10, the coefficients usually decrease in magnitude with increasing Keulegan Carpenter number.

10) For the low range of the Keulegan Carpenter number (KC=0-3.14) lift forces are approximately eight times smaller in magnitude than the in-line forces. Depending on the parameters of the flow conditions, lift may be ignored in this range.

11) Various researchers have contributed to the development of a unique and sophisticated apparatus to measure the effects of flow forces on objects close to a boundary in oscillatory flow.

12) Pressure measurement is an accurate and reliable method of obtaining the lift and drag forces indirectly. This method has the advantage that the pressure distribution around the cylinder can also be used whereas direct force measurement produces only the measured force.

11. RECOMMENDATIONS

The following recommendations for further work have been made.

1) A larger diameter test cylinder (300mm-500mm) should be used to investigate the results at larger values of the Reynolds number. Also, the possible change in results at the transition from laminar to turbulent boundary layers should be investigated, along with turbulent boundary layer results.

2) A smaller diameter test cylinder (±40mm) should be used to investigate the effect of βd more thoroughly. Reducing the test cylinder diameter will yield a lower range of βd and it would be most desirable if tests could be conducted where the oscillatory boundary layer is of a similar magnitude to the test cylinder diameter (ie. $\beta d=\pm 1$).

3) Since the force coefficients are most critical in the Keulegan Carpenter number range Kc=2-10, an extensive investigation of results in this range would be useful.

4) Tests could be performed with the test cylinder mounted on the boundary and partially embedded in the boundary. It would be even more desirable to conduct tests with the test cylinder partially embedded and covered by a protective mat, as sometimes used in the field. This, however would be difficult to achieve by using pressure measurement.

12. BIBLIOGRAPHY

REFERENCES CITED IN SCRIPT

Armitage N.P, *Determination of lift force on a sphere in oscillatory flow near a boundary using pressure measurement,* MSc dissertation, University of Cape Town, 1989

Bellamy M.R, *Lift forces on a sphere close to a boundary in oscillatory flow,* MSc dissertation, University of Cape Town, 1989

Bearman P.W, Downie M.J, Graham J.M.R and Obasaju E.D, *Forces on cylinders in viscous oscillatory flow at low Keulegan-Carpenter numbers,* J. Fluid Mech., vol. 154, pp337-356, 1985

Bearman P.W and Zdravkovich M.M, *Flow around a circular cylinder near a plane boundary,* J. Fluid Mech., vol. 89, Part 1, pp33-47, 1978

CERC - Coastal Engineering Research Centre, *Shore protection manual,* vol. 1,2 ,U.S. Government Printing Office, Washington,1977

Clauser F, *Turbulent boundary layer,* Advances in Applied Mechanics, Vol. 4, Academic Press, pp 1-51, 1956

Coleman N L, *Velocity profiles with suspended sediment,* J. Hydraulic Res.,(19), No. 3, pp 211-229, 1981

Horikawa K and Watanabe A, *Laboratory study on oscillatory boundary layer flow,* Coastal Eng. in Japan, vol. 11, pp13-28, 1968

Ikeda S and Yamamoto Y, *Oscillatory flow forces on cylinders placed on the bottom boundary,* J. Hydroscience and Hydr. eng., vol. 7, no. 1, pp35-49, 1989

Jonsson I G, *A new approach to oscillatory rough turbulent boundary layers,* Ocean Engineering, Vol. 7, Oxford England, pp109-152, 1980

Kajiura K, *A model of the bottom boundary layer in water waves,* Bull. Earthquake Inst., Vol. 46, University of Tokyo, pp75-123, 1968

Massey B.S, *Mechanics of fluids,* 4th edition, Van Nostrand Reinhold Company, 1979

Maull D.J and Milliner M.G, *Sinusoidal flow past a circular cylinder,* Coastal engineering, vol. 2, pp149-168, 1978

Milliner M G, *Forces on cylinders in oscillatory flow,* Phd dissertation, University of Cambridge, 1978

Milne-Thomson L.M, *Theoretical Hydrodynamics,* Macmillan and co., 1938

Rosenthal G.N, *Lift forces on spherical particles near a horizontal bed in oscillatory flow,* PhD dissertation,

Cambridge University, 1986

Rosenthal G.N and Sleath J.F.A, *Measurement of lift in oscillatory flow,* J. Fluid Mech., vol. 164, pp449-467, 1986

Sarpkaya T, *Forces on cylinders and spheres in a sinusoidally oscillating fluid,* Trans. ASME, J. Appl. Mech., vol. 42, Series E, pp32-37, 1975

Sarpkaya T, *Forces on cylinders near a plane boundary in a sinusoidally oscillating fluid,* Fluid Mech. in Petr. Ind., Symp. ASME Winter Annual Meet., Houston, Texas, pp43-47, 1975

Sarpkaya T, *Forces on cylinders near a plane boundary in a sinusoidally oscillating fluid,* Trans. ASME, J. Fluids Eng., Vol. 98, Series I, pp499-505, 1976

Sarpkaya T, *In-line and transverse forces on cylinders in oscillatory flow at high Reynolds numbers,* J. Ship Research, vol. 21, pp200-216, 1977

Sarpkaya T, *In-line and transverse forces on cylinders near a wall in oscillatory flow at high Reynolds numbers,* Paper no. OTC-2898, Ninth Annual Offshore Technology Conference, Houston, Texas, 1977

Sarpkaya T, *Force on a circular cylinder in viscous oscillatory flow at low Keulegan-Carpenter numbers,* J. Fluid Mech., vol.165, pp61-71, 1986

Sarpkaya T and Isaacson M, *Mechanics of wave forces on offshore structures,* Van Nostrand Reinhold, New York, 1981

Sawamoto M, Kikuchi K, Ohba M and Kashiwai J, *Forces on a circular cylinder in an oscillatory flow,* Coastal Engineering in Japan, Vol.12, pp147-158, 1980

Sleath J F A, Sea bed mechanics, John Wiley and Sons Inc., New York, 1984

Stokes G G, *On the effect of the internal friction of fluids on the motion of pendulums,* Trans. Cambridge Philos. Soc., Vol 9, pp20-21, 1851

Verley R.L.P, Lambrakos K.F and Reed K, *Hydrodynamic forces on seabed pipelines,* Proc. ASCE, J. Waterway, Port, Coastal and Ocean Eng., vol.115, pp190-204, 1989

Wright J.C and Yamamoto T, *Wave forces on cylinders near plane boundaries,* Proc. ASCE, J. Waterway, Port, Coastal and Ocean div., vol.105, pp1-13, 1979

Yamamoto T, Nath J.H and Slotta L.S, *Wave forces on cylinders near plane boundary,* ASCE, J. Waterways, Harbours and Coastal Eng. div., vol. 100, pp345-359, 1974

REFERENCES NOT CITED IN SCRIPT

Grace R.A and Zee G.T.Y, *Wave forces on rigid pipes using ocean test data,* Proc. ASCE, J. Waterway, Port, Coastal and Ocean div., vol. 107, pp71-92, 1981

Lugt H.J, *Vortex flow in nature and technology,* John Wiley and Sons, 1983

Murray C G, *Lift forces on stationary spheres in flow between Reynolds numbers 5,000 and 80,000,* Phd dissertation, University of Aberdeen, 1981

Nath J H and Yamamoto T, *Forces from fluid flow around objects,* Proc. 14th Conf. Coastal Engg., Copenhagen, pp1808-1827, 1974

Olson R.M, *Essentials of engineering fluid mechanics,* 4th edition, Harper and Row, New York, 1980

Potter M.C and Foss J.F, *Fluid mechanics,* John Wiley and Sons, 1975

Priest M.S, *Wave forces on exposed pipelines on the ocean bed,* Paper no. OTC-1383, Third Offshore Technology Conference, Houston, Texas, 1971

Schlichting H, *Boundary layer theory,* 6th edition, McGraw-Hill, 1968

Shaw T.L (ed), *Mechanics of wave induced forces on cylinders,* Pitman, California, 1979

Williamson C.H.K, *Sinusoidal flow relative to circular cylinders,* J. Fluid Mech., vol. 155, pp141-174, 1985

Wright J.C, *Wave forces on a horizontal circular cylinder near a plane boundary,* MSc. Dissertation, Oregon State University, 1976

Yuan S.W, *Foundations of fluid mechanics,* Prentice-Hall Inc., New Jersey, 1967

APPENDIX A - PERFORMANCE CHARACTERISTICS OF THE PRESSURE TRANSDUCERS

CHARACTERISTIC	MIN	TYP	MAX	UNIT
Operating pressure range	-	-	6.9	kPa
Sensitivity	-	2.6	-	mV/kPa
Full scale span	17	18	19	mV
Zero pressure offset	-1	0	+1	mV
Linearity and hysteresis	-	±0.2	±1	%FSO
Temperature effect on span	-	±0.4	±2	%FSO
Temperature effect on offset	-	±0.2	±1	mV
Repeatability	-	±0.2	±0.5	%FSO
Input impedance	-	4	-	kΩ
Output impedance	-	4	-	kΩ
Common mode voltage	4.7	5	5.3	V_{DC}
Response time	-	100	-	μsec
Long term stability of offset and span		±0.1	-	%FSO

APPENDIX B - DETAILS OF THE CONVERSION OF RAW TEST DATA TO PRESSURE UNITS

From the calibration process, we obtain a number of readings which allows a straight line representing the calibration curve to be drawn. See figure B.1.

When the test cylinder is stationary and the water in the flume is absolutely still, the offsets of each transducer are recorded by the A/D converter in A/D units. This may be interpreted as the A/D value that represents the static head on a particular transducer. This should not be confused with the zero reading which is the A/D value representing atmospheric pressure.

During data logging, the A/D converter records values that vary in the vicinity of the offset. Since only the kinematic pressures are of concern, the offset is subtracted from these instantaneously measured values. The conversion of A/D units to pressure is achieved as follows:

$$y = a + b\,x$$

$$\therefore \quad x = \frac{y - a}{b}$$

$$\therefore \quad \text{Kinematic pressure} = x_{\text{kinematic}} - x_{\text{static}}$$

$$= \left(\frac{\text{sample} - \text{zero}}{b}\right) - \left(\frac{\text{offset} - \text{zero}}{b}\right)$$

$$= (\text{Sample} - \text{offset}) \times 1/b$$

$$= (\text{Sample} - \text{offset}) \times \text{calib. factor}$$

Notice that the zero value has cancelled and is therefore not of great consequence in the conversion.

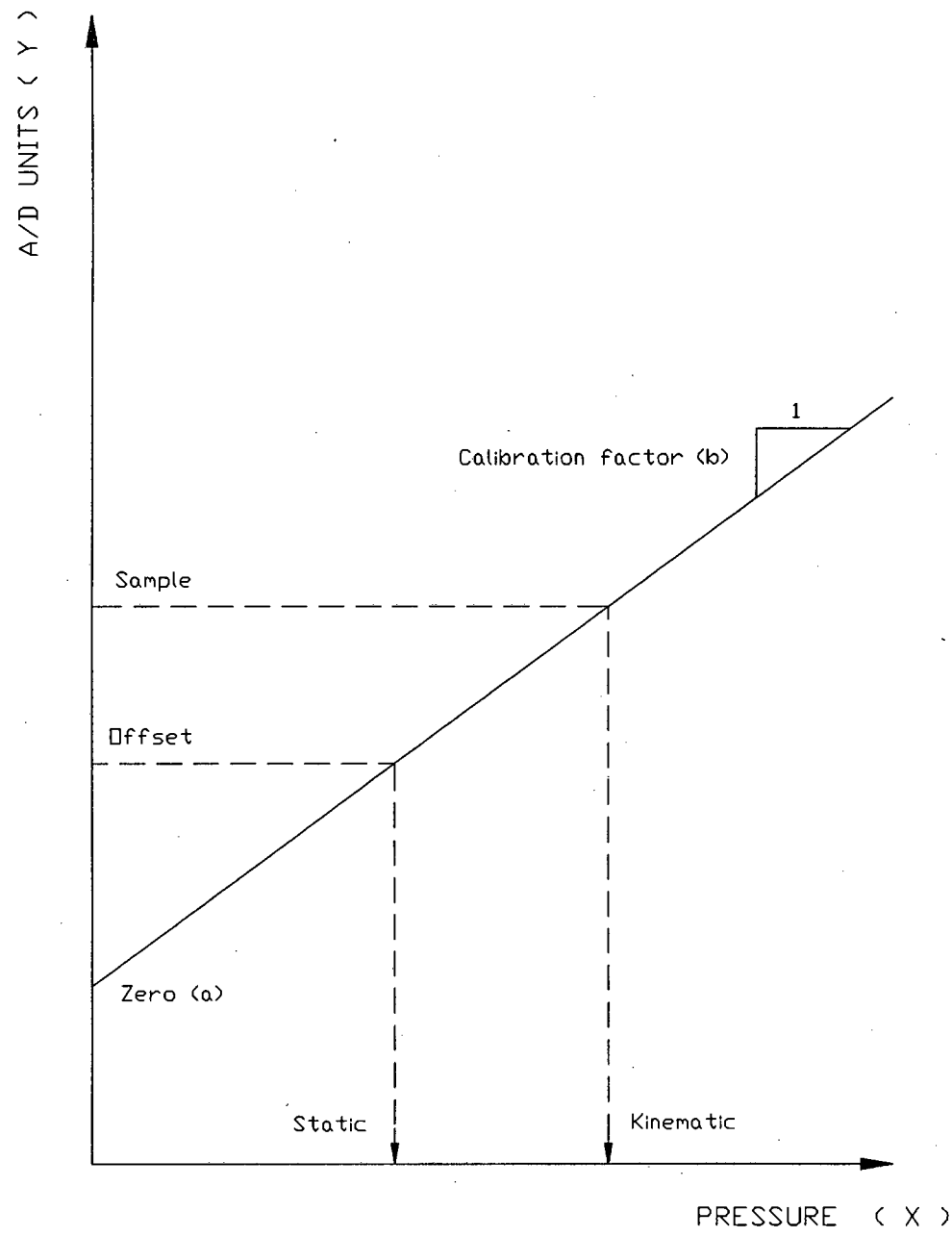

Figure B.1 : Calibration curve for the pressure unit conversion

APPENDIX C - DETAILS OF THE CONVERSION OF PRESSURE TO FORCE UNITS AND THE INTEGRATION PROCESS.

Consider a small wedge in the cross section of the test cylinder with an infinitesimally small included angle $d\Theta$. See figure C.1.

The arc length, $S = r \times d\theta$ with : r in m
: $d\theta$ in radians

Now consider that this arc length extends for 1m along the central axis of the cylinder. The area of the cylindrical arc is given by :

$$a = S\ (m) \times 1\ (m)$$
$$= r \times d\theta \quad (m^2)$$

The force acting on this area is determined by the measured pressure, which is assumed to be constant over the annulus.

$$f_{annulus} = P\ (N/m^2) \times a\ (m^2) \quad (N)$$

The lift and drag components of this force may be calculated by simple geometry. See figure C.2.

Now, to obtain the force acting over the entire surface of the hemisphere, the force equations are integrated over the respective orientation limits. i.e. for the lift force case,

$$f_L = P \times a \times \sin\theta$$
$$= P \times r \times \sin\theta\ d\theta$$

For a 30° wedge, $$F_L = \int_{\theta-15}^{\theta+15} f_L$$

$$= P \times r \times \left[-\cos \theta \right]_{\theta-15}^{\theta+15} \quad (N)$$

The net lift forces for each wedge are then algebraically added together to yield the total lift force.

Similarly, $$F_D = P \times r \times \left[\sin \theta \right]_{\theta-15}^{\theta+15} \quad (N)$$

Note that the above forces have units of Newtons for a metre wide strip.

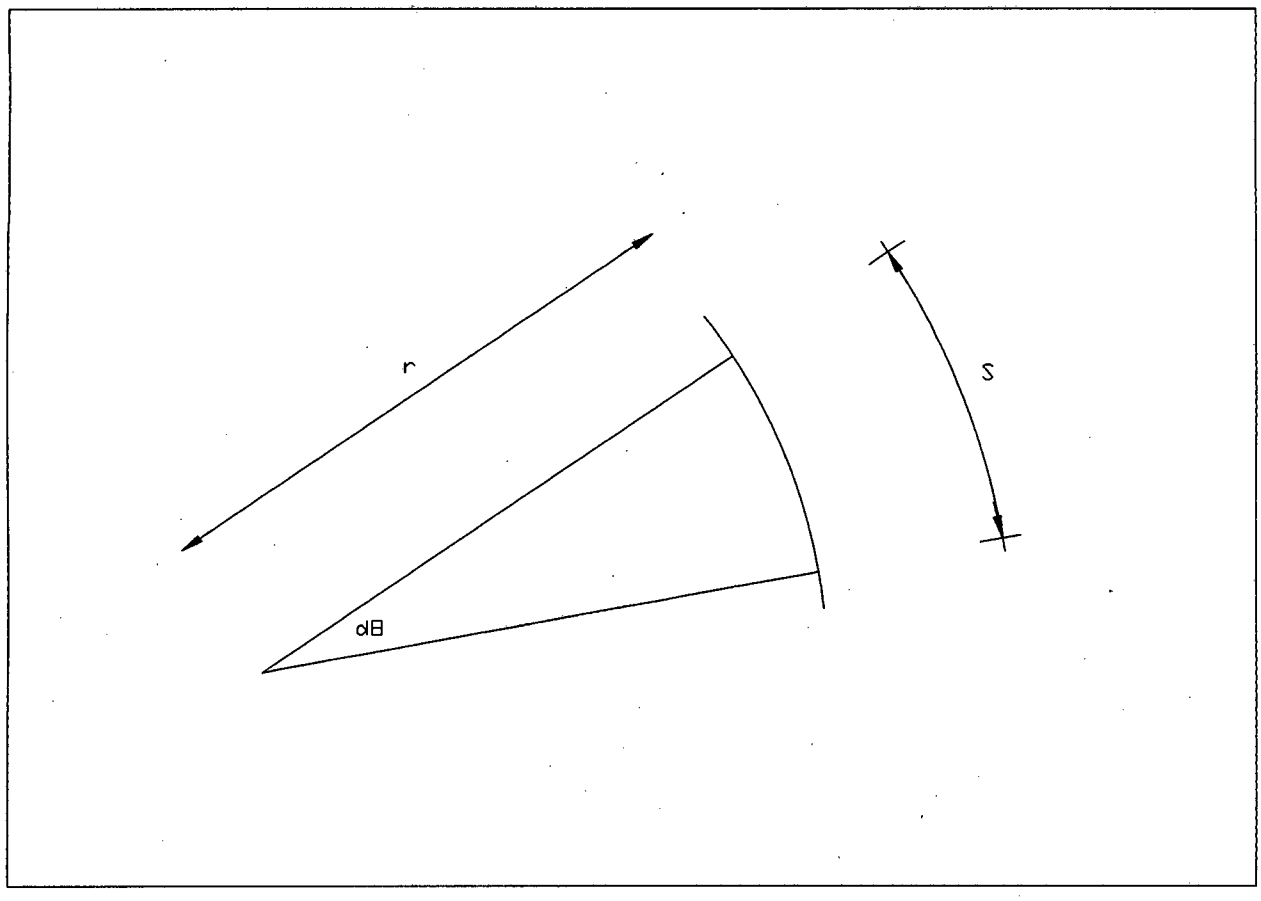

Figure C.1 : Small wedge of test cylinder cross section

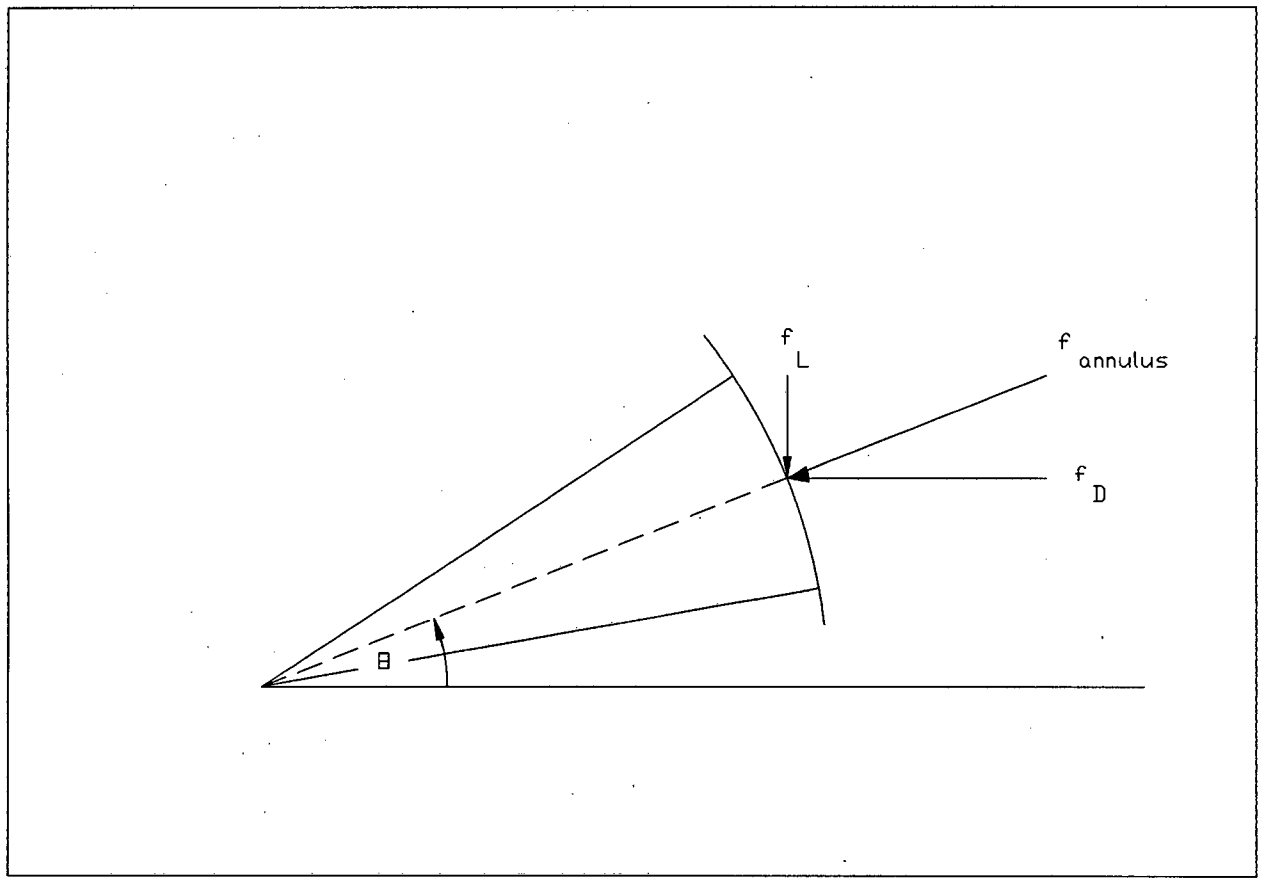

Figure C.2 : Lift and drag components of calculated force

APPENDIX D - IDENTIFICATION OF THE DATA FILES ON DISC

Due to the large number of files that were to be stored on disc, a coding system was developed so that by looking at the file name, the main parameters of the test could be determined.

A file name comprised three letters followed by three digits.

1. The first letter refers to the test cylinder diameter.
   A diameter = 90 mm was classed as "A".
   A diameter = 120 mm was classed as "B".

2. The second character refers to the gap ratio.
   A gap ratio of 0.01 was classed as "M".
   A gap ratio of 0.03125 was classed as "A".
   A gap ratio of 0.046875 was classed as "K".
   A gap ratio of 0.0625 was classed as "B".
   A gap ratio of 0.09375 was classed as "C".
   A gap ratio of 0.125 was classed as "D".
   A gap ratio of 0.25 was classed as "F".
   A gap ratio of 0.5 was classed as "H".
   A gap ratio of 0.6 was classed as "L".
   A gap ratio of 0.75 was classed as "I".
   A gap ratio of 1.0 was classed as "J".

3. The third character refers to the period of oscillation.
   A period of 2s was classed as "A".
   A period of 4s was classed as "B".
   A period of 6s was classed as "C".
   A period of 8s was classed as "D".

A period of 10s was classed as "E".

4. The digits following the letters equalled the amplitude of oscillation at which the test was performed.

For example: ABC120 - cylinder diameter = 90mm
gap ratio = 0.0625
period = 6s
amplitude = 120mm

Tests that were performed to check repeatability, phase lag, etc. were coded by CHK.

For example : CHK004 was the fourth check test.

APPENDIX E - PRINTOUT OF THE COMPUTER PROGRAMME " PIPEFORCES "

The following fourteen pages are a list of the computer programme which was written in Basic 3.0 on a Hewlett Packard HP9816. The programme was used primarily to calibrate the pressure transducers, run the data logging tests and plot the results shown in Appendices G and H.

The programme has undergone an evolutionary process. Bellamy(1989) wrote some of the subroutines in a similar manner to Rosenthal (1986). The "Force", "Amp_Measure", "Phase_lag" and "Microlink" subroutines were primarily written by Bellamy and edited by Tucker to adapt to pressure measurement. The remainder of the programme was written by Tucker.

```
  OPTION BASE 1
  RESET 7
  SEND 7;LISTEN 3 SEC 8 MTA
  OUTPUT 7 USING "#,B";0
  SEND 7;UNT UNL
  DEG
  DIM Filename$(4)[6],Param$(9)[11],Units$[20],Header(10),Transcalib(7)
  DIM Pulser(500),Sample(1400),Symmetry(1400),Dummy(1999),Samp(14000)
  DIM Average(1400),Total(1400),Pascal(1400),Offset(7)
  DIM Liftsample(1400),Dragsample(1400),Liftforce(200),Dragforce(200)
  DIM Clift(200),Cdrag(200),Zero(7),Ampp(2000),Phaselag(10)
  DIM Xstamp1(4),Xstamp2(4)
  DIM Ystamp1(4),Ystamp2(4)
  READ Xstamp1(*)
  DATA 0,5600,0,5600
  READ Xstamp2(*)
  DATA 5200,10800,5200,10800
  READ Ystamp1(*)
  DATA 4000,4000,600,600
  READ Ystamp2(*)
  DATA 7200,7200,3800,3800
!*****************************************************************************
Main_menu:      !
  PRINT CHR$(12)
  PRINT "*********************************************************************"
  PRINT "*                                                                   *"
  PRINT "*                MAIN MENU OF PIPEFORCES                            *"
  PRINT "*                                                                   *"
  PRINT "*                1. CALIBRATE TRANSDUCERS                           *"
  PRINT "*                                                                   *"
  PRINT "*                2. TEST PROCEDURE                                  *"
  PRINT "*                                                                   *"
  PRINT "*                3. PLOT FORCE vs PHASE                             *"
  PRINT "*                                                                   *"
  PRINT "*********************************************************************"
  PRINT
  PRINT "                CHOOSE ONE OF THE ABOVE OPTIONS"
  INPUT Optw
  IF Optw=1 THEN GOSUB Calibrate
  IF Optw=2 THEN GOSUB Testprocedure
  IF Optw=3 THEN GOSUB Force
  GOTO Main_menu
  STOP
!*****************************************************************************
Calibrate:    !
  PRINT CHR$(12)
  DISP "HOW MANY PRESSURE MEASUREMENTS PER CALIBRATION";
  INPUT N
  FOR Trans=1 TO 7
      RESET 7
      S1=2^Trans
      SEND 7;LISTEN 3 SEC 8 MTA
      OUTPUT 7 USING "#,B";S1
      GOSUB Calib
      GOSUB Regression
  NEXT Trans
  SEND 7;LISTEN 3 SEC 8 MTA
  OUTPUT 7 USING "#,B";0
  SEND 7;UNL UNT
  PRINT CHR$(12)
  PRINT "TRANSDUCER          ZERO          CALIBRATION FACTOR"
  PRINT "==========          ========      ======================"
  PRINT
  FOR I=1 TO 7
      PRINT USING "4X,D,15X,4D,15X,Z.5D";I;Zero(I);Transcalib(I)
      PRINT
  NEXT I
  PAUSE
  RETURN
 !*****************************************************************************
Calib:     !
  PRINT CHR$(12)
  PRINT
  PRINT "TRANSDUCER no. ";Trans
  PRINT
  PRINT "PRESS SOFTKEY 2 TO REPEAT READINGS"
  FOR I=1 TO N
      IF I=1 THEN
          WAIT 3
          DISP "1st POINT , ..... ZERO PRESSURE (ATMOSPHERIC)"
          Load(1)=0
      ELSE
          DISP "POINT (";I;")   PRESSURE IN mm (vertical)";
          INPUT Load(I)
          Load(I)=Load(I)*10
      END IF
      Count=1
Pulz: ENTER 70301 USING "#,W";Pulser(Count)
      WAIT .005
      IF Count<500 THEN
          Count=Count+1
          GOTO Pulz
      END IF
      Sumpulse(I)=SUM(Pulser)/500
      PRINT
      IF I=1 THEN
          PRINT "*************************RESULTS*************************
*"
          PRINT
      END IF
      PRINT "POINT( ";I;" )   PRESSURE = ";Load(I);" Pa   AVERAGE PULSER =
;Sumpulse(I)
      ON KEY 2 GOTO Calib
  NEXT I
  RETURN
  !*****************************************************************************
Regression:                                          !    LEAST SQUARE
  Sx=0
  Sy=0
  Sxy=0
  Sxx=0
  FOR I=1 TO N
      Sx=Sx+Load(I)
      Sy=Sy+Sumpulse(I)
      Sxy=Sxy+Load(I)*Sumpulse(I)
      Sxx=Sxx+Load(I)*Load(I)
  NEXT I
  Xbar=Sx/N
  Ybar=Sy/N
  B=(Sxy-N*Xbar*Ybar)/(Sxx-N*Xbar^2)
```

```
1190  A=Ybar-B*Xbar
1200  Zero(Trans)=A
1210  Transcalib(Trans)=1/B
1220  PRINT CHR$(12)
1230  PRINT
1240  PRINT "*************************************************************"
1250  PRINT "*                                                           *"
1260  PRINT "*          TRANSDUCER = ";Trans
1270  PRINT "*                                                           *"
1280  PRINT "*                    Y = ";A;"  +  ";DROUND(B,4);" X"
1290  PRINT "*                                                           *"
1300  PRINT "*       ZERO PRESSURE = ";A;"  COMPUTER UNITS"
1310  PRINT "*                                                           *"
1320  PRINT "*  CALIBRATION FACTOR = ";1/B
1330  PRINT "*                                                           *"
1340  PRINT "*************************************************************"
1350  PRINT
1360  DISP "PRESS CONT "
1370  PAUSE
1380  RETURN
1390 !*************************************************************************
1400 Testprocedure:!
1410  PRINT CHR$(12)
1420  PRINT "*************************************************************"
1430  PRINT "*                                                           *"
1440  PRINT "*               MENU FOR TEST PROCEDURE                     *"
1450  PRINT "*                                                           *"
1460  PRINT "*               1. PERIOD MEASUREMENT                       *"
1470  PRINT "*                                                           *"
1480  PRINT "*               2. AMPLITUDE MEASUREMENT                    *"
1490  PRINT "*                                                           *"
1500  PRINT "*               3. PHASE LAG MEASUREMENT                    *"
1510  PRINT "*                                                           *"
1520  PRINT "*               4. DATA LOGGING                             *"
1530  PRINT "*                                                           *"
1540  PRINT "*               5. EXIT TO MAIN MENU                        *"
1550  PRINT "*                                                           *"
1560  PRINT "*************************************************************"
1570  PRINT
1580  PRINT "               CHOOSE ONE OF THE ABOVE OPTIONS"
1590  INPUT Opt6
1600  IF Opt6=1 THEN GOSUB Measure_period
1610  IF Opt6=2 THEN GOSUB Amp_measure
1620  IF Opt6=3 THEN GOSUB Phase_lag
1630  IF Opt6=4 THEN GOSUB Logging
1640  IF Opt6=5 THEN GOSUB Main_menu
1650  GOTO Testprocedure
1660  RETURN
1670 !*************************************************************************
1680 Measure_period:                          ! SUBROUTINE TO MEASURE PERIOD
1690  PRINT CHR$(12)
1700  PRINT "*************************************************************"
1710  PRINT "*                                                           *"
1720  PRINT "*                  PERIOD MEASUREMENT                       *"
1730  PRINT "*                                                           *"
1740  PRINT "*************************************************************"
1750  PRINT
1760  ASSIGN @An0 TO 70300
1770  Threshold=2800
1780  SEND 7;TALK 3 SEC 0 MLA
1790  DISP "PRESS ANY KEY TO CONTINUE"
1800  Time1=TIMEDATE
1810 Pulse:                                   !   LOOKING FOR PULSES  (high
1820  ENTER @An0 USING "#,W";Pulse
1830  IF Pulse>=Threshold THEN
1840      Time2=TIMEDATE
1850      Period1=Time2-Time1
1860      IF Period1<.5 THEN BEEP
1870      Time1=Time2
1880      PRINT "PERIOD=";Period1
1890  END IF
1900  ON KBD GOTO Endperiod
1910  GOTO Pulse
1920 Endperiod:  !
1930  SEND 7;UNT
1940  OFF KBD
1950  RETURN
1960 !*************************************************************************
1970 Amp_measure:                          ! SUB ROUTINE TO MEASURE AMPLITUD
1980  PRINT CHR$(12)
1990  PRINT "*************************************************************"
2000  PRINT "*                                                           *"
2010  PRINT "*                  AMPLITUDE MEASUREMENT                    *"
2020  PRINT "*                                                           *"
2030  PRINT "*************************************************************"
2040  PRINT
2050  PRINT USING "23A,10X,15A";"AMPLITUDE IN A/D UNITS","AMPLITUDE IN mm"
2060  DISP "PRESS ANY KEY TO CONTINUE"
2070  Maxamp=-99999
2080  Minamp=99999
2090  ASSIGN @An3 TO 70303
2100  SEND 7;TALK 3 SEC 3 MLA
2110  Ampcount=0
2120  Diff=0
2130 Read_amp:                             ! TO READ NEXT AMPLITUDE READIN
2140  ENTER @An3 USING "#,W";Adamp
2150  IF Adamp>Minamp AND Ampcount=1 THEN
2160      Maxamp=-99999
2170      Ampcount=0
2180  END IF
2190  IF Adamp<Maxamp AND Ampcount=0 THEN
2200      IF Amp>40 THEN
2210          Amplit=.1801+.274631431*Diff
2220          PRINT USING "8X,4D,22X,4D,2A";Diff,Amplit,"mm"
2230      END IF
2240      Diff=0
2250      Minamp=99999
2260      Ampcount=1
2270  END IF
2280  Maxamp=MAX(Adamp,Maxamp)
2290  Minamp=MIN(Adamp,Minamp)
2300  Amp=Maxamp-Minamp
2310  IF Amp>Diff THEN Diff=Amp
2320  DISP "A/D  AMP = ";Diff
2330  ON KBD GOTO End_measure
2340  GOTO Read_amp
2350 End_measure:   !
2360  SEND 7;UNT
2370  OFF KBD
2380  RETURN
```

```
2390 !************************************************************************
2400 Phase_lag:!
2410  ASSIGN @An0 TO 70300
2420  ASSIGN @An1 TO 70301
2430  ASSIGN @An2 TO 70302
2440  ASSIGN @An3 TO 70303
2450  ASSIGN @Hsc TO 70330
2460  ASSIGN @Box TO 703
2470  GOSUB Measure_period
2480  PRINT CHR$(12)
2490  DISP "TURN AMPLITUDE SWITCH TO ZERO - PRESS CONTINUE"
2500  PAUSE
2510  DISP
2520  FOR I=1 TO 2000
2530      ENTER @An3 USING "#,W";Ampp(I)
2540  NEXT I
2550  Sinezero=SUM(Ampp)/2000
2560  Threshold=2800
2570  DISP "TURN UP AMPLITUDE PROPORTIONAL TO PERIOD - PRESS CONTINUE"
2580  SEND 7;UNT
2590  PAUSE
2600  DISP
2610  FOR I=1 TO 10
2620      Sinecount=0
2630 Start1:                          !WAITS FOR LF PULSE TO START MEASUREMENT
2640      ENTER @An0 USING "#,W";Pulse
2650      IF Pulse<Threshold THEN GOTO Start1
2660      OUTPUT @Hsc USING ",2(B)";8,0   !TIMING IS SETUP HERE(24 FOR TRIGGER)
2670      OUTPUT @An0 USING "#,B";1                          !SKIP THIS CHANNEL
2680      OUTPUT @An1 USING "#,B";1                          !SKIP THIS CHANNEL
2690      OUTPUT @An2 USING "#,B";1                          !SKIP THIS CHANNEL
2700      OUTPUT @An3 USING "#,B";2   !RETURN TO SCAN START AFTER TAKING READING
2710      SEND 7;TALK 3 SEC 3 MLA                    ! START POSITION OF SCAN
2720 Start2:                                    ! WAITING FOR ZERO SINEWAVE
2730      ENTER @Box USING "#,W";Sinewave
2740      IF Sinewave<(Sinezero+10) AND Sinewave>(Sinezero-10) THEN
2750          OUTPUT @Hsc USING "B,B";0,0
2760          SEND 7;UNL UNT
2770          Phaselag(I)=(Sinecount+50)*360/200
2780      ELSE
2790          Sinecount=Sinecount+1
2800          GOTO Start2
2810      END IF
2820  NEXT I
2830  Phase_lag=SUM(Phaselag)/10
2840  PRINT CHR$(12)
2850  PRINT
2860  PRINT "PERIOD = ";Period1
2870  PRINT
2880  PRINT "PHASE LAG = ";Phase_lag
2890  DISP "PRESS CONTINUE"
2900  PAUSE
2910  RETURN
2920 !************************************************************************
2930 Logging:                    ! SUBROUTINE TO RECORD TRANSDUCER READINGS
2940  PRINT CHR$(12)
2950  PRINT "*********************************************************"
2960  PRINT "*                                                       *"
2970  PRINT "*                    DATA LOGGING                       *"
2980  PRINT "*                                                       *"
2990  PRINT "*********************************************************"
3000  DISP "MEASURING OFFSETS ......PLEASE WAIT"
3010  GOSUB Measure_offset
3020 Next_set:  !
3030  GOSUB Parameters
3040  GOSUB Amp_measure
3050  GOSUB Rr8
3060  DISP "END OF SAMPLING  ......PLEASE WAIT"
3070  GOSUB Convertrawdata
3080  GOSUB Convertpressure
3090  GOSUB Saveforcefile
3100  DISP "ANOTHER DATA SET";
3110  INPUT Answer1$
3120  IF Answer1$="N" OR Answer1$="n" THEN Main_menu
3130  GOTO Next_set
3140  RETURN
3150 !************************************************************************
3160 Measure_offset:             !MEASURES STATIC HEADS ON SUBMERGED TRANSDUCER
3170  ASSIGN @An1 TO 70301
3180  FOR I=1 TO 7
3190      Samp_offset_sum=0
3200      S1=2^I
3210      SEND 7;LISTEN 3 SEC 8 MTA
3220      OUTPUT 7 USING "#,B";S1
3230      WAIT 3
3240      FOR J=1 TO 500
3250          ENTER @An1 USING "#,W";Sample_offset
3260          Samp_offset_sum=Samp_offset_sum+Sample_offset
3270      NEXT J
3280      Offset(I)=Samp_offset_sum/500
3290  NEXT I
3300  SEND 7;LISTEN 3 SEC 8 MTA
3310  OUTPUT 7 USING "#,B";0
3320  SEND 7;UNL UNT
3330  FOR I=1 TO 7
3340      DISP "ENTER CALIBRATION FACTOR FOR TRANSDUCER ";I;
3350      INPUT Transcalib(I)
3360  NEXT I
3370  PRINT CHR$(12)
3380  PRINT "TRANSDUCER          OFFSET          CALIBRATION FACTOR"
3390  PRINT "=============================================================="
3400  PRINT
3410  FOR J=1 TO 7
3420      PRINT USING "4X,D,16X,4D,15X,Z.5D";J;Offset(J);Transcalib(J)
3430      PRINT
3440  NEXT J
3450  DISP "ARE THESE CORRECT (Y/N) ";
3460  INPUT Qst$
3470  IF Qst$="N" THEN GOTO Measure_offset
3480  RETURN
3490 !************************************************************************
3500 Parameters:                              ! READ IN PARAMETERS OFF DATA DIS
3510  ASSIGN @Pathal TO "DATA_PARAM:HP9122,700,0"
3520  ENTER @Pathal;Header(*),Month$
3530  ASSIGN @Pathal TO *
3540 Try_again:   !
3550  PRINT CHR$(12)
3560  FOR I=1 TO 9
3570      READ Param$(I)
3580  NEXT I
```

```
3590  DATA "DATE","CYCLES","SAMPLES","DIAMETER","GAP","TEMPERATURE"
3600  DATA "PHASE LAG","PERIOD","AMPLITUDE"
3610  PRINT USING "11A,X,A,6X,DD,A,4A,A,DD";Param$(1),"=",Header(1)," ",Month$,"
 ",Header(2)
3620  FOR I=2 TO 9
3630      PRINT USING "11A,X,A,X,7D.DD  ";Param$(I),"=",Header(I+1)
3640  NEXT I
3650  RESTORE 3600
3660  RESTORE 3590
3670  DISP "ARE THESE CORRECT   (Y/N)";
3680  INPUT Yn$
3690  IF Yn$="N" OR Yn$="n" THEN
3700      DISP "DATE   eg  (10,MAY,88)";
3710      INPUT Header(1),Month$,Header(2)
3720      DISP "NUMBER OF CYCLES";
3730      INPUT Header(3)
3740      REM  "SAMPLES/CYCLE"
3750      Header(4)=200
3760      DISP "CYLINDER DIAMETER";
3770      INPUT Header(5)
3780      DISP "GAP DISTANCE  (mm)";
3790      INPUT Header(6)
3800      DISP "WATER TEMPERATURE (C)";
3810      INPUT Header(7)
3820      DISP "PHASE LAG   (degrees)";
3830      INPUT Header(8)
3840      DISP "PERIOD";
3850      INPUT Header(9)
3860      DISP "AMPLITUDE  (mm)";
3870      INPUT Header(10)
3880      GOTO Try_again
3890  END IF
3900  Cycles=Header(3)
3910  Diameter=Header(5)
3920  Gap=Header(6)
3930  Phase=Header(8)
3940  Period=Header(9)
3950  Amplitude=Header(10)
3960  Um=(2*PI*Amplitude/1000)/Period                              !      m/s
3970  Lag=INT(Phase/360*200+.5)                                !DEGREES TO SAMPLES
3980  ASSIGN @Patha2 TO "DATA_PARAM:HP9122,700,0"
3990  OUTPUT @Patha2;Header(*),Month$
4000  ASSIGN @Patha2 TO *
4010  RETURN
4020 !************************************************************************
4030 Rr8:                                !  USES RR8 A/D MODULE TO SWITCH SIGNAL
4040  ASSIGN @An0 TO 70300
4050  ASSIGN @An1 TO 70301
4060  ASSIGN @Hsc TO 70330
4070  ASSIGN @Box TO 703
4080  Threshold=2800
4090  Counter=1
4100  FOR I=1 TO 7
4110      S1=2^I
4120      Sampletot=I*2000
4130      SEND 7;LISTEN 3 SEC 8 MTA
4140      OUTPUT 7 USING "#,B";S1
4150      GOSUB Microlink
4160  NEXT I
4170  SEND 7;LISTEN 3 SEC 8 MTA
4180  OUTPUT 7 USING "#,B";0
4190  SEND 7;UNL UNT
4200  RETURN
4210 !************************************************************************
4220 Microlink:   !
4230  DISP "NEXT PULSE WILL START SAMPLING"
4240 Start11:                          !WAITS FOR LF PULSE TO START THE SAMPLIN
4250  ENTER @An0 USING "#,W";Pulse
4260  IF Pulse<Threshold THEN GOTO Start11
4270  DISP "SAMPLING TRANSDUCER  ";I
4280  OUTPUT @Hsc USING ",2(B)";8,0       !TIMING IS SETUP HERE(24 FOR TRIGGER
4290  OUTPUT @An0 USING "#,B";1                                !SKIP THIS CHANNE
4300  OUTPUT @An1 USING "#,B";2      !RETURN TO SCAN START AFTER TAKING READIN
4310  SEND 7;TALK 3 SEC 1 MLA                    ! START POSITION OF SCA
4320 Start22:                                    ! WAITING FOR NEXT SAMPL
4330  ENTER @Box USING "#,W";Samp(Counter)
4340  Counter=Counter+1
4350  IF Counter>Sampletot THEN GOTO Sample_end
4360  GOTO Start22
4370 Sample_end:                                              ! END OF SAMPLIN
4380  OUTPUT @Hsc USING "B,B";0,0
4390  SEND 7;UNT UNL
4400  RETURN
4410 !************************************************************************
4420 Convertrawdata:                        !  CONVERTS RAW DATA INTO PRESSUF
4430  FOR I=1 TO 7
4440      L=1+2000*(I-1)                          !2000 = 200 SAMPLES * 10 CYCLE
4450      FOR J=(1+200*(I-1)) TO (200*I)
4460          Total(J)=Samp(L)+Samp(L+200)+Samp(L+400)+Samp(L+600)
4470          Total(J)=Total(J)+Samp(L+800)+Samp(L+1000)+Samp(L+1200)
4480          Total(J)=Total(J)+Samp(L+1400)+Samp(L+1600)+Samp(L+1800)
4490          L=L+1
4500      NEXT J
4510  NEXT I
4520  FOR I=1 TO 1400                          ! TAKES AVERAGE OF 10 CYCLE
4530      Average(I)=Total(I)/Cycles
4540  NEXT I
4550  FOR I=1 TO 7                                !  PHASE LAG ADJUSTMEN
4560      J=I*200
4570      FOR K=1+200*(I-1) TO (200*I)
4580          Dummy(K)=Average(K)
4590      NEXT K
4600      FOR L=1 TO Lag
4610          Dummy(J+L)=Average(J-200+L)
4620      NEXT L
4630      FOR M=1+200*(I-1) TO (200*I)
4640          Sample(M)=Dummy(M+Lag)
4650      NEXT M
4660  NEXT I
4670  FOR I=1 TO 7                          ! OFFSET + CALIBRATION ADJUSTMEN
4680      FOR J=1+200*(I-1) TO (200*I)
4690          Pascal(J)=(Sample(J)-Offset(I))*Transcalib(I)
4700      NEXT J
4710  NEXT I
4720  RETURN
4730 !************************************************************************
4740 Convertpressure:                       ! INTEGRATES PRESSURE TO GIVE FORC
4750  FOR I=1 TO 7
4760      Lat=I*30-120
4770      Uplim=ABS(Lat)+15                          ! UPPER LIMIT IN DEG
```

```
4780      IF ABS(Lat)=90 THEN Uplim=90
4790      Lolim=ABS(Lat)-15                                  ! LOWER LIMIT IN DEGS
4800      Liftfactor=SGN(Lat)*Diameter/2000*(COS(Uplim)-COS(Lolim))
4810      Dragfactor=Diameter/2000*(SIN(Uplim)-SIN(Lolim))
4820      IF ABS(Lat)=90 THEN Dragfactor=0
4830      FOR J=1+200*(I-1) TO (200*I)
4840          IF J<(1+200*(I-.5)) THEN
4850              Symmetry(J)=Pascal(J+100)
4860          ELSE
4870              Symmetry(J)=Pascal(J-100)
4880          END IF
4890          Dragsample(J)=(Pascal(J)-Symmetry(J))*Dragfactor          !   N/m
4900          Liftsample(J)=(Pascal(J)+Symmetry(J))*Liftfactor          !   N/m
4910      NEXT J
4920  NEXT I
4930  FOR I=1 TO 200           ! ADD SAMPLES FROM ALL TRANSDUCERS - INTEGRATION
4940      FOR J=1 TO 6
4950          Dragsample(I)=Dragsample(I)+Dragsample(I+J*200)
4960          Liftsample(I)=Liftsample(I)+Liftsample(I+J*200)
4970      NEXT J
4980      Dragforce(I)=Dragsample(I)
4990      Liftforce(I)=Liftsample(I)
5000  NEXT I
5010  FOR I=1 TO 200
5020      Clift(I)=Liftforce(I)/(.5*Um^2*Diameter)
5030      Cdrag(I)=Dragforce(I)/(.5*Um^2*Diameter)
5040  NEXT I
5050  RETURN
5060 !*************************************************************************
5070 Saveforcefile:                                  ! Creates a new BDAT file
5080  MASS STORAGE IS ":HP9122X,700,1"
5090  BEEP
5100  DISP "D=";Diameter;"  :  G/D=";Gap/Diameter;"  :  T=";Period;"  :  A=";Amp
litude;"     :     ENTER FILE NAME ";
5110  INPUT Newfile$
5120  CREATE BDAT Newfile$,14,256                              ! 8*415/256=13
5130  DISP "DATA IS BEING TRANSFERRED TO FILE...   ";Newfile$
5140  ASSIGN @Path TO Newfile$
5150  OUTPUT @Path;Header(*),Month$,Clift(*),Cdrag(*)
5160  ASSIGN @Path TO *
5170  RETURN
5180 !*************************************************************************
5190 Force: !
5200  PRINT CHR$(12)
5210  PRINT "*****************************************************************"
5220  PRINT "*                                                               *"
5230  PRINT "*                    MENU FOR FORCE PLOTS                       *"
5240  PRINT "*                                                               *"
5250  PRINT "*                    1. PLOT LIFT FORCES                        *"
5260  PRINT "*                                                               *"
5270  PRINT "*                    2. PLOT DRAG FORCES                        *"
5280  PRINT "*                                                               *"
5290  PRINT "*                    3. EXIT TO MAIN MENU                       *"
5300  PRINT "*                                                               *"
5310  PRINT "*****************************************************************"
5320  PRINT
5330  PRINT "              CHOOSE ONE OF THE ABOVE OPTIONS"
5340  INPUT Opt
5350  IF Opt=1 THEN GOSUB Plotforce
5360  IF Opt=2 THEN GOSUB Plotforce
5370  IF Opt=3 THEN GOSUB Main_menu
5380  GOTO Force
5390  RETURN
5400 !*************************************************************************
5410 Plotforce:  !
5420  PRINT CHR$(12)
5430  DISP "HOW MANY FILES DO YOU WANT TO PLOT ON ONE PAGE";
5440  INPUT Nofiles
5450  IF Nofiles<1 OR Nofiles>4 THEN
5460      PRINT "REPEAT WITH A NUMBER BETWEEN 1 AND 4"
5470      GOTO Plotforce
5480  END IF
5490  Rapidplot=1
5500  DISP "DO YOU WANT THE LABELS PLOTTED      (Y/N)";
5510  INPUT Answer$
5520  IF Answer$="Y" OR Answer$="y" THEN
5530      Rapidplot=0
5540      DISP "WITH WHAT FIGURE NUMBER DO YOU WANT TO LABEL THE PLOT";
5550      INPUT Figno$
5560  END IF
5570  FOR I=1 TO Nofiles
5580      DISP "WHAT IS THE NAME OF FILE No. ";I;
5590      INPUT Filename$(I)
5600  NEXT I
5610  PRINT CHR$(12)
5620  PRINT
5630  PRINT "    ************************************************************"
5640  PRINT "    *                                                          *"
5650  PRINT "    *          THE FOLLOWING FILES WILL BE PLOTTED             *"
5660  PRINT "    *                                                          *"
5670  PRINT "    ************************************************************"
5680  PRINT
5690  PRINT
5700  PRINT
5710  FOR Q=1 TO Nofiles
5720      PRINT "            ";Q;".  ";Filename$(Q)
5730  NEXT Q
5740  PRINT
5750  PRINT
5760  IF Rapidplot=0 THEN
5770      PRINT "              Figure no. = ";Figno$
5780  END IF
5790  DISP "ARE THEY CORRECT   (Y/N)";
5800  INPUT Quiz$
5810  IF Quiz$="N" THEN Plotforce
5820  FOR J=1 TO Nofiles
5830      File$=Filename$(J)
5840      Stampno=J
5850      GOSUB Getfile
5860      GOSUB Multiblock2
5870      GOSUB Forcescales
5880      GOSUB Properties
5890      GOSUB Plotforcedata
5900  NEXT J
5910  IF Answer$="Y" THEN GOSUB Figlabel
5920  RETURN
5930 !*************************************************************************
5940 Getfile:  !
5950  MASS STORAGE IS ":HP9122X,700,1"
5960  DISP "ACCESSING FILE ... ";File$
```

```
5970  ASSIGN @Path TO File$
5980  ENTER @Path;Header(*),Month$,Clift(*),Cdrag(*)
5990  ASSIGN @Path TO *
6000  Day=Header(1)
6010  Year=Header(2)
6020  Cycles=Header(3)
6030  Samples=Header(4)
6040  Diameter=Header(5)
6050  Gap=Header(6)
6060  Temp=Header(7)
6070  Phase=Header(8)
6080  Period=Header(9)
6090  Amplitude=Header(10)
6100  Um=(2*PI*Amplitude/1000)/Period                              !      m/s
6110  Nu=10^(19.182-7.776*LGT(273+Temp))                           !   mm^2/s
6120  Reynoldsno=(Um*1000*Diameter)/Nu                             !ALL IN mm
6130  Bd=SQR(PI/Nu/Period)*Diameter                                !ALL IN mm
6140  Kc=2*PI*Amplitude/Diameter                                   !ALL IN mm
6150  Gapratio=Gap/Diameter
6160  Clplus=MAX(Clift(*))
6170  Clminus=MIN(Clift(*))
6180  Clamp=Clplus-Clminus
6190  Cdmax=MAX(Cdrag(*))
6200  RETURN
6210 !*************************************************************************
6220 Multiblock2:                          ! SEND SIZE OF EACH BLOCK TO PLOTTER
6230  OUTPUT 705;"VS,15"
6240  OUTPUT 705;"IP"&VAL$(Xstamp1(Stampno))&","&VAL$(Ystamp1(Stampno))&","&VAL$
(Xstamp2(Stampno))&","&VAL$(Ystamp2(Stampno))
6250  GINIT
6260  PLOTTER IS 705,"HPGL"
6270  RETURN
6280 !*************************************************************************
6290 Forcescales:   !
6300  IF Opt=1 THEN
6310      Cmax=MAX(ABS(Clplus),ABS(Clminus))
6320  ELSE
6330      Cmax=Cdmax
6340  END IF
6350  Fmax=Cmax*(.5*Um^2*Diameter)
6360  Diviscl=10                        !FINDS SCALE DIVISIONS FOR THE COEFFICIENTS
6370  IF Cmax<20 THEN Diviscl=5
6380  IF Cmax<8 THEN Diviscl=2
6390  IF Cmax<4 THEN Diviscl=1
6400  IF Cmax<2 THEN Diviscl=.5
6410  IF Cmax<.8 THEN Diviscl=.2
6420  IF Cmax<.4 THEN Diviscl=.1
6430  IF Cmax<.2 THEN Diviscl=.05
6440  IF Cmax<.008 THEN Diviscl=.002
6450  Divisforce=100                    !FINDS SCALE DIVISIONS FOR THE FORCES
6460  IF Fmax<250 THEN Divisforce=50
6470  IF Fmax<100 THEN Divisforce=20
6480  IF Fmax<50 THEN Divisforce=10
6490  IF Fmax<25 THEN Divisforce=5
6500  IF Fmax<10 THEN Divisforce=2
6510  IF Fmax<5 THEN Divisforce=1
6520  IF Fmax<2.5 THEN Divisforce=.5
6530  IF Fmax<1 THEN Divisforce=.2
6540  IF Fmax<.5 THEN Divisforce=.1
6550  IF Fmax<.25 THEN Divisforce=.05
6560  IF Fmax<.005 THEN Divisforce=.001
6570  Forcediv=Divisforce/(.5*Um^2*Diameter)
6580  RETURN
6590 !*************************************************************************
6600 Properties:                          !DRAWS FRAME AND LABELS CHARACTERISTIC
6610  GRAPHICS ON
6620  FRAME
6630  IF Rapidplot=1 THEN Labelaxes
6640  LDIR 90
6650  LORG 5
6660  MOVE 2.2,56
6670  CSIZE 3.4
6680  IF Opt=2 THEN
6690      LABEL USING "K";"DRAG COEFFICIENT "
6700      MOVE 5,56
6710      LABEL USING "K";"(+ve in one direction and -ve in the other)"
6720  ELSE
6730      LABEL USING "K";"LIFT COEFFICIENT "
6740      MOVE 5,56
6750      LABEL USING "K";"(+ve away from the boundary)"
6760  END IF
6770  MOVE 132,56
6780  Units$="(milliNewtons/metre)"
6790  IF Fmax>=1 THEN Units$="(Newtons/metre)"
6800  IF Opt=2 THEN
6810      LABEL USING "K";"DRAG FORCE ";Units$
6820  ELSE
6830      LABEL USING "K";"LIFT FORCE ";Units$
6840  END IF
6850  LORG 2
6860  LDIR 0
6870  MOVE 35,6.7
6880  LABEL USING "K";"PHASE ANGLE  (0 degrees = velocity reversal)"
6890  MOVE 0,4
6900  LDIR 0
6910  DRAW 133.4448,4
6920  MOVE 2,2
6930  CSIZE 3
6940  LABEL USING "K";"DISC FILE : ";File$
6950  MOVE 35,2
6960  LABEL USING "K";"CYCLES = ";Cycles
6970  MOVE 63,2
6980  LABEL USING "K";"SAMPLES/CYCLE = ";Samples
6990  MOVE 105,2
7000  LABEL USING "K";"DATE : ";Day;"-";Month$;"-";Year
7010  LORG 2
7020  CSIZE 3.1
7030  MOVE 84,96
7040  LABEL USING "4A,DD.DD,X,A";"T = ";Period;"s"
7050  MOVE 104,96
7060  LABEL USING "5A,4D,X,AA";"A  = ";Amplitude;"mm"
7070  MOVE 84,92
7080  LABEL USING "4A,3D,X,AA";"d = ";Diameter;"mm"
7090  MOVE 104,92
7100  LABEL USING "5A,.DD,X,3A";"Um = ";Um;"m/s"
7110  MOVE 84,88
7120  LABEL USING "5A,D.4D,X ";"G/d =";Gapratio
7130  MOVE 104,88
7140  LABEL USING "5A,5D";"Re = ";Reynoldsno
7150  MOVE 84,84
```

```
7160  LABEL USING "5A,3D.DD";"Bd = ";Bd
7170  MOVE 104,84
7180  LABEL USING "5A,DD.DD";"Kc = ";Kc
7190  IF Opt=1 THEN
7200      MOVE 84,80
7210      LABEL USING "6A,2D.3D";"Cl+ = ";Clplus
7220      MOVE 104,80
7230      LABEL USING "6A,3D.3D";"Cl- =";Clminus
7240      MOVE 84,76
7250      LABEL USING "8A,2D.3D";"Clamp = ";Clamp
7260  ELSE
7270      MOVE 84,76
7280      LABEL USING "8A,DD.3D";"Cdmax = ";Cdmax
7290  END IF
7300 !*************************************************************************
7310 Labelaxes:                                  !  SCALES AND LABELS ALL AXES
7320  VIEWPORT 17,150.,13,100
7330  WINDOW 0,378,(-Diviscl*5),((+Diviscl*5)+Diviscl/5)
7340  AXES 90,Diviscl,0,(-Diviscl*5),1,1,2          ! LABELS COEFFICIENT SCALE
7350  CLIP OFF
7360  CSIZE 2.7
7370  LDIR 0
7380  LORG 8
7390  Yd=INT((-Diviscl*5)*1000)/1000
7400  FOR I=1 TO 11
7410      MOVE -2,Yd
7420      LABEL USING "K";Yd
7430      Yd=Yd+Diviscl
7440      IF Yd<.000001 AND Yd>-.000001 THEN Yd=0
7450  NEXT I
7460  CLIP ON
7470  AXES 400,Forcediv,378,0,1,1,2                        !LABELS FORCE SCALE
7480  CLIP OFF
7490  LDIR 0
7500  Yf=0
7510  Yyy=0
7520  LORG 2
7530  CSIZE 2.8
7540  Factor=1000
7550  IF Fmax>=1 THEN Factor=1
7560  FOR I=1 TO 20
7570      MOVE 382,Yf
7580      LABEL USING "K";Yyy*Factor
7590      Yf=Yf+Forcediv
7600      IF Yf>Diviscl*5 THEN I=20
7610      Yyy=Yyy+Divisforce
7620  NEXT I
7630  Yf=-Forcediv
7640  Yyy=-Divisforce
7650  FOR I=1 TO 20
7660      MOVE 380,Yf
7670      LABEL USING "K";Yyy*Factor
7680      Yf=Yf-Forcediv
7690      IF Yf<-Diviscl*5 THEN I=20
7700      Yyy=Yyy-Divisforce
7710  NEXT I
7720  IF Rapidplot=1 THEN Axesout
7730  CSIZE 3.3                              ! LABELS VALUE OF THE PHASE ANGLE
7740  Xx=0
7750  LORG 6
7760  FOR I=1 TO 5
7770      MOVE Xx,-Diviscl*5*1.01
7780      LABEL USING "K";Xx
7790      Xx=Xx+90
7800  NEXT I
7810  LINE TYPE 4                    !  DRAWS DOTTED LINES AT PHASES 90,180,270,36
7820  MOVE 90,-Diviscl*5
7830  DRAW 90,+Diviscl*5
7840  MOVE 180,-Diviscl*5
7850  DRAW 180,+Diviscl*5
7860  MOVE 270,-Diviscl*5
7870  DRAW 270,+Diviscl*2.2
7880  MOVE 360,-Diviscl*5
7890  DRAW 360,+Diviscl*2.2
7900  LINE TYPE 3                    !DRAWS GRID LINES ACROSS PAGE AT VALUES OF C
7910  MOVE 0,-Diviscl*4
7920  DRAW 380,-Diviscl*4
7930  MOVE 0,-Diviscl*3
7940  DRAW 380,-Diviscl*3
7950  MOVE 0,-Diviscl*2
7960  DRAW 380,-Diviscl*2
7970  MOVE 0,-Diviscl
7980  DRAW 380,-Diviscl
7990  MOVE 0,Diviscl
8000  DRAW 380,Diviscl
8010  MOVE 0,Diviscl*2
8020  DRAW 380,Diviscl*2
8030  MOVE 0,Diviscl*3
8040  DRAW 230,Diviscl*3
8050  MOVE 0,Diviscl*4
8060  DRAW 230,Diviscl*4
8070  MOVE 0,Diviscl*5
8080  DRAW 230,Diviscl*5
8090 Axesout:              ! THIS IS FOR RAPIDPLOT TO LEAVE OUT LABELING OF AXE
8100  LINE TYPE 1
8110  RETURN
8120 !*************************************************************************
8130 Plotforcedata:                          !  PLOTS THE LIFT/DRAG vs PHASE CURV
8140  CLIP ON
8150  Xdiv=0
8160  Xdivis=360/200
8170  IF Opt=2 THEN
8180      MOVE 0,Cdrag(1)
8190      FOR I=1 TO 211
8200          IF I>200 THEN
8210              PLOT Xdiv,Cdrag(I-200)
8220          ELSE
8230              PLOT Xdiv,Cdrag(I)
8240          END IF
8250          Xdiv=Xdiv+Xdivis
8260      NEXT I
8270  ELSE
8280      MOVE 0,Clift(1)
8290      FOR I=1 TO 211
8300          IF I>200 THEN
8310              PLOT Xdiv,Clift(I-200)
8320          ELSE
8330              PLOT Xdiv,Clift(I)
8340          END IF
8350          Xdiv=Xdiv+Xdivis
```

```
8360       NEXT I
8370    END IF
8380    RETURN
8390 !*************************************************************************
8400 Figlabel:                              !LABELS DIAGRAM WITH DIAMETER,Bd AND G/
8410    IF Opt=2 THEN Ftp$="drag"
8420    IF Opt=1 THEN Ftp$="lift"
8430    Diam=Diameter
8440    Gd=Gapratio
8450    OUTPUT 705;"VS,15"
8460    OUTPUT 705;"IP"&VAL$(0)&","&VAL$(100)&","&VAL$(10800)&","&VAL$(500)
8470    GINIT
8480    PLOTTER IS 705,"HPGL"
8490    GRAPHICS ON
8500    FRAME
8510    CSIZE 50
8520    LORG 2
8530    LDIR 0
8540    FOR I=0 TO .15 STEP .15
8550       MOVE 2+I,50
8560       LABEL USING "7A,AAAAA,12A,4A,23A,K,7A,3D.DD,9A,D.4D";"Figure ";Fignc
" : Plots of ";Ftp$;" vs phase for diameter=";Diam;"mm, Bd=";Bd;" and G/d=";Gd
8570    NEXT I
8580    RETURN
8590 !*************************************************************************
8600    END
```

APPENDIX F - TEST RESULTS IN TABULAR FORM

Tables showing the force coefficients as a function of the dimensionless constants are given on the following pages.

Each page constitutes the results of tests performed at one gap ratio and they have been arranged in ascending order. The results of tests at a certain gap ratio have been arranged in ascending order of period (or descending βd). For each period, results are arranged in ascending amplitudes.

Diam.	G/d	T	Bd	Amp	Um	Re	KC	Cl+	Cl-	Clamp	Cd	Cm	Cdmax
90	0.01	4	79.79	30	0.05	4244	2.09	-3.861	-9.371	5.510	3.989	2.149	26.307
90	0.01	4	79.79	60	0.09	8489	4.19	-0.406	-4.783	4.376	2.044	2.098	10.324
90	0.01	4	79.79	90	0.14	12733	6.28	1.870	-2.172	4.043	1.940	1.865	5.799
90	0.01	4	79.79	120	0.19	16977	8.38	2.792	-0.937	3.729	1.857	1.737	4.027
90	0.01	4	79.79	150	0.24	21221	10.47	3.049	-0.508	3.558	1.880	1.722	3.161
90	0.01	4	79.79	180	0.28	25466	12.57	2.736	-0.246	2.982	1.813	1.672	2.654
90	0.01	4	79.79	210	0.33	29710	14.66	2.349	-0.672	3.020	1.786	1.849	2.400
90	0.01	4	79.79	240	0.38	33954	16.76	2.197	-0.500	2.697	1.808	1.863	2.346
90	0.01	6	65.15	50	0.05	4716	3.49	4.389	-0.453	4.842	6.764	3.158	23.823
90	0.01	6	65.15	100	0.10	9432	6.98	4.370	0.588	3.782	4.376	2.723	8.439
90	0.01	6	65.15	150	0.16	14148	10.47	4.365	0.628	3.737	3.586	2.364	4.797
90	0.01	6	65.15	200	0.21	18865	13.96	3.923	0.711	3.211	3.328	2.364	3.655
90	0.01	6	65.15	250	0.26	23581	17.45	3.445	0.427	3.018	3.112	2.377	3.157
90	0.01	6	65.15	300	0.31	28297	20.94	3.186	0.402	2.784	2.637	2.336	2.700
90	0.01	6	65.15	350	0.37	33013	24.43	2.646	0.437	2.209	2.524	2.374	2.410
90	0.01	6	65.15	400	0.42	37729	27.93	2.418	-0.123	2.541	2.492	1.399	2.205
90	0.01	8	56.42	75	0.06	5305	5.24	6.142	1.978	4.164	2.136	2.157	14.605
90	0.01	8	56.42	150	0.12	10611	10.47	5.459	1.512	3.947	2.158	1.975	4.970
90	0.01	8	56.42	225	0.18	15916	15.71	4.735	0.537	4.198	2.075	2.180	3.230
90	0.01	8	56.42	300	0.24	21221	20.94	4.237	0.448	3.789	2.032	2.563	2.655
90	0.01	8	56.42	375	0.29	26527	26.18	3.178	0.840	2.338	2.048	2.644	2.370
90	0.01	8	56.42	450	0.35	31832	31.42	1.651	-0.480	2.131	2.029	3.027	2.288
90	0.01	8	56.42	525	0.41	37138	36.65	1.713	0.072	1.641	2.091	3.179	2.124
90	0.01	8	56.42	600	0.47	42443	41.89	1.683	-0.032	1.716	1.955	3.601	2.026
90	0.01	10	50.47	100	0.06	5660	6.98	11.755	7.147	4.608	-0.718	-2.019	7.327
90	0.01	10	50.47	200	0.13	11321	13.96	7.726	4.018	3.707	0.519	-1.694	3.526
90	0.01	10	50.47	300	0.19	16981	20.94	2.249	-0.828	3.078	1.394	5.203	3.783
90	0.01	10	50.47	400	0.25	22642	27.93	1.651	-1.372	3.023	0.734	-0.916	2.034
90	0.01	10	50.47	500	0.31	28302	34.91	1.918	-0.898	2.816	0.704	-0.393	1.578
90	0.01	10	50.47	600	0.38	33963	41.89	2.296	0.120	2.177	0.562	-0.026	1.337
90	0.01	10	50.47	700	0.44	39623	48.87	1.469	-0.390	1.859	0.371	0.602	0.941
90	0.01	10	50.47	800	0.50	45284	55.85	1.591	0.091	1.500	0.218	0.058	1.025

Diam.	G/d	T	Bd	Amp	Um	Re	KC	Cl+	Cl-	Clamp	Cd	Cm	Cdmax
120	0.03125	2	150.46	15	0.05	5660	0.79	2.343	-8.101	10.444	22.120	1.217	37.693
120	0.03125	2	150.46	30	0.09	11319	1.57	2.479	-7.805	10.284	10.988	1.459	18.078
120	0.03125	2	150.46	45	0.14	16979	2.36	2.915	-6.170	9.085	7.335	1.564	11.478
120	0.03125	2	150.46	60	0.19	22638	3.14	3.403	-5.206	8.608	5.417	1.648	7.771
120	0.03125	2	150.46	75	0.24	28298	3.93	3.871	-4.237	8.108	4.304	1.760	5.969
120	0.03125	2	150.46	90	0.28	33957	4.71	3.829	-3.208	7.037	3.644	1.728	4.770
120	0.03125	2	150.46	105	0.33	39617	5.50	3.831	-2.833	6.664	3.157	1.669	3.902
120	0.03125	2	150.46	120	0.38	45276	6.28	3.860	-2.528	6.387	2.803	1.695	3.335
120	0.03125	4	106.39	30	0.05	5659	1.57	2.333	-7.463	9.796	8.082	1.850	31.161
120	0.03125	4	106.39	60	0.09	11319	3.14	3.413	-4.187	7.600	4.353	2.002	11.836
120	0.03125	4	106.39	90	0.14	16978	4.71	3.463	-2.554	6.018	2.857	2.030	6.951
120	0.03125	4	106.39	120	0.19	22638	6.28	3.592	-1.922	5.514	2.383	1.930	5.343
120	0.03125	4	106.39	150	0.24	28297	7.85	3.429	-1.281	4.710	2.369	1.771	4.310
120	0.03125	4	106.39	180	0.28	33956	9.42	3.076	-0.766	3.841	2.227	1.732	3.460
120	0.03125	4	106.39	210	0.33	39616	11.00	2.823	-0.575	3.398	2.171	1.612	3.102
120	0.03125	4	106.39	240	0.38	45275	12.57	2.659	-0.410	3.069	2.012	1.731	2.890
120	0.03125	6	86.87	50	0.05	6289	2.62	12.658	4.058	8.600	10.622	3.092	27.186
120	0.03125	6	86.87	100	0.10	12577	5.24	5.998	0.645	5.352	5.615	2.905	9.752
120	0.03125	6	86.87	150	0.16	18866	7.85	4.335	0.138	4.197	4.468	2.565	6.378
120	0.03125	6	86.87	200	0.21	25155	10.47	3.524	0.216	3.307	3.912	2.224	4.590
120	0.03125	6	86.87	250	0.26	31443	13.09	2.930	0.191	2.739	3.495	2.083	3.518
120	0.03125	6	86.87	300	0.31	37732	15.71	2.697	0.096	2.600	3.118	1.946	2.874
120	0.03125	6	86.87	350	0.37	44021	18.33	2.541	0.106	2.435	2.852	1.731	2.647
120	0.03125	6	86.87	400	0.42	50309	20.94	2.129	0.030	2.099	2.616	1.449	2.453
120	0.03125	8	75.23	75	0.06	7074	3.93	3.673	-2.302	5.975	3.026	2.407	12.356
120	0.03125	8	75.23	150	0.12	14149	7.85	3.152	-0.432	3.583	2.378	2.211	5.741
120	0.03125	8	75.23	225	0.18	21223	11.78	2.633	0.013	2.620	2.384	2.120	3.783
120	0.03125	8	75.23	300	0.24	28298	15.71	2.734	-0.003	2.737	2.307	2.236	2.746
120	0.03125	8	75.23	375	0.29	35372	19.63	2.698	0.082	2.616	2.079	2.122	2.356
120	0.03125	8	75.23	450	0.35	42447	23.56	2.251	0.152	2.099	2.108	2.076	2.351
120	0.03125	8	75.23	525	0.41	49521	27.49	1.890	-0.087	1.978	2.022	2.270	1.960
120	0.03125	8	75.23	600	0.47	56596	31.42	1.520	-0.193	1.713	1.911	1.811	1.866

Diam.	G/d	T	Bd	Amp	Um	Re	KC	Cl+	Cl-	Clamp	Cd	Cm	Cdmax
120	0.046875	2	146.51	15	0.05	5366	0.79	0.774	-6.759	7.533	19.529	1.149	38.512
120	0.046875	2	146.51	30	0.09	10733	1.57	-0.241	-1.022	0.781	5.753	0.405	6.888
120	0.046875	2	146.51	45	0.14	16099	2.36	2.222	-7.032	9.254	7.312	1.283	10.735
120	0.046875	2	146.51	60	0.19	21465	3.14	3.009	-6.523	9.532	5.942	1.366	8.339
120	0.046875	2	146.51	75	0.24	26831	3.93	3.463	-5.412	8.875	5.087	1.445	6.365
120	0.046875	2	146.51	90	0.28	32198	4.71	3.736	-4.537	8.273	4.387	1.471	5.118
120	0.046875	2	146.51	105	0.33	37564	5.50	3.591	-3.714	7.305	3.732	1.493	4.399
120	0.046875	2	146.51	120	0.38	42930	6.28	3.960	-3.247	7.207	3.332	1.485	3.916
120	0.046875	4	103.60	30	0.05	5366	1.57	1.798	-8.022	9.820	7.403	1.579	28.462
120	0.046875	4	103.60	60	0.09	10733	3.14	2.868	-6.187	9.055	4.534	1.834	12.802
120	0.046875	4	103.60	90	0.14	16099	4.71	3.212	-4.271	7.483	3.141	1.912	7.070
120	0.046875	4	103.60	120	0.19	21466	6.28	3.206	-2.902	6.107	2.642	1.901	5.406
120	0.046875	4	103.60	150	0.24	26832	7.85	3.049	-1.859	4.908	2.412	1.818	4.296
120	0.046875	4	103.60	180	0.28	32199	9.42	2.937	-1.464	4.402	2.415	1.693	3.686
120	0.046875	4	103.60	210	0.33	37565	11.00	2.766	-1.038	3.804	2.435	1.644	3.383
120	0.046875	4	103.60	240	0.38	42932	12.57	2.577	-0.846	3.424	2.237	1.708	2.933
120	0.046875	6	84.59	50	0.05	5963	2.62	3.246	-6.473	9.719	10.912	2.694	27.619
120	0.046875	6	84.59	100	0.10	11926	5.24	3.419	-3.237	6.656	6.041	2.739	10.346
120	0.046875	6	84.59	150	0.16'	17889	7.85	2.902	-1.416	4.318	4.701	2.394	6.388
120	0.046875	6	84.59	200	0.21	23852	10.47	2.703	-0.818	3.521	4.168	2.139	4.751
120	0.046875	6	84.59	250	0.26	29814	13.09	2.299	-0.522	2.821	3.682	1.996	3.824
120	0.046875	6	84.59	300	0.31	35777	15.71	1.995	-0.504	2.499	3.259	1.830	2.946
120	0.046875	6	84.59	350	0.37	41740	18.33	2.006	-0.410	2.416	2.933	1.593	2.536
120	0.046875	6	84.59	400	0.42	47703	20.94	1.947	-0.445	2.392	2.707	1.285	2.419
120	0.046875	8	73.25	75	0.06	6707	3.93	3.632	-4.517	8.149	3.549	2.377	15.600
120	0.046875	8	73.25	150	0.12	13414	7.85	2.779	-1.135	3.914	2.601	2.187	6.751
120	0.046875	8	73.25	225	0.18	20121	11.78	2.306	-0.374	2.680	2.617	2.183	4.108
120	0.046875	8	73.25	300	0.24	26828	15.71	1.956	-0.291	2.247	2.393	2.286	3.248
120	0.046875	8	73.25	375	0.29	33535	19.63	1.937	-0.247	2.183	2.247	2.017	2.552
120	0.046875	8	73.25	450	0.35	40242	23.56	1.961	-0.339	2.299	2.111	2.047	2.154
120	0.046875	8	73.25	525	0.41	46949	27.49	1.606	-0.296	1.903	2.030	2.051	2.053
120	0.046875	8	73.25	600	0.47	53656	31.42	1.484	-0.201	1.685	1.937	1.893	1.883

Diam.	G/d	T	Bd	Amp	Um	Re	KC	Cl+	Cl-	Clamp	Cd	Cm	Cdmax
120	0.0625	2	148.47	15	0.05	5511	0.79	-0.257	-4.340	4.082	13.935	1.254	29.453
120	0.0625	2	148.47	30	0.09	11022	1.57	0.348	-4.828	5.176	6.841	1.324	12.540
120	0.0625	2	148.47	45	0.14	16533	2.36	1.419	-5.390	6.809	4.560	1.276	7.987
120	0.0625	2	148.47	60	0.19	22043	3.14	2.373	-5.686	8.060	3.887	1.292	6.009
120	0.0625	2	148.47	75	0.24	27554	3.93	3.710	-5.608	9.318	3.623	1.492	5.035
120	0.0625	2	148.47	90	0.28	33065	4.71	3.742	-4.909	8.652	3.274	1.533	4.819
120	0.0625	2	148.47	105	0.33	38576	5.50	3.951	-4.251	8.202	3.003	1.542	4.052
120	0.0625	2	148.47	120	0.38	44087	6.28	3.991	-3.531	7.521	2.732	1.532	3.352
120	0.0625	4	104.99	30	0.05	5511	1.57	0.570	-5.140	5.710	6.312	1.474	24.829
120	0.0625	4	104.99	60	0.09	11023	3.14	3.015	-5.784	8.799	4.209	1.618	9.433
120	0.0625	4	104.99	90	0.14	16534	4.71	3.550	-4.337	7.887	3.190	1.755	6.297
120	0.0625	4	104.99	120	0.19	22046	6.28	3.434	-3.060	6.494	2.511	1.794	4.622
120	0.0625	4	104.99	150	0.24	27557	7.85	3.352	-2.271	5.623	2.539	1.686	4.185
120	0.0625	4	104.99	180	0.28	33069	9.42	2.951	-1.567	4.517	2.427	1.564	3.717
120	0.0625	4	104.99	210	0.33	38580	11.00	2.777	-0.937	3.714	2.203	1.563	3.280
120	0.0625	4	104.99	240	0.38	44092	12.57	2.630	-0.833	3.463	2.062	1.643	2.934
120	0.0625	6	85.72	50	0.05	6123	2.62	2.934	-5.282	8.215	9.881	2.566	23.002
120	0.0625	6	85.72	100	0.10	12247	5.24	3.502	-3.577	7.079	5.796	2.624	8.998
120	0.0625	6	85.72	150	0.16	18370	7.85	3.320	-1.682	5.001	4.466	2.456	6.017
120	0.0625	6	85.72	200	0.21	24493	10.47	2.676	-0.731	3.406	3.955	2.109	4.638
120	0.0625	6	85.72	250	0.26	30616	13.09	2.343	-0.395	2.738	3.507	1.959	3.666
120	0.0625	6	85.72	300	0.31	36740	15.71	2.043	-0.259	2.302	3.184	1.752	2.923
120	0.0625	6	85.72	350	0.37	42863	18.33	2.043	-0.337	2.381	2.821	1.609	2.475
120	0.0625	6	85.72	400	0.42	48986	20.94	2.011	-0.177	2.188	2.590	1.313	2.309
120	0.0625	8	74.24	75	0.06	6889	3.93	0.892	-6.942	7.833	3.629	2.152	12.963
120	0.0625	8	74.24	150	0.12	13779	7.85	2.453	-2.378	4.831	2.524	2.150	5.850
120	0.0625	8	74.24	225	0.18	20668	11.78	2.045	-0.793	2.838	2.498	2.073	3.603
120	0.0625	8	74.24	300	0.24	27558	15.71	1.980	-0.449	2.429	2.304	2.077	2.720
120	0.0625	8	74.24	375	0.29	34447	19.63	1.946	-0.250	2.197	2.035	1.868	2.188
120	0.0625	8	74.24	450	0.35	41337	23.56	1.626	-0.201	1.827	1.975	1.790	1.926
120	0.0625	8	74.24	525	0.41	48226	27.49	1.420	-0.092	1.512	1.857	1.606	1.818
120	0.0625	8	74.24	600	0.47	55116	31.42	1.402	-0.121	1.524	1.827	1.707	1.681

Diam.	G/d	T	Bd	Amp	Um	Re	KC	Cl+	Cl-	Clamp	Cd	Cm	Cdmax
90	0.09375	4	77.70	30	0.05	4025	2.09	0.674	-5.247	5.921	5.707	1.503	25.249
90	0.09375	4	77.70	60	0.09	8050	4.19	3.681	-4.858	8.539	4.065	1.774	9.712
90	0.09375	4	77.70	90	0.14	12075	6.28	3.548	-2.786	6.333	3.059	1.831	5.852
90	0.09375	4	77.70	120	0.19	16099	8.38	3.234	-1.550	4.784	2.612	1.733	4.669
90	0.09375	4	77.70	150	0.24	20124	10.47	2.887	-0.819	3.706	2.518	1.548	3.947
90	0.09375	4	77.70	180	0.28	24149	12.57	2.721	-0.548	3.269	2.047	1.516	3.113
90	0.09375	4	77.70	210	0.33	28174	14.66	2.595	-0.418	3.013	2.097	1.439	2.668
90	0.09375	4	77.70	240	0.38	32199	16.76	2.434	-0.004	2.438	1.995	1.510	2.447
90	0.09375	6	63.44	50	0.05	4472	3.49	4.133	-5.095	9.228	9.499	2.594	18.905
90	0.09375	6	63.44	100	0.10	8944	6.98	3.651	-1.605	5.256	5.262	2.501	7.495
90	0.09375	6	63.44	150	0.16	13415	10.47	3.128	-0.036	3.164	4.226	2.128	4.993
90	0.09375	6	63.44	200	0.21	17887	13.96	3.193	-0.007	3.200	3.435	1.733	3.723
90	0.09375	6	63.44	250	0.26	22359	17.45	3.169	0.105	3.064	3.041	1.514	3.079
90	0.09375	6	63.44	300	0.31	29058	20.94	1.752	-0.367	2.119	3.094	2.472	2.911
90	0.09375	6	63.44	350	0.37	33901	24.43	1.663	-0.266	1.929	2.784	2.345	2.547
90	0.09375	6	63.44	400	0.42	38744	27.93	1.362	-0.296	1.658	2.580	1.967	2.455
90	0.09375	8	54.94	75	0.06	5031	5.24	4.289	-3.013	7.302	2.963	2.021	9.902
90	0.09375	8	54.94	150	0.12	10061	10.47	3.179	-0.163	3.342	2.425	1.868	4.265
90	0.09375	8	54.94	225	0.18	15092	15.71	3.126	0.088	3.038	2.340	1.991	3.190
90	0.09375	8	54.94	300	0.24	20123	20.94	2.868	0.164	2.704	2.204	2.108	2.688
90	0.09375	8	54.94	375	0.29	27242	26.18	1.855	-0.137	1.992	2.120	2.454	2.234
90	0.09375	8	54.94	450	0.35	32690	31.42	1.467	-0.050	1.517	2.118	2.493	2.225
90	0.09375	8	54.94	525	0.41	38138	36.65	1.201	-0.096	1.296	1.900	2.520	1.818
90	0.09375	8	54.94	600	0.47	43587	41.89	0.984	-0.117	1.102	1.818	2.550	1.768
90	0.09375	10	50.47	100	0.06	5660	6.98	4.547	-0.737	5.283	-0.675	-2.607	7.270
90	0.09375	10	50.47	200	0.13	11321	13.96	3.575	0.277	3.298	0.264	-2.609	3.682
90	0.09375	10	50.47	300	0.19	16981	20.94	2.927	0.133	2.794	0.472	-2.460	2.453
90	0.09375	10	50.47	400	0.25	22638	27.93	2.446	0.042	2.404	0.492	-2.136	1.620
90	0.09375	10	50.47	500	0.31	28298	34.91	1.977	0.023	1.954	0.474	-1.750	1.491
90	0.09375	10	50.47	600	0.38	33958	41.89	1.465	0.076	1.389	0.460	-1.261	1.316
90	0.09375	10	50.47	700	0.44	39617	48.87	1.117	0.007	1.110	0.369	-0.972	1.091
90	0.09375	10	50.47	800	0.50	45277	55.85	1.063	0.028	1.035	0.332	-0.325	1.183

Diam.	G/d	T	Bd	Amp	Um	Re	KC	Cl+	Cl-	Clamp	Cd	Cm	Cdmax
120	0.125	2	150.46	15	0.05	5660	0.79	-0.726	-2.078	1.352	19.221	0.869	32.283
120	0.125	2	150.46	30	0.09	11319	1.57	-0.263	-1.868	1.605	8.166	1.093	12.240
120	0.125	2	150.46	45	0.14	16979	2.36	0.158	-2.285	2.443	5.380	1.121	8.397
120	0.125	2	150.46	60	0.19	22638	3.14	0.935	-3.360	4.295	4.355	1.038	6.107
120	0.125	2	150.46	75	0.24	28298	3.93	2.172	-4.676	6.848	4.106	0.957	4.552
120	0.125	2	150.46	90	0.28	33957	4.71	3.208	-4.845	8.053	3.870	0.960	4.103
120	0.125	2	150.46	105	0.33	39617	5.50	3.693	-4.908	8.600	3.496	1.005	4.149
120	0.125	2	150.46	120	0.38	45276	6.28	3.501	-4.281	7.783	3.156	1.041	3.799
120	0.125	4	106.39	30	0.05	5659	1.57	-3.166	-4.990	1.824	5.180	1.467	25.621
120	0.125	4	106.39	60	0.09	11319	3.14	1.479	-4.443	5.921	3.461	1.357	8.878
120	0.125	4	106.39	90	0.14	16978	4.71	3.189	-5.352	8.542	3.277	1.482	5.180
120	0.125	4	106.39	120	0.19	22638	6.28	3.463	-4.620	8.083	2.896	1.535	4.159
120	0.125	4	106.39	150	0.24	28297	7.85	3.579	-3.546	7.125	2.702	1.534	4.189
120	0.125	4	106.39	180	0.28	33956	9.42	3.227	-2.413	5.640	2.477	1.439	3.716
120	0.125	4	106.39	210	0.33	39616	11.00	2.867	-1.700	4.568	2.173	1.412	3.259
120	0.125	4	106.39	240	0.38	45275	12.57	2.603	-1.415	4.018	2.186	1.340	2.991
120	0.125	6	86.87	50	0.05	6289	2.62	1.035	-3.567	4.602	8.908	2.212	22.557
120	0.125	6	86.87	100	0.10	12577	5.24	3.525	-4.732	8.256	5.999	2.224	8.009
120	0.125	6	86.87	150	0.16	18866	7.85	3.388	-2.985	6.373	4.734	2.059	5.691
120	0.125	6	86.87	200	0.21	25155	10.47	2.900	-1.759	4.659	4.128	1.746	4.470
120	0.125	6	86.87	250	0.26	31443	13.09	2.353	-0.962	3.315	3.638	1.469	3.494
120	0.125	6	86.87	300	0.31	37732	15.71	1.927	-0.367	2.294	3.101	1.206	2.836
120	0.125	6	86.87	350	0.37	44021	18.33	1.884	-0.385	2.269	2.678	0.978	2.455
120	0.125	6	86.87	400	0.42	50309	20.94	1.787	-0.255	2.042	2.434	0.719	2.254
120	0.125	8	75.23	75	0.06	7074	3.93	2.778	-4.649	7.428	3.600	1.666	12.809
120	0.125	8	75.23	150	0.12	14149	7.85	3.122	-2.824	5.946	2.819	1.892	5.430
120	0.125	8	75.23	225	0.18	21223	11.78	2.354	-0.848	3.202	2.648	1.836	3.496
120	0.125	8	75.23	300	0.24	28298	15.71	1.953	-0.405	2.358	2.340	1.777	2.597
120	0.125	8	75.23	375	0.29	35372	19.63	2.002	-0.199	2.201	2.165	1.550	2.226
120	0.125	8	75.23	450	0.35	42447	23.56	1.691	-0.213	1.904	1.890	1.439	1.807
120	0.125	8	75.23	525	0.41	49521	27.49	1.703	-0.125	1.828	1.826	1.487	1.840
120	0.125	8	75.23	600	0.47	56596	31.42	1.362	-0.060	1.422	1.709	1.395	1.636

Diam.	G/d	T	Bd	Amp	Um	Re	KC	Cl+	Cl-	Clamp	Cd	Cm	Cdmax
120	0.25	2	150.46	15	0.05	5660	0.79	0.268	-1.356	1.624	15.869	0.901	28.048
120	0.25	2	150.46	30	0.09	11319	1.57	0.048	-0.754	0.802	7.311	1.038	12.328
120	0.25	2	150.46	45	0.14	16979	2.36	0.077	-0.683	0.760	4.859	1.063	8.150
120	0.25	2	150.46	60	0.19	22638	3.14	0.184	-0.958	1.141	3.657	1.015	5.553
120	0.25	2	150.46	75	0.24	28298	3.93	0.428	-1.307	1.735	2.927	0.991	4.159
120	0.25	2	150.46	90	0.28	33957	4.71	0.712	-1.814	2.527	2.443	0.944	3.082
120	0.25	2	150.46	105	0.33	39617	5.50	1.651	-2.685	4.335	2.38	0.817	2.454
120	0.25	2	150.46	120	0.38	45276	6.28	2.807	-3.482	6.289	2.8	0.585	2.867
120	0.25	4	106.39	30	0.05	5659	1.57	-0.620	-1.834	1.213	4.392	1.387	22.129
120	0.25	4	106.39	60	0.09	11319	3.14	0.071	-1.296	1.367	2.319	1.297	8.137
120	0.25	4	106.39	90	0.14	16978	4.71	1.211	-2.533	3.745	2.06	1.148	4.886
120	0.25	4	106.39	120	0.19	22638	6.28	2.867	-4.074	6.940	2.603	1.062	3.562
120	0.25	4	106.39	150	0.24	28297	7.85	3.150	-3.829	6.979	2.452	1.138	2.949
120	0.25	4	106.39	180	0.28	33956	9.42	3.217	-3.180	6.396	2.3	1.127	3.133
120	0.25	4	106.39	210	0.33	39616	11.00	2.913	-2.487	5.401	2.142	1.115	2.769
120	0.25	4	106.39	240	0.38	45275	12.57	2.608	-1.665	4.273	1.944	1.097	2.338
120	0.25	6	86.87	50	0.05	6289	2.62	-0.043	-1.436	1.393	7.587	2.203	19.054
120	0.25	6	86.87	100	0.10	12577	5.24	1.982	-3.502	5.484	5.028	1.752	6.999
120	0.25	6	86.87	150	0.16	18866	7.85	3.037	-3.773	6.811	4.435	1.604	4.866
120	0.25	6	86.87	200	0.21	25155	10.47	3.042	-2.744	5.785	3.936	1.266	4.141
120	0.25	6	86.87	250	0.26	31443	13.09	2.633	-1.794	4.427	3.483	1.071	3.285
120	0.25	6	86.87	300	0.31	37732	15.71	2.063	-1.201	3.264	3.015	0.971	2.707
120	0.25	6	86.87	350	0.37	44021	18.33	1.455	-0.314	1.769	2.547	0.413	2.482
120	0.25	6	86.87	400	0.42	50309	20.94	1.312	-0.468	1.780	2.154	0.550	1.989
120	0.25	8	75.23	75	0.06	7074	3.93	0.750	-2.202	2.952	2.5	1.313	11.002
120	0.25	8	75.23	150	0.12	14149	7.85	2.466	-3.686	6.152	2.747	1.359	4.256
120	0.25	8	75.23	225	0.18	21223	11.78	2.270	-2.410	4.679	2.667	1.455	3.073
120	0.25	8	75.23	300	0.24	28298	15.71	1.839	-1.187	3.026	2.371	1.313	2.426
120	0.25	8	75.23	375	0.29	35372	19.63	1.485	-0.452	1.937	1.898	1.149	2.072
120	0.25	8	75.23	450	0.35	42447	23.56	1.349	-0.381	1.730	1.762	1.134	1.749
120	0.25	8	75.23	525	0.41	49521	27.49	1.220	-0.216	1.437	1.677	1.100	1.611
120	0.25	8	75.23	600	0.47	56596	31.42	1.040	-0.212	1.253	1.529	1.079	1.401

Diam.	G/d	T	Bd	Amp	Um	Re	KC	Cl+	Cl-	Clamp	Cd	Cm	Cdmax
120	0.5	2	150.46	15	0.05	5660	0.79	1.293	-0.580	1.873	0.967	0.928	16.741
120	0.5	2	150.46	30	0.09	11319	1.57	0.419	-0.096	0.514	-1.235	1.055	7.014
120	0.5	2	150.46	45	0.14	16979	2.36	0.337	-0.270	0.607	-0.749	1.129	5.121
120	0.5	2	150.46	60	0.19	22638	3.14	0.298	-0.183	0.480	-0.446	1.144	3.530
120	0.5	2	150.46	75	0.24	28298	3.93	0.030	-0.331	0.361	0.067	1.262	3.455
120	0.5	2	150.46	90	0.28	33957	4.71	0.176	-0.345	0.521	0.305	1.270	3.077
120	0.5	2	150.46	105	0.33	39617	5.50	0.489	-0.871	1.360	0.444	1.223	2.513
120	0.5	2	150.46	120	0.38	45276	6.28	0.937	-1.429	2.365	0.499	1.160	2.219
120	0.5	4	106.39	30	0.05	5659	1.57	0.062	-0.888	0.950	3.948	1.261	19.966
120	0.5	4	106.39	60	0.09	11319	3.14	-0.024	-0.433	0.410	2.120	1.196	7.124
120	0.5	4	106.39	90	0.14	16978	4.71	0.095	-0.626	0.721	1.610	1.130	4.614
120	0.5	4	106.39	120	0.19	22638	6.28	0.737	-1.497	2.234	1.459	0.966	3.146
120	0.5	4	106.39	150	0.24	28297	7.85	1.680	-2.246	3.926	1.670	0.727	2.651
120	0.5	4	106.39	180	0.28	33956	9.42	2.139	-2.268	4.406	2.003	0.622	2.082
120	0.5	4	106.39	210	0.33	39616	11.00	2.318	-2.206	4.523	1.863	0.688	1.867
120	0.5	4	106.39	240	0.38	45275	12.57	2.147	-1.693	3.840	1.706	0.719	1.740
120	0.5	6	86.87	50	0.05	6289	2.62	0.446	-1.050	1.496	8.180	2.501	18.005
120	0.5	6	86.87	100	0.10	12577	5.24	0.345	-1.306	1.651	4.718	2.123	7.341
120	0.5	6	86.87	150	0.16	18866	7.85	1.999	-2.599	4.598	4.317	1.596	4.593
120	0.5	6	86.87	200	0.21	25155	10.47	2.564	-2.234	4.799	3.875	1.334	3.892
120	0.5	6	86.87	250	0.26	31443	13.09	2.358	-1.695	4.053	3.455	1.073	3.460
120	0.5	6	86.87	300	0.31	37732	15.71	1.895	-1.328	3.223	2.822	0.992	2.825
120	0.5	6	86.87	350	0.37	44021	18.33	1.460	-0.814	2.274	2.432	0.833	2.442
120	0.5	6	86.87	400	0.42	50309	20.94	1.156	-0.434	1.590	2.159	0.760	2.302
120	0.5	8	75.23	75	0.06	7074	3.93	-0.074	-0.994	0.920	1.998	1.581	8.867
120	0.5	8	75.23	150	0.12	14149	7.85	2.002	-2.432	4.434	2.447	1.150	4.282
120	0.5	8	75.23	225	0.18	21223	11.78	2.458	-2.109	4.567	2.546	1.091	2.965
120	0.5	8	75.23	300	0.24	28298	15.71	1.850	-1.449	3.300	2.043	1.116	2.454
120	0.5	8	75.23	375	0.29	35372	19.63	1.313	-0.693	2.006	1.735	1.014	1.867
120	0.5	8	75.23	450	0.35	42447	23.56	0.974	-0.337	1.311	1.534	1.118	1.725
120	0.5	8	75.23	525	0.41	49521	27.49	0.904	-0.321	1.225	1.453	1.113	1.491
120	0.5	8	75.23	600	0.47	56596	31.42	0.700	-0.185	0.884	1.341	1.141	1.413

Diam.	G/d	T	Bd	Amp	Um	Re	KC	Cl+	Cl-	Clamp	Cd	Cm	Cdmax
90	0.6	2	112.85	15	0.05	4245	1.05	0.314	-0.503	0.818	-3.330	0.623	11.736
90	0.6	2	112.85	30	0.09	8490	2.09	-0.019	-0.415	0.395	-1.802	0.563	4.196
90	0.6	2	112.85	45	0.14	12735	3.14	0.116	-0.251	0.367	-1.581	0.682	2.910
90	0.6	2	112.85	60	0.19	16980	4.19	0.210	-0.421	0.631	-1.113	0.630	2.180
90	0.6	2	112.85	75	0.24	21225	5.24	0.286	-0.854	1.139	-0.959	0.665	1.845
90	0.6	2	112.85	90	0.28	25470	6.28	0.776	-1.336	2.111	-0.631	0.646	1.327
90	0.6	2	112.85	105	0.33	29715	7.33	1.655	-2.176	3.830	-0.236	0.653	1.056
90	0.6	2	112.85	120	0.38	33960	8.38	2.375	-2.288	4.663	0.455	0.543	1.005
90	0.6	8	56.42	75	0.06	5305	5.24	-1.244	-3.620	2.375	2.203	1.687	10.047
90	0.6	8	56.42	150	0.12	10611	10.47	2.257	-1.910	4.166	2.790	1.705	3.952
90	0.6	8	56.42	225	0.18	15916	15.71	1.248	-1.033	2.281	2.245	1.728	2.471
90	0.6	8	56.42	300	0.24	21221	20.94	0.806	-0.806	1.613	1.860	1.625	2.134
90	0.6	8	56.42	375	0.29	26527	26.18	0.533	-0.290	0.824	1.667	1.710	1.722
90	0.6	8	56.42	450	0.35	31832	31.42	0.721	-0.324	1.045	1.631	1.772	1.738
90	0.6	8	56.42	525	0.41	37138	36.65	0.746	-0.332	1.078	1.541	1.638	1.524
90	0.6	8	56.42	600	0.47	42443	41.89	0.542	-0.304	0.846	1.493	1.840	1.497
90	0.75	2	112.85	15	0.05	4245	1.05	0.994	-0.001	0.995	-6.363	0.500	14.092
90	0.75	2	112.85	30	0.09	8490	2.09	0.108	-0.274	0.382	-3.378	0.456	5.243
90	0.75	2	112.85	45	0.14	12735	3.14	0.132	-0.131	0.263	-2.291	0.474	3.097
90	0.75	2	112.85	60	0.19	16980	4.19	0.095	-0.318	0.412	-1.901	0.560	2.360
90	0.75	2	112.85	75	0.24	21225	5.24	0.190	-0.572	0.762	-1.458	0.640	2.129
90	0.75	2	112.85	90	0.28	25470	6.28	0.391	-0.763	1.154	-1.020	0.652	1.648
90	0.75	2	112.85	105	0.33	29715	7.33	1.417	-1.946	3.362	-0.690	0.691	1.150
90	0.75	2	112.85	120	0.38	33960	8.38	2.339	-2.164	4.503	-0.035	0.495	0.889
90	0.75	8	56.42	75	0.06	5305	5.24	-0.750	-2.622	1.872	2.204	1.815	10.638
90	0.75	8	56.42	150	0.12	10611	10.47	2.078	-1.918	3.996	2.788	1.672	4.411
90	0.75	8	56.42	225	0.18	15916	15.71	1.546	-1.318	2.864	2.262	1.618	2.496
90	0.75	8	56.42	300	0.24	21221	20.94	0.862	-0.725	1.587	1.813	1.646	1.973
90	0.75	8	56.42	375	0.29	26527	26.18	0.740	-0.628	1.368	1.692	1.657	1.765
90	0.75	8	56.42	450	0.35	31832	31.42	0.616	-0.318	0.934	1.562	1.771	1.511
90	0.75	8	56.42	525	0.41	37138	36.65	0.541	-0.281	0.822	1.501	1.700	1.473
90	0.75	8	56.42	600	0.47	42443	41.89	0.532	-0.235	0.767	1.443	1.675	1.448

Diam.	G/d	T	Bd	Amp	Um	Re	KC	Cl+	Cl-	Clamp	Cd	Cm	Cdmax
90	1	2	112.85	15	0.05	4245	1.05	0.765	-0.719	1.484	-3.385	0.516	13.517
90	1	2	112.85	30	0.09	8490	2.09	0.181	-0.129	0.310	-1.817	0.495	4.144
90	1	2	112.85	45	0.14	12735	3.14	0.096	-0.197	0.293	-1.250	0.490	2.499
90	1	2	112.85	60	0.19	16980	4.19	0.081	-0.150	0.230	-1.096	0.566	2.096
90	1	2	112.85	75	0.24	21225	5.24	0.089	-0.340	0.429	-0.882	0.616	1.716
90	1	2	112.85	90	0.28	25470	6.28	0.152	-0.381	0.534	-0.676	0.642	1.389
90	1	2	112.85	105	0.33	29715	7.33	0.955	-1.653	2.609	-0.358	0.653	0.979
90	1	2	112.85	120	0.38	33960	8.38	1.744	-1.946	3.690	-0.012	0.463	0.732
90	1	8	56.42	75	0.06	5305	5.24	1.134	-0.029	1.163	2.116	1.755	10.506
90	1	8	56.42	150	0.12	10611	10.47	2.225	-1.525	3.750	2.543	1.349	3.786
90	1	8	56.42	225	0.18	15916	15.71	1.522	-1.032	2.554	2.271	1.441	2.532
90	1	8	56.42	300	0.24	21221	20.94	0.748	-0.752	1.500	1.850	1.625	2.029
90	1	8	56.42	375	0.29	26527	26.18	0.590	-0.555	1.145	1.582	1.431	1.655
90	1	8	56.42	450	0.35	31832	31.42	0.238	-0.185	0.423	1.451	1.567	1.471
90	1	8	56.42	525	0.41	37138	36.65	0.361	-0.268	0.629	1.453	1.433	1.473
90	1	8	56.42	600	0.47	42443	41.89	0.443	-0.233	0.676	1.369	1.419	1.365

APPENDIX G - PLOTS OF LIFT vs PHASE

Plots of lift versus phase have been given, showing both lift coefficient and lift force versus the phase angle.

The plots are arranged in ascending order of gap ratio. For each gap ratio, tests are arranged in increasing period and for each period they are arranged in increasing amplitude.

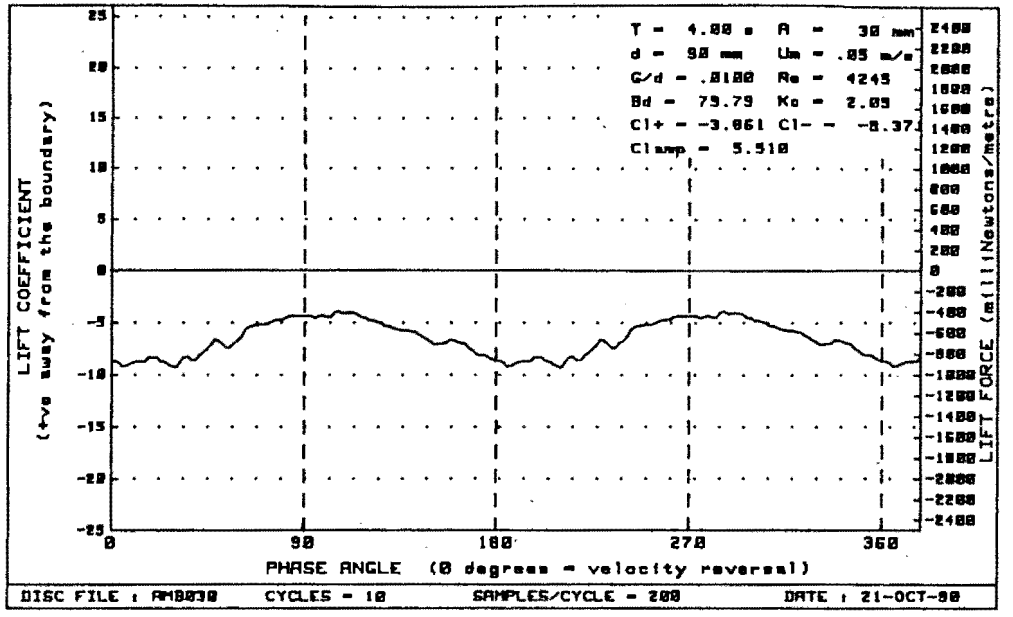

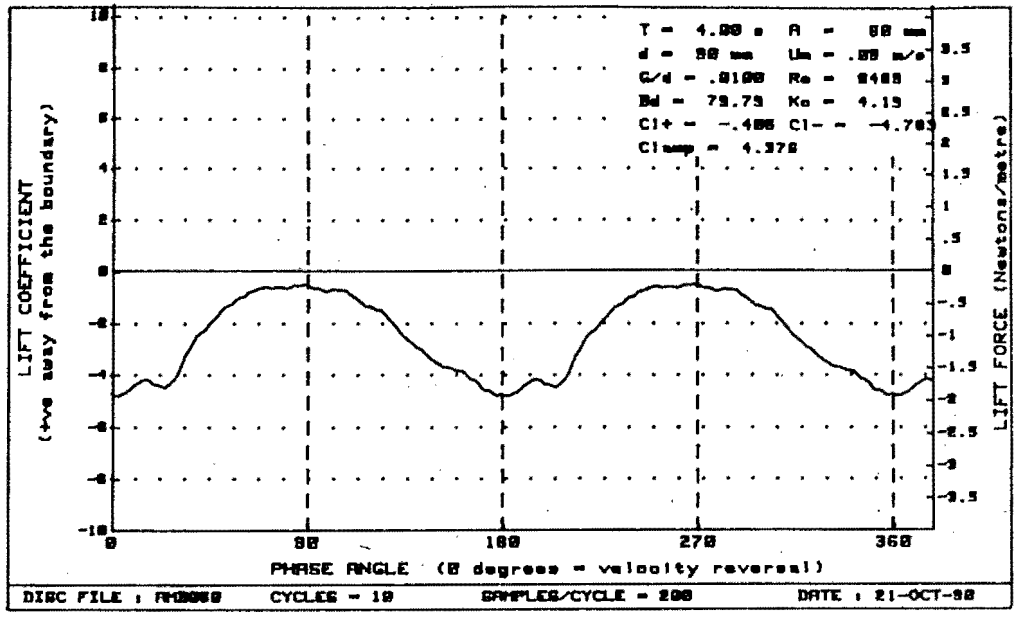

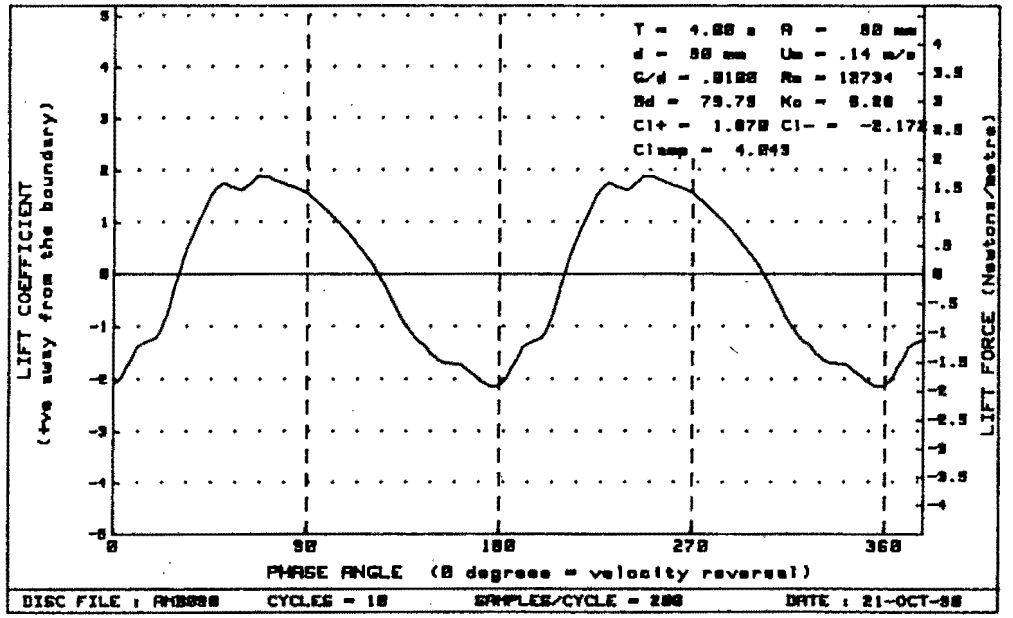

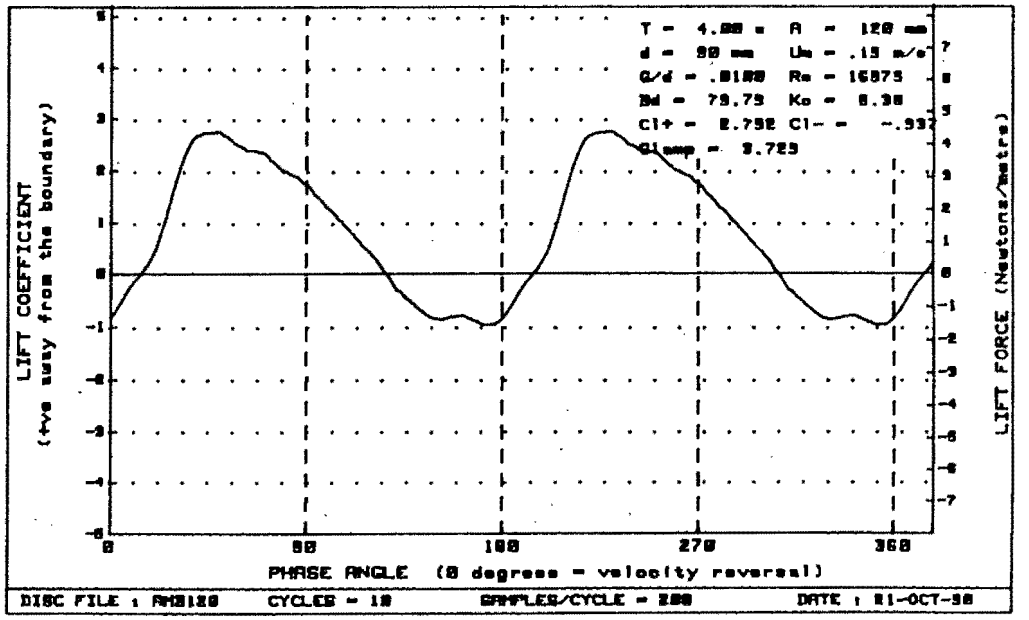

Figure G-1 : Plots of lift vs phase for diameter=90mm, Bd= 79.79 and G/d= .0100

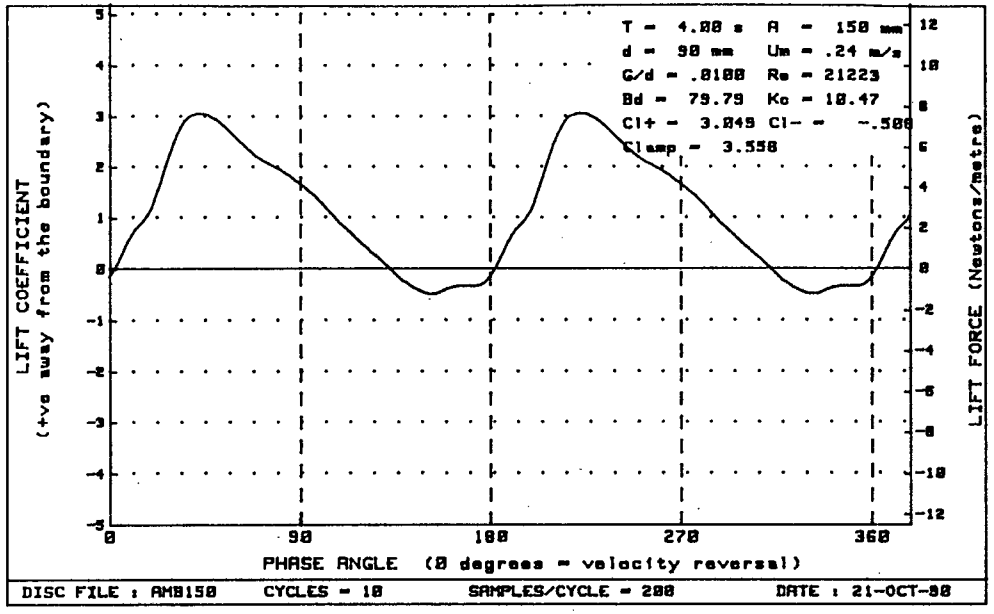

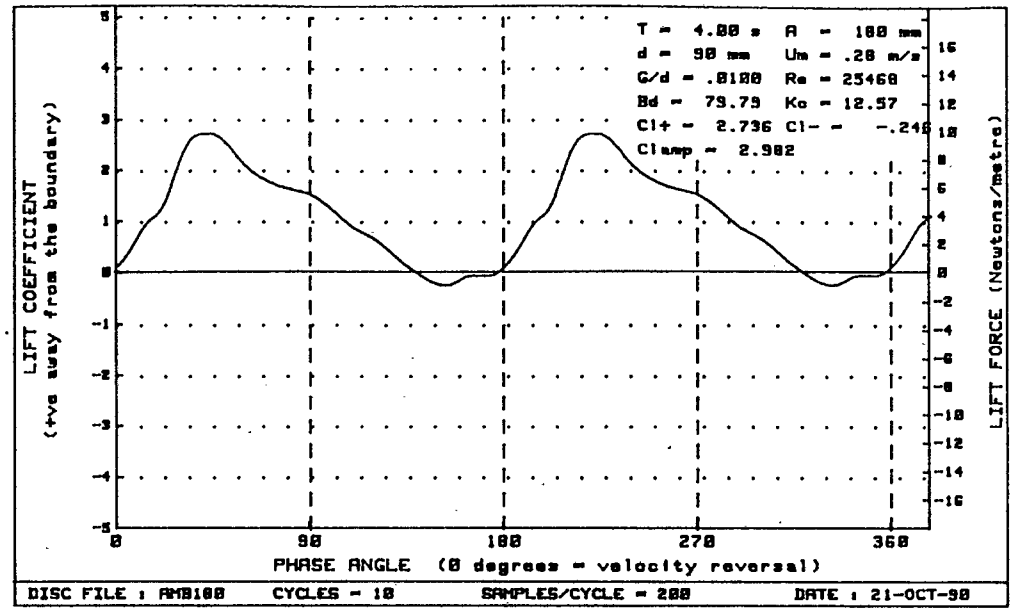

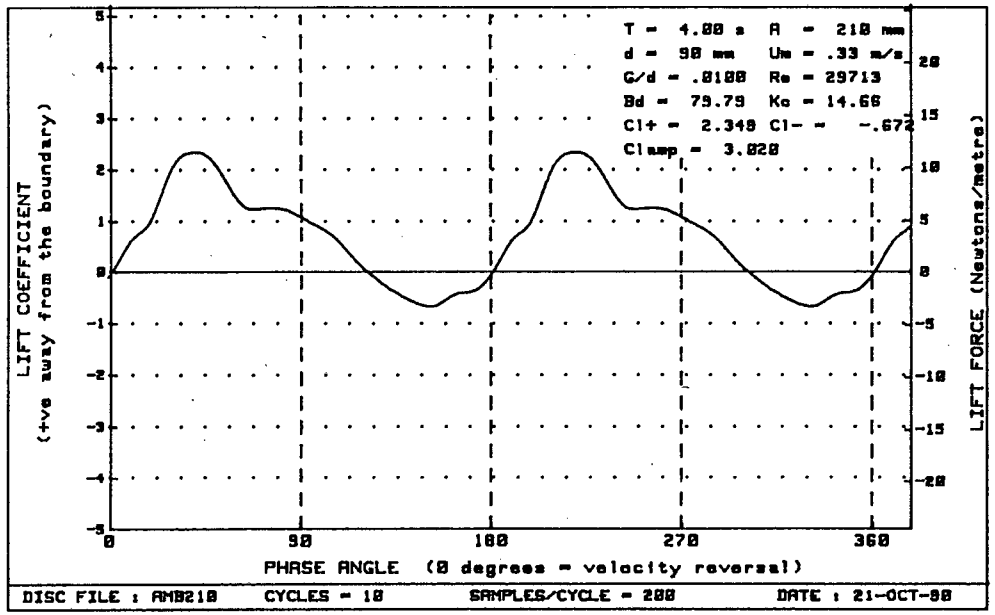

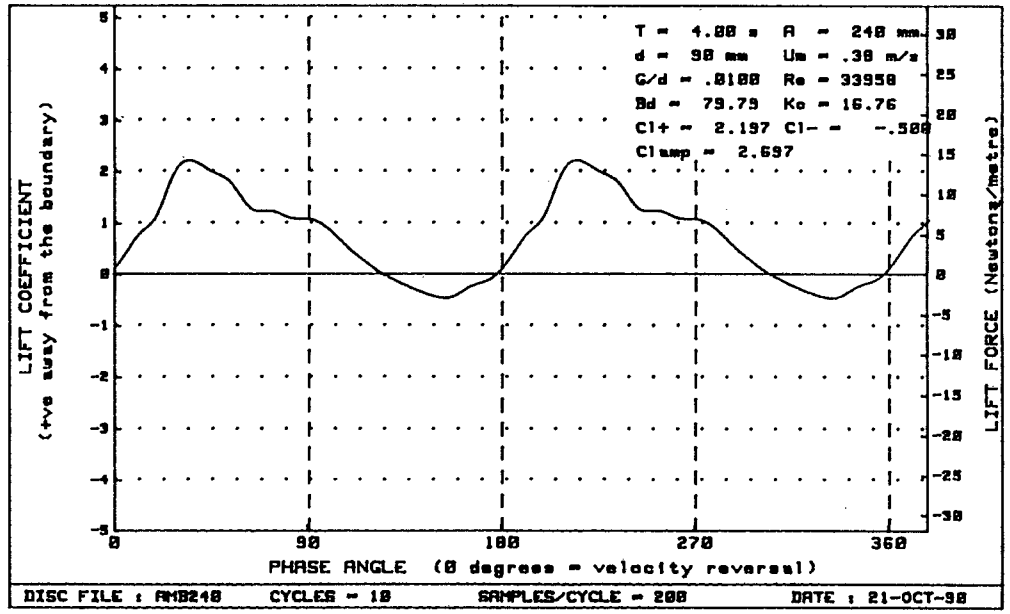

Figure G-2 : Plots of lift vs phase for diameter=90mm, Bd= 79.79 and G/d= .0100

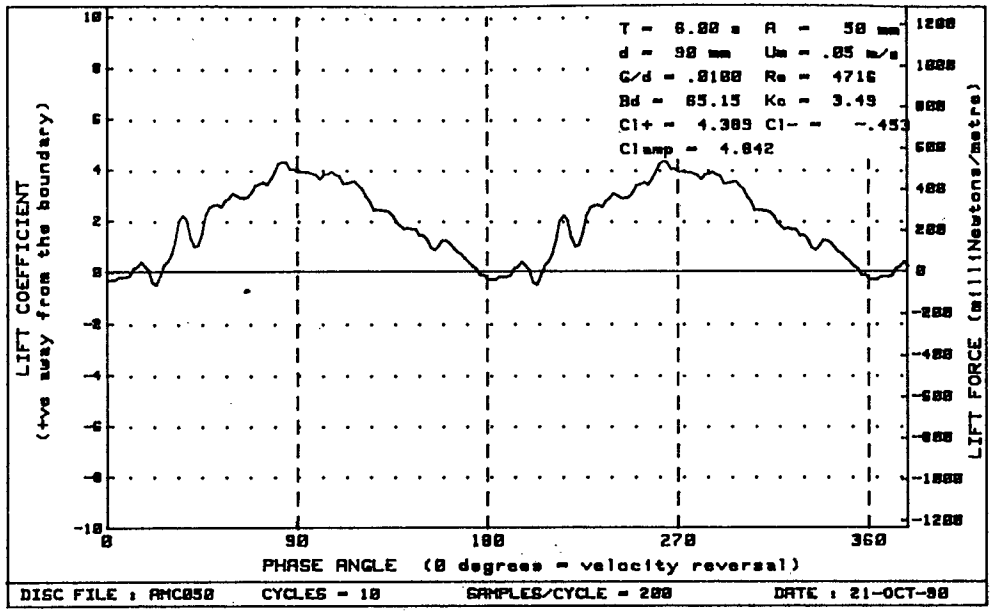

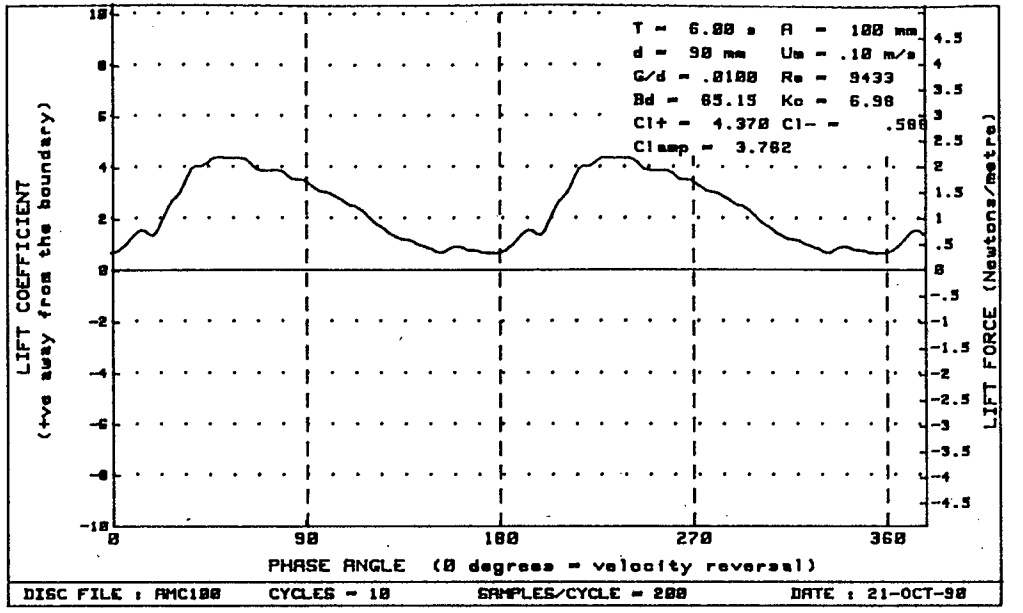

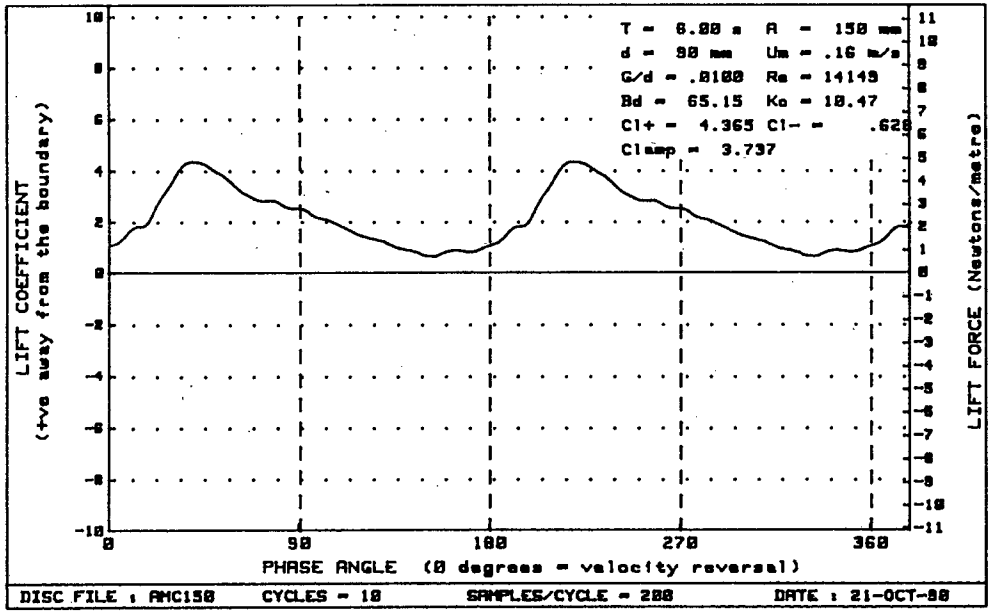

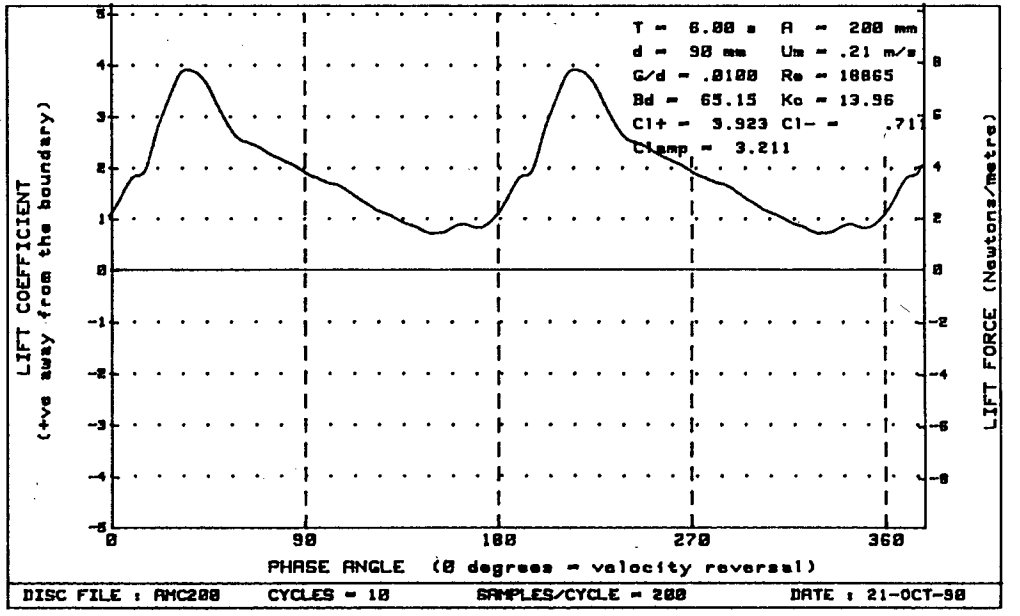

Figure G-3 : Plots of lift vs phase for diameter=90mm, Bd= 65.15 and G/d= .0100

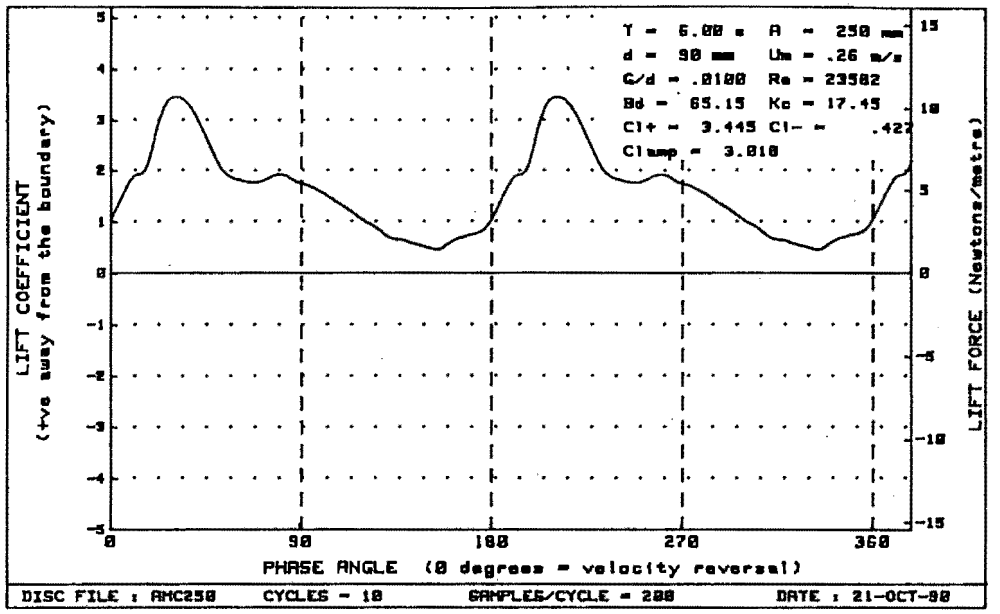

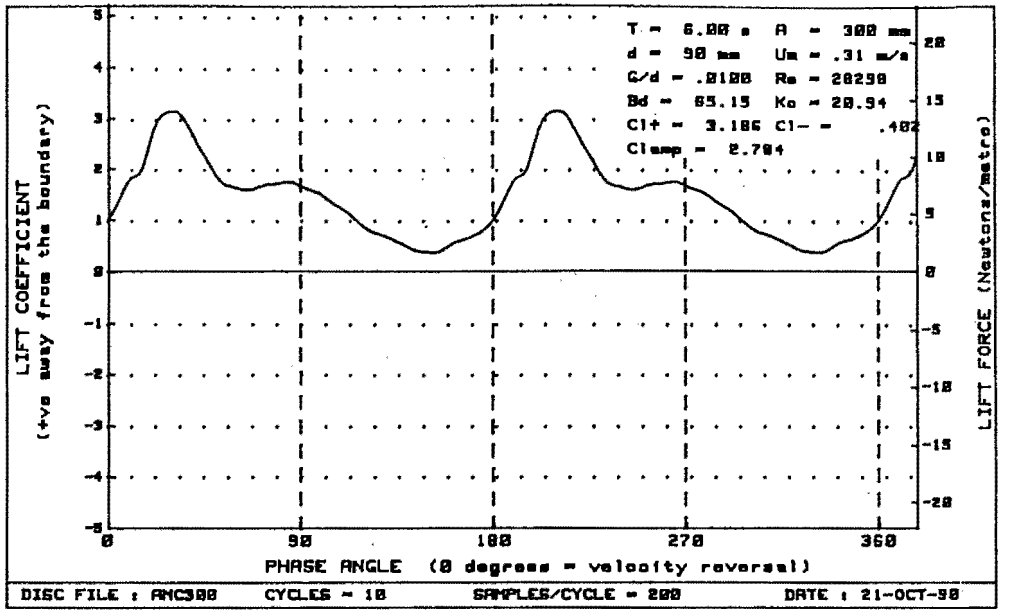

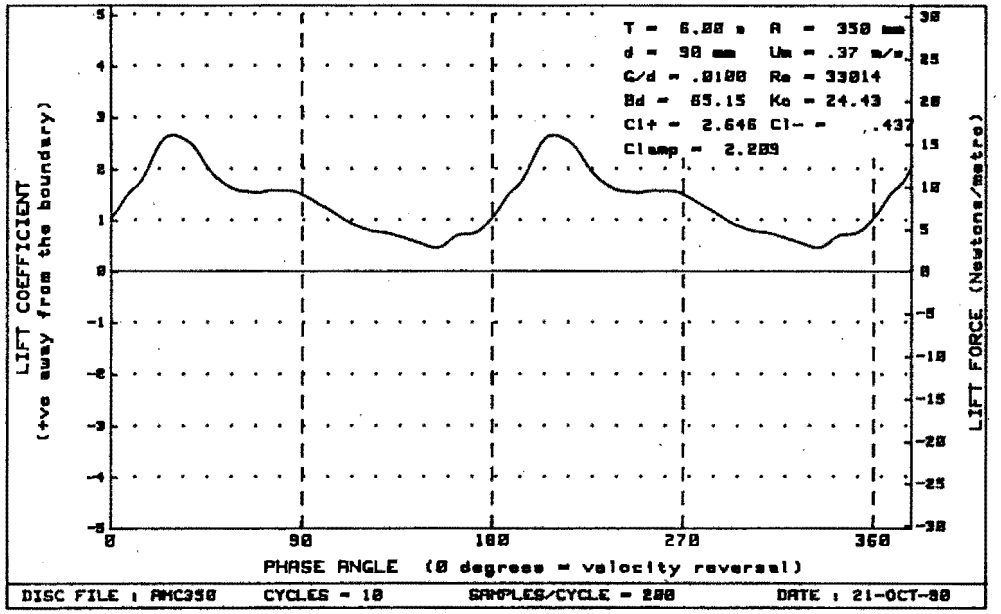

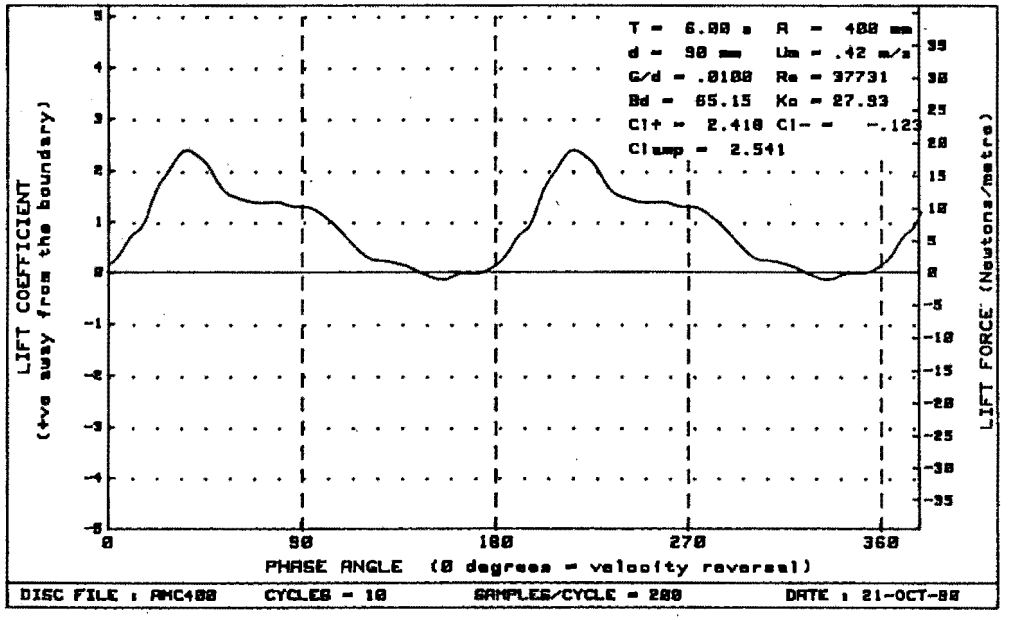

Figure G-4 : Plots of lift vs phase for diameter=90mm, Bd= 65.15 and G/d= .0100

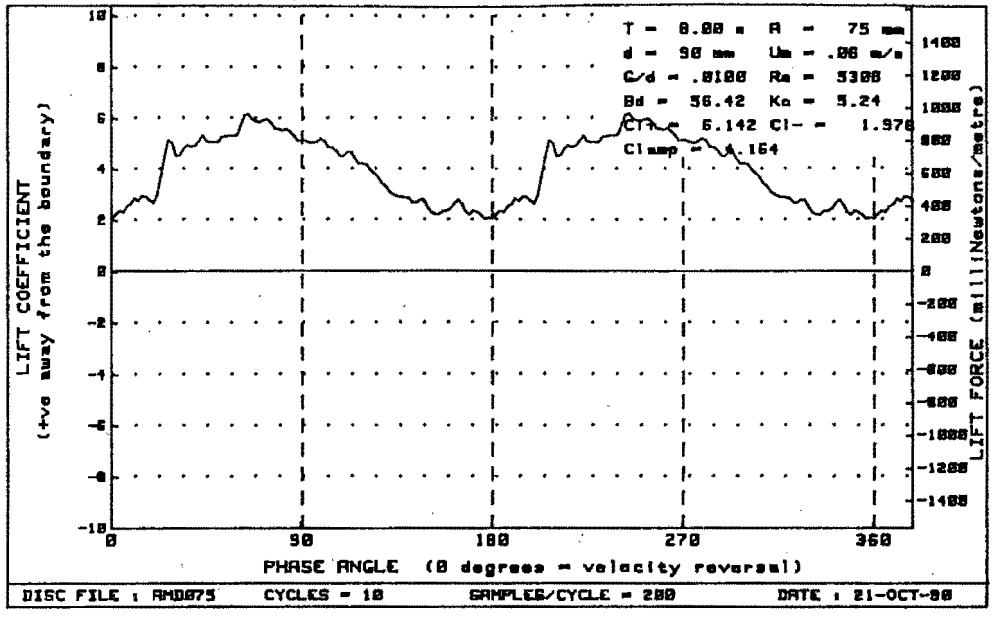

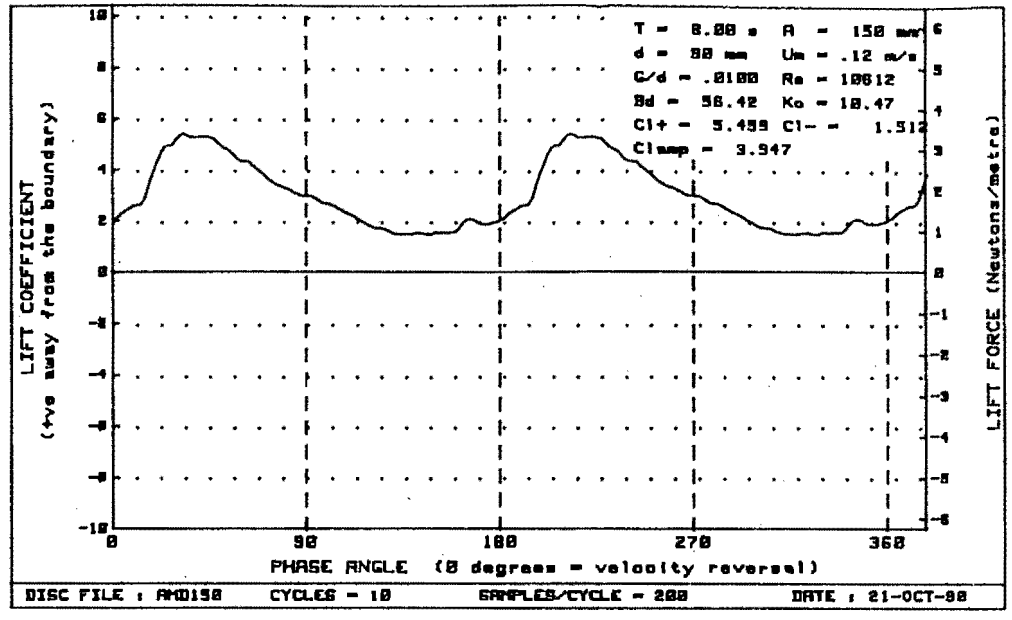

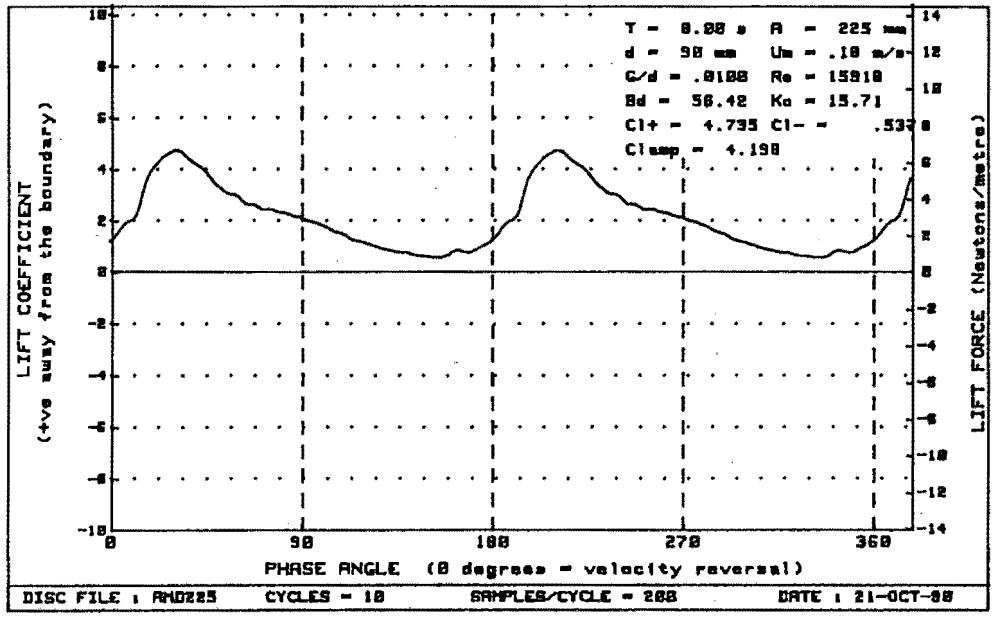

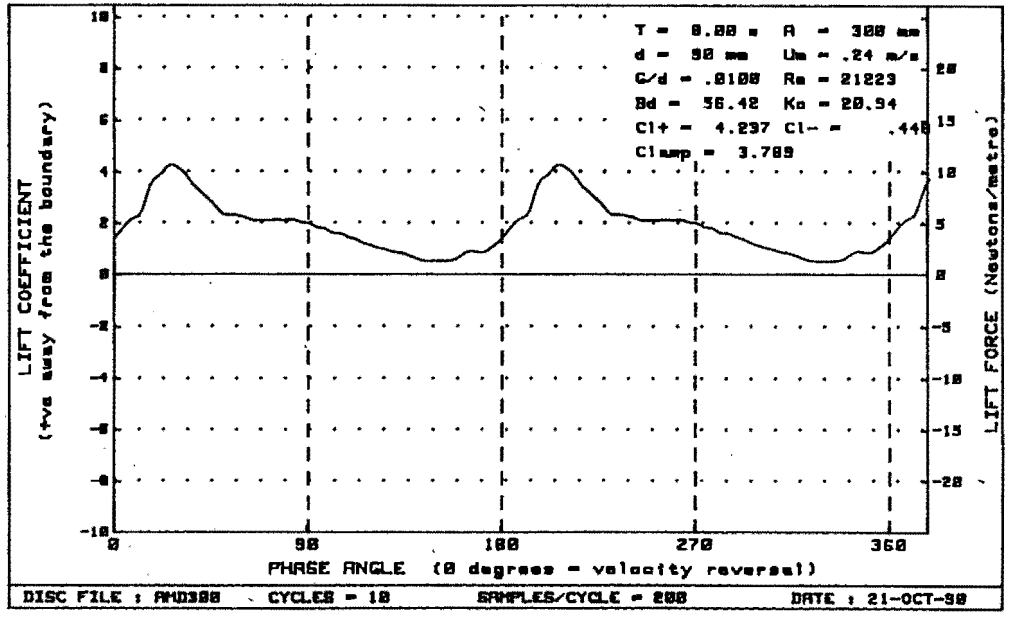

Figure G-5 : Plots of lift vs phase for diameter=90mm, Bd= 56.42 and G/d= .0100

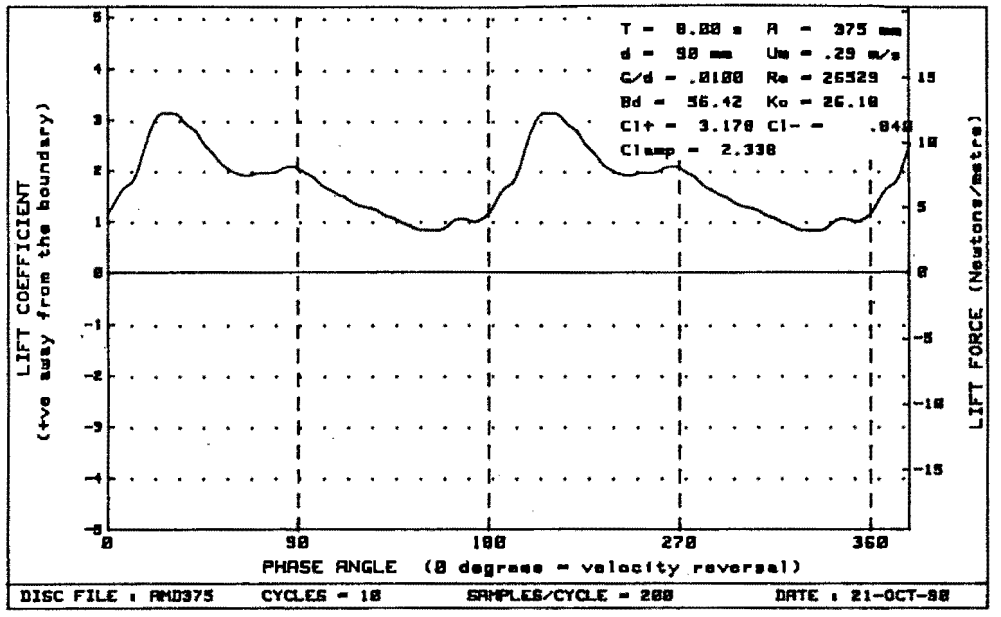

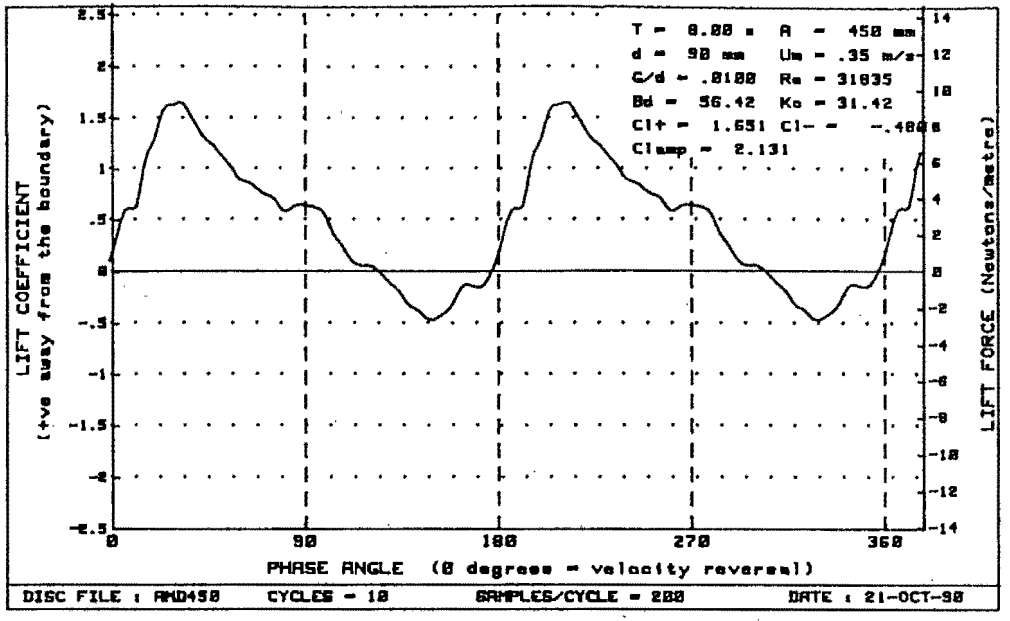

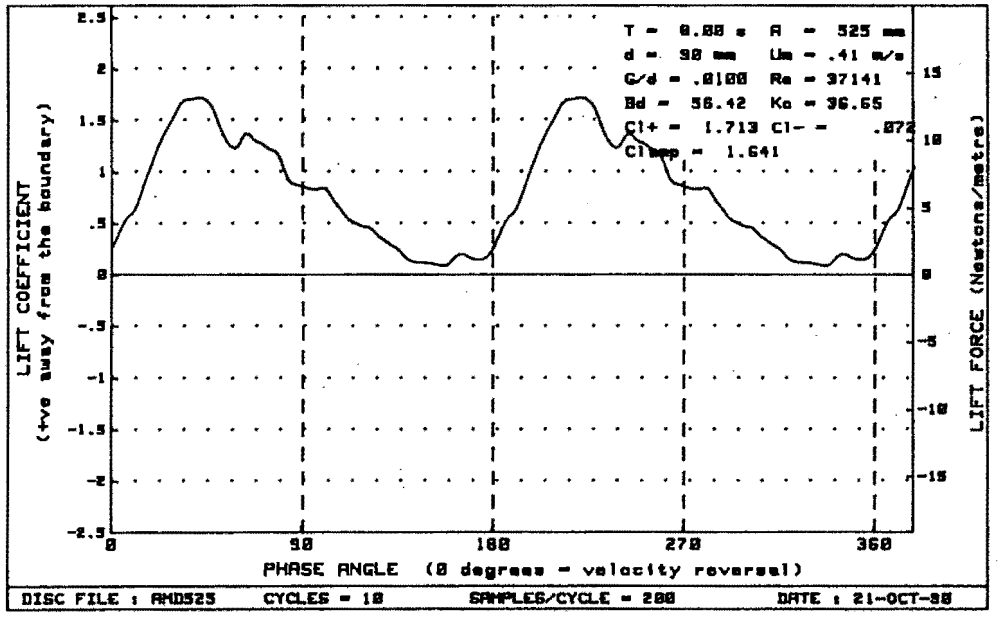

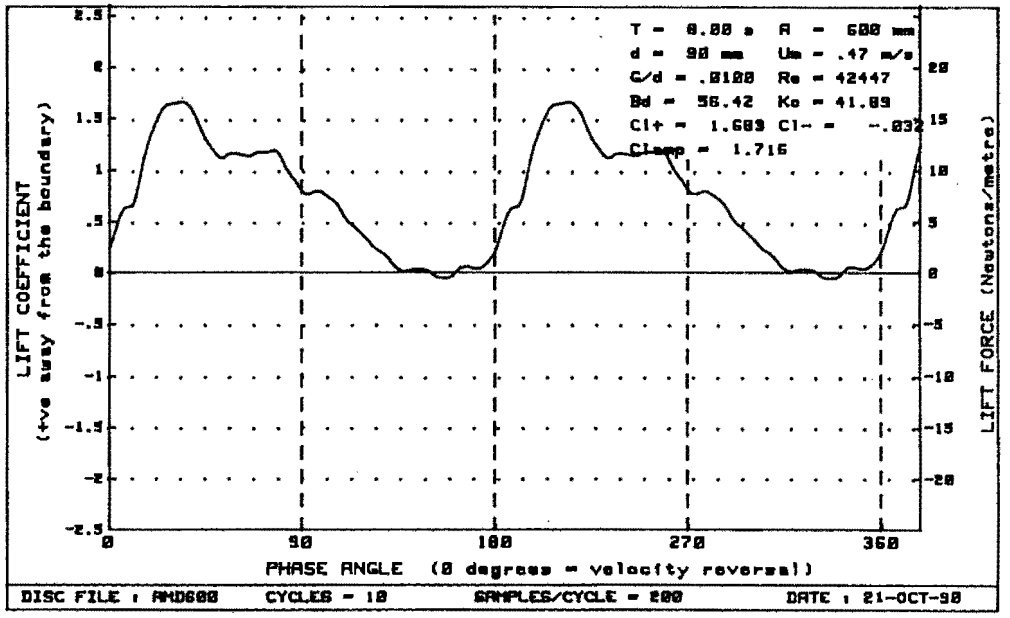

Figure G-6 : Plots of lift vs phase for diameter=90mm, Bd= 56.42 and G/d= .0100

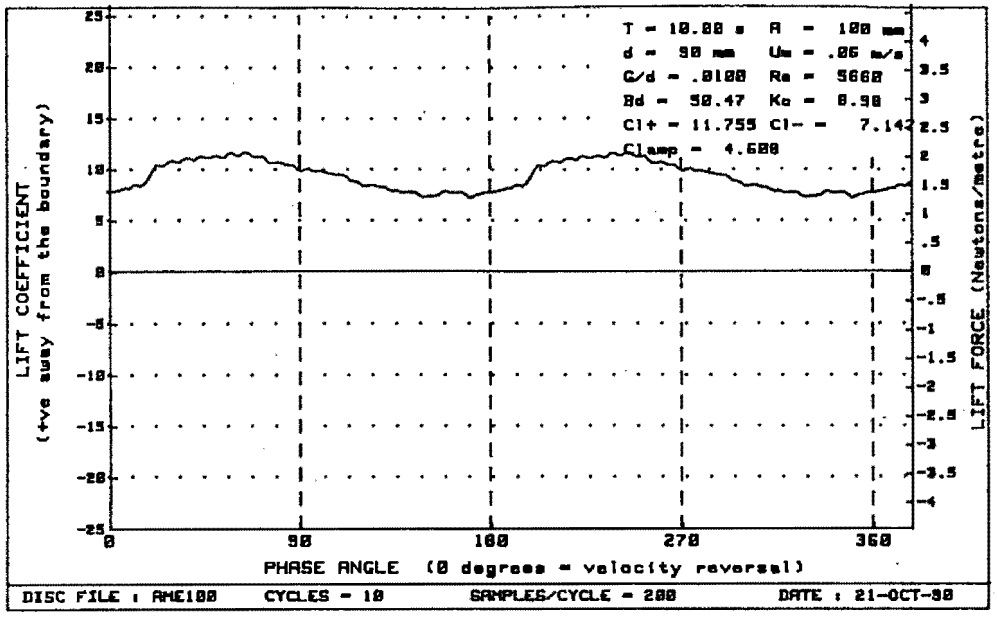

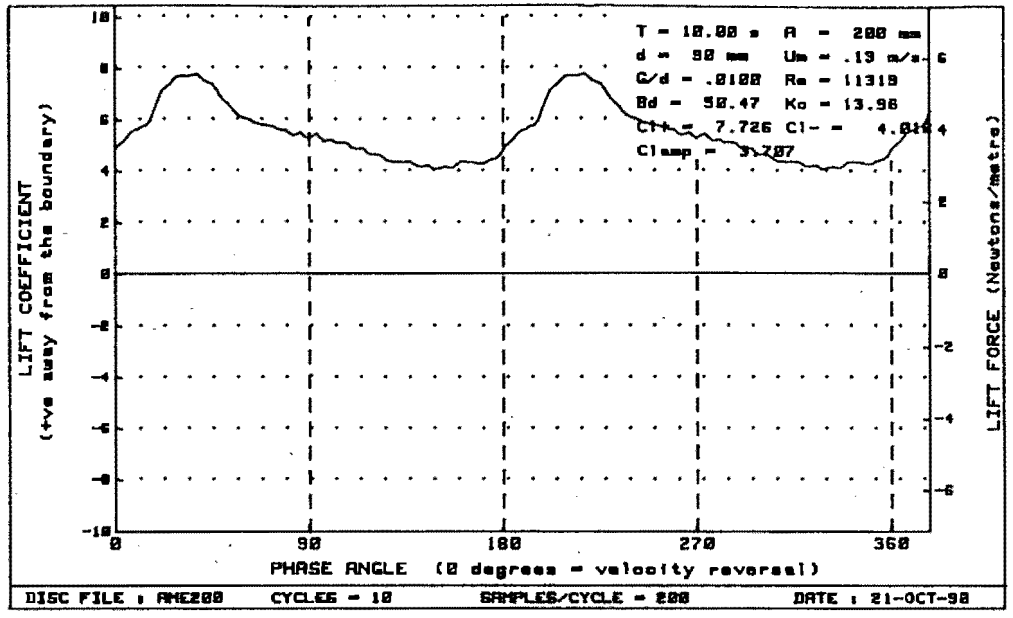

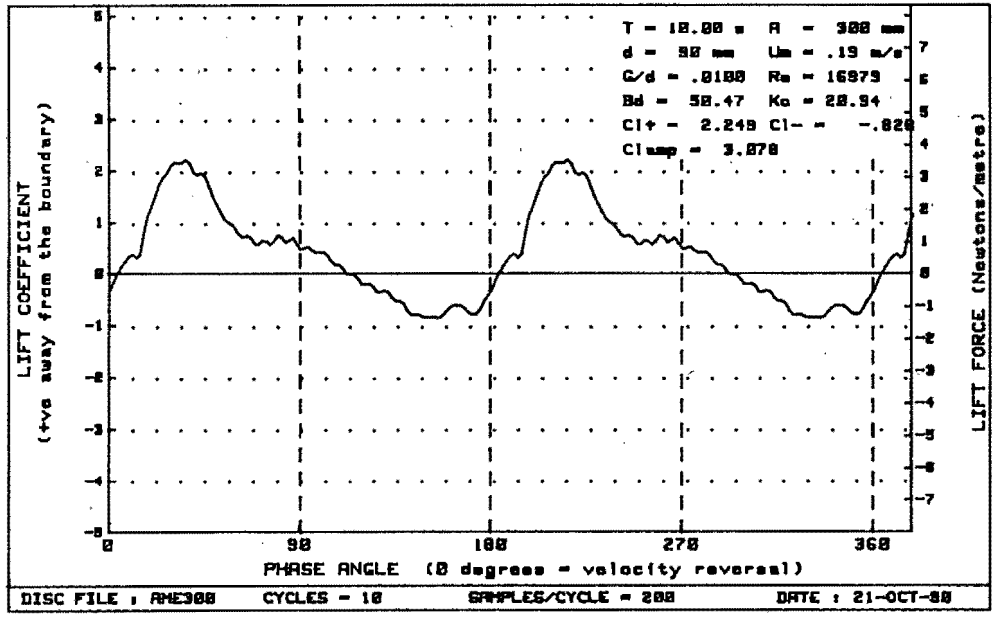

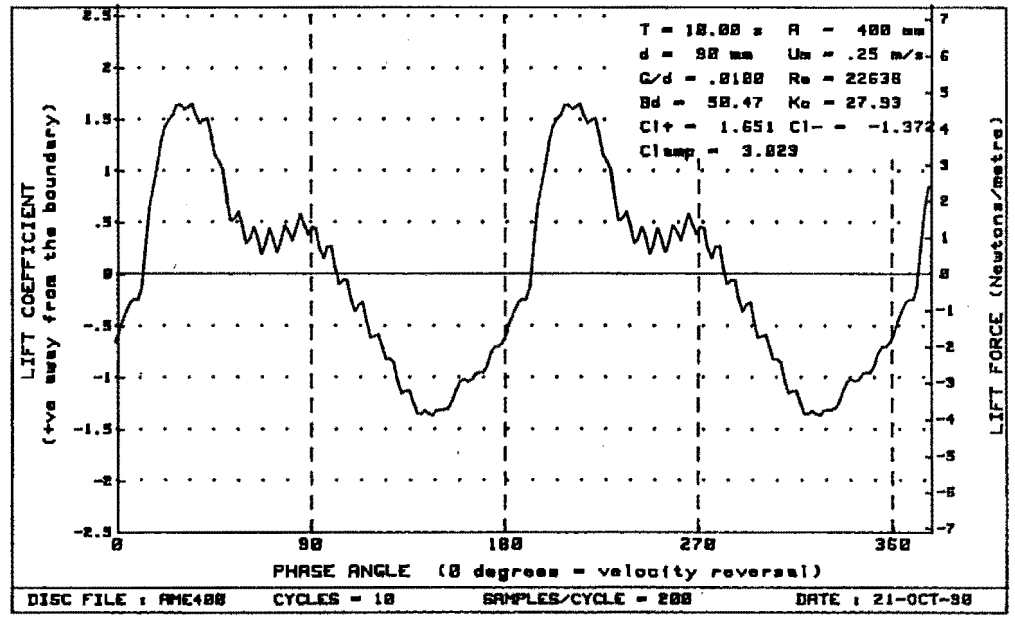

Figure G-7 : Plots of lift vs phase for diameter=90mm, Bd= 50.47 and G/d= .0100

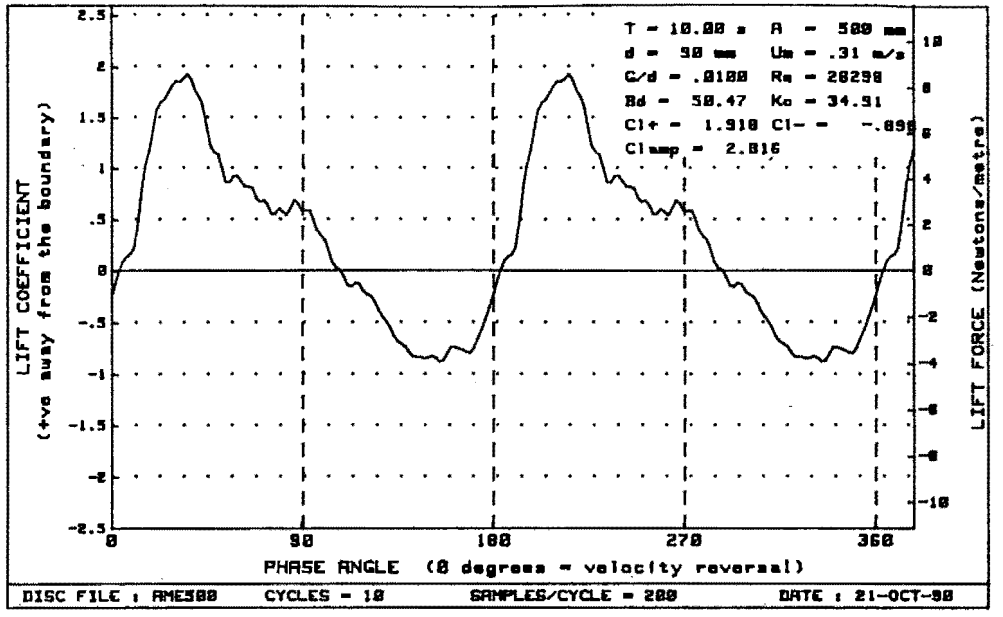

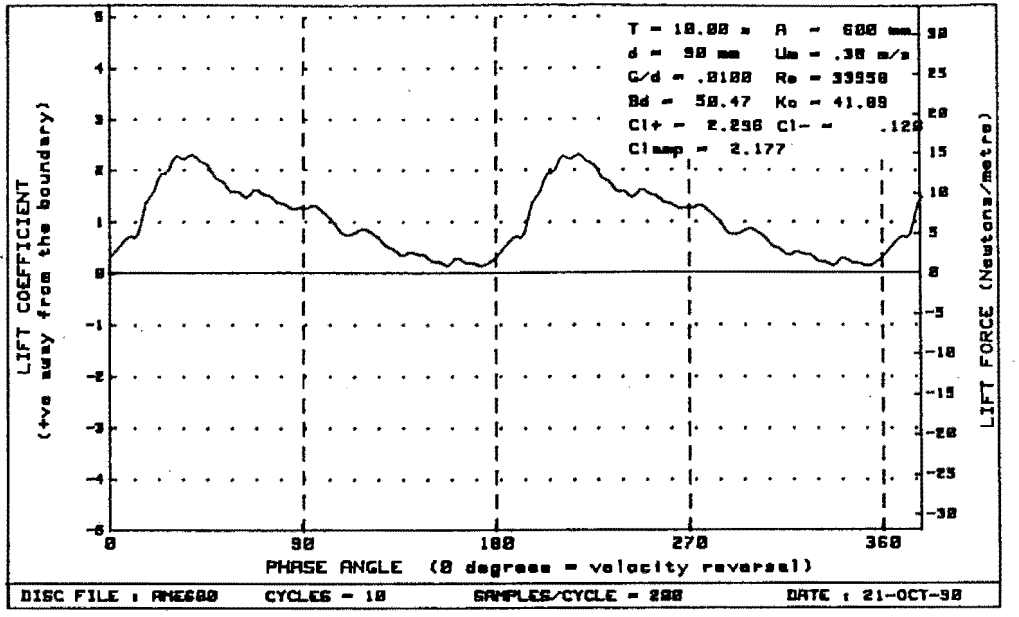

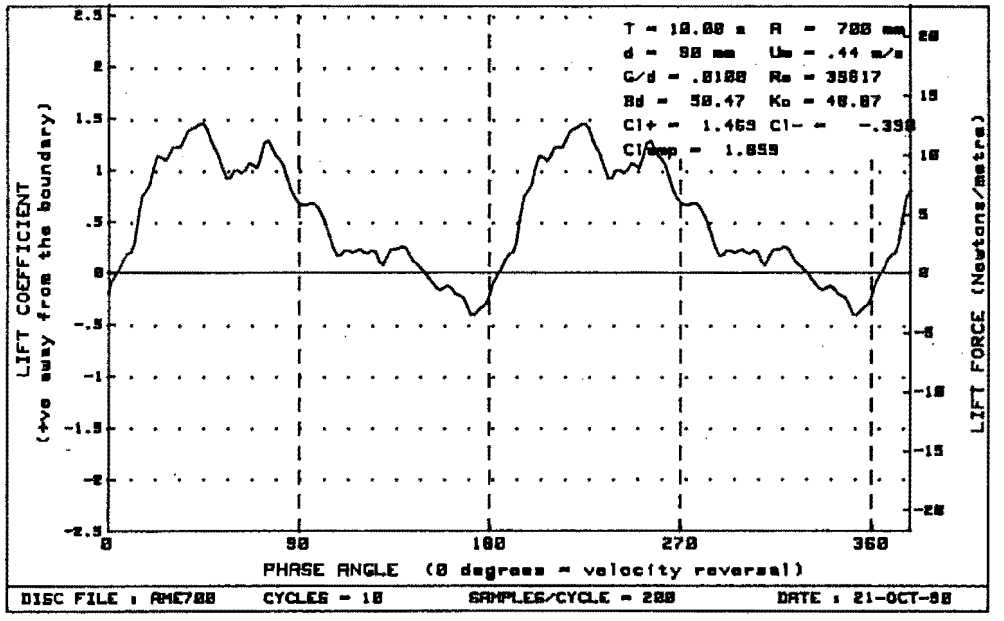

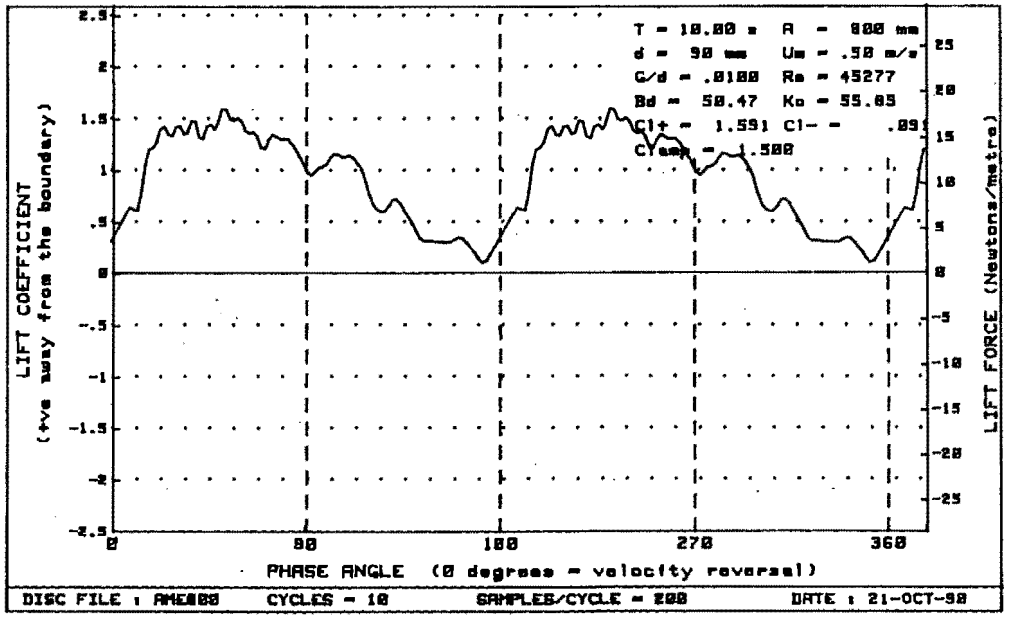

Figure G-8 : Plots of lift vs phase for diameter=90mm, Bd= 50.47 and G/d= .0100

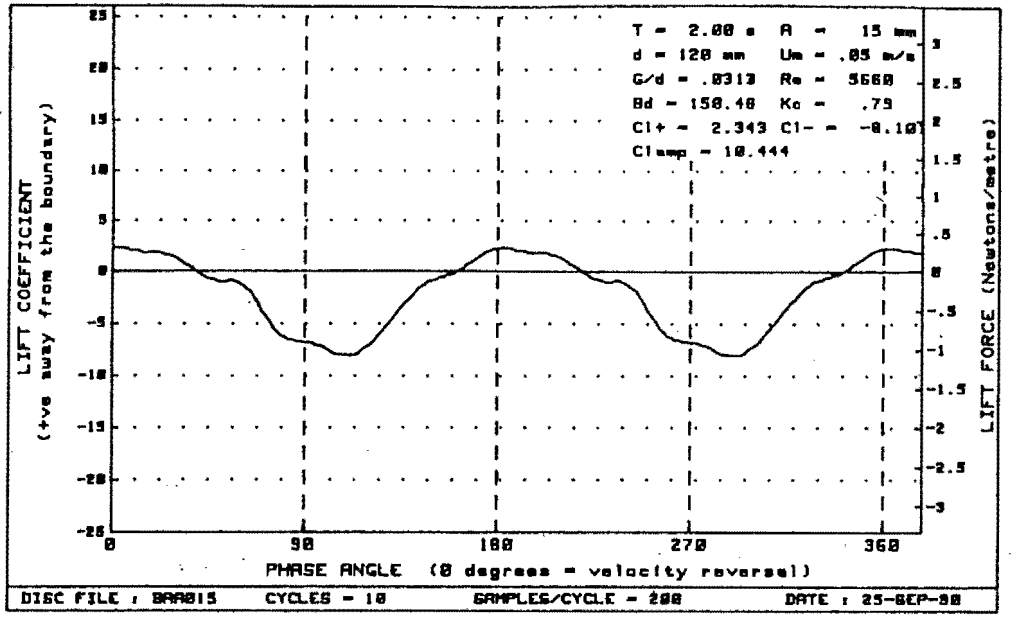

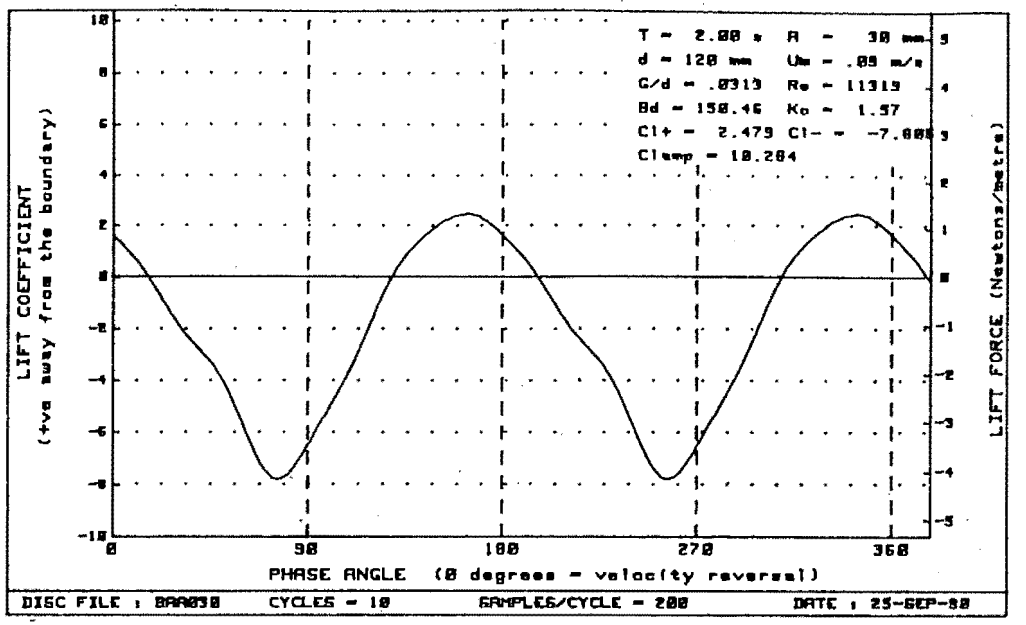

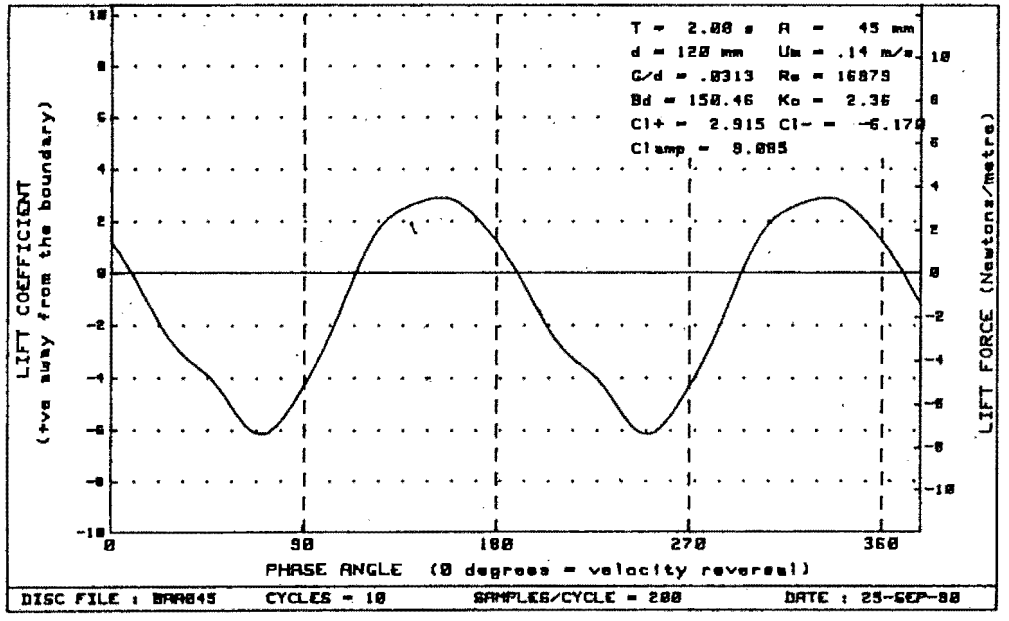

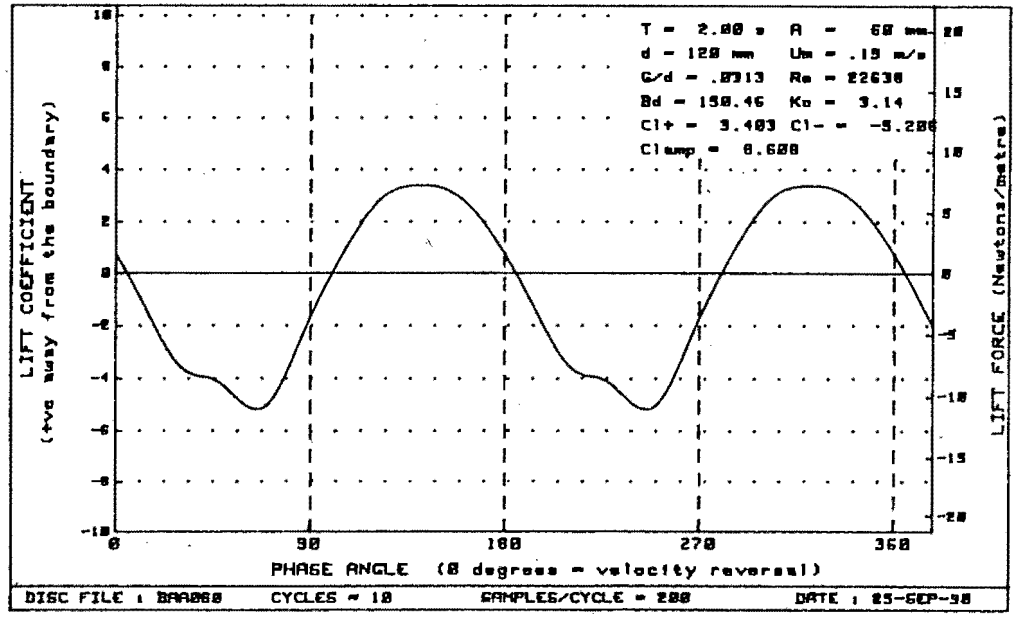

Figure G-9 : Plots of lift vs phase for diameter=120mm, Bd=150.46 and G/d= .0313

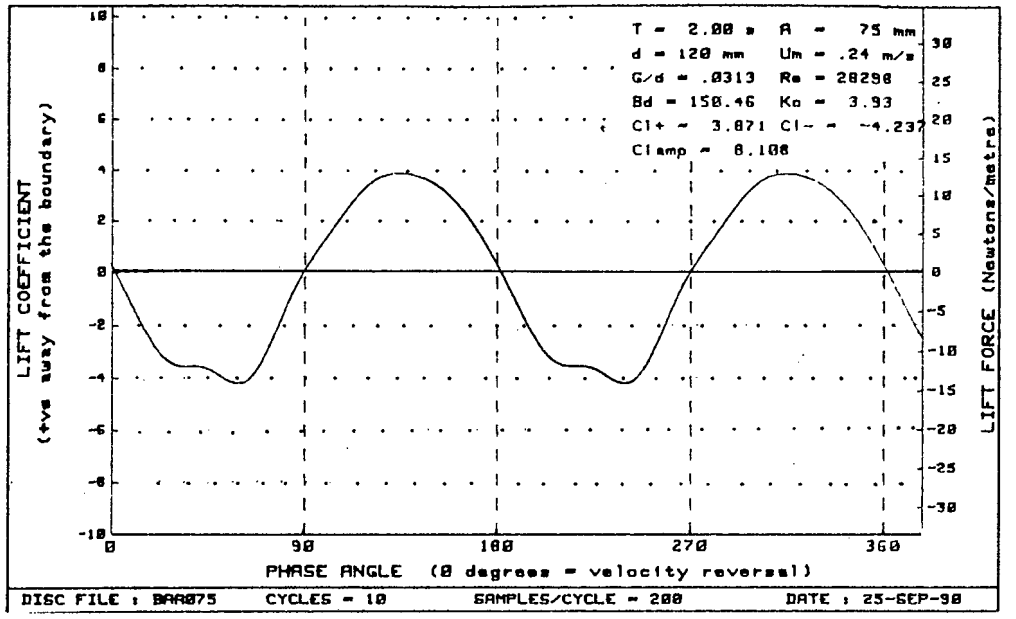

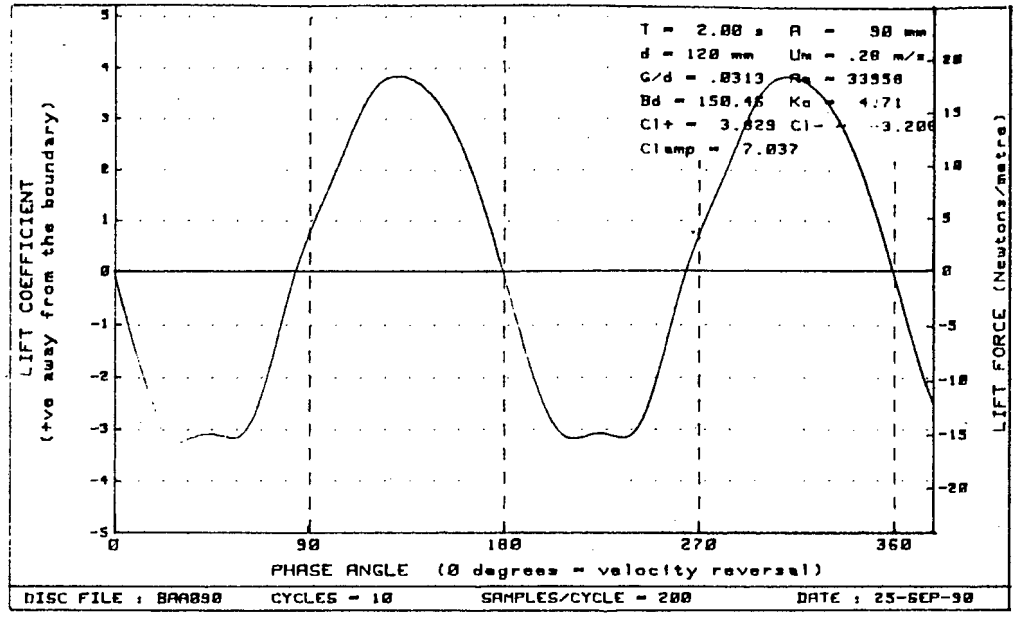

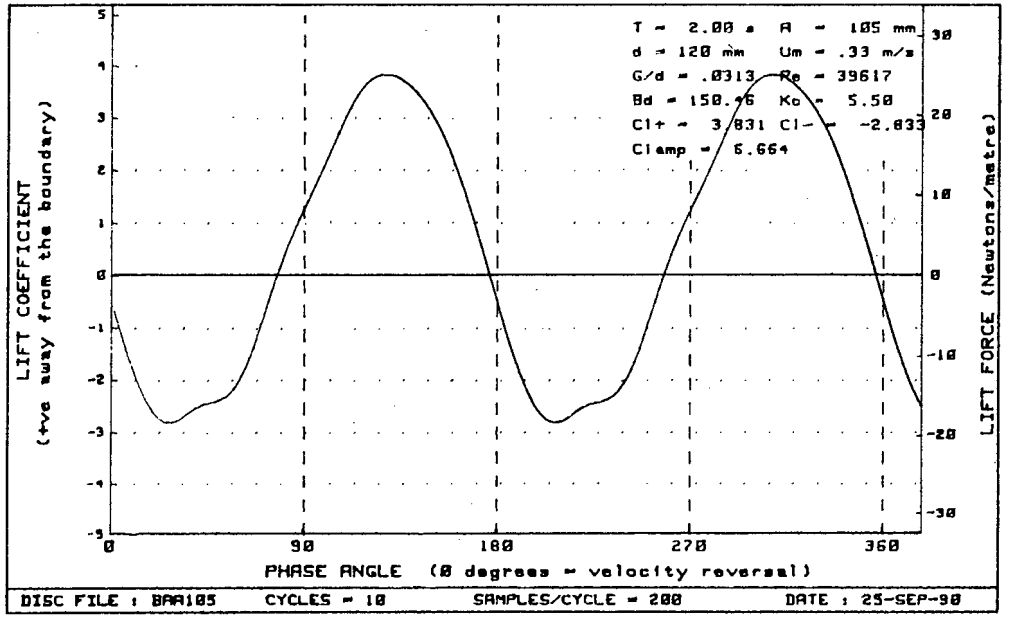

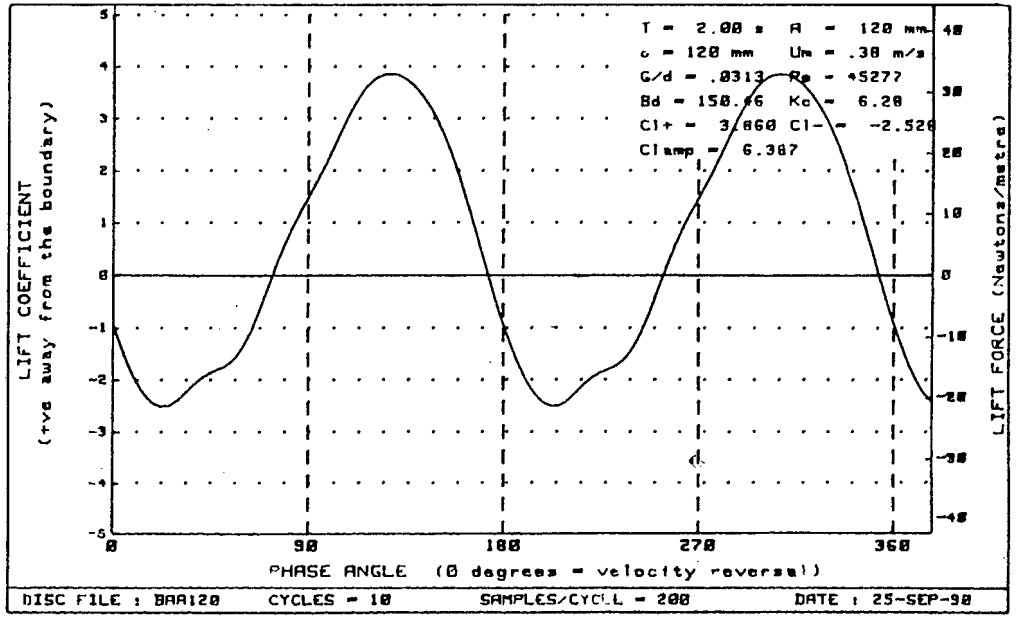

Figure G-10 : Plots of lift vs phase for diameter=120mm, Bd=150.46 and G/d= .0313

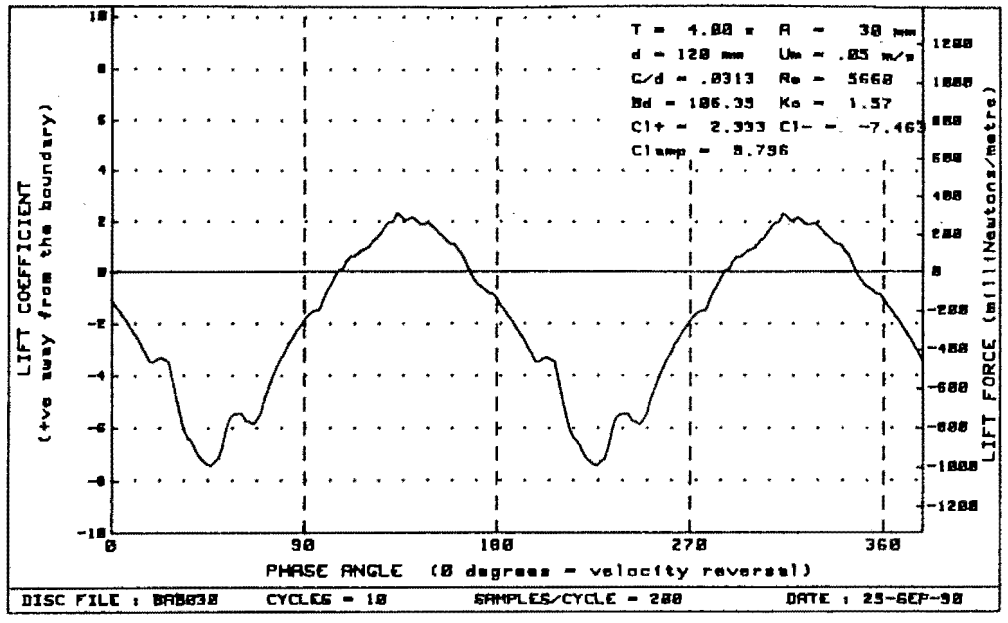

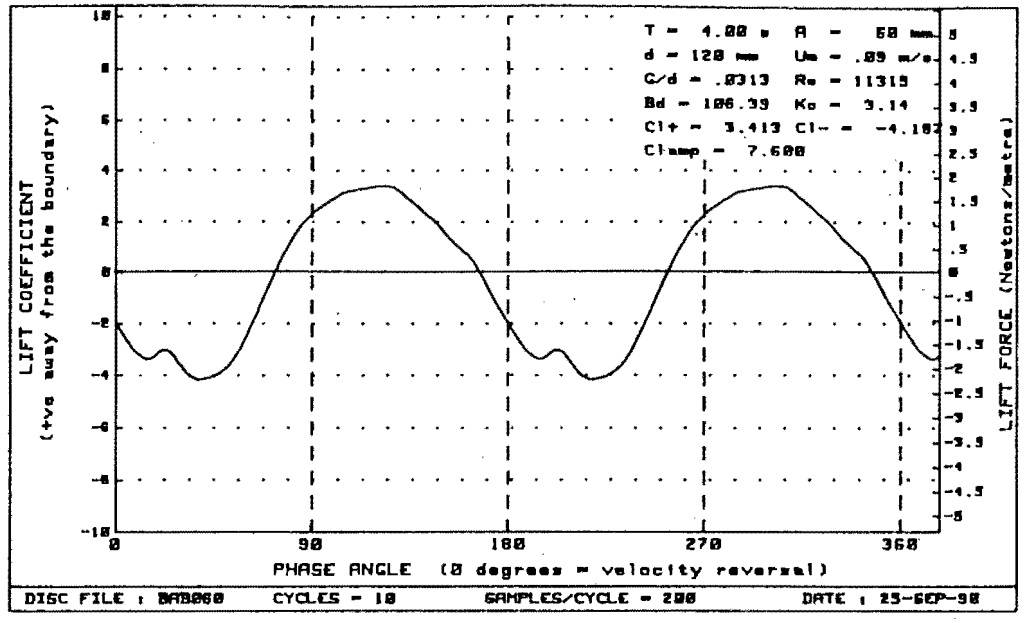

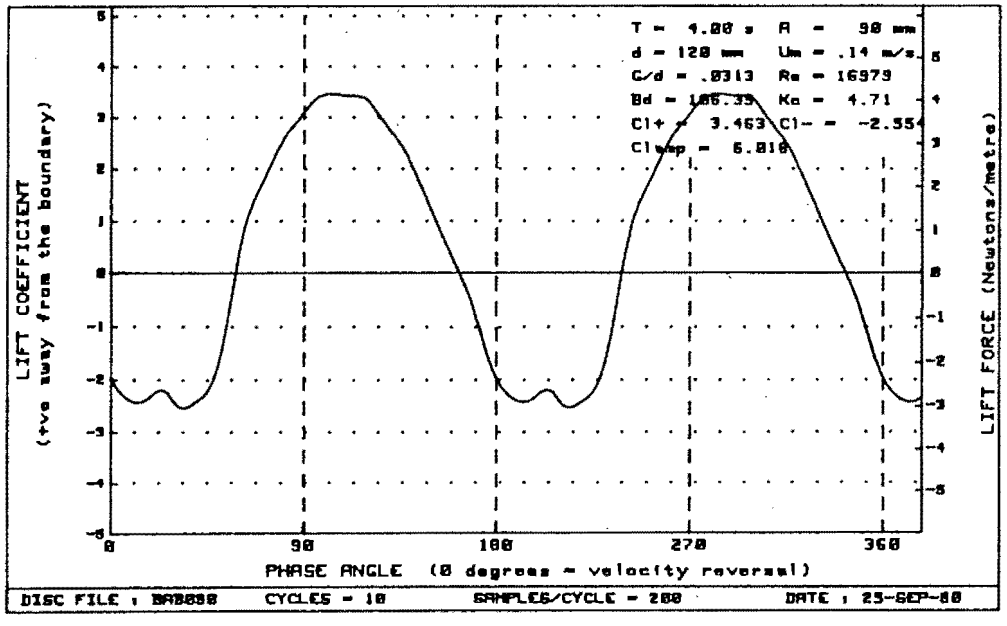

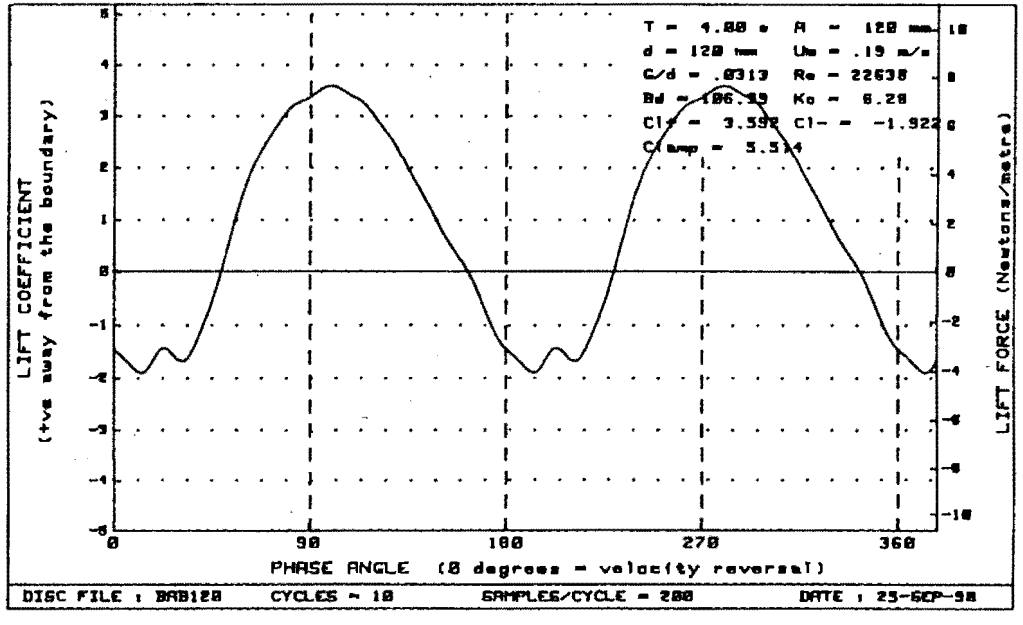

Figure G-11 : Plots of lift vs phase for diameter=120mm, Bd=106.39 and G/d= .0313

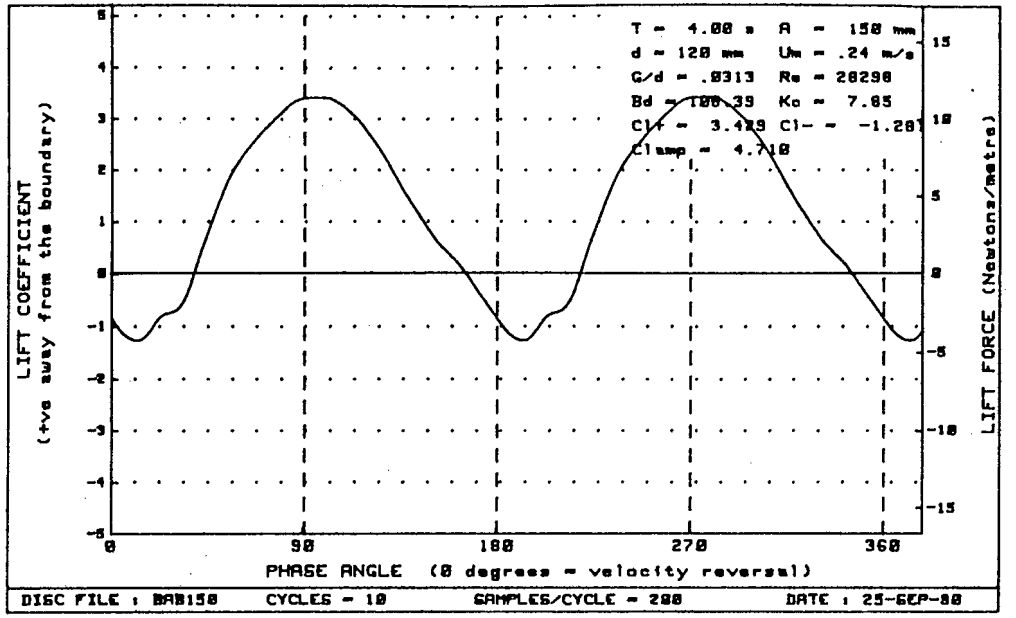

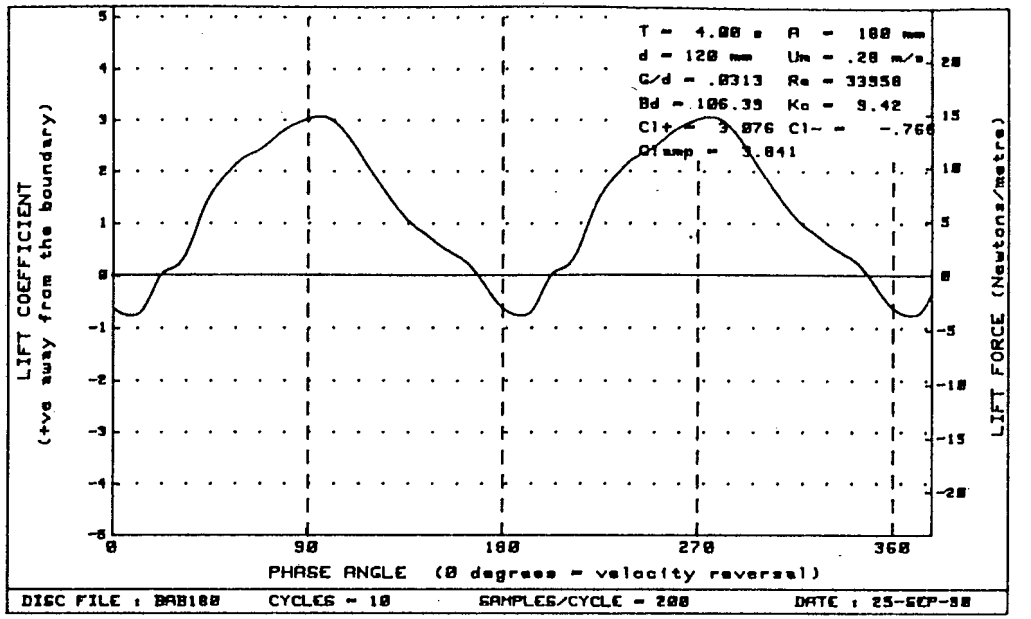

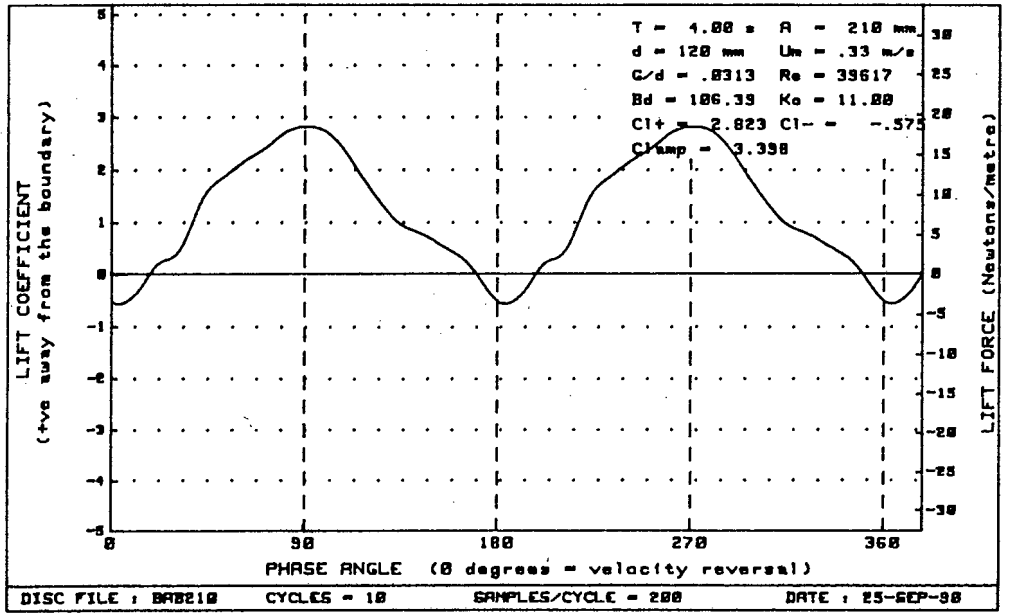

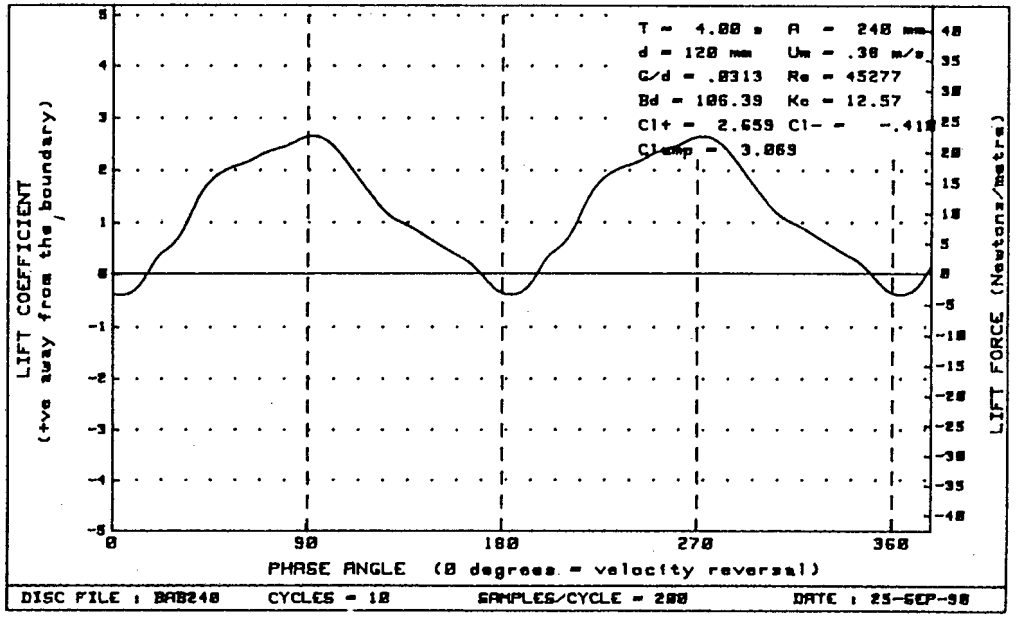

Figure G-12 : Plots of lift vs phase for diameter=120mm, Bd=106.39 and G/d= .0313

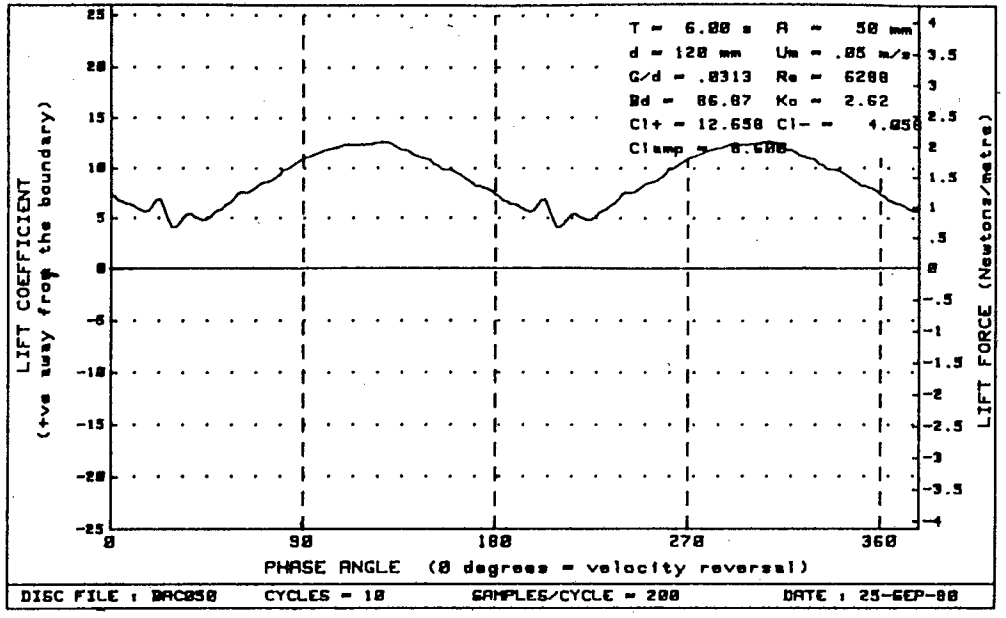

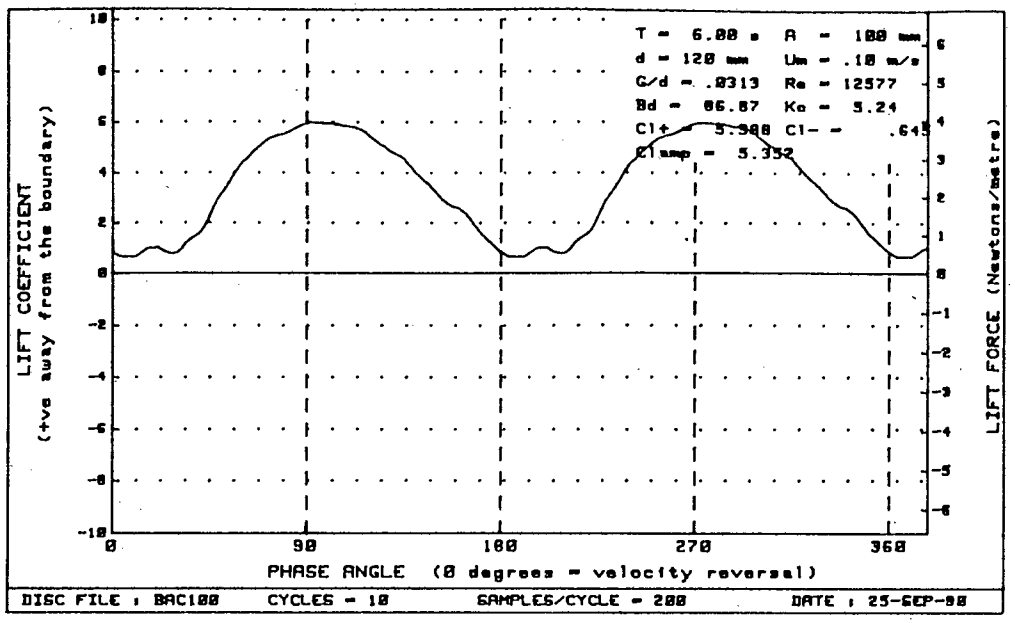

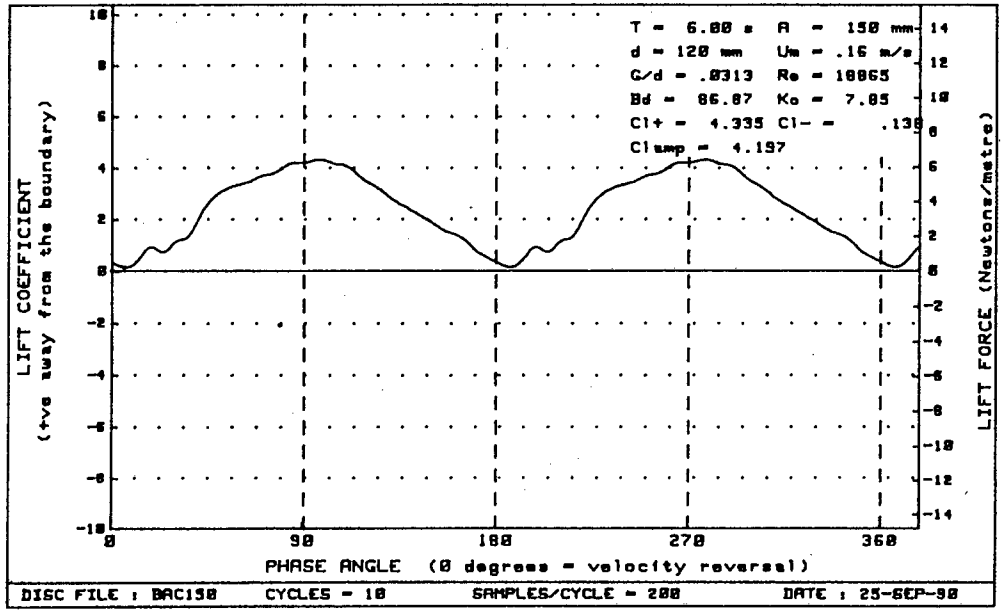

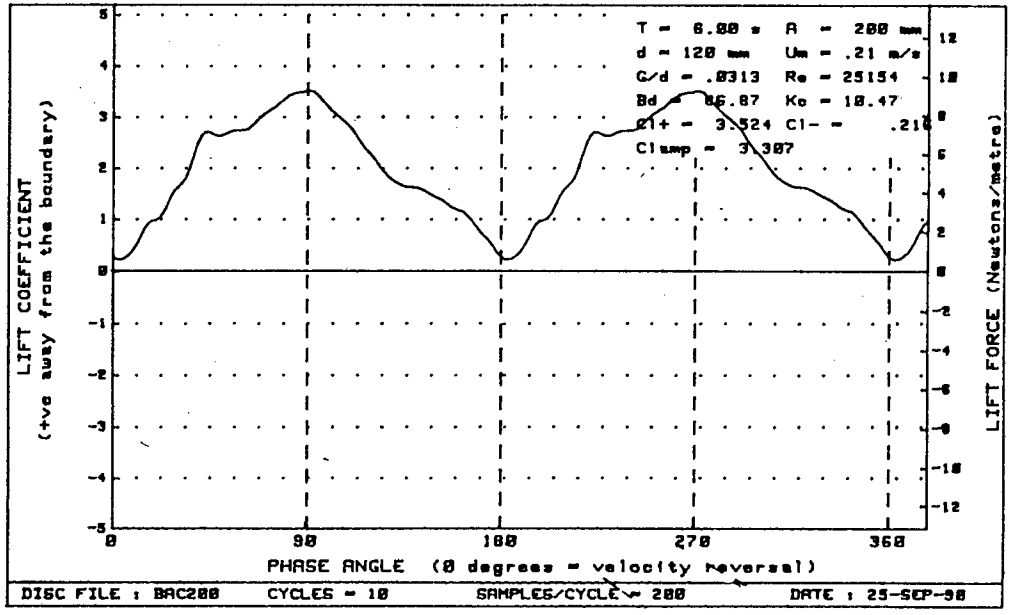

Figure G-13 : Plots of lift vs phase for diameter=120mm, Bd= 86.87 and G/d= .0313

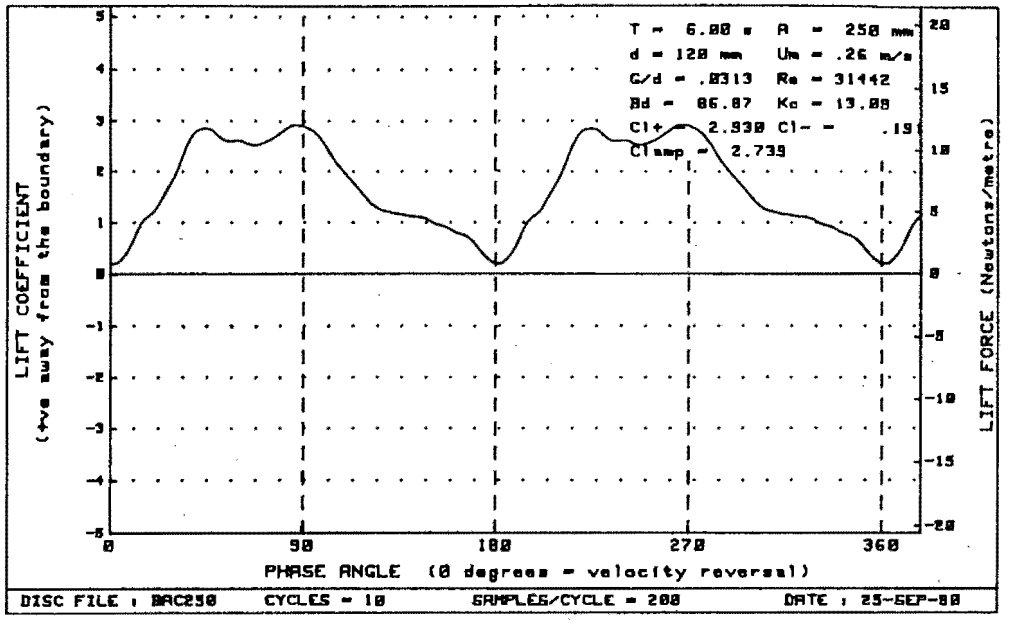

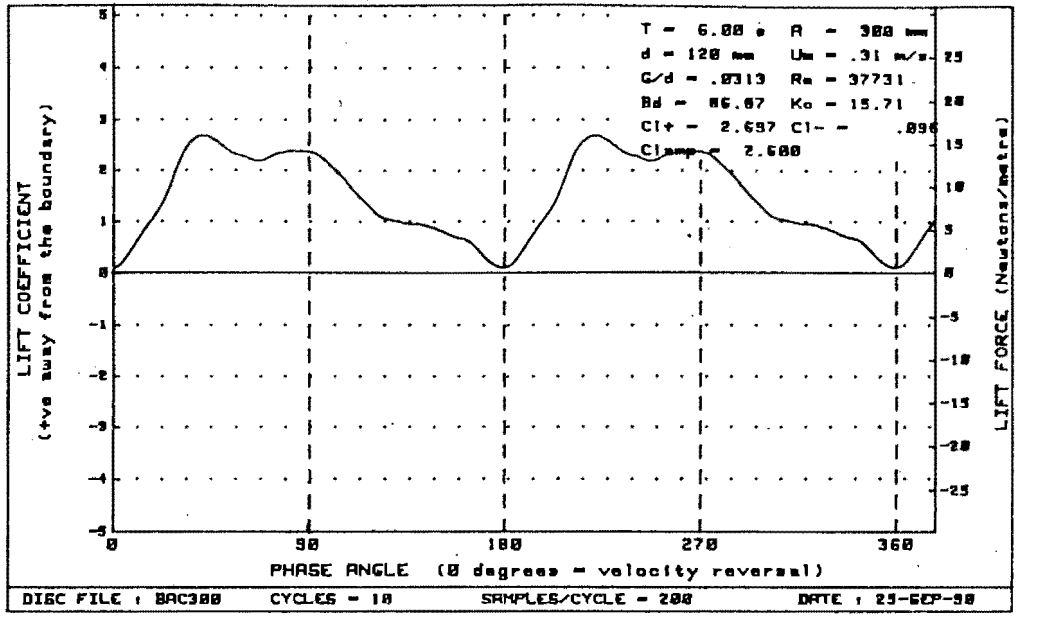

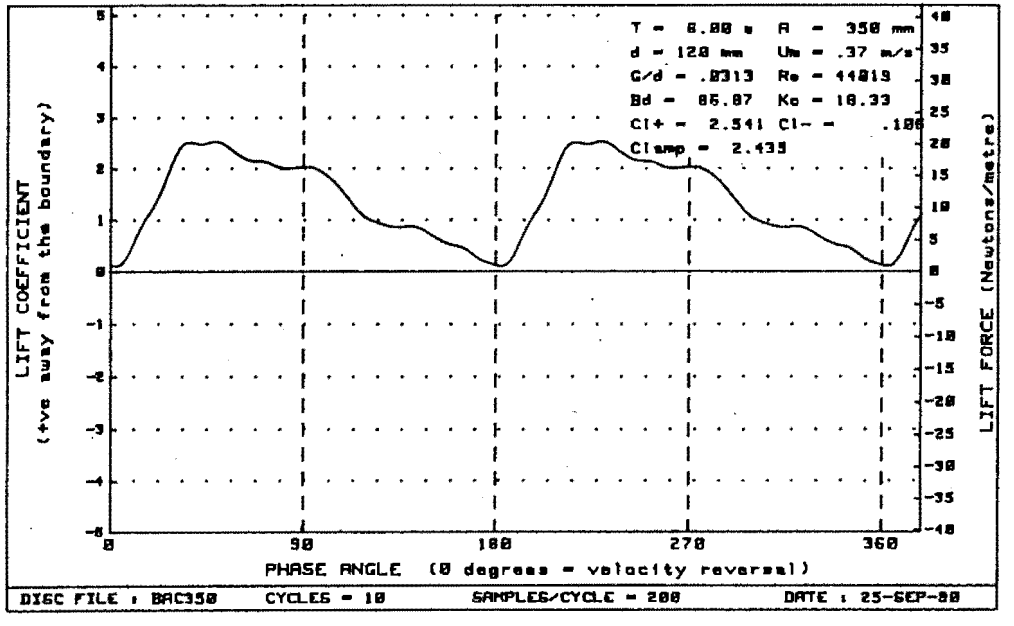

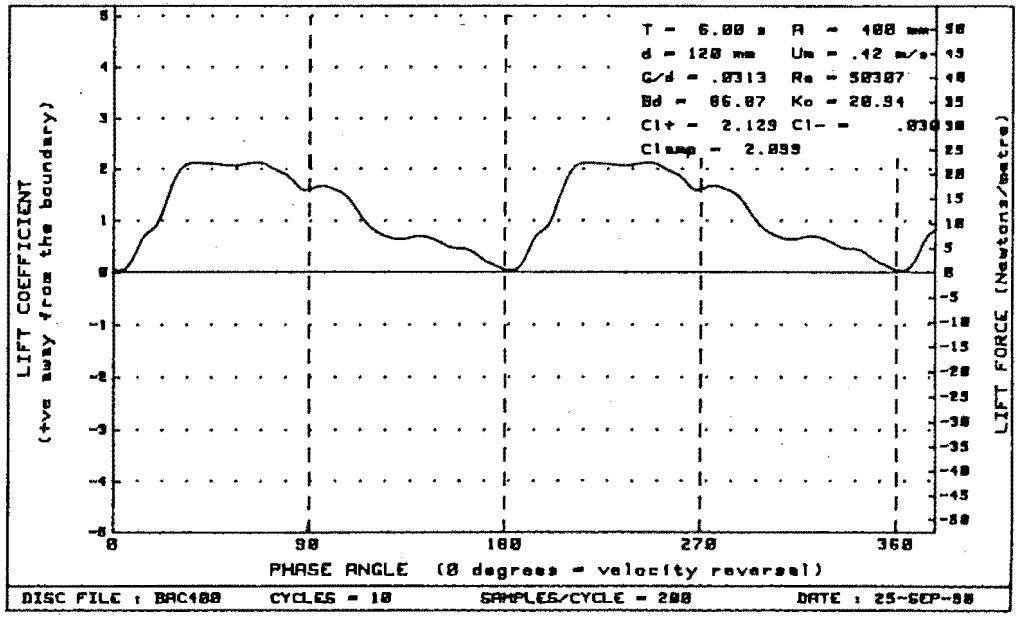

Figure G-14 : Plots of lift vs phase for diameter=120mm, Bd= 86.87 and G/d= .0313

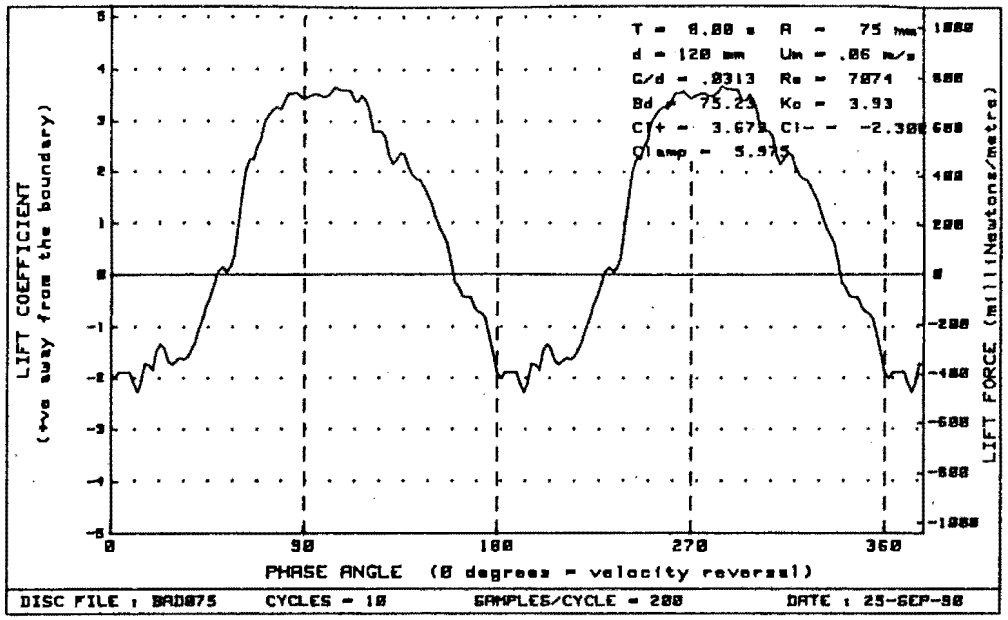

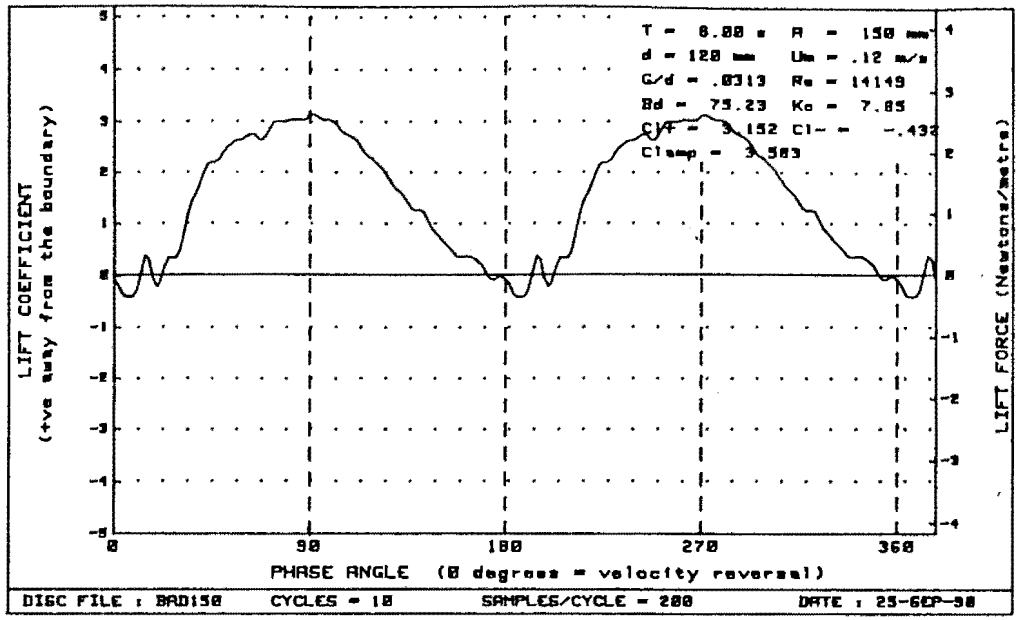

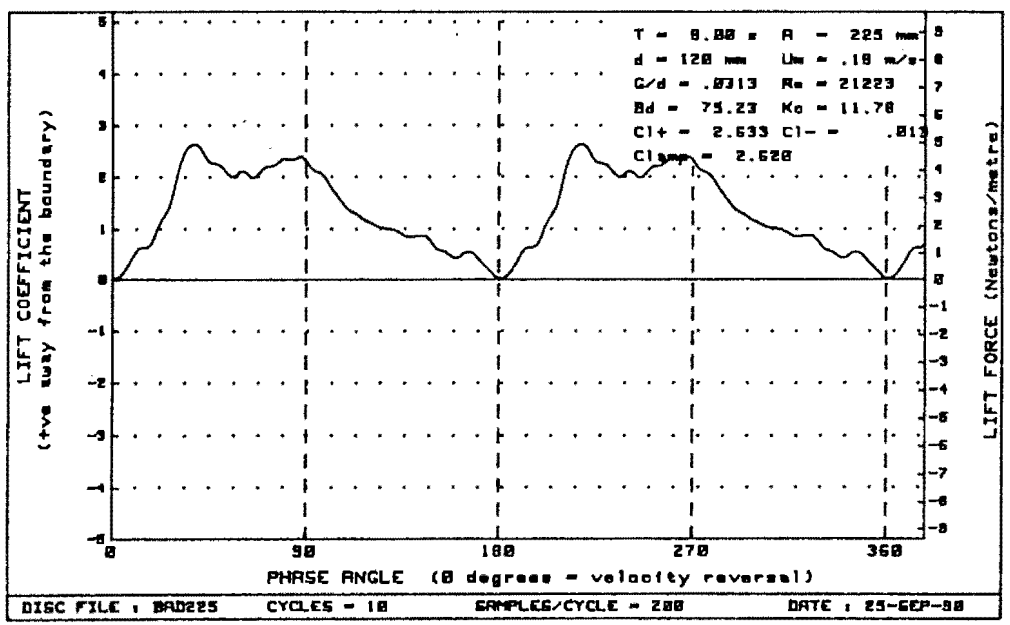

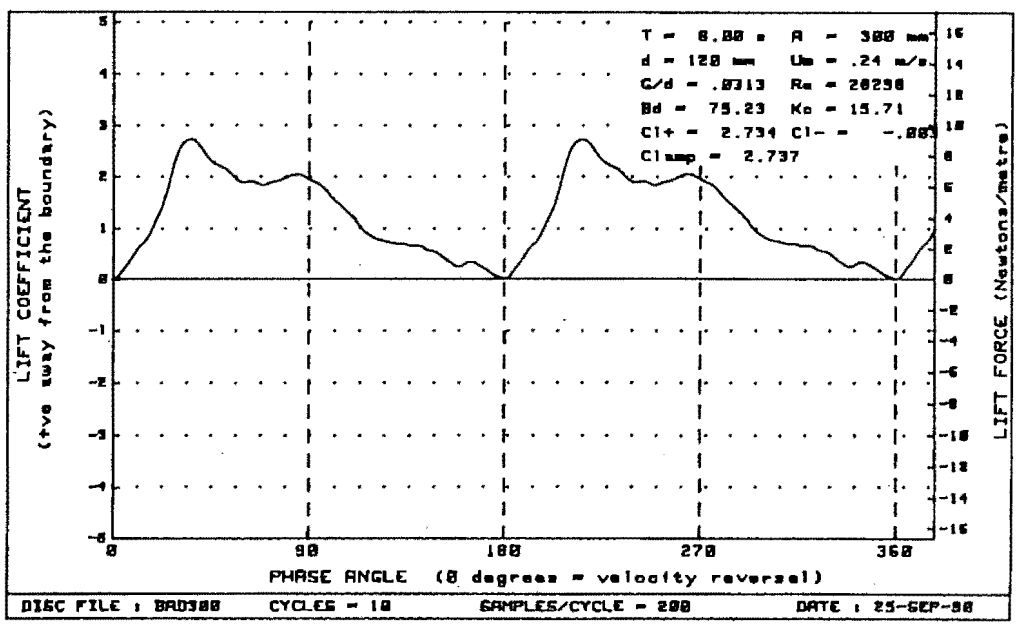

Figure G-15 : Plots of lift vs phase for diameter=120mm, Bd= 75.23 and G/d= .0313

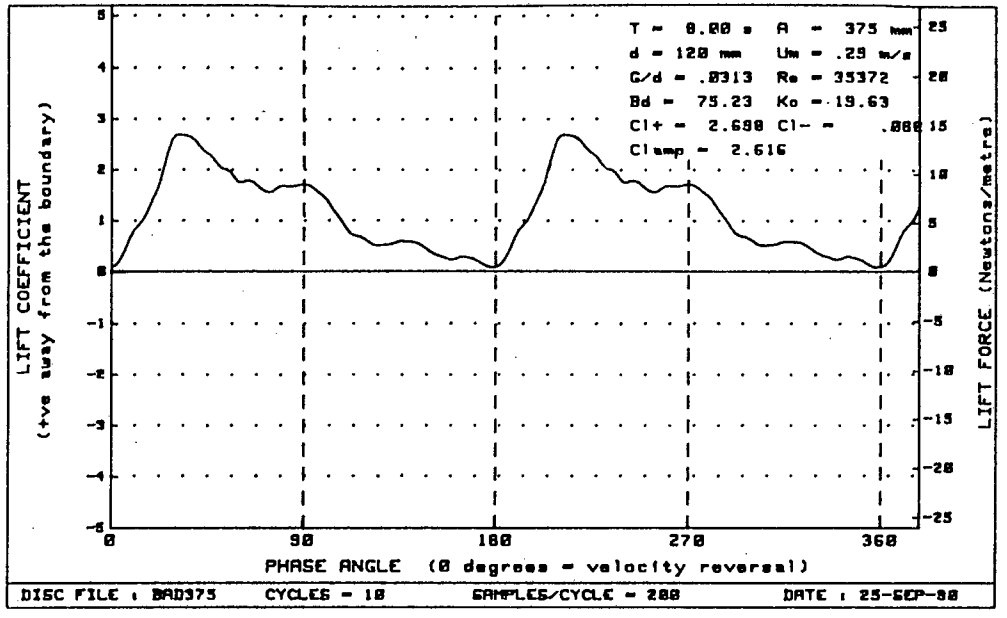

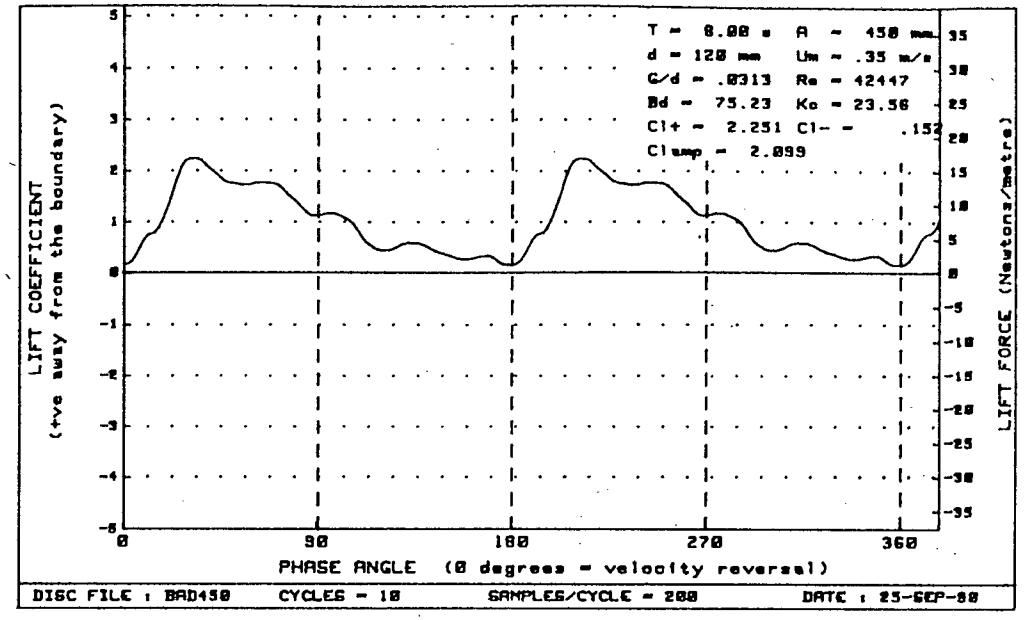

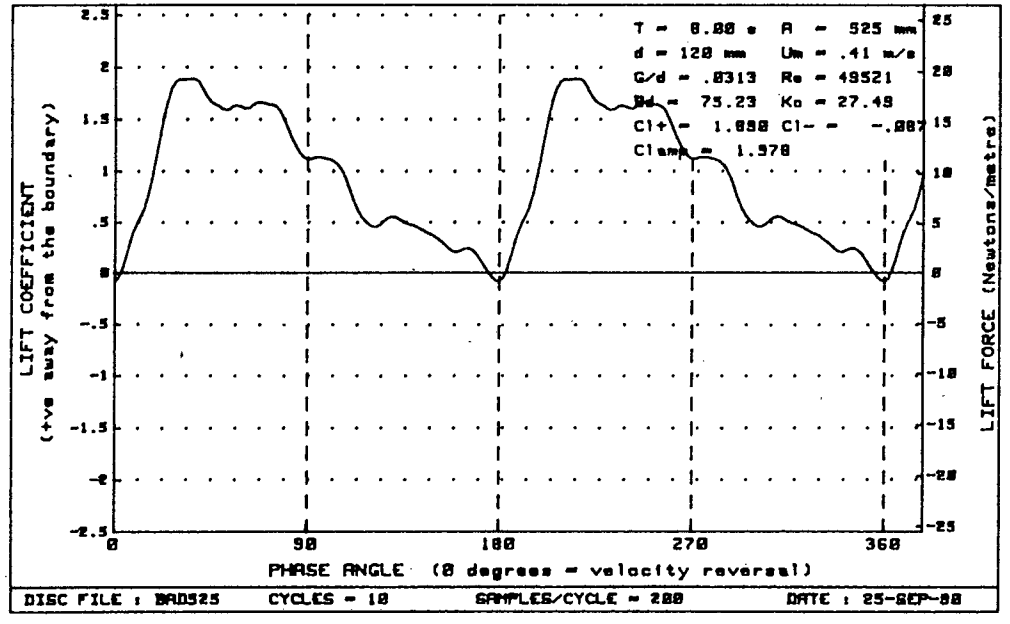

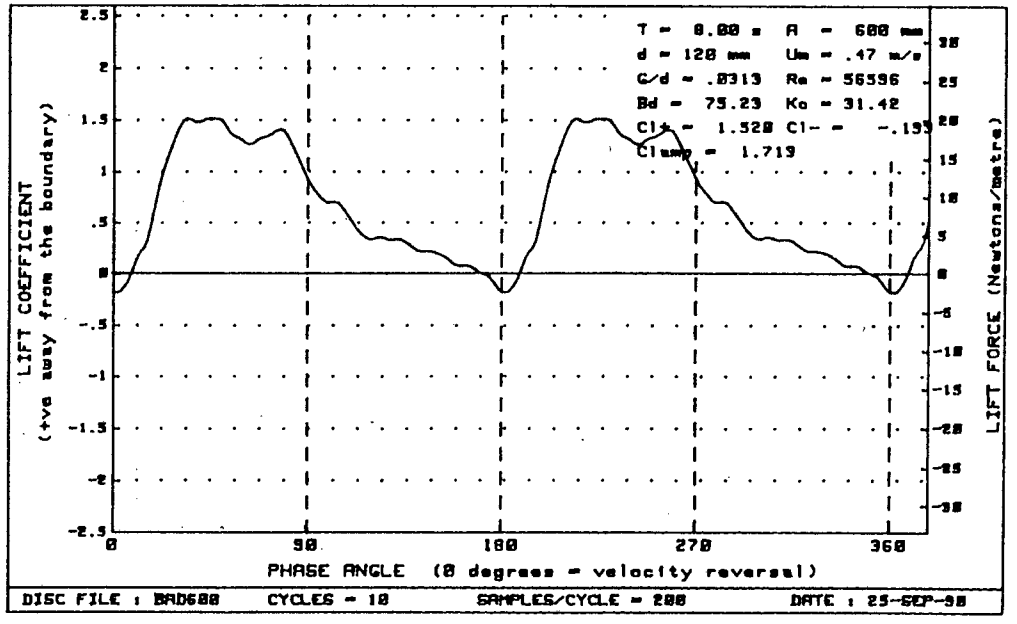

Figure G-16 : Plots of lift vs phase for diameter=120mm, Bd= 75.23 and G/d= .0313

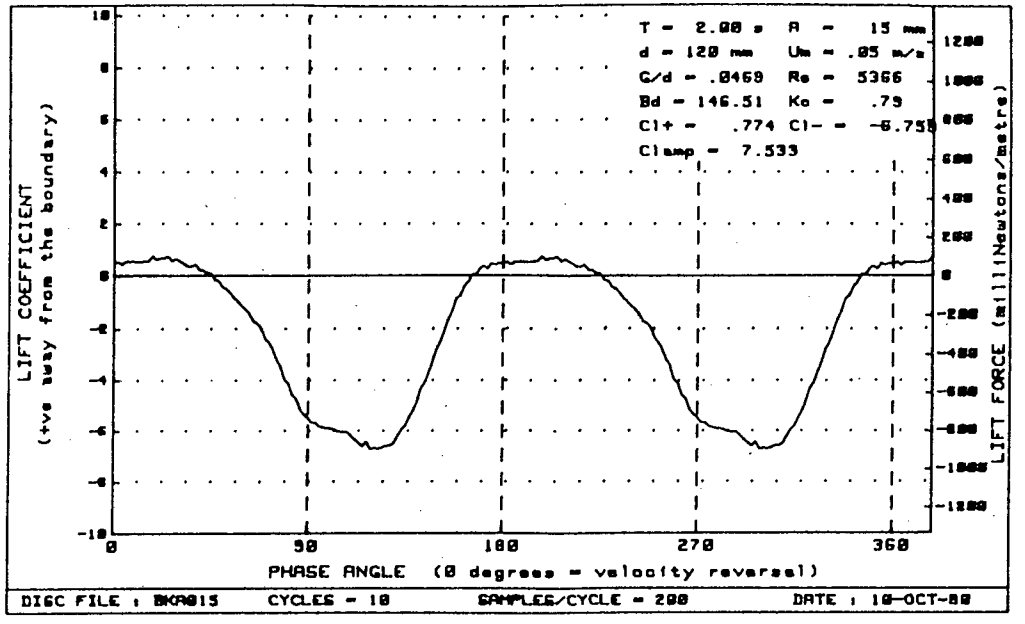

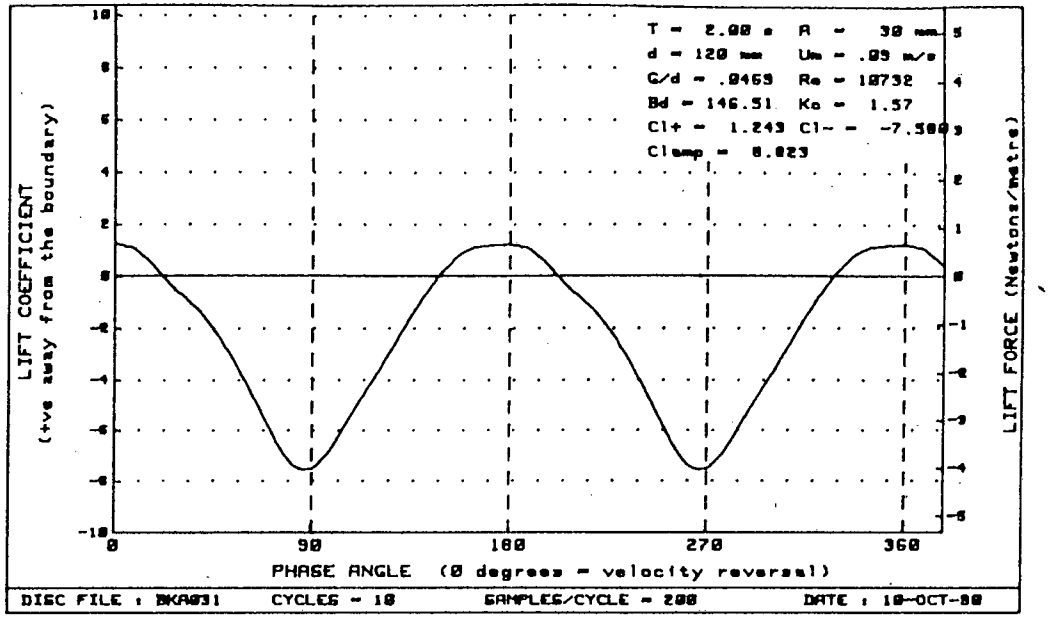

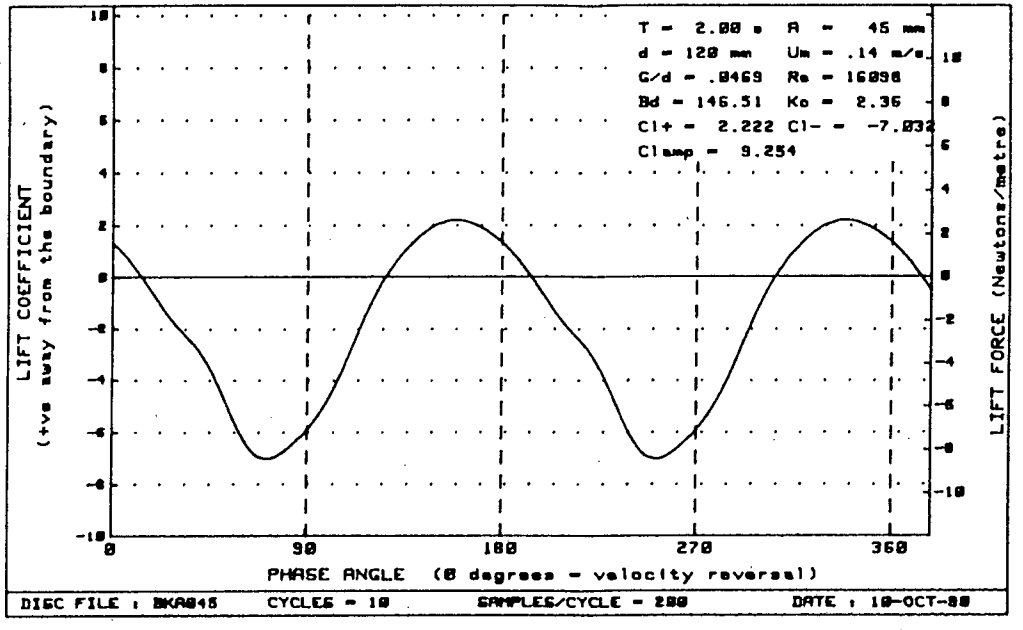

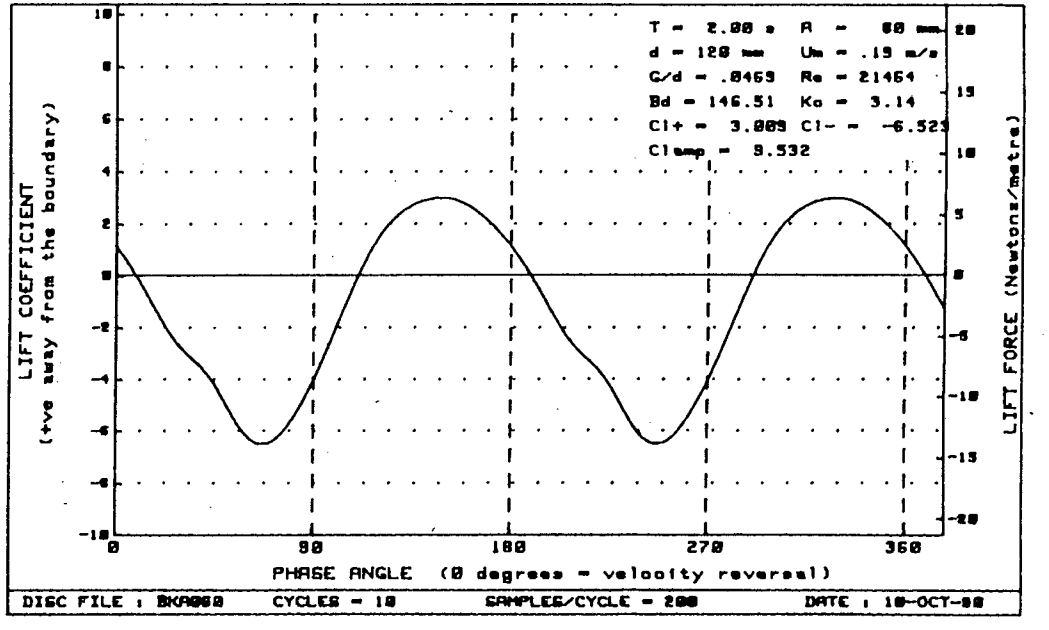

Figure G-17 : Plots of lift vs phase for diameter=120mm, Bd=146.51 and G/d= .0469

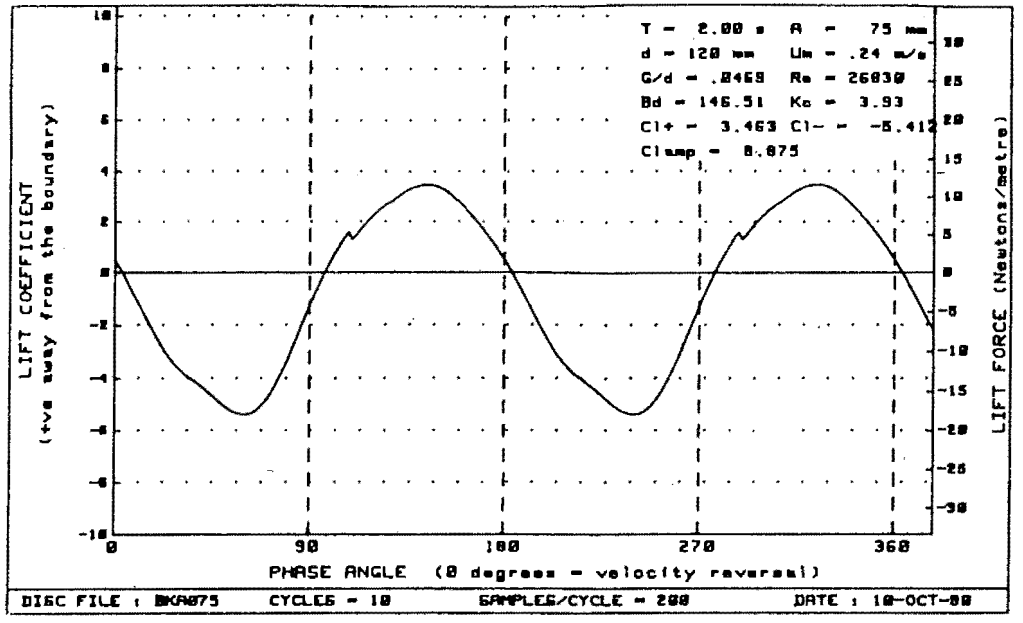

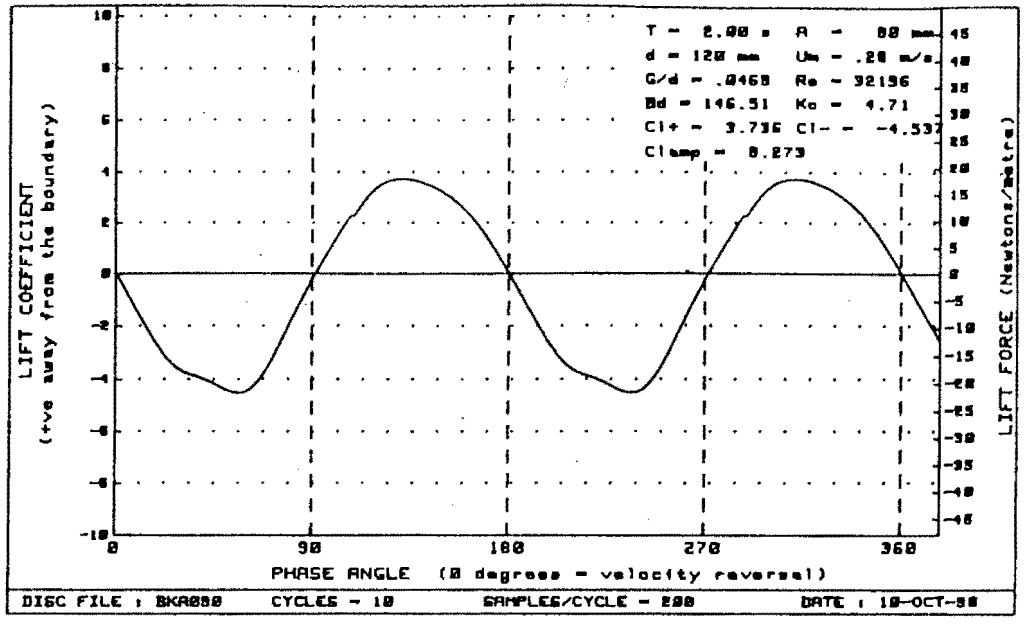

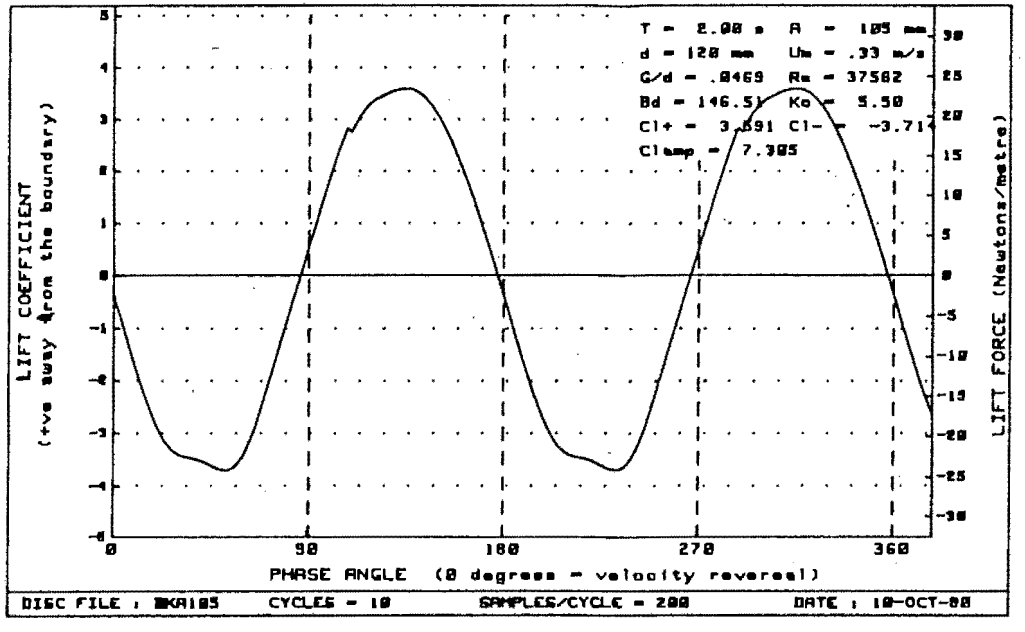

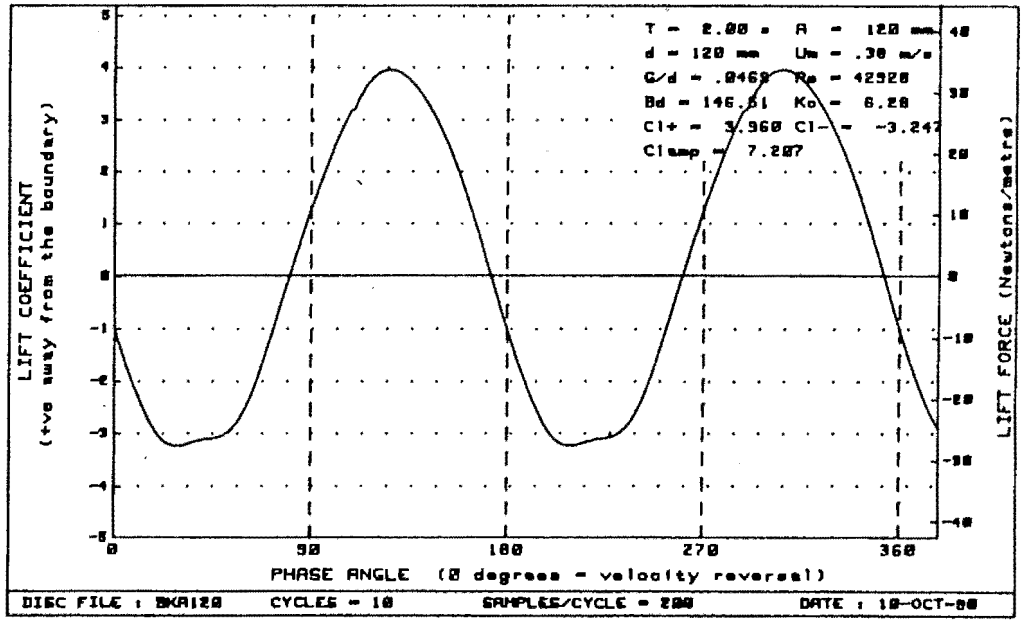

Figure G-18 : Plots of lift vs phase for diameter=120mm, Bd=146.51 and G/d= .0469

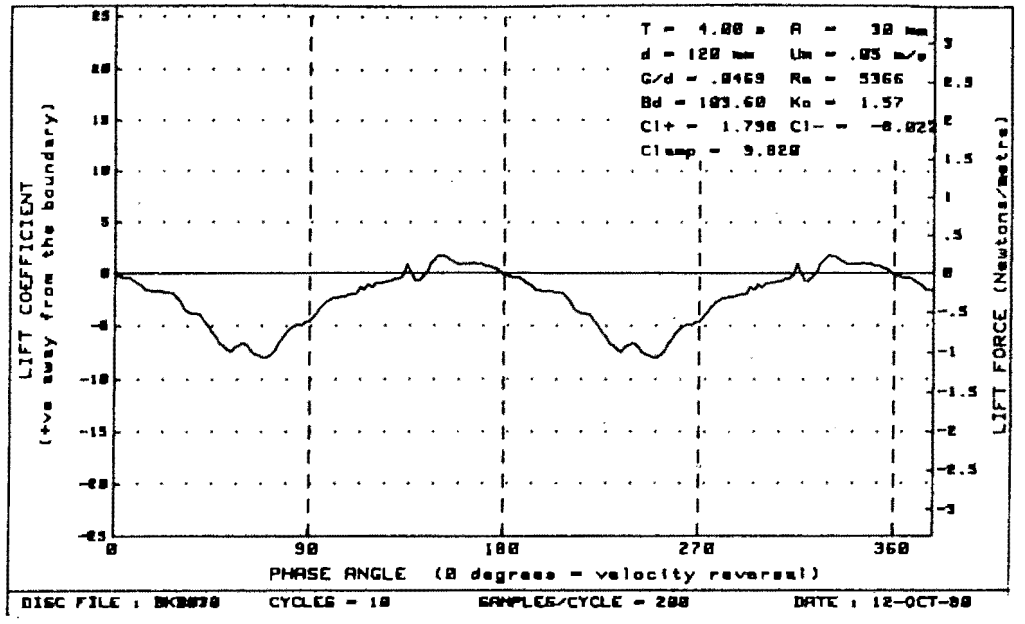

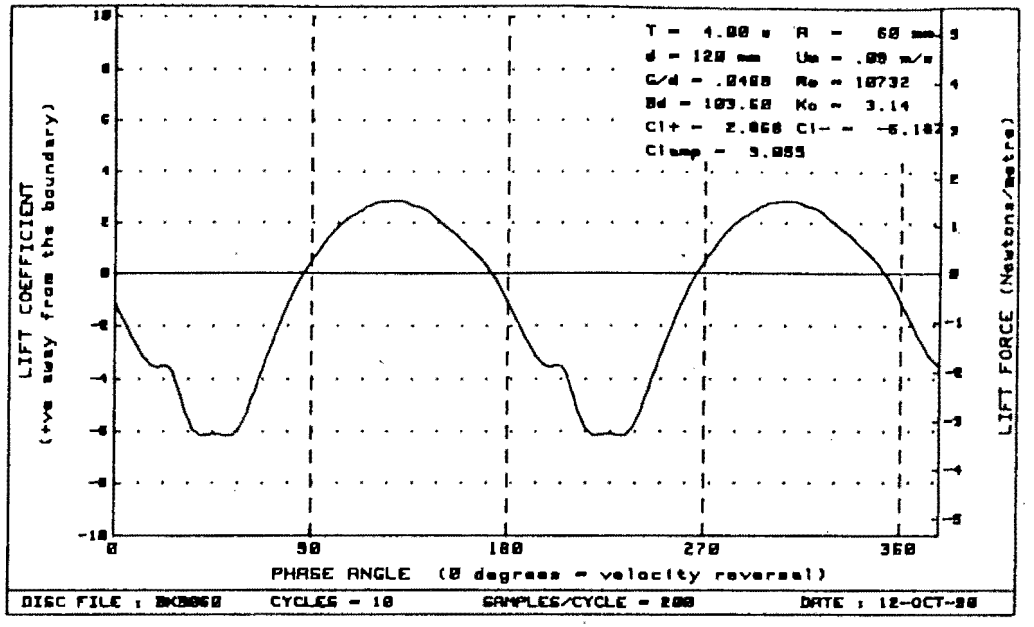

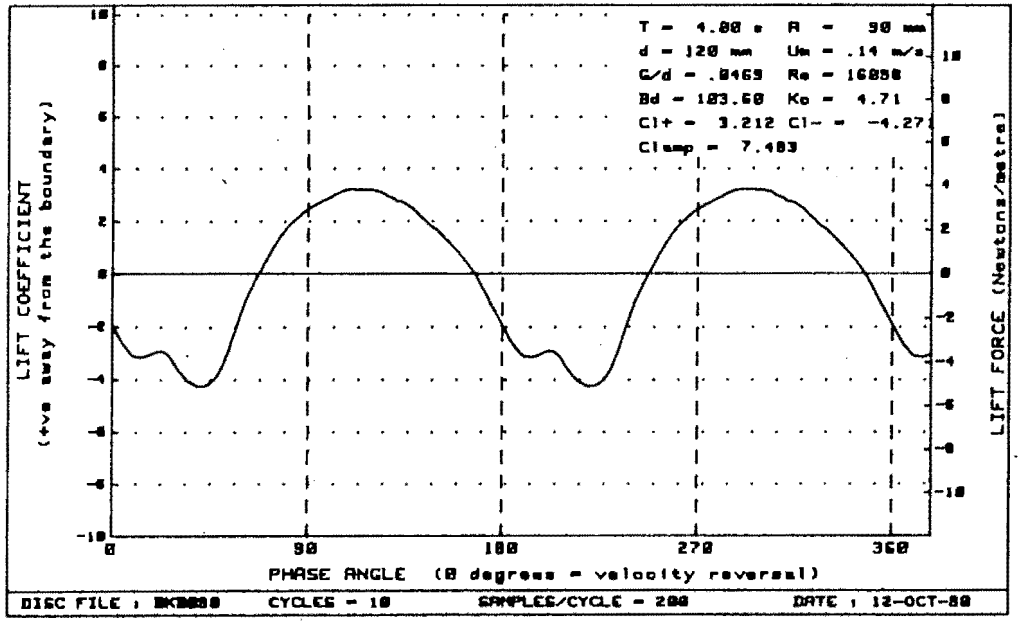

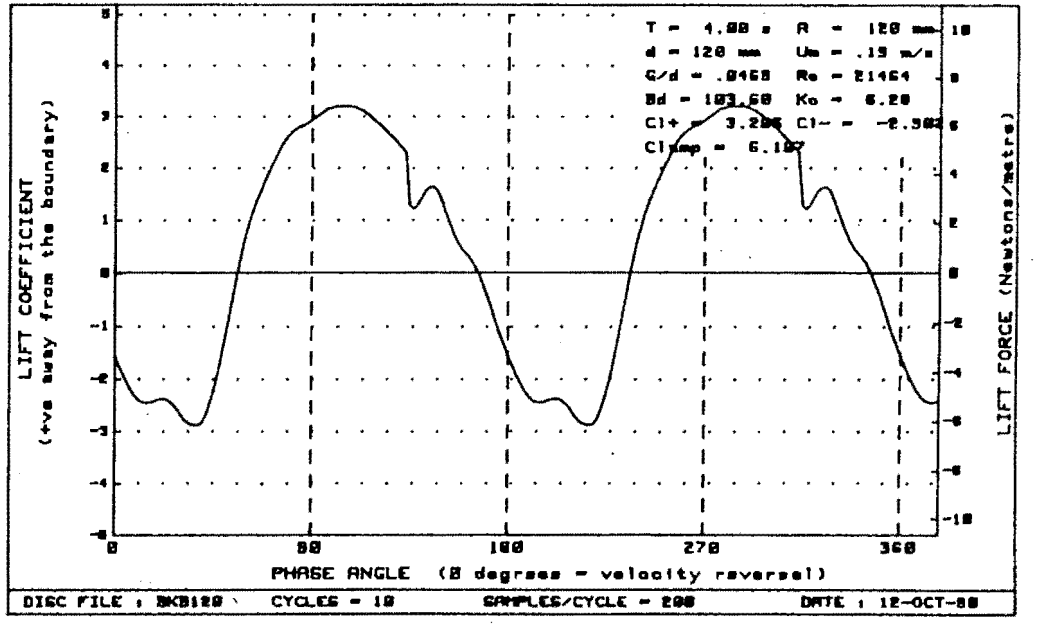

Figure G-19 : Plots of lift vs phase for diameter=120mm, Bd=103.60 and G/d= .0469

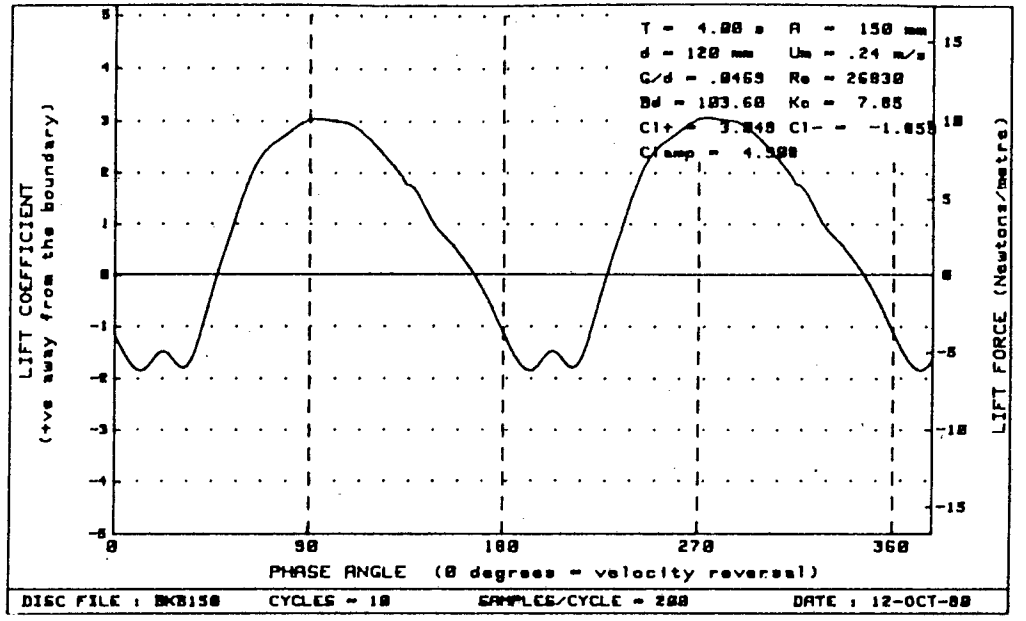

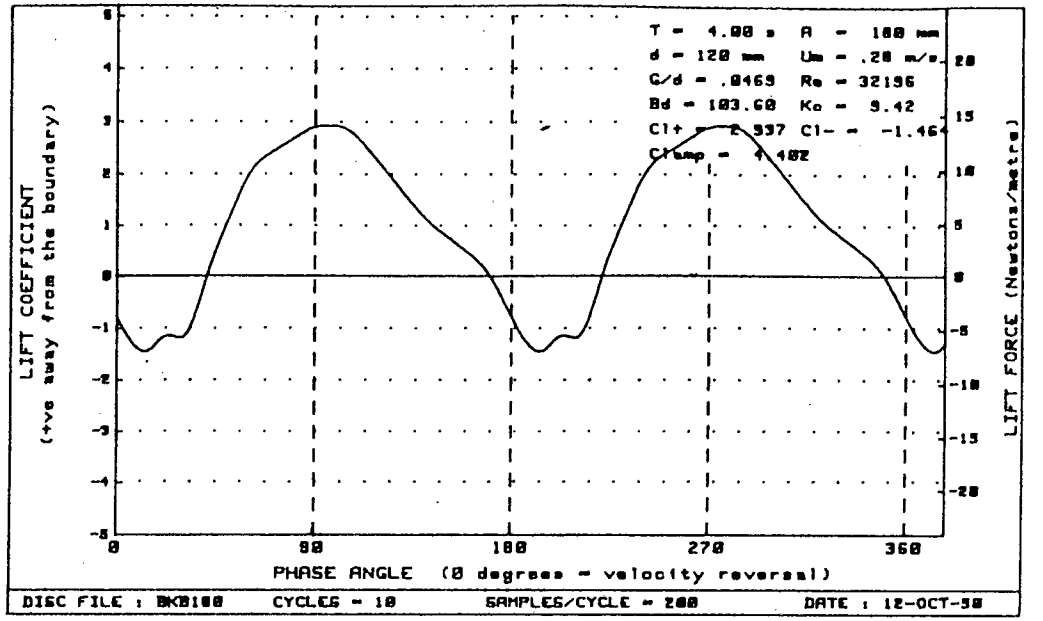

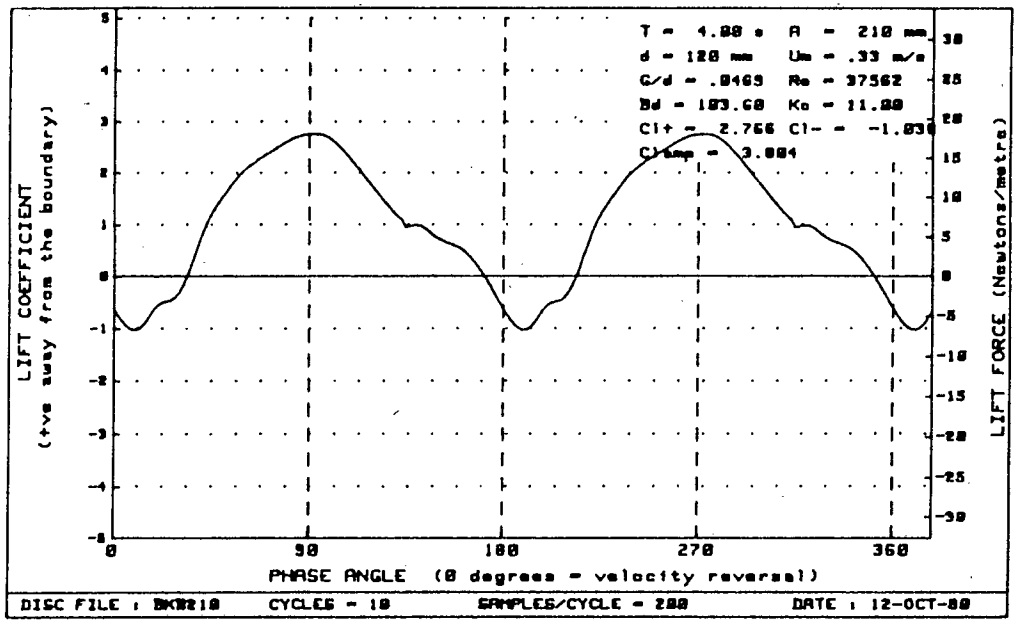

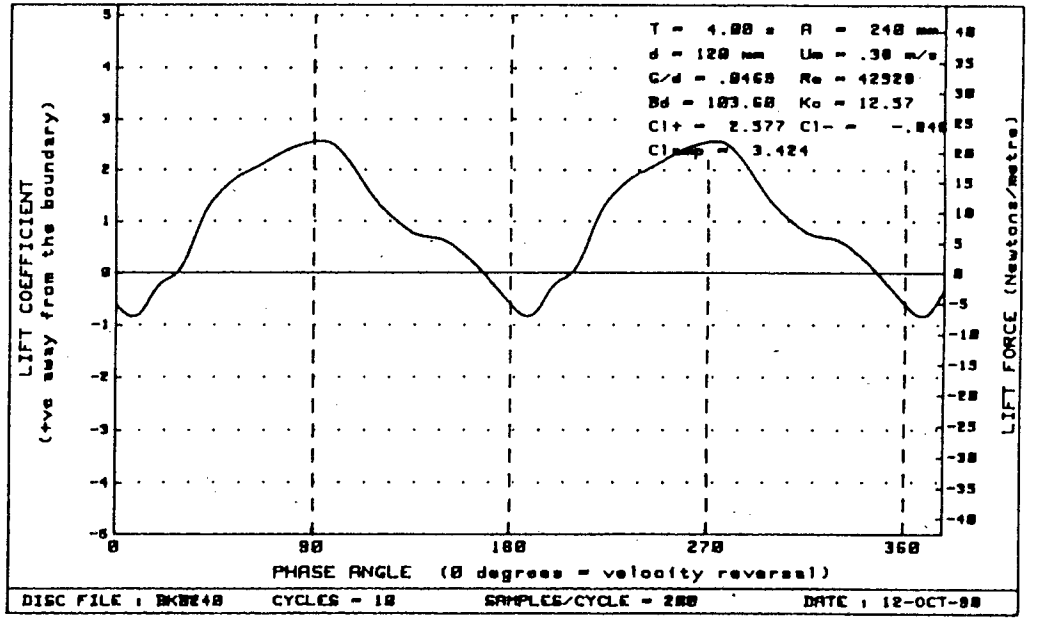

Figure G-20 : Plots of lift vs phase for diameter=120mm, Bd=103.60 and G/d= .0469

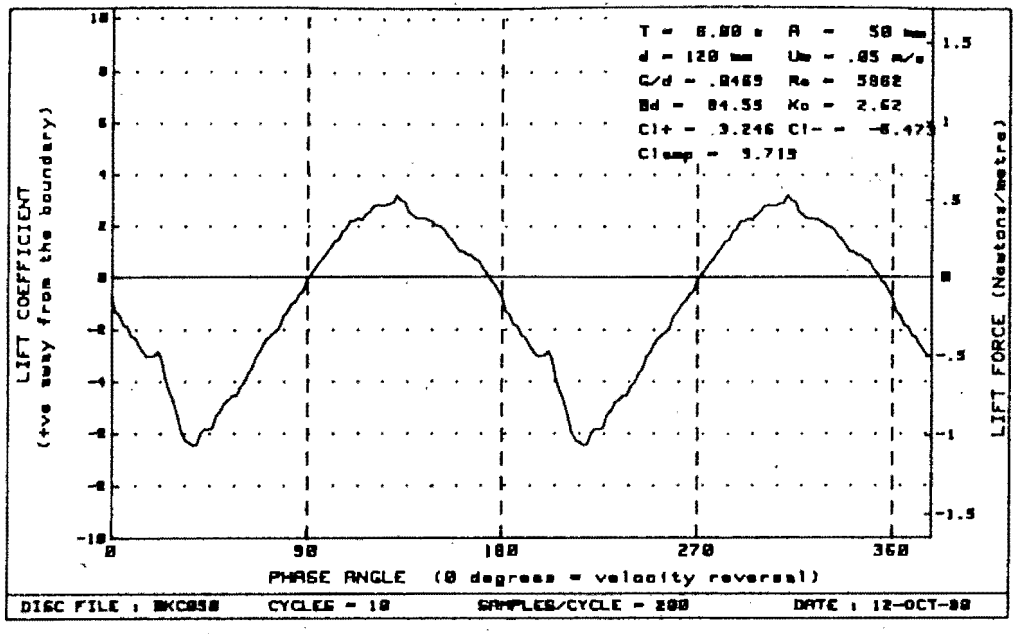

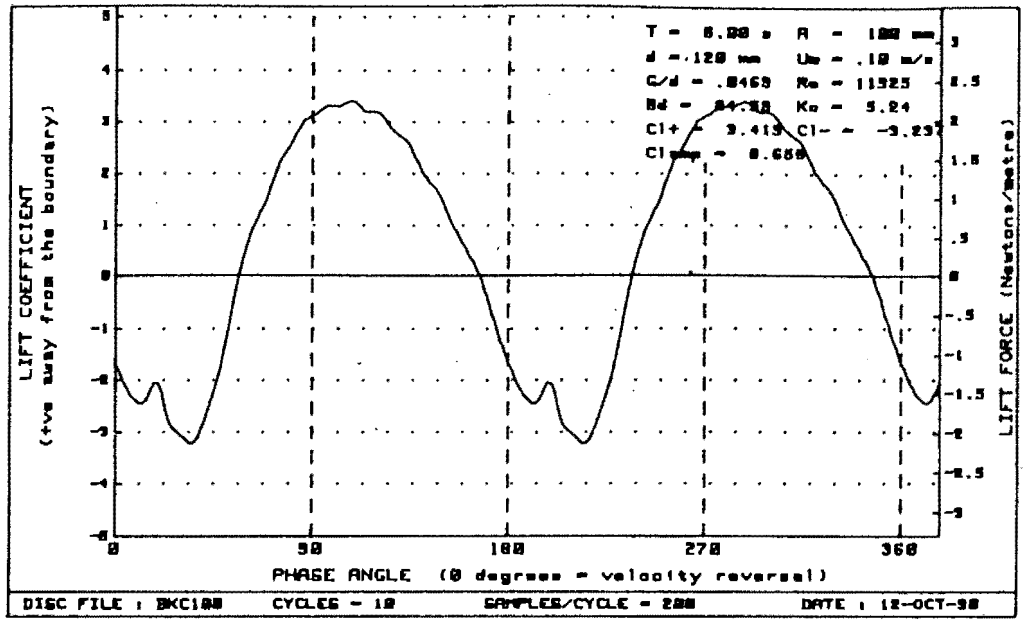

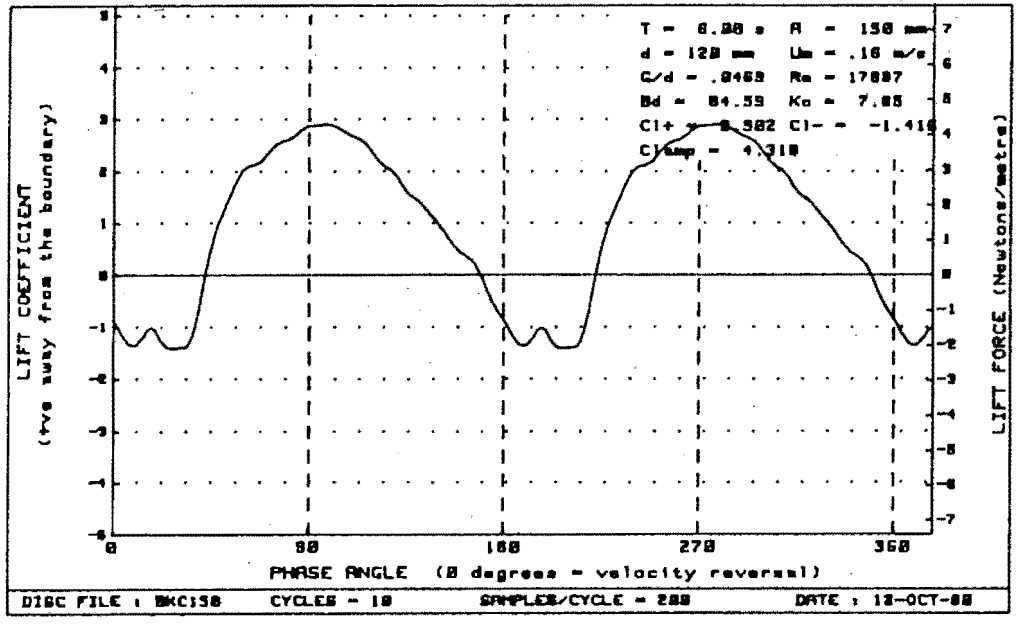

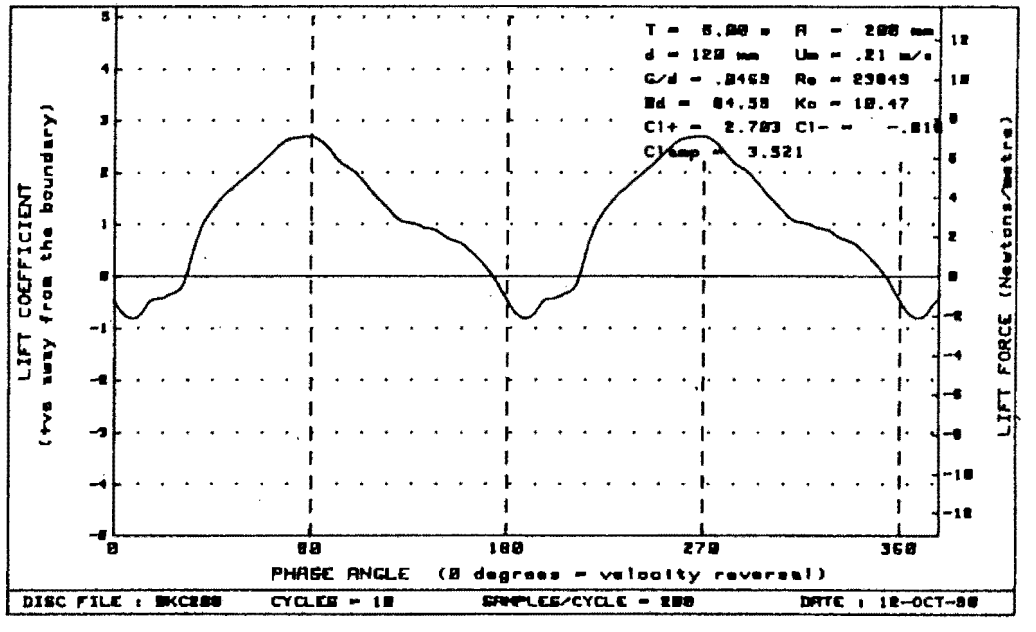

Figure G-21 : Plots of lift vs phase for diameter=120mm, Bd= 84.59 and G/d= .0469

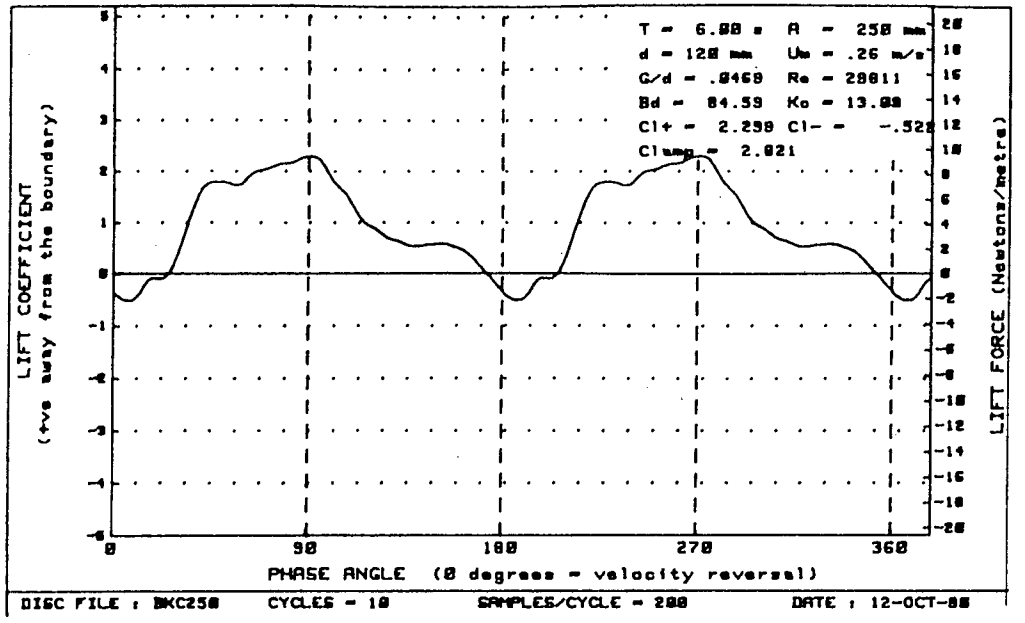

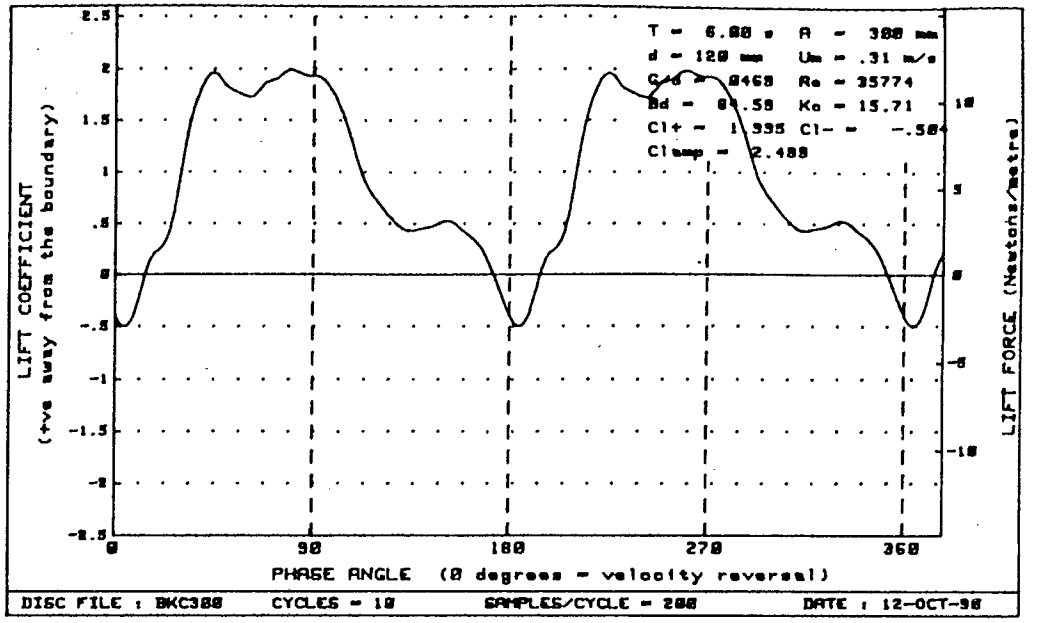

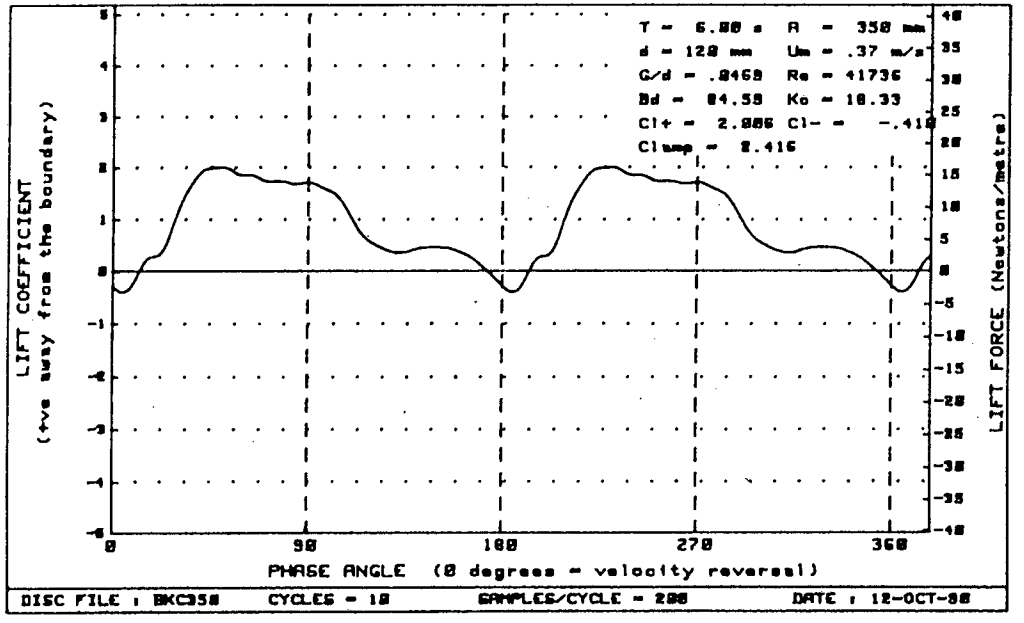

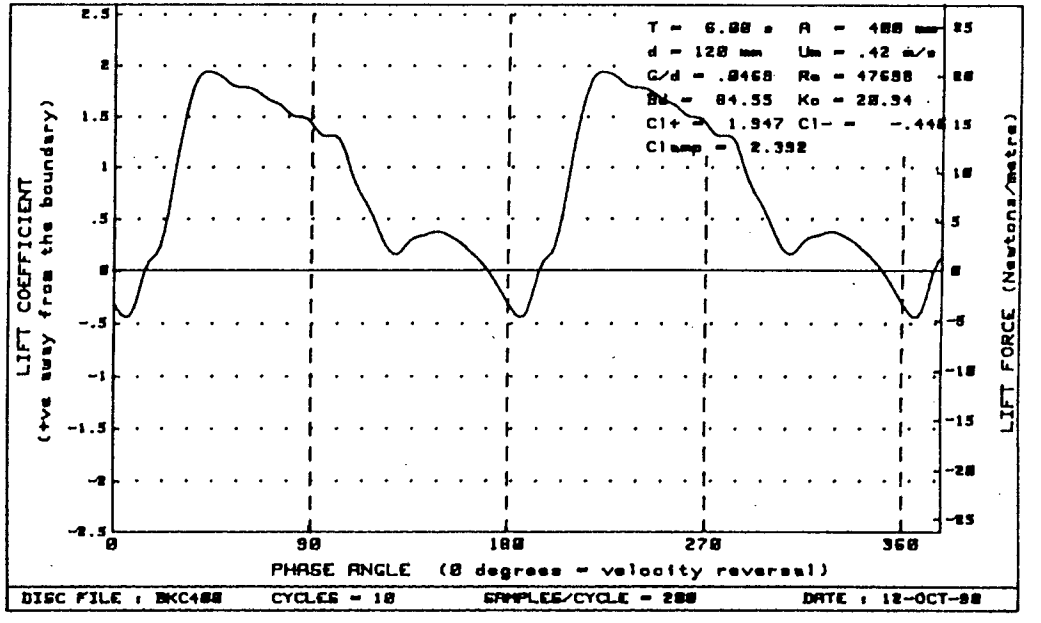

Figure G-22 : Plots of lift vs phase for diameter=120mm, Bd= 84.59 and G/d= .0469

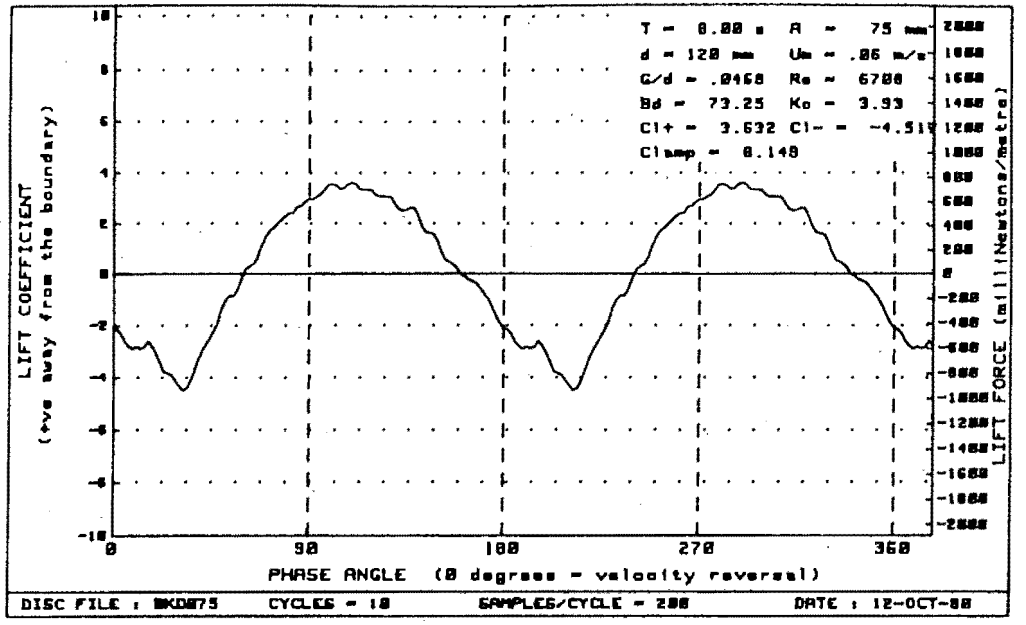

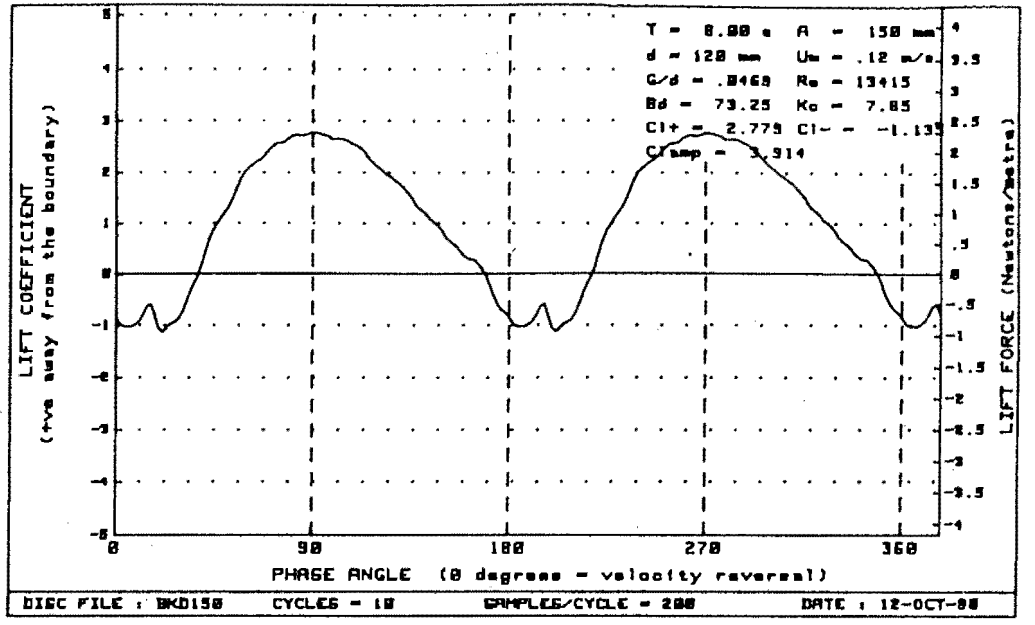

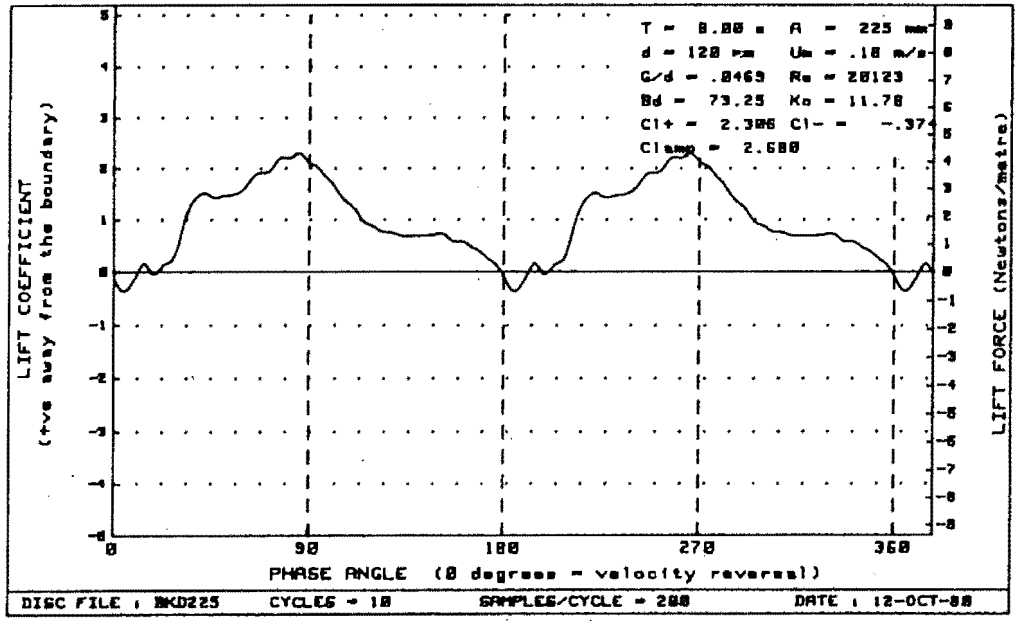

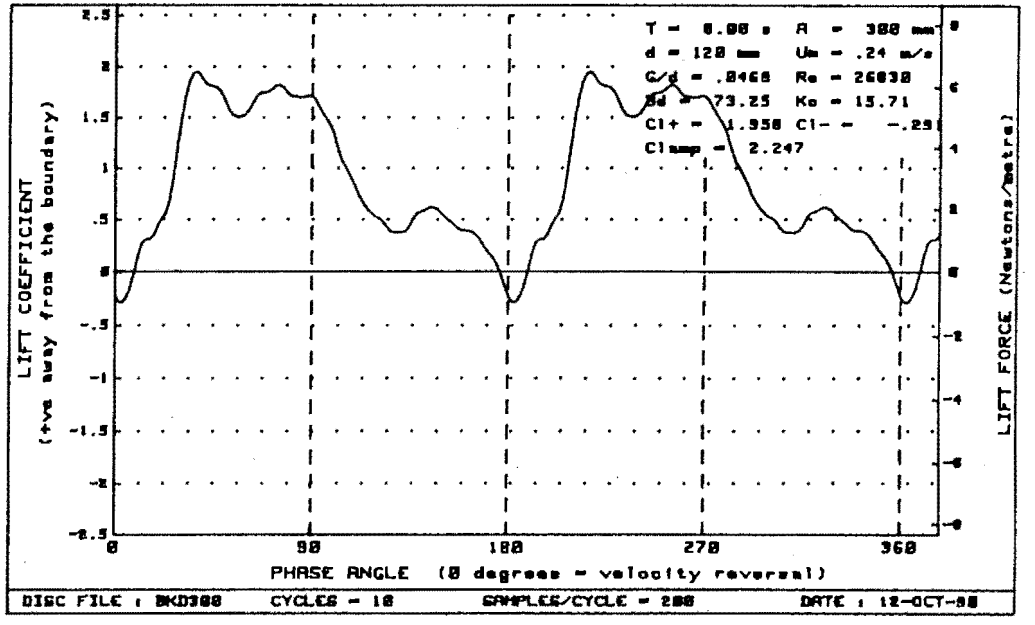

Figure G-23 : Plots of lift vs phase for diameter=120mm, Bd= 73.25 and G/d= .0469

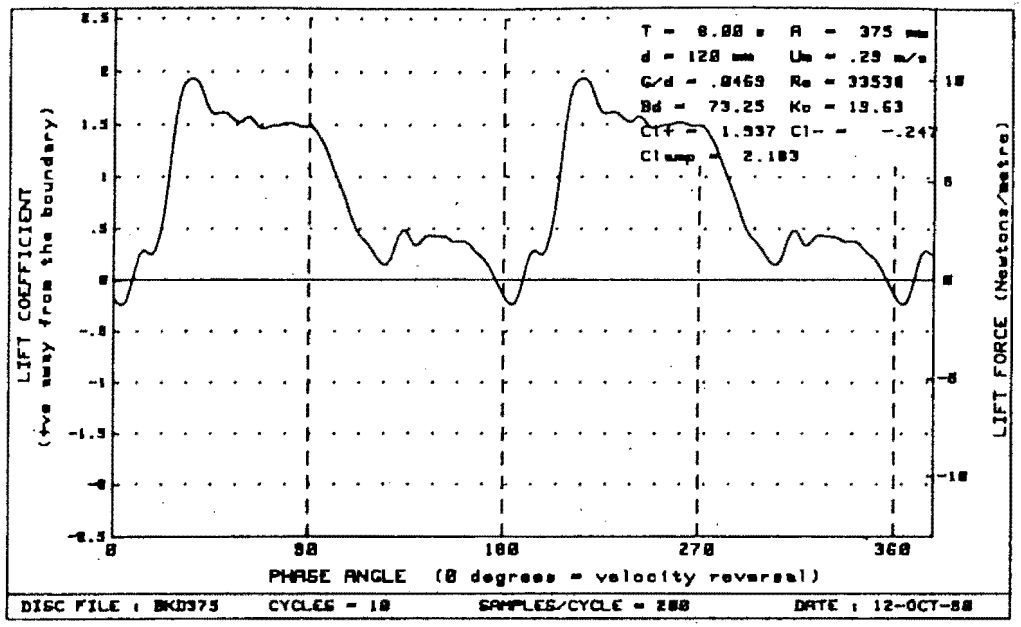

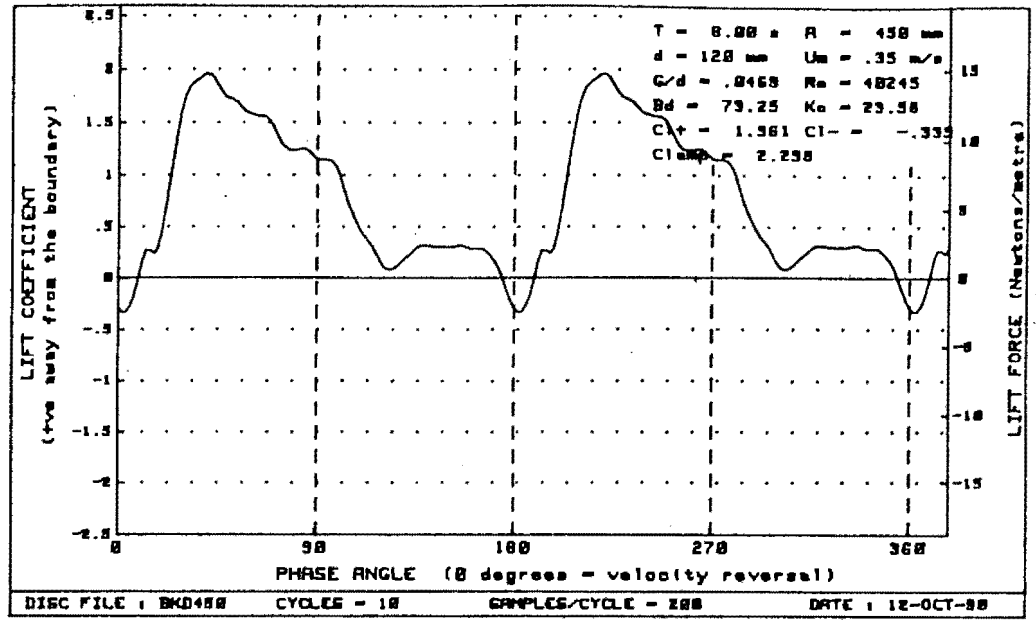

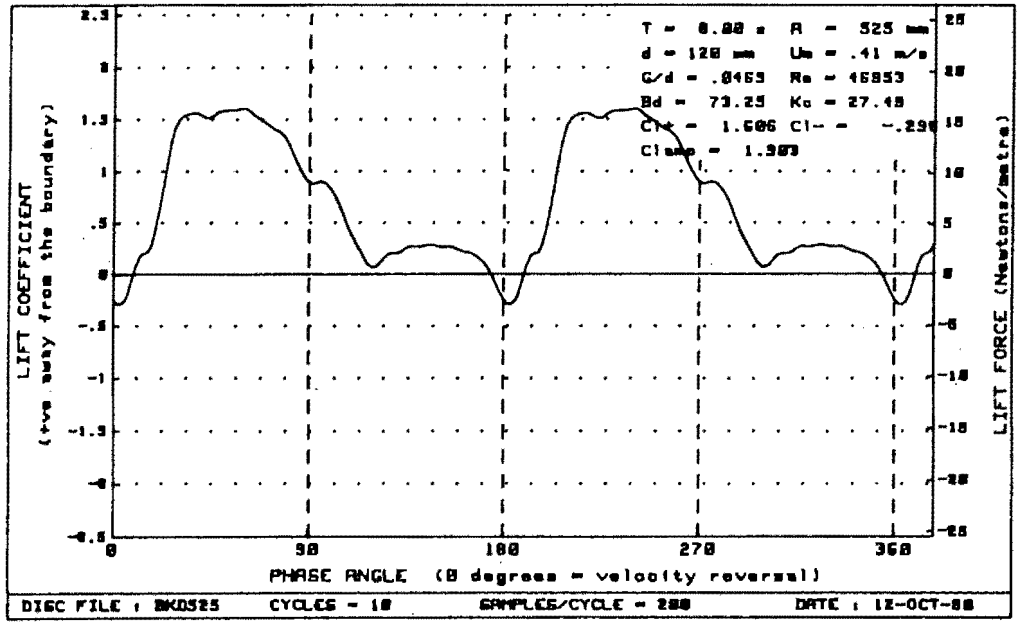

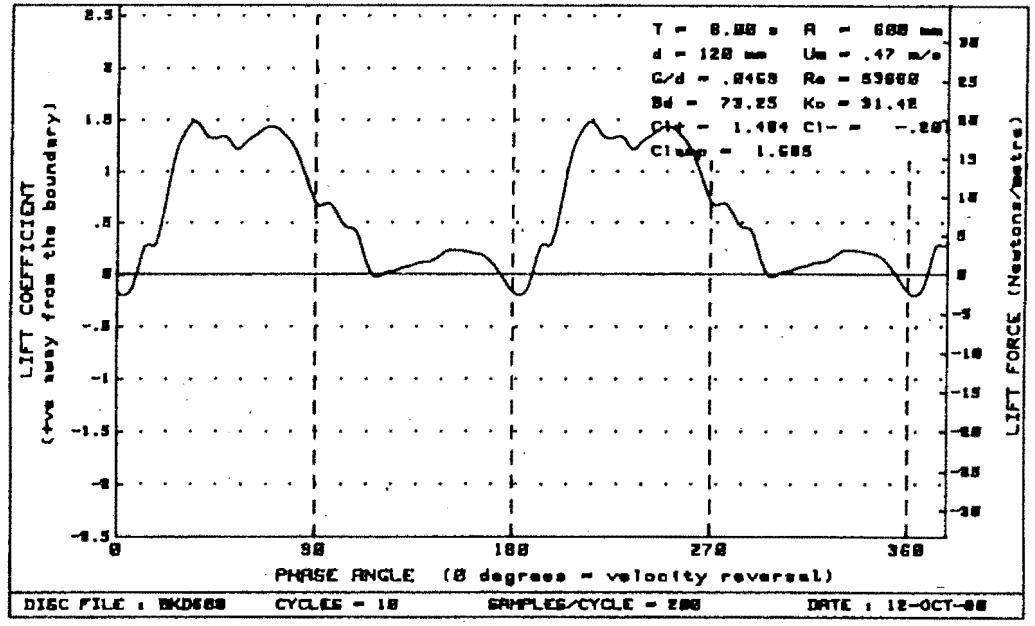

Figure G-24 : Plots of lift vs phase for diameter=120mm, Bd= 73.25 and G/d= .0469

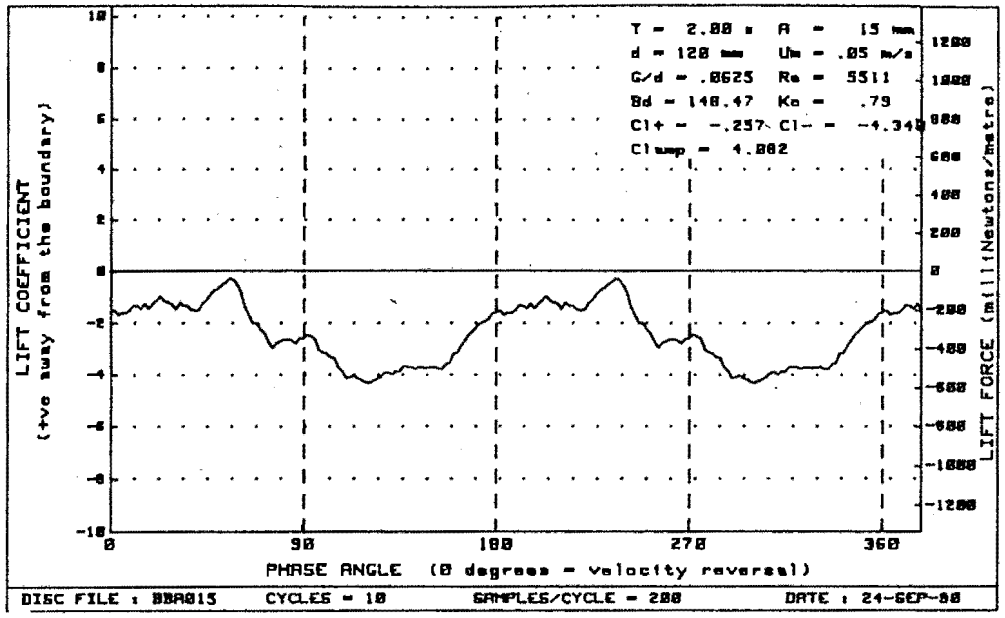

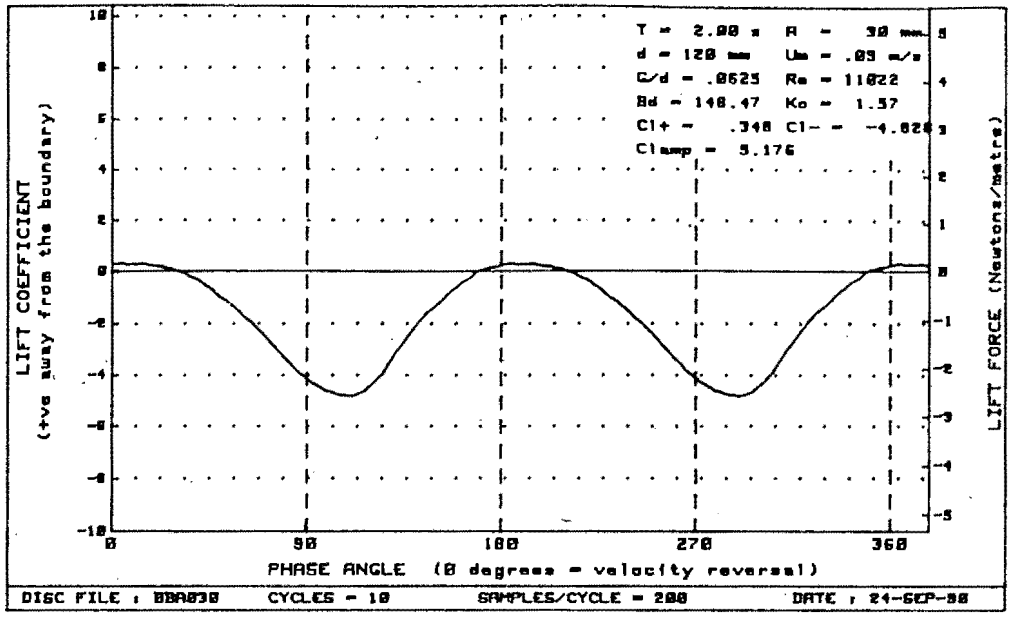

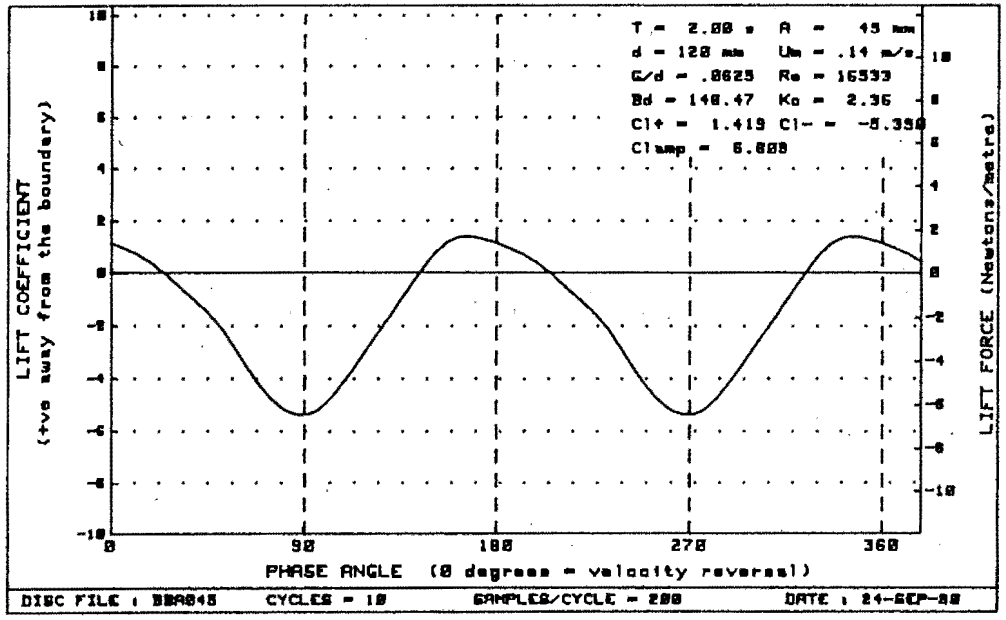

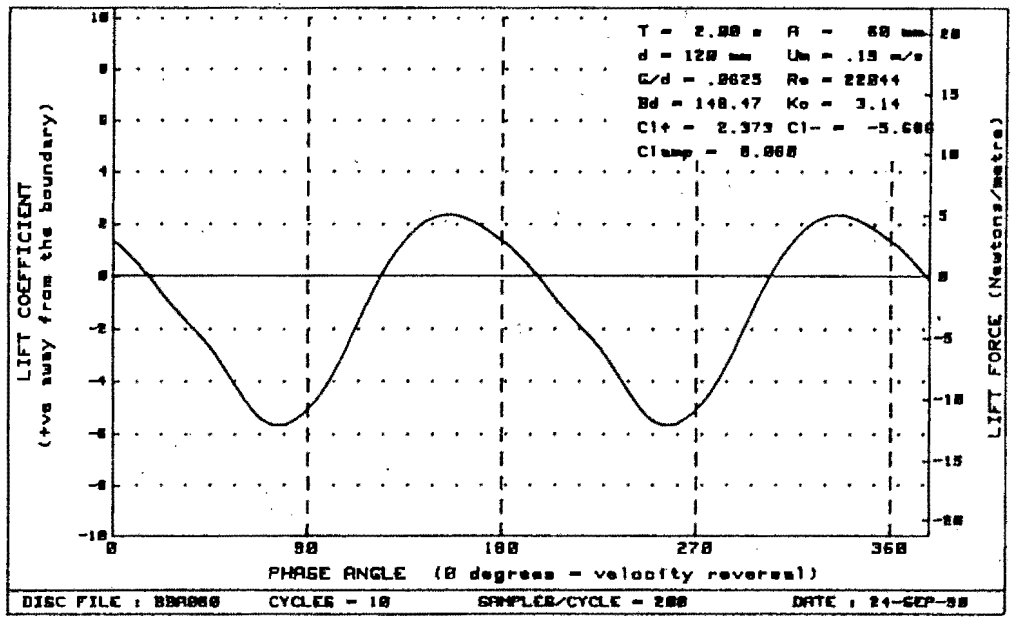

Figure G-25 : Plots of lift vs phase for diameter=120mm, Bd=148.47 and G/d= .0625

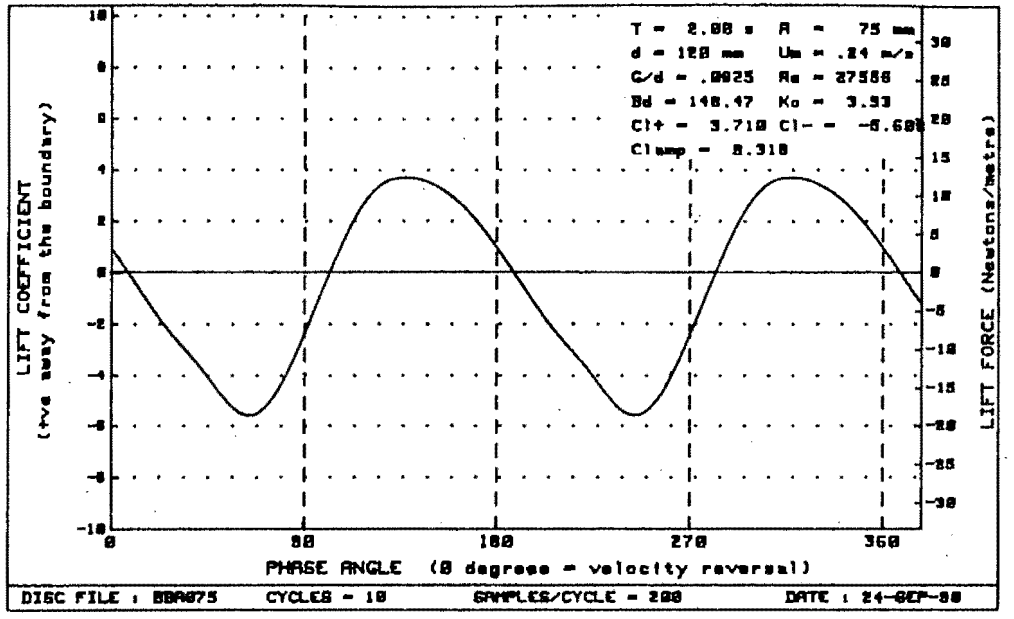

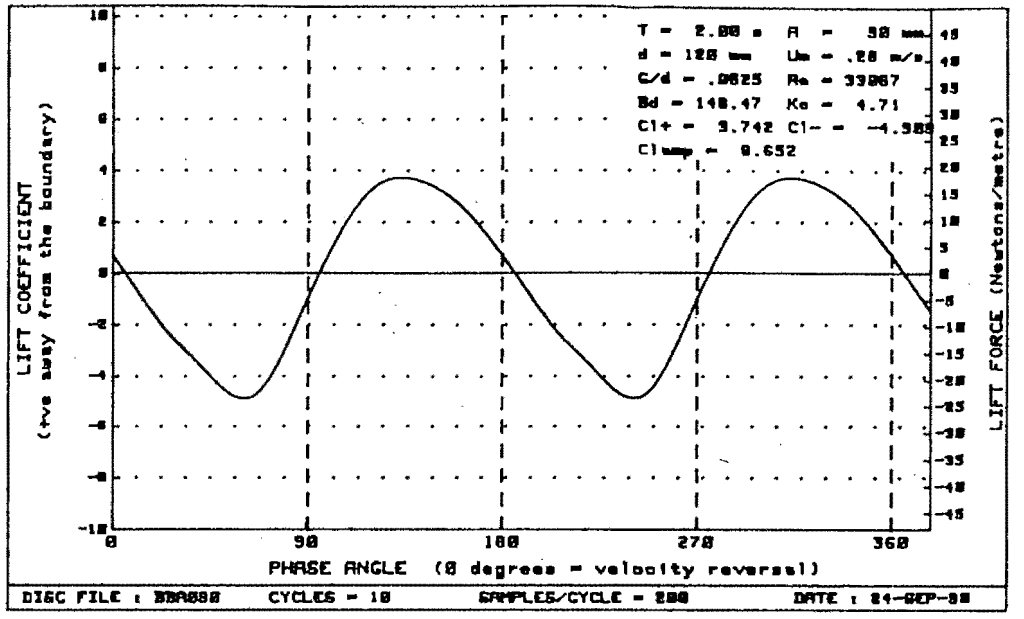

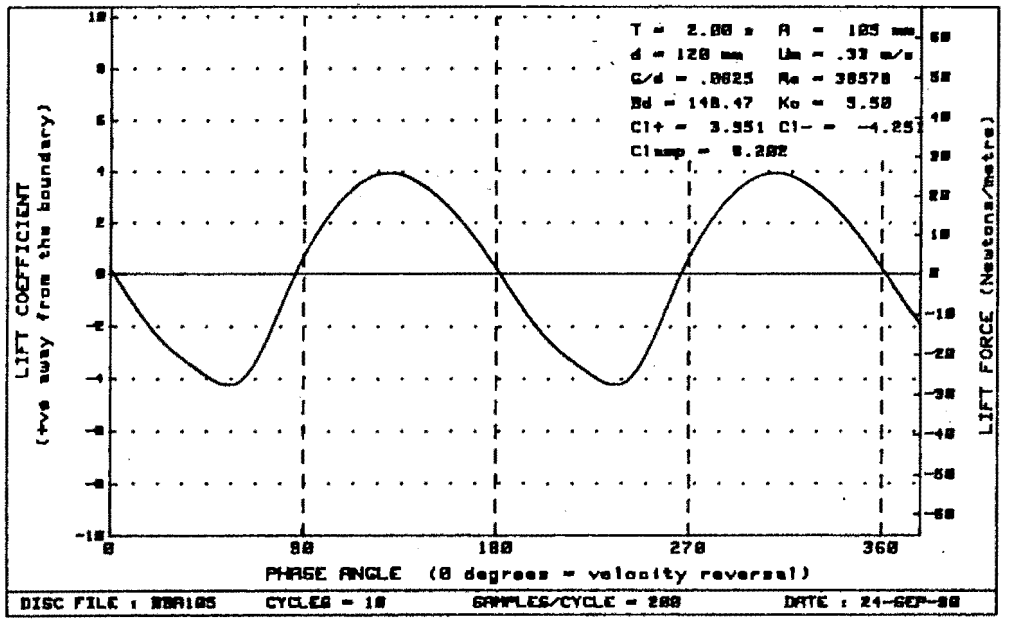

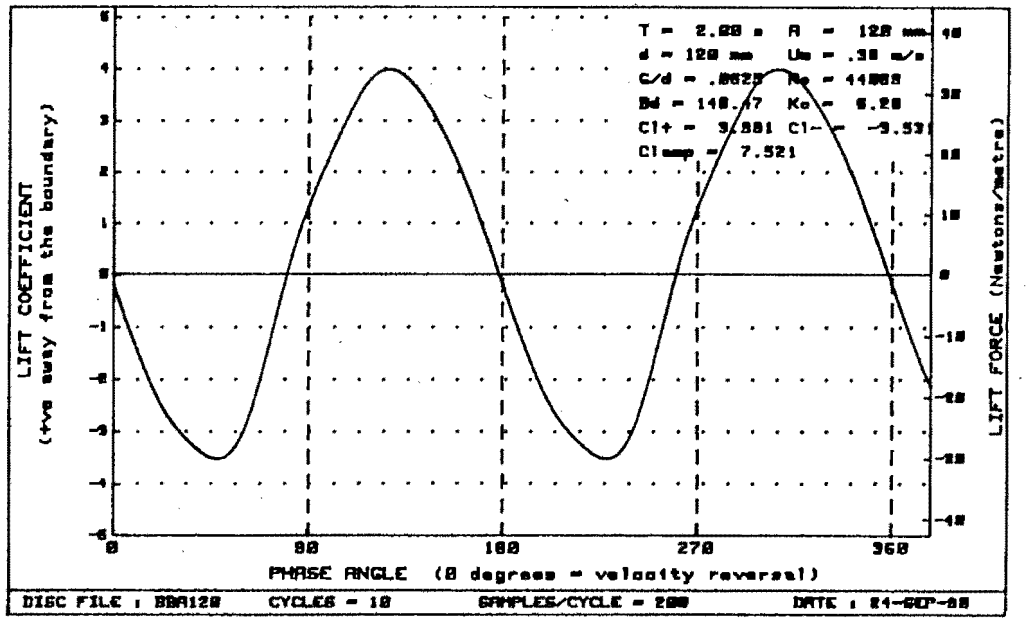

Figure G-26 : Plots of lift vs phase for diameter=120mm, Bd=148.47 and G/d= .0625

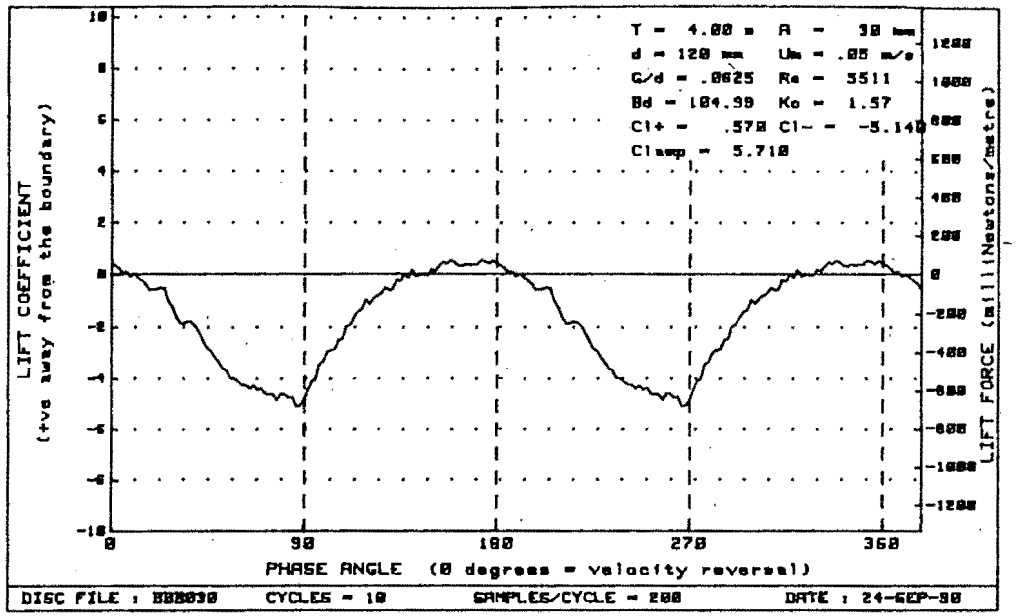

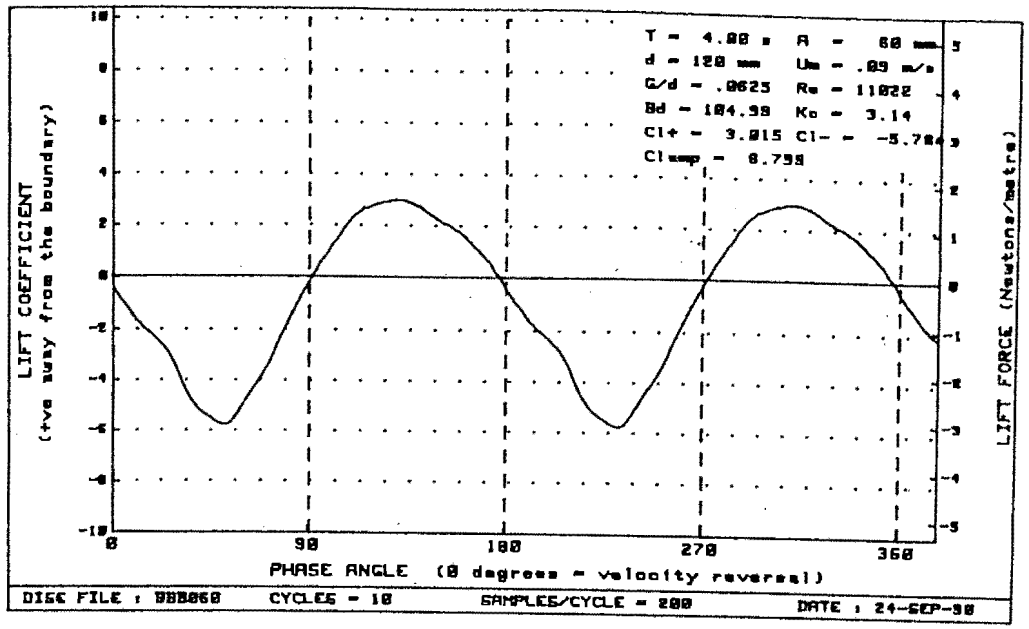

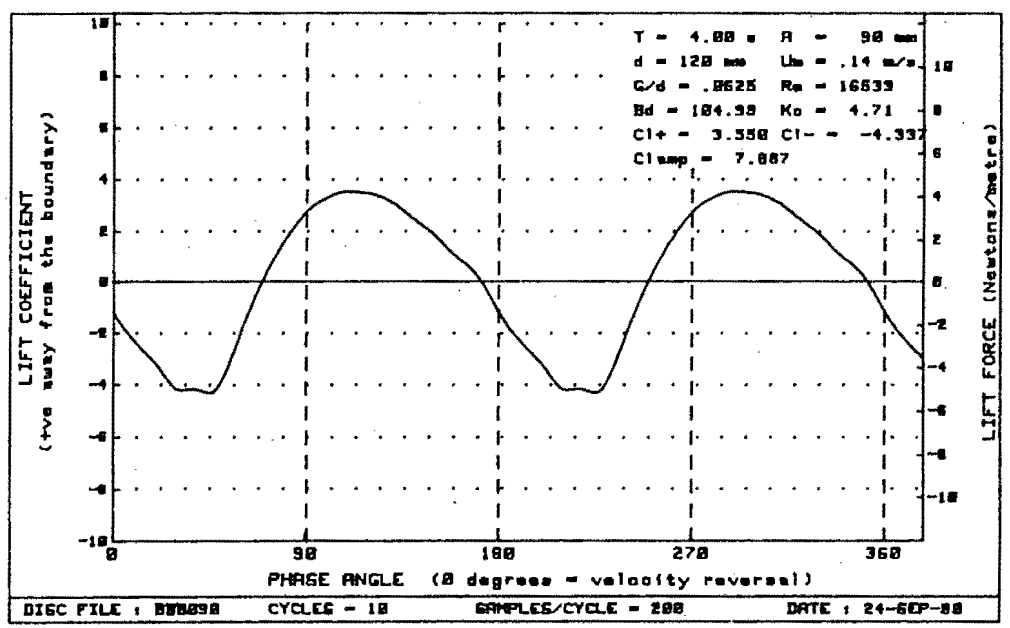

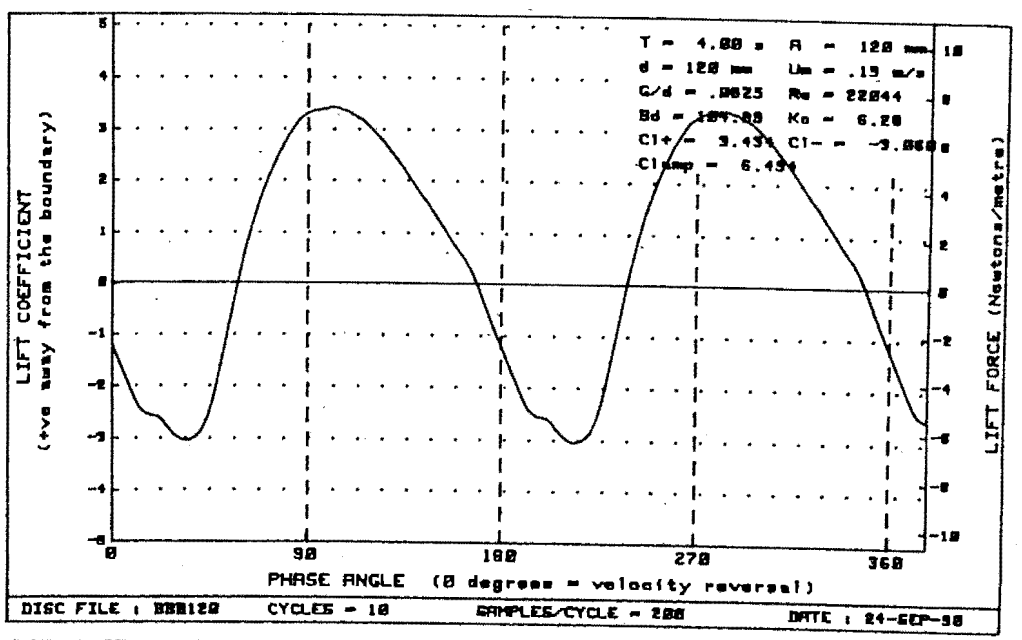

Figure G-27 : Plots of lift vs phase for diameter=120mm, Bd=104.99 and G/d= .0625

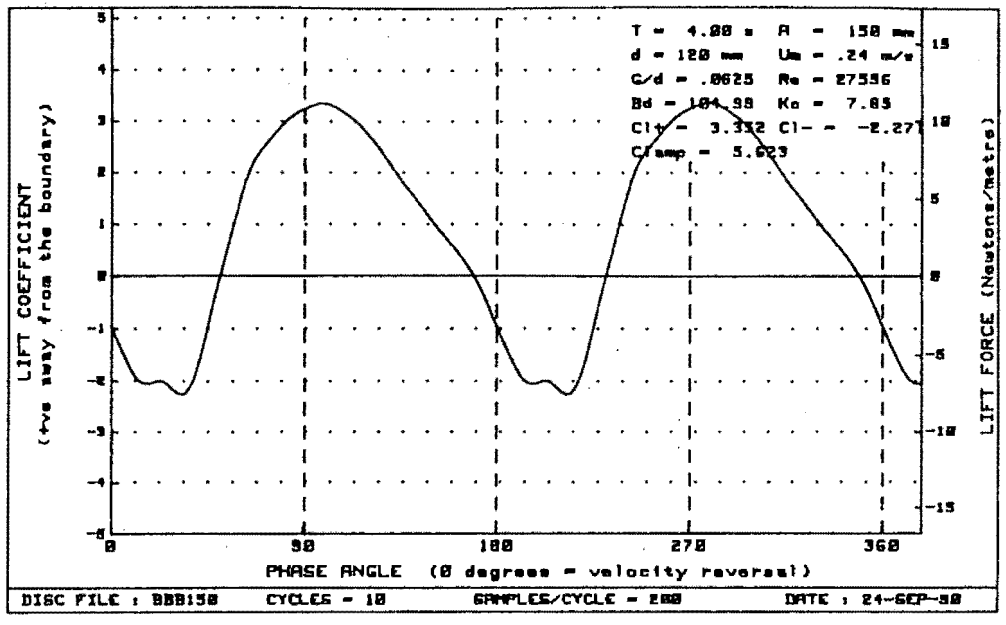

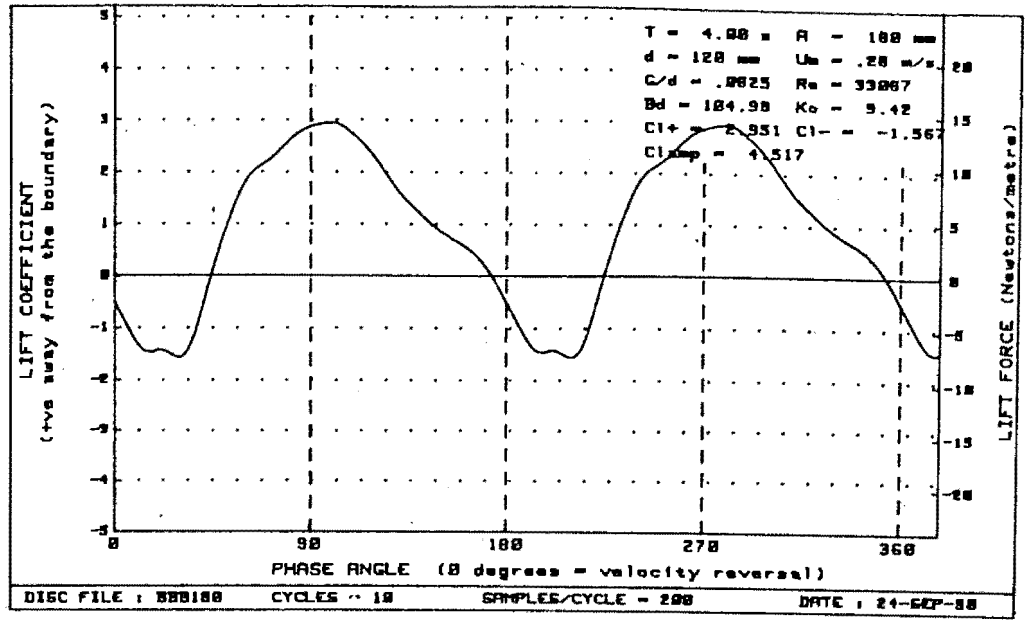

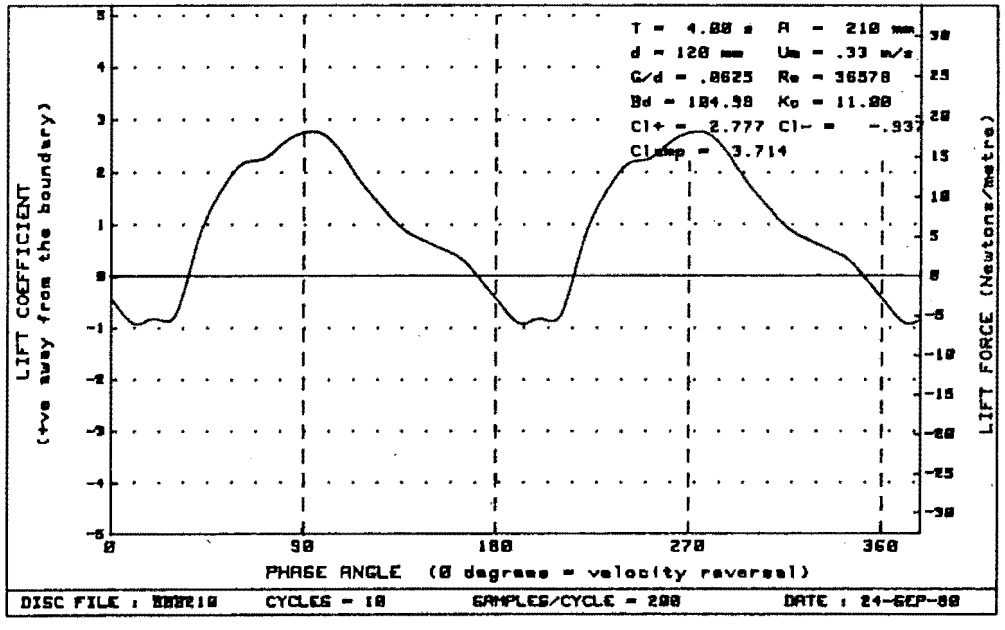

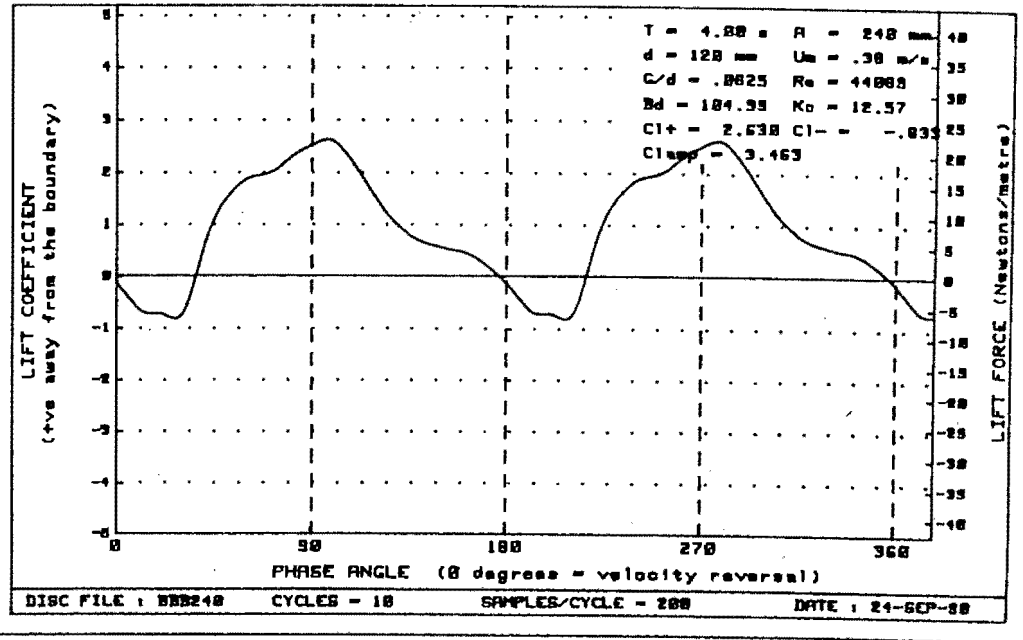

Figure G-28 : Plots of lift vs phase for diameter=120mm, Bd=104.99 and G/d= .0625

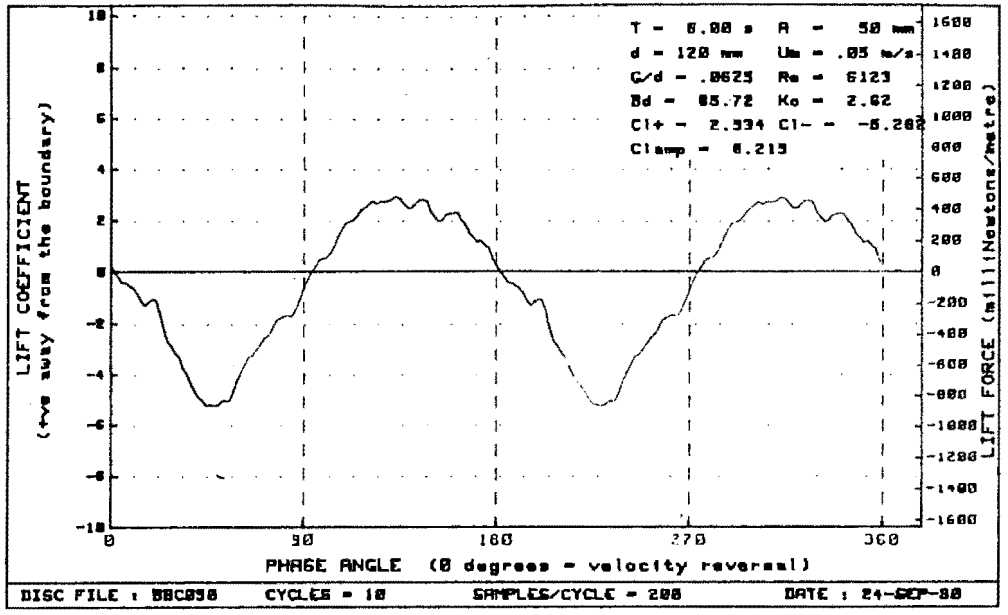

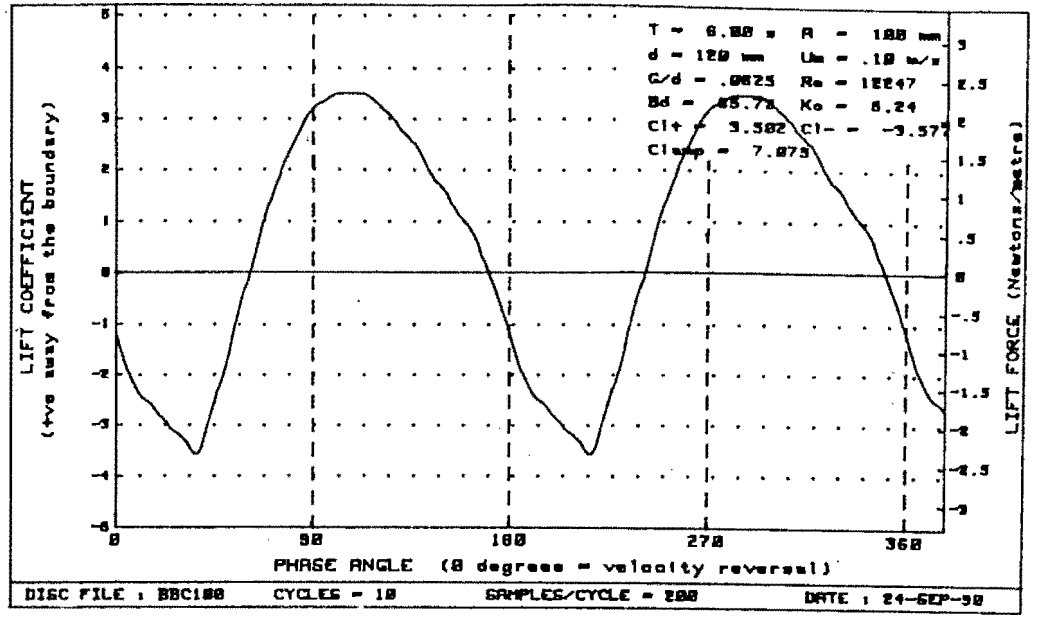

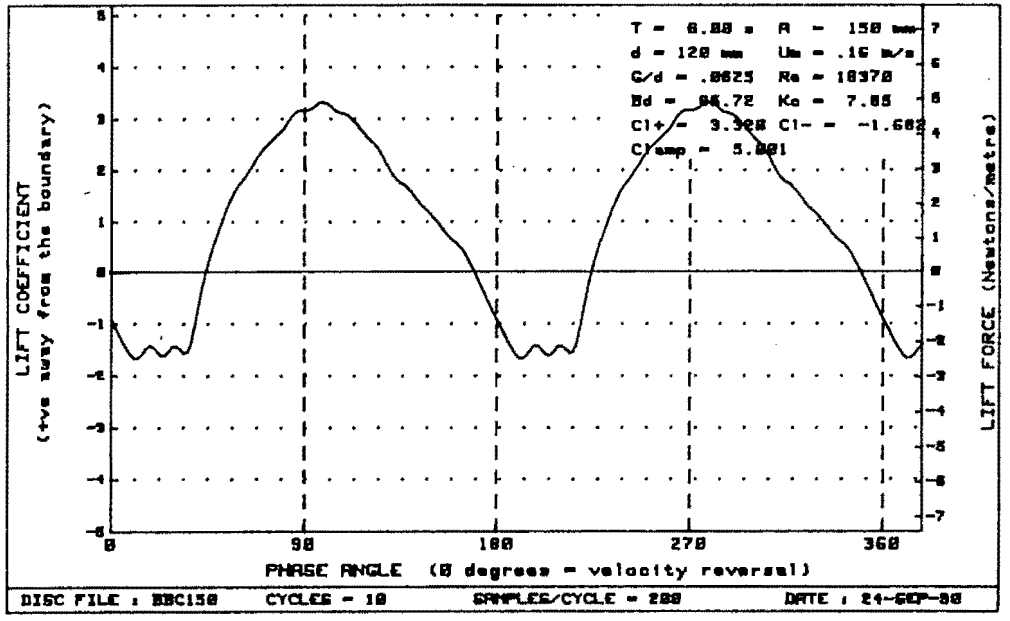

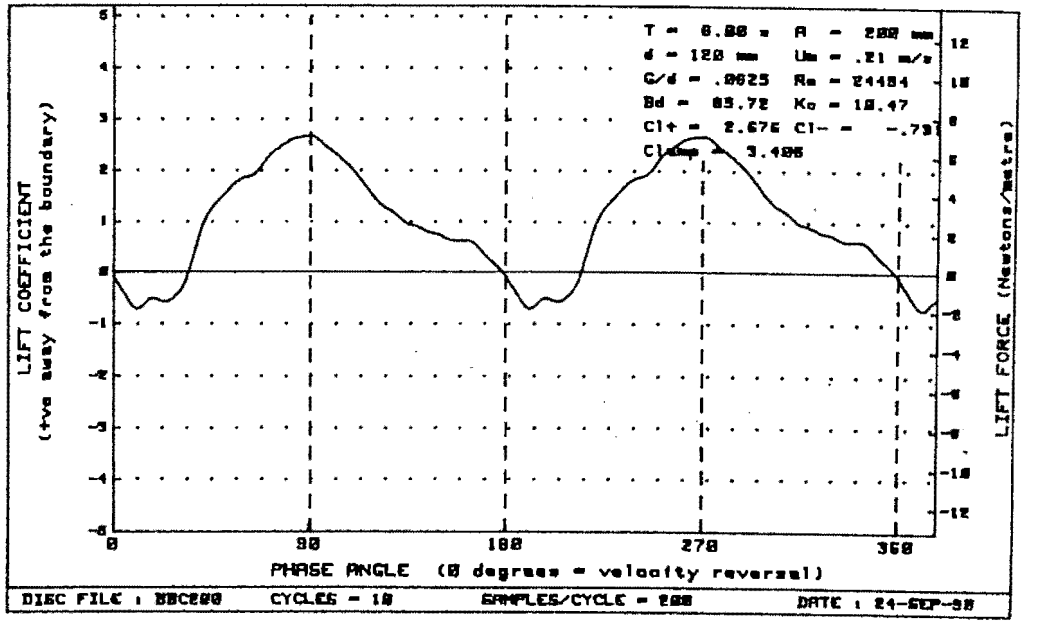

Figure G-29 : Plots of lift vs phase for diameter=120mm, Bd= 85.72 and G/d= .0625

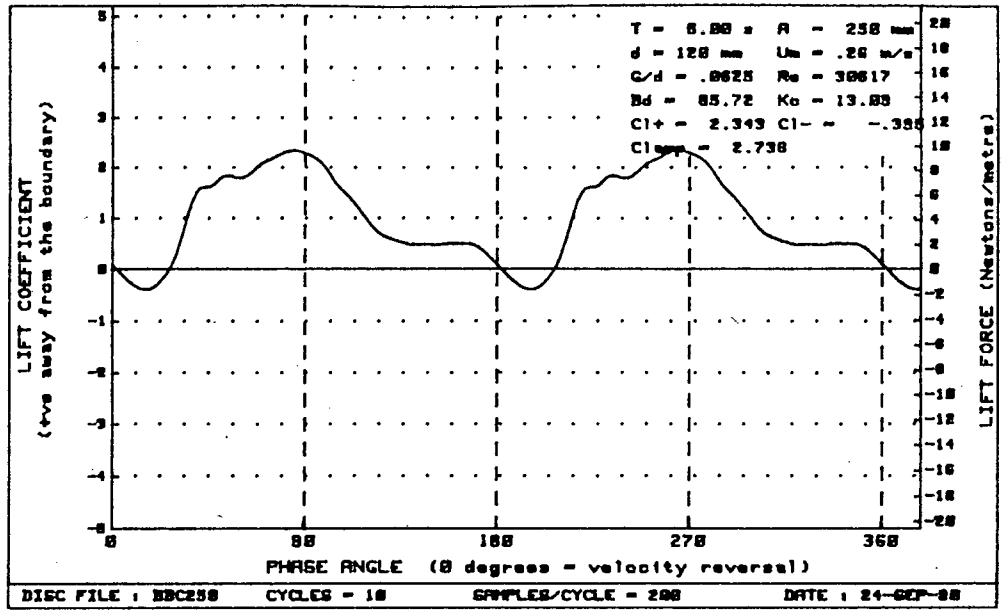

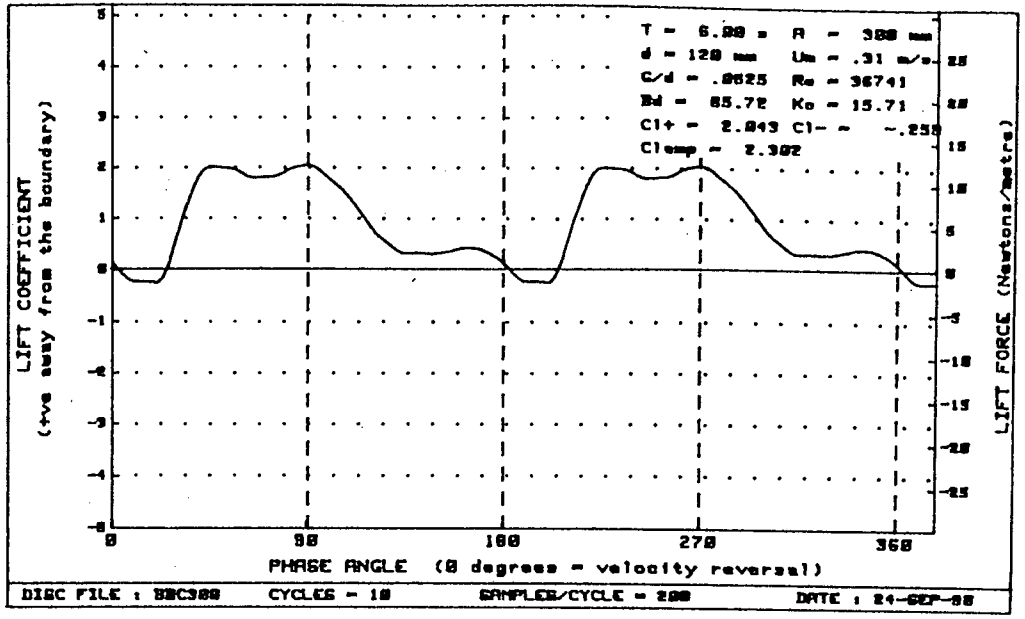

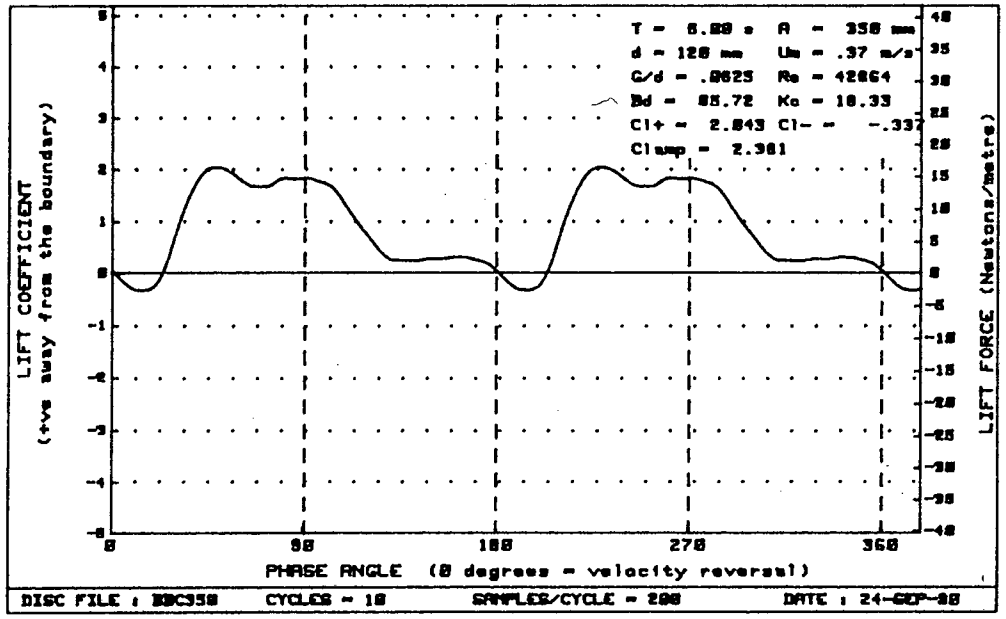

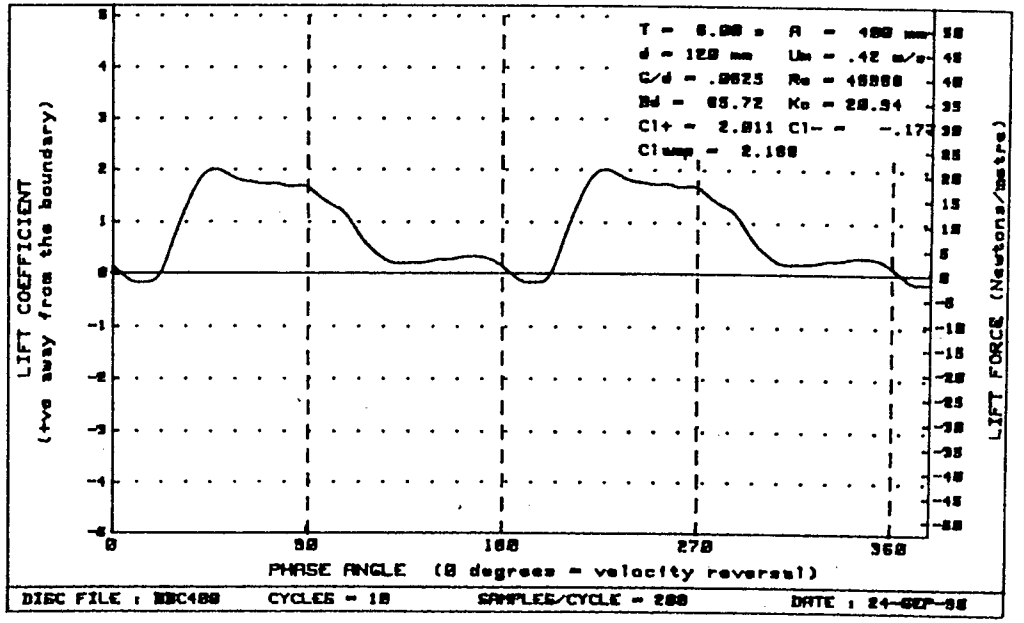

Figure G-30 : Plots of lift vs phase for diameter=120mm, Bd= 85.72 and G/d= .0625

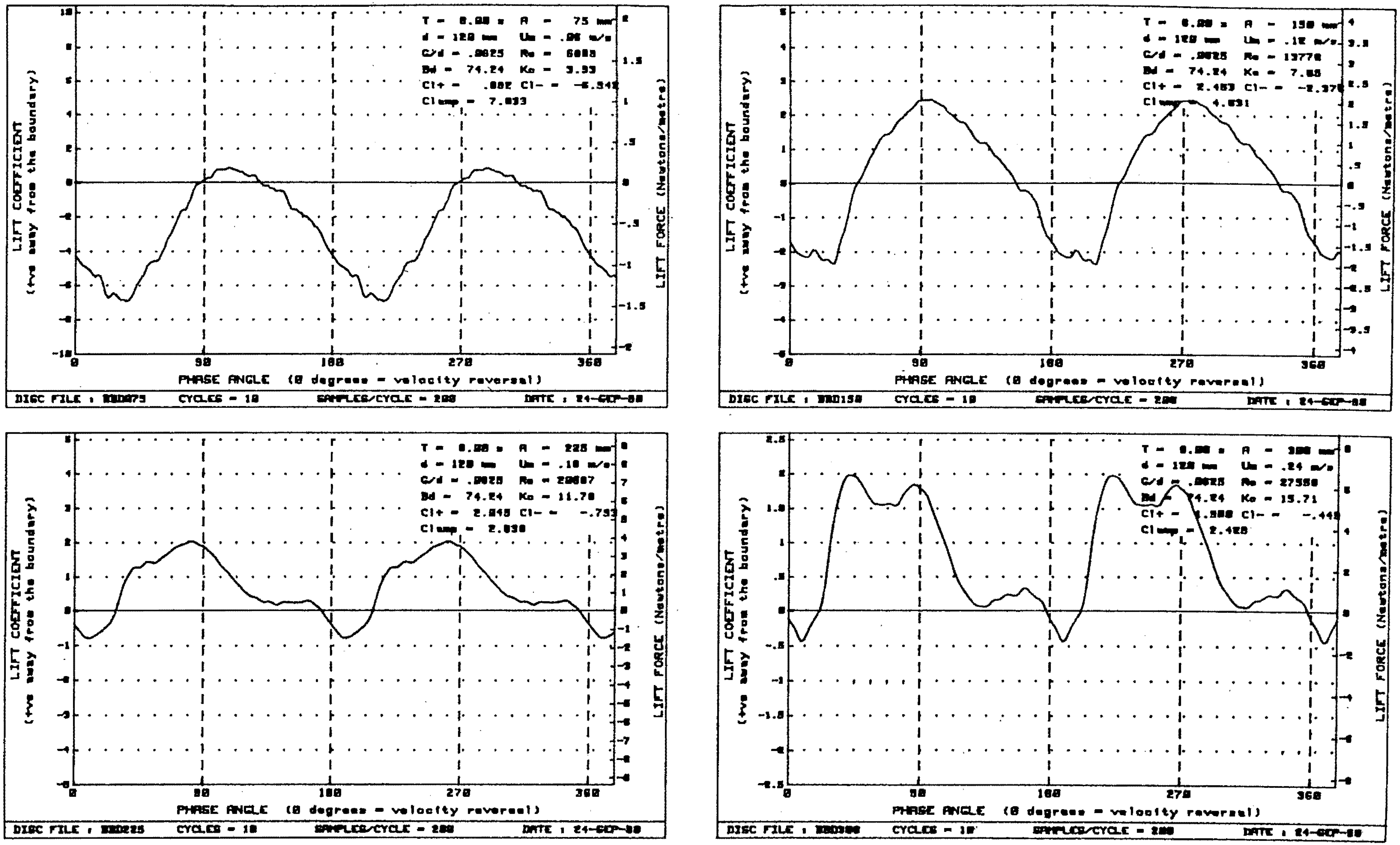

Figure G-31 : Plots of lift vs phase for diameter=120mm, Bd= 74.24 and G/d= .0625

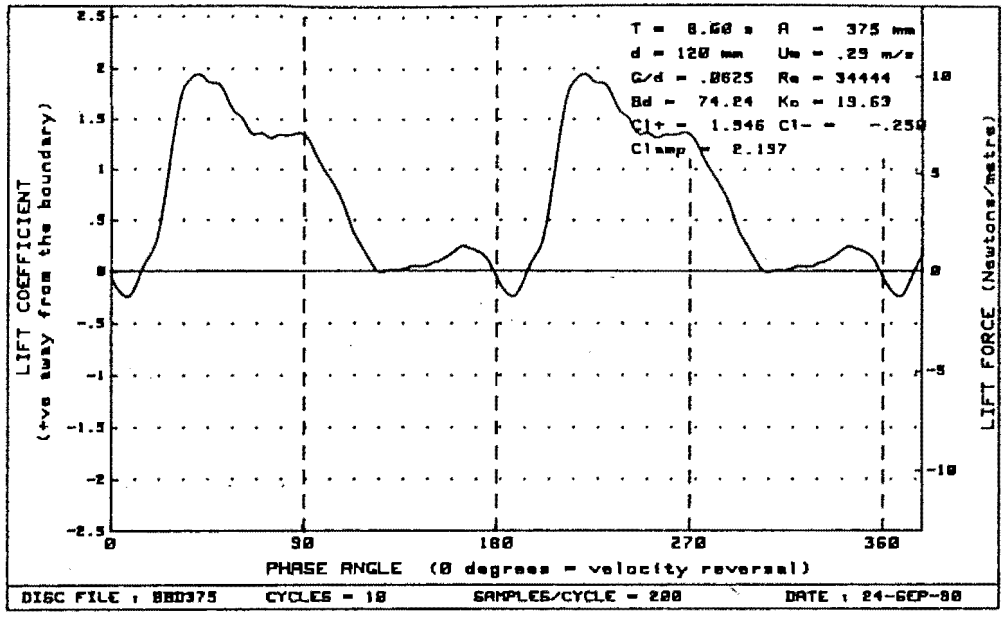

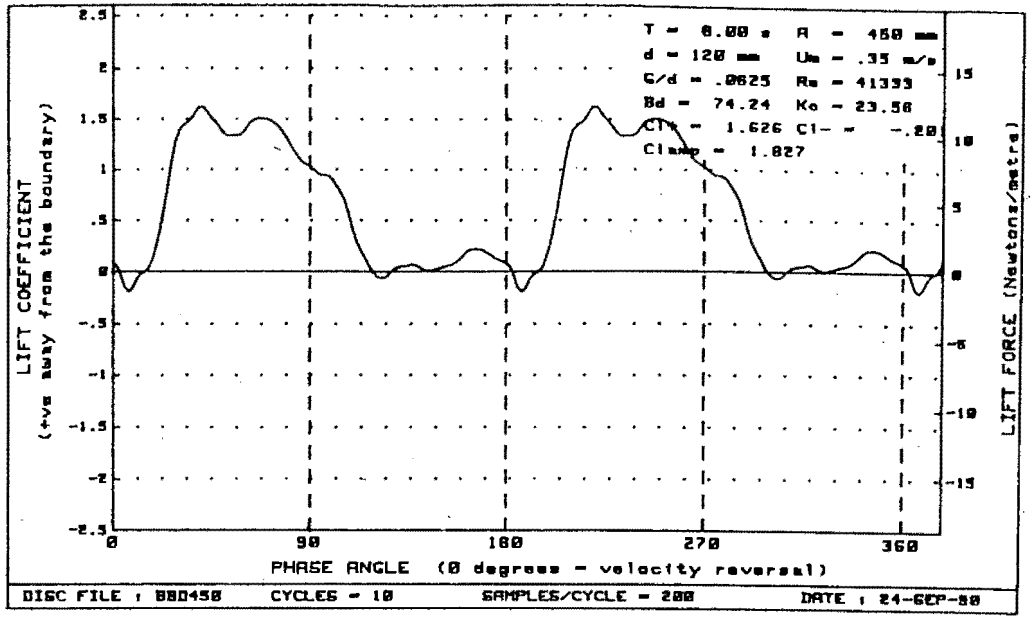

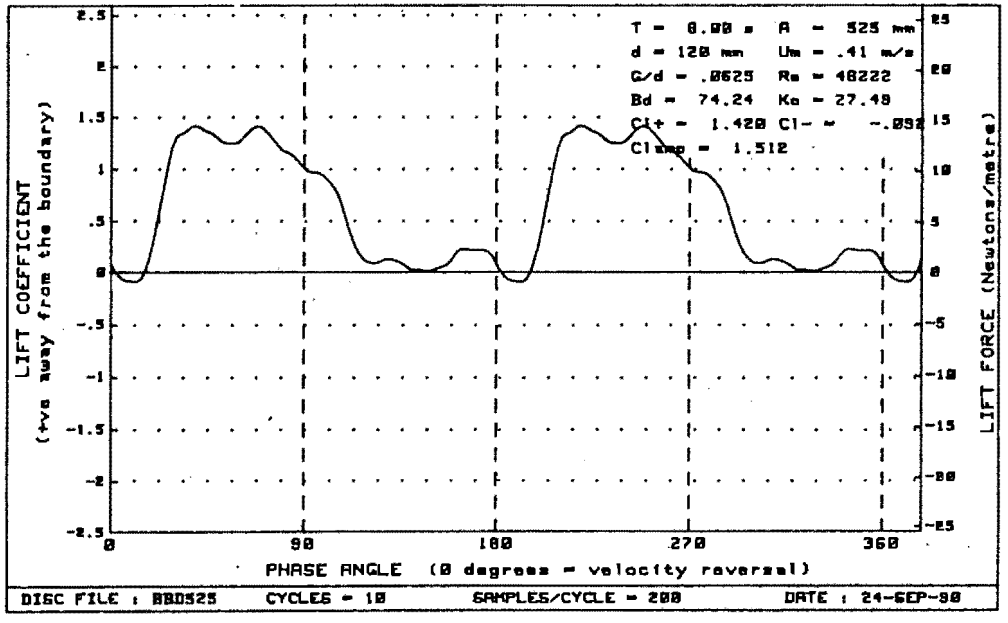

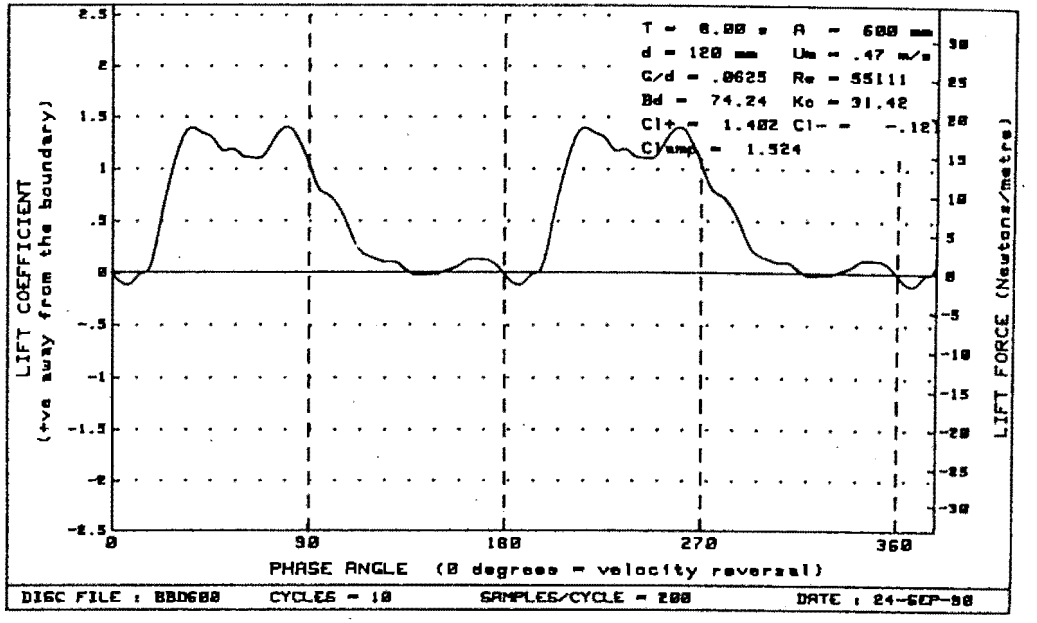

Figure G-32 : Plots of lift vs phase for diameter=120mm, Bd= 74.24 and G/d= .0625

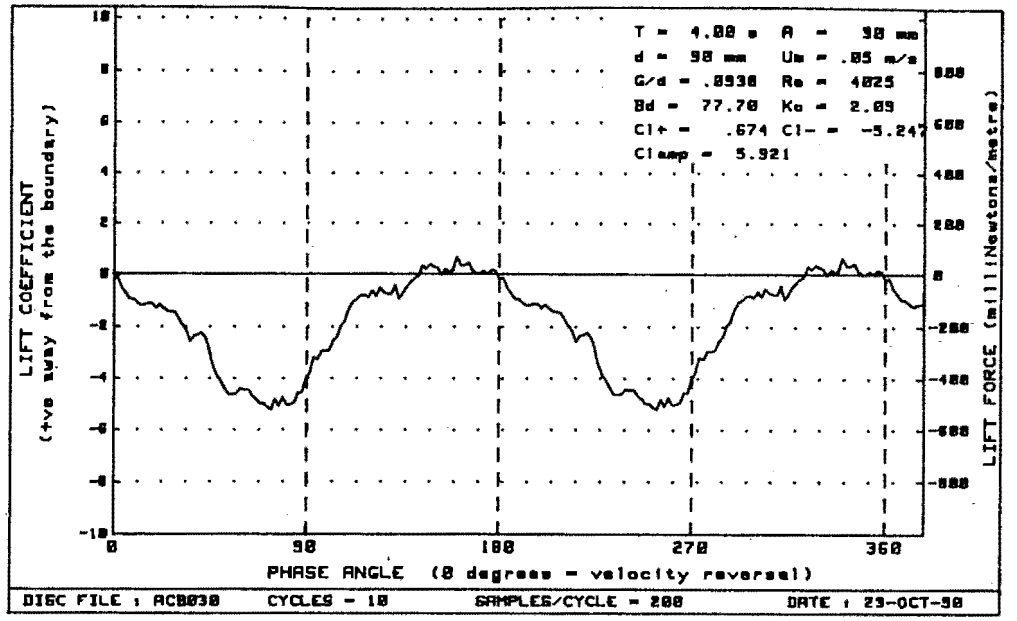

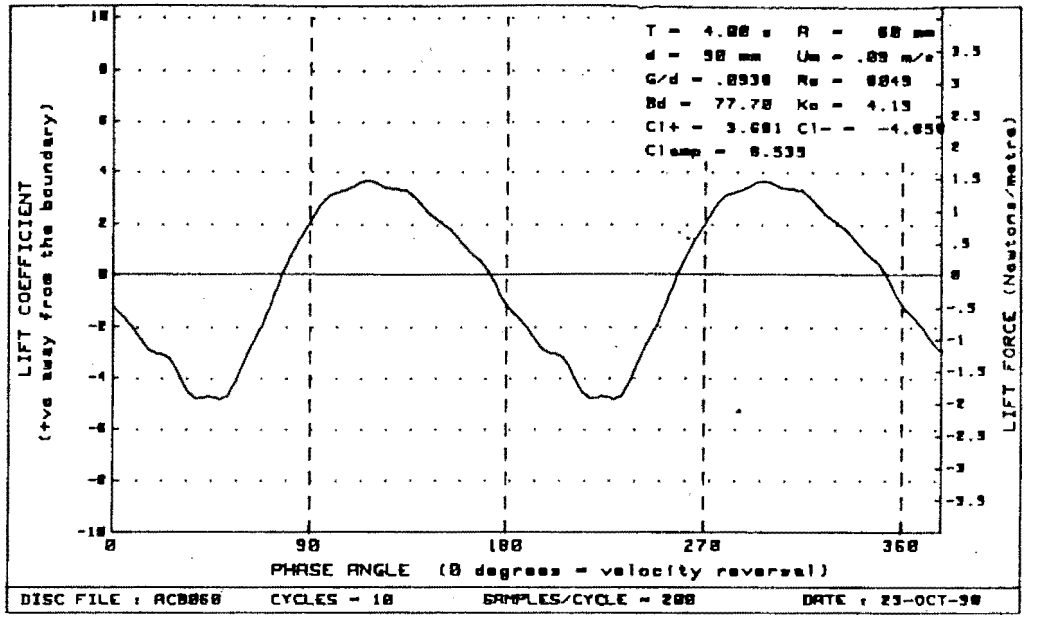

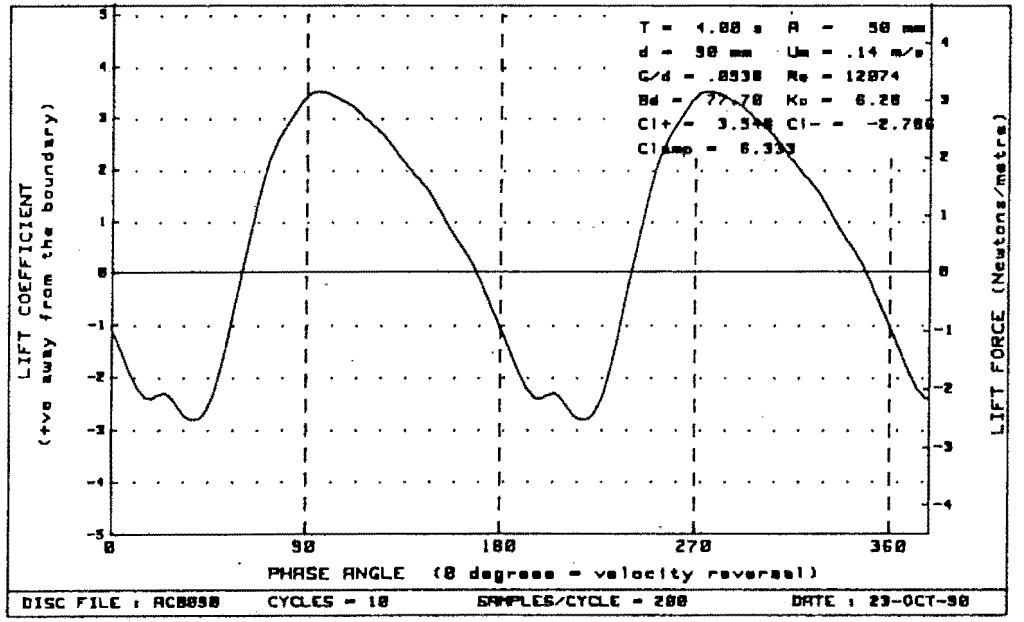

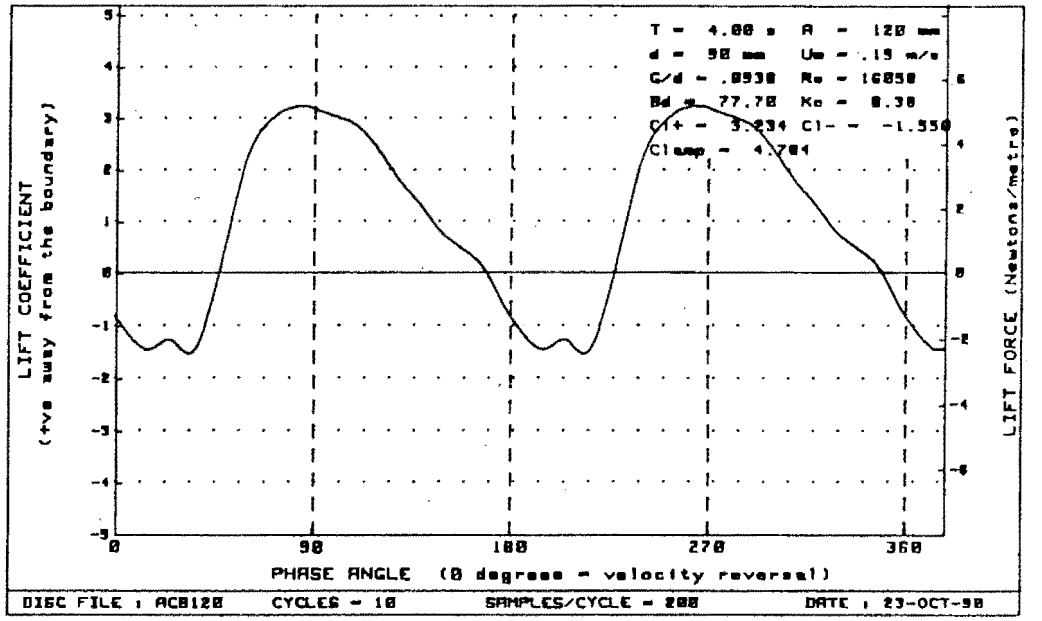

Figure G-33 : Plots of lift vs phase for diameter=90mm, Bd= 77.70 and G/d= .0938

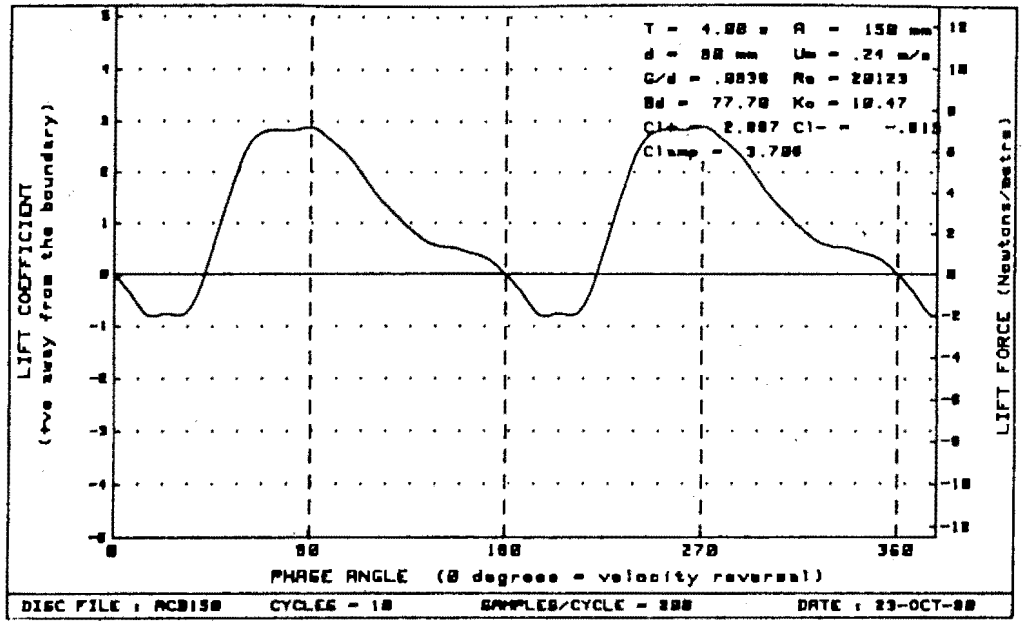

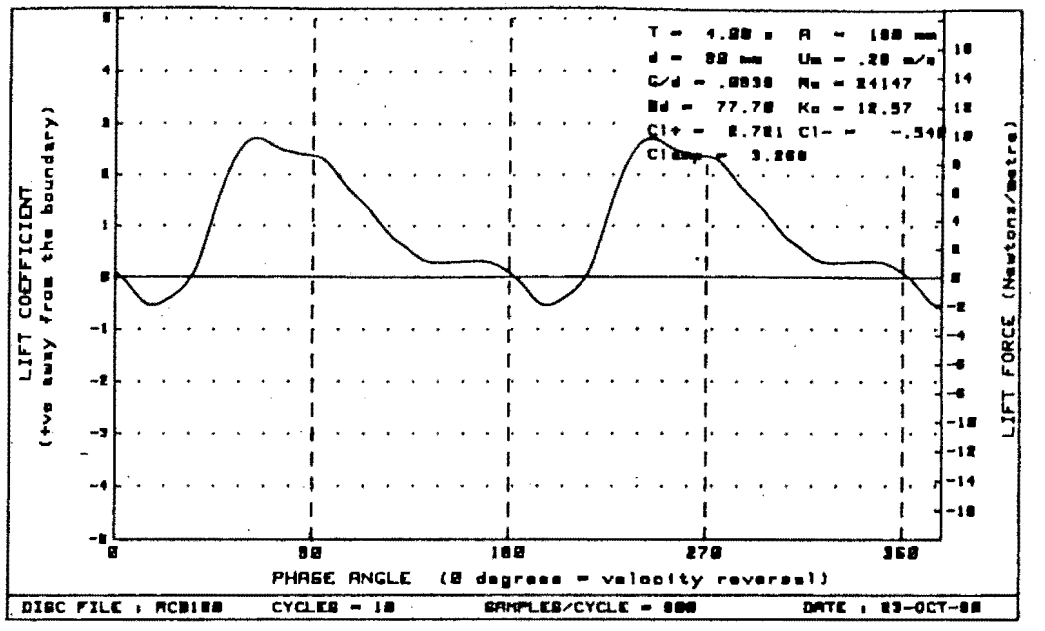

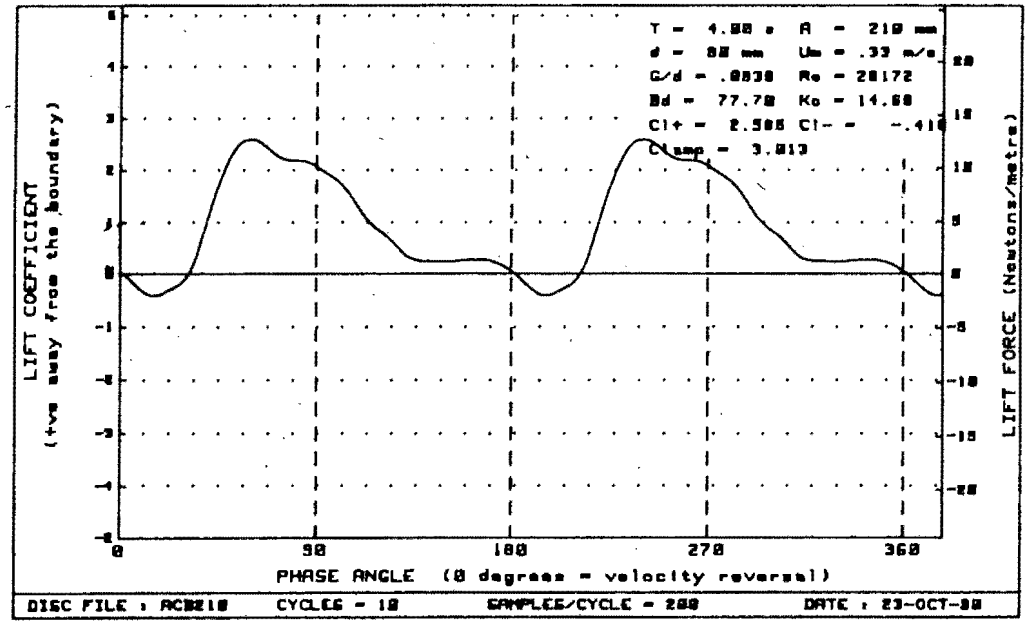

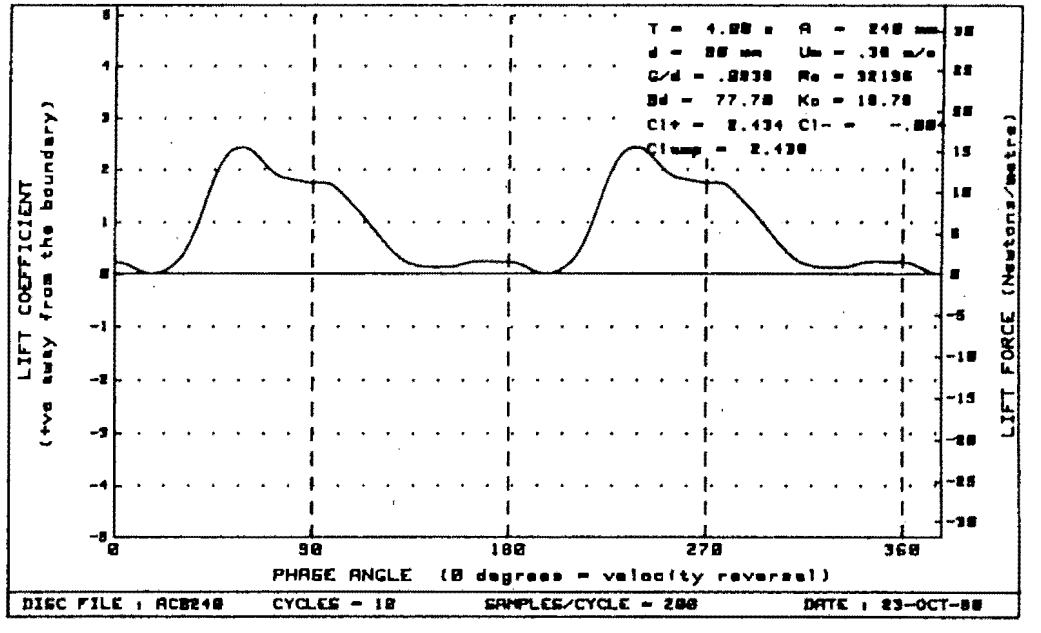

Figure G-34 : Plots of lift vs phase for diameter=90mm, Bd= 77.70 and G/d= .0938

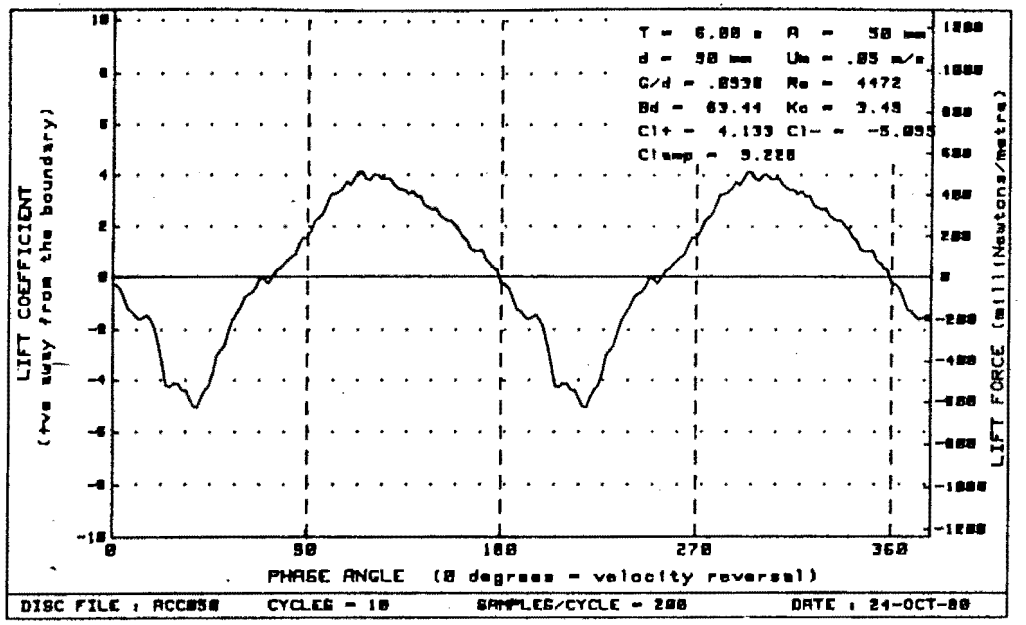

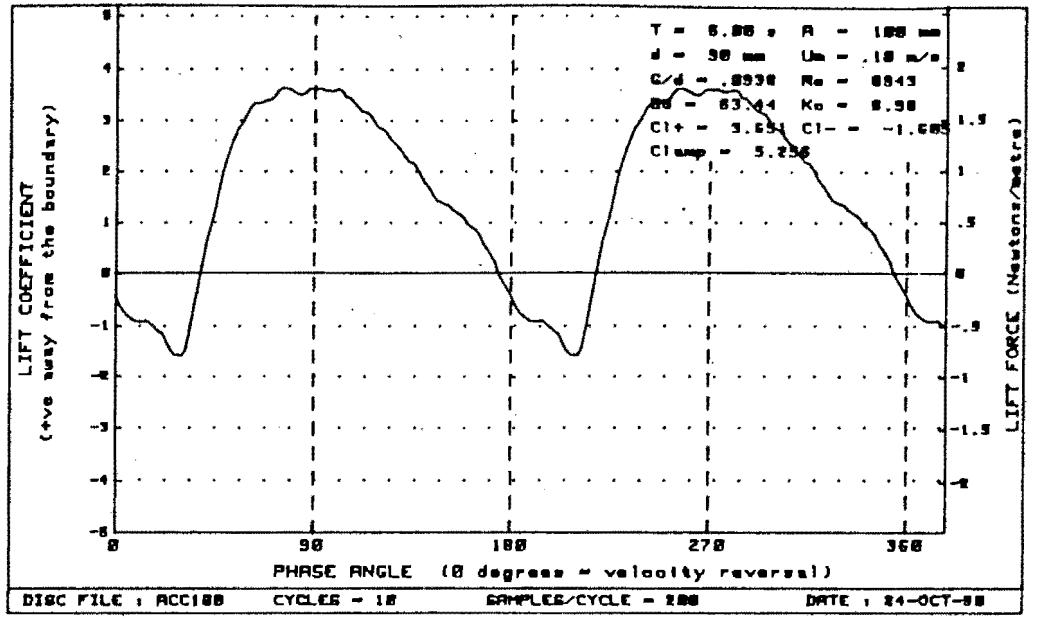

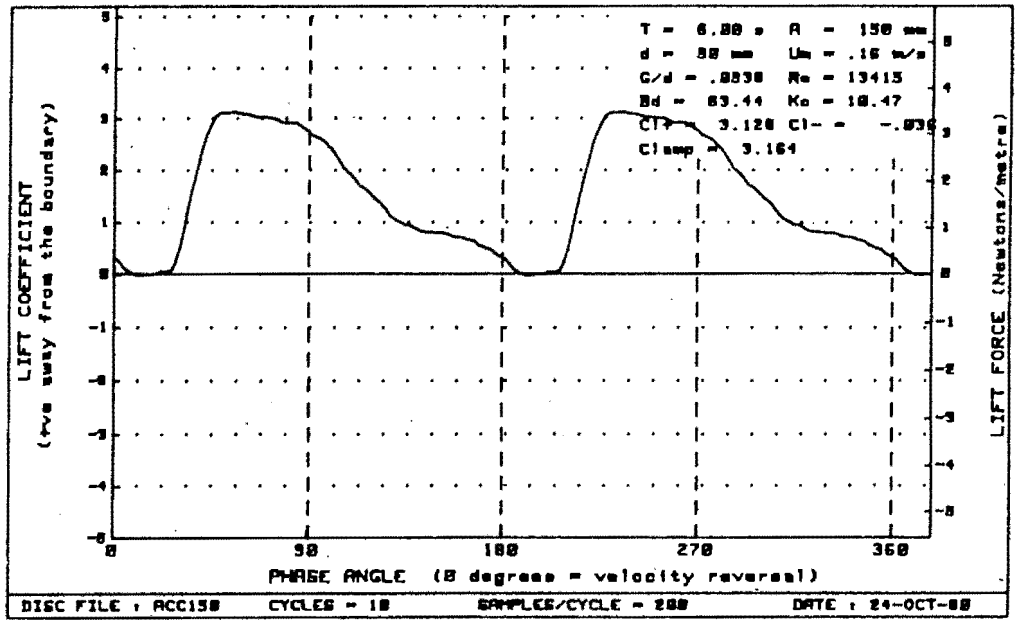

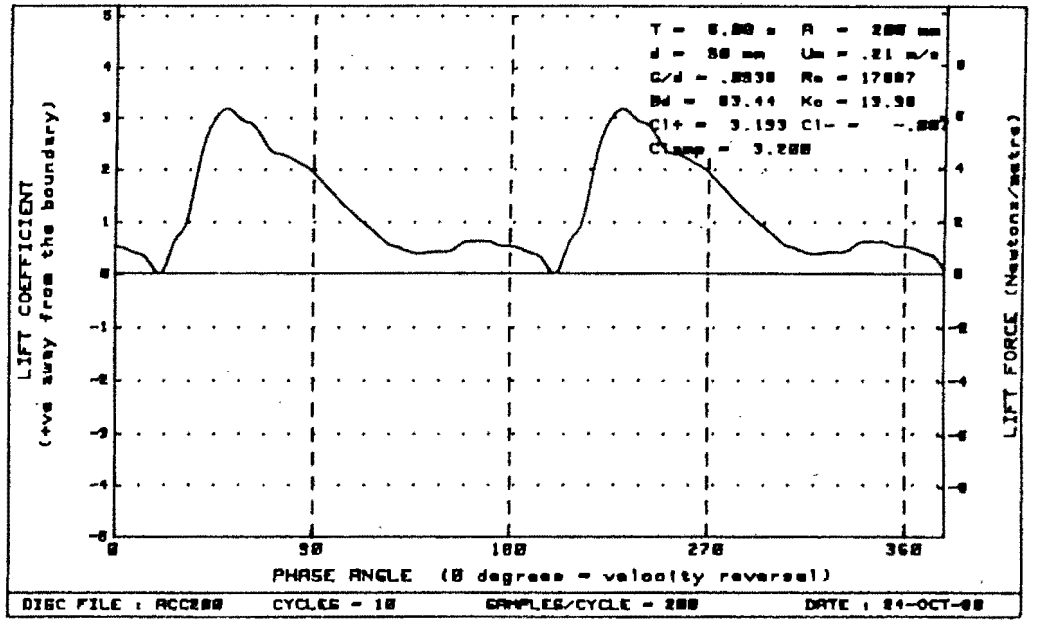

Figure G-35 : Plots of lift vs phase for diameter=90mm, Bd= 63.44 and G/d= .0930

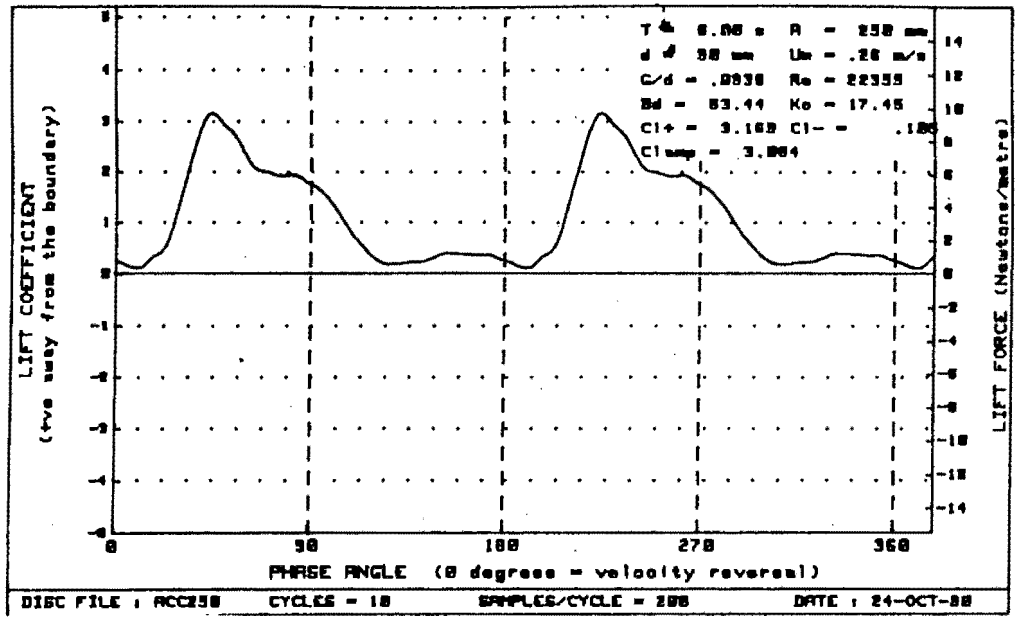

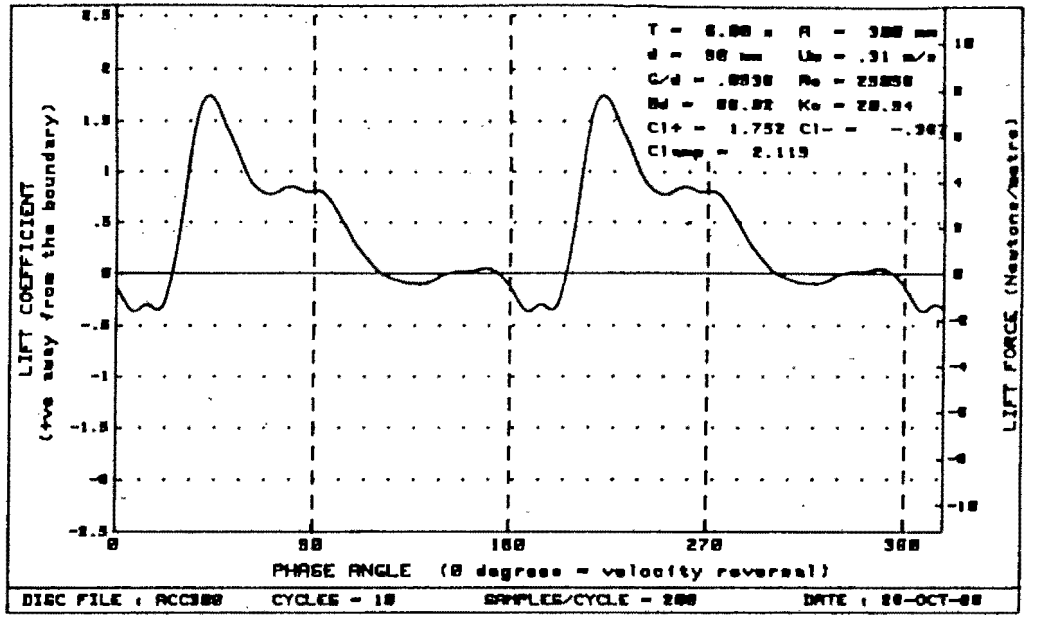

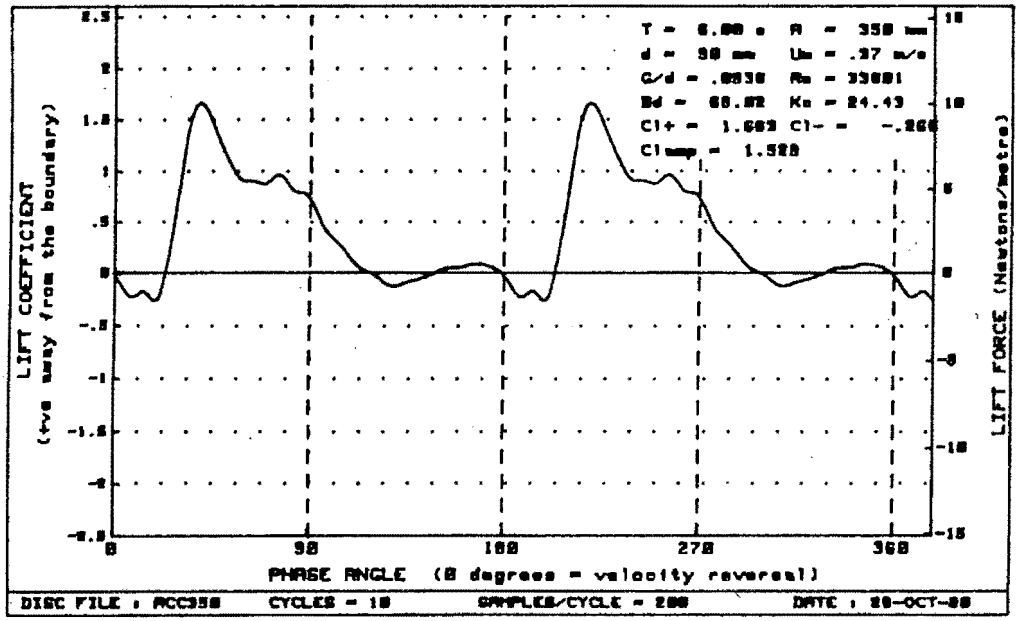

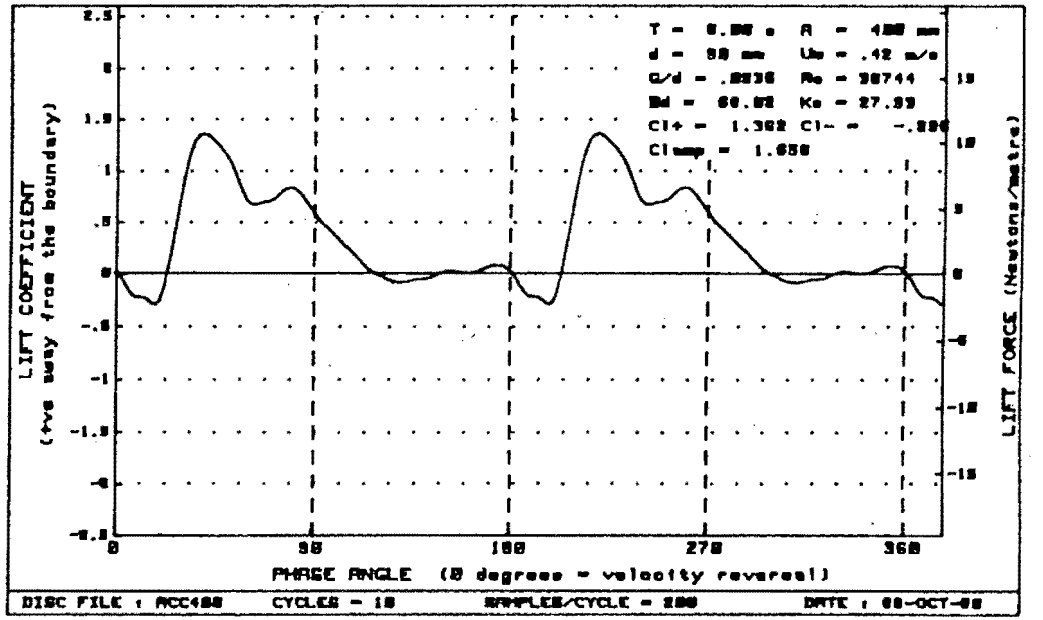

Figure G-36 : Plots of lift vs phase for diameter=90mm, Bd= 66.02 and G/d= .0938

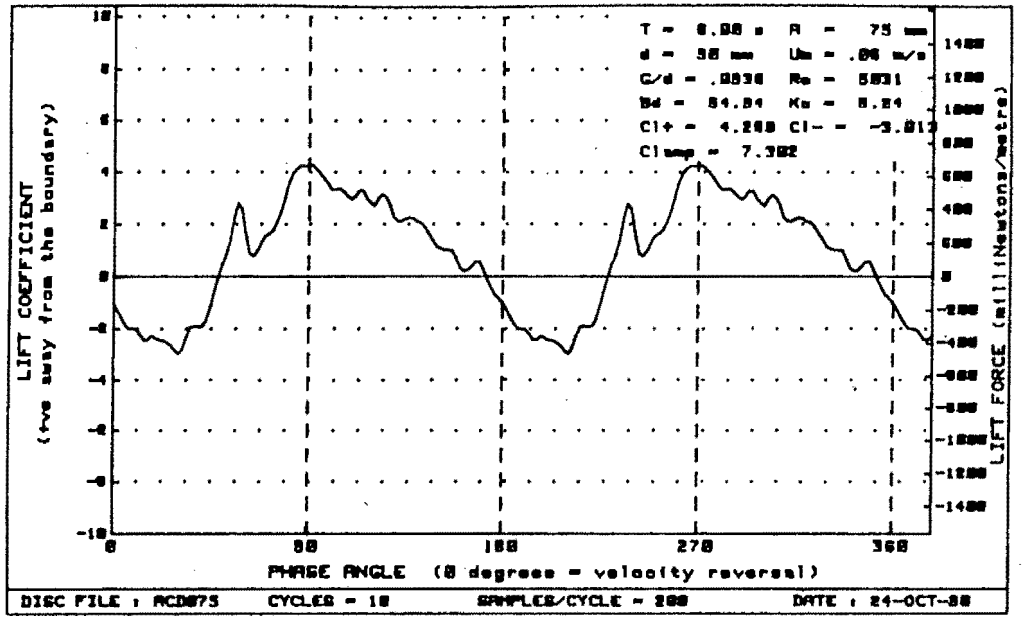

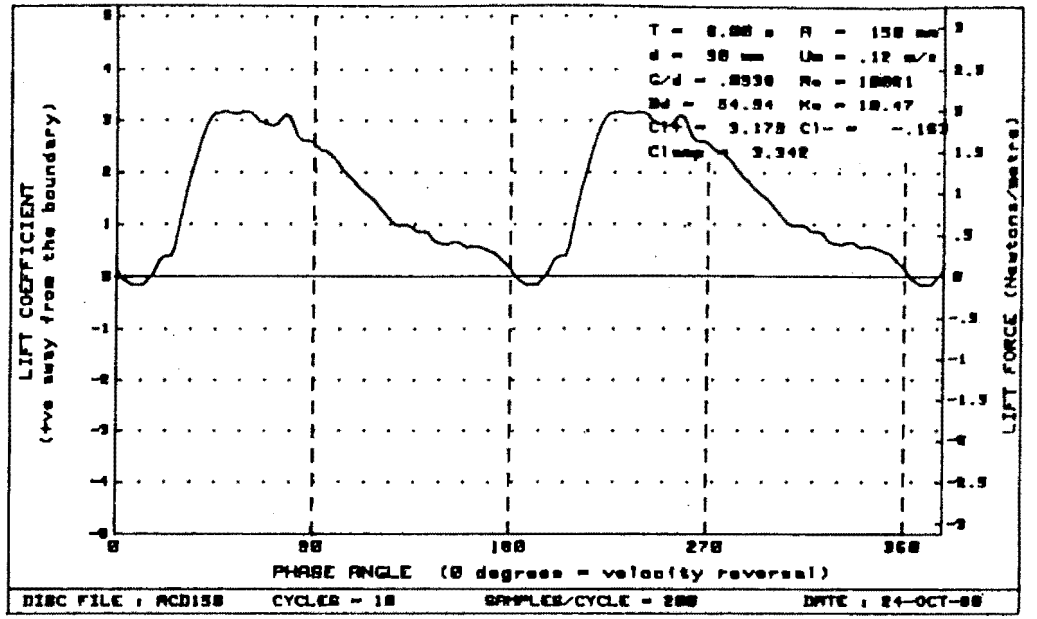

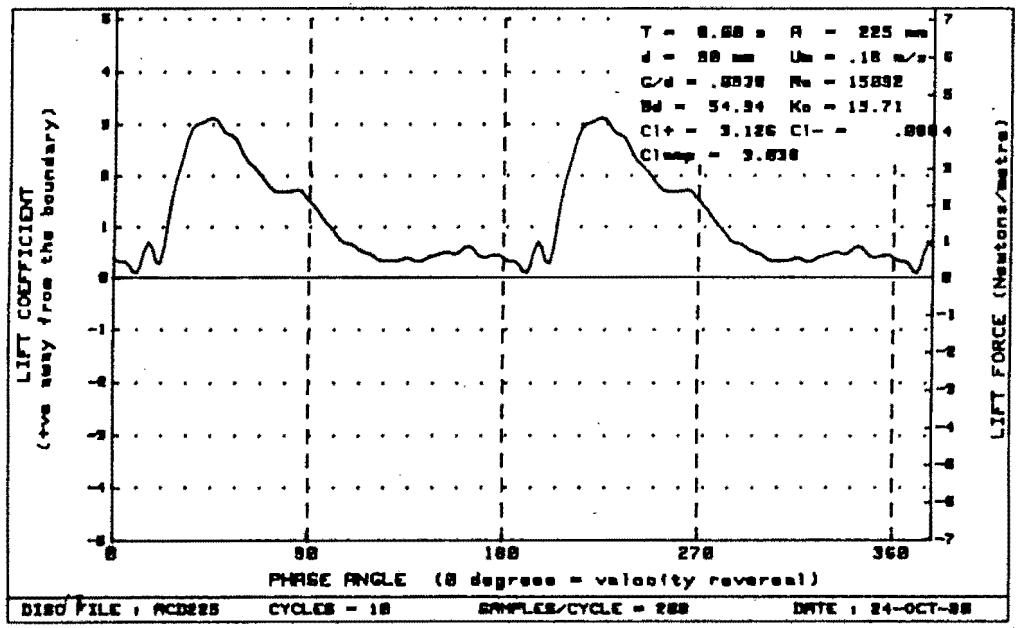

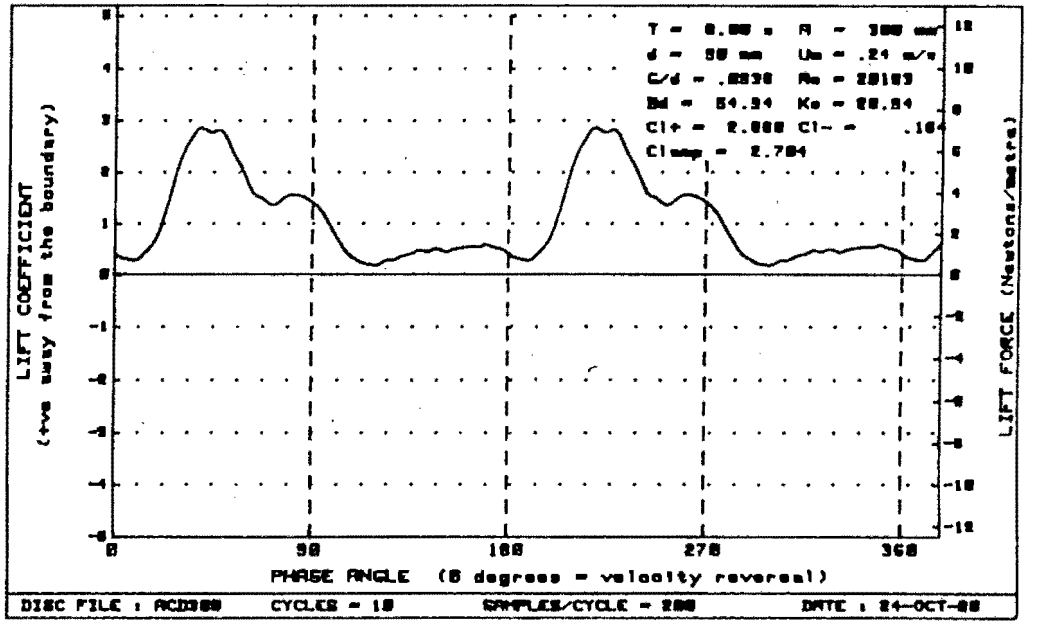

Figure G-37 : Plots of lift vs phase for diameter=90mm, Bd= 54.94 and G/d= .0938

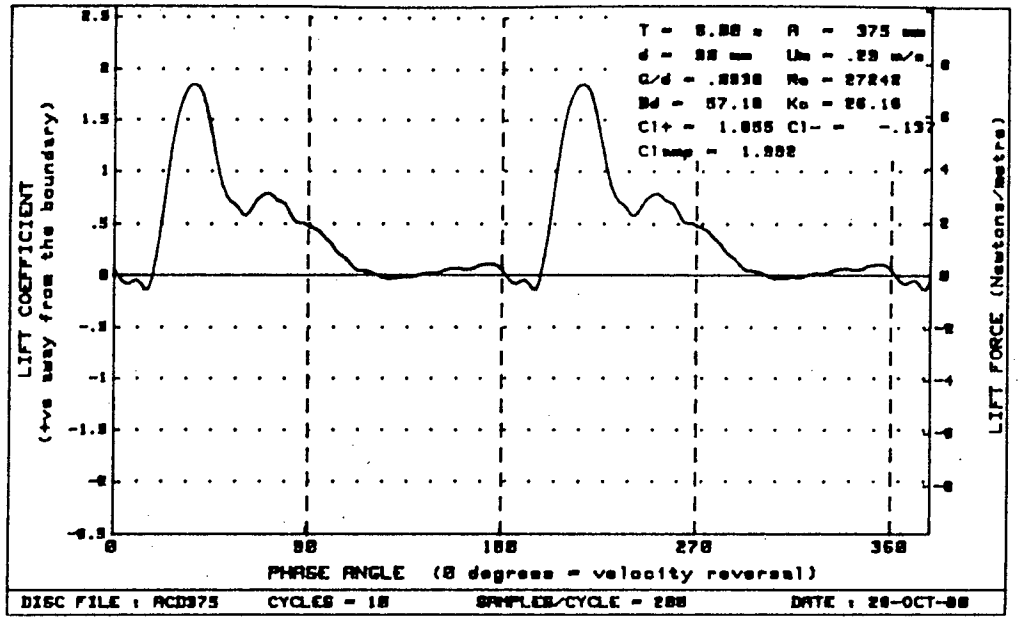

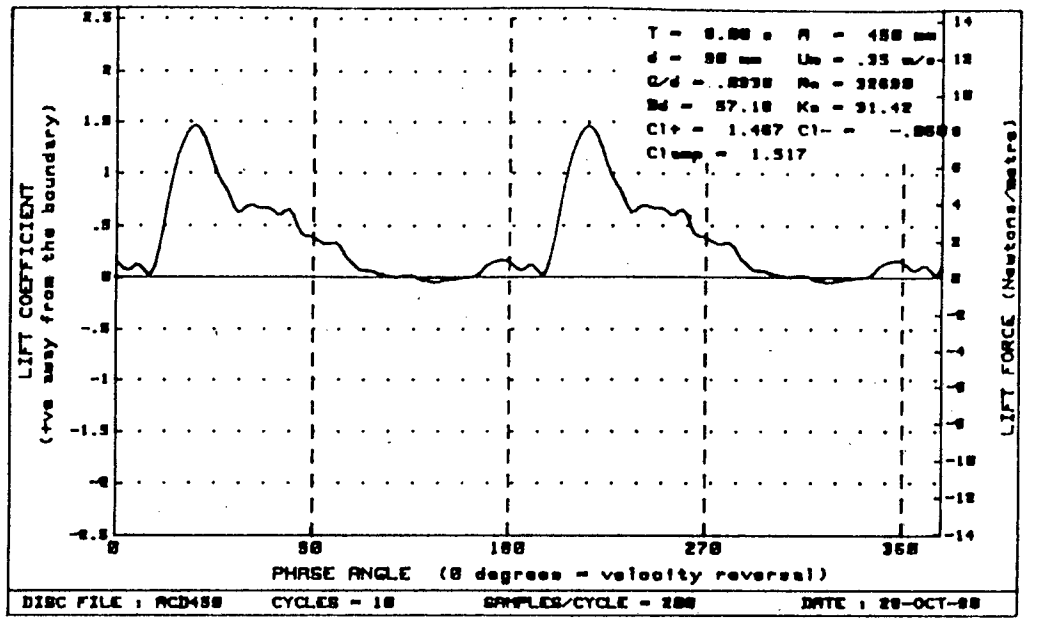

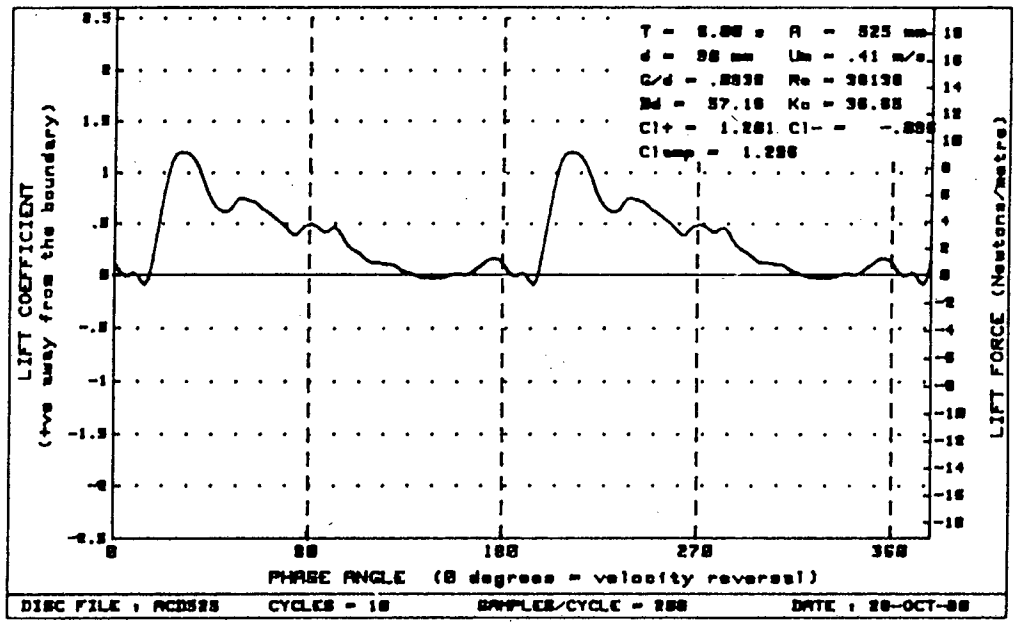

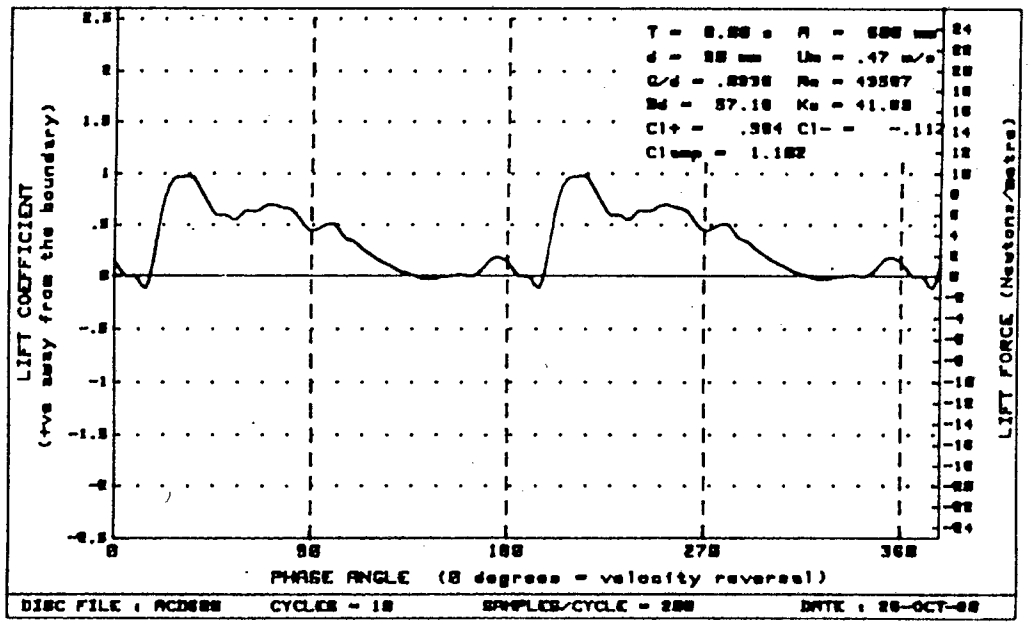

Figure G-38 : Plots of lift vs phase for diameter=90mm, Bd= 57.18 and G/d= .0938

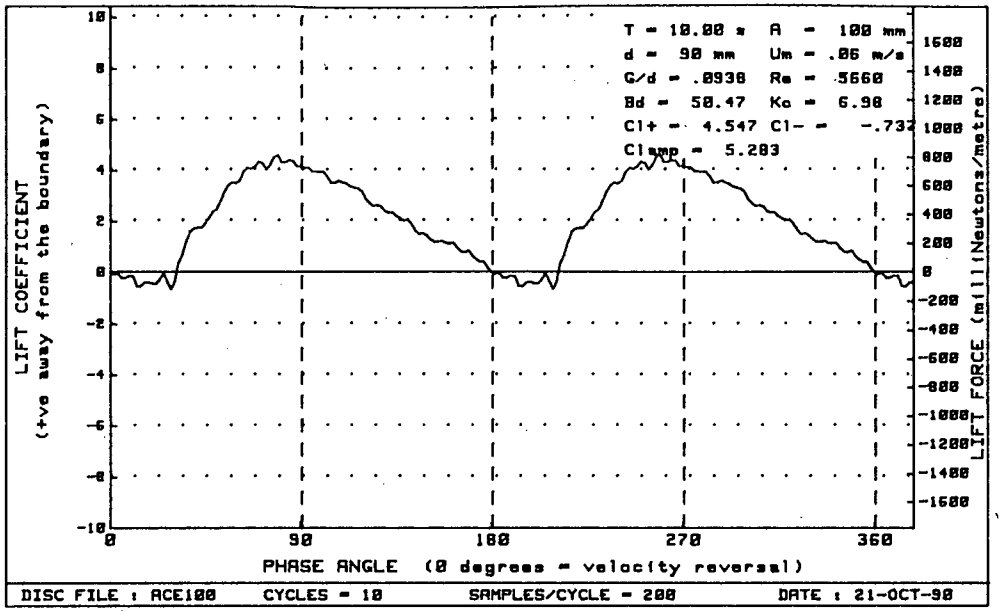

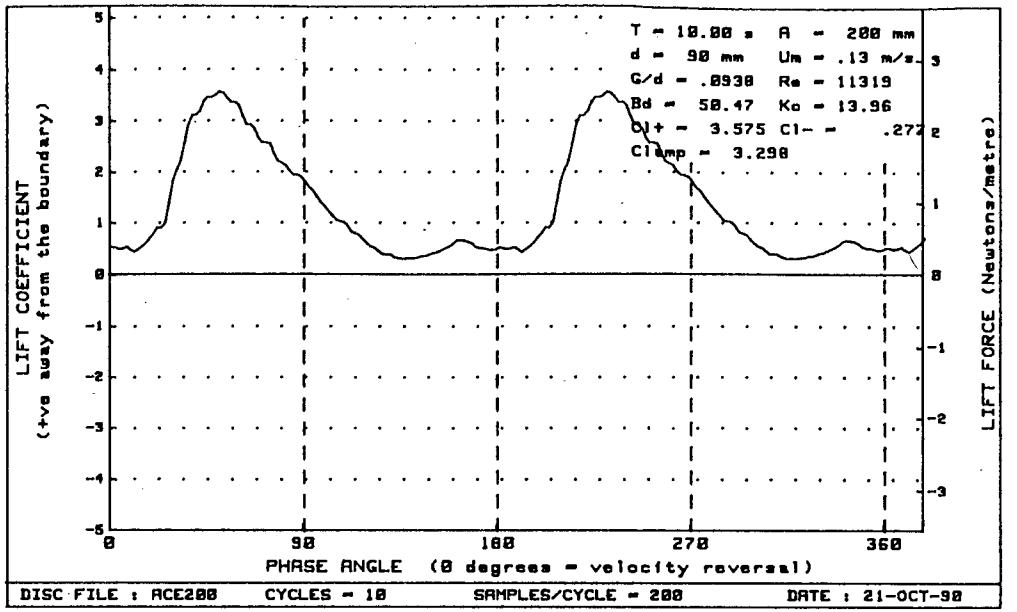

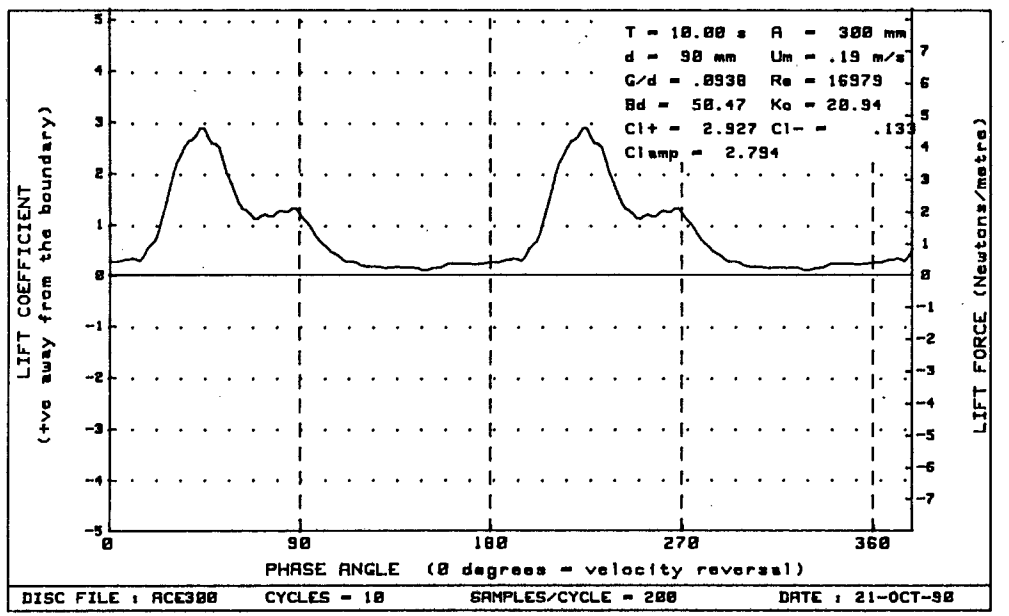

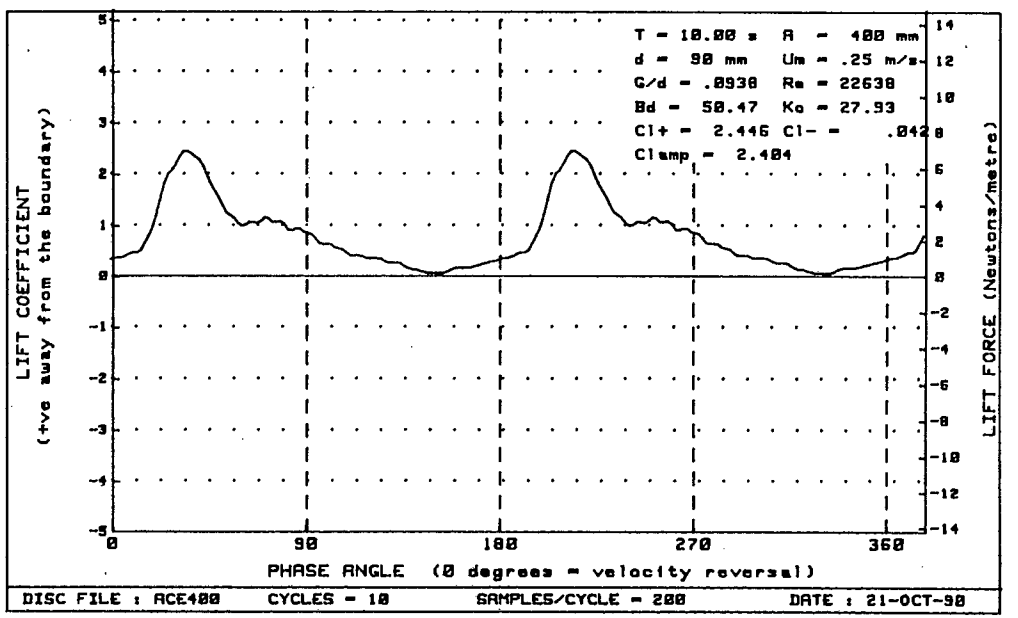

Figure G-39 : Plots of lift vs phase for diameter=90mm, Bd= 50.47 and G/d= .0938

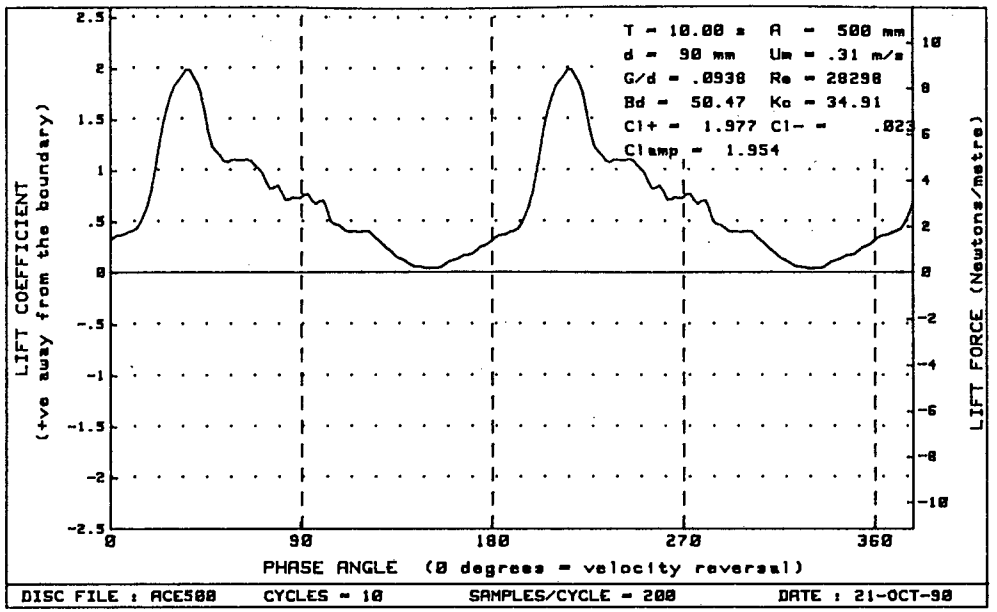

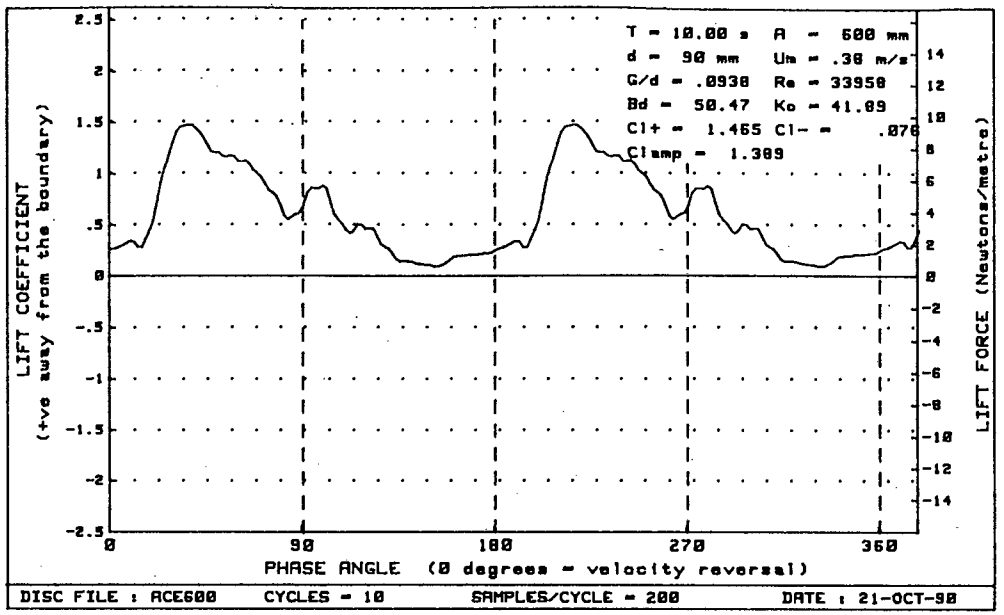

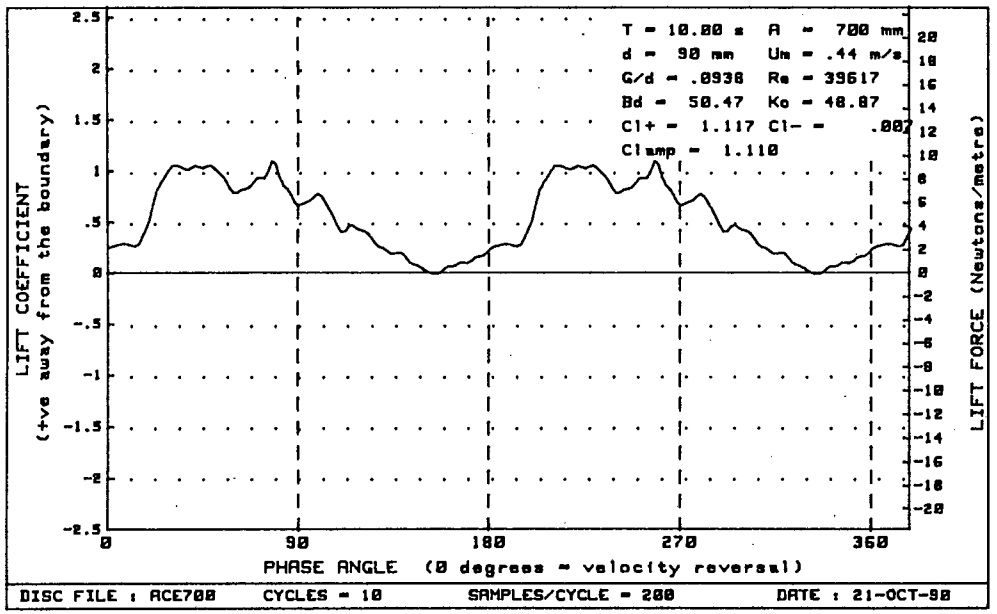

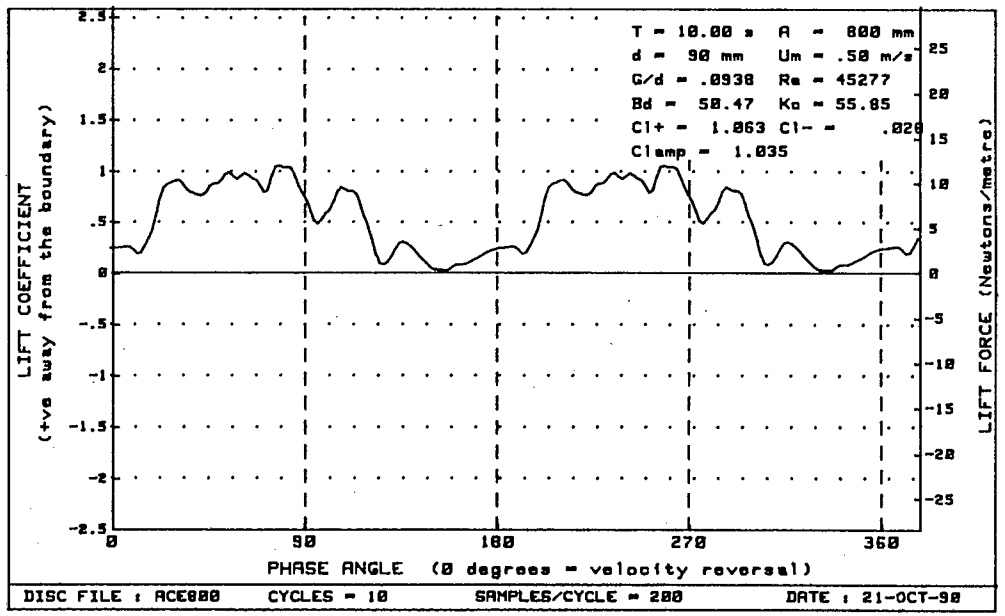

Figure G-40 : Plots of lift vs phase for diameter=90mm, Bd= 50.47 and G/d= .0938

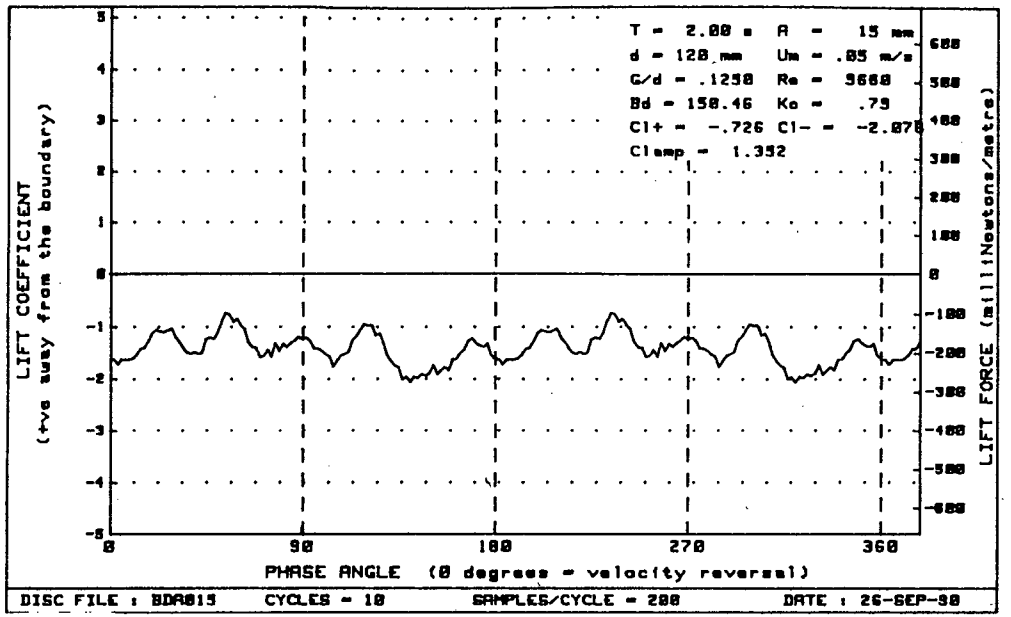

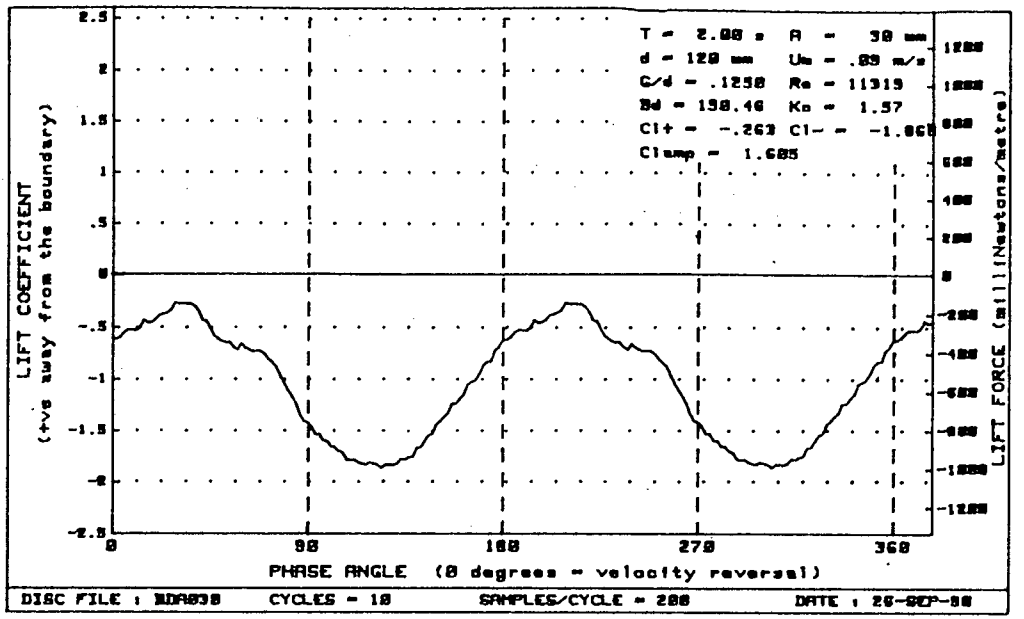

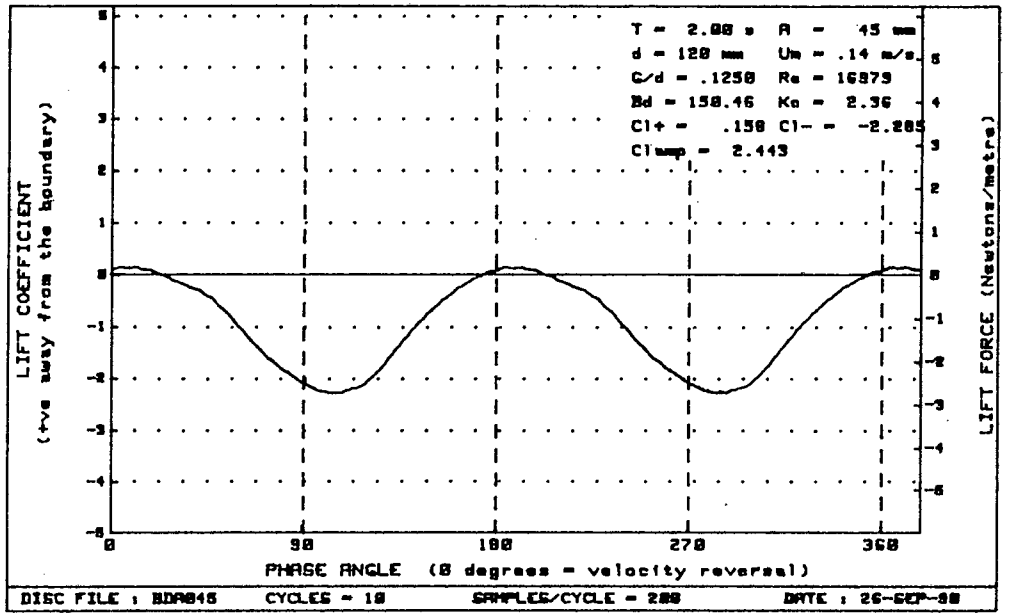

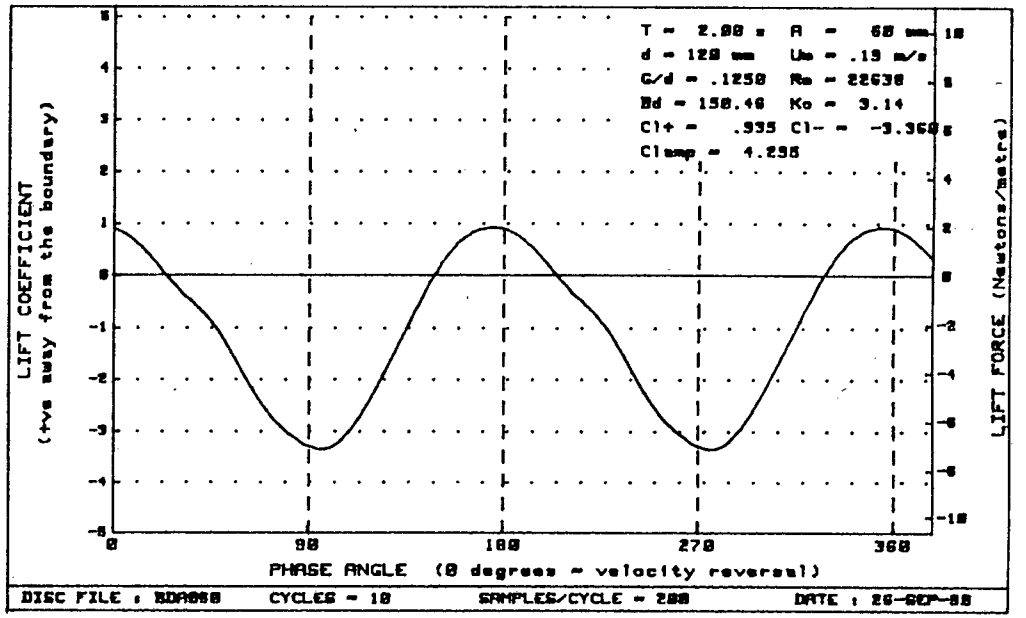

Figure G-41 : Plots of lift vs phase for diameter=120mm, Bd=150.46 and G/d= .1250

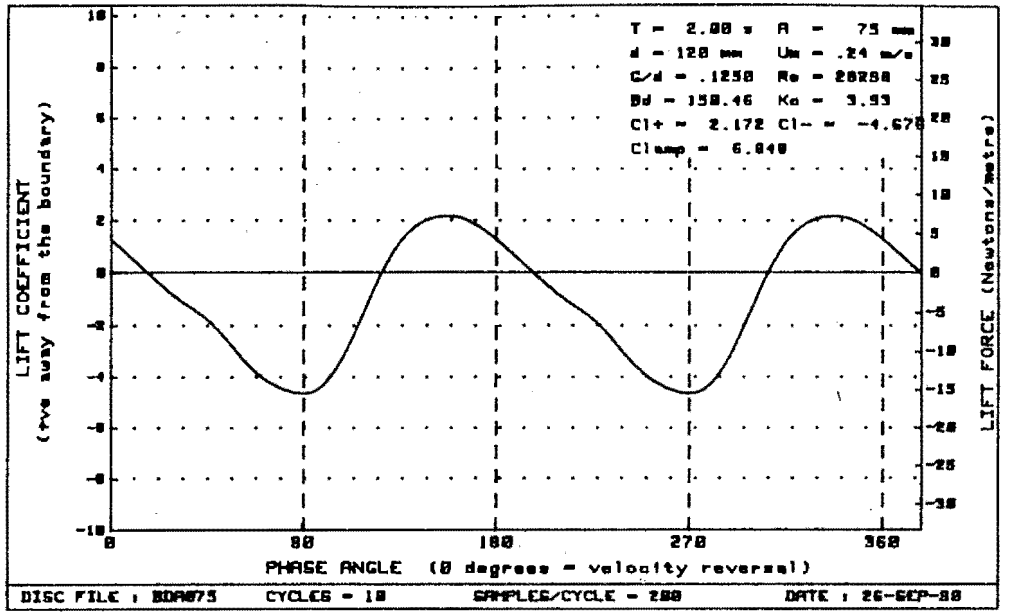

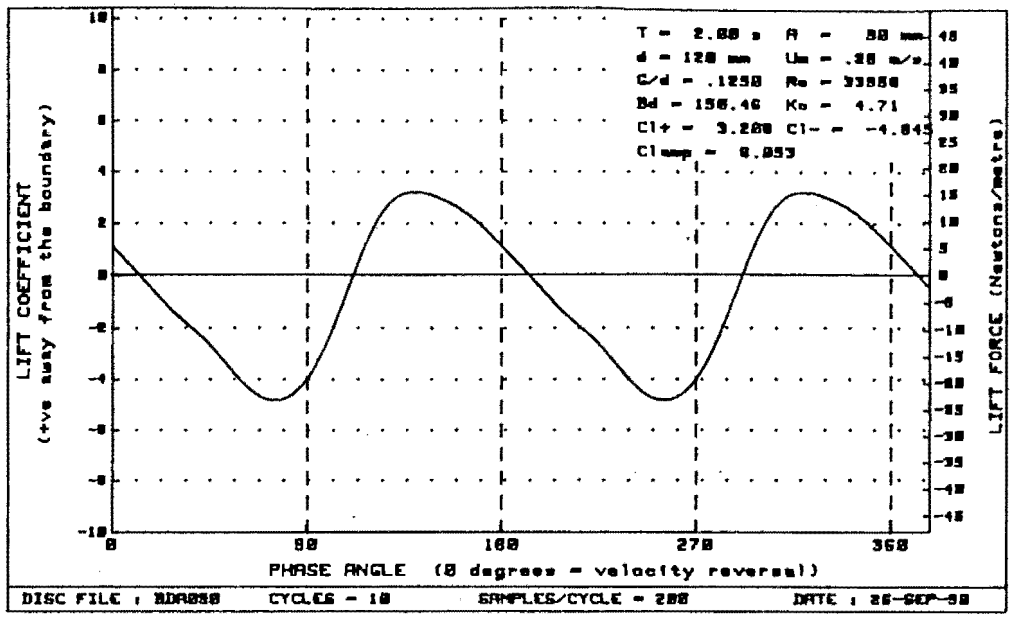

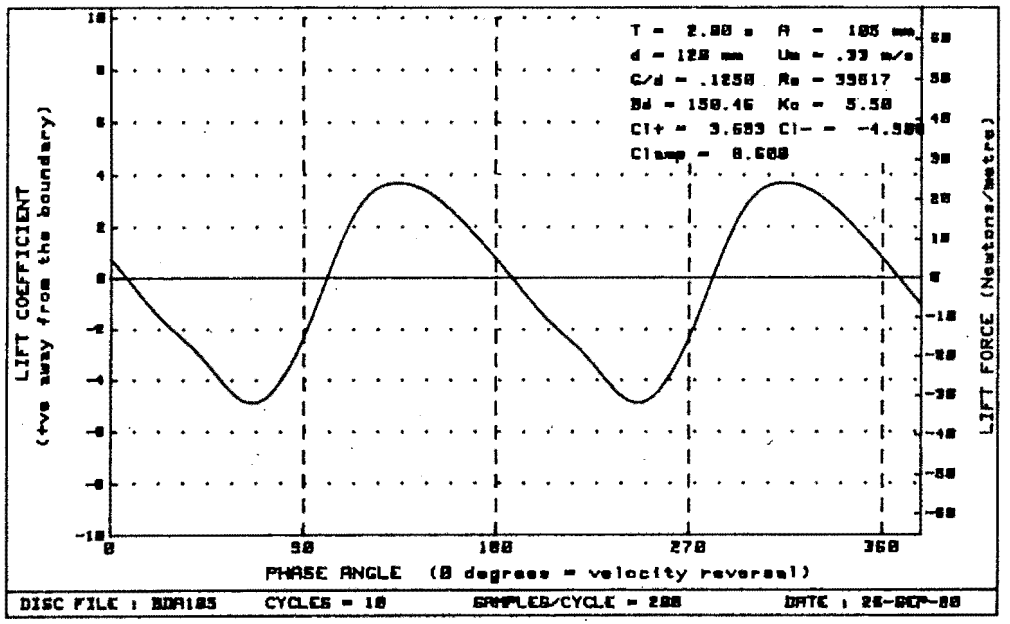

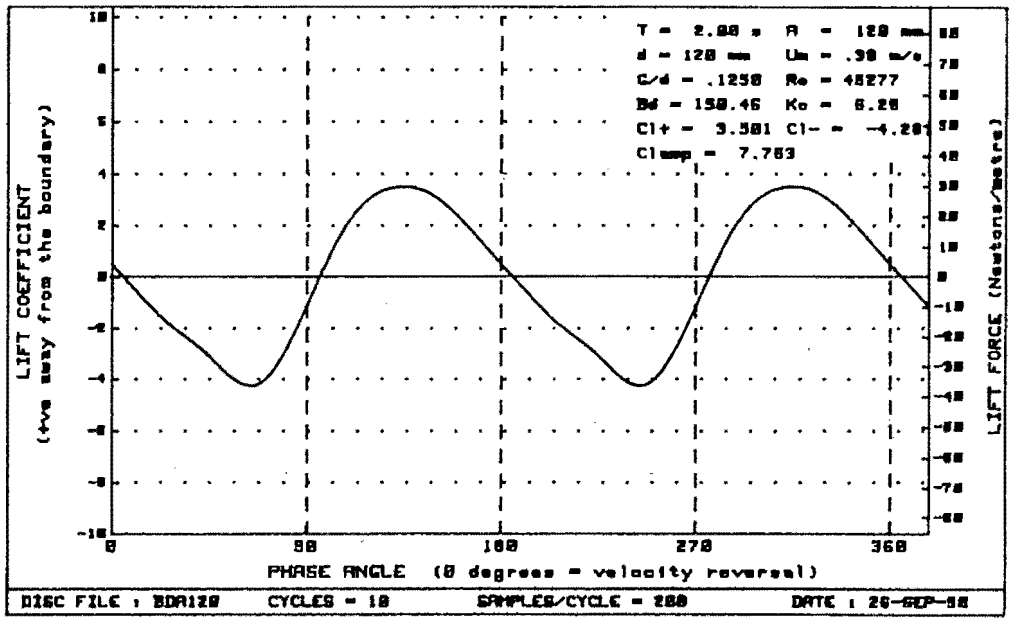

Figure G-42 : Plots of lift vs phase for diameter=120mm, Bd=150.46 and G/d= .1250

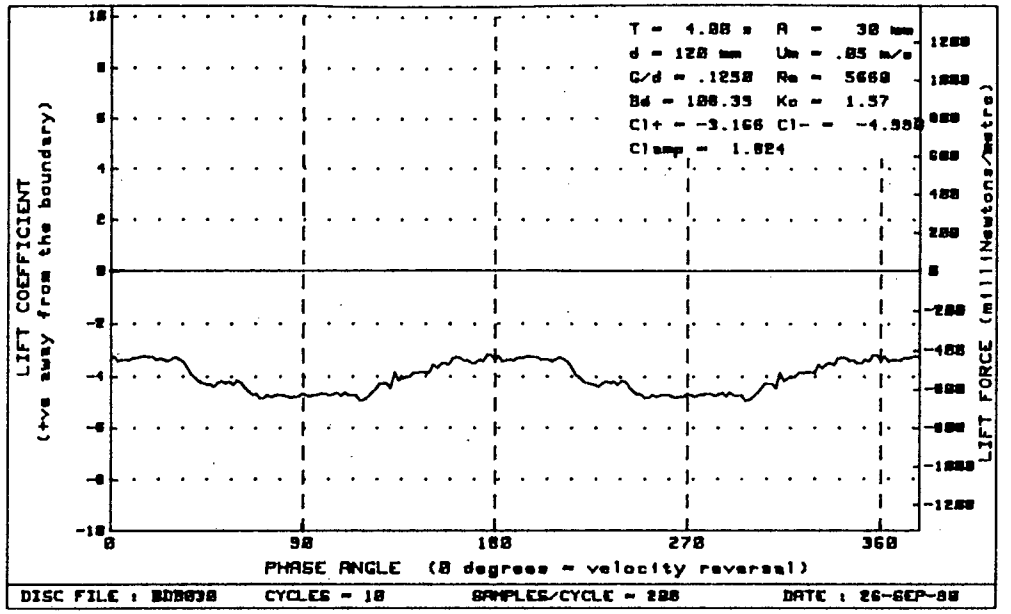

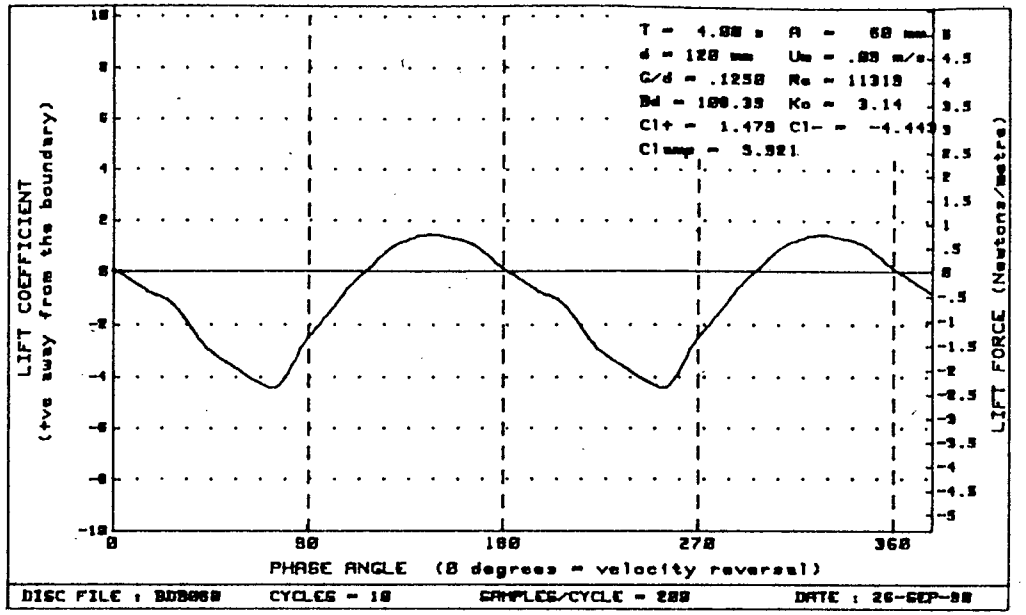

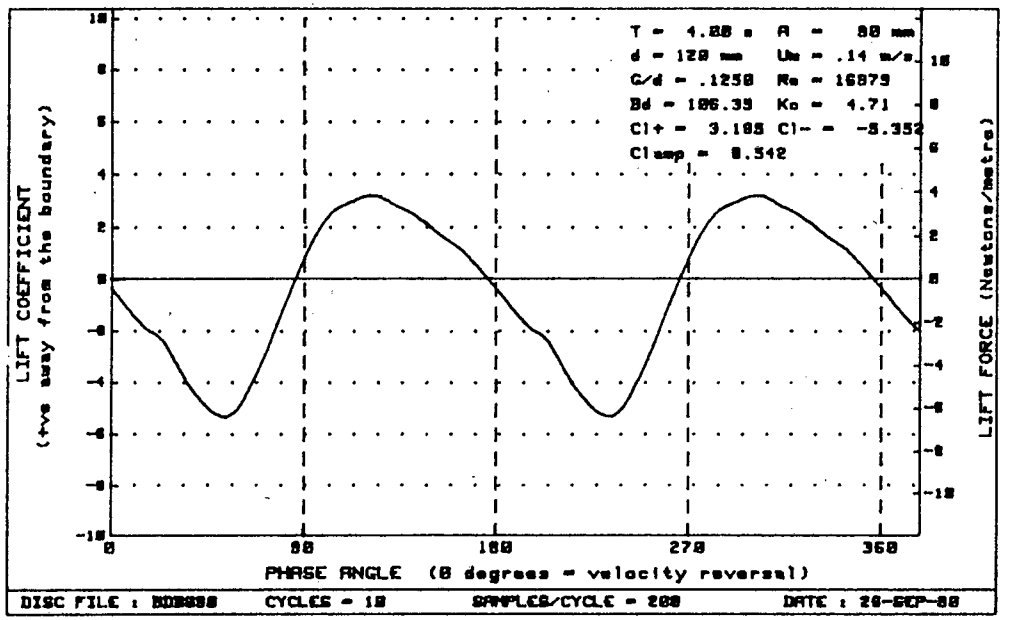

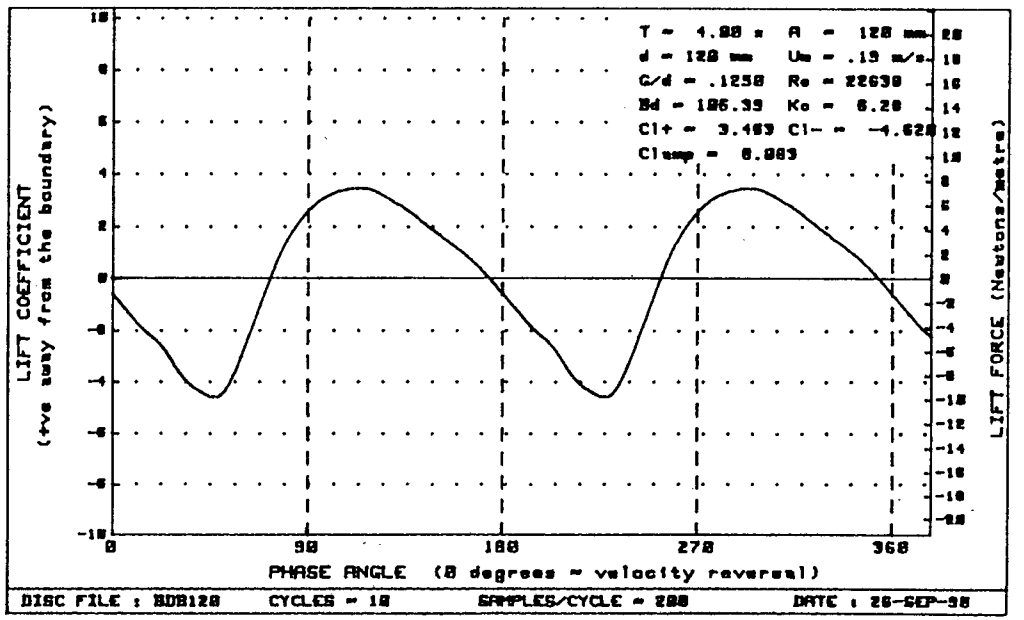

Figure G-43 : Plots of lift vs phase for diameter=120mm, Bd=106.39 and G/d= .1250

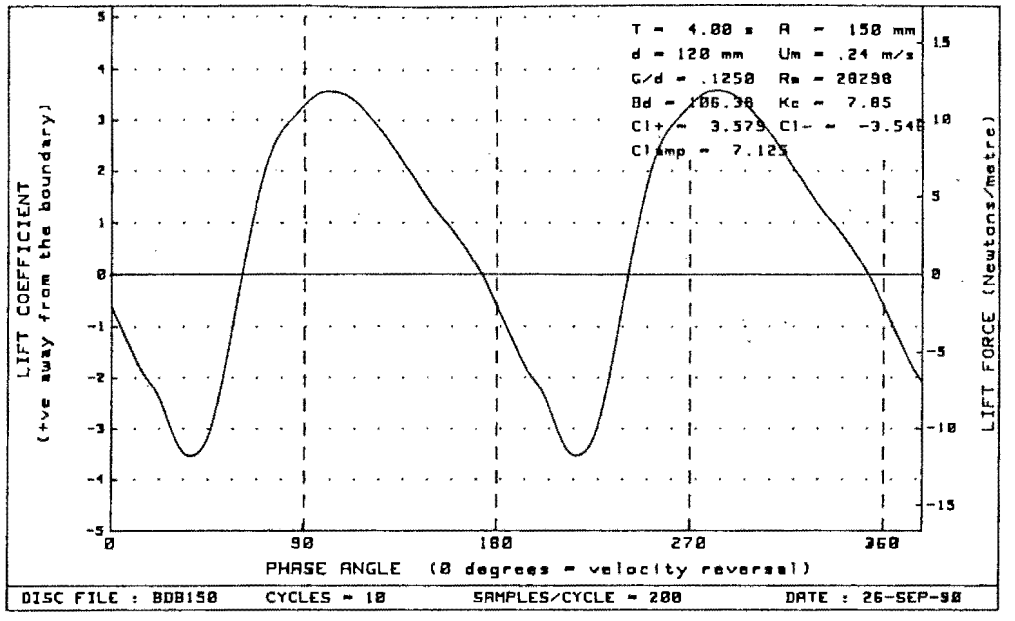

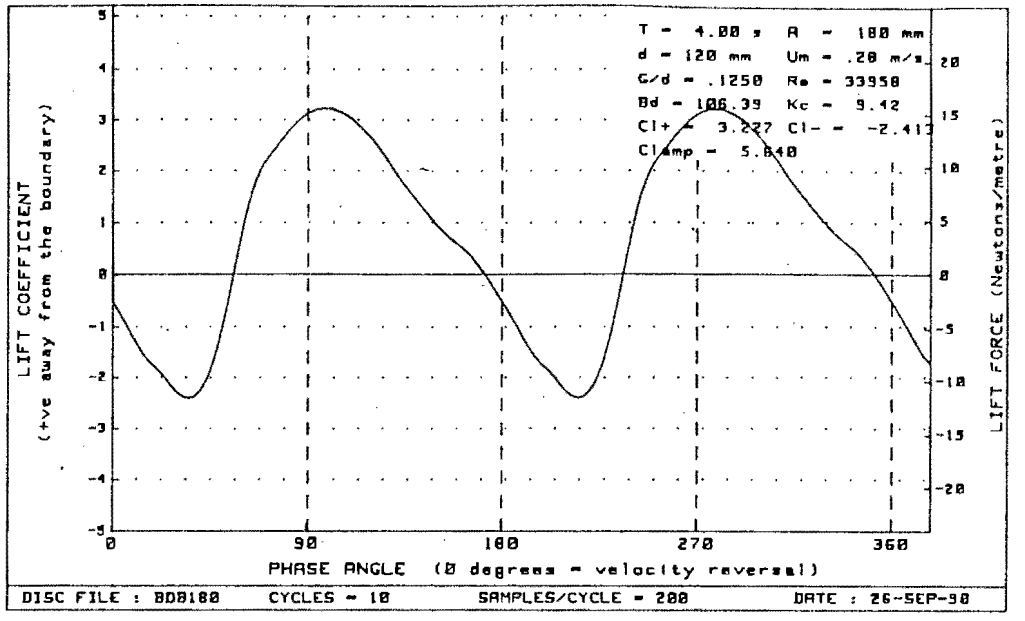

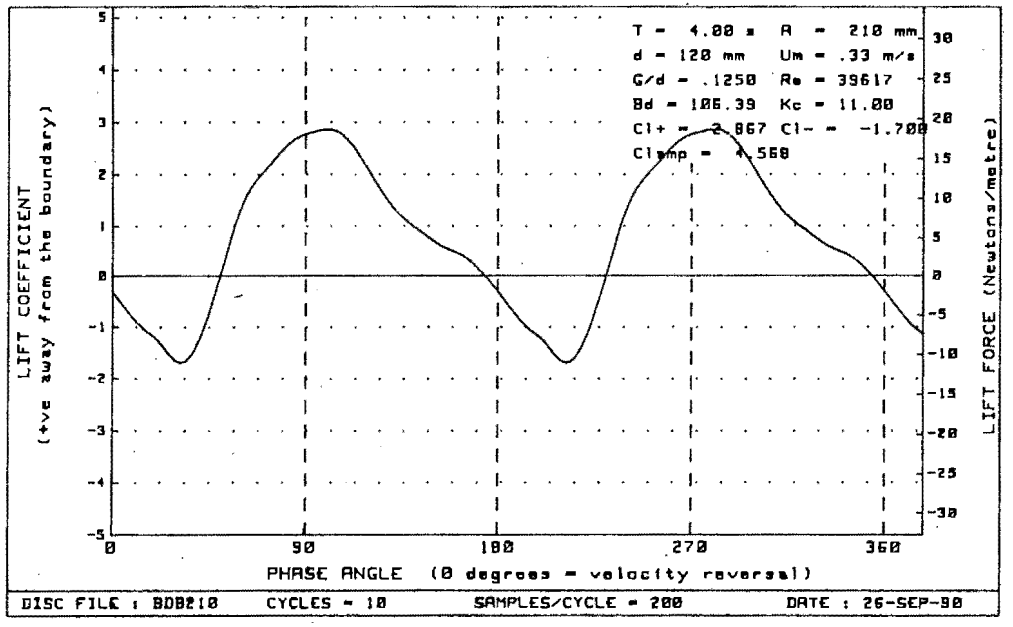

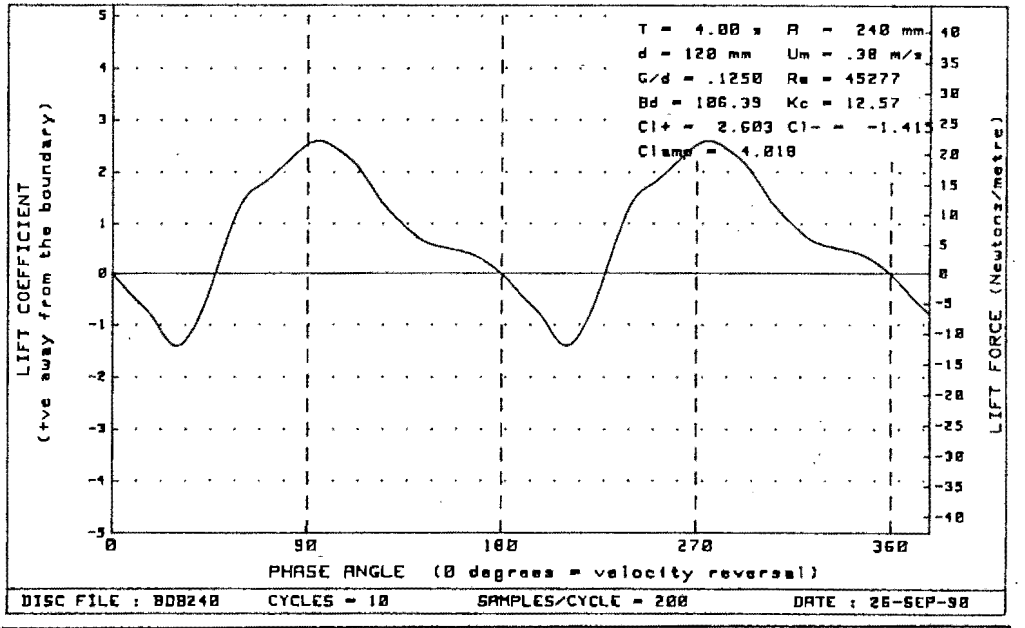

Figure G-44 : Plots of lift vs phase for diameter=120mm, Bd=106.39 and G/d= .1250

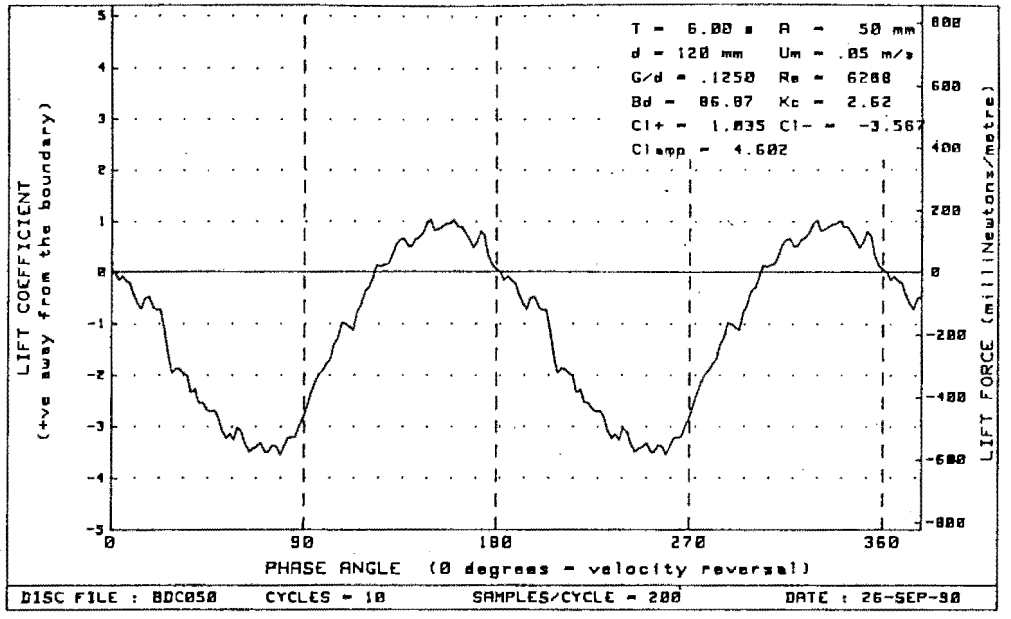

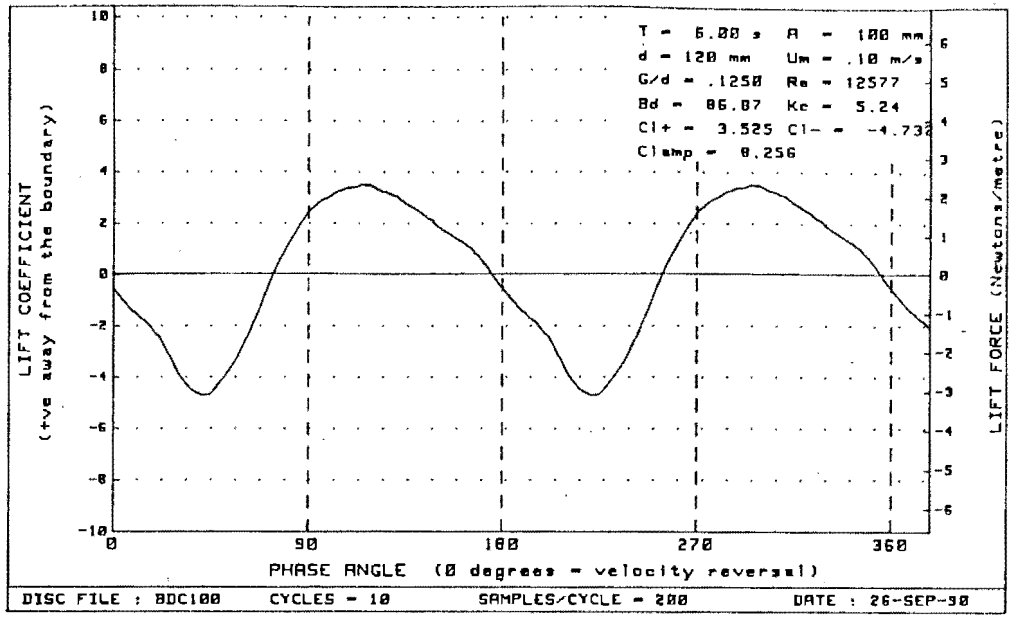

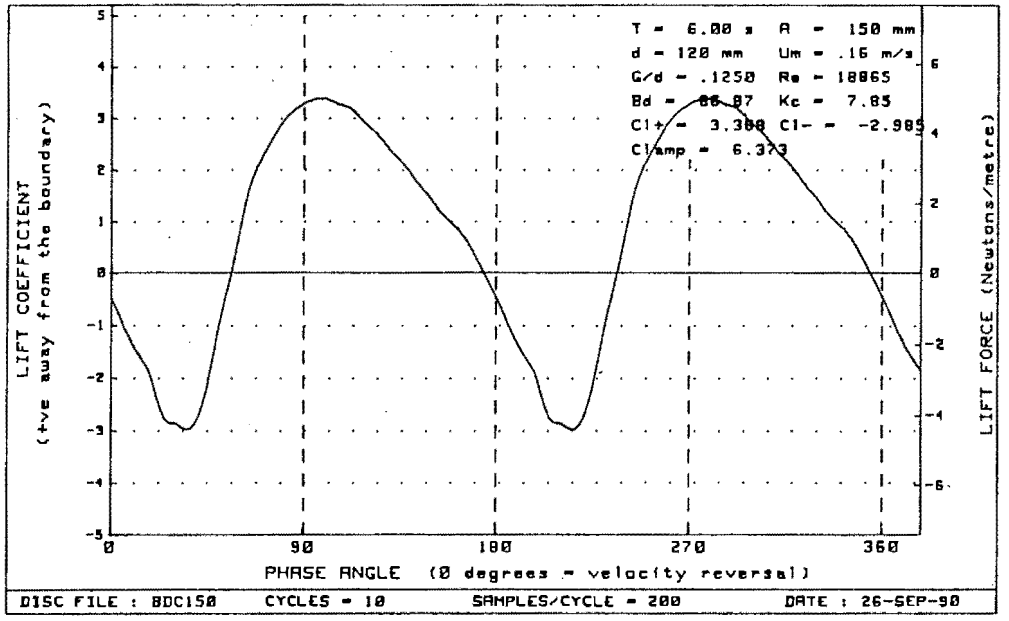

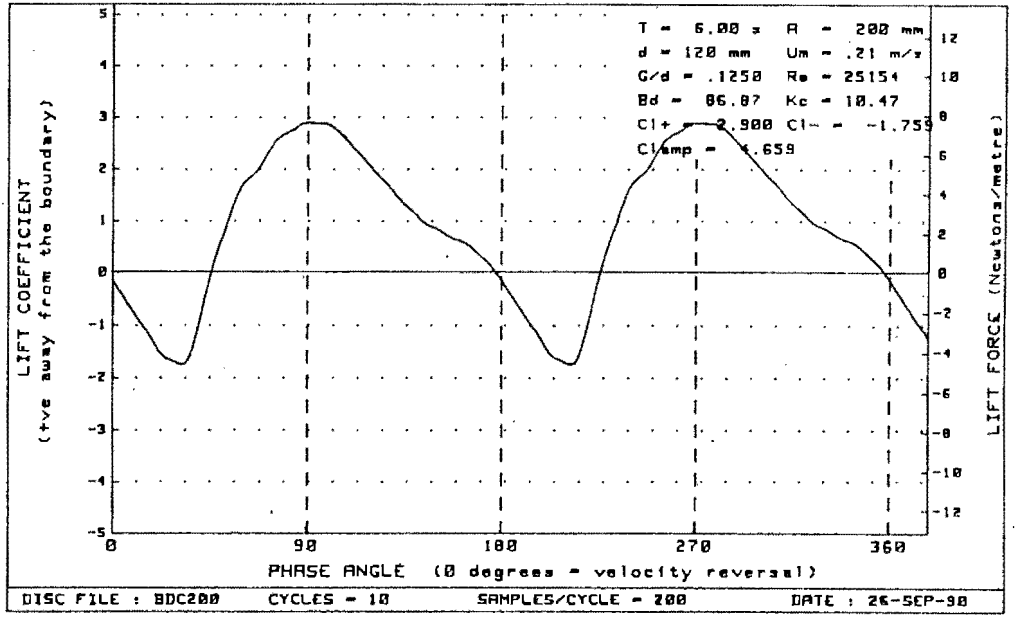

Figure G-45 : Plots of lift vs phase for diameter=120mm, Bd= 86.87 and G/d= .1250

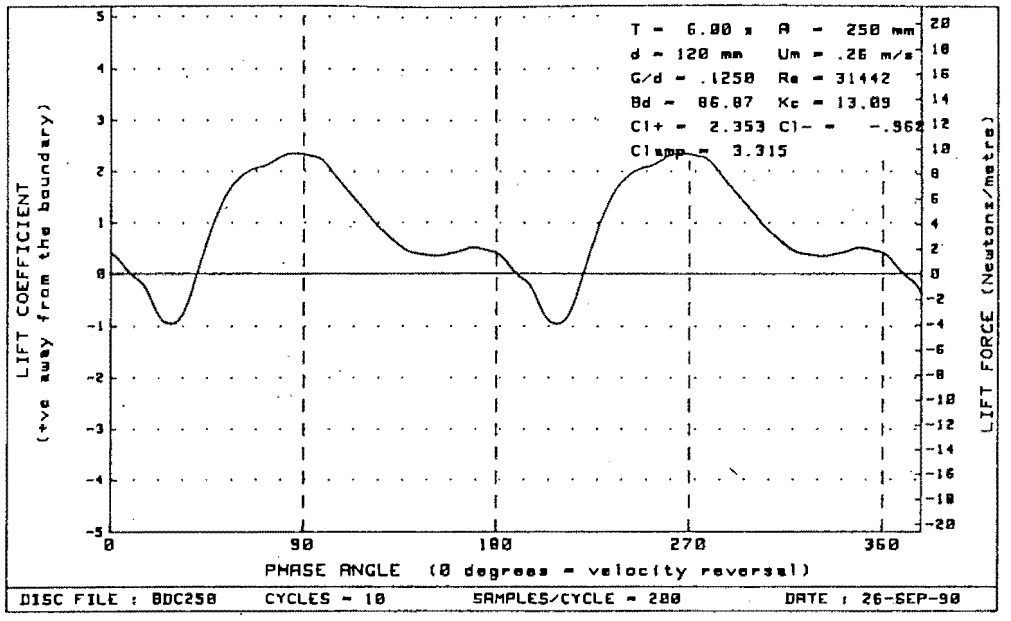

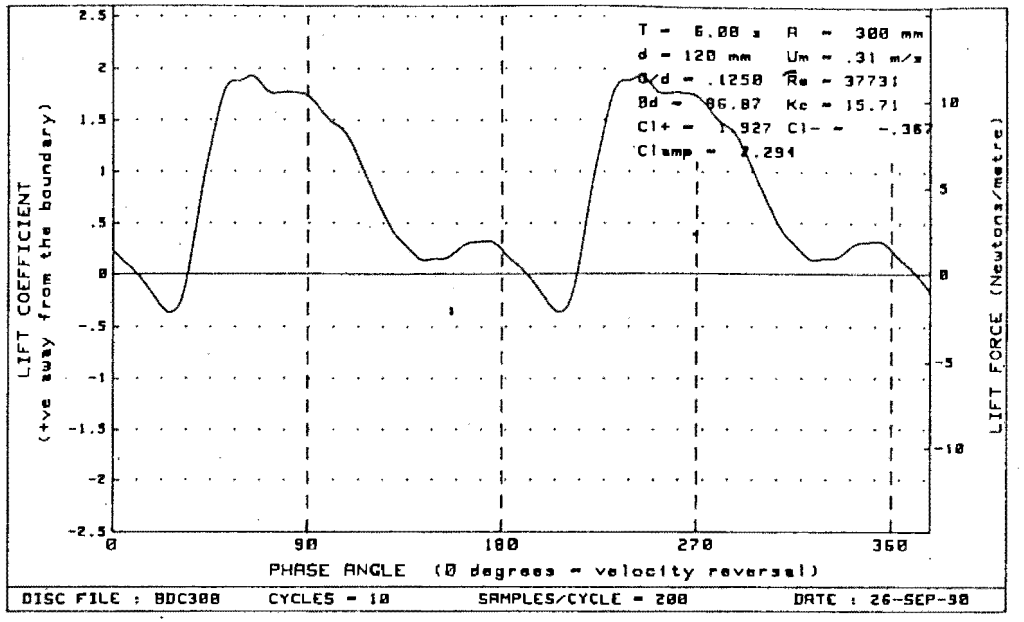

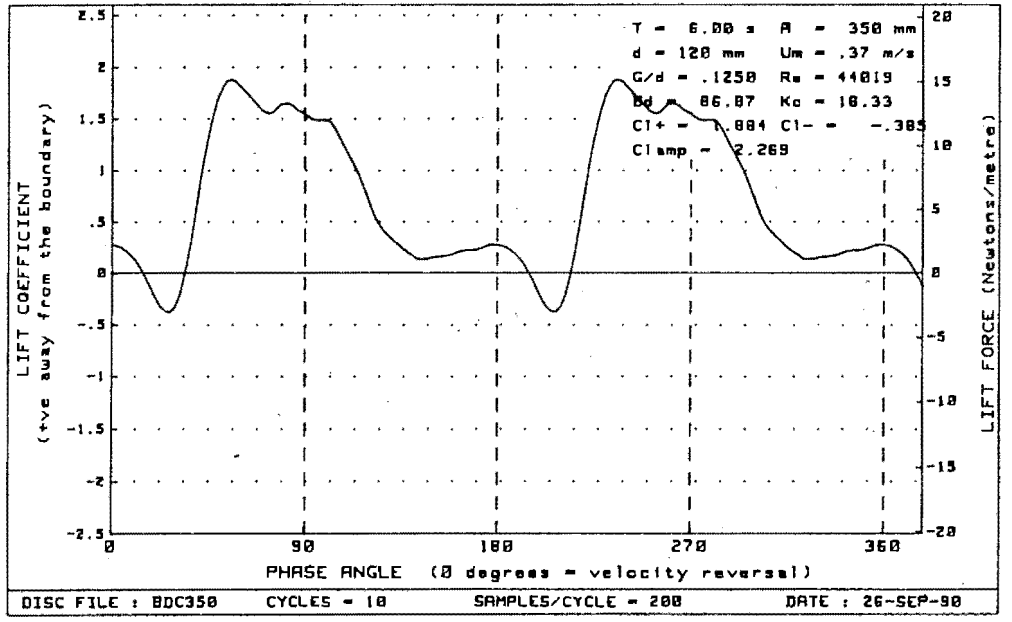

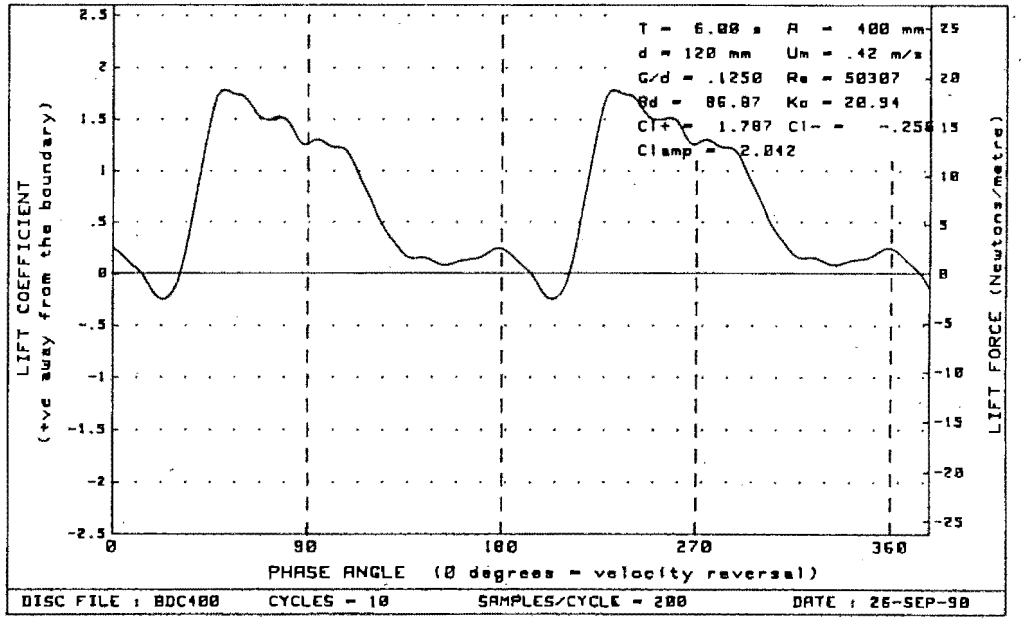

Figure G-46 : Plots of lift vs phase for diameter=120mm, Bd= 86.87 and G/d= .1250

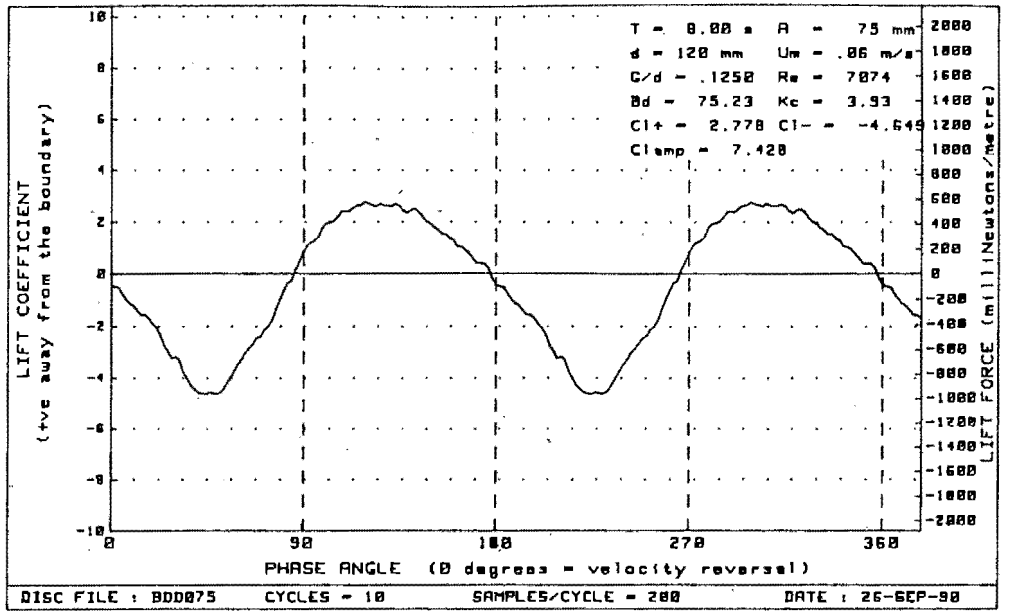

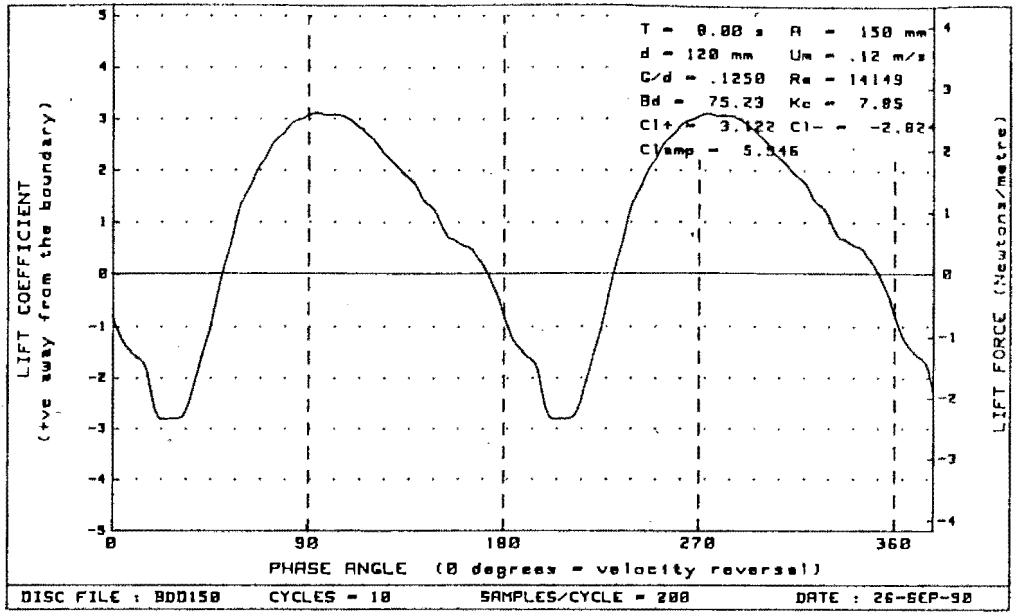

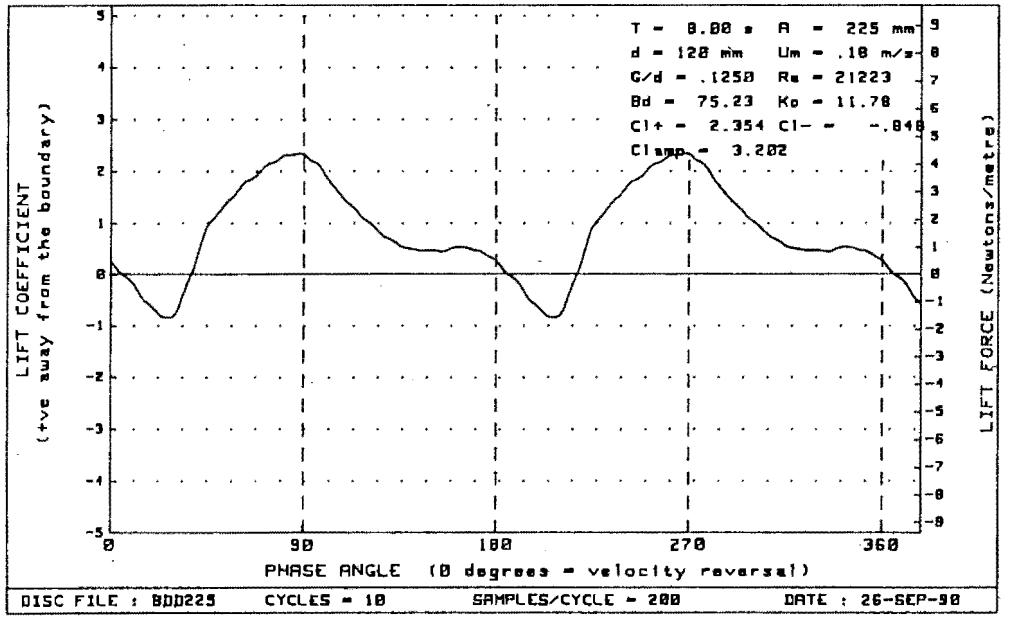

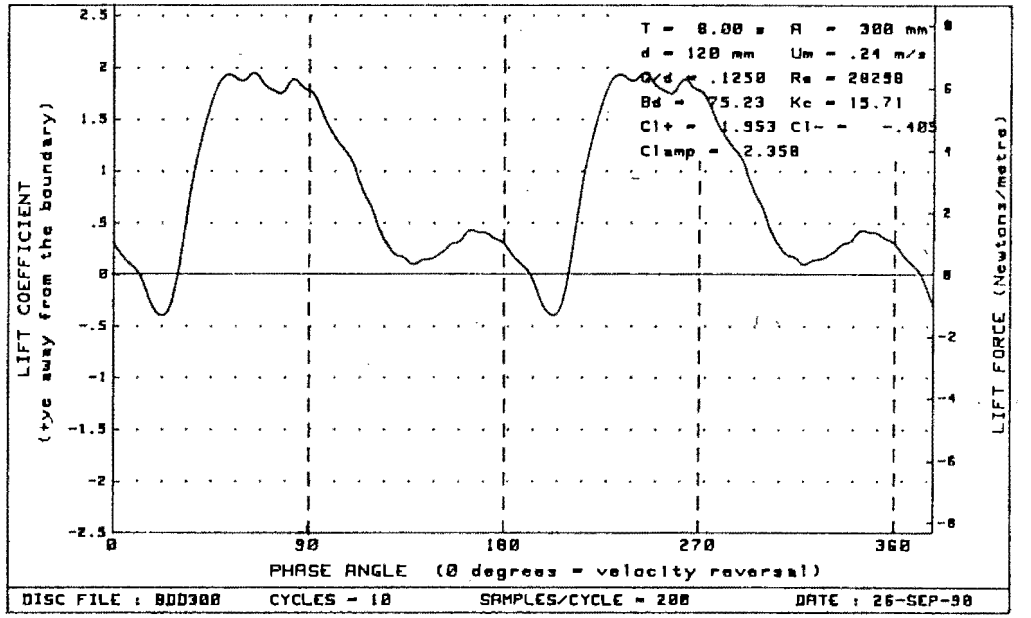

Figure G-47 : Plots of lift vs phase for diameter=120mm, Bd= 75.23 and G/d= .1250

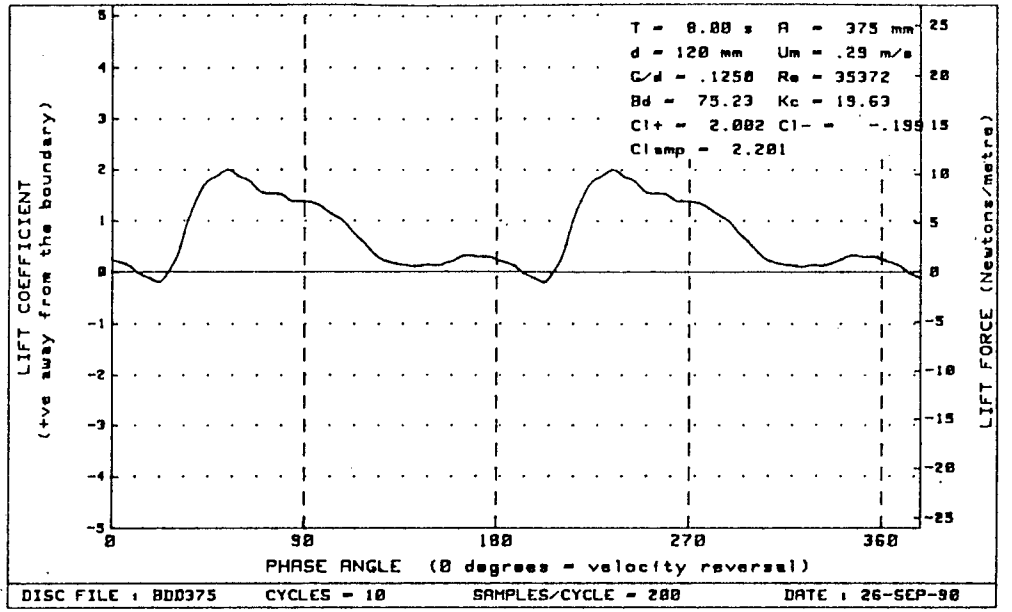

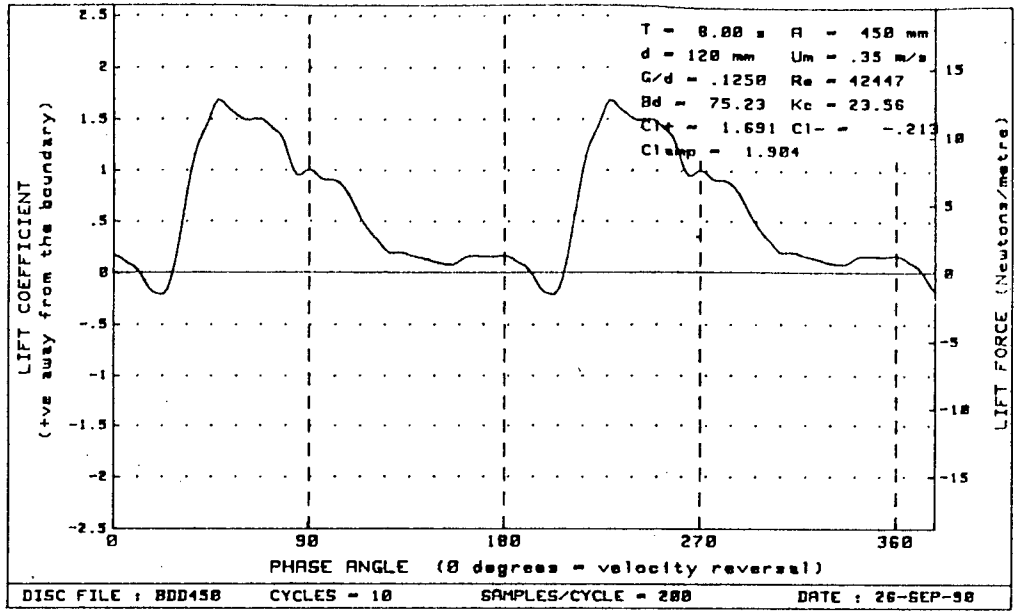

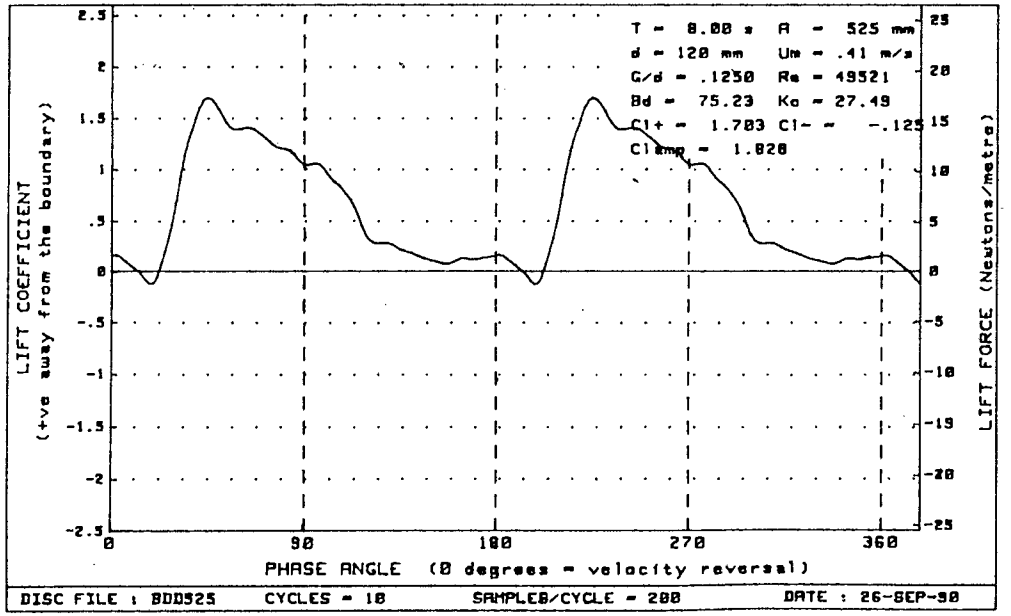

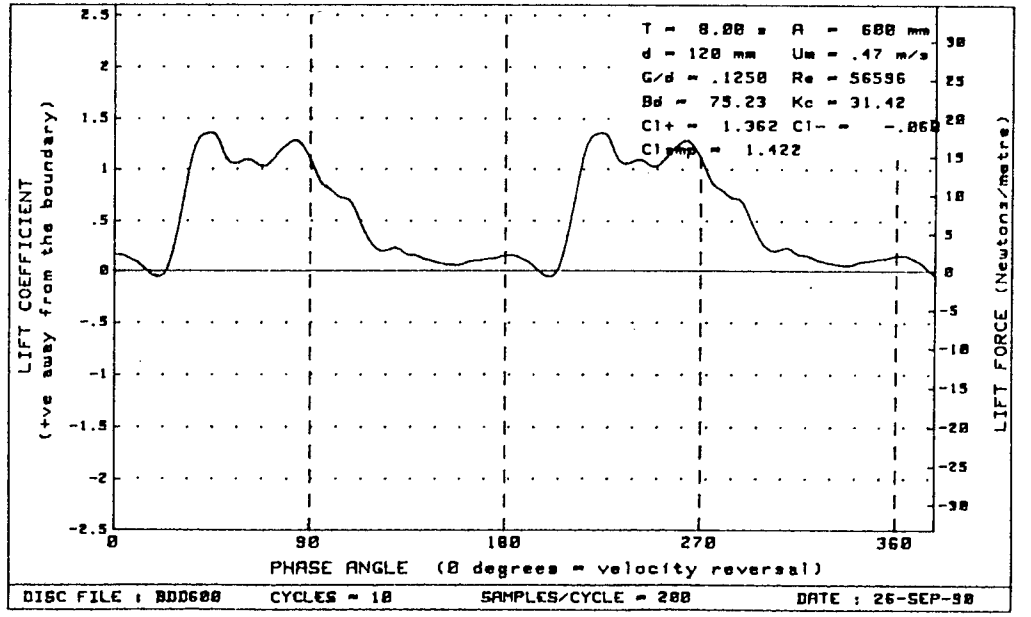

Figure G-48 : Plots of lift vs phase for diameter=120mm, Bd= 75.23 and G/d= .1250

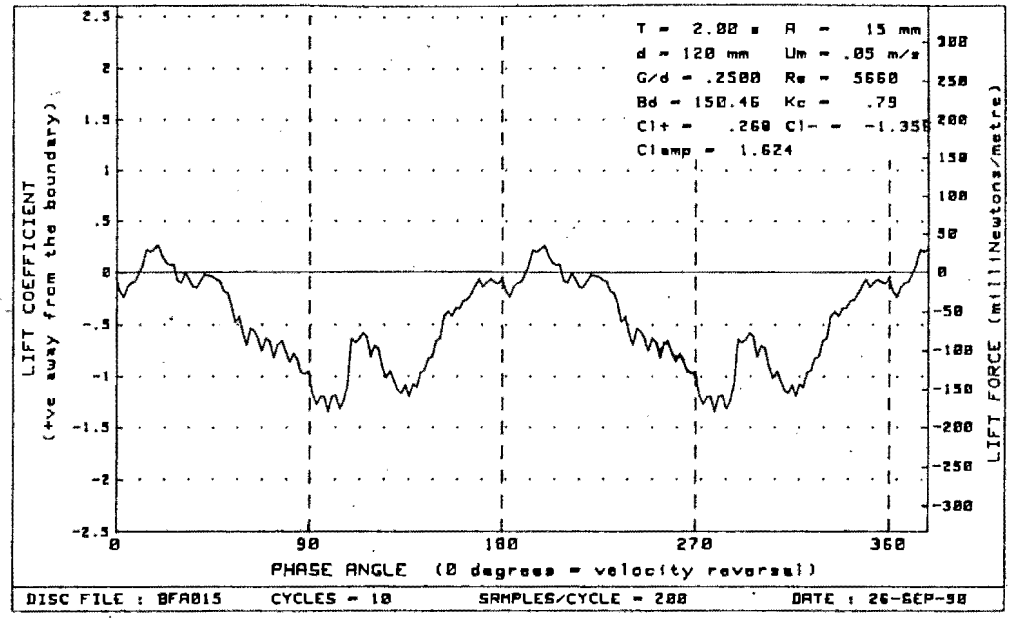

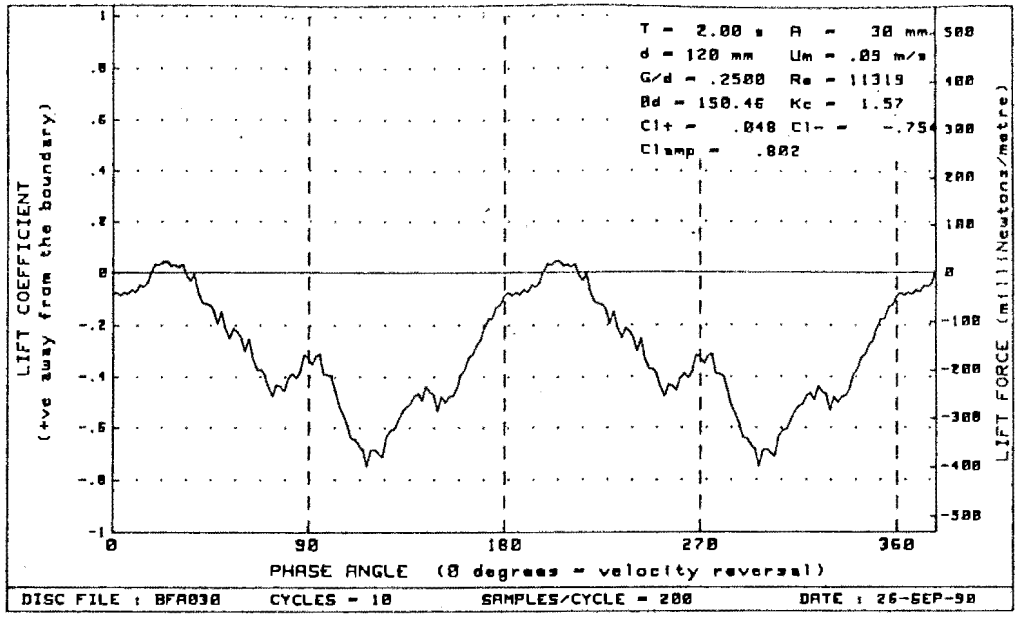

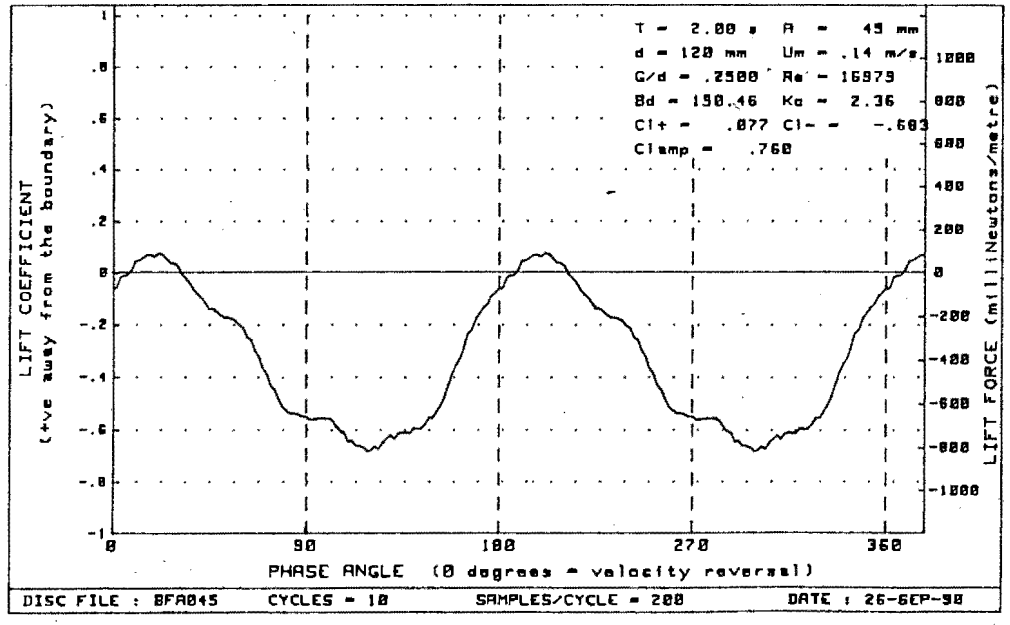

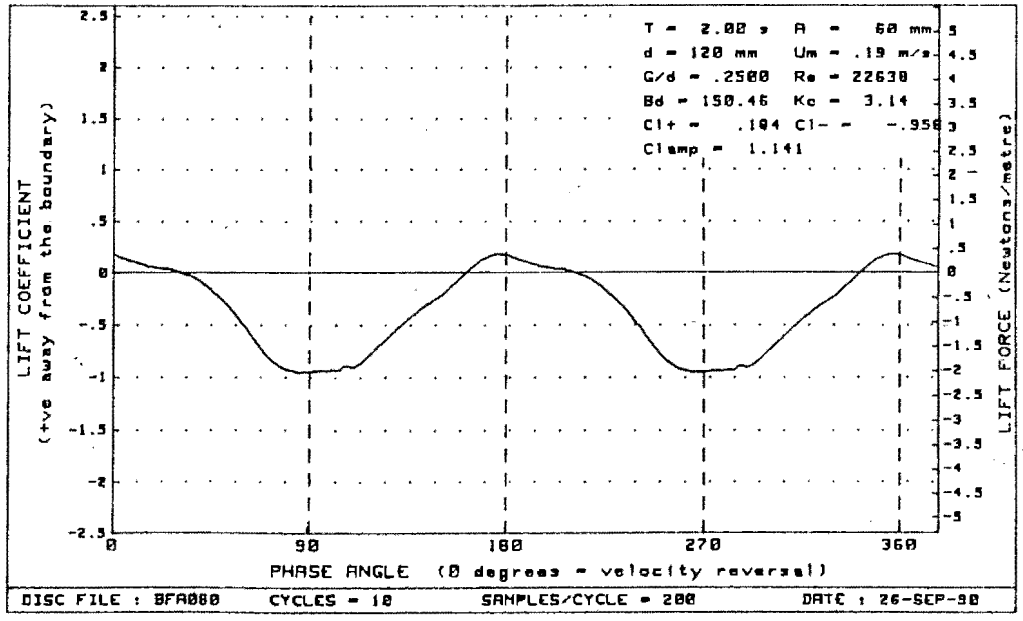

Figure G-49 : Plots of lift vs phase for diameter=120mm, Bd=150.46 and G/d= .2500

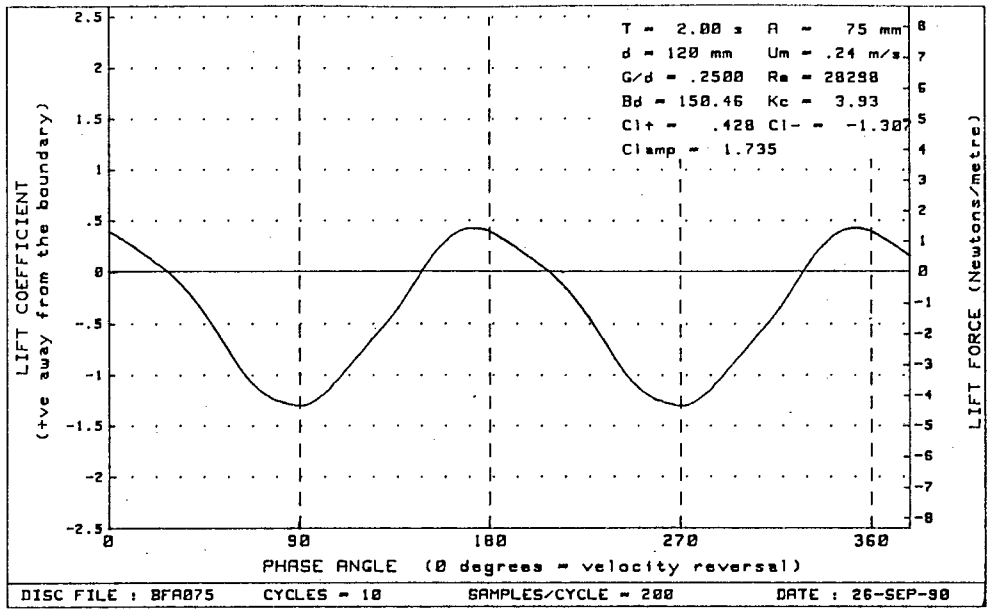

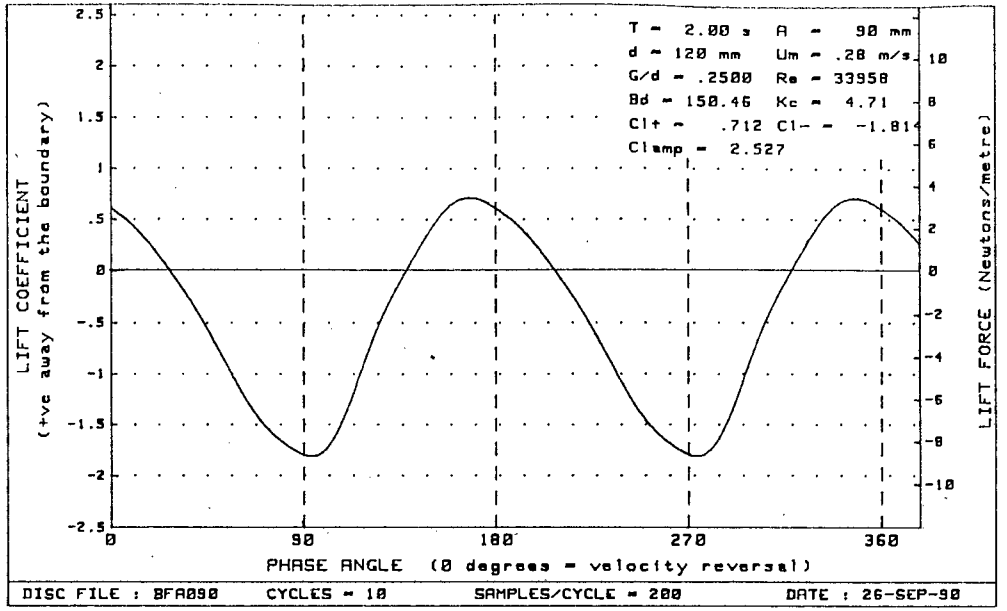

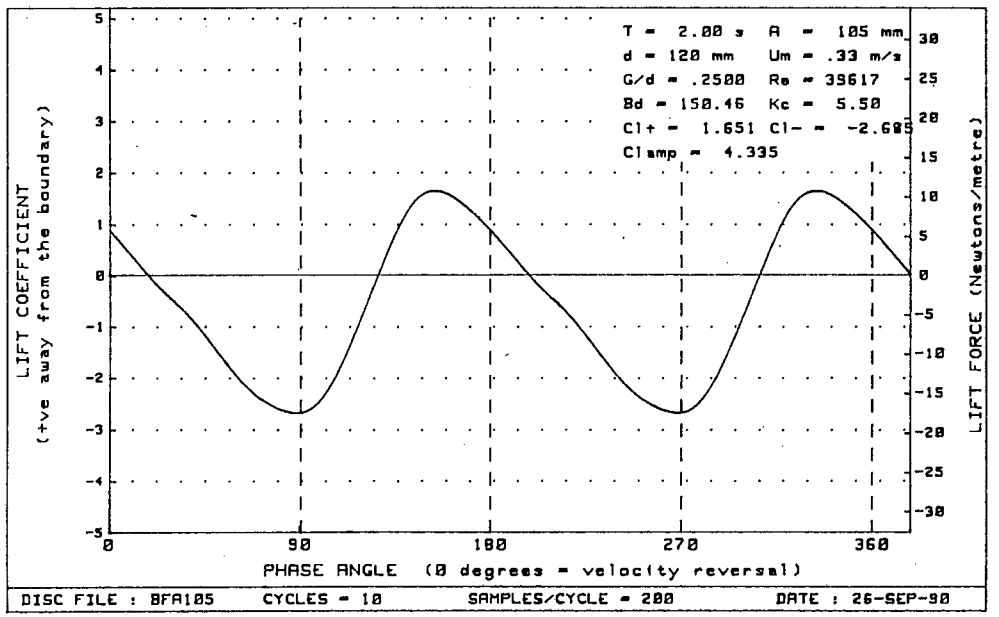

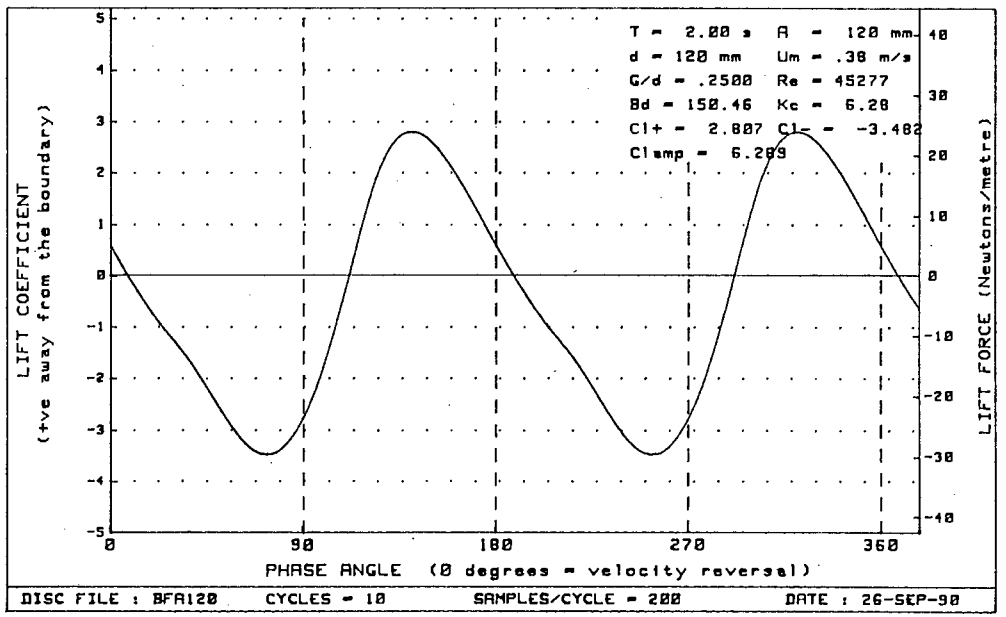

Figure G – 50 : Plots of lift vs phase for diameter=120mm, Bd=150.46 and G/d= .2500

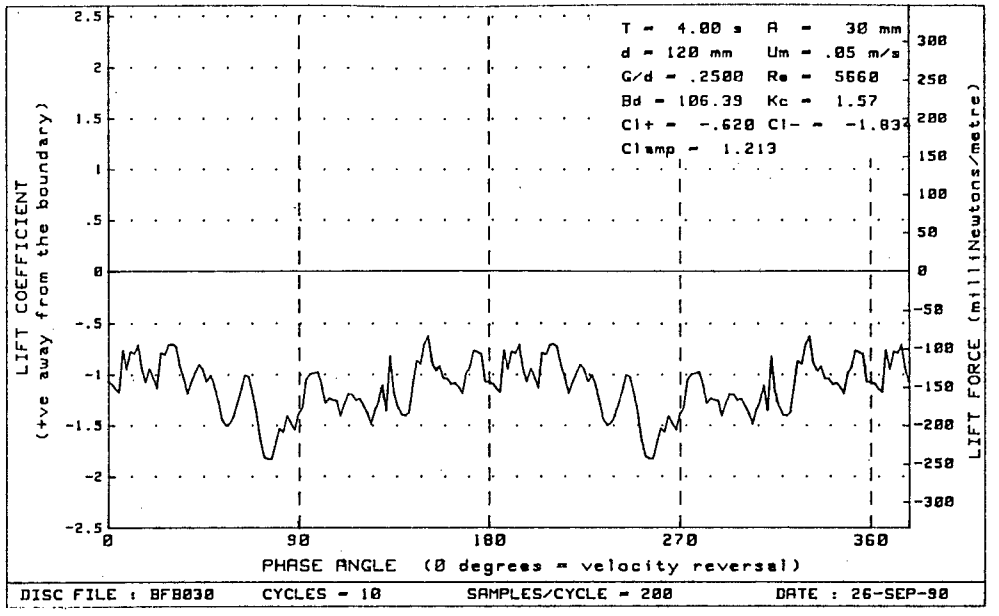

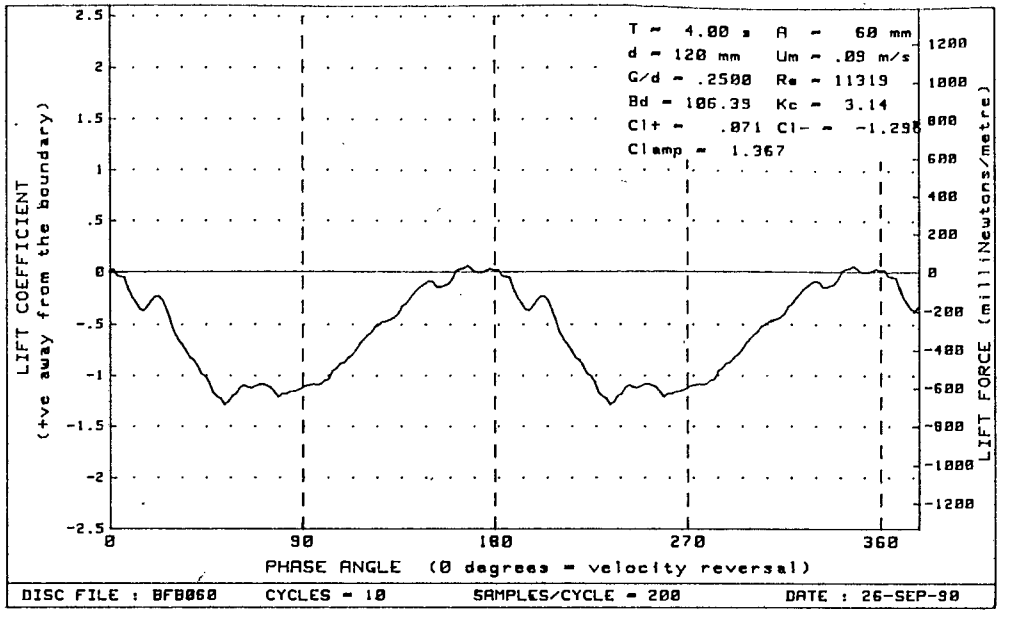

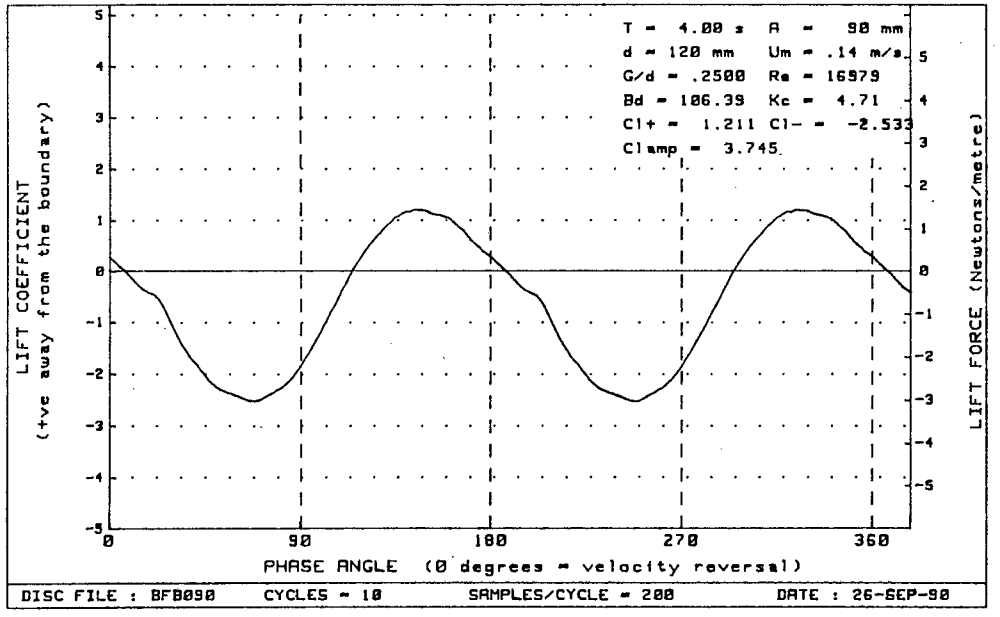

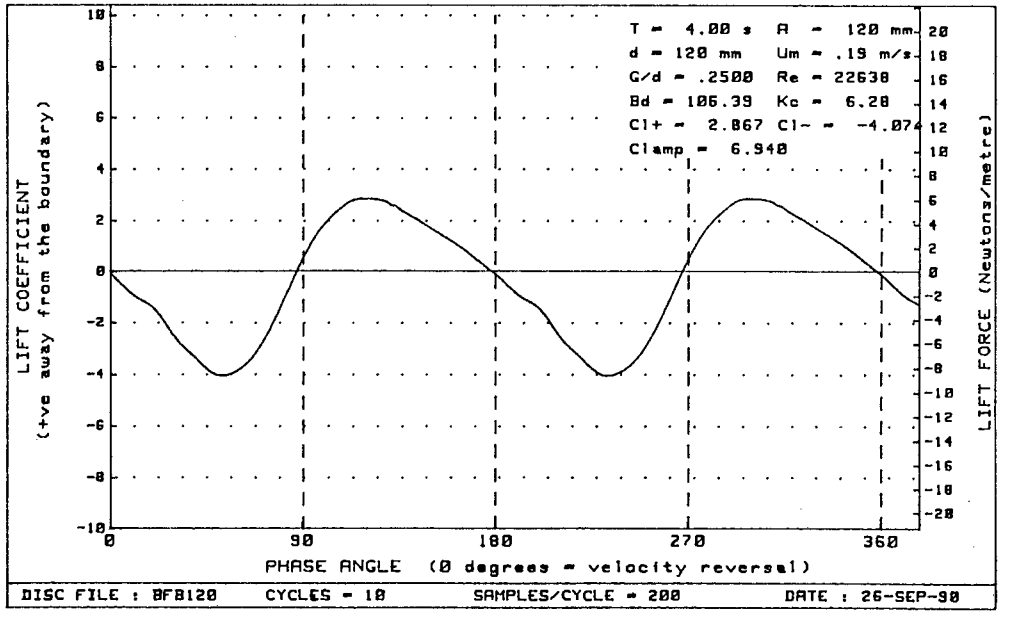

Figure G – 51 : Plots of lift vs phase for diameter=120mm, Bd=106.39 and G/d= .2500

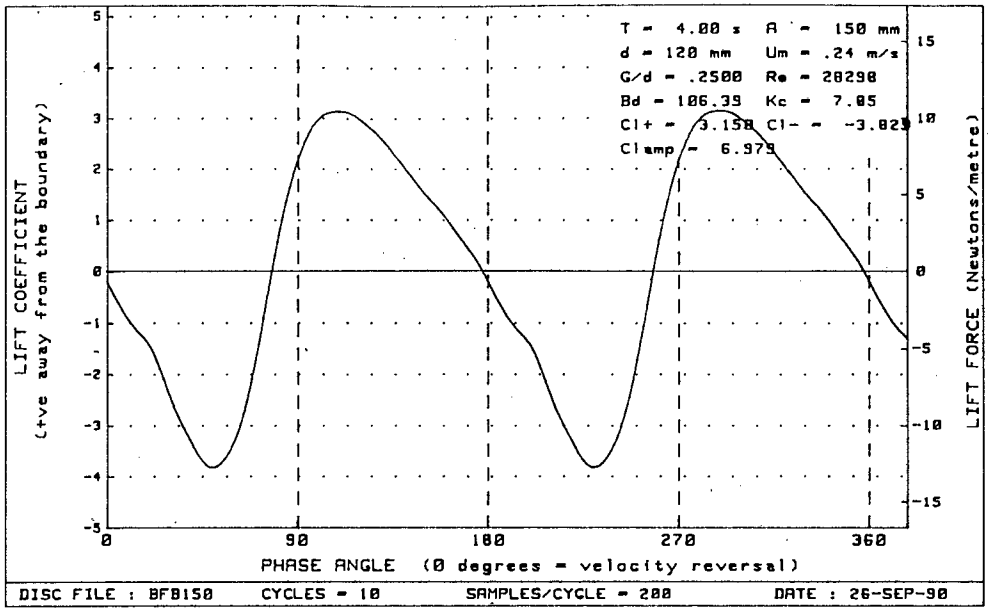

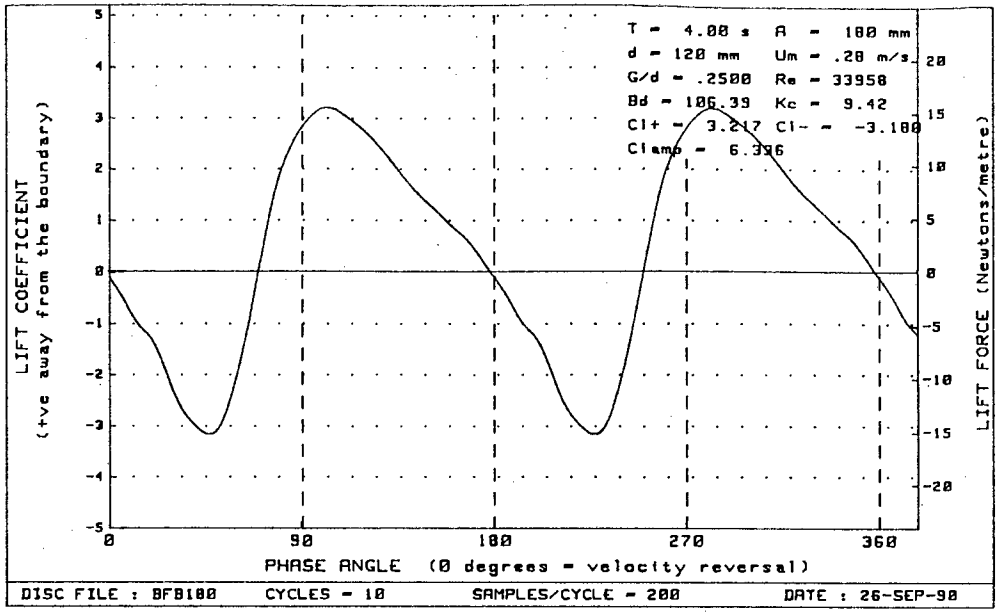

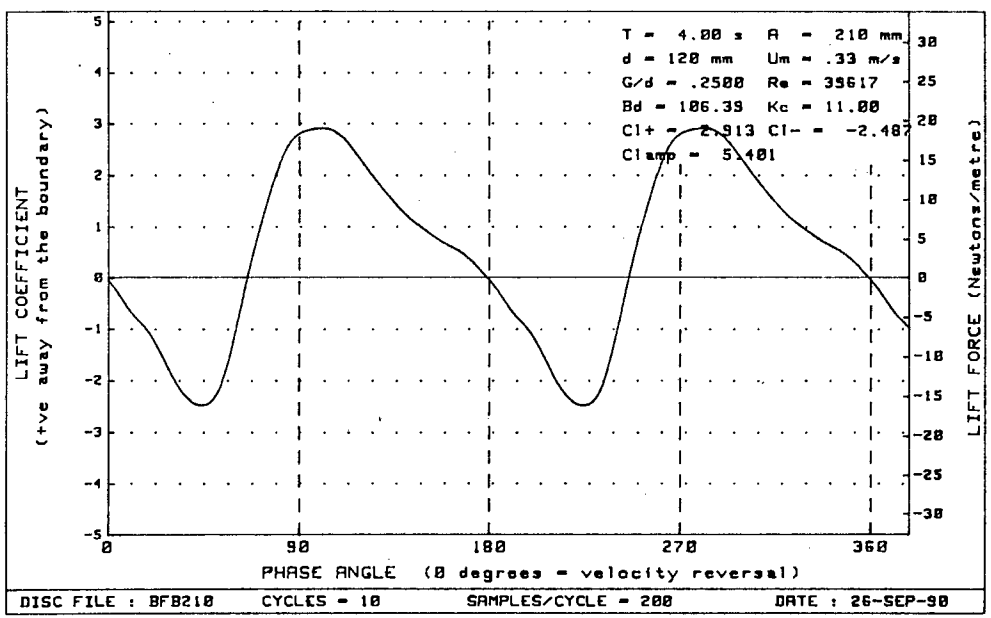

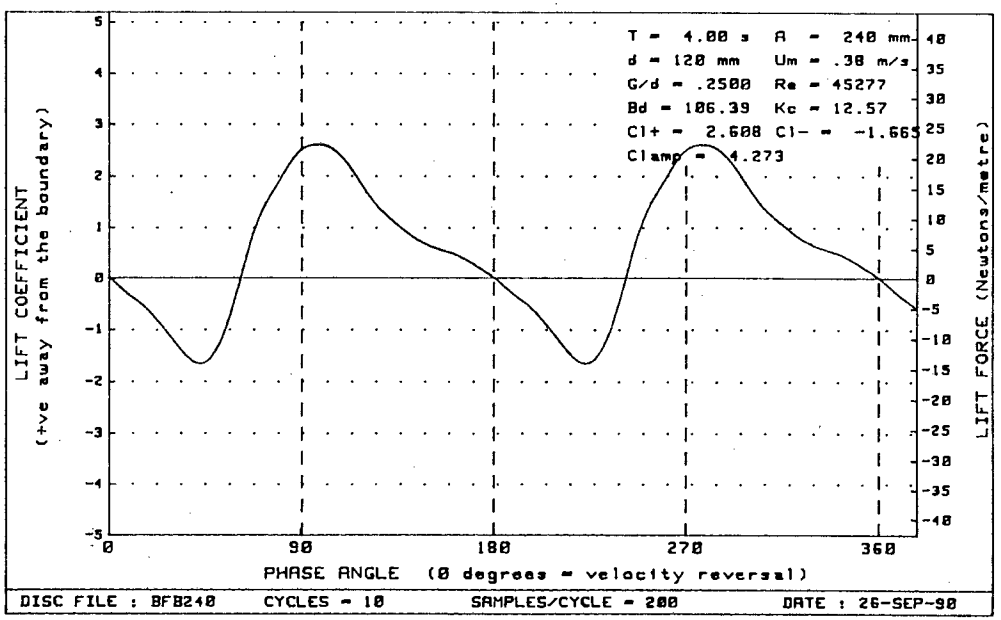

Figure G - 52 : Plots of lift vs phase for diameter=120mm, Bd=106.39 and G/d= .2500

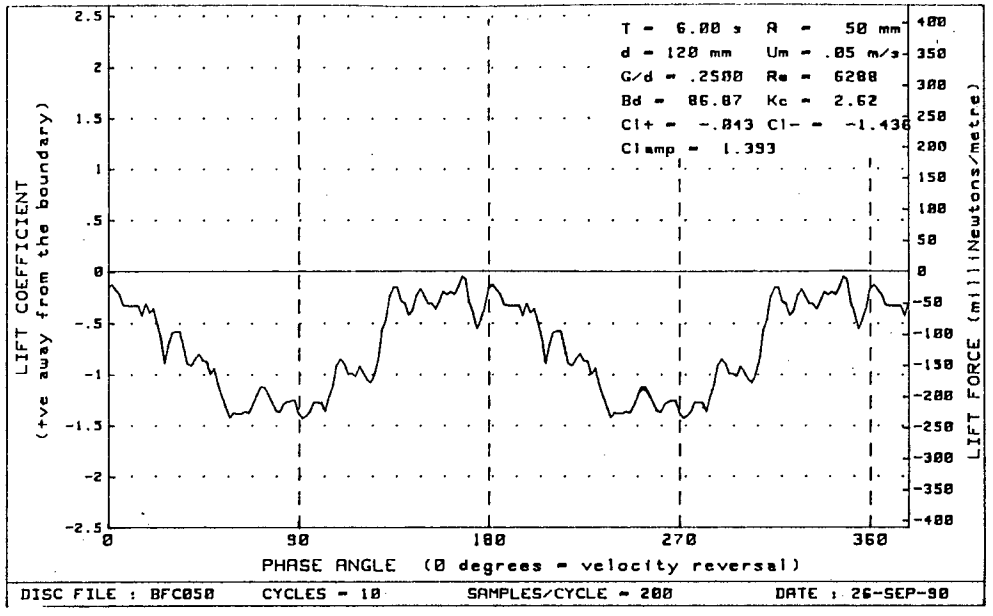

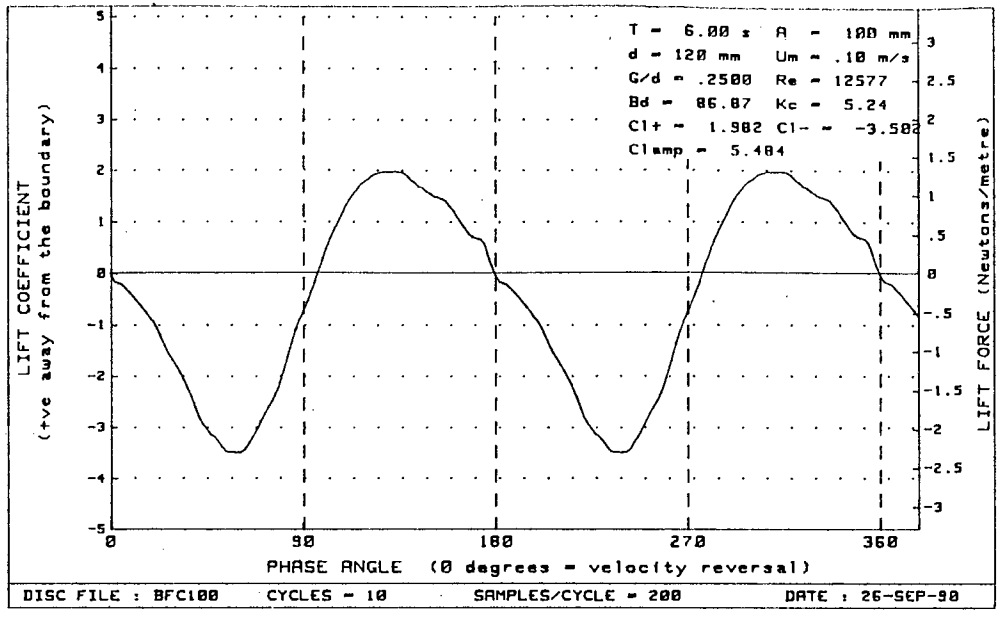

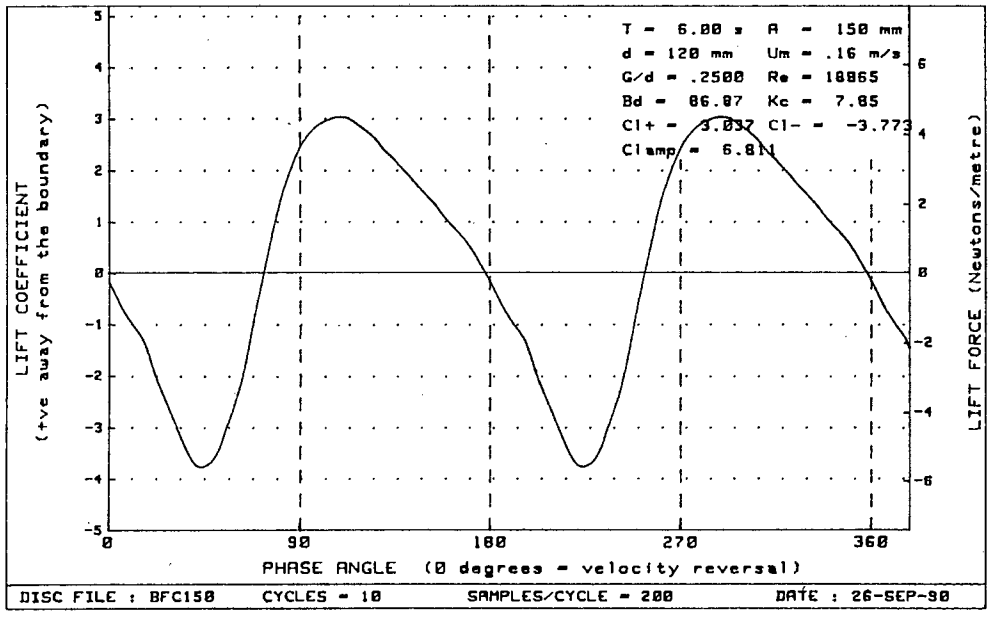

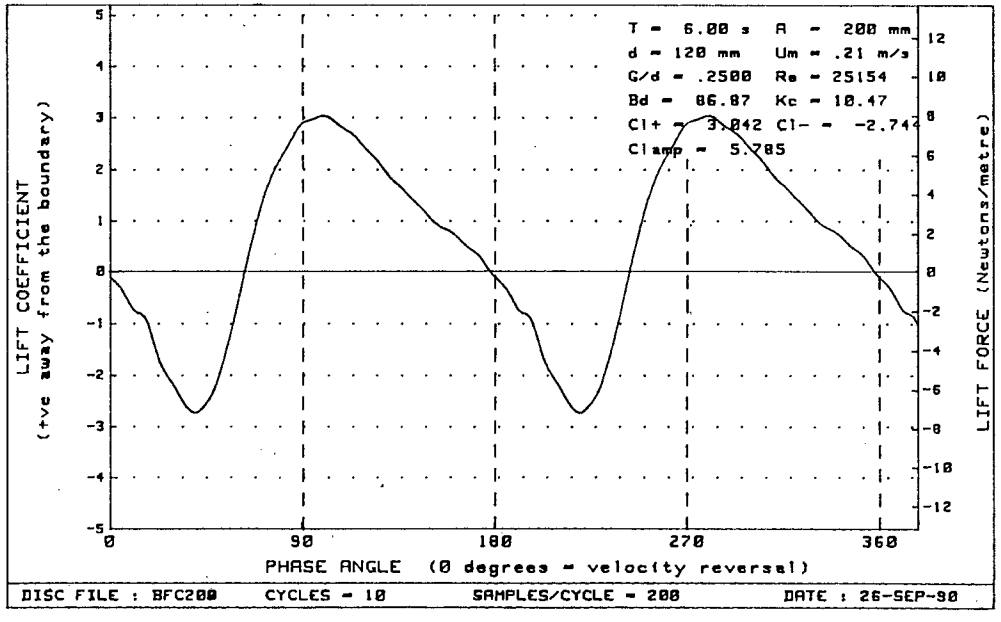

Figure G – 53 : Plots of lift vs phase for diameter=120mm, Bd= 86.87 and G/d= .2500

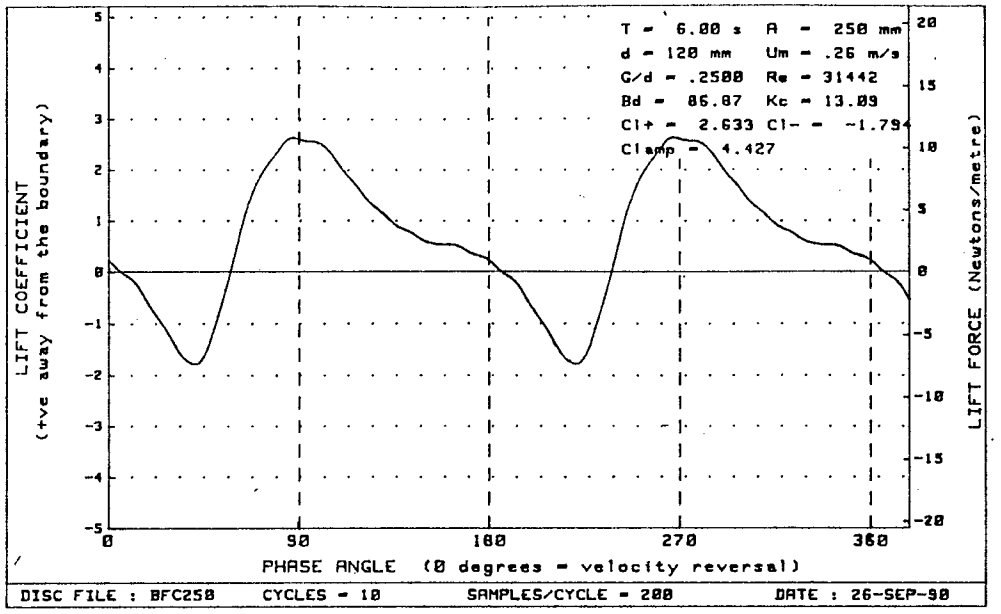

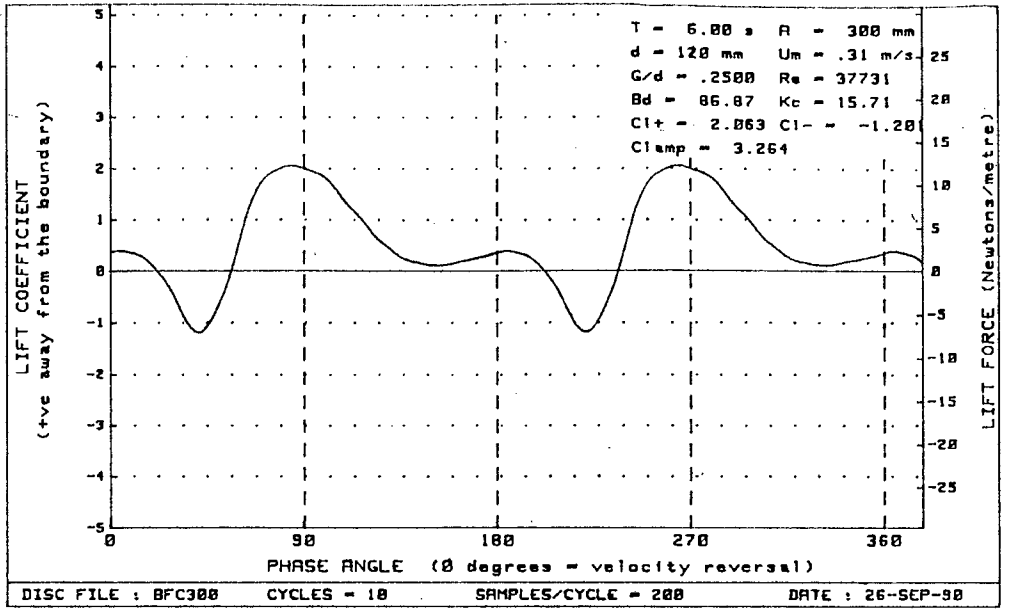

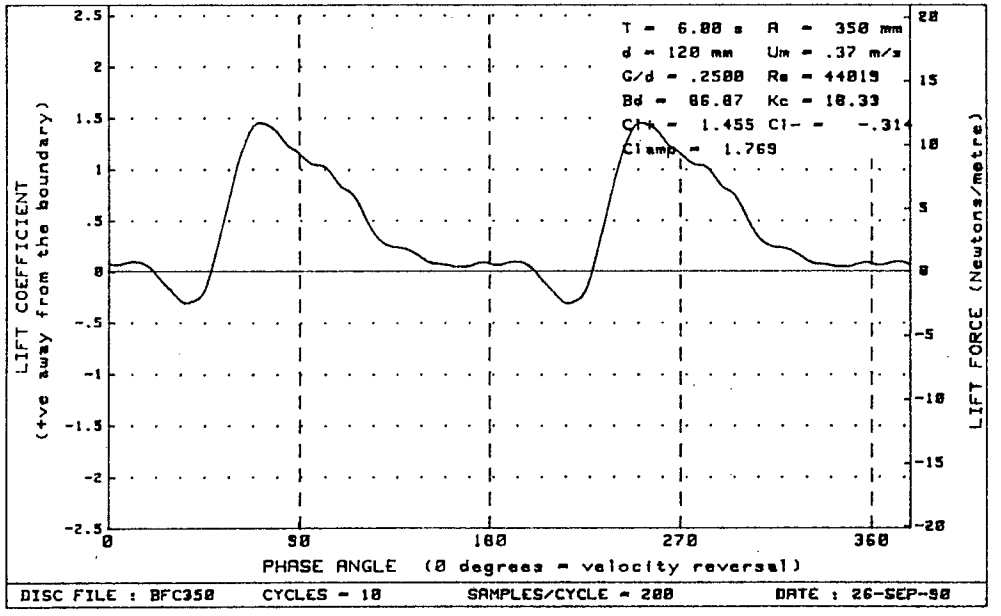

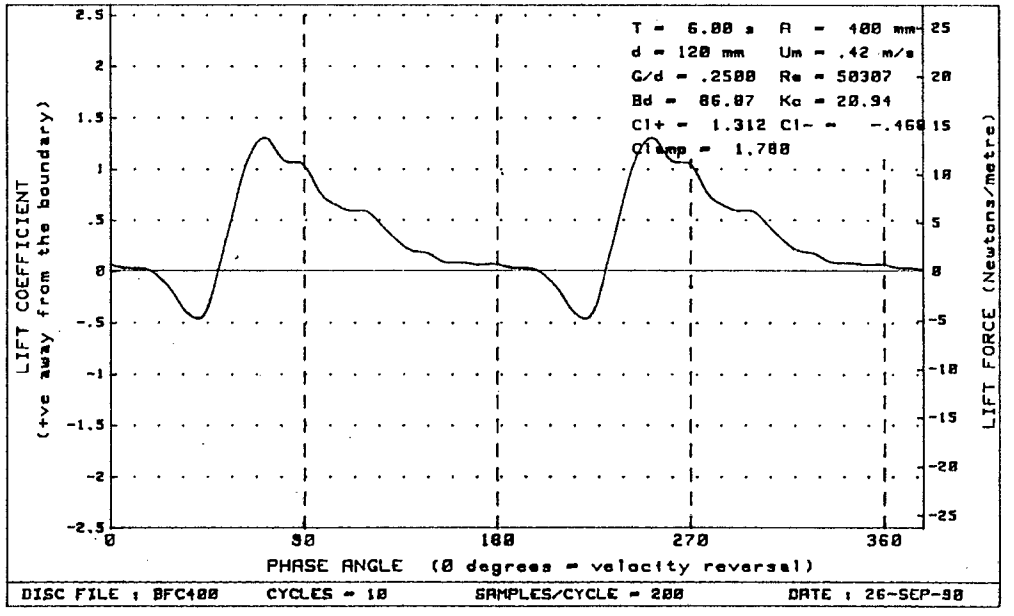

Figure G - 54 : Plots of lift vs phase for diameter=120mm, Bd= 86.87 and G/d= .2500

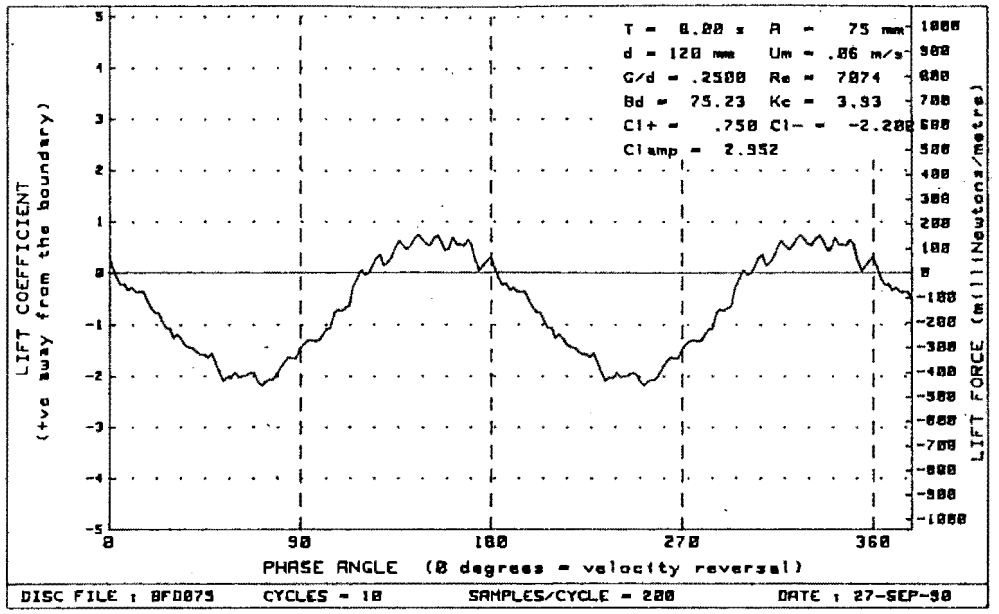

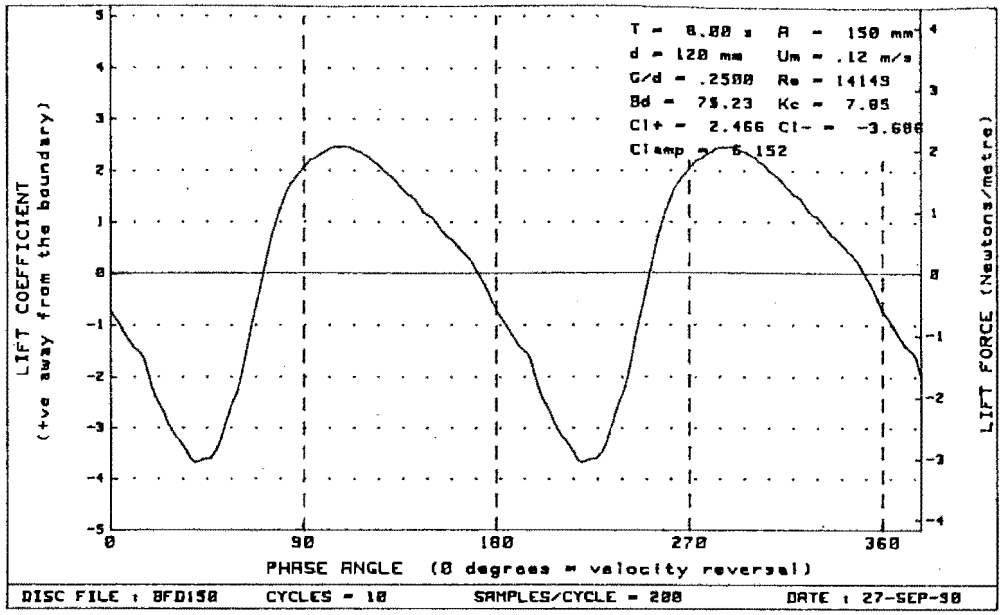

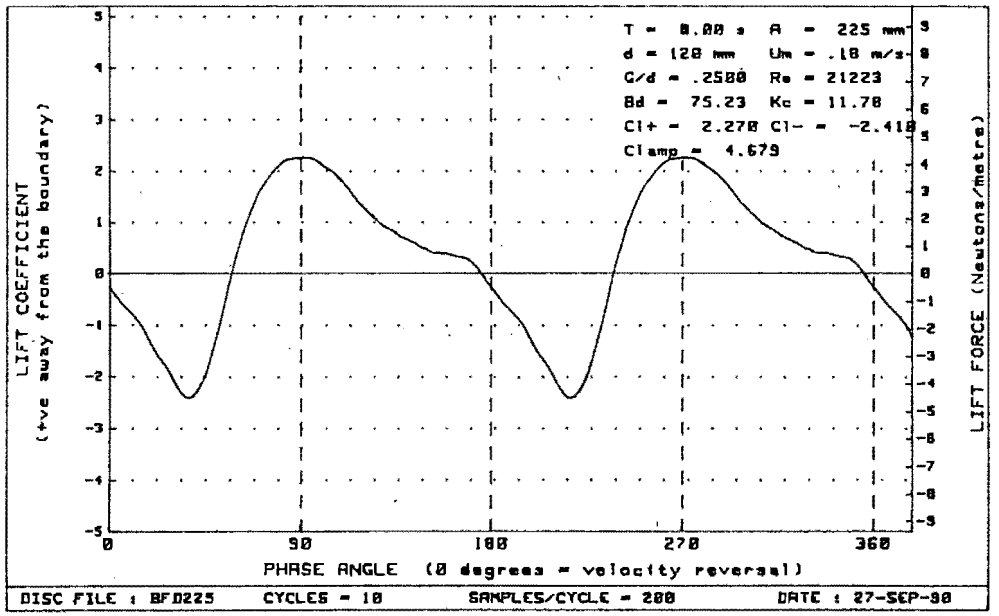

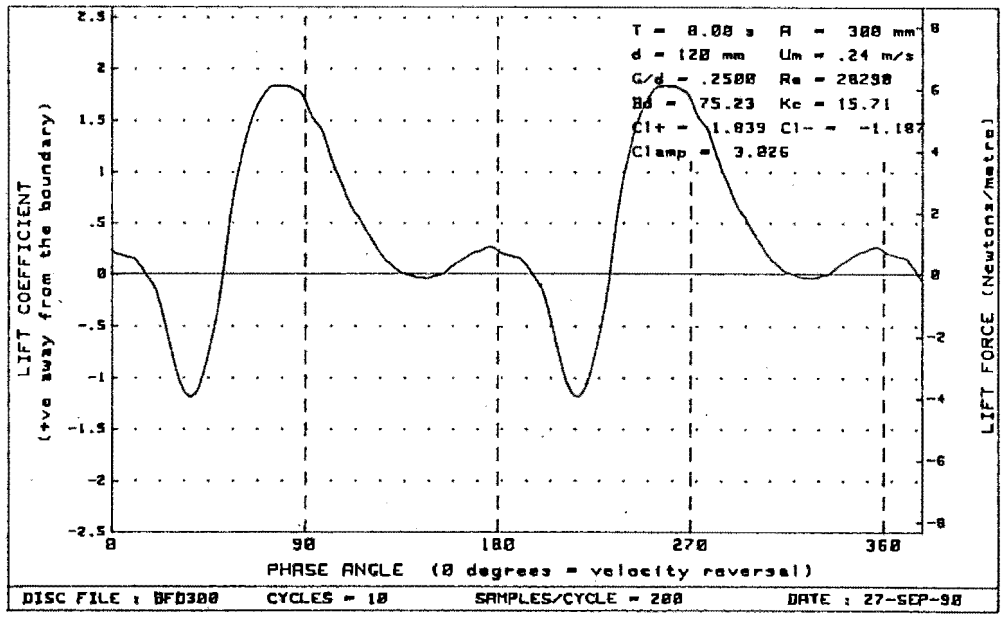

Figure G - 55 : Plots of lift vs phase for diameter=120mm, Bd= 75.23 and G/d= .2500

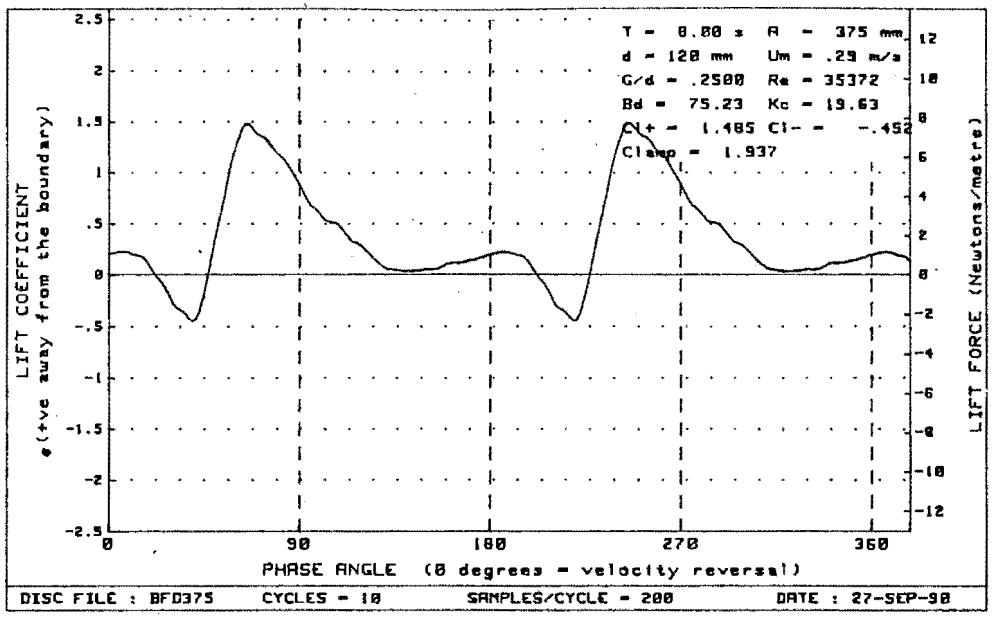

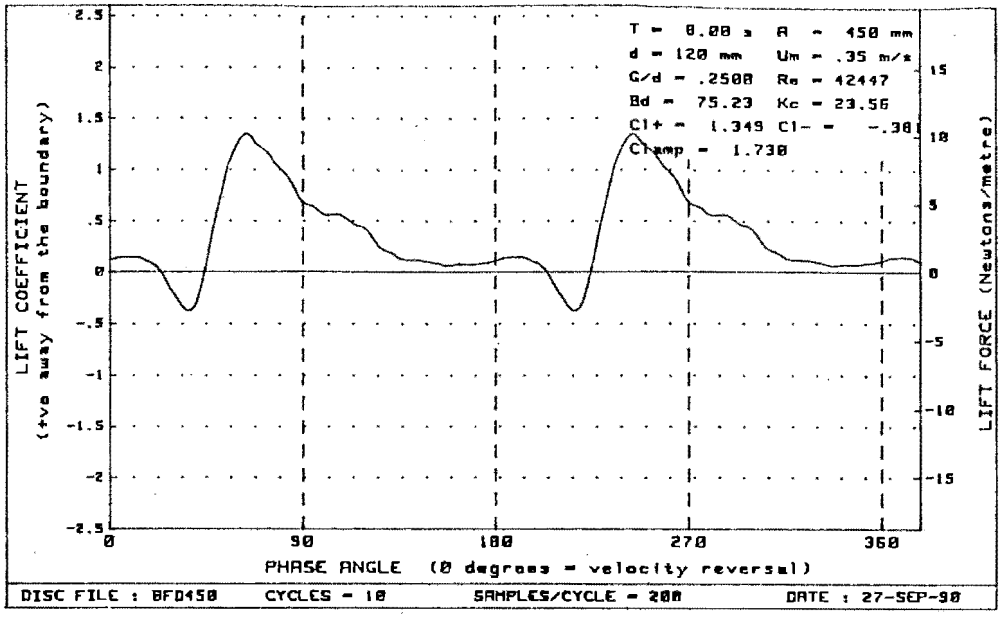

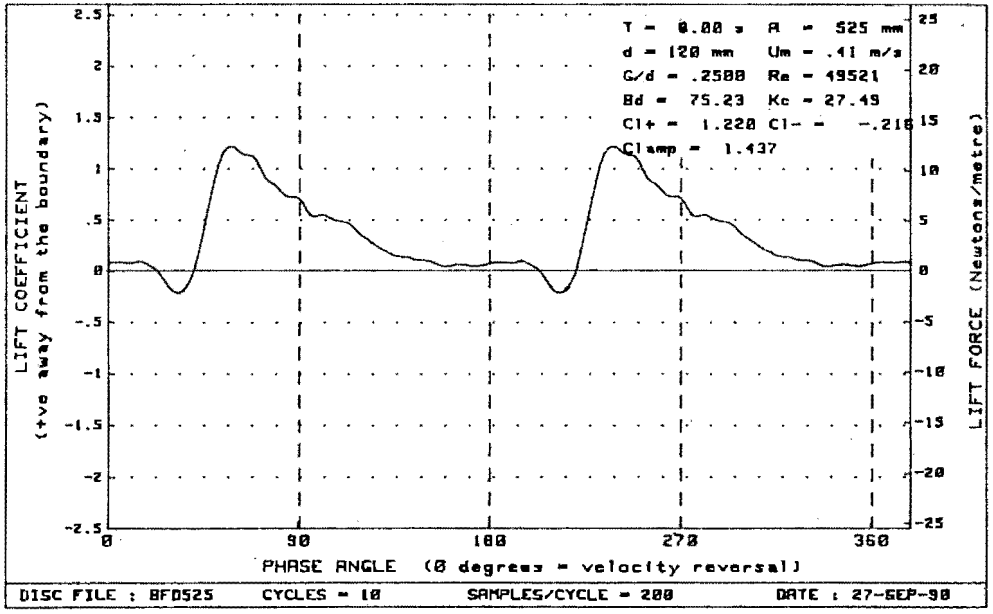

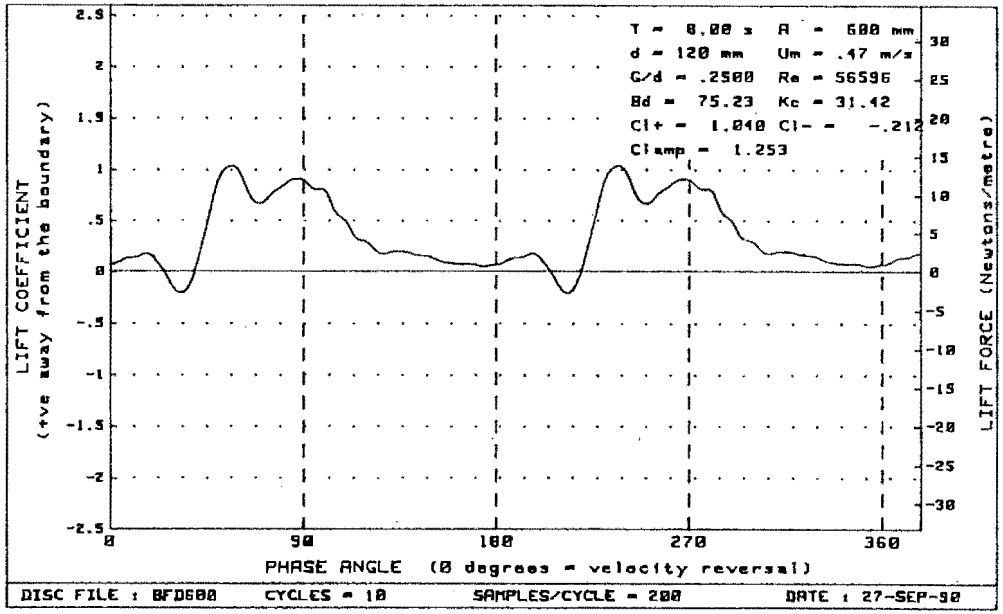

Figure G - 56 : Plots of lift vs phase for diameter=120mm, Bd= 75.23 and G/d= .2500

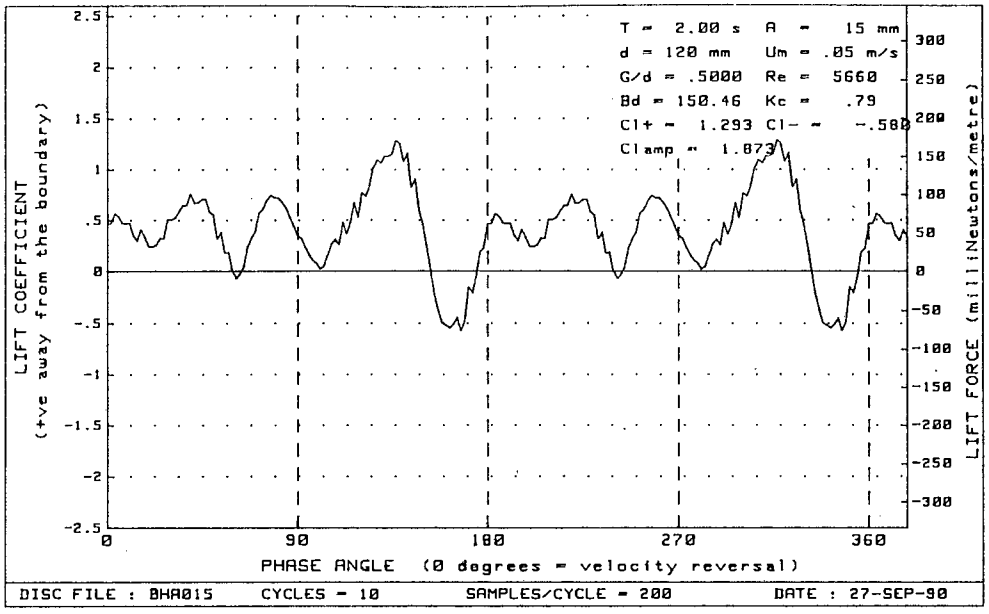

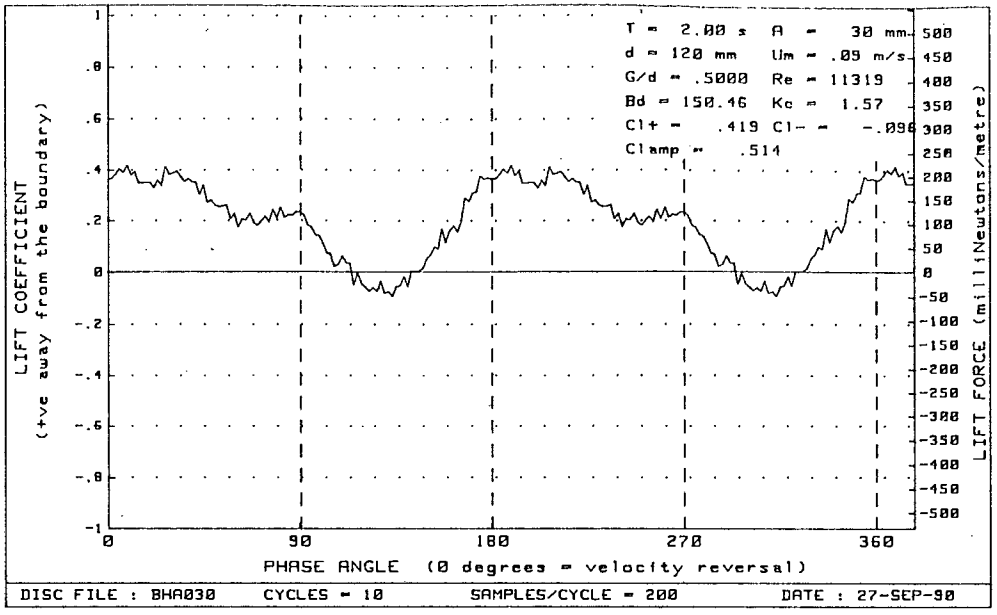

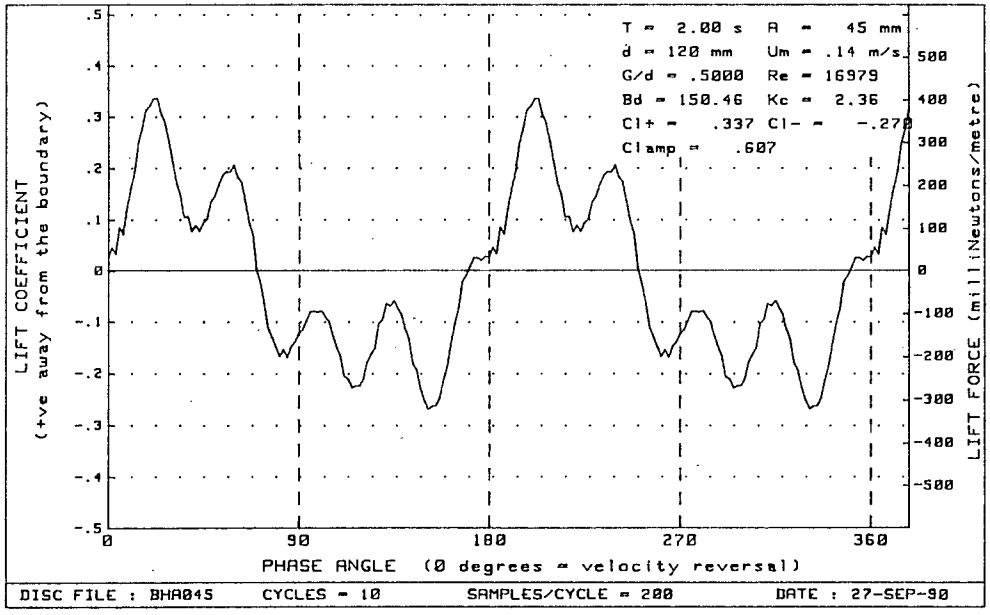

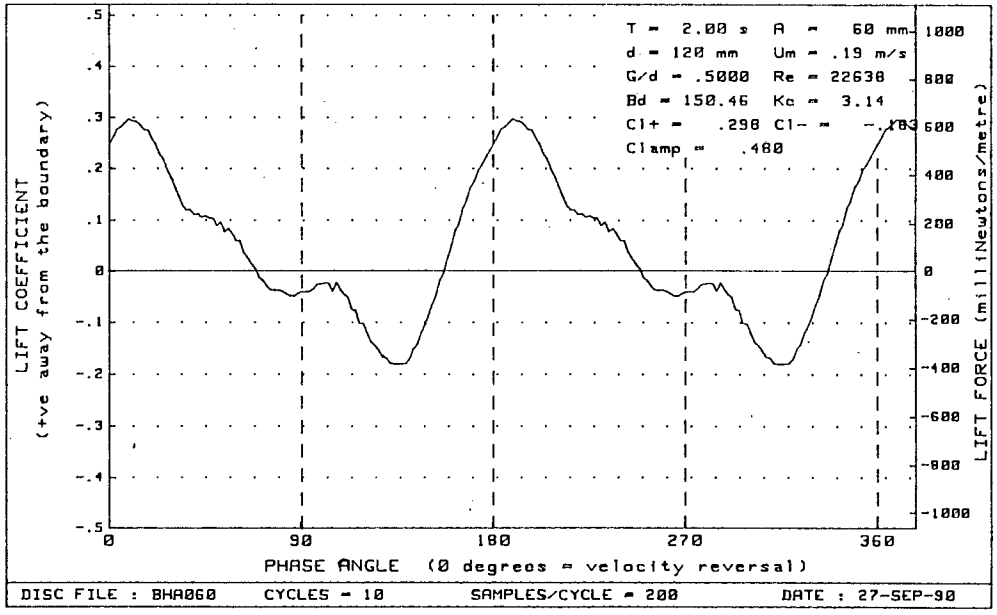

Figure G - 57 : Plots of lift vs phase for diameter=120mm, Bd=150.46 and G/d= .5000

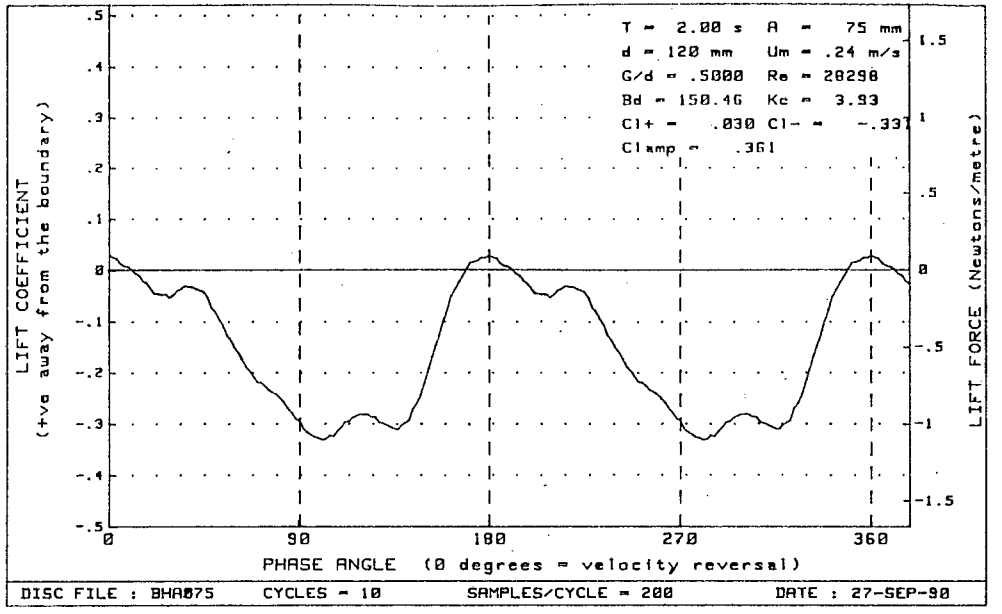

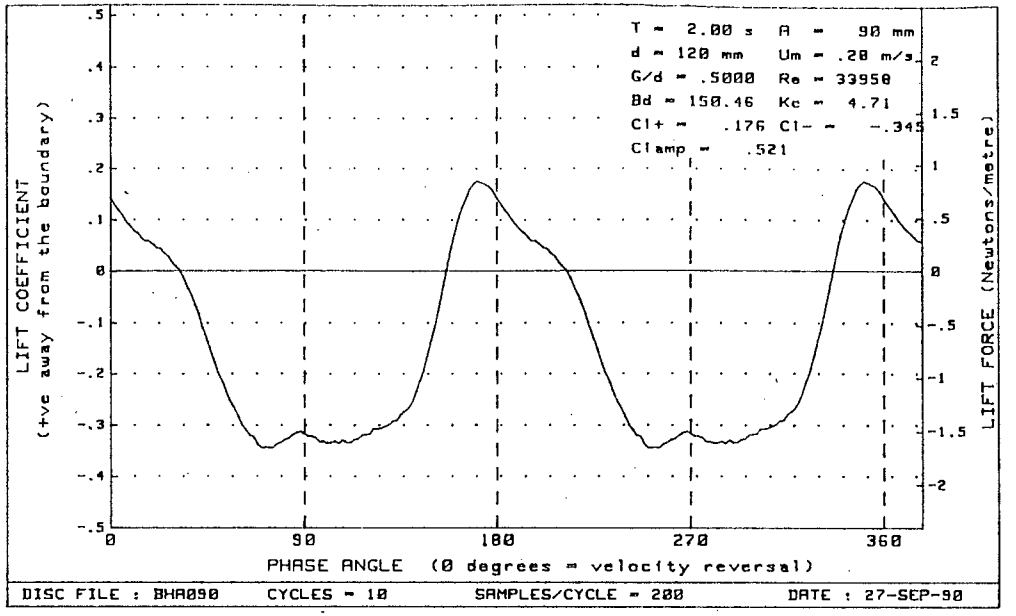

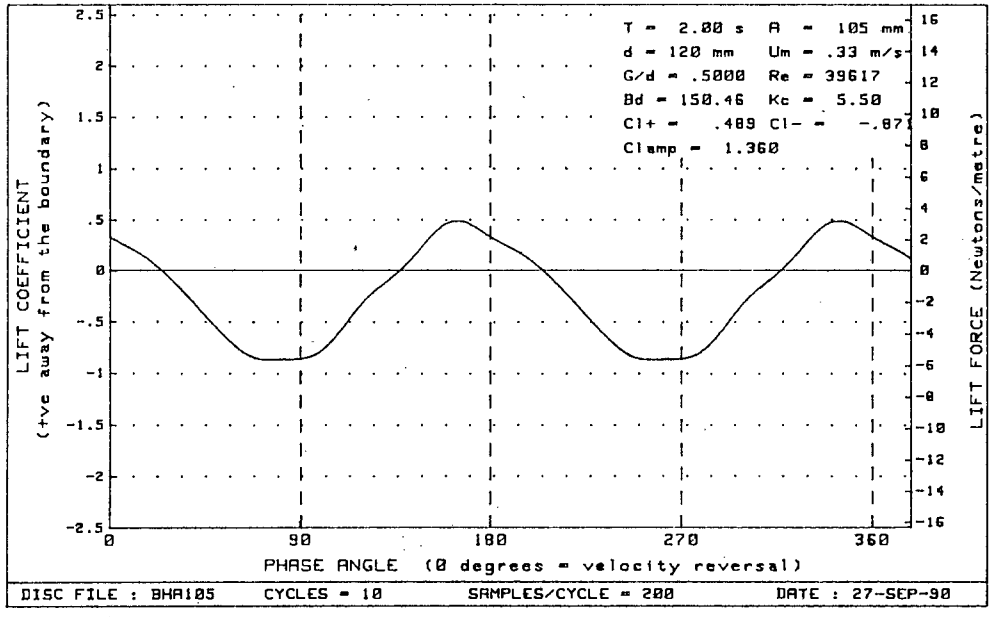

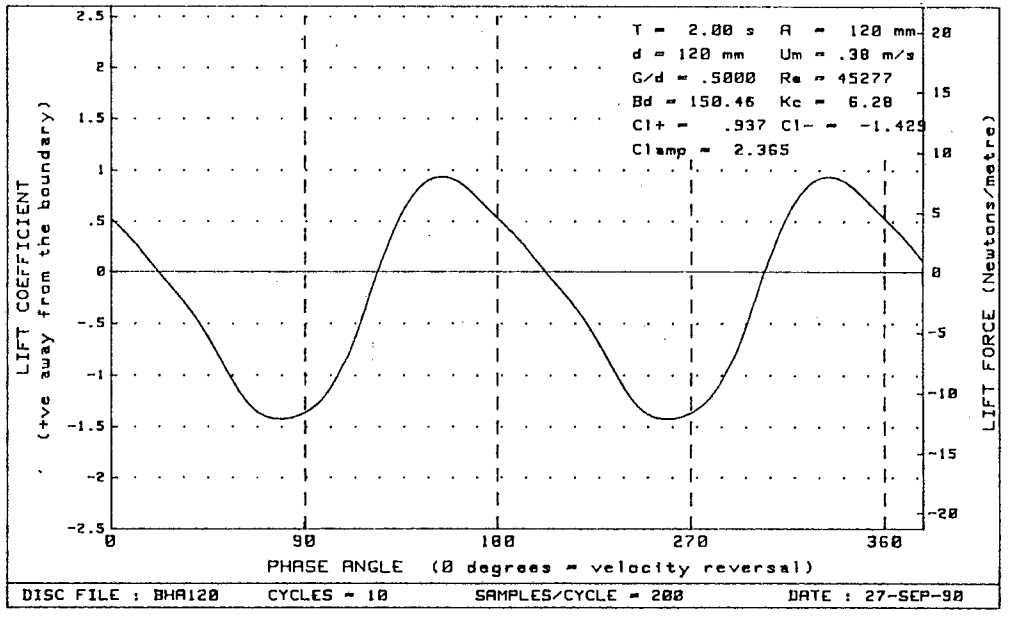

Figure G – 58 : Plots of lift vs phase for diameter=120mm, Bd=150.46 and G/d= .5000

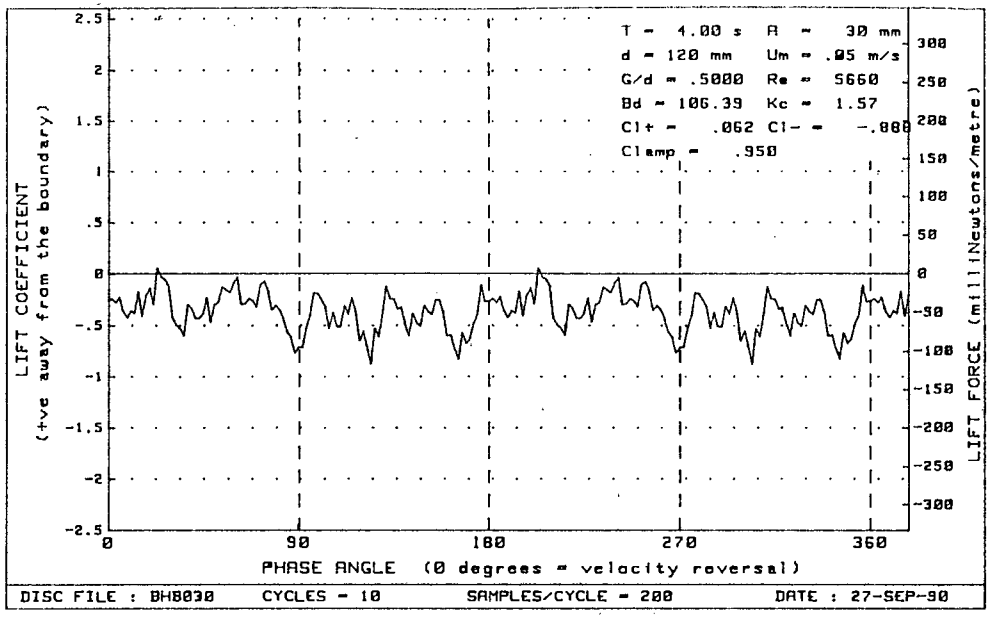

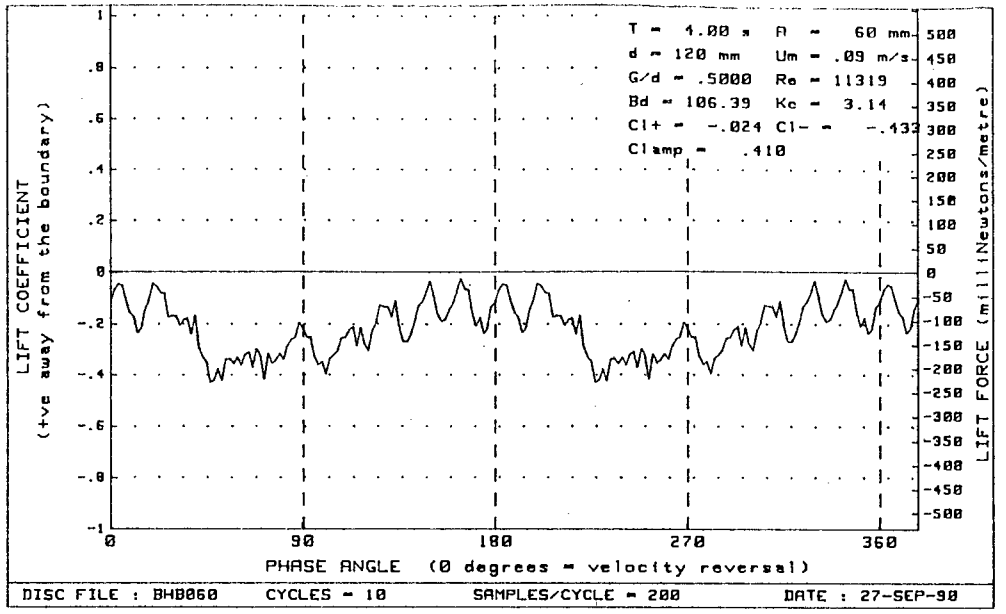

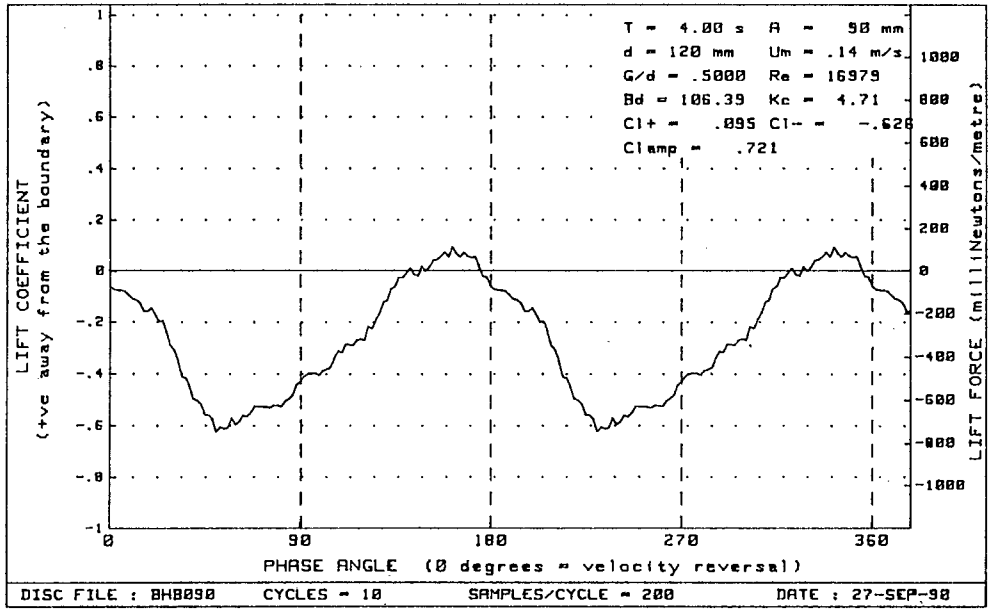

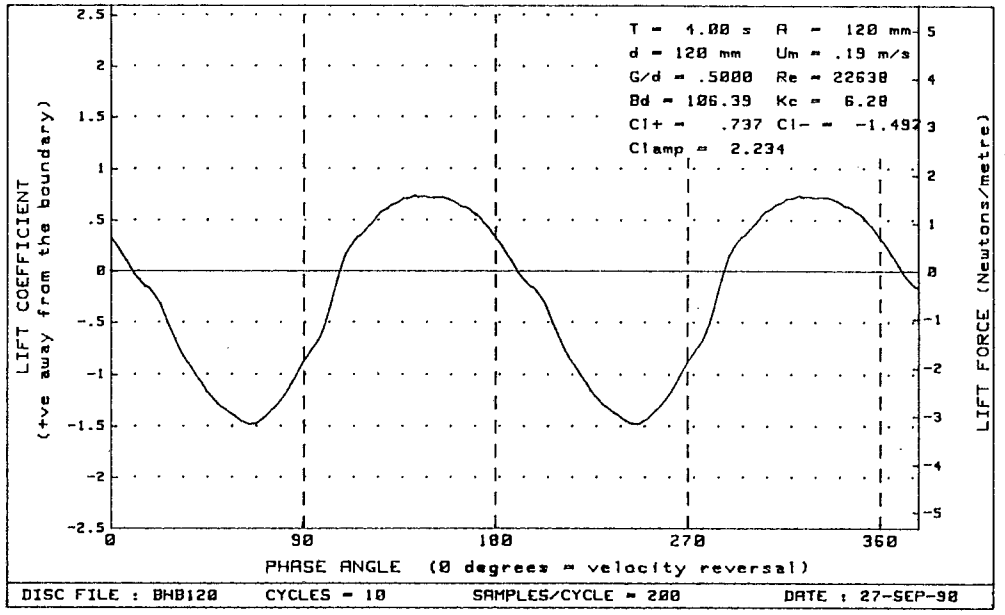

Figure G - 59 : Plots of lift vs phase for diameter=120mm, Bd=106.39 and G/d= .5000

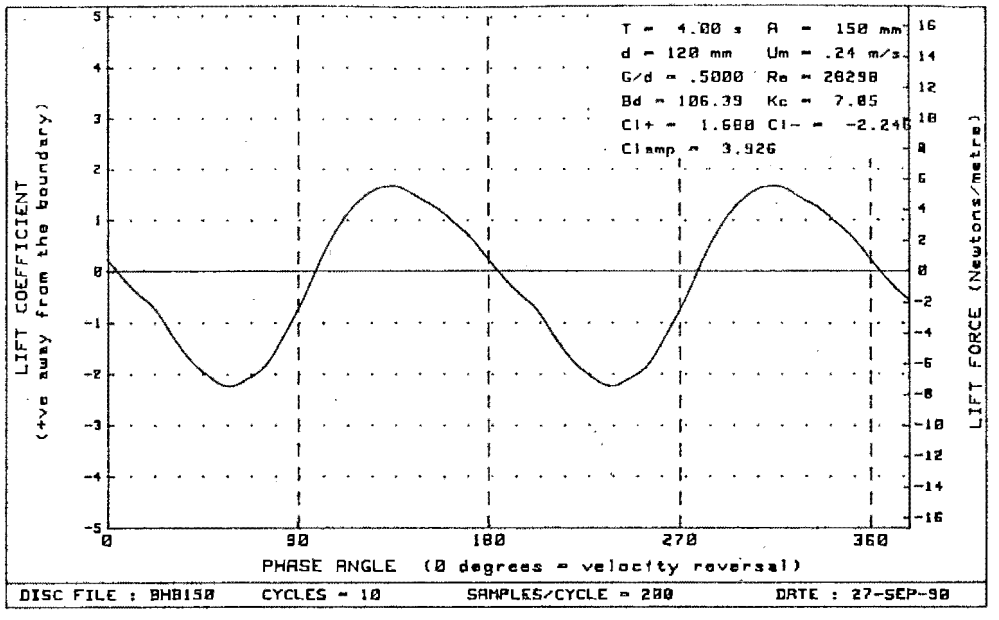

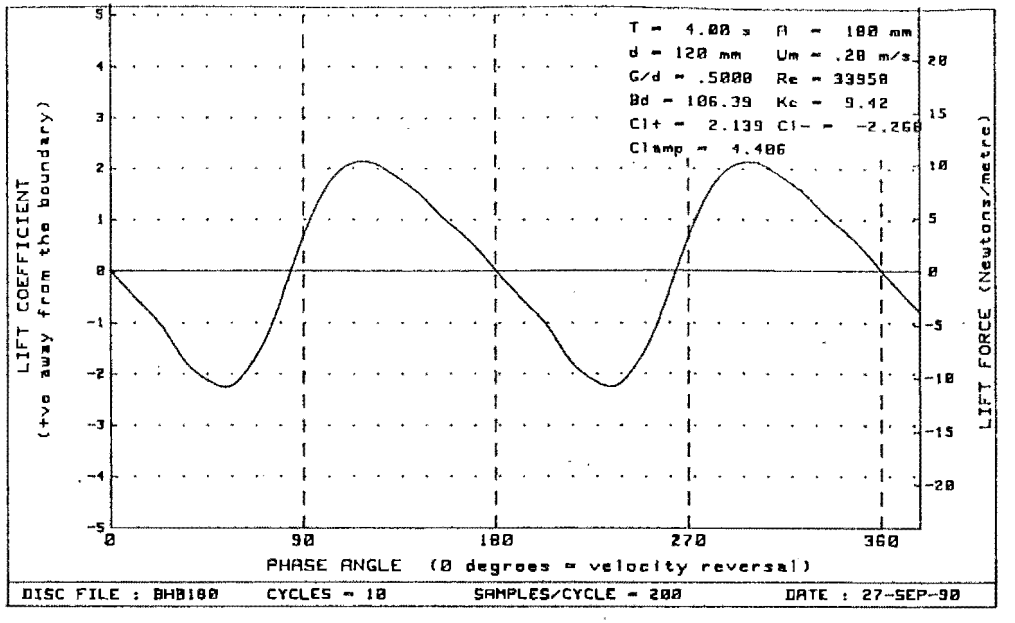

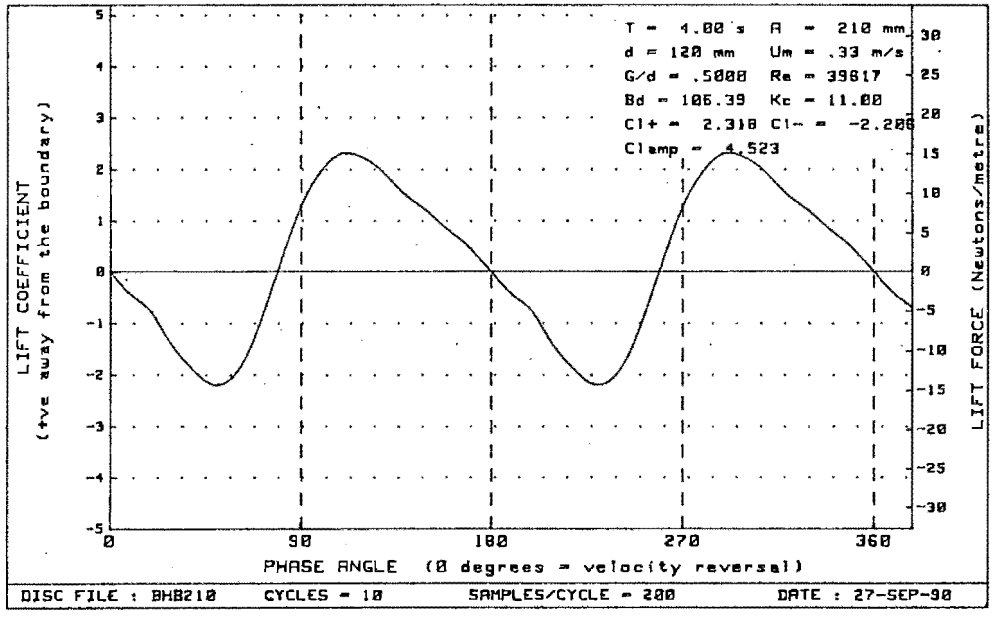

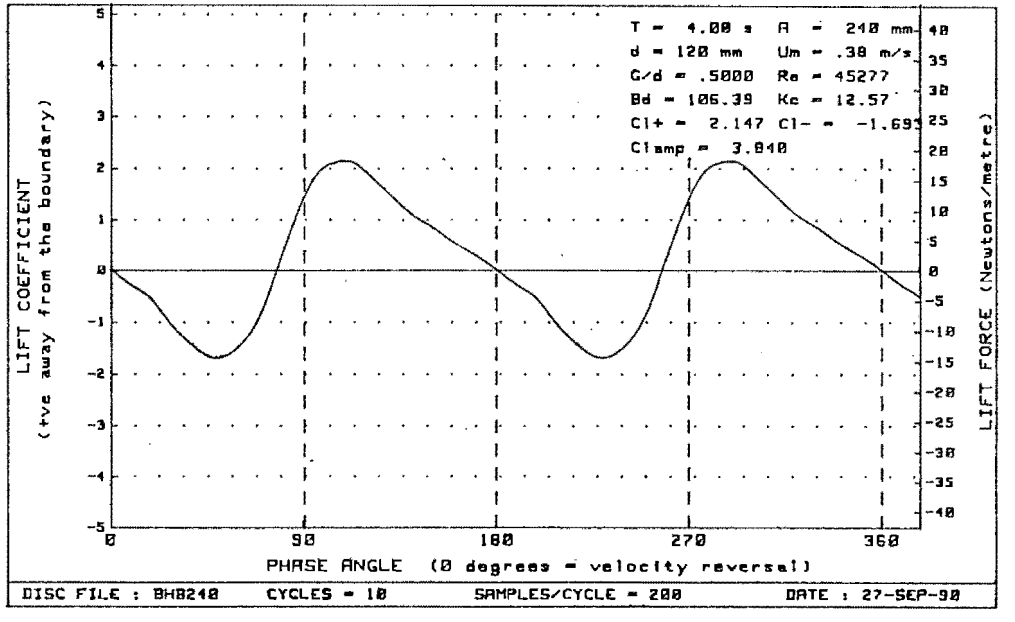

Figure G - 60 : Plots of lift vs phase for diameter=120mm, Bd=106.39 and G/d= .5000

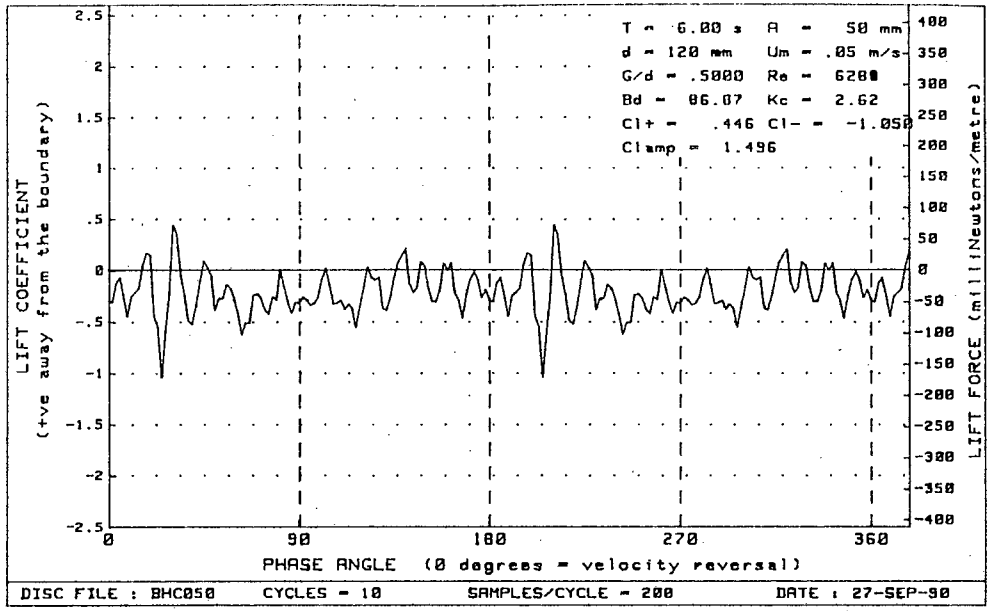

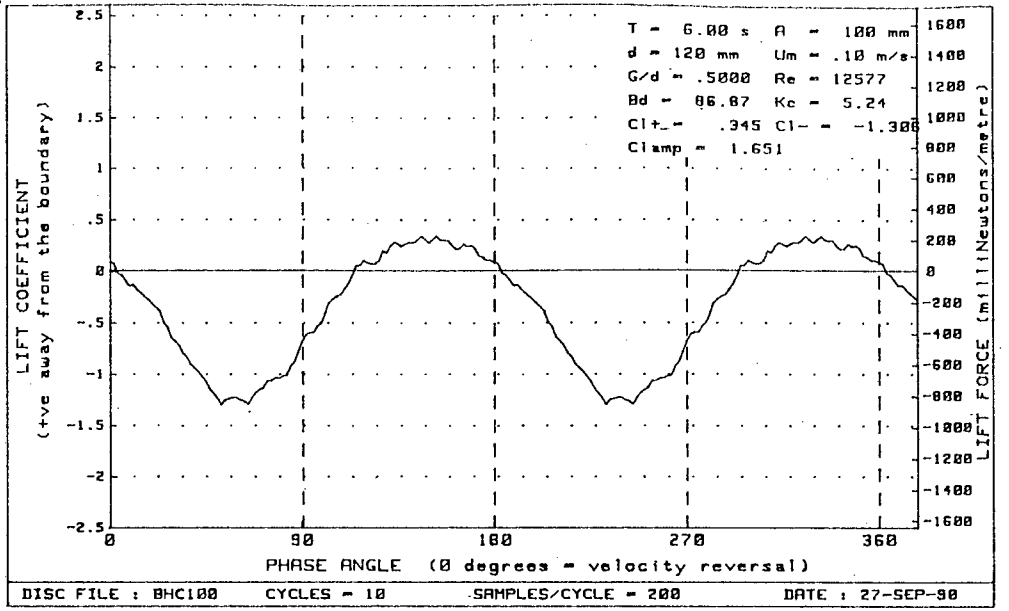

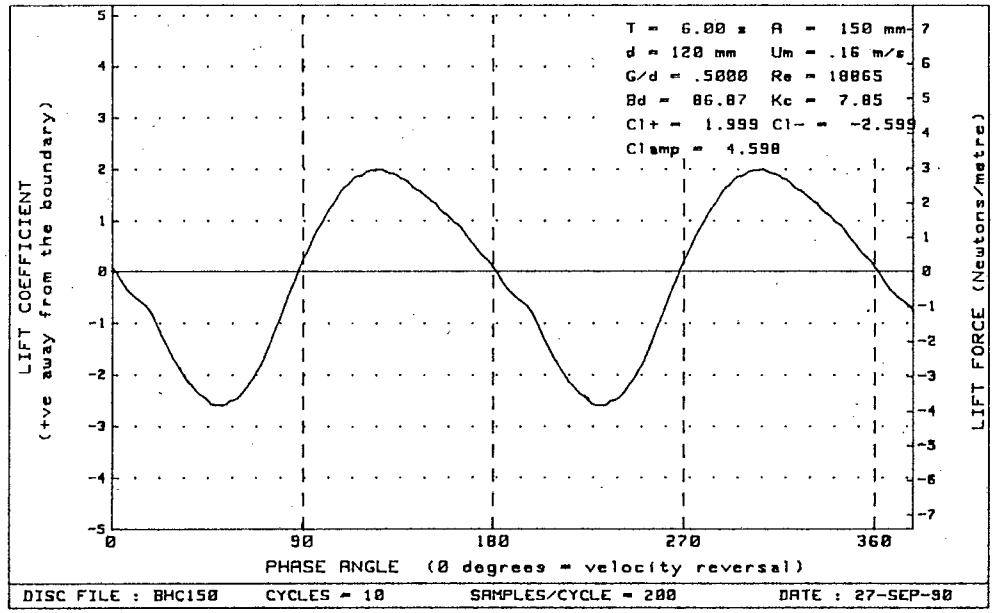

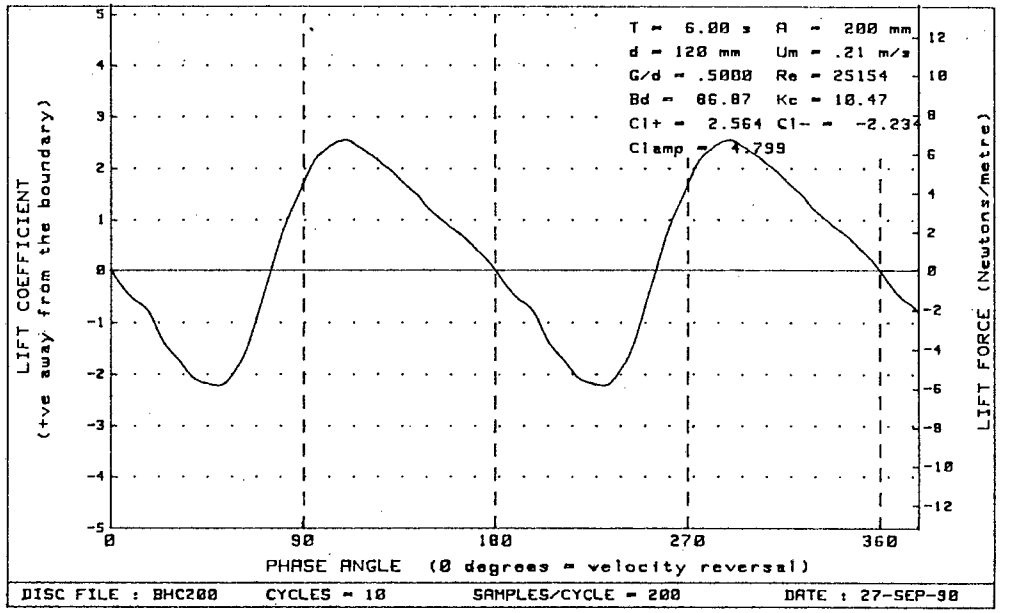

Figure G – 61 : Plots of lift vs phase for diameter=120mm, Bd= 86.87 and G/d= .5000

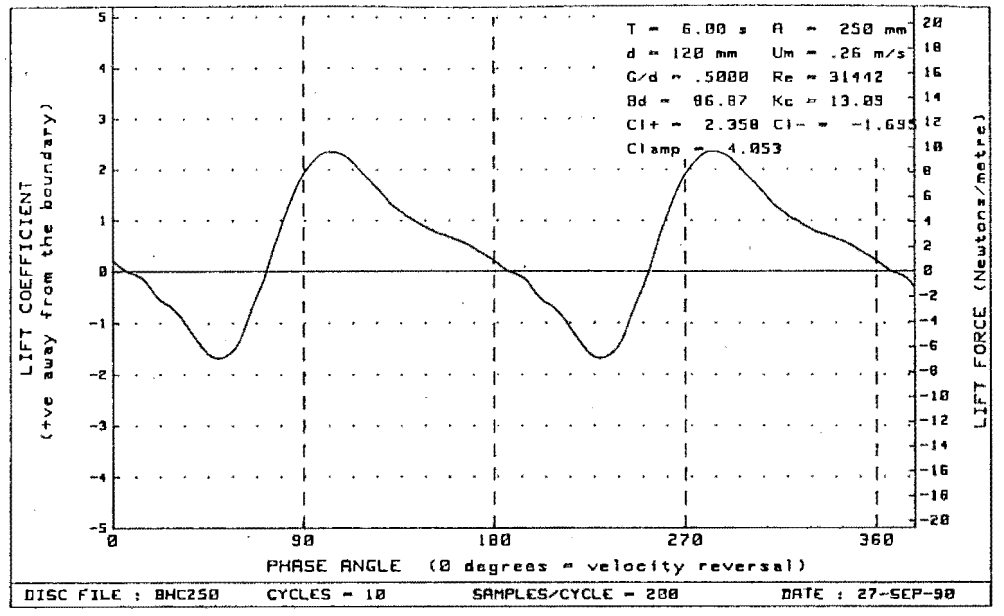

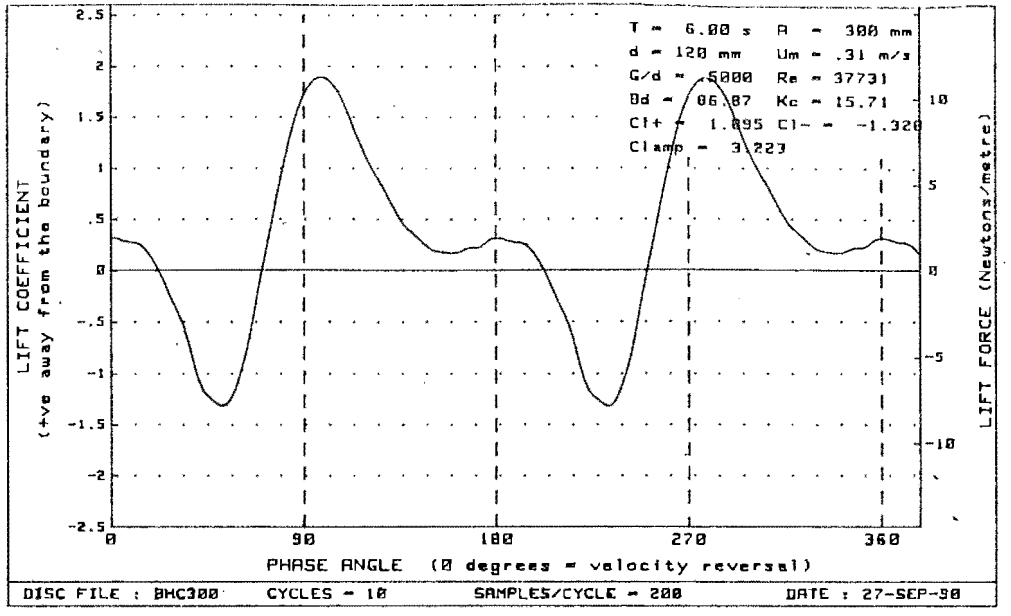

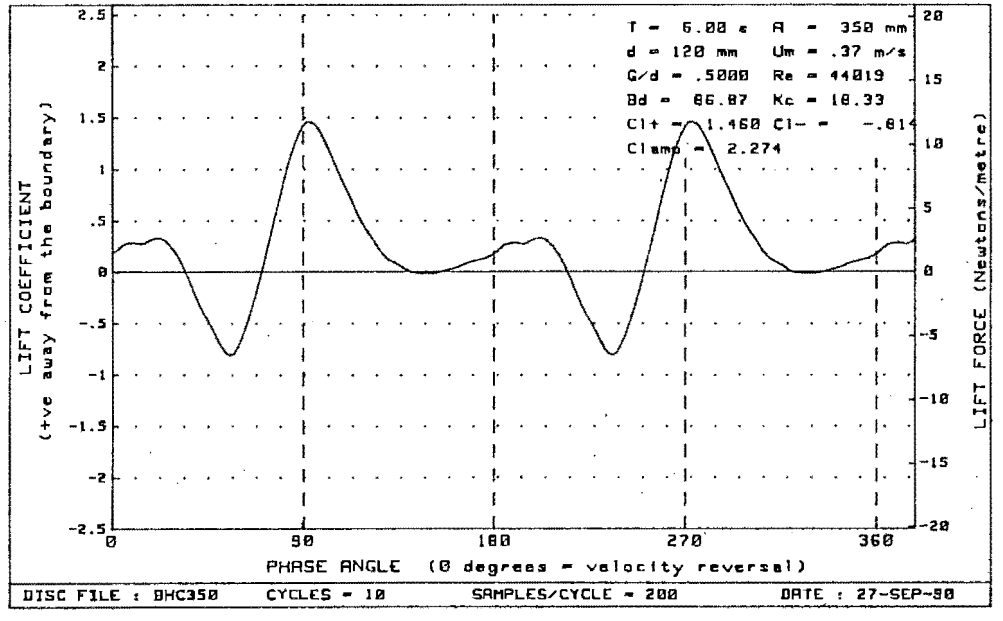

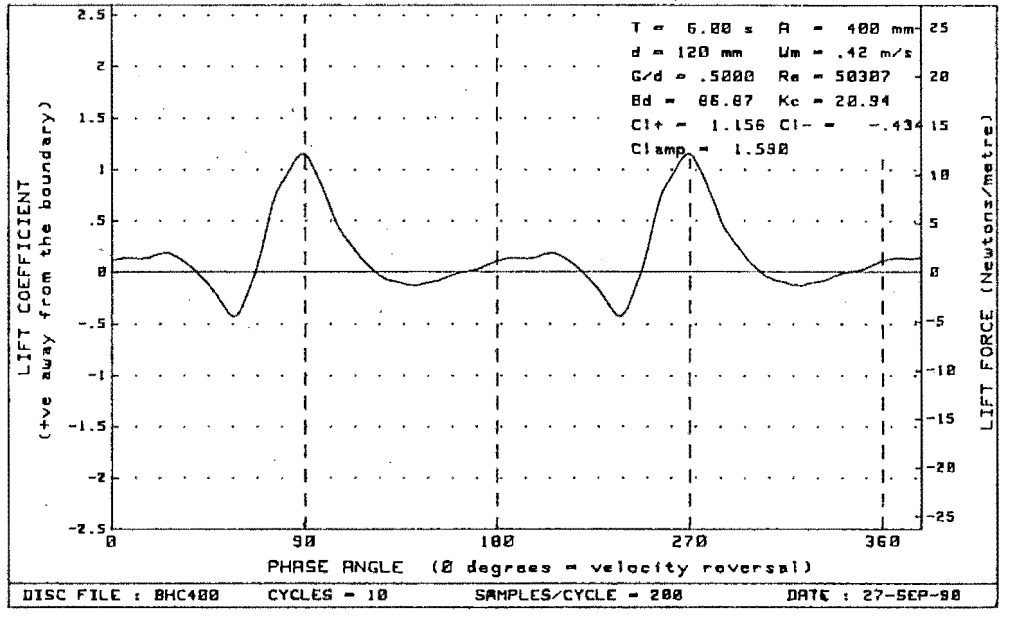

Figure G - 62 : Plots of lift vs phase for diameter=120mm, Bd= 86.87 and G/d= .5000

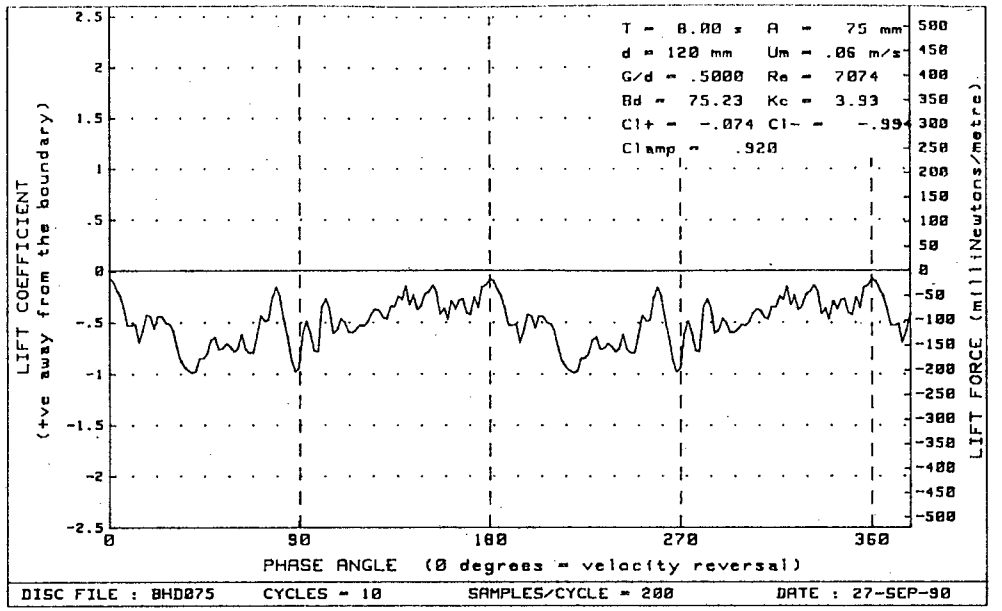

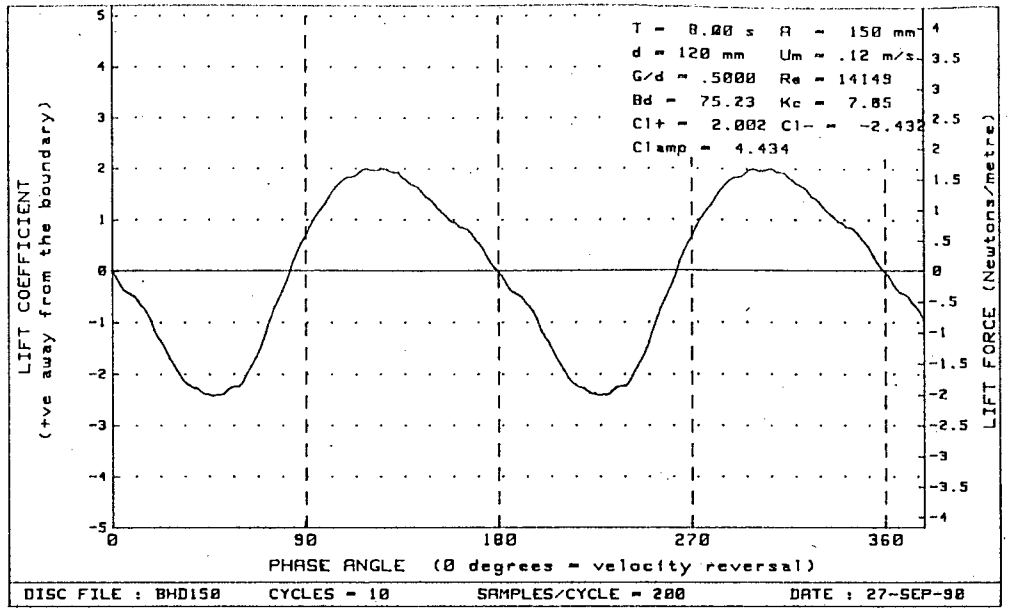

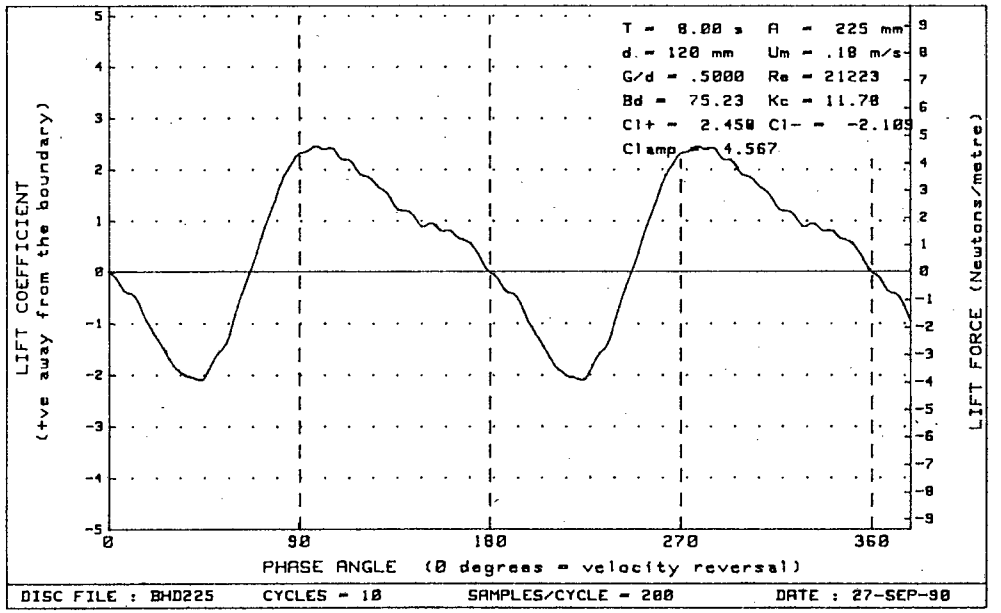

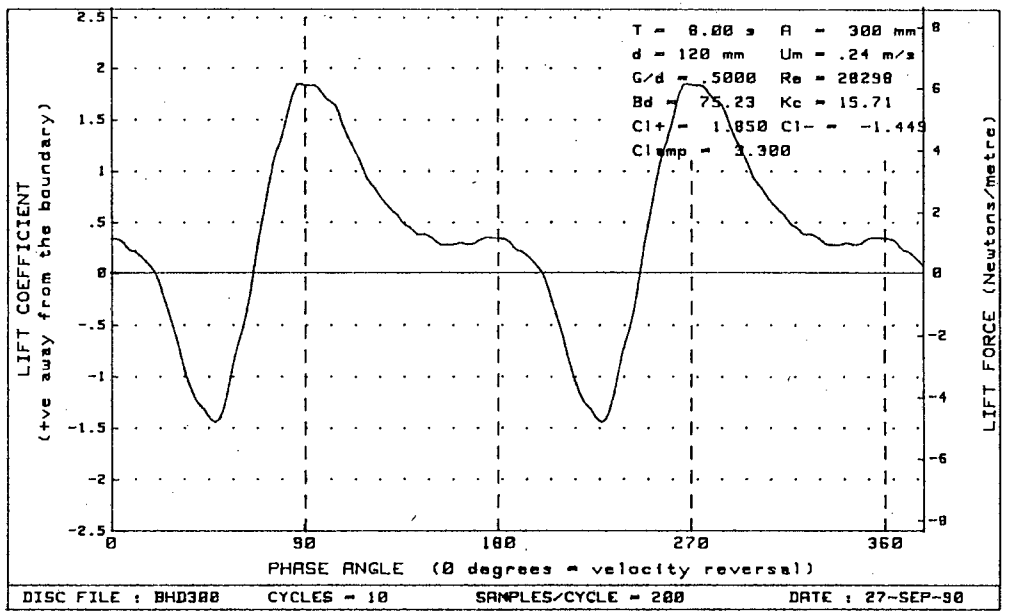

Figure G – 63 : Plots of lift vs phase for diameter=120mm, Bd= 75.23 and G/d= .5000

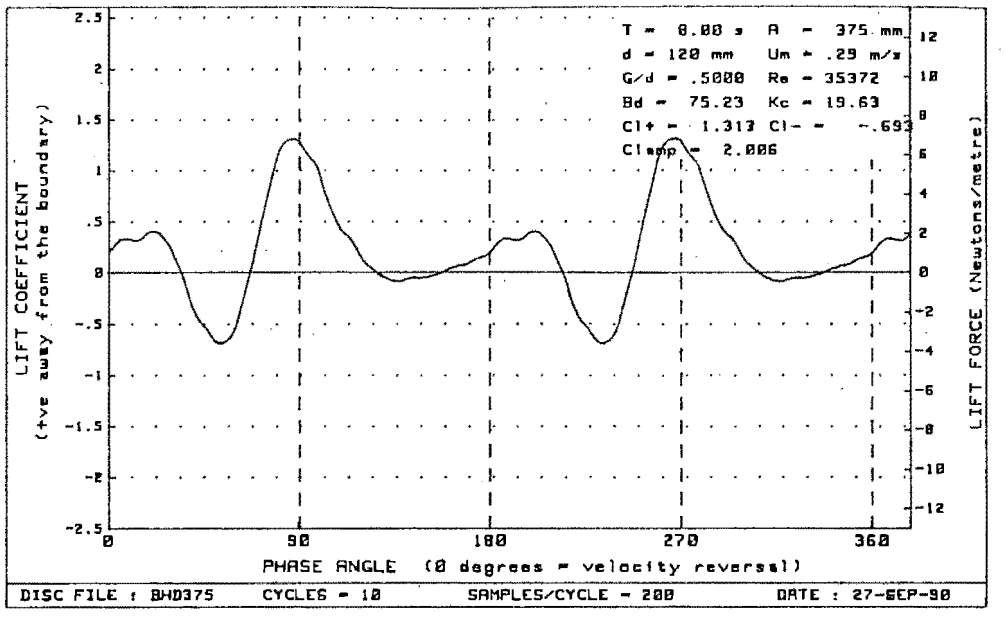

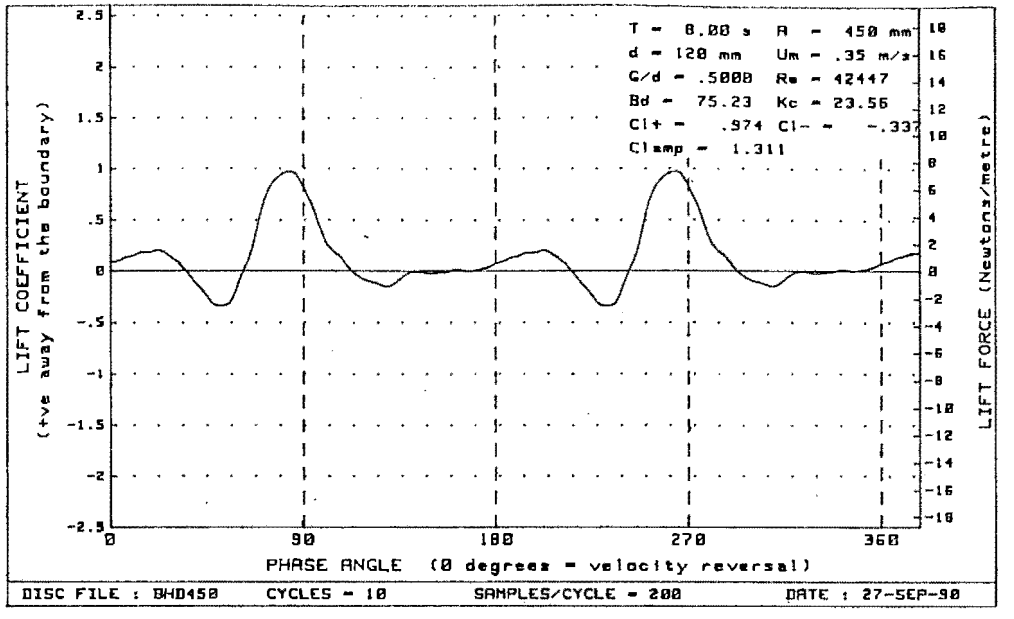

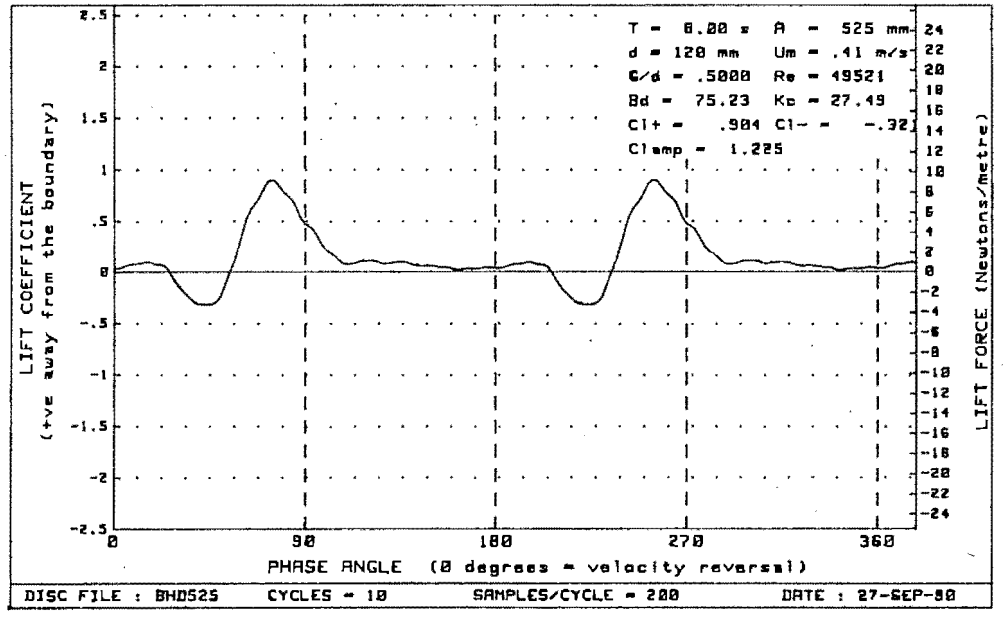

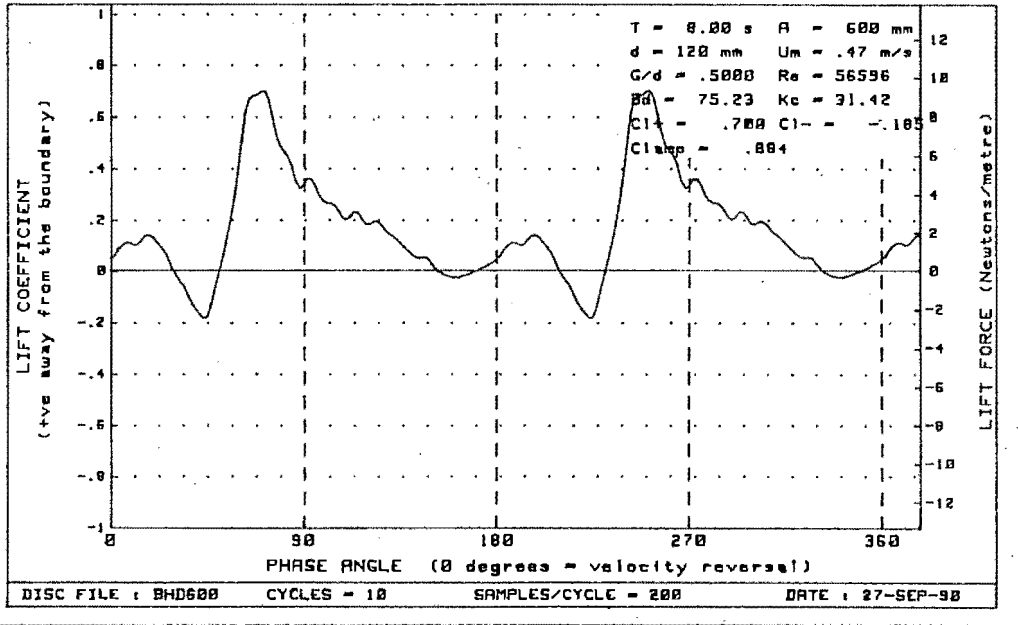

Figure G – 64 : Plots of lift vs phase for diameter=120mm, Bd= 75.23 and G/d= .5000

APPENDIX H - PLOTS OF DRAG vs PHASE

Plots of drag versus phase have been given, showing both drag coefficient and drag force versus the phase angle.

The plots are arranged in ascending order of gap ratio. For each gap ratio the results are arranged in ascending period and for each period they are arranged in ascending amplitude.

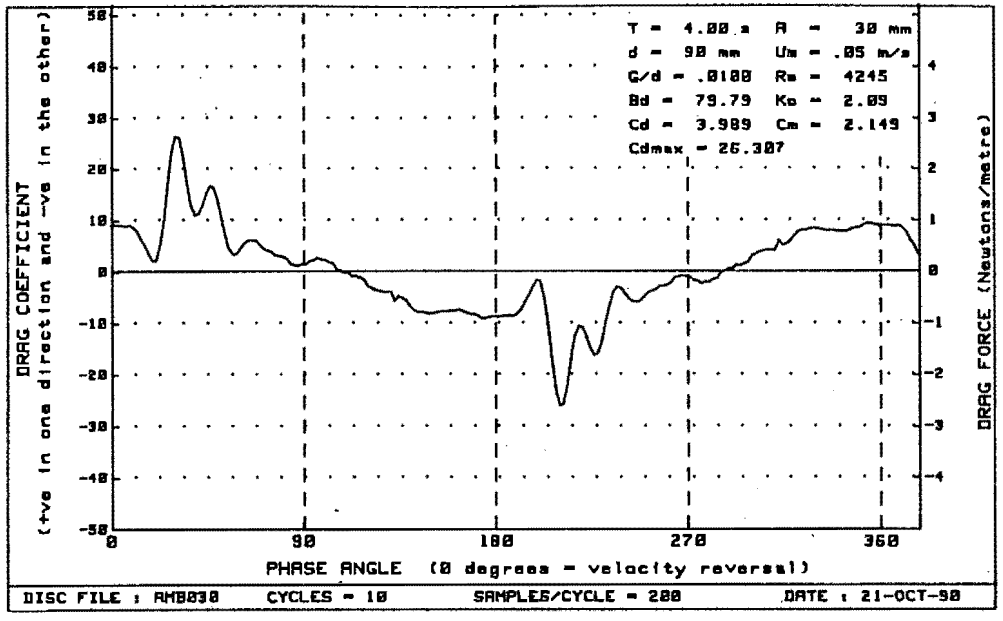

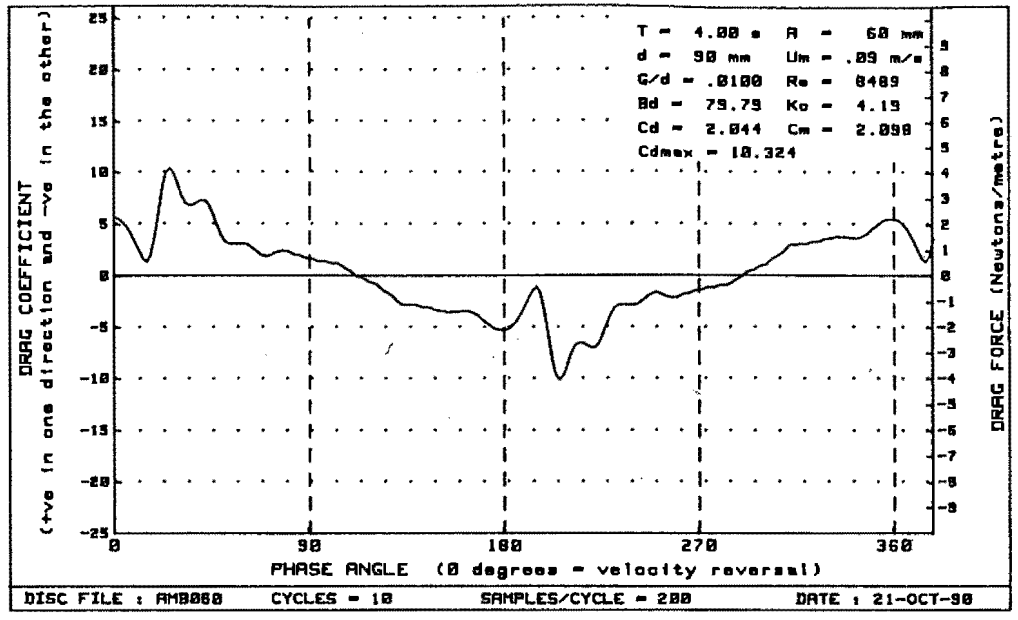

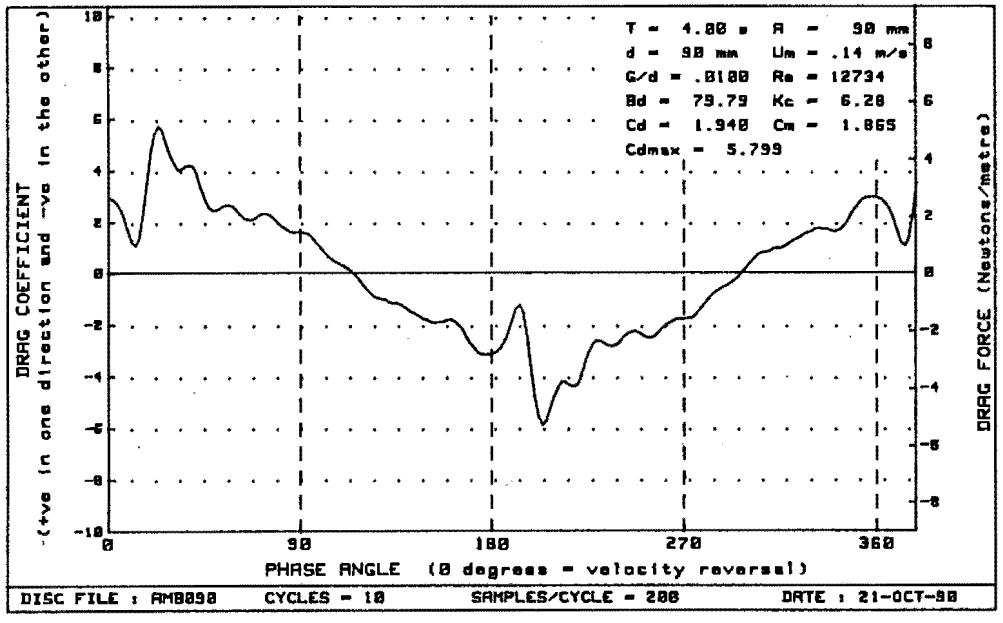

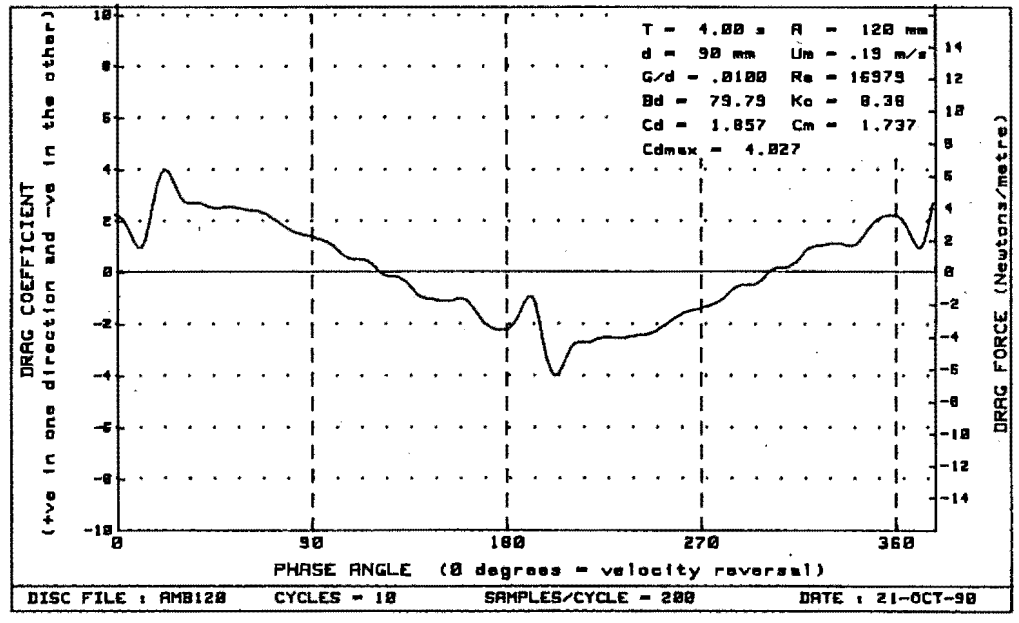

Figure H-1 : Plots of drag vs phase for diameter=90mm, Bd= 79.79 and G/d= .0100

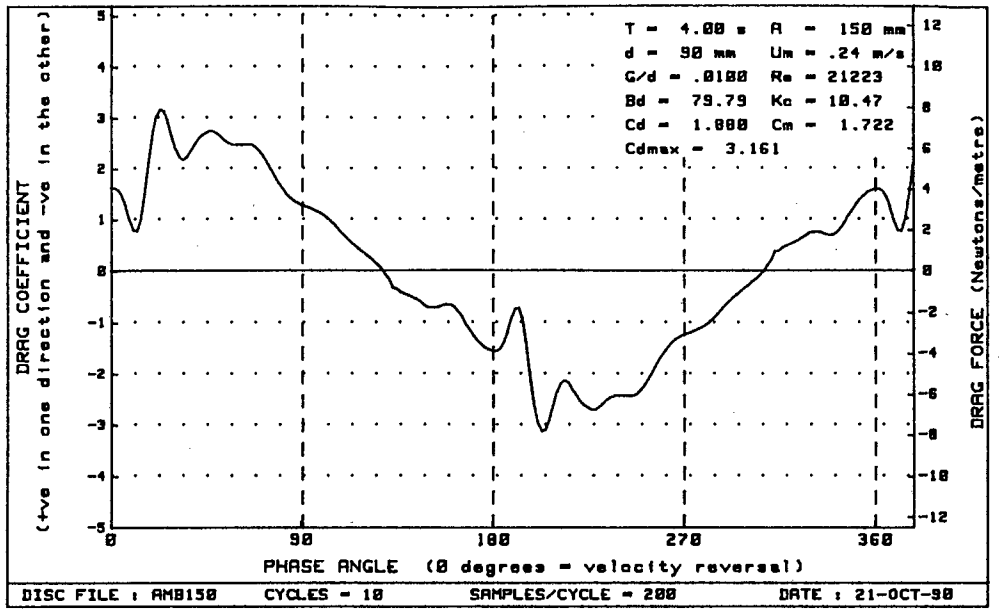

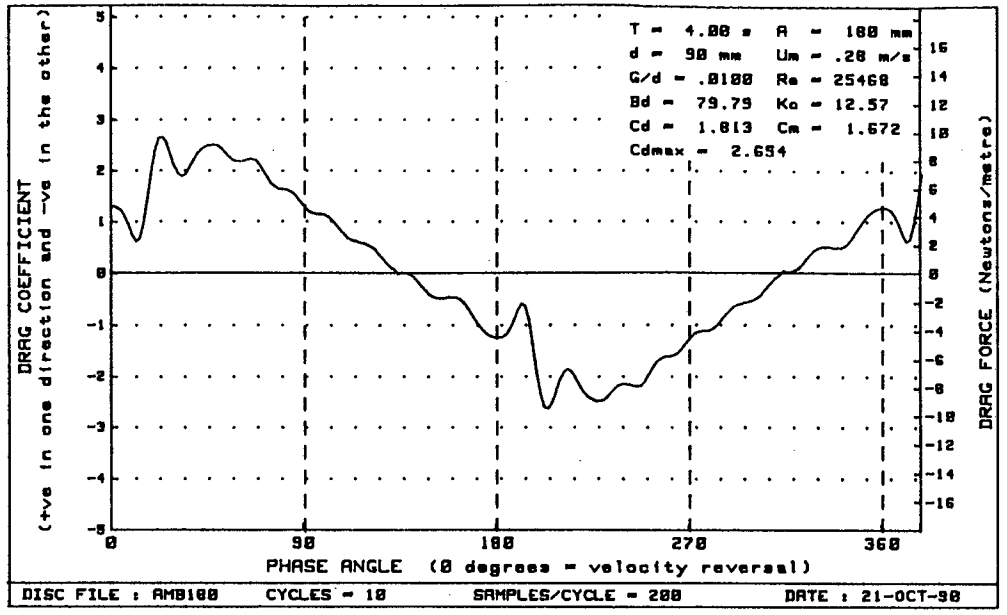

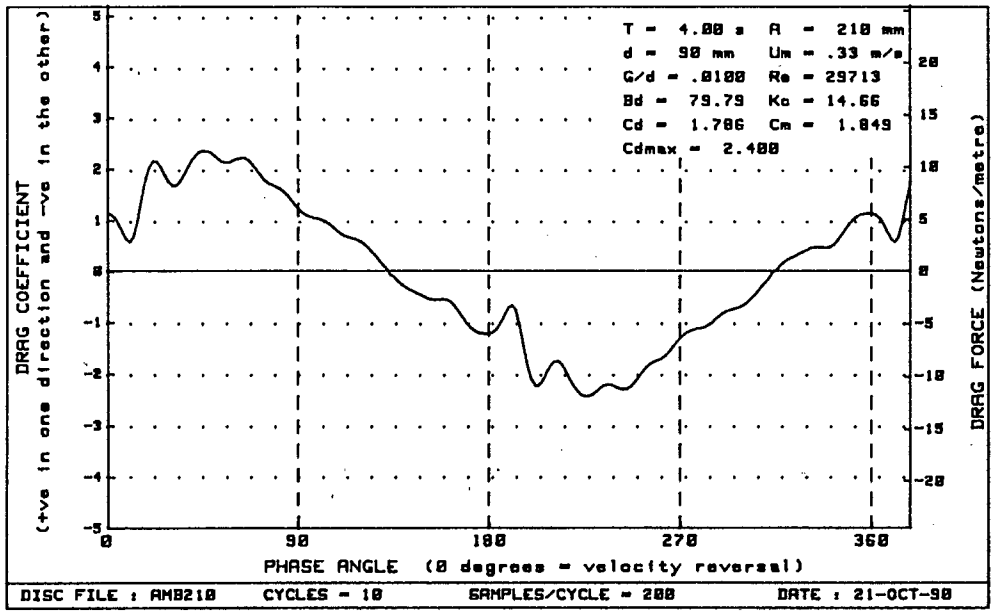

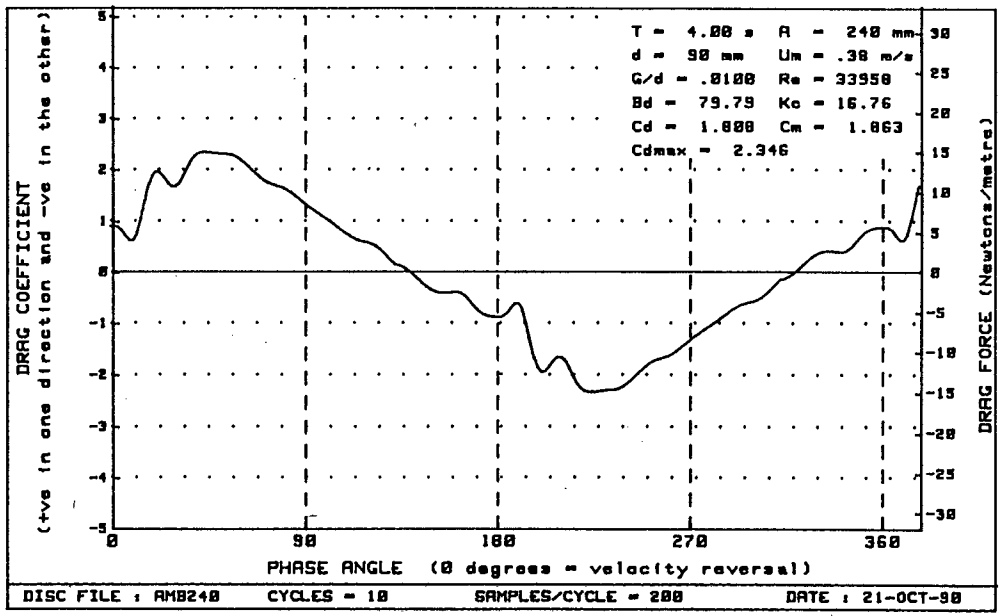

Figure H-2 : Plots of drag vs phase for diameter=90mm, Bd= 79.79 and G/d= .0100

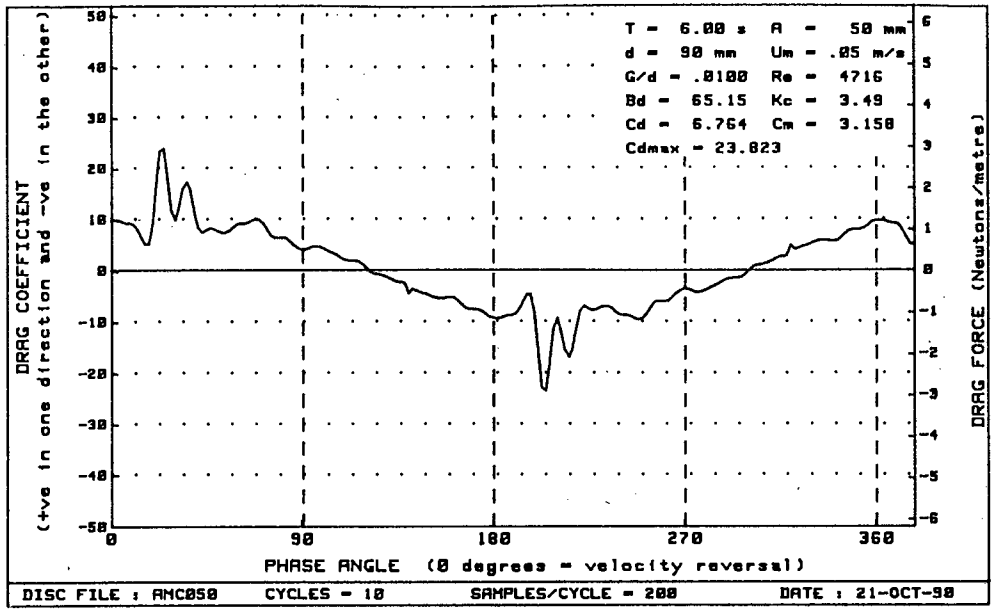

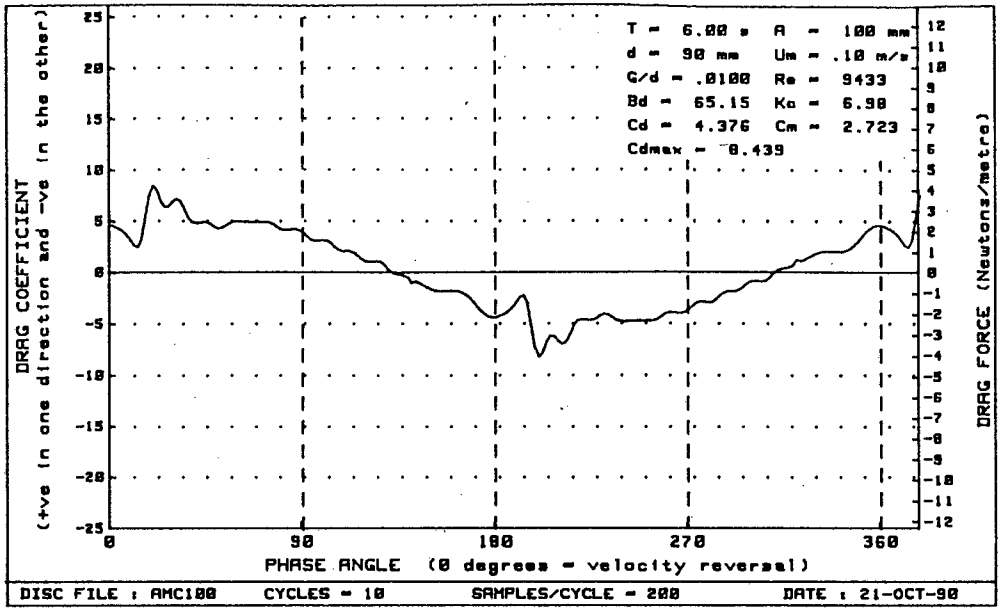

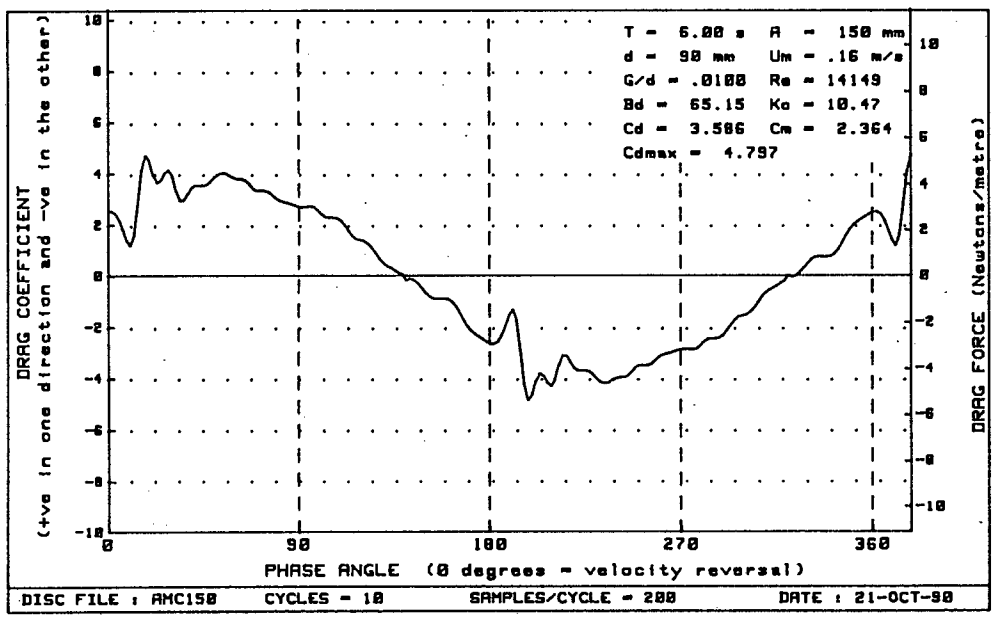

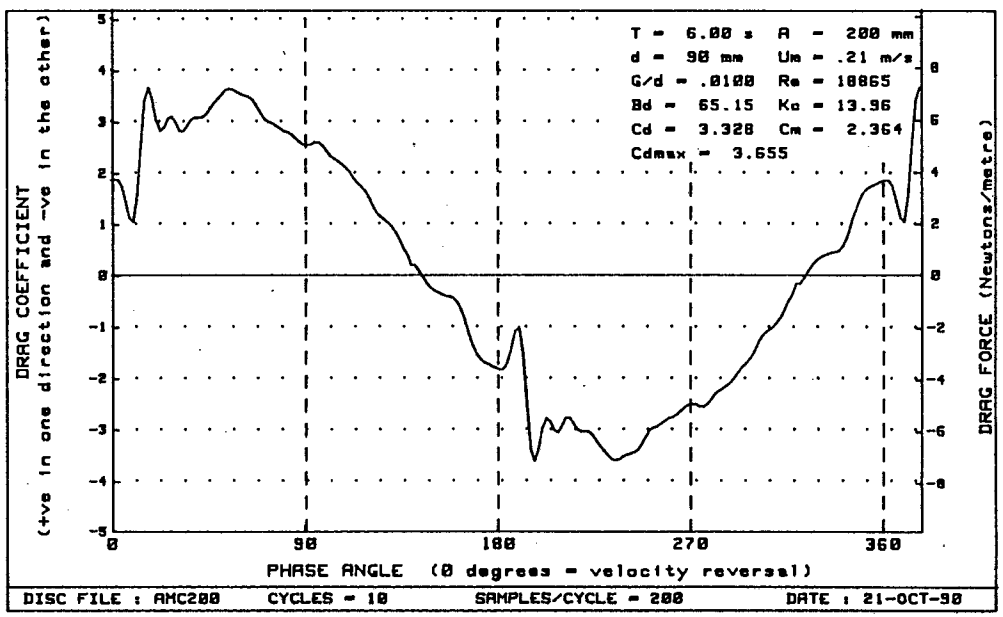

Figure H-3 : Plots of drag vs phase for diameter=90mm, Bd= 65.15 and G/d= .0100

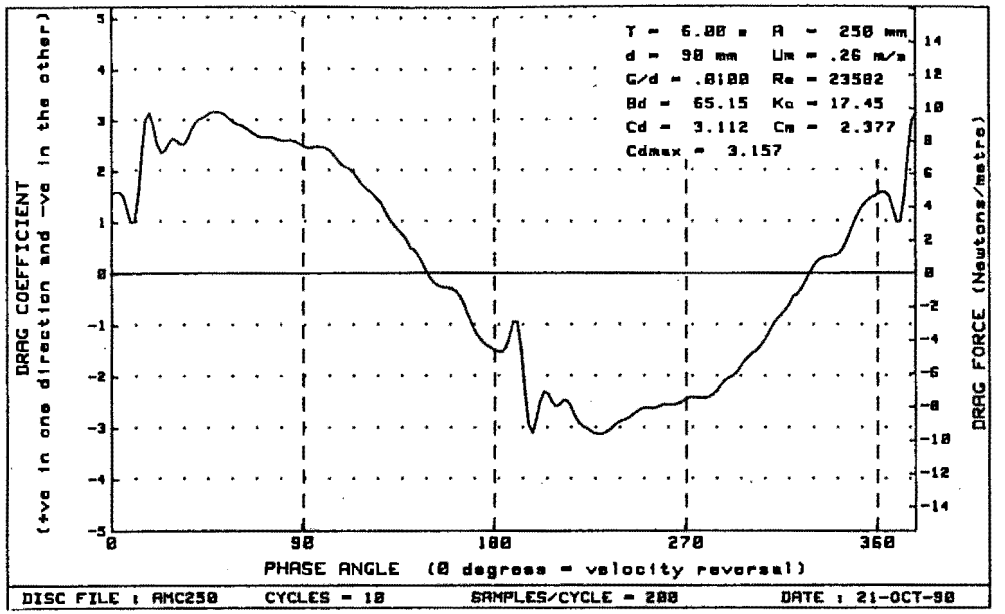

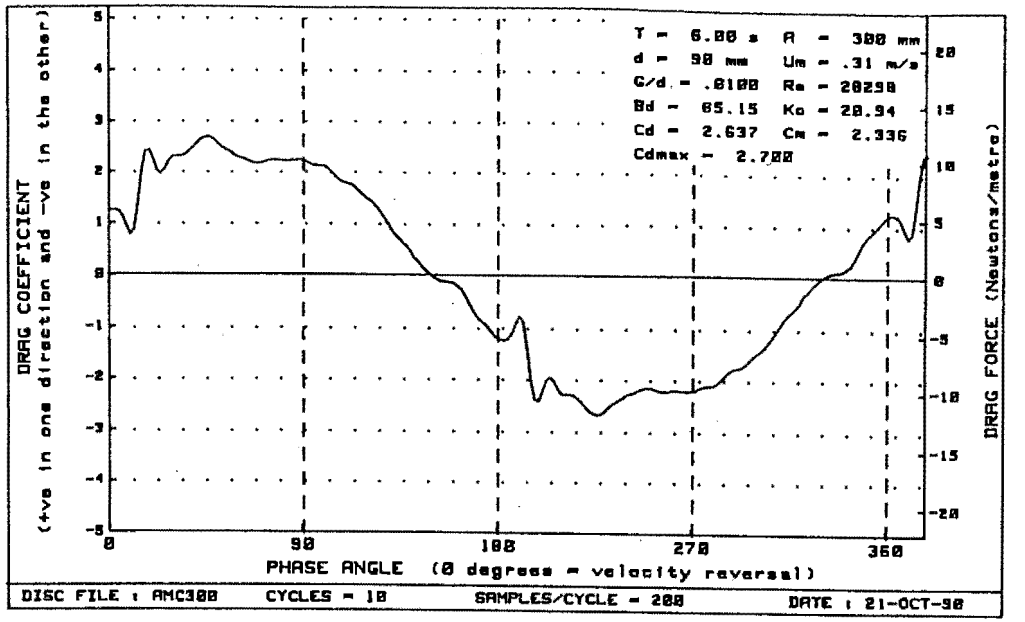

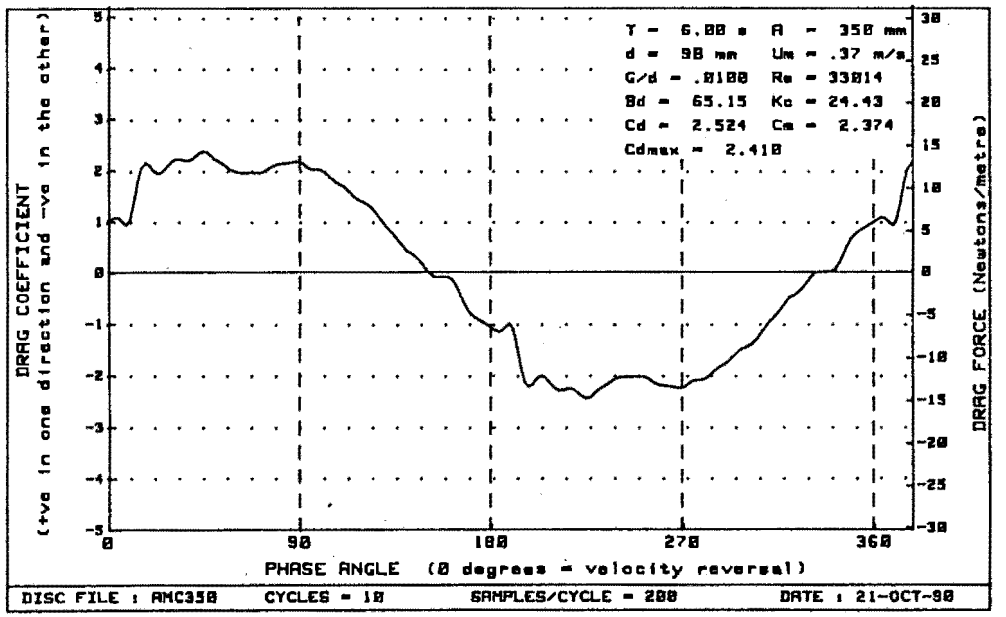

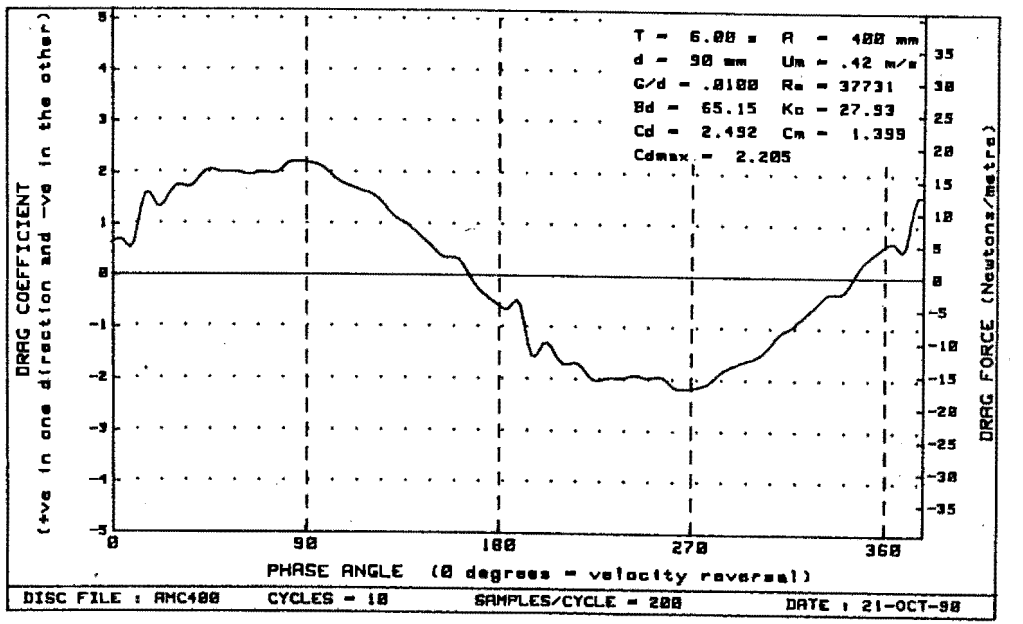

Figure H-4 : Plots of drag vs phase for diameter=90mm, Bd= 65.15 and G/d= .0100

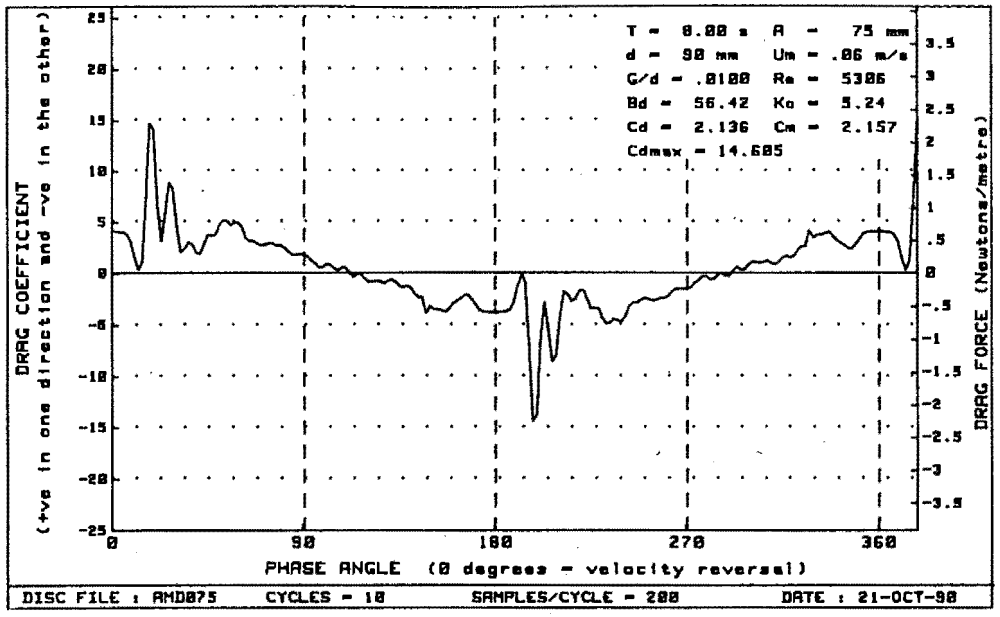

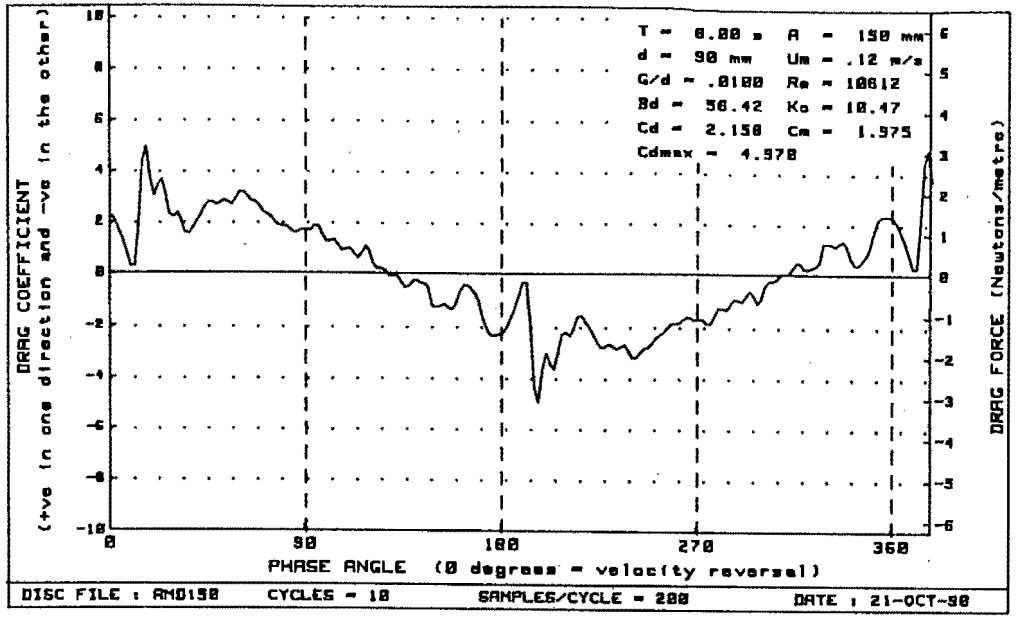

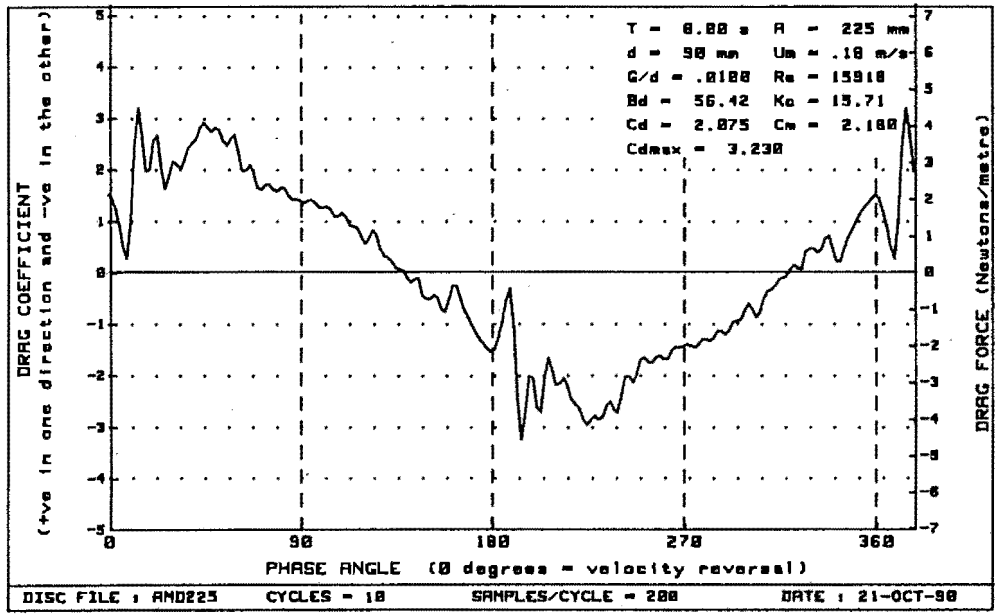

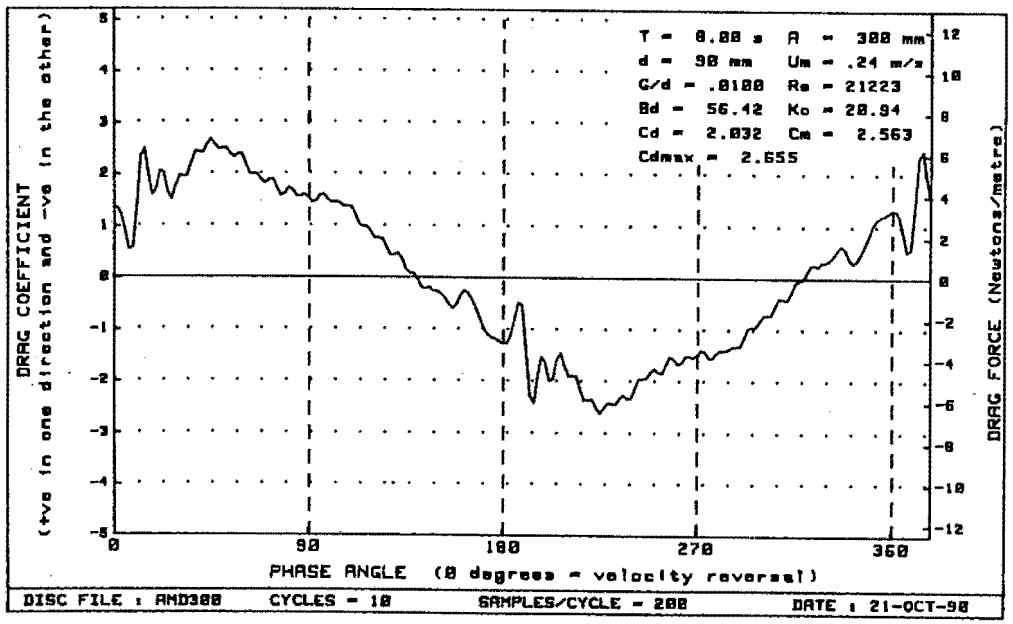

Figure H-5 : Plots of drag vs phase for diameter=90mm, Bd= 56.42 and G/d= .0100

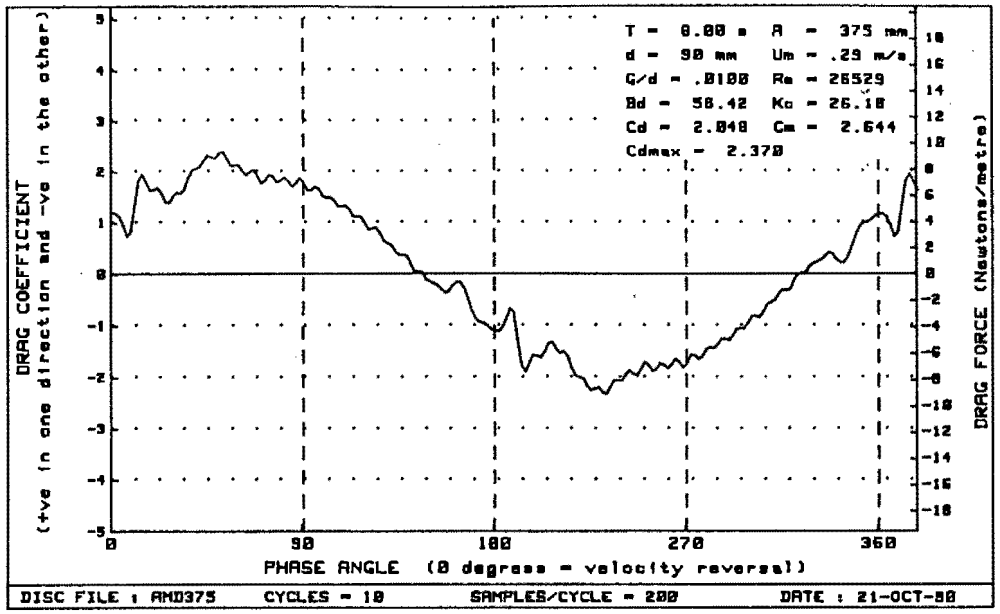

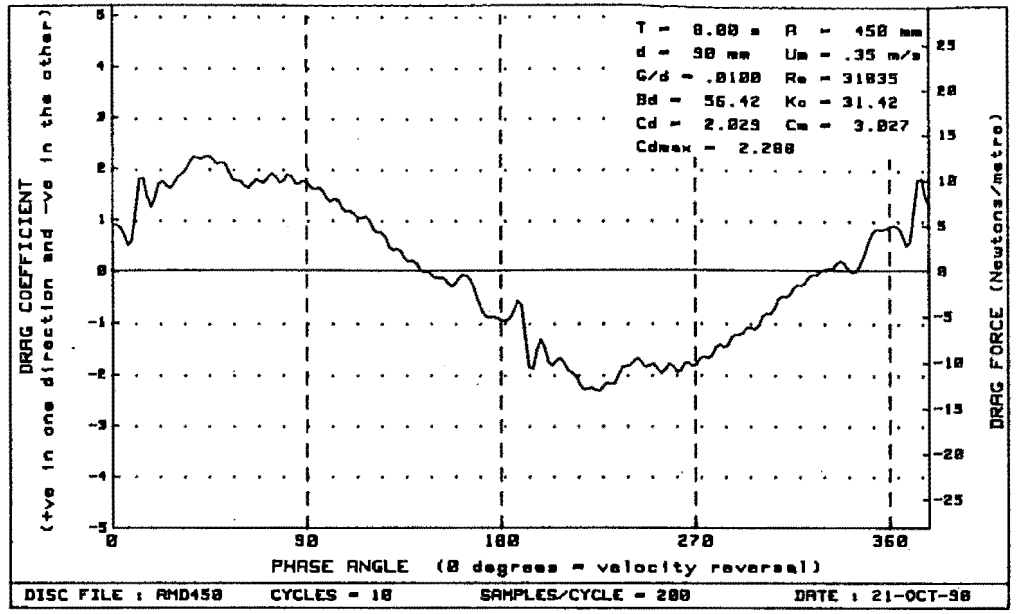

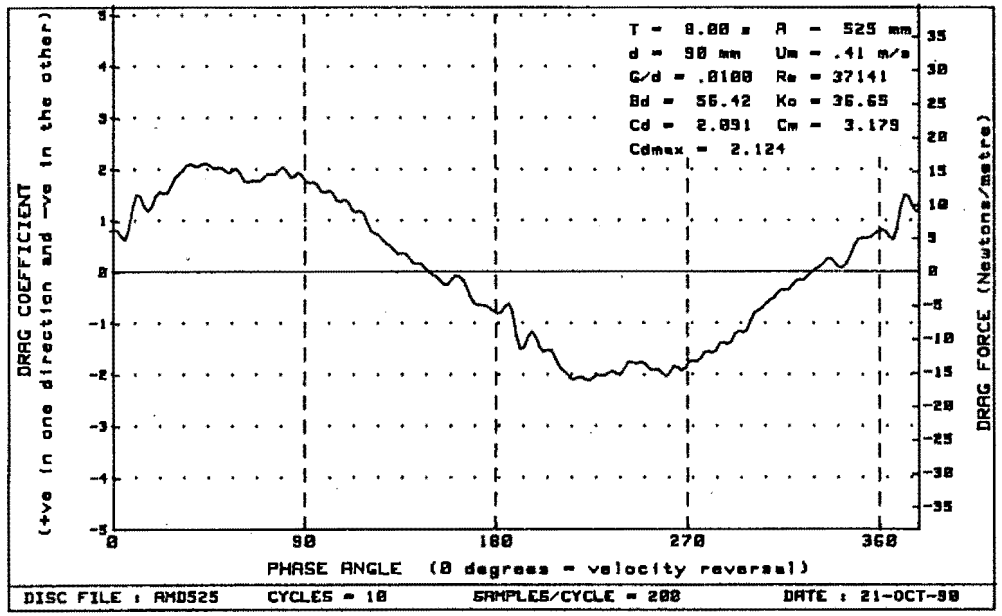

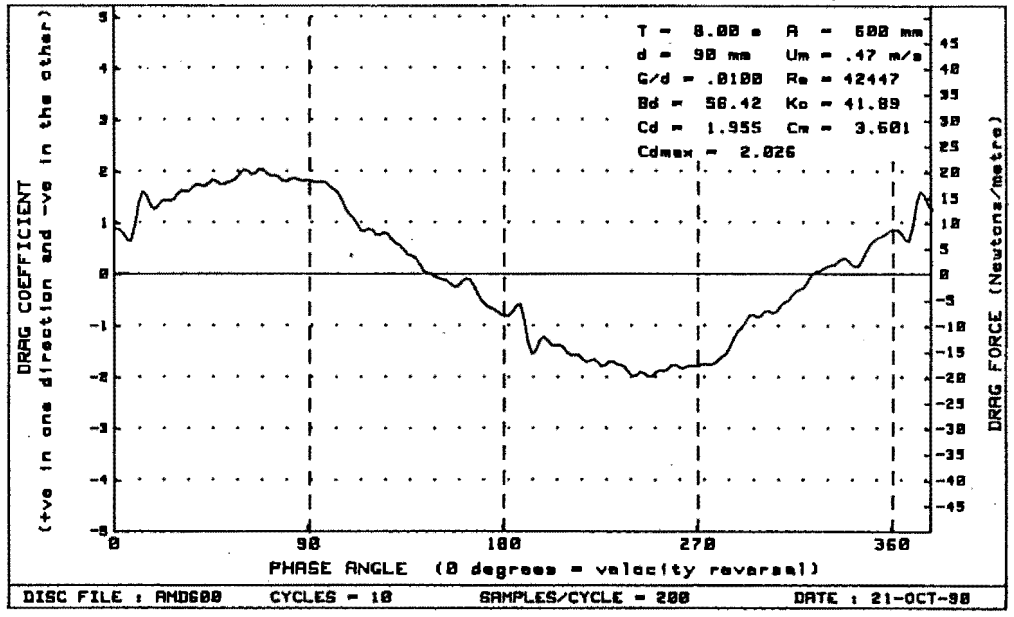

Figure H-6 : Plots of drag vs phase for diameter=90mm, Bd= 56.42 and G/d= .0100

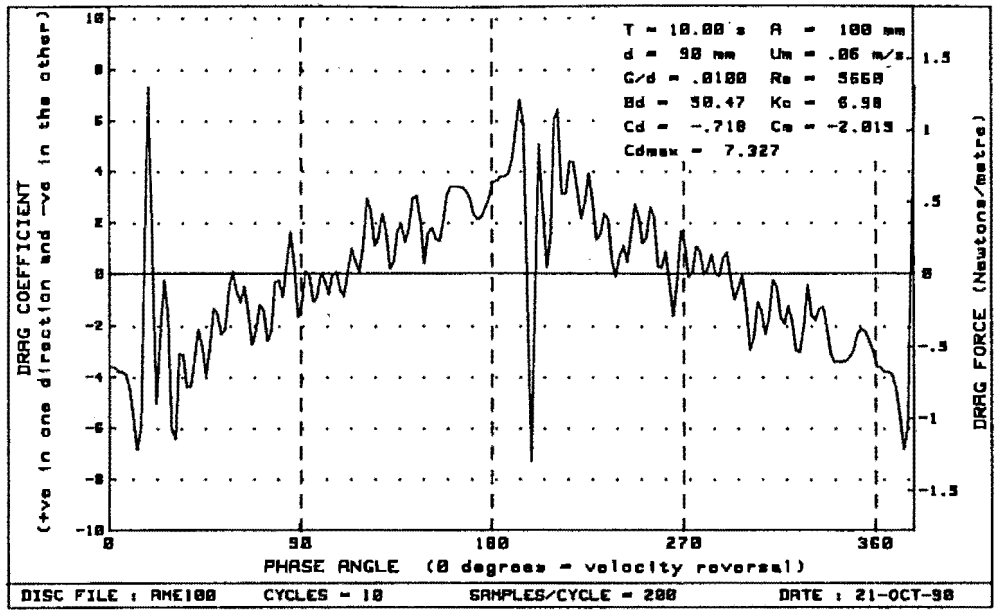

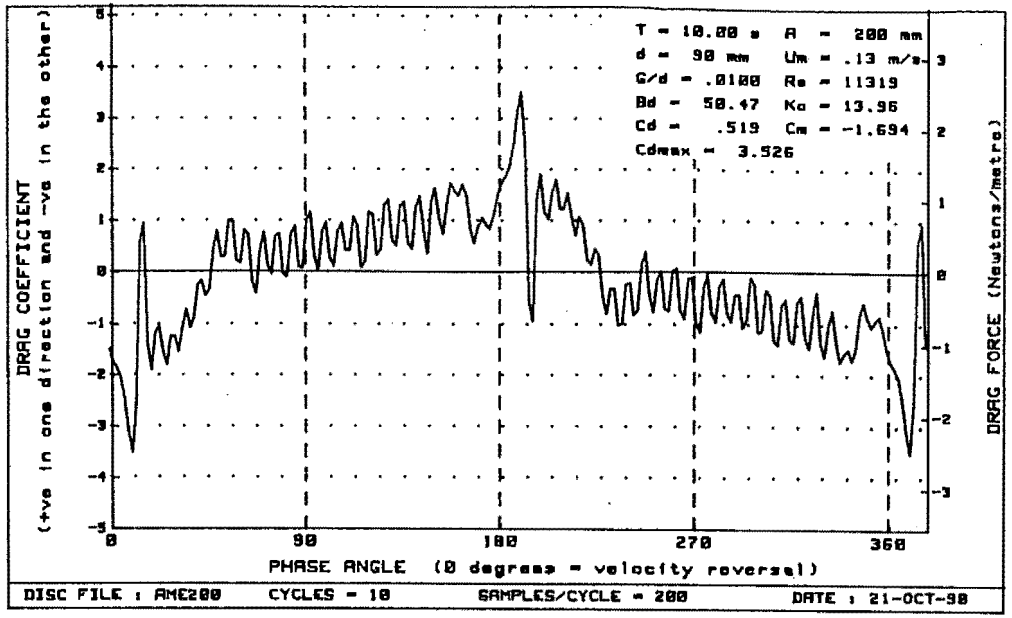

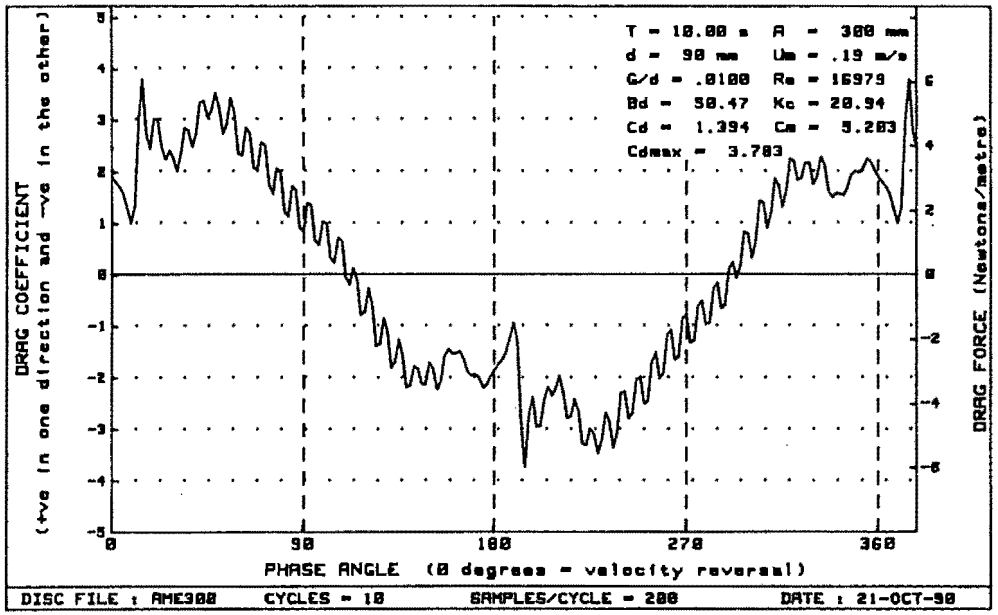

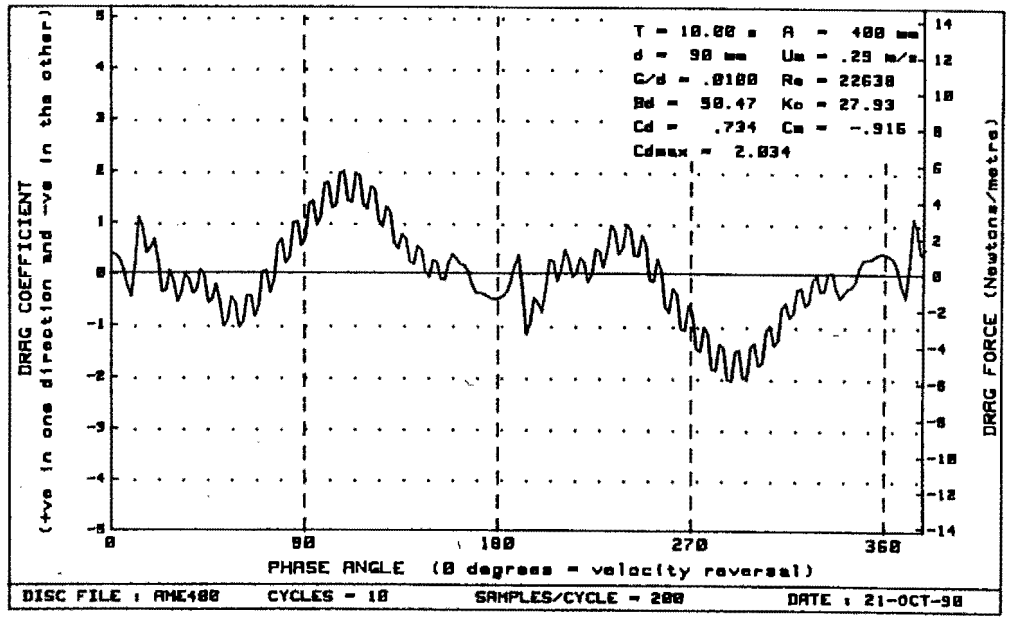

Figure H-7 : Plots of drag vs phase for diameter=90mm, Bd= 50.47 and G/d= .0100

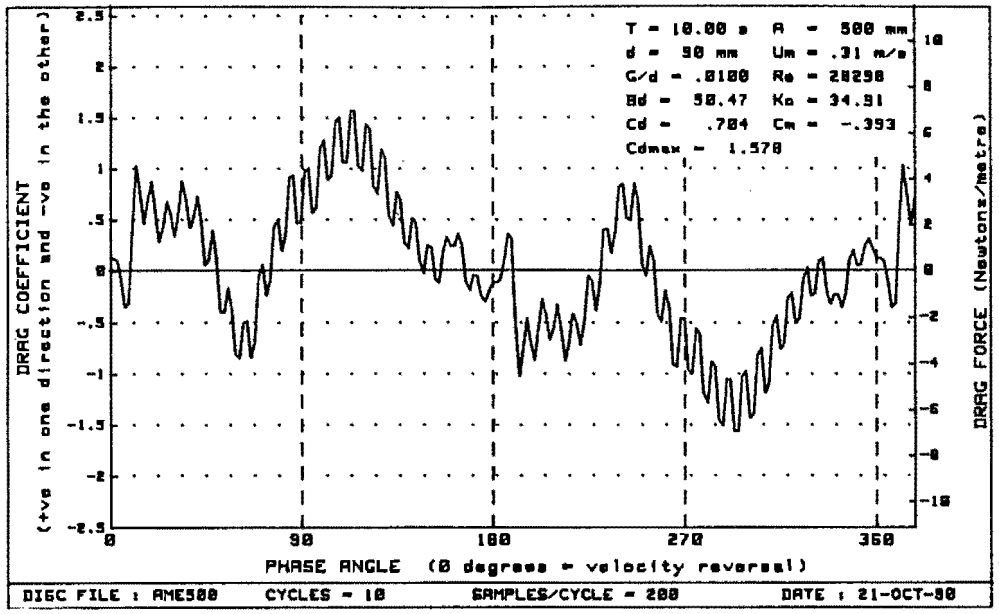

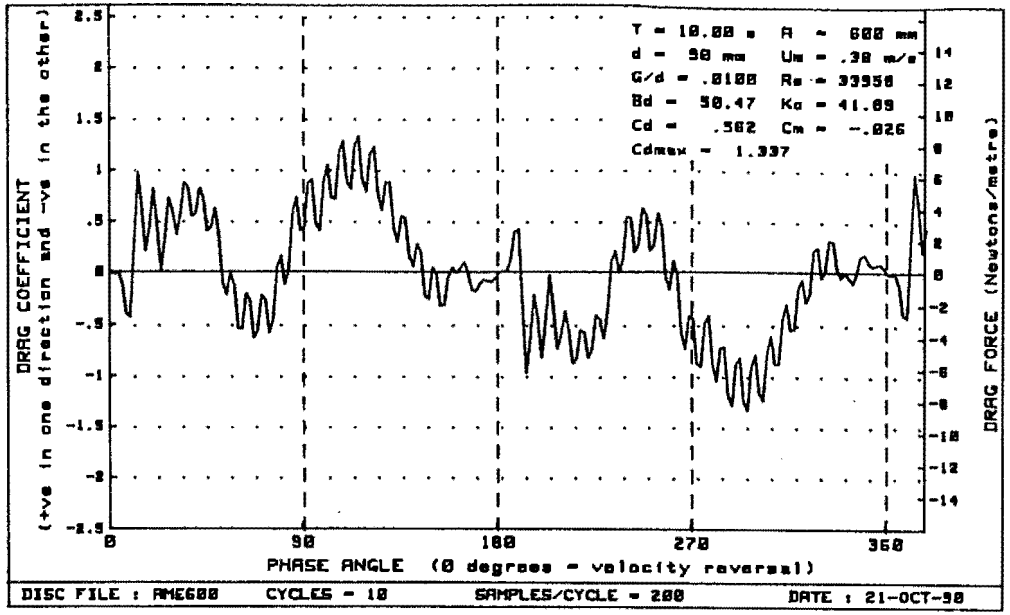

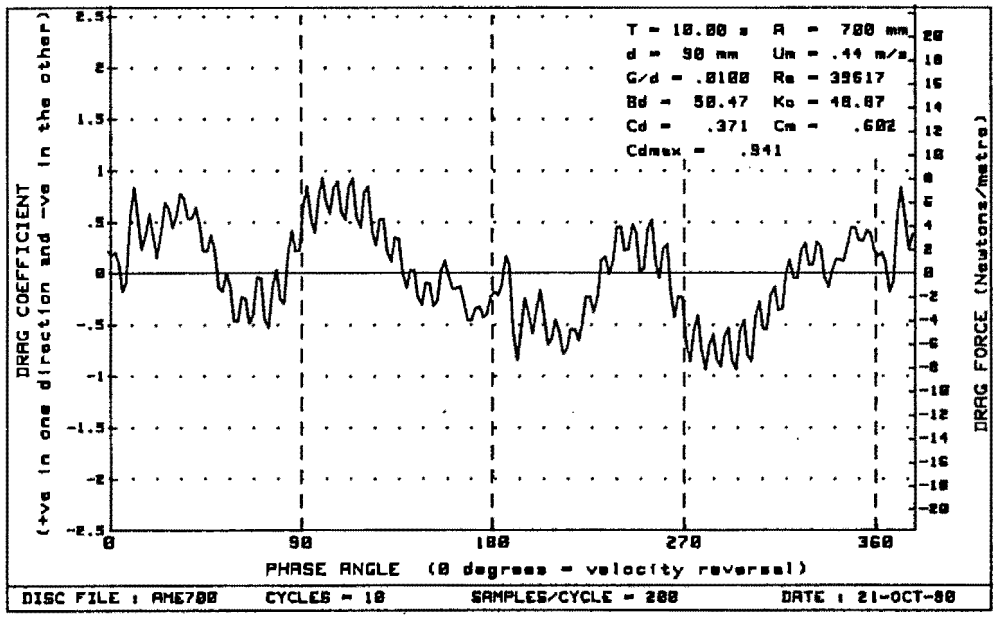

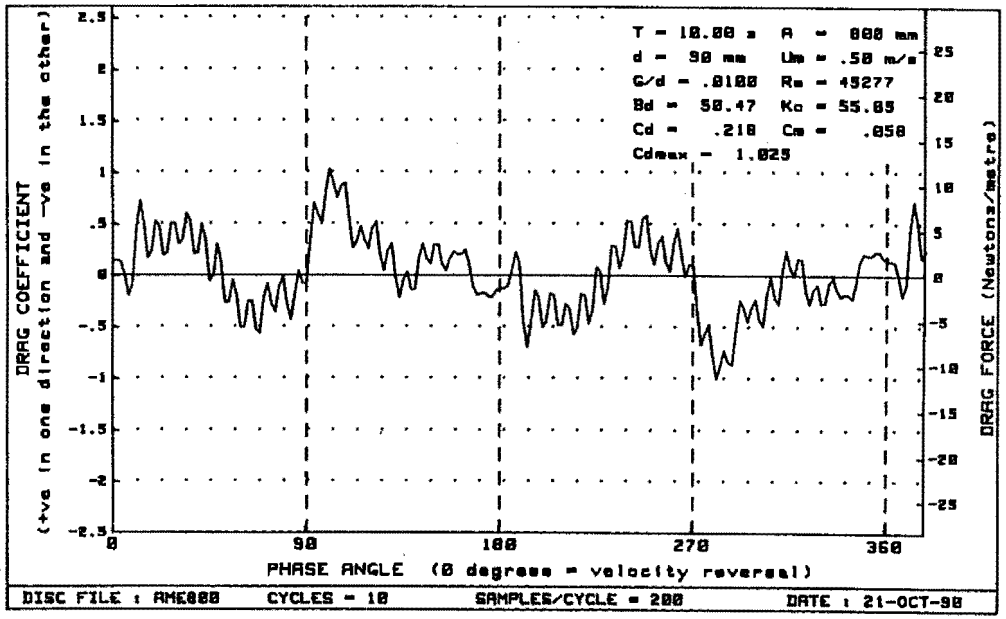

Figure H-8 : Plots of drag vs phase for diameter=90mm, Bd= 50.47 and G/d= .0100

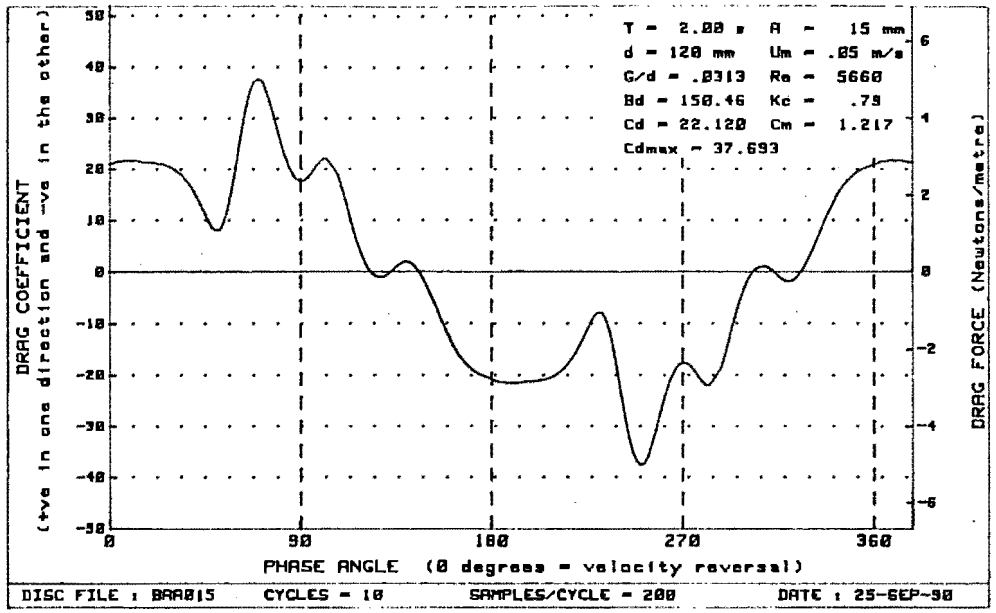

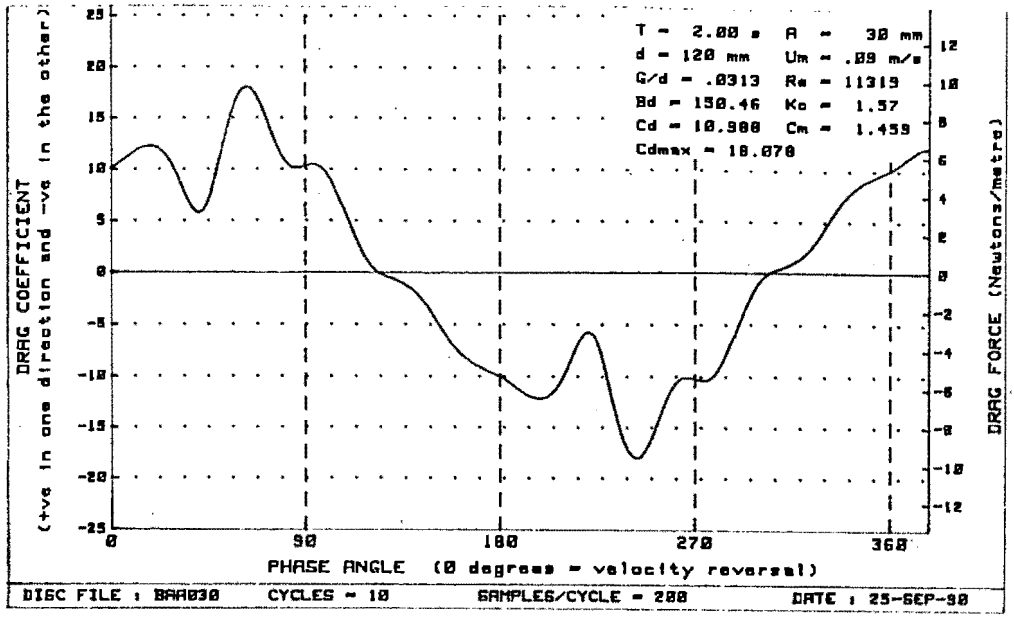

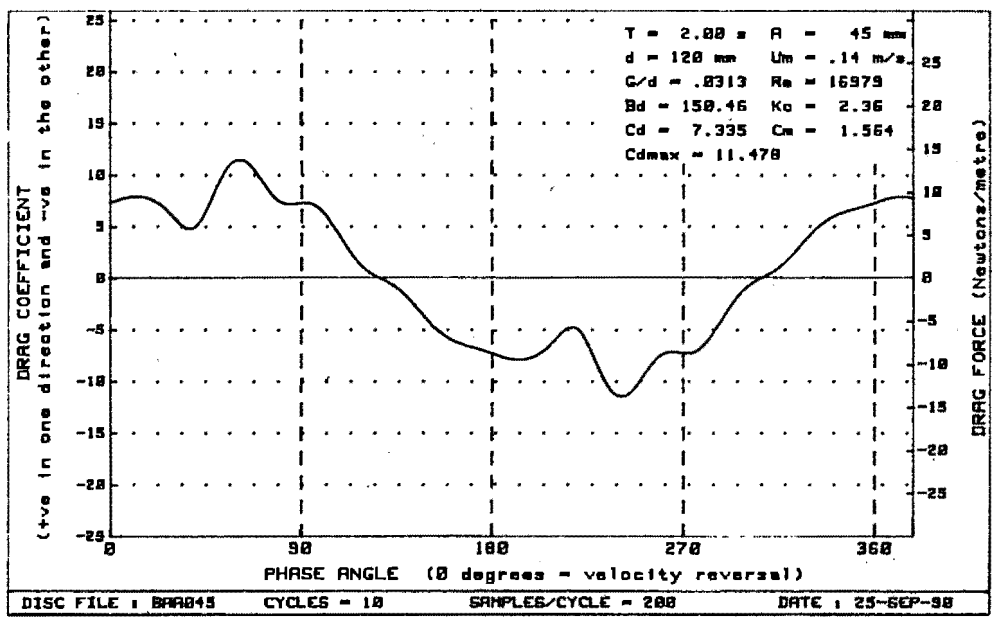

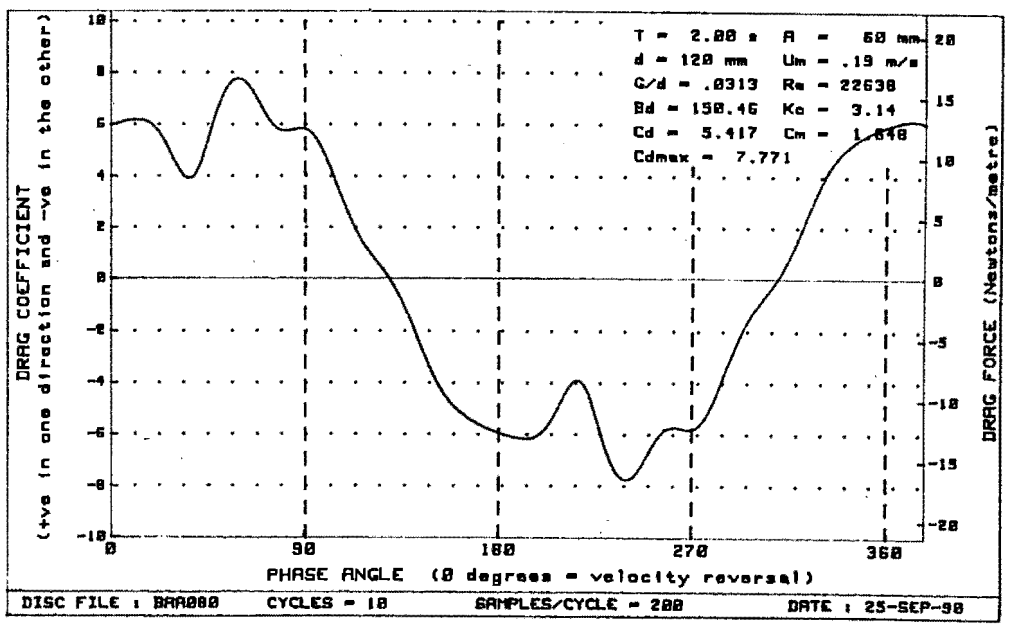

Figure H - 9 : Plots of drag vs phase for diameter=120mm, Bd=150.46 and G/d= .0313

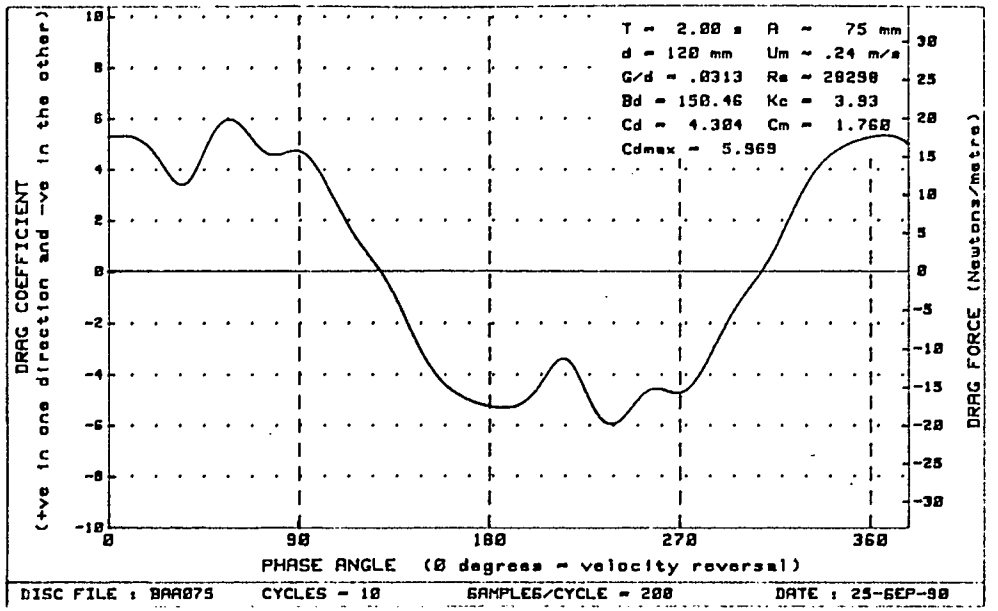

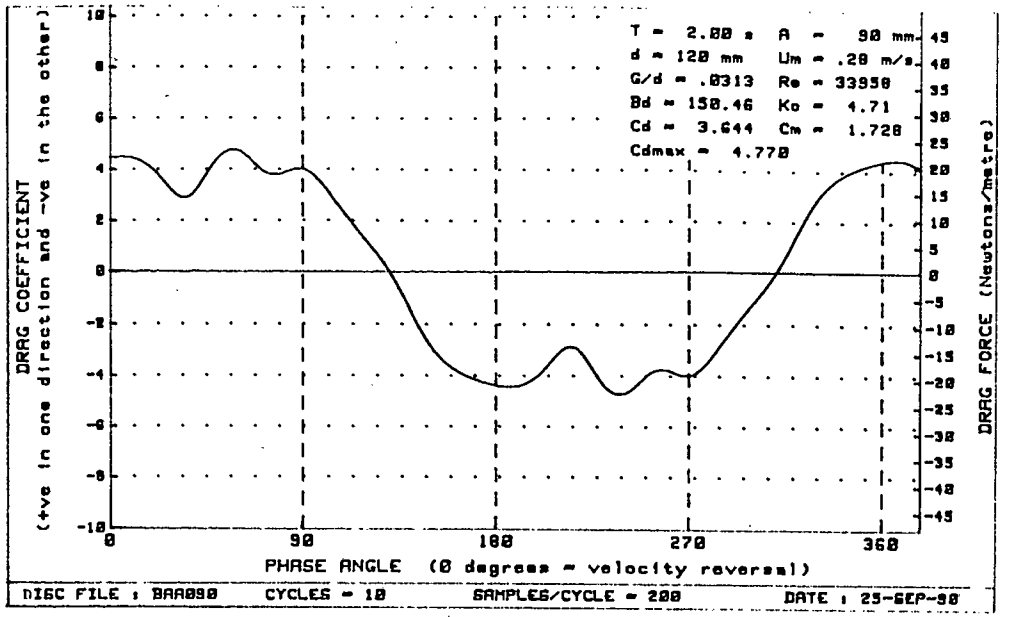

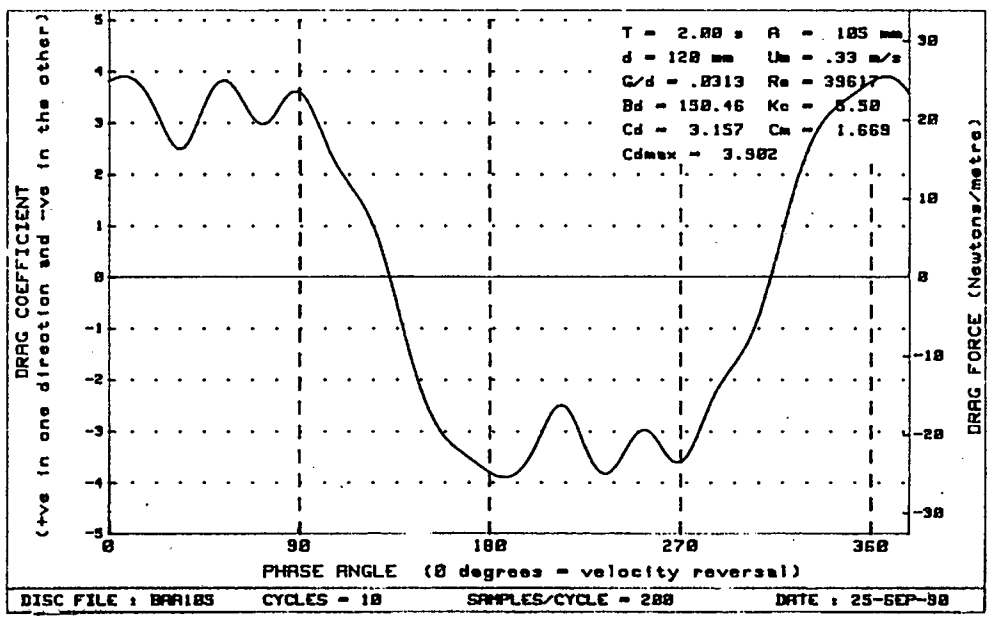

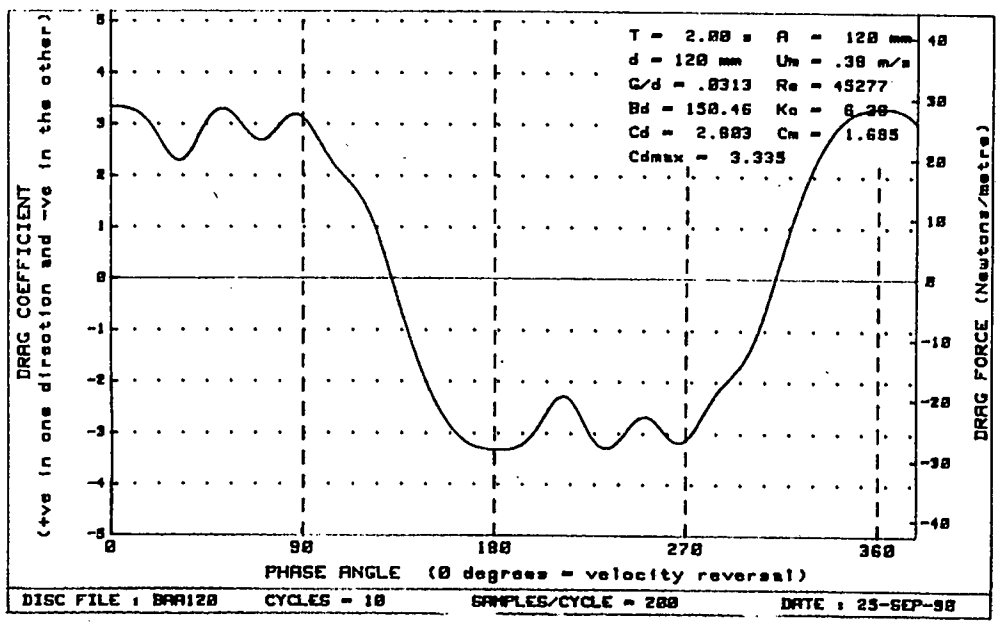

Figure H - 10 : Plots of drag vs phase for diameter=120mm, Bd=150.46 and G/d= .0313

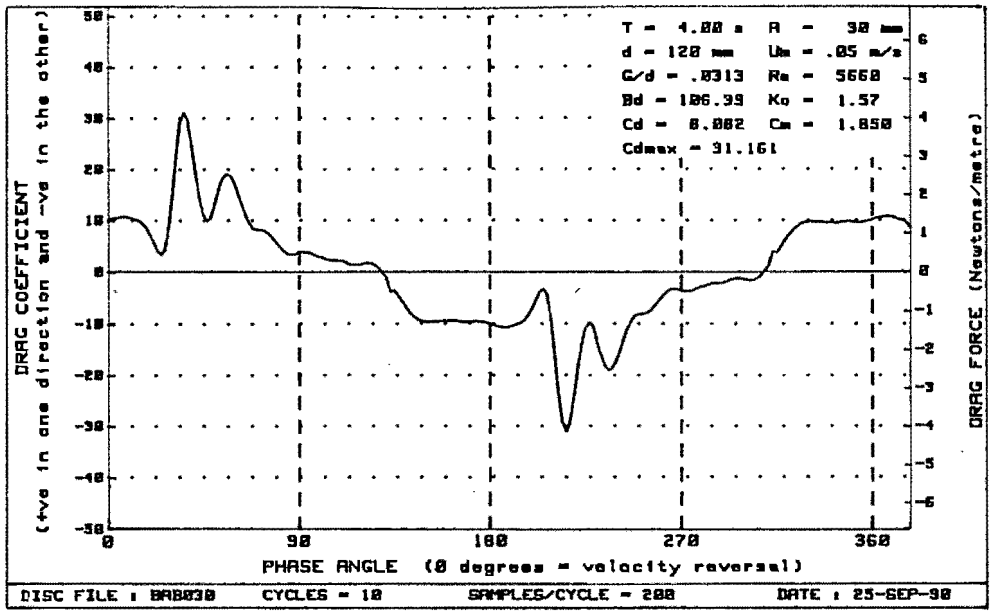

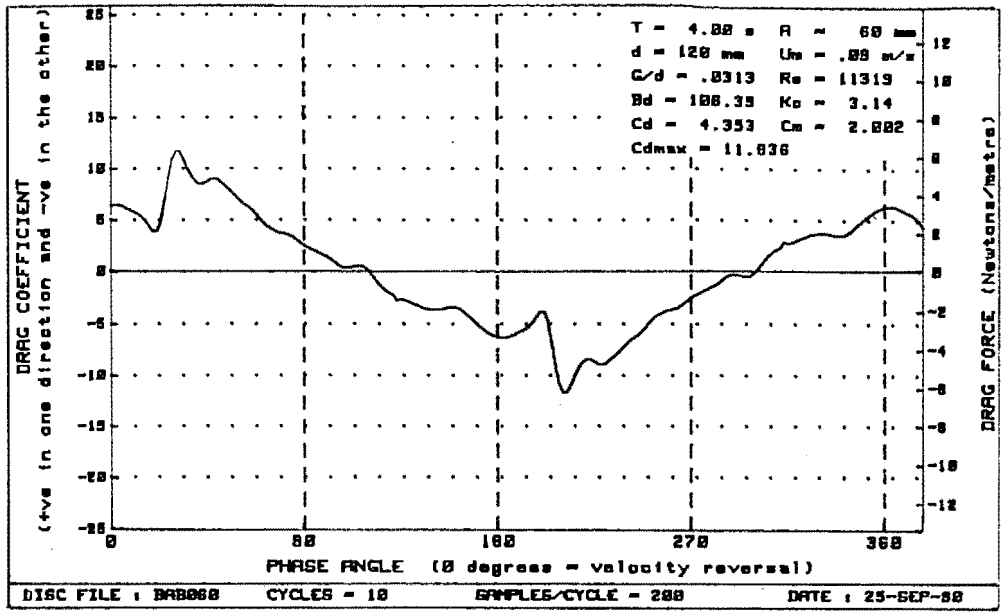

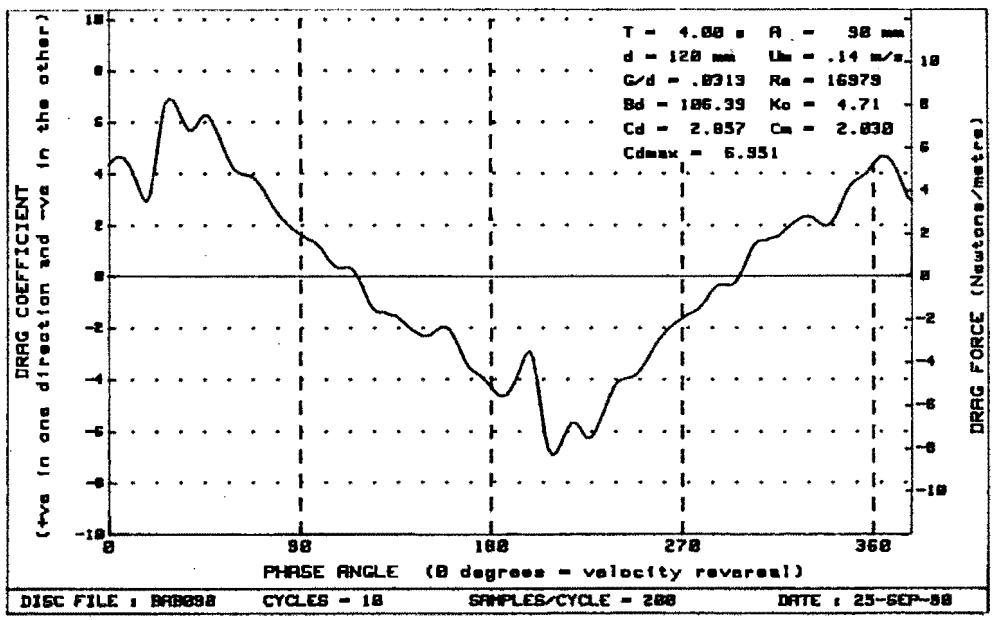

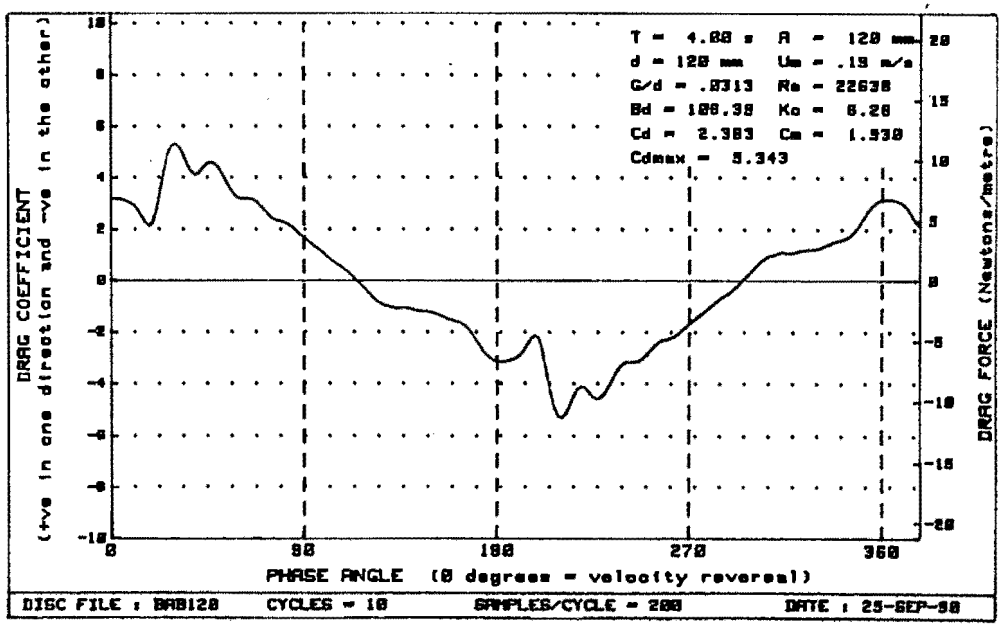

Figure H – 11 : Plots of drag vs phase for diameter=120mm, Bd=106.39 and G/d= .0313

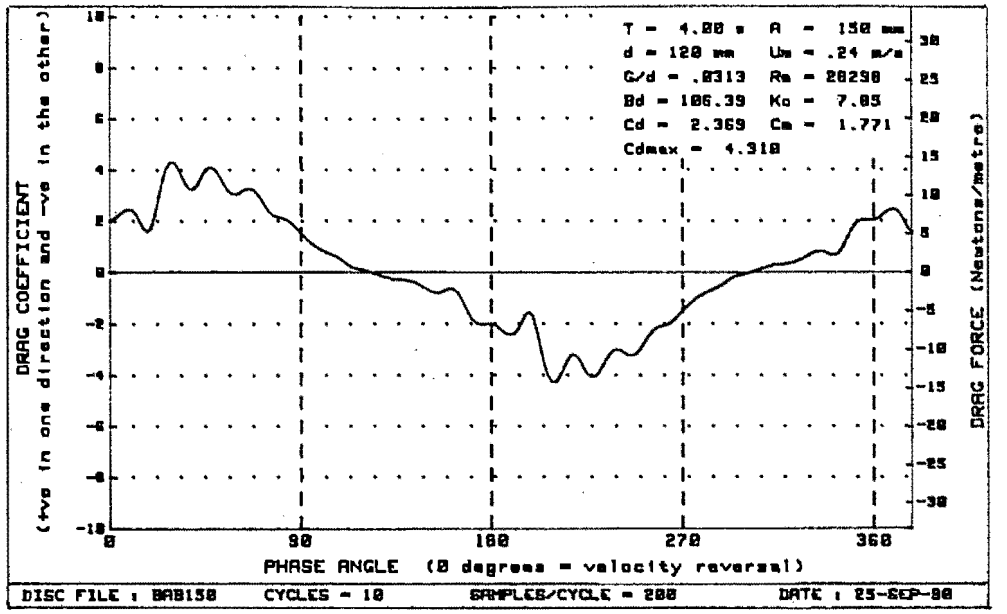

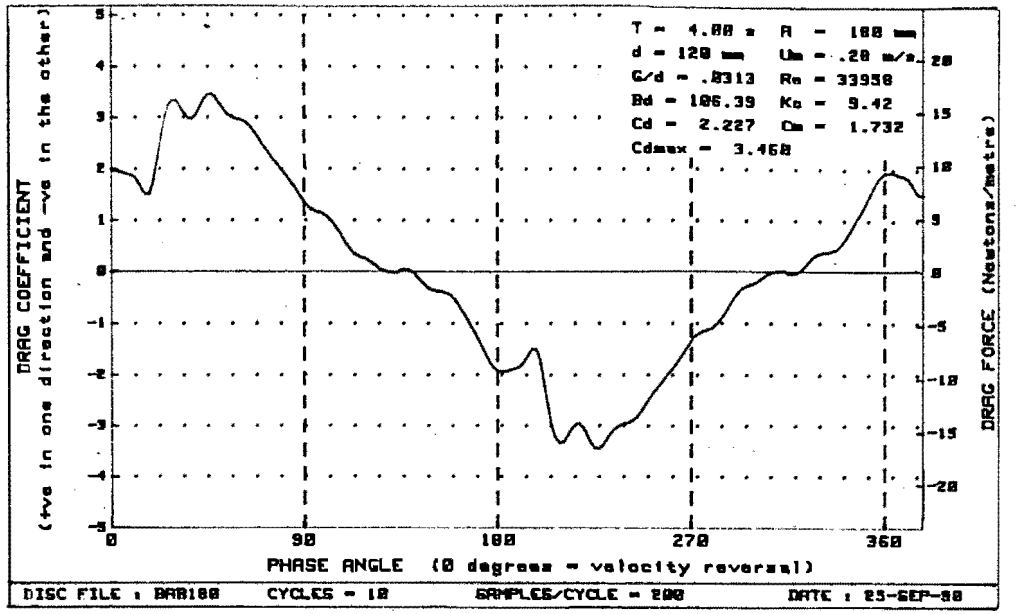

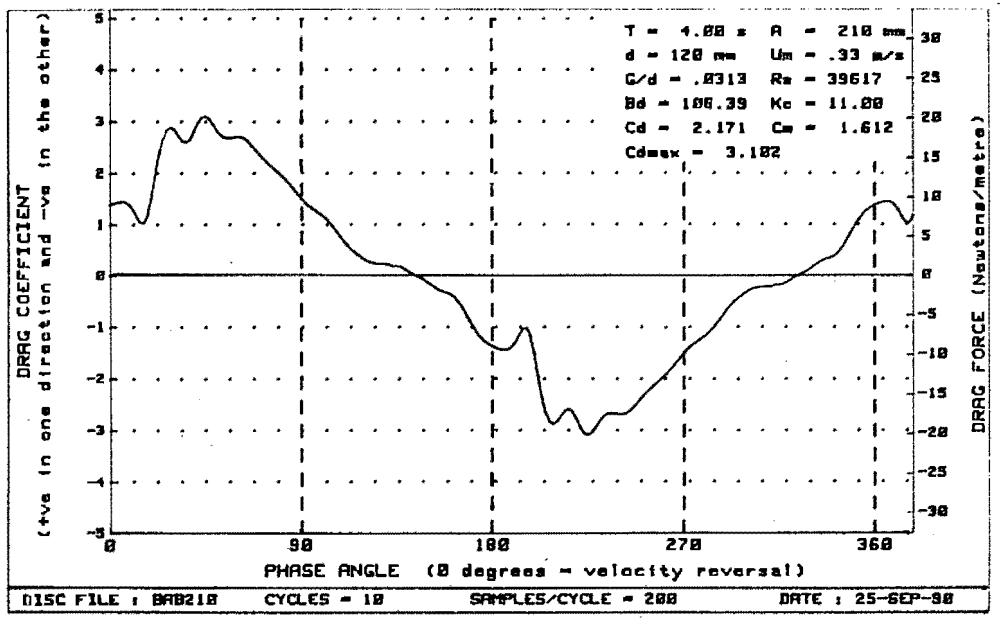

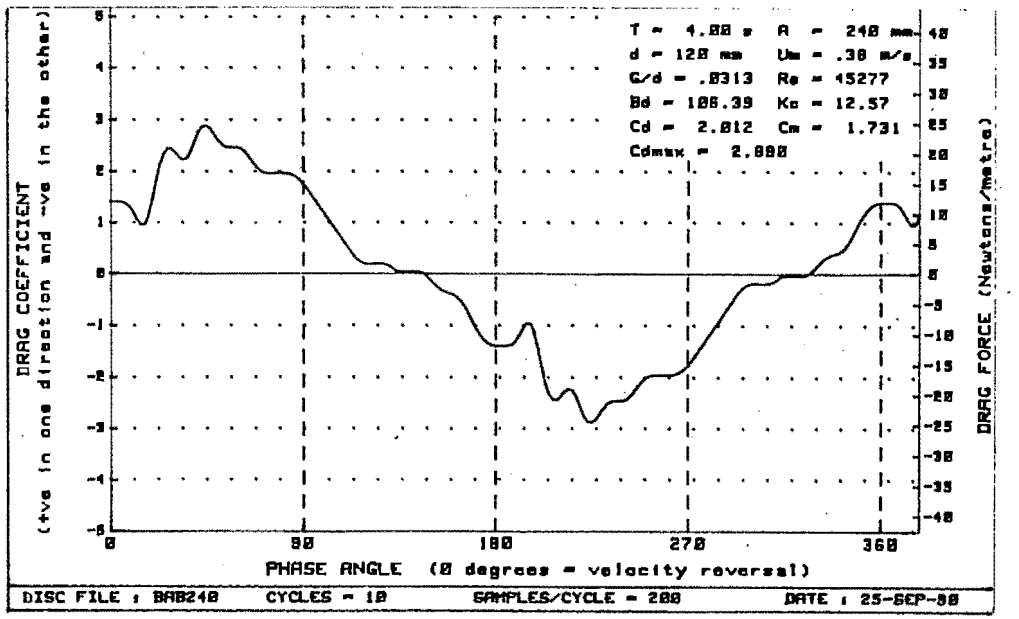

Figure H - 12 : Plots of drag vs phase for diameter=120mm, Bd=106.39 and G/d= .0313

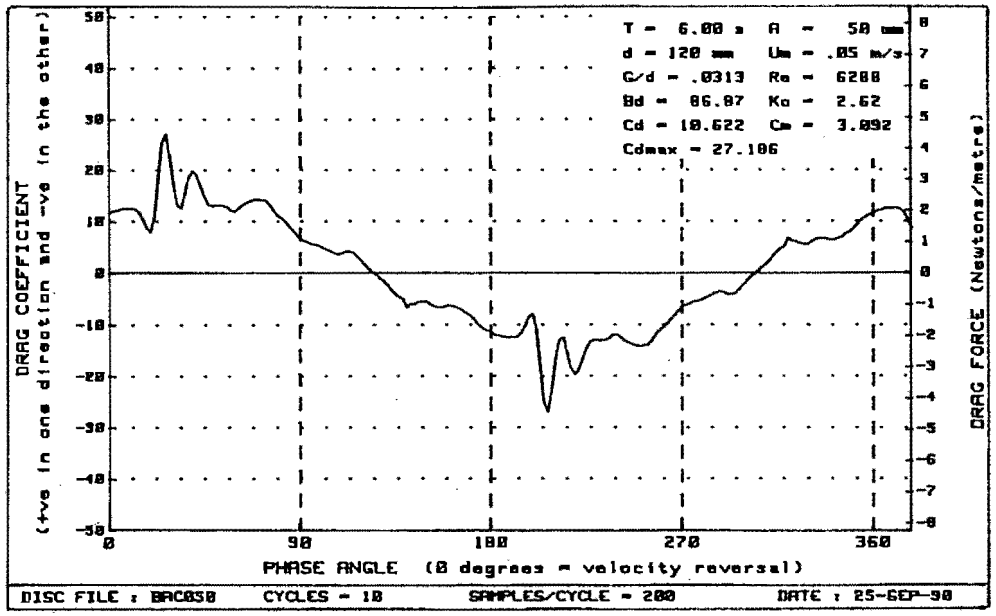

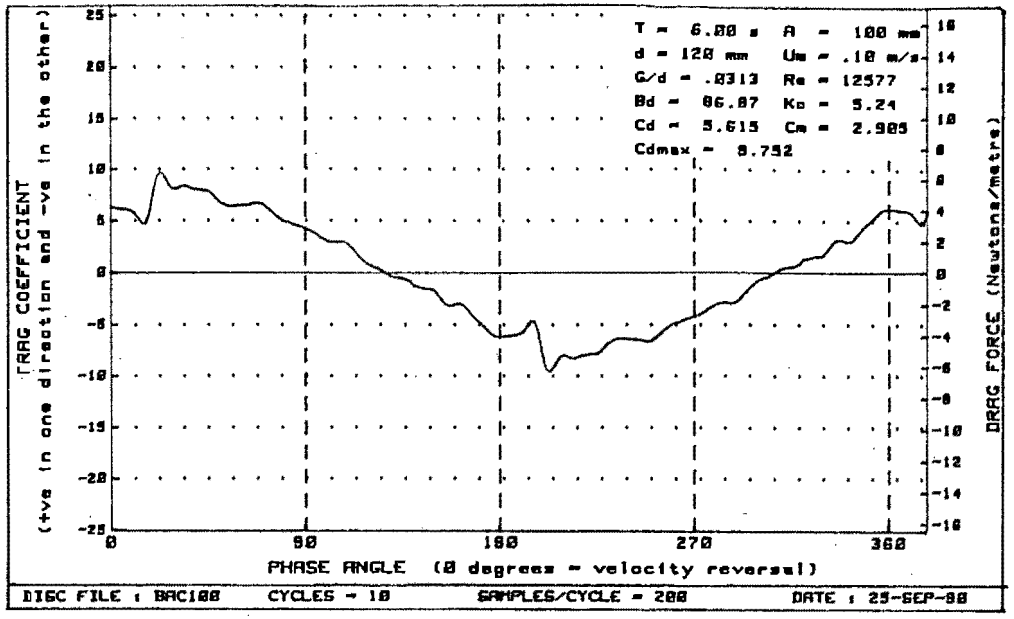

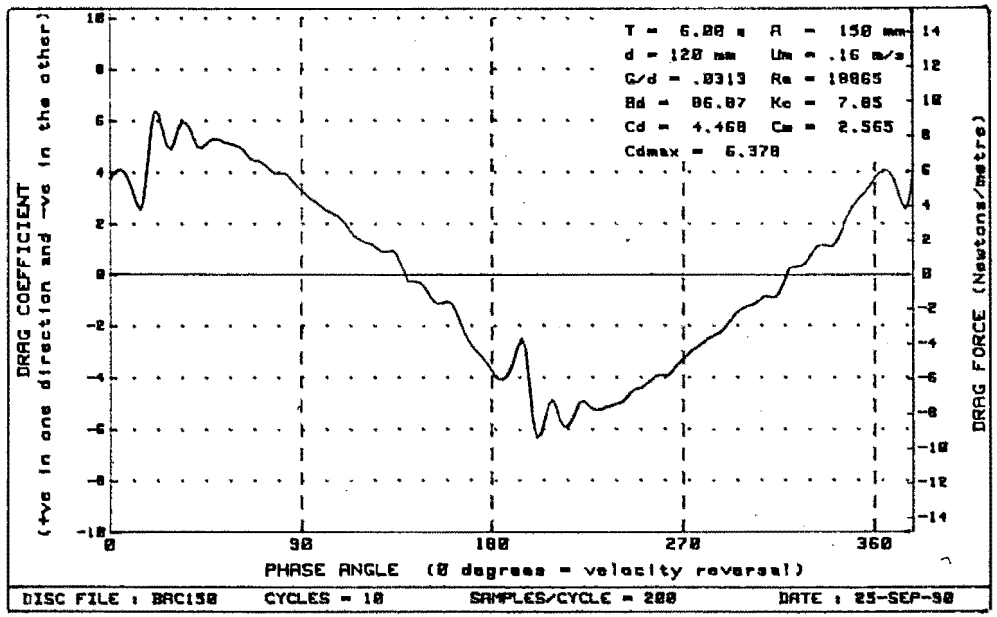

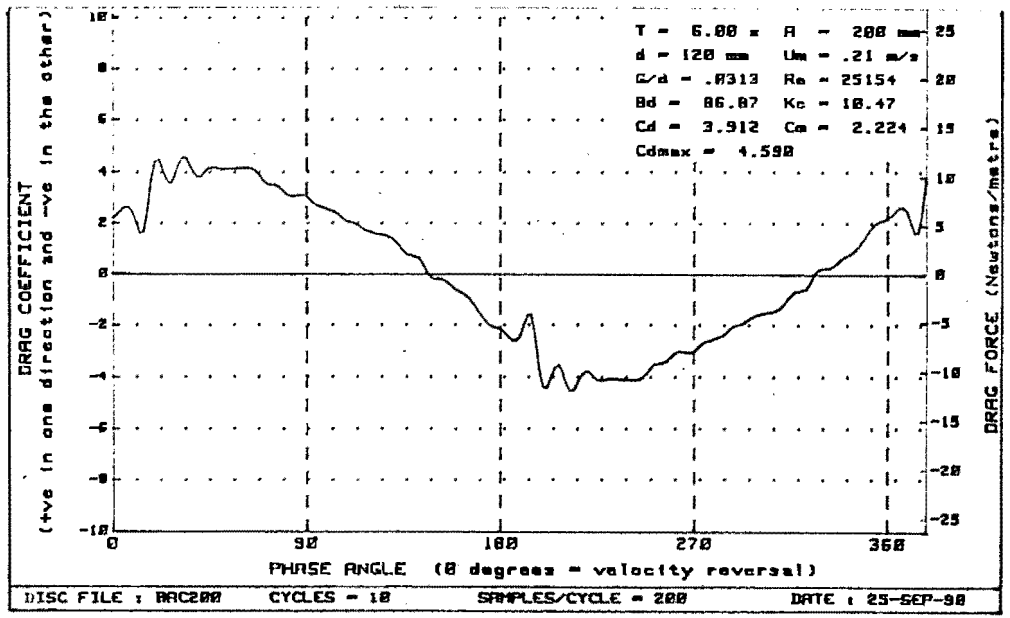

Figure H - 13 : Plots of drag vs phase for diameter=120mm, Bd= 86.87 and G/d= .0313

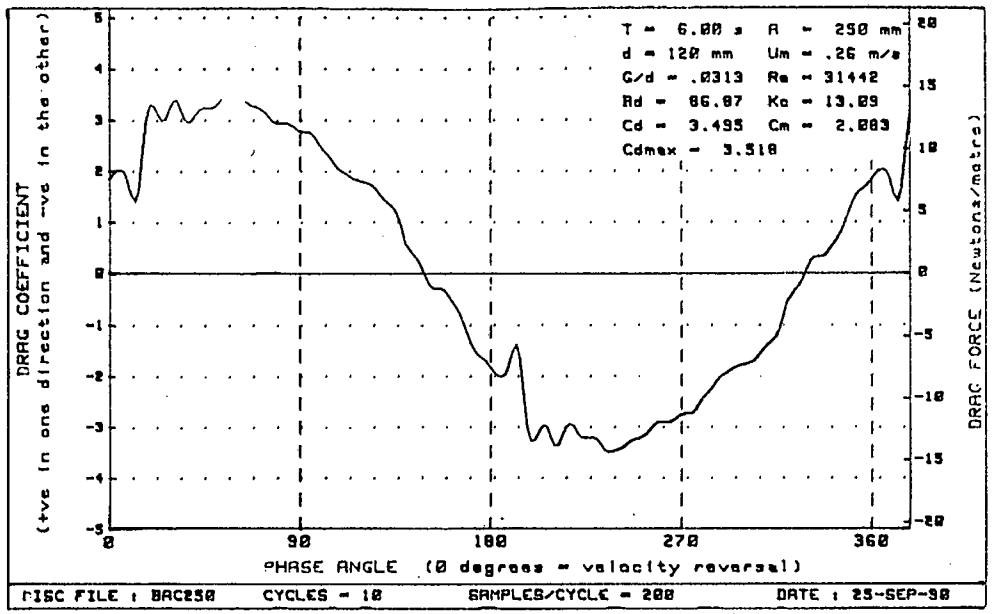

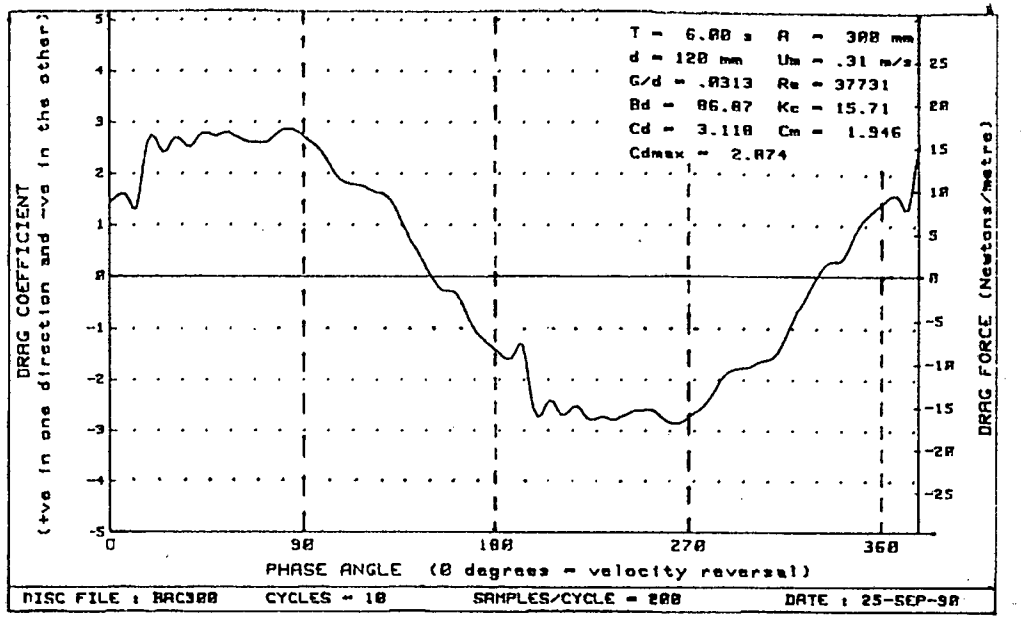

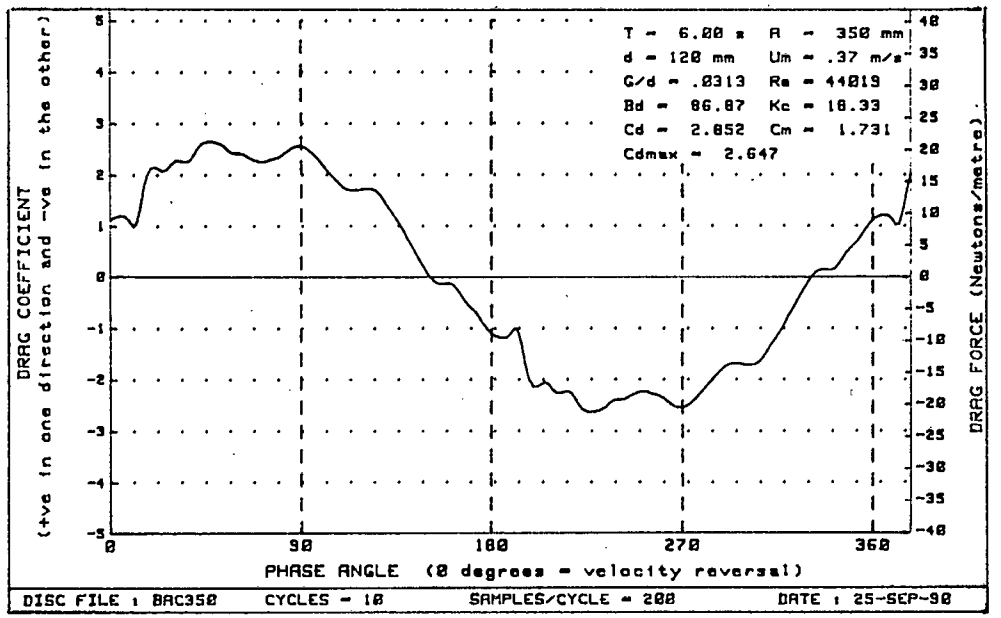

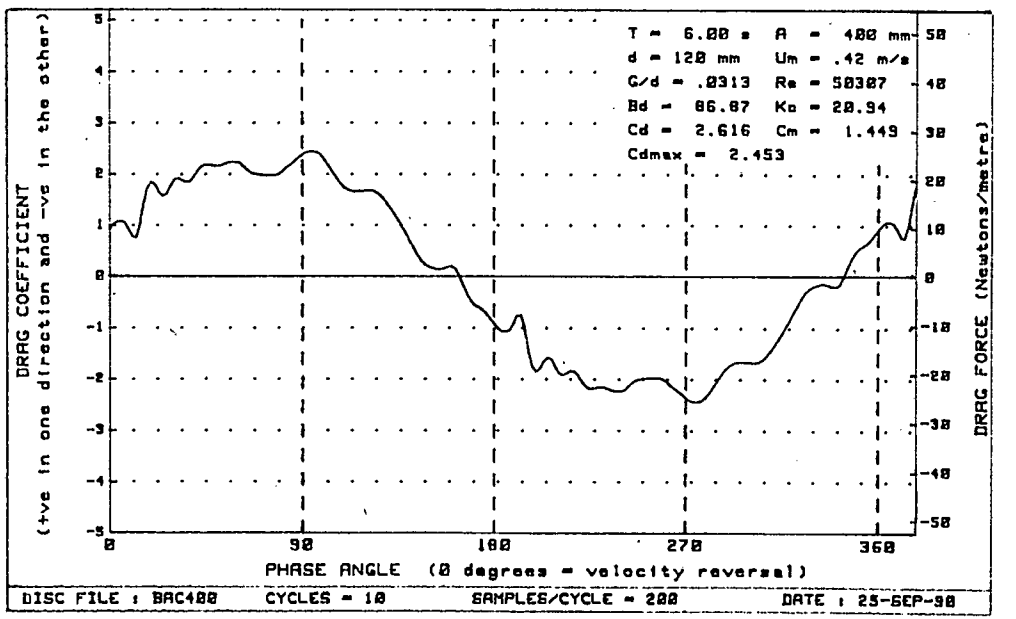

Figure H – 14 : Plots of drag vs phase for diameter=120mm, Bd= 86.87 and G/d= .0313

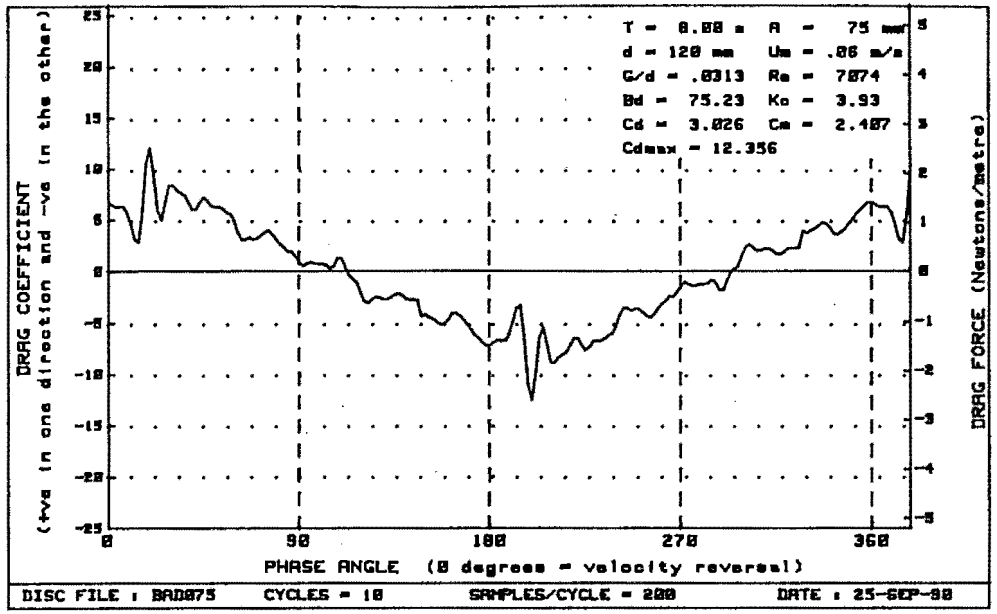

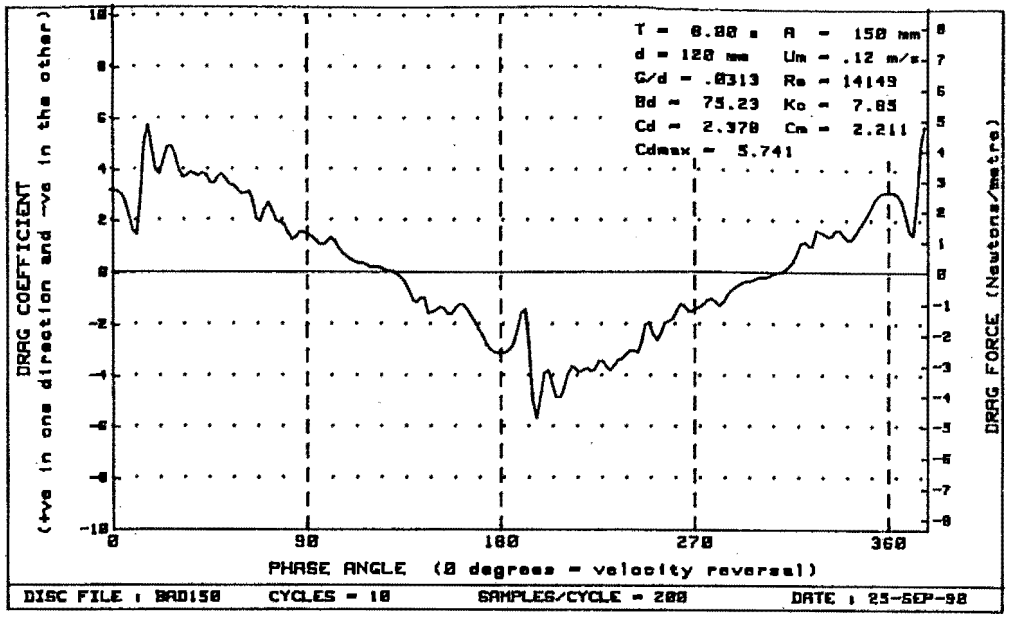

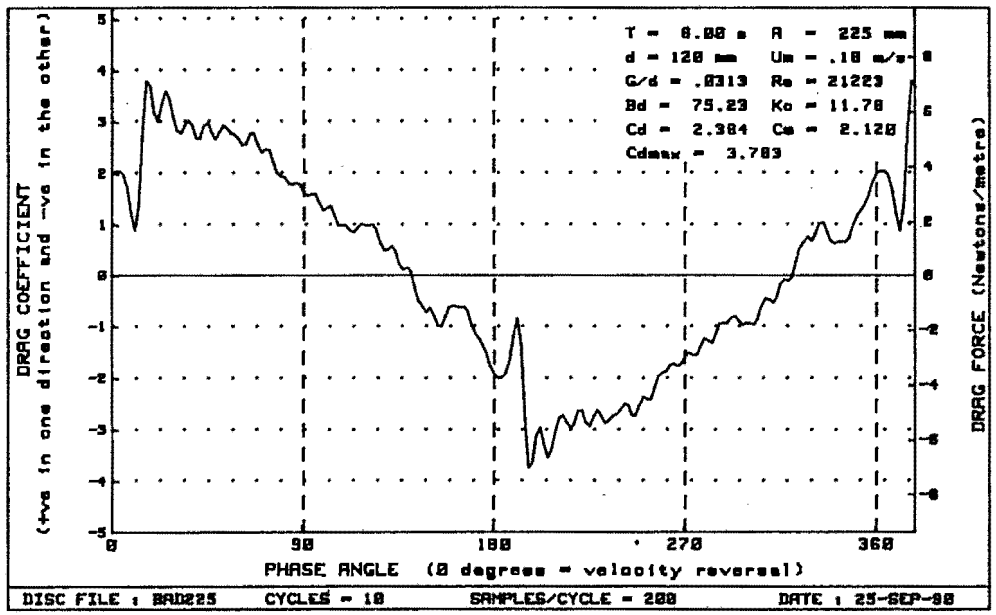

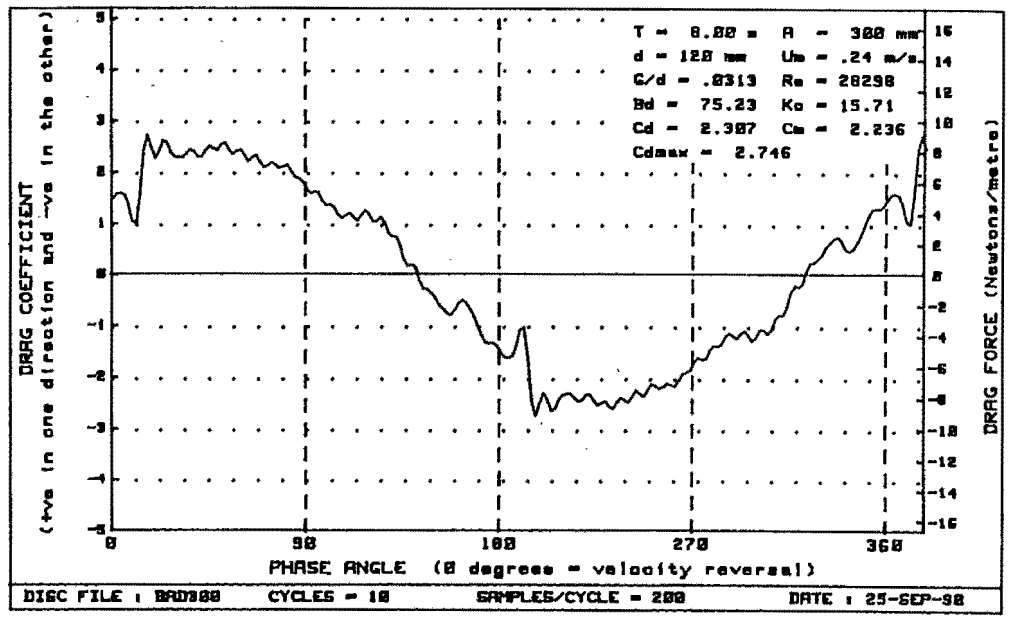

Figure H-15 : Plots of drag vs phase for diameter=120mm, Bd= 75.23 and G/d= .0313

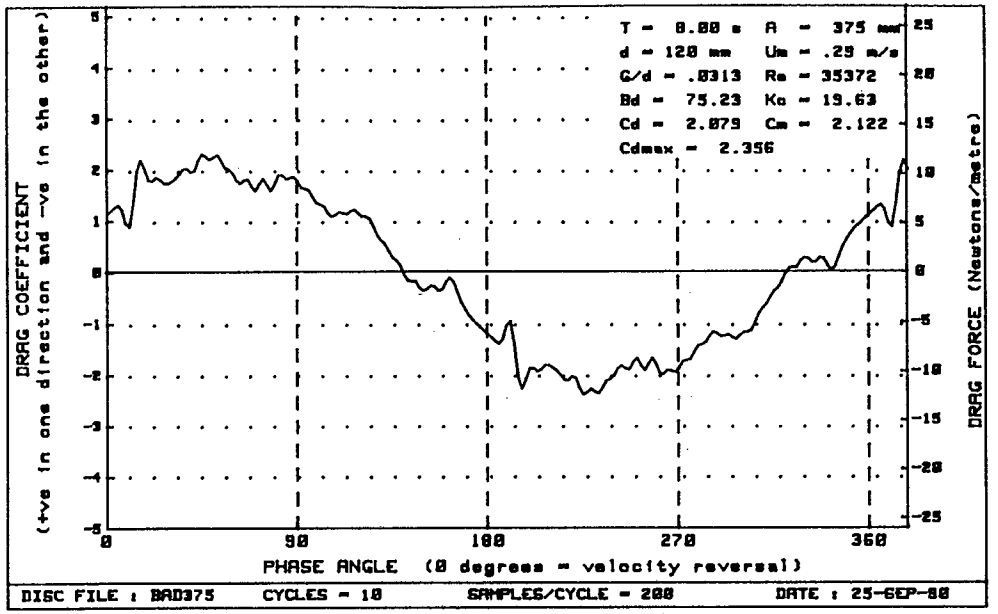

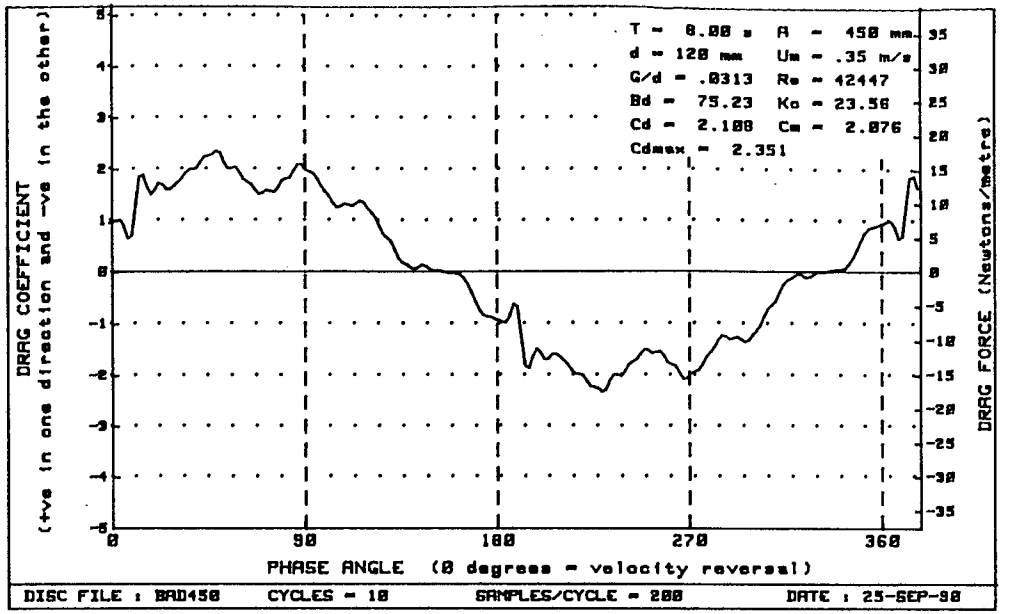

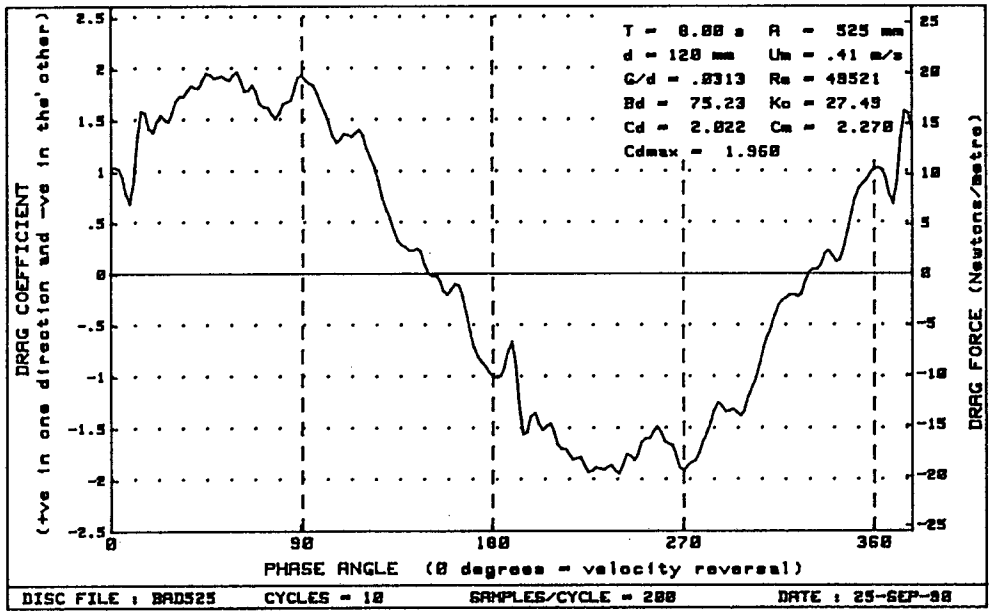

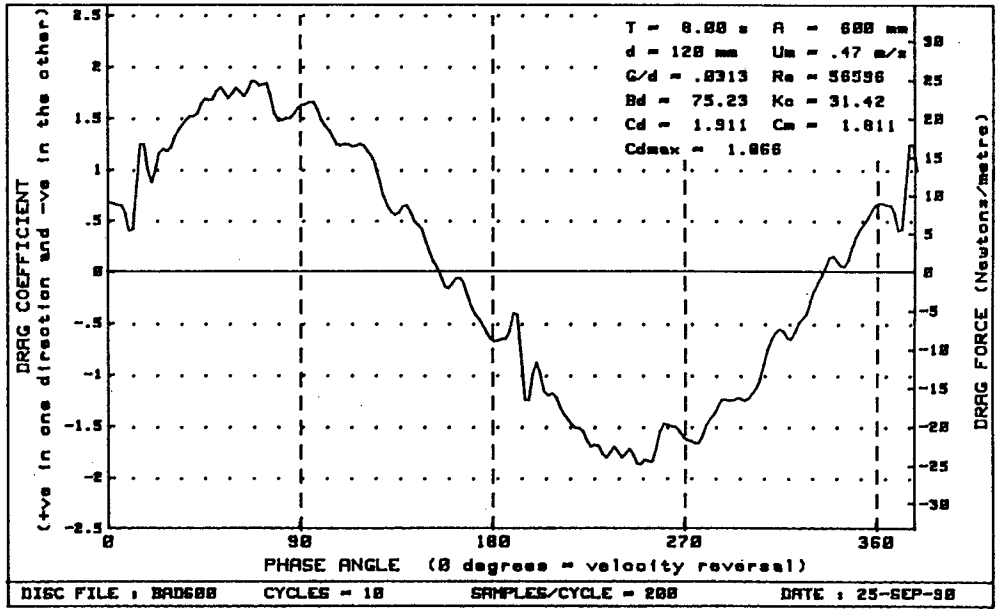

Figure H-16 : Plots of drag vs phase for diameter=120mm, Bd= 75.23 and G/d= .0313

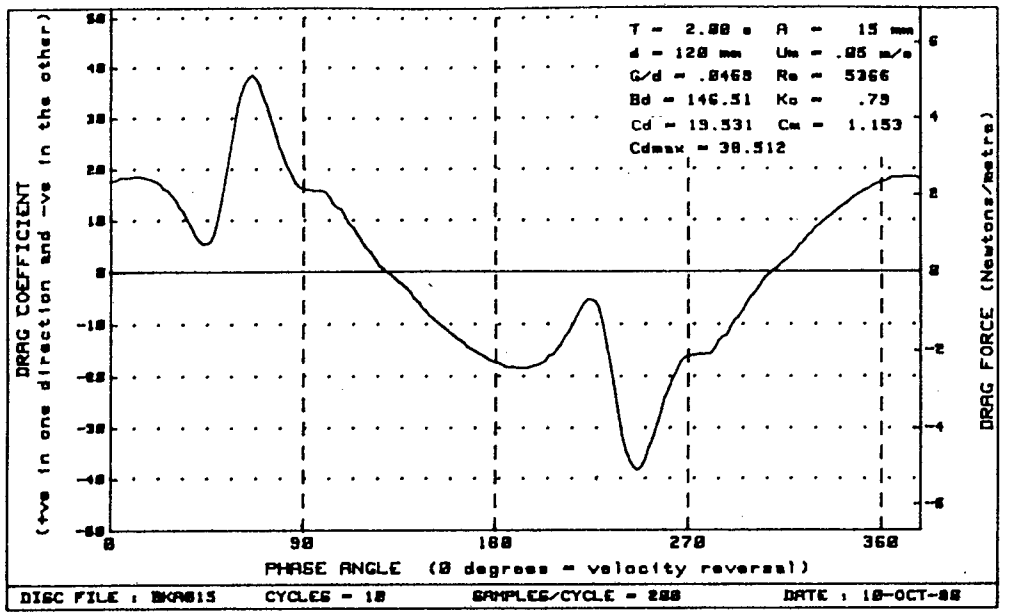

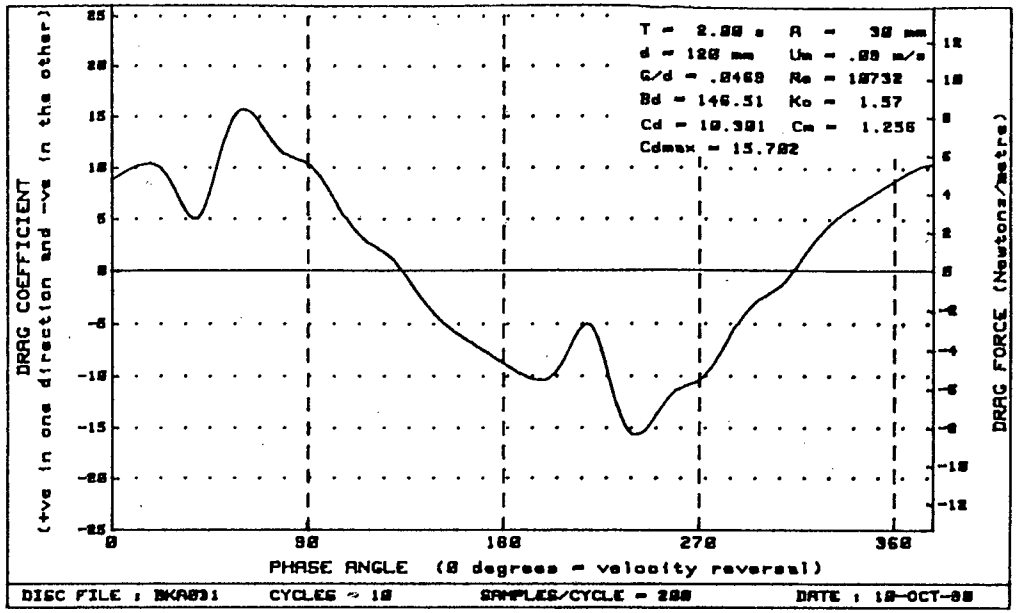

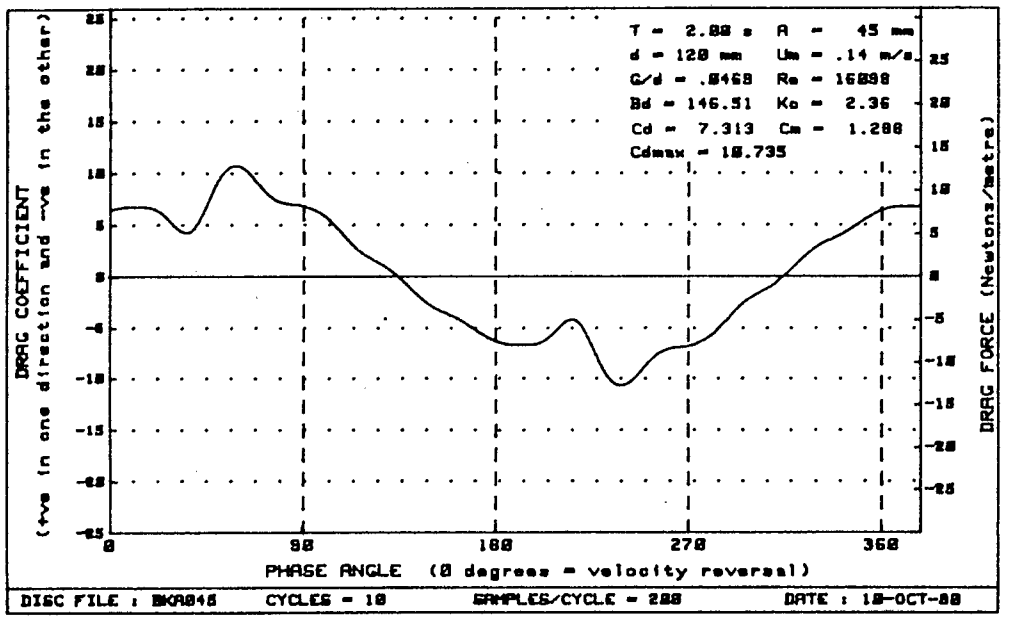

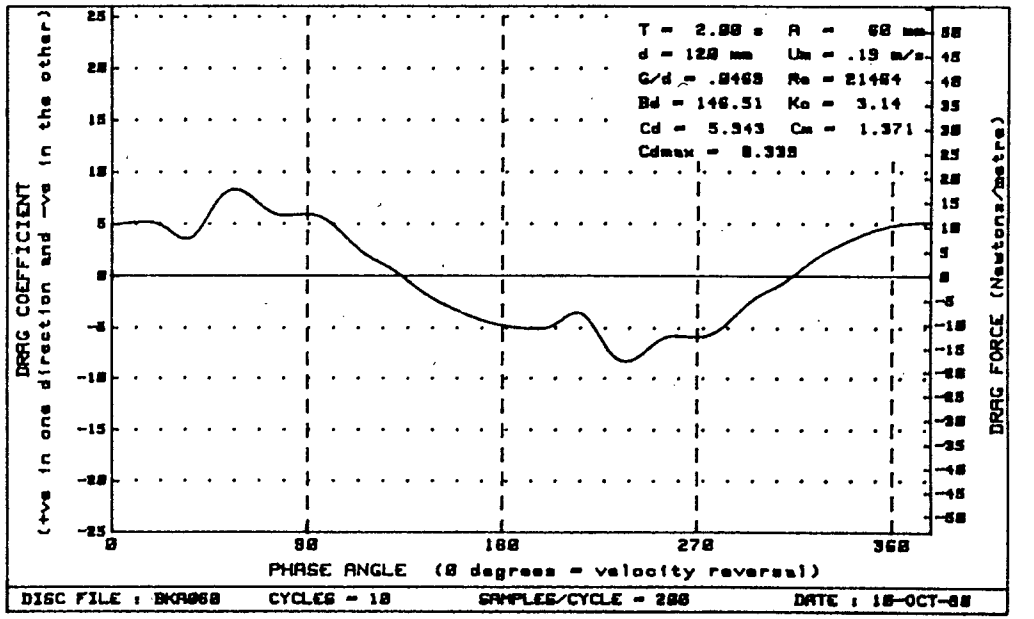

Figure H-17 : Plots of drag vs phase for diameter=120mm, Bd=146.51 and G/d= .0469

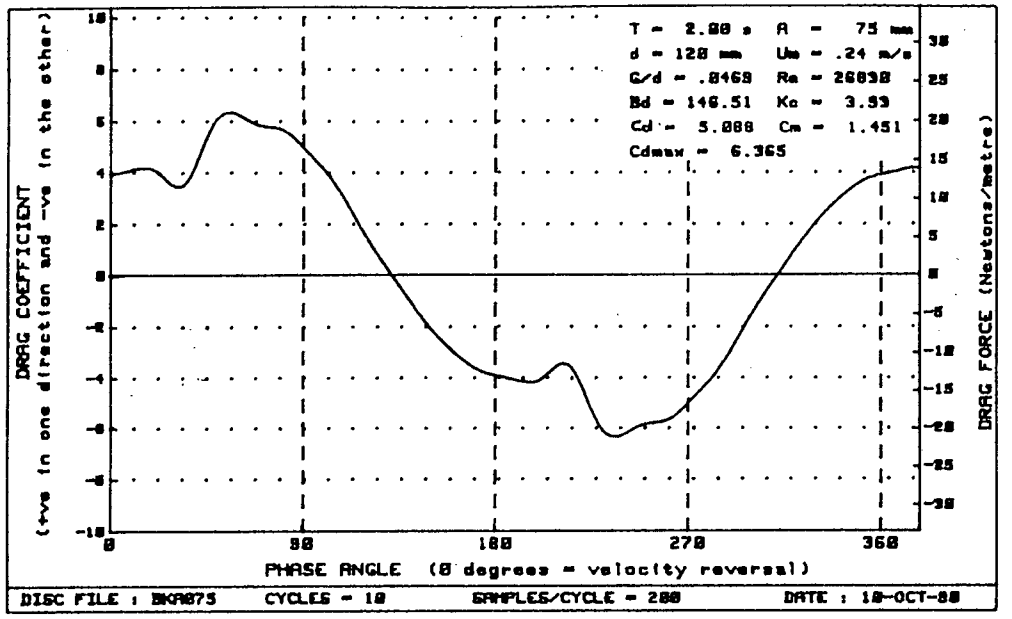

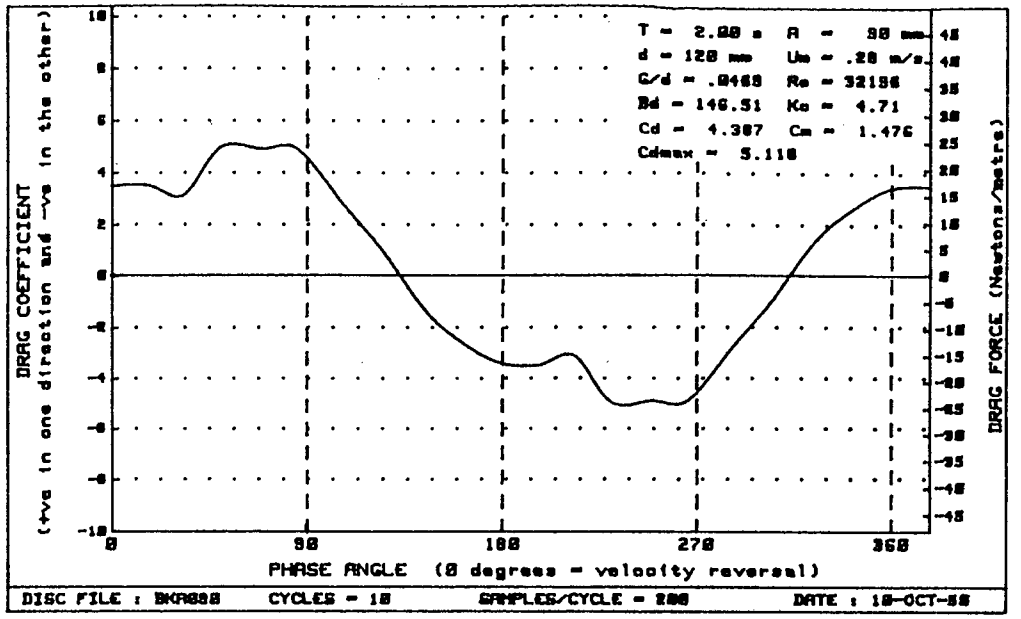

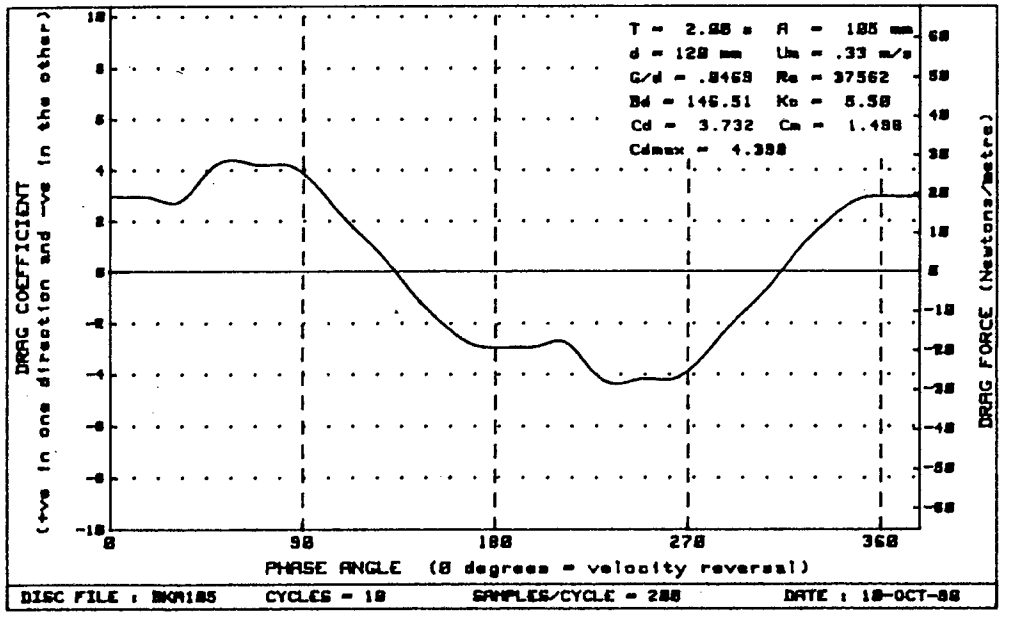

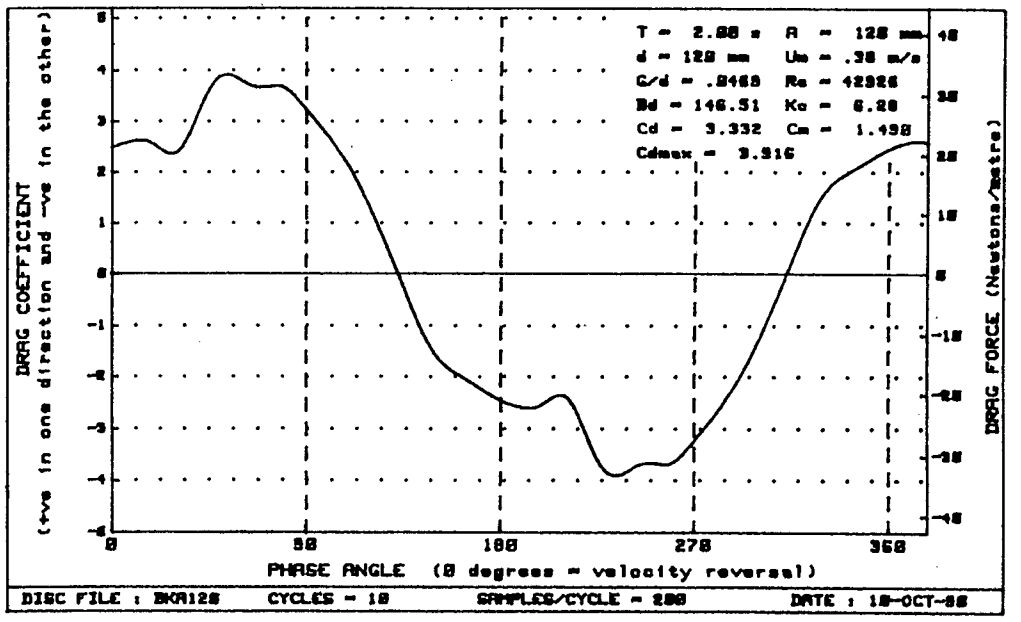

Figure H-18 : Plots of drag vs phase for diameter=120mm, Bd=146.51 and G/d= .0469

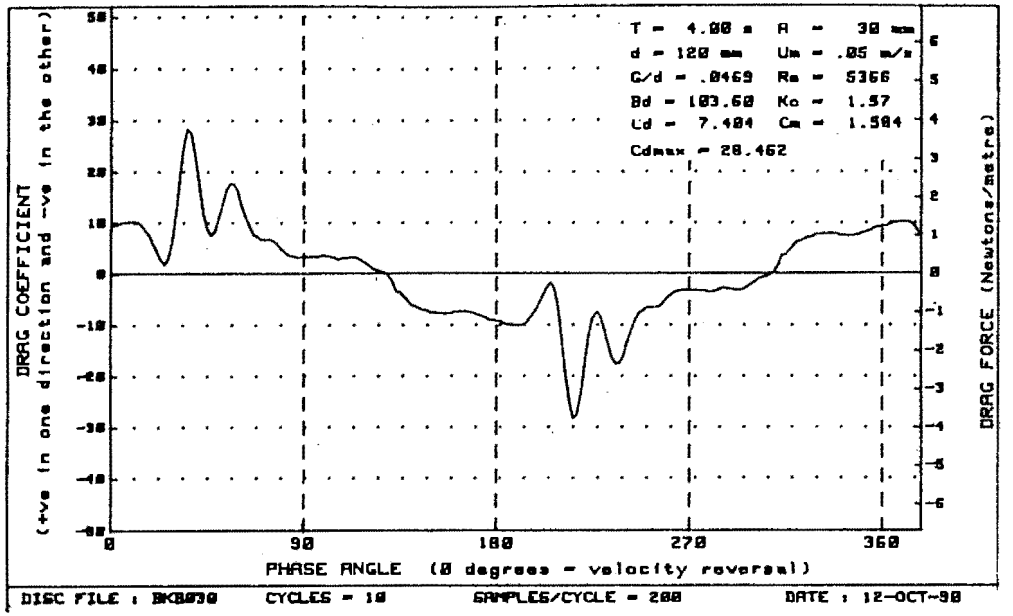

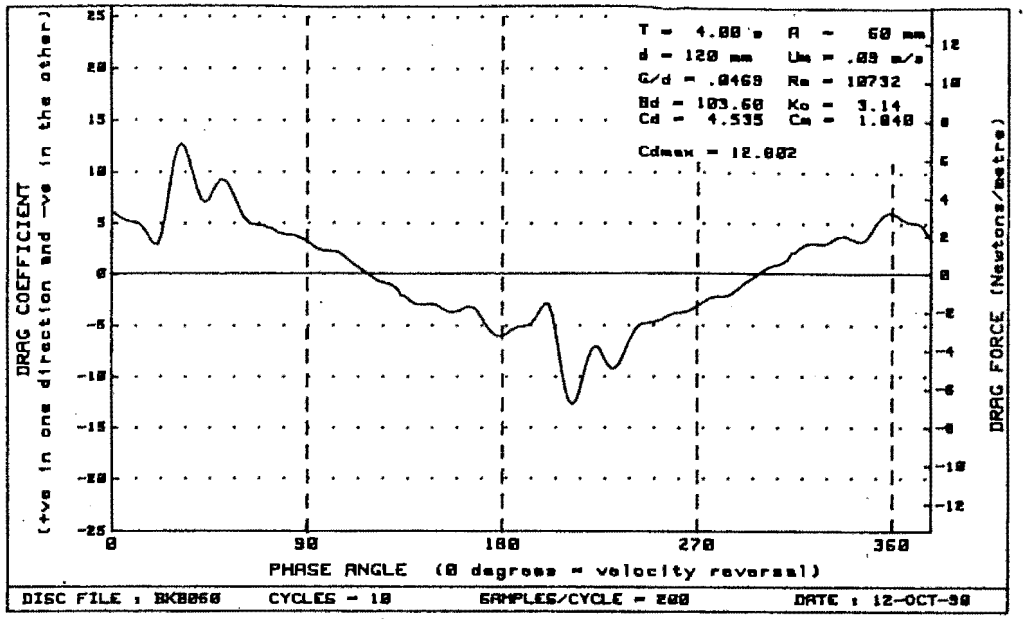

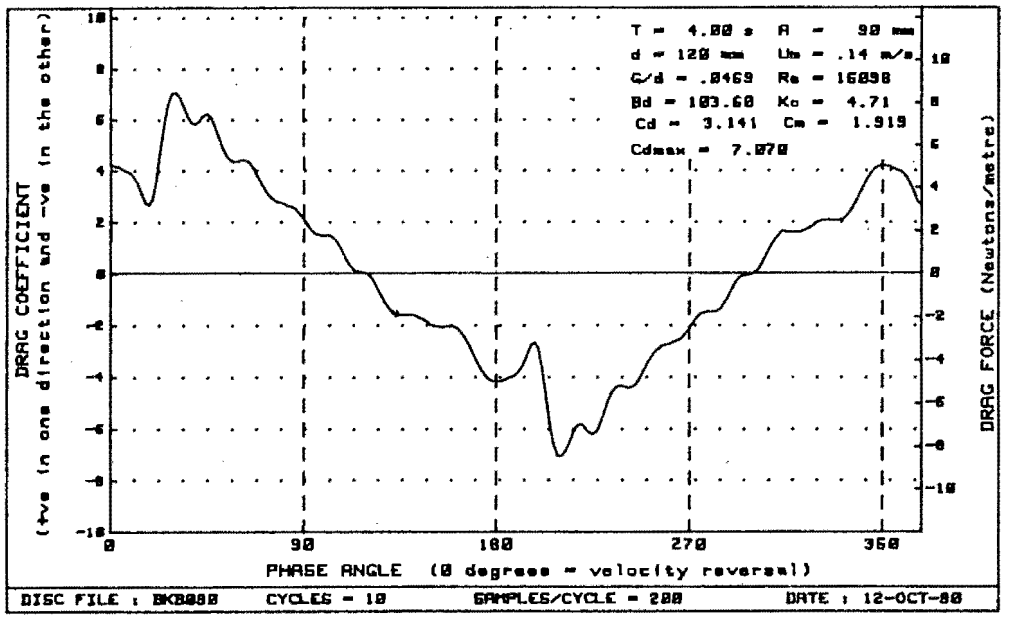

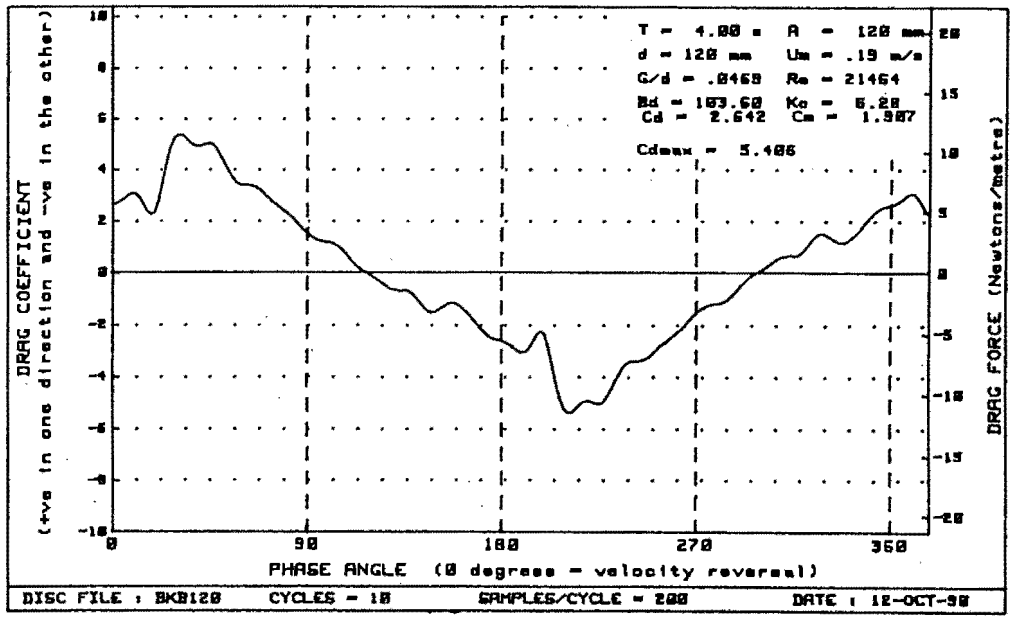

Figure H-19 : Plots of drag vs phase for diameter=120mm, Bd=103.60 and G/d= .0469

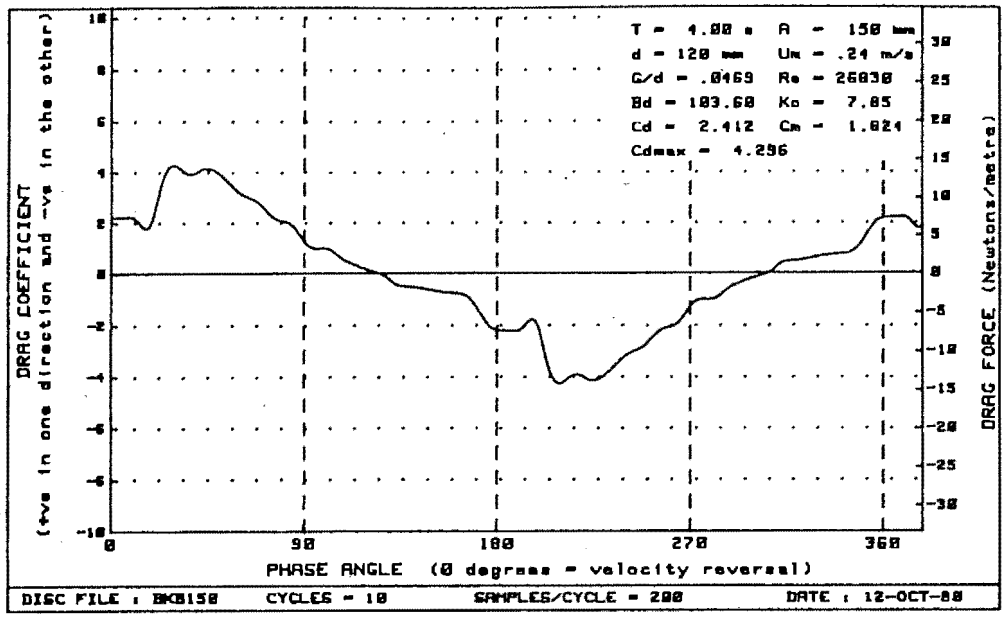

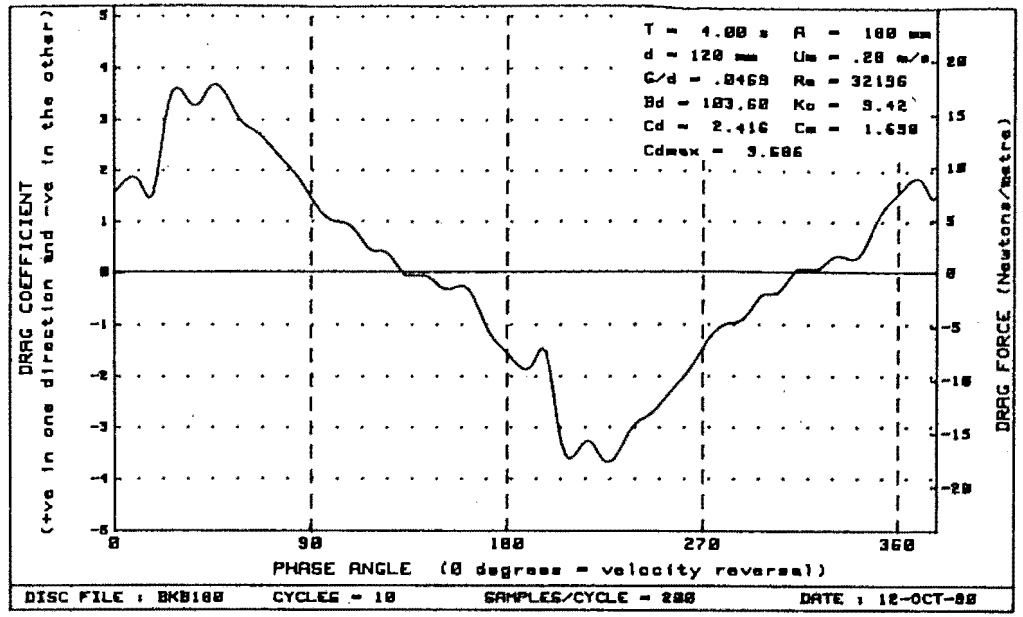

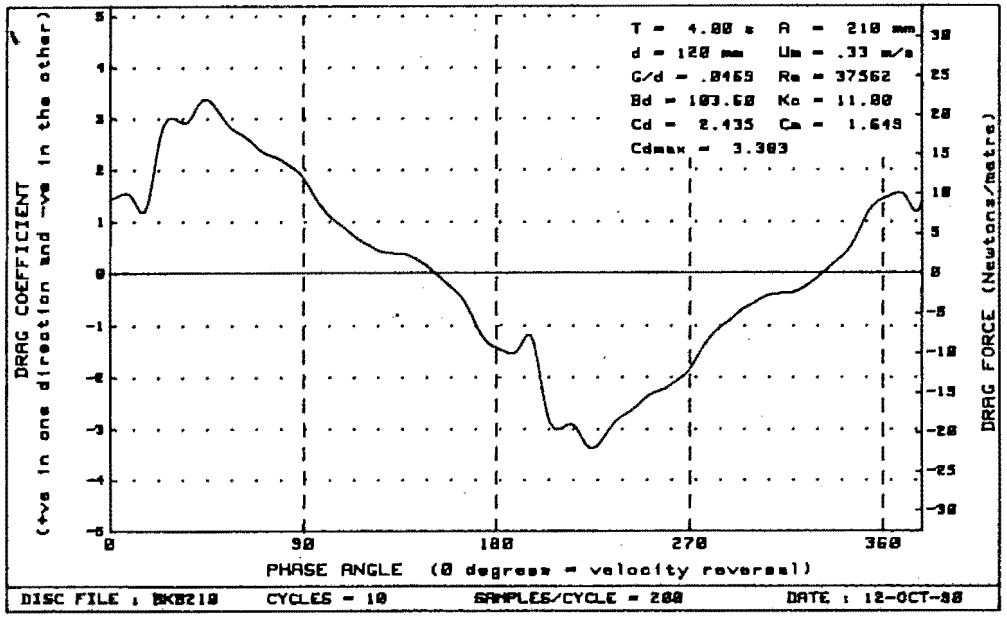

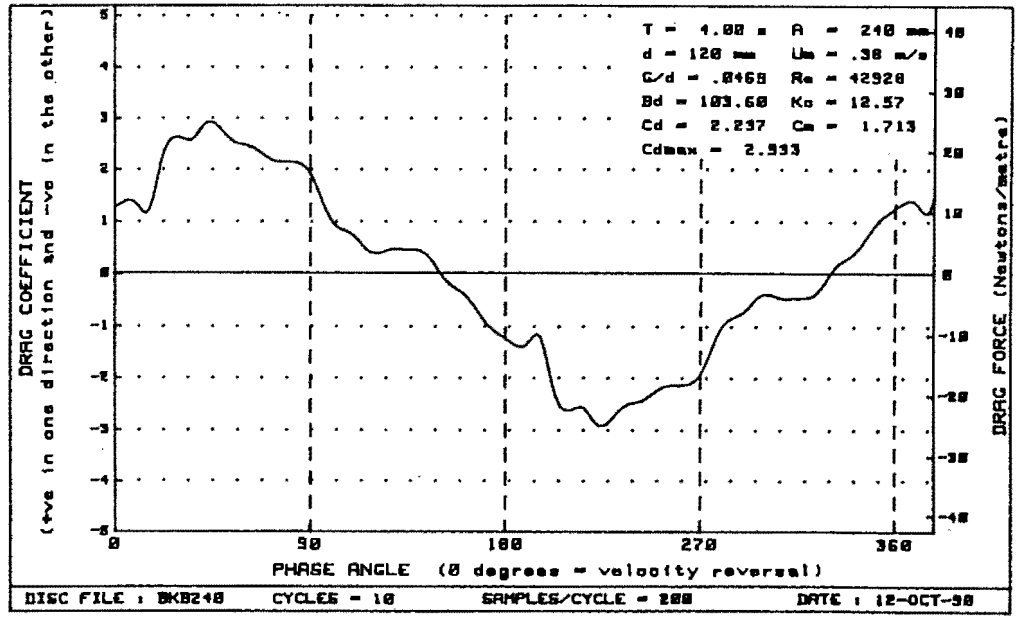

Figure H-20 : Plots of drag vs phase for diameter=120mm, Bd=103.60 and G/d= .0469

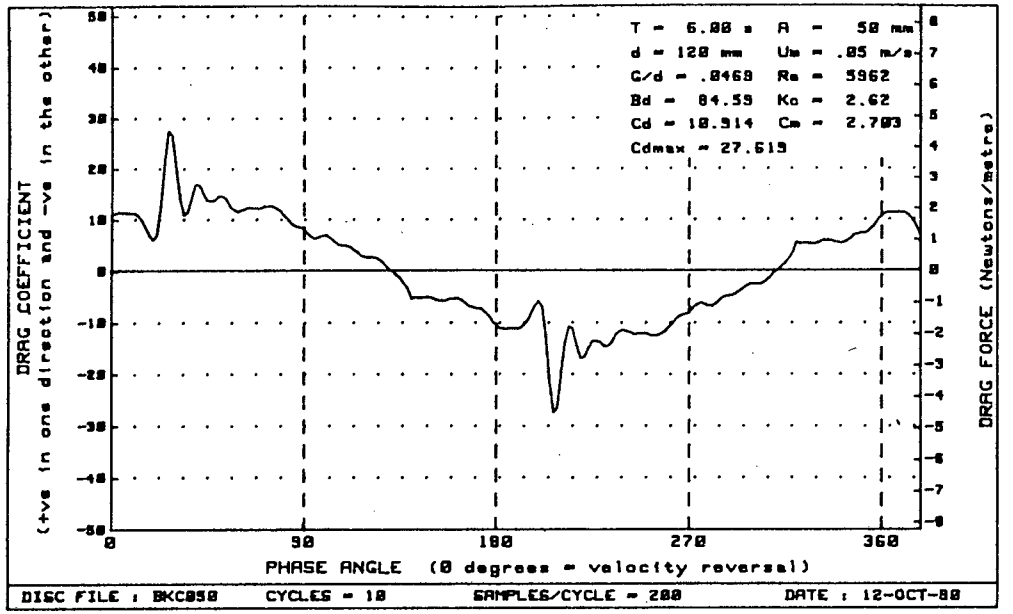

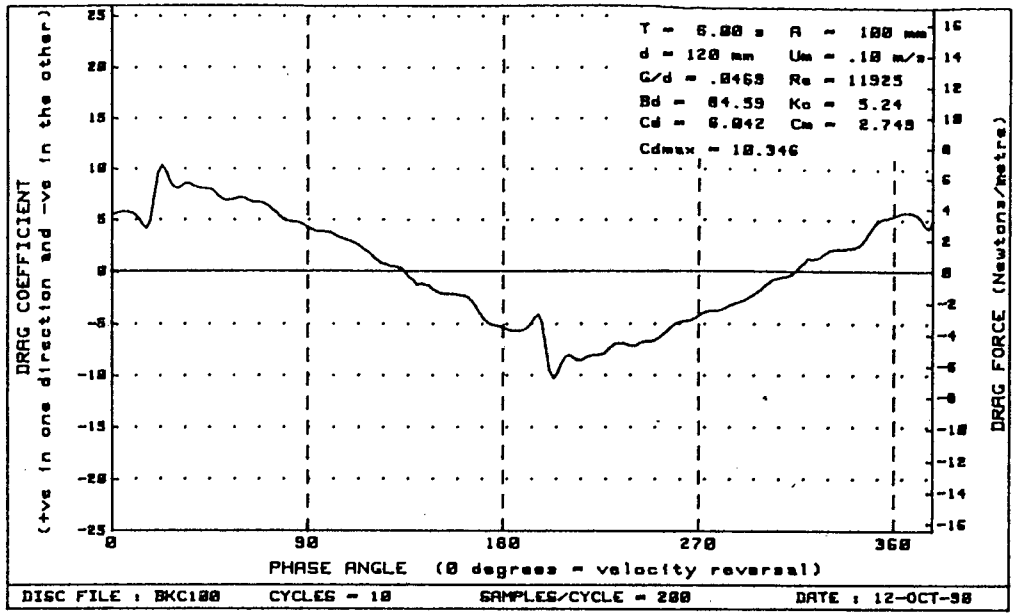

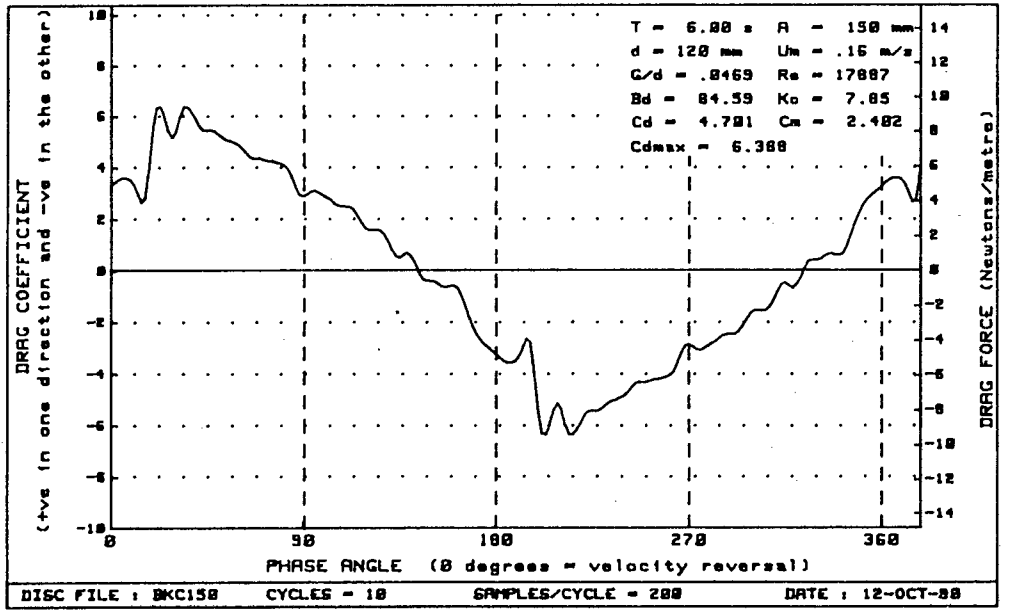

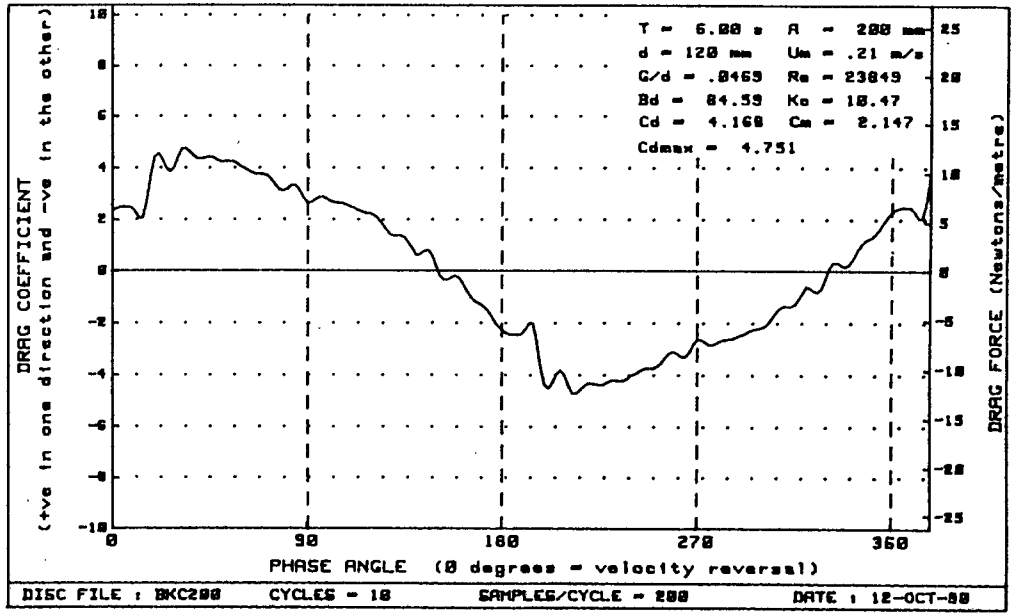

Figure H-21 : Plots of drag vs phase for diameter=120mm, Bd= 84.59 and G/d= .0469

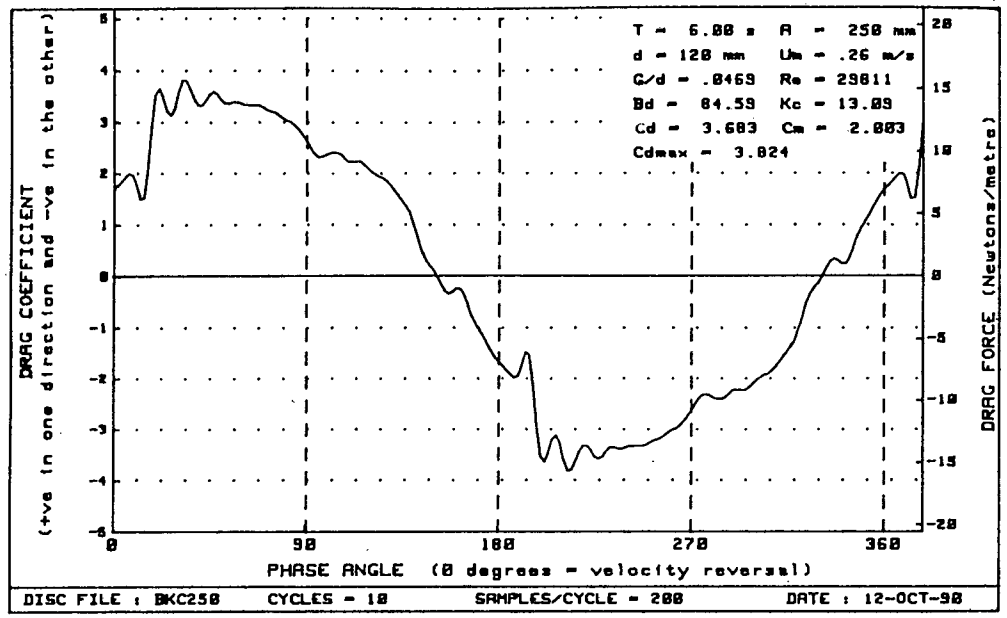

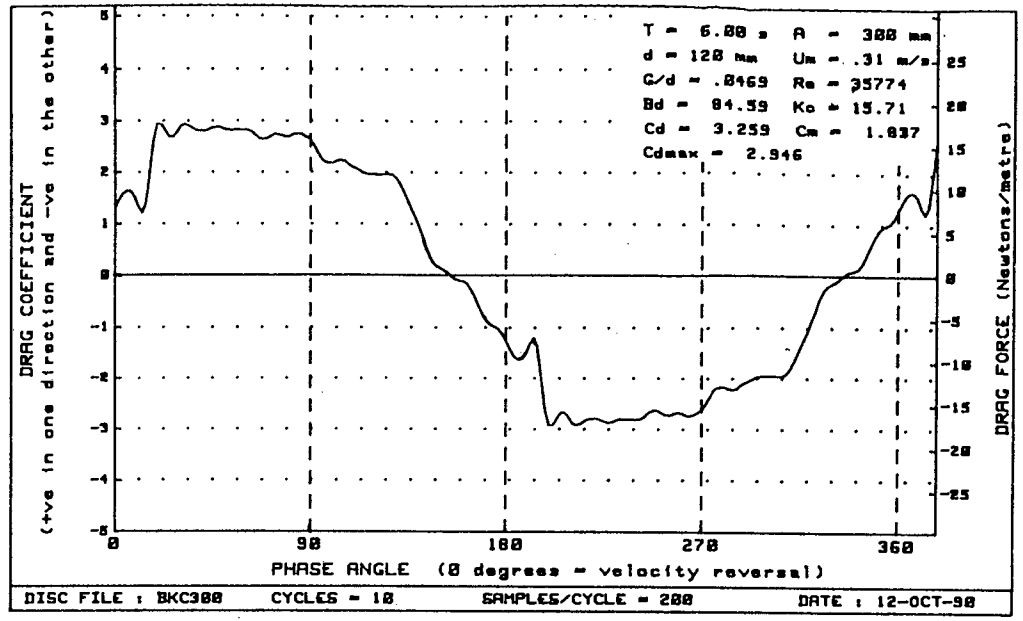

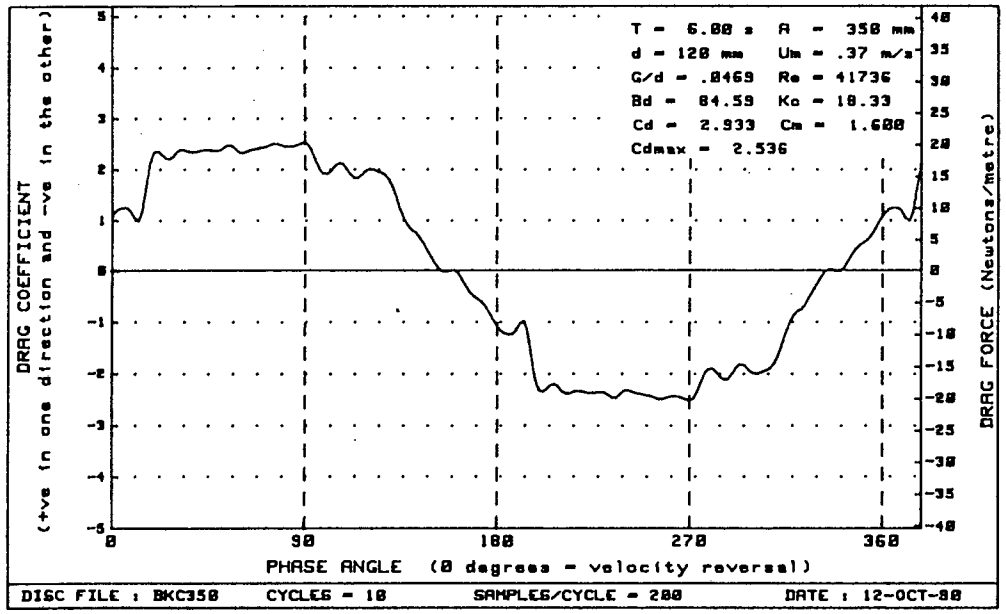

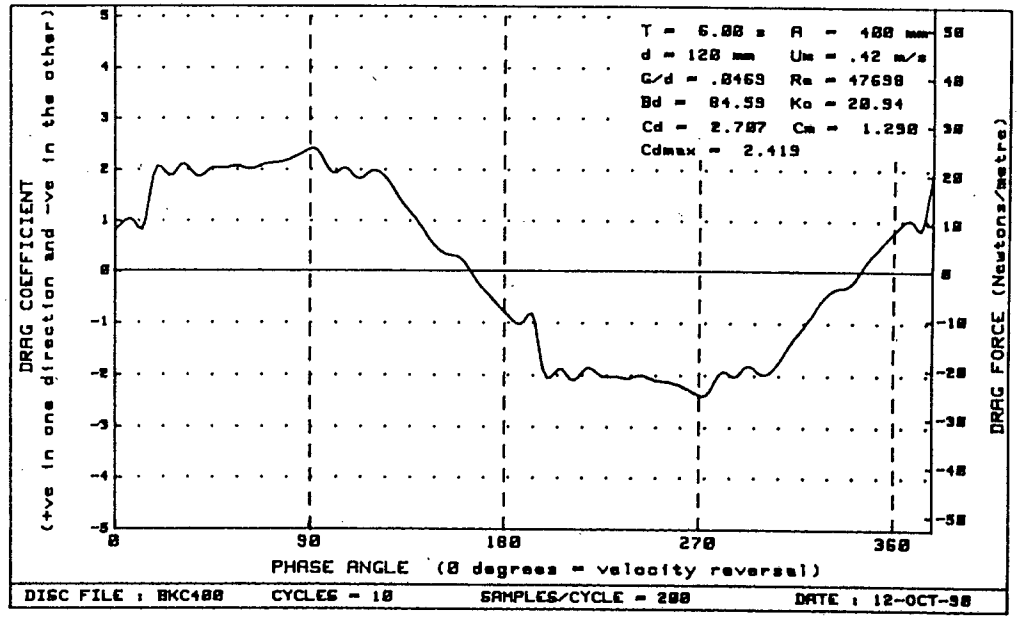

Figure H-22 : Plots of drag vs phase for diameter=120mm, Bd= 84.59 and G/d= .0469

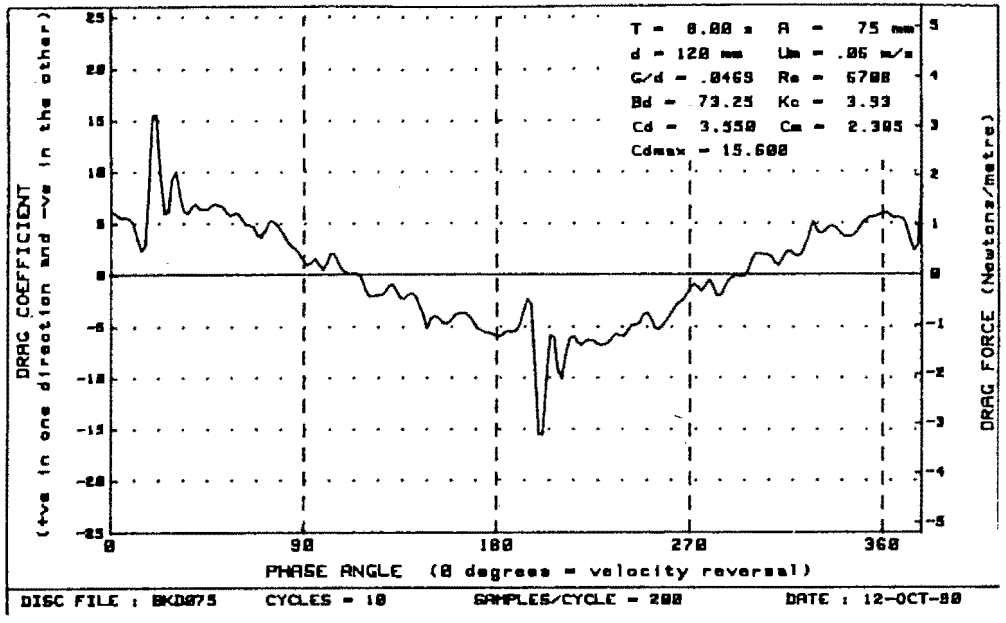

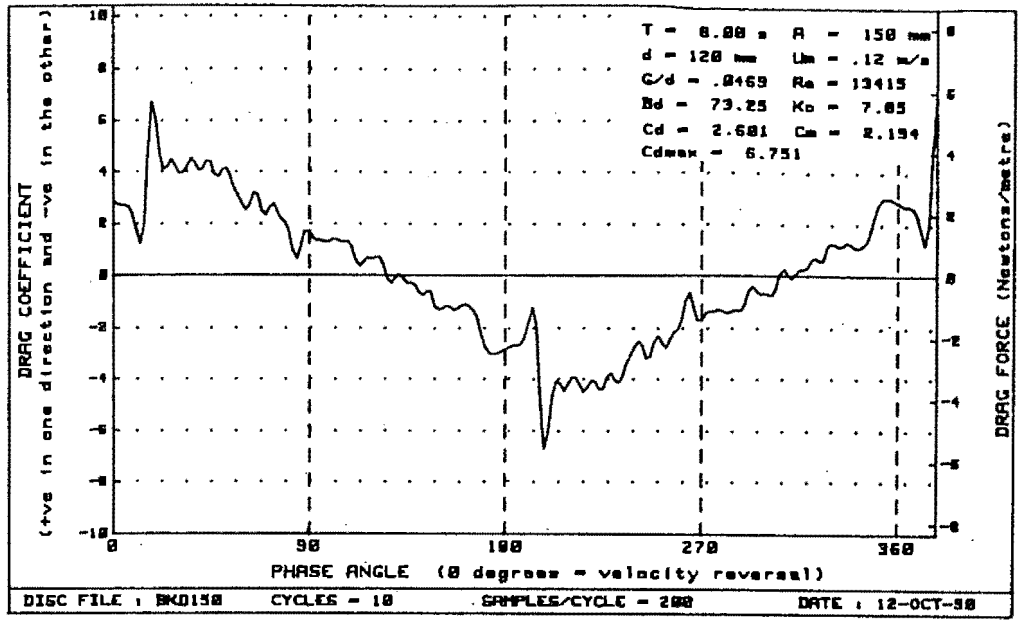

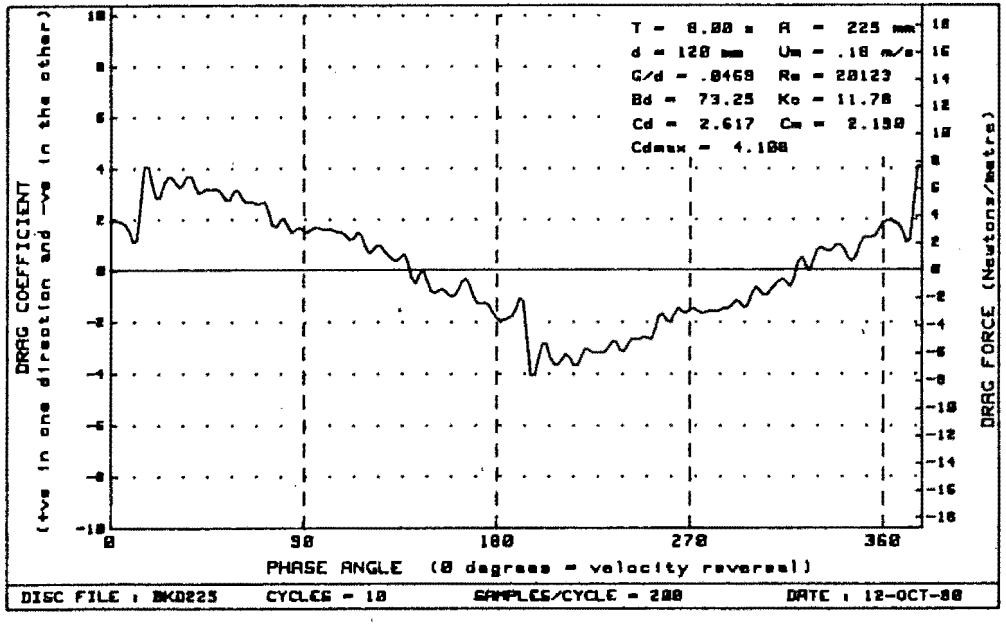

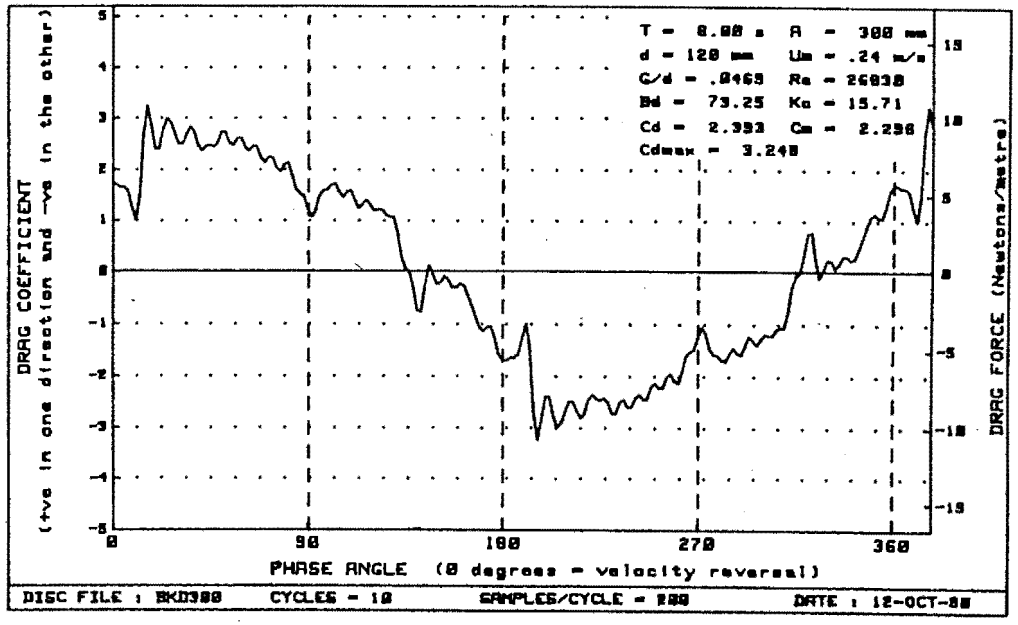

Figure H-23 : Plots of drag vs phase for diameter=120mm, Bd= 73.25 and G/d= .0469

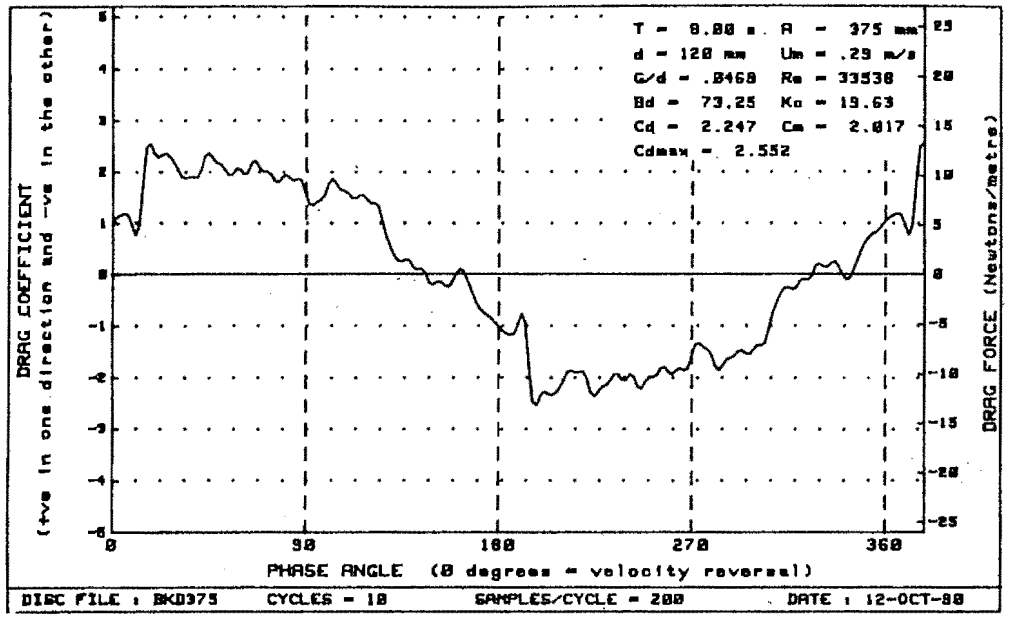

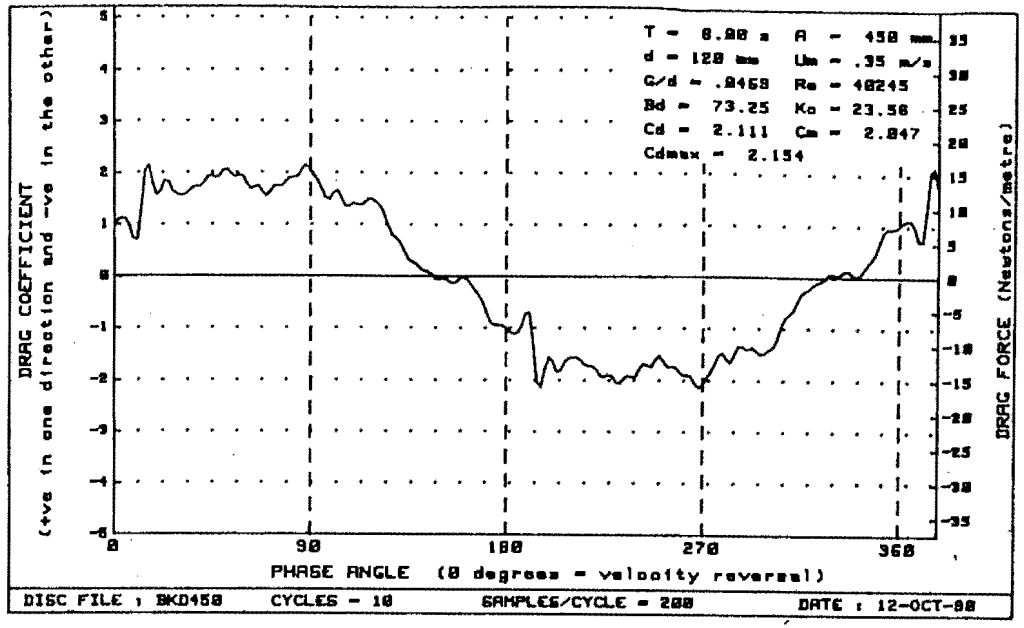

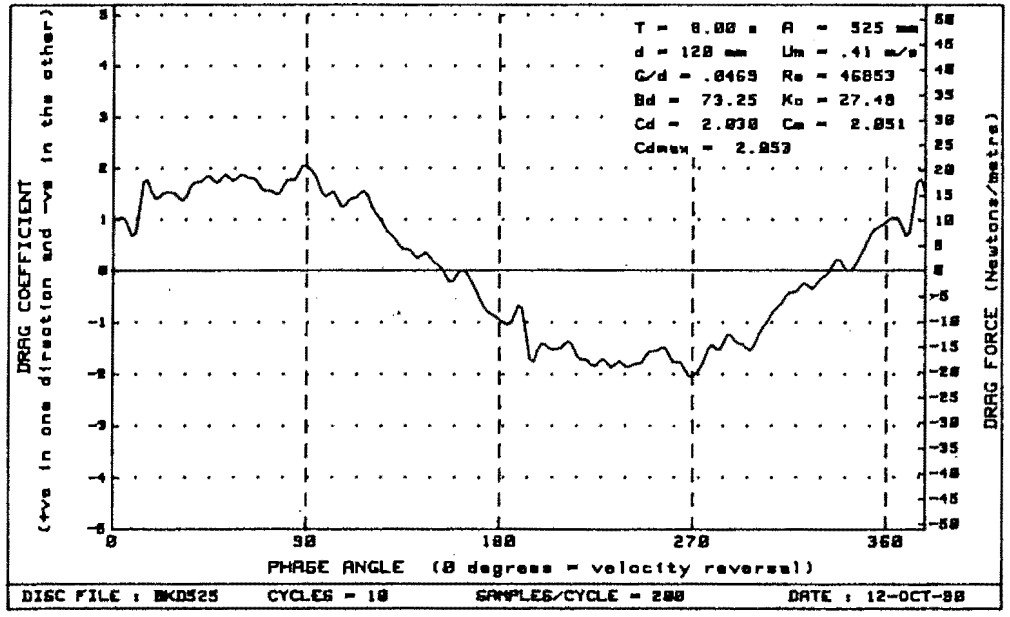

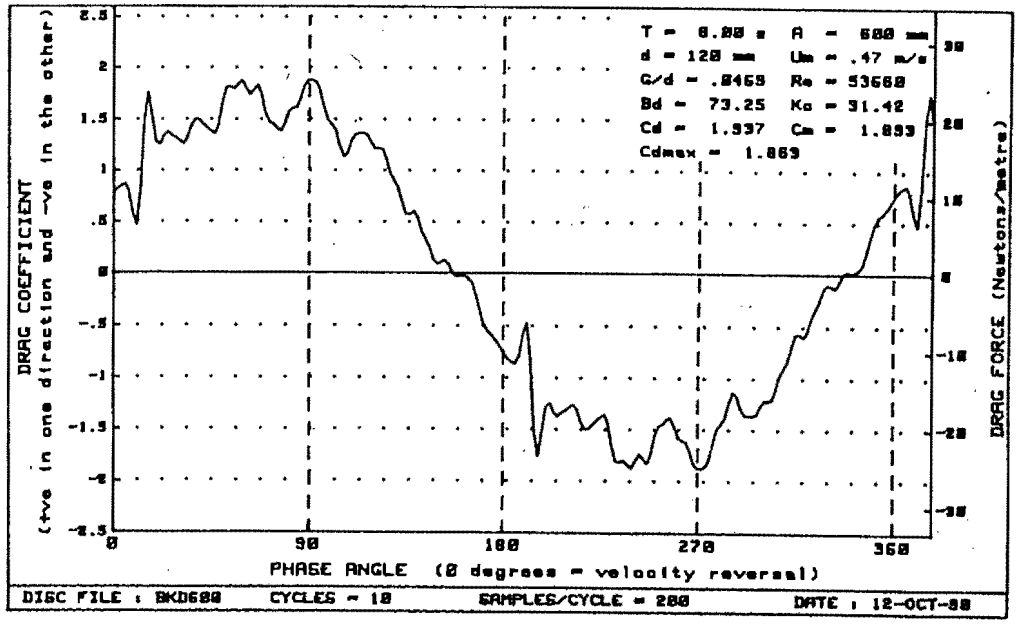

Figure H-24 : Plots of drag vs phase for diameter=120mm, Bd= 73.25 and G/d= .0469

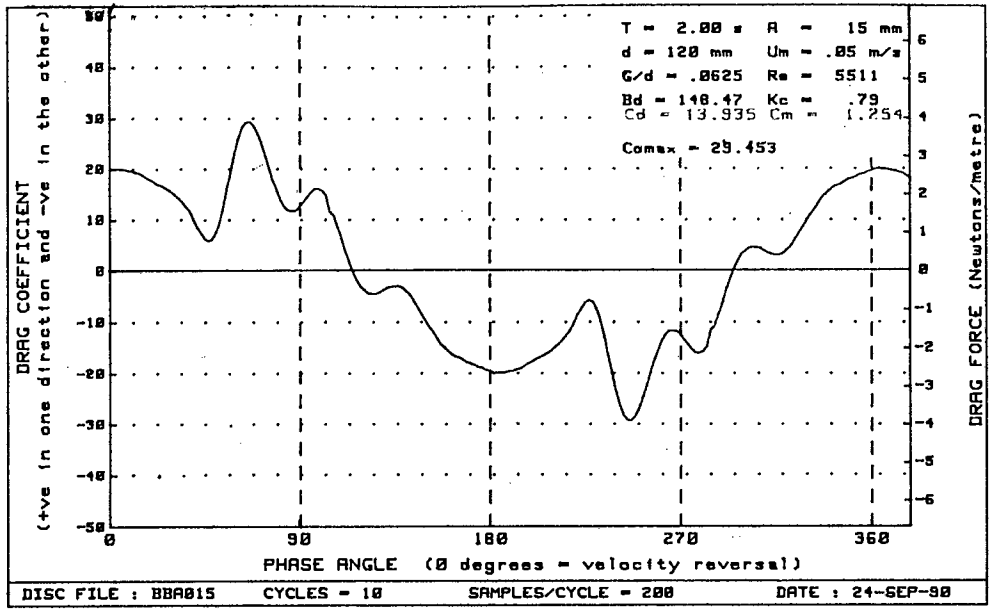

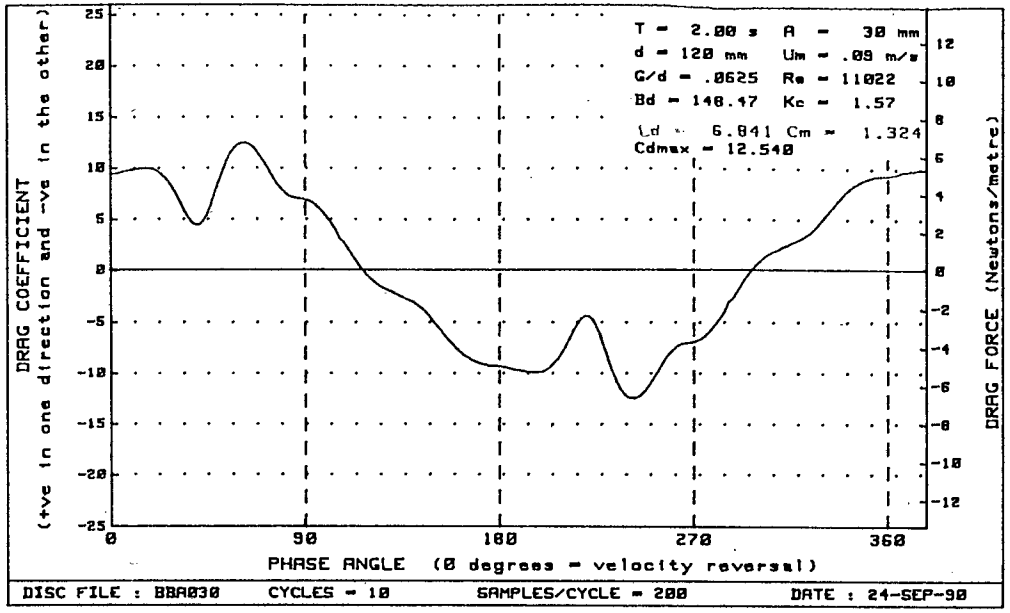

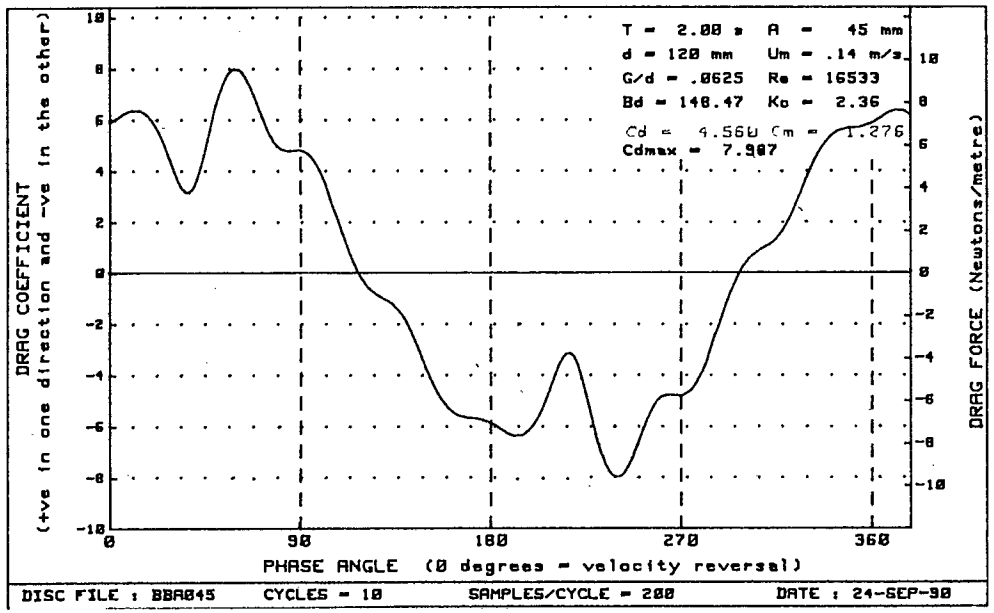

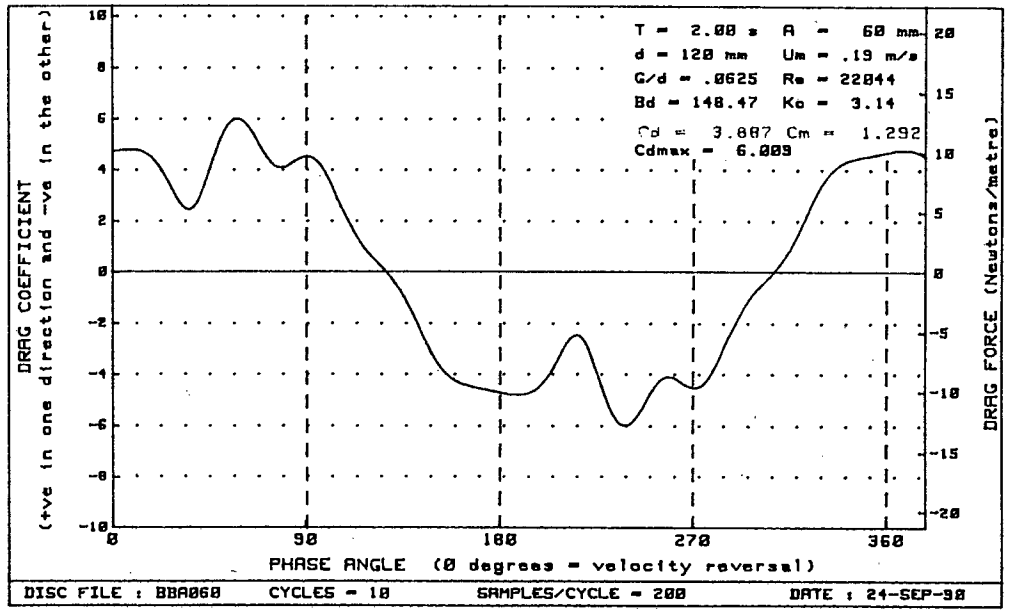

Figure H-25 : Plots of drag vs phase for diameter=120mm, Bd=148.47 and G/d= .0625

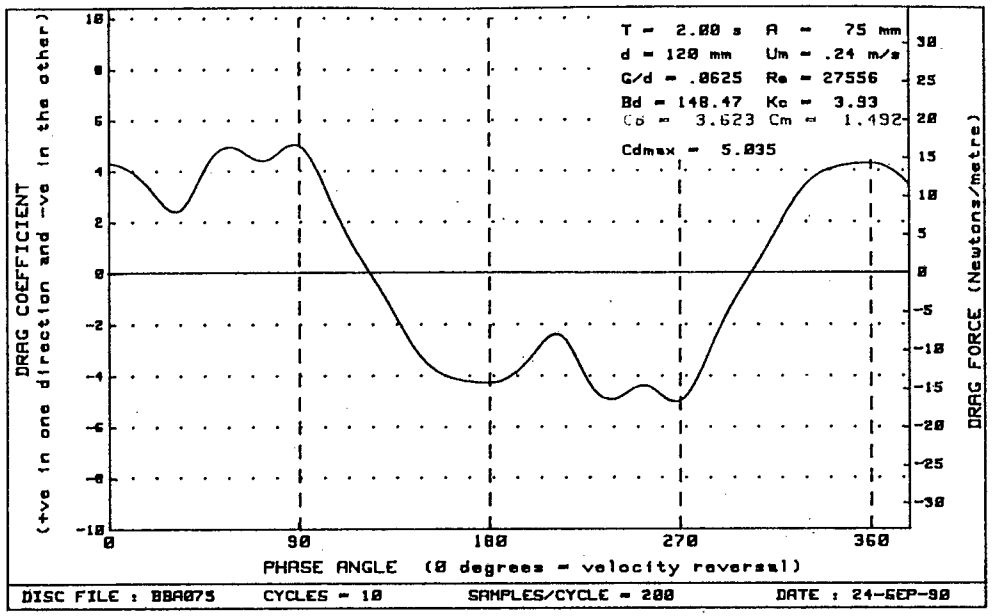

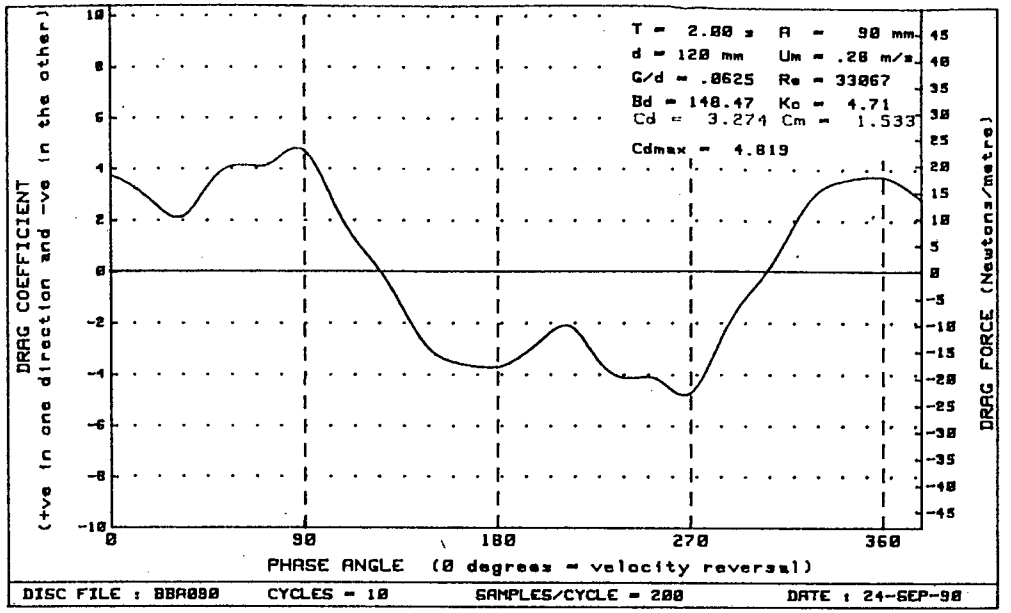

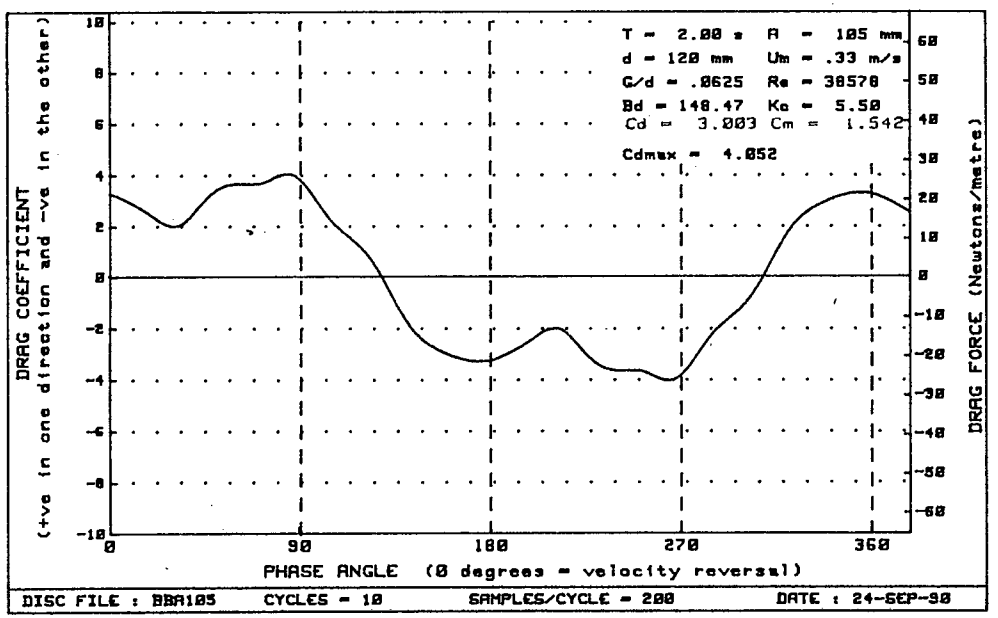

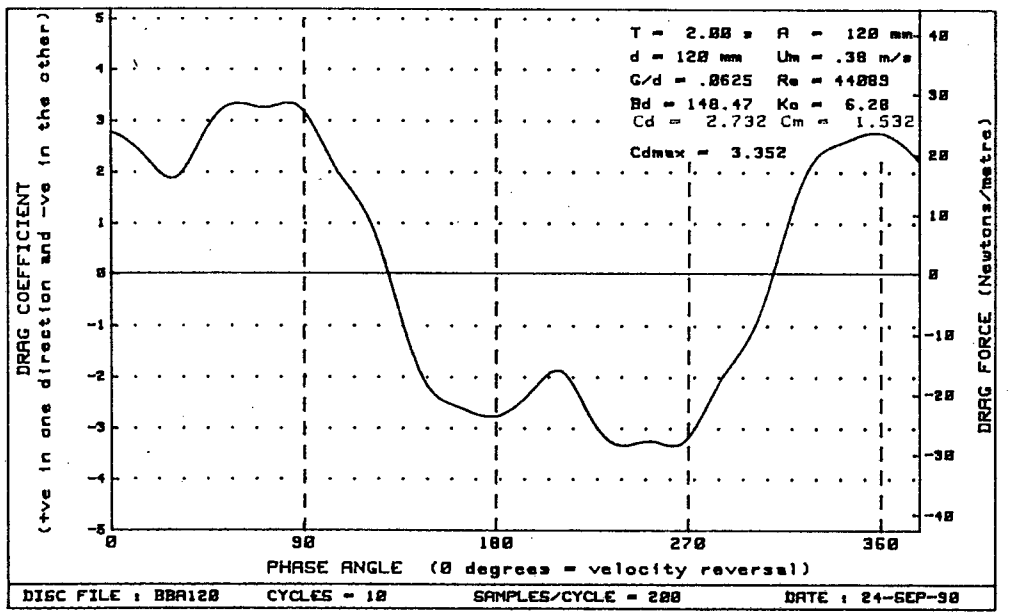

Figure H-26 : Plots of drag vs phase for diameter=120mm, Bd=148.47 and G/d= .0625

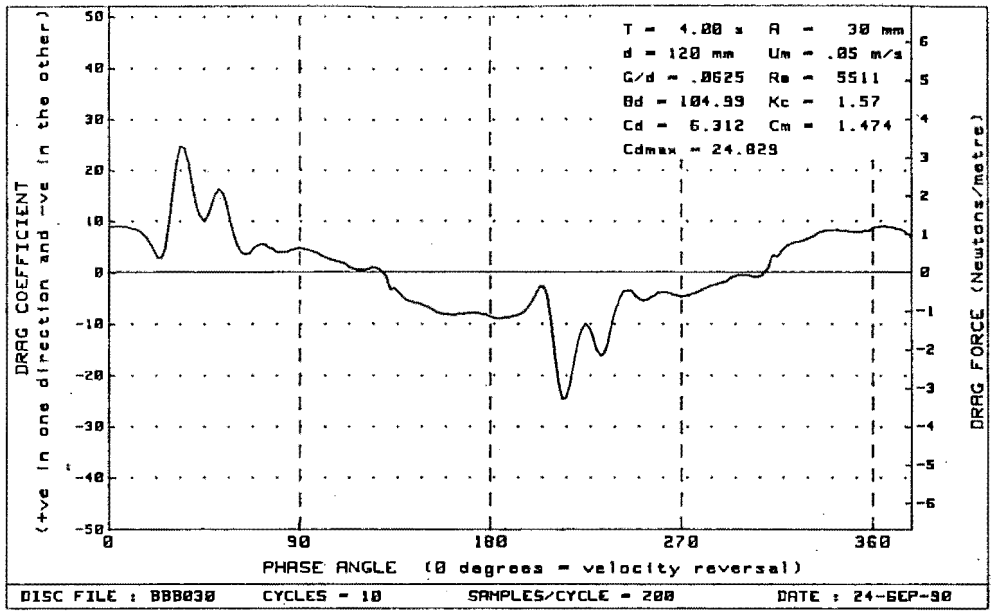

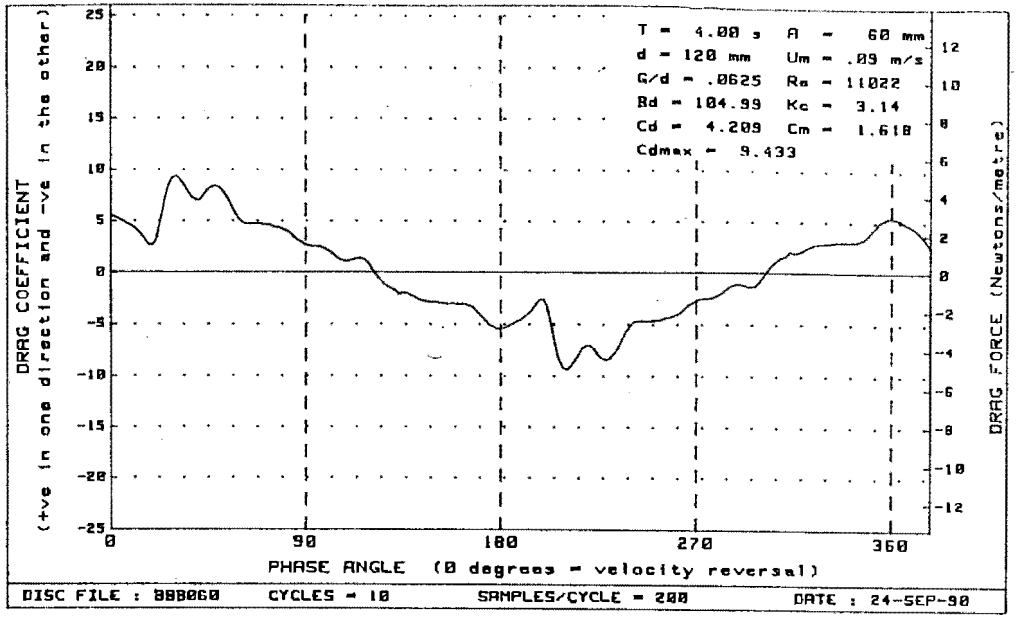

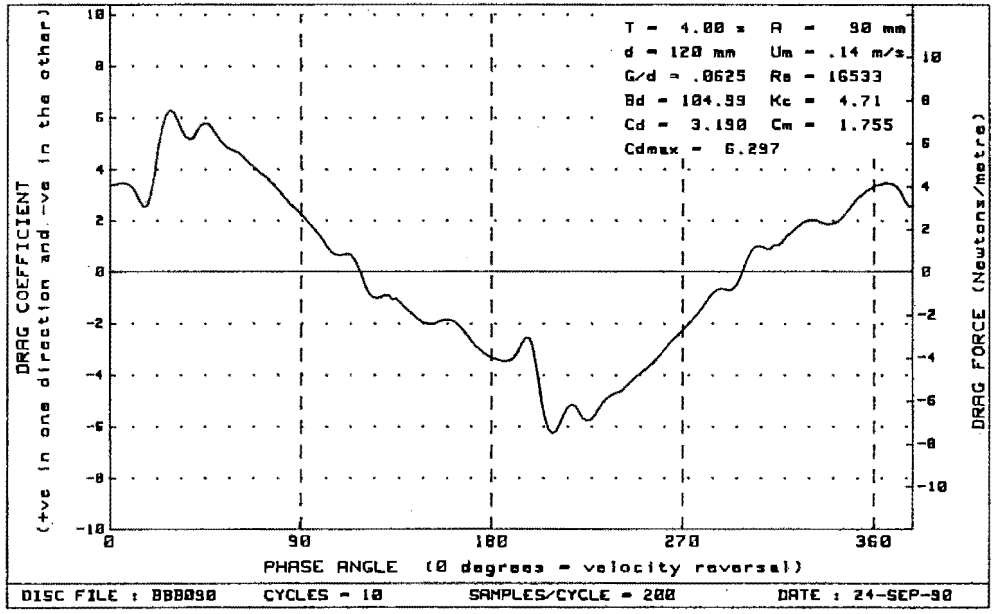

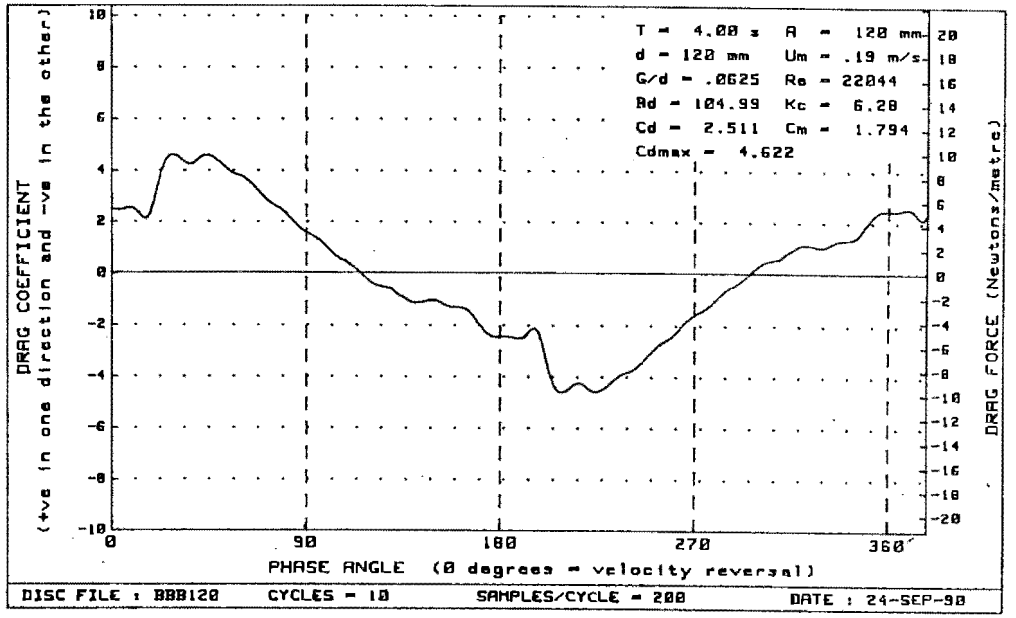

Figure H – 27 : Plots of drag vs phase for diameter=120mm, Bd=104.99 and G/d= .0625

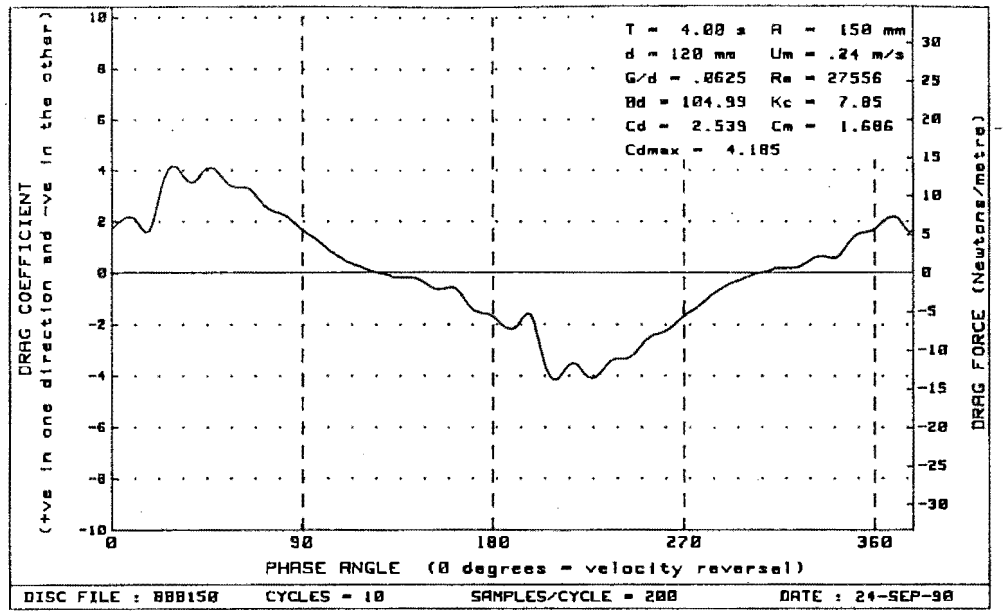

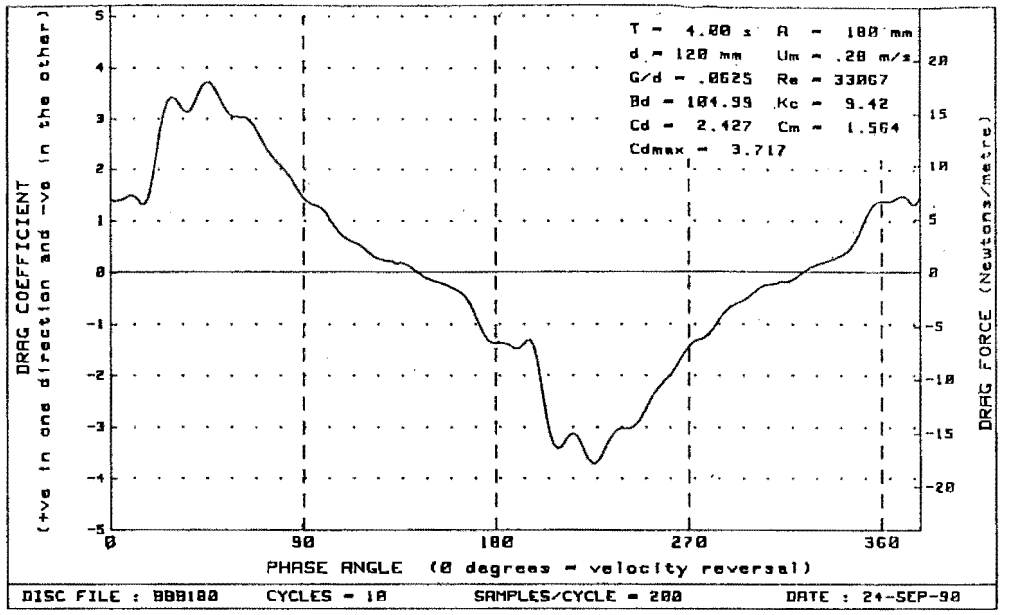

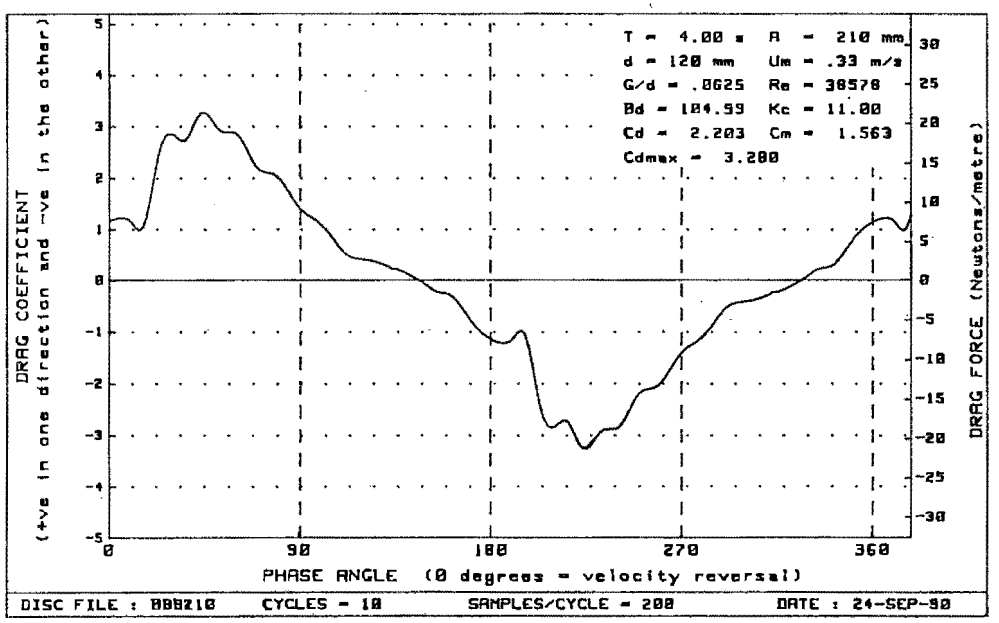

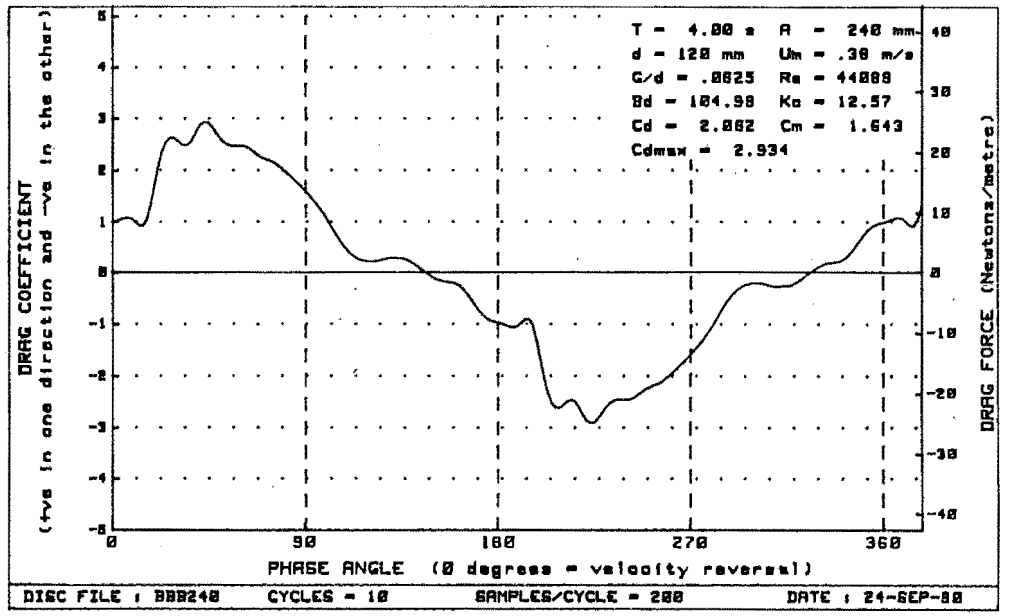

Figure H – 28 : Plots of drag vs phase for diameter=120mm, Bd=104.99 and G/d= .0625

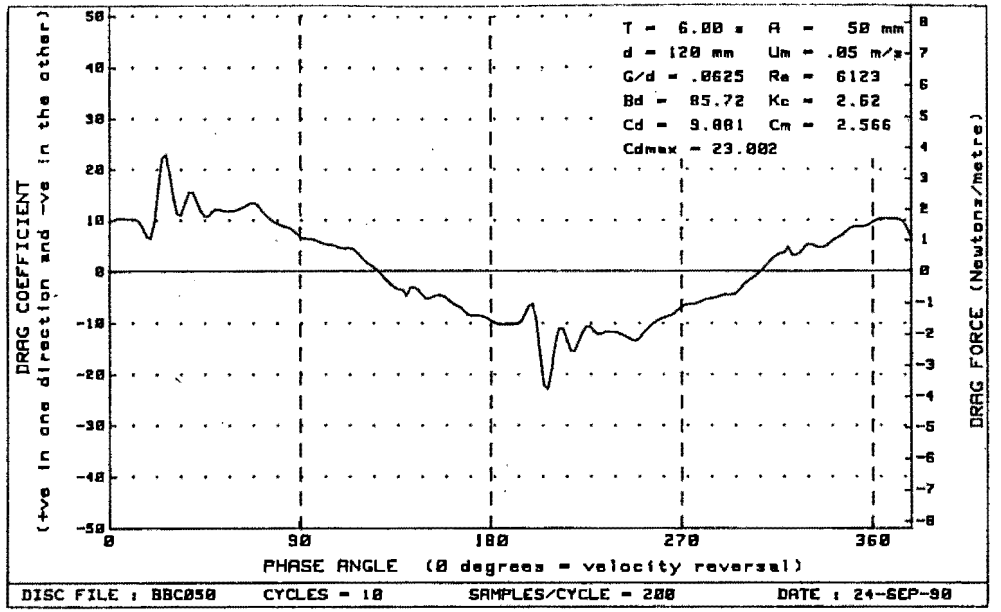

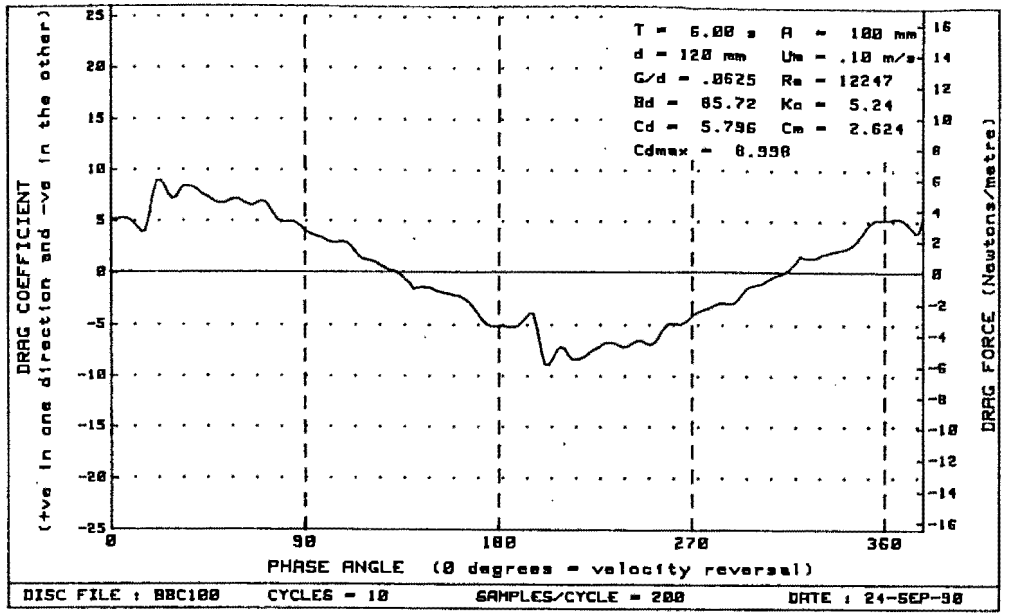

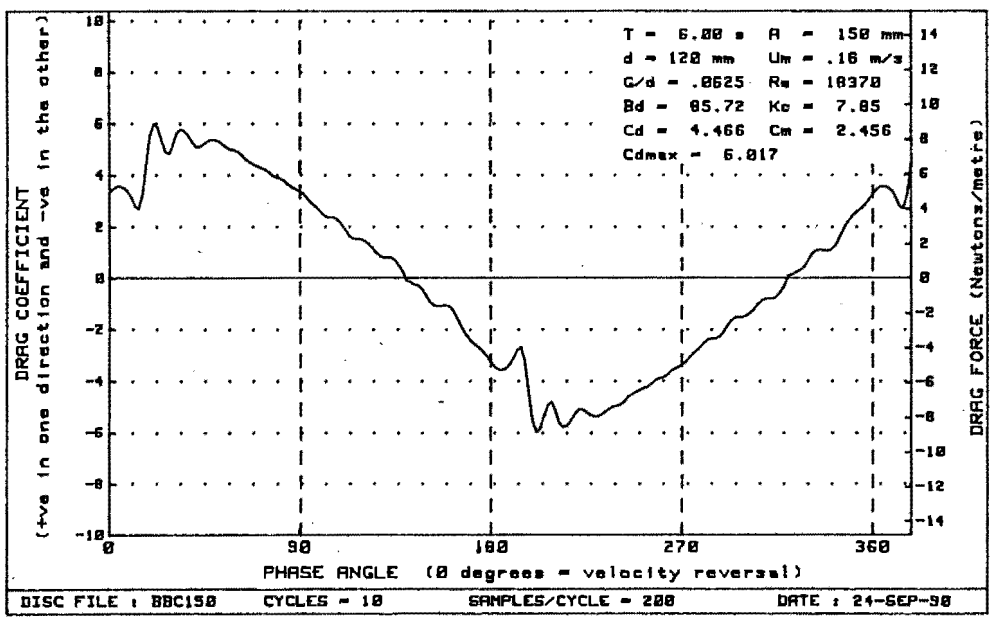

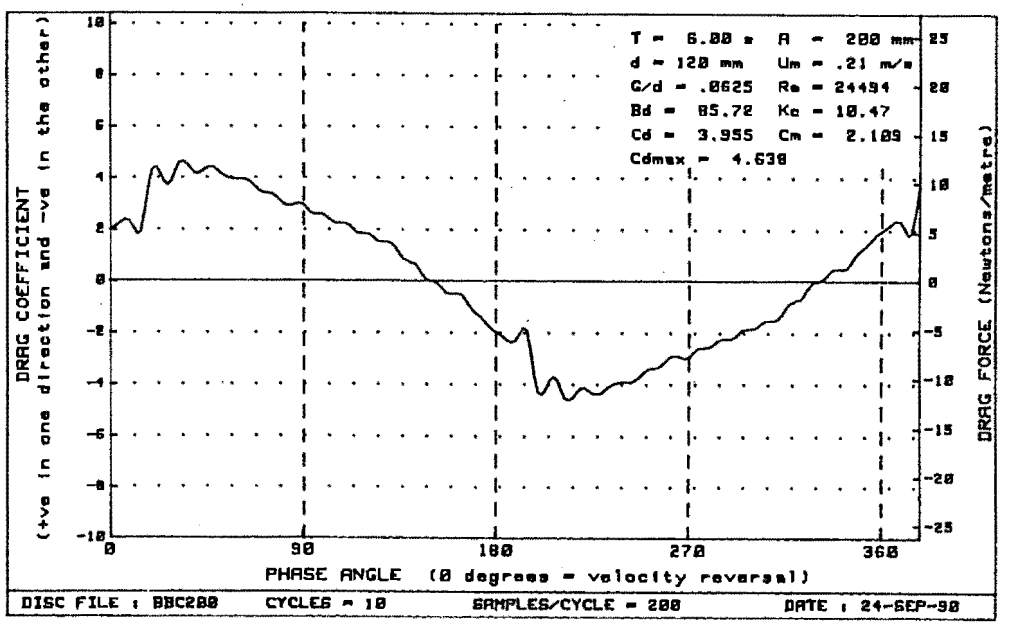

Figure H - 29 : Plots of drag vs phase for diameter=120mm, Bd= 85.72 and G/d= .0625

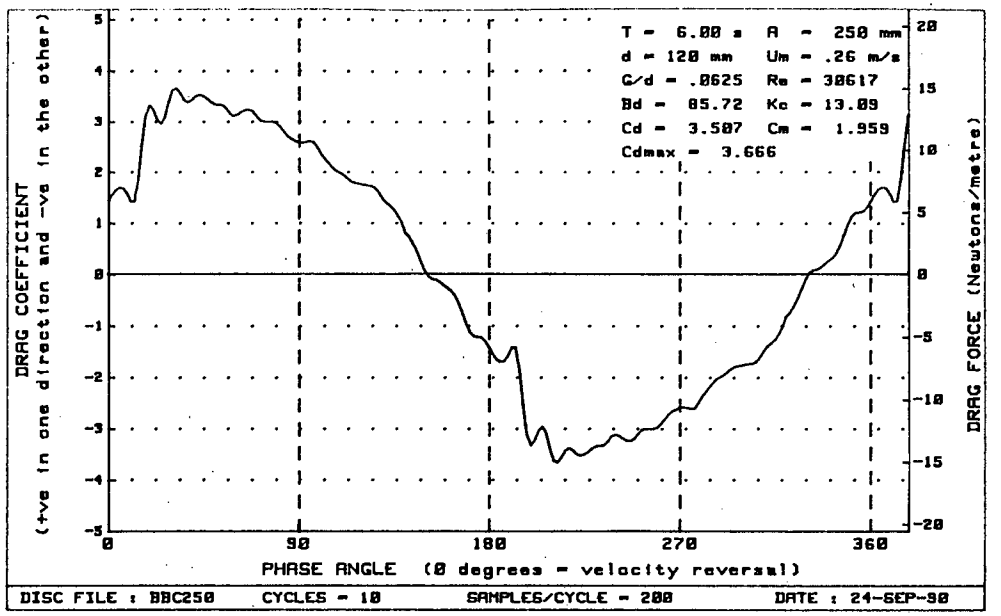

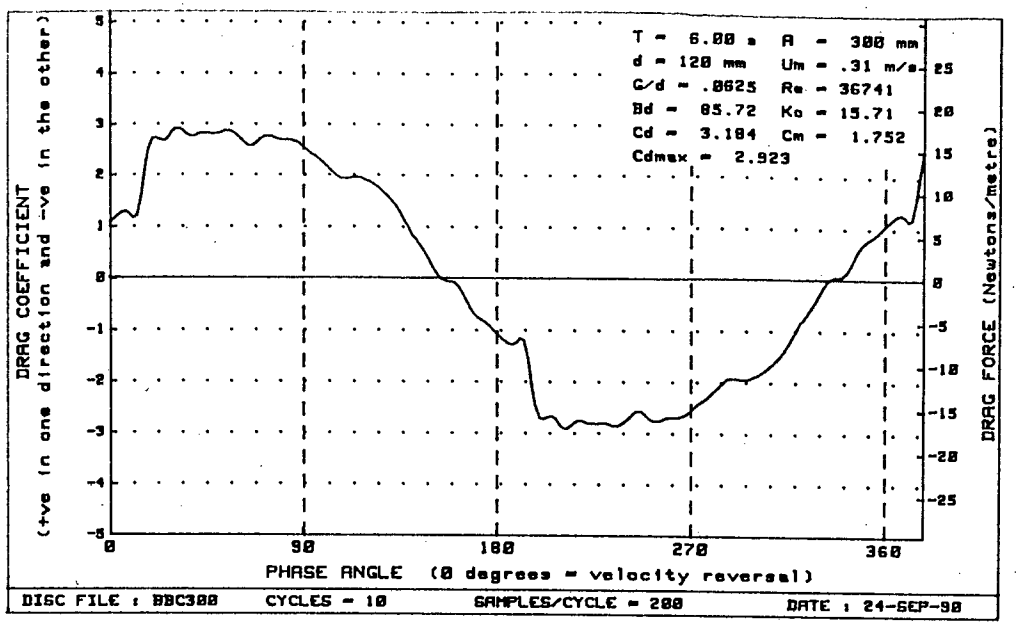

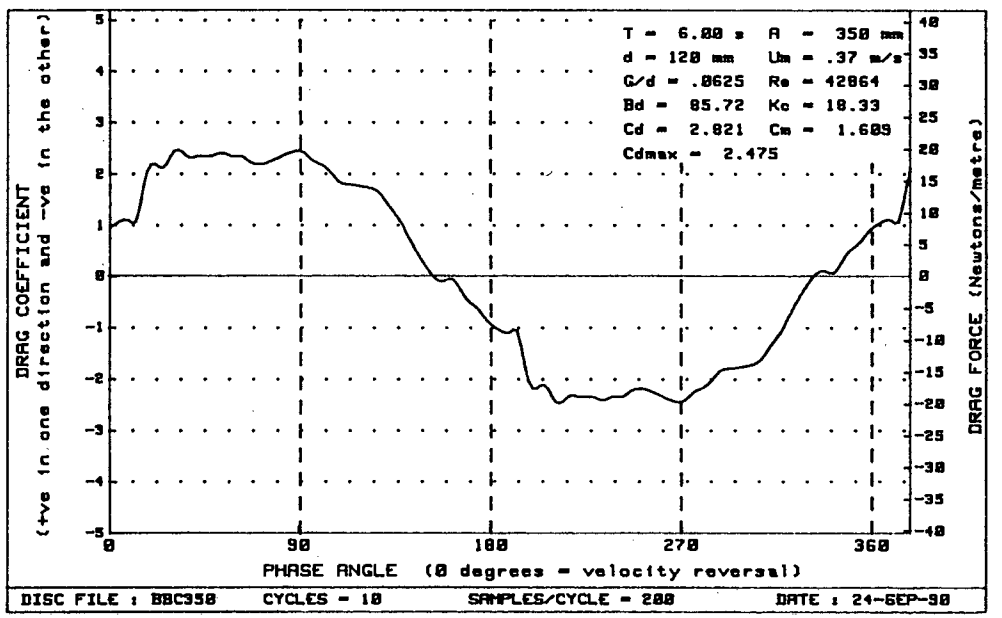

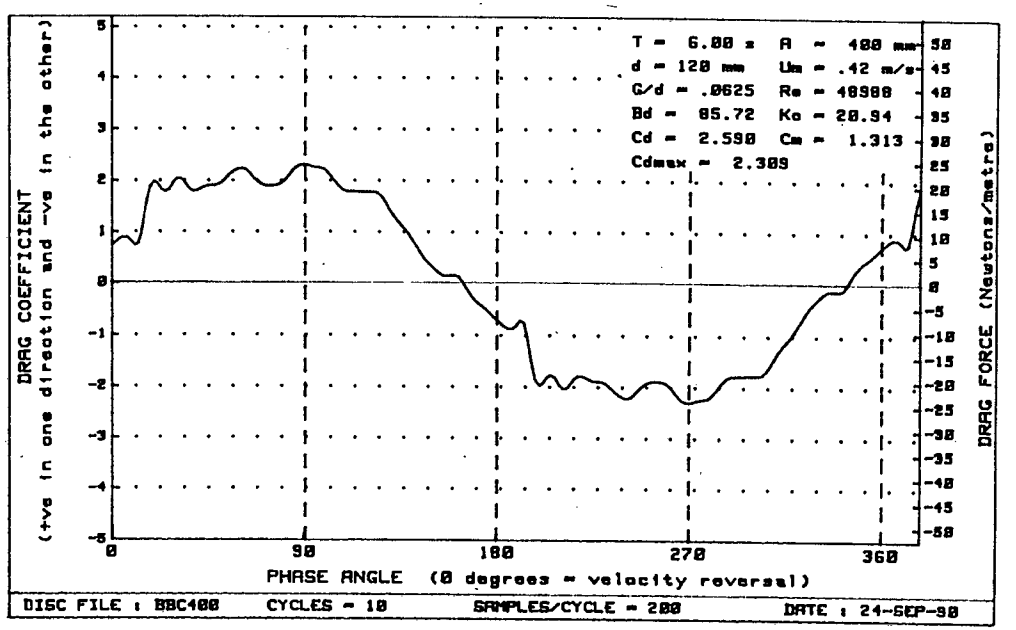

Figure H - 30 : Plots of drag vs phase for diameter=120mm, Bd= 85.72 and G/d= .0625

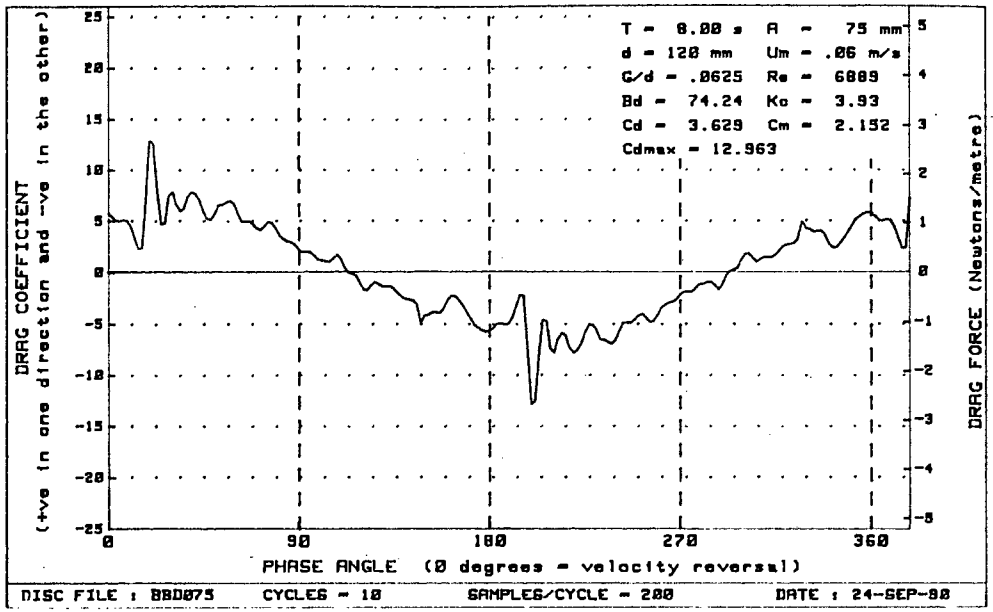

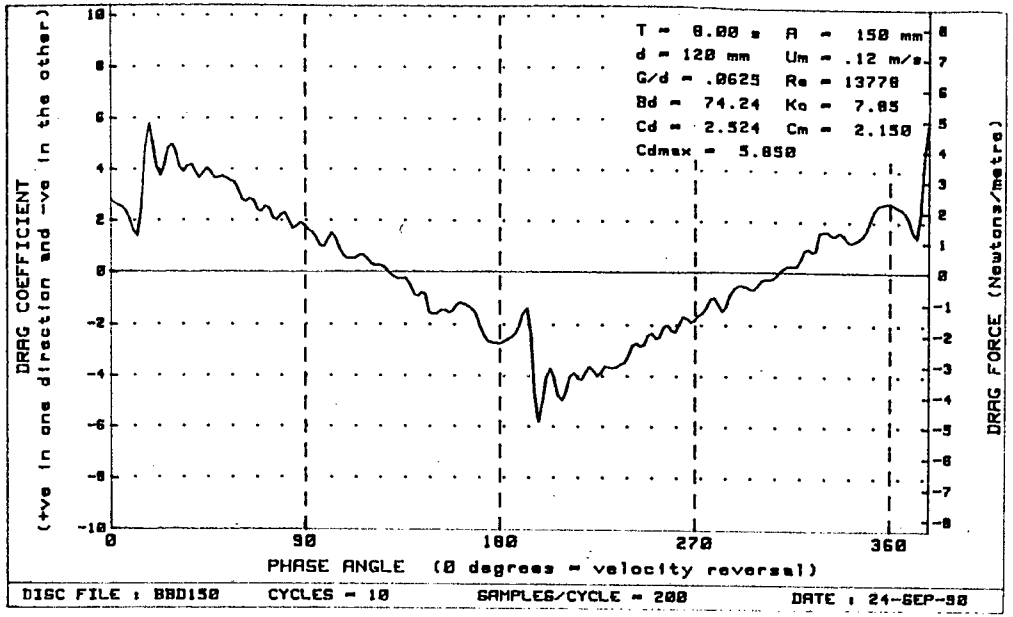

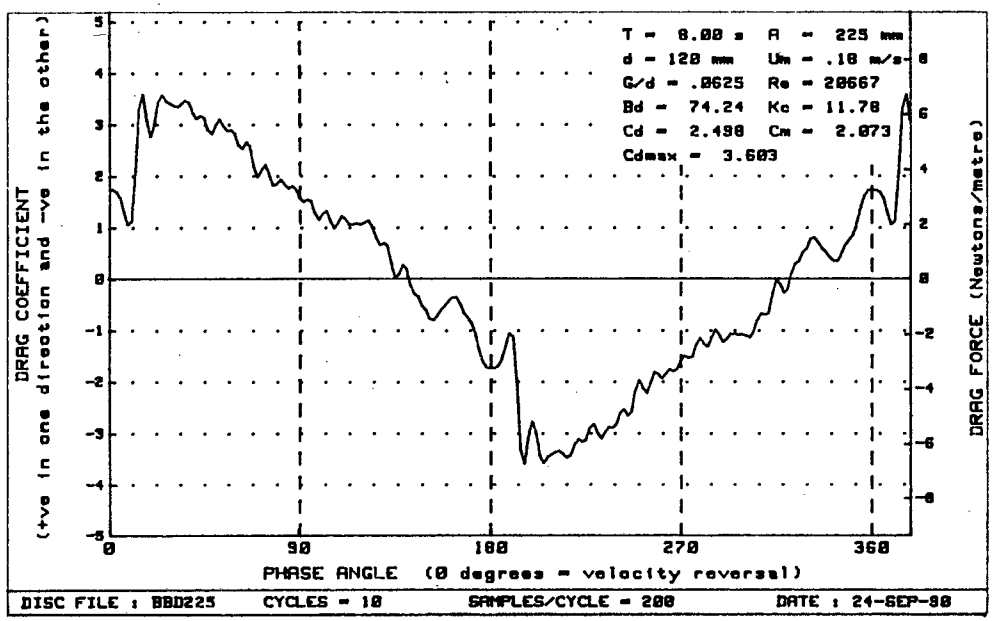

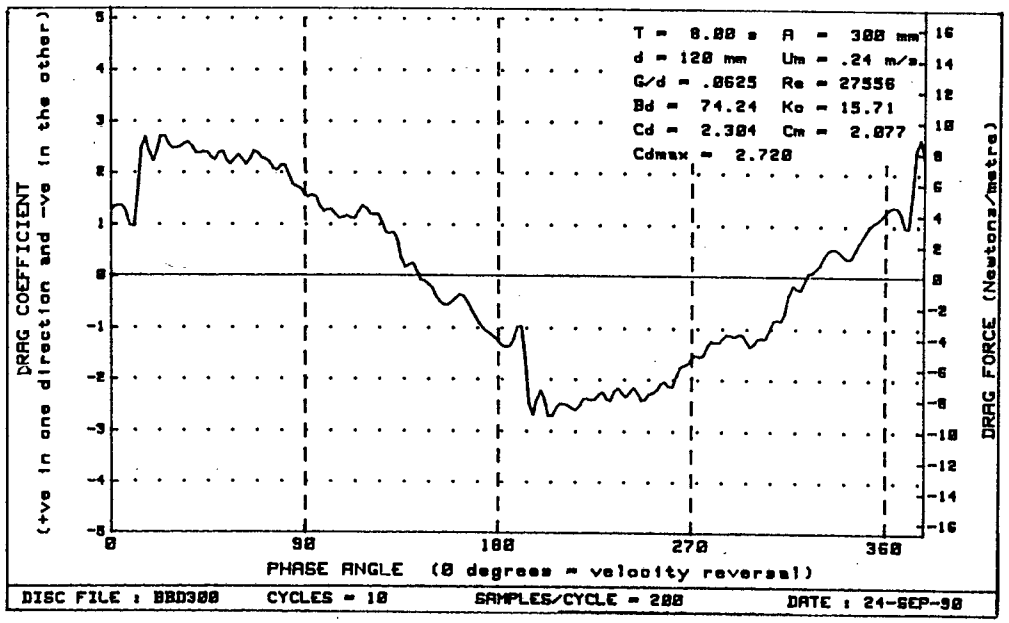

Figure H – 31 : Plots of drag vs phase for diameter=120mm, Bd= 74.24 and G/d= .0625

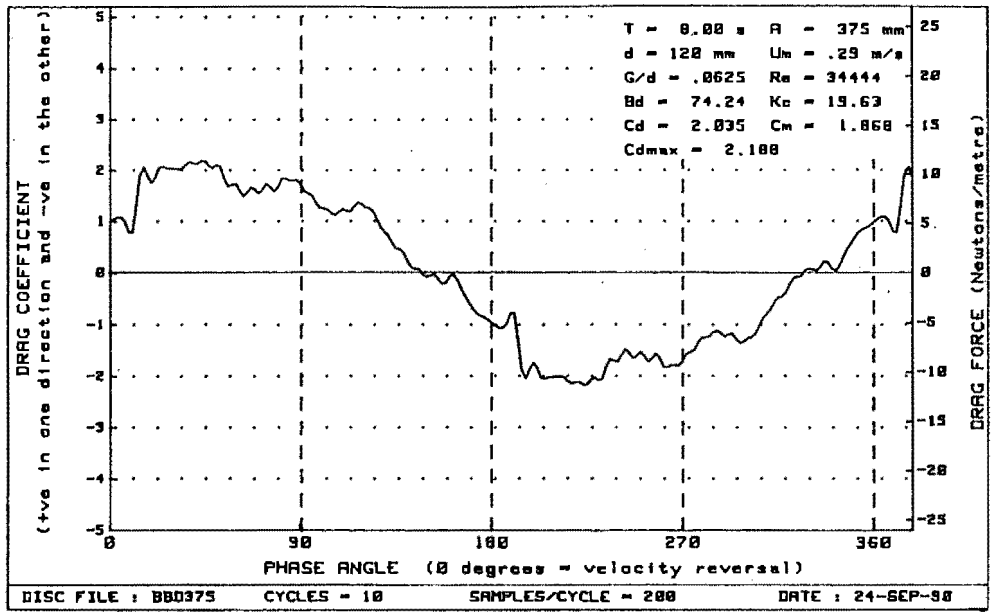

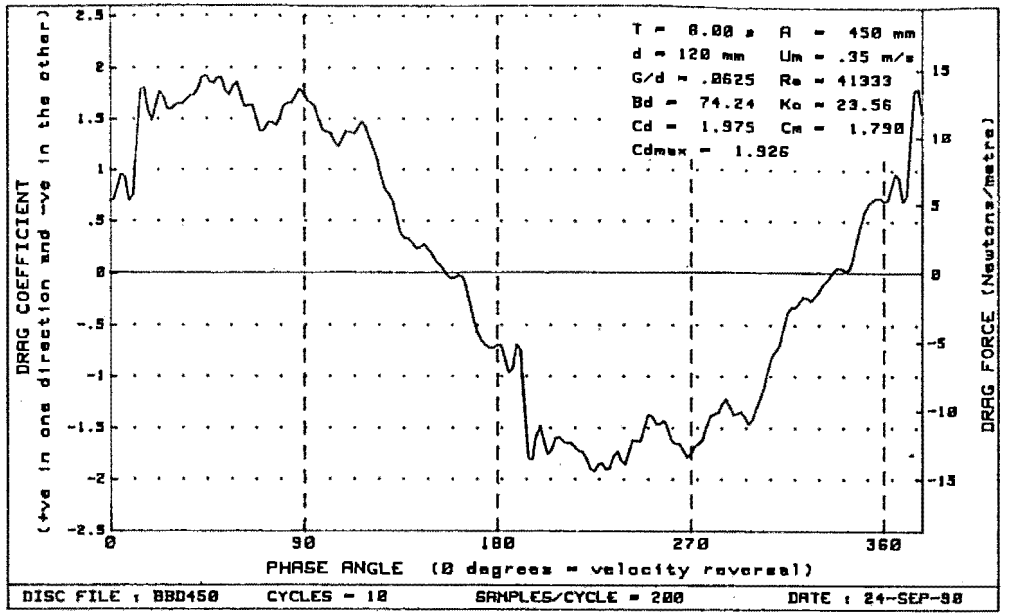

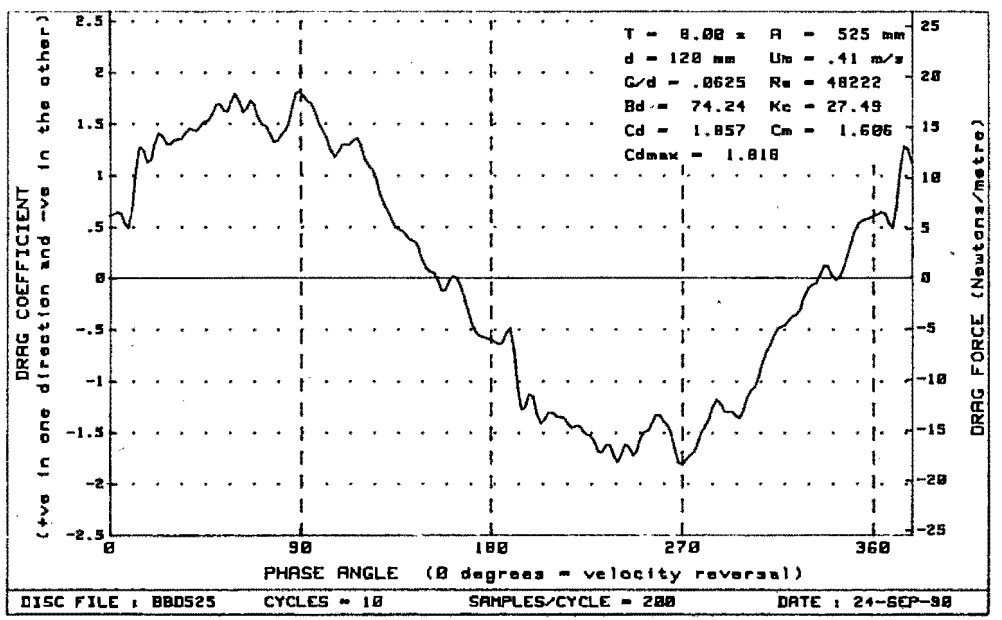

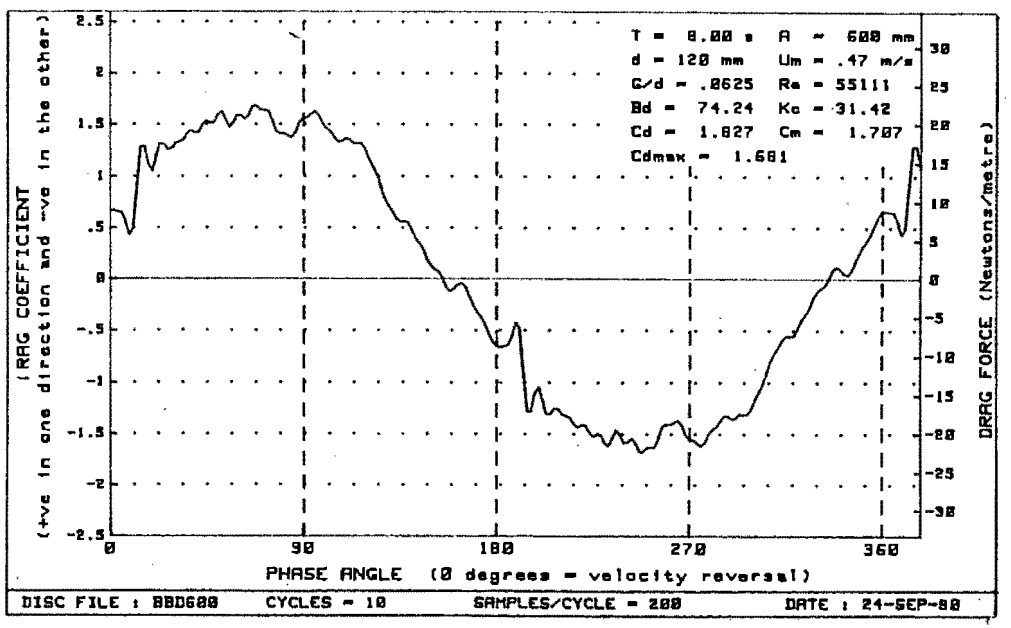

Figure H – 32 : Plots of drag vs phase for diameter=120mm, Bd= 74.24 and G/d= .0625

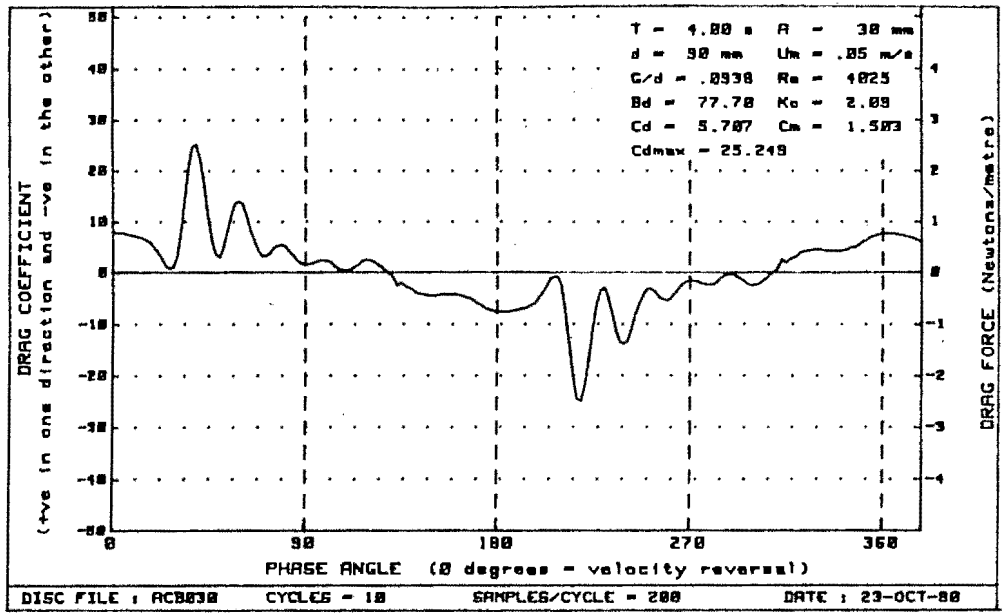

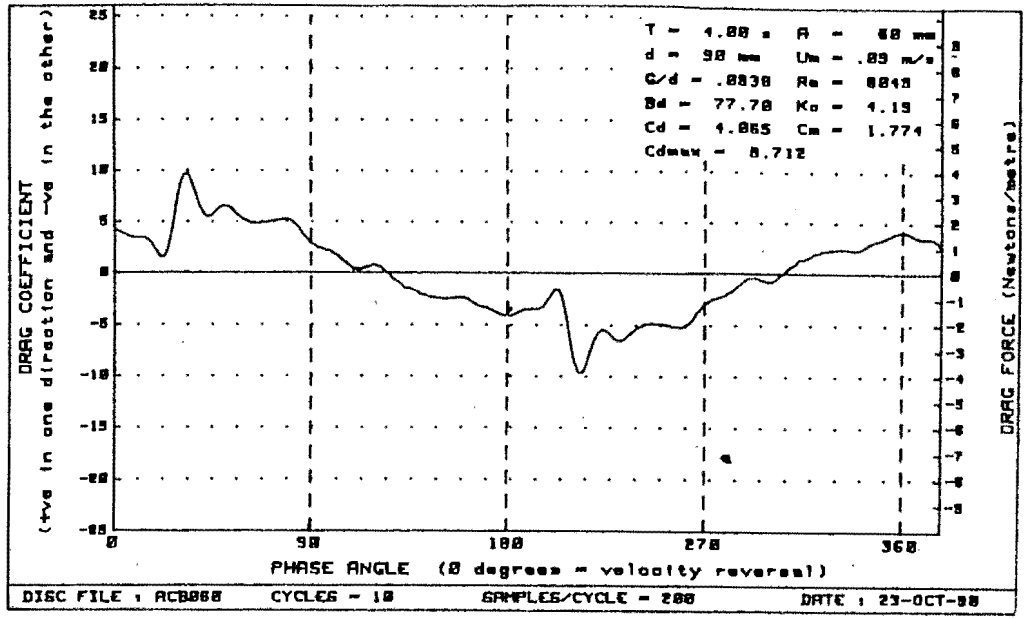

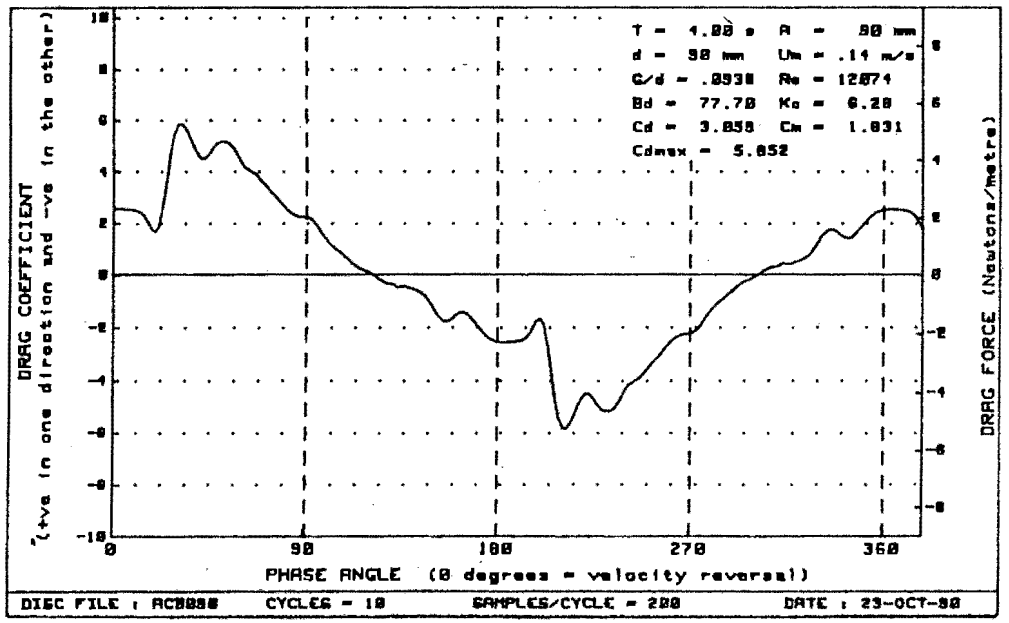

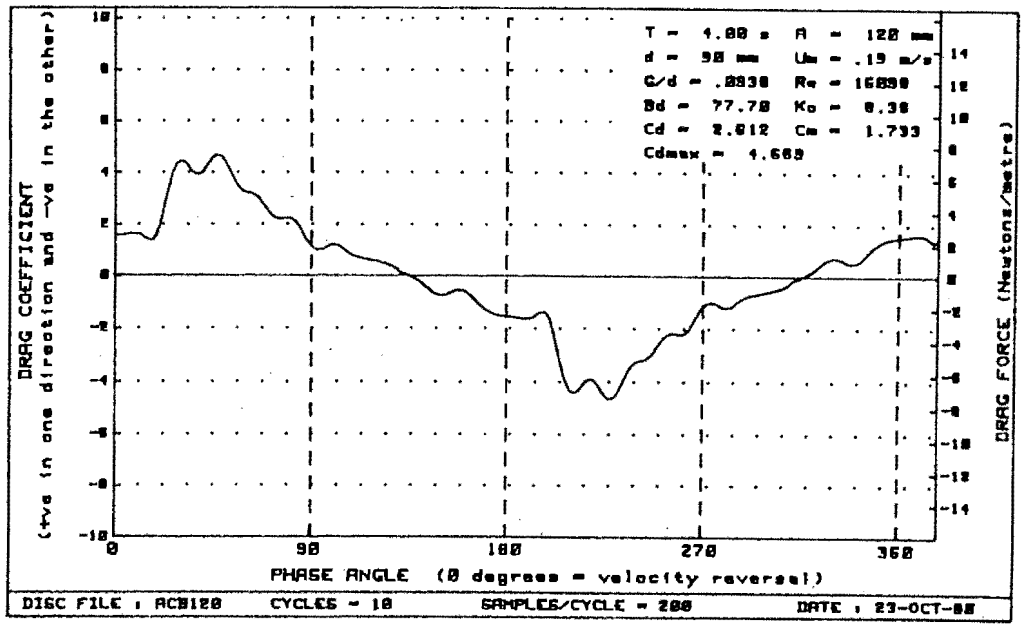

Figure H-33 : Plots of drag vs phase for diameter=90mm, Bd= 77.70 and G/d= .0938

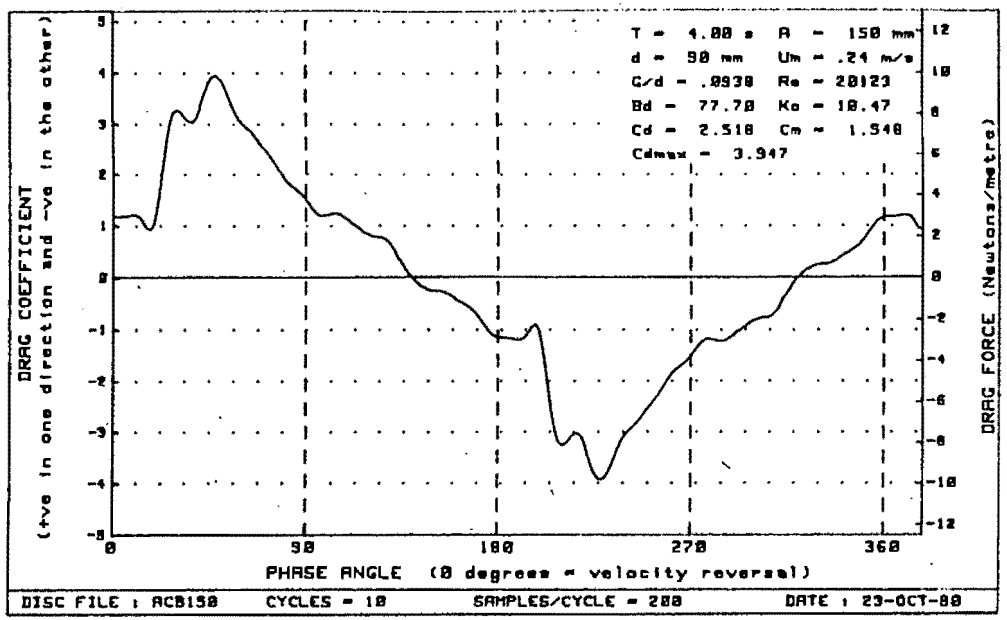

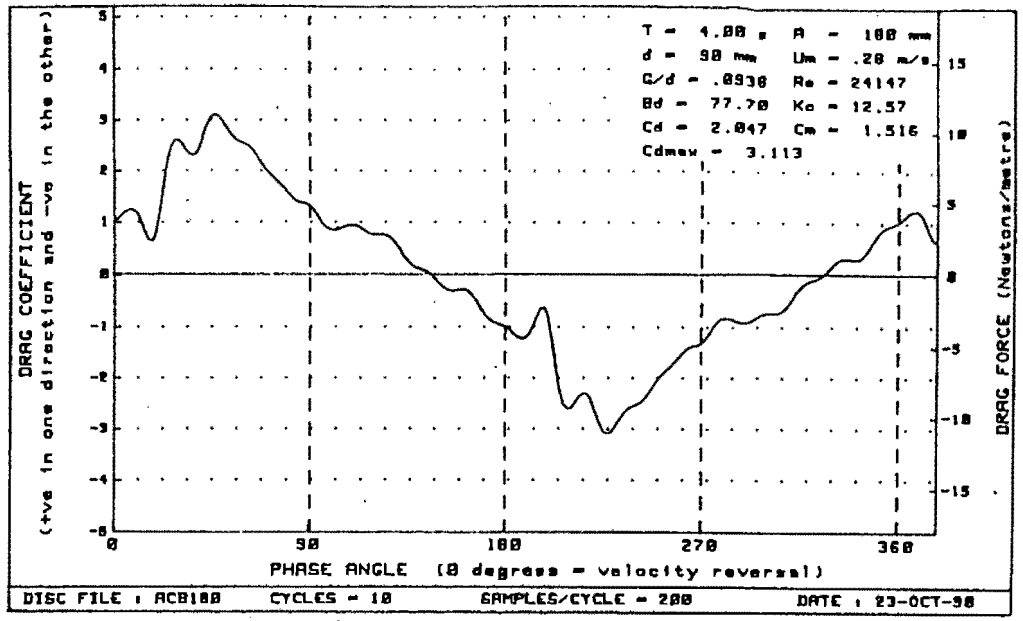

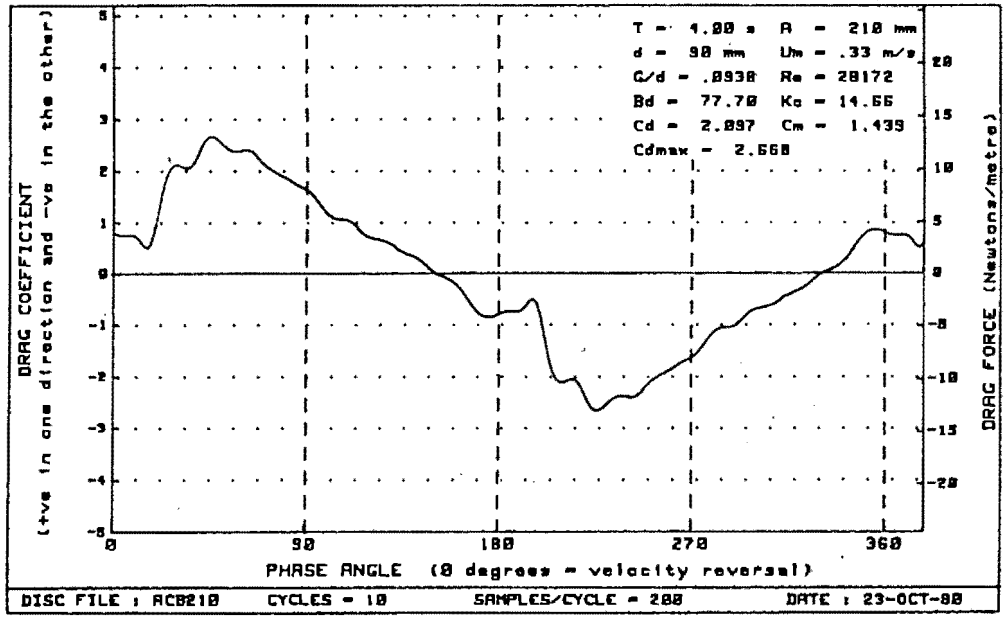

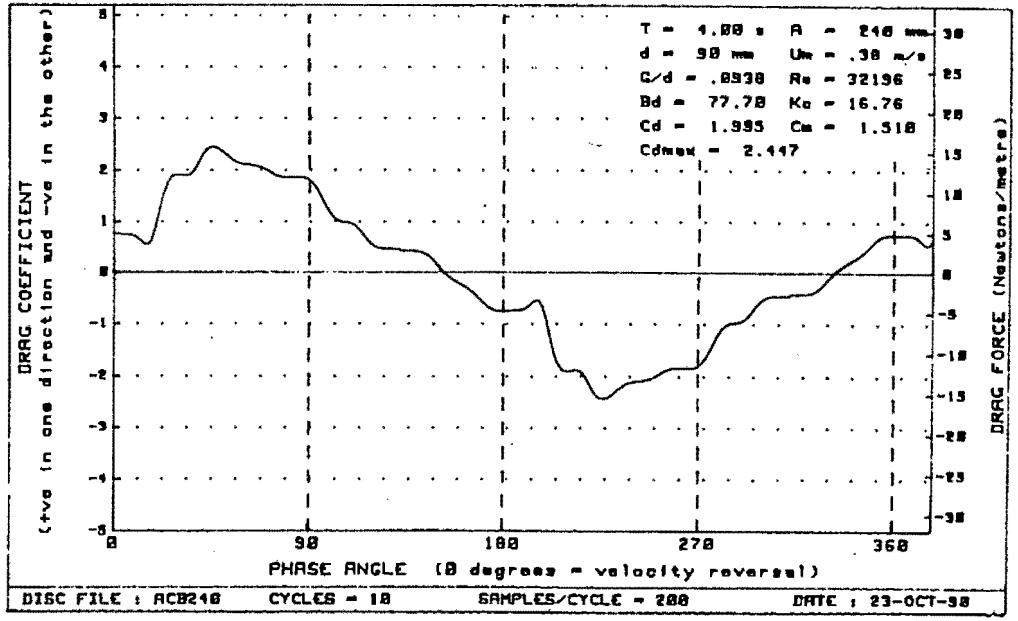

Figure H-34 : Plots of drag vs phase for diameter=90mm, Bd= 77.70 and G/d= .0938

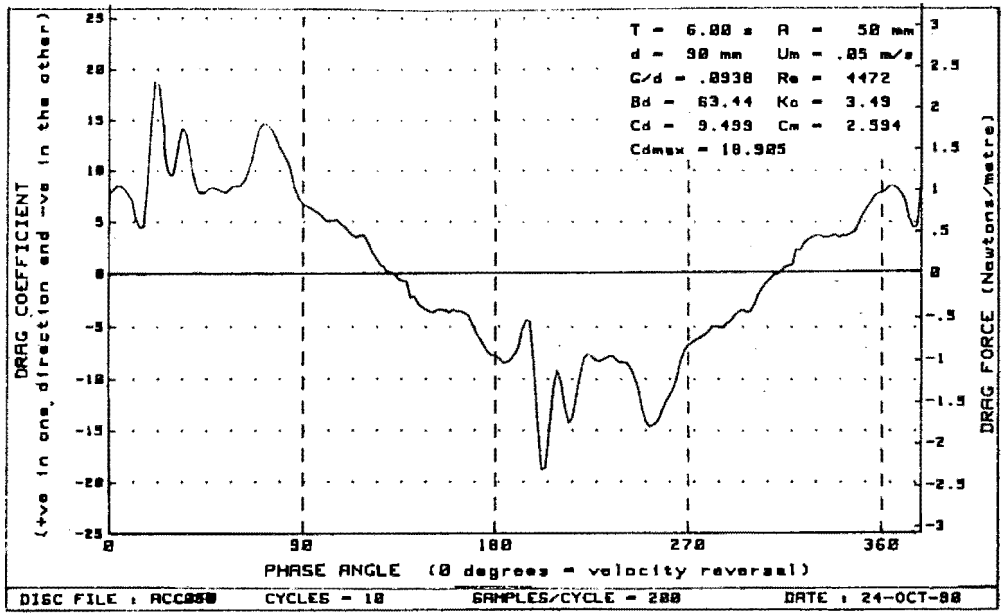

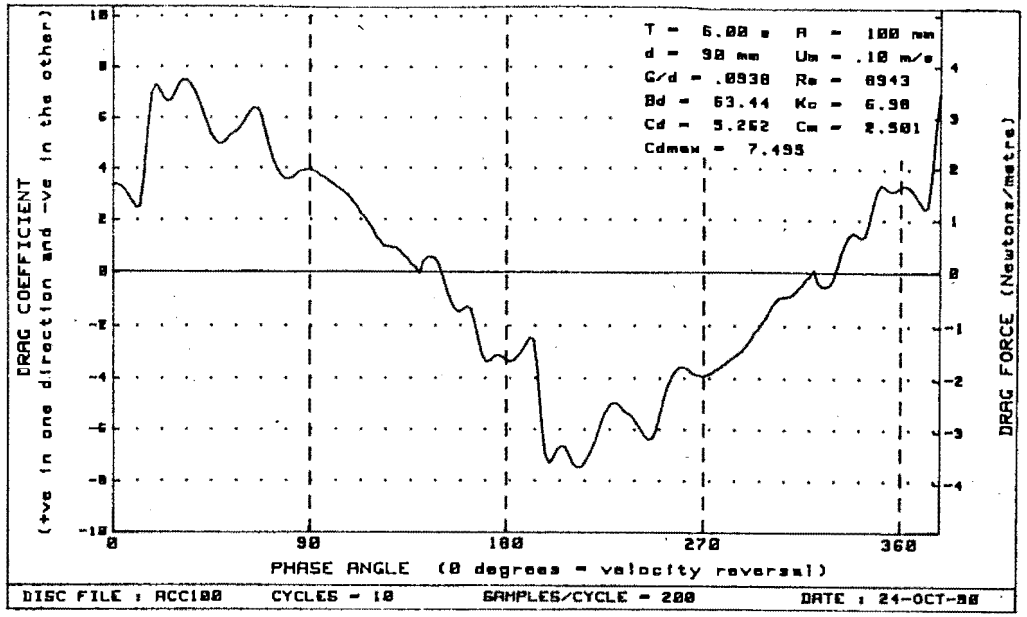

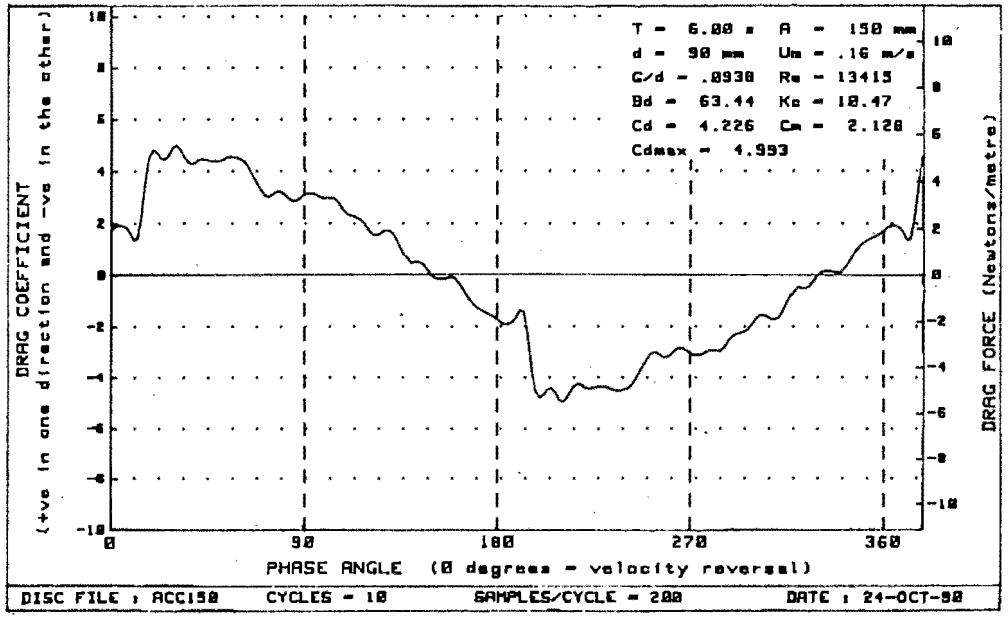

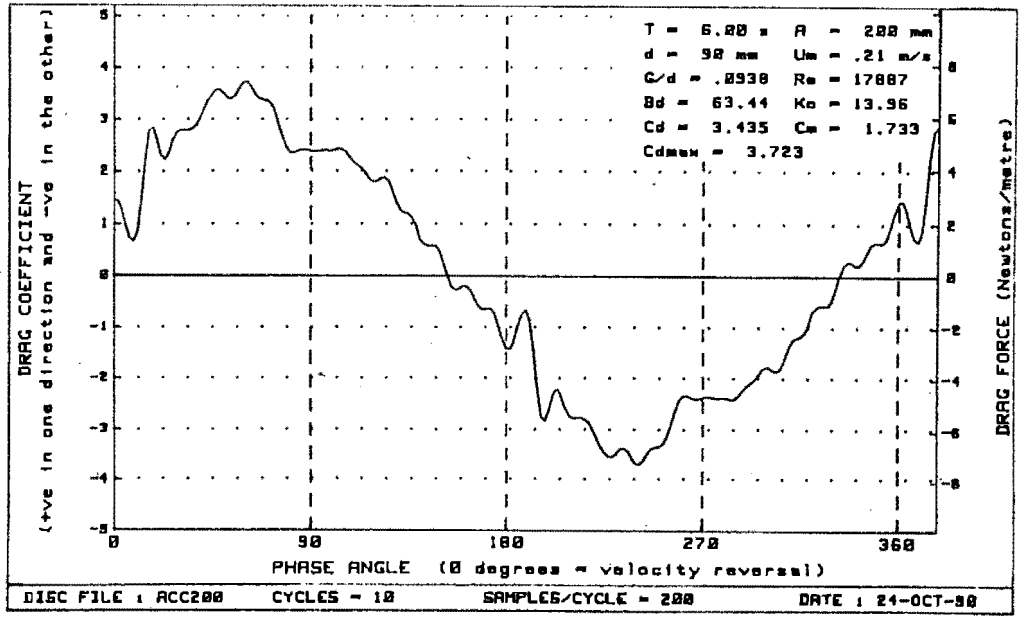

Figure H-35 : Plots of drag vs phase for diameter=90mm, Bd= 63.44 and G/d= .0938

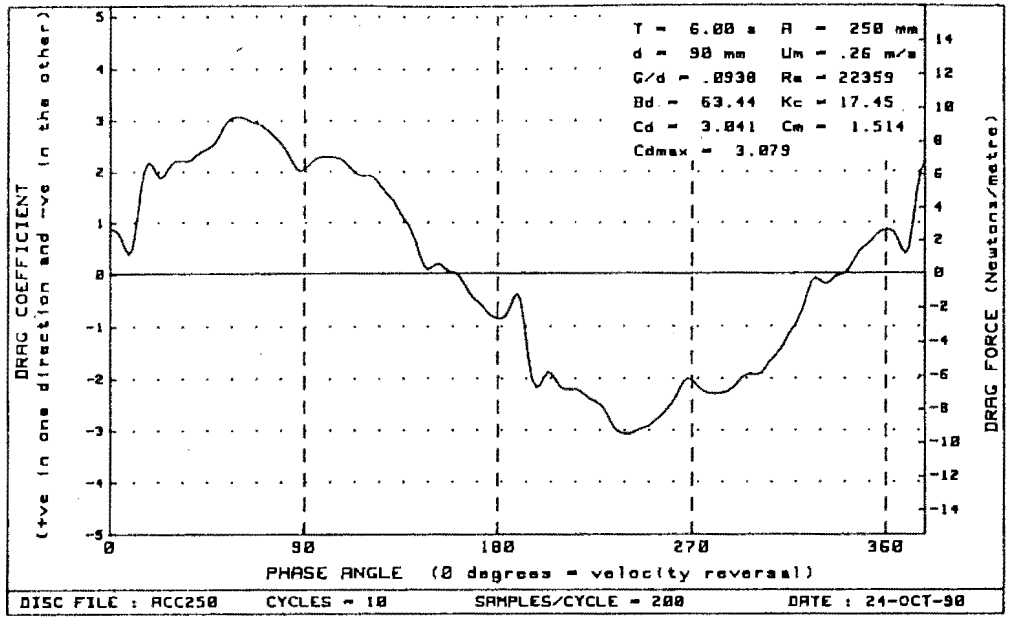

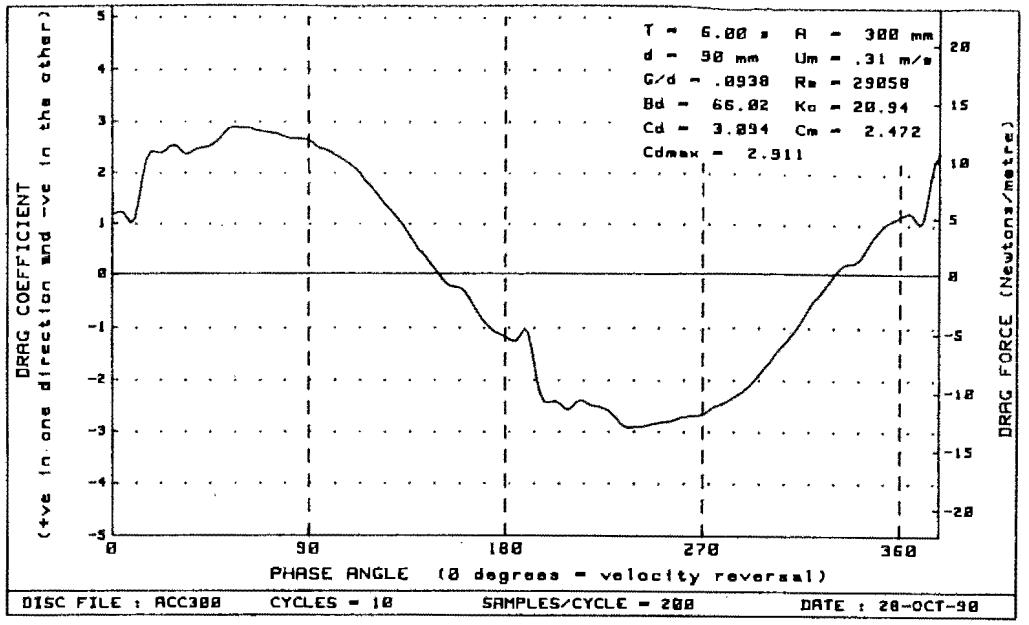

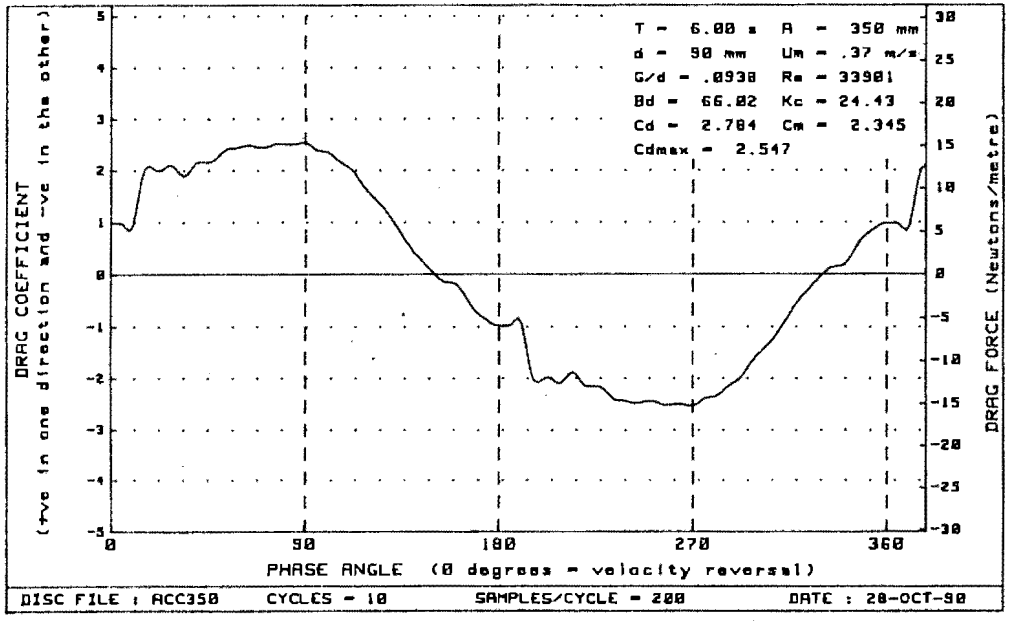

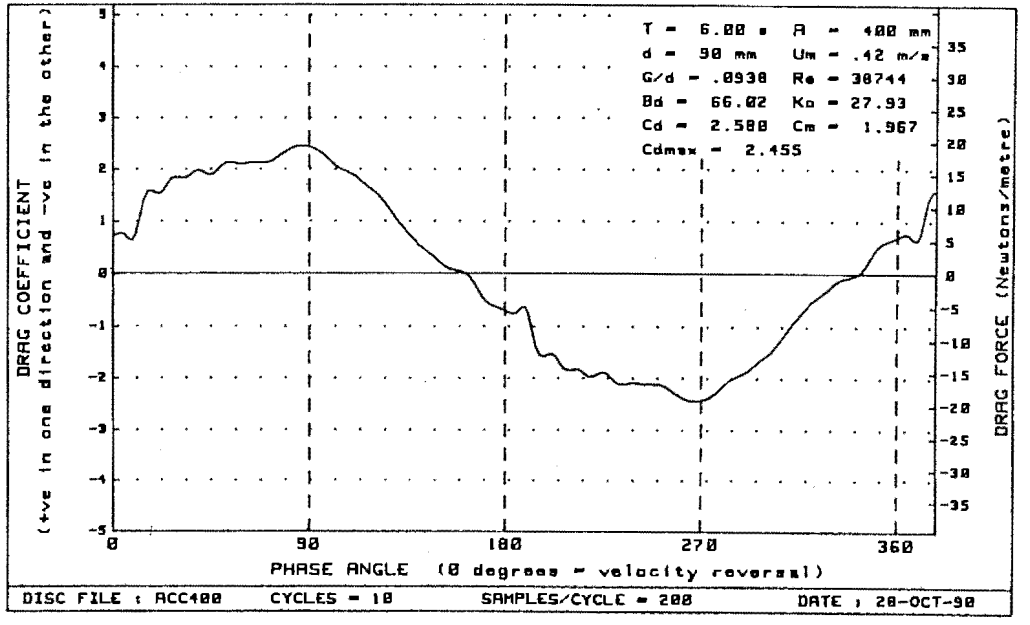

Figure H-36 : Plots of drag vs phase for diameter=90mm, Bd= 66.02 and G/d= .0938

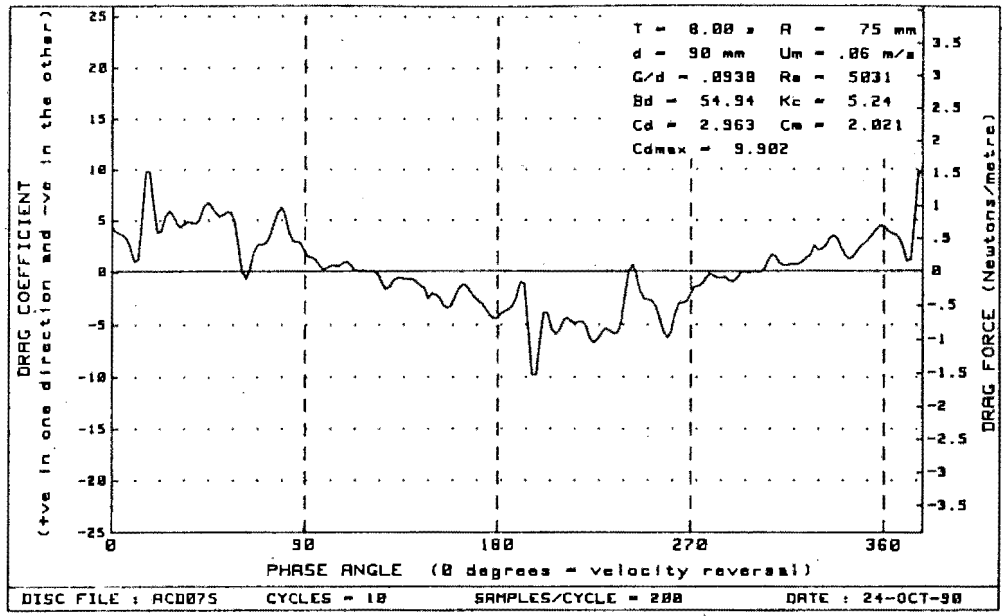

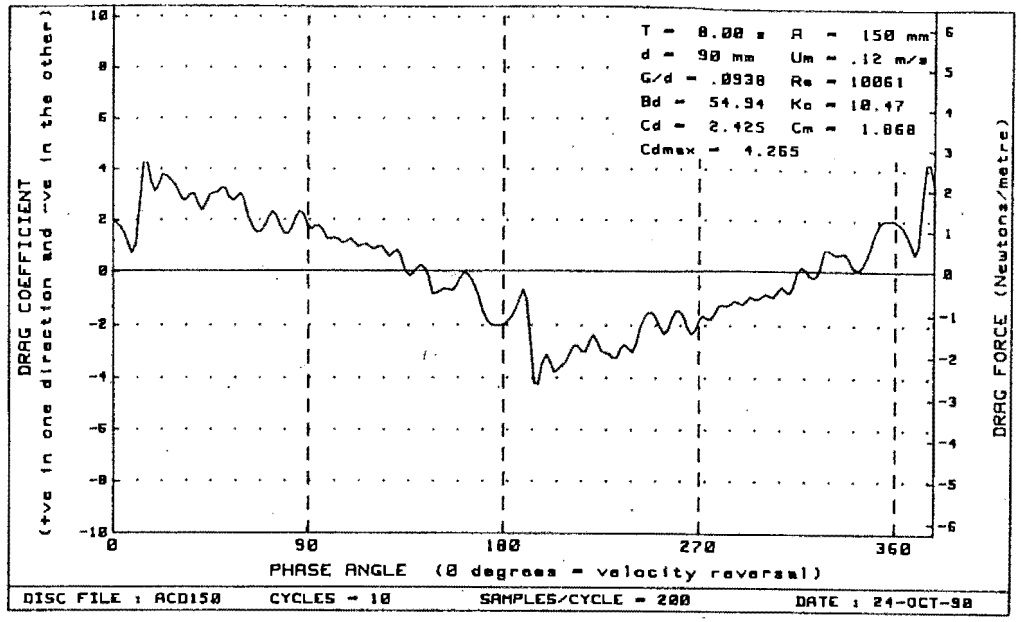

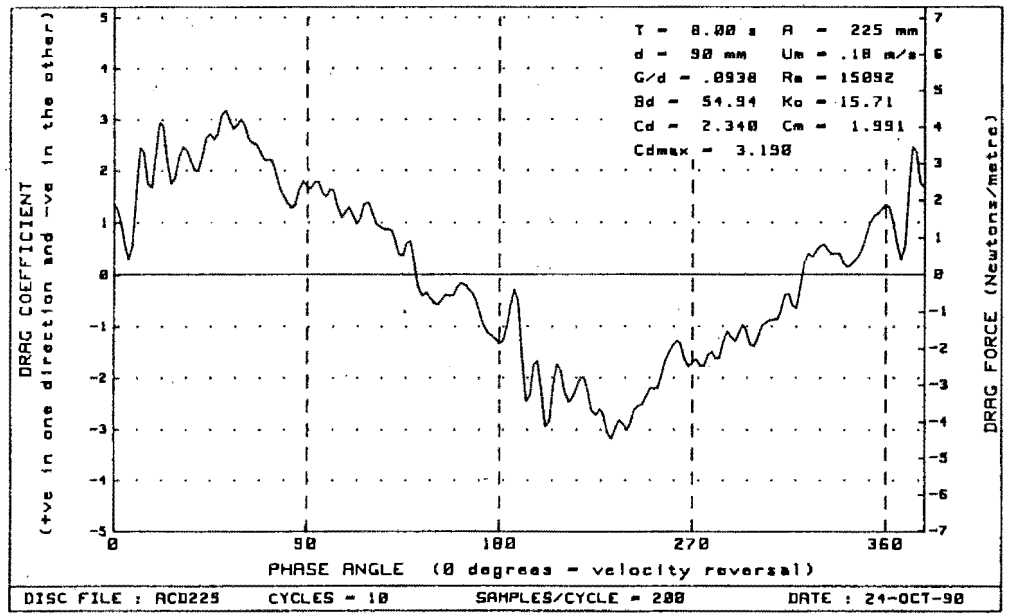

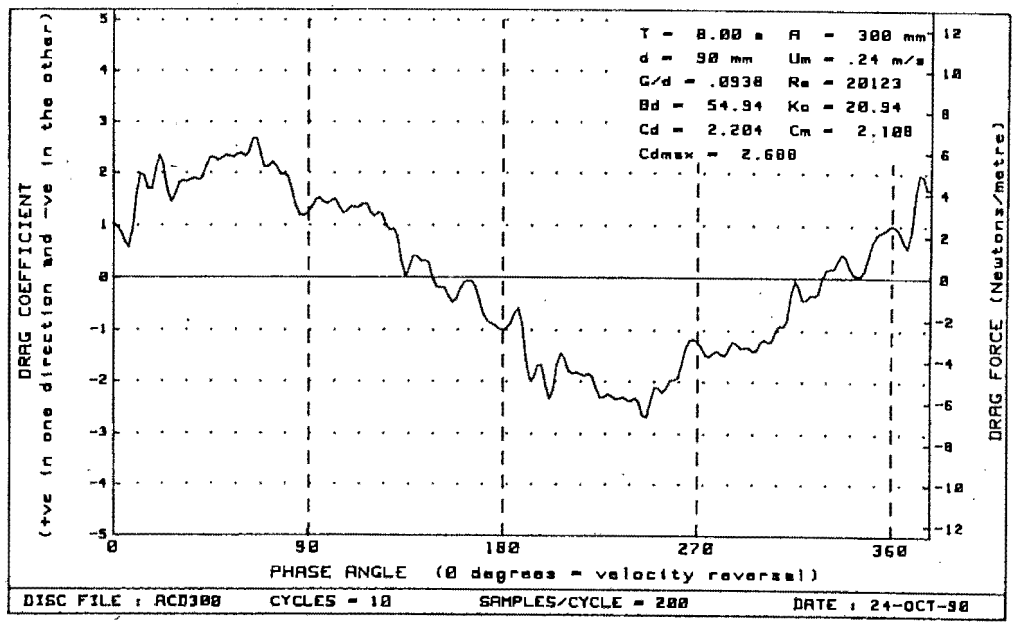

Figure H-37 : Plots of drag vs phase for diameter=90mm, Bd= 54.94 and G/d= .0938

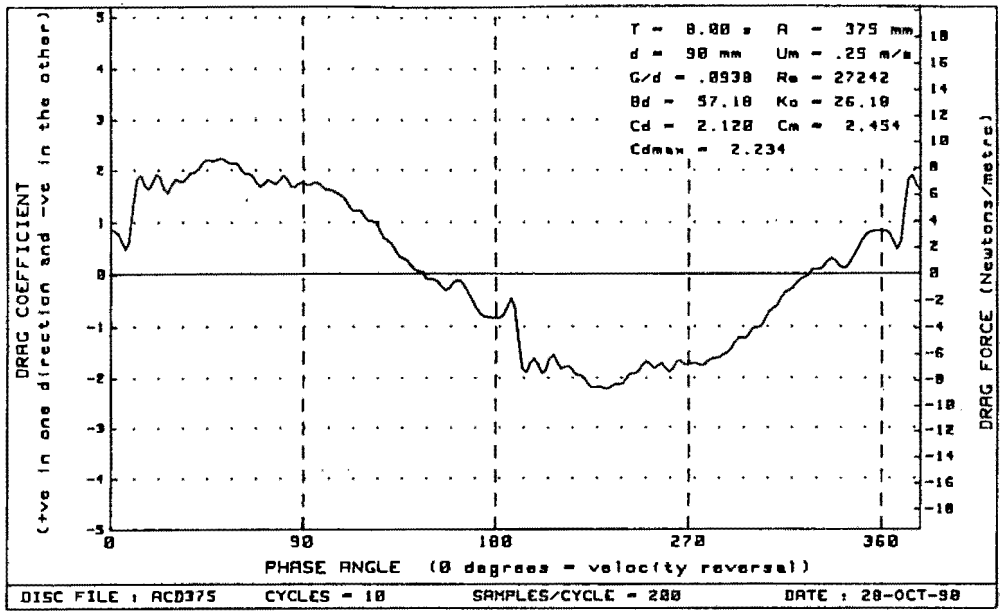

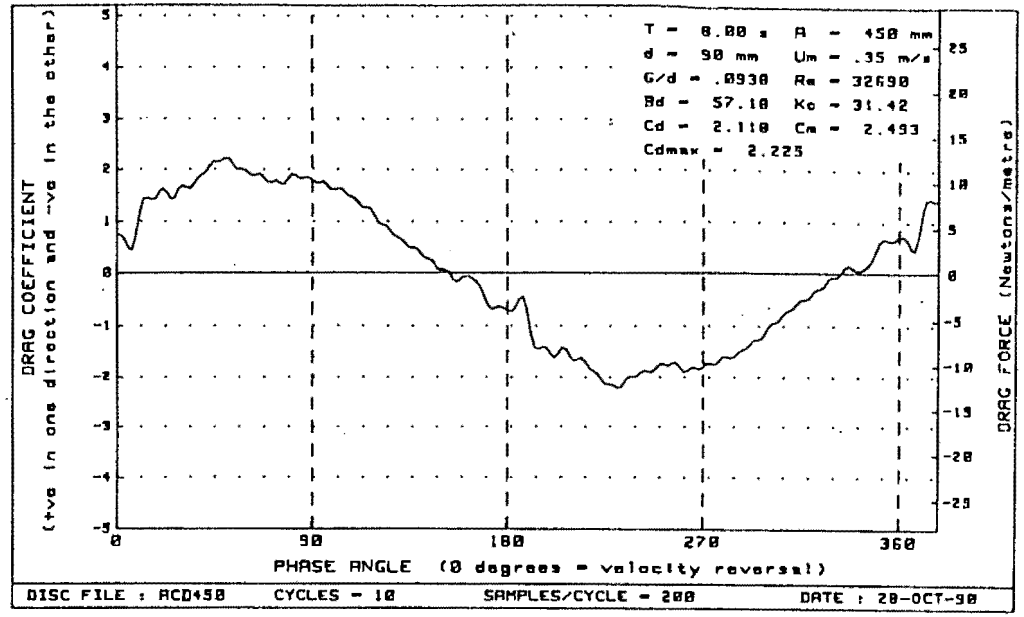

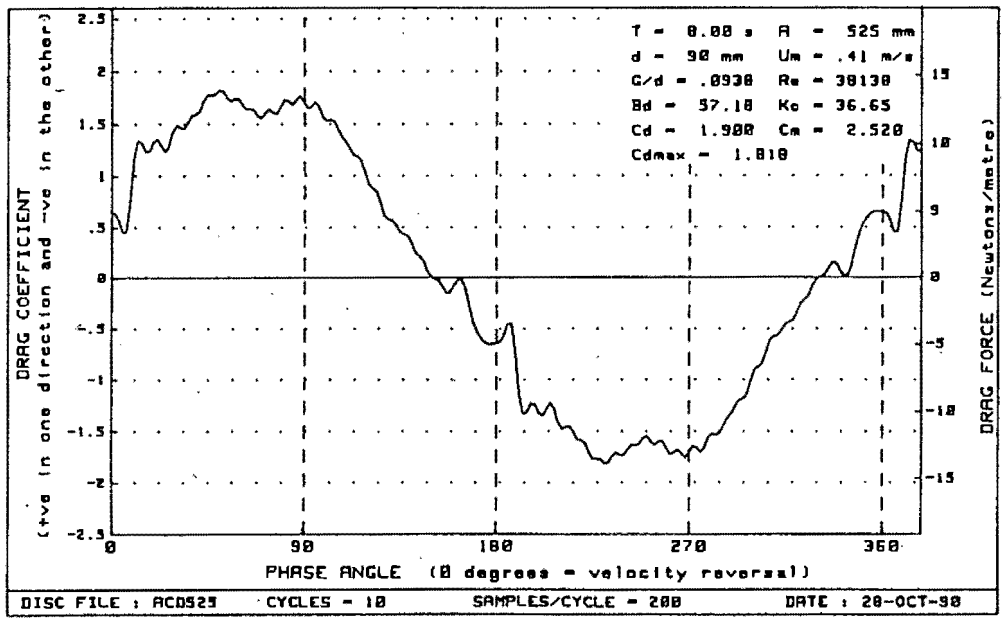

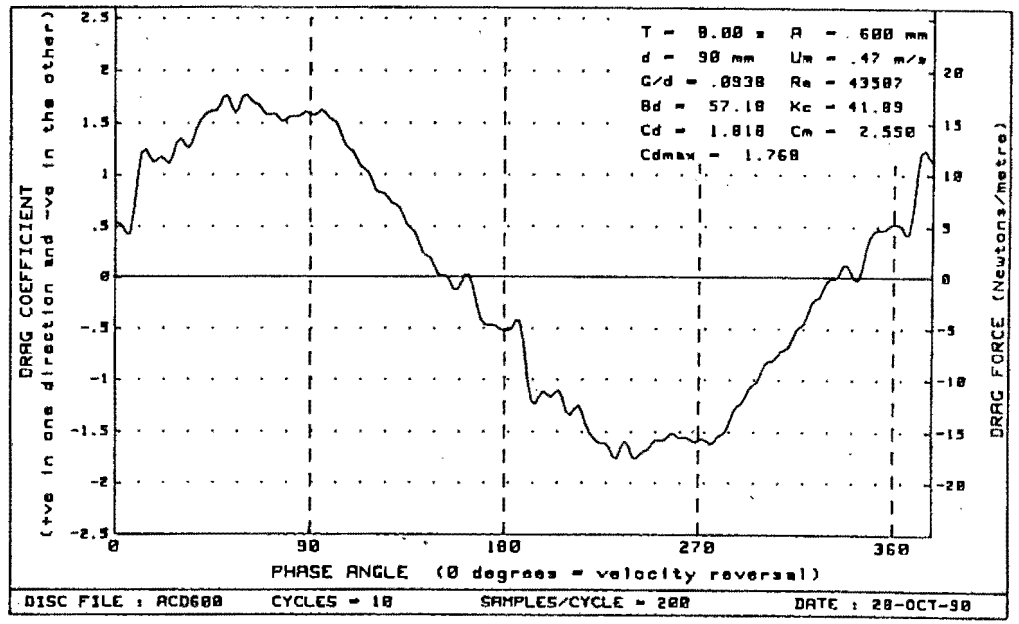

Figure H-38 : Plots of drag vs phase for diameter=90mm, Bd= 57.18 and G/d= .0938

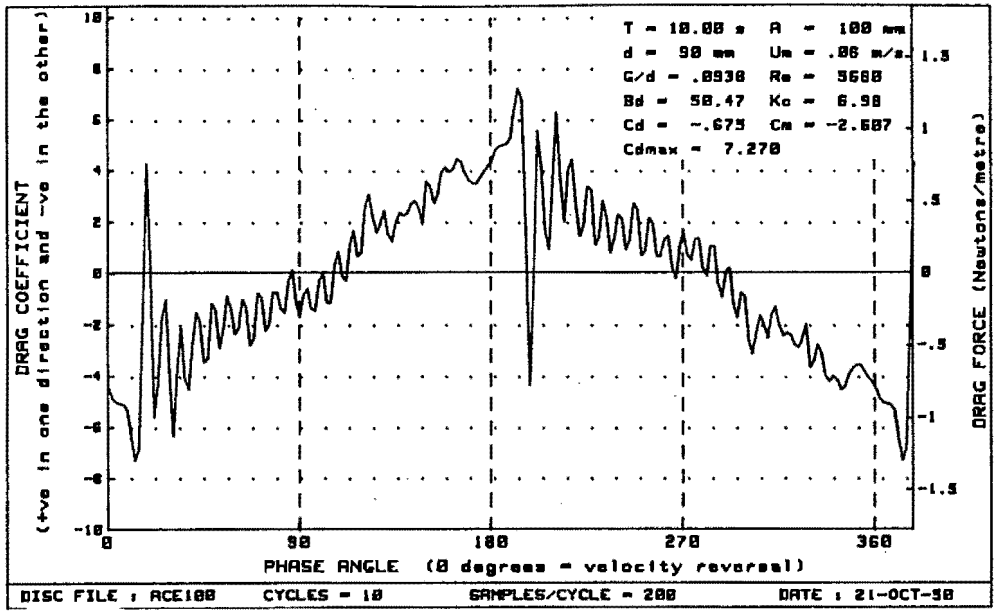

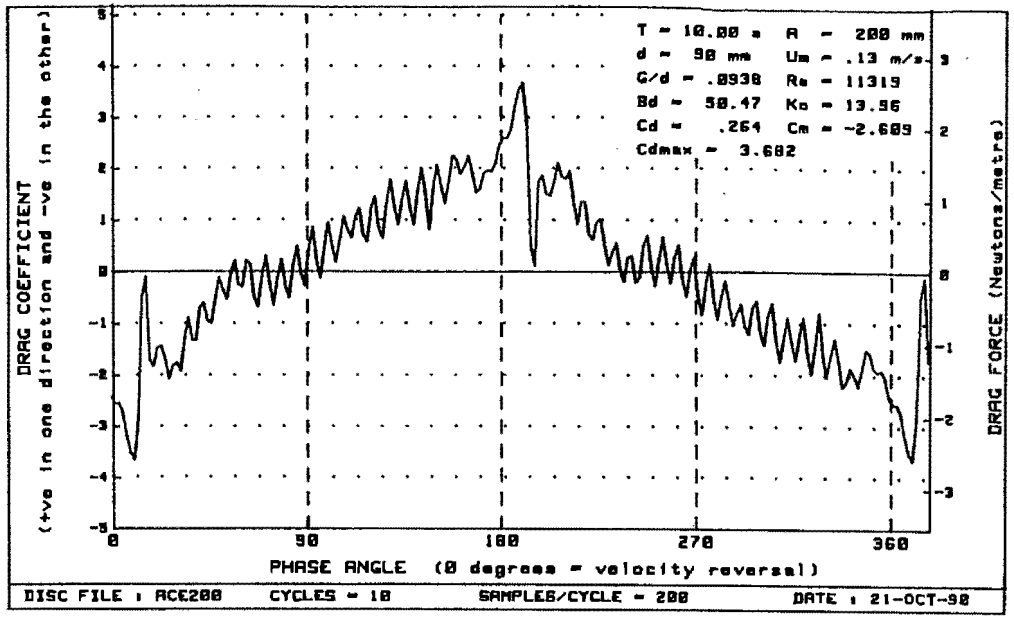

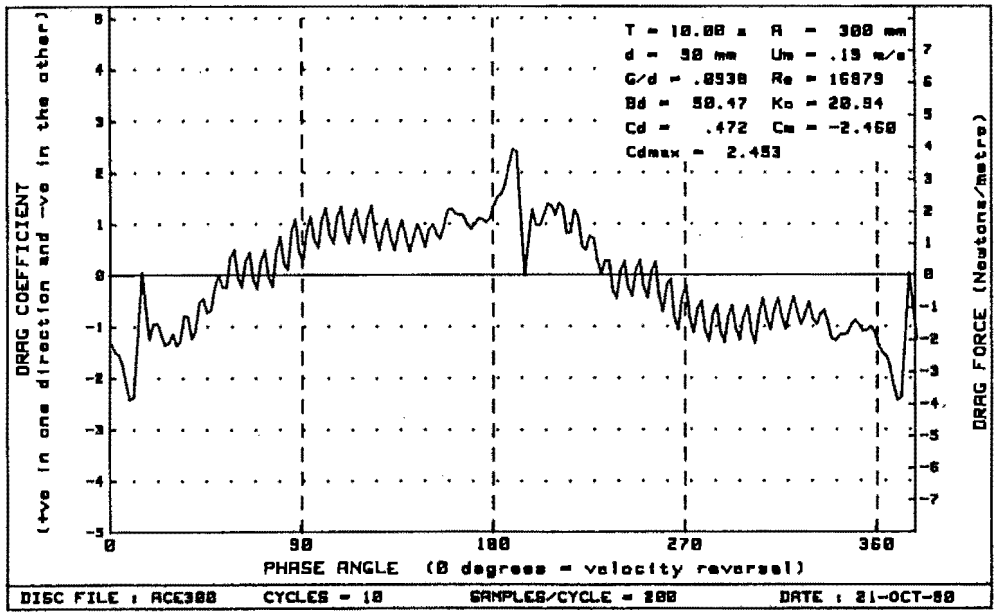

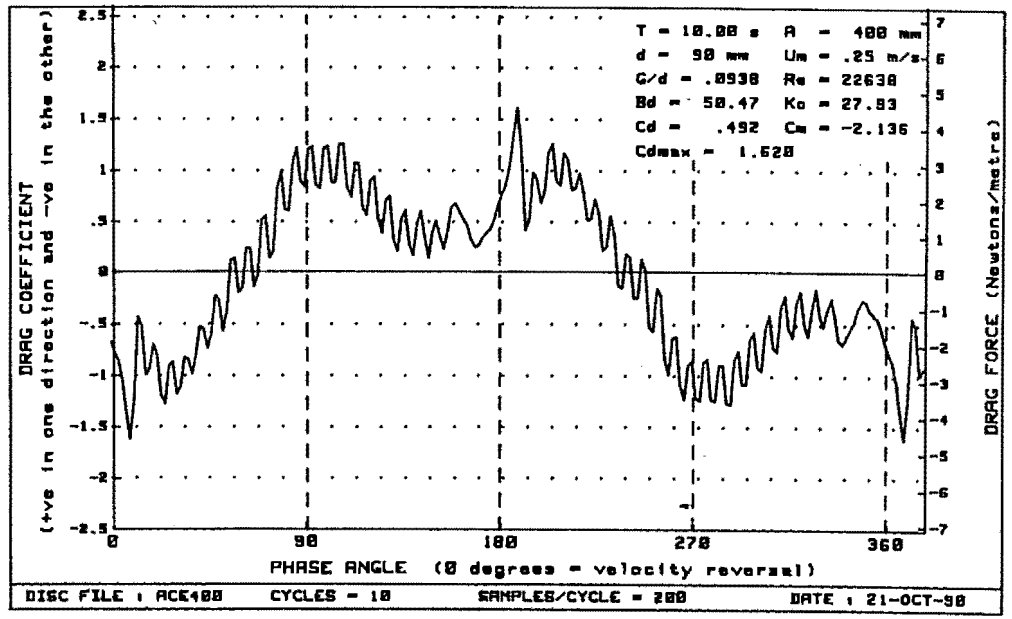

Figure H-39 : Plots of drag vs phase for diameter=90mm, Bd= 50.47 and G/d= .0938

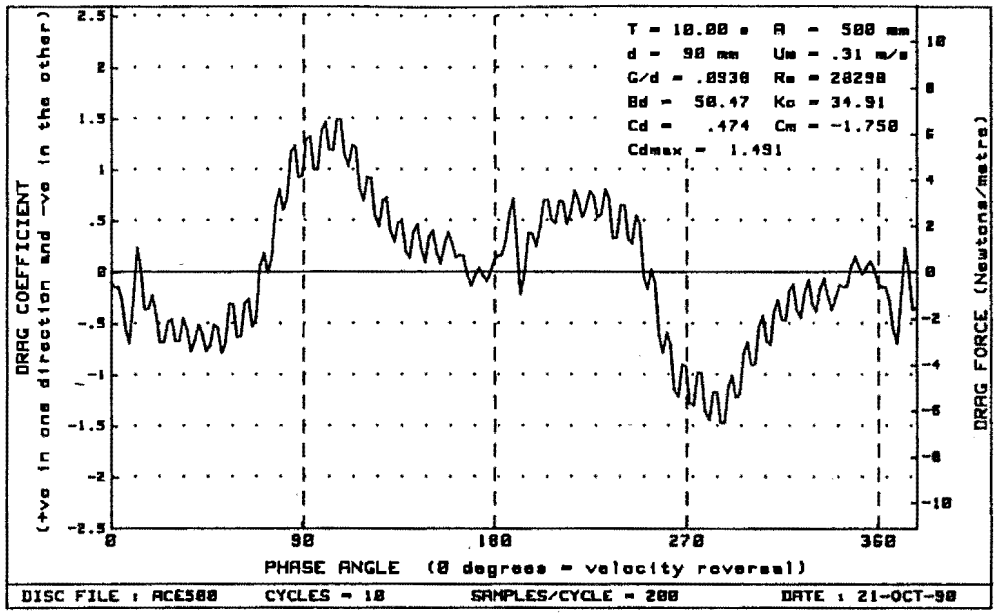

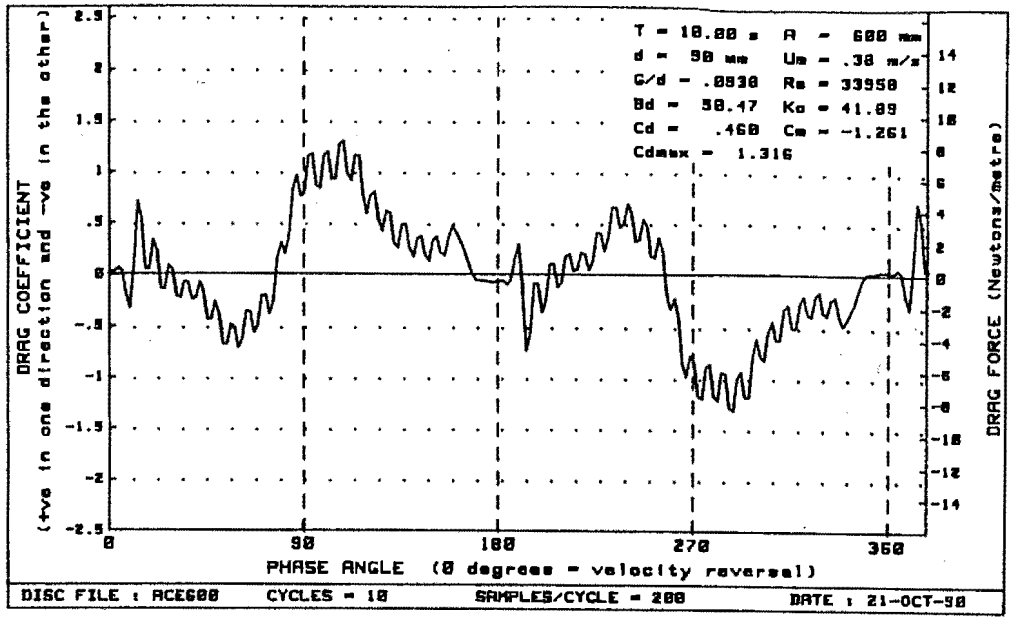

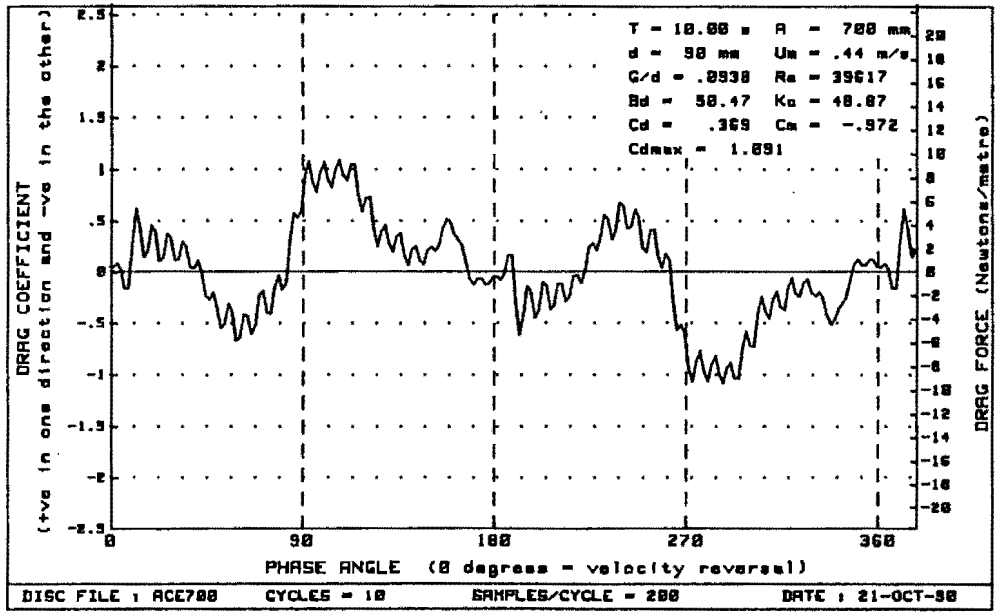

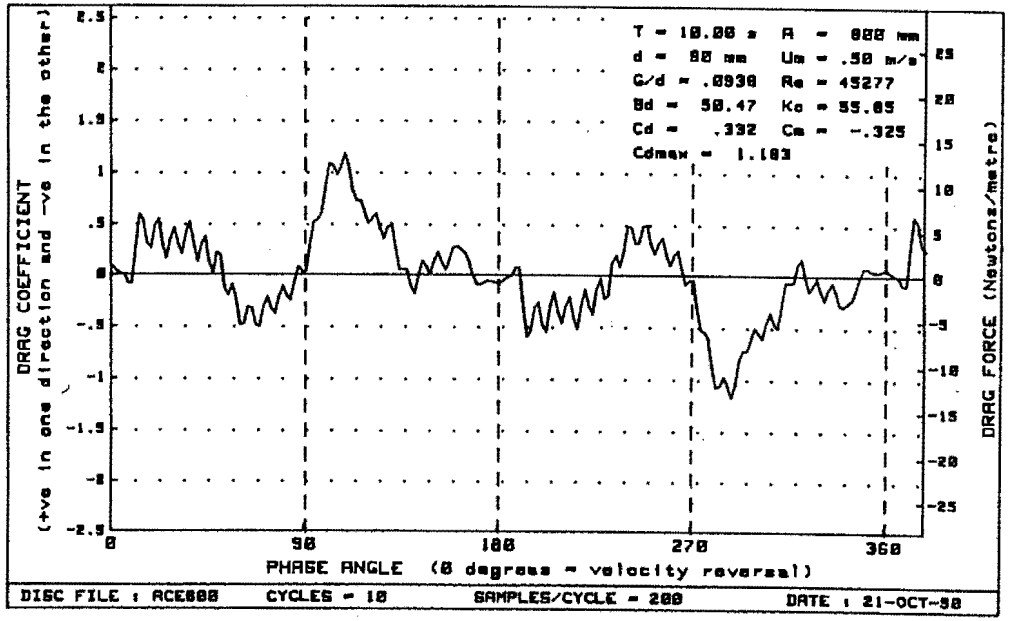

Figure H-40 : Plots of drag vs phase for diameter=90mm, Bd= 50.47 and G/d= .0938

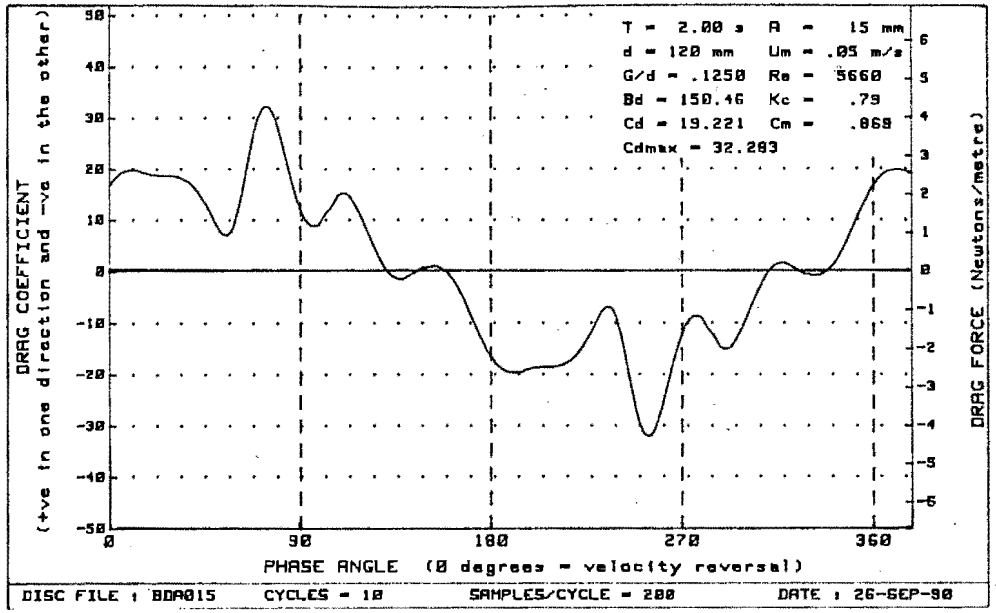

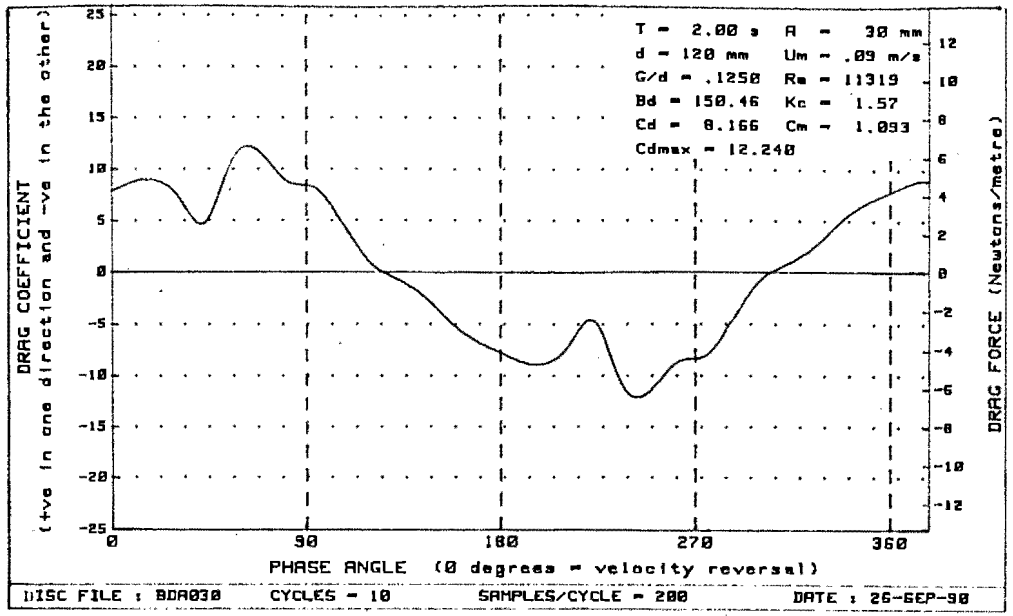

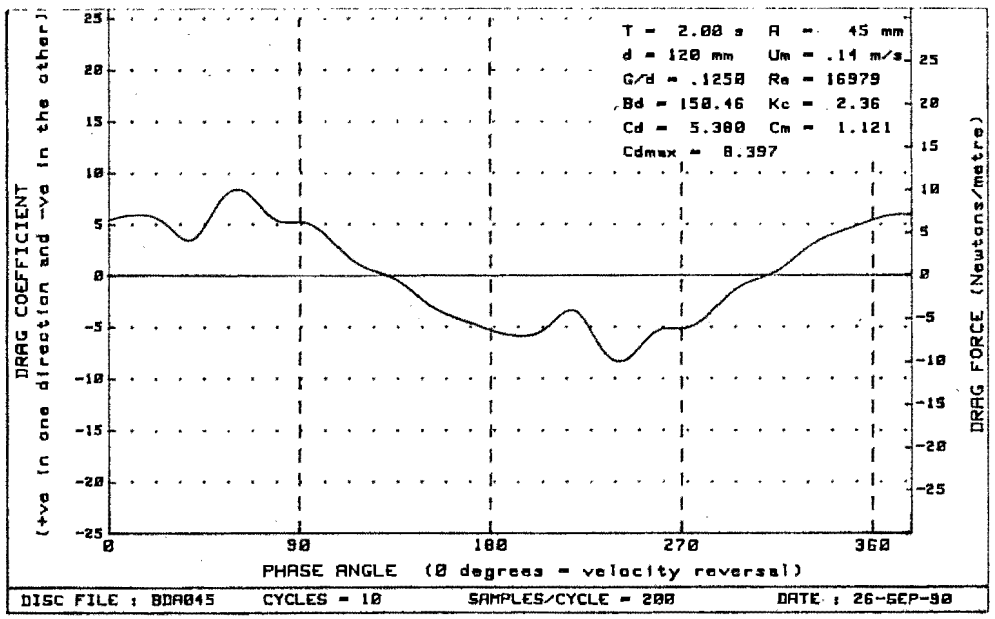

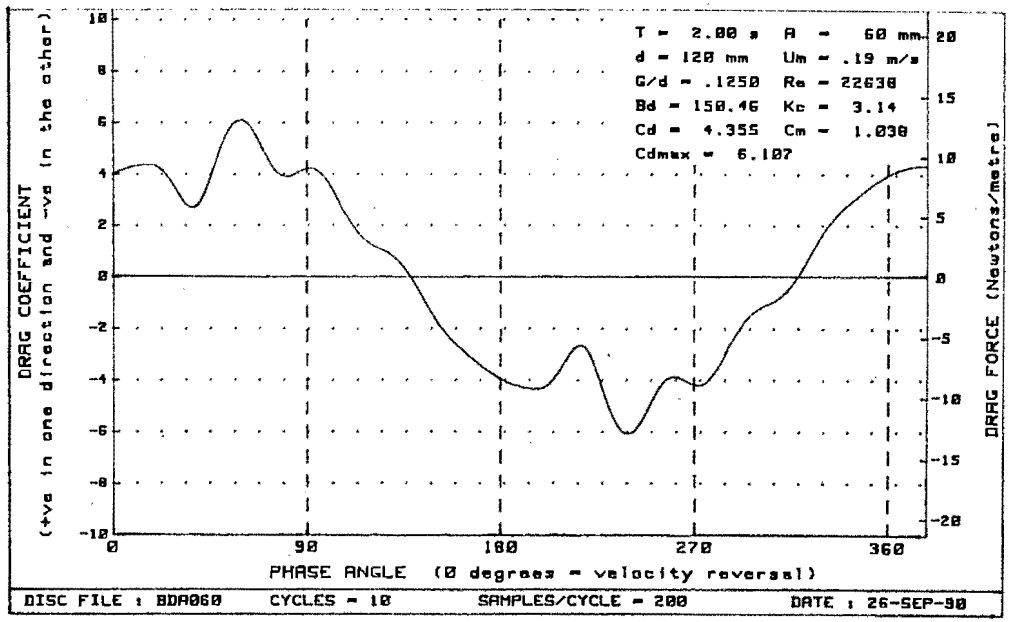

Figure H-41 : Plots of drag vs phase for diameter=120mm, Bd=150.46 and G/d=0.125

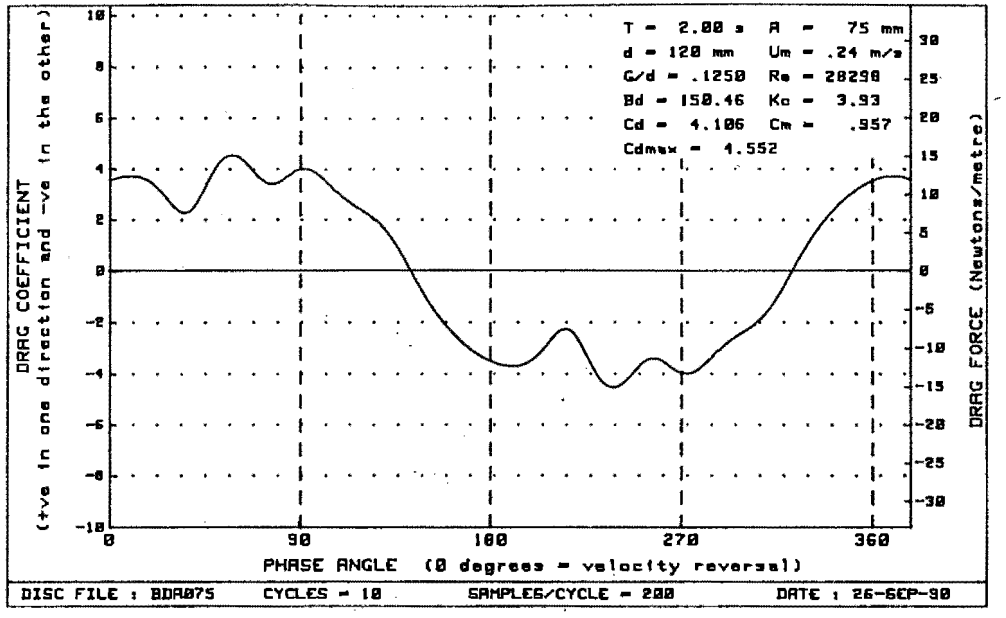

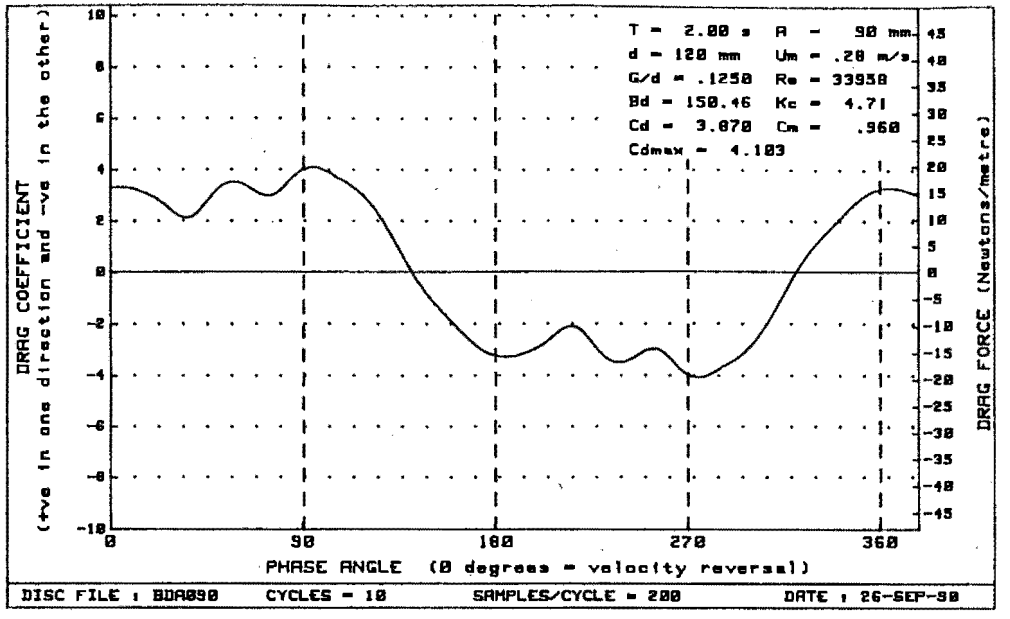

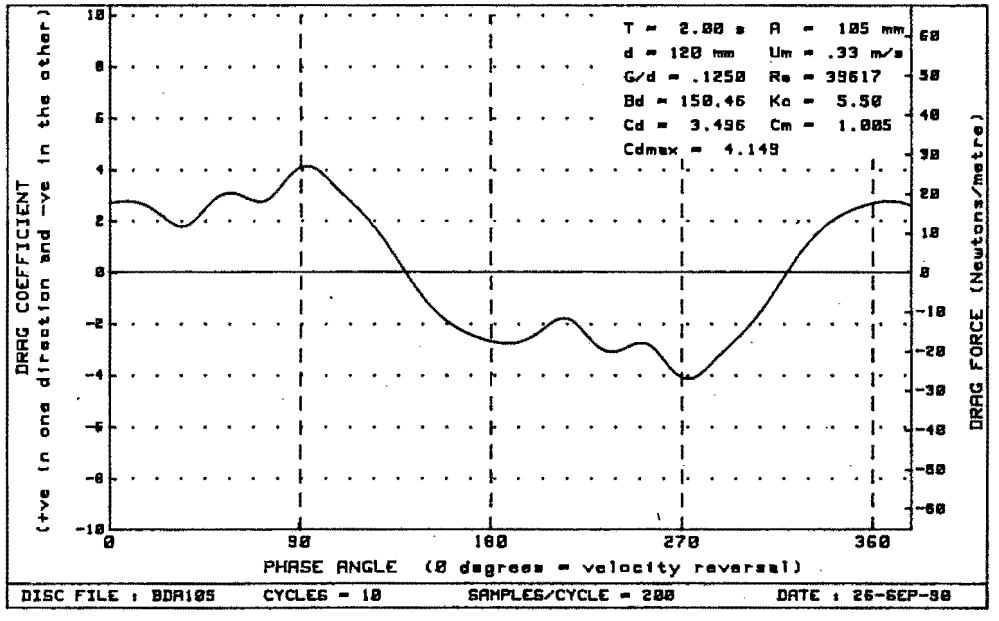

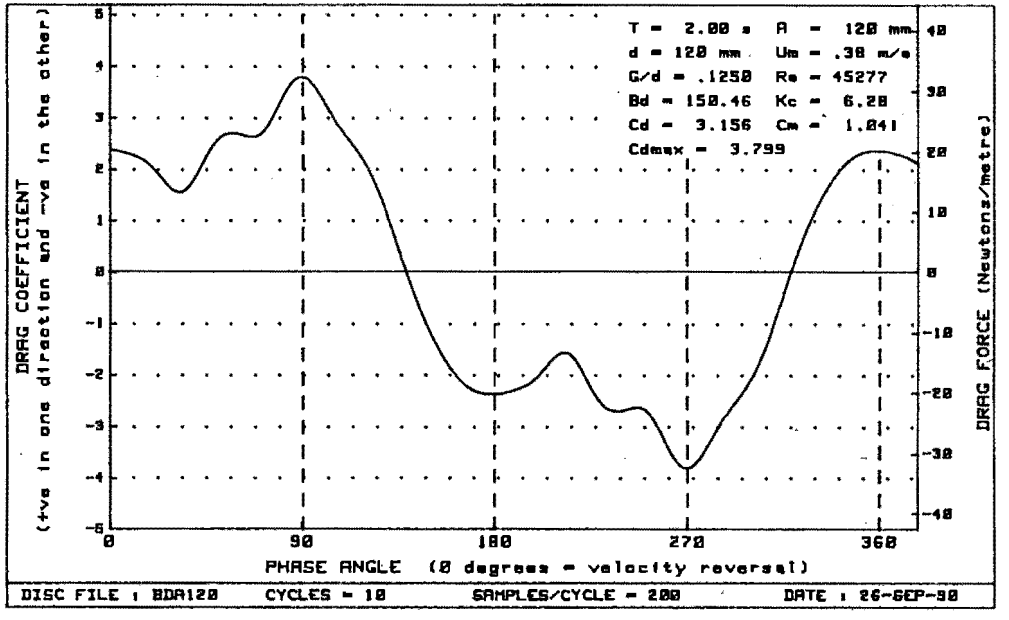

Figure H-42 : Plots of drag vs phase for diameter=120mm, Bd=150.46 and G/d=0.125

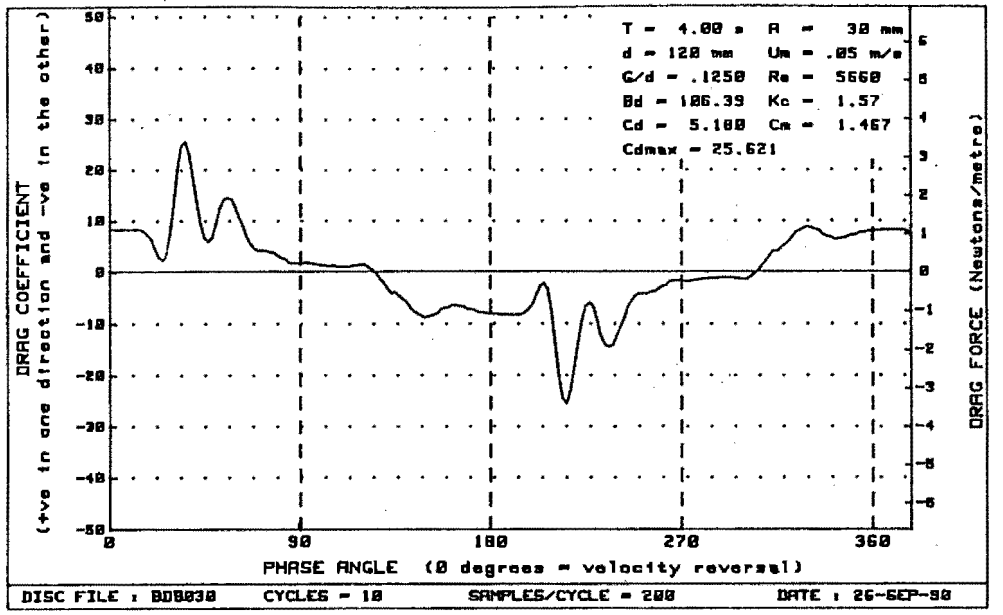

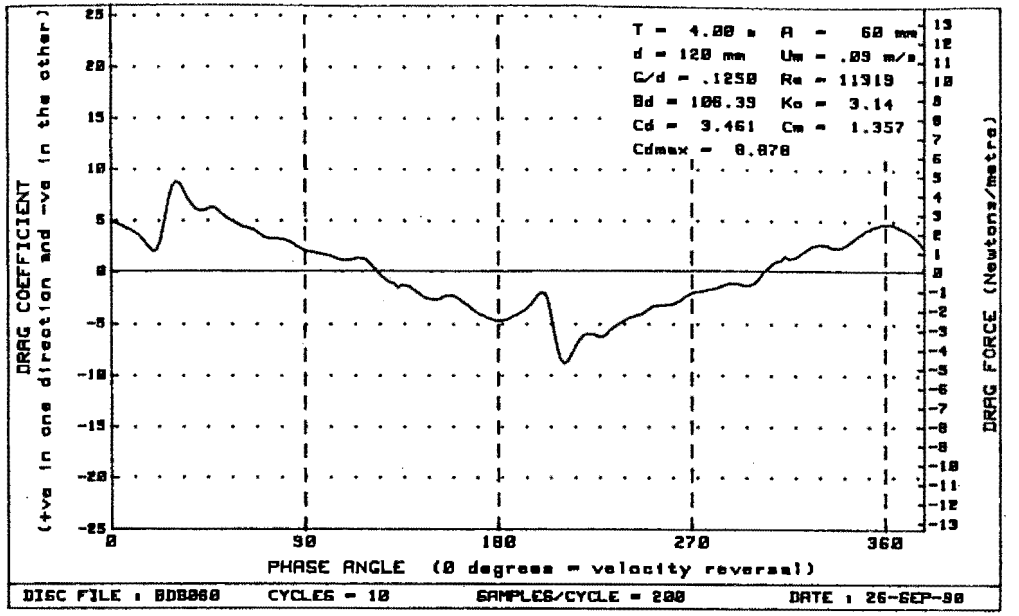

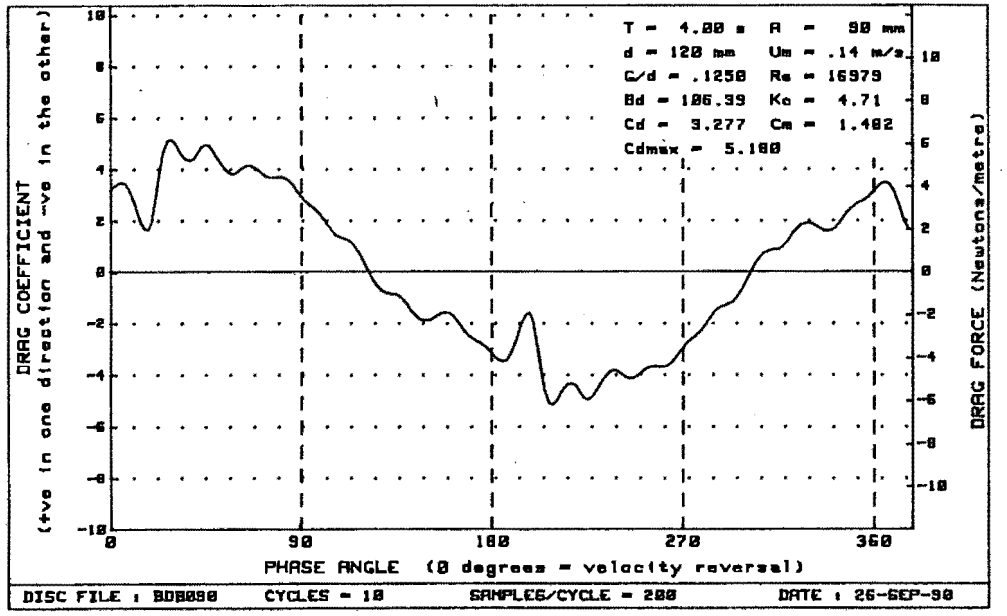

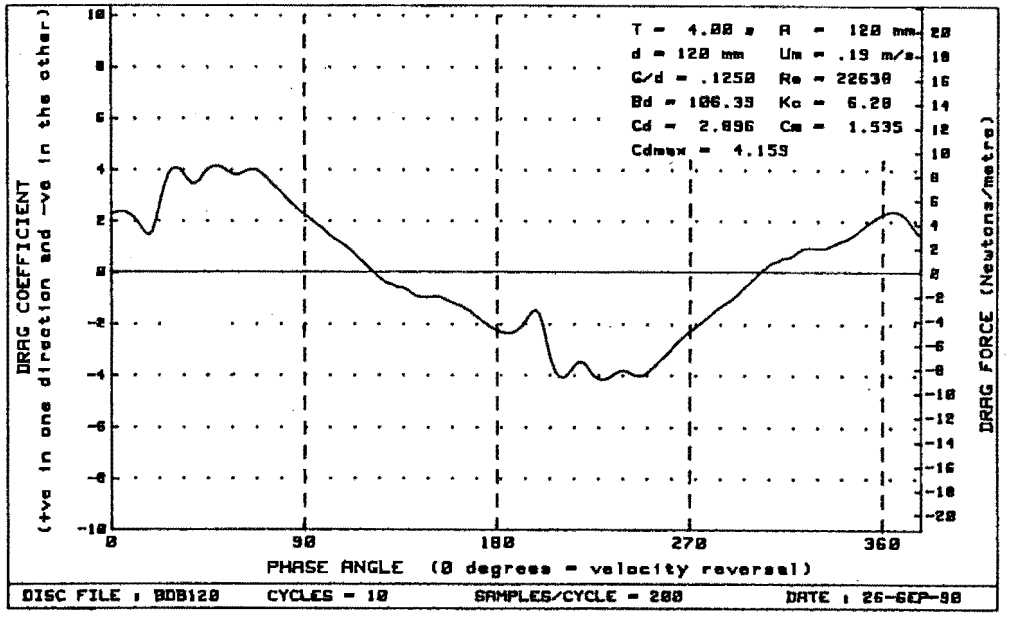

Figure H-43 : Plots of drag vs phase for diameter=120mm, Bd=106.39 and G/d= .1250

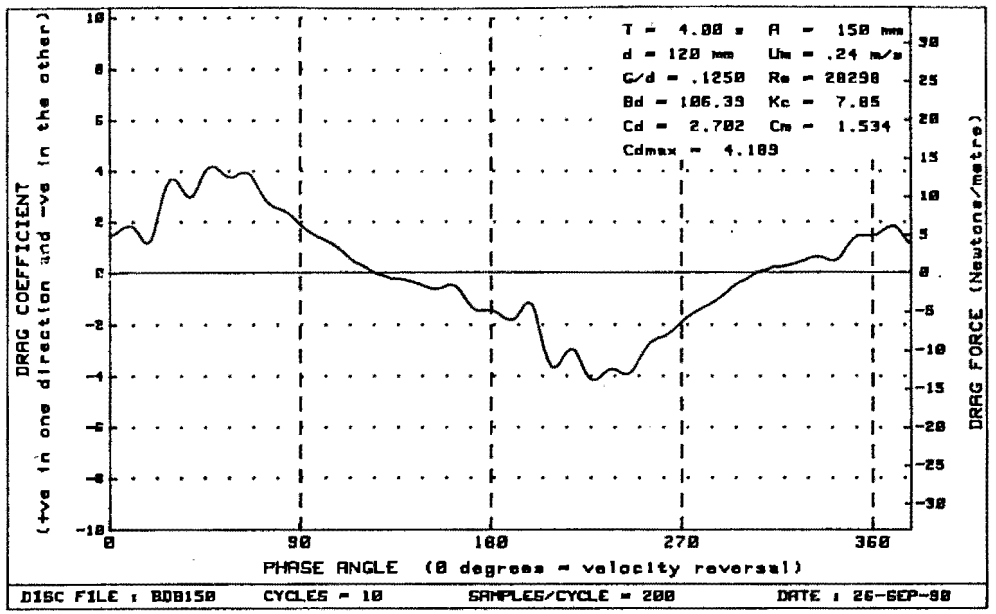

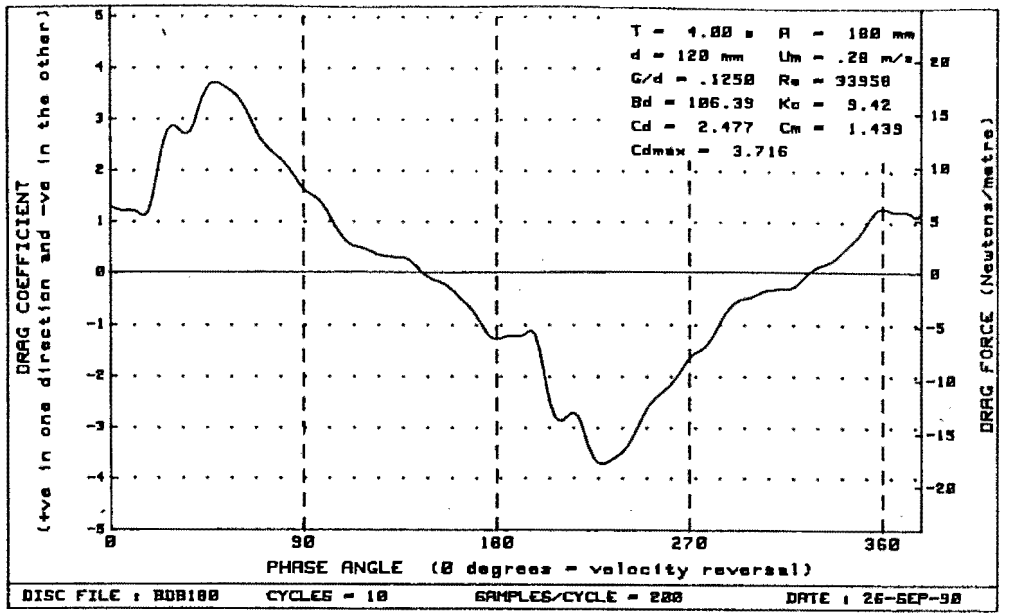

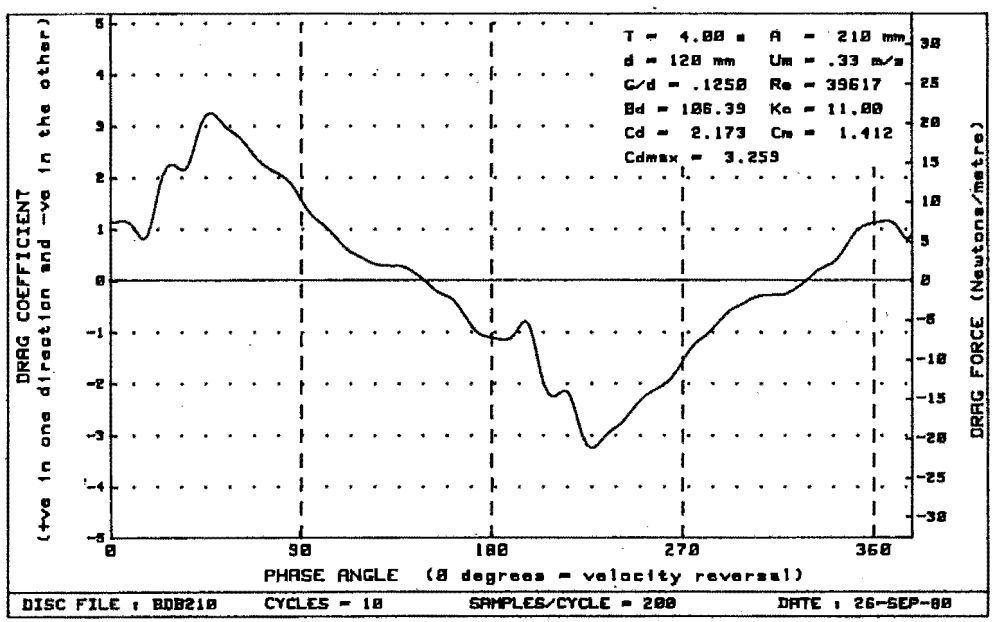

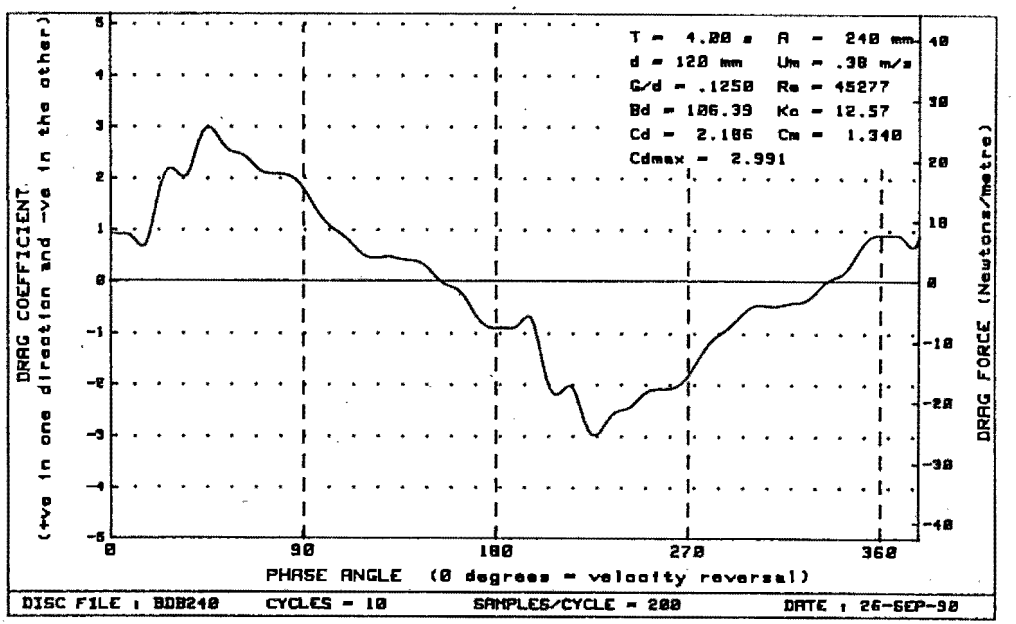

Figure H-44 : Plots of drag vs phase for diameter=120mm, Bd=106.39 and G/d= .1250

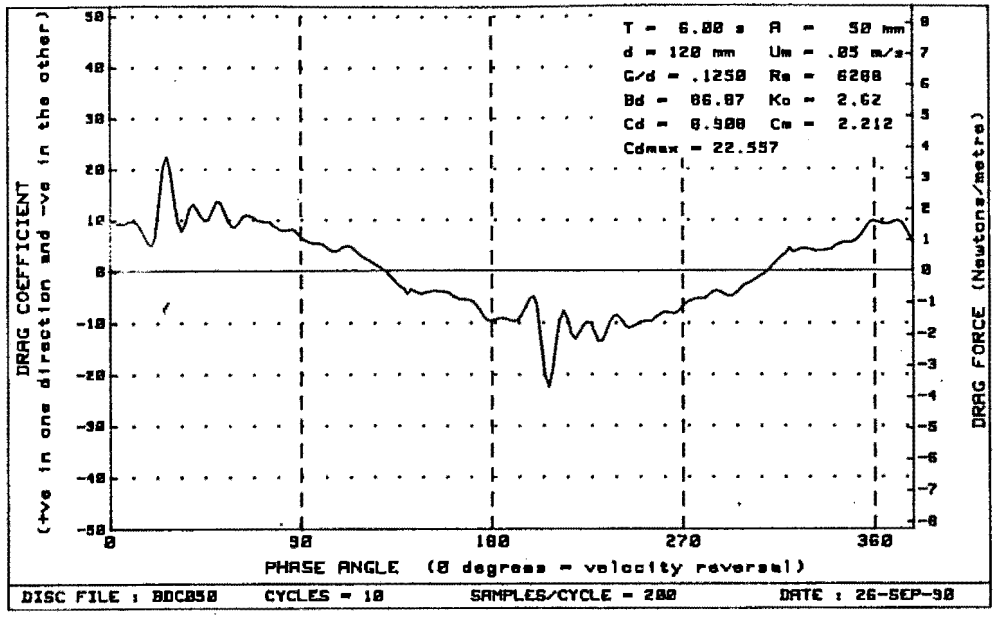

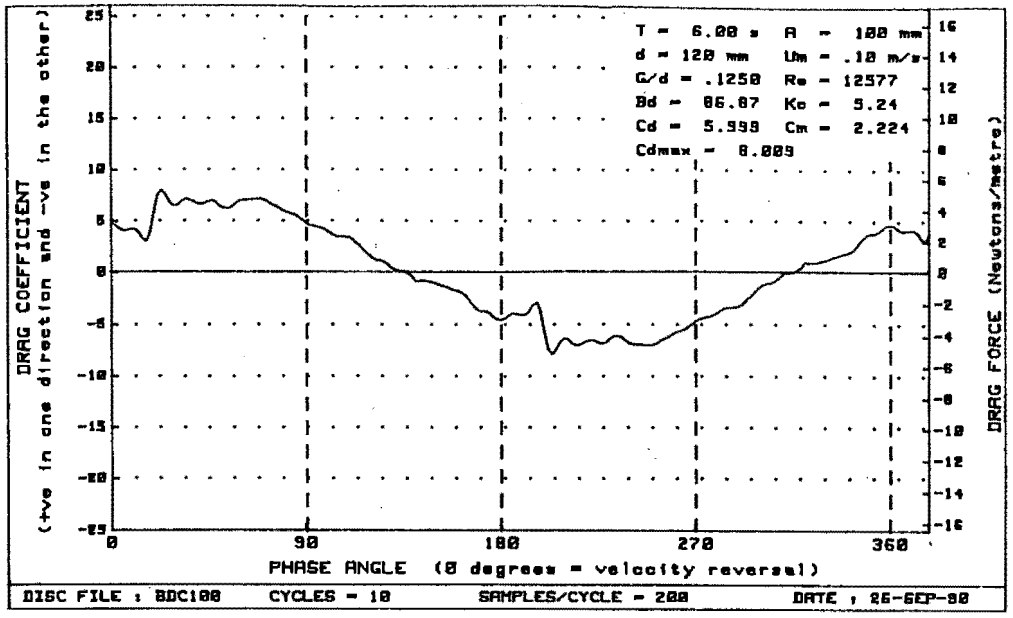

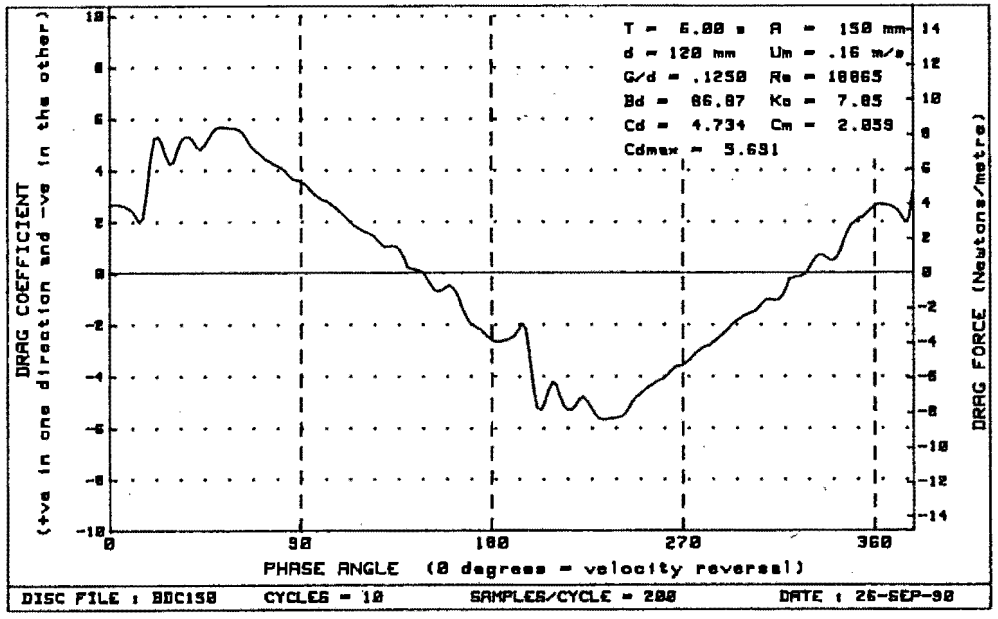

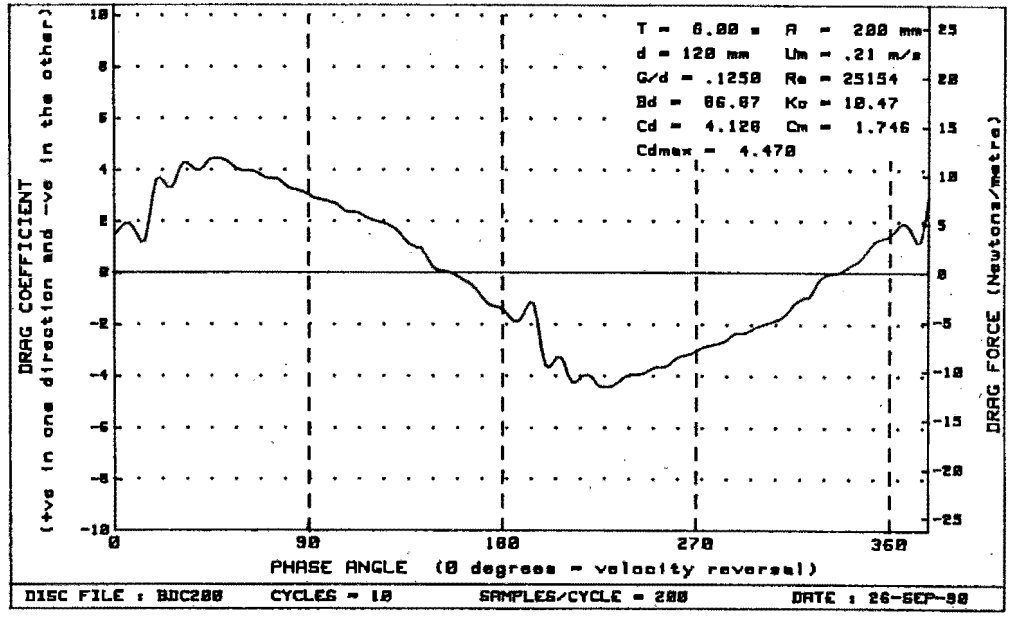

Figure H-45 : Plots of drag vs phase for diameter=120mm, Bd= 86.87 and G/d= .1250

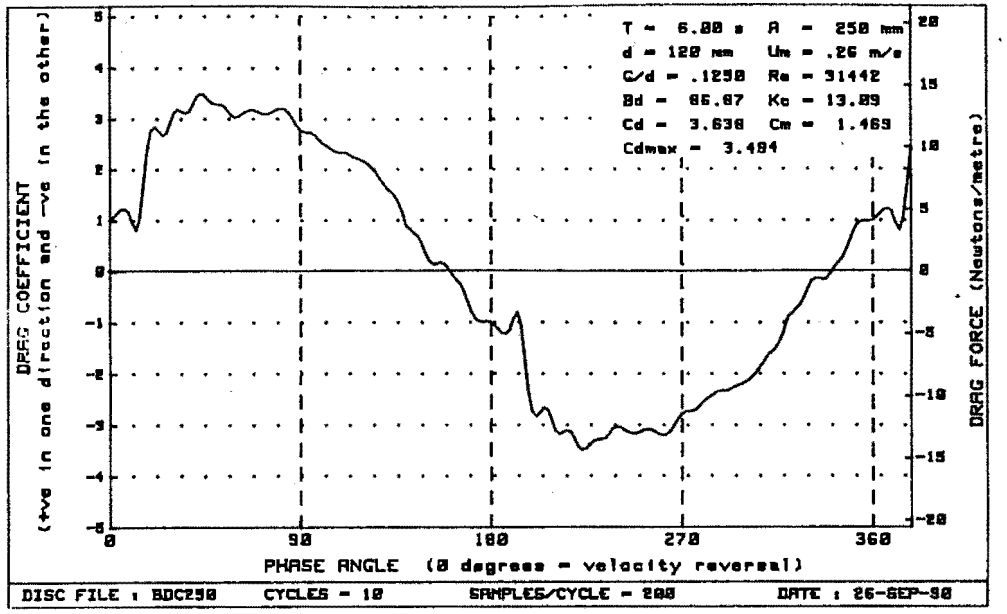

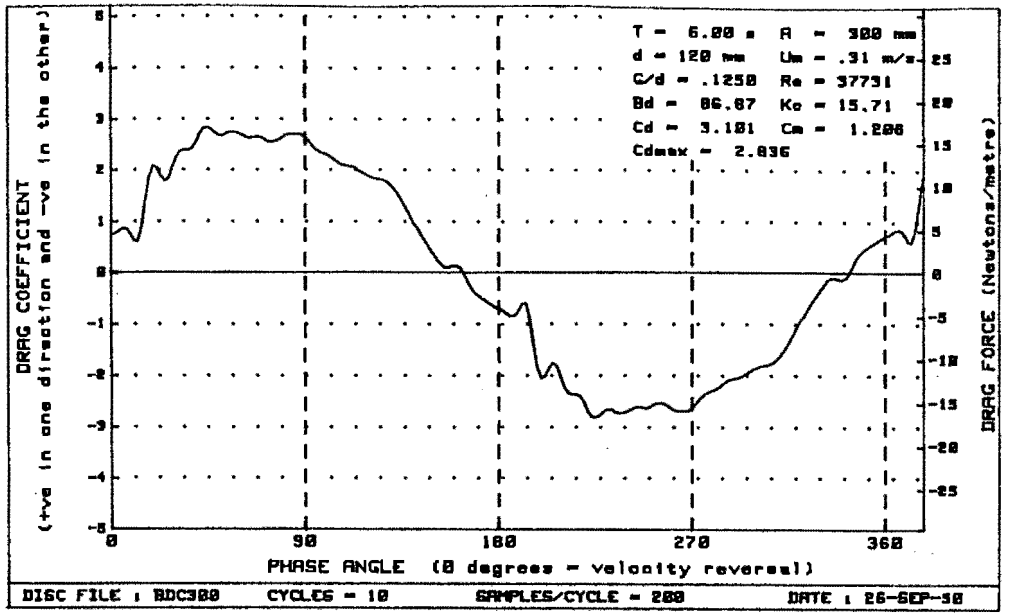

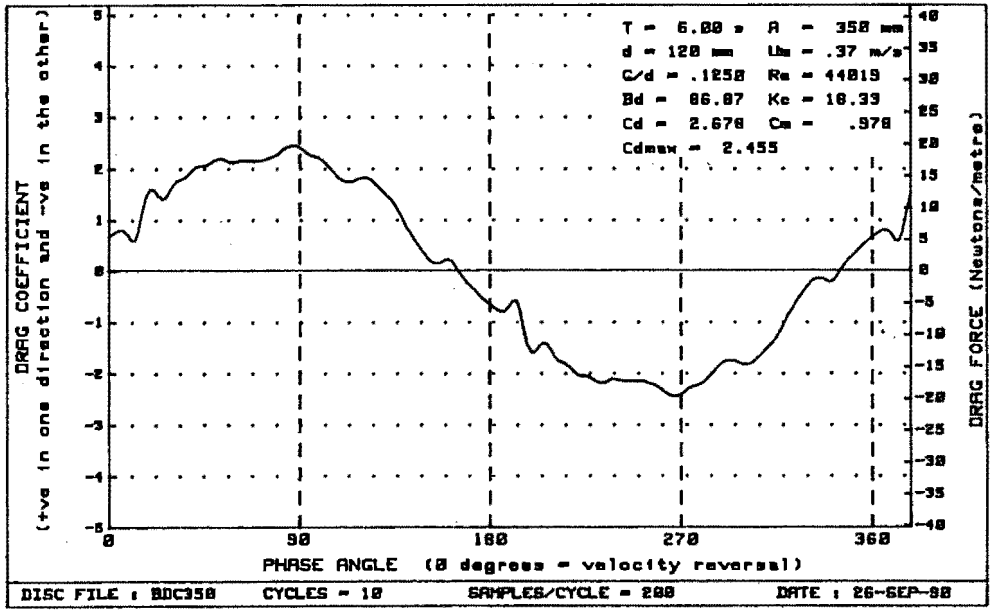

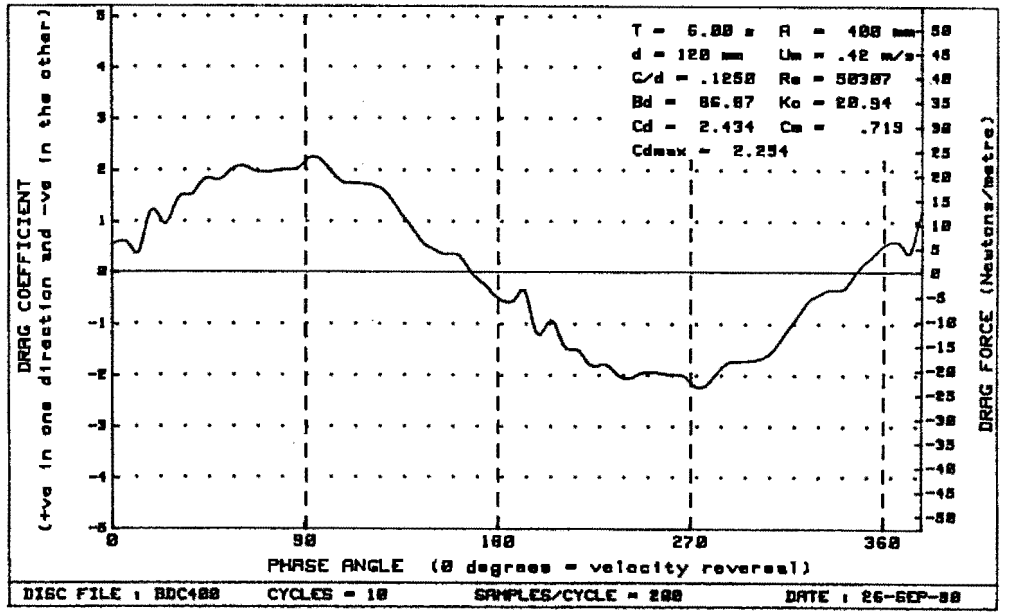

Figure H-46 : Plots of drag vs phase for diameter=120mm, Bd= 86.87 and G/d= .1250

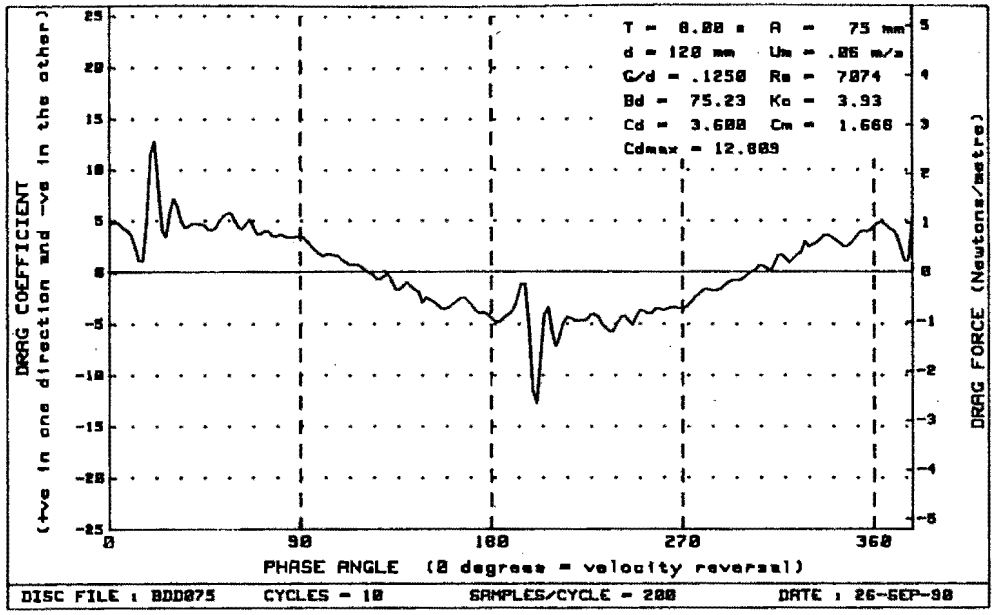

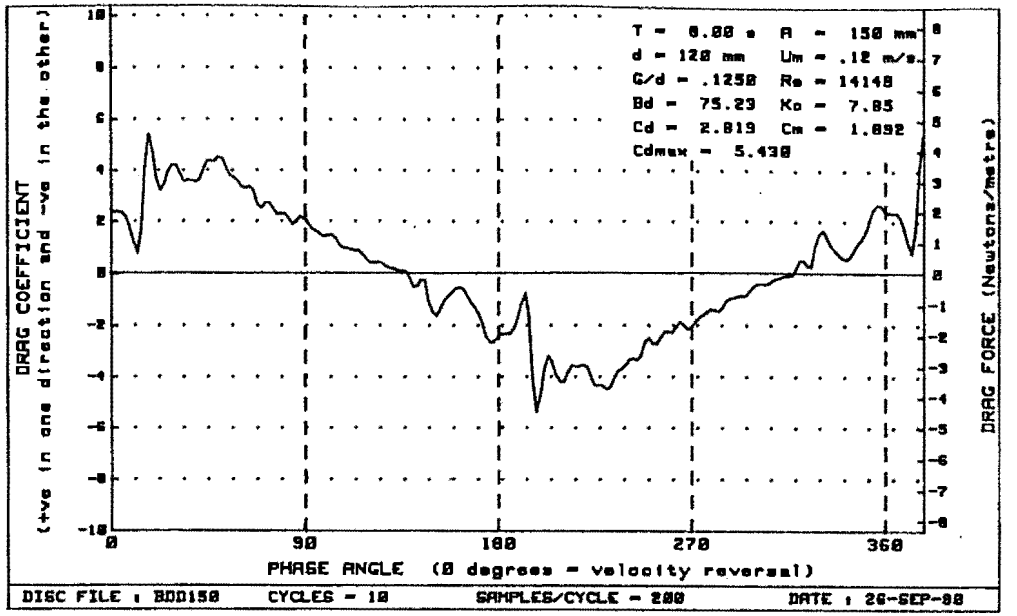

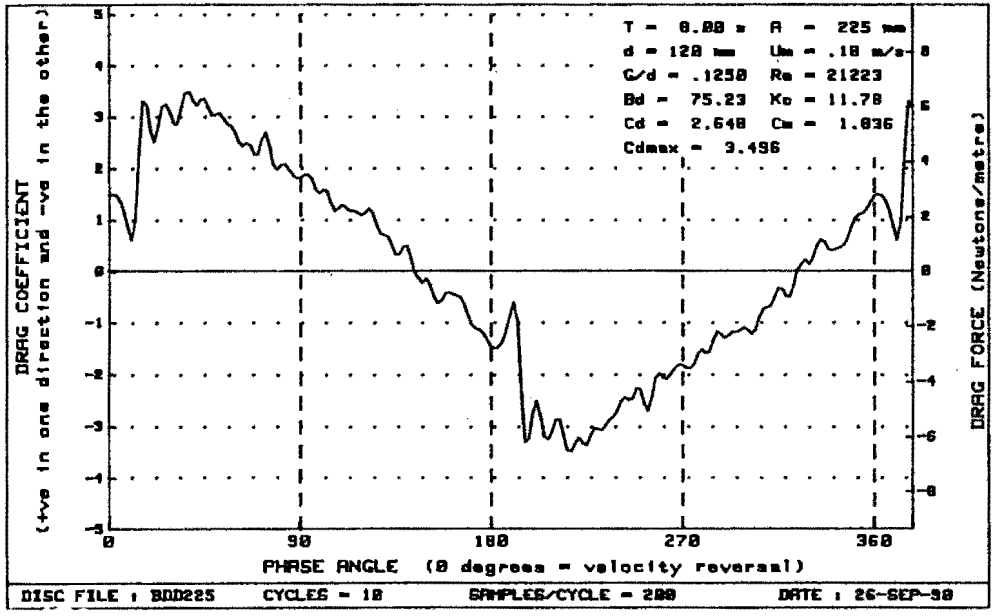

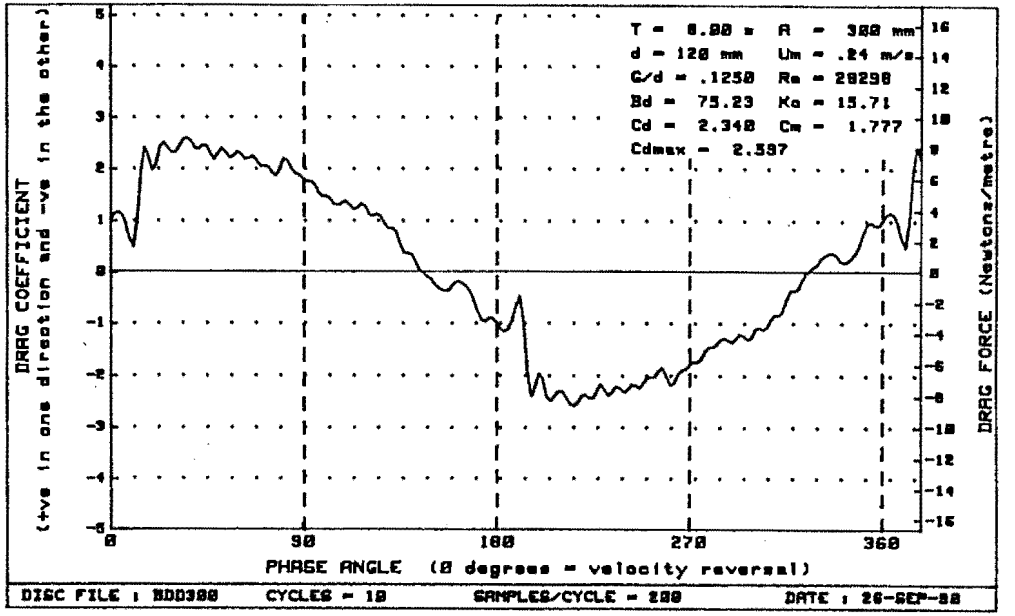

Figure H-47 : Plots of drag vs phase for diameter=120mm, Bd= 75.23 and G/d= .1250

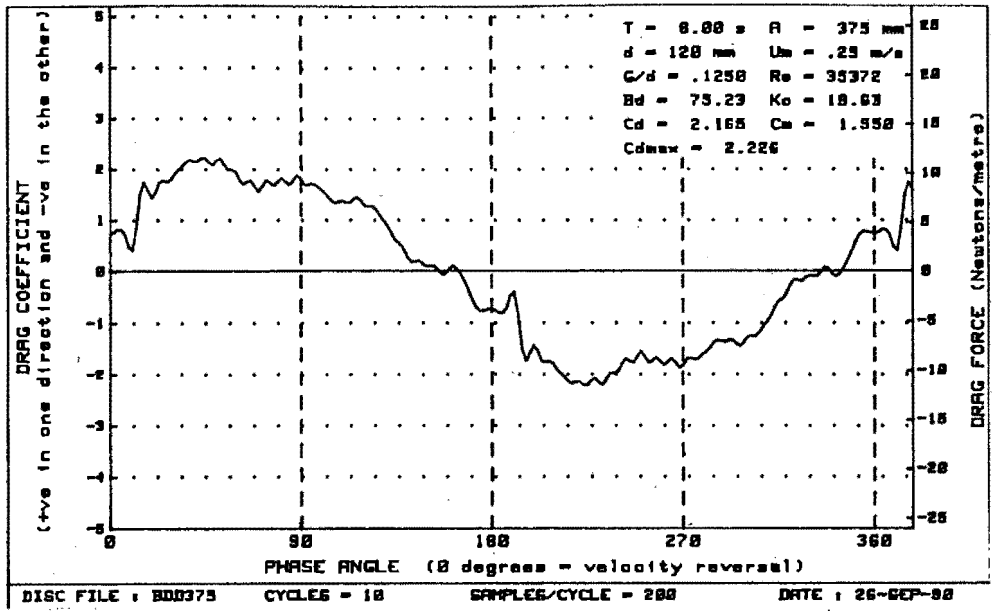

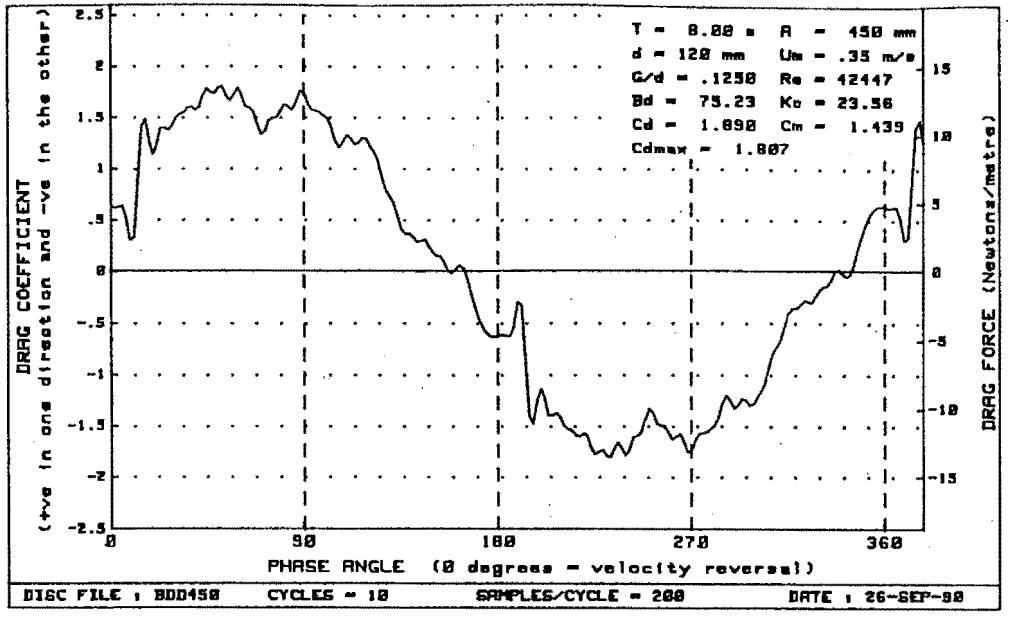

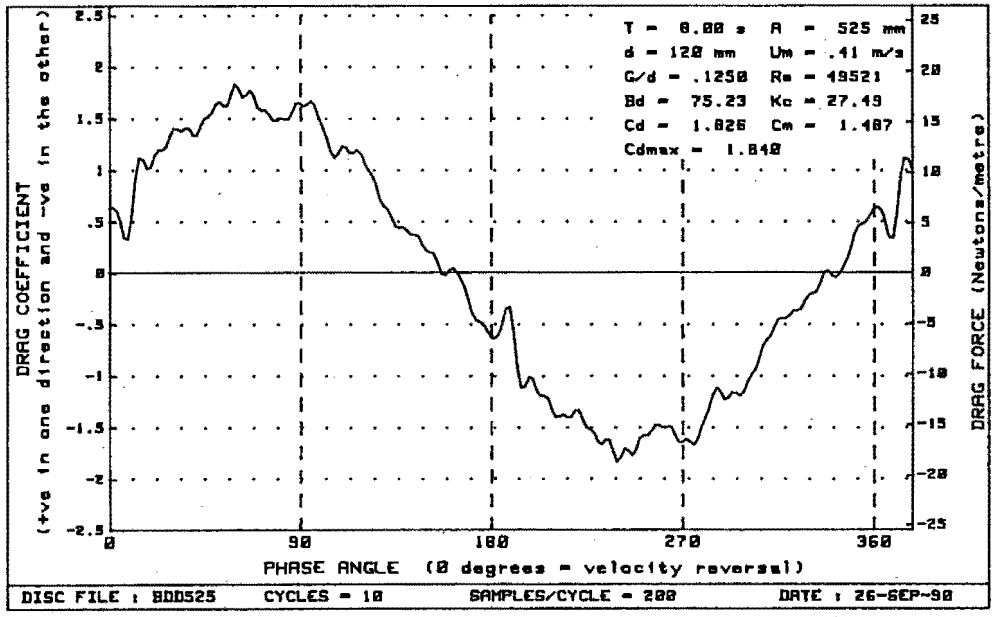

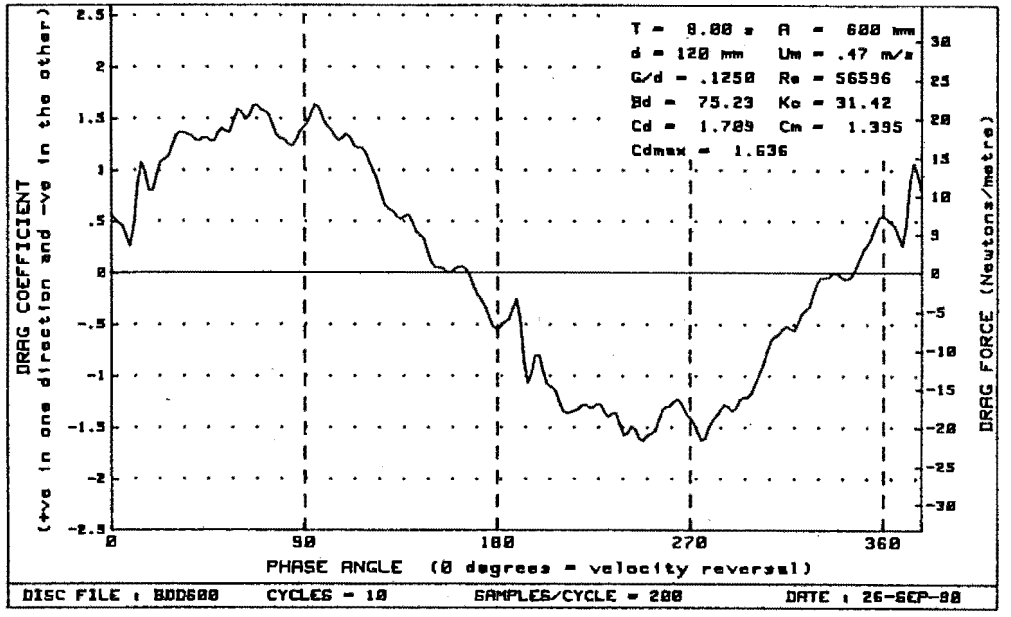

Figure H-48 : Plots of drag vs phase for diameter=120mm, Bd= 75.23 and G/d= .1250

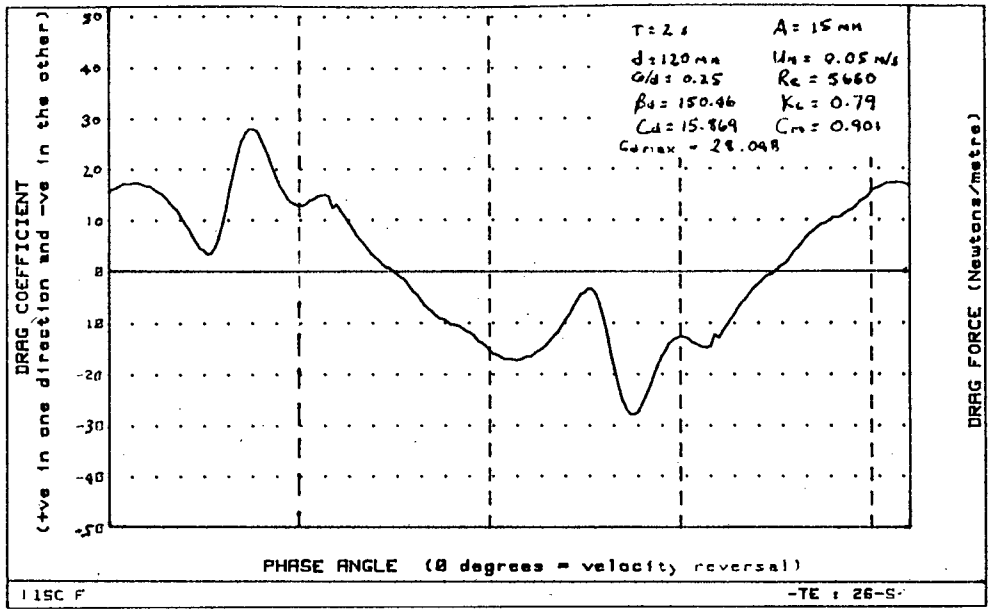

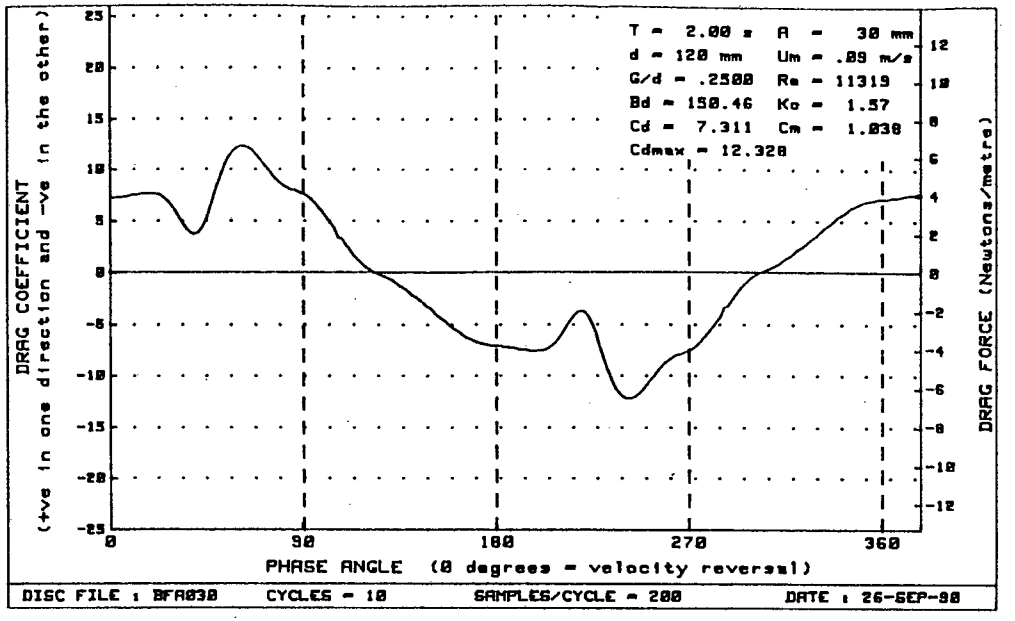

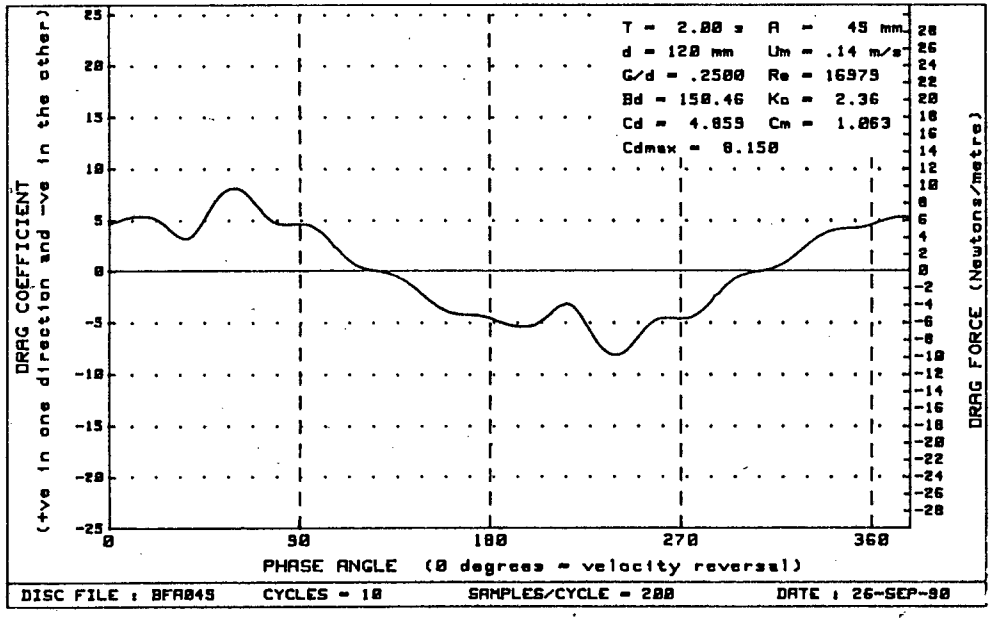

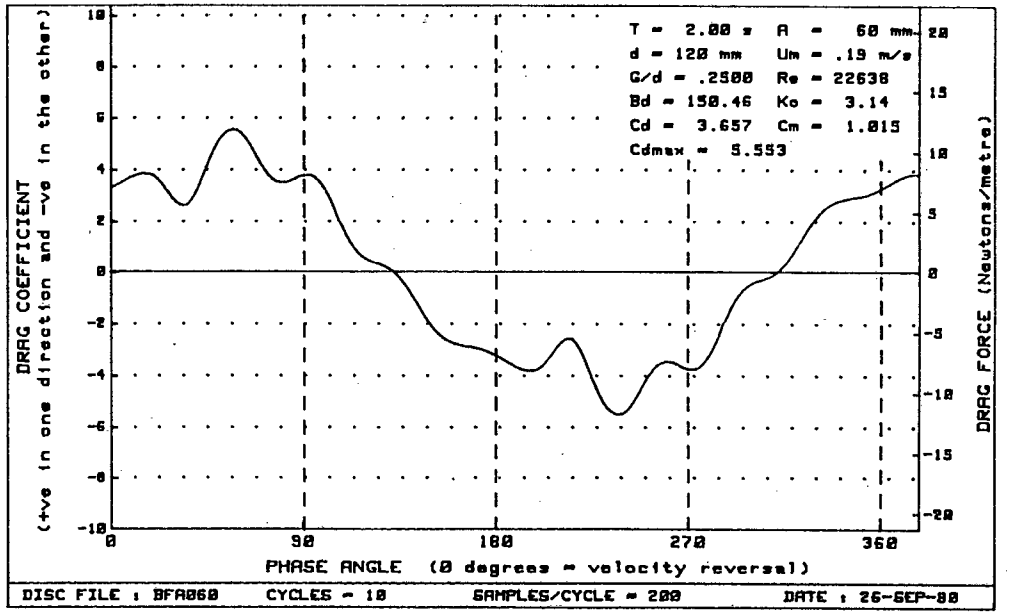

Figure H-49 : Plots of drag vs phase for diameter=120mm, Bd=150.46 and G/d= .2500

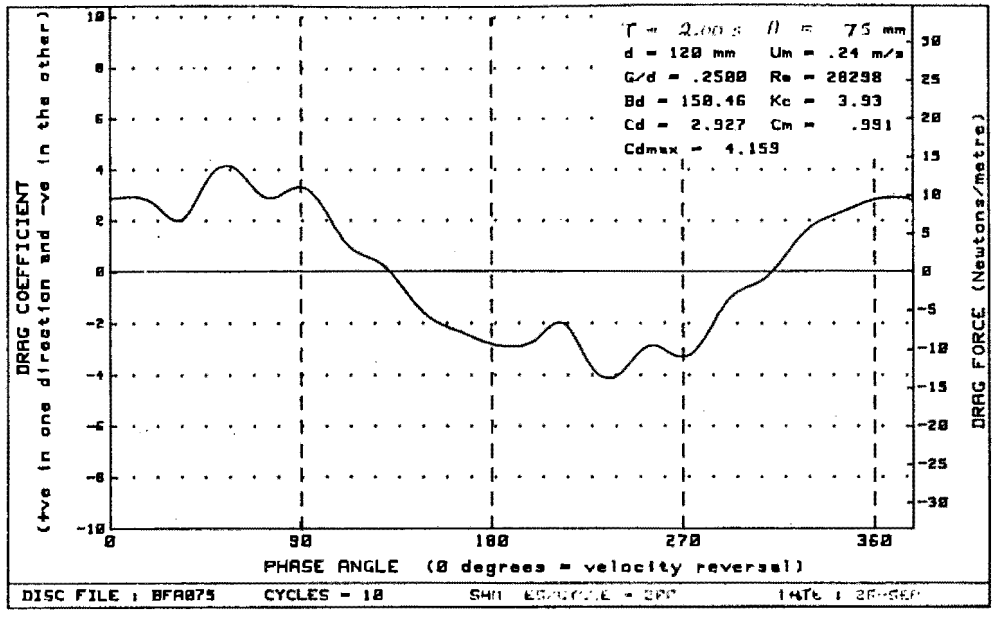

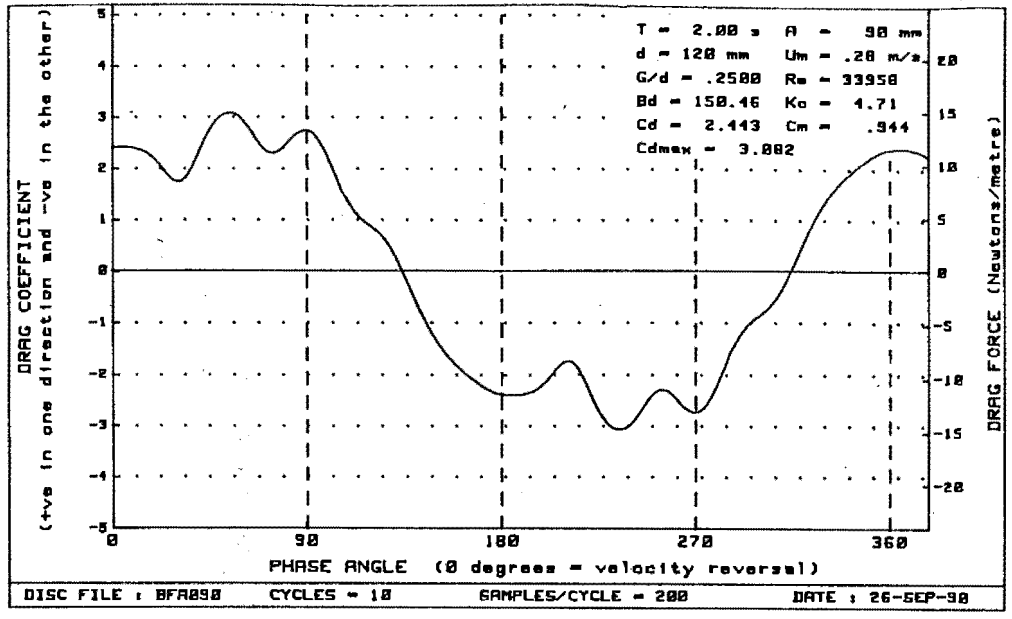

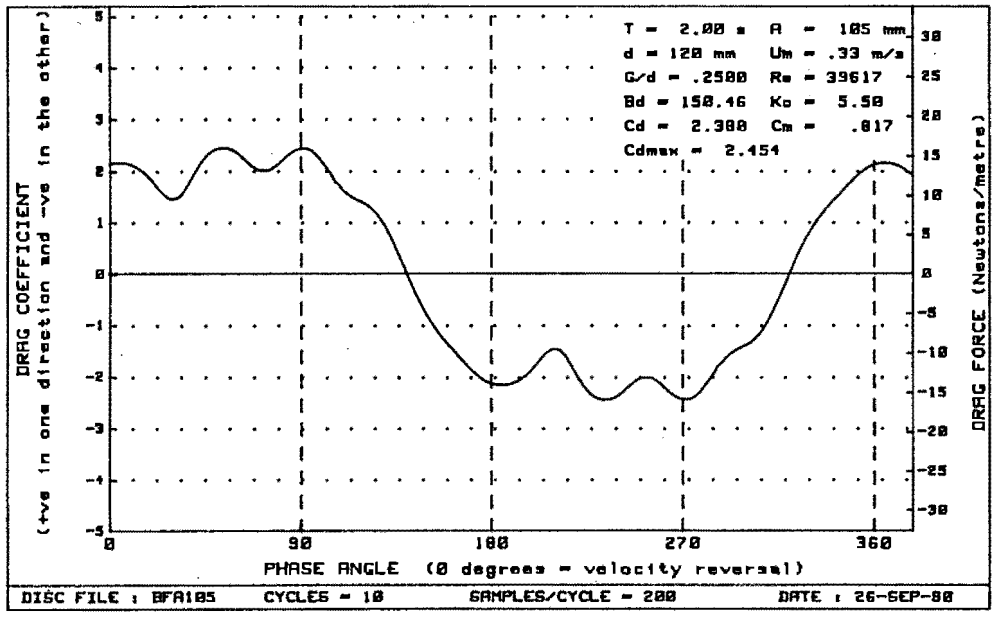

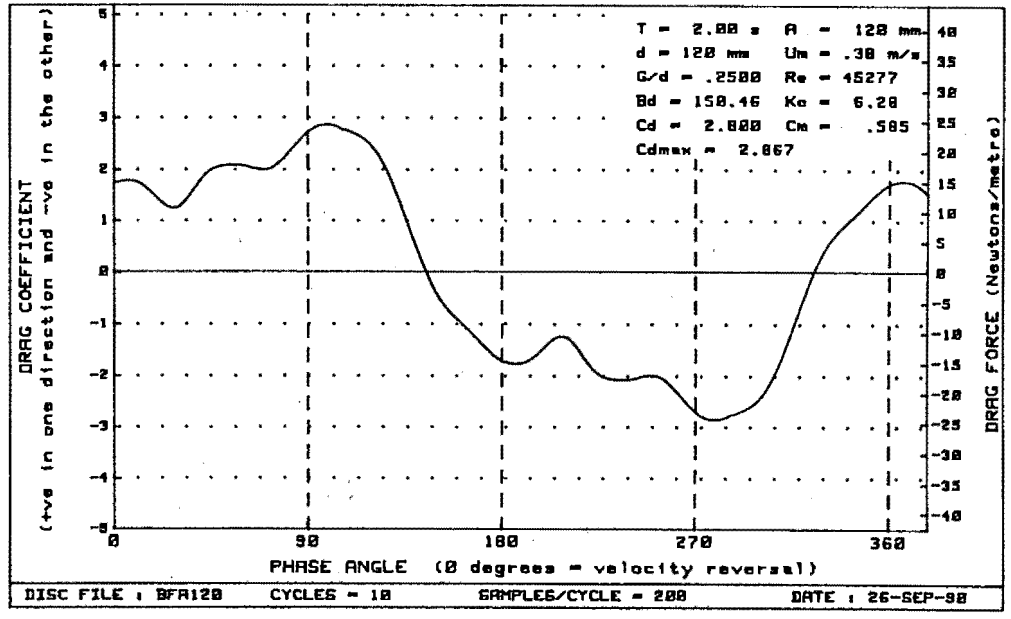

Figure H-50 : Plots of drag vs phase for diameter=120mm, Bd=150.46 and G/d= .2500

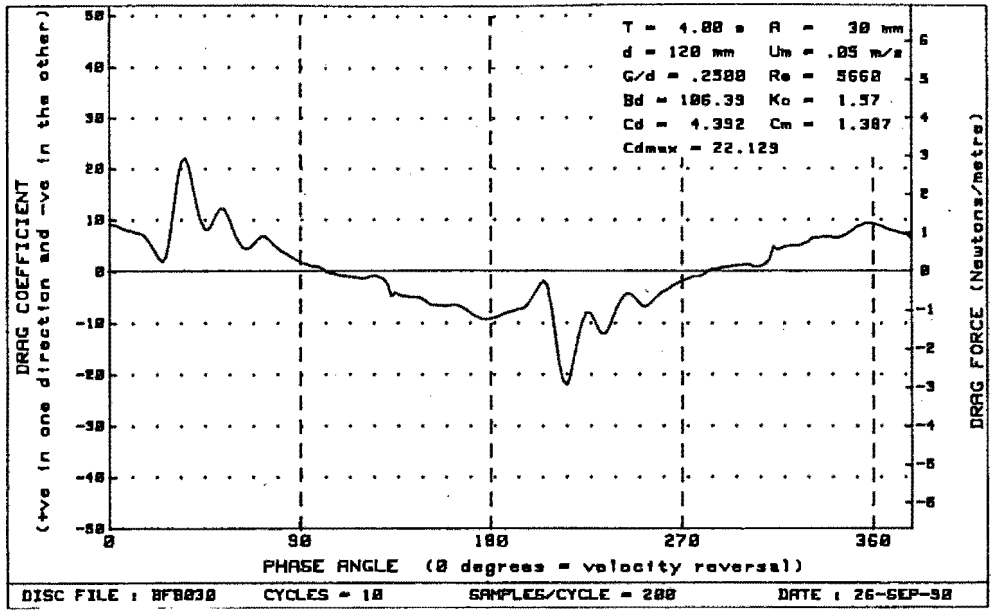

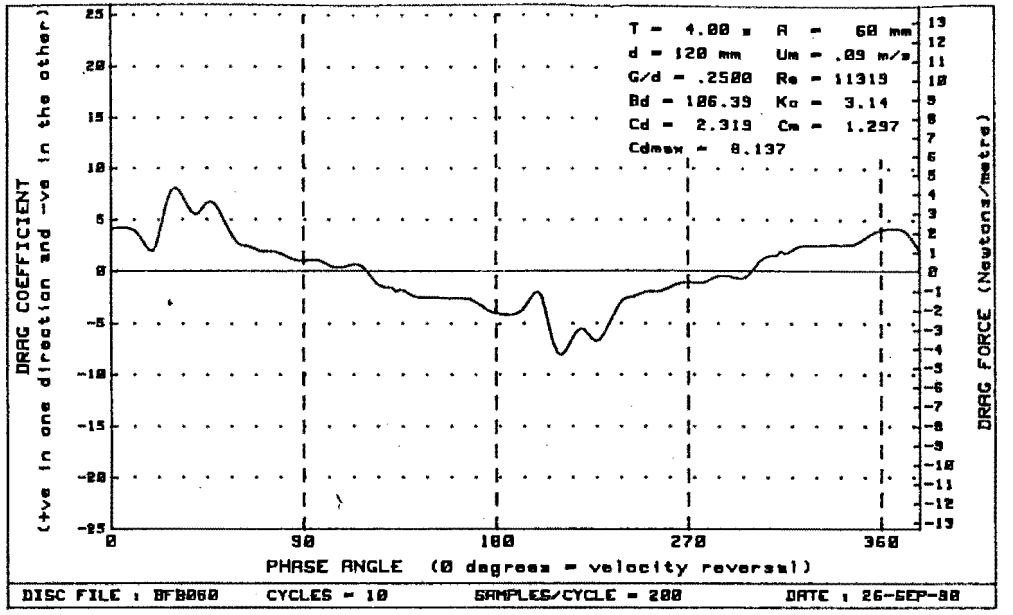

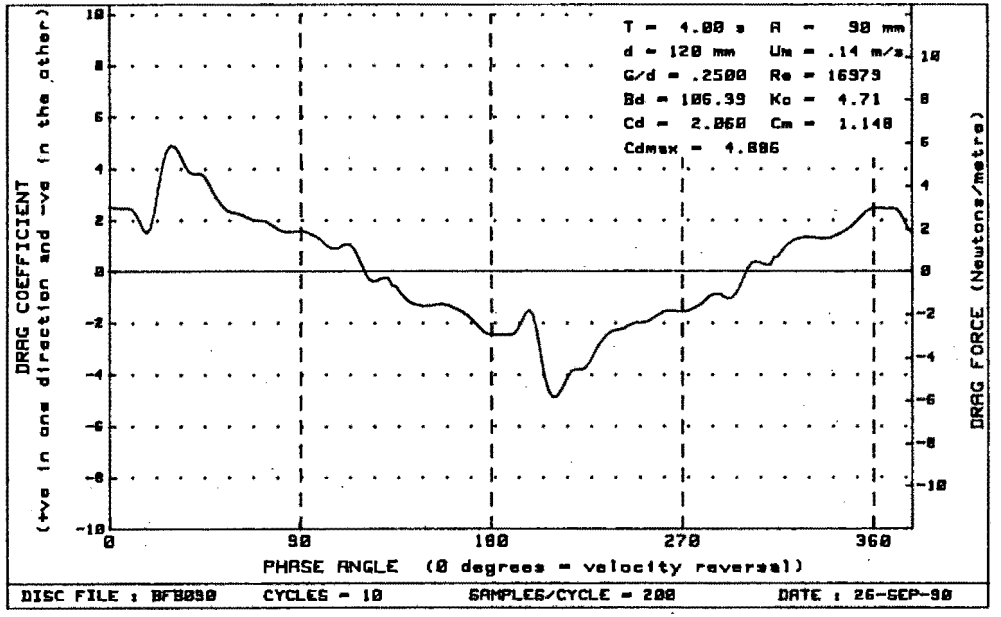

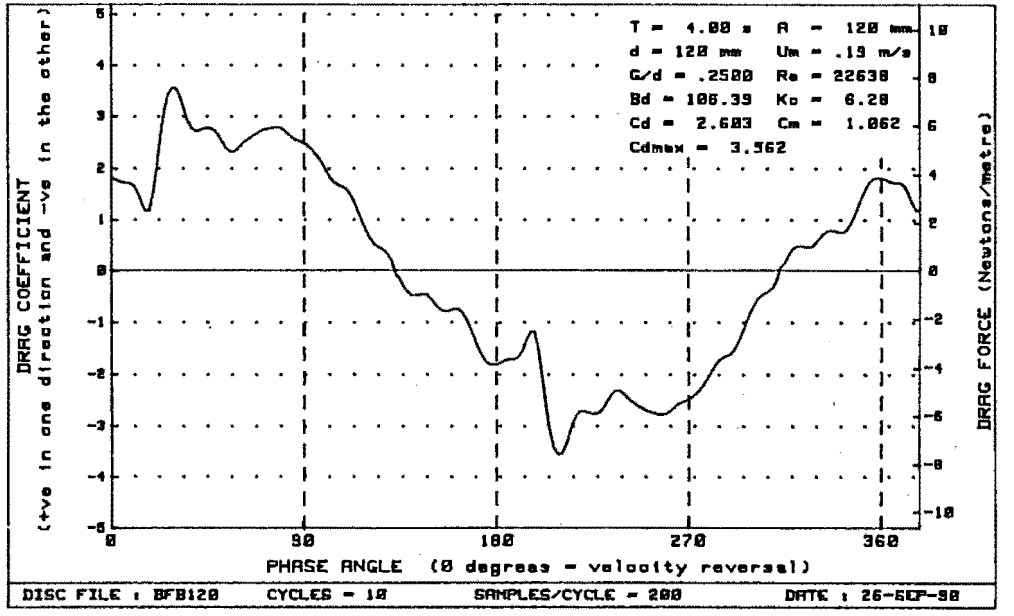

Figure H-51 : Plots of drag vs phase for diameter=120mm, Bd=106.39 and G/d= .2500

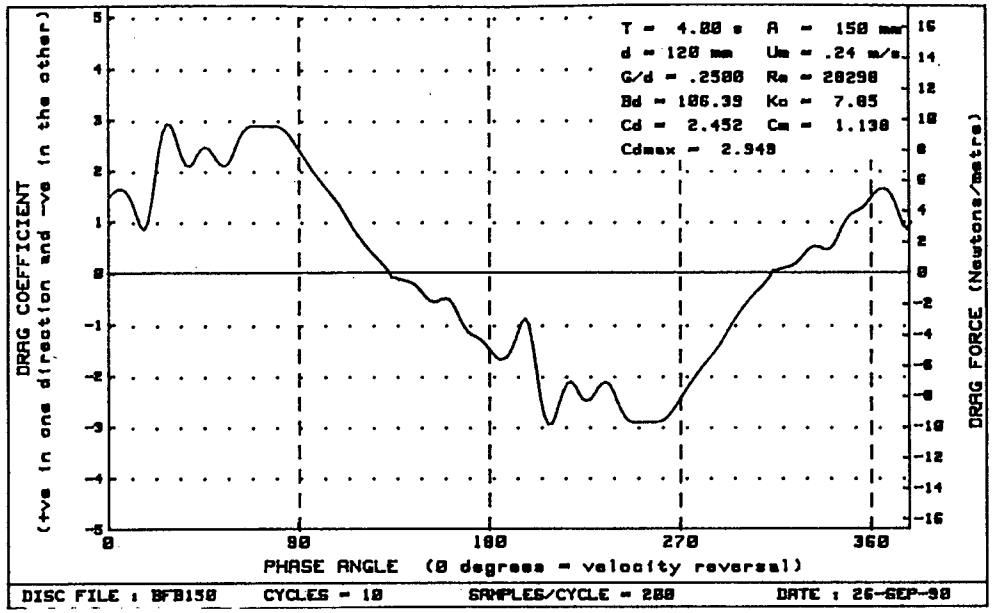

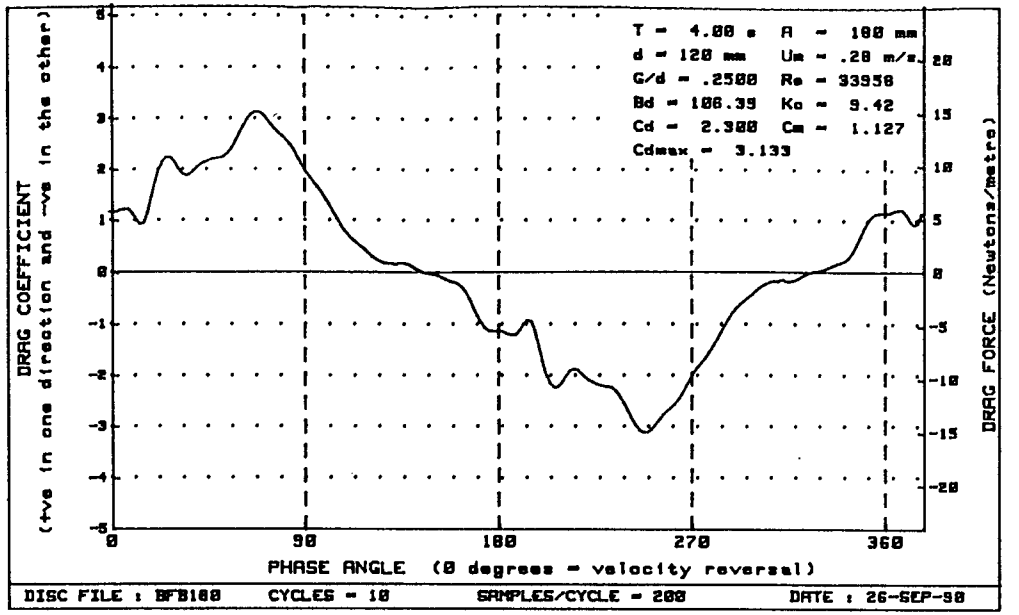

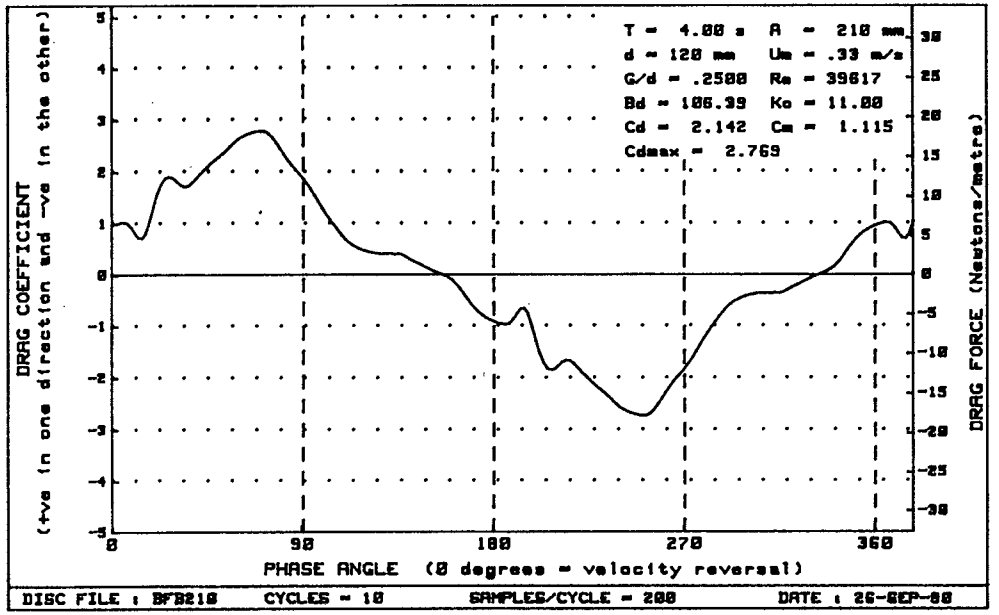

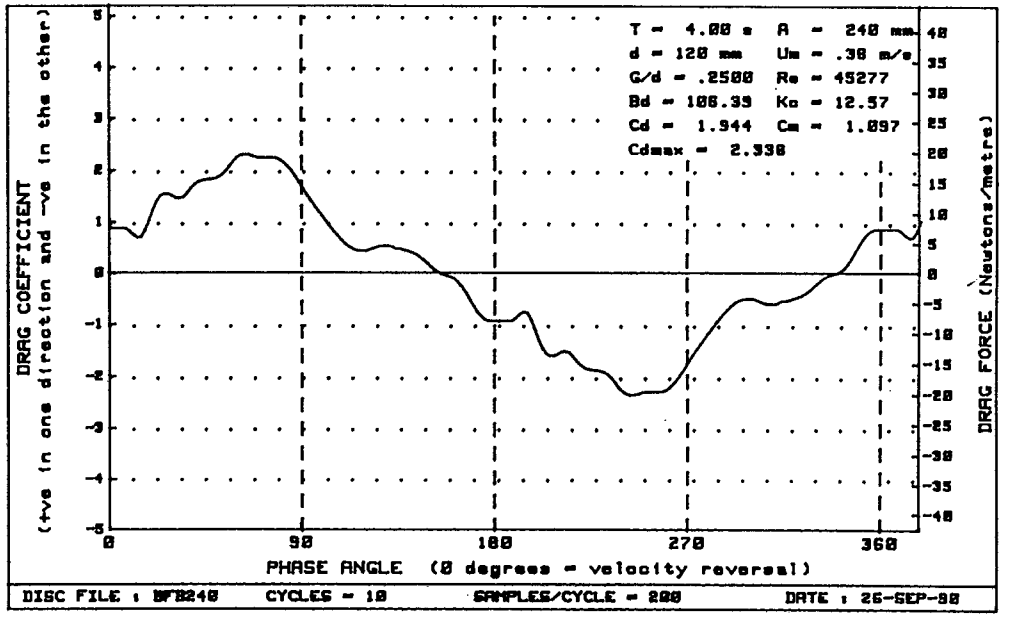

Figure H-52 : Plots of drag vs phase for diameter=120mm, Bd=106.39 and G/d= .2500

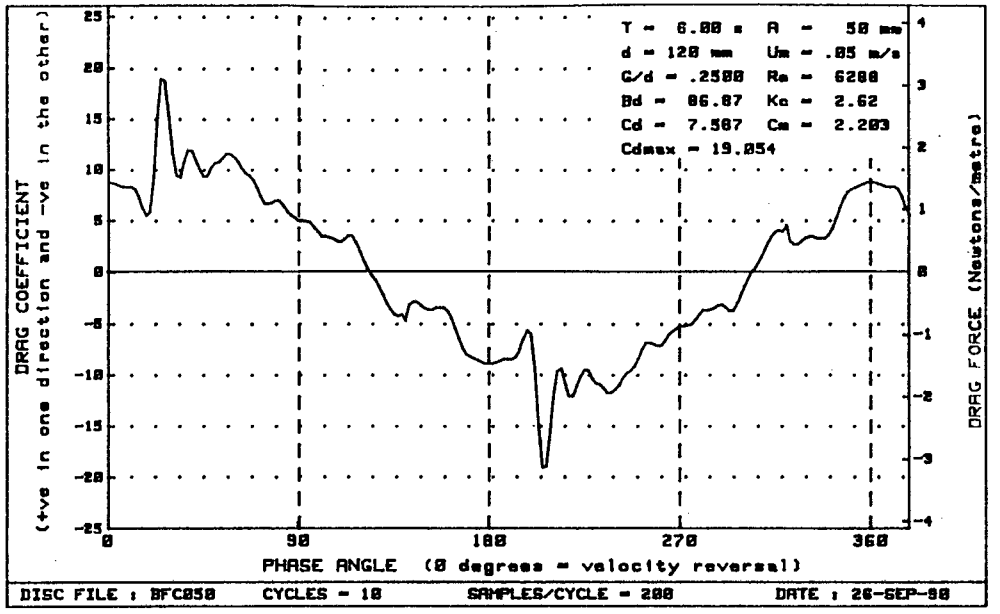

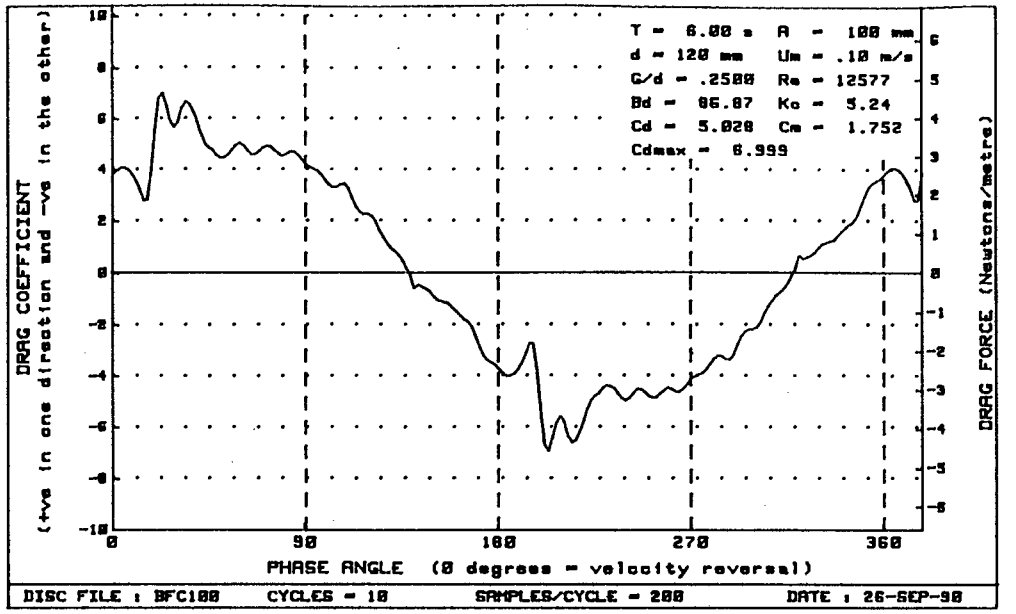

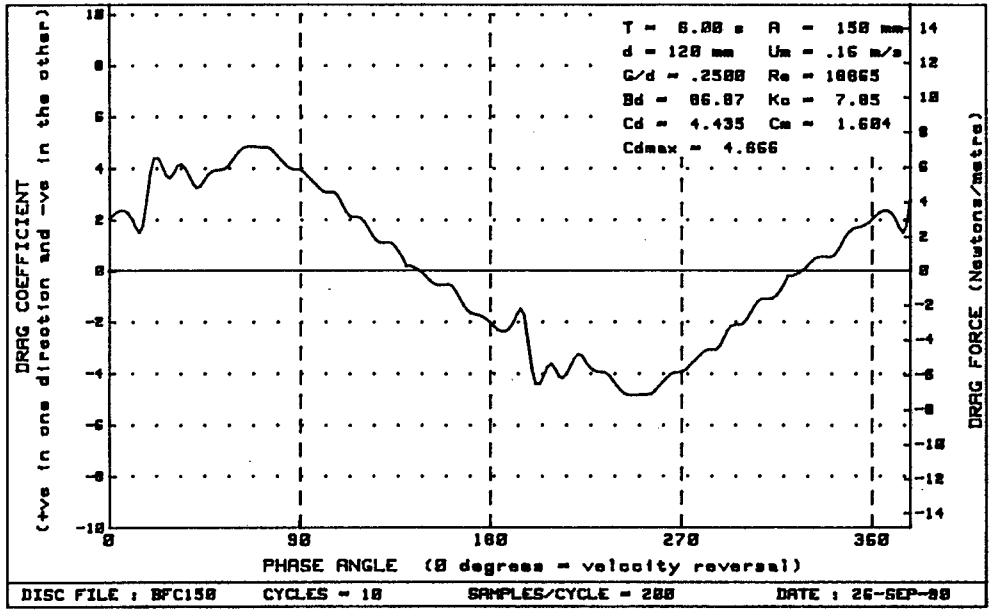

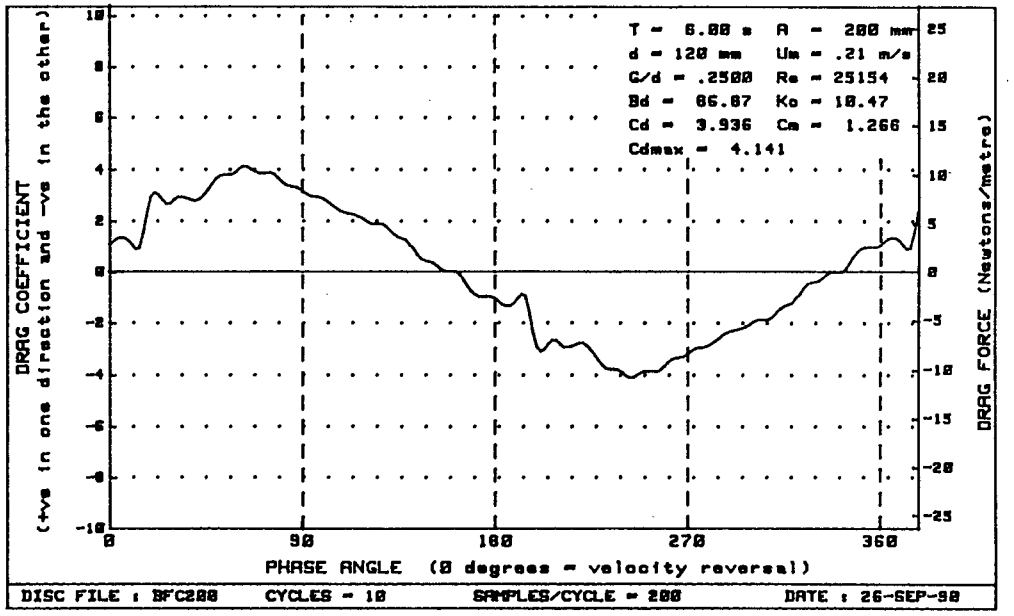

Figure H-53 : Plots of drag vs phase for diameter=120mm, Bd= 86.87 and G/d=0.25

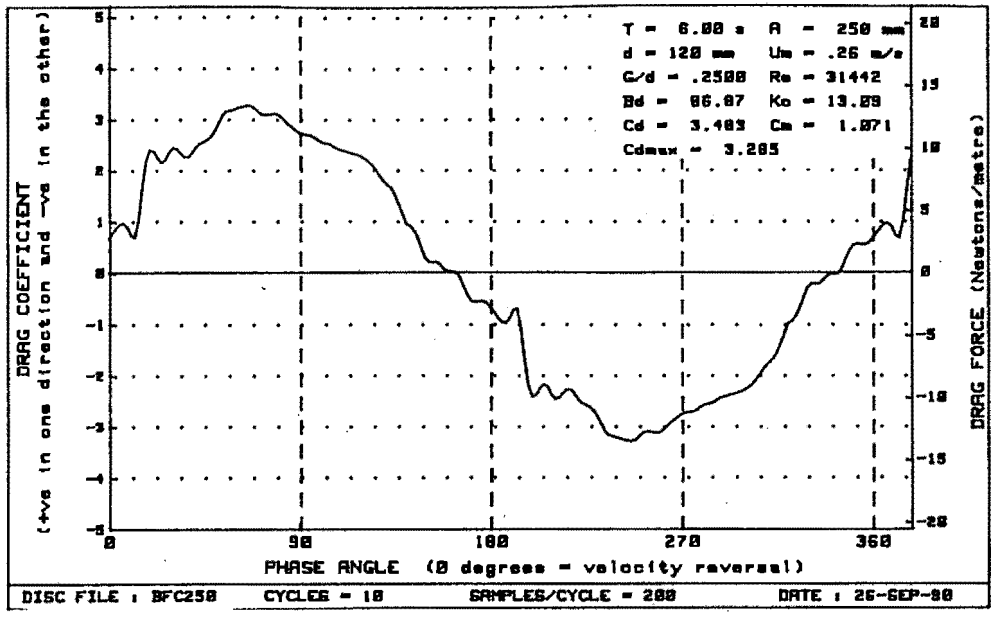

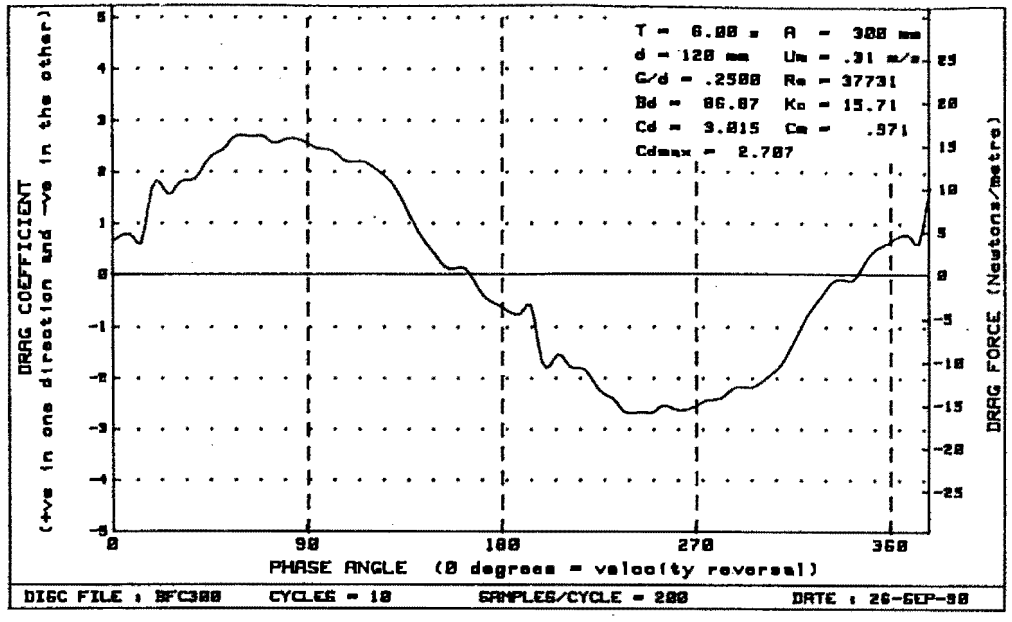

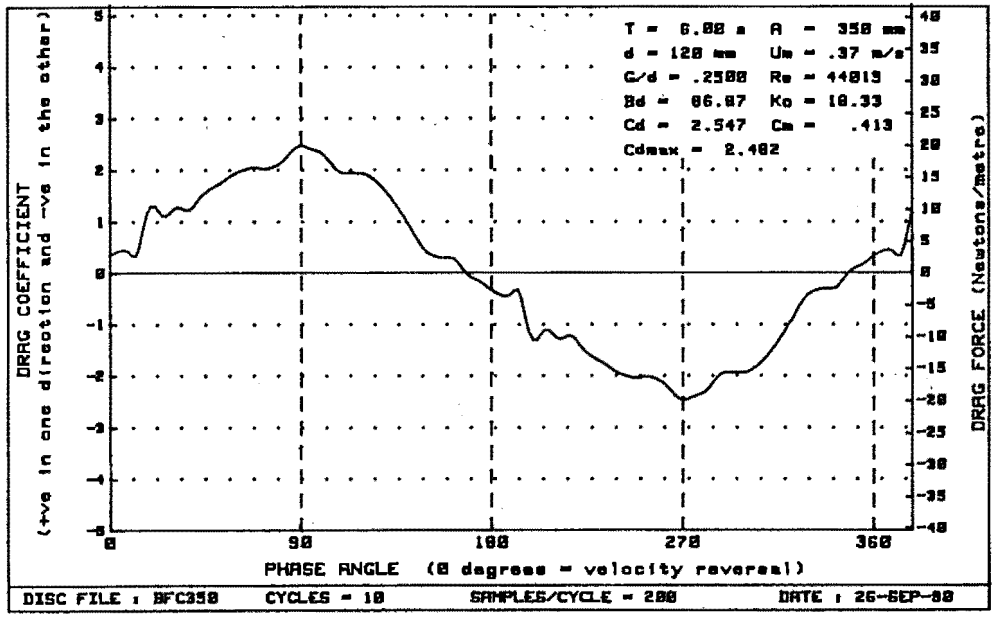

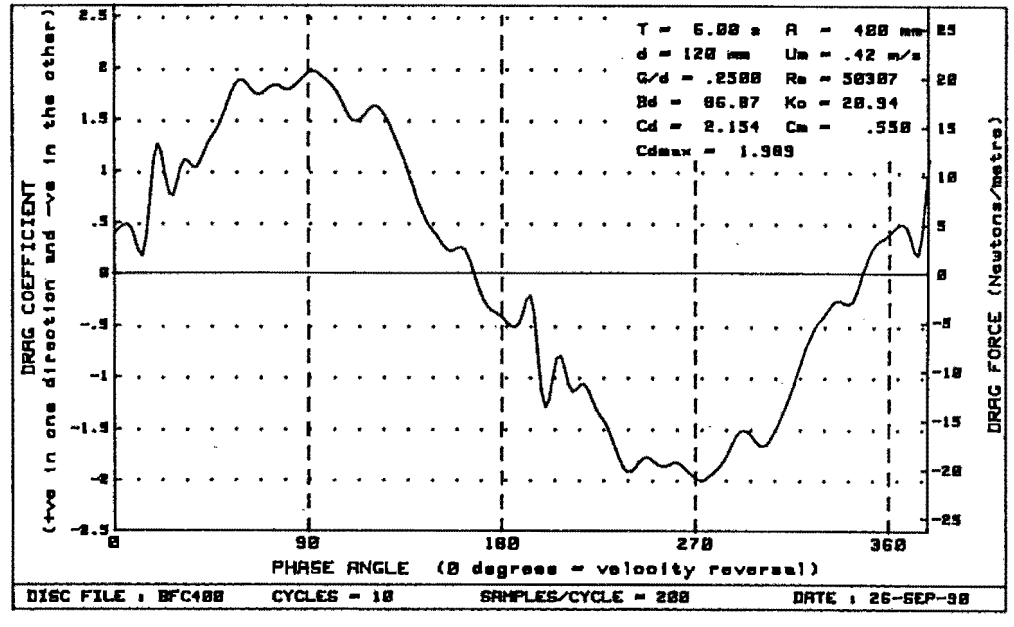

Figure H-54 : Plots of drag vs phase for diameter=120mm, Bd= 86.87 and G/d=0.25

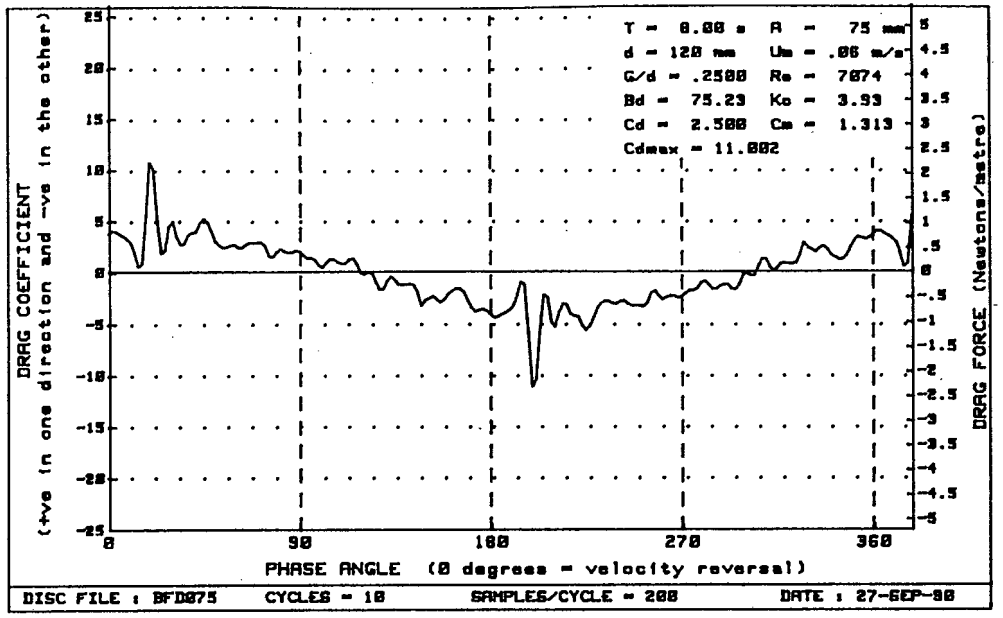

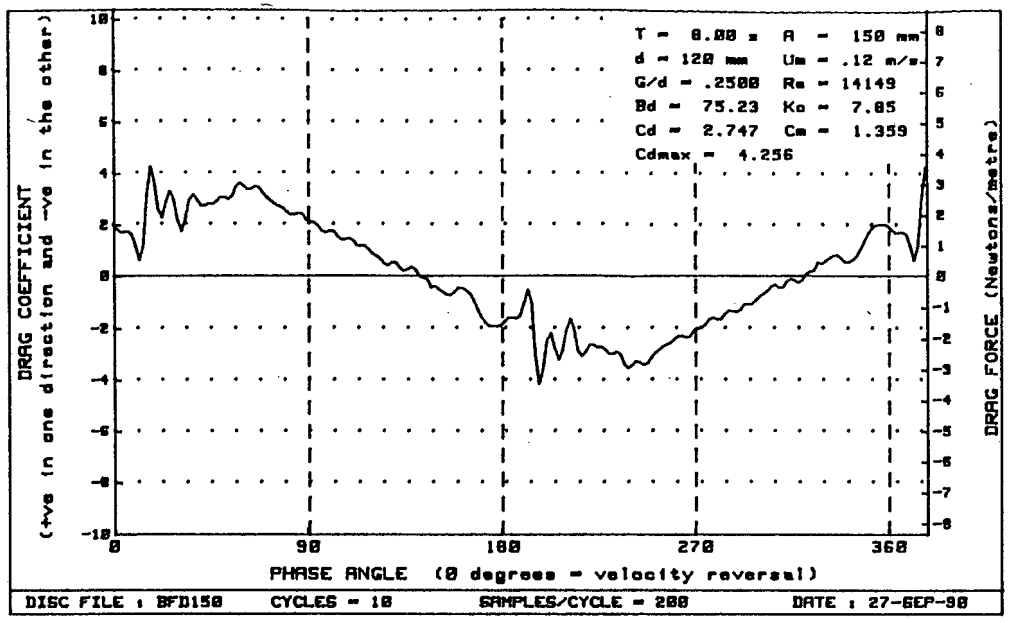

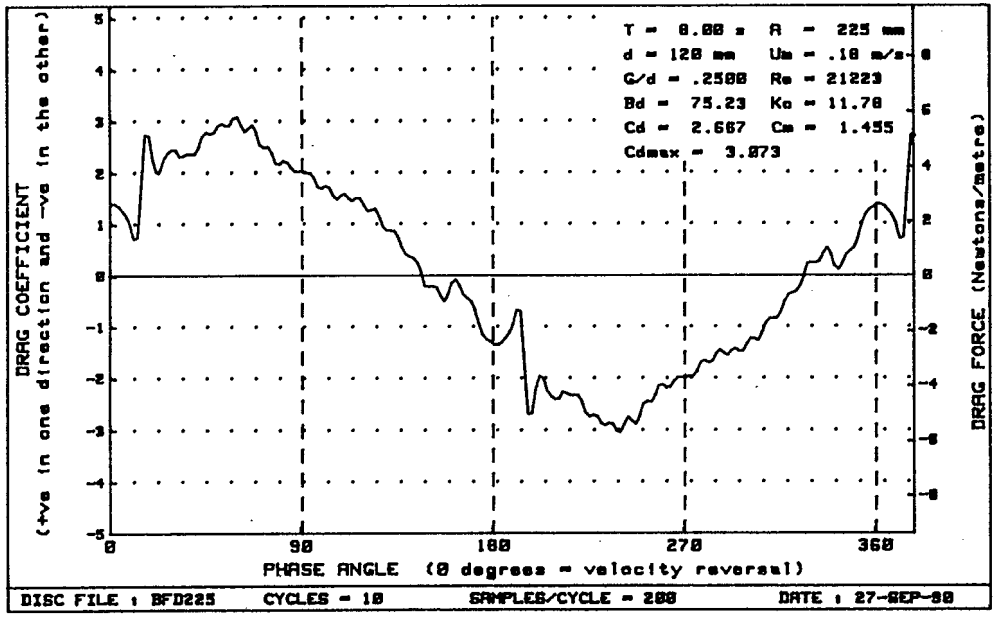

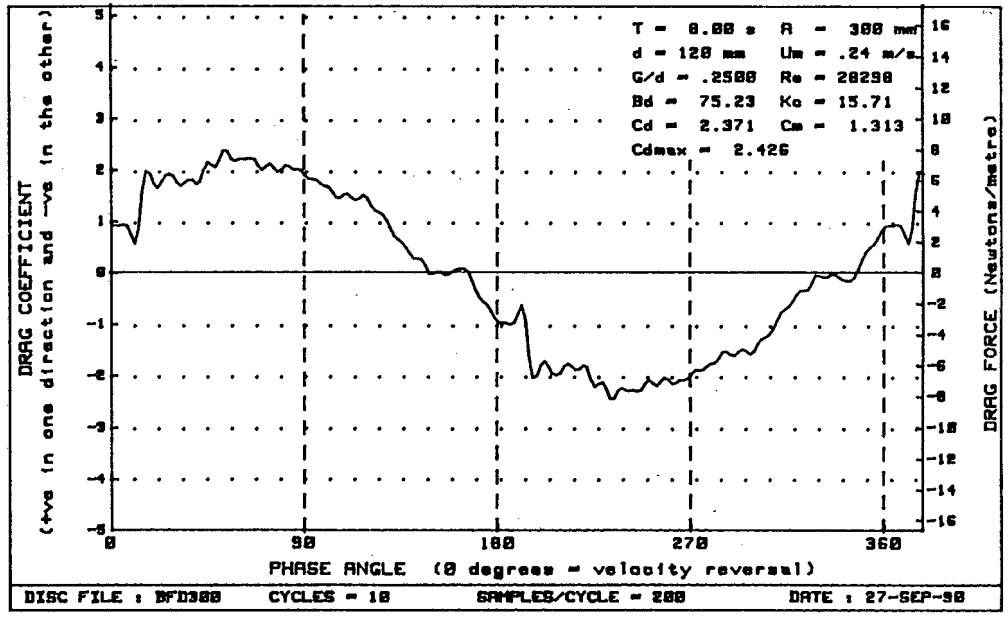

Figure H-55 : Plots of drag vs phase for diameter=120mm, Bd= 75.23 and G/d= .2500

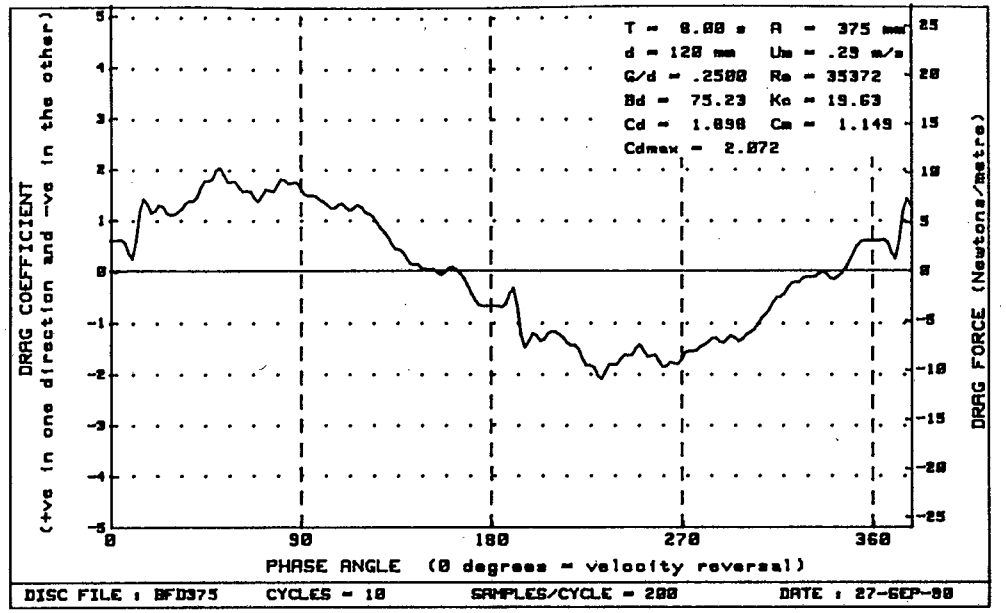

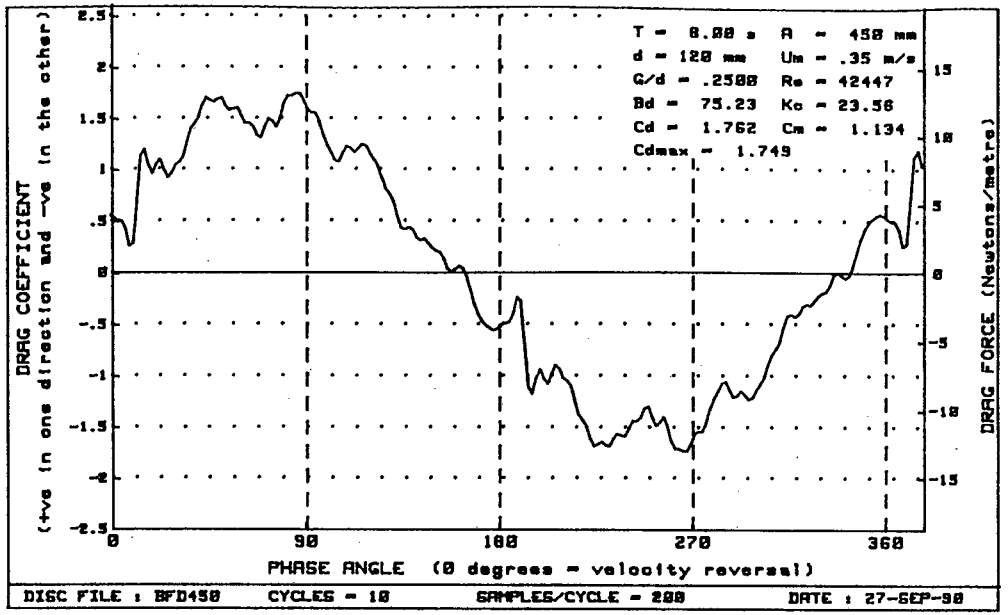

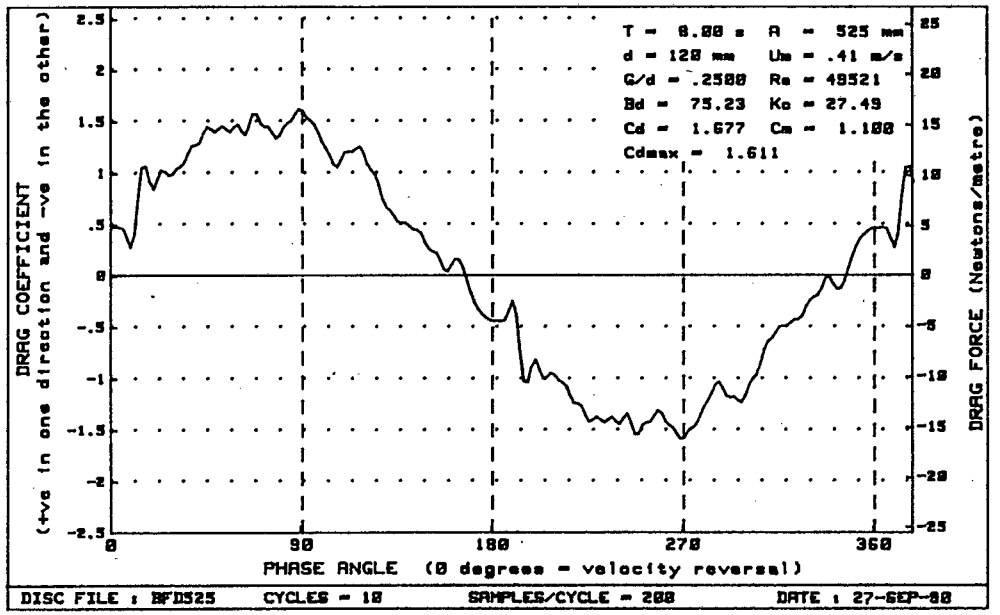

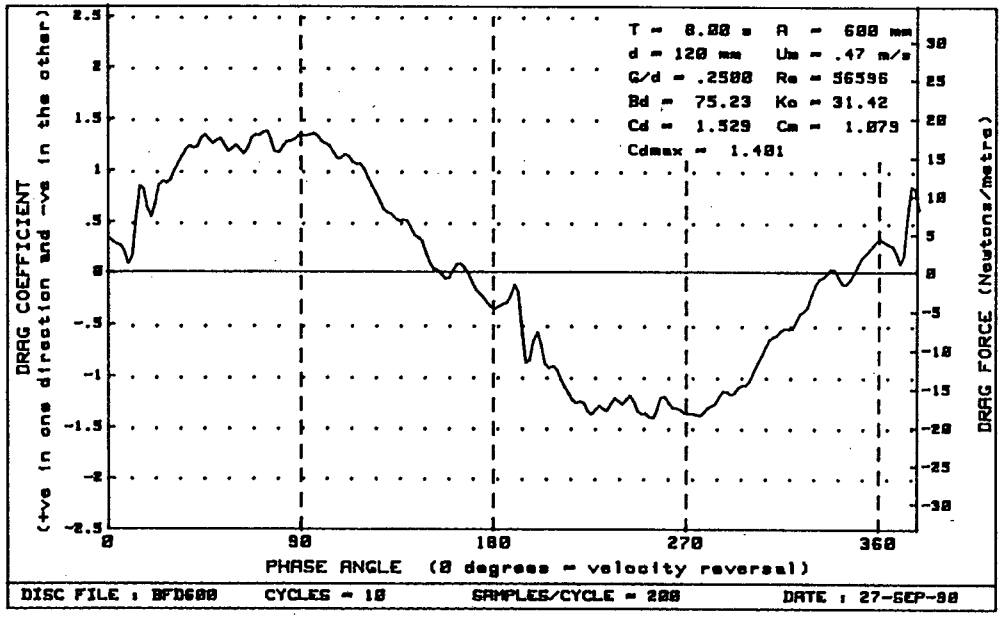

Figure H-56 : Plots of drag vs phase for diameter=120mm, Bd= 75.23 and G/d= .2500

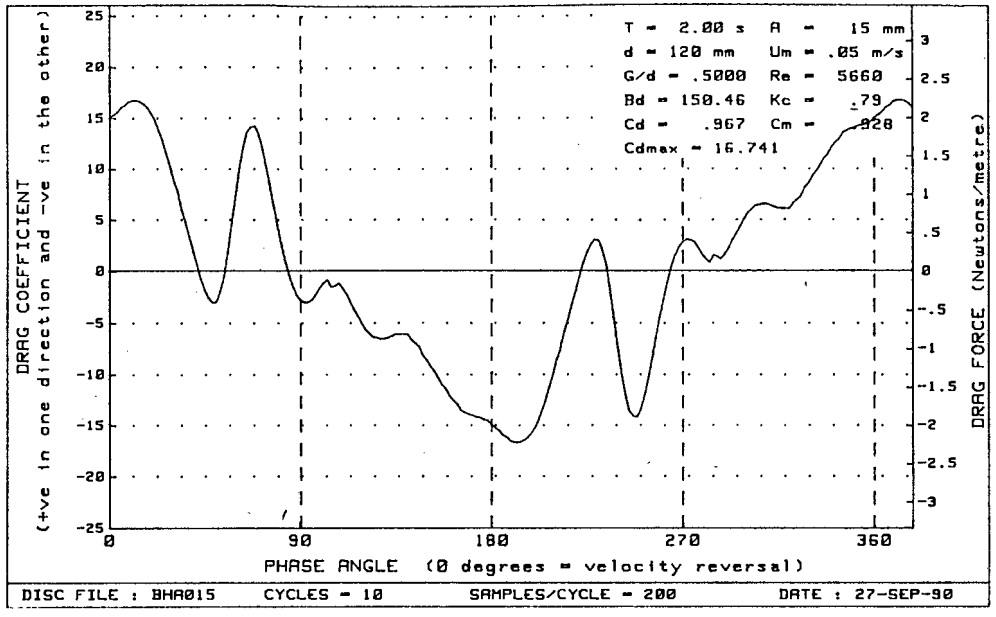

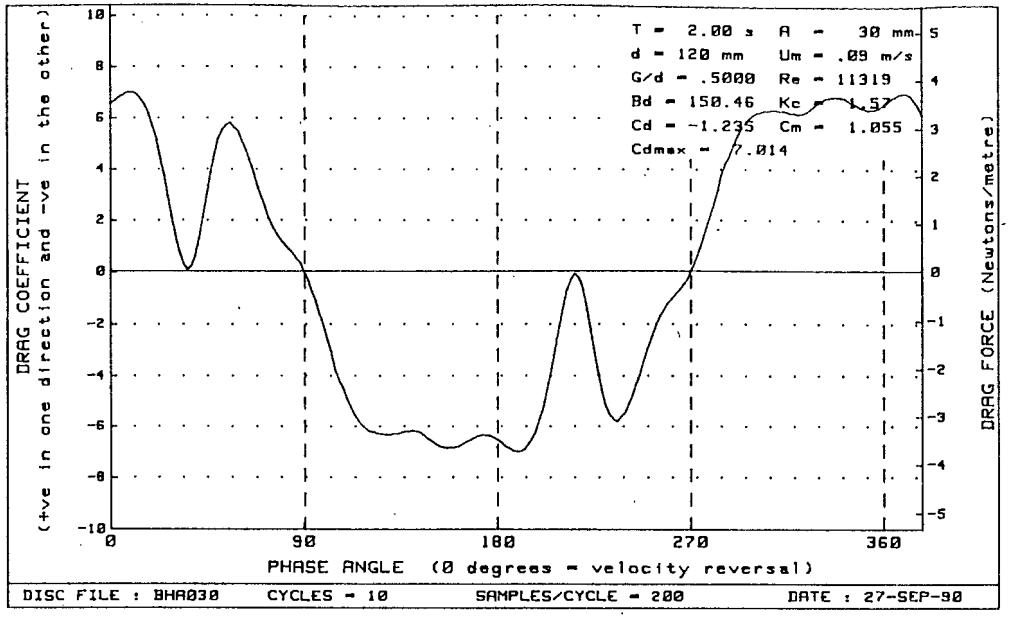

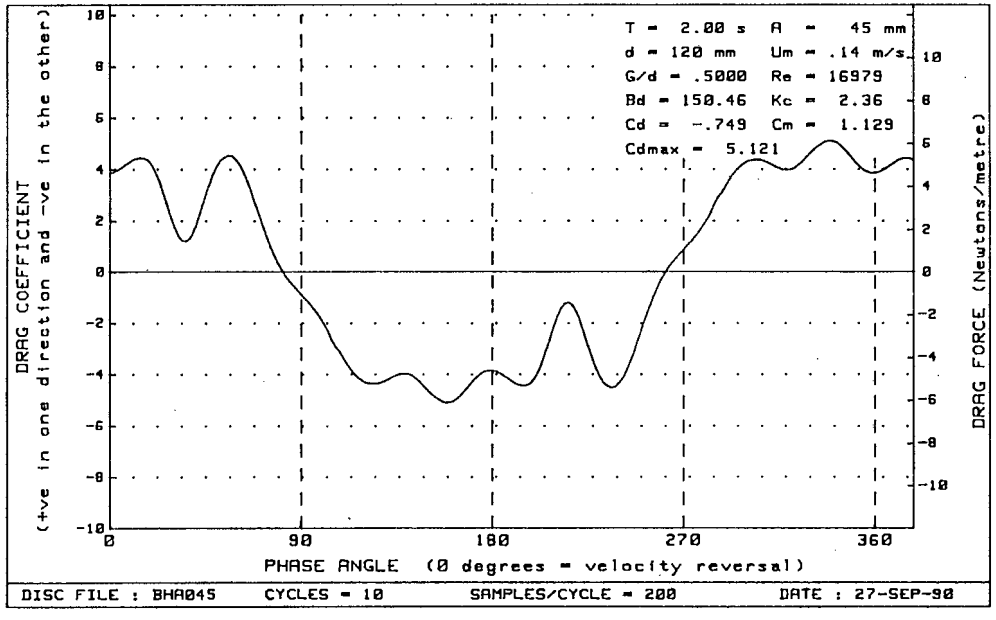

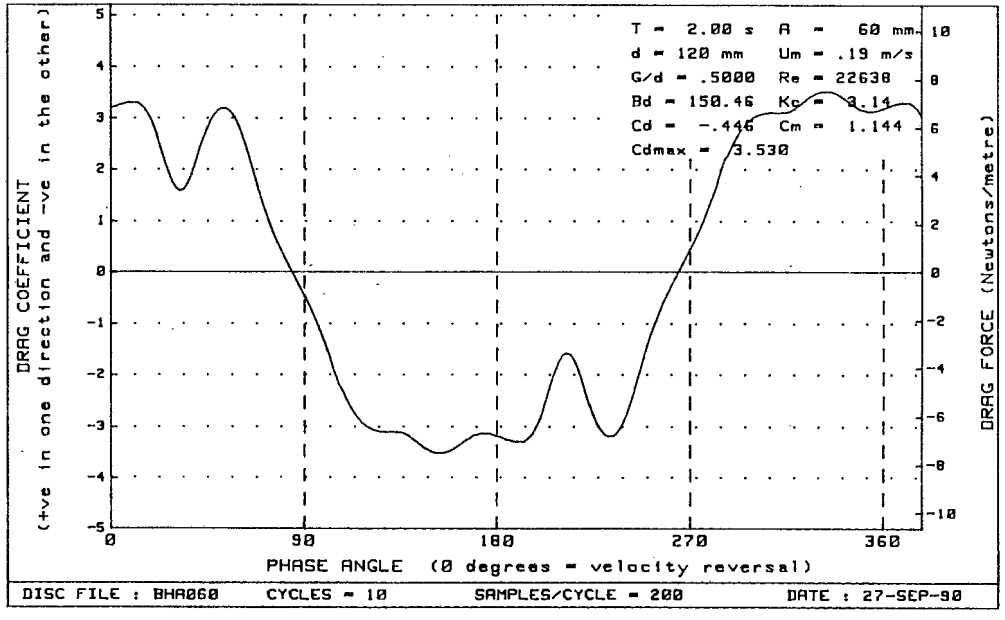

Figure H – 57:: Plots of drag vs phase for diameter=120mm, Bd=150.46 and G/d= .5000

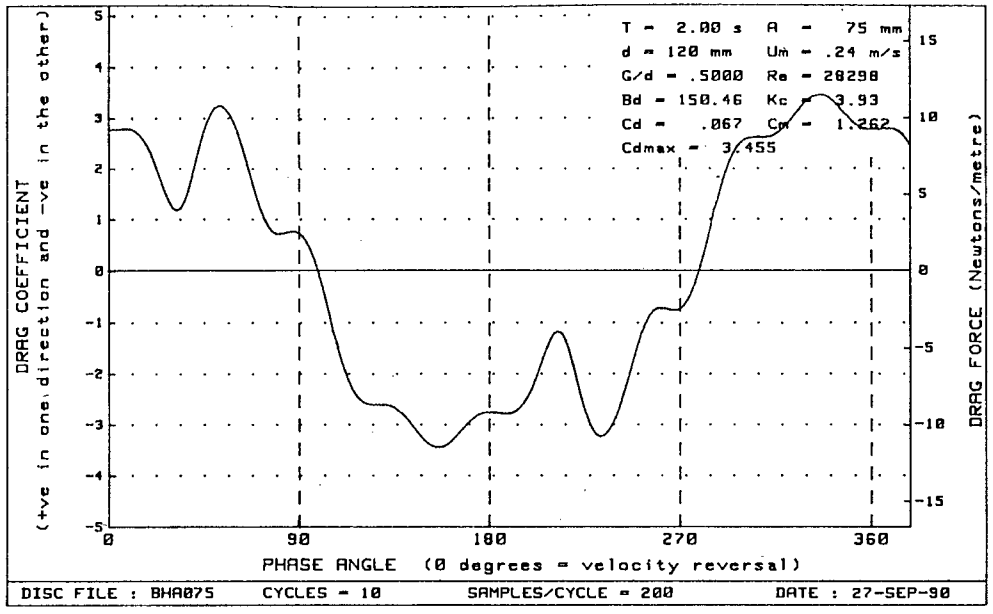

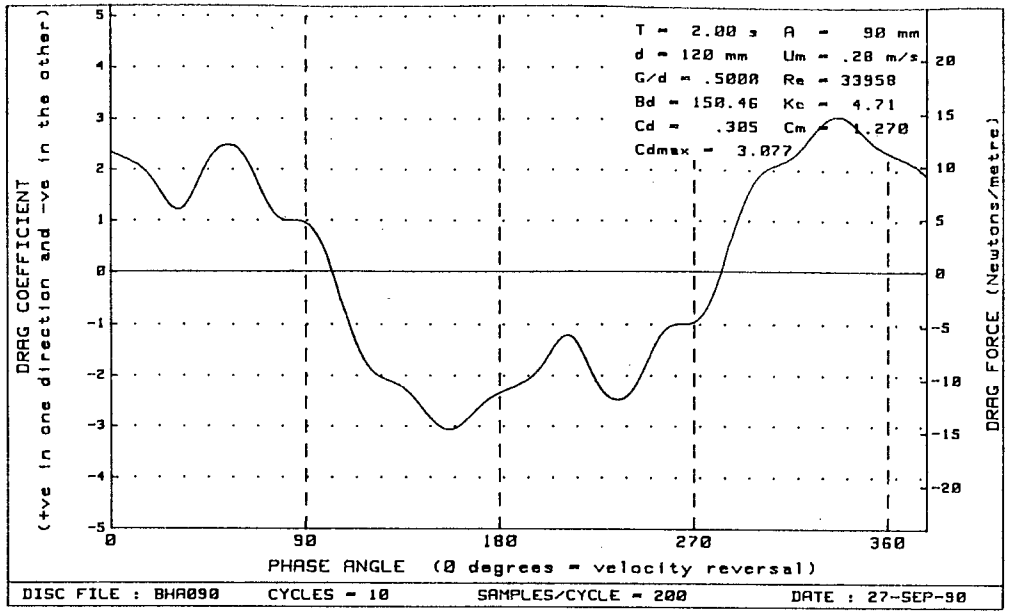

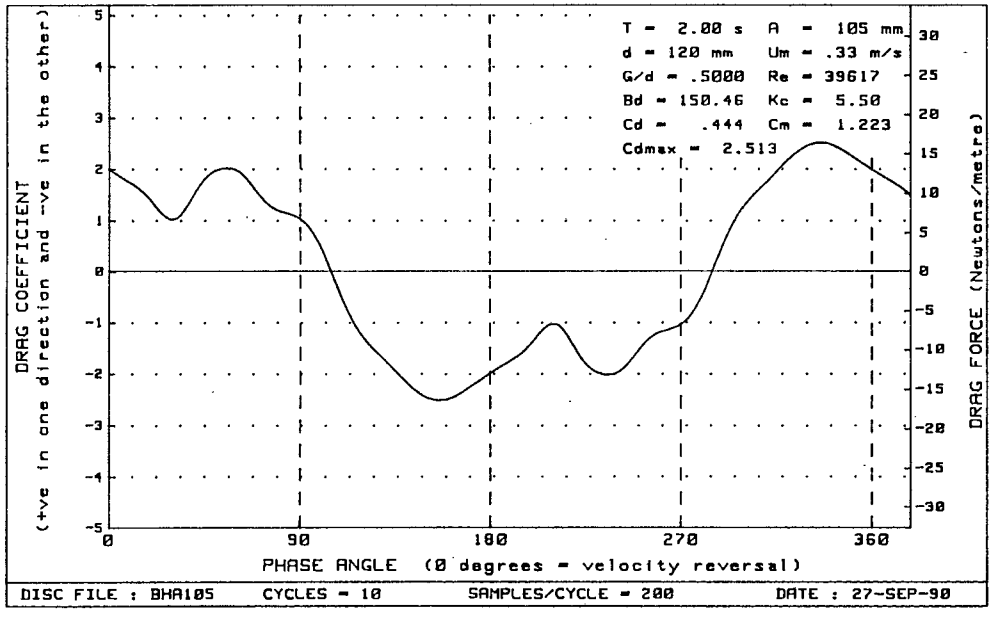

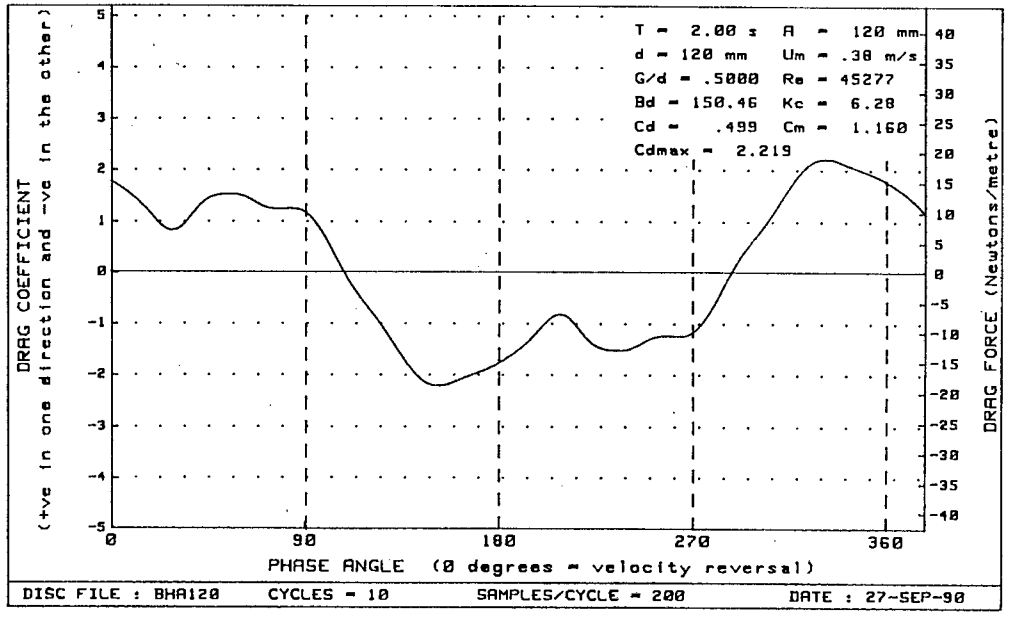

Figure H – 58 : Plots of drag vs phase for diameter=120mm, Bd=150.46 and G/d= .5000

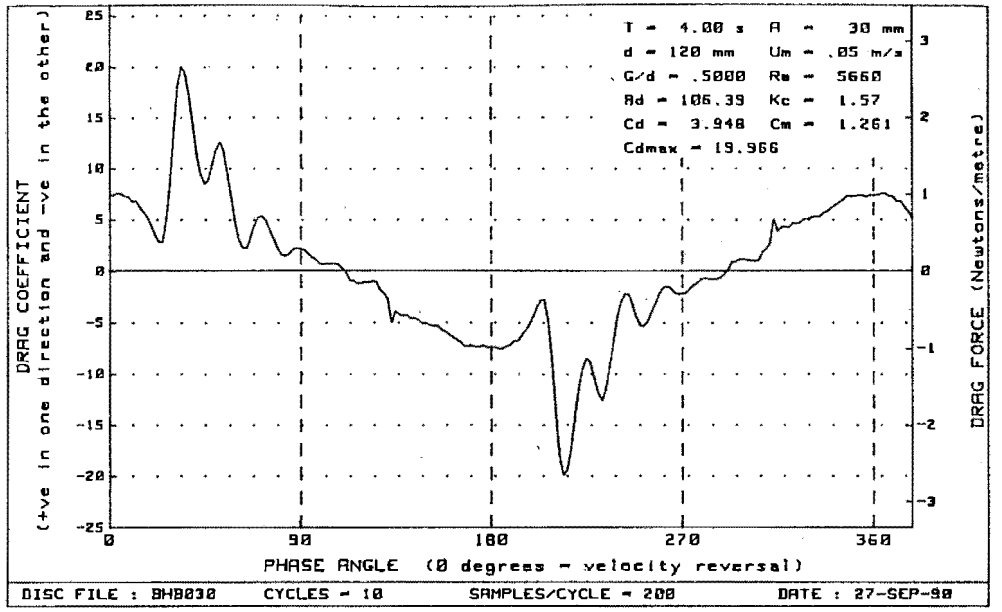

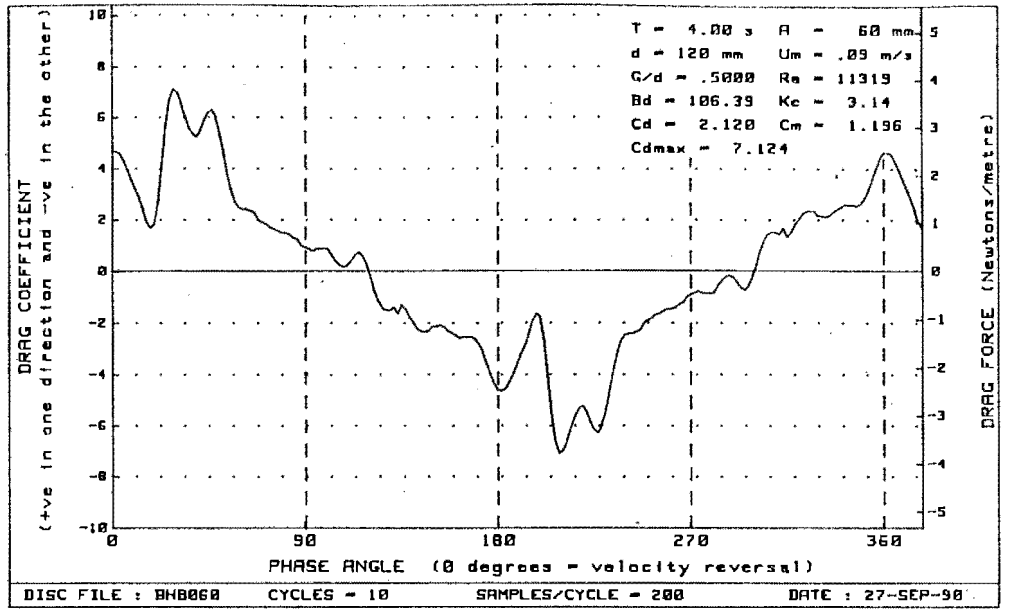

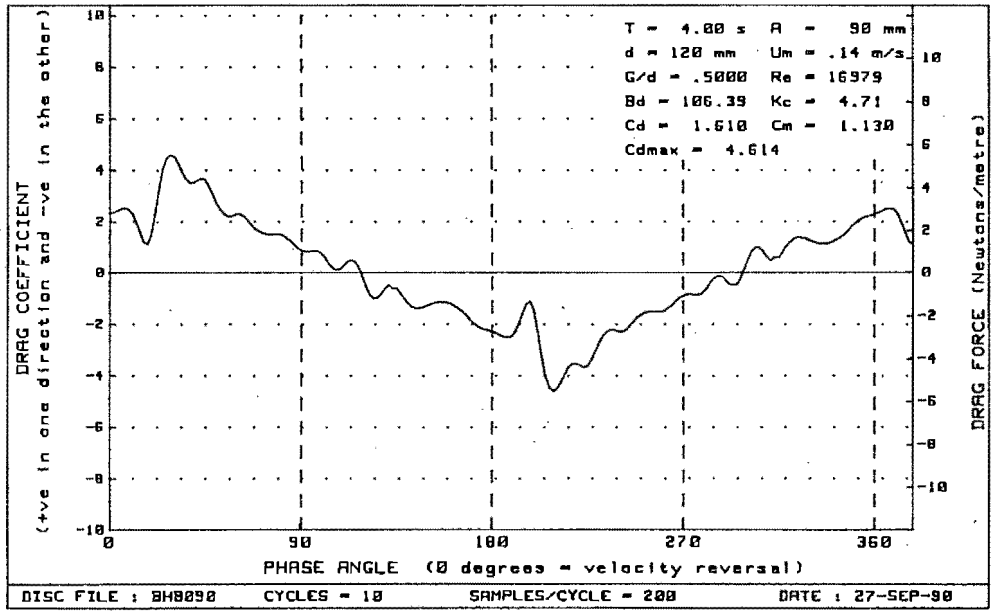

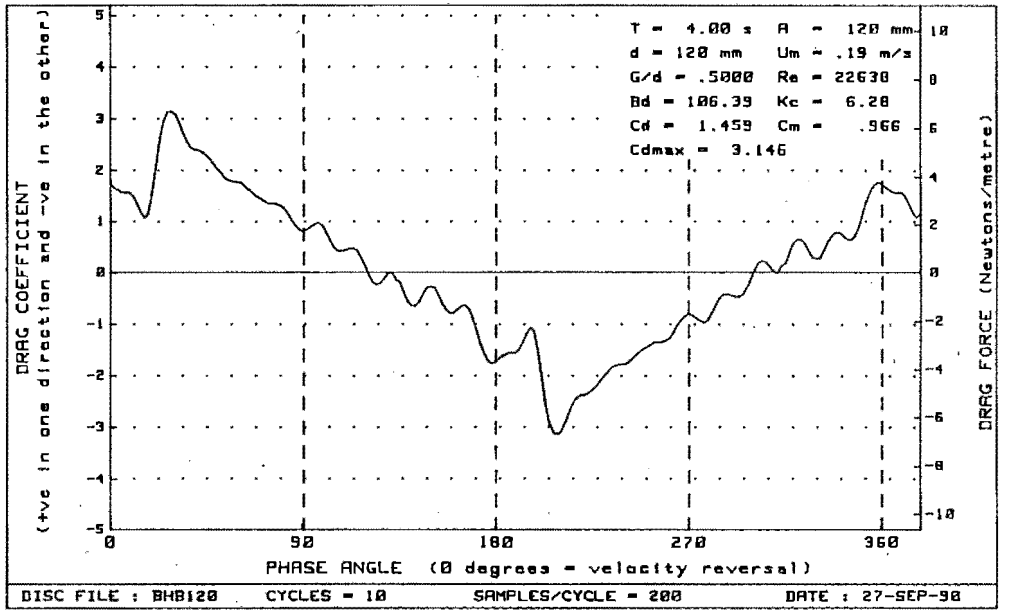

Figure H – 59 : Plots of drag vs phase for diameter=120mm, Bd=106.39 and G/d= .5000

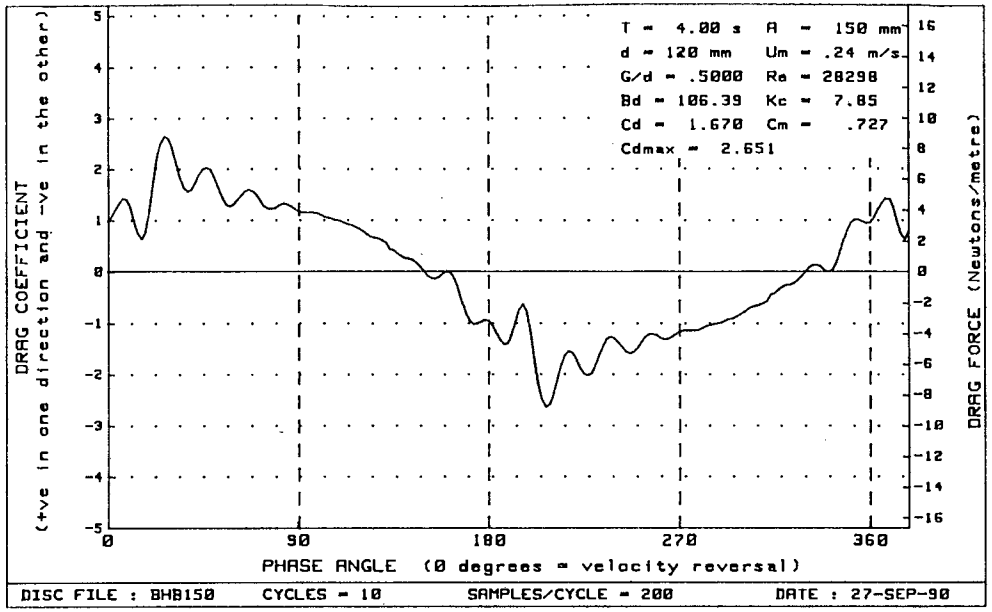

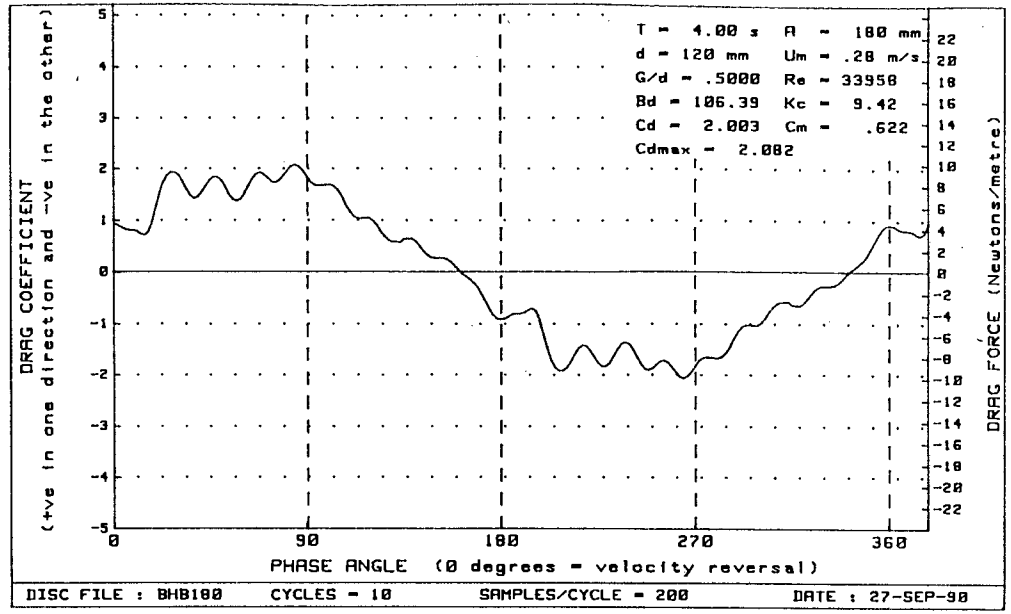

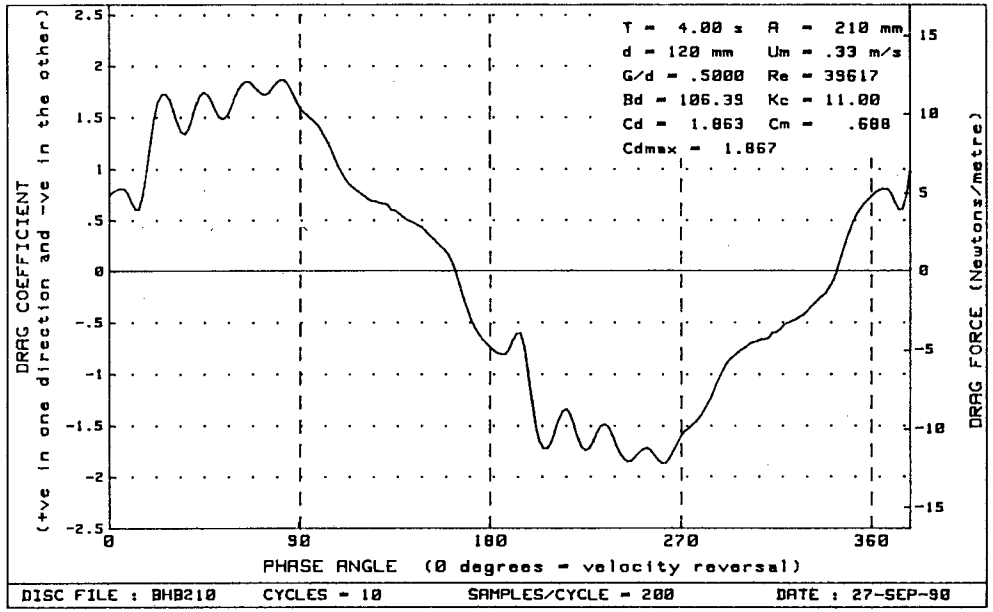

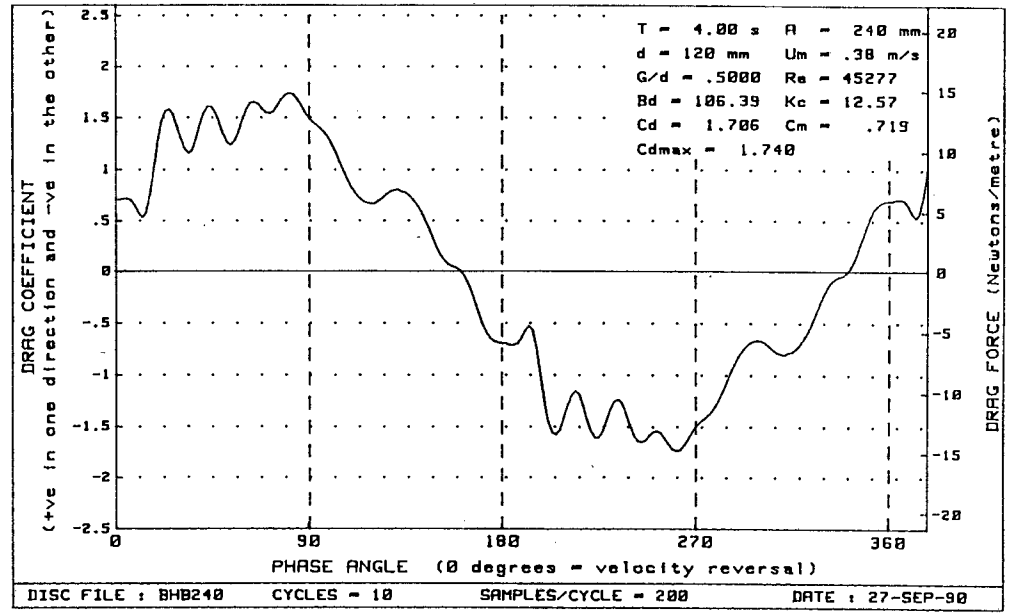

Figure H – 60 : Plots of drag vs phase for diameter=120mm, Bd=106.39 and G/d= .5000

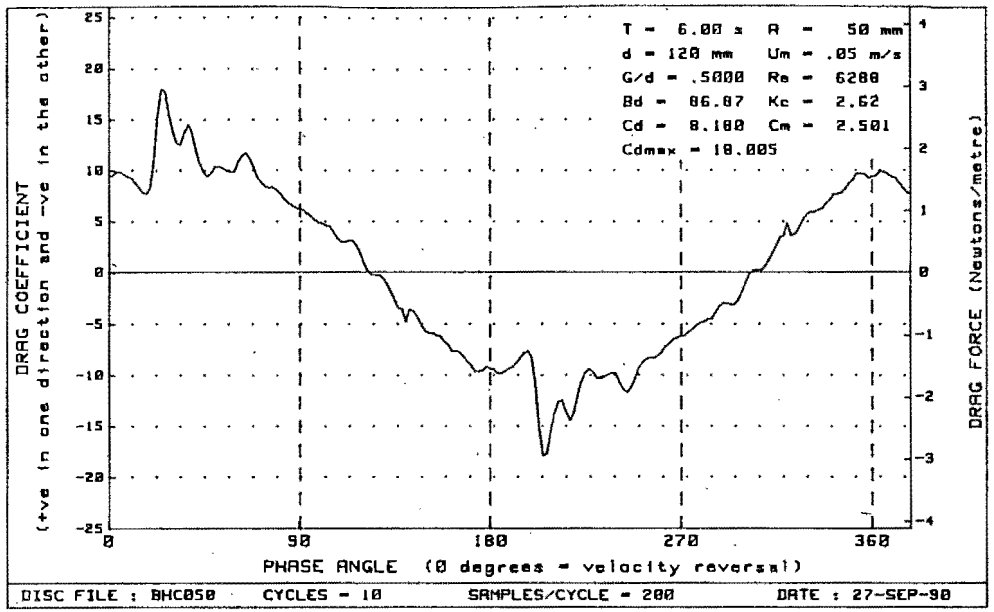

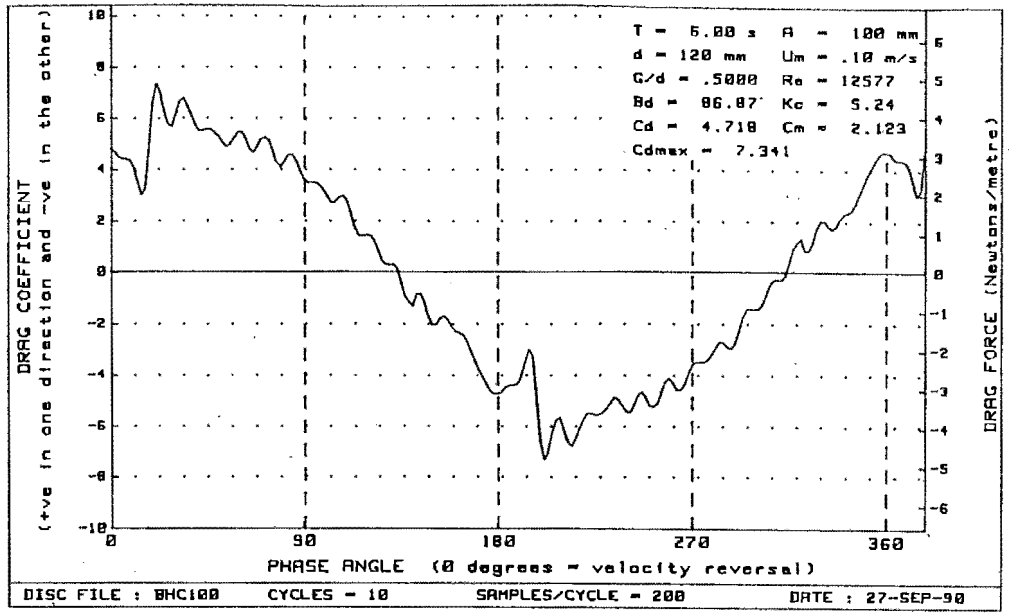

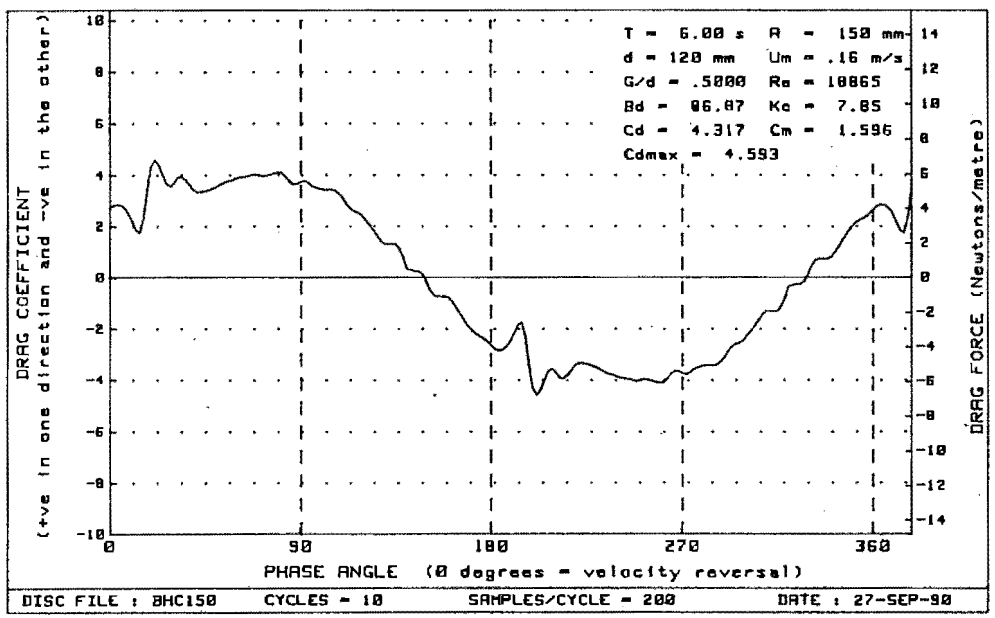

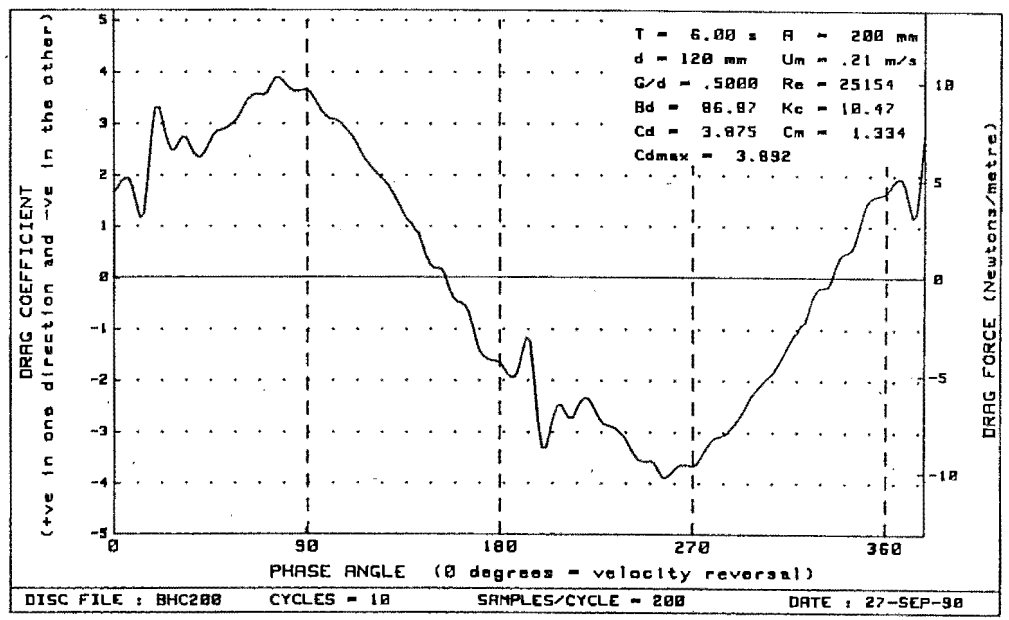

Figure H – 61 : Plots of drag vs phase for diameter=120mm, Bd= 86.87 and G/d= .5000

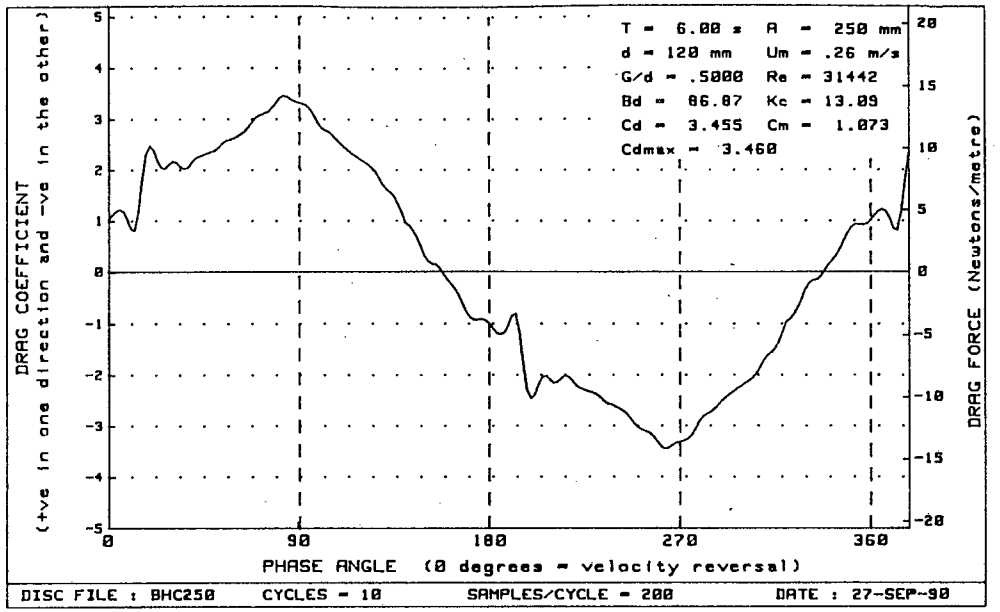

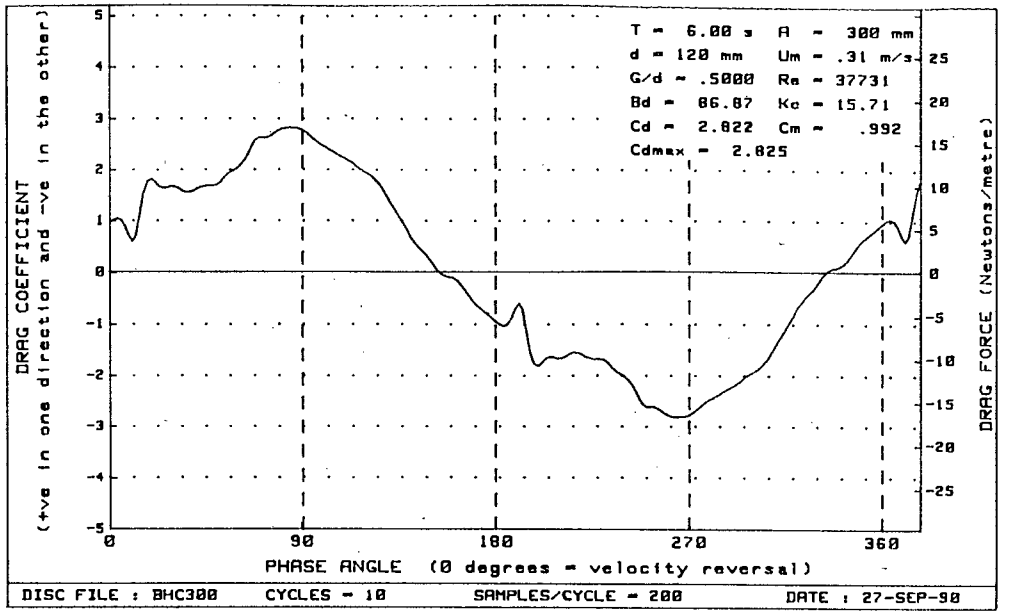

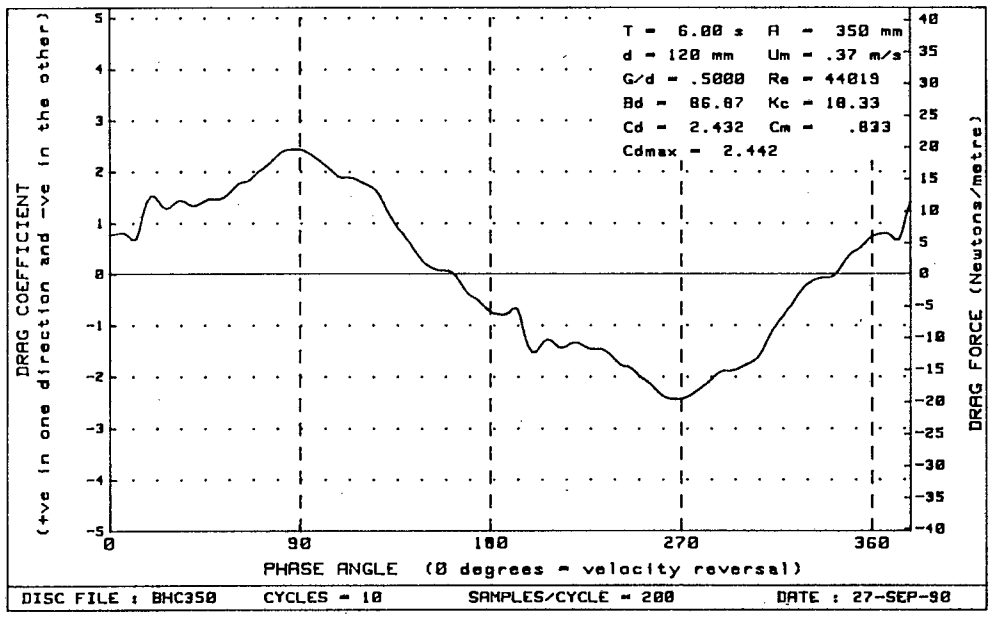

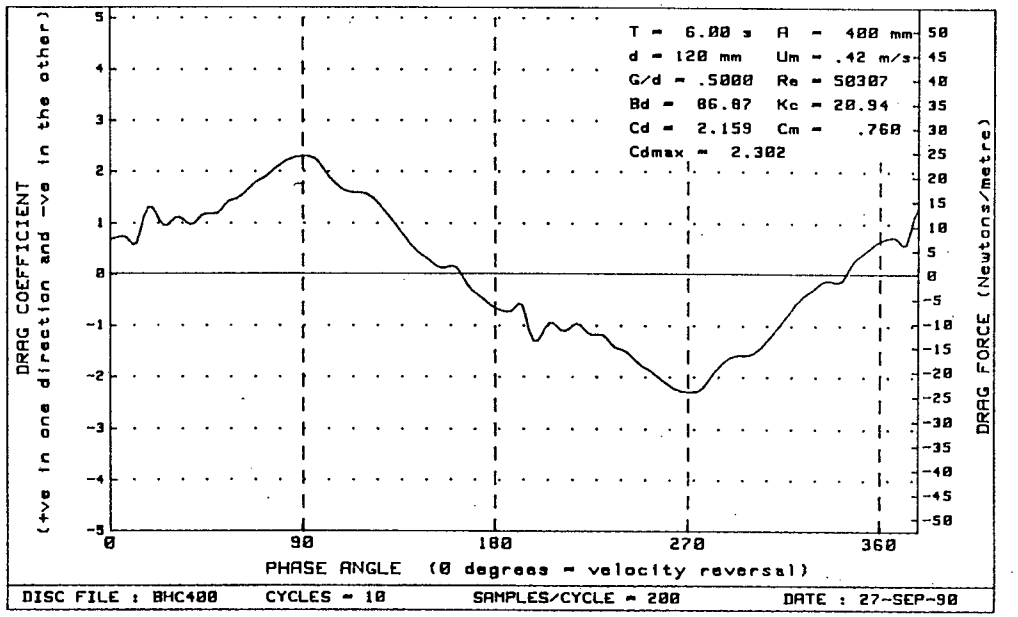

Figure H – 62 : Plots of drag vs phase for diameter=120mm, Bd= 86.87 and G/d= .5000

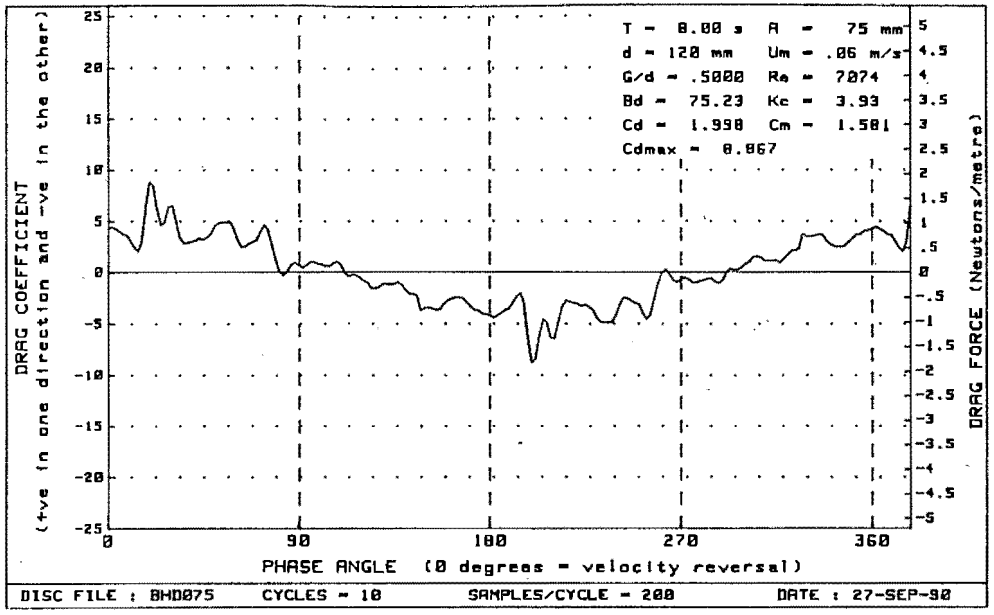

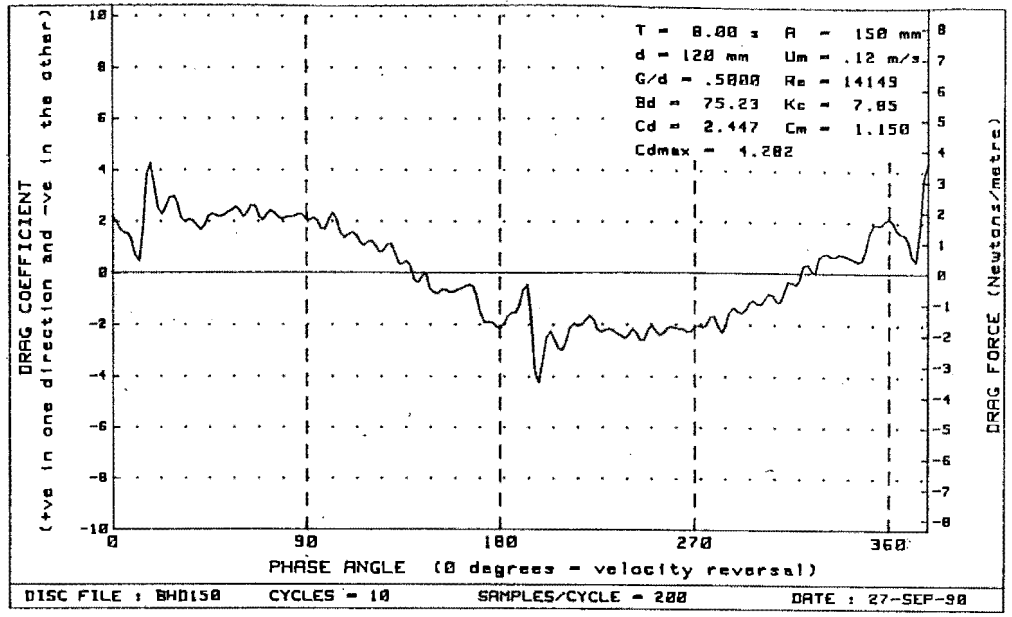

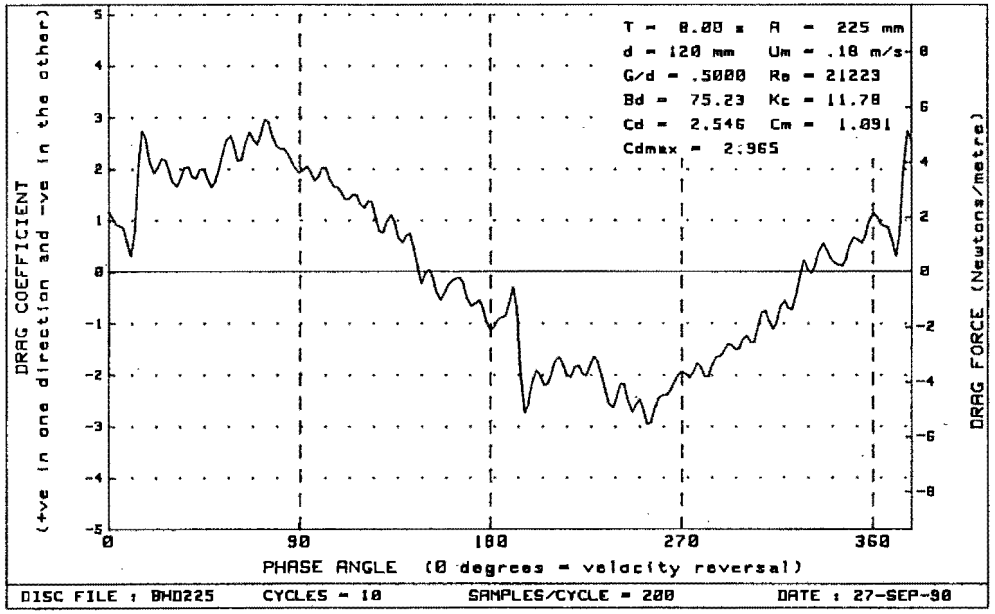

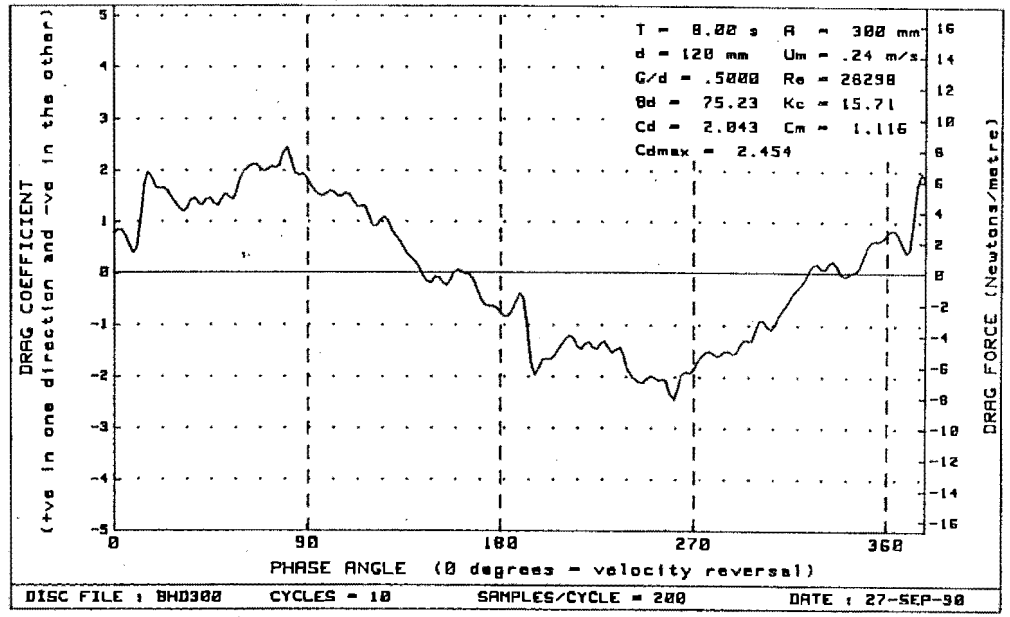

Figure H - 63 : Plots of drag vs phase for diameter=120mm, Bd= 75.23 and G/d= .5000

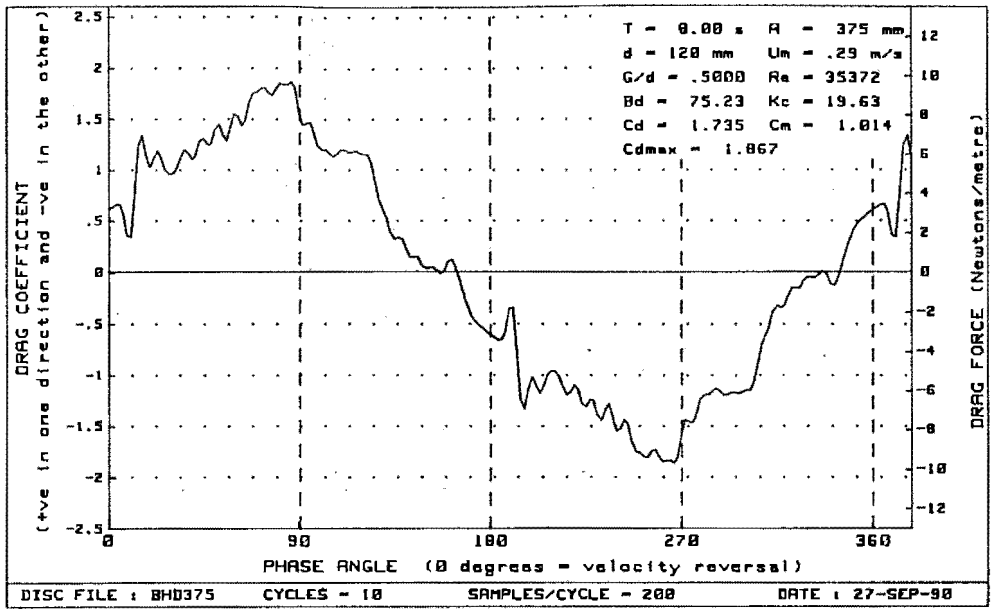

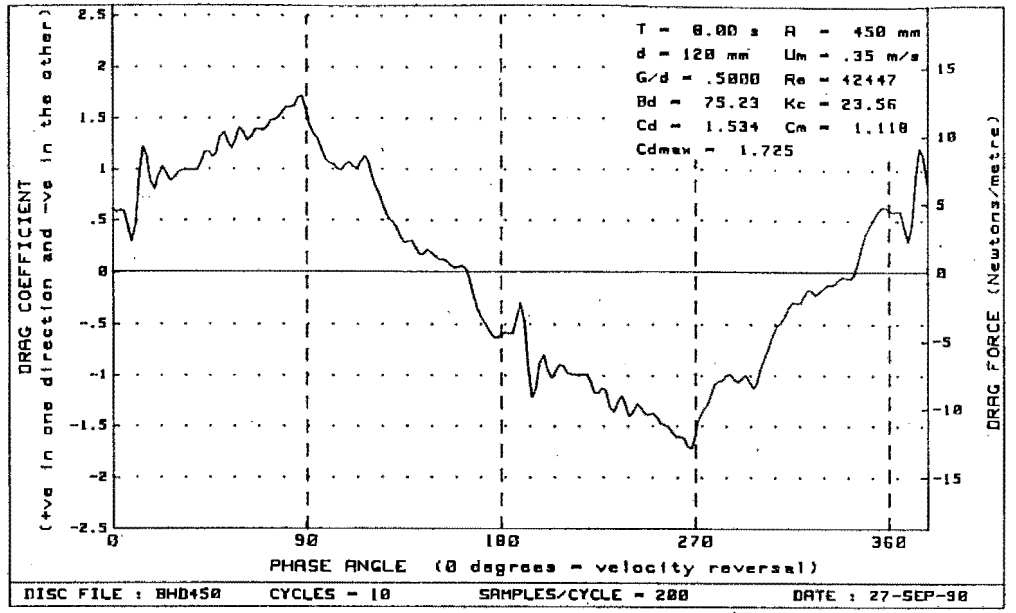

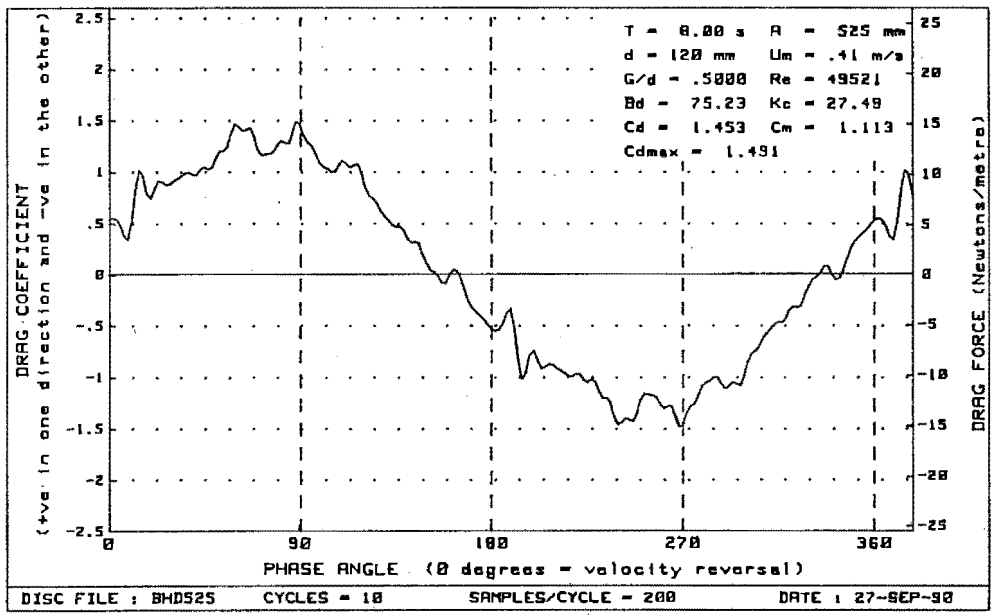

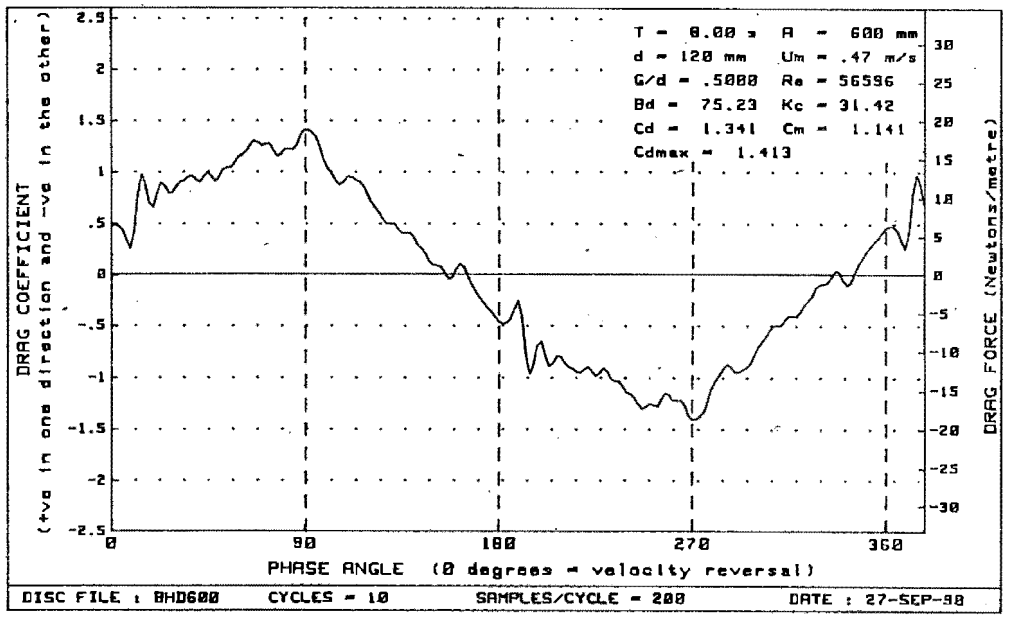

Figure H – 64 : Plots of drag vs phase for diameter=120mm, Bd= 75.23 and G/d= .5000

APPENDIX I - TEST RESULTS IN GRAPHICAL FORM

The following graphs show the test results plotted as a function of lift and drag coefficients, Keulegan Carpenter no., Reynolds no., gap ratio and βd.

LEGEND :

Figure number	Graph
1-4	Cl+ vs Kc for const. βd and varying gap ratios.
5-8	Cl- vs Kc for const. βd and varying gap ratios.
9-12	Clamp vs Kc for const. βd and varying gap ratios.
13-16	Cl+ vs Kc for const. βd and varying gap ratios.(d=90mm)
17-20	Cl+ vs Kc for const. βd and varying gap ratios.(d=90mm)
21-24	Clamp vs Kc for const. βd and varying gap ratios.(d=90)
25-26	Cl+ vs Kc for const. βd ,G/d = 0.6, 0.75, 1.0
27-28	Cl- vs Kc for const. βd ,G/d = 0.6, 0.75, 1.0
29-30	Clamp vs Kc for const. βd ,G/d = 0.6, 0.75, 1.0
31-34	Cd vs Kc for const. βd and varying gap ratios.
35-38	Cm vs Kc for const. βd and varying gap ratios.
39-42	Cdmax vs Kc for const. βd and varying gap ratios.
43-46	Cd vs Kc for const. βd and varying gap ratios.(d=90mm)
47-50	Cm vs Kc for const. βd and varying gap ratios.(d=90mm)
51-54	Cdmax vs Kc for const. βd and varying gap ratios.(d=90mm)

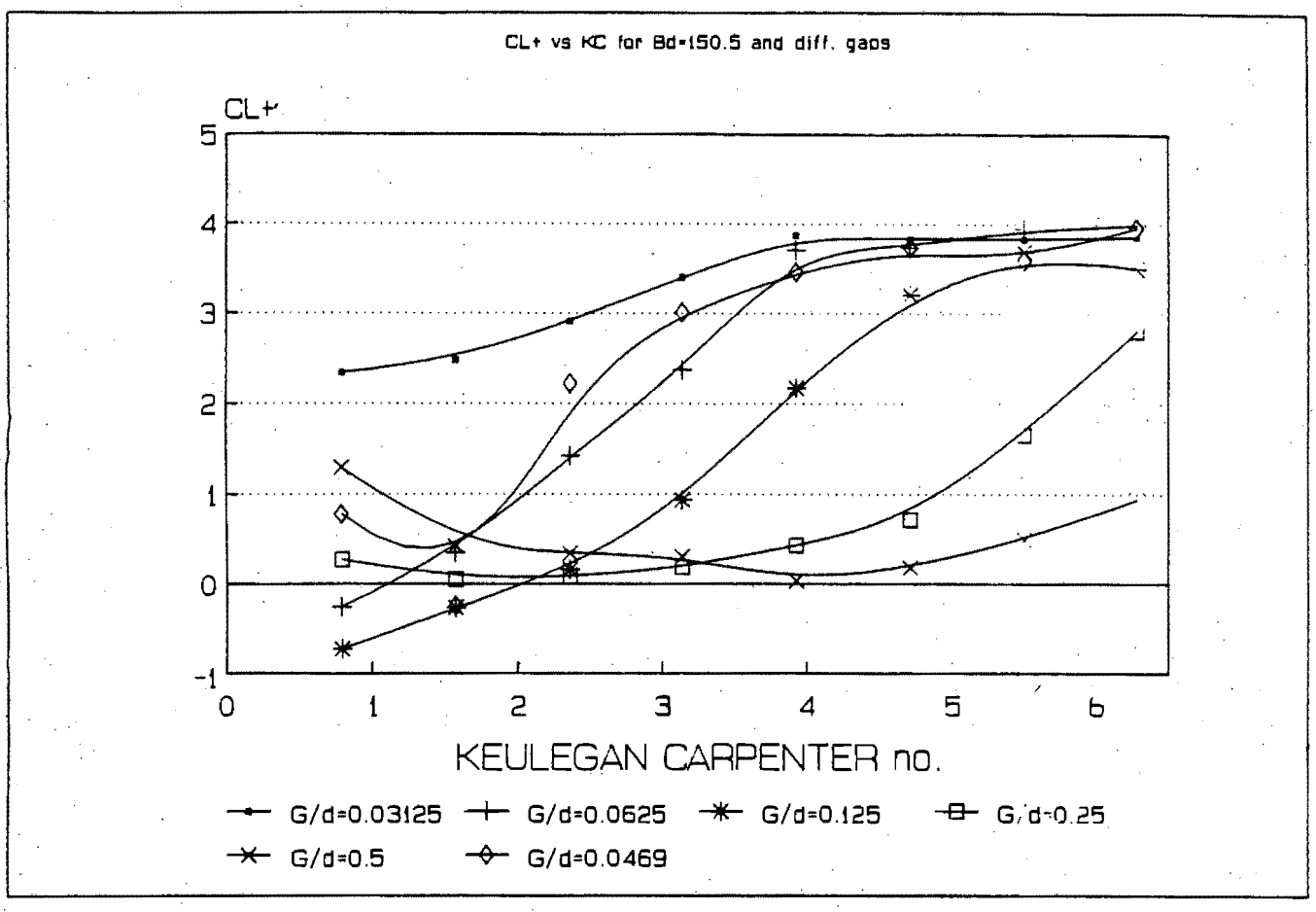

Figure I-1 : Cl+ vs KC for diameter=120mm, T=2s, ave Bd=150.5 and different gap ratios.

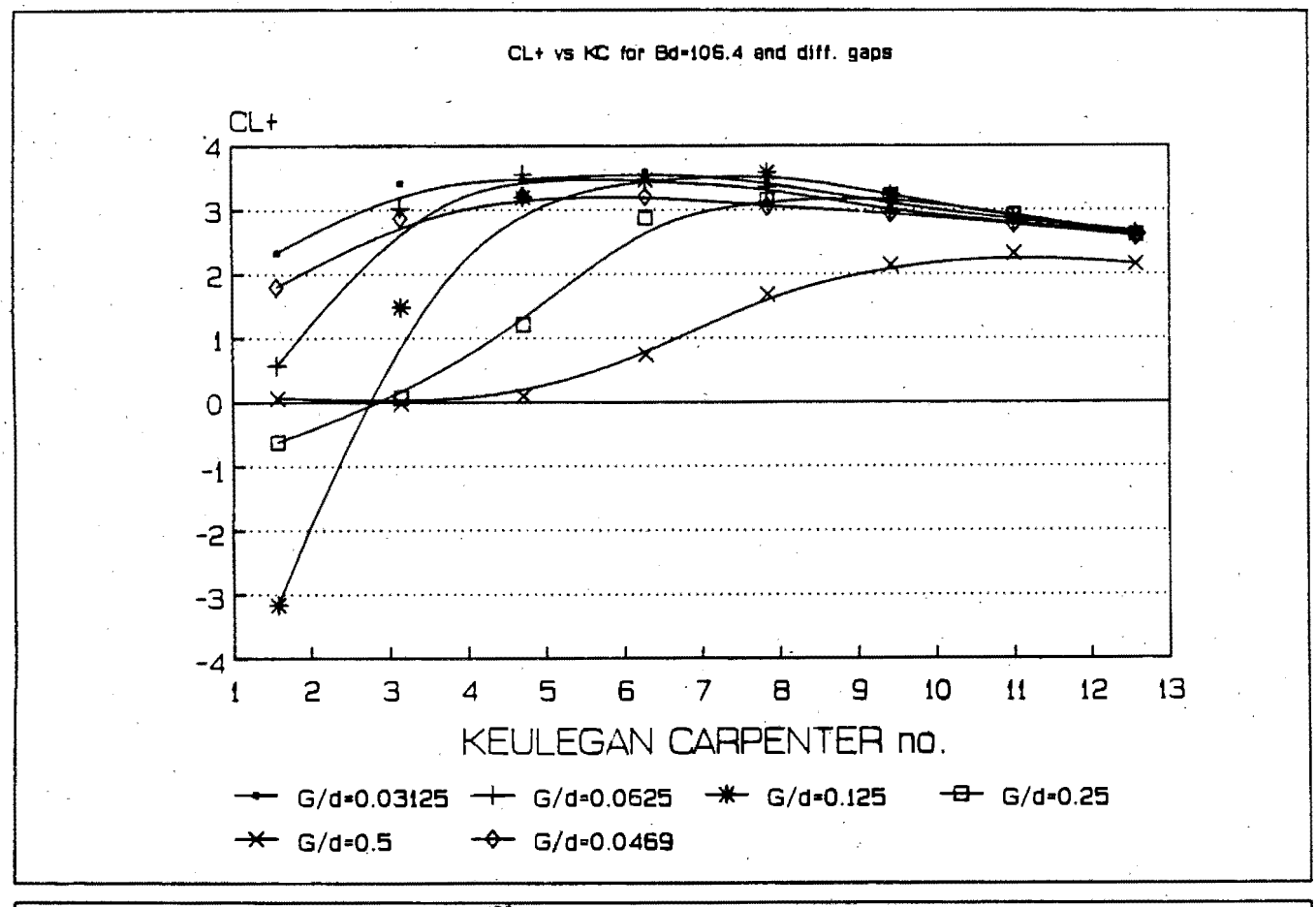

Figure I-2 :Cl+vs KC for diameter=130mm, T=4s, ave Bd=106.4 and different gap ratios.

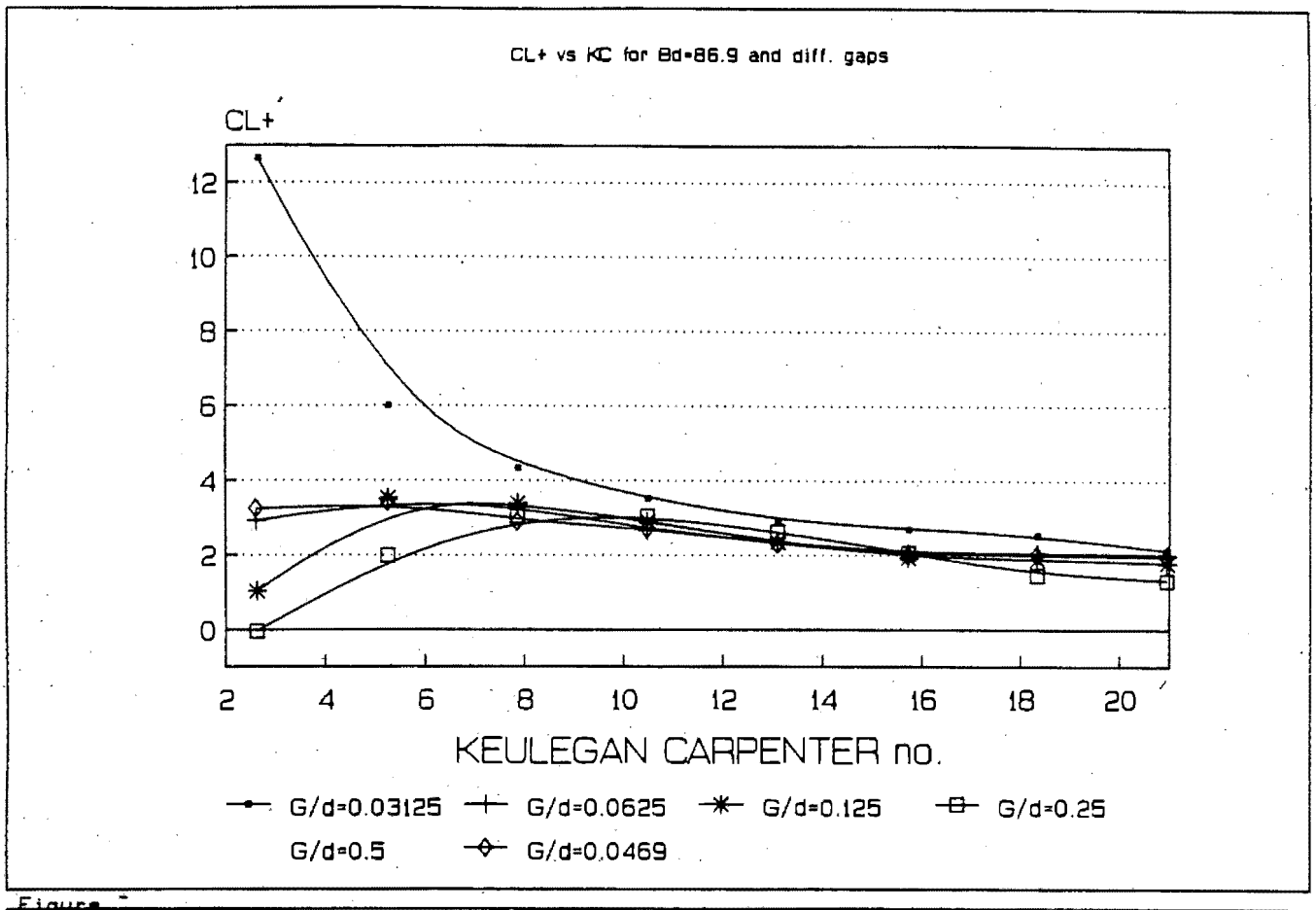

Figure I-3 : Cl+ vs KC for diameter=120mm, T=6s, ave Bd=86.9 and different gap ratios.

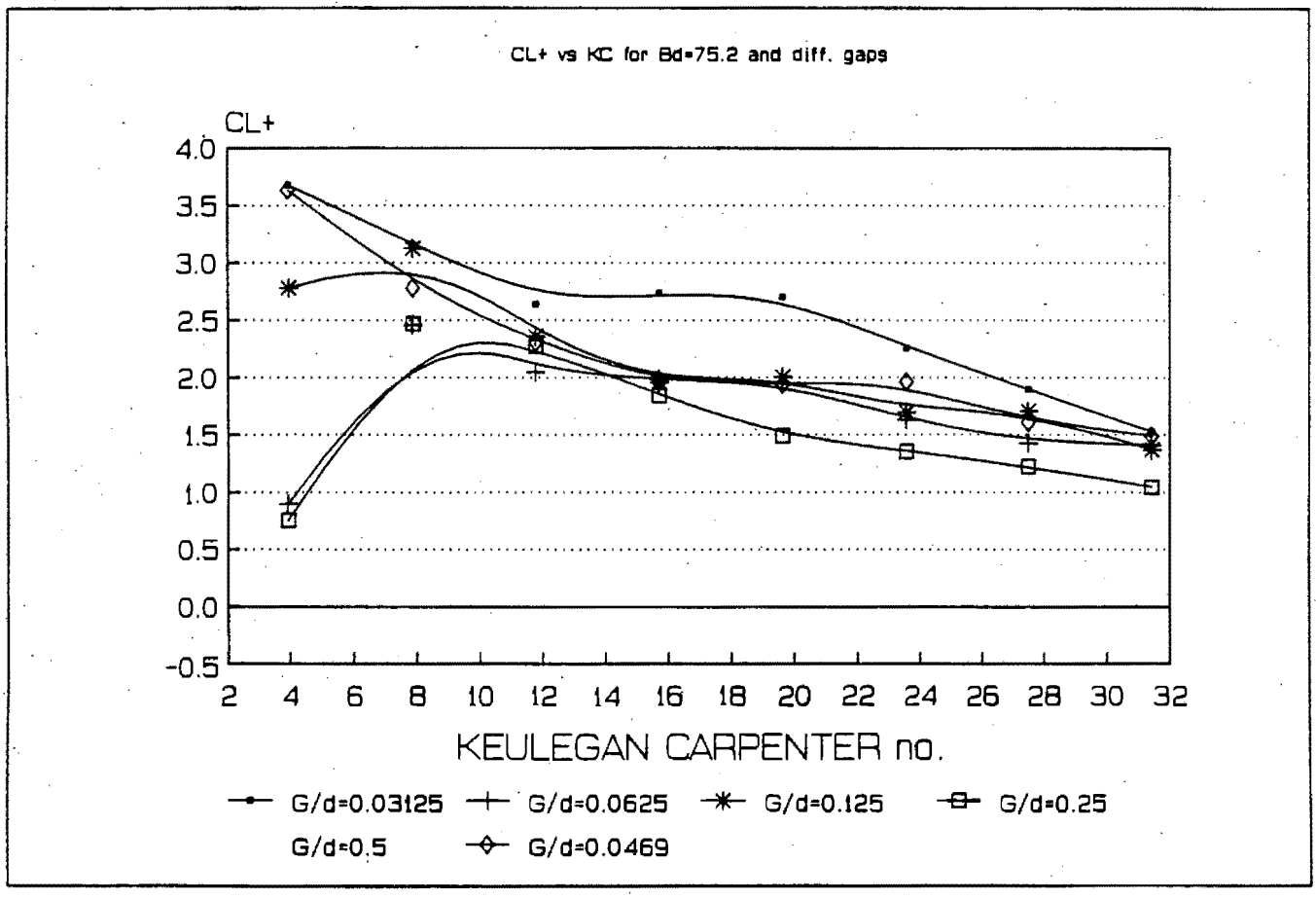

Figure I-4 : Cl+ vs KC for diameter=120mm, T=8s, ave Bd=75.2 and different gap ratios.

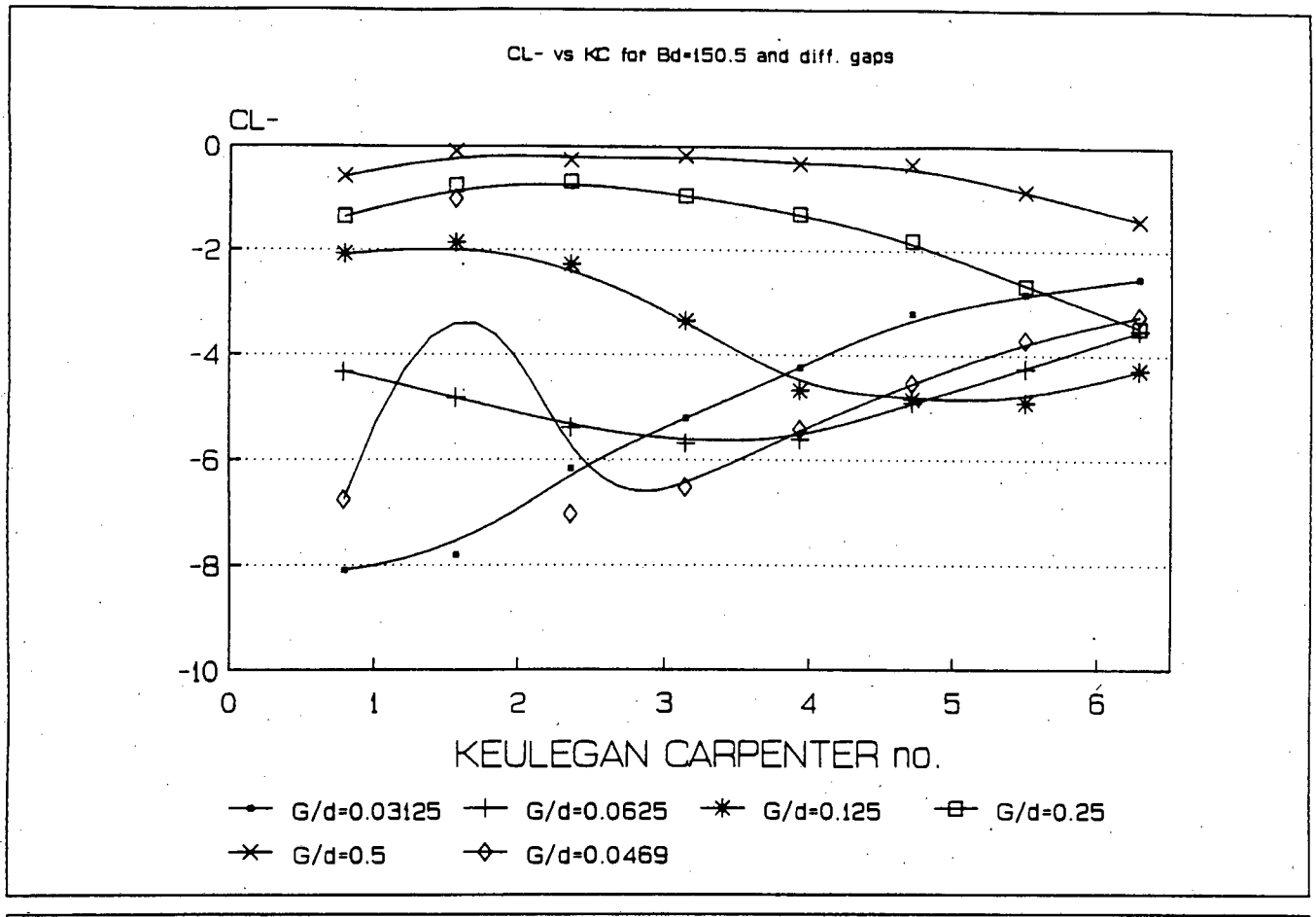

Figure I-5 : Cl- vs KC for diameter=120mm, T=2s, ave Bd=150.5 and different gap ratios.

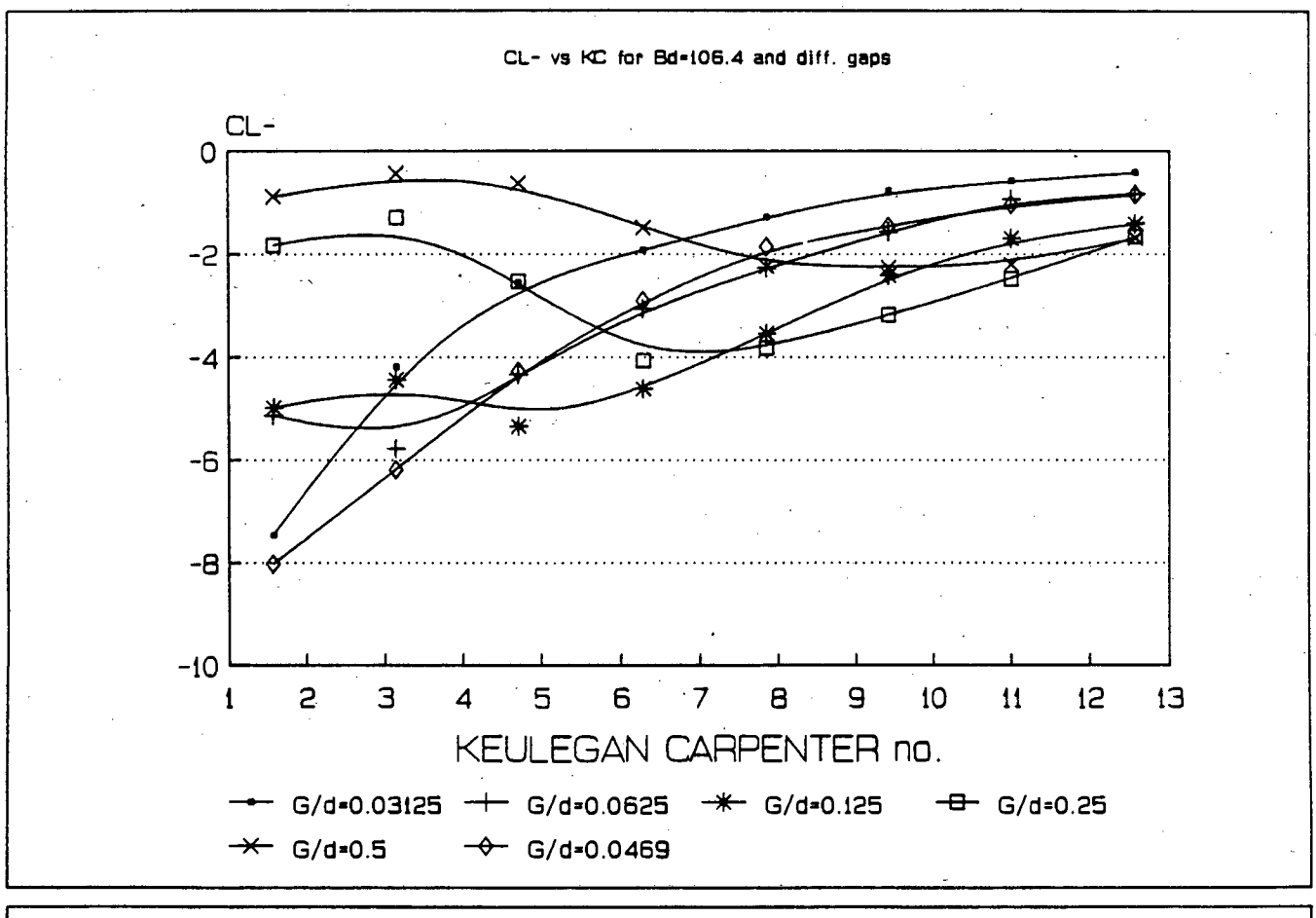

Figure I-6 : Cl- vs KC for diameter=120mm, T=4s, ave Bd=106.4 and different gap ratios.

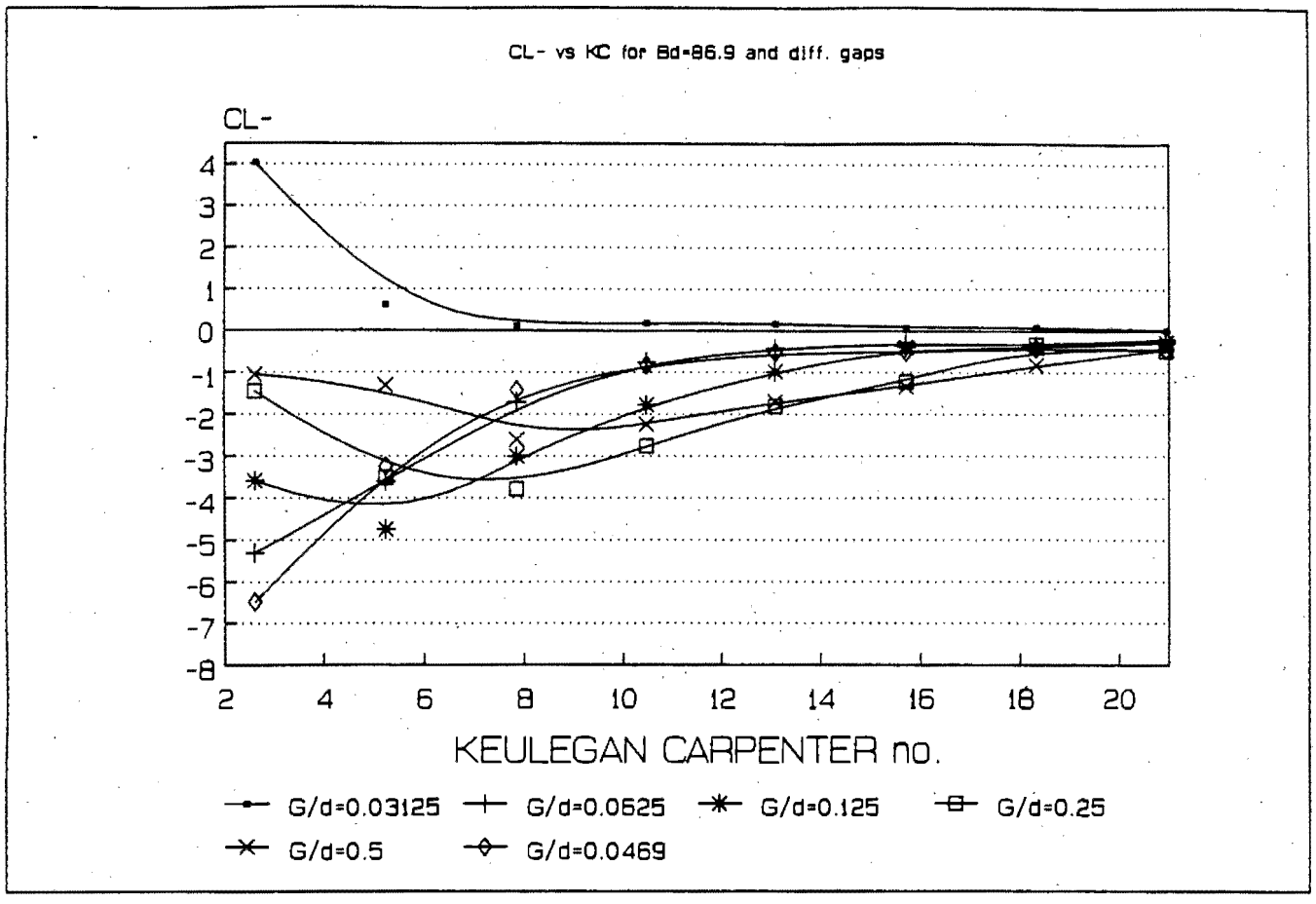

Figure I-7 : Cl- vs KC for diameter=120mm, T=6s, ave Bd=86.9 and different gap ratios.

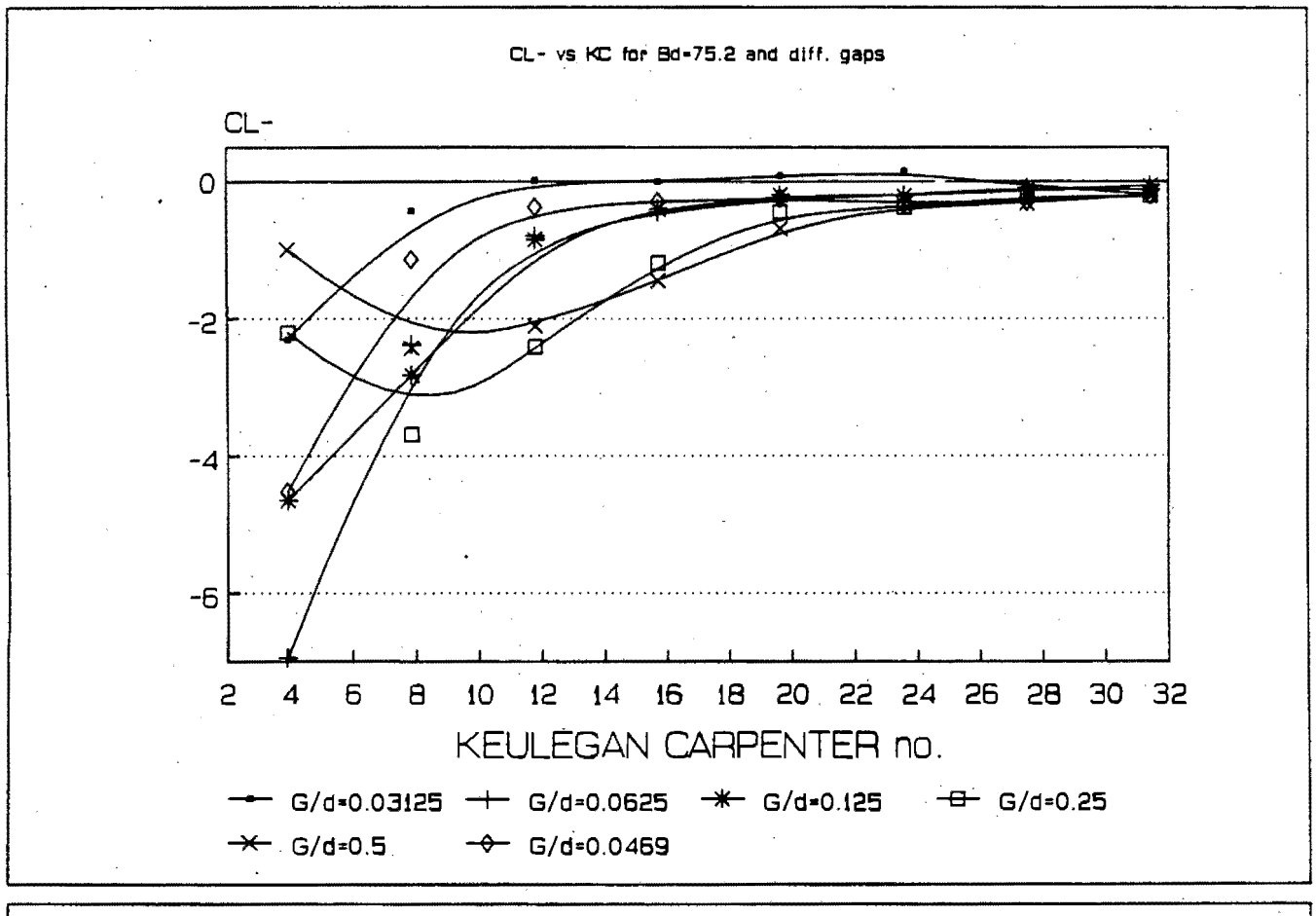

Figure I-8 : Cl- vs KC for diameter=120mm, T=8s, ave Bd=75.2 and different gap ratios.

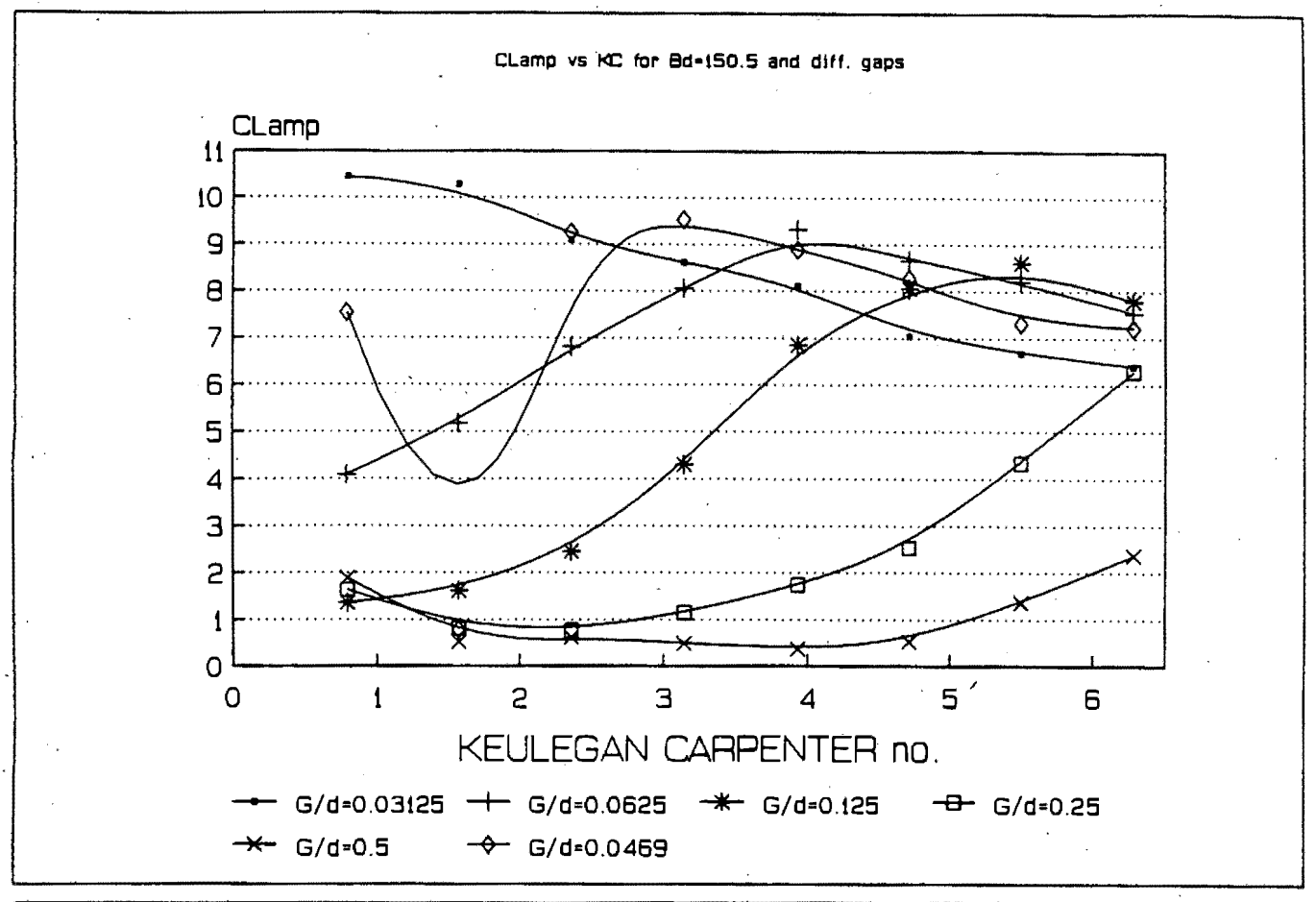

Figure I-9 : Clamp vs KC for diameter=120mm, T=2s, ave Bd=150.5 and different gap ratios.

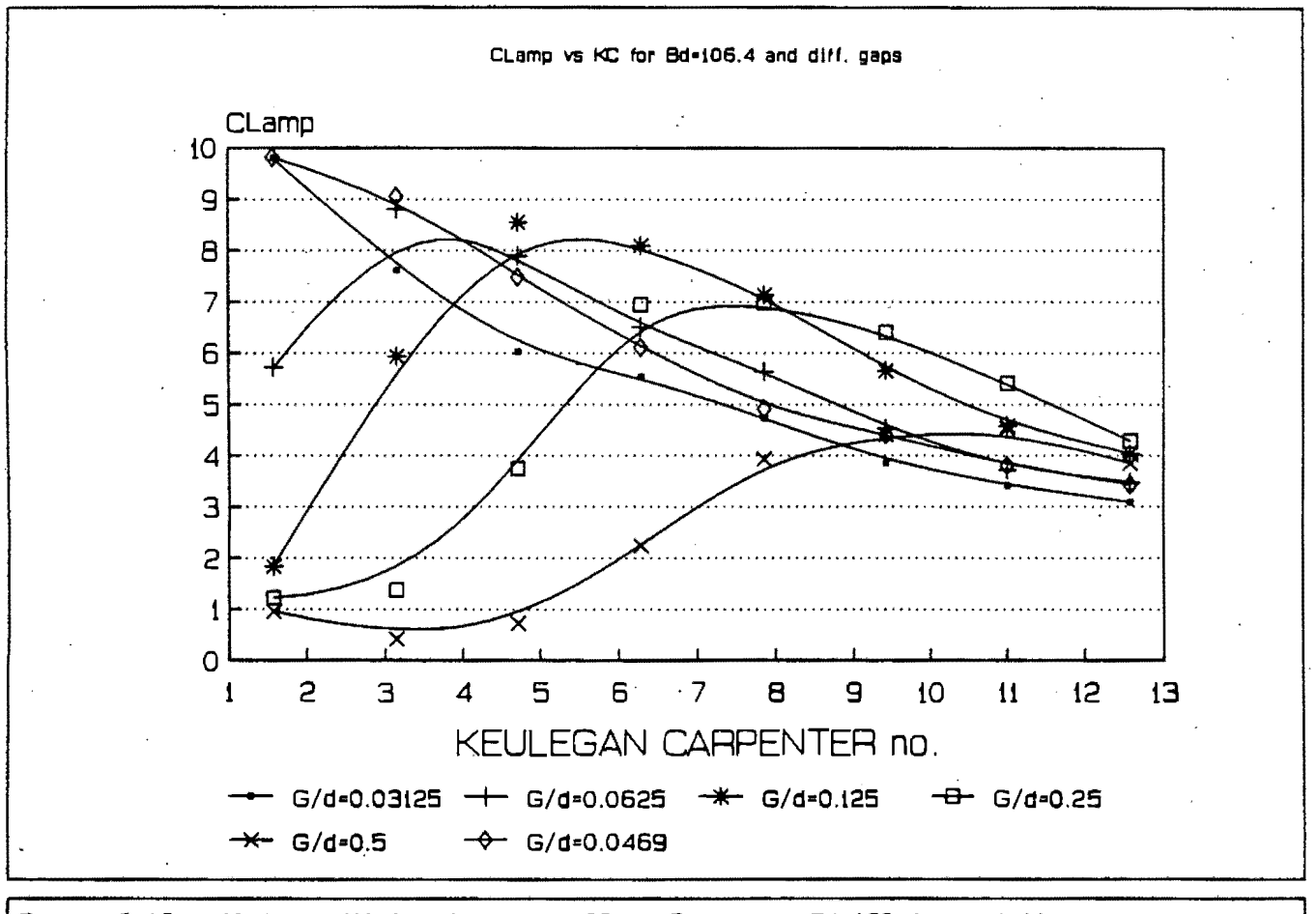

Figure I-10 : Clamp vs KC for diameter=120mm, T=4s, ave Bd=106.4 and different gap ratios.

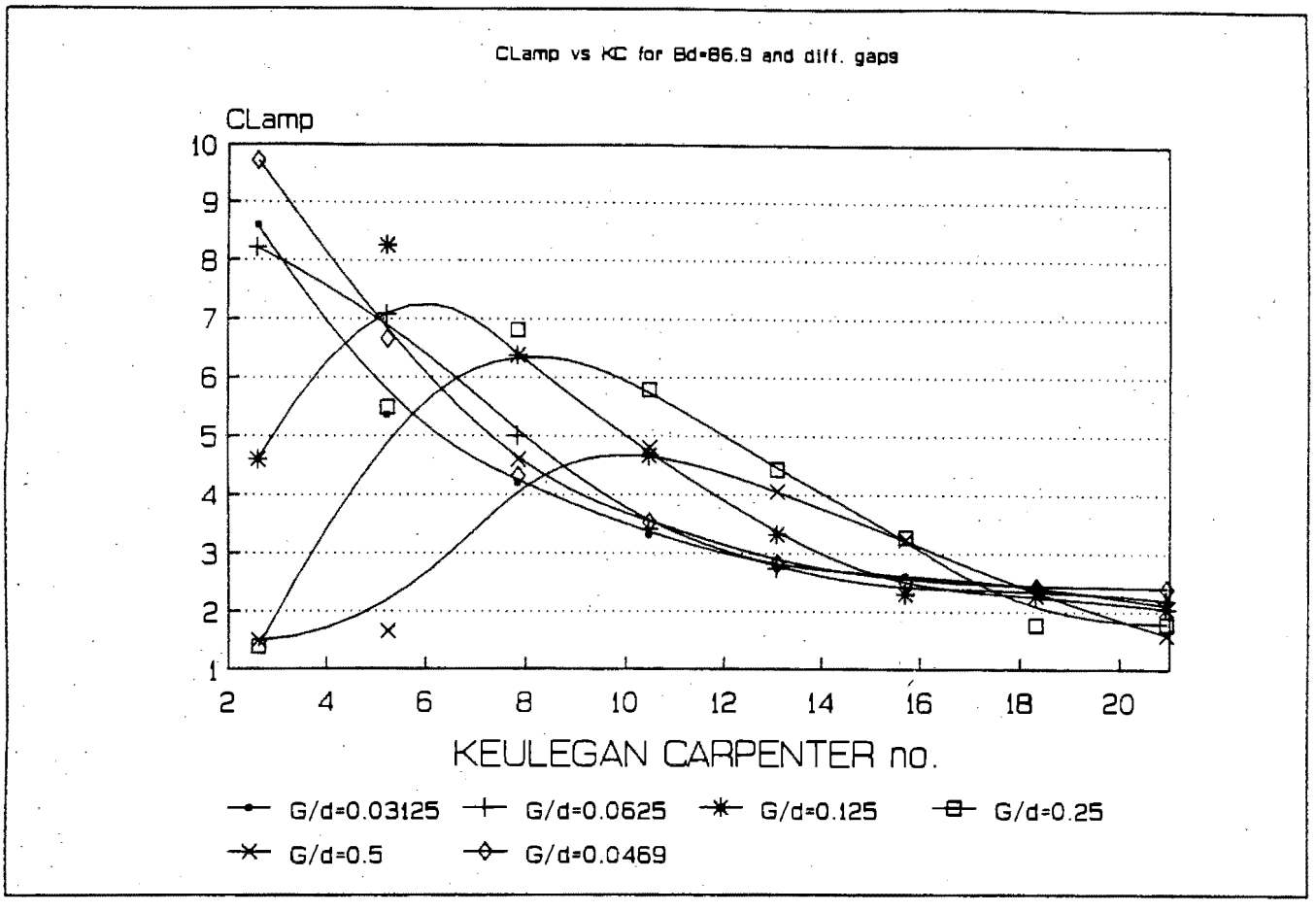

Figure I-11 : Clamp vs KC for diameter=120mm, T=6s, ave Bd=86.9 and different gap ratios.

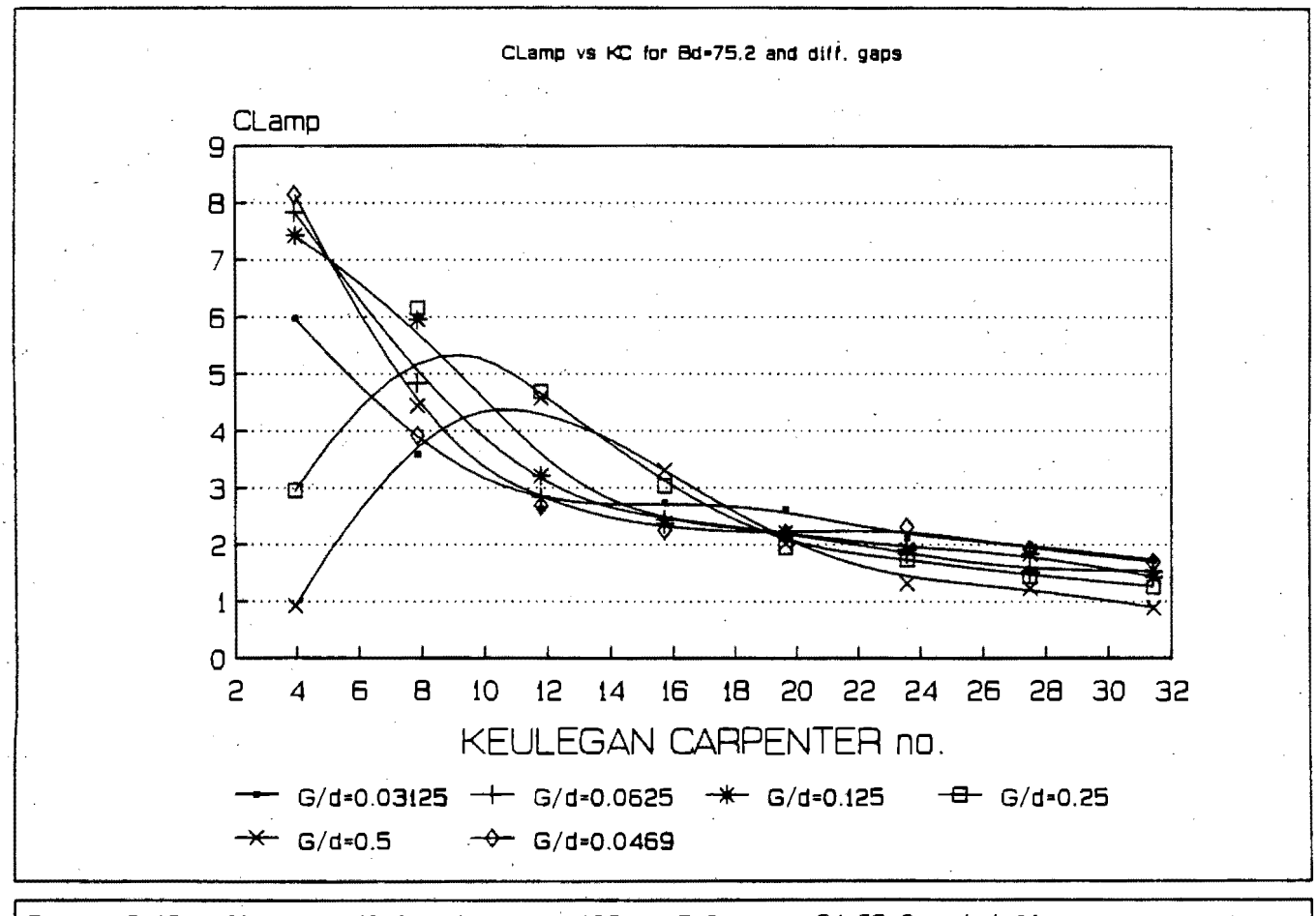

Figure I-12 : Clamp vs KC for diameter=120mm, T=8s, ave Bd=75.2 and different gap ratios.

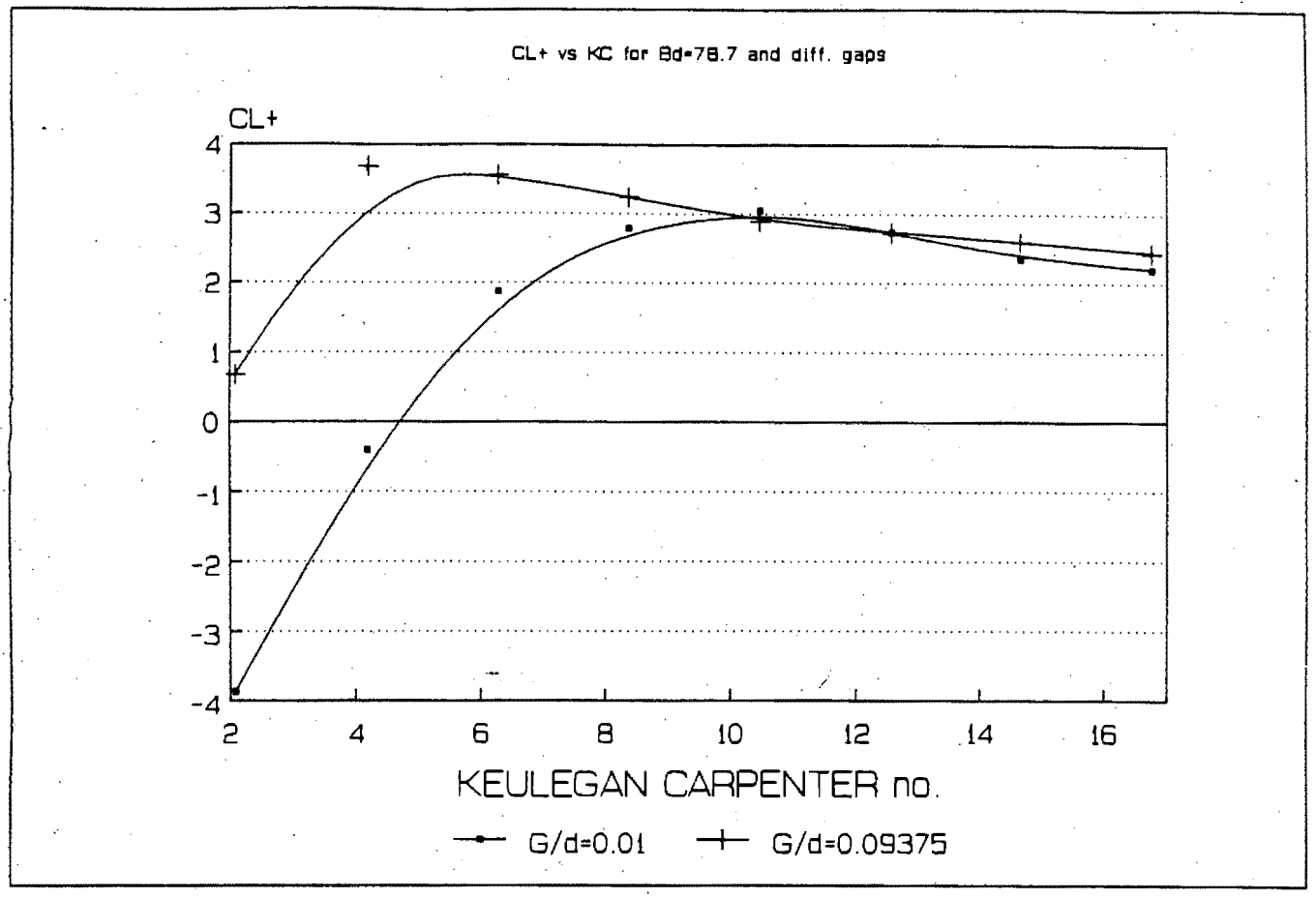

Figure I-13 : Cl+ vs KC for diameter=90mm, T=4s, ave Bd=78.7 and different gap ratios.

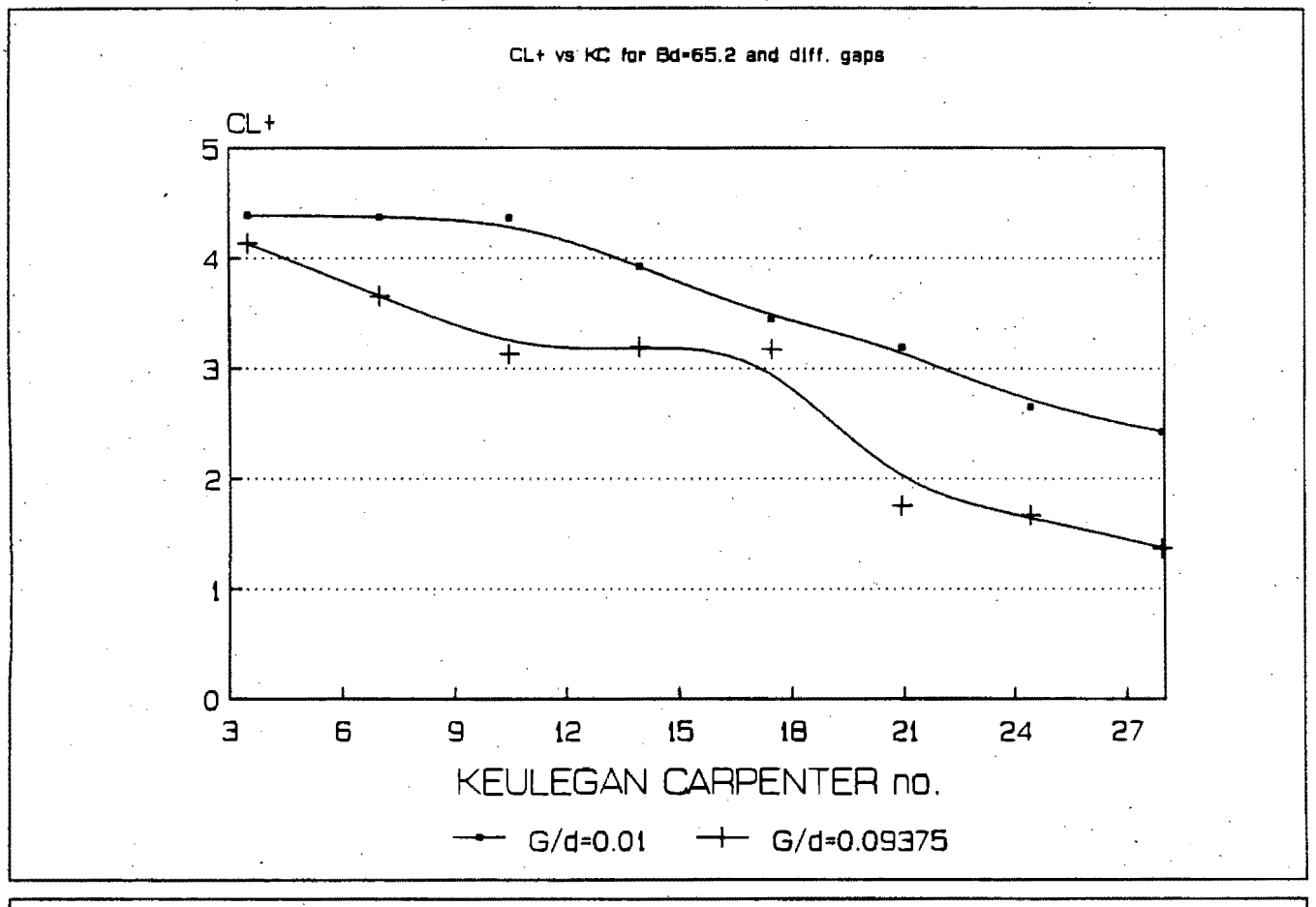

Figure I-14 : Cl+ vs KC for diameter=90mm, T=6s, ave Bd=65.2 and different gap ratios.

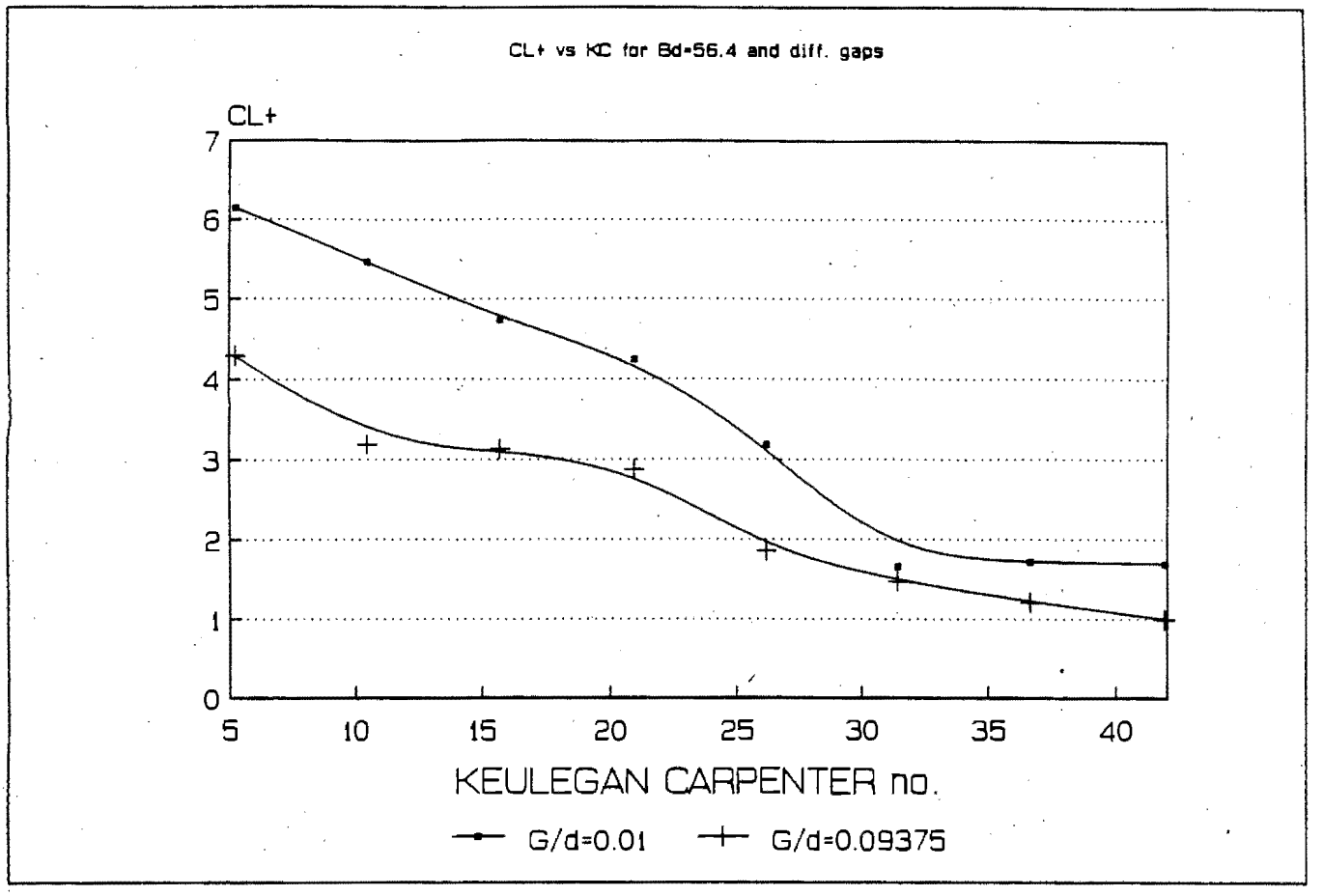

Figure I-15 : Cl+ vs KC for diameter=90mm, T=8s, ave Bd=56.4 and different gap ratios.

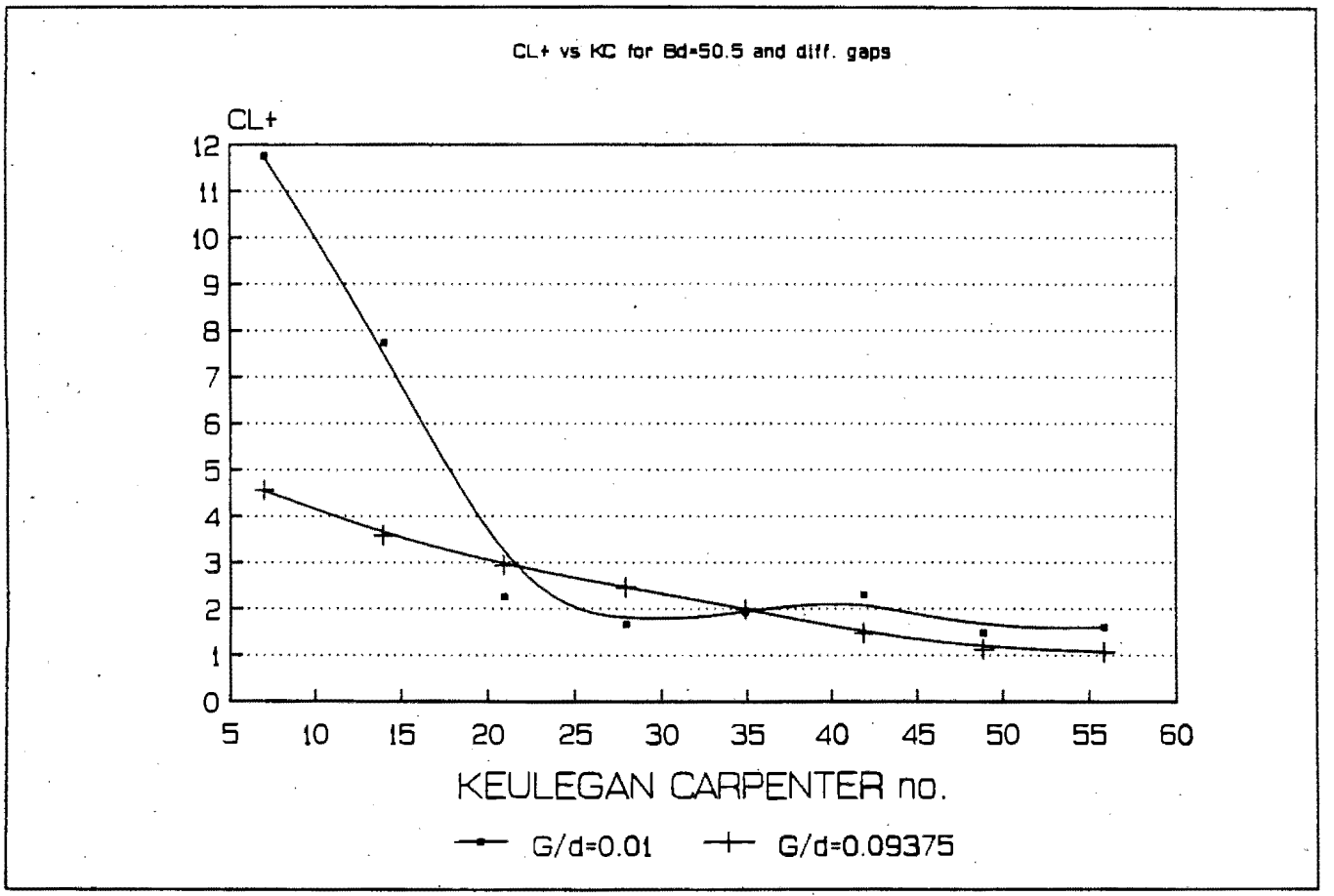

Figure I-16 : Cl+ vs KC for diameter=90mm, T=10s, ave Bd=50.5 and different gap ratios.

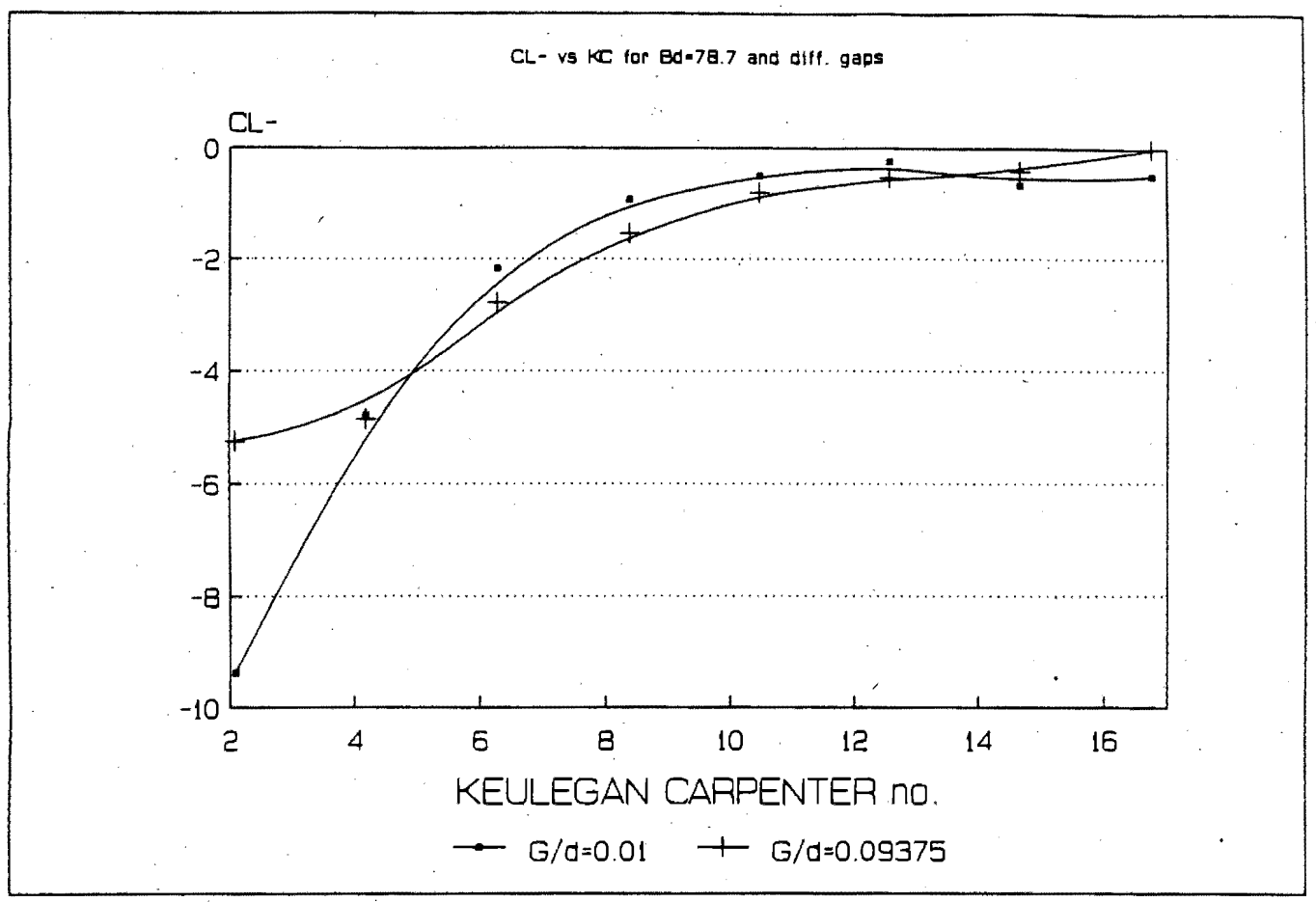

Figure I-17 : Cl- vs KC for diameter=90mm, T=4s, ave Bd=78.7 and different gap ratios.

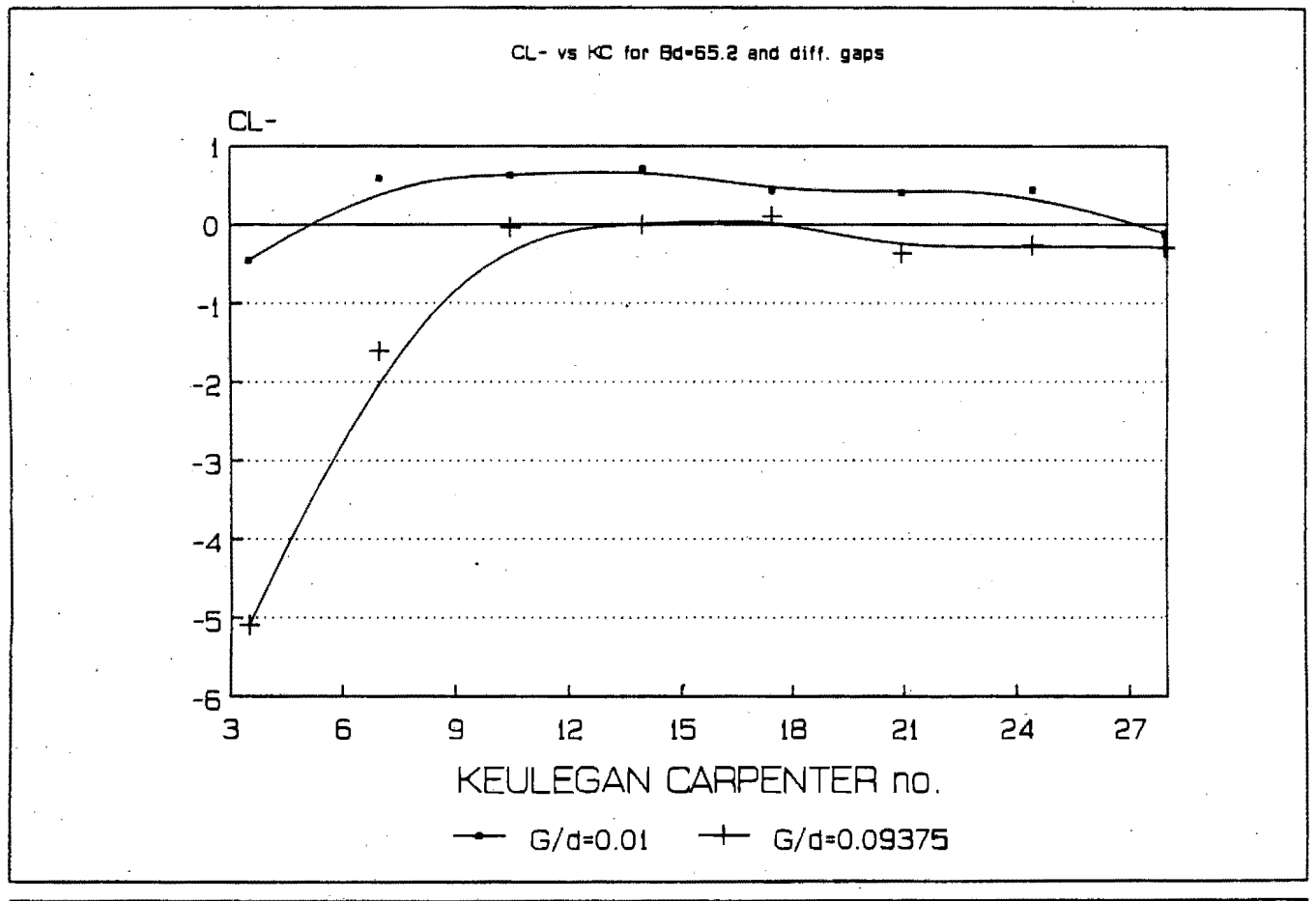

Figure I-18 : Cl- vs KC for diameter=90mm, T=6s, ave Bd=65.2 and different gap ratios.

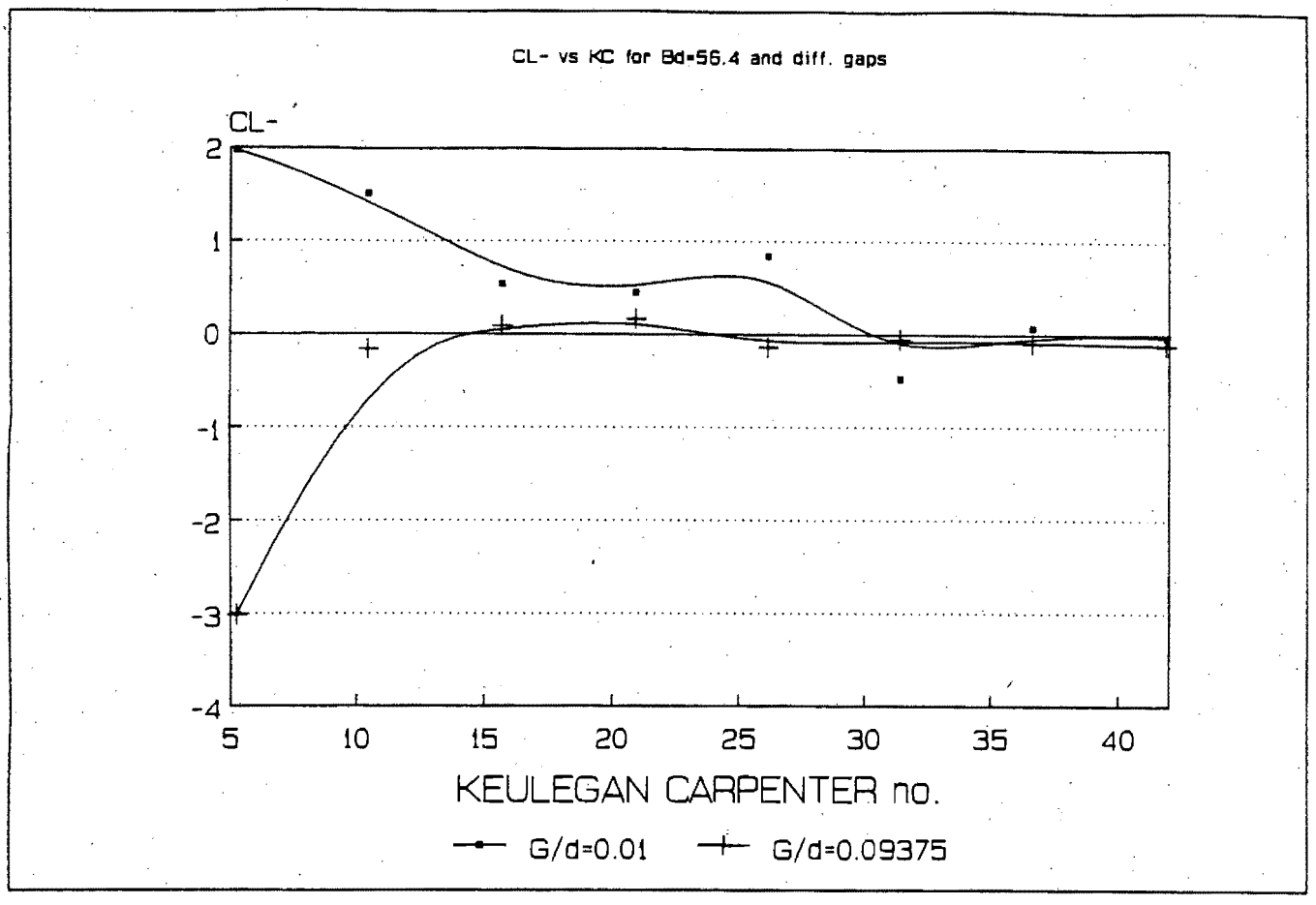

Figure I-19 : Cl- vs KC for diameter=90mm, T=8s, ave Bd=56.4 and different gap ratios.

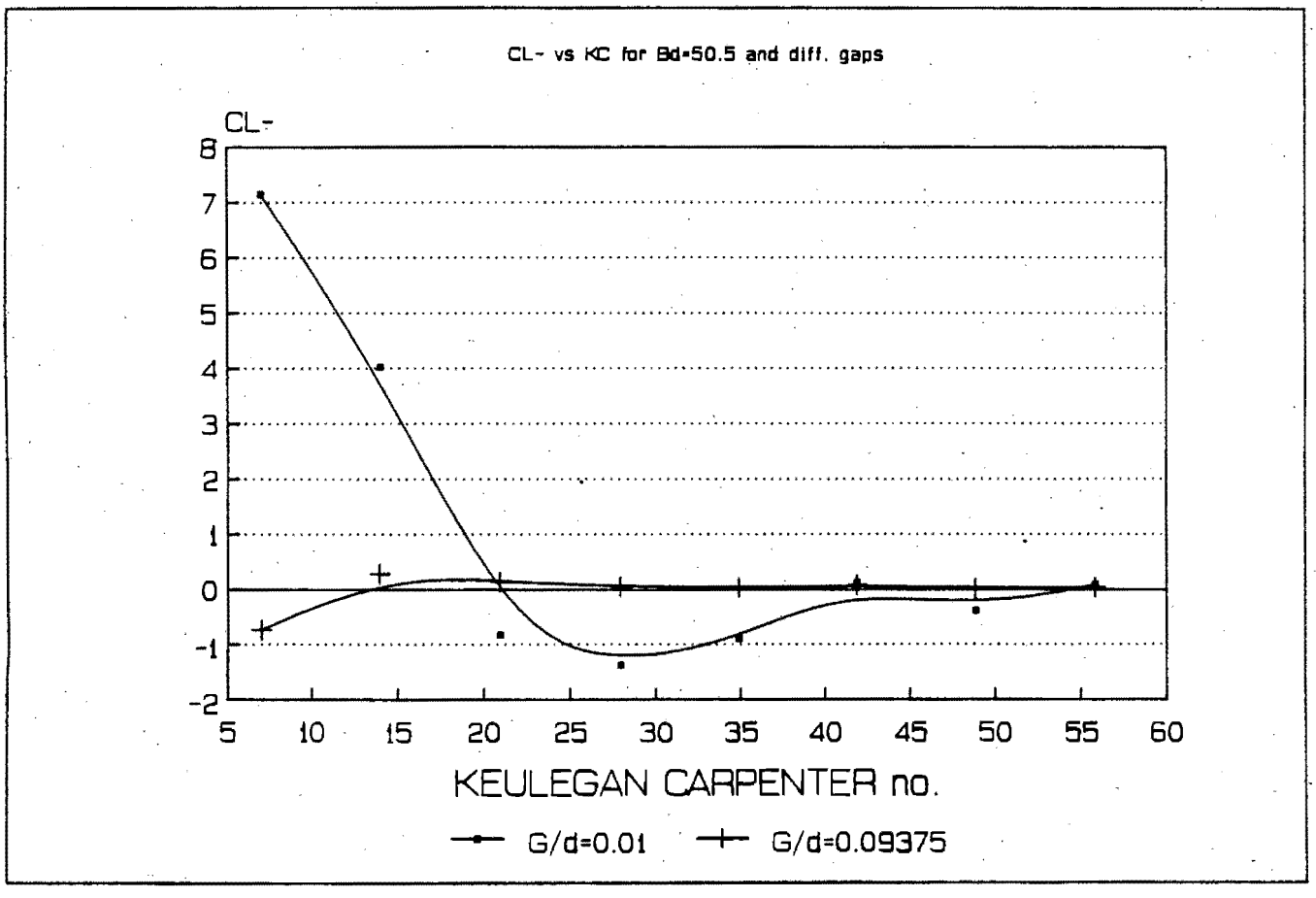

Figure I-20 : Cl- vs KC for diameter=90mm, T=10s, ave Bd=50.5 and different gap ratios.

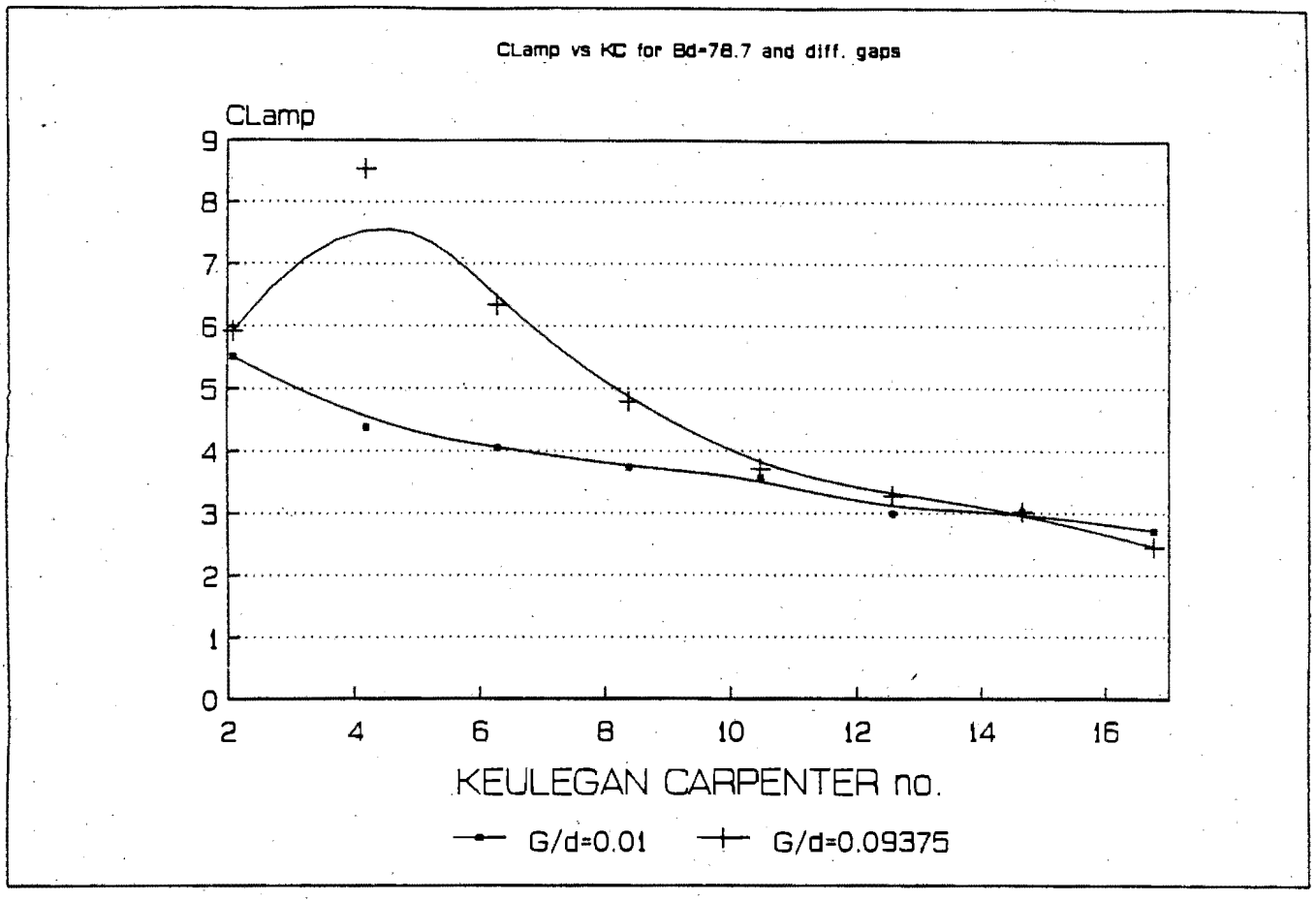

Figure I-21 : Clamp vs KC for diameter=90mm, T=4s, ave Bd=78.7 and different gap ratios.

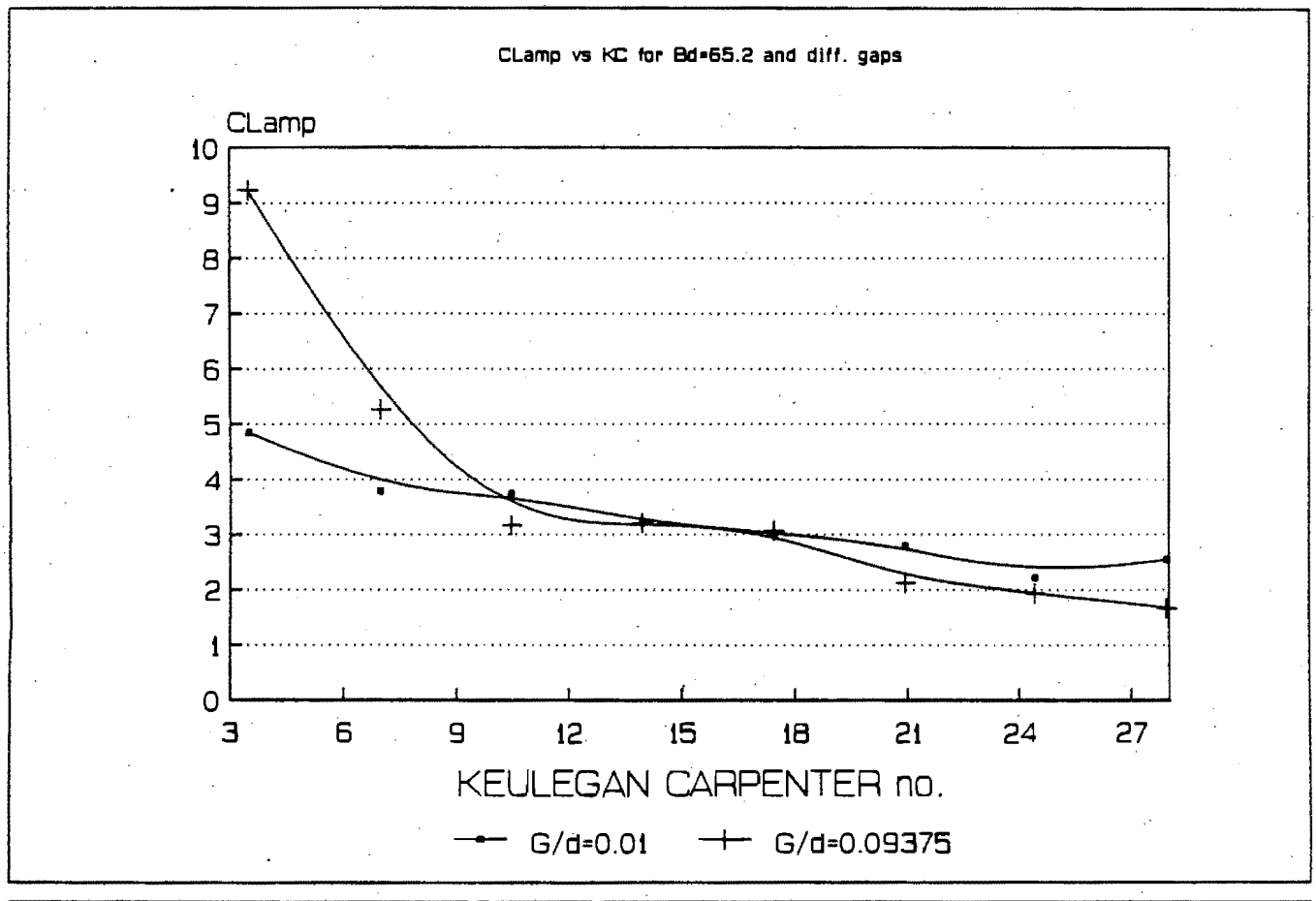

Figure I-22 : Clamp vs KC for diameter=90mm, T=6s, ave Bd=65.2 and different gap ratios.

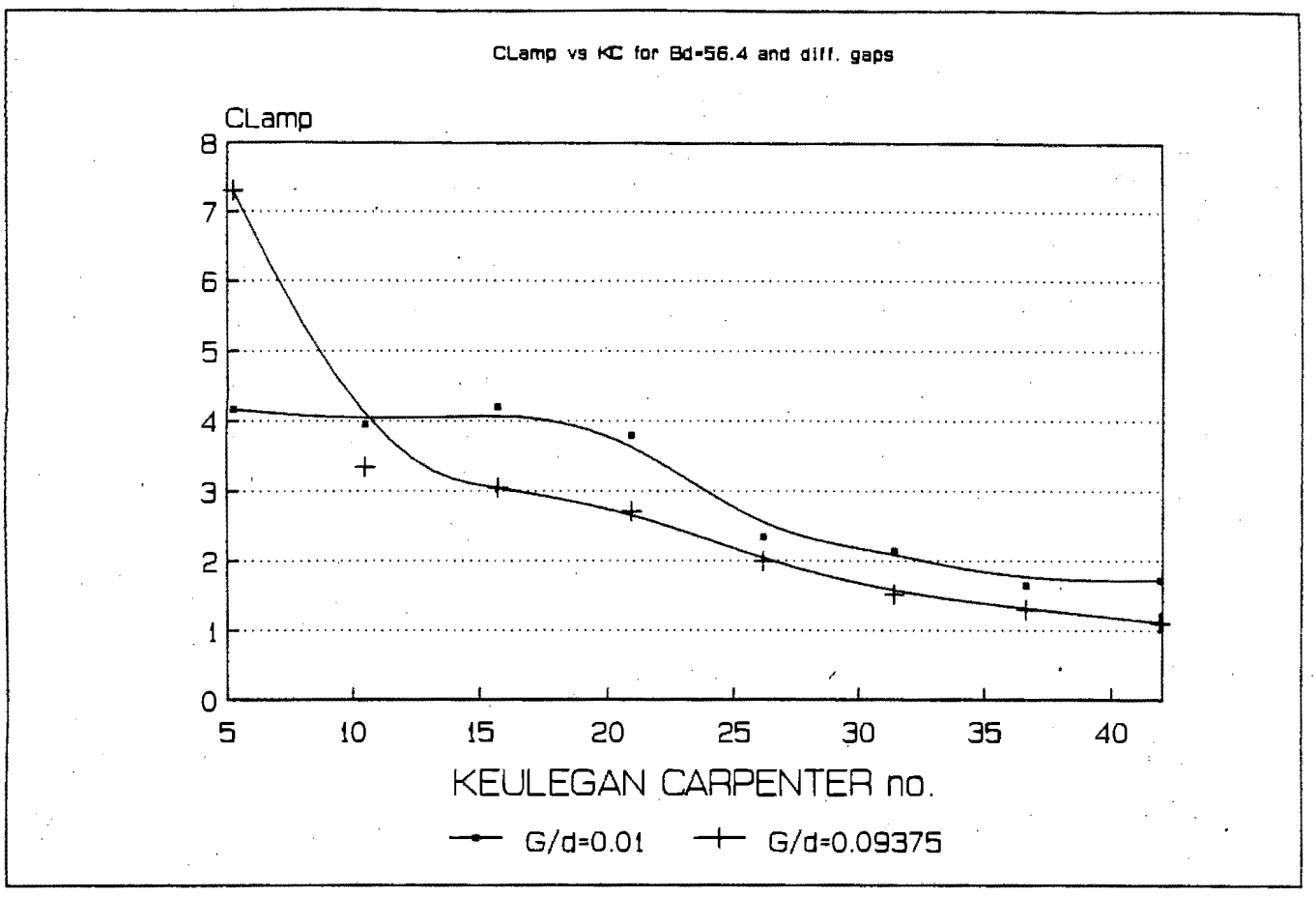

Figure I-23 : Clamp vs KC for diameter=90mm, T=8s, ave Bd=56.4 and different gap ratios.

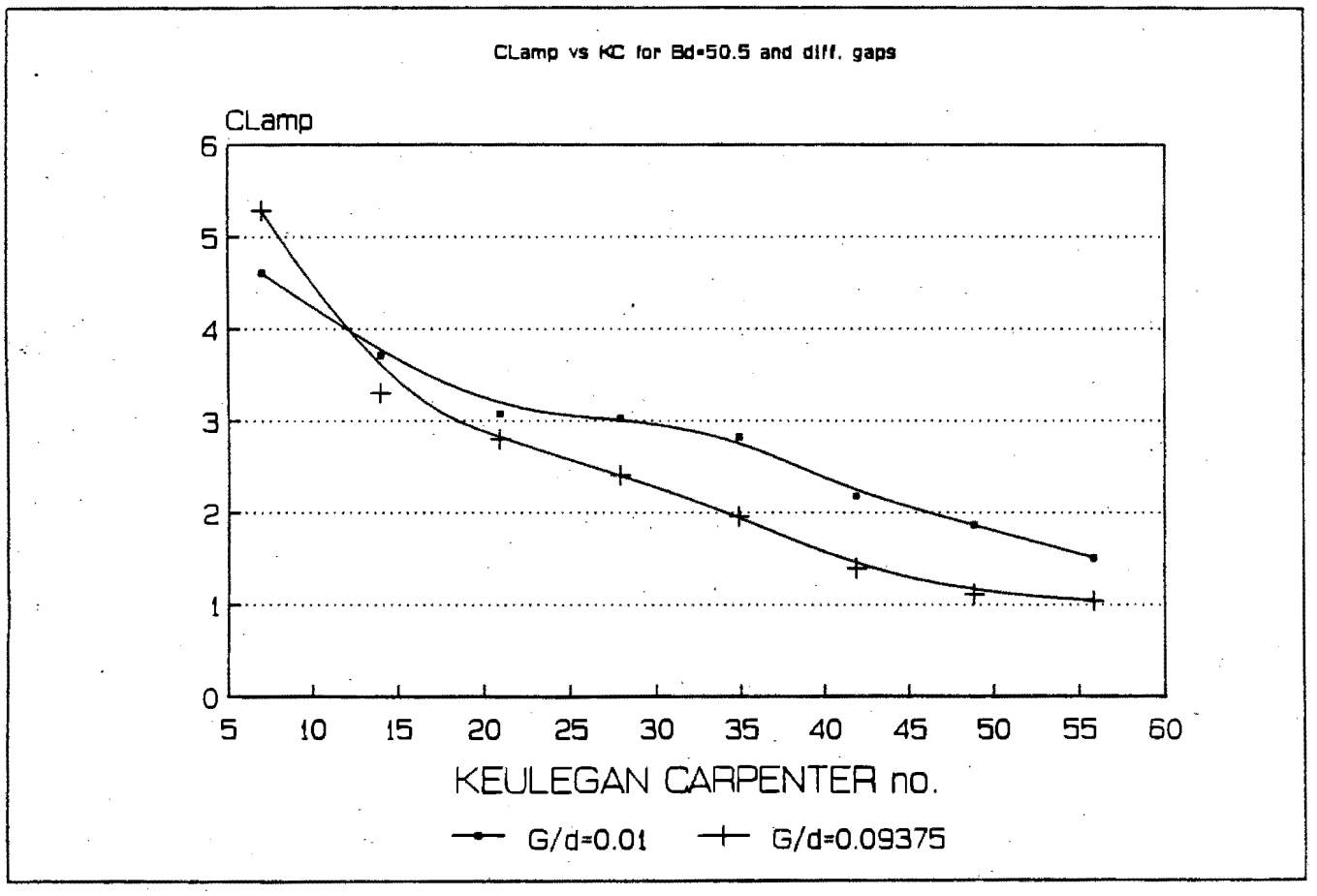

Figure I-24 : Clamp vs KC for diameter=90mm, T=10s, ave Bd=50.5 and different gap ratios.

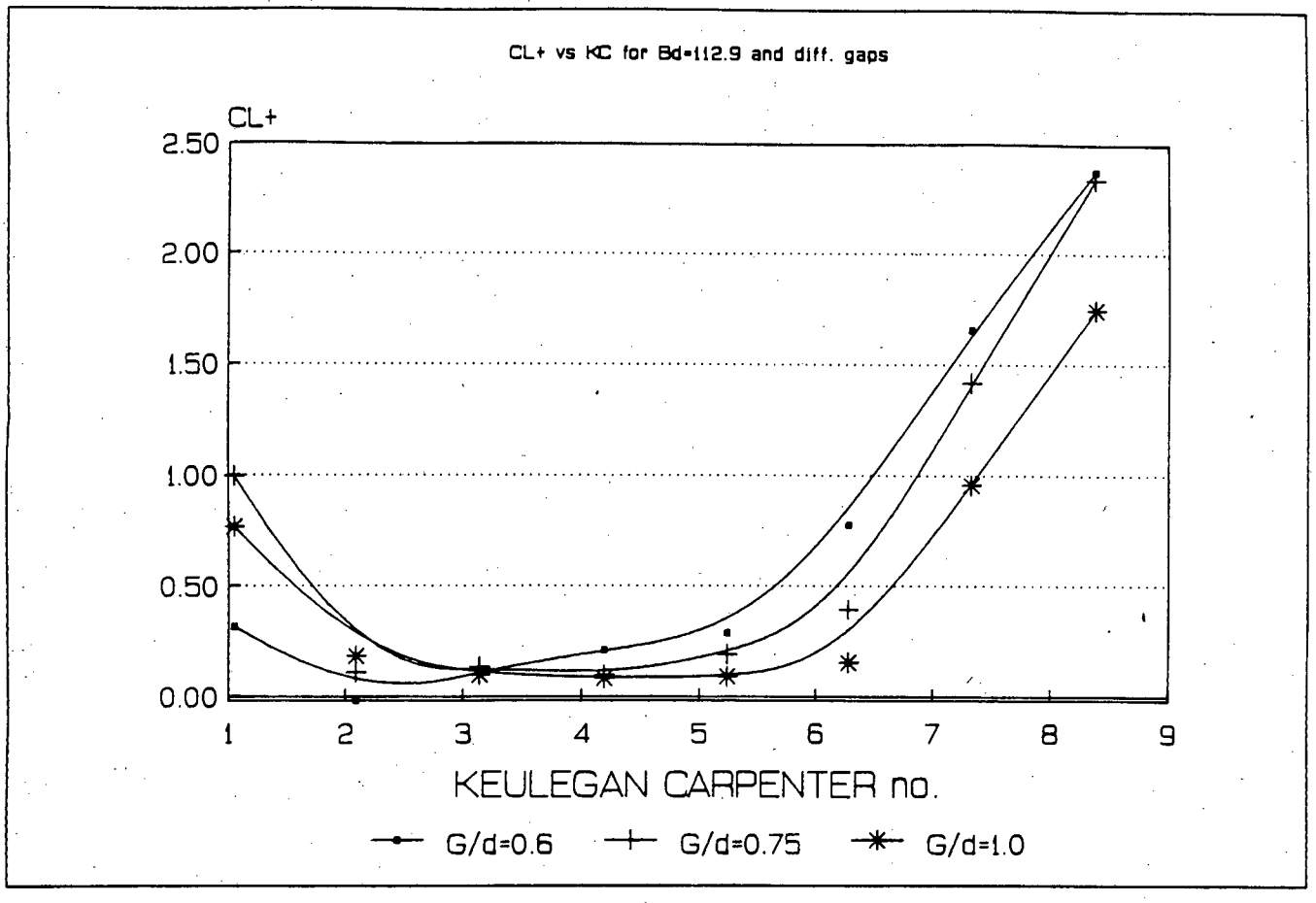

Figure I-25 : Cl+ vs KC for diameter=90mm, T=2s, ave Bd=112.9 and different gap ratios.

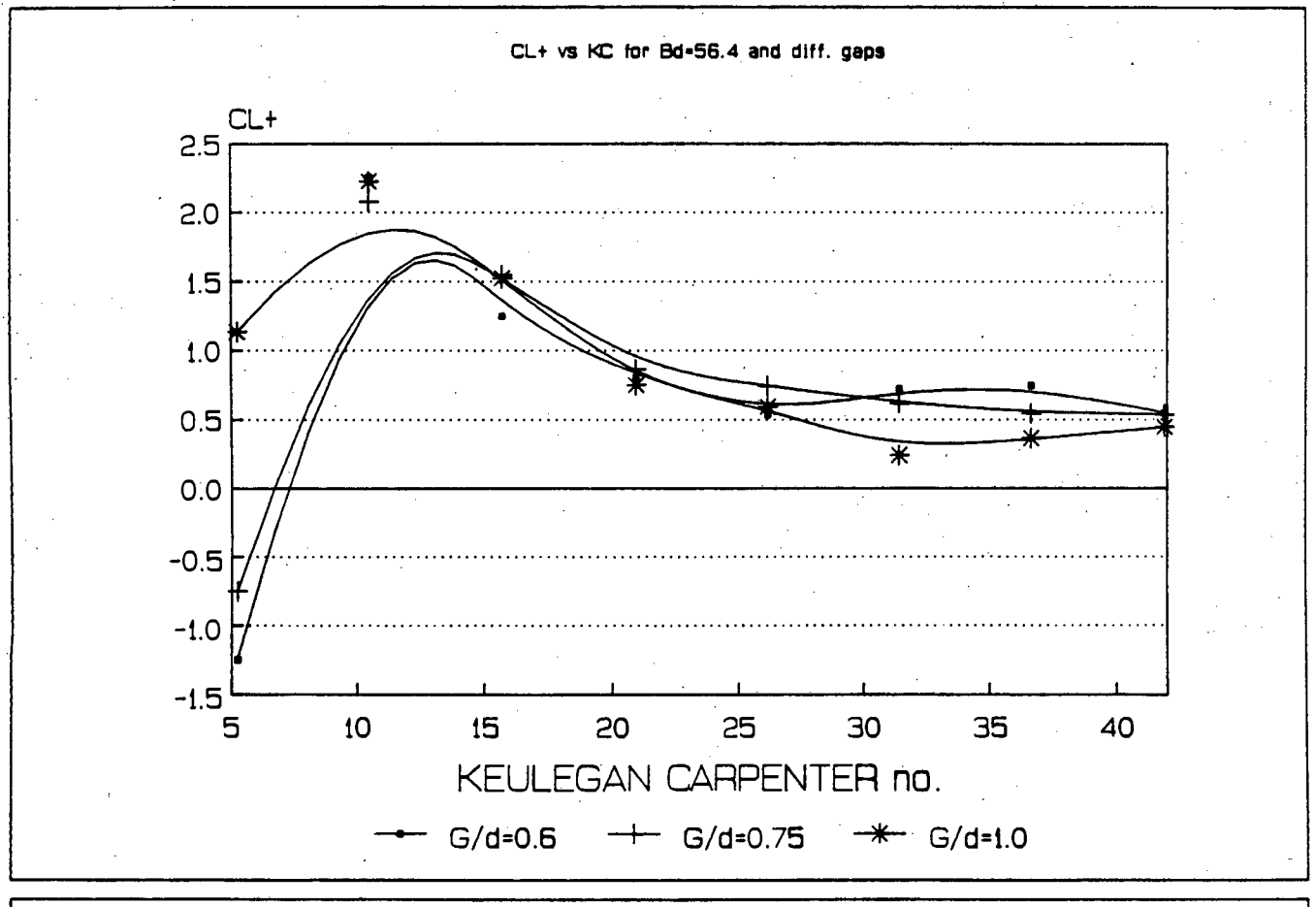

Figure I-26 : Cl+ vs KC for diameter=90mm, T=8s, ave Bd=56.4 and different gap ratios.

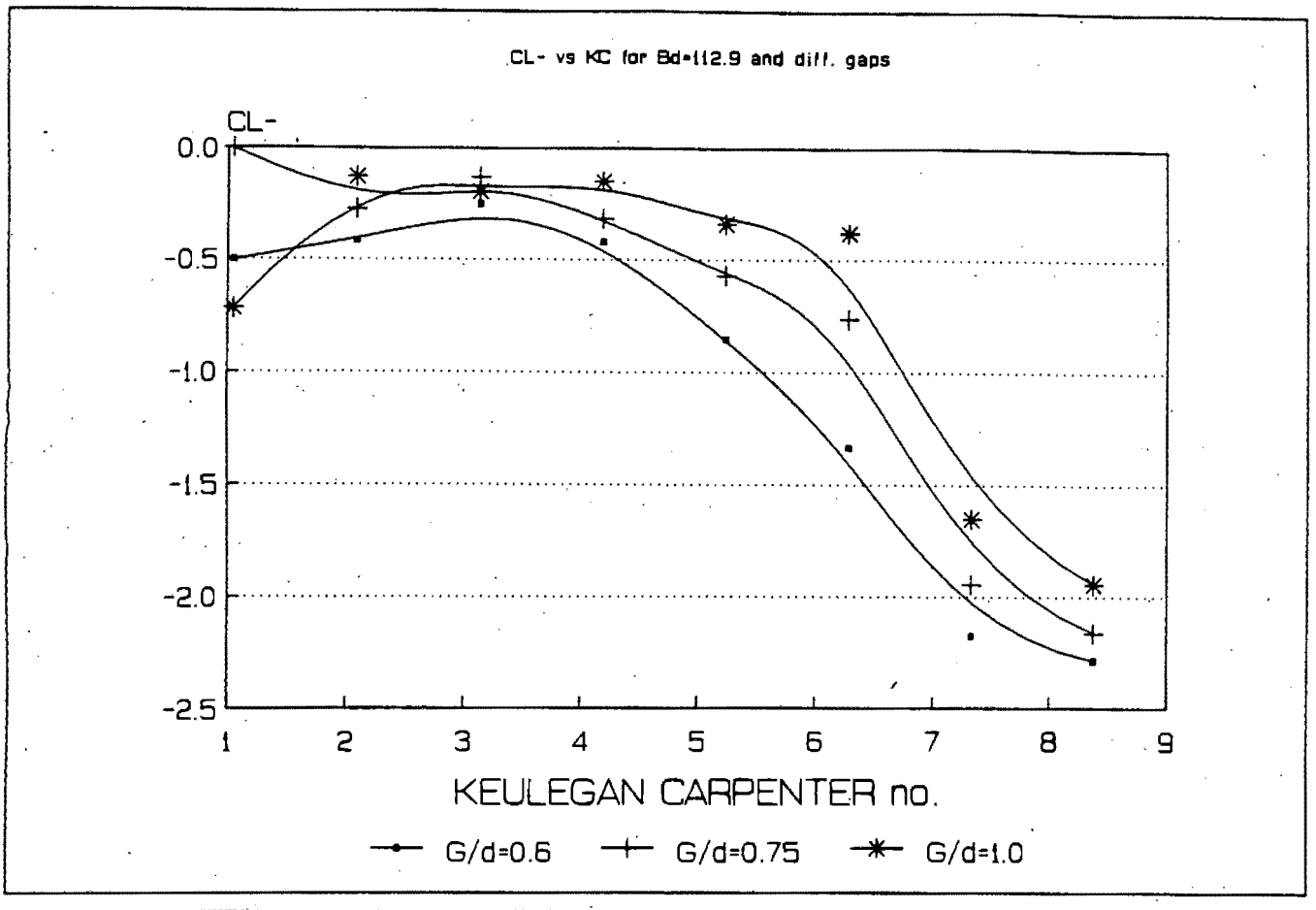

Figure I-27 : Cl- vs KC for diameter=90mm, T=2s, ave Bd=112.9 and different gap ratios.

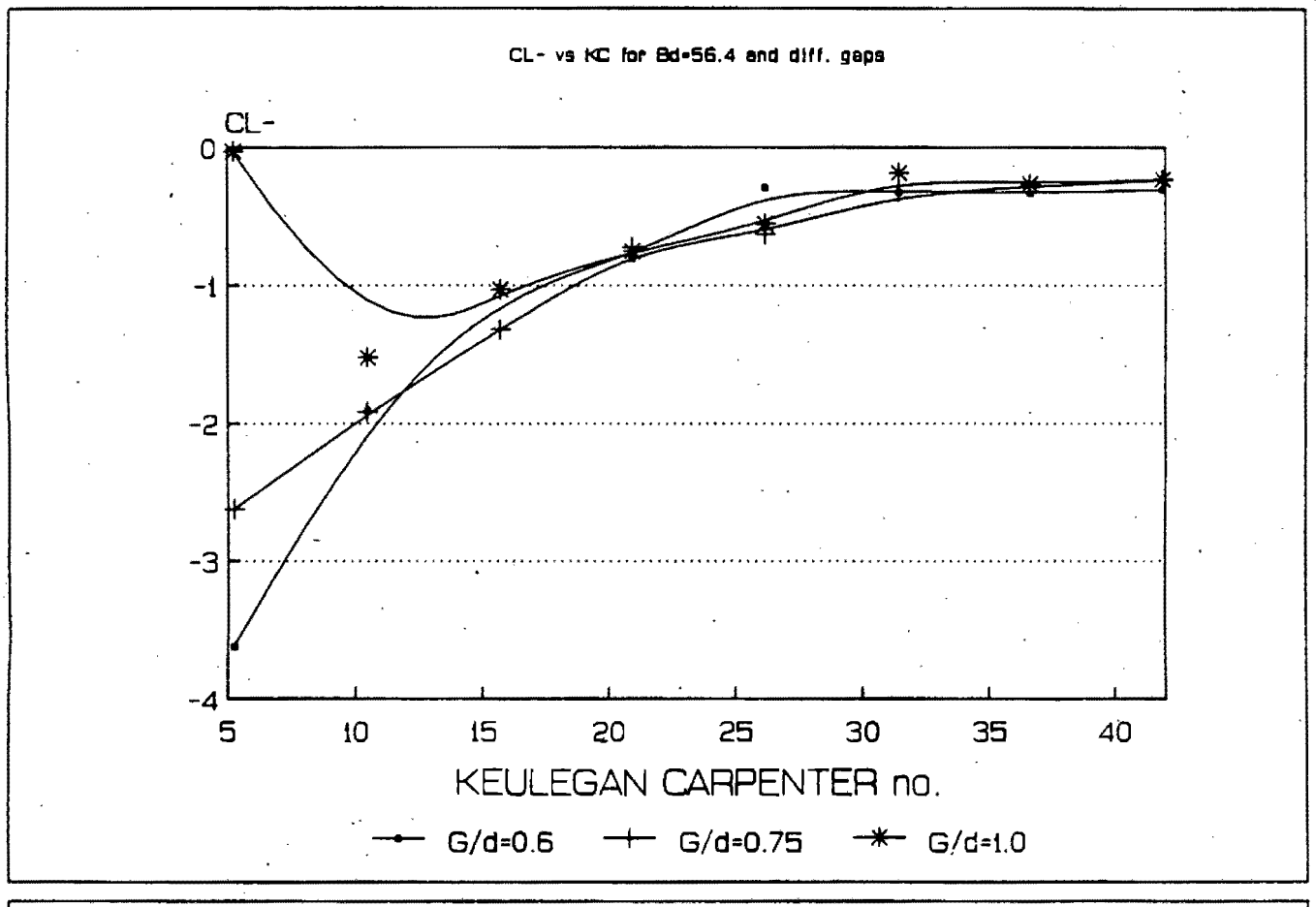

Figure I-28 : Cl- vs KC for diameter=90mm, T=8s, ave Bd=56.4 and different gap ratios.

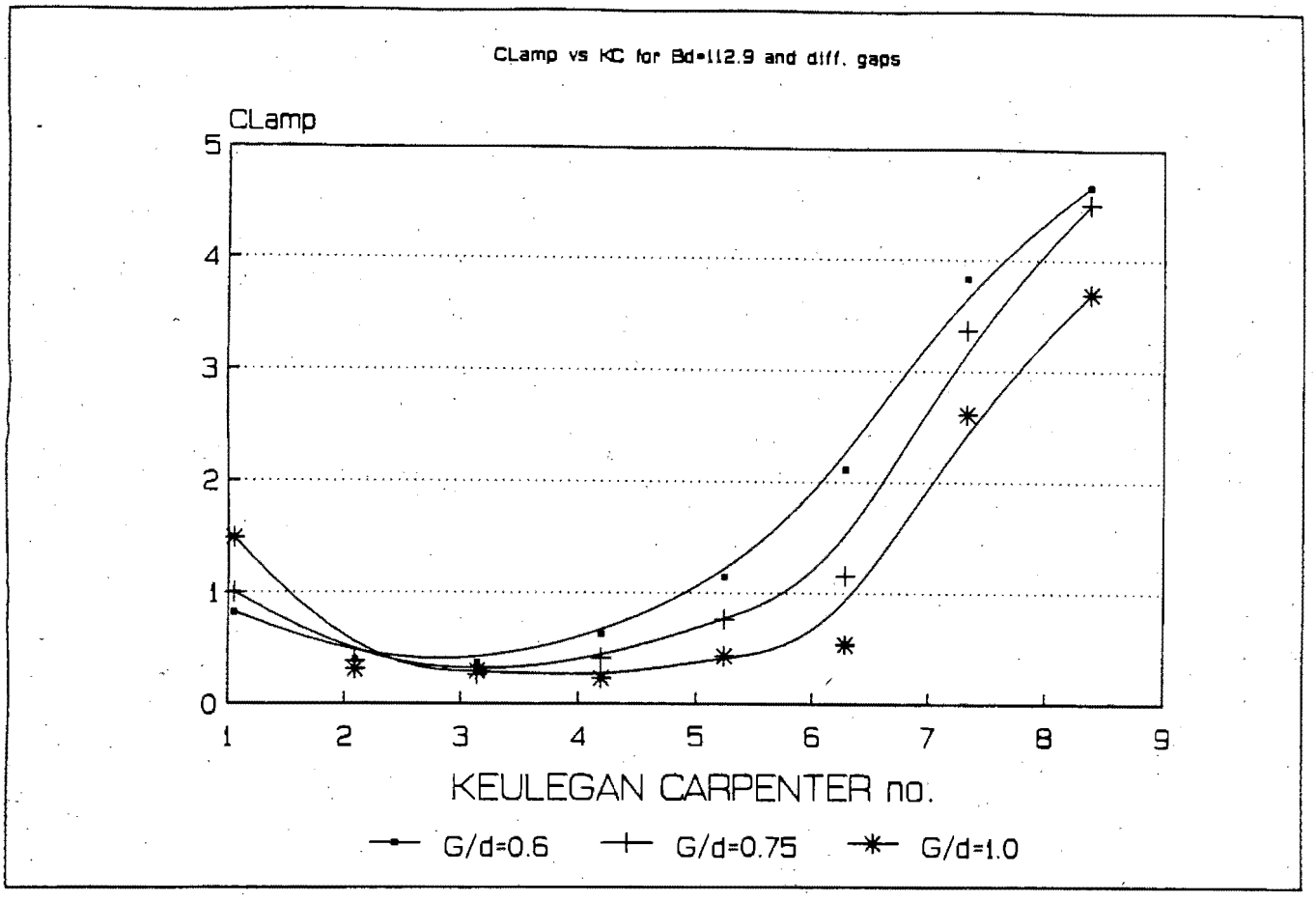

Figure I-29 : Clamp vs KC for diameter=90mm, T=2s, ave Bd=112.9 and different gap ratios.

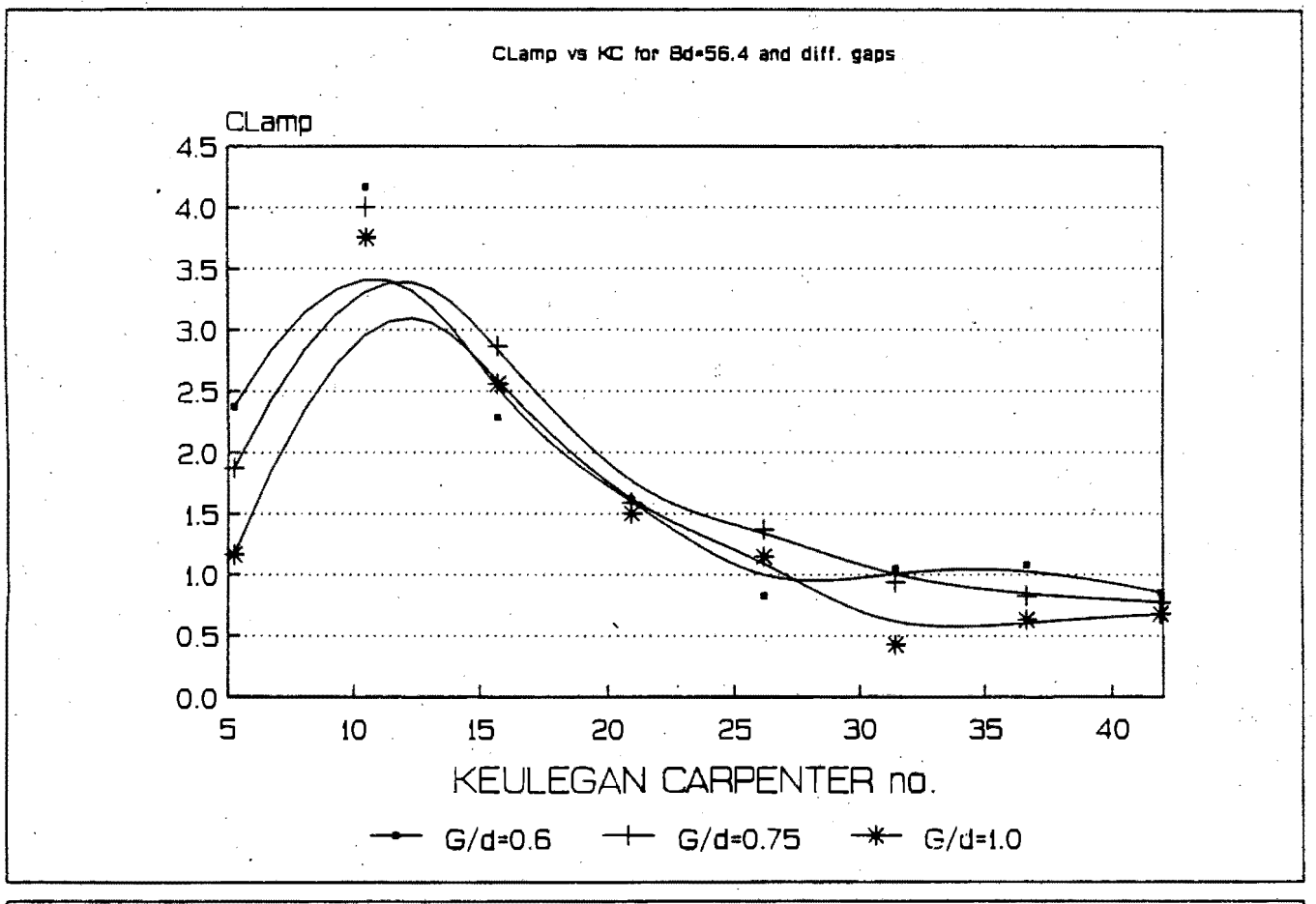

Figure I-30 : Clamp vs KC for diameter=90mm, T=8s, ave Bd=56.4 and different gap ratios.

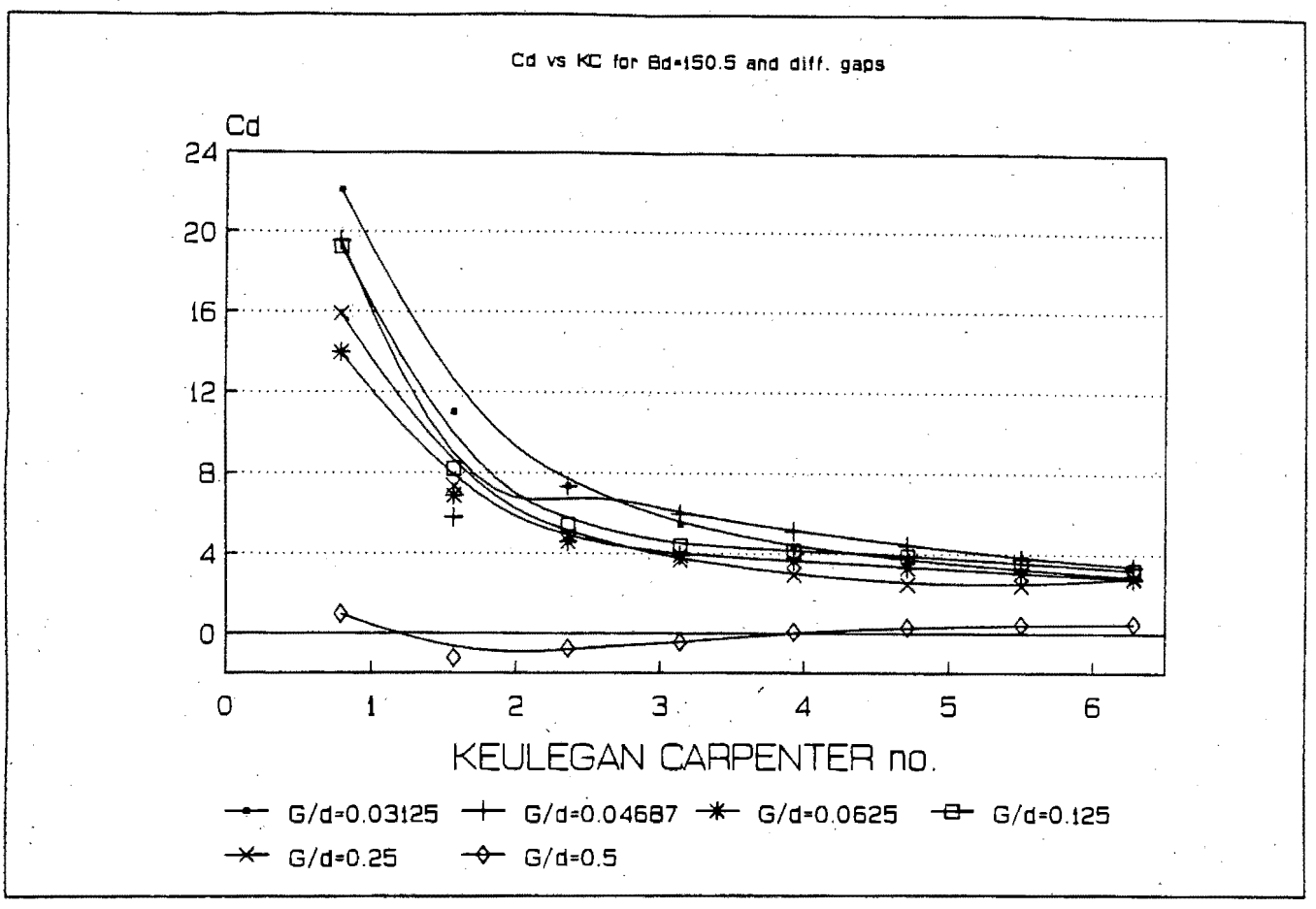

Figure I-31 : Cd vs KC for diameter=120mm, T=2s, ave Bd=150.5 and different gap ratios.

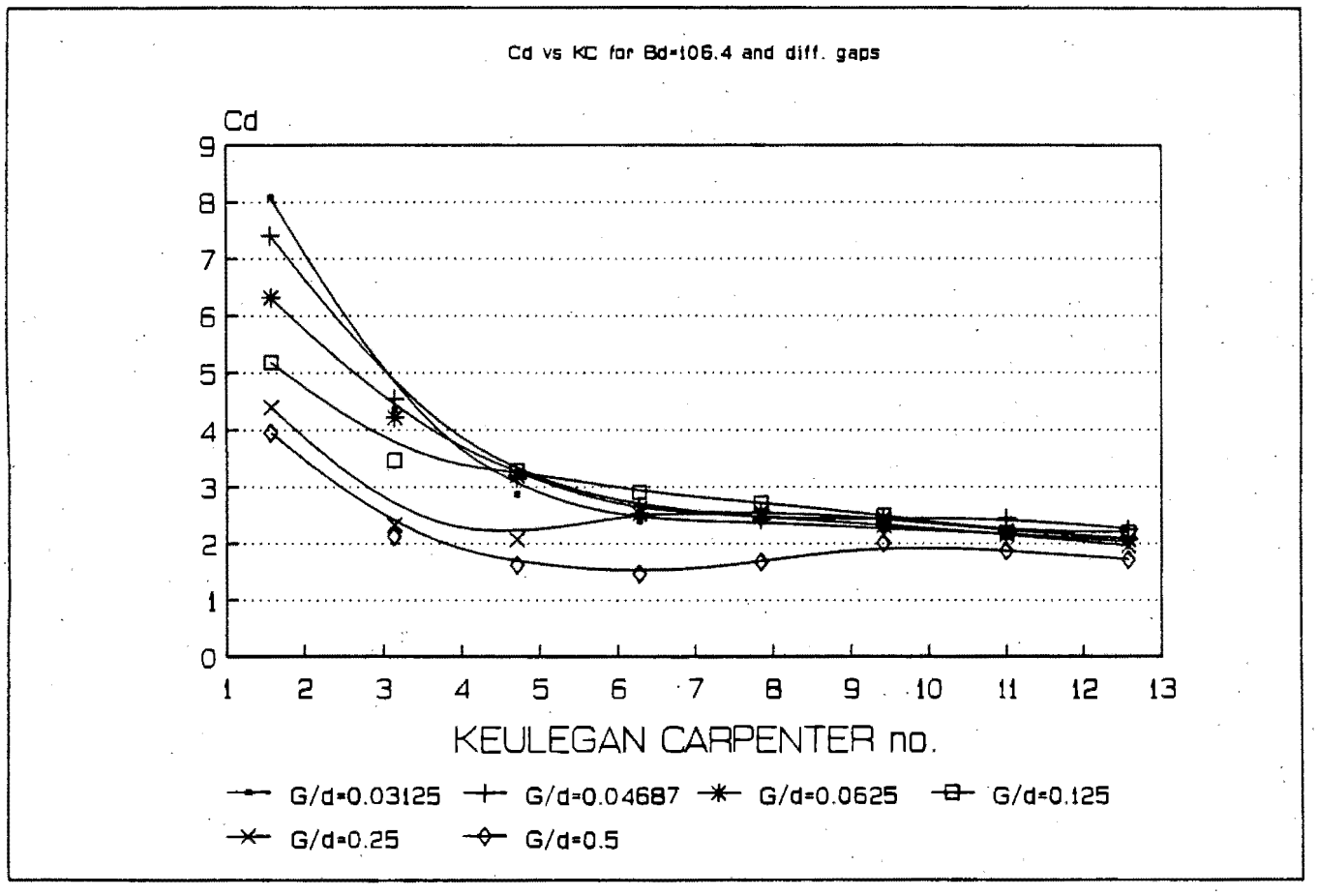

Figure I-32 : Cd vs KC for diameter=120mm, T=4s, ave Bd=106.4 and different gap ratios.

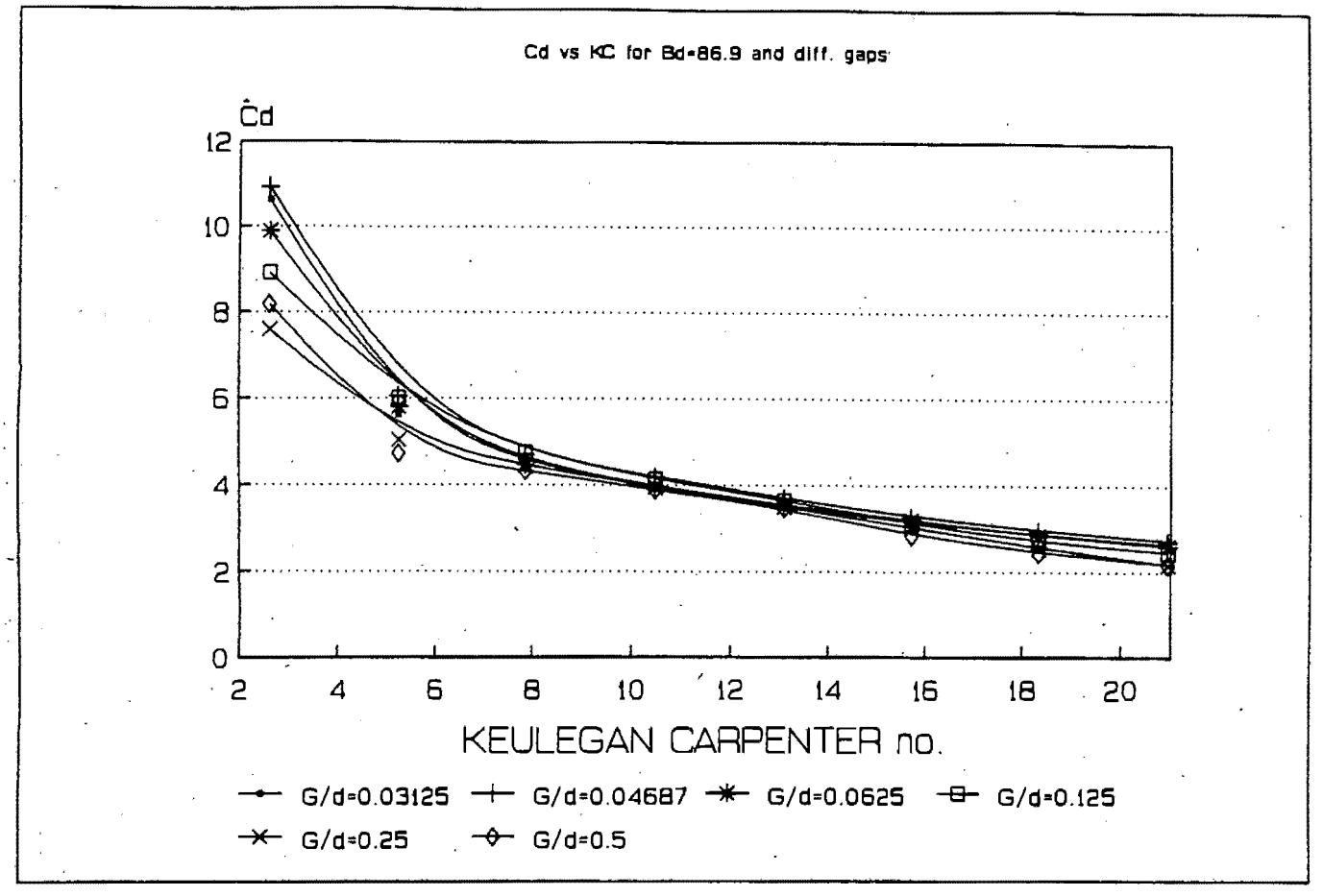

Figure I-33 : Cd vs KC for diameter=120mm, T=6s, ave Bd=86.9 and different gap ratios.

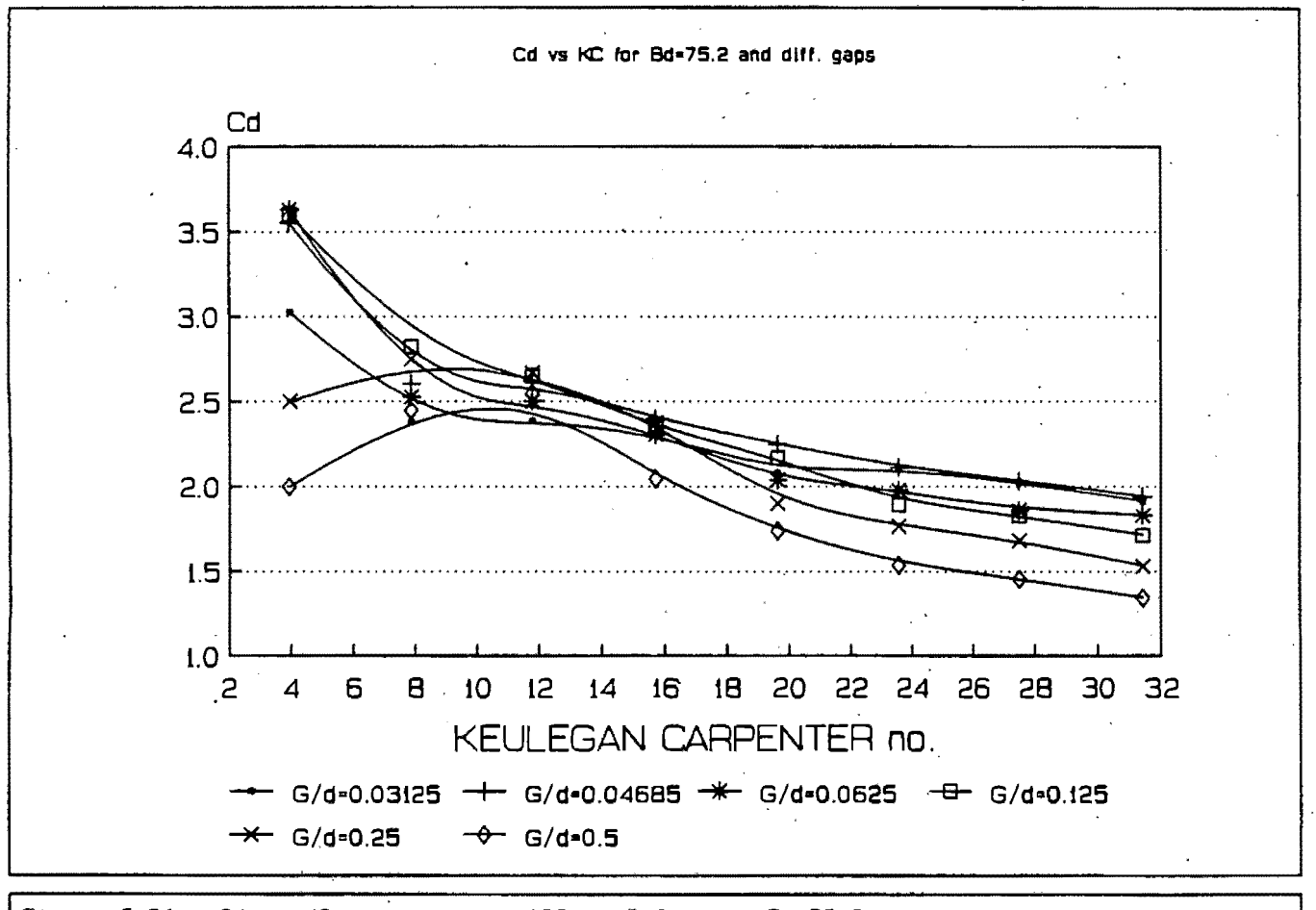

Figure I-34 : Cd vs KC for diameter=120mm, T=8s, ave Bd=75.2 and different gap ratios.

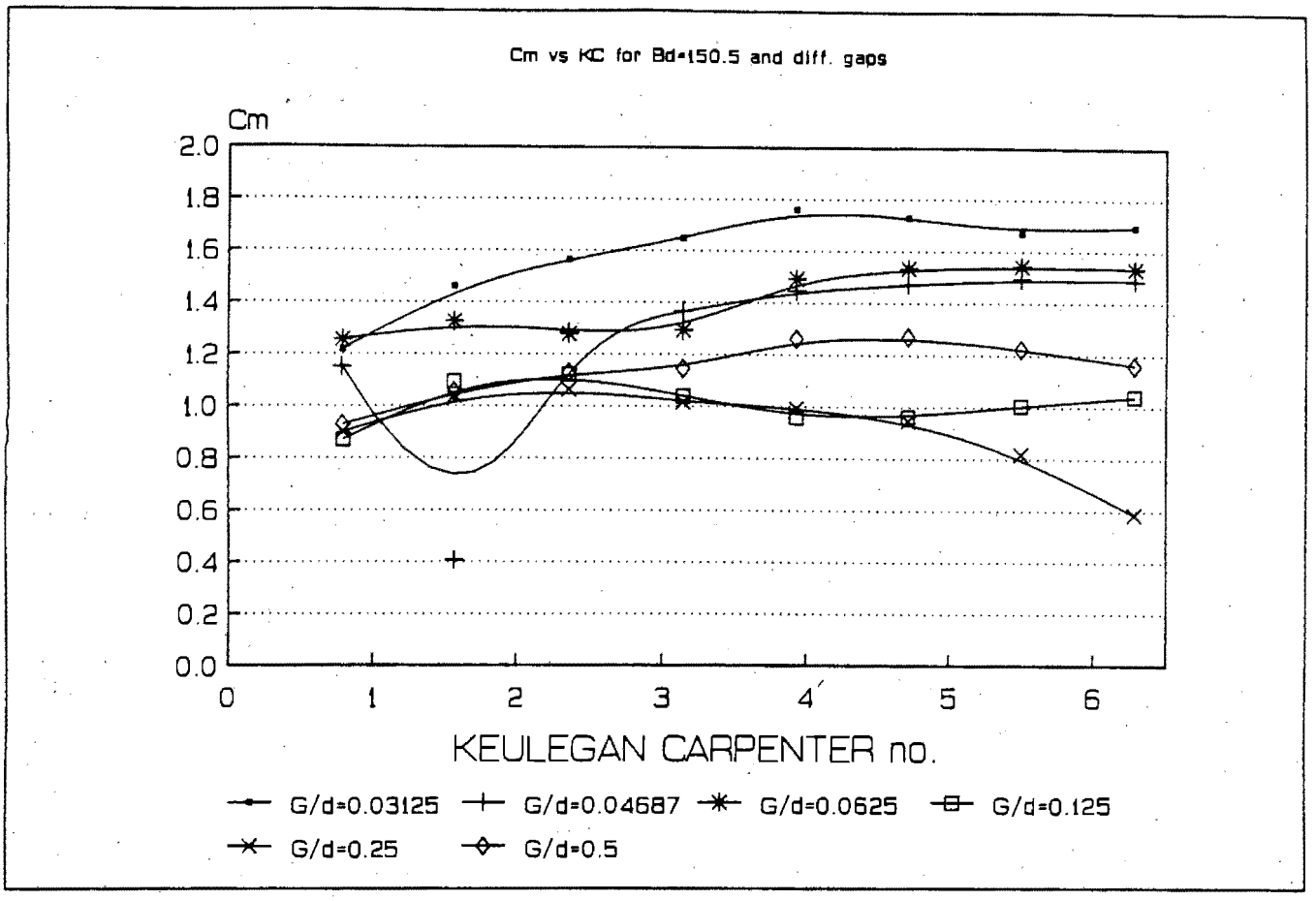

Figure I-35 : Cm vs KC for diameter=120mm, T=2s, ave Bd=150.5 and different gap ratios.

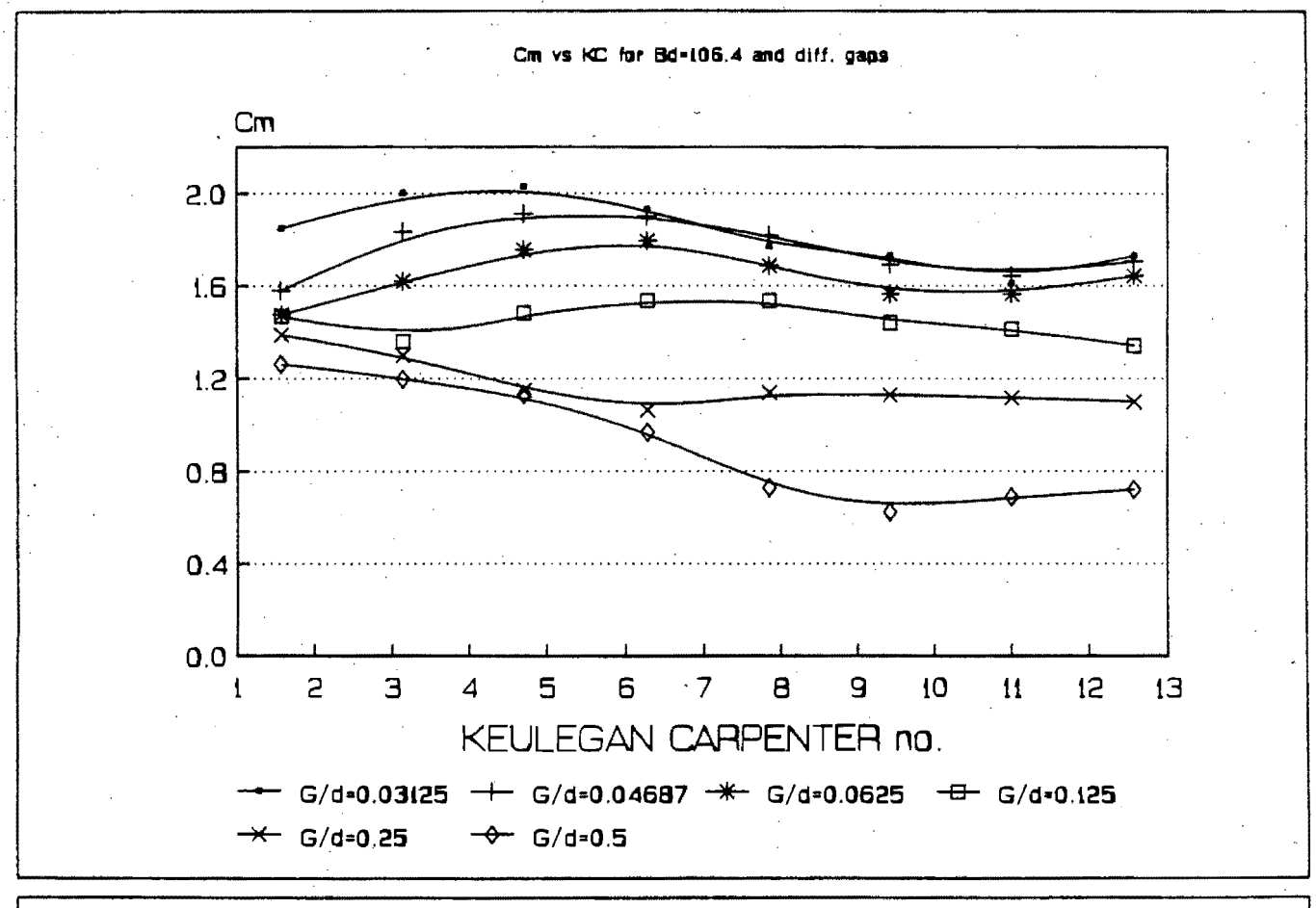

Figure I-36 : Cm vs KC for diameter=120mm, T=4s, ave Bd=106.4 and different gap ratios.

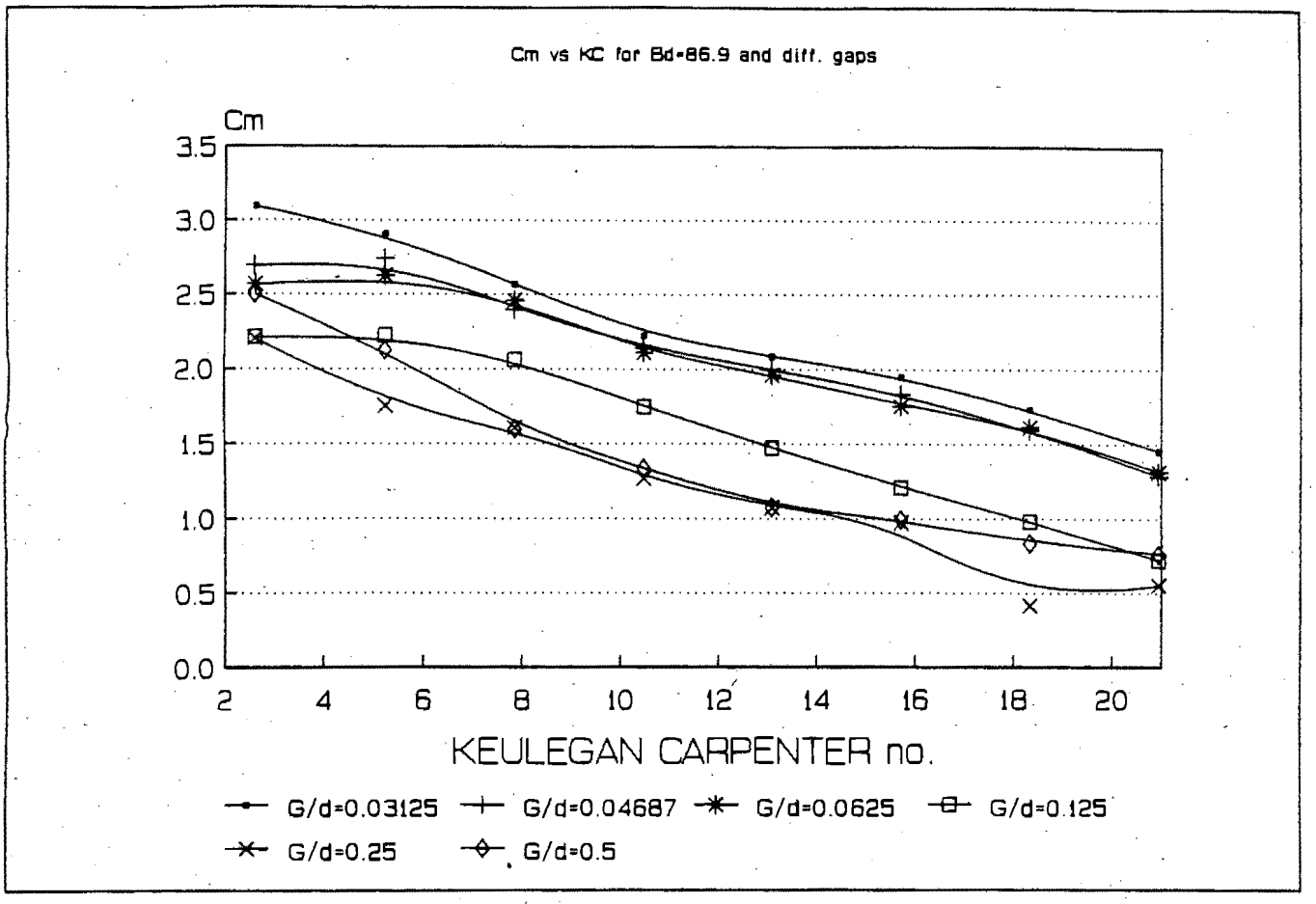

Figure I-37 : Cm vs KC for diameter=120mm, T=6s, ave Bd=86.9 and different gap ratios.

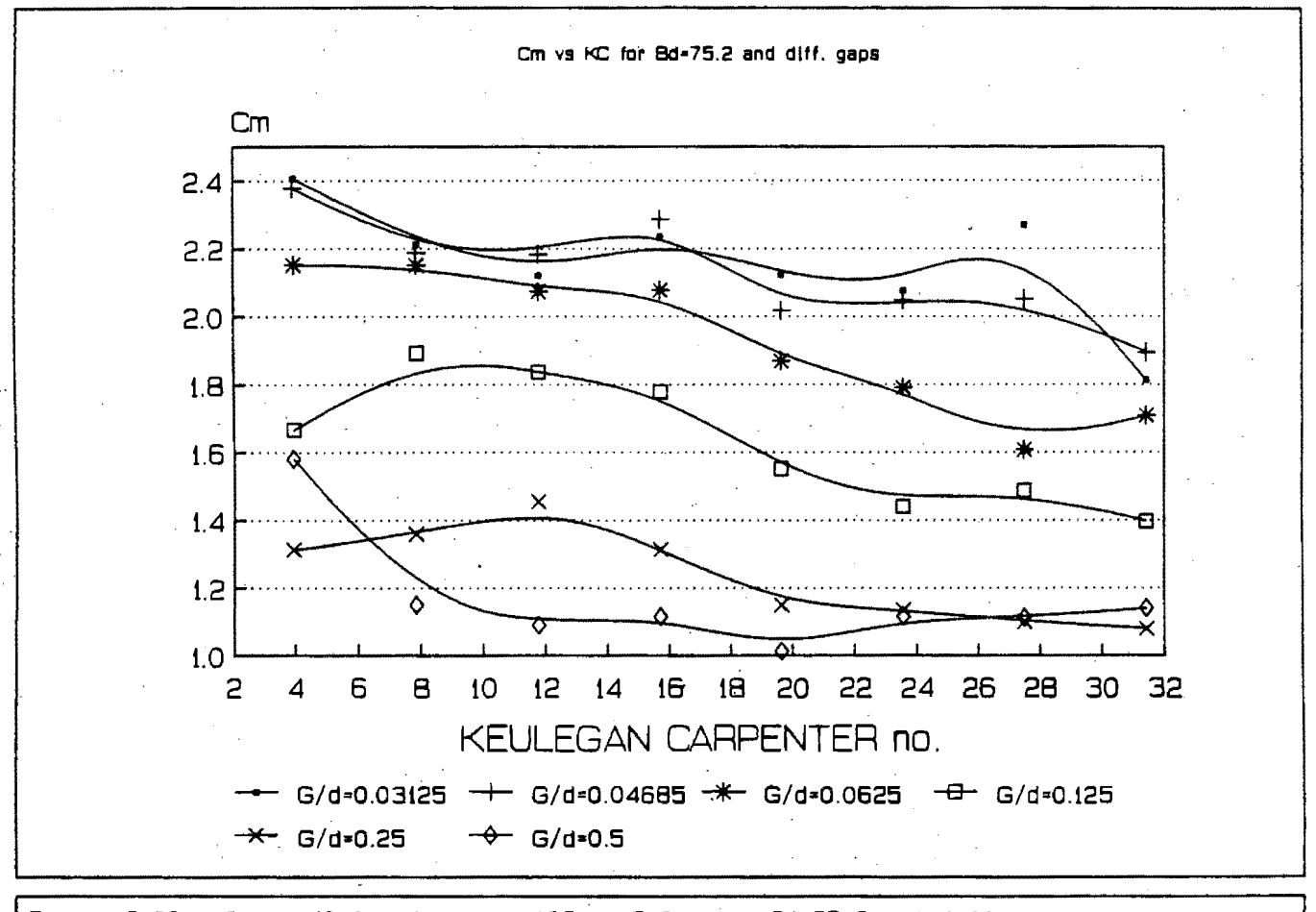

Figure I-38 : Cm vs KC for diameter=120mm, T=8s, ave Bd=75.2 and different gap ratios.

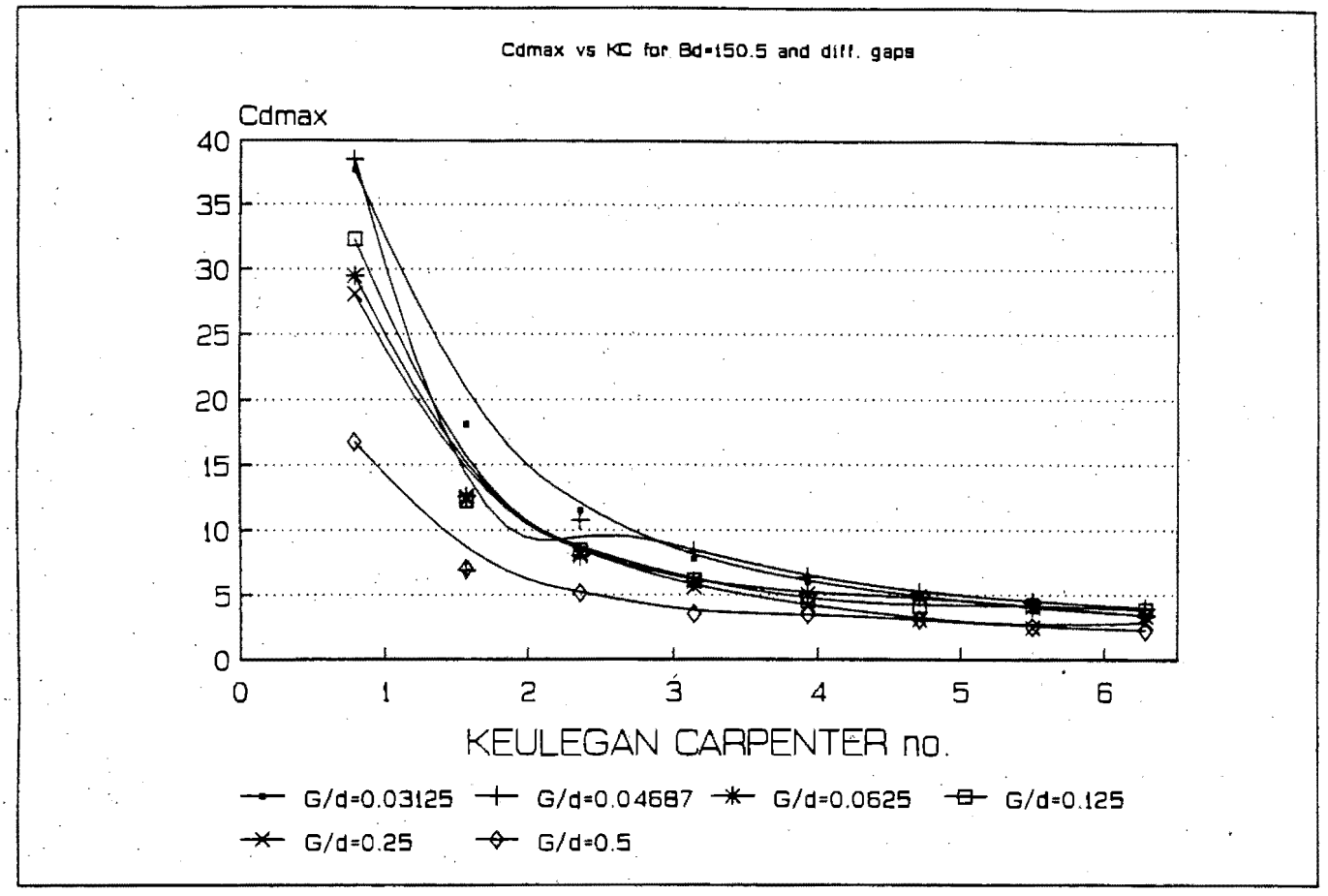

Figure I-39 : Cdmax vs KC for diameter=120mm, T=2s, ave Bd=150.5 and different gap ratios.

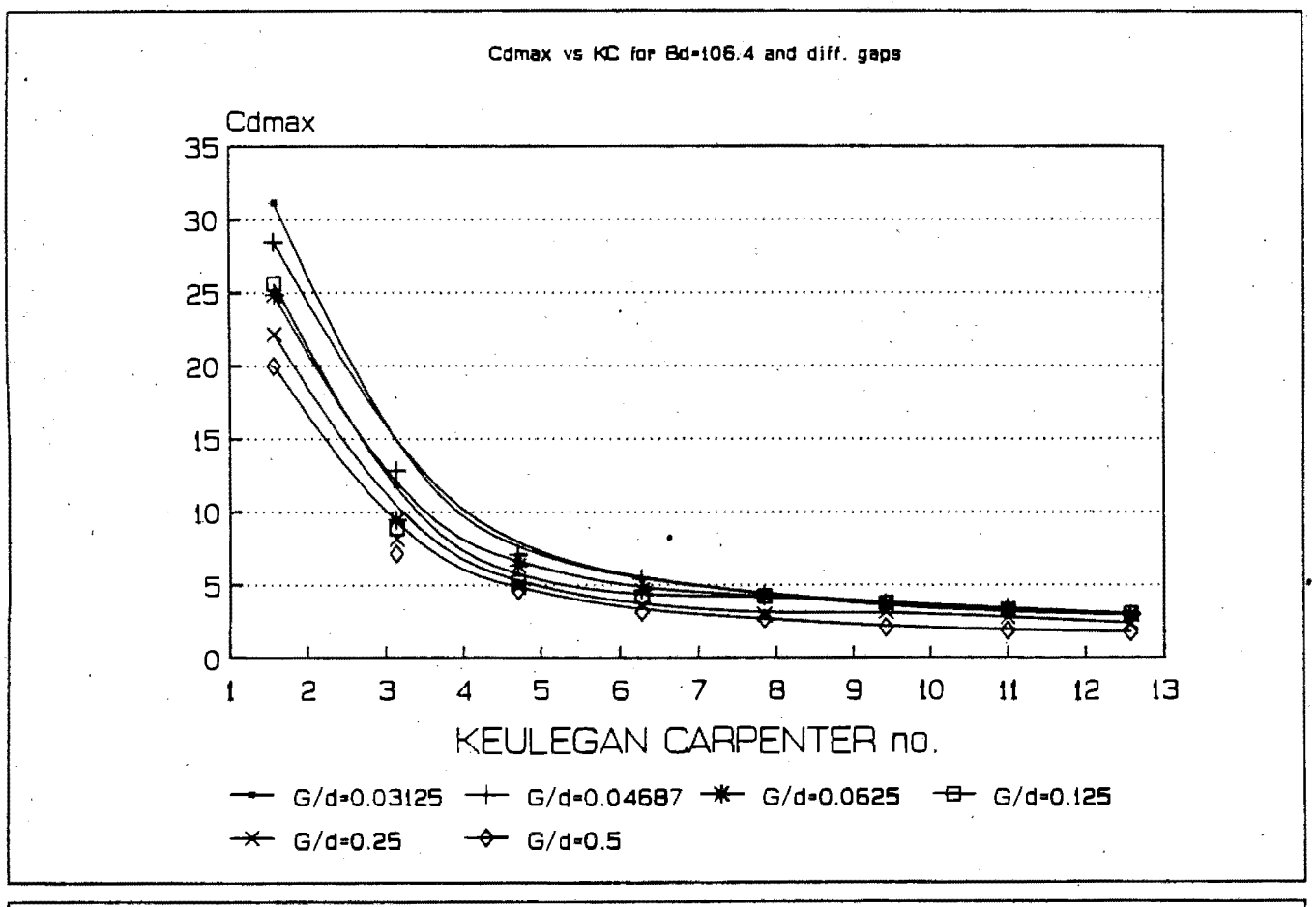

Figure I-40 : Cdmax vs KC for diameter=120mm, T=4s, ave Bd=106.4 and different gap ratios.

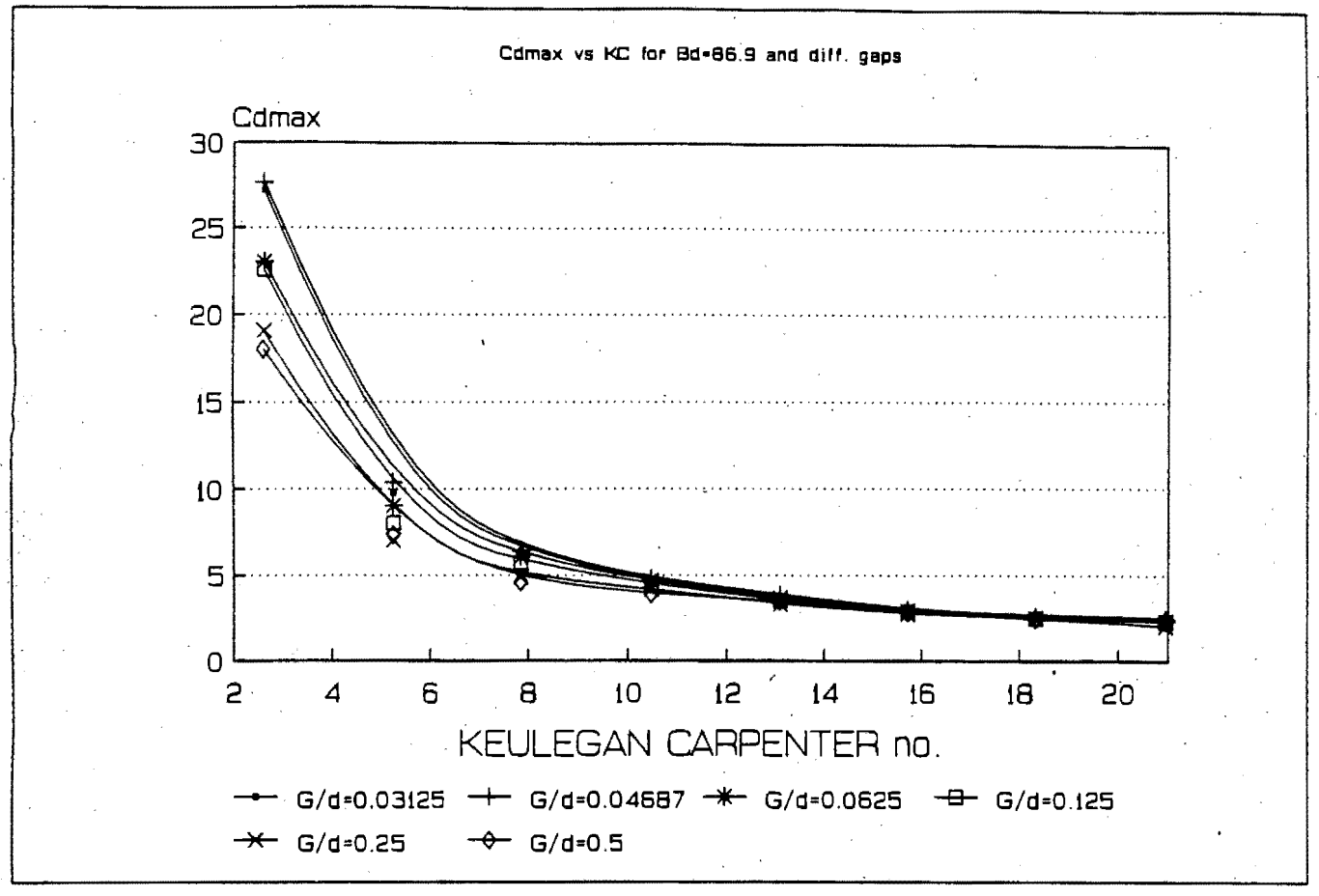

Figure I-41 : Cdmax vs KC for diameter=120mm, T=6s, ave Bd=86.9 and different gap ratios.

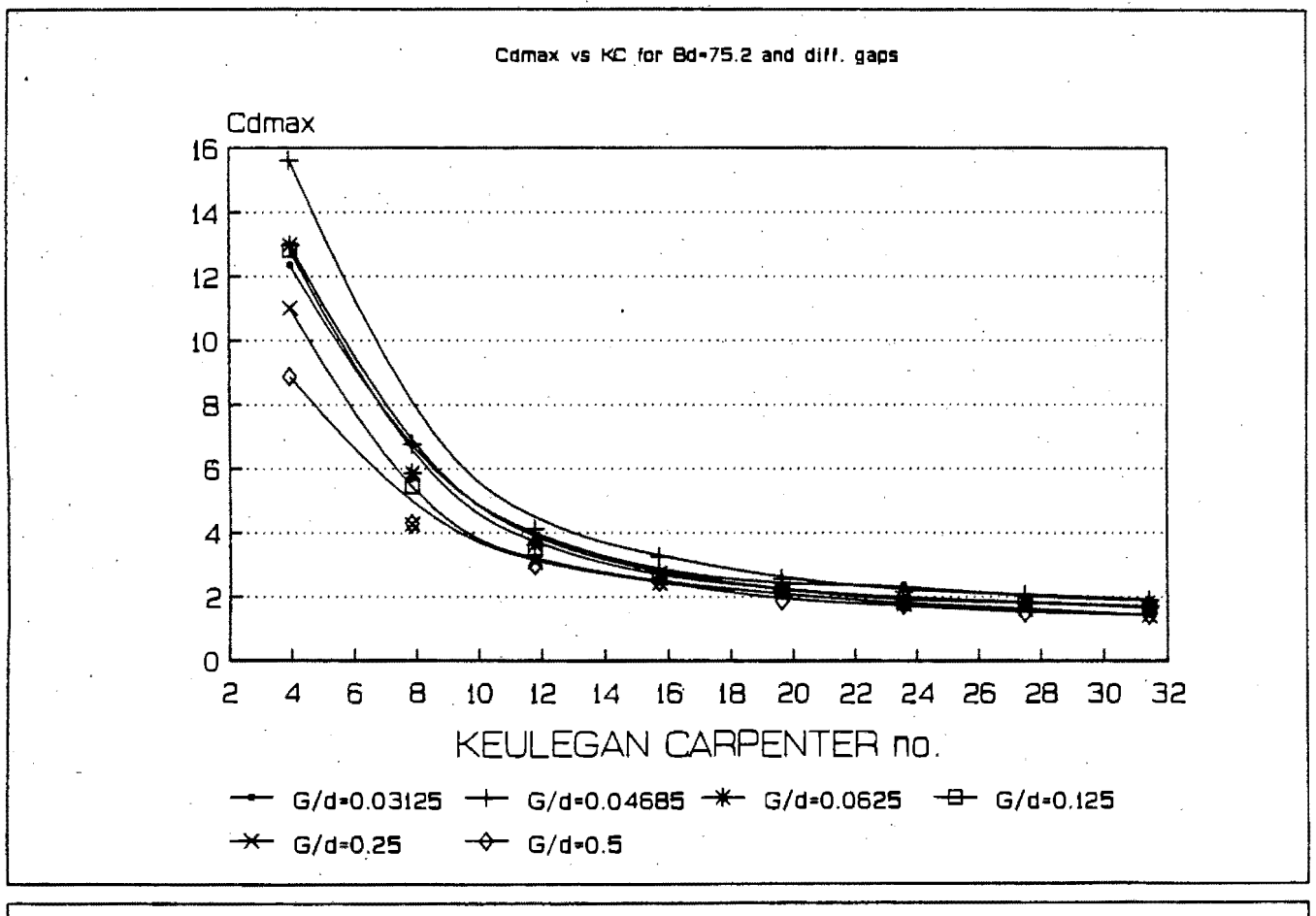

Figure I-42 : Cdmax vs KC for diameter=120mm, T=8s, ave Bd=75.2 and different gap ratios.

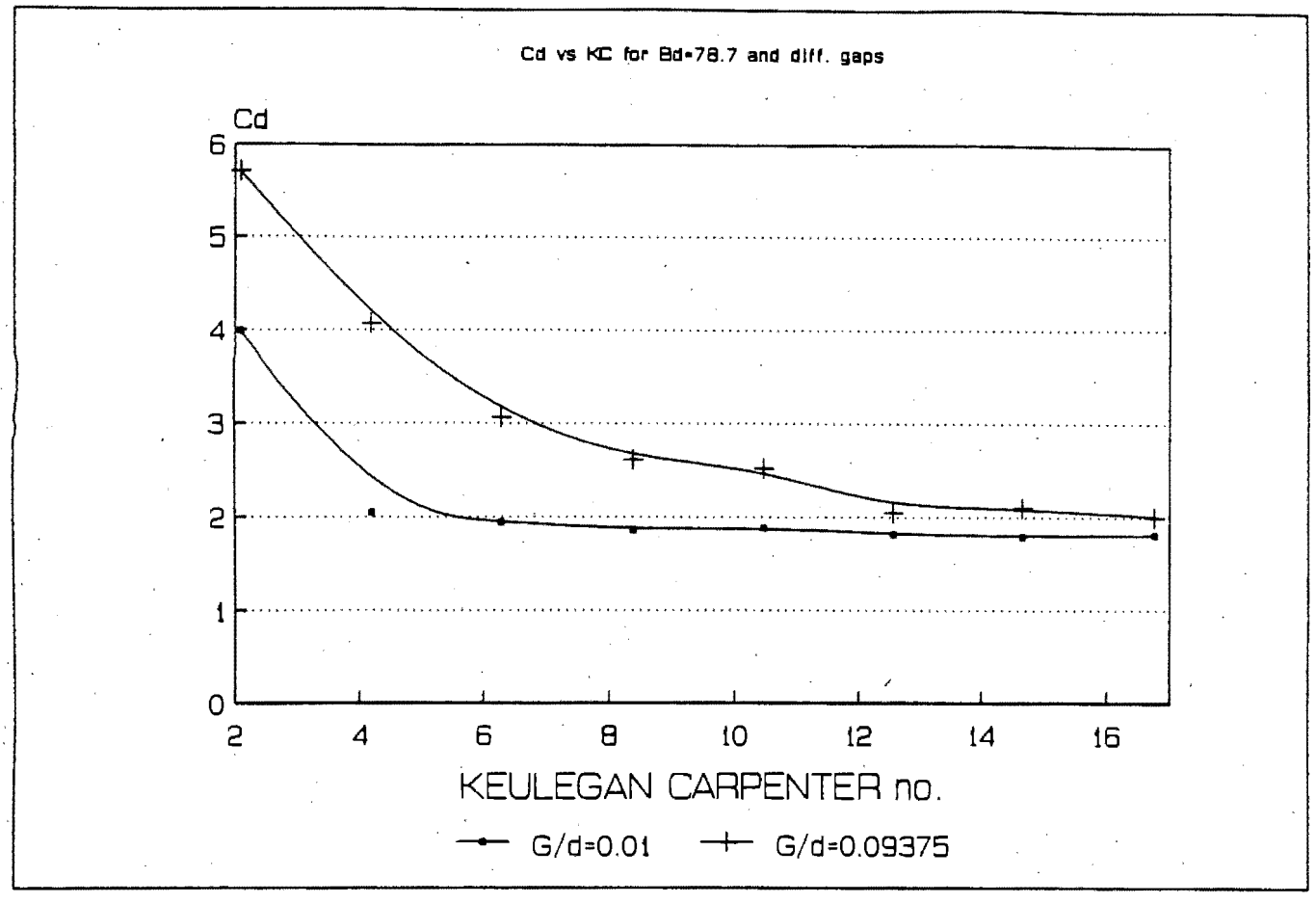

Figure I-43 : Cd vs KC for diameter=90mm, T=4s, ave Bd=78.7 and different gap ratios.

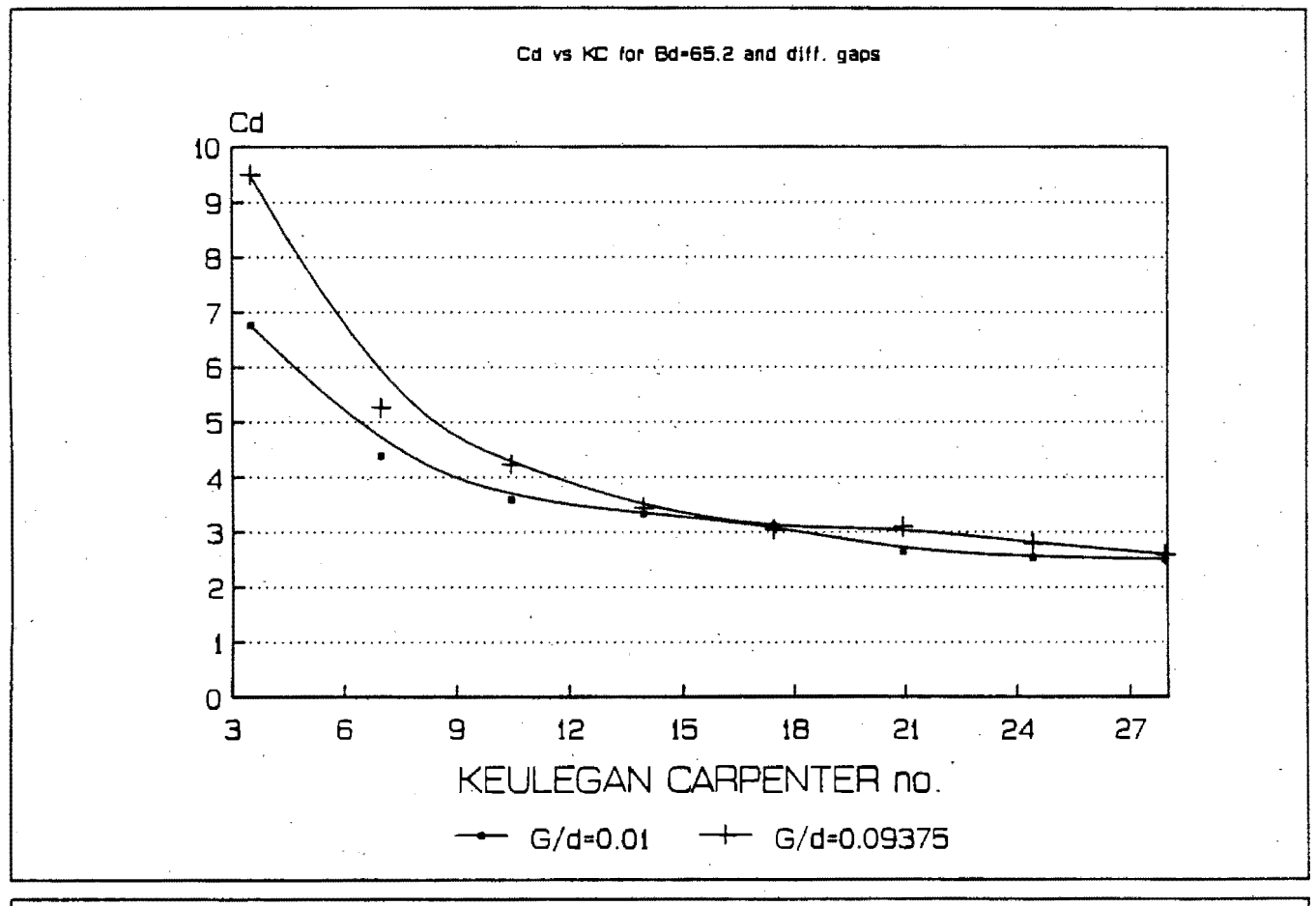

Figure I-44 : Cd vs KC for diameter=90mm, T=6s, ave Bd=65.2 and different gap ratios.

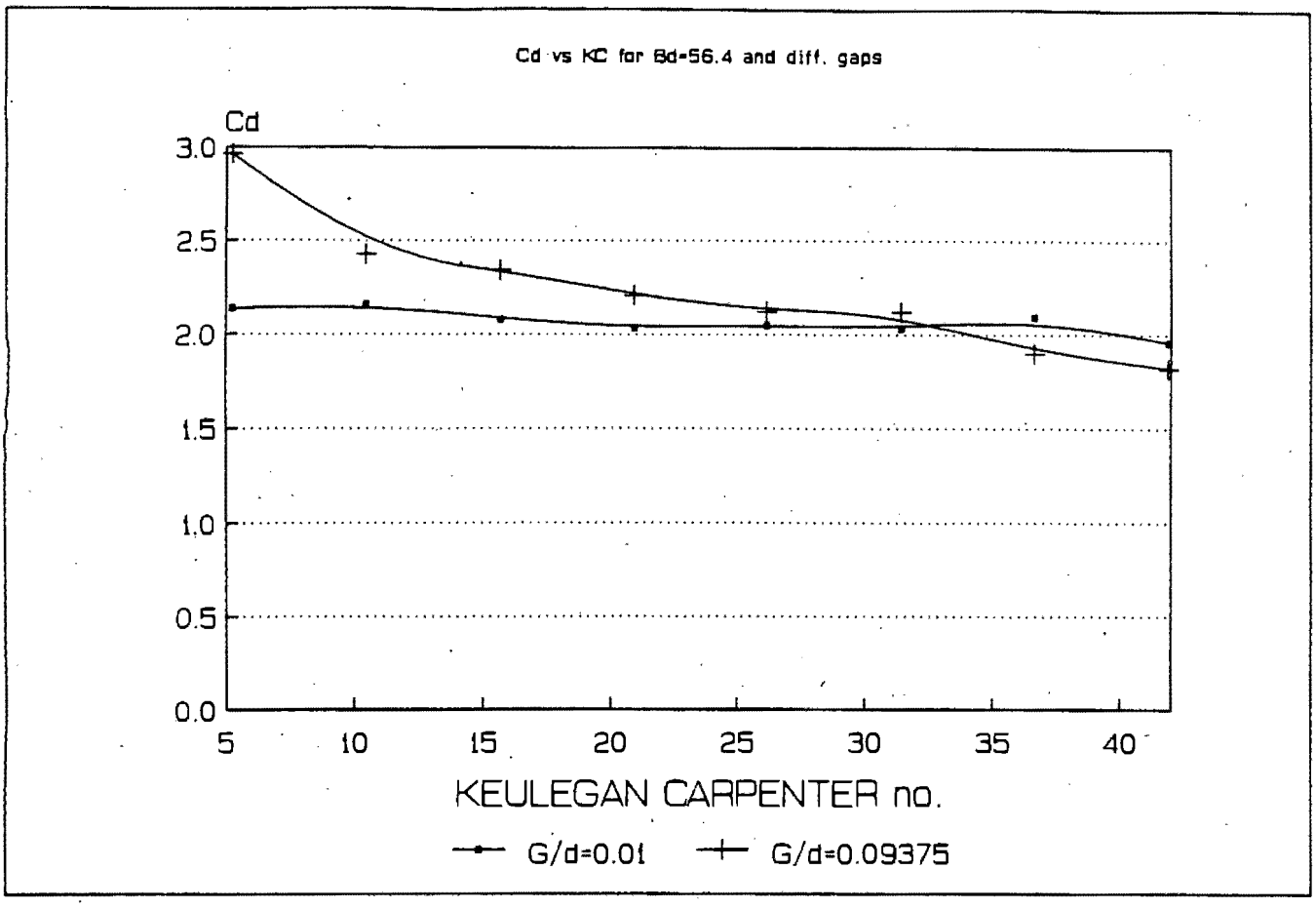

Figure I-45 : Cd vs KC for diameter=90mm, T=8s, ave Bd=56.4 and different gap ratios.

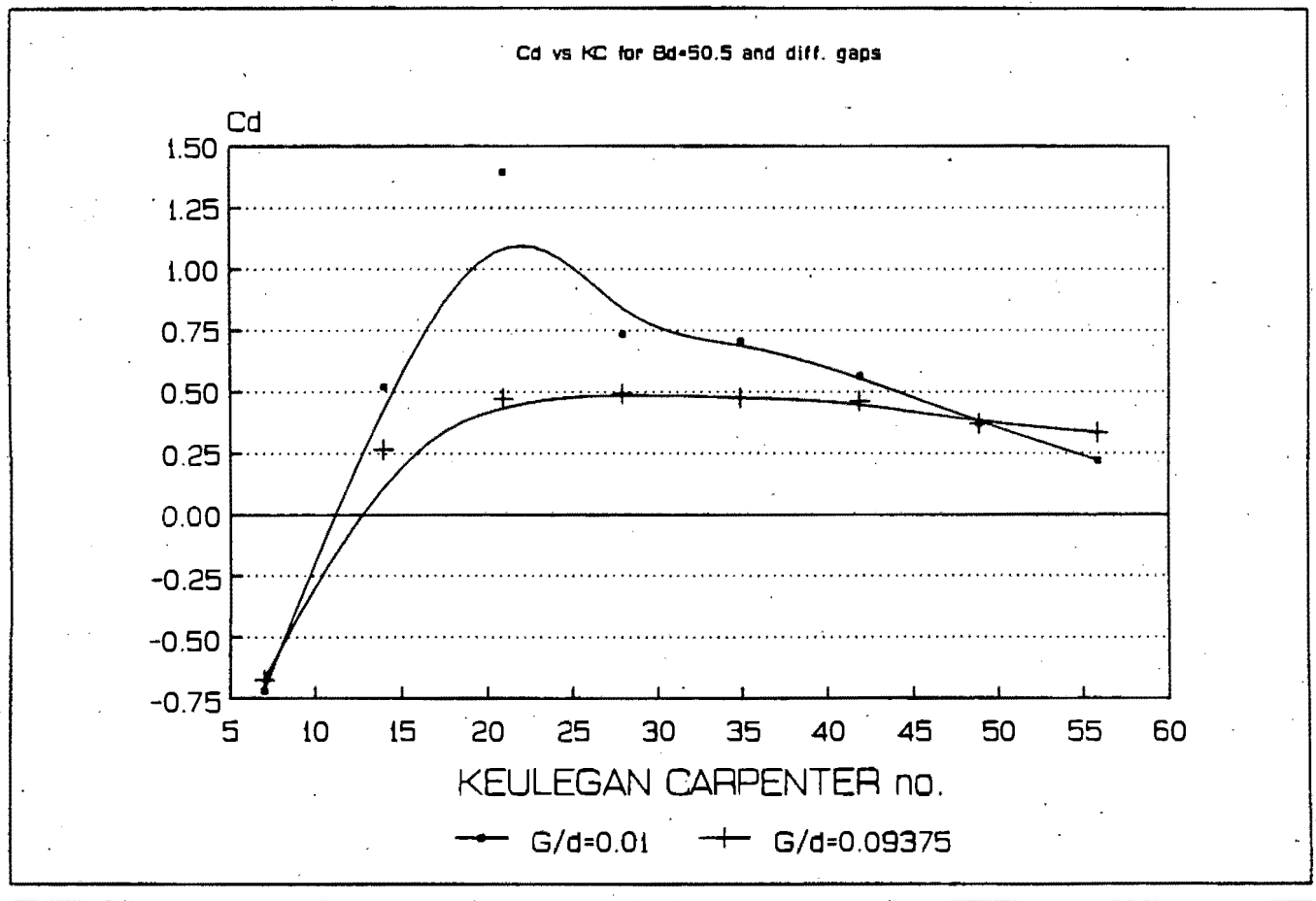

Figure I-46 : Cd vs KC for diameter=90mm, T=10s, ave Bd=50.5 and different gap ratios.

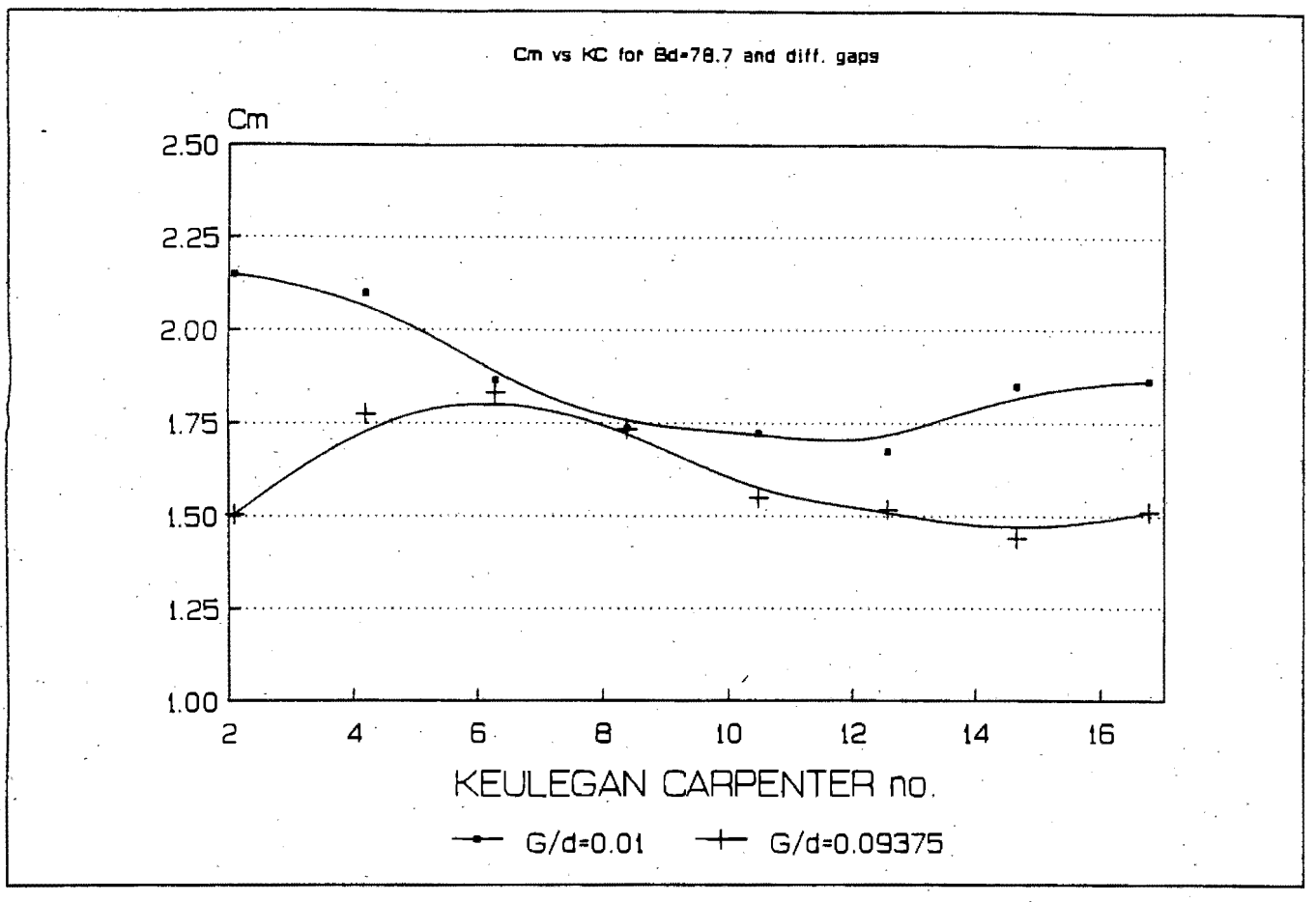

Figure I-47 : Cm vs KC for diameter=90mm, T=4s, ave Bd=78.7 and different gap ratios.

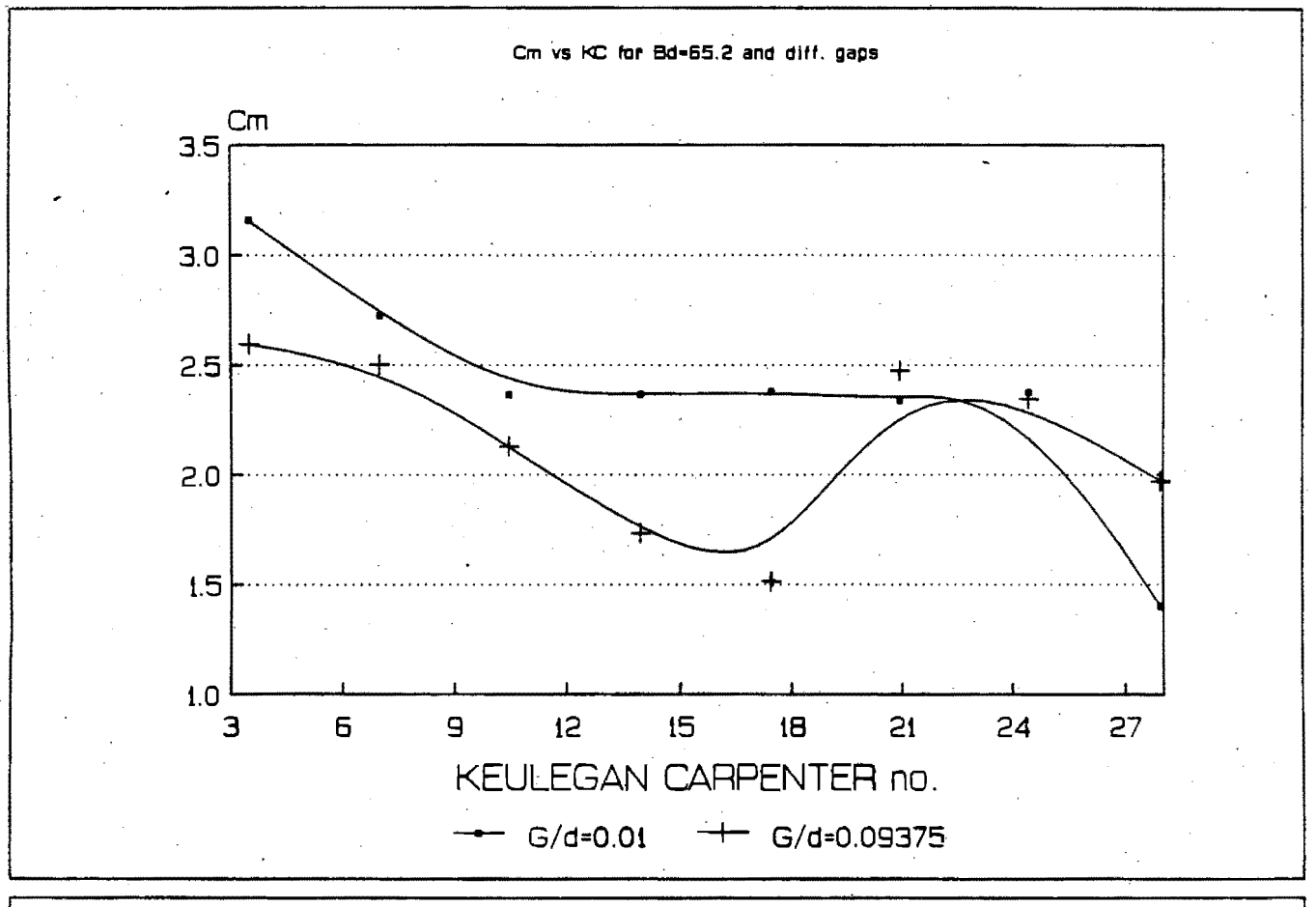

Figure I-48 : Cm vs KC for diameter=90mm, T=6s, ave Bd=65.2 and different gap ratios.

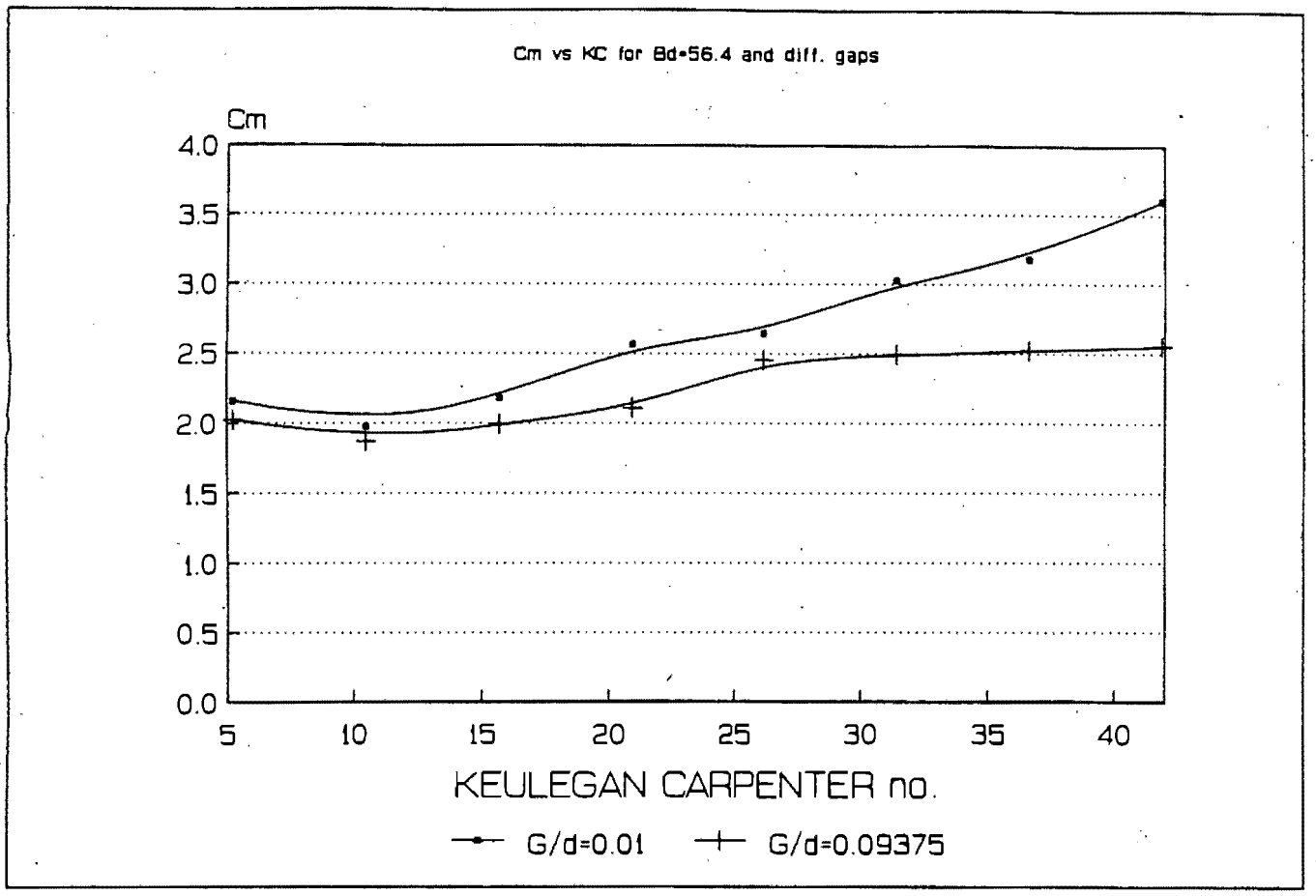

Figure I-49 : Cm vs KC for diameter=90mm, T=8s, ave Bd=56.4 and different gap ratios.

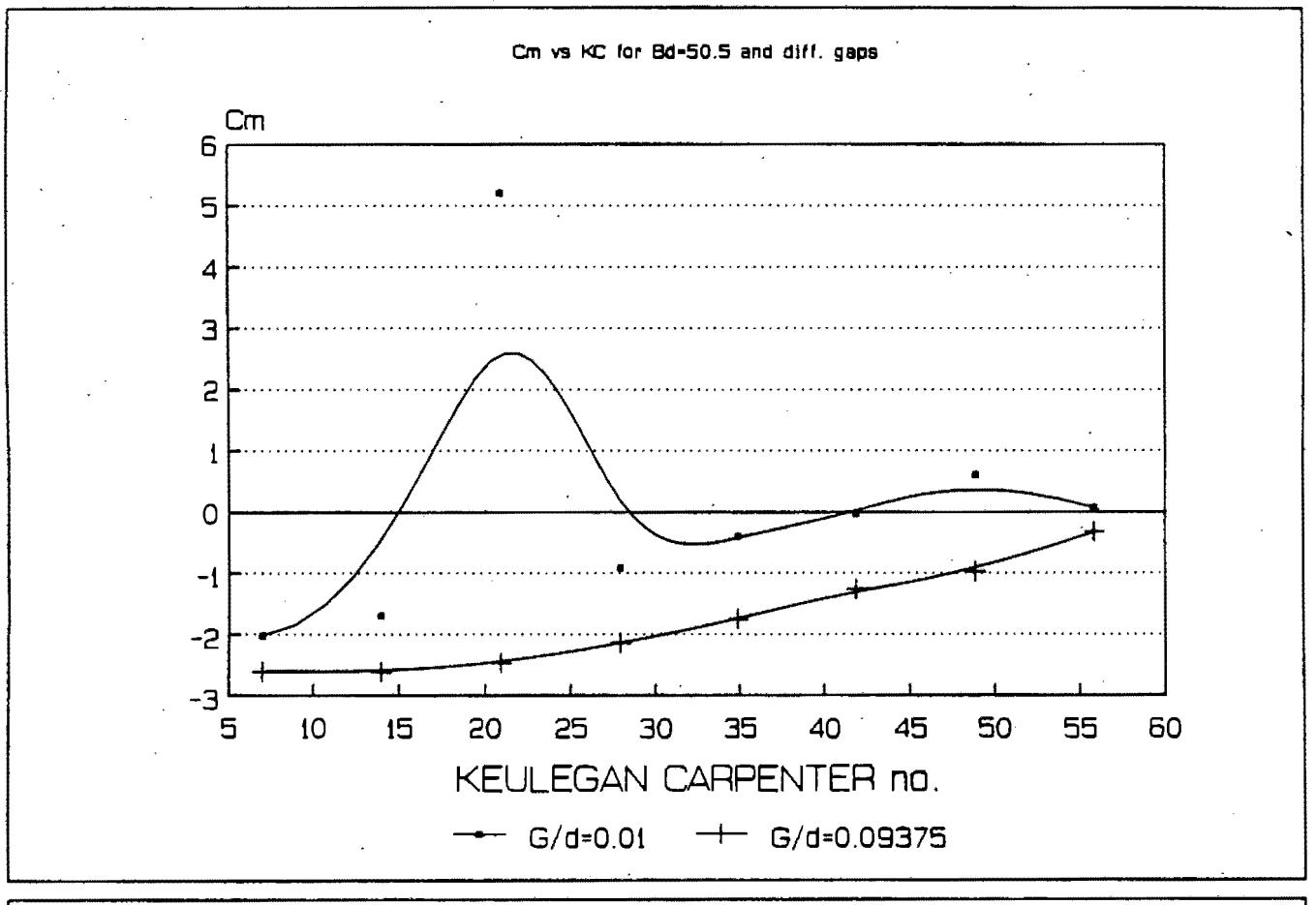

Figure I-50 : Cm vs KC for diameter=90mm, T=10s, ave Bd=50.5 and different gap ratios.

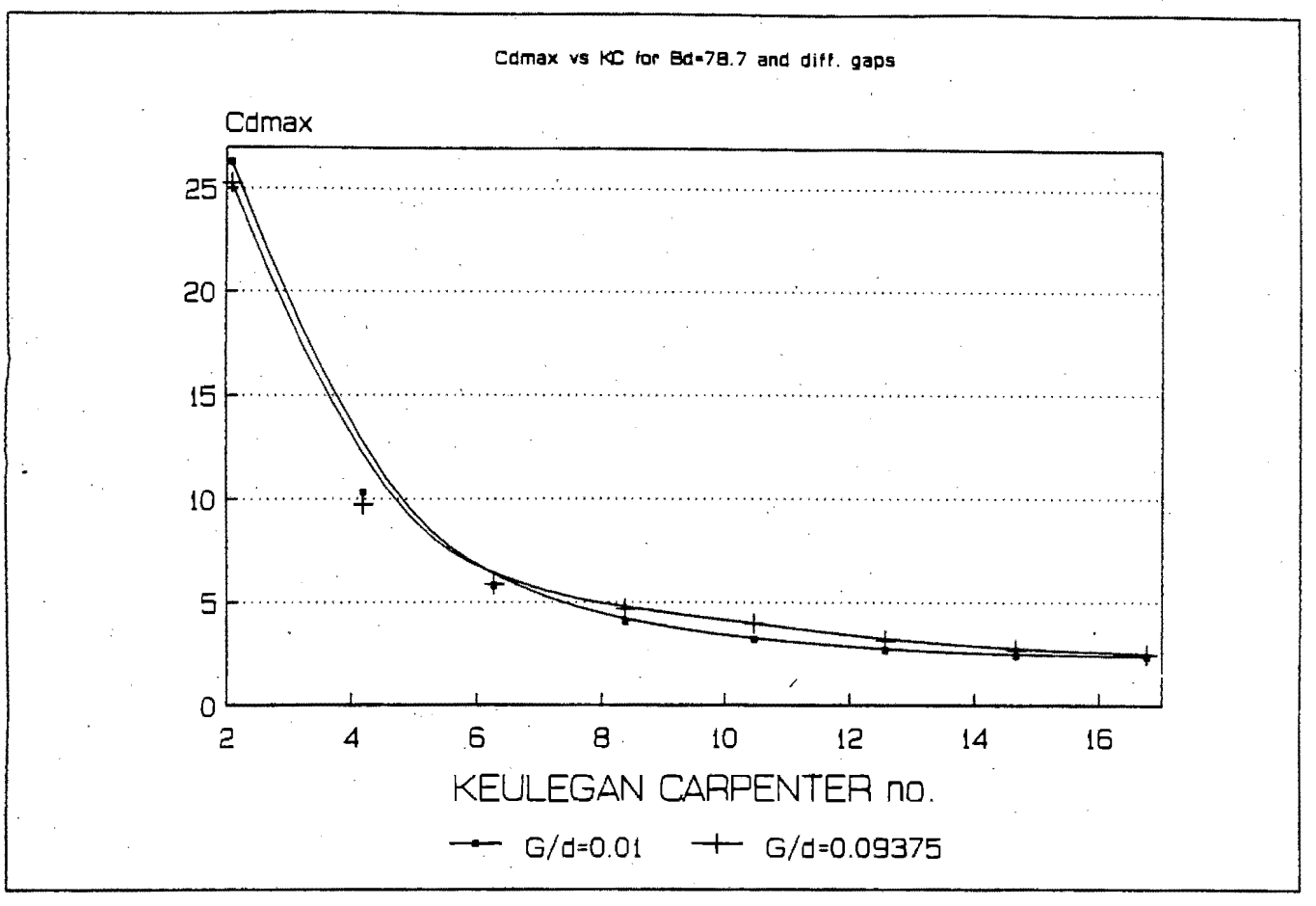

Figure I-51 : Cdmax vs KC for diameter=90mm, T=4s, ave Bd=78.7 and different gap ratios.

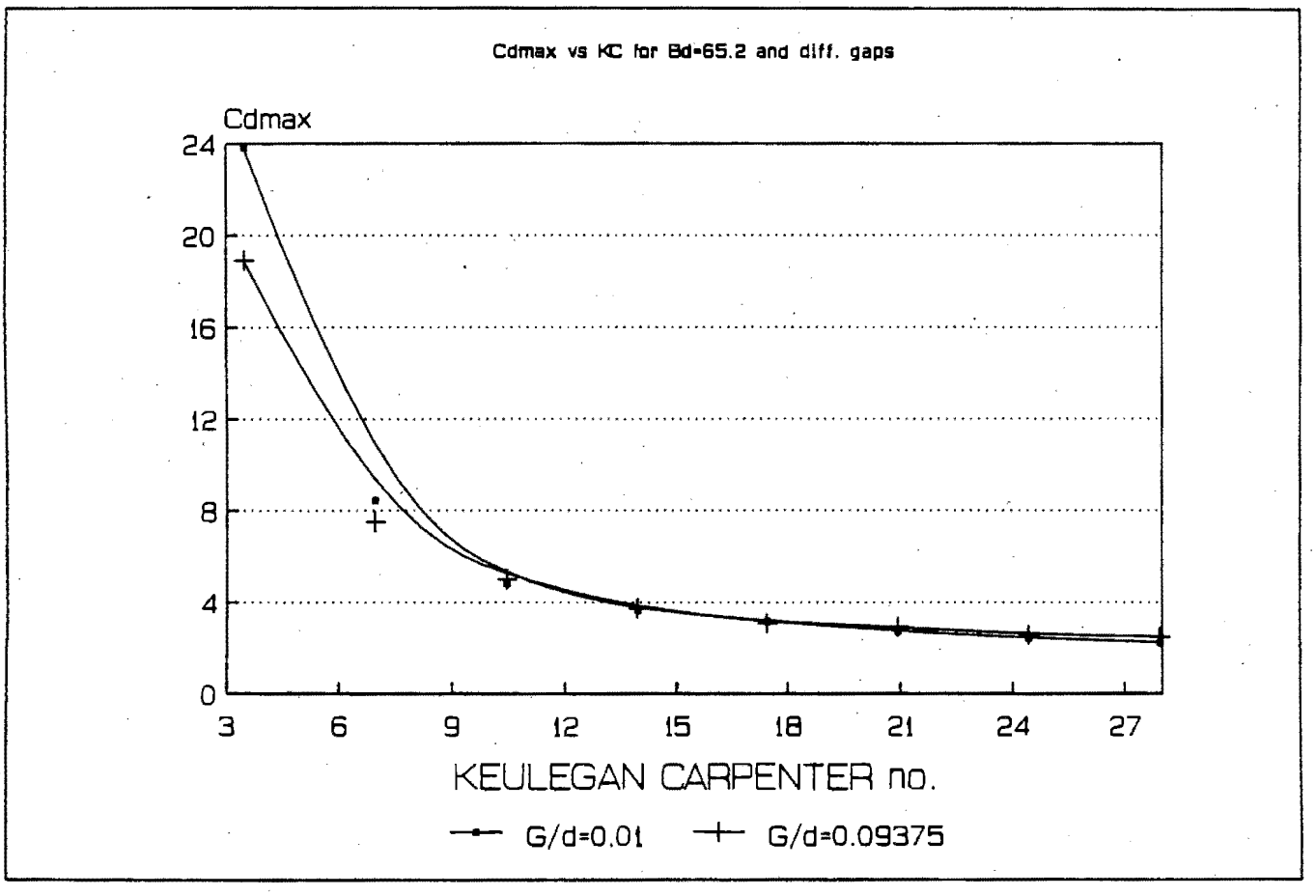

Figure I-52 : Cdmax vs KC for diameter=90mm, T=6s, ave Bd=65.2 and different gap ratios.

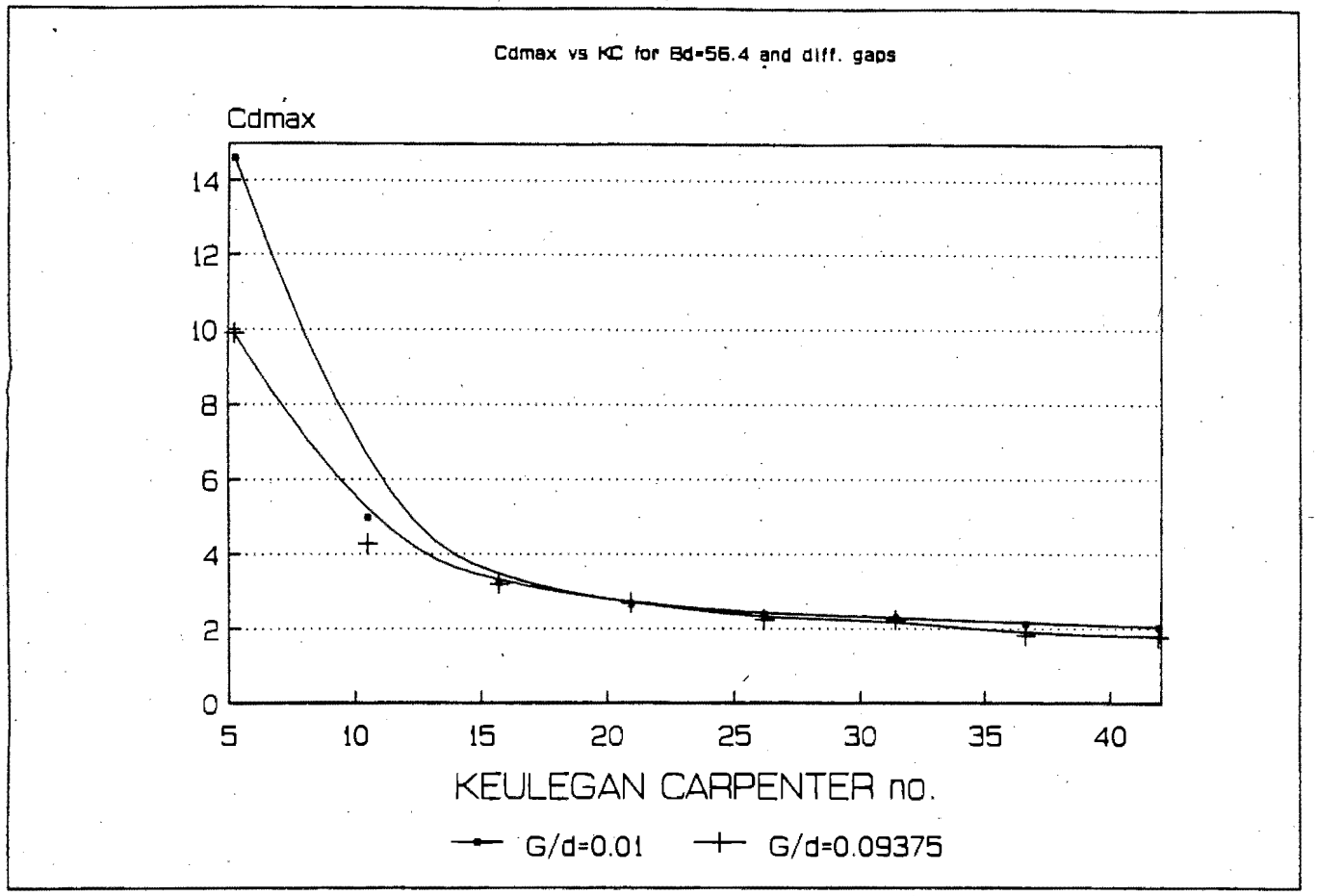

Figure I-53 : Cdmax vs KC for diameter=90mm, T=8s, ave Bd=56.4 and different gap ratios.

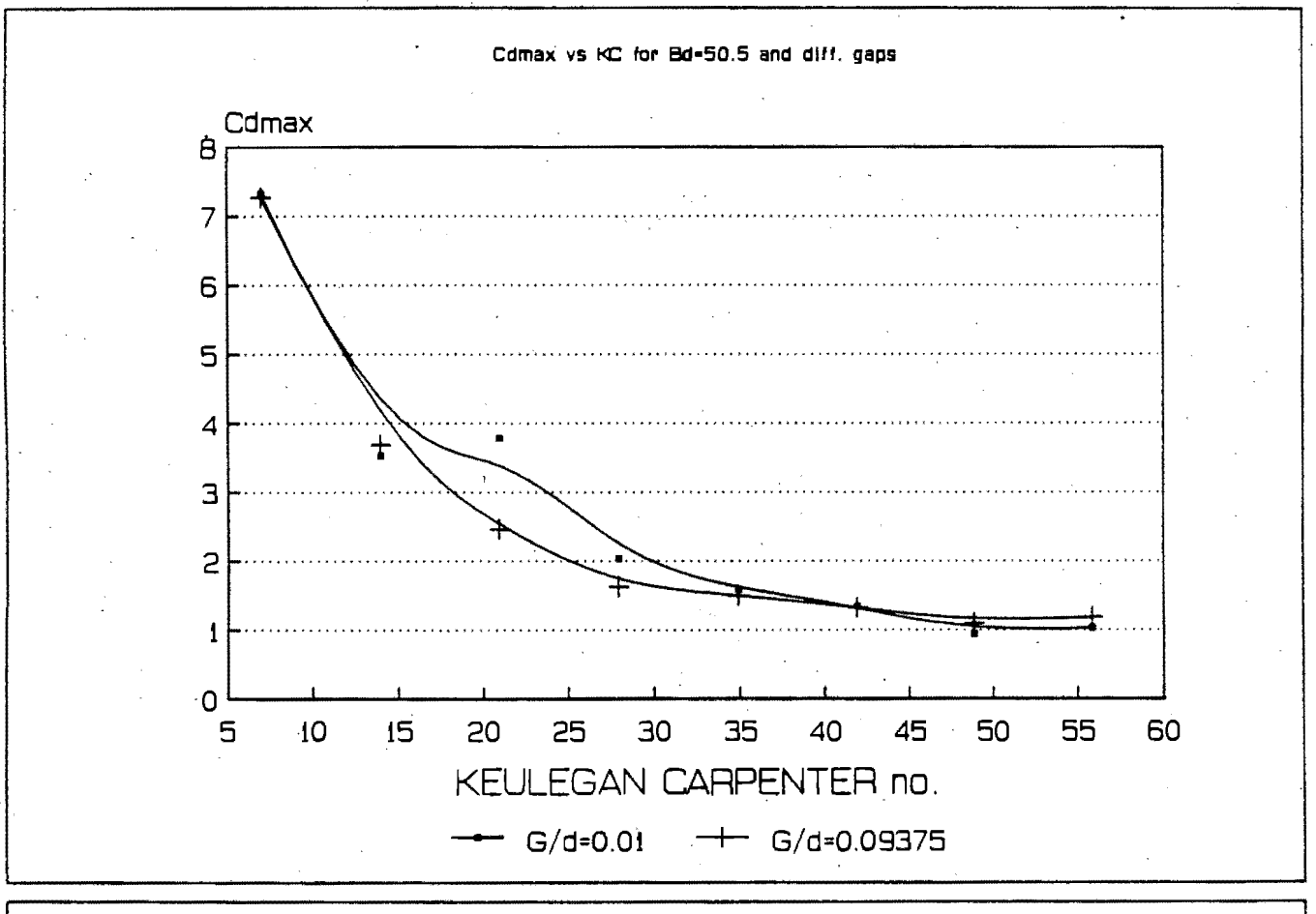

Figure I-54 : Cdmax vs KC for diameter=90mm, T=10s, ave Bd=50.5 and different gap ratios.

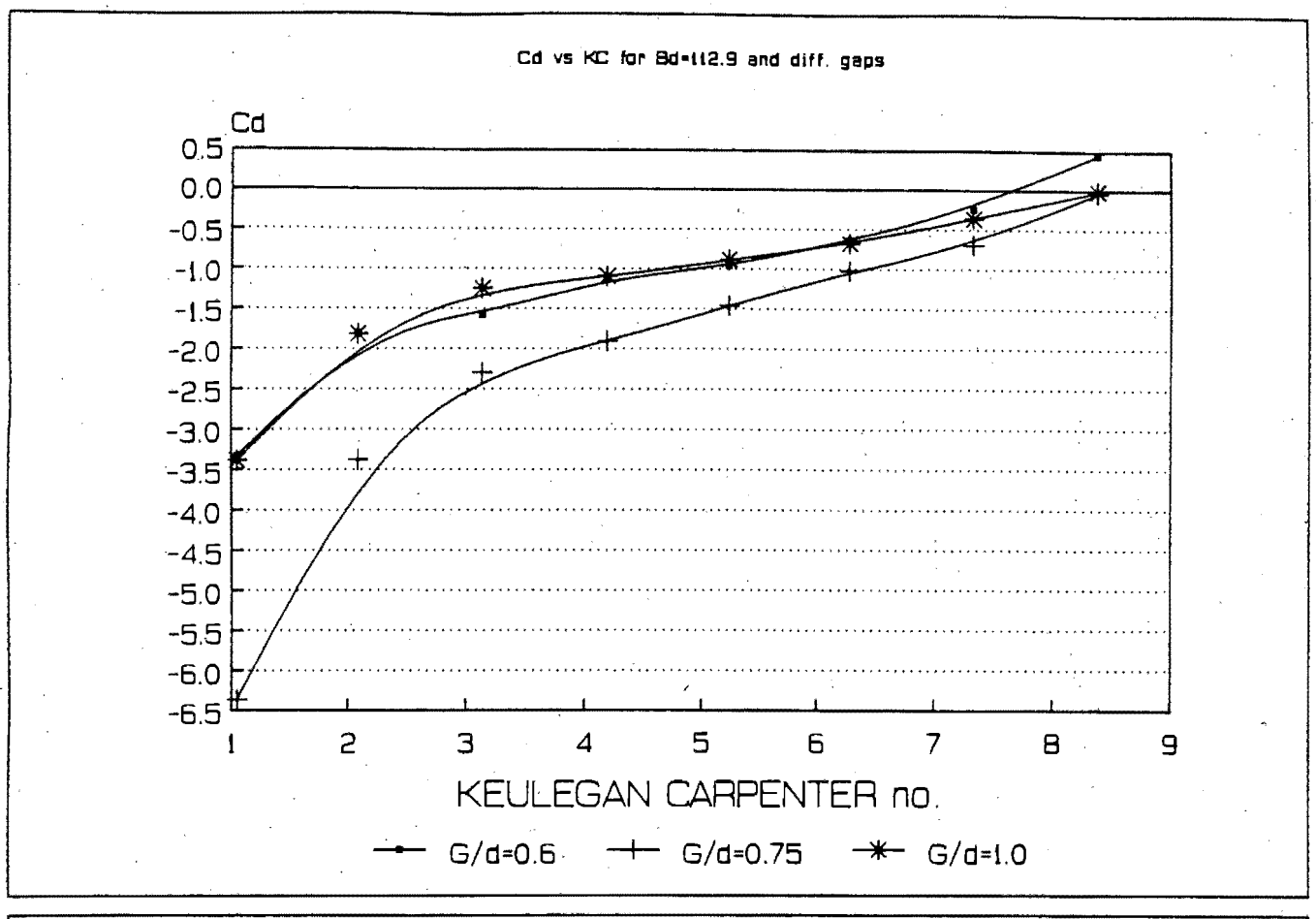

Figure I-55 : Cd vs KC for diameter=90mm, T=2s, ave Bd=112.9 and different gap ratios.

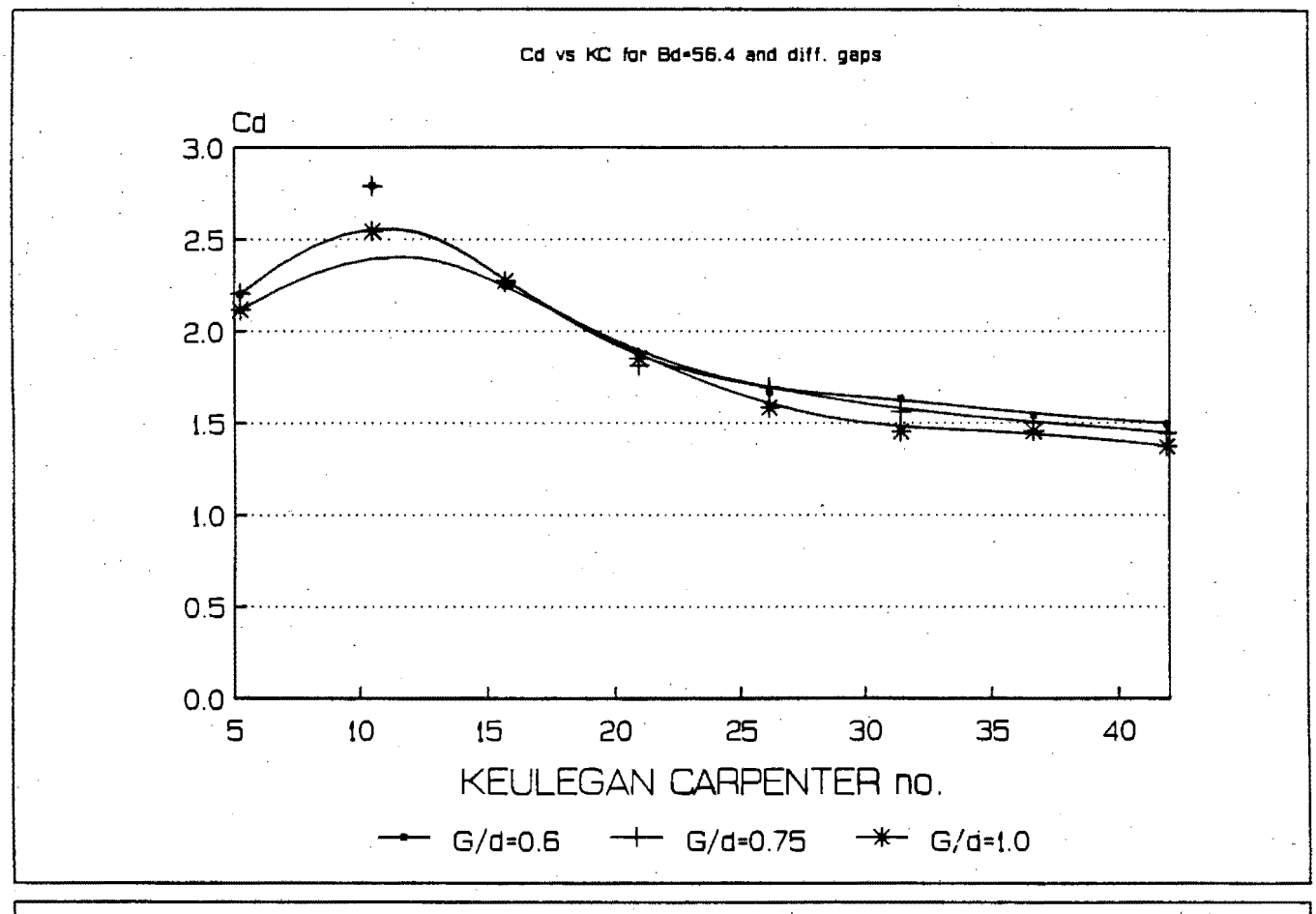

Figure I-56 : Cd vs KC for diameter=90mm, T=8s, ave Bd=56.4 and different gap ratios.

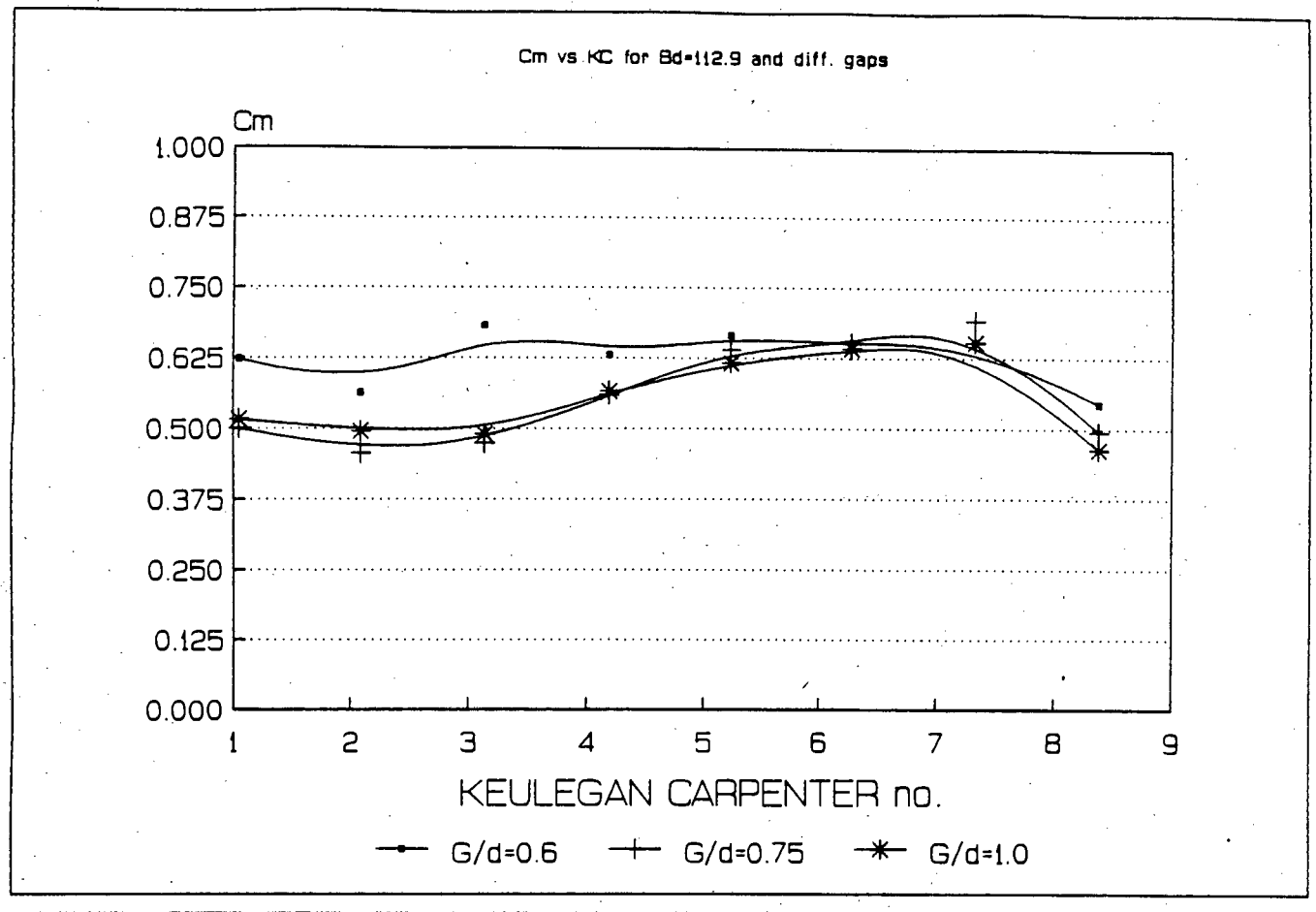

Figure I-57 : Cm vs KC for diameter=90mm, T=2s, ave Bd=112.9 and different gap ratios.

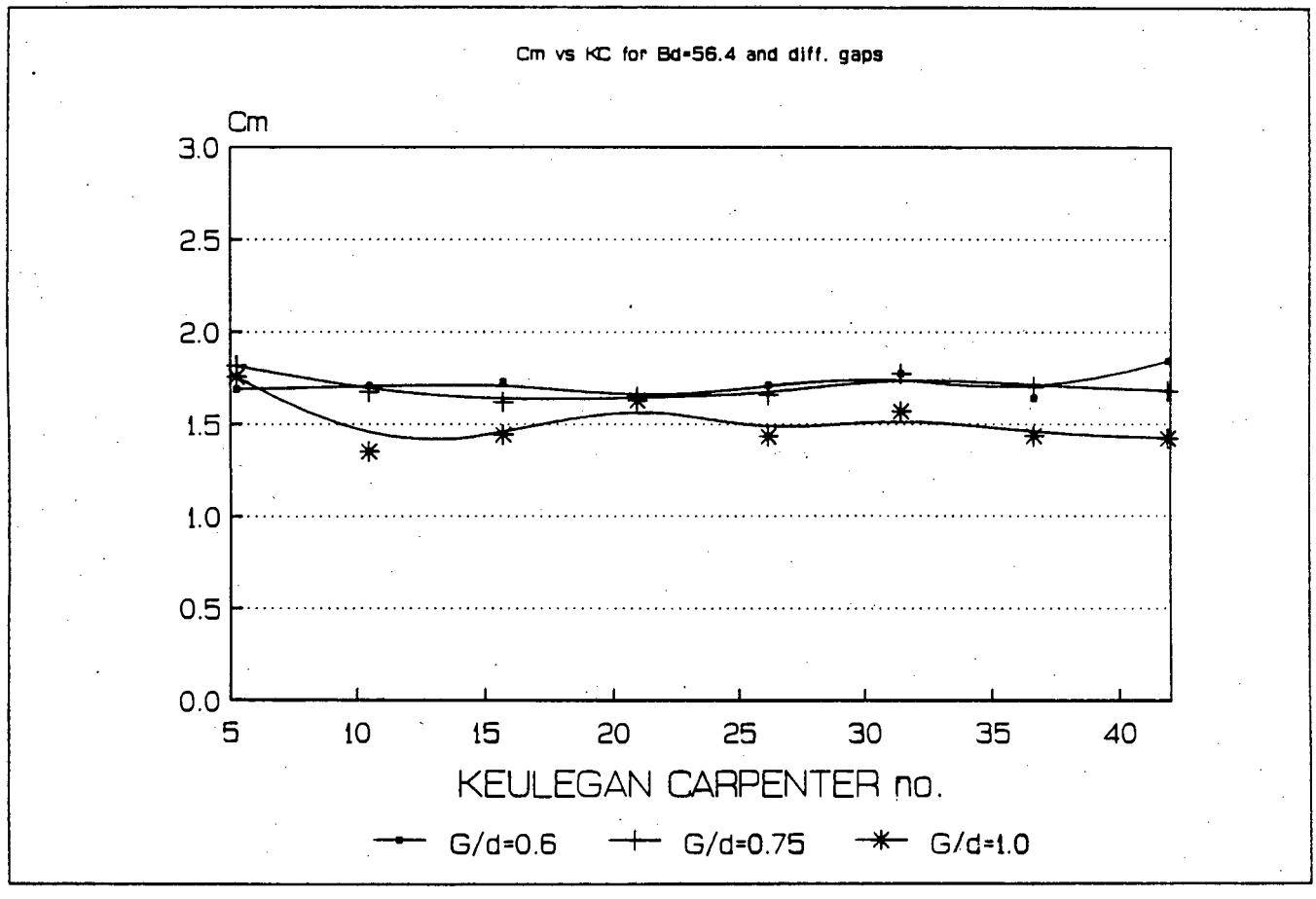

Figure I-58 : Cm vs KC for diameter=90mm, T=8s, ave Bd=56.4 and different gap ratios.

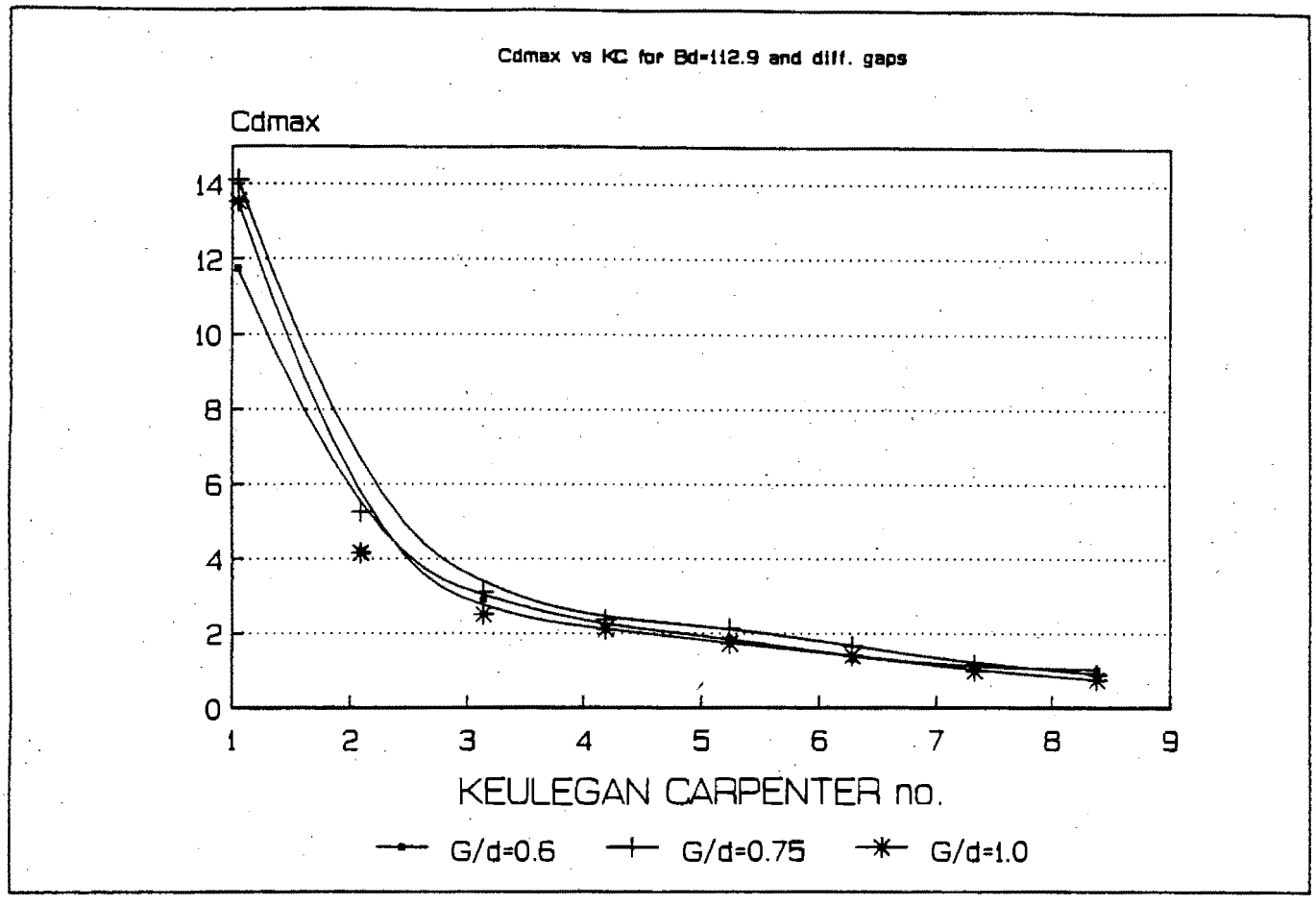

Figure I-59 : Cdmax vs KC for diameter=90mm, T=2s, ave Bd=112.9 and different gap ratios.

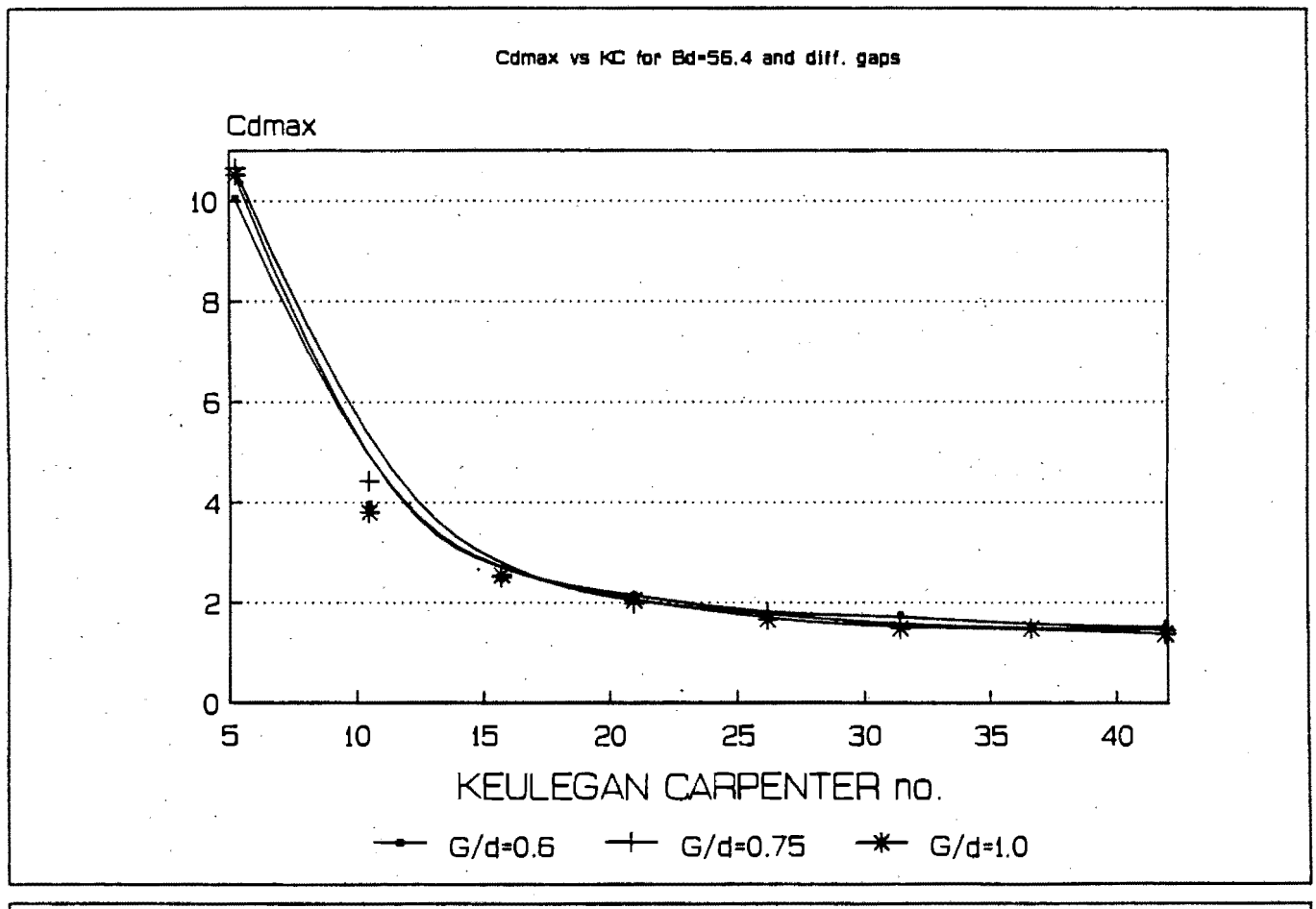

Figure I-60 : Cdmax vs KC for diameter=90mm, T=8s, ave Bd=56.4 and different gap ratios.

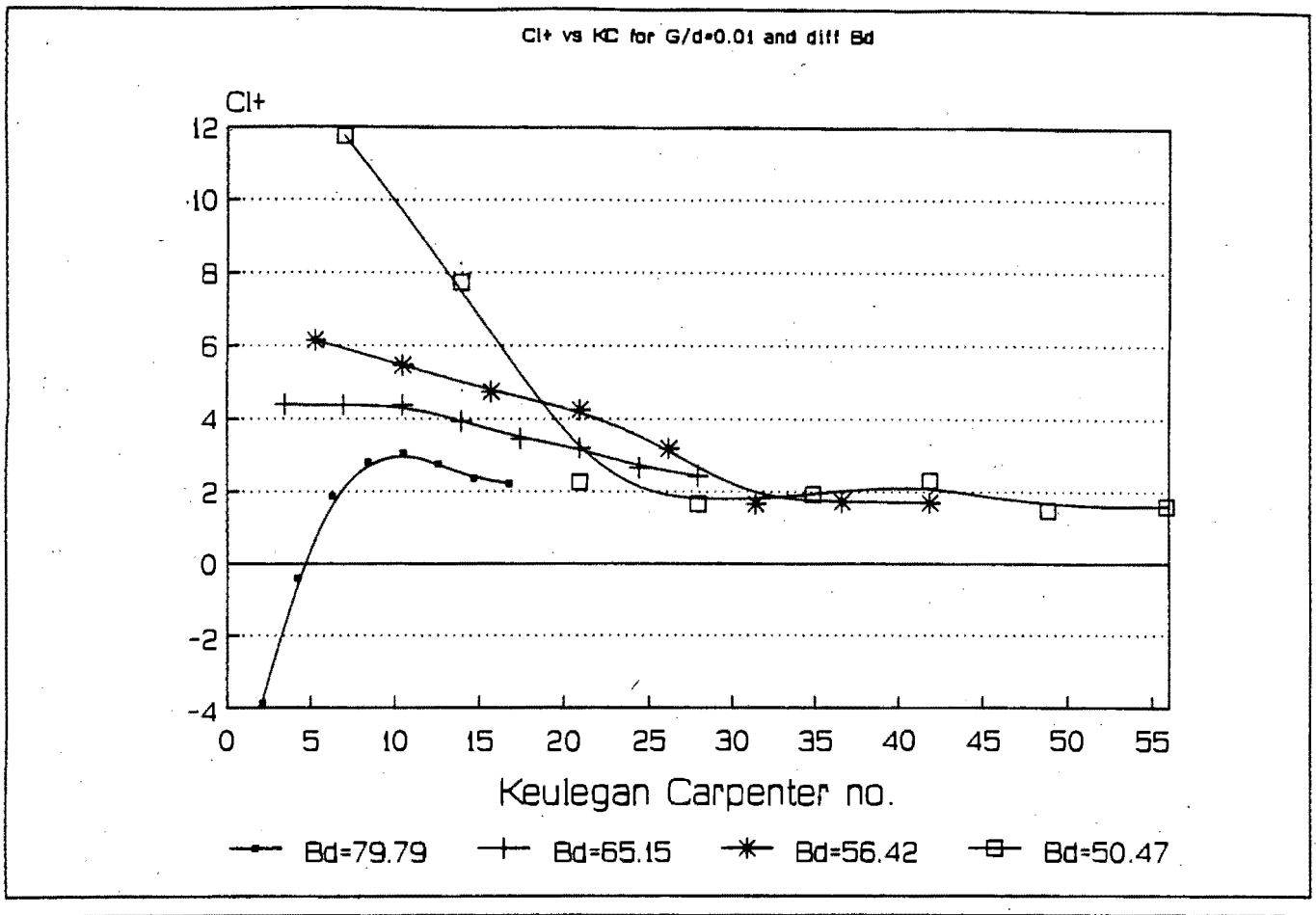

Figure I-61 : Cl+ vs KC for diameter=90mm, G/d=.01 and different Bd.

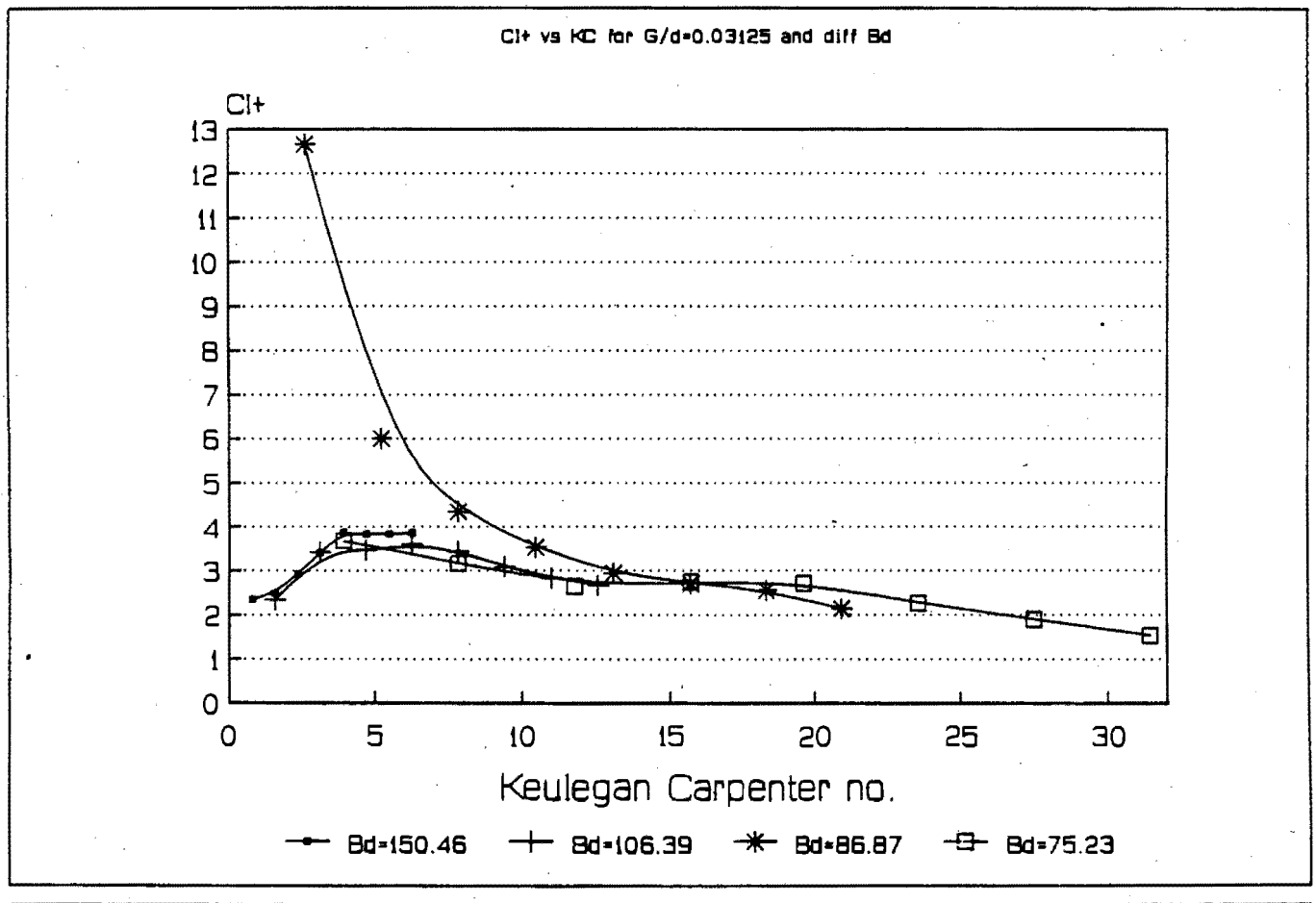

Figure I-62 : Cl+ vs KC for diameter=120mm, G/d=.03125 and different Bd.

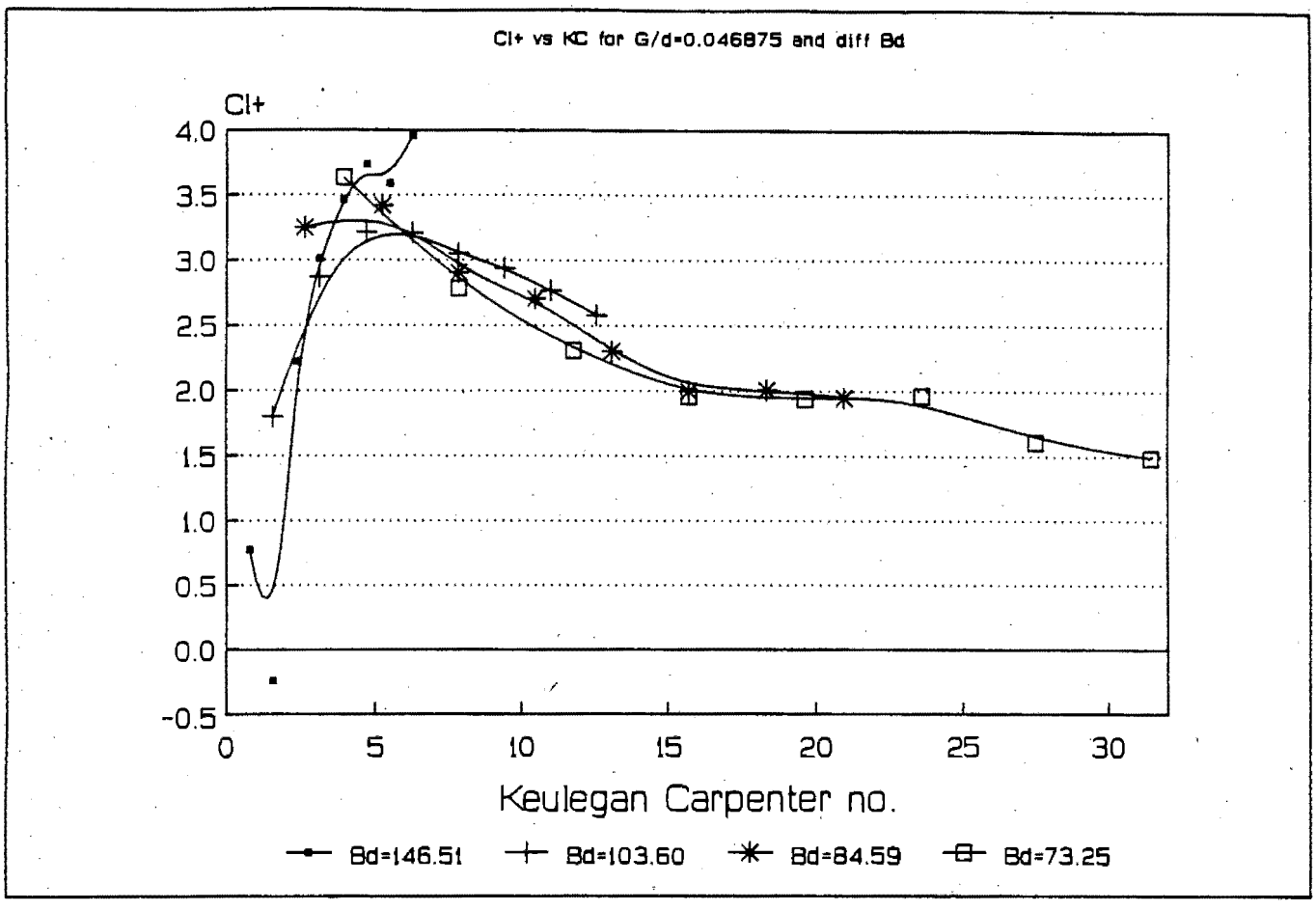

Figure I-63 : Cl+ vs KC for diameter=120mm, G/d=.046875 and different Bd.

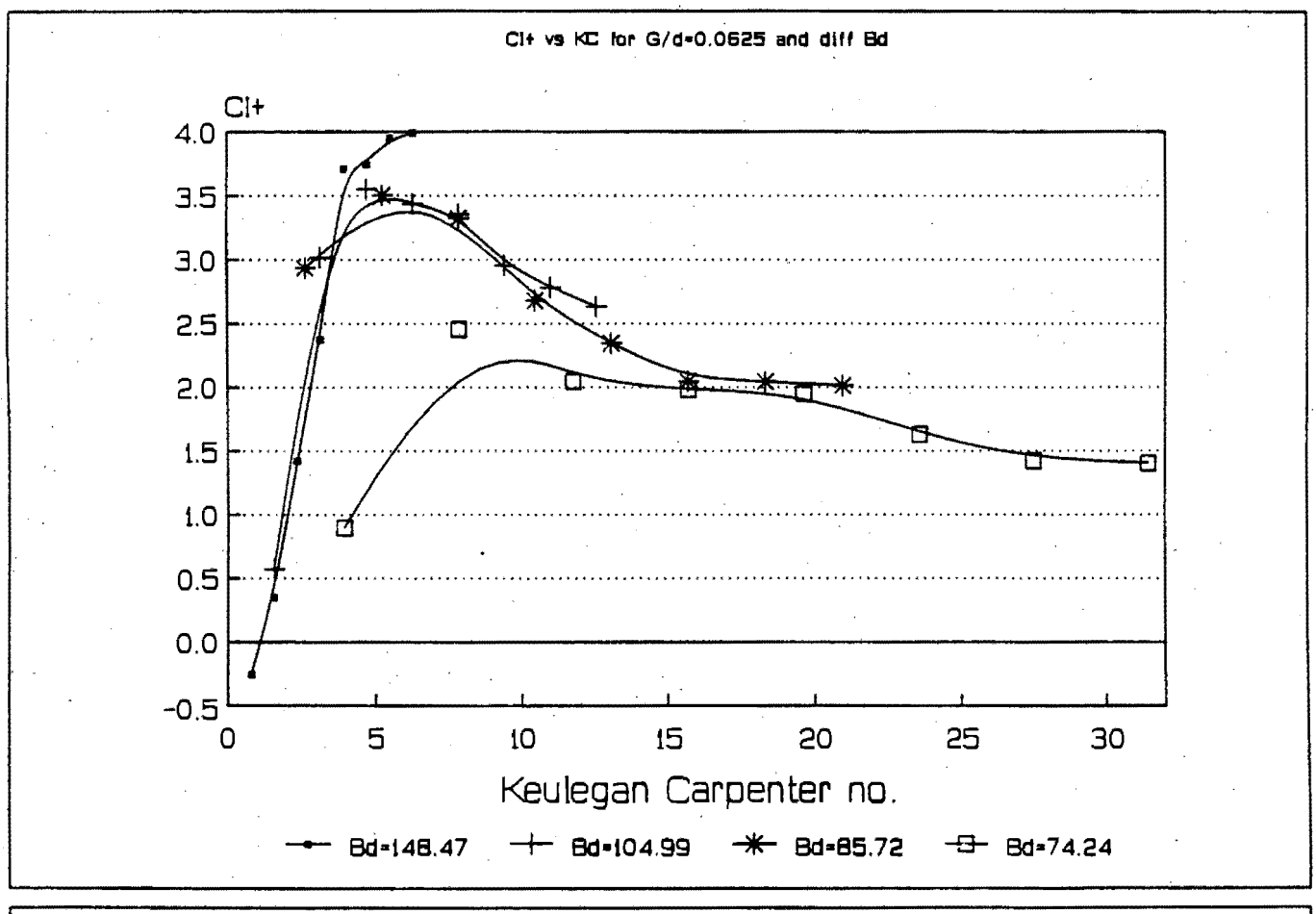

Figure I-64 : Cl+ vs KC for diameter=120mm, G/d=.0625 and different Bd.

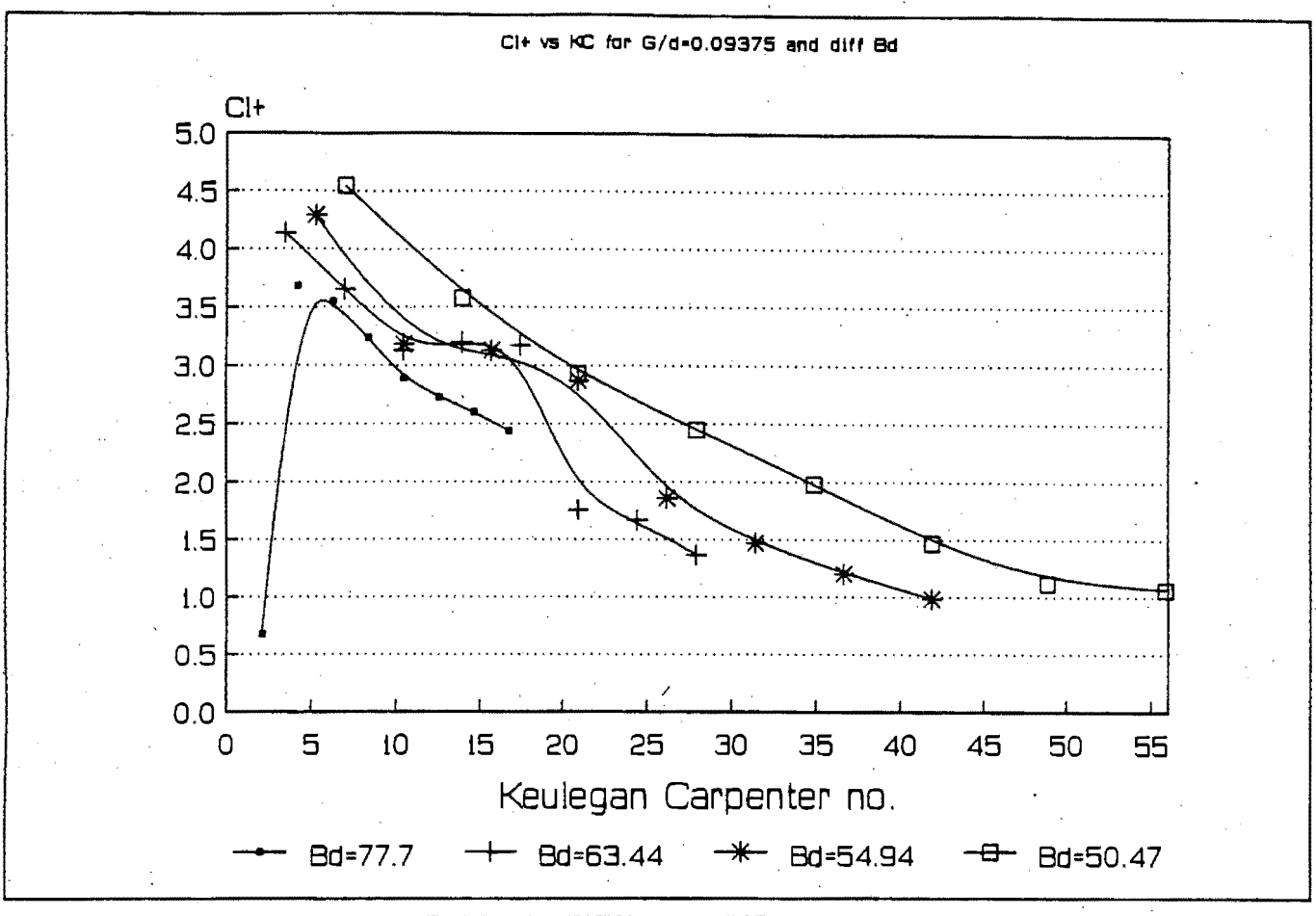

Figure I-65 : Cl+ vs KC for diameter=90mm, G/d=.09375 and different Bd.

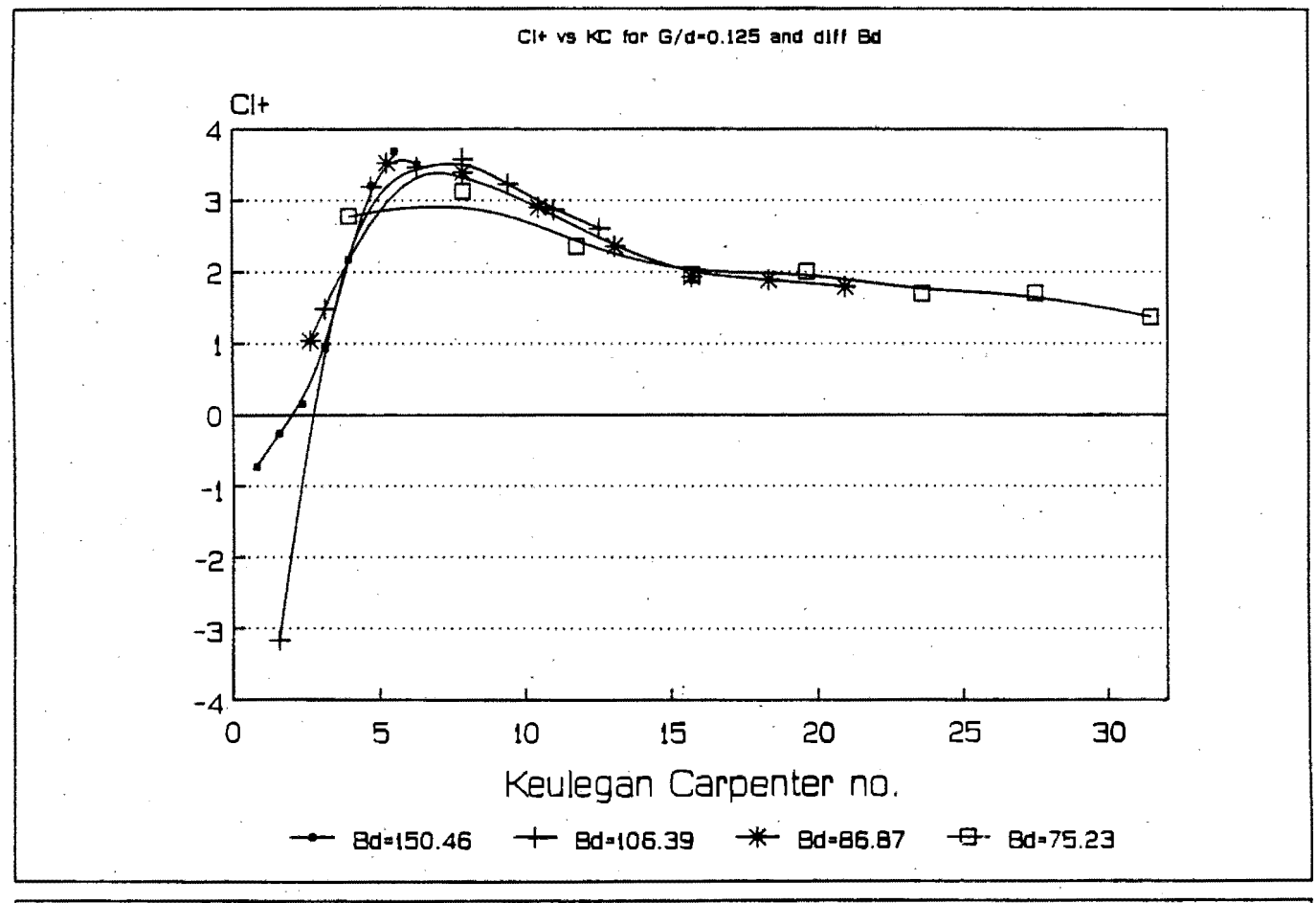

Figure I-66 : Cl+ vs KC for diameter=120mm, G/d=.125 and different Bd.

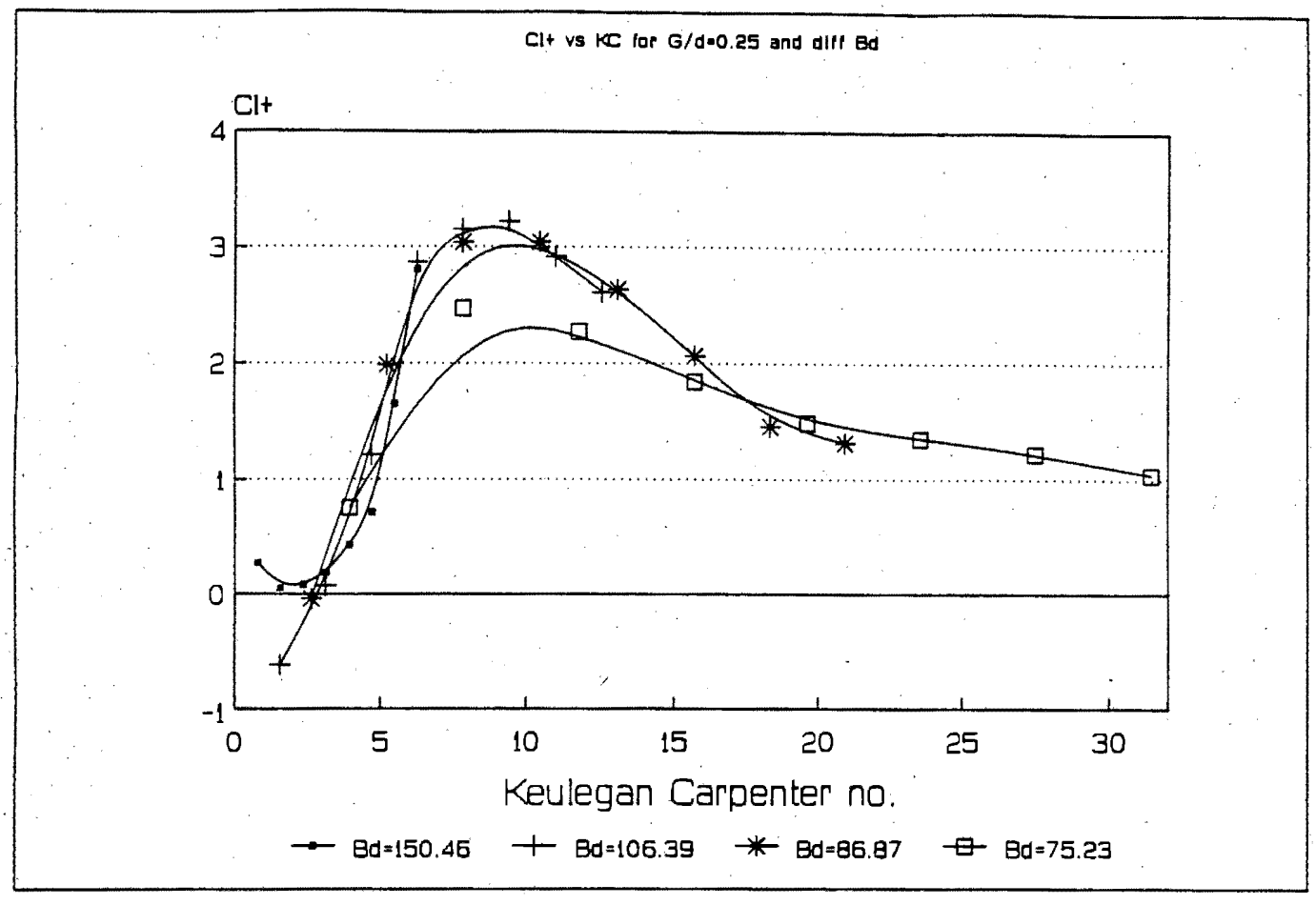

Figure I-67 : Cl+ vs KC for diameter=120mm, G/d=.25 and different Bd.

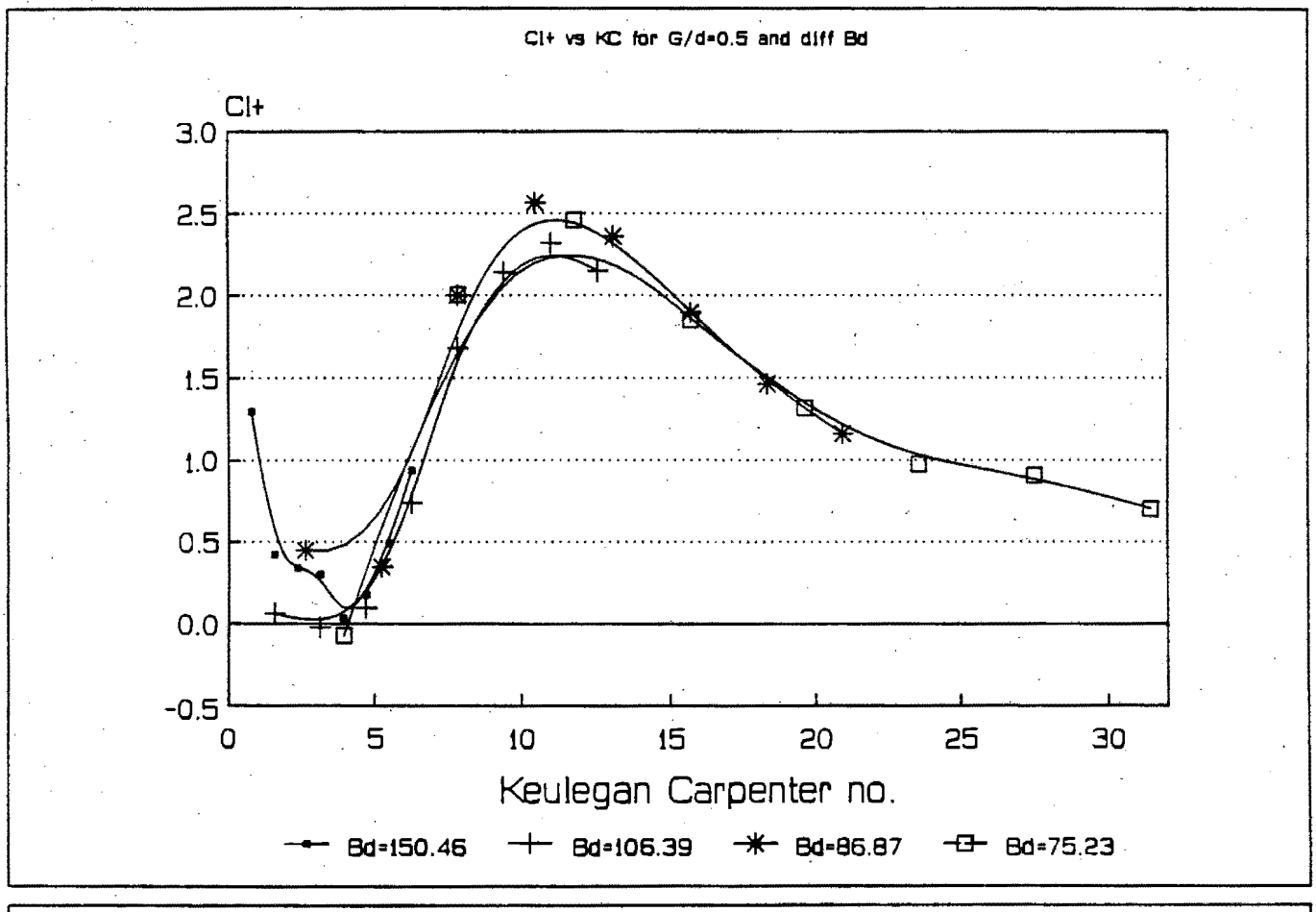

Figure I-68 : Cl+ vs KC for diameter=120mm, G/d=.5 and different Bd.

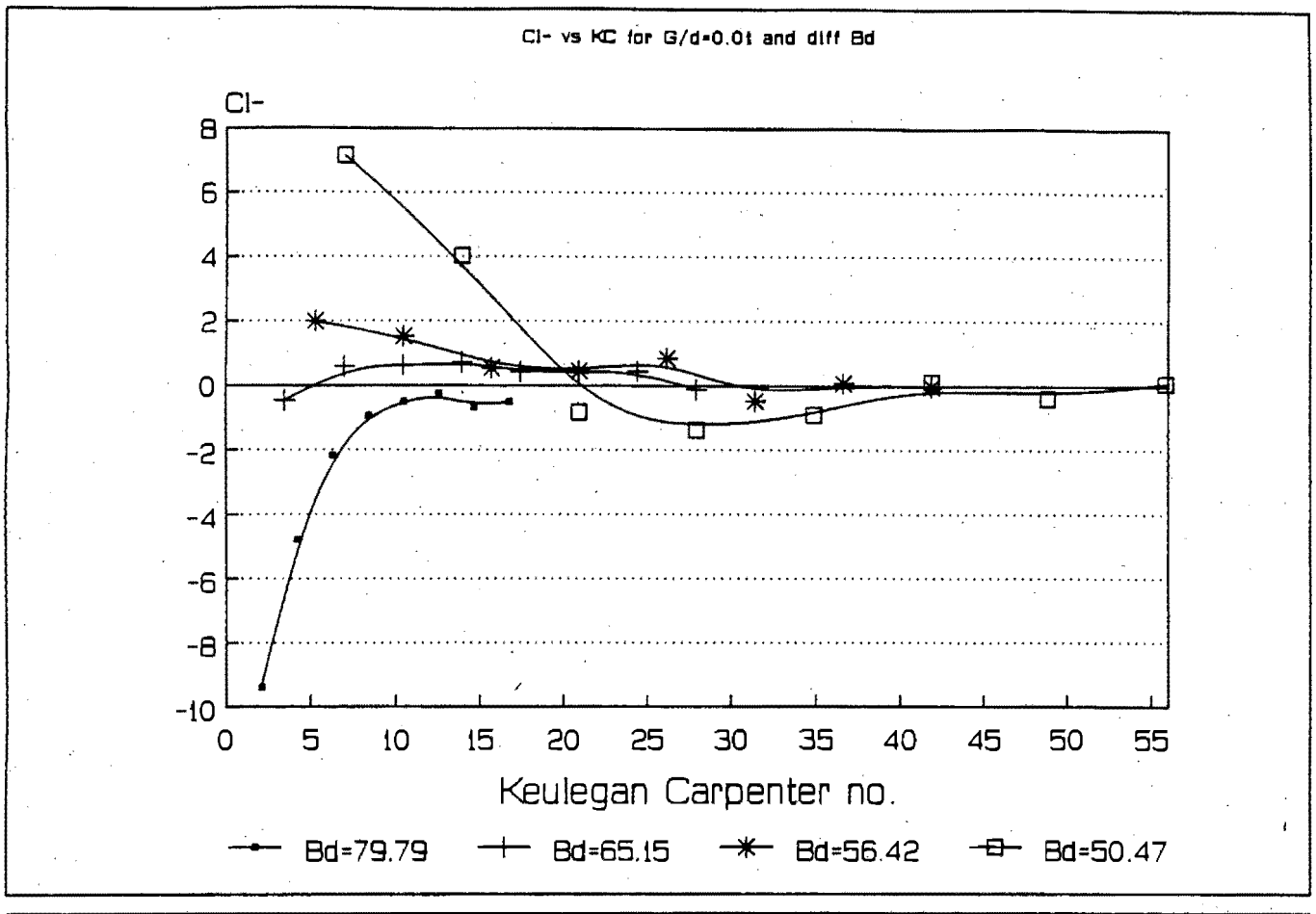

Figure I-69 : Cl- vs KC for diameter=90mm, G/d=.01 and different Bd.

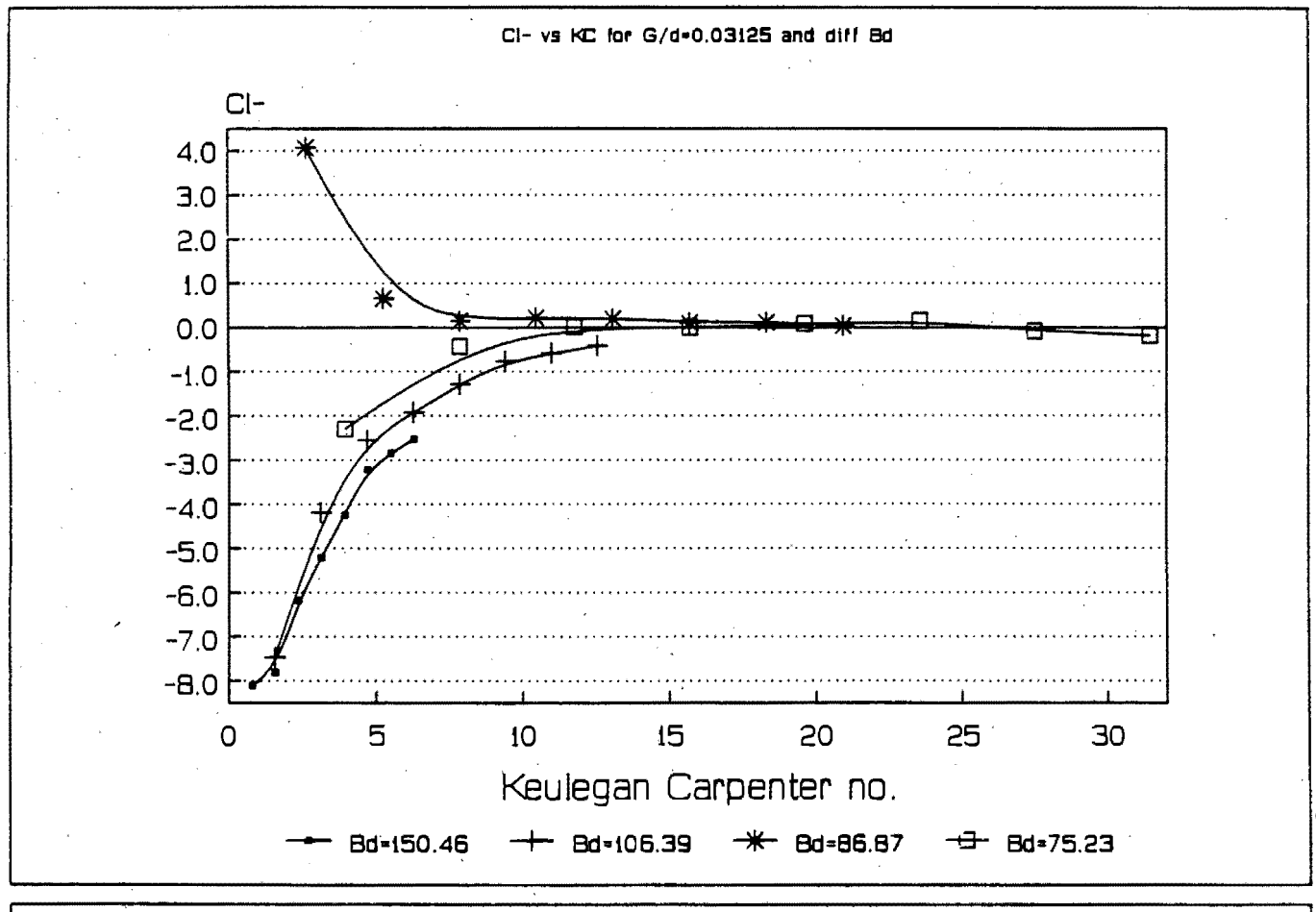

Figure I-70 : Cl- vs KC for diameter=120mm, G/d=.03125 and different Bd.

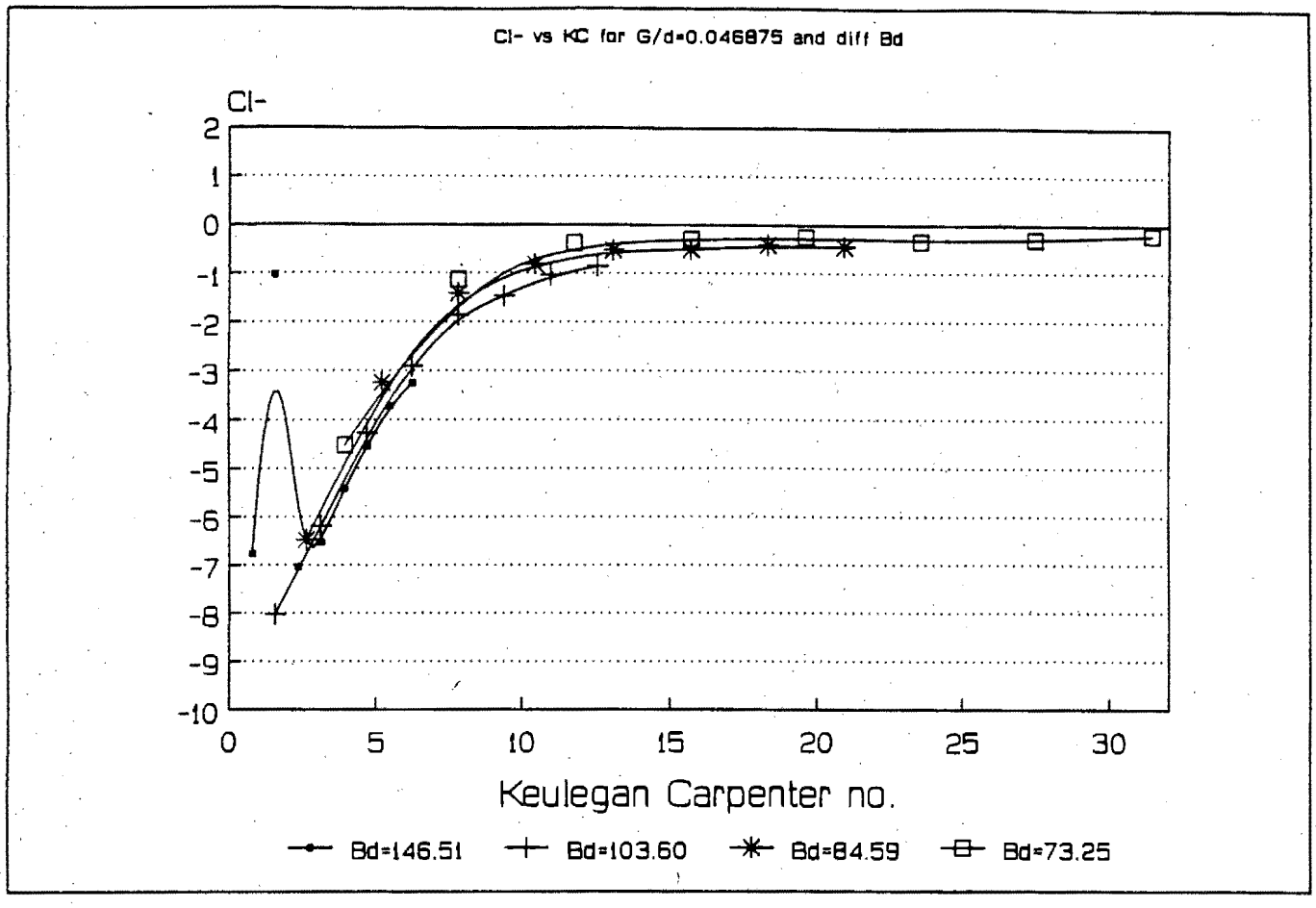

Figure I-71 : Cl- vs KC for diameter=120mm, G/d=.046875 and different Bd.

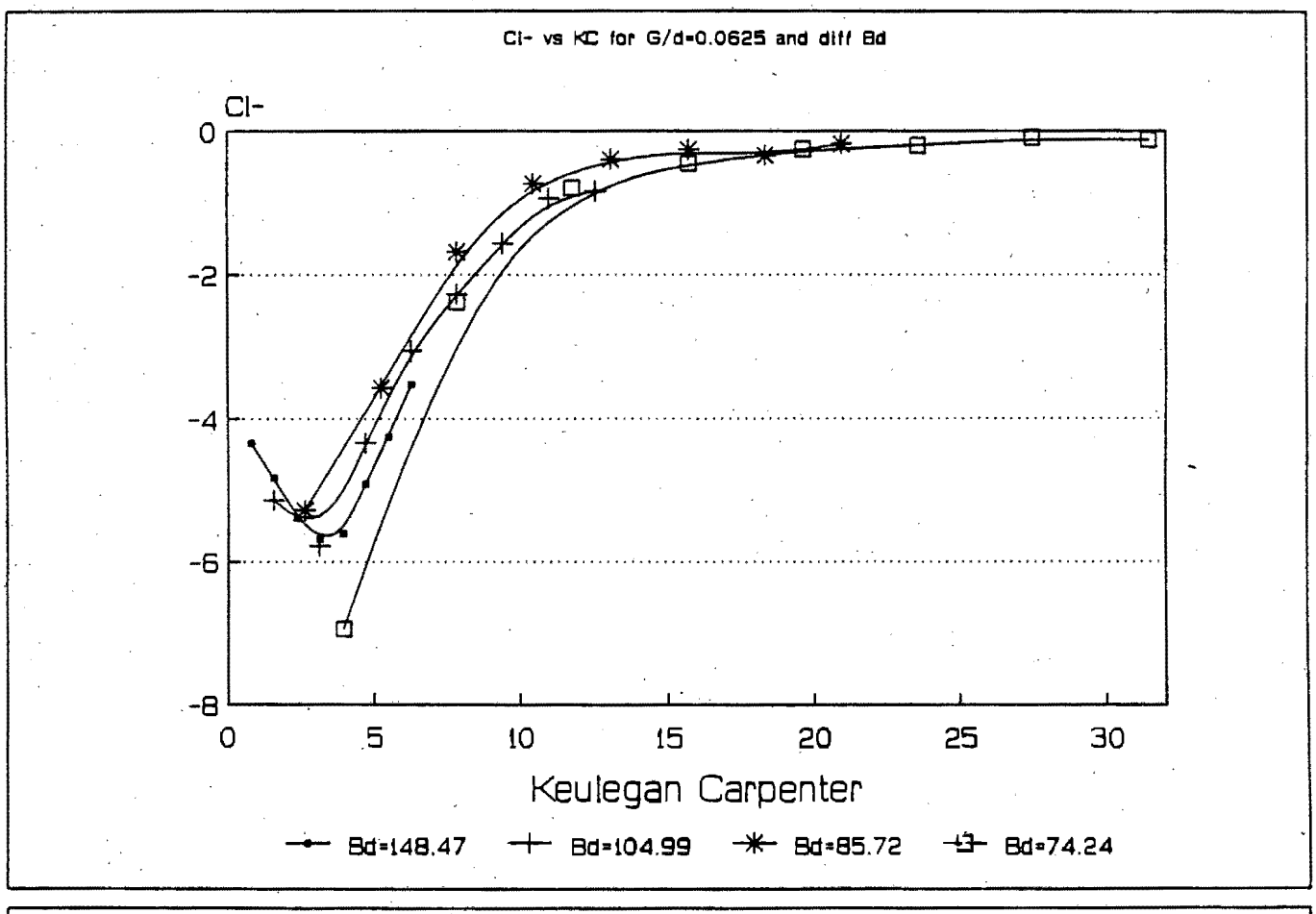

Figure I-72 : Cl- vs KC for diameter=120mm, G/d=.0625 and different Bd.

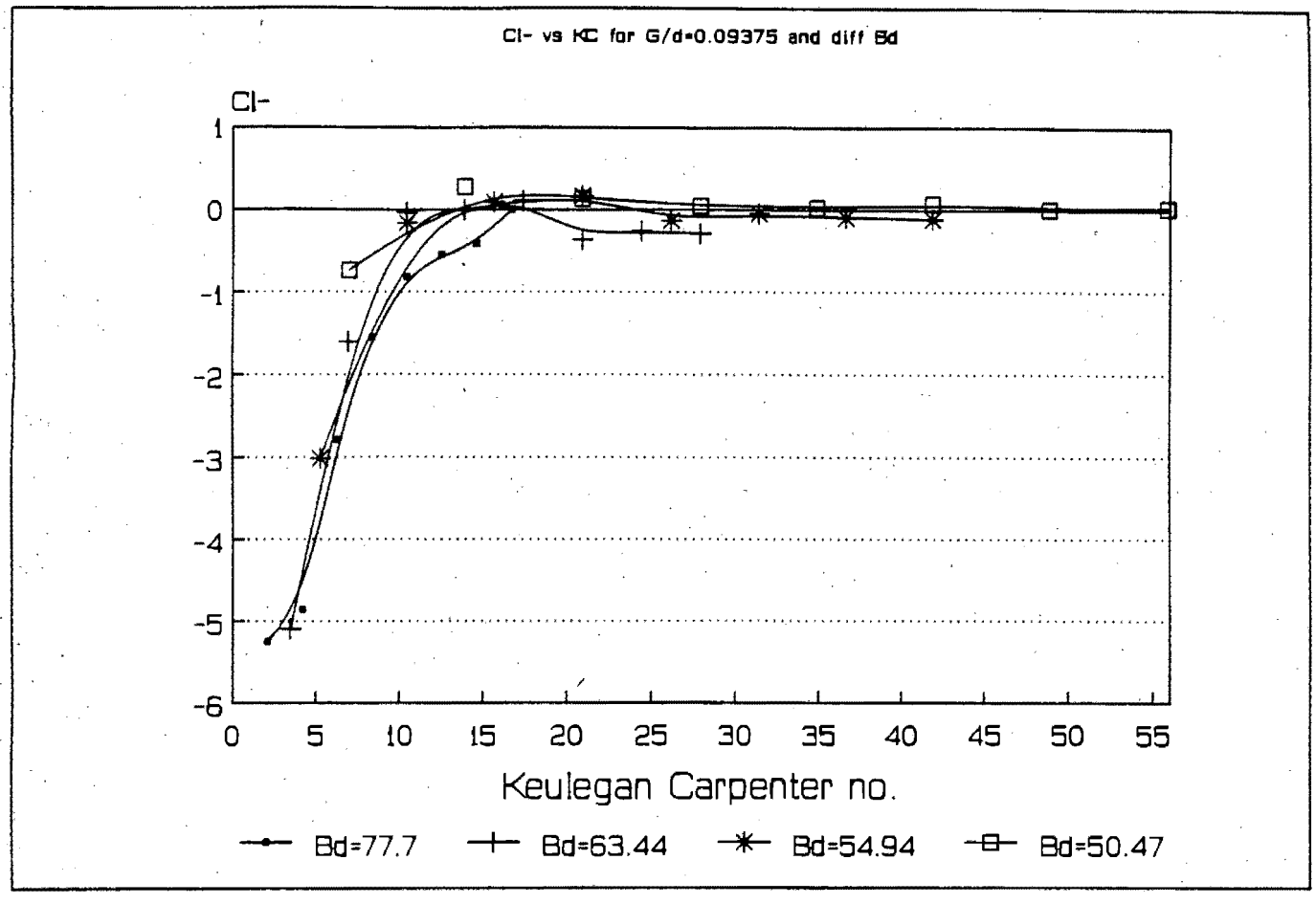

Figure I-73 : Cl- vs KC for diameter=90mm, G/d=.09375 and different Bd.

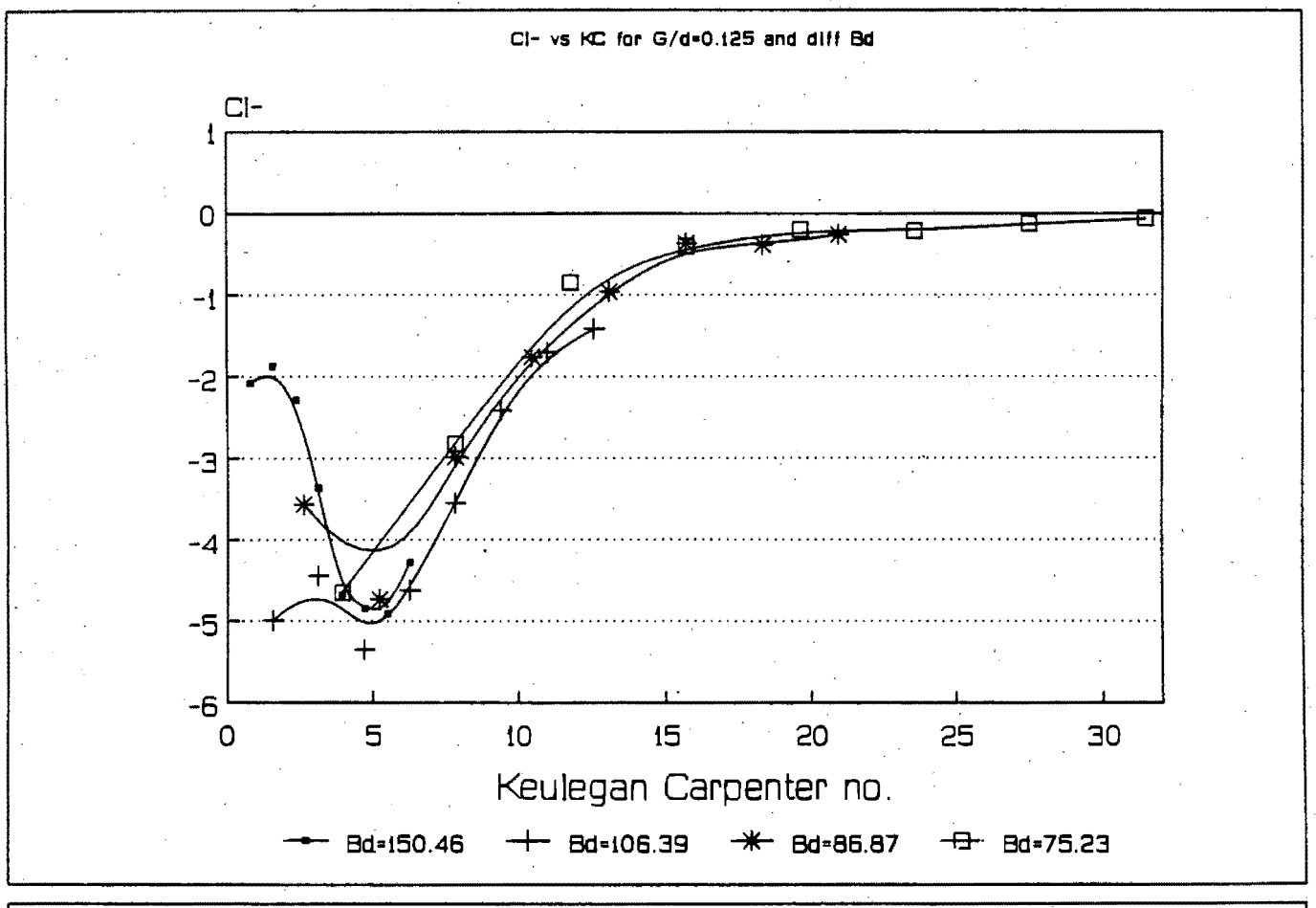

Figure I-74 : Cl- vs KC for diameter=120mm, G/d=.125 and different Bd.

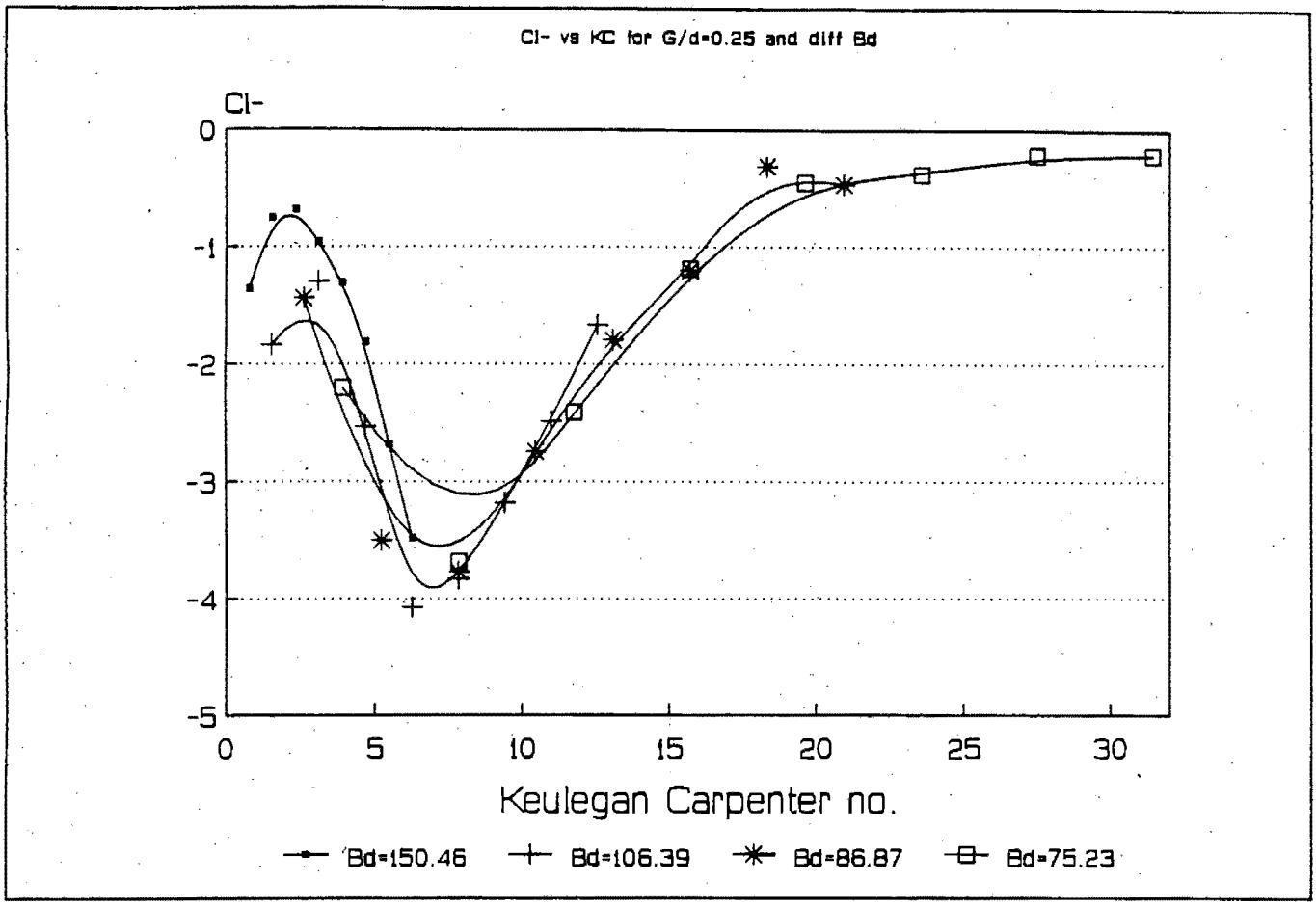

Figure I-75 : Cl- vs KC for diameter=120mm, G/d=.25 and different Bd.

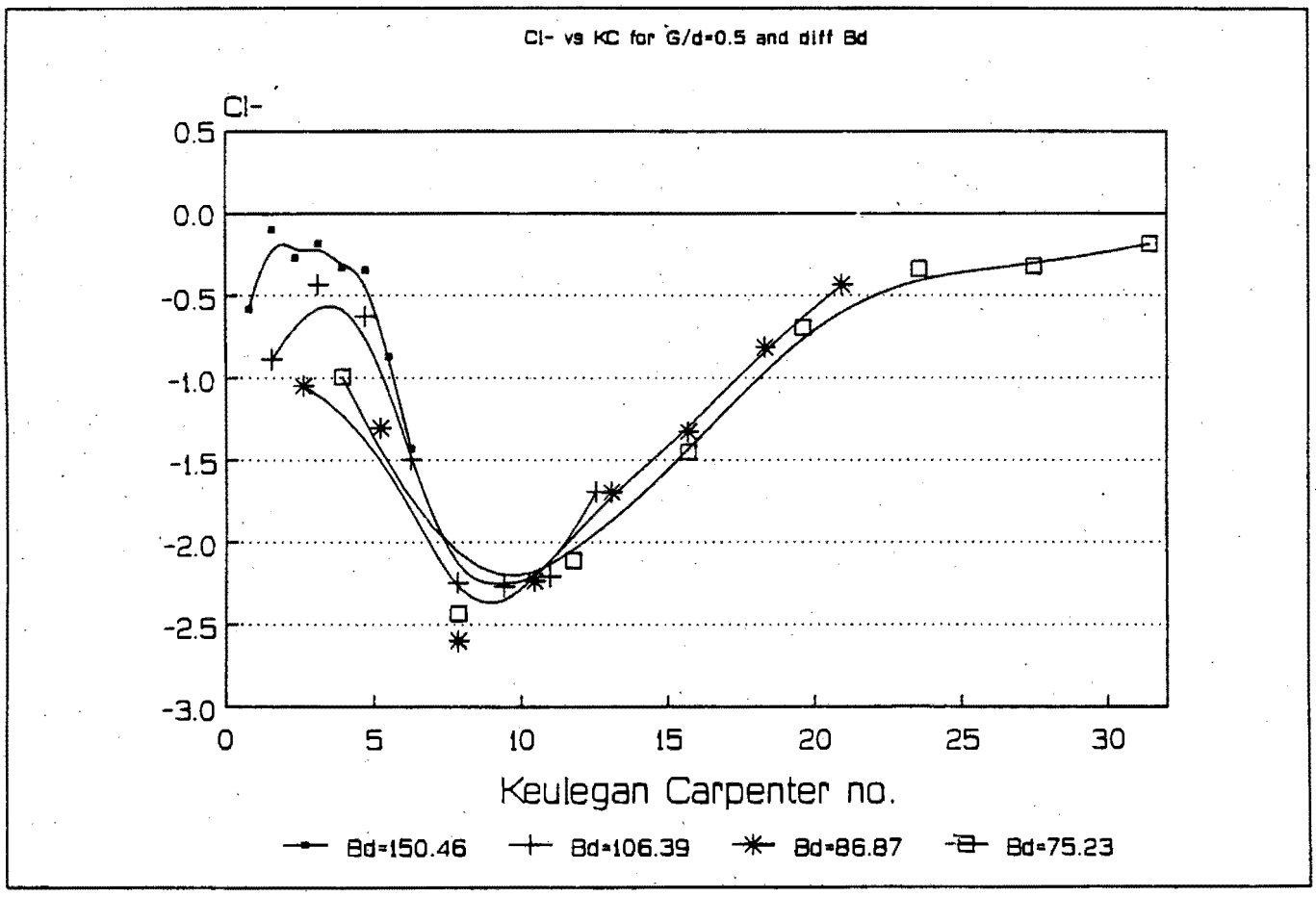

Figure I-76 : Cl- vs KC for diameter=120mm, G/d=.5 and different Bd.

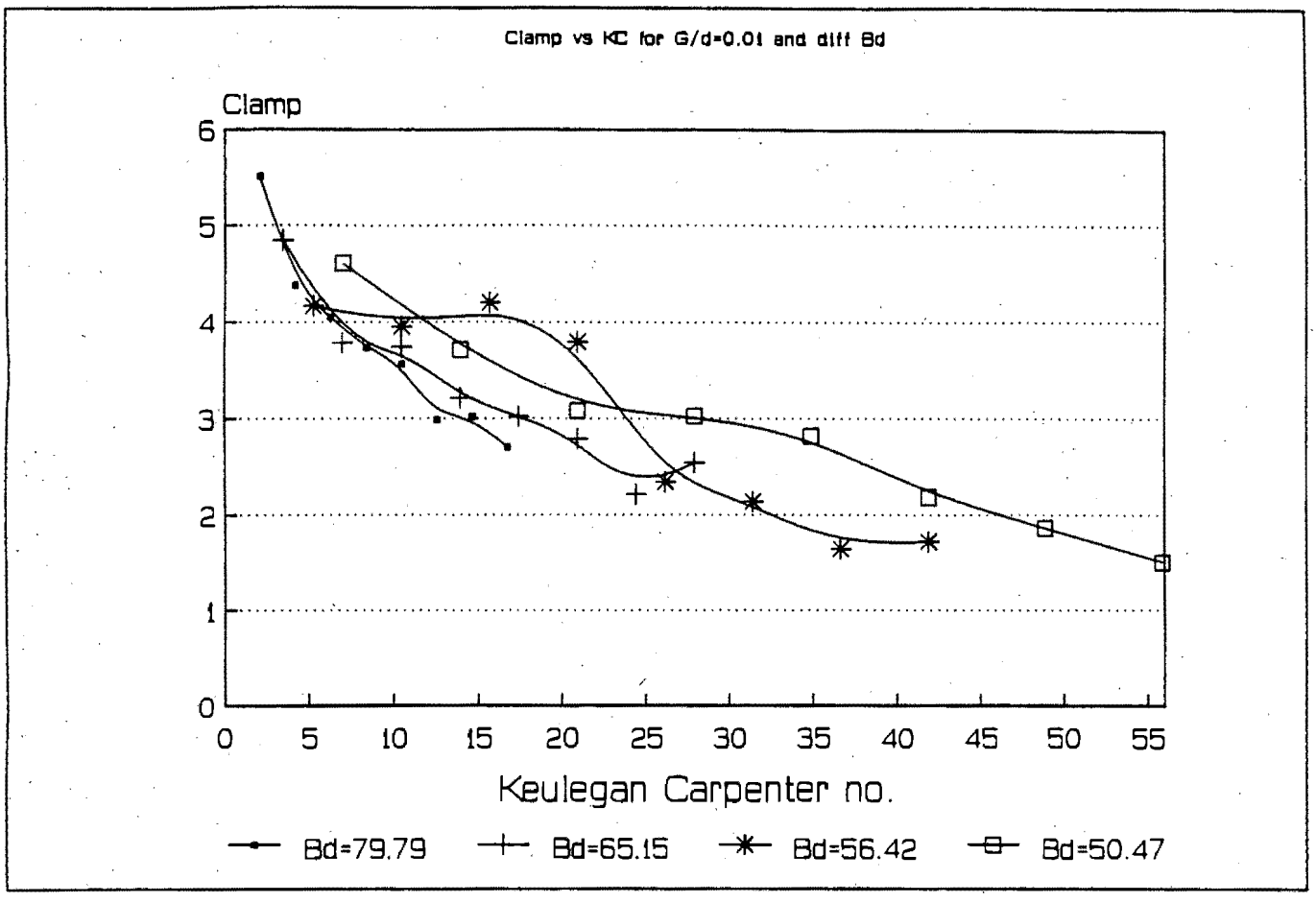

Figure I-77 : Clamp vs KC for diameter=90mm, G/d=.01 and different Bd.

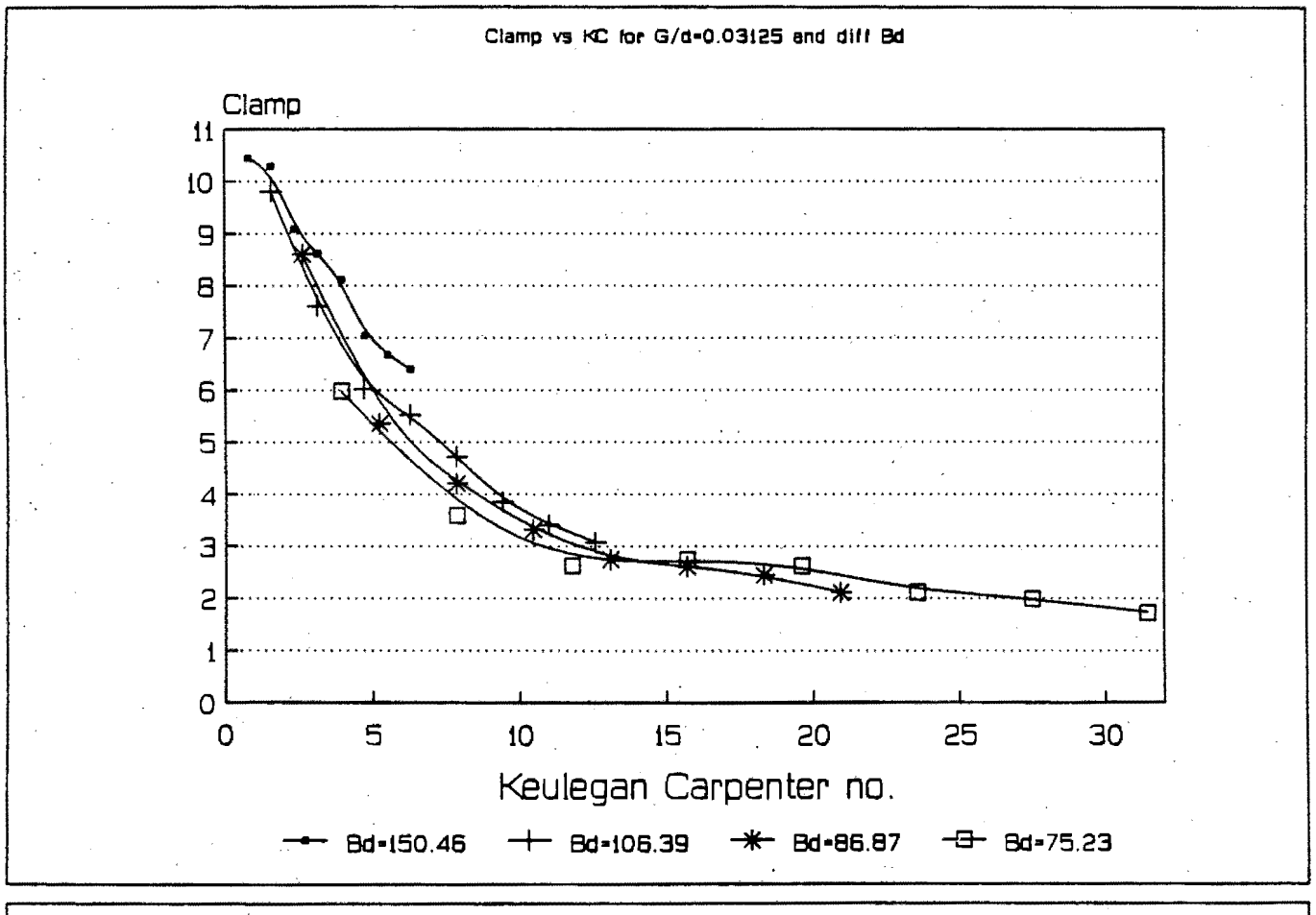

Figure I-78 : Clamp vs KC for diameter=120mm, G/d=.03125 and different Bd.

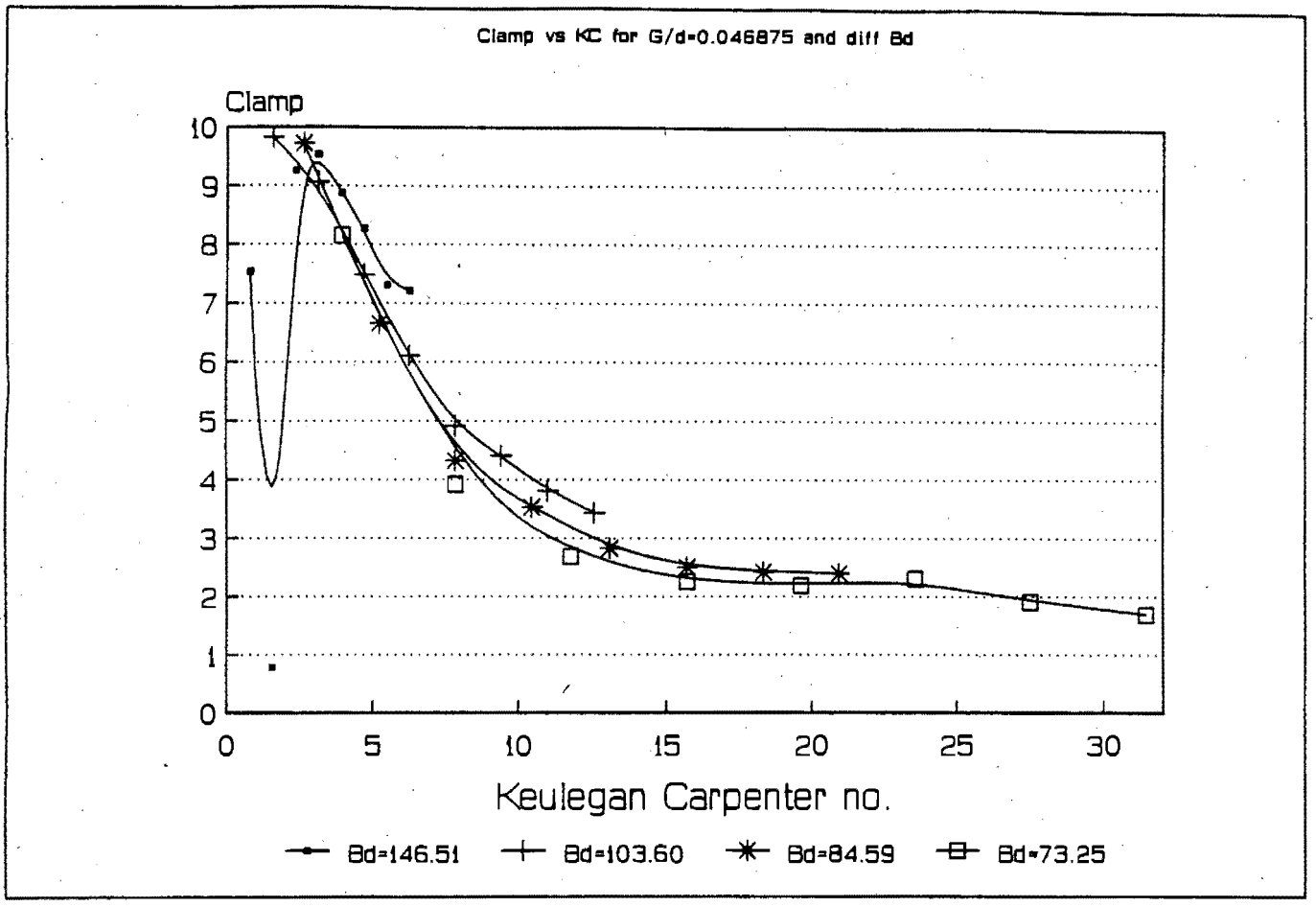

Figure I-79 : Clamp vs KC for diameter=120mm, G/d=.046875 and different Bd.

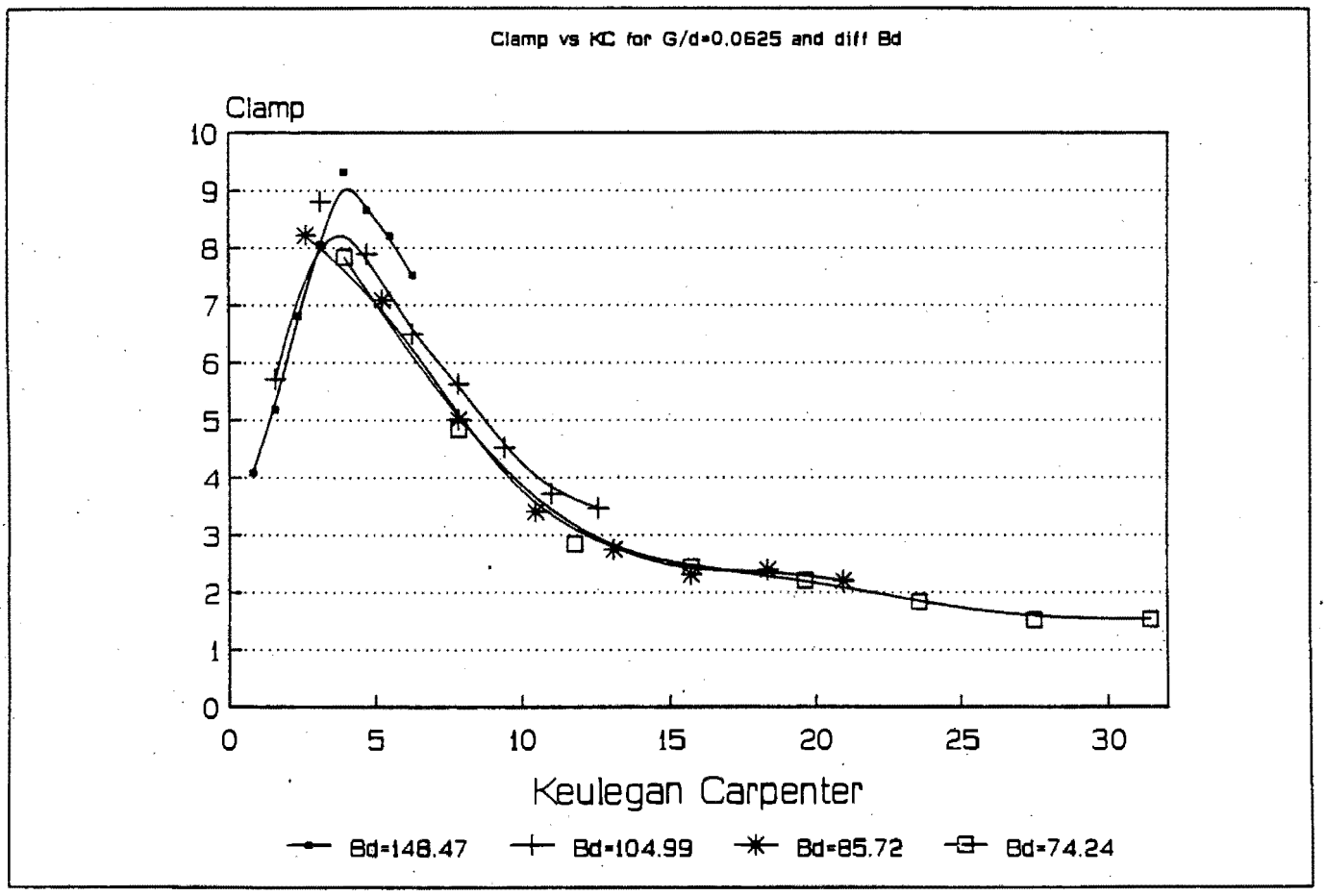

Figure I-80 : Clamp vs KC for diameter=120mm, G/d=.0625 and different Bd.

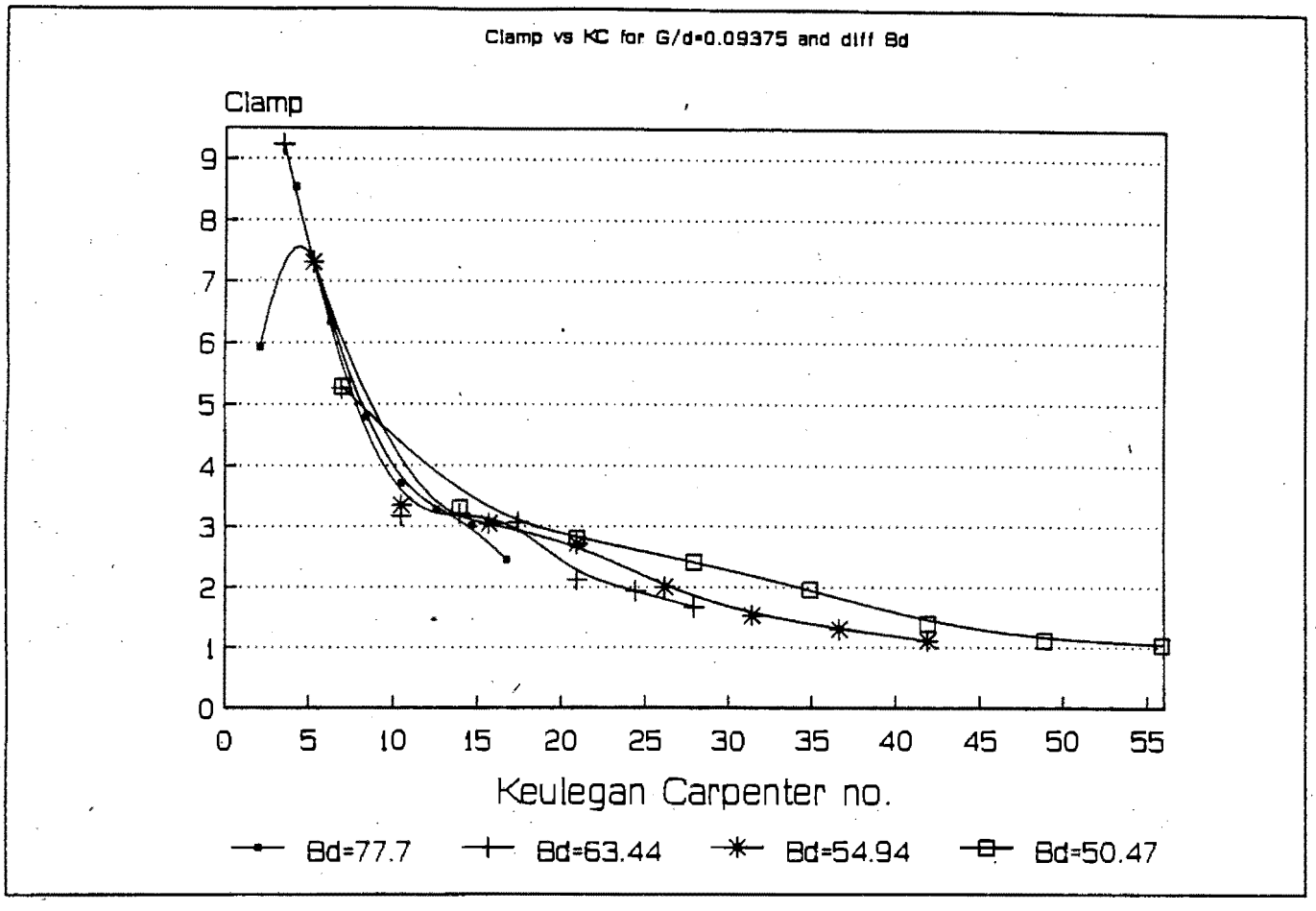

Figure I-81 : Clamp vs KC for diameter=90mm, G/d=.09375 and different Bd.

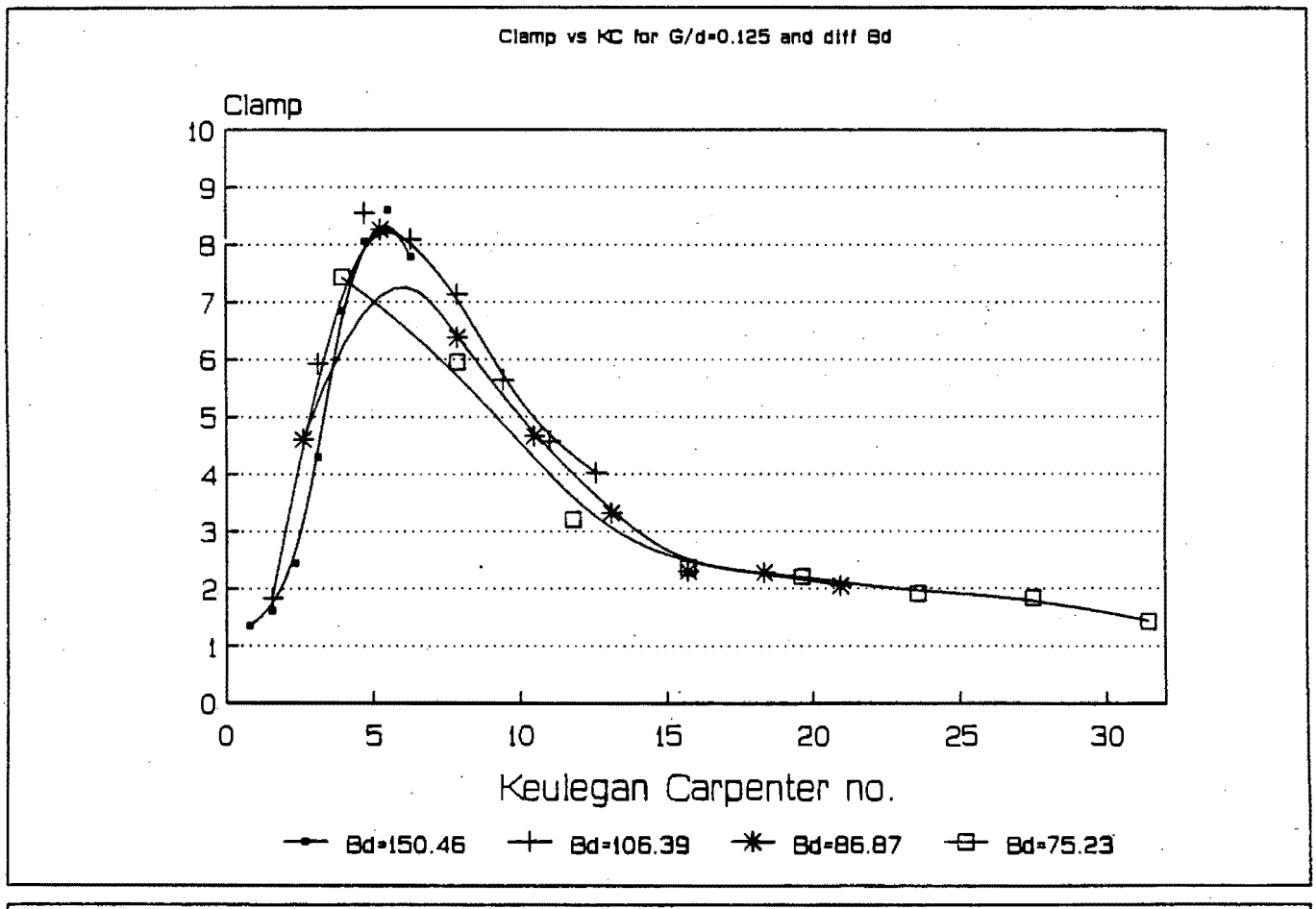

Figure I-82 : Clamp vs KC for diameter=120mm, G/d=.125 and different Bd.

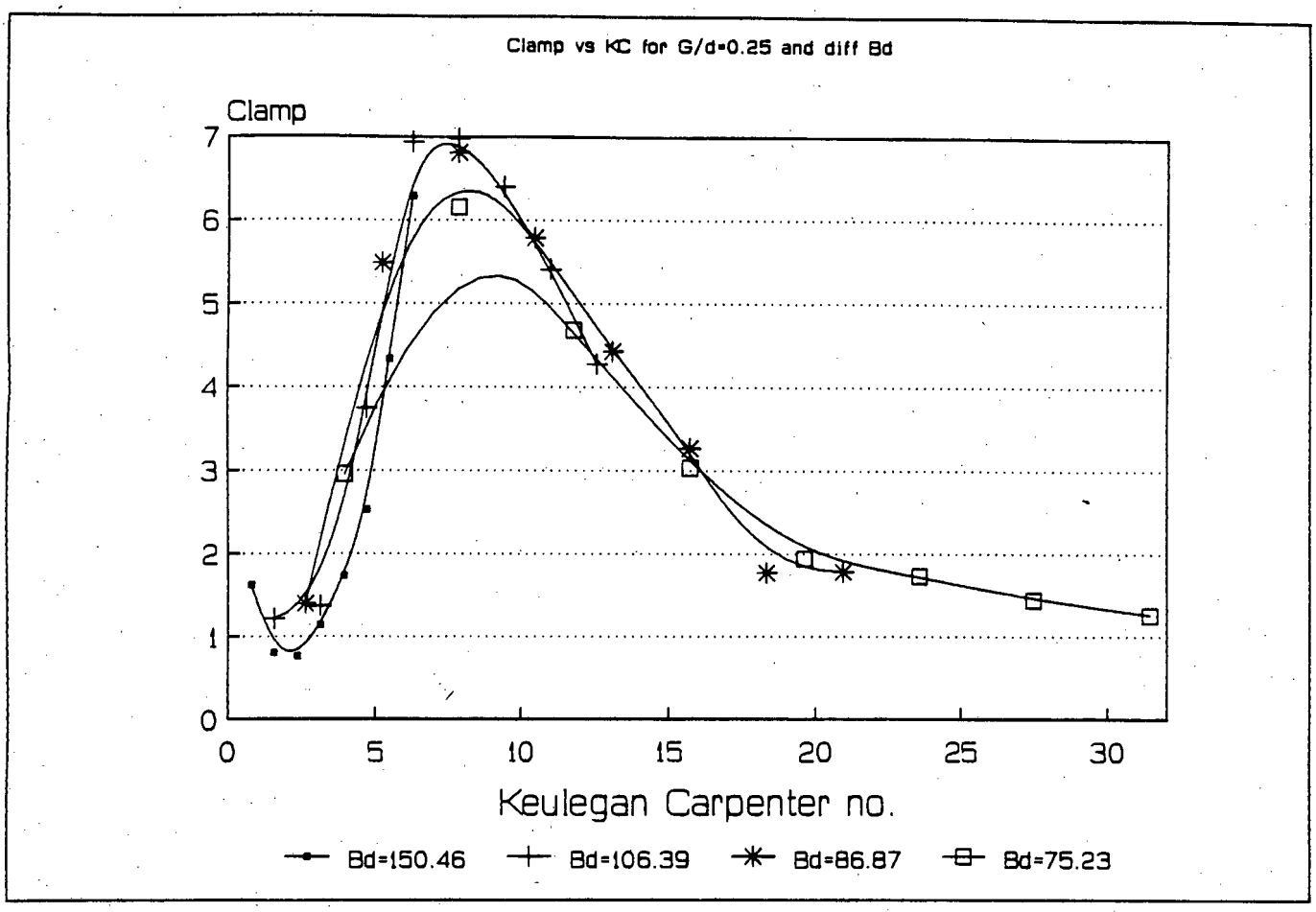

Figure I-83 : Clamp vs KC for diameter=120mm, G/d=.25 and different Bd.

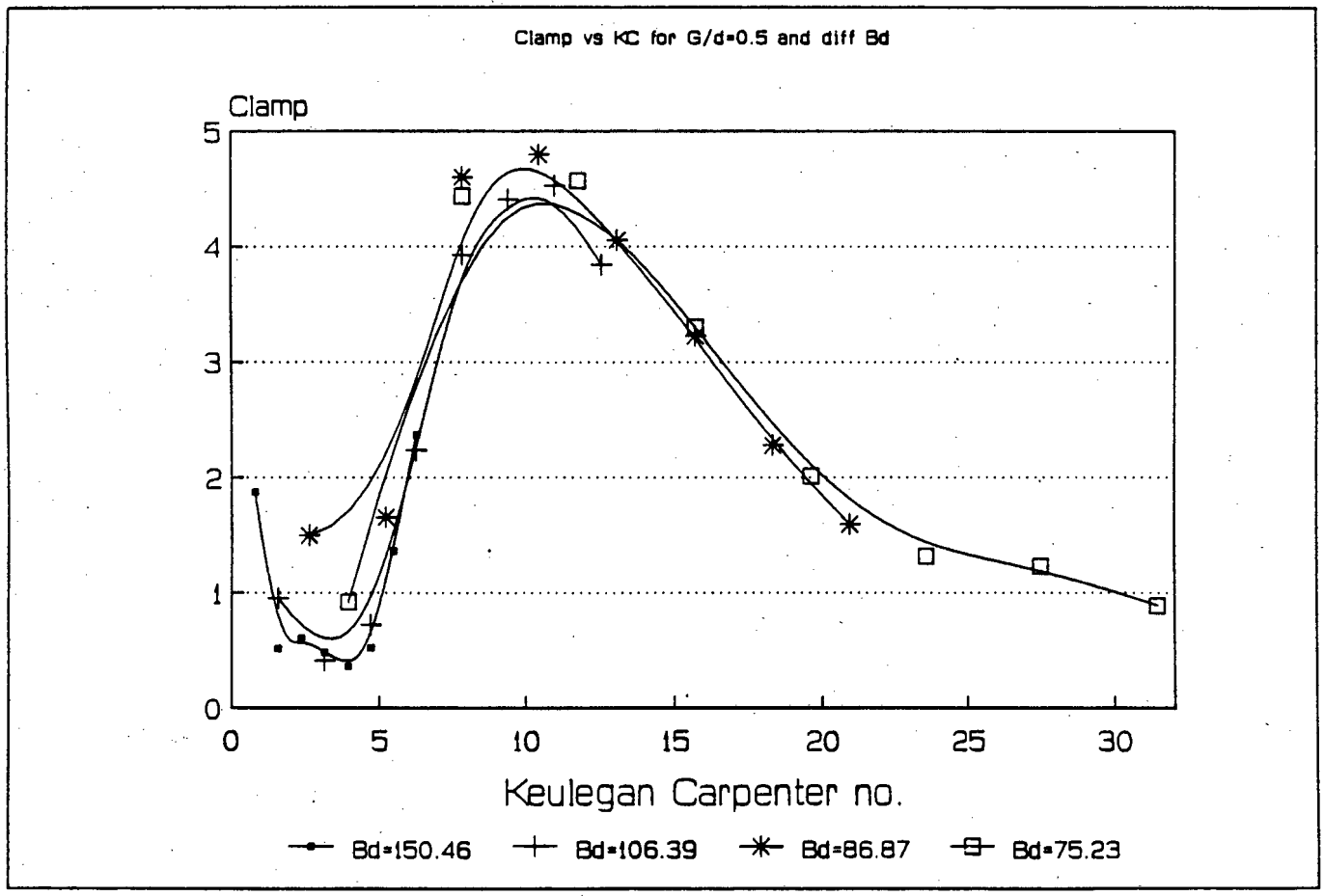

Figure I-84 : Clamp vs KC for diameter=120mm, G/d=.5 and different Bd.

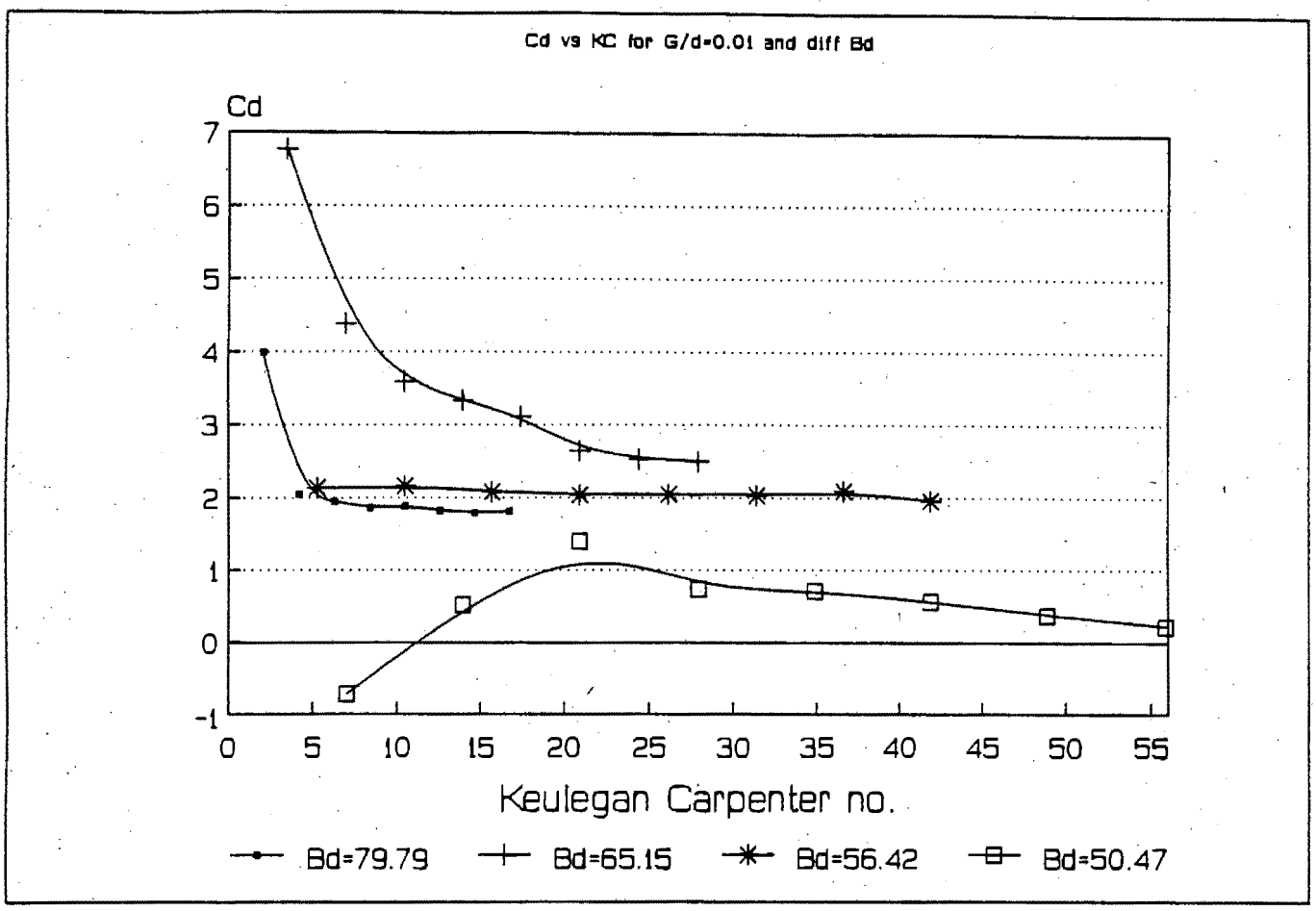

Figure I-85 : Cd vs KC for diameter=90mm, G/d=.01 and different Bd.

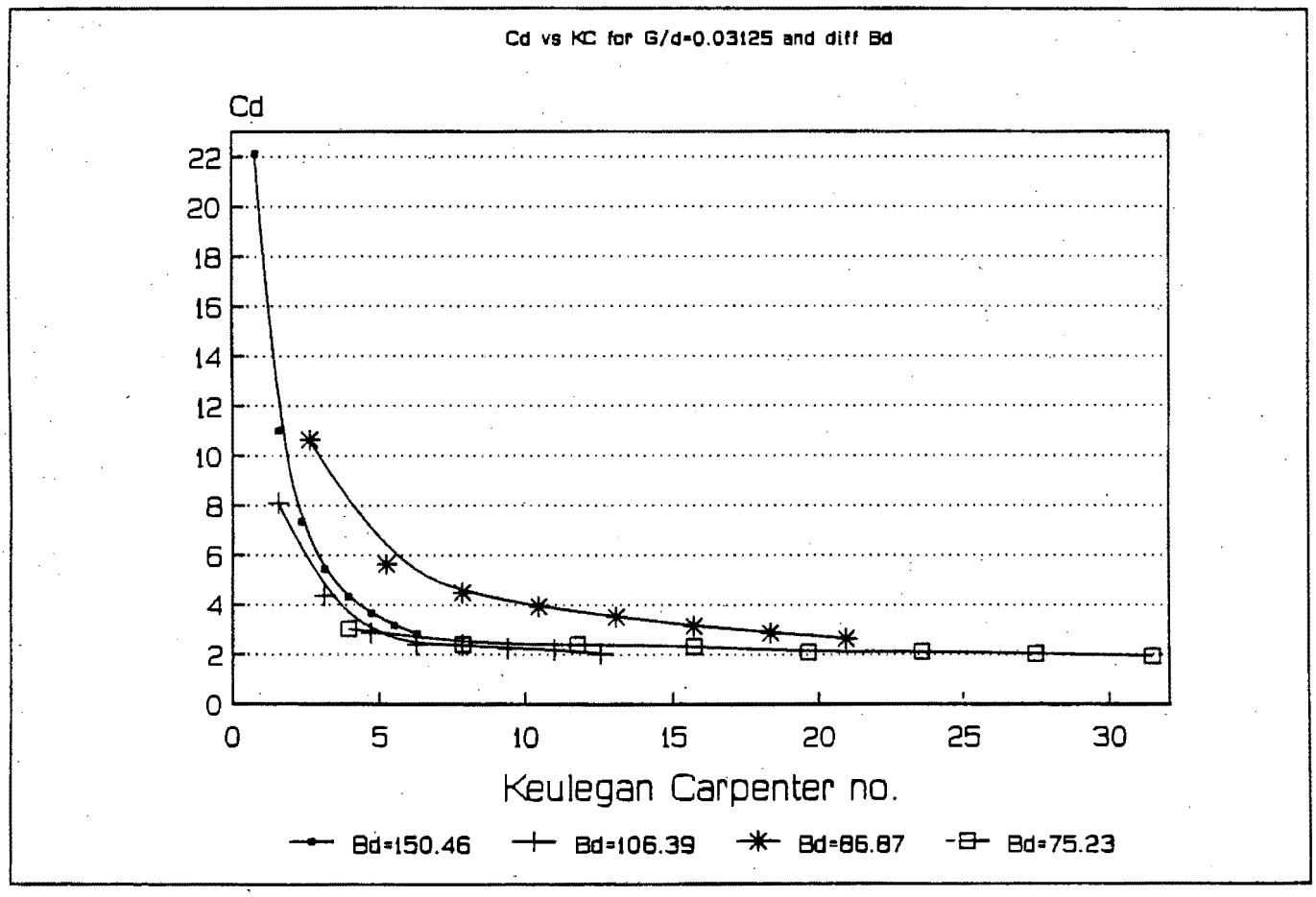

Figure I-86 : Cd vs KC for diameter=120mm, G/d=.03125 and different Bd.

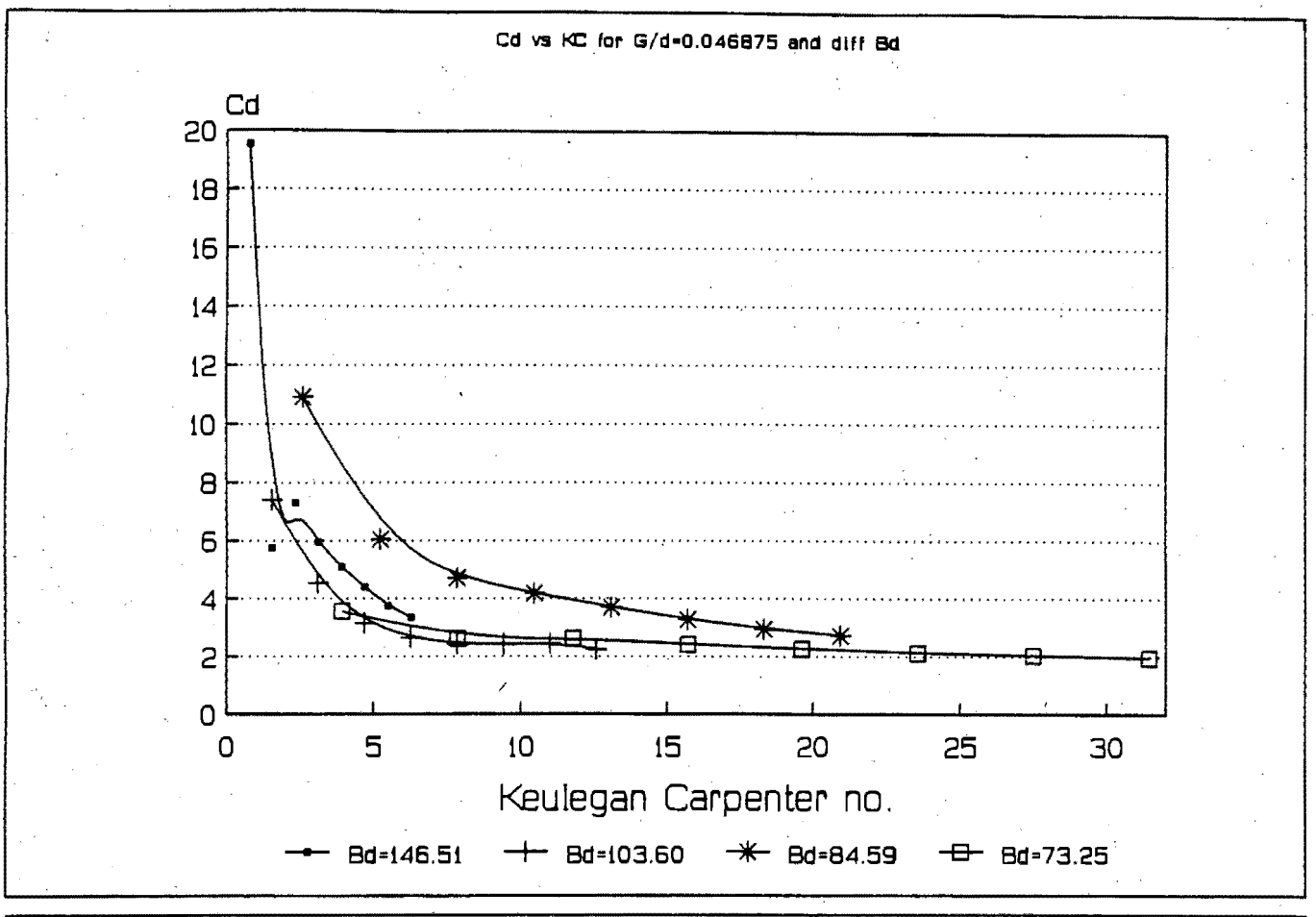

Figure I-87 : Cd vs KC for diameter=120mm, G/d=.046875 and different Bd.

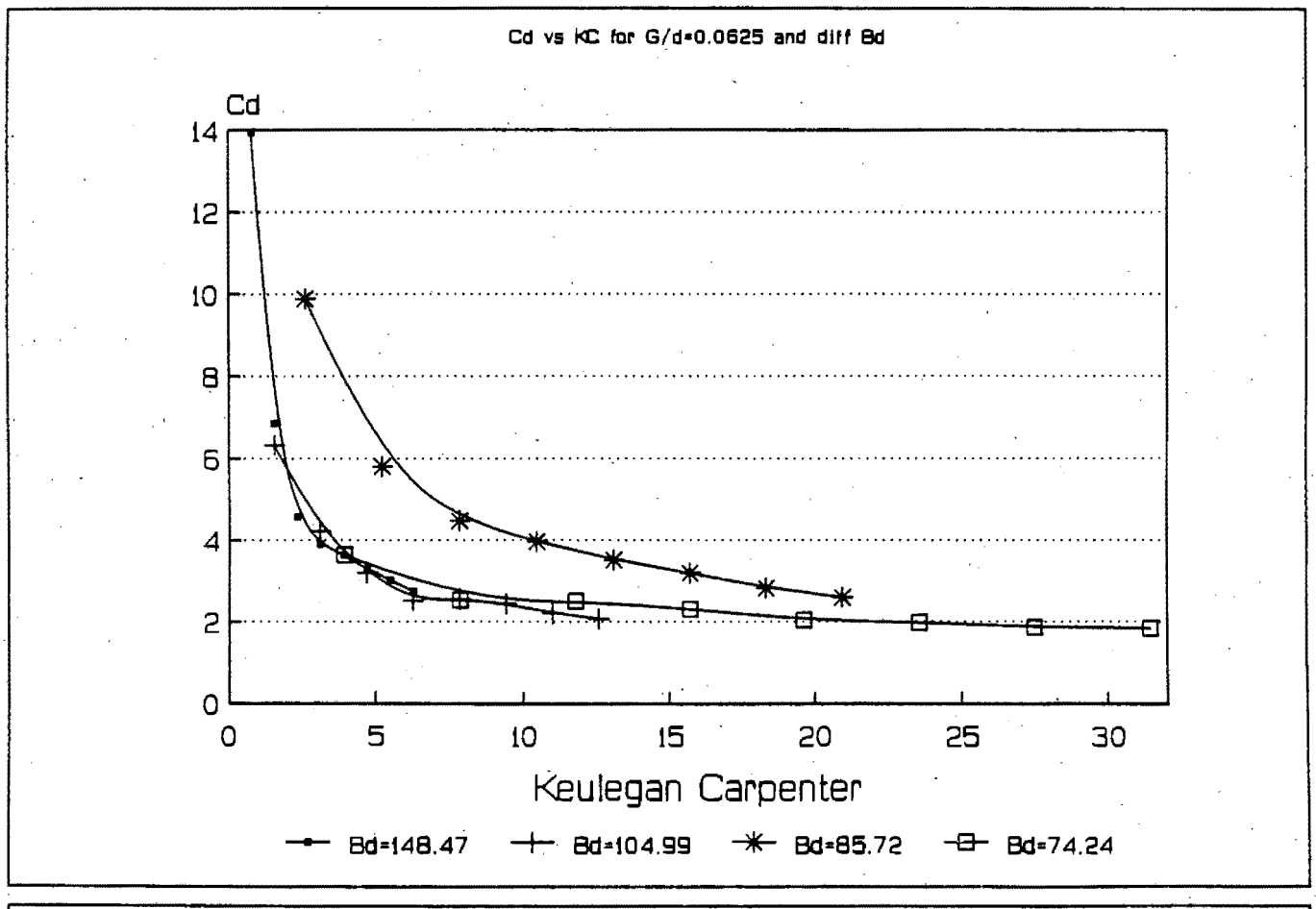

Figure I-88 : Cd vs KC for diameter=120mm, G/d=.0625 and different Bd.

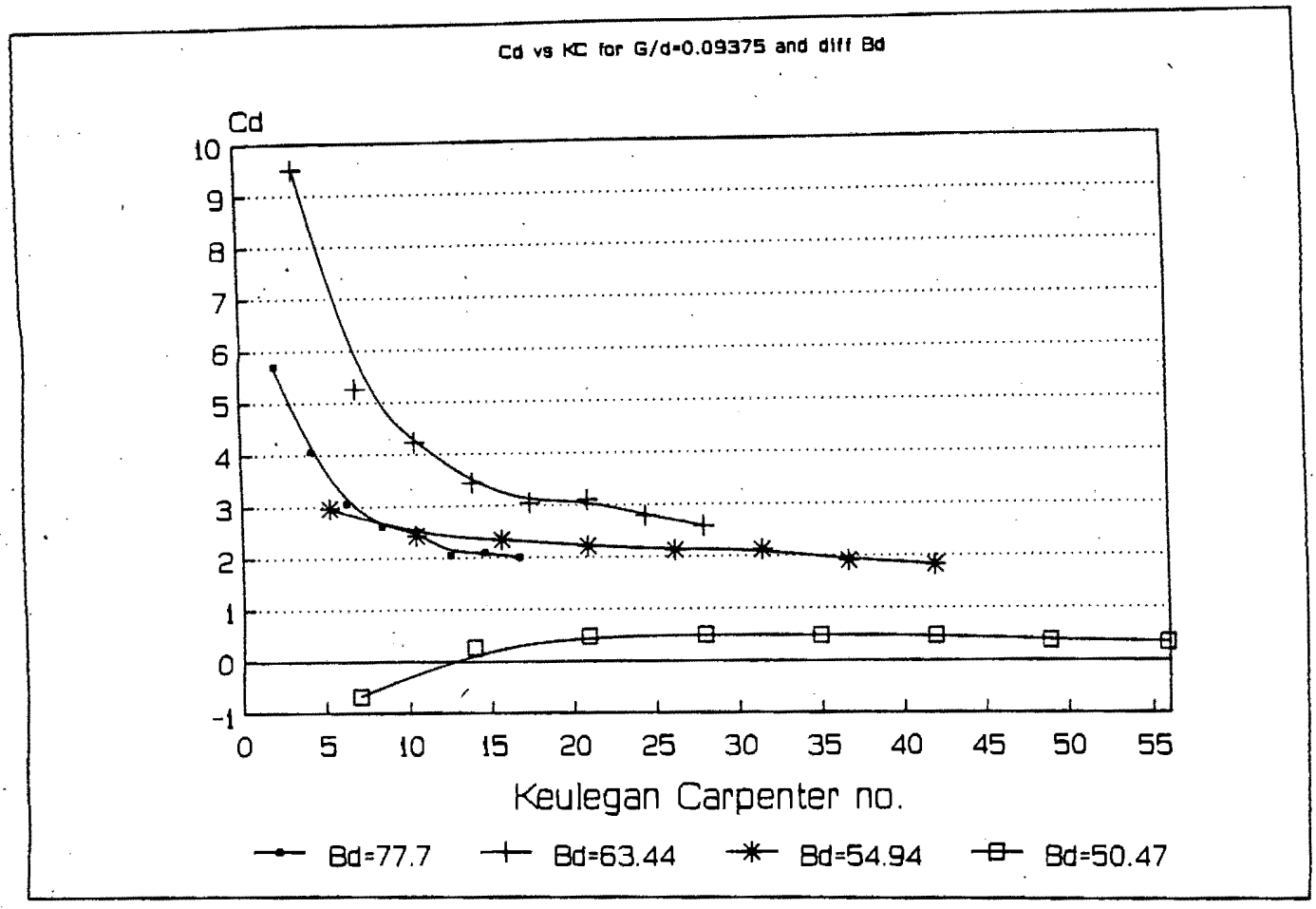

Figure I-89 : Cd vs KC for diameter=90mm, G/d=.09375 and different Bd.

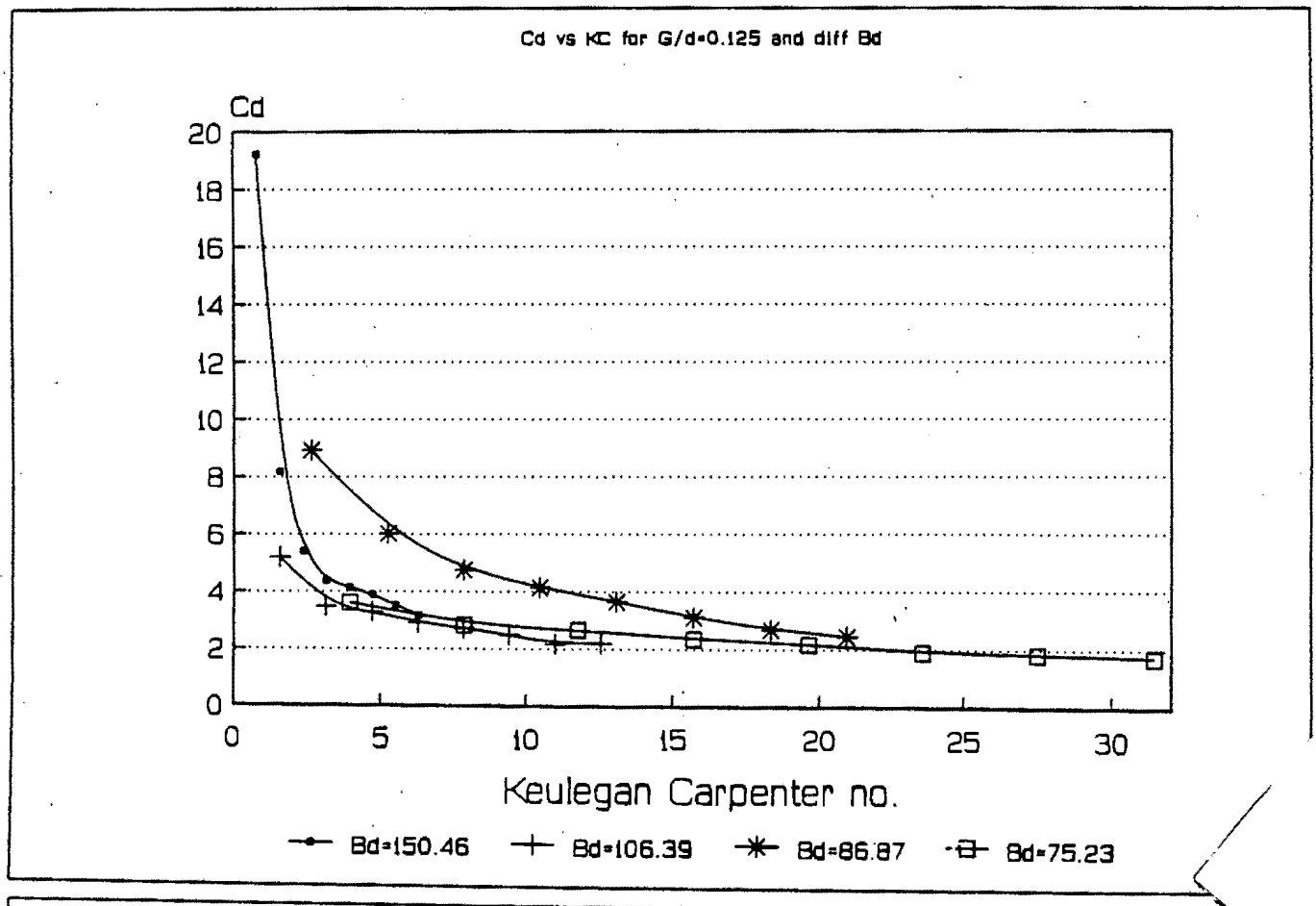

Figure I-90 : Cd vs KC for diameter=120mm, G/d=.125 and different Bd.

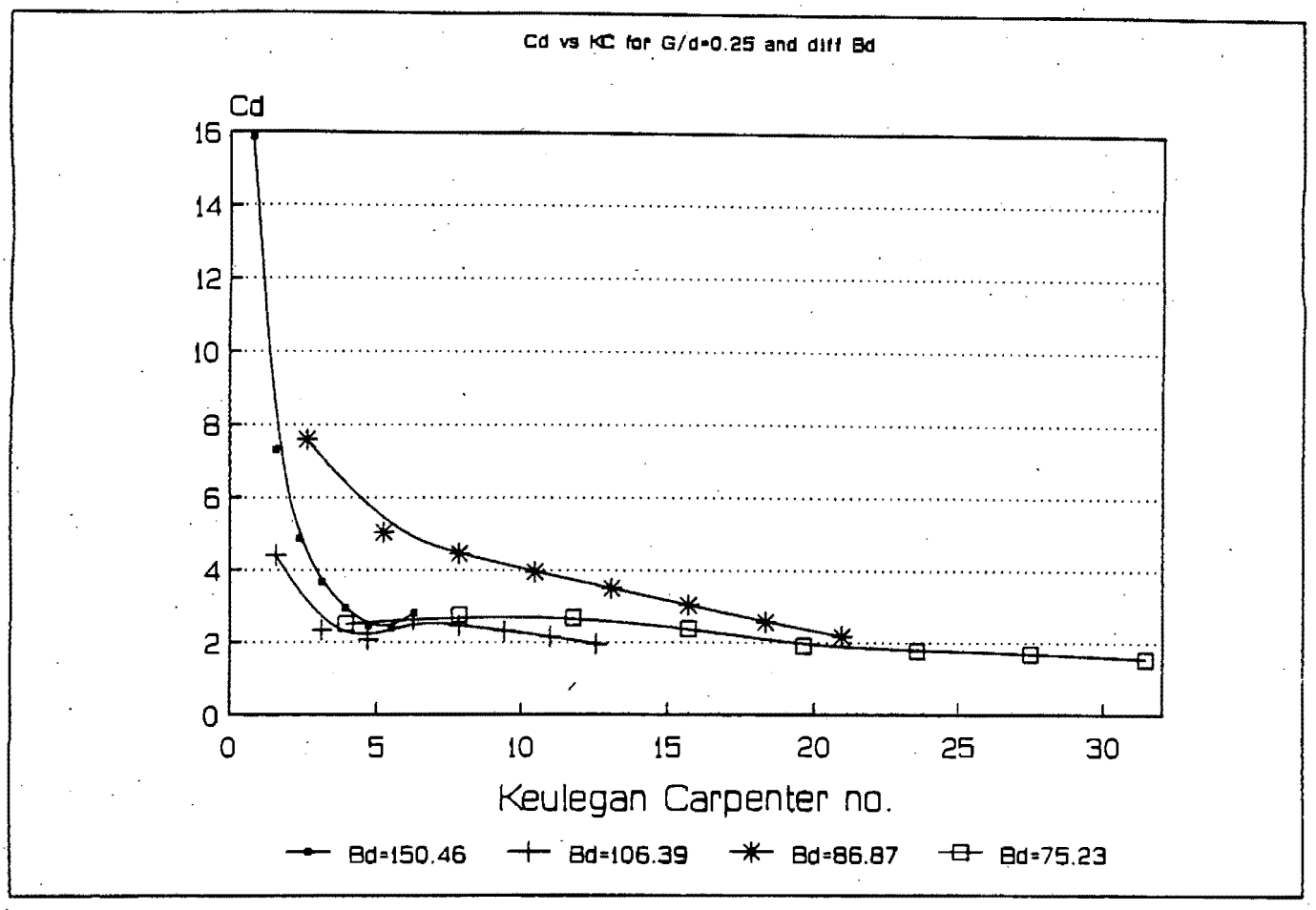

Figure I-91 : Cd vs KC for diameter=120mm, G/d=.25 and different Bd.

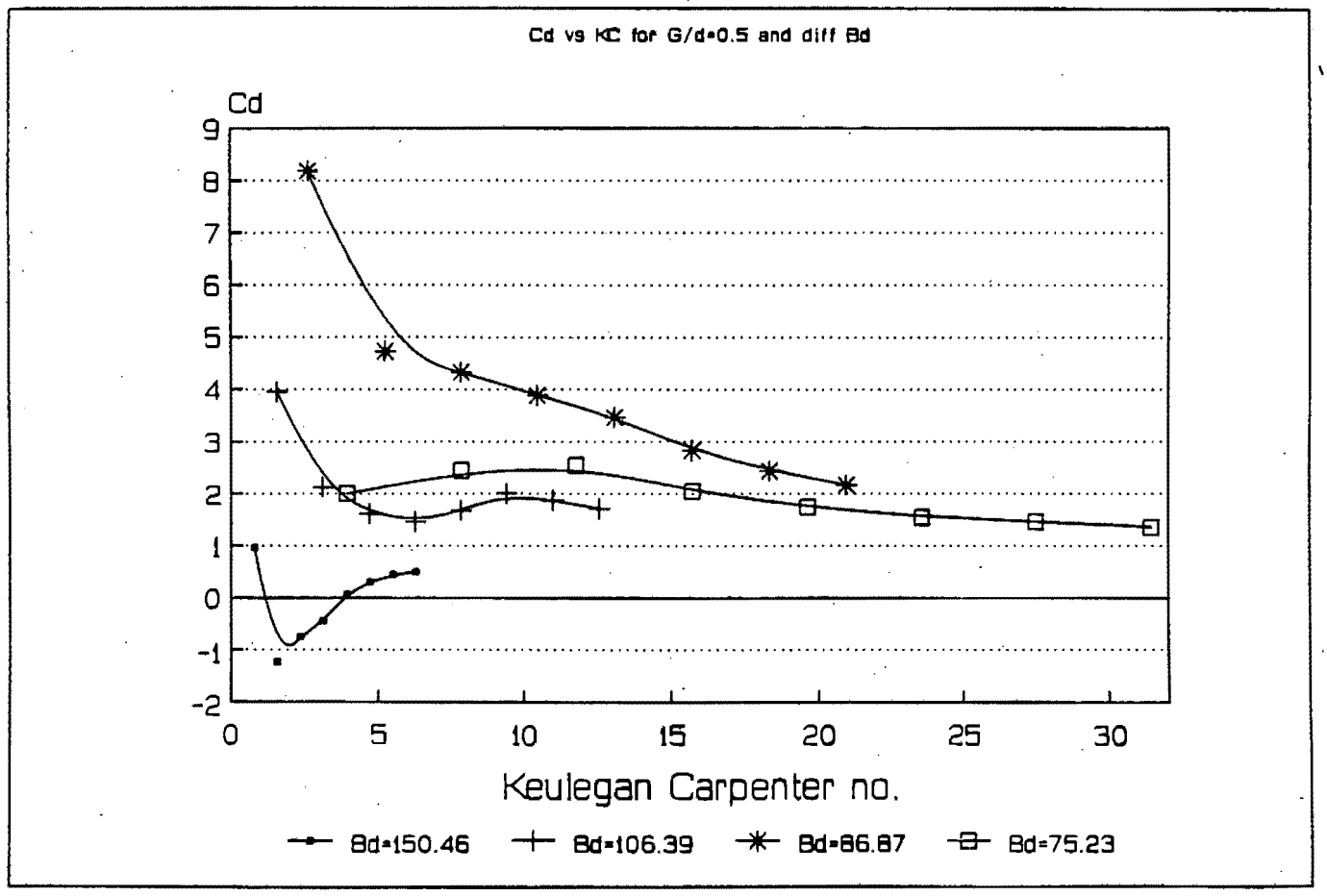

Figure I-92 : Cd vs KC for diameter=120mm, G/d=.5 and different Bd.

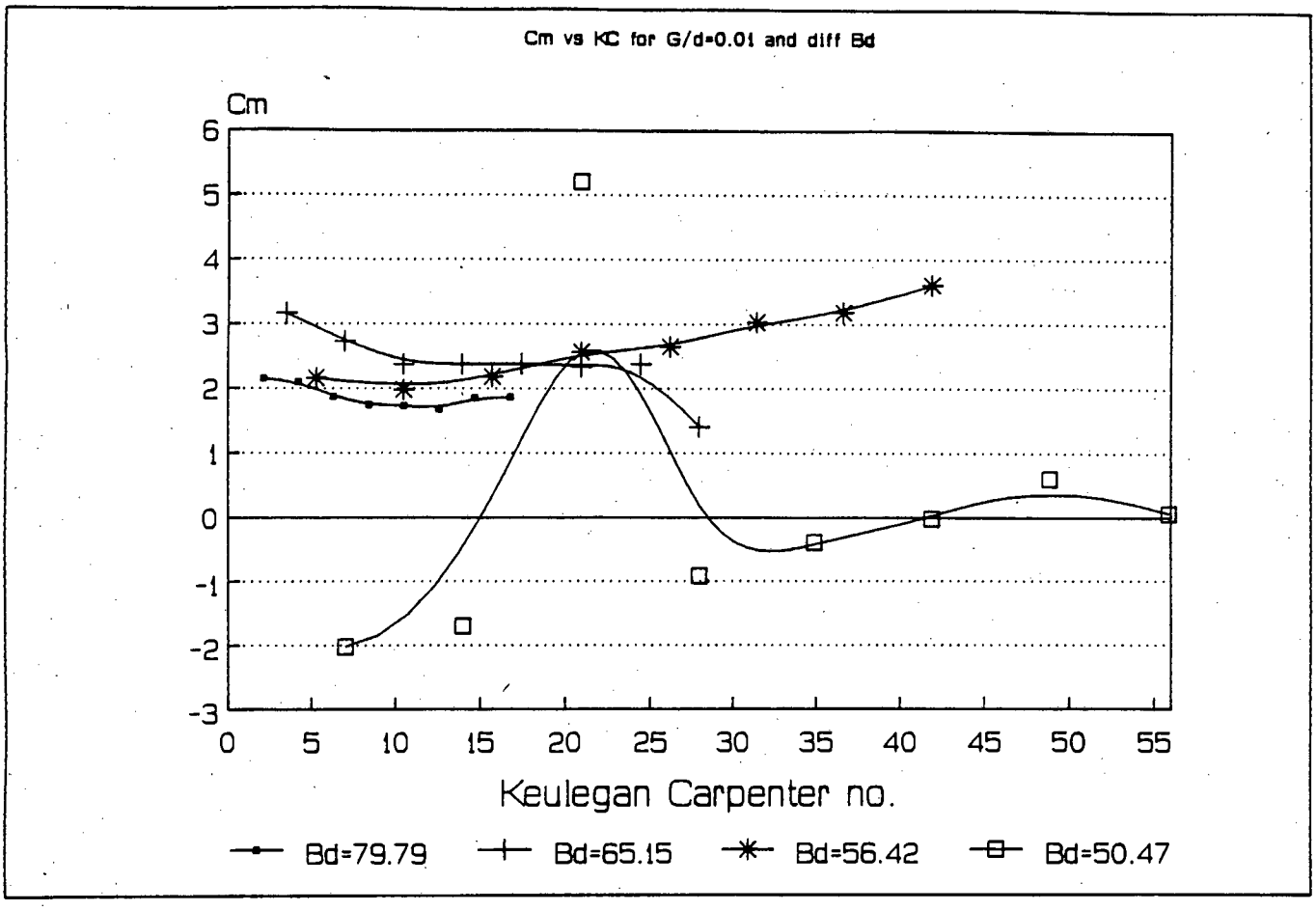

Figure I-93 : Cm vs KC for diameter=90mm, G/d=.01 and different Bd.

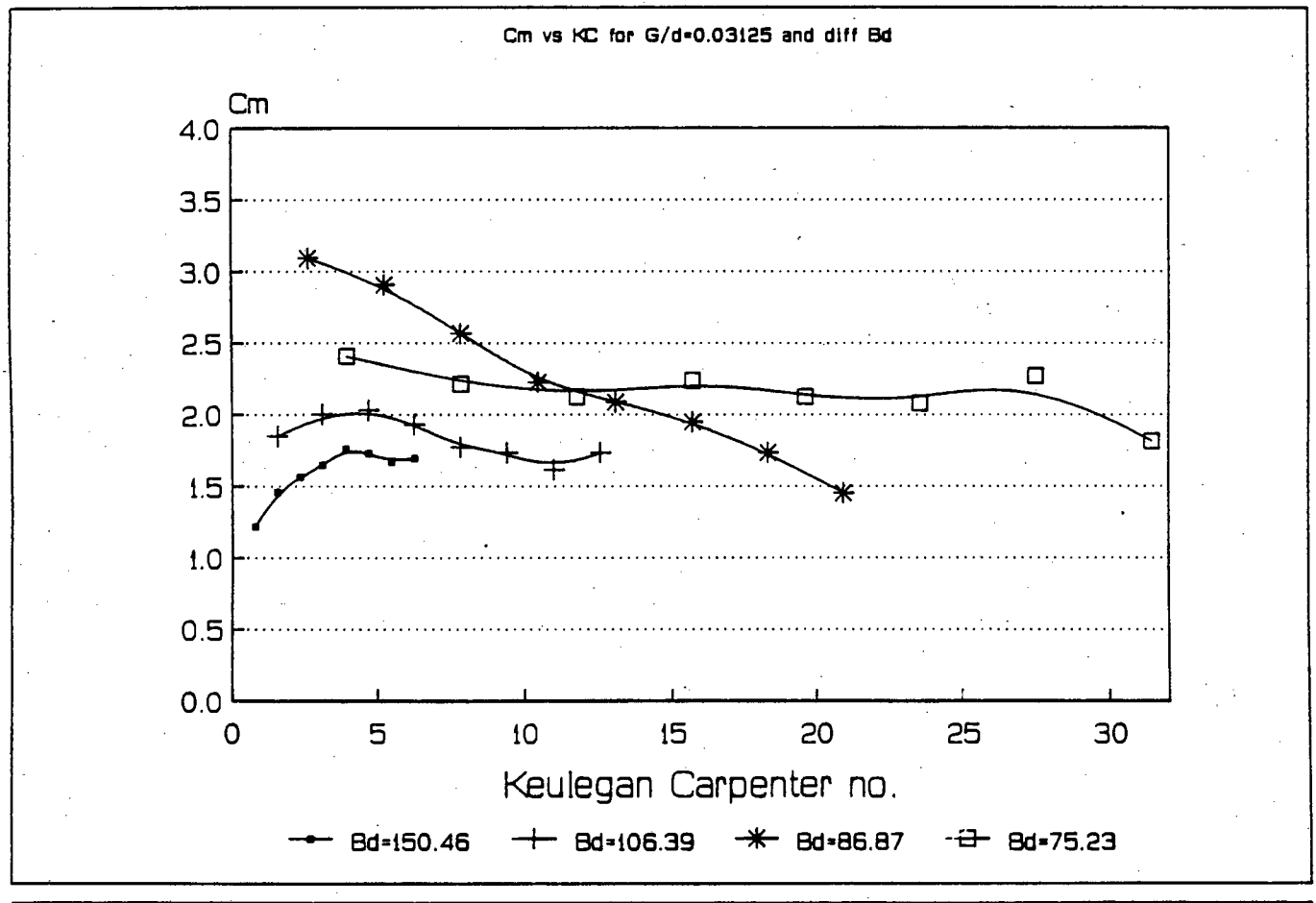

Figure I-94 : Cm vs KC for diameter=120mm, G/d=.03125 and different Bd.

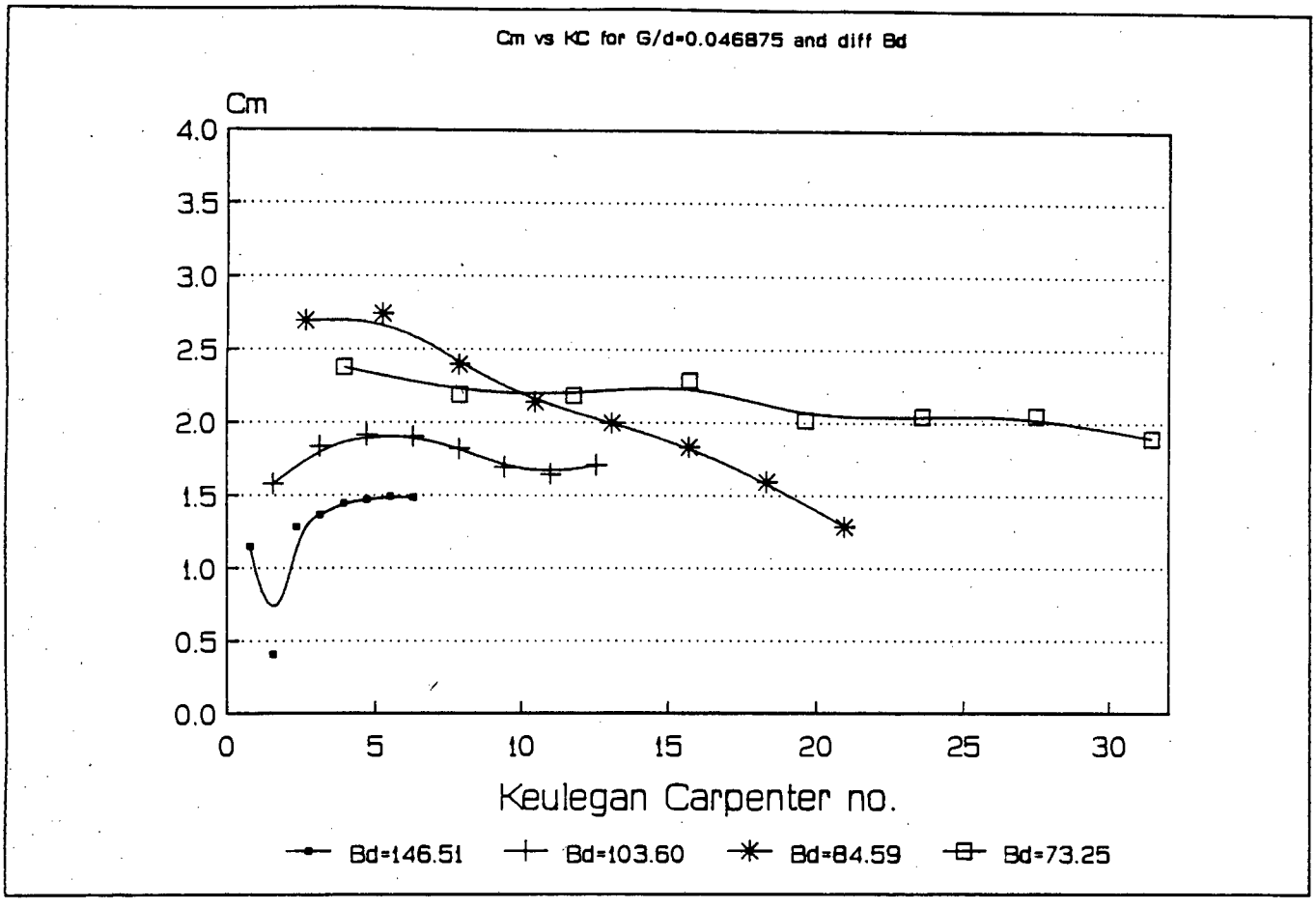

Figure I-95 : Cm vs KC for diameter=120mm, G/d=.046875 and different Bd.

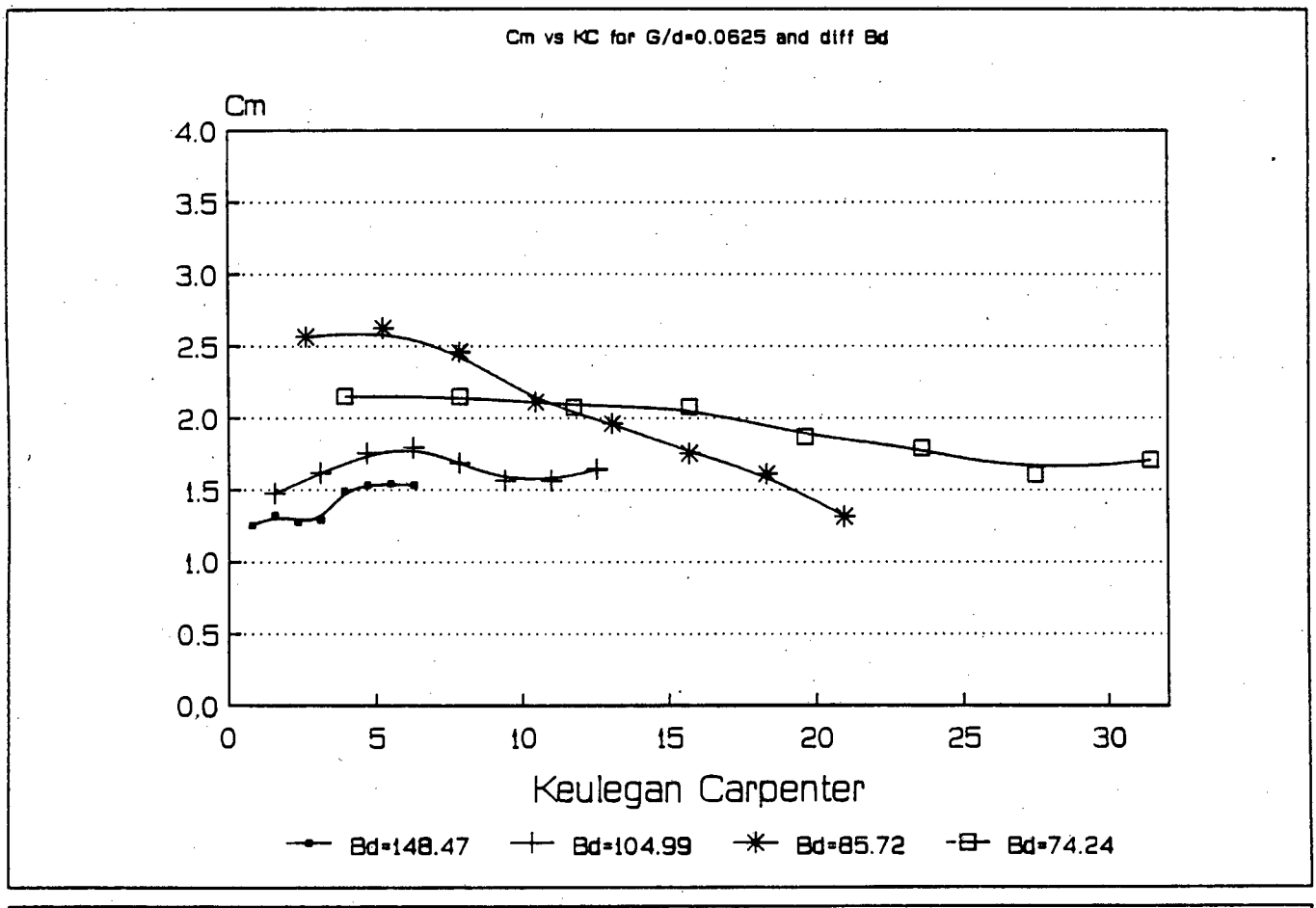

Figure I-96 : Cm vs KC for diameter=120mm, G/d=.0625 and different Bd.

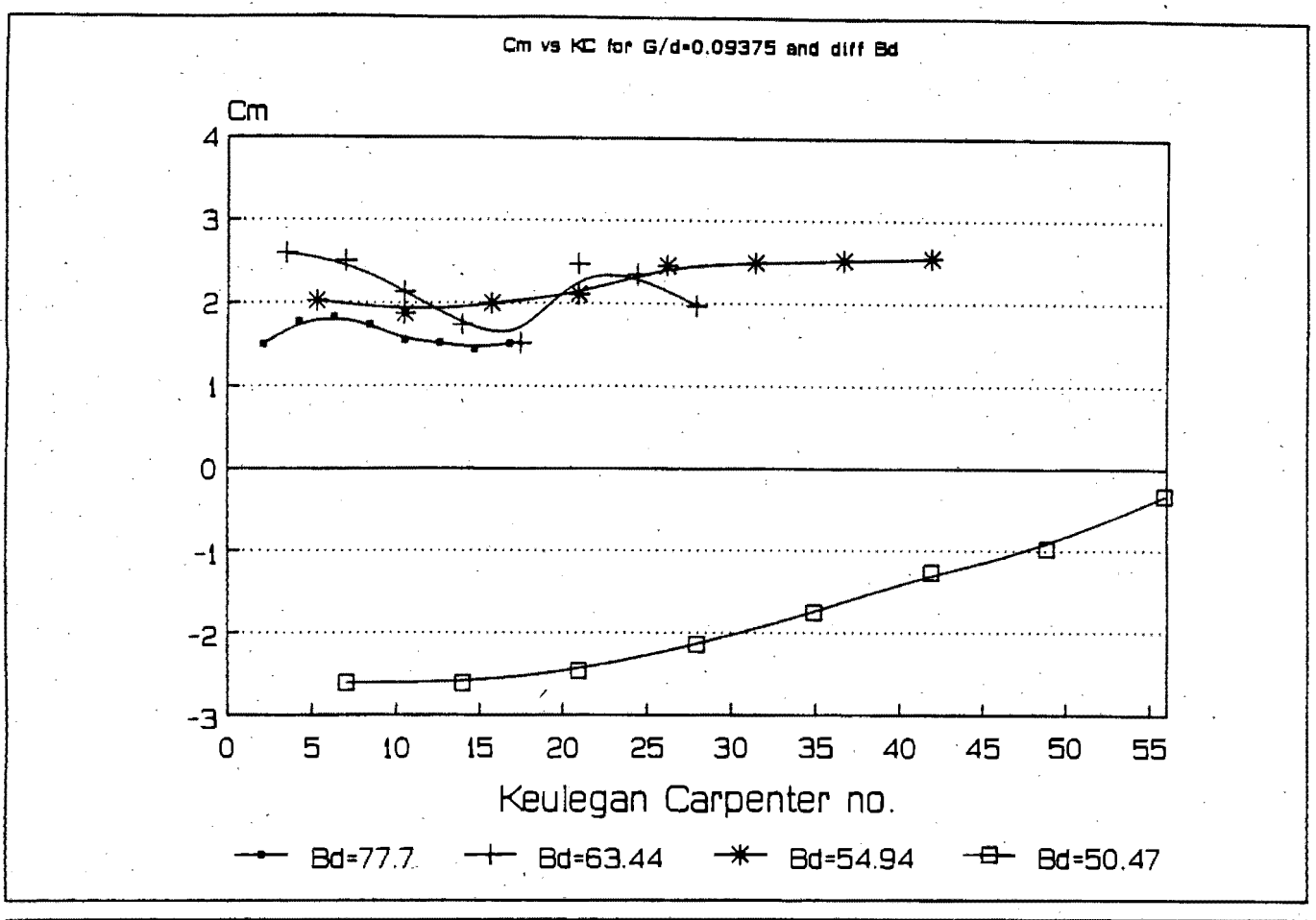

Figure I-97 : Cm vs KC for diameter=90mm, G/d=.09375 and different Bd.

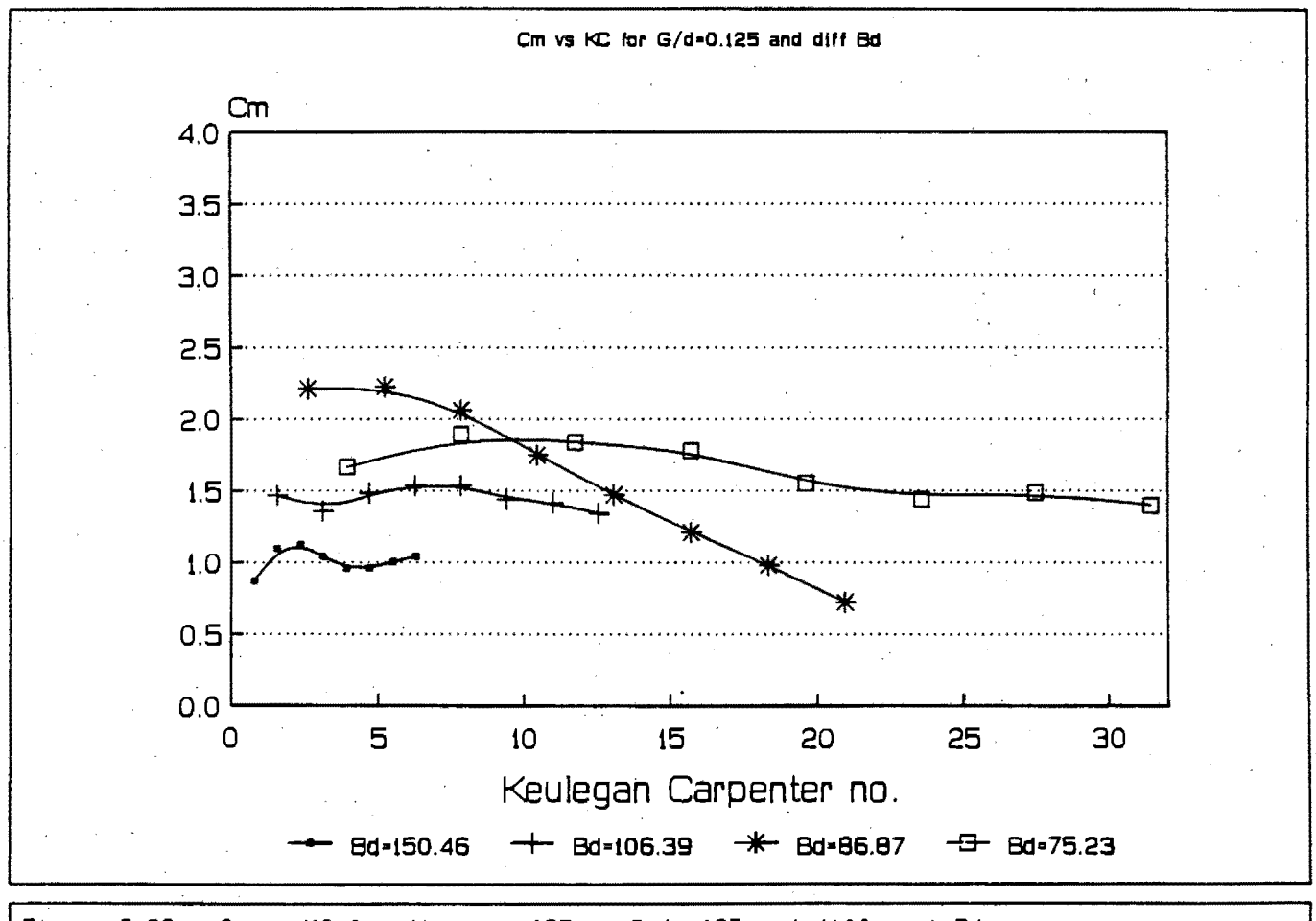

Figure I-98 : Cm vs KC for diameter=120mm, G/d=.125 and different Bd.

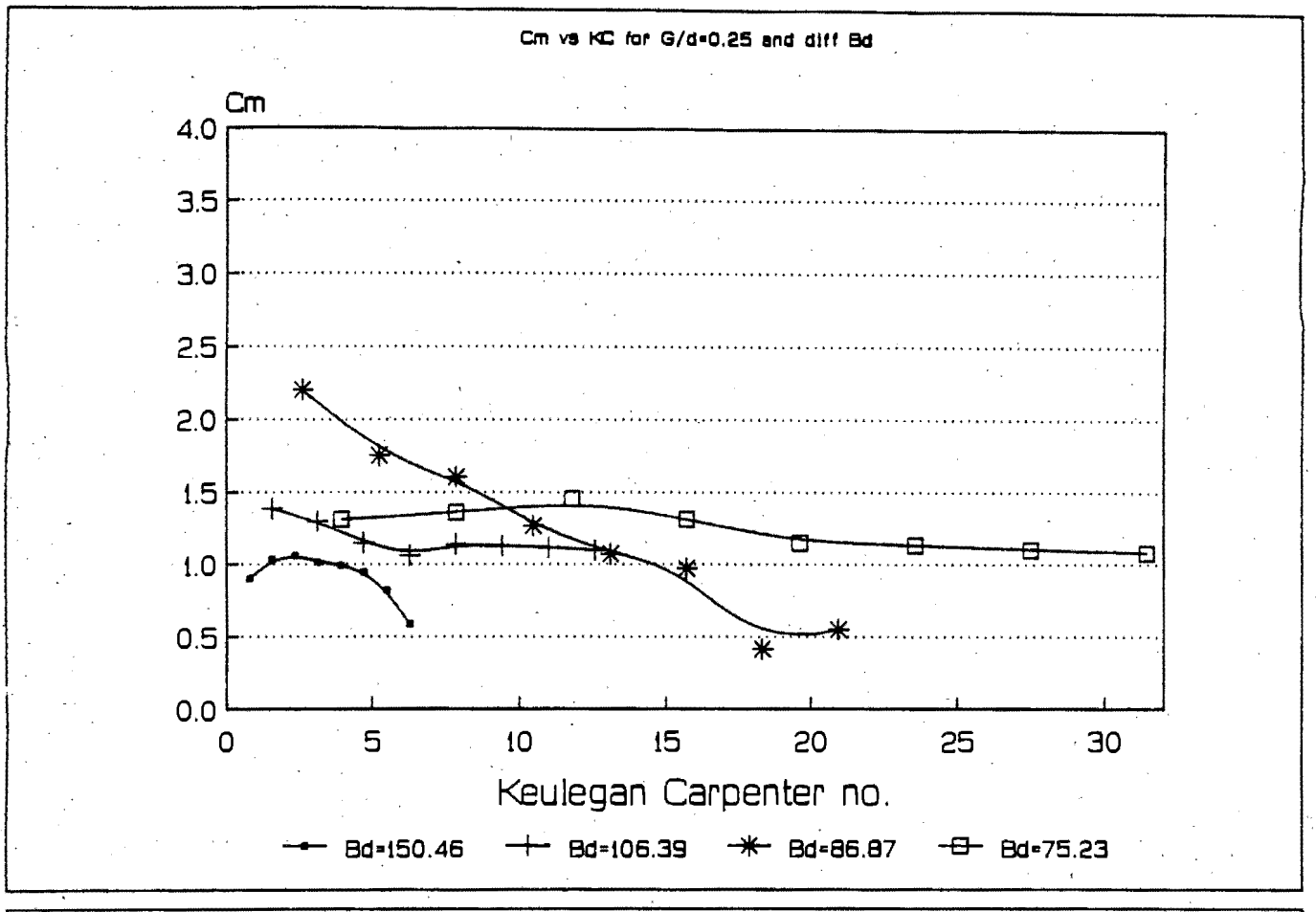

Figure I-99 : Cm vs KC for diameter=120mm, G/d=.25 and different Bd.

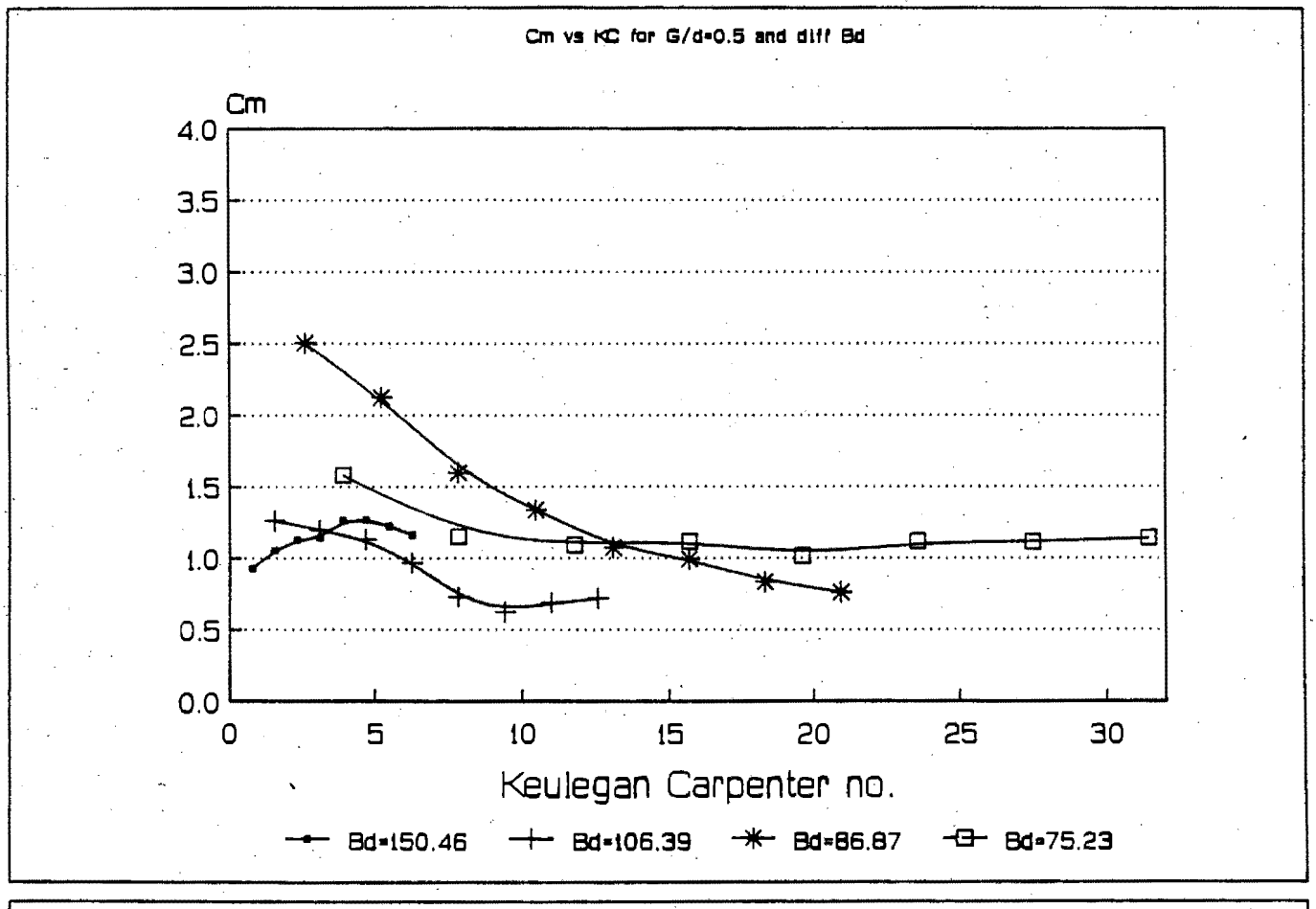

Figure I-100 : Cm vs KC for diameter=120mm, G/d=.5 and different Bd.

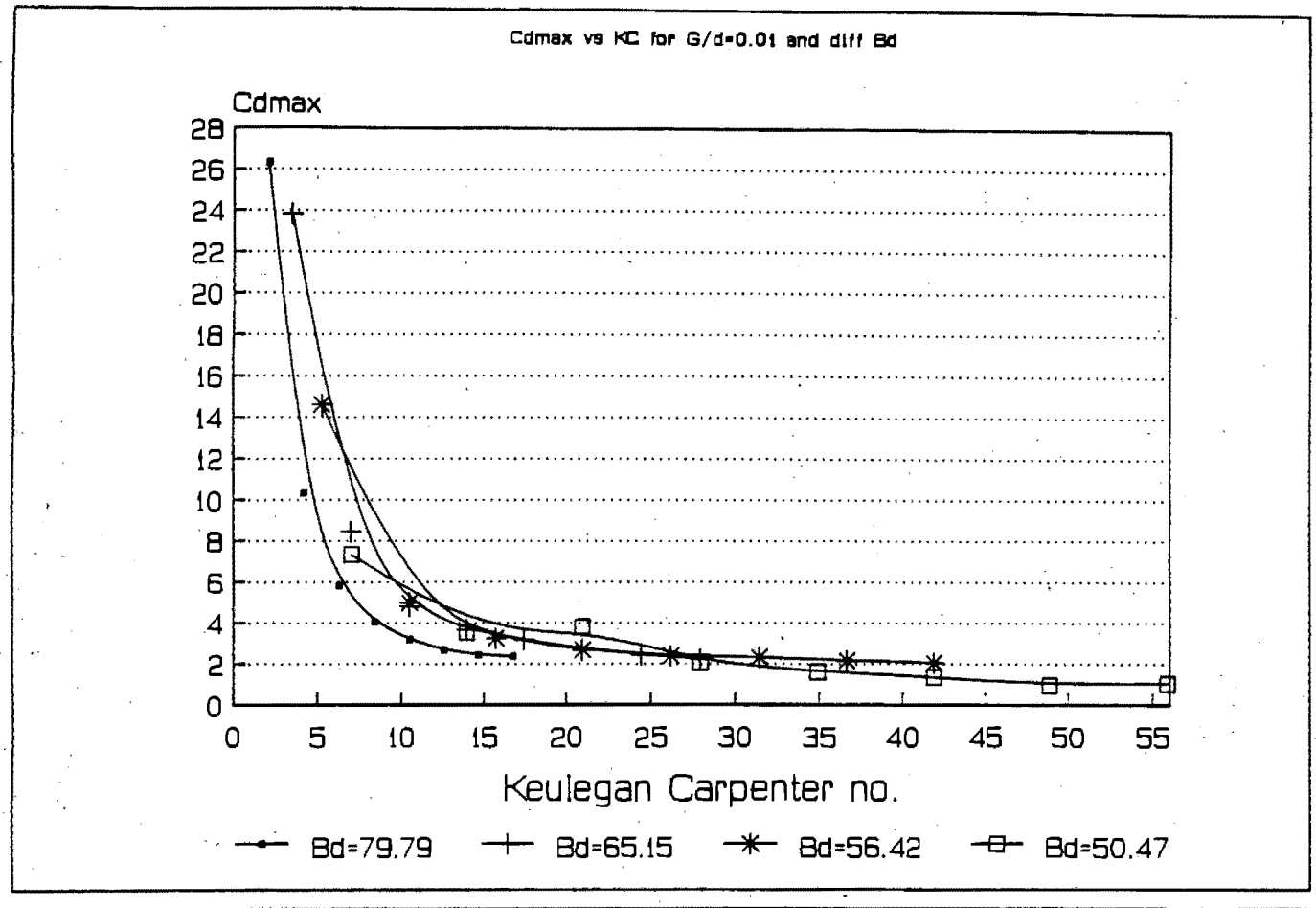

Figure I-101 : Cdmax vs KC for diameter=90mm, G/d=.01 and different Bd.

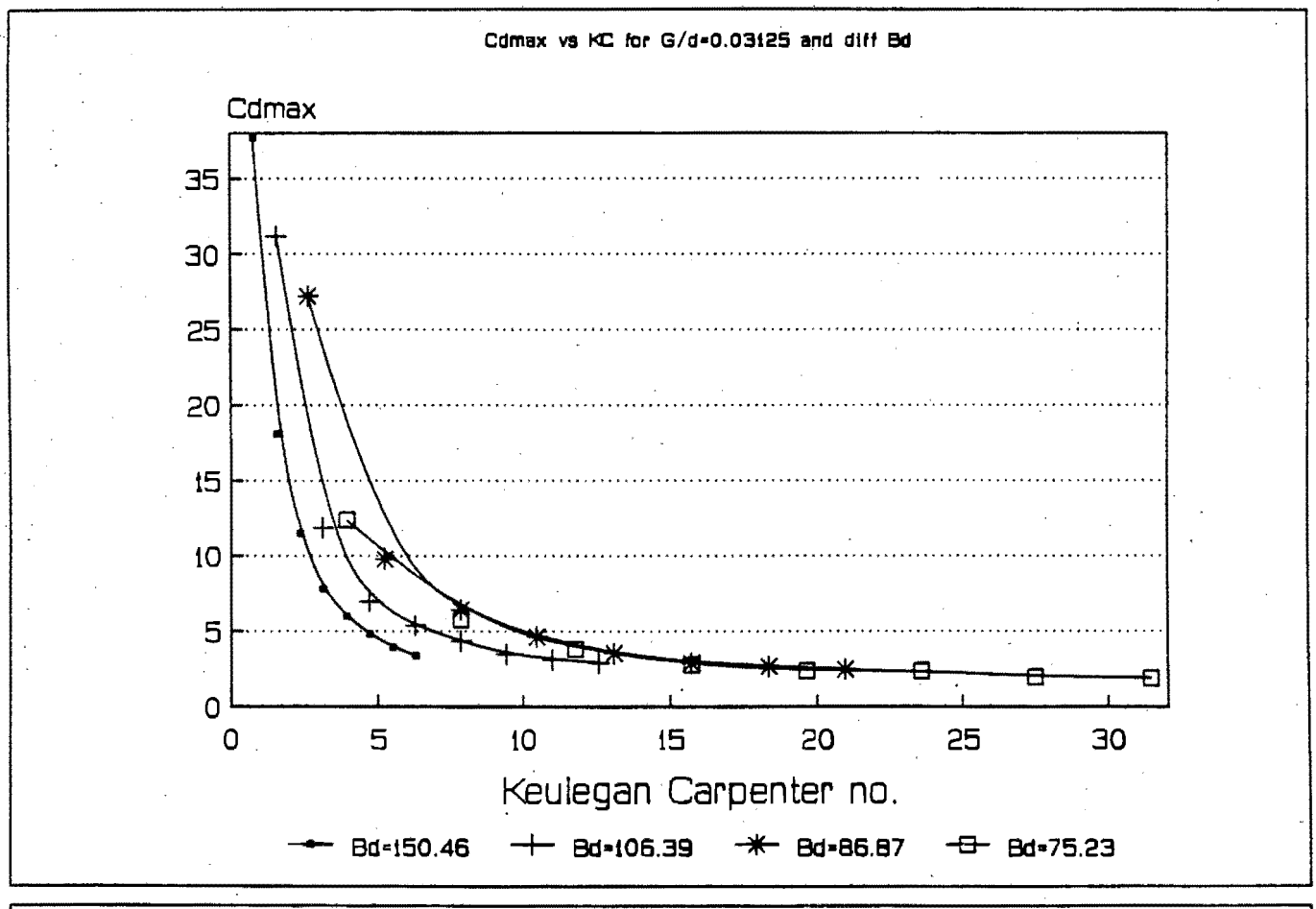

Figure I-102 : Cdmax vs KC for diameter=120mm, G/d=.03125 and different Bd.

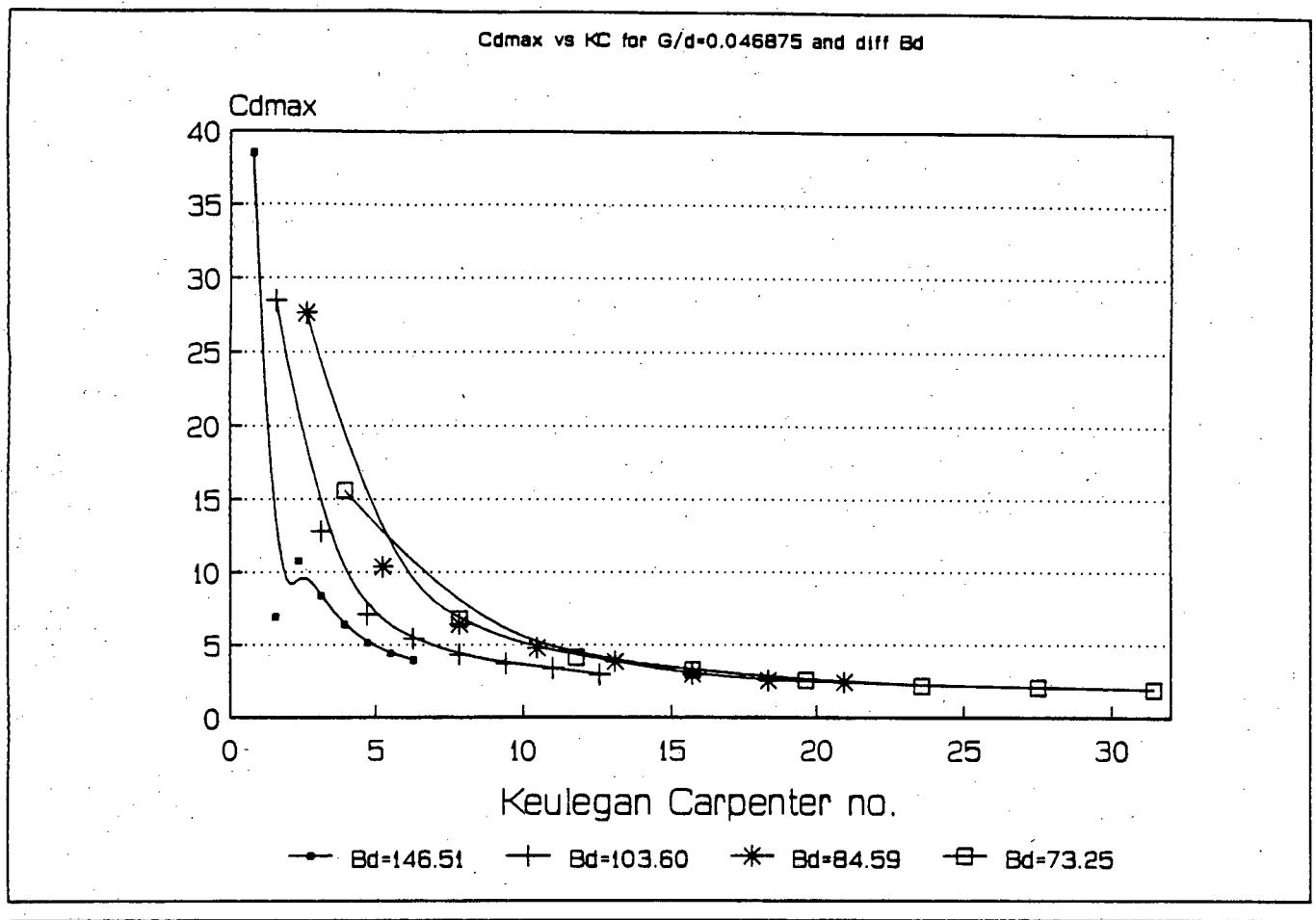

Figure I-103 : Cdmax vs KC for diameter=120mm, G/d=.046875 and different Bd.

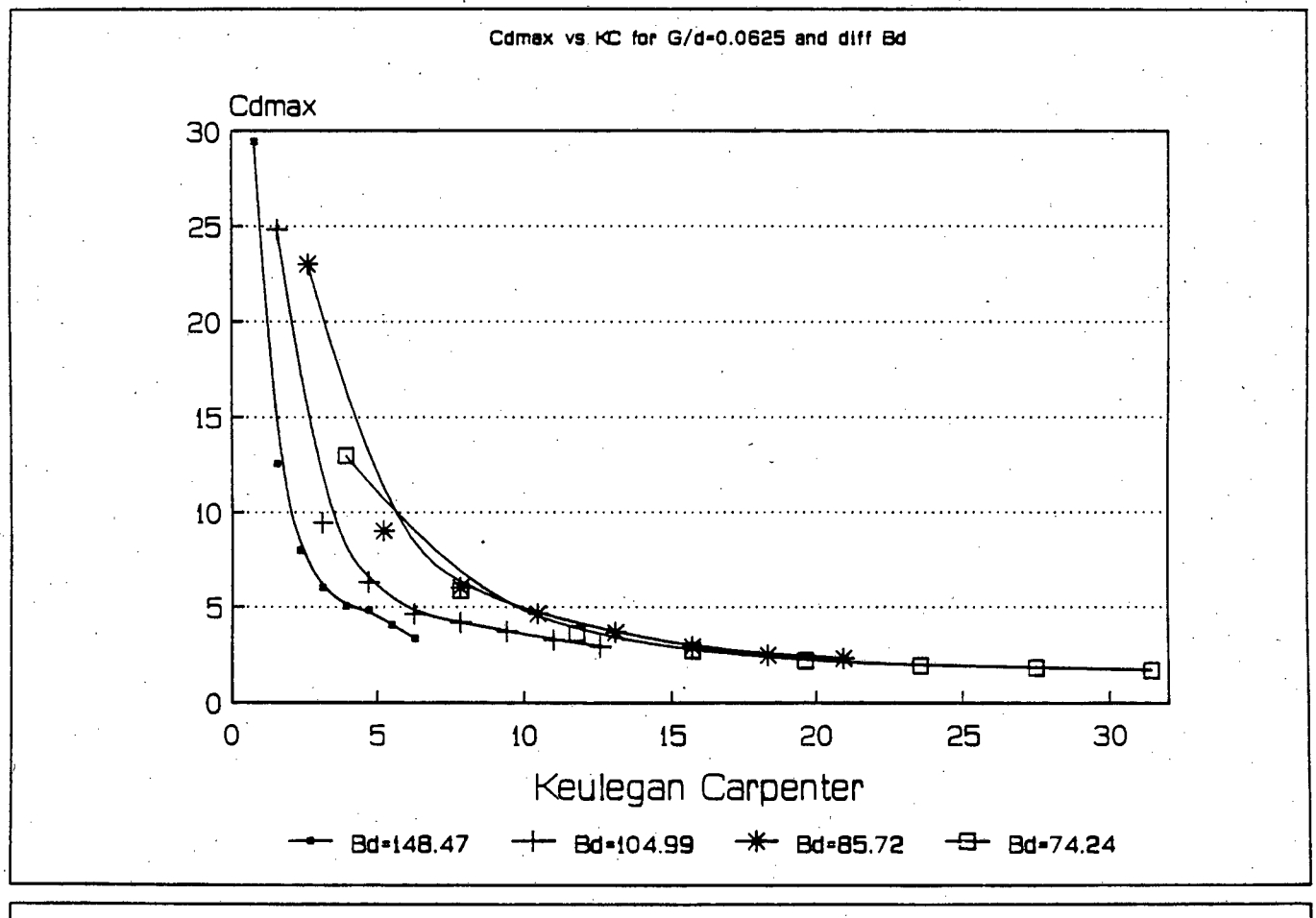

Figure I-104 : Cdmax vs KC for diameter=120mm, G/d=.0625 and different Bd.

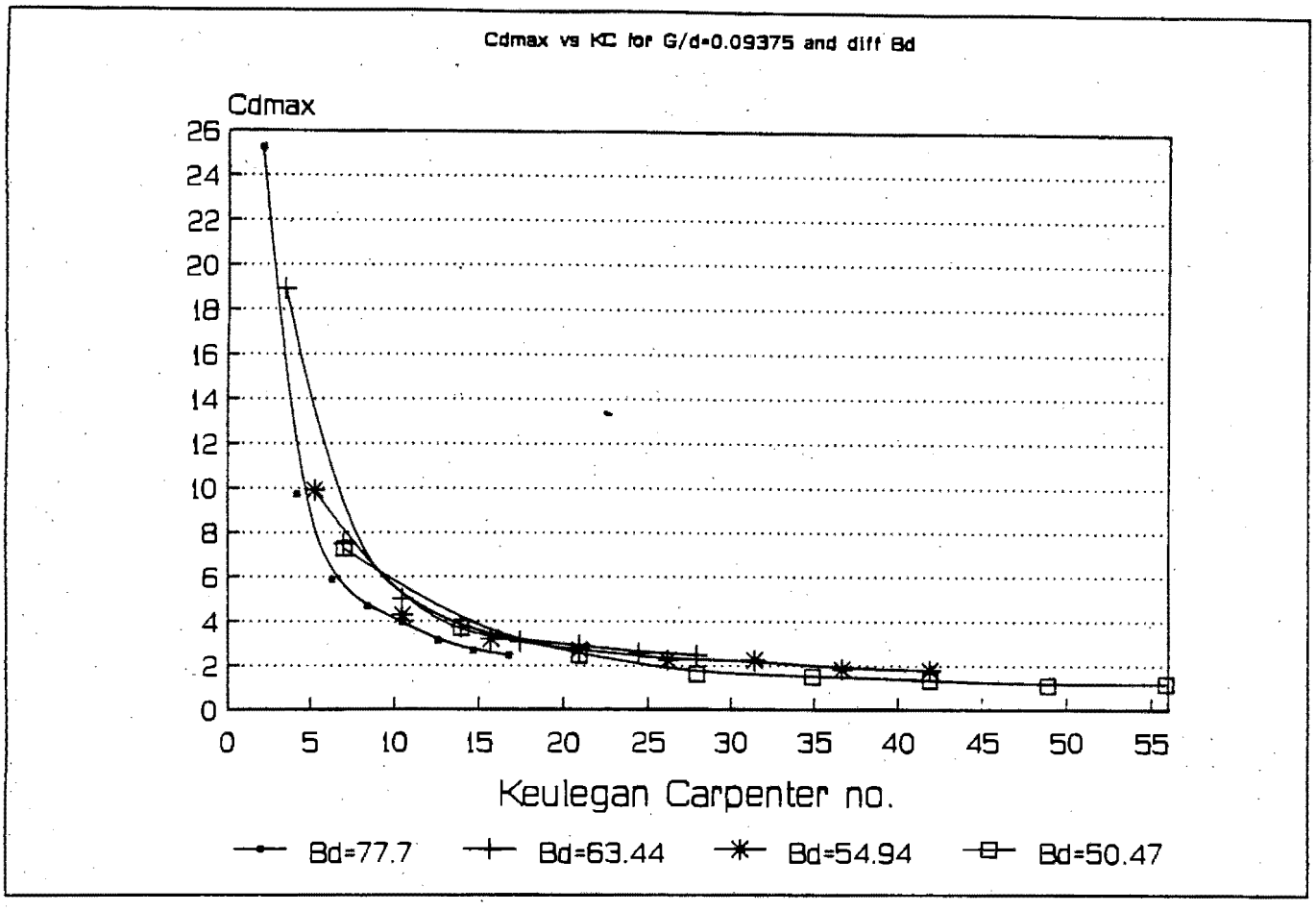

Figure I-105 : Cdmax vs KC for diameter=90mm, G/d=.09375 and different Bd.

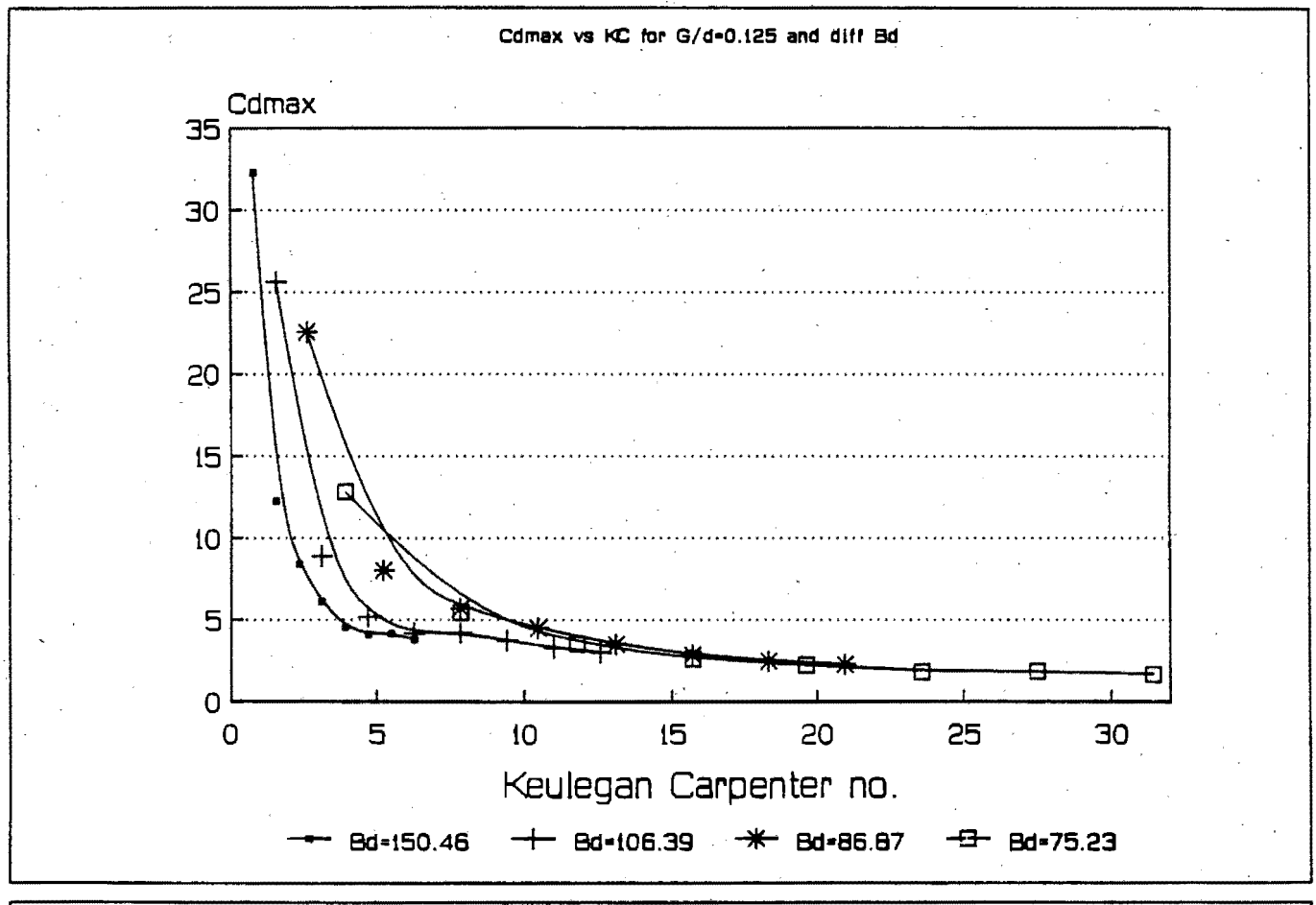

Figure I-106 : Cdmax vs KC for diameter=120mm, G/d=.125 and different Bd.

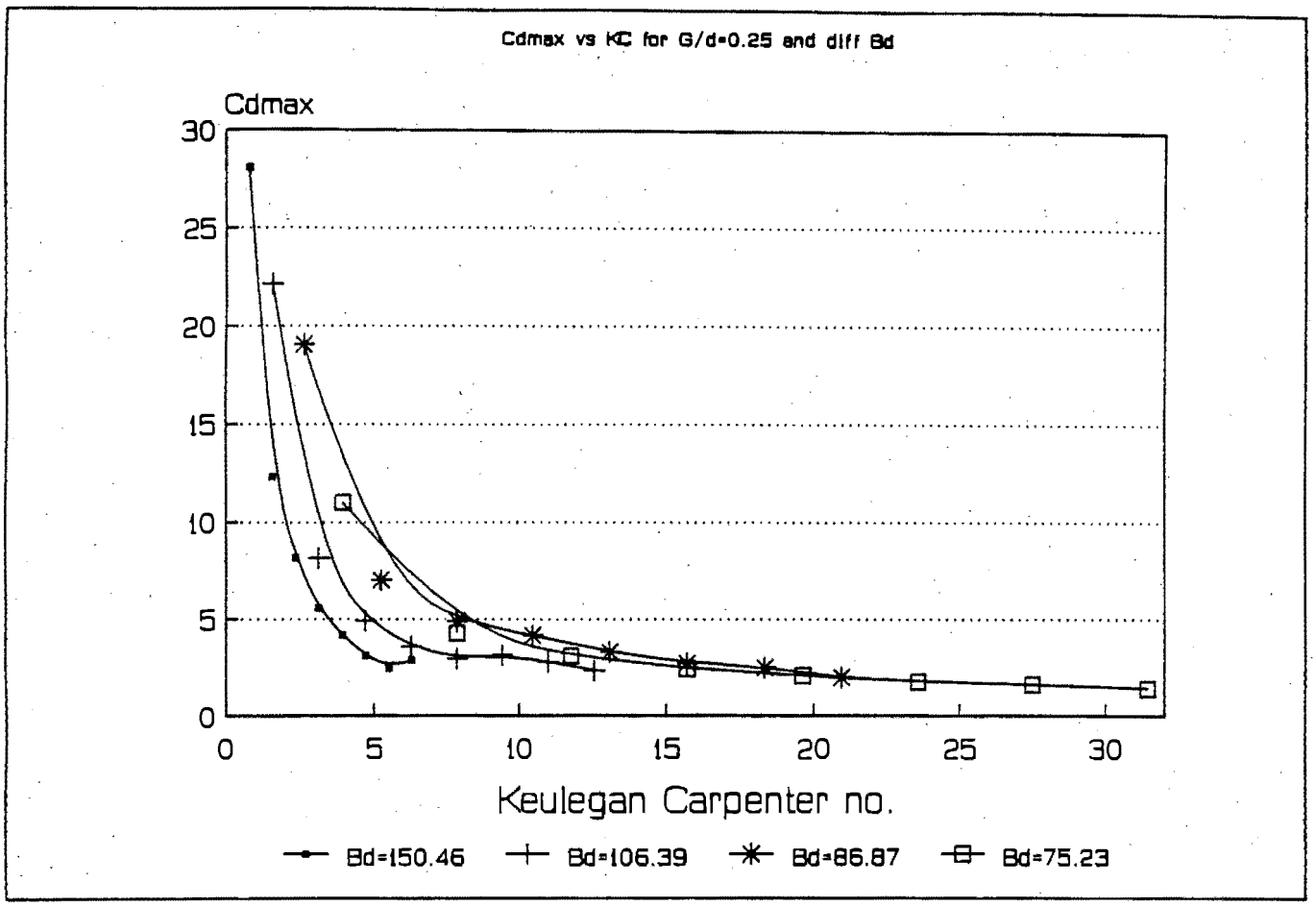

Figure I-107 : Cdmax vs KC for diameter=120mm, G/d=.25 and different Bd.

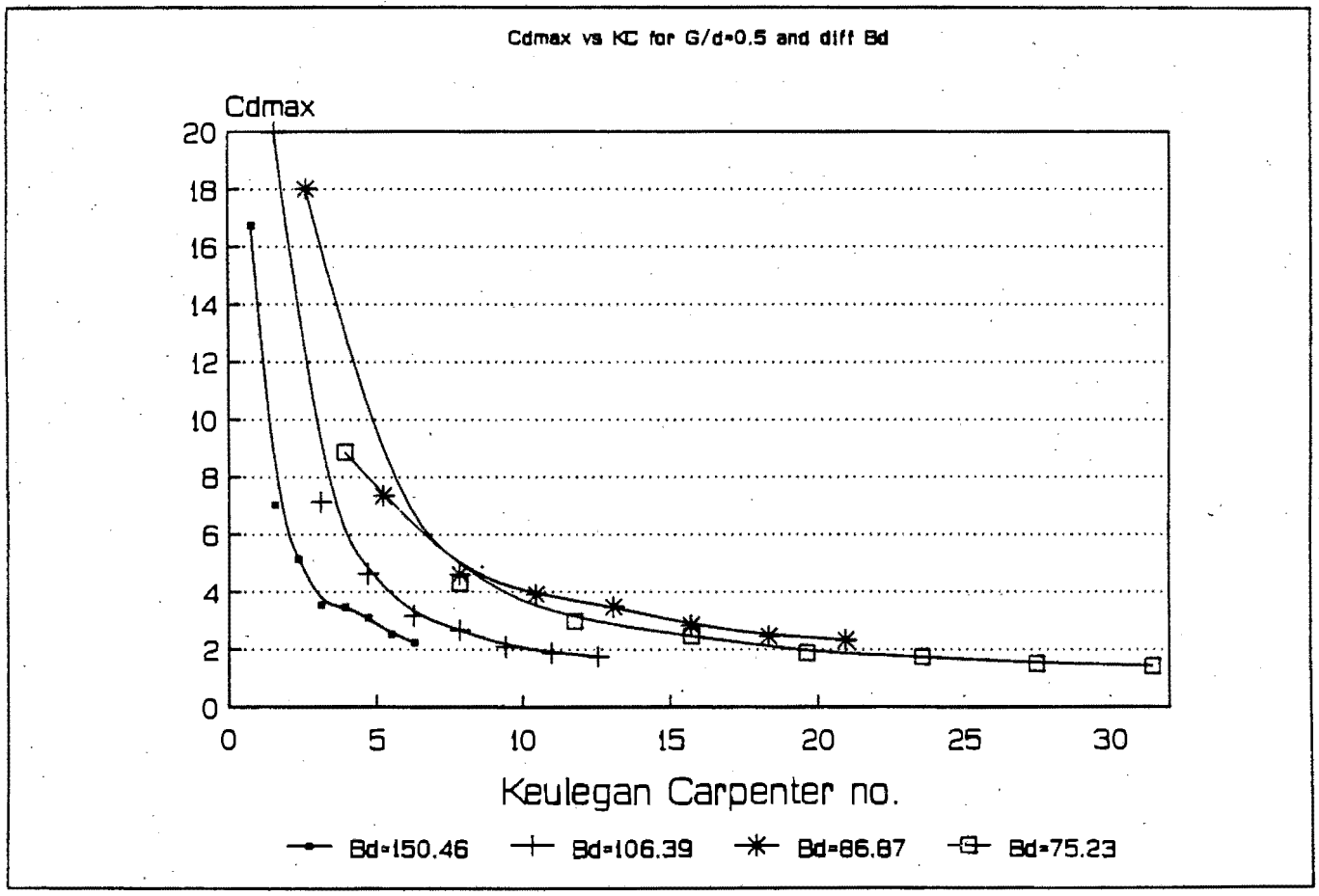

Figure I-108 : Cdmax vs KC for diameter=120mm, G/d=.5 and different Bd.

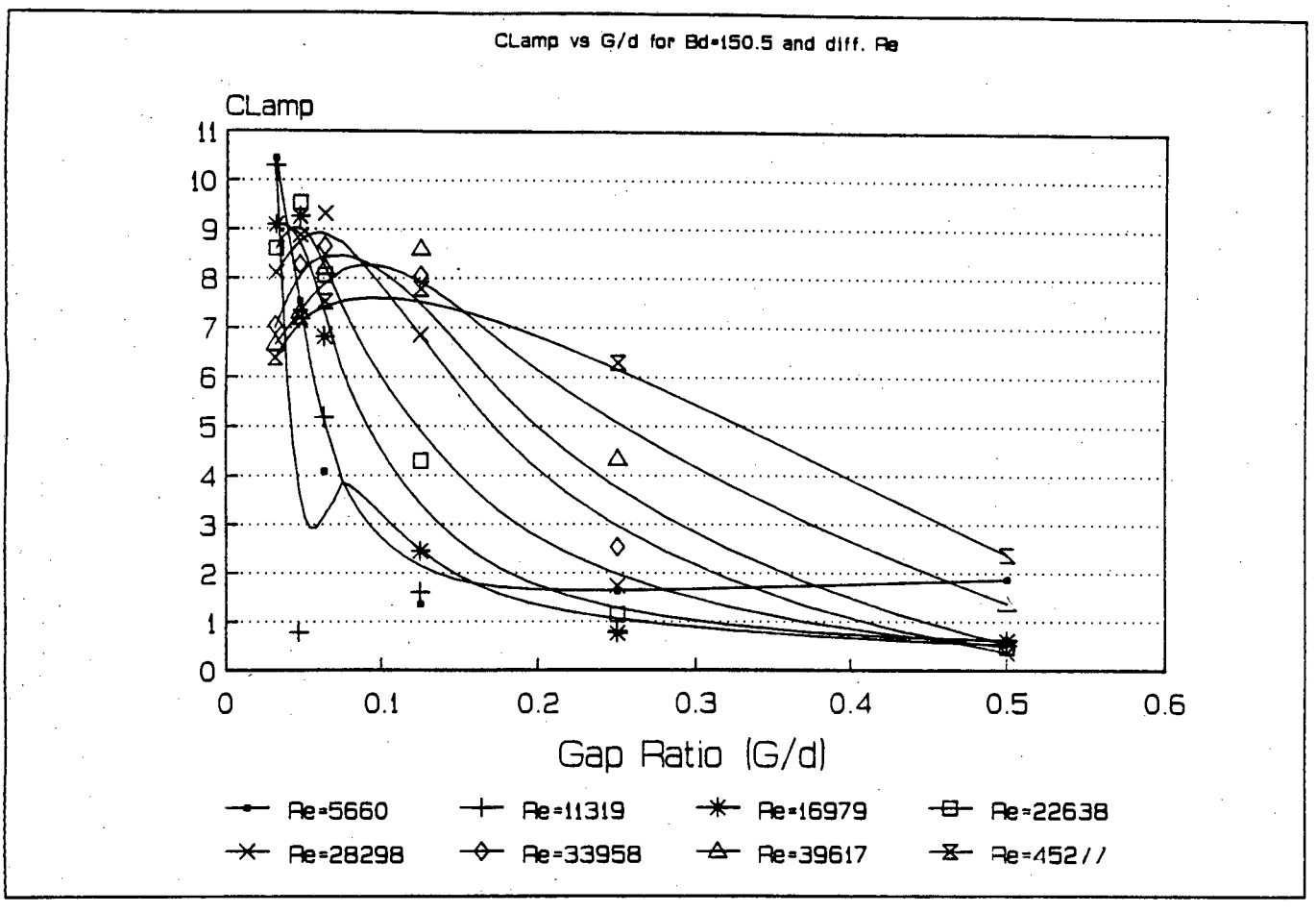

Figure I-109 : Clamp vs G/d for diameter=120mm, T=2s, Bd=150.5 and different Re.

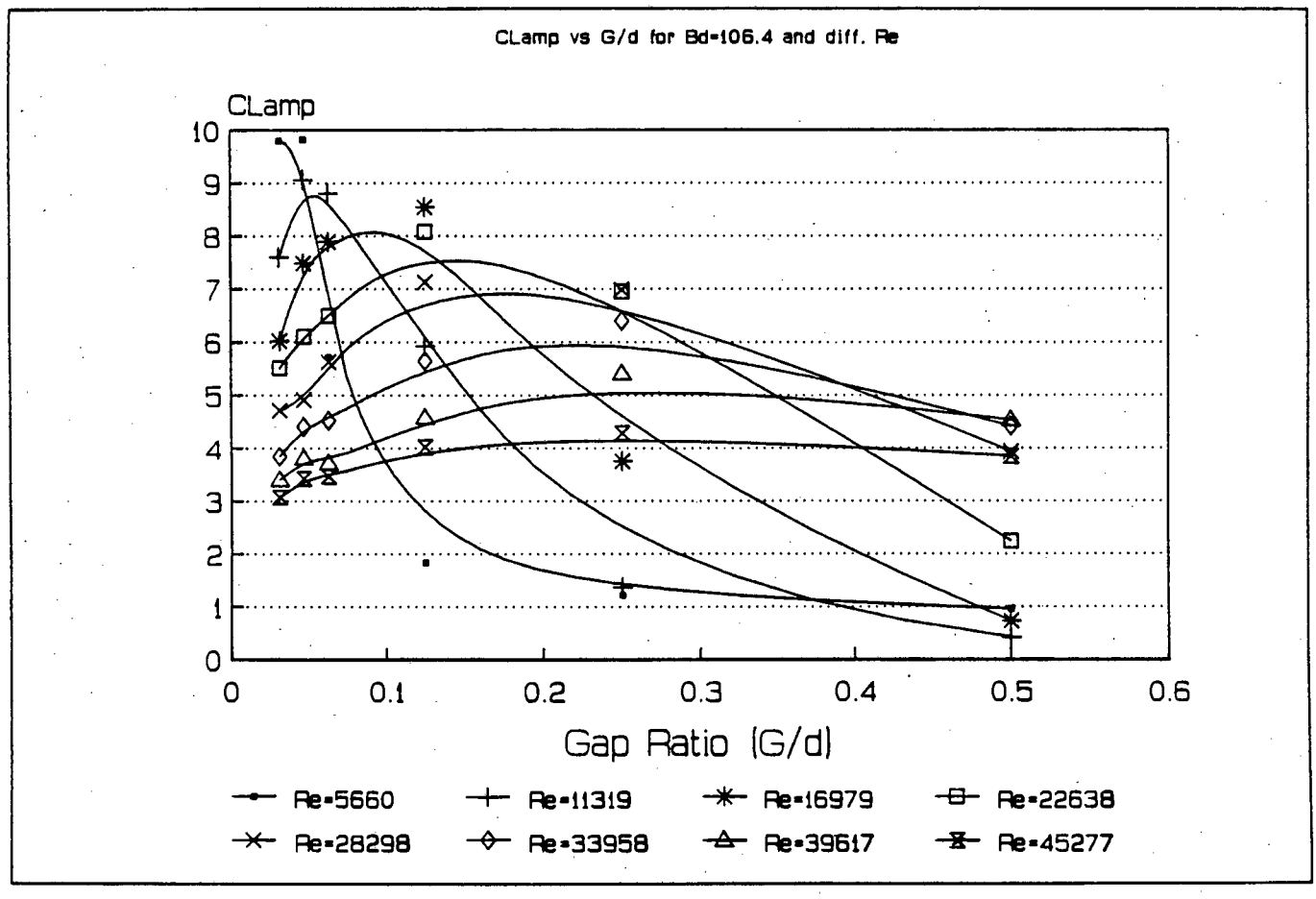

Figure I-110 : Clamp vs G/d for diameter=120mm, T=4s, Bd=106.4 and different Re.

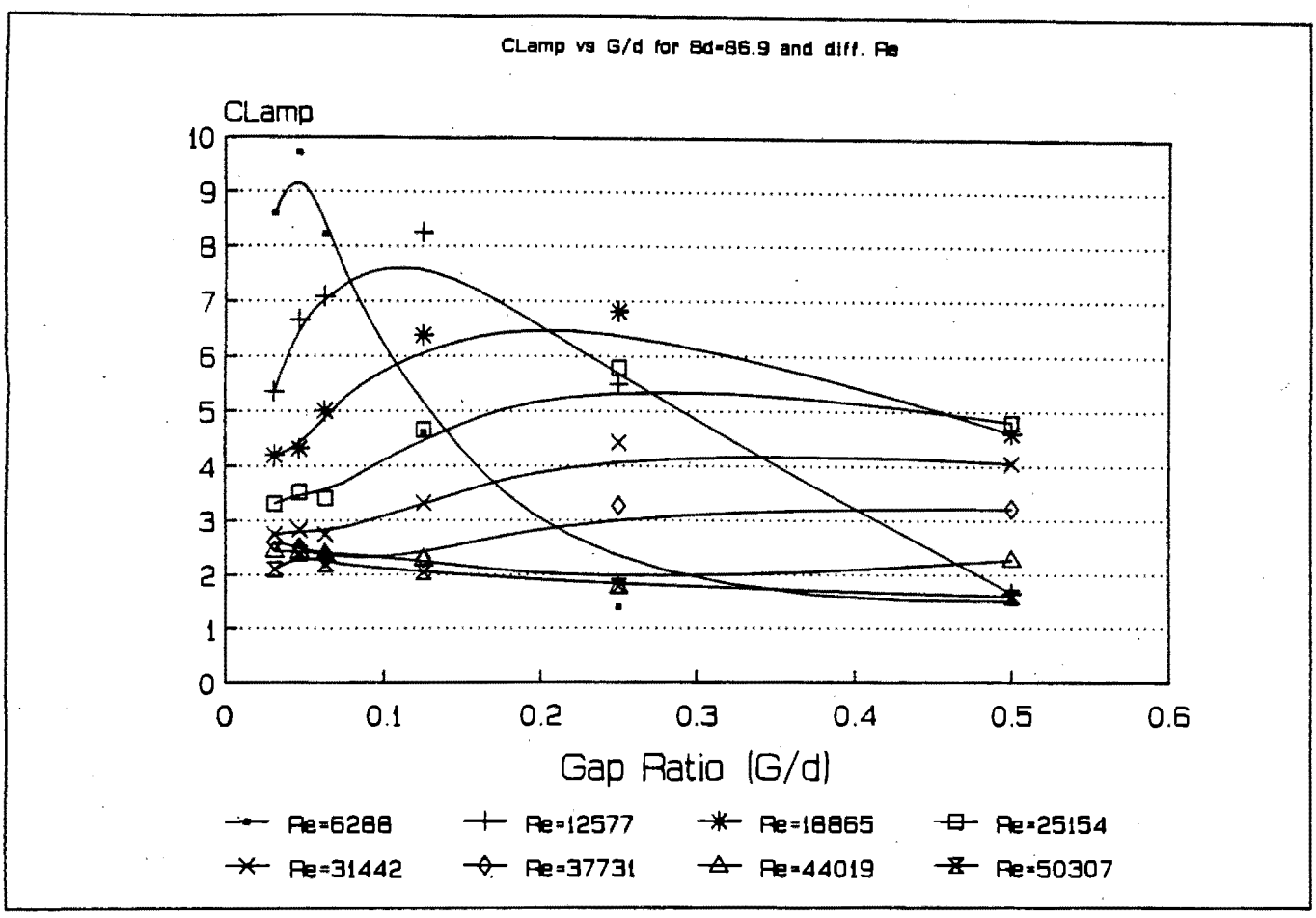

Figure I-111 : Clamp vs G/d for diameter=120mm, T=6s, Bd=86.9 and different Re.

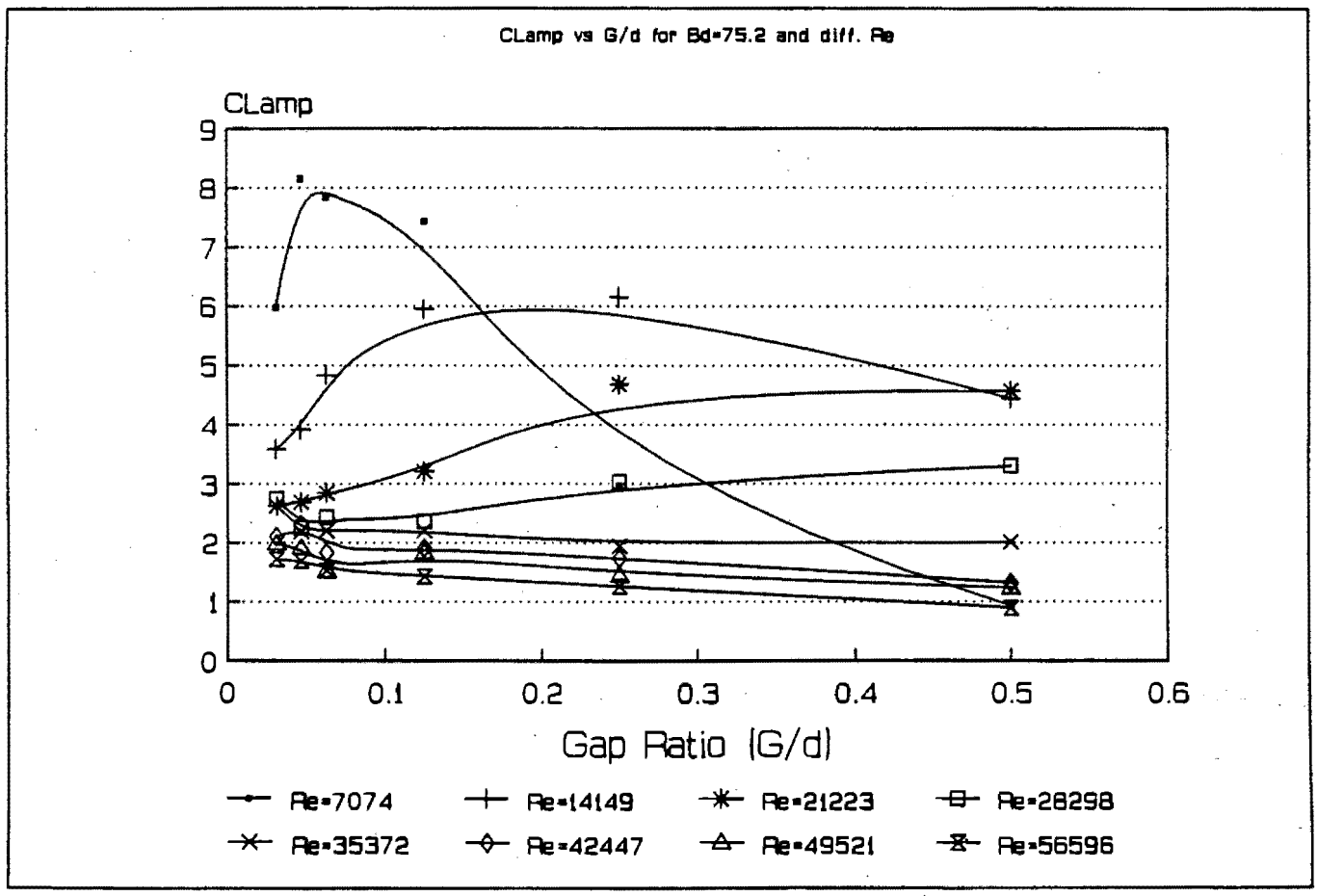

Figure I-112 : Clamp vs G/d for diameter=120mm, T=8s, Bd=75.2 and different Re.

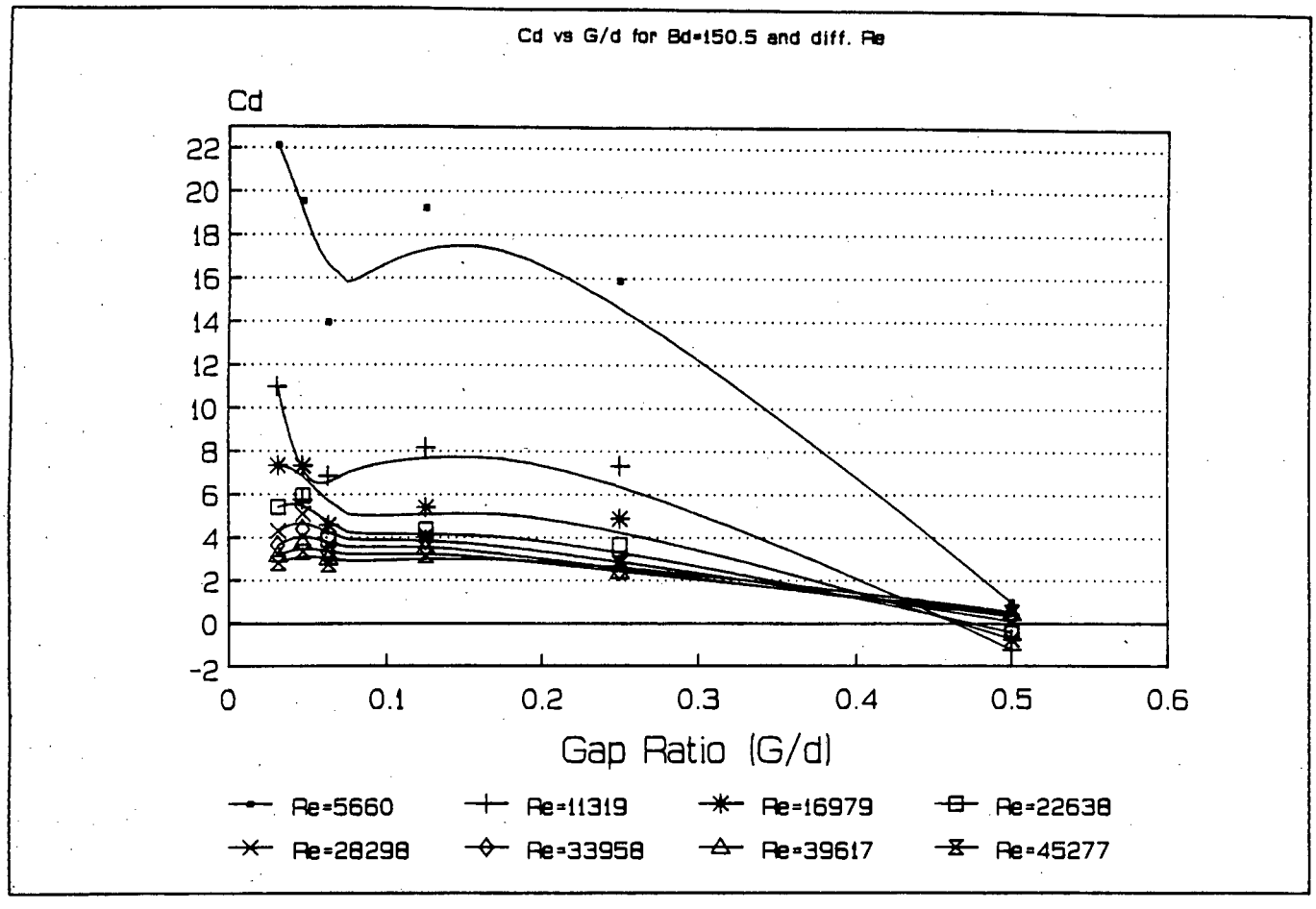

Figure I-113 : Cd vs G/d for diameter=120mm, T=2s, Bd=150.5 and different Re.

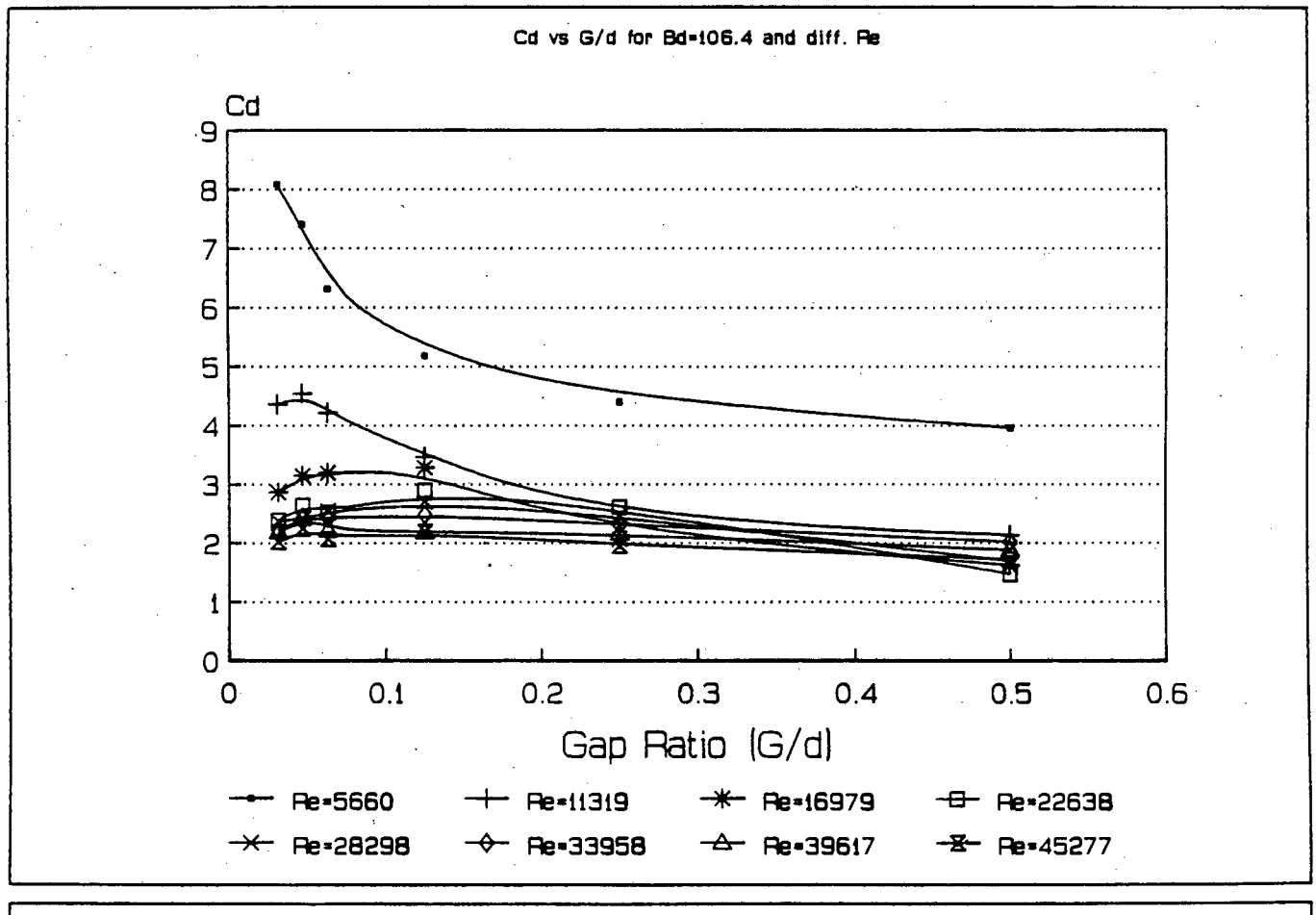

Figure I-114 : Cd vs G/d for diameter=120mm, T=4s, Bd=106.4 and different Re.

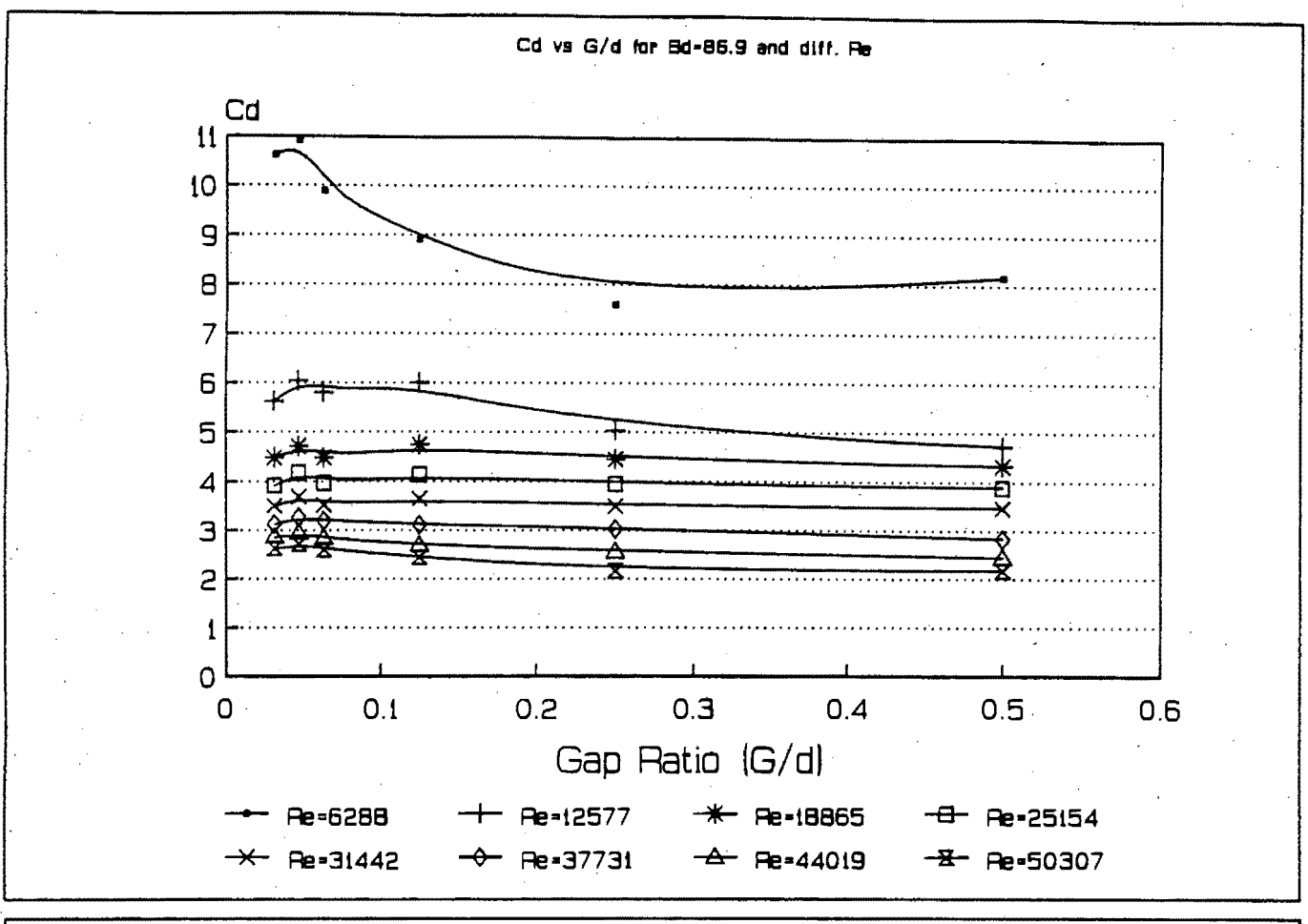

Figure I-115 : Cd vs G/d for diameter=120mm, T=6s, Bd=86.9 and different Re.

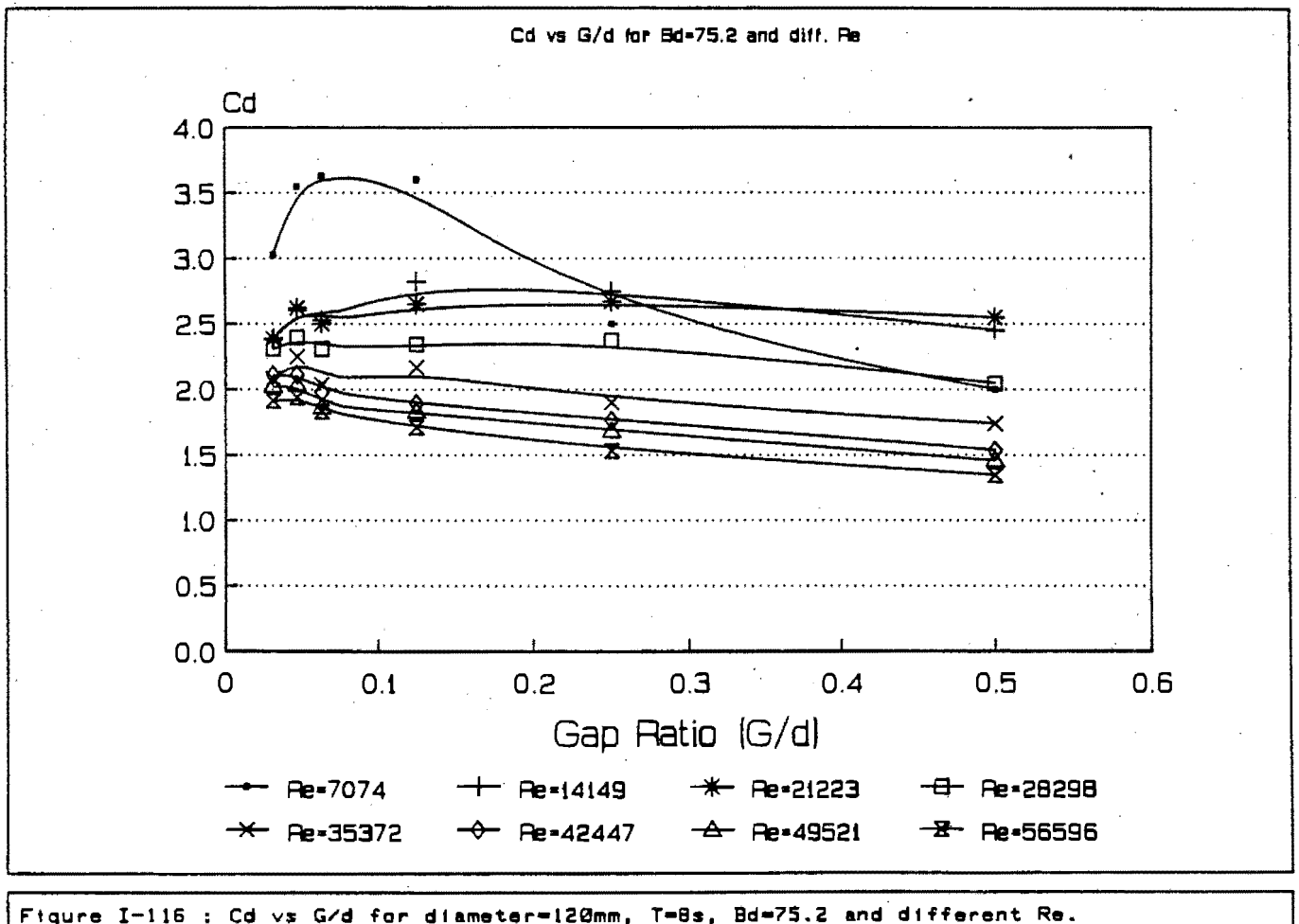

Figure I-116 : Cd vs G/d for diameter=120mm, T=8s, Bd=75.2 and different Re.

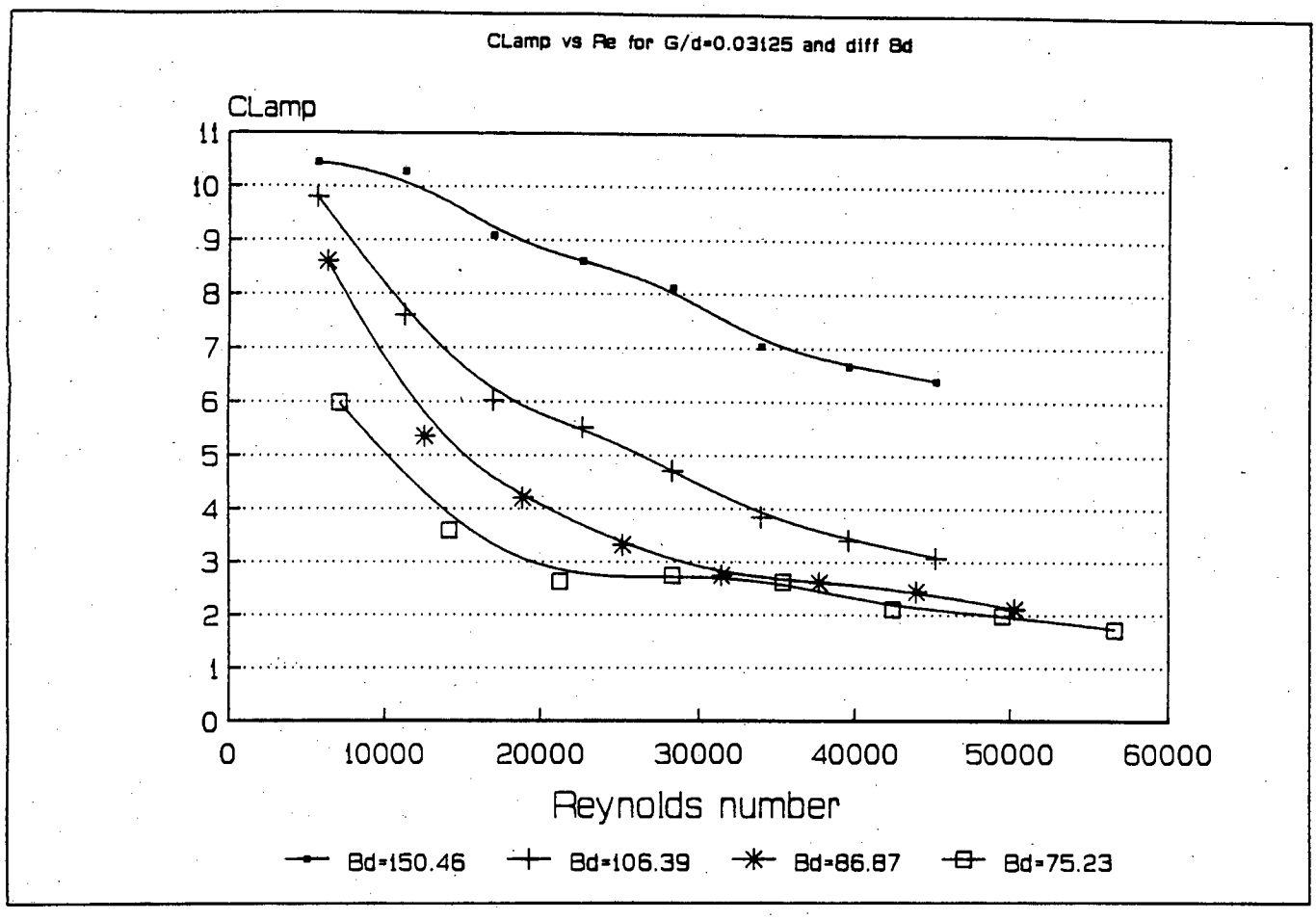

Figure I-117 : Clamp vs Re for diameter=120mm, G/d=.03125 and different Bd.

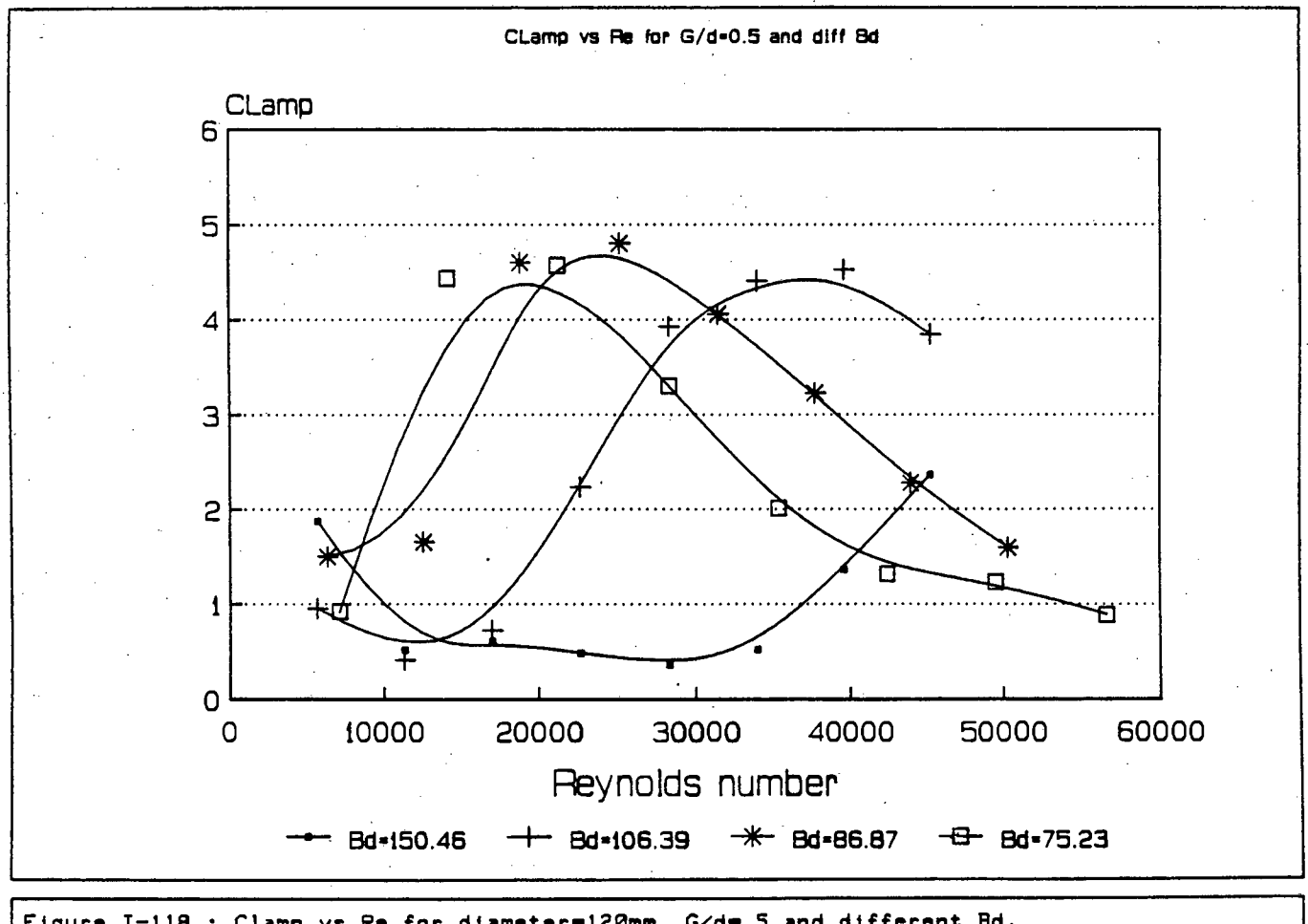

Figure I-118 : Clamp vs Re for diameter=120mm, G/d=.5 and different Bd.

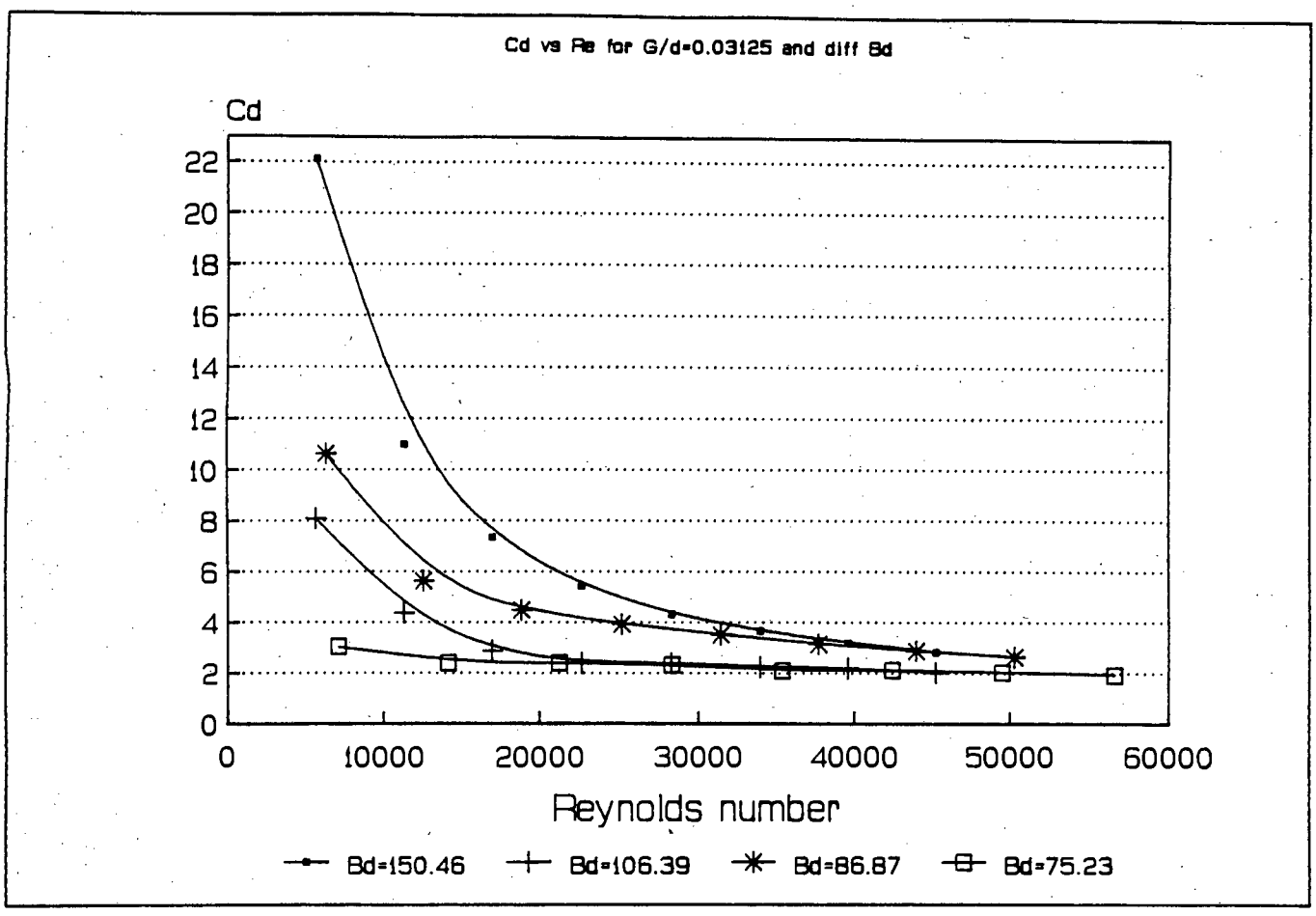

Figure I-119 : Cd vs Re for diameter=120mm, G/d=.03125 and different Bd.

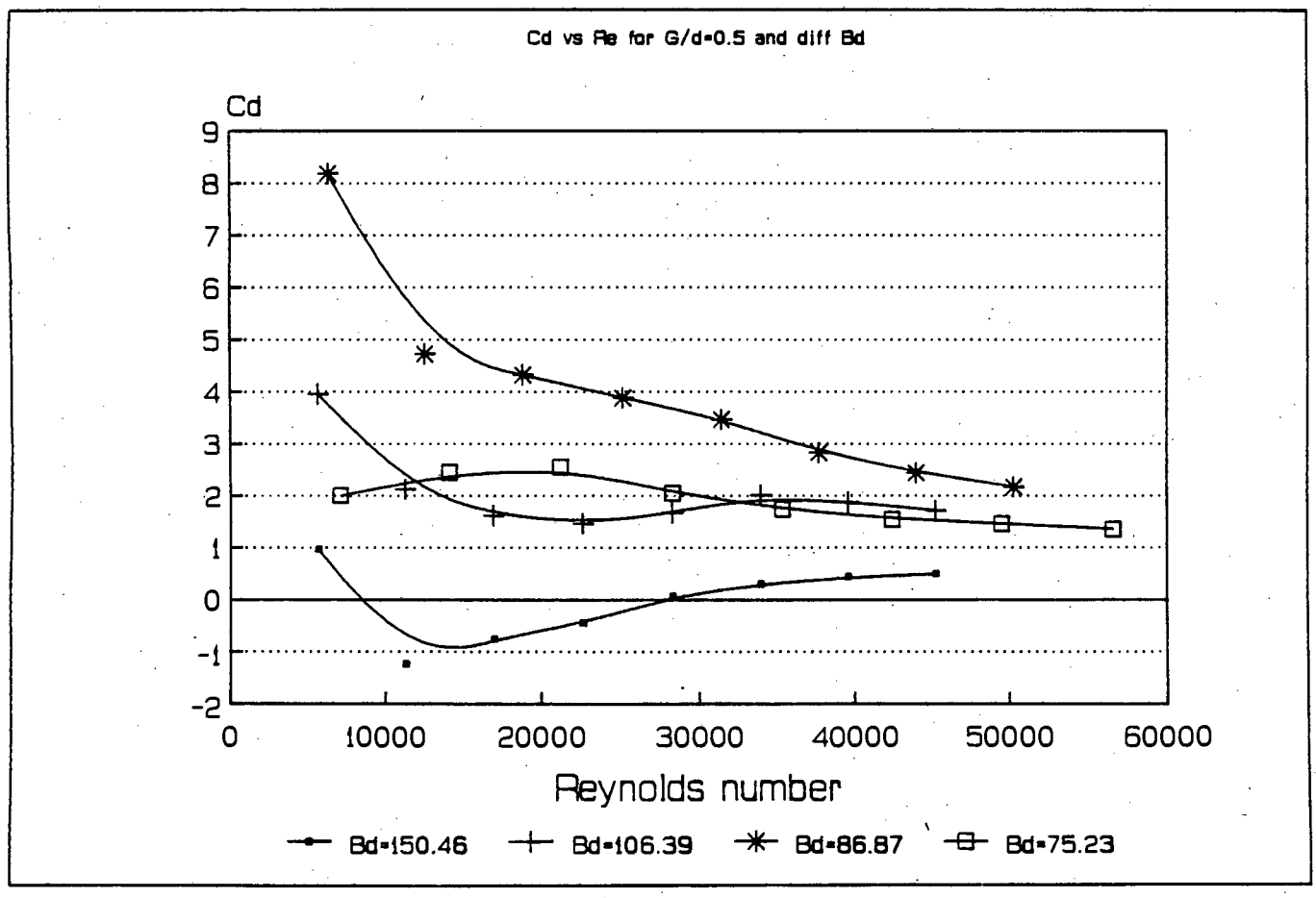

Figure I-120 : Cd vs Re for diameter=120mm, G/d=.5 and different Bd.

APPENDIX J - EXAMINATIONS WRITTEN BY THE AUTHOR TO COMPLETE THE REQUIREMENTS OF THE DEGREE OF MASTER OF SCIENCE IN CIVIL ENGINEERING.

EXAMINATION	CREDITS OBTAINED
Advanced hydraulic structures (CIV 519F)	5
Township services (CIV559F)	4
Pumps (CIV518S)	5
Contract law (CIV525S)	3
Constitutive modelling of soils (CIV544S)	3
	20
Dissertation	20
Total	40
Credits required	40